N00228-85-G-3262

DTIC FILE COPY

1

AD-A220 917

FULLY-NONLINEAR SIMULATION OF A PLUNGING BREAKING WAVE IMPACTING A VERTICAL WALL

by

Philip Wayne Taylor

B.S., Mech. Eng., United States Naval Academy (1980)

SUBMITTED TO THE DEPARTMENT OF OCEAN ENGINEERING IN PARTIAL FULFILLMENT OF THE REQUIREMENTS FOR THE DEGREE OF

MASTER OF SCIENCE IN NAVAL ARCHITECTURE AND MARINE ENGINEERING

at the

MASSACHUSETTS INSTITUTE OF TECHNOLOGY

February 1990

DTIC
ELECTE
APR 19 1990
S D
D

Copyright © Philip W. Taylor, 1990. All rights reserved.

The author hereby grants to MIT permission to reproduce and to distribute copies of this thesis in whole or in part.

The author grants this same right to the U.S. Government.

DISTRIBUTION STATEMENT A
Approved for public release;
Distribution Unlimited

Signature of Author Philip W. Taylor
Department of Ocean Engineering
February 21, 1990

Certified by Dick Yue
Professor Dick K. P. Yue
Thesis Supervisor

Accepted by _____
Professor A. Douglas Carmichael
Chairman, Ocean Engineering Department Graduate Committee

04 17 073

FULLY-NONLINEAR SIMULATION OF A PLUNGING BREAKING WAVE IMPACTING A VERTICAL WALL

by

Philip Wayne Taylor

Submitted to the Department of Ocean Engineering on December 29, 1989 in partial fulfillment of the requirements for the degree of Master of Science in Naval Architecture and Marine Engineering.

Abstract

The primary objective of this research is to extend fully nonlinear potential flow theory to the problem of breaking wave impact upon a vertical wall. The validity of this theory as a basis for the simulation of a deep-water plunging breaking wave has recently been demonstrated by comparison of numerical results with experiments by Chan. The numerical approach used was a mixed Eulerian-Lagrangian method based upon application of Cauchy's integral theorem to the fluid domain. This same approach is applied to the wave impact problem in the present work. The experimental results of Chan on the kinematics and dynamics of wave impact on a vertical wall provide a basis for comparison.

As a preliminary study, the simulation of a plunging breaker in a long tank is repeated to examine the difficulties involved more closely and to investigate the influence of point regridding and smoothing routines upon the results. Next, the a shorter numerical tank is used with the same wavemaker input in order to force overturning to occur near the end of the tank. Several difficulties with simulation are revealed which were not present with the longer tank, and techniques are developed to address them. A simulation is finally achieved in which the overturning wave reaches the end of the tank before re-entry into the free surface occurs. This allows the imposition of an impact condition at the end of the tank. Various techniques for simulating the impact process are then investigated.

The preliminary results obtained for the impact simulations show qualitatively plausible flows in some cases, with the formation of upward and downward moving jets along the wall after impact. The computed impact pressures on the wall, however, are initially negative and are found to be dependent on the number of points used to define the impact region on the wall. Further investigation is required to assess the ability of this potential flow model to simulate wave impact.

Thesis Supervisor: ProfessorDickK.P.Yue
Title: AssociateProfessor

Dedication

To Athena

Accesion For
NTIS CRA&I ☑
DTIC TAB ☐
Unannounced ☐
Justification
By per form 50
Distribution /
Availability Codes
Dist | Avail and / or Special
A-1

DTIC COPY INSPECTED 4

Table of Contents

Abstract 2
Dedication 3
Table of Contents 4
List of Figures 6

1. Introduction 7

2. Mathematical Formulation 9

3. Numerical Implementation 13
- 3.1 Discretization, Solution and Time Integration 13
- 3.2 Regridding and Smoothing; Time Step Control 14
- 3.3 Conservation of Mass and Energy 15
- 3.4 Structure of Program 17
- 3.5 Wavemaker Input 24
- 3.6 Convergence Tests 26
  - 3.6.1 Typical Computing Times 28

4. Simulation of a Plunging Breaker in a Long Tank 29
- 4.1 Results Using Modified Code 30
  - 4.1.1 Summary of Runs and Failure Types 30
  - 4.1.2 Comparison of Successful Runs 32
- 4.2 Summary 34

5. Simulation of a Plunging Wave Near a Wall: Pre-Impact Flow 36
- 5.1 Results: L=11.667 37
  - 5.1.1 Summary of Attempted Runs and Failure Types 37
  - 5.1.2 Comparison of Successful Run with Experiment 40
- 5.2 Results: Variation of Tank Lengths 41
  - 5.2.1 Summary of Attempted Runs and Failure Types 42
  - 5.2.2 Comparison of Run L=11.60 with Experiment 43
- 5.3 Results: Effort to Increase Point Resolution 43
  - 5.3.1 Techniques Investigated 43
    - 5.3.1.1 Point addition 43
    - 5.3.1.2 Modified smoothing 48
    - 5.3.1.3 Alternate finite difference for wall point velocity 52
    - 5.3.1.4 Alternate finite difference plus modified smoothing 54
  - 5.3.2 Comparison of Successful Run with Experiment 58
- 5.4 Summary 58

6. Simulation of a Plunging Wave Near a Wall: Impact Process 60
- 6.1 Results 62
  - 6.1.1 Summary of Attempted Runs 64
  - 6.1.2 Computation of Pressures 69
  - 6.1.3 Comparison with Experiment 70

6.2 Summary 70

7. Investigation of Criteria for a Robust Point Distribution Scheme **73**

7.1 Selection of Parameters and Test Cases 76
7.2 Definition of Criteria 77
7.3 Summary 80

8. Conclusions **81**

8.1 Summary of Work 81
8.1.1 Simulations for Long Tank 81
8.1.2 Simulations for Short Tank: Pre-impact 82
8.1.3 Simulations for Short Tank: Post Impact 84
8.2 Recommendations for Future Work 84
8.2.1 Point Distribution Schemes 84
8.2.2 Impact Problem 85

Appendix A. **87**

Appendix B. **137**

Appendix C. **199**

Appendix D. **240**

Appendix E. **327**

Appendix F. **372**

Appendix G. **382**

Appendix H. **439**

Appendix I. **460**

Appendix J. **536**

List of Figures

Figure 2-1: Fluid domain for pre-impact flow. 10
Figure 2-2: Fluid domain for post-Impact flow 11
Figure 3-1: Wavemaker velocity input time history. 25
Figure 7-1: Comparison of SAW for runs B1 and B4. 79

Chapter 1

Introduction

Two natural processes which are little understood from a theoretical viewpoint are the evolution of steep and overturning water waves and the impact of such waves upon rigid structures. The development of numerical models to gain insight into these processes is of great interest, especially in the case of wave impact on structures.

The ability of a fully nonlinear potential flow model to describe the motion of steep and overturning gravity waves was confirmed in the work of Dommermuth, Yue, Lin, Rapp, Chan and Melville [3],in which numerical simulations based upon nonlinear potential theory reproduced experimental measurements of surface elevations and fluid velocities at various depths for a plunging breaker generated in a wave tank by a piston-type wavemaker. The numerical approach used was a mixed Eulerian-Lagrangian scheme similar to that developed by Vinje and Brevig [9]. The success of a model which ignores such physical phenomena as viscosity and surface tension also implies that these mechanisms are relatively unimportant for plunging breaking waves [3], at least far from surface-piercing boundaries and prior to re-entry of the overturning crest into the free surface.

The kinematics and dynamics of deep-water plunging waves impacting on a vertical wall were investigated experimentally by Chan [1] using the same wavemaker and tank setup. In the experiment, a computer-controlled wave generator was first used to consistently reproduce a plunging breaker at location in the tank far from either end. A movable surface piercing plate was then positioned at various locations in the observed zone of "open-water" wave breaking so that a range of impact conditions on the wall was achieved. Systematic measurements of wall pressures, fluid velocities and surface

elevations were made for each condition which allowed the correlation of the kinematic and dynamic properties of the impact process. One of the main observations made was that wave impact occurs as the wave front is "focused" toward a zone on the wall termed the "impact zone", and that air is trapped in the impact process to varying degrees. It was found that the impulsive pressures measured at impact were highest when a relatively large pocket of air was trapped at impact. Pressure oscillations were also measured at impact and were attributed to the dynamics of the trapped air, and it was concluded that the impact dynamics could be decomposed into a non-oscillating hydrodynamic component and an oscillating pressure component due to trapped air. The impact pressure characteristics were found to be strongly dependent on the wall location relative to the wave breaking location, although significant variation in impact pressures was observed at a given wall location due primarily to the random nature of the trapped air dynamics [2].

The main purpose of the present work is to investigate the application of fully nonlinear potential flow theory to the problem of a plunging breaker impacting a vertical wall, using the experimental results of Chan [1, 2] as a basis for comparison. The starting point for the investigation is the same mathematical and numerical approach and computer program used for the plunging breaker simulation in a long tank [3]. From this point the primary objectives of the research are to:

1. Extend the program developed by Dommermuth et al. [3] to permit simulation of the impact of an overturning wave upon a vertical wall; and

2. Investigate criteria based upon local flow characteristics which may be used to develop a robust rule to automatically control the distribution of Lagrangian points on the free surface during the simulation.

The second objective is important if a general algorithm is to be found which will reduce or eliminate the need for trial-and-error approaches to the use of such numerical techniques as regridding and smoothing in order to complete a simulation.

Chapter 2

Mathematical Formulation

The assumptions which allow potential theory to be applied are that the fluid flow is irrotational and inviscid. The fluid is also assumed to be incompressible and homogeneous with gravity as the only body force acting. Surface tension is also neglected. The fluid is confined to a two-dimensional rectangular tank of length $L(t)$ with a vertical piston wavemaker at one end which undergoes a prescribed time-dependent horizontal motion with velocity $U(t)$.

There are two problems to examine: the case of flow prior to impact with the wall and the case of flow after impact. The mathematical formulation for the two cases differs only in the boundary conditions used, and is similar to the approach used by Vinje and Brevig [9] in that it is based upon Cauchy's integral theorem. The equations below are presented in the form given by Dommermuth et al. [3]. Note that mass, length and time units are chosen such that the non-dimensionalized gravitational acceleration, density and tank depth have a value of unity. This applies to all equations and results presented hereafter.

A sketch of the fluid domain is given in Figure 2-1 for the case where wave impact with the right boundary has not yet occurred.

The complex potential is defined as $\beta(z,t) = \phi(x,y,t) + i\psi(x,y,t)$, where both ϕ and ψ are functions which satisfy Laplace's equation and $z = x + iy$. If the entire boundary is denoted as $C(z,t) = B_L \cup F \cup B_R \cup B_B$, then Cauchy's integral theorem yields

$$2\pi i\, \beta(\zeta,t) = \int_C \frac{\beta(z,t)}{z-\zeta}\, dz \qquad 2.1$$

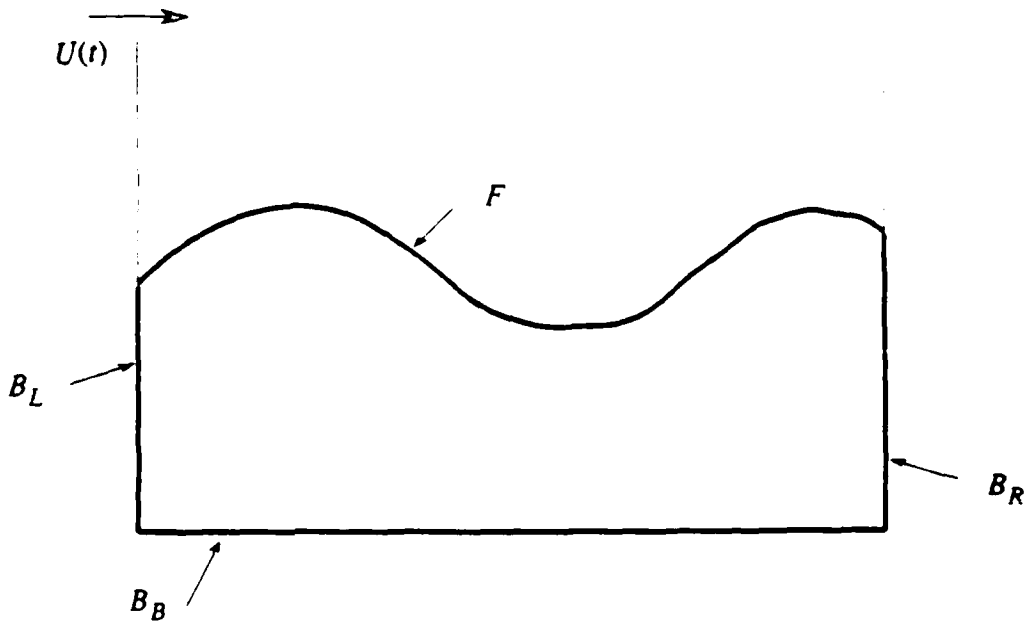

Figure 2-1: Fluid domain for pre-impact flow.

where ζ is inside the contour of integration. The boundary conditions for the pre-impact problem are given below:

$$\psi = U(t)\,(y+1) \quad \text{on} \quad B_L(x,t) \tag{2.2}$$

$$\psi = 0 \quad \text{on} \quad B_R\,,\,B_B \tag{2.3}$$

$$\frac{Dz}{Dt} = \frac{\partial \beta^*}{\partial z} \quad \text{on} \quad F(z,t) \tag{2.4a}$$

$$\frac{D\phi}{Dt} = 0.5\,V^2 - y - p \quad \text{on} \quad F(z,t) \tag{2.4b}$$

In the pre-impact case the pressure p on the free surface is set to zero. Note that that $D/Dt \equiv \partial/\partial t + \nabla\phi \cdot \nabla$ is the material derivative and that * represents the complex conjugate. Note also that $V^2 = u^2 + v^2 = (\partial\beta/\partial z)\,(\partial\beta/\partial z)^*$, where V is the velocity magnitude, u is the horizontal component of velocity and v is the vertical component. The specification of the problem for $\beta(z,t)$ and $F(z,t)$ is complete when initial conditions are given which correspond to a fluid at rest at $t = 0$.

As in Dommermuth et al. [3], the fact that ϕ is even with respect to the bottom boundary B_B and ψ is odd with respect to B_B is used to reduce the number of unknowns by the method of images. If the contour of integration is reflected about the bottom line $y = -1$ and the bottom is then removed, Cauchy's integral theorem then yields

$$2\pi i\, \beta(\zeta,t) = \int_{C'} \left[\frac{\beta(z,t)}{z-\zeta} - \frac{\beta^*(z,t)}{z^* - \zeta - 2i} \right] dz \qquad 2.5$$

where $C' = B_L \cup F \cup B_R$. Numerically, for a tank with $L >> 1$, the number of unknowns is substantially reduced by the number of points defined originally along the bottom.

In case of wall impact, the fluid domain is modified as shown in Figure 2-2.

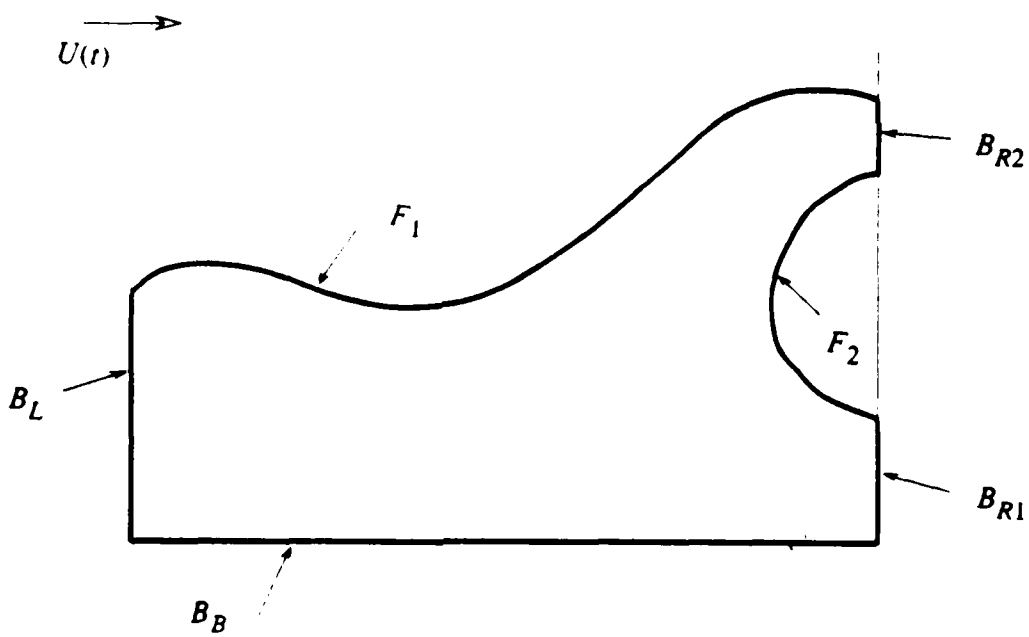

Figure 2-2: Fluid domain for post-Impact flow

Now $C(z,t) = B_L \cup F_1 \cup B_{R1} \cup F_2 \cup B_{R2} \cup B_B$. The boundary conditions for the post-impact problem are the same except that B_R is divided into B_{R1} and B_{R2}, and F is divided into F_1 and F_2. In equation (2.4b), a non-zero pressure p along F_2 would represent

air being trapped at impact, in which case an additional relationship between p and the volume of the trapped air pocket is necessary. For the post-impact case, equation (2.5) is the same with C' modified appropriately. In both cases, if ζ is allowed to approach C' from the interior, a Fredholm integral equation of the second kind for the unknowns ψ on F and ϕ on B is obtained by taking the real part of (2.5) when ζ is on F. Similarly, a Fredholm integral equation of the second kind for the unknowns is obtained by taking the imaginary part of (2.5) when ζ is on B [9].

At a given value of time t, the exact solution of the boundary value problem is approximated by the solution of the system of equations obtained by discretization of the contour of integration in equation (2.5) to obtain the values of ψ on the free surface and ϕ on the tank boundaries. The complex velocity potential β is then known on the free suface so that the velocity at the free surface points can then be computed from $\partial\beta/\partial z = u - iv$. Using these velocities, numerical time integration of the kinematic and dynamic boundary conditions on the free surface, equations (2.4a) and (2.4b), gives the position and velocity potential on $F(z,t + \Delta t)$ to be used in solving the BVP at time $t + \Delta t$. The wavemaker velocity $U(t)$ is always a known input to the problem. The solution of the BVP is independent of time, all points being considered Eulerian points, while the time integration step treats the free surface points as Lagrangian points; hence the description of solution as a mixed Eulerian-Lagrangian approach.

Chapter 3

Numerical Implementation

3.1 Discretization, Solution and Time Integration

The discretization of equation (2.5) is achieved by dividing the modified contour of integration C' into linear segments or panels. The complex potential β is assumed to vary linearly between the endpoints of each panel, which are referred to as nodes. At a given node z_k, which corresponds to ζ in (2.5), integration along the panelized contour with nodes z_j, which correspond to the variable of integration z in (2.5), yields one equation relating the unknowns on the boundary. The real or imaginary part of the resulting discretized equation is used appropriately to maintain the form of a Fredholm integral equation of the second kind, as discussed in Chapter 2. When this is repeated for all z_k, an $N \times N$ linear system of equations $\mathbf{A}\mathbf{x} = \mathbf{b}$ for the N unknowns is obtained where $\mathbf{A}$ is the matrix of influence coefficients. The formulas for these influence coefficients and their asymptotic approximations for z_j far from z_k are given in Vinje and Brevig [9].

In this numerical approach, the treatment of the singularity of the solution at the intersection point between the rigid boundaries and the free surface is the same as that developed by Lin [5, 6]: both ϕ and ψ are considered known values at the contact points. This approach is also used in extending the program used by Dommermuth et al. [3] to the case for wave impact in Chapter 6, where two new contact points are considered to be created at the right wall when the plunging crest tip impacts the wall.

The solution of the boundary value problem at each time step is performed using the standard LINPACK routines SGEFA for factorization and SGESL for back-substitution. After solution, the complex potential β is known at all points on the boundary. A three-

point finite difference formula is then used to compute the velocities of the Lagrangian points on the free surface, since $\partial\beta/\partial z = u - iv$. The horizontal and vertical velocities u and v then specify the right-hand sides of equations (2.4), allowing time integration of these equations to obtain new known values of ϕ and z on F at the next time step.

The method of time integration used is a combination of a fourth-order Runge- Kutta (RK4) scheme to integrate values for three initial time steps followed by a fourth-order Adams-Moulton-Bashforth (ABM4) scheme for an arbitrary number of steps. This technique was also used by Longuet-Higgins and Cokelet [7], and the linear stability aspects of each scheme are addressed in Dommermuth et al. [3].

3.2 Regridding and Smoothing; Time Step Control

The program developed by Dommermuth et al. [3], which will henceforth be referred to as the "original" program, uses two techniques to avoid or supress "sawtooth" instabilities in the evolution of the free surface which have been observed by several investigators (e.g., [7]) using the mixed Eulerian-Lagrangian approach. One technique is a five-point smoothing formula identical to that used by Longuet-Higgins and Cokelet [7], which is applied to values of position and velocity potential at the free surface points. The other is a regridding algorithm [3, 4] which uses quadratic interpolation of position and velocity potential at the free surface points to create a new set of equally distributed points using the linear distance between the original points as a parameter. Both smoothing and regridding tend to suppress the effects of higher-wavenumber components; qualitatively, smoothing treats any oscillatory type of variation as noise and simply finds an average curve through the input values, while regridding tends to prevent the resolution of higher wavenumbers by arresting the concentration of Lagrangian points in regions of higher velocity gradients and wavenumbers. The cause of "sawtooth" instablities is thought to be

related in part to possible growth of errors in computed velocities due to small errors in computed velocity potential in such regions [3]. In the original program, the regridding alogorithm is applied to all points on the free surface between the wavemaker and far wall. As a wave steepens and eventually overturns, a certain degree of spatial resolution is required to define regions of high velocities and curvature, such as the crest tip. For this reason, the approach taken in the simulation of a plunging breaker using the original program is to employ regridding until more resolution is required, at which time smoothing is invoked in order to allow the free surface points to "cluster" in the overturning region. A dynamic time-step control algorithm is also used which limits the time step size so that no panel moves more than 10% of its length in one time step [3].

In Chapter 4, the original program is used to do further simulations for a plunging breaker using the same wavemaker input and tank length (L=20) as Dommermuth et al. [3]. The purpose of these numerical experiments is to investigate the dependence of results on the particular times when regridding is stopped and smoothing is started. In Chapter 5, modification in the use of smoothing at the free surface-wall intersection point is found necessary to simulate a plunging breaking wave just prior to impact with a vertical wall. The regridding algorithm is also modified to add points in the curl region to obtain sufficient resolution. This trial-and-error approach to the use of smoothing and regridding is the motivation for Chapter 7, which investigates the possibility of developing a robust method of free surface point distribution based upon criteria related to local flow properties.

3.3 Conservation of Mass and Energy

The conservation of mass is is checked by comparing the original fluid area (volume) with a numerical computation of area based on the following formula:

$$A = -\int_C y \, dx \qquad 3.1$$

In this formula, C represents the original closed contour $B_L \cup F \cup B_R \cup B_B$ and a trapezoidal rule is used for the free surface integration.

The conservation of energy is checked in one form by comparing the computed power input from the wavemaker with the rate of change of fluid energy, represented in continuous form as follows:

$$\int_{B_L} pU \, ds = \frac{1}{2}\frac{d}{dt}\left[\int_{B_L \cup F} \phi \, d\psi + \int_F y^2 n_y \, ds \right] + \frac{U}{2} \qquad 3.2$$

The left-hand side represents the power input from the wavemaker. The first term in brackets on the right hand side represents the kinetic energy of the fluid and the second term is the potential energy contribution from the free surface. The last term represents the rate of change of potential energy due the changing tank length, and in practice is subtracted from both sides to improve the accuracy of the estimate [3]. A trapezoidal rule is again used for the integrations, and the normal vector $\mathbf{n} = n_x\mathbf{i} + n_y\mathbf{j}$ at each point on the free surface (which points outward from the fluid) is approximated by the average of the normal vectors to the adjacent panels, except at the contact points where the normal to the first or last free surface panel is used. A second check of energy conservation is obtained by comparing the total fluid energy computed directly at each time step with the total work input obtained by integrating in time the left-hand side of equation (3.2) using a three-point integration routine.

Note that both (3.1) and (3.2) are valid for both the pre-impact and post-impact cases, the only difference being integration over two free surface regions in the post-impact case.

3.4 Structure of Program

The original program is written in two parts: a start program for time equal to zero to some later value t_n and a restart program from time t_{n-1} to some time t_f. The basic logic of the programs is given below:

1. INPUT: known values of x, y and ϕ on F and ψ on B at time step N.

2. RK4 integration for steps N+1 to N+3. For each sub-step k=1 to k=4 in the RK computation at a given time step do the following:

   a. Compute value of x, y and ϕ on F at sub-step k using the values from step (g) below; or, if k=1, just save values from previous time step.

   b. Reposition nodes on wavemaker and far wall so that they are evenly spaced based on elevation of contact points.

   c. Compute the value of wavemaker velocity using linear interpolation of given velocity time history, assign values of ψ on B_L.

   d. Compute the influence coefficients and set up the A matrix and **b** vector.

   e. Solve the system for ϕ on B and ψ on F.

   f. Compute the velocities u and v at the free surface points by defining complex potential β and position z at each point and using three-point difference along F (one-sided for contact points and centered for interior points). Compute value of $D\phi/Dt$ in equation (2.4a).

   g. Compute $\Delta t \cdot u$, $\Delta t \cdot v$ and $\Delta t \cdot D\phi/Dt$ at free surface points for use in (a).

h. If k=1, save values of computed in (g) for later use in ABM4 integration. If current time step is N+1, values are saved corresponding to N, etc.

i. If k=1, write output for previous time step: x, y, ϕ, and ψ at all nodes. For example, if current time step is N+2, then values are saved for time step N+1.

j. If k=1 and N is the initial time step, call time step control alogorithm to set value of Δt using the velocities computed in step (f).

k. If k=4, complete RK integration for x, y and ϕ on F for current time step. If current step is N+3, then proceed to ABM4 integration.

3. ABM4 integration for time steps N+4 to N+M, where M is arbitrary. For each sub-step k=1 to k=2 in the ABM computation at a given time step do the following:

a. Compute value of x, y and ϕ on F at sub-step k ("predictor" step) using the values from step (g) below; or, if k=1, just save values from previous time step.

b. Reposition nodes on wavemaker and far wall so that they are evenly spaced based on elevation of contact points.

c. Compute the value of wavemaker velocity using linear interpolation of given velocity time history, assign values of ψ on B_L.

d. Compute the influence coefficients and set up the A matrix and b vector.

e. Solve the system for ϕ on B and ψ on F.

f. Compute the velocities u and v at the free surface points by defining complex potential β and position z at each point and using three-point difference along F (one-sided for contact points and centered for interior points). Compute value of $D\phi/Dt$ in equation (2.4a).

g. Compute $\Delta t \cdot u$, $\Delta t \cdot v$ and $\Delta t \cdot D\phi/Dt$ for use in (a).

h. If k=1, write output for previous time step: x, y, ϕ, and ψ at all nodes. For example, if current time step is N+4, then values are saved for time step N+3. Note that if the program stops at step (4) below, then the last values saved are for time step N+M-1.

i. If k=2, complete RK integration for current time step ("corrector" step). If current time step is N+M, then proceed to step (4).

4. If maximum number of time steps or maximum value of simulation time is exceeded, then STOP.

5. Regrid or smooth values of x, y and ϕ for free surface points.

6. Call time step control algorithm to set new value of Δt using the most recent computed velocities of free surface points in step (2)(f), k=2.

7. Return to start of RK integration loop at step (2) with N=N+M.

Note that the integer M determines the frequency at which the RK integration is restarted. In principle, it is necessary to return to the RK integration routine to provide new initial values for the ABM routine if either (1) the size of the time step changes, or (2) regridding or smoothing free surface points, or any other operation which changes the identity of the points being "tracked" in the integration, is used. In the original programs and all modified versions discussed in this work the time step control routine as well as any

smoothing, regridding or other routines which change the identity of free surface points are called every M^{th} time step even though the specific routines and the sequence of calling them may differ from one version to another. The RK routine is therefore also restarted at that time step.

Using the original start program, regridding and smoothing of the free surface points occurs every M^{th} time step just before the final solution and output is completed for that time step. As noted above, if the program stops at step (4) at current time step N+M, the last values saved are for time step N+M-1. The values of ϕ, x and y on the free surface at time step N+M-1 have not yet been smoothed or regridded. When the original restart program is then used, the values at time step N+M-1 are read and smoothing or regridding is immediately applied to the free surface point values. The program then proceeds as in the start program. Because the regridding or smoothing occurrence is shifted back one time step on restart, solution values at a given time t using the start program alone, for instance, may differ slightly from values obtained using the restart program one or more times (M is assumed the same). Also, there will not necessarily be an exact matching of time and time step values between runs which restart at different points, since computed velocities may also be slightly different and because the time step control routine computes Δt based upon velocities and positions of free surface points.

One error in both original programs is that an initial value of Δt is not input; therefore at step (2)(g), for k=1, the first sub-step in the ABM integration incorrectly uses Δt=0. In step (2)(j), the time step control routine is called and a value of Δt is computed and there are no further problems. This error is corrected by switching steps (2)(g) and (2)(j). Since this error only occurs at the initial step of the start or restart programs, the effect of the error is probably not significant; the results using the start program alone would be essentially unaffected since at the initial time step the values computed for u, v and $D\phi/Dt$ in step

(2)(g) are near zero at all free surface points. Note also in the original programs that the time step control routine is called in (6) after the final integration step (3)(i) for the values of ϕ, x and y on the free surface, but before free surface point velocities are computed based upon these final values after return to the start of the RK integration loop in step (2)(f) with k=1. Thus the positions of the free surface points used in the time step control routine are the current positions, but the velocities used are not current. Although this is not an error, it is more consistent to call the time step control routine after the current velocities are computed.

Modified versions of the original start and restart programs were created which allow for a "consistent" restart. Using the above example, this means that the last values saved when either program stops are those for time step N+M, after any regridding or smoothing has occurred, rather than for N+M-1. On restart, these values from step N+M are used as input and the solution at time step N+M is duplicated so that the program yields results as if no restart had been necessary. This is desirable when program run time is limited or when it is necessary to restart a run at an earlier time step but using different input parameters.

The error mentioned above as well as the inconsistency in use of the time step control routine are also eliminated. The logic of the modified programs is given below:

1. INPUT: known values of x, y and ϕ on F and ψ on B at time step N.

2. RK4 integration for steps N+1 to N+3. For each sub-step k=1 to k=4 in the RK computation at a given time step do the following:

    a. If k=1 and time step N=N+M from step (4), regrid or smooth values of x, y and ϕ for free surface points.

    b. Compute value of x, y and ϕ on F at sub-step k using the values from step (k) below; or, if k=1, just save values from previous time step.

c. Reposition nodes on wavemaker and far wall so that they are evenly spaced based on elevation of contact points.

d. Compute the value of wavemaker velocity using linear interpolation of given velocity time history, assign values of ψ on B_L.

e. Compute the influence coefficients and set up the A matrix and **b** vector.

f. Solve the system for ϕ on B and ψ on F.

g. Compute the velocities u and v at the free surface points by defining complex potential β and position z at each point and using three-point difference along F (one-sided for contact points and centered for interior points). Compute value of $D\phi/Dt$ in equation (2.4a).

h. If k=1, write output for previous time step: x, y, ϕ, and ψ at all nodes. For example, if current time step is N+2, then values are saved for time step N+1.

i. Call time step control algorithm to set new value of Δt using the most recent computed velocities of free surface points at step (g).

j. If maximum number of time steps or maximum value of simulation time is exceeded, then STOP.

k. Compute $\Delta t \cdot u$, $\Delta t \cdot v$ and $\Delta t \cdot D\phi/Dt$ at free surface points for use in (b).

l. If k=1, save values of computed in (k) for later use in ABM4 integration. If current time step is N+1, values are saved corresponding to N, etc.

m. If k=4, complete RK integration for x, y and ϕ on F for current time step. If current step is N+3, then proceed to ABM4 integration.

3. ABM4 integration for time steps N+4 to N+M, where M is arbitrary. For each sub-step k=1 to k=2 in the ABM computation at a given time step do the following:

   a. Compute value of x, y and ϕ on F at sub-step k ("predictor" step) using the values from step (g) below ; or, if k=1, just save values from previous time step.

   b. Reposition nodes on wavemaker and far wall so that they are evenly spaced based on elevation of contact points.

   c. Compute the value of wavemaker velocity using linear interpolation of given velocity time history, assign values of ψ on B_L.

   d. Compute the influence coefficients and set up the A matrix and **b** vector.

   e. Solve the system for ϕ on B and ψ on F.

   f. Compute the velocities u and v at the free surface points by defining complex potential β and position z at each point and using three-point difference along F (one-sided for contact points and centered for interior points). Compute value of $D\phi/Dt$ in equation (2.4a).

   g. Compute $\Delta t \cdot u$, $\Delta t \cdot v$ and $\Delta t \cdot D\phi/Dt$ for use in (a).

   h. If k=1, write output for previous time step: x, y, ϕ, and ψ at all nodes. For example, if current time step is N+4, then values are saved for time step N+3. Note that if the program stops at step (4) below, then the last values saved are for time step N+M-1.

i. If k=2, complete RK integration for current time step ("corrector" step). If current time step is N+M, then proceed to step (4).

4. Return to start of RK integration loop at step (2) with N=N+M.

3.5 Wavemaker Input

The only input to the original programs used by Dommermuth et al. [3] is the velocity time history of the vertical wavemaker. This time history was obtained by taking a centered finite difference of the measured wavemaker displacement in the experiment and applying Fourier analysis to the data to obtain the following Fourier cosine series:

$$U(t) = \sum_{n=1}^{72} U_n \cos(\omega_n t - \theta_n) \qquad 3.3$$

A plot of the velocity time history is shown in Figure 3-1. The values of U_n, ω_n and θ_n are given in Appendix B of [3].

The same input is used in all simulations in the present work, and corresponds to the wavemaker input used by Chan in the experiments which are used for comparison with simulated results.

The electrical input signal to the wavemaker in the experiment is plotted in Figure 1 of [2]. It should be noted that the wavemaker veloctity input used in the simulations shown in Figure 3-1 starts about 4.3 s later than the input wave signal to the wavemaker at a point when this signal first becomes non-zero. This difference corresponds to a non-dimensional time difference of about 17.0. When any references are made in this work to time values in the actual experiment, the values given will reflect a correction of -17.0 so that they will compare directly to the simulated time values.

Figure 3-1: Wavemaker velocity input time history.

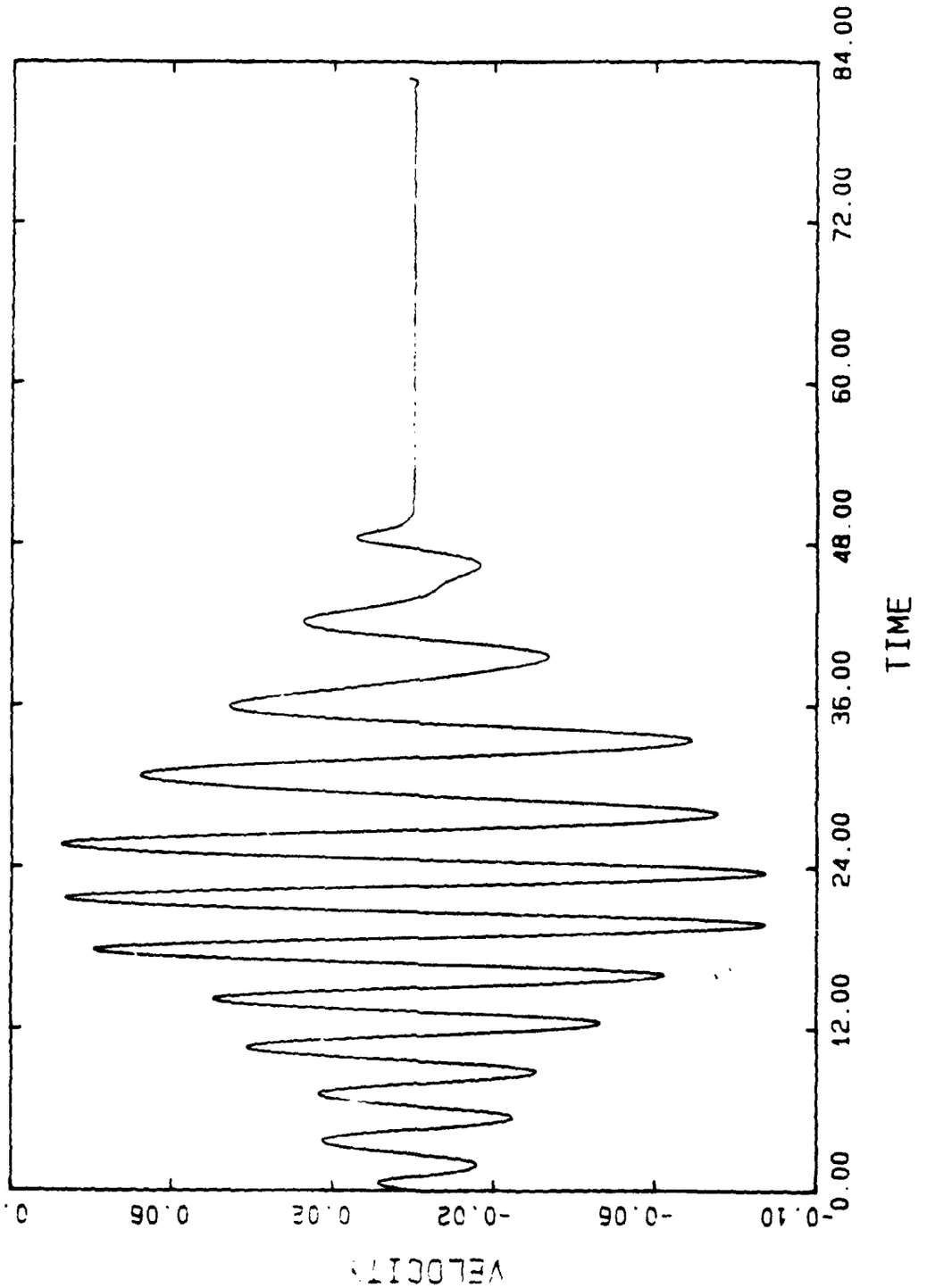

3.6 Convergence Tests

The accuracy of the boundary value problem solution step in the original programs is evaluated in Dommermuth et al. [3] using exact deep-water Stokes waves for comparison with the program results. The convergence of relative error with panel size is shown to be quadratic, and for wave steepnesses ε less than about 0.2, a density of 40 panels per wavelength is found to yield a relative error in free surface velocity of approximately 0.5%. The modified programs for the pre-impact cases do not alter the setup of the system of equations, so the same convergence is expected. The only difference between the original and modified programs in the solution step is that the modified programs use the standard LINPACK routines SGEFA and SGESL to solve the system of equations. The original program also uses a vectorized Gaussian elimination routine with partial pivoting, and there is negligible difference between results using the two solvers.

The overall accuracy of the time simulation is also evaluated for the original programs in Dommermuth et al. [3]. The convergence of free surface elevation with decreasing panel size and time step size is demonstrated by comparing computed free surface elevations with and without regridding applied to the free surface points with the elevation measured in the experiment at a time midway to the wave breaking event. To check the validity the program modifications described above, the same convergence test is performed using the modified programs, and in addition two additional cases of smoothing only and regridding plus smoothing are considered. For all runs M = 15, where M is defined in Section 3.4. The tank length used for the convergence test is L = 8, compared to L = 20 used in the full simulation for the plunging breaker. The position along the tank length is $x = 3.17$, and the time from the start of the wavemaker is $t = 25$.The results are presented in Table 3.1 below for an initially even distribution of panels along the wavemaker, free surface and far wall. N represents the total number of panels.

TABLE 3.1: EVEN PANEL DISTRIBUTION					
N	Δt	No Regrid	Regrid	Smooth	Reg.+Sm.
100	.100	-.06174	-.06033	-.06204	-.06011
150	.075	-.06572	-.06519	-.06547	-.06496
200	.075	-.06517	-.06520	-.06523	-.06524
250	.050	-.06574	-.06557	-.06576	-.06561

For comparison, another test is run where the number of panels on the wavemaker and wall is fixed at 25 and the total number of panels in each case is the same as in Table 1. In other words, the width of panels on the free surface is larger and the number of free surface panels smaller than in the first test for a given total number of panels, except in the last case of 250 panels which again are evenly distributed. The results are presented in Table 3.2 below.

TABLE 3.2: UNEVEN PANEL DISTRIBUTION					
N	Δt	No Regrid	Regrid	Smooth	Reg.+Sm.
100	.100	-.05507	-.04244	-.05075	-.04148
150	.075	-.06433	-.06365	-.06414	-.06333
200	.075	-.06512	-.06528	-.06521	-.06526
250	.050	-.06574	-.06557	-.06576	-.06561

The measured value in the experiment was -.0670.

In both Table 3.1 and Table 3.2 convergence is demonstrated with increasing total number of panels and decreasing time step size. For the case of 250 panels, which has even initial panel distribution, the values have converged to within 1.0% for all combinations of regridding and smoothing based on comparison with the case of 200 panels in each table. Note also that for the case of 250 panels the run which uses no smoothing or regridding and that which uses smoothing alone give results closest to the experimental value. This suggests that the use of regridding may cause a greater loss of fidelity in the numerical solution. In the cases having uneven initial panel distribution, the computed values for 100 and 150 total panels are farther from the experimental value than those for the

corresponding cases with even panel distribution. In the case of 250 panels, the number of panels per wave is about 40 based on a linear wave having a frequency of $\omega = 2$, the frequency below which most of the input energy is concentrated based on the harmonic content of the wavemaker velocity input spectrum [3]. This is roughly the panel density used in all the simulations described in later chapters for both the long and short tank cases.

In the case of even panel distribution, the first two columns of Table 3.1 should be identical to Table 2 in [3]; however, the convergence shown in Table 3.1 is not quite as fast. As a check, the original program used in [3] was also run using regridding alone, and the results for free surface elevation, velocity potential and stream function agreed with the modified program up to at least five significant figures. One possible explanation for the discrepancy could then be that a different method of interpolation of the program output in time and in x may have been used in [3] to obtain values at the desired point. The method used here is a linear interpolation first in time followed by a linear interpolation in x.

3.6.1 Typical Computing Times

All simulations discussed in this work were performed on a Cray 2 supercomputer. As mentioned in Dommermuth et al. [3], about 80% of the computational time required for the solution of the system of equations for the boundary value problem is devoted to the assembly of the matrix of influence coefficients and about 20% is devoted to the *LU* decomposition of the matrix solution. In Chapter 4, where the simulations involve 549 unknowns for tank length L = 20, a typical run (e.g., run A3C)requires about 21 hours for 4200 time steps. In Chapter 5, where the number of unknowns is reduced to 349 for the shorter tank lengths, a typical run requires about 8 hours for 3600 time steps (e.g., run C4).

Chapter 4

Simulation of a Plunging Breaker in a Long Tank

The simulation of a plunging breaker performed by Dommermuth et al. [3] involved use of regridding every 15 time steps (corresponding to M = 15 in the discussion of program structure in Chapter 3) for the initial phase (about 3000 time steps) and smoothing every 5 steps for the last phase (about 1000 steps). Determination of the time at which regridding stopped and smoothing started was somewhat difficult and a matter of trial and error; in fact, an intermediate phase during which both regridding and smoothing were applied was required in order to allow the simulation to progress to overturning.

The purpose of this chapter is to repeat the simulation of the plunging breaker in a tank of L = 20 (non-dimensionalized on a depth h of 0.6 m) using the modified programs to illustrate the difficulties encountered for this case, and also to investigate the dependence of results on various combinations of regridding, regridding plus smoothing and smoothing alone. Note that the total number of panels on the free surface is 500 and that there are 25 panels on both the wavemaker and right wall. For L = 20 and h = 1 this gives an initial panel size of 0.04.

In this and following chapters, the point of run failure refers to the point at which the computation breaks down. This usually coincides with the simulation becoming physically invalid, such as when an overturning crest re-enters the free surface or if the free surface intersects itself.

Note that plots of free surface profiles for the runs referred to below are located in Appendix A. The run names start with a letter which corresponds to the appropriate appendix. This same convention is used for all runs in later chapters as well. Each free

surface profile plot in the appendix has a heading at the top of the page which gives the run name, time step number, and time value at that time step. Numbers in parentheses immediately following time values in the text are the corresponding number of time steps in the simulation.

4.1 Results Using Modified Code

4.1.1 Summary of Runs and Failure Types

Run A1 is made with regridding alone applied every 15 steps. Run A1 fails at time t = 44.88 (2149). The plot of free surface profile from x = 0 - 20 at step 2049, 100 steps before failure, shows two predominant peaks; the first peak, nearest the right wall around x = 9.5 is the steepest (note the horizontal and vertical scale) and is followed by a second peak around x = 6.6. The failure occurs at the first peak as the two panels at the top of the peak begin to overturn but then collapse into one another as shown in the detailed plots. It is the second peak noted above which, in successful simulations such as runs A3A - A3D below, eventually steepens and overturns after t = 51.

Run A2 is a restart of run A1 at t = 42.15 (1770) with smoothing alone applied every 5 steps. Failure occurs at t = 43.54 (3575). Again, the failure is at the first peak around x = 9.1. The nature of the failure is different, though, from run A1 because the free surface points have become more dense at the top of the first peak since regridding is no longer applied. The crest overturns, forming a thin cusp which eventually self-intersects. This failure suggests that in the actual experiment the first crest may itself have been a weakly overturning or "spilling" breaking wave which may not be accurately simulated by the present method. The failure in run A1 appears to be a manifestation of a breaking tendency in the absence of adequate resolution of the free surface. The *a priori* knowledge that the second peak is the one of interest in this case necessitates some means of suppressing the tendency of the first peak to break long enough for the second to develop to overturning.

Run A3 restarts run A1 at t = 42.01 (1755) with regridding plus smoothing applied every 5 steps. This run is arbitrarily stopped at t = 54.29 (3260) since the time when overturning of the second peak is expected to occur has been exceeded. In this case overturning of both peaks is suppressed by the combination of regridding and smoothing.

Runs A3A, A3B, A3C and A3D are restarts of run A3 at the following respective times with smoothing every 5 steps: 45.98 (2155), 47.04 (2225), 48.01 (2285) and 49.02 (2360). These runs successfully continue to overturning and plunging of the second peak and are summarized in the next section. A sequence of free surface profiles showing the overturning process is plotted for each run in Appendix A.3.

Runs A3E, A3F and A3G are restarts of run A3 at the following respective times using smoothing only every 5 steps: 44.03 (1970), 44.60 (2030) and 45.00 (2070). In these cases, the breaking tendency of the first peak has not been successfully suppressed and failure occurs in a way similar to run A2. The breaking of the first peak occurs later than in run A2 and the peak has a smaller amplitude. In these three cases, the later smoothing alone is started, the later breaking occurs.

Run A4 restarts run A1 at an earlier time than run A3, at t = 40.09 (1575). Regridding plus smoothing is again applied every 5 steps. This run is arbitrarily stopped at t = 50.93 (2575).

Runs A4A, A4B, A4C and A4D are restarts of run A4 at the following respective times with smoothing every 5 steps: 45.99 (2140), 46.99 (2205), 48.03 (2270) and 49.03 (2345). These runs successfully continue to overturning and plunging of the second peak and are summarized in the next section. Because of their similarity to runs A3, A3A, A3B, A3C and A3D , runs A4 through A4D are not plotted.

4.1.2 Comparison of Successful Runs

The following table summarizes the time and position of crest tip contact with the free surface (re-entry point) for runs A3A - A3D and A4A - A4D.

TABLE 3.1

RUN	Trs	Ts	Tc	Xc	Yc	Δt	STEP
A3A	42.0	46.0	51.51	11.95	2.55	.00041	4560
A3B	42.0	47.0	51.32	11.82	2.75	.00048	4417
A3C	42.0	48.0	51.31	11.81	3.65	.00047	4217
A3D	42.0	49.0	51.26	11.76	4.71	.00002	4450
A4A	40.1	46.0	51.48	11.91	3.05	.00040	4501
A4B	40.1	47.0	51.31	11.82	3.40	.00006	4479
A4C	40.1	48.0	51.30	11.80	3.90	.00011	4229
A4D	40.1	49.0	51.25	11.75	4.56	.00034	4386

Trs is the time when regridding plus smoothing is started, Ts is the time when smoothing alone is started, Tc is the contact time, Xc and Yc are the contact position, Δt is the time step size at contact and STEP is the time step number. The contact points above are determined by finding the first time step at which a point on the crest tip passes below a line segment connecting two free surface points.

There is little difference in the contact time and position between corresponding runs (i.e., A3A and A4A). This indicates that the time at which regridding plus smoothing is invoked, Trs, has the least effect on the results. The greatest dependence is on the time at which smoothing only is started, Ts. The latest re-entry time at the greatest distance from the wavemaker occurs when Ts is a minimum and there is a consistent trend toward re-entry occurring earlier and closer to the wavemaker as Ts increases, although the difference in re-entry time and position between runs A3B and A3C or between A4B and A4C is relatively small.

In the actual experiment, contact of the crest tip with the free surface occurred at approximately Tc = 52.2 (12.9 s) and Xc = 12.1 (7.25 m), and in the simulation of

Dommermuth et al. [3] contact occurred at approximately Tc = 52 and Xc = 12.2. As in the original simulation, all of the above simulations yield re-entry of the plunging breaker at an earlier time than the experiment.

Examination of quantities at free surface points such as velocity, acceleration and energy shows that just prior to contact the maximum computed velocity magnitude shifts from values on the order of 1.0 in the curl of the wave to values an order of magnitude higher at the crest tip or cusp, suggesting that computational error begins to dominate at the tip where the panel size is about 10 times smaller than the original panel length. Computed maximum acceleration magnitudes are on the order of 5 - 10 g in the wave curl just prior to this discontinuity in velocity; Dommermuth et al. [3] observed a maximum acceleration of about 6 g in the curl of the wave in their simulation just before re-entry.

For runs A3A - A3D the table below gives energy-related quantities at the time step just before the discontinuity in computed velocity occurs.

TABLE 3.2

RUN	STEP	Vm	Ec	-Wc/Ec
A3A	4558	1.18	.04173	0.929
A3B	4416	1.04	.03922	1.023
A3C	4215	1.06	.03974	1.010
A3D	4419	1.31	.04341	0.924

Vm is the maximum velocity magnitude at contact, Ec is the total fluid energy at contact and Wc is the total work input to the fluid from the wavemaker at contact. The ratio -Wc/Ec is a measure of conservation of energy and will equal to unity if the the computed work input and fluid energy have the same magnitude (Ec + Wc = 0). In all cases above the computed work input to the fluid Wc = .04013, which means that the variation in total energy between runs is due only to the variation in free surface position and velocity. There is a direct correspondence between the maximum velocity in the curl of the wave at contact and the total energy at contact. Although the energy conservation check is only

relative, since both work and fluid energy quantities are derived from the simulation, runs A3B and A3C seem to be the most consistent from a global energy conservation standpoint. It should be noted that for all the above simulations the area or "mass" of the fluid domain varies less that 0.1% from the initial area.

4.2 Summary

In repeating the simulation of the plunging breaker for a tank length of L = 20, a "weak breaking" event appears to occur at the peak leading the peak which eventually becomes the plunging breaker. Regridding alone every 15 steps fails in the vicinity of this event as the first peak steepens, although there is not sufficient resolution to clearly show a breaking phenomenon. When regridding is stopped and smoothing alone started at a time before the weak breaking event, the Lagrangian points become more dense as the first peak steepens and the breaking event is more clearly resolved into a thin plunging cusp. The simulation then fails when the cusp self-intersects.

An intermediate application of regridding plus smoothing every 5 steps until the time of the weak breaking event has passed followed by smoothing alone every 5 steps allows the second peak to develop to overturning. The time and position at which re-entry occurs is seen to be most dependent upon the time at which the regridding plus smoothing application is stopped and smoothing only begins; as this time Ts is decreased, the time of re-entry is observed to increase. There is a minimum value of Ts, however, below which the tendency of the first peak to break is not sufficiently suppressed and the simulation fails.

Runs A3A, A3B, A4A and A4B are very close to one another in time and position of crest tip contact with the free surface; runs A3A and A3B also show the best global (relative) energy conservation and show a net loss of fluid energy compared to work input of one to two percent. The differences in final fluid energy at contact can be attributed

primarily to variations in free surface velocities and position which occur with the changing duration of the regridding plus smoothing phase between runs.

When tank length is shortened and the wavemaker input remains the same, similar difficulties in simulation are encountered which will be described in the next chapter.

Chapter 5

Simulation of a Plunging Wave Near a Wall: Pre-Impact Flow

In this chapter the same wavemaker input is used with a shorter tank length in an attempt to simulate a plunging breaking wave near the wall at the end of the tank. The initial choice of tank length, L = 11.667, is identical to one of the three tank lengths used by Chan in investigating the influence of wall position on wave impact pressure [1]. The shortest length of the three is chosen because of the observed tendency of the simulated wave to break sooner than in the actual experiment for the plunging breaker in the longer tank, coupled with the fact that in the actual experiment for wave impact this tank length corresponded to the least developed breaking prior to impact. Anticipating earlier breaking than experiment for the short tank cases as well, it was thought that choice of the shortest might still permit simulation of a wave that has started to overturn but has not yet contacted the free surface prior to wall impact. In fact, as described below, re-entry is imminent prior to reaching the end of the tank for L = 11.667, and a series of experiments with different tank lengths is required to obtain a simulation wherein the overturning crest tip is approximately horizontal as it approaches the end of the tank so that eventual simulation of impact with the wall prior to re-entry will be possible. The case where L = 11.60 is finally chosen to continue the impact study in the next chapter. In all cases, the number of panels on the free surface is 300 and the number of panels on the wavemaker and wall is 25. The initial free surface panel size is slightly smaller than the runs where L = 20; it would be identical if the short tank length were L = 12.

In conducting these simulations using shorter tank lengths, it is discovered that a problem arises as the crest approaches the end of the tank. The original Lagrangian points closest to the wall tend to be convected away from the wall so that resolution of the free

surface near the wall and in the lower part of the wave curl becomes poor. In order to improve the resolution in this regime, a routine is developed to add points in the wave curl region based on a quadratic interpolation scheme similar to that used in the original regridding routine for the free surface points. This technique is found to introduce new difficulties with excessive upward motion of the wall contact point as adjacent points are added. Another problem arises because the increased density of Lagrangian points upon point addition in some cases allows excessive "clustering" of points in the curl as the simulation proceeds since the points still tend to be convected away from the wall and into into the center of the curl. The approaches used to eliminate or alleviate these difficulties are also addressed.

5.1 Results: L=11.667

5.1.1 Summary of Attempted Runs and Failure Types

The plots of free surface profiles for the runs referred to below are located in Appendix B.

Run B1 is made using regridding alone every 15 time steps. Like run A1 in Chapter 4, the simulation breaks down at the first peak when the overturning process is not adequately resolved. The time of failure is later at $t = 47.68$ (2736) around $x = 11.0$.

Run B2 is made using smoothing alone every 15 time steps as a comparison with run B1. This run fails in a manner similar to that in run A2 of Chapter 4 when the first peak begins to overturn. A thin cusp is formed which eventually self-intersects before re-entry, causing failure at $t = 43.97$ (5769) around $x = 9.3$. This weak breaking event at the first peak, as in Chapter 4, necessitates some means of artificial suppression in order to allow the second peak to develop to the point of breaking near the end of the tank.

Run B3 is a restart of run B1 at $t = 42.00$ (1800) with smoothing every 5 time steps.

It is analagous to run A2 of Chapter 4. Failure occurs at t = 43.50 (3865) at the first peak when the overturning crest re-enters the free surface at about x = 9.0. Qualitatively, runs B2 and B3 are similar in the formation of a thin cusp. The overturning in run B3 is delayed due to the initial phase of regridding.

Run B4 starts the simulation from t = 0, but with no smoothing or regridding used. The RK4 scheme followed by the ABM scheme is repeated every 15 time steps (M = 15) when the time step control routine is called to compute a new Δt. This run is of particular interest, as its objective is to confirm the development of a "sawtooth" type of instability in the absence of any smoothing or regridding. This type of instability does indeed occur in the vicinity of the wavemaker and causes failure at t = 31.7 (1476). The profiles show the development of the instability, which is first detectable at the scale of the plots at about t = 27.0 (1000).

Run B5 is a restart of run B1 at t = 42.00 (1800) without using regridding or smoothing. As in run B4 the time integration returns to the RK4 scheme every 15 time steps when the time step size is recomputed. Although no sawtooth instability is observed in this run, failure occurs at the first peak at t = 43.88 (4639) as the crest overturns and the cusp self-intersects before touching the free surface. This run restarts at the same point as run B3, and a comparison shows that the cusp is much sharper and less physical in appearance in the case without smoothing applied.

Run B6 restarts run B1 at t = 42.00 (1800) and proceeds using regridding plus smoothing every 5 time steps in an attempt to suppress the overturning tendency of the first peak observed in runs B2 through B5 above. It is analogous to run A3 in Chapter 4, and the result is the same in that overturning of both the first and second peaks is suppressed. This run does eventually break down at about t = 52.01 (3380) as the second peak "sloshes" up the right wall.

Runs B6A through B6F are restarts of run B6 at the following respective times with smoothing alone every 5 steps: 43.84 (2000), 45.03 (2130), 45.99 (2215), 46.94 (2280) and 49.01 (2420). As in runs A3A - A3F and A4A - A4D in Chapter 4, the objective in these runs is to capture the overturning of the second peak after having suppressed the overturning of the first peak through the use of combined regridding and smoothing every 5 steps.

Run B6A fails at t = 44.76 (2840) when the overturning second peak self-intersects before touching the free surface. It is important to note that the overturning occurs around x = 9.8, well before the end of the tank. It appears as though there is insufficient resolution in the curl of the wave, which may cause errors to grow in this region of high velocities and velocity gradients and lead to the observed failure at the top of the curl.

Run B6B fails at t = 49.02 (2922) when the overturning peak self-intersects before touching the free surface. In this case also it appears that there is insufficient density of Lagrangian points along the crest tip and curl to accurately capture the overturning. The overturning occurs later than run B6A and closer to the right wall, around x = 10.4.

Run B6C fails at t = 51.06 (3740) when the overturning crest again self-intersects in a manner similar to runs B6A and B6B. The overturning occurs even closer to the right wall, around x = 11.63.

Run B6D is identical to B6C except that the minimum allowable time step size is set to 0.00001 instead of 0.0001, which was used in all of the above cases. The purpose of this is to see if, in the overturning phase, reducing the restriction on time step size will affect the results. Although more time steps are required because of reduced Δt, failure still occurs in essentially the same fashion at t = 51.06 (3766). No profiles are plotted for this case.

Run B6E continues until the overturning crest is almost at the point of re-entry when failure occurs. One difference between this run and the previous runs is that the density of

Lagrangian points at the crest tip and in the curl is somewhat higher, and could explain the fact that the run does not fail as soon; however, the curl does distort in a way similar to runs 6A - 6D just prior to failure. The crest tip is just above the free surface at approximately t = 51.034 (3792) and x = 11.63. The panel adjacent to the wall is 0.7 times the size of the original panel size at t = 0 by this point. The panels decrease in size with distance from the right wall, and reach a minimum size at the crest tip of 0.08 times the original panel size. Failure occurs at t = 51.035 (3802).

Run B6F fails at t = 50.96 (3662) as the overturning crest self-intersects around x = 11.56. Compared to run B6E, the resolution of the curl region is worse by roughly one panel, and distortion at the top of the curl similar to runs B6A - B6D continues until failure occurs.

Run B7 duplicates run B6 except that smoothing is applied just before regridding rather than just after. The switch has no appreciable effect on the results, and profile plots are not given.

5.1.2 Comparison of Successful Run with Experiment

From the above runs, B6E is considered successful since the simulation fails just before re-entry occurs, even though resolution of the wave curl region is questionable. As anticipated, overturning does occur earlier than in the actual experiment, and the crest tip nears re-entry before the crest reaches the right wall. At this point it is of interest to compare free surface elevations with the profiles given for the actual experiment prior to impact by Chan [2] in Figure 6 for the wall position (tank length) of L = 11.667. At t =51.49, the maximum crest height is about 0.18 and the run-up at the right wall is about 0.13 just as overturning begins. At t = 51.53, just before impact occurs, the maximum crest height is about 0.21 and the run-up is about 0.16. In the simulation, just as overturning begins, the maximum crest height is about 0.17 and the wall run-up is about 0.10. The

maximum crest height at the end of the run is about 0.17 and the run-up at the right wall is about 0.11. The crest height and run-up for the simulation are thus comparable to experiment as overturning starts, but because the simulated wave never reaches the wall the rapid increase in crest height and elevation at the wall observed in the experiment just prior to impact does not occur.

In the simulation, the height of the curl region as the wave overturns is on the order of 0.01 - 0.02. Assuming that a simulation can eventually be achieved where overturning has started but re-entry has not occurred as the crest reaches the wall boundary, the height of the space "trapped" between the impacting crest and free surface at the wall at the bottom of the curl should be on the same order. Using the same profiles from the actual experiment an estimate of the trapped air pocket height at impact is about 0.02 - .04 for L = 11.667.

In order to achieve the desired simulated result, an obvious choice is to try decreasing the tank length until the overturning wave reaches the wall before re-entry. This approach is described in the next section.

5.2 Results: Variation of Tank Lengths

In the following runs, the same sequence of regridding and smoothing is used as for run B6E. The initial run is made using regridding alone every 15 steps until Trs = 42.0, followed by regridding plus smoothing every 5 steps until Ts = 47.0, after which smoothing alone is used every 5 steps until the end of the simulation. In all runs the minimum allowable time step size is set to 0.0001. Plots of the final free surface profiles for these runs are located in Appendix C

5.2.1 Summary of Attempted Runs and Failure Types

The following table summarizes the runs for varying tank length.

TABLE 5.1					
RUN	LENGTH	Nrs	Ns	Nf	Tf
C1	11.525	1815	2310	3282	50.86
C2	11.55	1815	2305	3350	50.90
C3	11.59	1810	2300	3525	50.95
C4	11.60	1800	2295	3590	50.97
C5	11.63	1805	2290	3652	51.00
C6	11.65	1800	2285	3740	50.02

Nrs and Ns are the time steps corresponding to Ts and Trs; Tf and Nf are the time and time step at which the run fails.

Runs C1 and C2 fail in a similar fashion. In these cases, the tank length is so short that the free surface at the wall rises rapidly relative to the forward motion of the wave crest; as a result, overturning never occurs. The runs fail when the point adjacent to the wall contact point is convected to the left and eventually overtakes the points to its left.

In runs C3 and C4, overturning does begin due to longer tank lengths. The profiles for run C3 are very similar to run C4 at the start of overturning, only earlier in time by about 0.016. At comparable points of t = 50.94 (3425) for run C3 and t = 50.96 (3500) for run C4, just after overturning has begun, the panel next to the right wall is about 0.4 times the original panel length. Both simulations eventually fail as the point adjacent to the wall point moves so far to the left that there is no resolution at all of the the lower part of the curl. Accurate simulation of overturning is no longer possible and the curl is distorted in such a way that the crest "folds" down on itself instead of plunging.

In runs C5 and C6 overturning also begins, but in these cases the tank is too long because the crest is too far from the wall. They fail in a way similar to runs B6A - B6D and run B6F in section 5.1.1. The overturning in these cases is later than in runs C3 and C4,

and it is interesting to note that in these four cases the overturning time is delayed as tank length increases.

Despite the failure of runs C3 and C4, they are still potentially useful. Before failure, the trajectory of the overturning crest tip is roughly horizontal and close enough to the wall to suggest that solving the problem with resolution near the wall in these cases may allow the simulation to continue to impact. Run C4 with L = 11.60 is chosen to continue efforts to achieve an impact case.

5.2.2 Comparison of Run L=11.60 with Experiment

At t = 50.958 (3500), the profile of run C4 shows a maximum crest height of 0.18 and wall run-up of 0.15. This compares reasonably well to the profile of Chan [2] for L = 11.667 and t = 51.49 which shows a maximum crest height of about 0.18 and wall run-up of about 0.13 at roughly the same stage of overturning. Before failure occurs it appears that the simulation might continue to form a "pocket" between the overturning crest and wall at impact with an initial height of about 0.01.

5.3 Results: Effort to Increase Point Resolution

5.3.1 Techniques Investigated

The following sections describe the approach that is taken to address the problem of insufficient resolution near the wall and in the curl. Run C4 is used as the baseline run from which changes are made.

5.3.1.1 Point addition

Addition of Lagrangian points is the first technique used to increase point resolution near the wall and in the wave curl. A subroutine is developed which first finds the smallest panel on the free surface and then adds points at the midpoints of subsequent panels when

their length exceeds a specified multiple of the minimum panel length; in these runs two is the multiple. The points are added using quadratic interpolation for position and velocity potential with the linear distance between panels as the parameter. This subroutine is called immediately before the smoothing subroutine is called, in these cases every five time steps.

In the first series of runs, run C4 is restarted at t = 50.958 (3500) just after overturning has begun. The free surface profiles for these runs are located in Appendix D.

In run D1, smoothing is used every 5 steps and points addition is applied once, causing the addition of 3 points at step 3505 at the midpoints of the three panels which are nearest the right wall. The miminum panel size used for comparison in the point addition routine occurs at the tip of the overturning crest where the Lagrangian points have concentrated, and is 0.05 times the original panel size.

Examining the sequence of profiles for run D1 from steps 3510 to 3570, and comparing them with the same sequence of profiles for run C4 without point addition, it is apparent that point addition has improved resolution in part of the curl farthest from the wall but at the same time caused the contact point at the right wall to move rapidly upward in a non-physical way with an average velocity of about 4.0 until the overturning crest tip contacts this upward-moving surface and the run fails.

Run D2 is identical to D1 except that the minimum allowable time step size is set to 0.00001 instead of 0.0001, because in run D1 the miminum time step size was reached. The new minimum time step is never reached but the results of the run are indistiguishable from run D1 at a given time value, eliminating time step size restriction as a possible cause of the problem.

Run D3 is an extreme case in that point addition is applied 10 times starting at step 3505 and ending at 3600, resulting in a total addition of 15 points in the curl-wall region. Examining the sequence of plots from step 3515 to 3575 shows that the rapid upward

movement at the wall is more pronounced and more localized near the wall with the addition of points, and the run fails sooner than runs D1 and D2 due to the anomalous behavior of the points nearest the wall in the "jet".

Run D4 is identical to runs D1 and D2 except that no smoothing is applied after restart. It is important to note here that the smoothing routine used thus far smooths not only interior points on the free surface but the contact points as well using a one-sided formula instead of a centered formula. The values smoothed are the position and velocity potential. Comparing the profile of run D1 at step 3570 with run D4 at 3565, the position of the contact point is almost identical. The crest tip in run D4 is thinner and turned more downward than in D1, and there is evidence of instability in run D4 due to lack of smoothing in the slightly jagged appearance of points at the crest tip and in the curl. For the above cases, the conclusion is that a jet at the wall is formed regardless of whether smoothing is applied.

The following five runs restart run C4 earlier, at $t = 50.846$ (3100) before overturning occurs to see if there is any dependence on the time of point addition.

Run D5 uses smoothing every 5 steps after restart and applies point addition once, resulting in the addition of seven points at step 3105. Examining the profiles for steps 3130 to 3530 reveals that although there is still a local upward deformation of the free surface at the wall after point addition, it is less pronounced with an average velocity of about 1.0 over this range. As the wave overturns and approaches the wall, the disparity in elevation of the contact point and adjacent points becomes less marked. From steps 3630 to 3930, ($t = 50.960$ to $t = 50.973$) the overturning process appears much more physical than in run C4 over a similar range from steps 3500 to 3580 ($t = 50.958$ to $t = 50.966$) with no points added. However, failure of run D5 eventually does occur in a way similar to run C4 when the point next to the wall contact point begins to move to the left and eventually leaves no

resolution of the region near the wall; the crest then "folds" down on itself as the crest tip reaches the wall. The time of failure is later than run C4 by about 0.006.

Run D6 is identical to run D5 except point addition is applied twice, resulting in addition of 12 points, seven at step 3105 and five at 3110. The density of points near the wall is doubled relative to run D5 and quadrupled relative to run C4. Examining the profiles from steps 3145 to 3445 reveals that the upward deformation at the wall has an initial average velocity of about 1.0, as in run D5. This run also fails because of eventual interference of the point next to the wall with other points as it moves to the left, causing loss of resolution near the wall and deformation at the bottom of the curl. The time of failure is about 0.004 later than run C4.

Run D7 is identical to run D6 except point addition is applied three times, resulting in the addition one more point at step 3255 for a total of 13 points added instead of 12. The results are very similar to run D6.

The next two runs are made to see what affect no smoothing has on the results.

Run D8 is identical to run D5 except that smoothing is not used; point addition is applied once, resulting in the addition of seven points. Examining the profiles for steps 3101 to 3501, there is still an upward deformation of the free surface at the wall which again has an average velocity of about 1.0 over this range. The striking aspect of this run, however, is the failure due to the sawtooth instability which develops in the curl region and near the wall as the wave overturns. In this case failure occurs just below the crest tip at one of the original points having an added point on either side. It is not possible from this run alone to say what affect point addition has on the development of the sawtooth instability. The time of failure is about 0.018 sooner than run C4.

Run D9 is identical to run D7 except that smoothing is not used; point addition is applied three times, resulting in the addition of 13 points. Sawtooth instability is also

evident in the wave curl, but this run fails about 0.01 earlier than run D4 due to an anomaly at the wall where the the characteristic jet has developed. The time of failure is about 0.026 sooner than run C4.

In summary, runs D1 through D9 reveal the following:

1. Point addition causes the velocity of the wall contact point to increase in a non-physical way, causing upward deformation of the free surface at the wall.

2. The formation of this "jet" is dependent on when point addition occurs. In runs D1 - D4 the distortion of the jet is most severe and clearly non- physical; in runs D5 - D9 the distortion is less pronounced when points are added near the wall point earlier in the overturning process.

3. This jet is formed whether smoothing is applied or not.

4. In cases D4 - D7, where the jet at the wall is less dominant an effect, the simulation is improved relative to run C4 due the better resolution in the curl; however, as in run C4, leftward movement of the point next to the wall point eventually causes loss of resolution near the wall and distortion of the curl, leading to failure.

5. Because of relatively early failure of runs D8 and D9, it is not yet clear if the motion of this point to the left is affected by the smoothing of points near the wall.

6. Sawtooth instabilities do occur if no smoothing is applied upon restart.

The difficulty with the leftward movement of the point closest to the wall is apparent both before and after point addition is attempted, whereas the formation of the jet at the wall occurs only after point addition.

5.3.1.2 Modified smoothing

Because both problems involve the motion of the wall contact point and immediately adjacent points, it is conceivable that the application of smoothing may need to be modified in some way. As demonstrated in runs D8 and D9, some amount of smoothing is clearly necessary in order to prevent sawtooth instability. The original smoothing routine smooths the position and velocity potential of all points on the free surface, including the wall contact points. For the interior points, a centered 5-point formula is used; for the point adjacent to the wall point, a skewed 5-point formula is used; and for the wall point a one-sided 5-point formula is used. The smoothed values at each point are computed using the original (unsmoothed) values at adjacent points, and subsitution of the new values for original values is done as the final step.

The runs in this section investigate the effect of variations in use of the original smooting routine and changes to the original routine with regard to how the wall points and adjacent points are handled. The free surface profiles for these runs are located in Appendix E.

All these runs have identical input to run D6: they restart run C4 at step 3500 and apply point addition twice, adding seven points at step 3505 and five points at 3510.

In run E1, the order of subroutines is switched so that smoothing of free surface points occurs first followed by the addition of any points. The affect upon the free surface profiles is negligible when compared to run D6. Plots of profiles are not given for this run.

In run E2, the original smoothing routine is used but the arguments are changed so that the values of velocity potential and position at the wall point are neither smoothed themselves nor used in the formula for smoothing the adjacent points; in other words, the point adjacent to the wall is taken as the end point and the wall point is ignored. The results of this run are significantly different from run D6. In examining the profiles from step

3161 to 3861, note that the wall point still moves rapidly upward after point addition, but that the adjacent points do not. By ignoring the wall point in using the smoothing routine, the motion of the adjacent points is no longer coupled "artificially" to the wall point motion through smoothing, though there is still a coupling to the wall point motion in the solution of the boundary value problem and subsequent computation of velocities. The adjacent points do eventually "catch up" to the wall point, as seen at step 3761 when the crest tip is about 0.01 from the wall, then the wall point again moves upward relative to the adjacent points.

Another significant difference from run D6 is seen in the behavior of the point adjacent to the wall. In run D6 the movement of this point to the left becomes noticable around step 3445 (t = 50.946), and it eventually interferes with the points to its left to cause deformation of the bottom of the curl and failure. By step 3645 (t = 50.960), for instance, the adjacent point to the wall is extremely close to the second point from the wall, producing a panel of length 0.001, about 37 times smaller than the original panel size, while the panel between the wall and the adjacent point has a length of 0.128, about 0.3 times the size of the original panel (0.039). In contrast, run D6 at step 3661 (t = 50.961) shows no large deviation in position of the point next to the wall. The panel next to the wall has length 0.018 and the second panel from the wall has length 0.015. Although the point closest to the wall is moving to the left, the motion is not nearly as apparent.

The failure of run E2 is characterized by the clustering together of points into the center of the curl until the spacing becomes extremely small and computation breaks down. Comparison of the profiles at steps 3861 and 3961 shows the motion of points at the bottom of the curl into the center. Note also that the wall point is again significantly higher than the adjacent point by the end of the run, as it was at the beginning, and that the adjacent point has moved noticeably away from the wall but not so far as to cause the kind of failure in run D6. Failure occurs at t = 50.975, about 0.004 later than run D6.

In summary, the omission of the wall point in use of the original smoothing routine leads to the following observations:

1. The increase in wall point velocity upon point addition still occurs, but unlike previous runs the adjacent points do not move upward with it. The wall point motion seems effectively independent of the adjacent point motion when the wall point is not used as the end point in the smoothing computation.

2. The simulation proceeds considerably farther than run D6 due to the fact that the point adjacent to the wall does not move rapidly to the left. The overturning crest tip even passes the end of the tank since the program has not yet been modified to define impact at the end of the tank.

3. The addition of points to increase the resolution in the curl and near the wall eventually causes difficulty as the simulation proceeds because of the observed tendency of the points at the bottom of the curl and near the wall to move toward the center of the curl, causing failure when the point spacing becomes extremely small.

The fact that the anomalous upward acceleration of the wall point occurs whether or not the wall point is used in smoothing, along with the fact that the adjacent point moves rapidly to the left only when smoothing does include the wall point, suggest that non-physical motion of the wall point might induce error in the adjacent point velocity when coupled through the smoothing operation.

In run E3, the original smoothing routine is again used. In this case, the position of all points is smoothed (except the x-position of the wall point, which can only move vertically) but the velocity potential is not smoothed. For this run, each plot of the free surface profile is followed by a corresponding plot of velocity potential versus x-position. Examination of plots for steps 3150 to 3230 show that a jet is again formed by the wall

point and adjacent points, but that upward deformation is greater than in runs where velocity potential and position were smoothed. At step 3230 (t = 50.899), just as the crest is starting to overturn, note that the wall point elevation is comparable to the crest height and that the tip of the crest is not "smooth" but a sharp corner. There is a corresponding distortion in the velocity potential plot at the crest tip and wall. The free surface points also have a slightly jagged appearance, suggesting that instability may result when smoothing of velocity potential does not occur, even if smoothing of position does occur. This run eventually fails at t = 50.907, sooner than run D6 by about 0.065.

In run E4, the smoothing routine itself is modified so that the wall point position and velocity potential are not smoothed themselves but are used in the smoothing formula for the adjacent two points. This run differs from run E2, where the wall point values are not used at all in smoothing. Examining profiles for steps 3183 to 3983, the initial jet at the wall again develops, but another problem is observed to occur when the fourth, fifth and sixth points from the wall become very closely spaced as the points closest to the wall move to the left. This leads to local deformation of the free surface at these points and eventual failure around t = 50.968. The degree of deformation can be seen, for instance, by comparing the profile at step 3983 (t = 50.967) with run E2 at step 3761 (t = 50.967).

Although the jet at the wall still occurs in run E4, it is significant to note that the point closest to the wall does not move as rapidly to the left as it does in run D6, but that the motion still is greater than in run E2 where the wall point is not used at all in smoothing. This observation supports the conjecture that the anomalous wall point behavior may corrupt the computation of values at the adjacent points since the smoothing operation couples the values of these points, even though in run E4 the wall point values themselves are not smoothed. Conversely, the adjacent point motion could significantly affect the wall point motion through the smoothing operation.

5.3.1.3 Alternate finite difference for wall point velocity

The increase in wall point velocity upon point addition, evident from the plots of free surface profile, is confirmed by checking actual velocity values. For example, in run C4, which does not add points, the change in vertical velocity at the wall point from step 3104 to 3105 is 0.003, and from step 3105 to step 3106 is 0.002. In run D6, which adds seven points at step 3105 then smooths values, the respective changes in wall point velocity are 0.064 and 0.003. In run D9, which adds seven points at 3105 but does not smooth any values, the respective changes in wall point velocity are 0.062 and 0.003. In run E2, which excludes the wall point from smoothing, seven points are also added at 3105, and the respective changes in wall point velocity are 0.064 and 0.003. In all cases of point addition the jump in velocity from step 3104 to 3105 is about eight per cent, compared to a jump of 0.4 per cent in run C4 without point addition. From step 3105 to 3106 the change in velocity returns to a value comparable to run C4. When points are added again at step 3110, there is again a jump in velocity from step 3109 to 3110 of about sixteen percent based on the average velocity. For the range of time steps under consideration the time step size is about 0.0007.

Note that in the original and modified programs used thus far, the wall contact point velocity is computed by a one-sided three-point difference formula applied to the complex potential along the free surface. Therefore, when a point is added between the wall point and the original point adjacent to the wall, the subsequent computation of contact point velocity is now based in part on the interpolated position and velocity potential at this new point. The magnitude of the difference Δz used in the difference formula is also cut in half upon addition of the point. If a second point is later added between the wall point and the previous new point, as it is in the cases above, computation of the wall point velocity no longer uses any original adjacent points, and the magnitude of Δz is again cut in half. It should be pointed out that the identities of the points used in the smoothing routines discussed so far also change when points are added.

It is possible that point addition could cause the observed jumps or errors in the wall point velocity because of the introduction of quadratically interpolated values and smaller point spacing into the present formula for computing wall point velocity. The computation of velocity at interior points might also be significantly affected when new adjacent points are added.

It is interesting to recall that when points are added later in the overturning process the deformation at the wall is much more pronounced that when points are added earlier 5.3.1.1. This suggests that any error introduced in the wall point velocity upon point addition is larger when points are added at a later time, corresponding to greater velocities of the free surface near the wall.

An alternate method of computing the vertical velocity of the wall points after each solution step is to use a one-sided finite difference of the velocity potential only along the right wall, since $\partial\phi/\partial y = v$. This approach differs significantly in that the points used are always evenly spaced, points are never added to this region, and the values of velocity potential and position at the points below the wall point are not directly affected by the smoothing of the free surface points.

Based on this approach, 3-point, 4-point and 5-point finite difference formulas are subsituted for the original scheme when computing the wall point vertical velocity in the following runs. The original smoothing routine is still used in which the wall point values are smoothed as well as the interior free surface points. These runs restart run C4 at t = 50.846 (3100) and apply smoothing every five steps. All the runs apply point addition twice, adding seven points at step 3105 and five points at 3110. The free surface profiles for these runs are found in Appendix F.

In run F1, the 3-point formula is used. The free surface profiles show no significant change in the vertical motion of the wall point compared to run D6 which uses the original

velocity computation at the wall point. This run fails at t = 50.973 (3985) in a way very similar to run D6 as the point adjacent to the wall moves rapidly to the left as overturning proceeds, eventually interfering with adjacent points and causing deformation at the bottom of the curl.

Runs F2 and F3 use the 4-point and 5-point formulas, respectively. Again, there is little difference in the outcome compared to run D6. The failure times for run F2 and F3 are, respectively, t = 50.973 (4046) and t = 50.972 (4065). No profiles are plotted for these runs.

5.3.1.4 Alternate finite difference plus modified smoothing

The new method of computing wall point velocity appears to have little effect on the results using the original smoothing technique. The following runs use the new method in combination with variations of smoothing already used in runs E2 and E4 with the original method of velocity computation. The free surface profiles for all runs in this section are found in Appendix G.

The next three runs change the smoothing routine to prevent smoothing of the wall point vertical position and velocity potential but do use these values in smoothing the adjacent two points. This smoothing technique is identical to that used in run E4, in which the point adjacent to the wall is seen to move left much less than in run D6, although failure still occurs due to problems with the clustering of points near the wall. These runs again restart run C4 at step 3100 and apply smoothing every five steps. Point addition is applied twice, adding seven points at step 3105 and five points at step 3110.

In run G1, which uses the 3-point velocity formula for the wall point, there is a significant difference in the behavior of the wall point and adjacent points. Examining the profiles for steps 3110 to 4210 shows that initially (i.e., through step 3210) the wall point and adjacent points remain essentially even in elevation, with no jet formed. From steps

3310 through 3810 the wall point is seen to lag behind the adjacent points slightly in upward velocity and position. Note that at step 3810 the crest tip has nearly reached the boundary of the wall, and the simulation looks reasonable except for the low postion of the wall point compared to the adjacent points. It is also significant that by this step there has been no marked change in spacing of the points near the wall which characterize the later stages of previous runs. As the crest tip passes the wall boundary, an anomaly occurs at the wall in which the points closest to the wall point pass over the wall point, creating a deformation which eventually leads to failure. The time of failure is t = 50.995 (4410); however, this relatively late time is due to the abnormal evolution of the free surface and is not a good basis of comparison with previous runs.

In run G2, which uses the 4-point formula, the profiles for steps 3152 through 4052 show that the difficulty in wall point motion observed in run G1 is not present. The wall point never exhibits a marked difference in elevation relative to the adjacent points, and the crest tip passes the wall boundary without any anomaly developing in the motion of points near the wall contact point. This run finally fails in a way similar to run E4, in which the points in the center of the curl eventually become so closely spaced that the simulation breaks down. The time of failure is t = 50.978 (4152).

In run G3, which uses the 5-point formula, the results are nearly identical to run G2. The time of failure is t = 50.977 (4093).

Another run is done to see if decreasing the number of points added initially might prevent the type of failure in runs G2 and G3 due to clustering of points in the curl.

Run G4 is identical in input to run G3 except that point addition is only applied once at step 3105, adding five points. Examining the profiles for steps 3139 to 3839, the simulation appears comparable to run G3 as the crest tip nears the wall boundary. However, soon after the tip passes the distance corresponding to the end of the tank, the

lack of resolution in the curl produces a failure most like runs C5 and C6, which had better resolution in the curl than run C4 due to the longer tank lengths used. This failure is clearly shown in steps 3849 to 3909. The failure time is $t = 50.975$ (3939).

To test the combination of the new finite difference approach with another variation of smoothing, the following run is done using the 5-point difference formula and the same smoothing operation as in run E2, in which the wall point is not used at all. Recall that in run E2 the wall point motion appears essentially independent of the adjacent point motion, and does exhibit an increase in velocity upon point addition.

In run G5, run C4 is again restarted at step 3100 with smoothing every five steps. Point addition is applied twice, adding seven points at 3105 and five points at 3110. Examining the profiles for steps 3150 to 3250, the jump in wall point velocity is not evident; however, the points closest to the wall point begin to move to the right and the point next to the wall has passed the wall point by step 3250. This abnormal motion continues until failure. The change in computation of wall point velocity causes a drastic difference in results compared to run E2. The other 3- and 4-point formulas were not tried in combination with this type of smoothing, since the 5-point formula had worked well in run G3.

Run G6 attempts to solve the clustering problem observed in run G3 by using a routine which locally regrids the points in the curl region when the point spacing becomes less than the smallest panel at the crest tip. The resulting run is identical to run G3 until step 3870, when the local regridding routine is called. As seen in the profiles, the points in the curl are evenly redistributed using quadratic interpolation. The run then proceeds until an anomaly develops in the flow at the points nearest the wall, similar to run G1. The run fails at $t = 50.977$ (4003). The reason for this anomaly is not known, but it should be noted that the failure occurs after the crest has passed the position corresponding to the end of the tank.

The above observations are summarized below.

1. Runs G1 through G3 represent an improvement over previous attempts in that the increase in wall point velocity upon point addition is no longer present. Also, there is no significant motion of wall points to the left in the later stage of overturning as in previous runs. Although run G1 fails due to abnormal motion of the points near the wall after the crest tip has passed the wall boundary, runs G2 and G3 exhibit no such abnormality and fail only when the points in the center of the curl become too closely spaced.

2. The use of the new finite difference approach for computing wall point velocity, in combination with smoothing which does not directly alter the present values of the wall point position and velocity potential but does use these values to smooth adjacent points appears to achieve a realistic simulation until the crest tip has passed the end of the tank. The 4- and 5-point formulas yield nearly identical results.

3. Run G4 shows again that a minimum resolution in the curl region is required or the later stage of overturning will not be simulated correctly.

4. Run G5 suggests that omission of the wall point in smoothing is not desirable when the wall point velocity is computed using the new finite difference technique. The jump in wall point velocity is still eliminated as in runs G1 - G3, but motion of the adjacent points becomes distorted. This suggests that coupling to the wall point through smoothing may be a necessary constraint for correct velocity computation at the adjacent points.

5.3.2 Comparison of Successful Run with Experiment

In run C4 in Section 5.2.2, it appeared that the height of the pocket at impact would be about 0.01 providing the simulation could continue. From the profile at step 3793 (i(t) = 50.969) in run G3, the estimated pocket height at impact will be closer to 0.015. Note that this height is smaller than the initial length of the free surface panels, 0.039. The maximum crest height at impact will be about 0.19 and the wall run-up will be about 0.16. Referring to the comparison of run B6E with experiment in Section 5.1.2, the surface profile in the actual experiment for L = 11.667 showed a crest height of about 0.21 and a wall run-up of about 0.16 just prior to impact, and the pocket height at impact is estimated from the sketch to be about 0.02 - 0.04. The profile of the simulated wave as it approaches the wall is thus comparable to the actual experiment, except that the tank length used in the simulation is L = 11.60 instead of 11.667.

Run G3 is considered a successful run, since curl resolution appears sufficient and there are no apparent abnormalities by the time the crest tip reaches x = 11.60, corresponding to the end of the tank. This run is therefore chosen to continue the simulation of impact in the next chapter.

5.4 Summary

This effort to simulate wave breaking in a shorter tank has shown that certain difficulties arise when overturning occurs near the vertical wall at the end of the tank. In the long tank, the use of the original smoothing routine every five time steps is sufficient to allow the free surface points to concentrate in the wave cusp and curl to give good resolution of the overturning process. As the wave approaches the wall in the shorter tank and begins to overturn, the resolution in the curl and at the crest tip is not as fine and the original points nearest the wall tend to move to the left into the curl of the wave, causing a further loss of resolution near the wall.

In order to adequately simulate the overturning process, which is characterized by an upward velocity of the free surface at the wall comparable to the approaching crest horizontal velocity, points are added prior to overturning to increase resolution and both the smoothing routine and velocity computation for the wall contact point are modified to eliminate anomalous motion of the wall contact point and adjacent points. With these modifications to the program, a simulation with L = 11.60 is finally obtained in which the crest tip reaches the wall boundary position prior to re-entering the free surface and without any abnormalities in the flow up to that point.

The problem of insufficient resolution of the free surface in the cases of wave breaking near the wall is solved by the addition of points prior to overturning and the elimination of abnormal motion of the wall contact point and adjacent points. Note, however, that these added points eventually lead to failure because they tend to cluster together in the curl. In Run G3, this failure occurs well after the crest tip has passed the end of the wall where impact will be defined to occur, so that simulation of the impact process in the next chapter should not be affected by this problem. Run G6 is an attempt to alleviate the clustering problem by automatically regridding the points in the curl region when the point spacing becomes too close. The initial regridding appears satisfactory, but an anomaly eventually occurs near the wall which leads to failure.

The fact that the addition of points as described above must be done in a trial and error fashion and still can have an undesirable "side effect" of excessive clustering suggests the need for a more robust point distribution scheme, especially in the overturning regime.

Chapter 6

Simulation of a Plunging Wave Near a Wall: Impact Process

The idealized impact problem is posed numerically by creating a wall contact region at the crest at some arbitrary instant of time after the tip of the crest has passed the position $x = L$, as represented in Figure 2-2. The essential changes to the program in order to model impact are the modification of existing subroutines to include the two free surfaces and two right wall contact regions after impact occurs, along with the development of new subroutines to define the initial values of vertical position and velocity potential at the new free surface-wall intersection points created at impact of the crest with the wall. Note that in this chapter, the pressure in the pocket formed at impact between the wave front and the wall is assumed to be zero; i.e., there is no air "trapped" in the pocket.

It is important to note that the new wall contact points on the free surfaces of the crest are treated numerically in the same way as the original two intersection points are prior to impact: the values of both velocity potential ϕ and stream function ψ are specified in computing influence coefficients and setting up the system of equations. Also, they are treated as Lagrangian points, meaning that their vertical position and velocity potential are obtained by integration of equations 2.4.

The time at which impact is defined to occur depends on how much of the crest tip is allowed to pass the postion $x = L$ before imposing the impact conditions. This can either be done, for instance, by specifying a minimum value of horizontal crest tip overshoot after which impact will be imposed, or by specifying a maximum allowable overshoot before which impact must be imposed, or both. In the present programs, a maximum allowable overshoot is specified and impact is imposed at the first time step at which the crest tip passes $x = L$ but is still less than this tolerance. If the crest tip both passes $x = L$ and

exceeds the tolerance in the same time step, the simulation is restarted with time step size cut in half until condition for impact is met.

Once the time step at impact is determined, the vertical postion of the crest intersection points is set by using quadratic interpolation using values at the point which has just passed $x = L$ as the right endpoint and the two points to its left as the other two nodes. The x-position of the intersection points is of course $x = L$, and the value of $\psi = 0$ is assigned to the points. This results in the portion of the crest tip greater than $x = L$ being "cut off". The lost fluid area or volume is small relative to the original volume, typically no more than 0.0001%.

In order to eventually compute pressures at the wall due to crest impact, interior points on the wall must be added in the crest contact region. This is because the pressures at the intersection points alone will always be close to zero if computed correctly. In one version of the impact program described below, points are initially added with even spacing at the impact step, and the spacing is set by dividing the height of the contact region between the intersection points by the average of the lengths of the two free surface panels whose right endpoints are the intersection points. Like the points on the wavemaker boundary and right wall boundary, these new points are always evenly spaced by regridding the crest contact region at every solution step (this regridding is not be confused with the regridding of free surface points). The value of $\psi = 0$ is assigned to these points and the velocity potential is computed at each solution step.

Two methods of assigning initial values of the velocity potential to the crest intersection points are investigated. In the first method, the velocity potential value is obtained by quadratic interpolation just as the y-position. In this case the velocity potential is assigned without any impact condition constraint, and the fact that impact is occurring is reflected initially only by the $\psi = 0$ values assigned to the intersection points and to any

added points in the contact region. In the second method, the velocity potential at the intersection point is computed subject to the additional constraint that $\partial\beta/\partial z = 0 - iv$ at that point. This constraint is imposed by solving the one-sided 3-point difference formula expressing $\partial\beta/\partial z = u - iv$ for ϕ at the intersection point given the position and complex potential at the two points closest to the wall on the crest, the position of the intersection point, and the condition that $\psi = 0$ at the intersection point. This technique in a sense is a stronger imposition of the impact condition in its redundant specification of zero normal velocity through the initial value of the velocity potential as well as the condition $\psi = 0$.

6.1 Results

The results using three versions of the impact programs are presented. The primary characteristics of each program are given below.

1. Program 1 defines the impact process only as the creation of two new intersection points. No points are added on the wall in the impact region. The purpose of this version is to obtain an initial idea of how the impact simulation will work with no other changes.

2. Program 2 is the same as program 1 but adds a routine to check of the free surfaces of the crest at each time step to determine if any points nearest the two new intersection points have passed the position corresponding to the end of the tank. If such a point is found, a new intersection point is defined at that point using one of the two methods described in the introduction and the old intersection point is eliminated along with any intervening points. This leads to two possible cases, using the top of the crest as an example:

    a. The new intersection point is above the old intersection point.

Physically, this corresponds to the initial contact region being "enfolded" by fluid which moves to contact the boundary before the initial contact region can "spread out". For a spherical drop of fluid impacting a plane surface, Oguz and Prosperetti [8] give a simplified analysis using mass conservation and the momentum equation to show that the initial line of contact cannot move radially outward fast enough to prevent further contact of the wall by the fluid surface, unless the impact velocity is very small. For a wave crest impacting a wall, similar loss or destruction of the free surface may well occur, although the process is clearly complex.

b. The new intersection point is below the old intersection point. In this case, this amounts to ignoring effect of fluid between the old and new intersection points. If this neglected fluid is part of a thin jet which has formed as the initial impact region spreads out (the opposite case of the region being enfolded), then physically this may be acceptable because the contribution to impact pressure in a thin jet should be small.

3. Program 3 is the same as program 1 but initially adds points to the contact region in the impact step as described in the introduction. The purpose of this version is to allow the computation of impact pressures on the wall. For simplicity, the creation of new intersection points after initial impact as done in program 2 is not considered in order to keep the number of points on the wall constant during the impact process.

Each of these programs is also run both with and without smoothing of free surface points. The smoothing formulas used are identical to those in the modified routine used in

run G3 prior to impact. Smoothing is applied over both free surfaces every five time steps after initial impact occurs, unless a subsequent impact occurs (as in program 2) in which case the time step count starts over and smoothing is delayed until five uninterrupted steps have passed.

6.1.1 Summary of Attempted Runs

In run G3 of Chapter 5, the crest tip first passes the wall at step 3836 at $t = 50.972$. For the following runs, impact is imposed at two different time steps by restarting run G3 at steps 3850 ($t = 50.9729$) and 3870 ($t = 50.9738$), respectively. The overshoot tolerance is set large enough so that no backing up and restart of the simulation is necessary and the size of the time step is fixed at the value before impact occurs. The impact time steps are then 3851 and 3871. At 3851, impact is imposed when the crest tip position exceeds L = 11.60 by 0.0014, creating an initial contact length of 0.0037; Δt is set to 0.000048. At step 3871, impact is imposed when the crest tip exceeds L = 11.60 by 0.0028, creating an initial contact length of 0.0054; $\Delta t = 0.000038$.

The runs corresponding to impact at 3851 are designated by "H", and those corresponding to impact at 3871 by "I". The run numbers have the following meaning:

1 - Program 1, first method of computing ϕ at new points;

2 - Program 1, second method of computing ϕ at new points;

3 - Program 2, first method of computing ϕ at new points;

4 - Program 2, second method of computing ϕ at new points;

5 - Program 3, first method of computing ϕ at new points;

6 - Program 3, second method of computing ϕ at new points.

The further breakdown of run numbers refers to whether smoothing is used. For

example, I1.1 does not use smoothing and I1.2 does use smoothing. The run numbers correspond to the free surface profiles given in Appendices H and I. The abbreviation "IP" will be used below in referring to the intersection points between the wall and free surface.

In run H1.1, the point next to the top IP immediately overtakes the top IP at step 3852, leading to failure at step 3856. The initial velocities of both the top and bottom IP's are upward, 29.1 and 19.6, respectively. There is an initial jump in the upward velocity at the IP at the bottom of the curl from 16.5 to 17.9 at step 3851 when impact is defined, a change of 8%.

In run H2.1, the top free surface points do not tend to overtake the top IP as in H1.1, but the point next to the top IP moves rapidly downward, deforming the crest and causing failure at step 3858. The initial velocities of the top and bottom IP's are 49.0 and 24.3, respectively. The jump in velocity at the IP at the bottom of the curl is from 16.5 to 18.4, a change of 12%.

In run H3.1, the point next to the top IP which overtakes the IP in run H1.1 at step 3852 is instead defined as the new top IP at the same step. At step 3851, the initial velocities of the top and bottom IP's are 29.1 and 19.6. When the new top IP is defined in step 3852, the velocity of the top IP is increased to 31.0 and the bottom IP assumes a downward velocity of -98.8, starting a downward jet. The top IP also begins an upward jet. New intersection points continue to be defined as the simulation progresses. Note that at step 3854 the point next to the wall at the bottom of the curl has been disturbed by the influence of the downward moving jet. Failure occurs at step 3857. The initial velocity jump at the IP at the bottom of the curl is the same as in run H1.1.

In run H4.1, the same failure occurs as in run H2.1 as the point next to the top IP moves rapidly downward.

In run H5.1 two interior points are added in the contact region The profiles show

that the free surface points at the top of the crest overtake the top IP, while the free surface points near the wall at the bottom of the crest form a downward moving jet. The velocity of the top IP is initially 29.7 and that of the bottom point is -25.0. The simulation only proceeds for 2 time steps before failure. At the first impact step, 3851, there is a jump in the upward velocity at the IP at the bottom of the curl from 16.5 before impact to 17.7 after impact is imposed, a change of 7%.

In run H6.1, the top free surface points do not tend to move past the top IP and the bottom free surface points again form a downward jet. The initial velocities of the top and bottom IP's are 58.4 and -24.6, respectively. This run fails when the point next to the top IP moves rapidly downward, deforming the crest, as in runs H2.1 and H4.1. The initial jump in velocity at the IP at the bottom of the curl is 11%.

The runs H1.2, H2.2, H3.2, H4.2, H5.2 and H6.2 which use smoothing are essentially the same as their counterparts above which do not use smoothing because of the short duration of the simulations. For this reason profile plots are not given for these runs in Appendix H.

In run I1.1, the point next to the top IP overtakes the top IP at step 3875, causing failure. The initial velocities of both the top and bottom crest IP's are upward, 11.0 and 10.5, respectively, after which they both decelerate. The jump in velocity at the IP at the bottom of the curl is 10%.

Run I1.2 fails just as I1.1; smoothing does not occur prior to failure. The initial velocities are the same as in I1.1. No plots are given for this run.

Run I2.1 differs significantly from I1.1 in that the point next to the top IP does not overtake the IP, but it does move rapidly downward, leading to failure. Both top and bottom IP's initially move upward at velocities of 12.8 and 14.2, and then decelerate. Note also that the curl begins to deform as clustering becomes more pronounced. This

simultaneous upward motion of both IP's does not seem physical. The jump in velcity at bottom of the curl is 12%.

Run I2.2 is very similar to I2.1, but the effect of smoothing can be seen in the fact that the point next to the top IP does not tend to move downward as in I2.1. Because no restrictions are imposed on points other than the initial IP's, the point below the bottom crest IP has passed $x = 11.6$ in step 3911. The initial velocities at impact are the same as in I2.1.

Run I3.1 is identical to I1.1 up to step 3875, at which the point which passes over the top IP is defined as the new top IP. The result is that failure does not occur as in I1.1; instead, the simulation proceeds with the bottom crest IP moving downward to form a jet which eventually re-enters the free surface at step 3880. The top IP eventually forms an upward jet as well. The initial velocities of the top and bottom crest IP's are 11.0 and 10.5, after which the top IP accelerates and the bottom IP decelerates. At step 3875, when the new top IP is defined, new top IP velocity jumps from 21.6 to 9.8 followed by rapid upward acceleration and the bottom IP velocity jumps from 9.6 to -3.5, which starts the downward jet. The jump in velocity at the bottom of the curl at impact is 10%.

Run I3.2 is identical to run I3.1 until step 3880, the first step at which smoothing occurs; however, this is also the step at which the bottom of the jet re-enters the free surface, rendering the simulation invalid there.

Run I4.1 is identical to run I2.1 until step 3893, when the point next to the top IP which has moved rapidly downward eventually passes $x = 11.60$, at which time it is defined as the new top IP; however, it actually is below the bottom IP and the simulation fails.

Run I4.2 is identical to run I2.2 until step 3900, when the point below the bottom crest IP pass $x = 11.60$ and is defined as the new bottom IP. When this occurs, the top IP velocity jumps from 12.9 to 10.7 and the velocity of the bottom IP jumps from 8.8 to 3.5, after which they both decelerate.

Run I5.1 differs from run I1.1 in that four interior points are added in the contact region at impact. The results are similar in that the points next to the top IP overtakes the top IP, in this case at step 3876. An important difference, however, is that the bottom IP tends to form a downward jet, unlike run I1.1. The initial velocities of the top and bottom IP's at impact are 10.6 and -16.8, and the initial jump in velocity at the IP at the bottom of the curl is 10%.

Run I5.2 is very similar to run I5.1. The application of smoothing at step 3876 is seen to delay the overtaking of the top IP until one time step later at 3857. The initial velocities of the IP's are the same, and the downward jet tends to form in the same way.

Run I6.1 differs from run I2.1 only in that four interior points are added in the contact region at impact; both runs use the second method of assigning the velocity potential at the crest IP's. The difference in the result, however, is dramatic. This run continues until the jet formed at the bottom of the crest re-enters the free surface at the bottom of the curl. The points at the top of the crest do not form a jet but do move upward while decelerating. The initial velocities of the top and bottom crest IP's are 13.2 and -14.5, respectively. The initial jump in velocity at the IP at the bottom of the curl is 12%. Compared to run H2, the initial contact region is larger but the number of added points is smaller. Qualitativlely, this simulation appears physically plausible, in contrast to runs I2 and I4 which use the same method of assigning velocity potential to the IP's but add no points to the contact region on impact.

Run I6.2 is identical to run I6.1 through step 3875. Smoothing is applied at step 3876, but there is little effect on the result compared to run I6.1. The initial velocities of the IP's are the same as run I6.1.

6.1.2 Computation of Pressures

For run I6.1, the pressures are computed at the crest impact region. At the first step after impact, the initial pressures at the interior points are negative with a maximum magnitude of 39.9. The pressures at the top and bottom intersection points at this step are -0.15 and -6.6. The pressures at the interior points remain negative but decrease until step 3874, where there is a positive value of 29.9. For all subsequent steps the interior pressures are positive, attaining a maximum value of 48.9 at step 3876.

In order to obtain more imformation about the computed impact pressure, a series of variations on run I6.1 is done in which the time step size and number of points in the contact region are changed. The time step sizes used are 0.00004, 0.00001 and 0.000001. At each time step size, the number of points added are either two or five. Plots showing the time history of the pressure profile on the impact region of the wall for the case of Δt = 0.00001 are shown in Appendix J. It is found that the change in time step size has negligible effect on the results for a given number of points; however, changing the number of points has a marked difference on the pressures computed at a given time step. For the case of four total points (two added) in the contact region, although the pressure values are initially negative they eventually turn positive with a maximum of about 50. When five points are added, the initial negative pressures are almost three times as large. The pressure values never become completely positive as they do in the case with fewer points, and the maximum positive value attained is about one third as large.

It should be noted that the pressure computations are performed after the simulation using a separate analysis program; there is a possibility that the simulations could be valid and the analysis inaccurate. However, the same basic computation of pressure is done for the impact region as is used in computing the work input from the wavemaker, which has been reasonably well-tested. Examining the components of the pressure calculation show

that the large negative values are associated with the term $D\phi/Dt$ in Bernoulli's equation which is computed using a three- point difference in time.

6.1.3 Comparison with Experiment

In the experiment of Chan, the typical range of peak impact pressures measured is given as $5\rho C^2$ - $10\rho C^2$ where ρ is the water density and C is the linear wave phase speed corresponding to the center frequency of the wavemaker velocity spectrum, or 1.70 m/s [1, 2]. The largest impact pressure measure was $21\rho C^2$. In terms of the non-dimensionalization described at the beginning of Chapter 2, the measured non-dimensional impact pressures are in a range from 2.5 - 5 with the largest value being about 10. No large negative pressures were noted in the experiment.

The positive pressures computed for the simulation are of the same order of magnitude as those measured in the experiment, but there is as yet no explanation for the computed negative pressures. The duration of impact in the simulation is about 0.0003, defined from impact until the jet at the bottom of the crest re-enters the free-surface.

Recall that air compressibility in the pocket has not yet been included in the model. Another unknown factor is the effect of using a shorter tank length than the experiment in order to get impact to occur.

6.2 Summary

The following observations are made concerning the techniques tried in the simulation of wave impact on a vertical wall:

1. Although the use of the second method of computing velocity potential at the new crest intersection points tends to prevent adjacent points from overtaking them, the resulting flow when no points are added to the interior of the crest contact region at impact appears non-physical.

2. When the first method of computing velocity potential at the intersection points is used, coupled with the definition of new intersection points as adjacent points overtake the original points (e.g., runs I3.1 and I3.2), the flow appears plausible even though no interior points are added at impact. A downward jet forms at the bottom of the crest which eventually re-enters the free surface, while the free surface at the top of the crest accelerates upward.

3. When the second method of computing velocity potential is used coupled with the addition of points in the contact region at impact, the flow again appears plausible (run I6.1). If the first method is used, then the adjacent points will overtake the new intersection points. This could be remedied by defining these overtaking points to become new intersection points when they reach the wall boundary position, as use of program 2 did in runs I3.1 and I3.2. This was not attempted due to the desire to keep the number of points on the wall constant for the pressure computations.

Note that the "H" runs which use the second method of computing velocity potential at new intersection points fail due to the rapid downward motion of the point next to the top crest intersection point. This could probably be improved if smoothing were applied more often, such as every time step, since similar motion of this same point is "corrected" by smoothing in run I2.2.

The computations of pressure show results independent of time step size but highly dependent on the number of points added at impact to the contact region. The initial pressures computed are negative in all test cases, and in general grow more positive with time. The highest positive pressure computed is about 50 for the case with only two points added, while the negative pressures of largest magnitude occur in the case of five points added. The positive pressures obtained are comparable in order of magnitude to the

experimental values, but there is no explanation as yet for the initial negative pressures. These simulations do not include the compression of air in the pocket formed by the impacting wave.

Chapter 7

Investigation of Criteria for a Robust Point Distribution Scheme

The results of simulations of plunging breaking waves in Chapter 4 and Chapter 5 have shown that the distribution of points on the free surface has a major effect on the outcome of a simulation. "Distribution" is meant here in a general sense, referring to the variation of both the position and complex potential from point to point. The distribution of points is initially given at $t = 0$ by setting the velocity potential at all points equal to zero and using a total number of points so that the initial panel density is about 40 panels per wavelength based on a linear wave with a frequency of$\omega = 2.0$, the frequency below which most of the input energy is concentrated. As the simulation proceeds, the point distribution obviously changes in time. The regridding, smoothing and point addition routines used thus far change the point distribution in some way when they are applied at a particular time step. The regridding routine has been used as a method of suppressing sawtooth instabilities by intermittently redistributing points more or less evenly using quadratic interpolation with the linear distance between points as a parameter. Consequently, regridding is not desired when better resolution of the free surface is required in the overturning phase. Smoothing is then substituted for regridding to capture the overturning event by allowing the concentration of Lagrangian points while still serving to suppress sawtooth instabilities. Smoothing is in a sense a local redistribution of points which finds a mean quadratic curve through five points and then redefines the points to be on this curve. In the runs using the short tank lengths, the need for even better resolution in the overturning phase than that provided by the existing points is met by using a routine which redistributes points by adding points based on quadratic interpolation when point spacing exceeds an arbitrary multiple of the minimum panel size at the crest tip.

The application of these point distribution routines in the simulations discussed thus far has been essentially a trial and error process. In order to develop a program which can ultimately simulate wave breaking and impact without such an *ad hoc* use of separate point distribution techniques, development of a more robust point distribution scheme is necessary which can automatically control the distribution of points to optimize the simulation from the standpoint of computational time and accuracy. Such a scheme would need certain criteria for distributing points based upon comparison of selected parameters with critical values of these parameters. It could conceivably use the existing point distribution routines in a more sophisticated way or could even be fundamentally different from them.

The objective of this chapter is to examine possible parameters and types of criteria which may eventually prove useful in such a robust distribution scheme. The approach taken is to examine representative cases where simulations have failed in an attempt to find quantities which exhibit marked changes near the failure point. Such quantities may then be candidates for use as parameters in defining the criteria. The types of observed failures are summarized below.

1. Without the application of any smoothing or regridding routine at all, a simulation will fail due to a "sawtooth" type of instability in the free surface. In run B4 the simulation is started at $t = 0$ without regridding or smoothing, and sawtooth instability develops near the wavemaker which causes failure; in run D8 smoothing is stopped just before overturning and a sawtooth instability forms in the curl of the wave and near the wall which leads to failure.

2. When regridding alone is used from the start of the simulation, failure occurs as a wave crest steepens and tends to overturn. Such failures occur at the

peak of the crest and seem to suggest insufficient resolution of the free surface in this region due to regridding. Run B1 is an example.

3. In simulations where smoothing is being applied and overturning is progressing, failure can occur due to insufficient resolution in the curl of the wave and near the wall. Runs B6E and C4 are examples.

4. In simulations where smoothing is being applied and overturning is progressing, point addition in the curl region to improve resolution can eventually lead to failure due to "excessive" resolution as points at the bottom of the curl tend to be convected upward into the center of the curl. Failure occurs when these points become too closely spaced. Runs E2 and G3 are examples.

Recall in both Chapters 4 and 5 that several simulations "fail" due to an apparent "weak breaking" of the peak preceeding the one which is known to overturn in experiment. In physical terms these runs are not necessarily failures; they could be accurate at least in that the first peak may actually have experienced a degree of breaking; this cannot be verified without repeating the experiment. In order to permit the simulation to proceed to the overturning of the second peak, a combination of regridding and smoothing is used to suppress the overturning of the first peak. The point is that the use of regridding plus smoothing in these cases is an artificial means of achieving an end, and in general may be of limited use trying to simulate problems without any *a priori* knowledge of the outcome.

7.1 Selection of Parameters and Test Cases

All of the observed failure types described above are localized in some way. This fact suggests that any criteria which will be used to determine point distribution on the free surface should be based upon parameters related to local flow properties and local point distribution rather than on global quantities. Three such parameters are defined below.

One parameter to be examined is designated SAW and is intended to provide an indication of the presence of sawtooth instability on the free surface. It is defined as follows:

$$\mathrm{SAW} = \sum_{n=1}^{N} (-1)^n (\Delta\alpha)$$

where the free surface panels are numbered from 1 to N and $\Delta\alpha$ is the relative radian angle between a panel and the previous panel (positive counterclockwise) divided by π. The idea is that a "sawtooth" geometry of the panels will cause an alternating sign on $\Delta\alpha$ from panel to panel, which will tend to increase the magnitude of SAW.

The second parameter to be examined is a non-dimensional estimate of local curvature, designated CUR, and is defined at each panel vertex as follows:

$$\mathrm{CUR} = \frac{\Delta\alpha}{S} S_0$$

where S is the sum of the half-panel lengths on either side of the vertex and S_0 is the original panel length at $t = 0$.

The third parameter is a measure of the rate of contraction or expansion of a panel relative to the average velocity of the panel endpoints. It is designated CON and is defined as follows:

$$\mathrm{CON} = \frac{\Delta l}{\Delta t}\,\frac{1}{V}$$

where Δl is the change in panel length and V is the average velocity magnitude of the endpoints of the panel.

There are essentially two approaches to examining such parameters. One is to track the value of the parameter, or perhaps its maximum or minimum, in time. The other is to choose a particular time step and look how the value of the parameter varies spatially along the free surface, assuming it is defined at each free surface point or panel.

The runs selected as representative cases are runs B1, B4, C4 and G3.

7.2 Definition of Criteria

Once parameters of interest have been identified, their correlation with the failure of a simulation must be determined. If a parameter value changes markedly as failure approaches, then it may be related to the reason for failure. This is especially true if the values of the same parameter in a run which does not fail at the same point are considerably different from the values associated with failure.

If a strong correlation does exist between a parameter and failure, then critical values of the parameter can conceivably be found to define a criterion for the redistribution of points in such a way as to prevent failure. The robust point distribution algorithm would control the starting, stopping, frequency and method of redistribution based upon such criteria. Ideally, it should cause minimal distortion of the solution while preventing instabilities.

In the following examples using the runs cited above, simple criteria are suggested based upon the three parameters described which could improve the use of the existing

point distribution routines by making their application more automated and rational. The actual implementation of these suggested criteria has not yet been attempted.

In the first example, the failure due to sawtooth instablity is addressed. The values of SAW are compared between run B1, which shows no sawtooth instabilities, and run B4, which does develop such instability near the wavemaker.

Figure 7-1 shows time histories of SAW for the two runs. Note that around $t = 27$ the value of SAW in run B4 becomes significantly larger than the value in run B1, exceeding 0.1. Examination of the free surface profiles for run B4 in Appendix B shows that this is also roughly the time when the sawtooth instability becomes apparent in the plots (i.e., at step 1000). This suggests that SAW could be used in a criterion which will start smoothing or regridding only when the value of SAW exceeds, for instance, 0.1, and stop once the value falls below 0.1 again.

In the second example, failure due to lack of resolution associated with regridding is considered by examining values of the curvature parameter CUR in run B1. The issue here is whether a criterion can be found which can control when to stop regridding and start smoothing so that sufficient resolution of an overturning event can be achieved. It is possible that regridding may fail when the curvature of the steepening crest becomes too large. About 100 steps prior to failure at the first peak, the value of CUR at the points defining the peak is about two orders of magnitude larger than at neighboring points. At step 2636, for example, the variation in CUR at the first peak is from -0.0067 to -0.455 and then back to 0.0061 over a span of eight points. This suggests that a criterion could be defined which locates a peak and stops regridding and starts smoothing when the magnitude of CUR exceeds a critical value at the peak, such as 0.01.

In the third example, the type of failure due to lack of resolution in the curl of an overturning wave near a wall is addressed. Run C4, which fails due to such lack of

Figure 7-1: Comparison of SAW for runs B1 and B4.

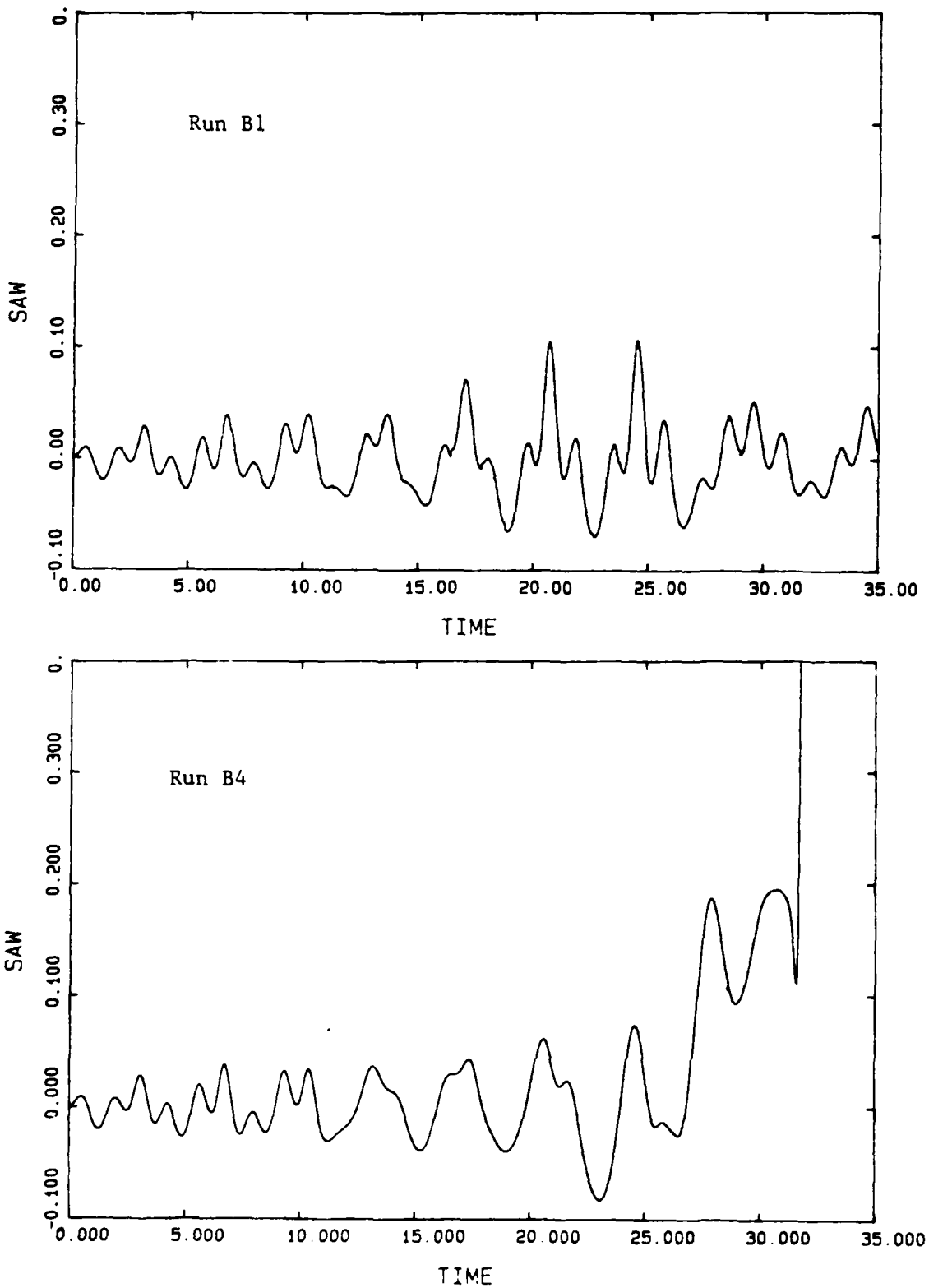

resolution, is compared with run G3, which proceeds further than C4 because of the addition of points prior to overturning. The main difference here is the value of the parameter CON at panels near the wall. In run C4, at step 3540 (t = 50.962) the values of CON at the three panels closest to the wall from left to right are -0.41, -3.37 and 2.60. At this step overturning is in progress (see profiles in Appendix C). The value of 2.60 for the panel next to the wall indicates that it is expanding rapidly relative to other panels, while the negative values indicate contraction of the adjacent panels. This is consistent with the observed motion to the left of the point next to the wall in the profiles. In contrast, for run G3 at step 3693 (t = 50.963) the corresponding values of CON are -0.06, -0.07 and 0.03. This suggests that a criterion might be developed which would add points to increase resolution based on the increasing magnitude of CON at panels near the wall. It is not clear what a critical value of this parameter might be.

The fourth type of observed failure which occurs when points in the curl cluster together has not yet been linked to a parameter. However, the method of local reridding used in run G6 to alleviate the clustering problem observed in run G3 still may be worth pursuing as a means of redistribution once an improved criterion for invoking it is developed.

7.3 Summary

Although a robust point distribution scheme has yet to be developed, some non-dimesional parameters related to local flow characteritics have been identified which are correlated with various observed types of failure. Criteria based upon these parameters have been suggested which may improve the application of the existing types of distribution routines and thereby lay the groundwork for the desired robust scheme.

Chapter 8

Conclusions

8.1 Summary of Work

This research attempts to extend the use of fully nonlinear potential flow theory from the simulation of a deep-water plunging breaking wave by Dommermuth et al. [3] to the simulation of a deep-water plunging breaking wave impacting a vertical wall. The experimental basis for this numerical study is the work of Chan [1, 2] done on the measurement of impact pressures and kinematics of a deep-water plunging wave impacting a vertical wall. The numerical wavemaker velocity input used is the same as that used by Dommermuth et al., only the numerical tank is shortened as the actual tank was in the experiment in order to force overturning of the wave to occur near the wall so that wall impact is possible.

8.1.1 Simulations for Long Tank

The simulation of a deep water plunging wave in a long tank of L = 20 is repeated in order to investigate the dependence of results upon the use of smoothing, regridding or both. It is confirmed that sawtooth instabilities develop on the free surface in this case when the simulation is started without the use of any smoothing or regridding. The simulation is complicated by the apparent "weak breaking" tendency of the peak preceding the peak which eventually overturns and plunges. This difficulty is overcome by the use of regridding plus smoothing for a limited interval which suppresses the breaking of the first peak, after which smoothing alone is used which allows simulation of the overturning of the second peak to continue.

The results of the simulations are found to be most dependent upon the ending time of the regridding plus smoothing interval. As the time of starting smoothing alone decreases, the time at which re-entry occurs is observed to increase. For the simulations which continue to re-entry, the maximum difference in time of re-entry is 0.15, or about 0.3% of the average total simulation time. The maximum deviation in re-entry x-position is 0.2, or about 1.7% of the average x-position at re-entry.

The relative global conservation of energy is also dependent on the timing of regridding and smoothing application. The runs with the longest and shortest re-entry times are found to have the worst conservation of energy, gaining about 7% in fluid energy relative to total wavemaker work over the duration of the simulation.

8.1.2 Simulations for Short Tank: Pre-impact

The same time sequence of regridding, regridding plus smoothing and smoothing alone that is used in run A3B to successfully simulate a plunging breaker in the long tank is applied to the short tank simulations after noting that the difficulty with the weak breaking tendency of the first peak still exists. In runs where no regridding and smoothing is used, the development of a sawtooth instability of the free surface is observed.

As in the simulation for the tank of L = 20, breaking in the simulations using a shorter tank occurs sooner than in the actual experiment. Initially, a length of L = 11.667 is used to coincide with one of the cases of wall impact investigated by Chan [1, 2], but overturning and near re-entry in the successful simulation occurs before the crest tip reaches the horizontal postion corresponding to the end of the tank. After experimenting with several shorter tank lengths, a simulation is achieved with L = 11.60 in which the overturning crest appears as though it will reach the end of the tank, but failure occurs due to lack of resolution of the free surface near the wall.

In order to finally obtain a simulation with L = 11.60 which continues to the point of impact without any apparent abnormalities in the flow, the following techniques are used:

1. Points are added in the curl region and near the wall prior to the start of overturning to increase resolution.

2. The smoothing of points near the wall is changed so that the position and velocity potential at the intersection point are not smoothed themselves but are used in smoothing the adjacent two points. The original method smoothed the wall point values as well.

3. The computation of vertical velocity at the intersection point is modified from a one-sided 3-point difference of complex potential along the free surface to a one-sided 5-point difference of velocity potential along the right wall.

Important observations from these simulations are the following:

1. There is a minimum degree of resolution required in the curl region to successfully simulate the overturning process.

2. Point addition prior to overturning can cause difficulty later in the overturning process as points tend to cluster in the center of the curl. When spacing becomes too close the simulation breaks down.

3. The modified finite difference scheme for computing intersection point velocity coupled with the modified smoothing routine eliminates the problems of the jump in intersection point velocity upon point addition and anomalous motion of points nearest the wall. In this case, the 3-point finite difference scheme eventually allows abnormal flow near the wall, but the 4- and 5-point schemes appear sufficient and give nearly identical results.

At the point where the crest tip reaches the wall, the crest height, wall run-up and curl

dimensions for the simulated wave with L = 11.60 are comparable to the experiment for the case where L = 11.667.

8.1.3 Simulations for Short Tank: Post Impact

The idealized impact problem is initially posed by creating two new wall-free surface intersection points at the crest after the crest has passed the horizontal position corresponding to the end of the tank. Two techniques are examined for assigning the initial velocity potential to these new intersection points, and a technique is tried for defining new intersection points as other free surface points later reach the wall boundary. The effect of adding interior points to the contact region at impact is also investigated, and such point addition is observed to produce the most plausible flows in a qualitative sense.

The preliminary results of pressure computations for the impact region without the effect of air compressibility are puzzling. The initial pressures are negative, and tend to become more positive with time. Also, the magnitude of the initial pressures is seen to be highly dependent on the number of points added to the contact region at impact. Although positive pressures are eventually obtained which are of the same order of magnitude as those measured in the experiment, there is as yet no explanation for the computed negative pressures.

8.2 Recommendations for Future Work

8.2.1 Point Distribution Schemes

The further investigation of parameters which may be correlated to observed types of failure should be continued with the objective of improving the methods of distributing points on the free surface and ultimately developing a robust algorithm which can ensure effective simulations for a variety of nonlinear water wave problems. In particular, the criteria suggested in Chapter 7 could be implemented to determine their effectiveness.

8.2.2 Impact Problem

The idealized impact problem using potential flow is observed in some cases to yield qualitatively plausible flows. The preliminary computations of pressure, however, are not easily accepted as physical. The negative pressures obtained on impact could be the result of the following:

1. An error in the main program which solves the BVP and integrates the free surface boundary conditions.

2. An error in the analysis program which computes the pressures from the main program output.

3. Basic assumptions concerning how the initial impact condition is to be imposed; for example, the method of initially assigning velocity potentials to the new intersection points and the discontinuity introduced by "cutting off" an arbitrary amount of the crest tip to define the impact region Note that a value of $\psi = 0$ is assigned to the points on the wall in the impact region; other constant values of ψ should be tried to see if there is any affect on the results.

In addition to investigating the above issues, the following suggestions are made:

1. Include air compressibility in the simulation by modifying the dynamic free surface boundary condition in the "pocket" to impose a pressure based upon the volume of air in the pocket and an ideal gas law, perhaps adiabatic. This is an essential next step if results are to be carefully compared with those of Chan [1, 2], who surmised that measured pressure oscillations during impact were due to the dynamics of the air trapped at impact.

2. Investigate possible point addition techniques and time step control particularly suited to the impact regime, where high velocities are computed

for the intersection points created at impact. In the computations done so far, the time step size has been held constant throughout impact.

3. Investigate the possible scaling of the computational problem to match experimental results.

Appendix A

Refer to Chapter 4 for discussion.

A1 2049 44.3294

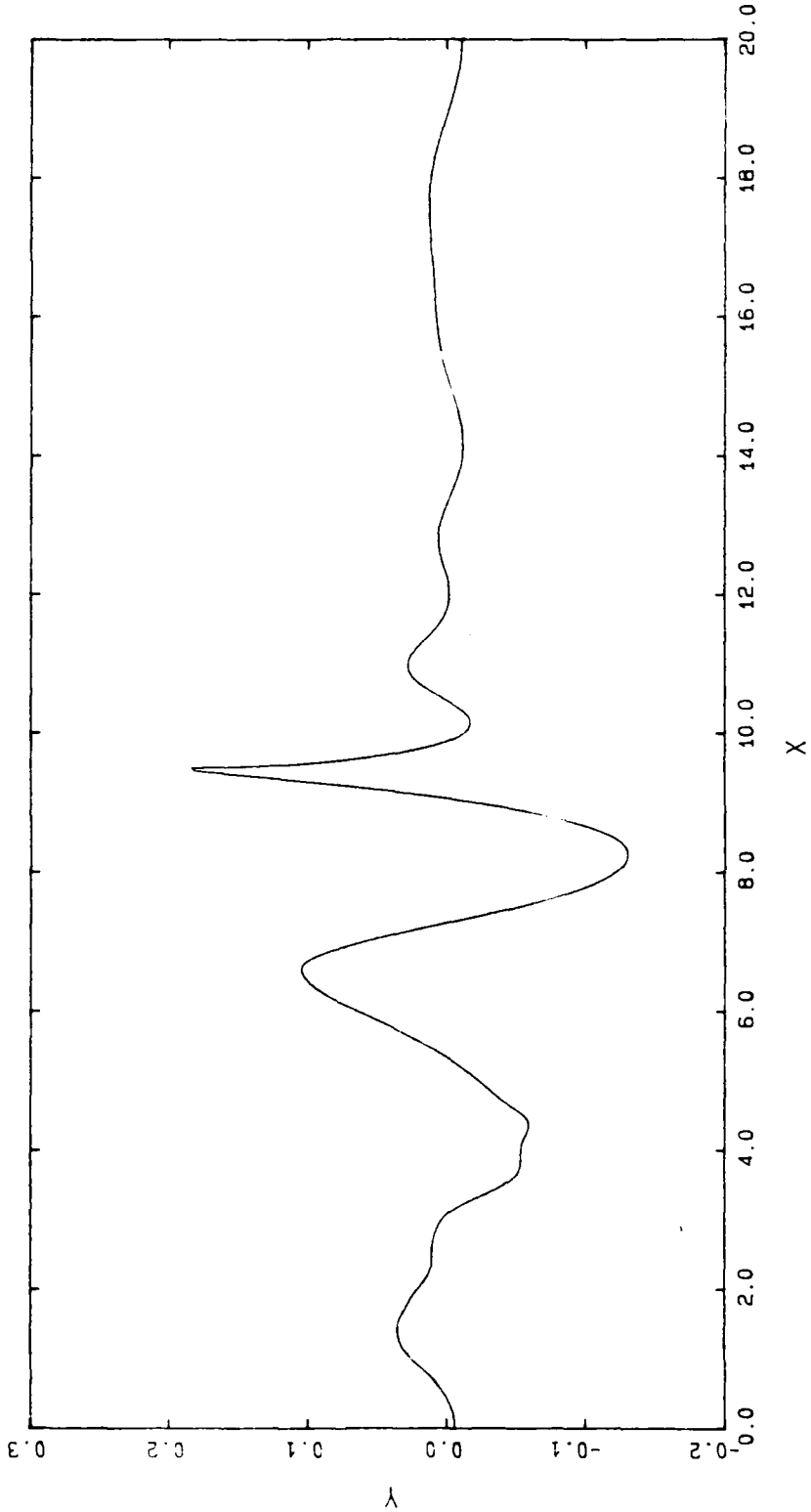

A1 2049 44.3294

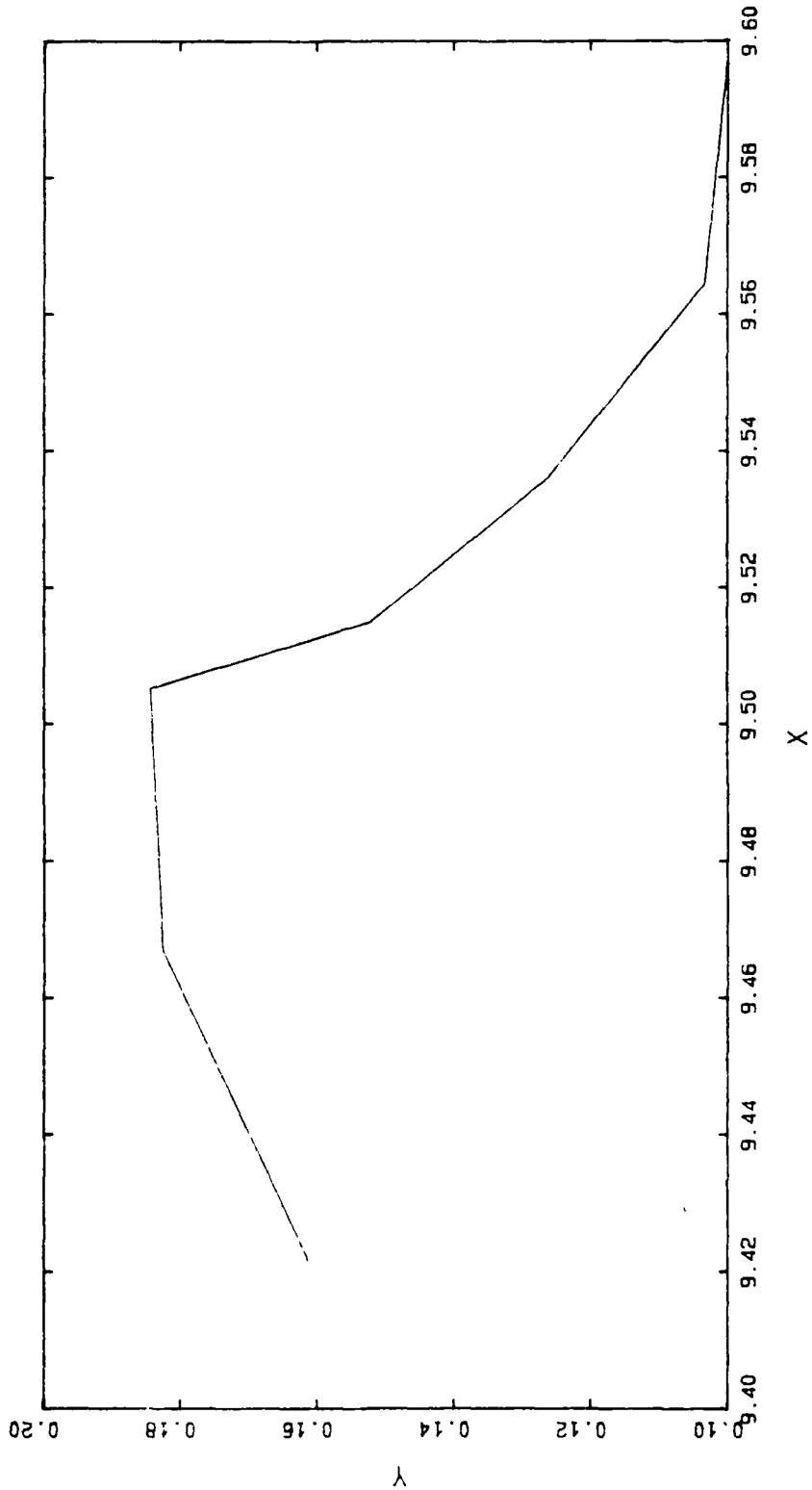

Al 2069 44.4469

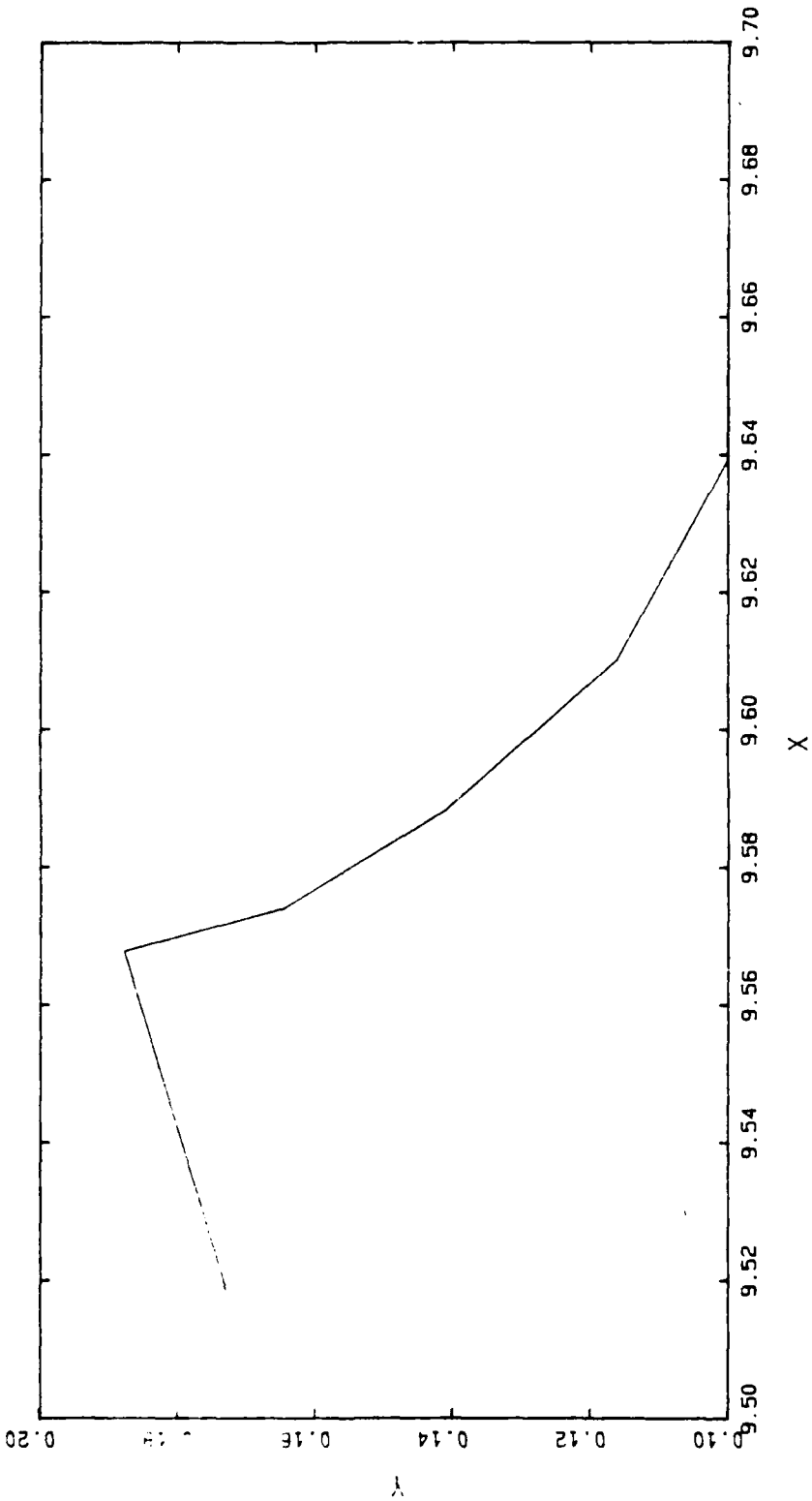

A1 2089 44.5455

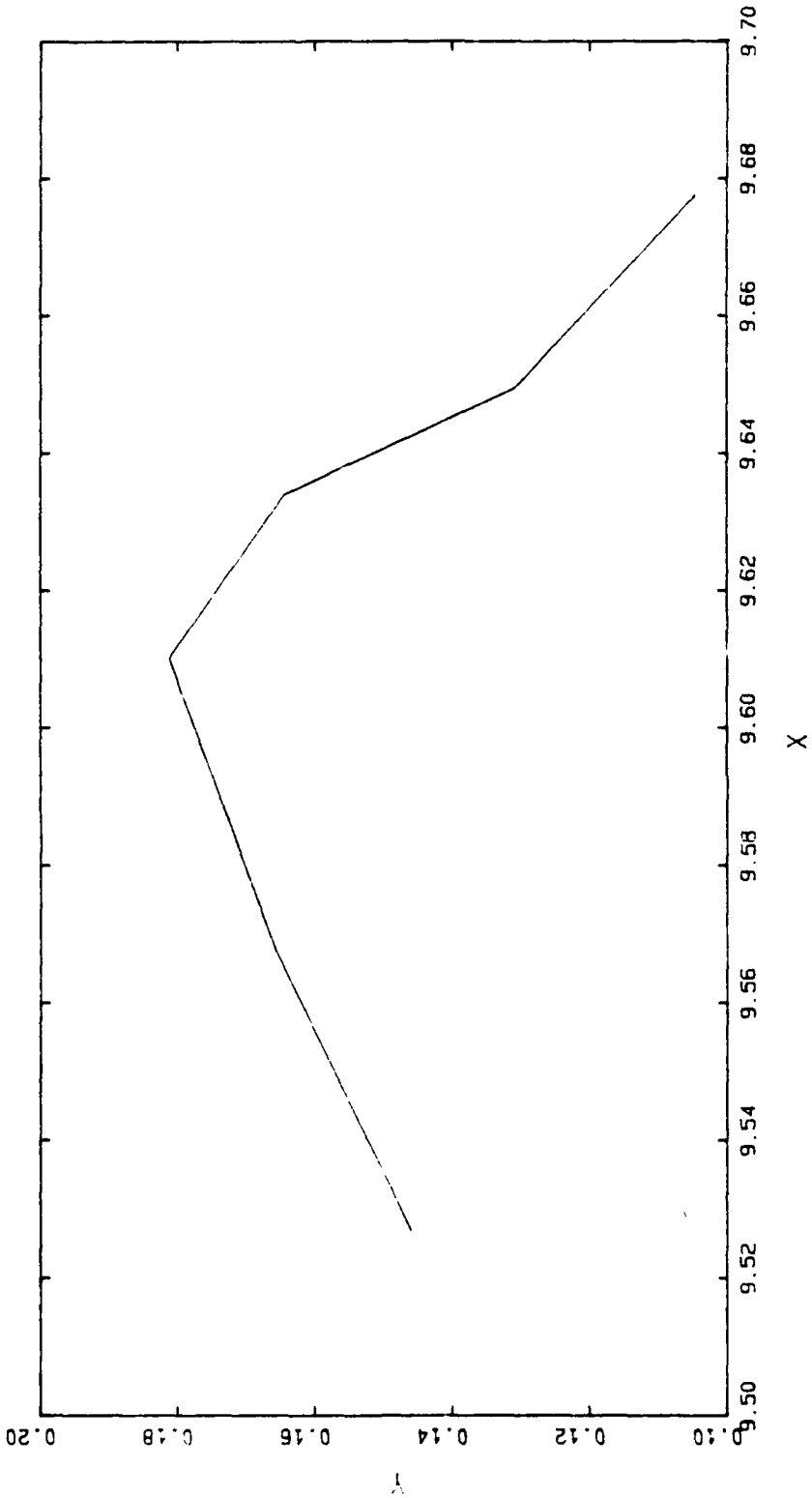

A1 2109 44.6535

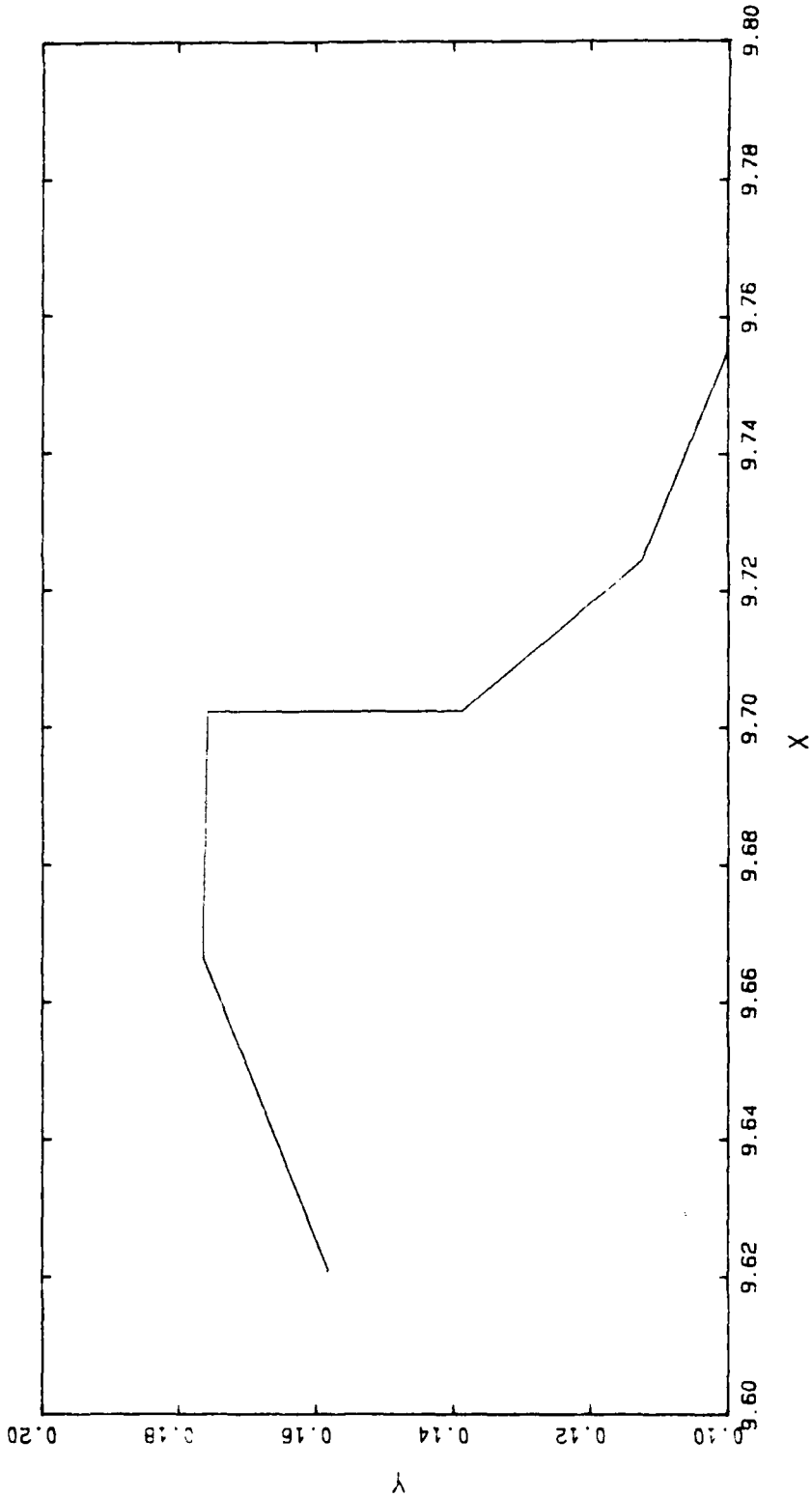

Al 2129 44.7686

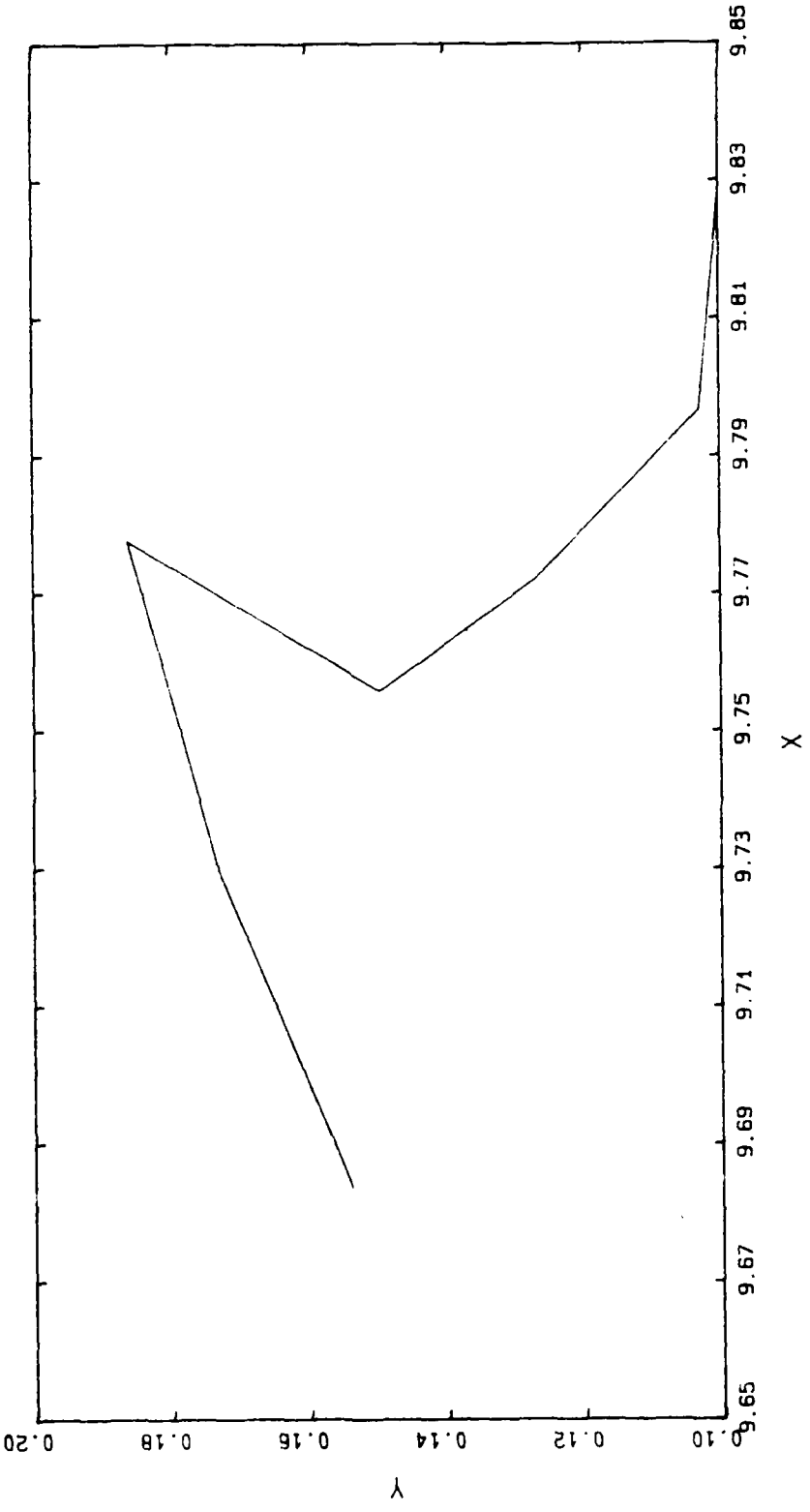

A1 2139 44.8271

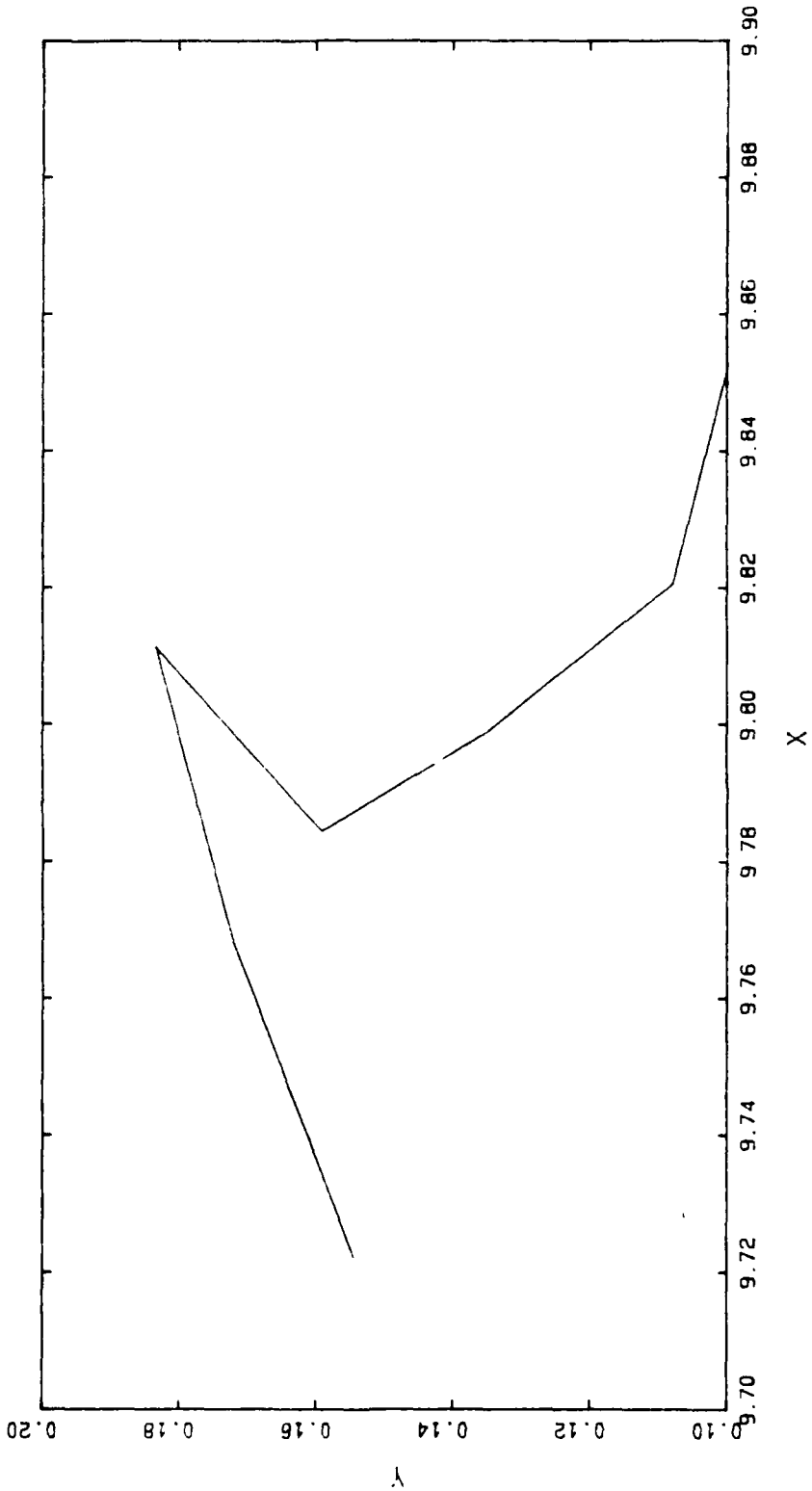

A1 2144 44.8562

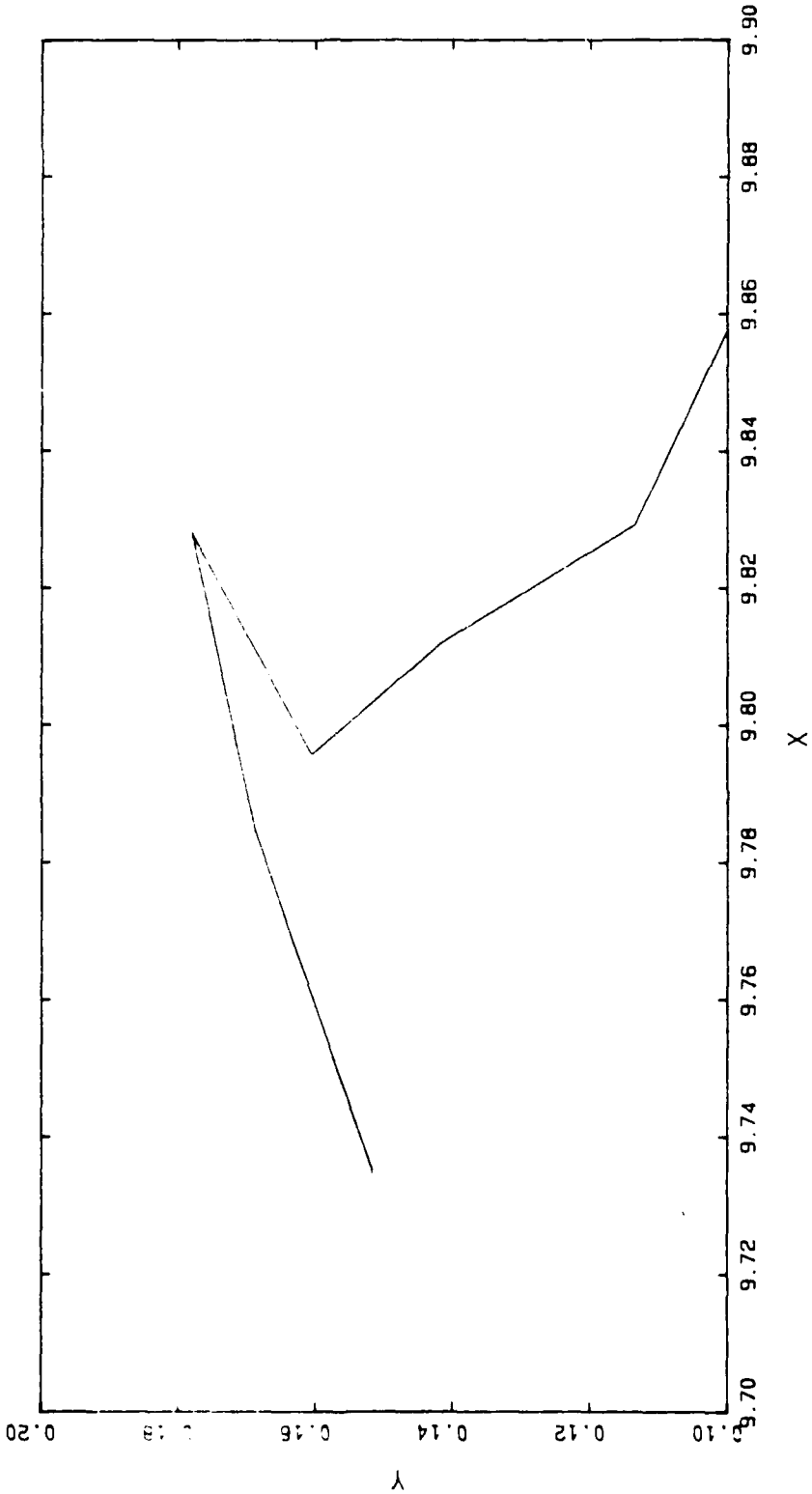

A1 2146 44.8673

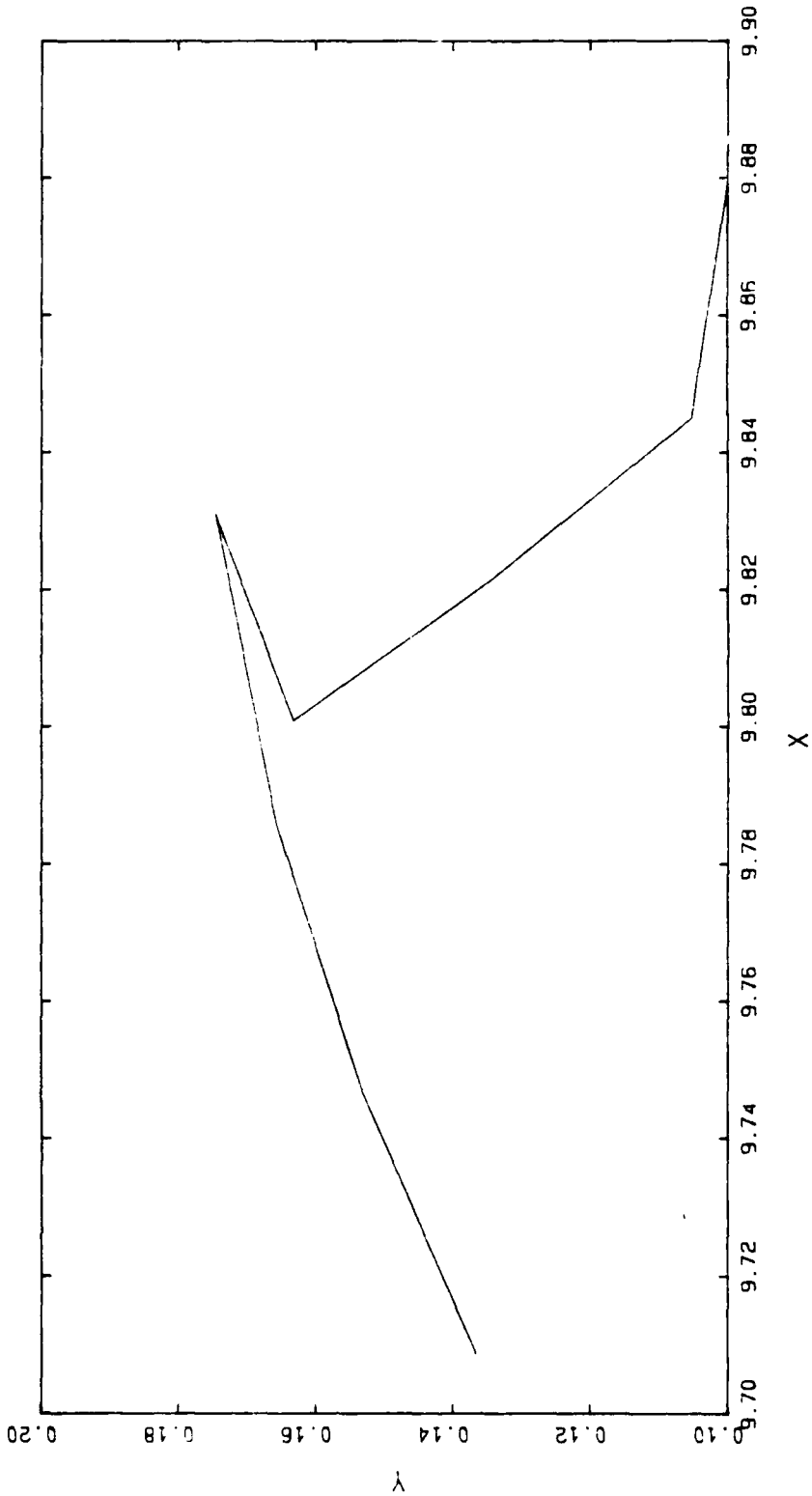

A1 2148 44.8777

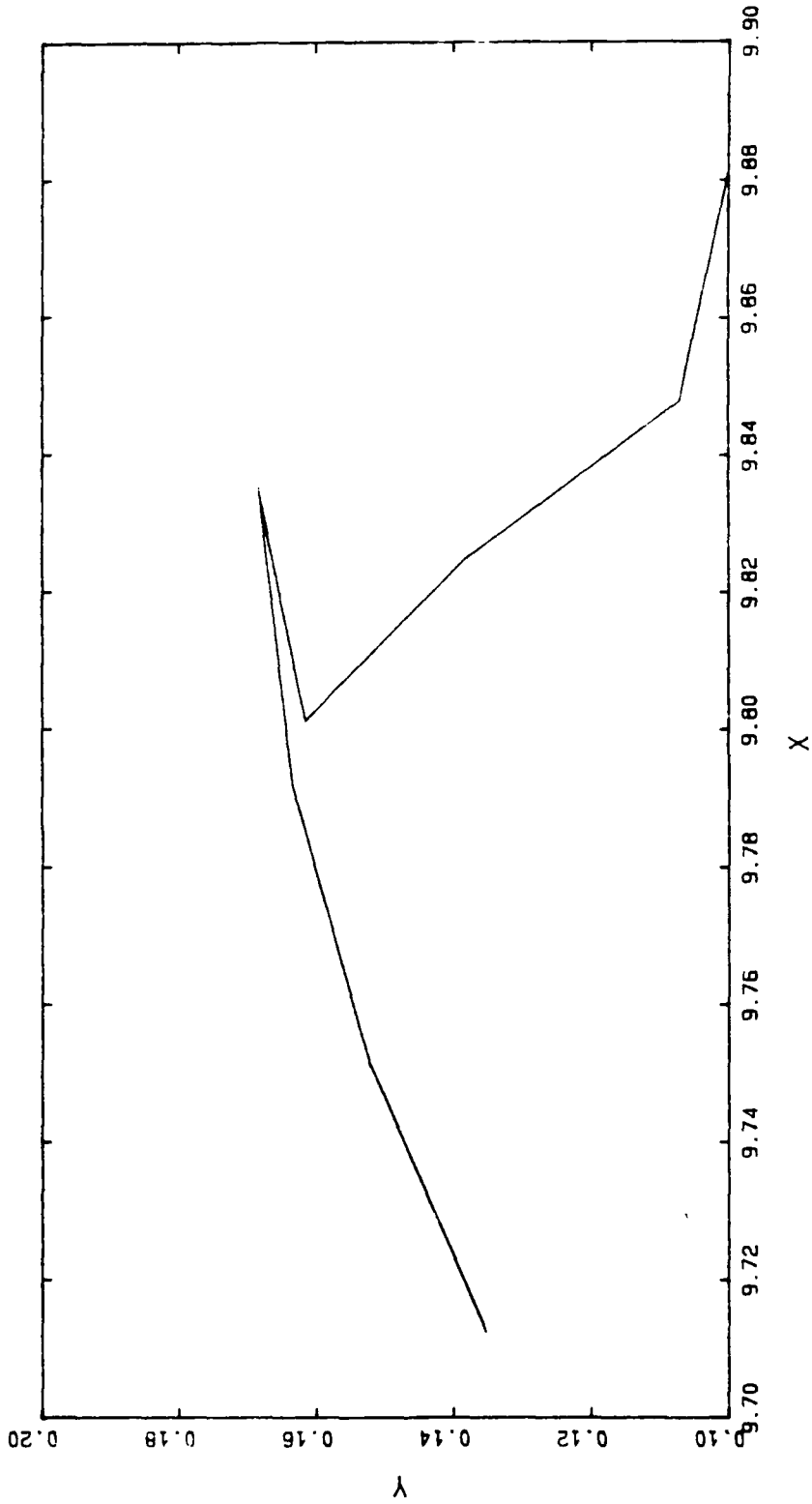

A1 2149 44.8829

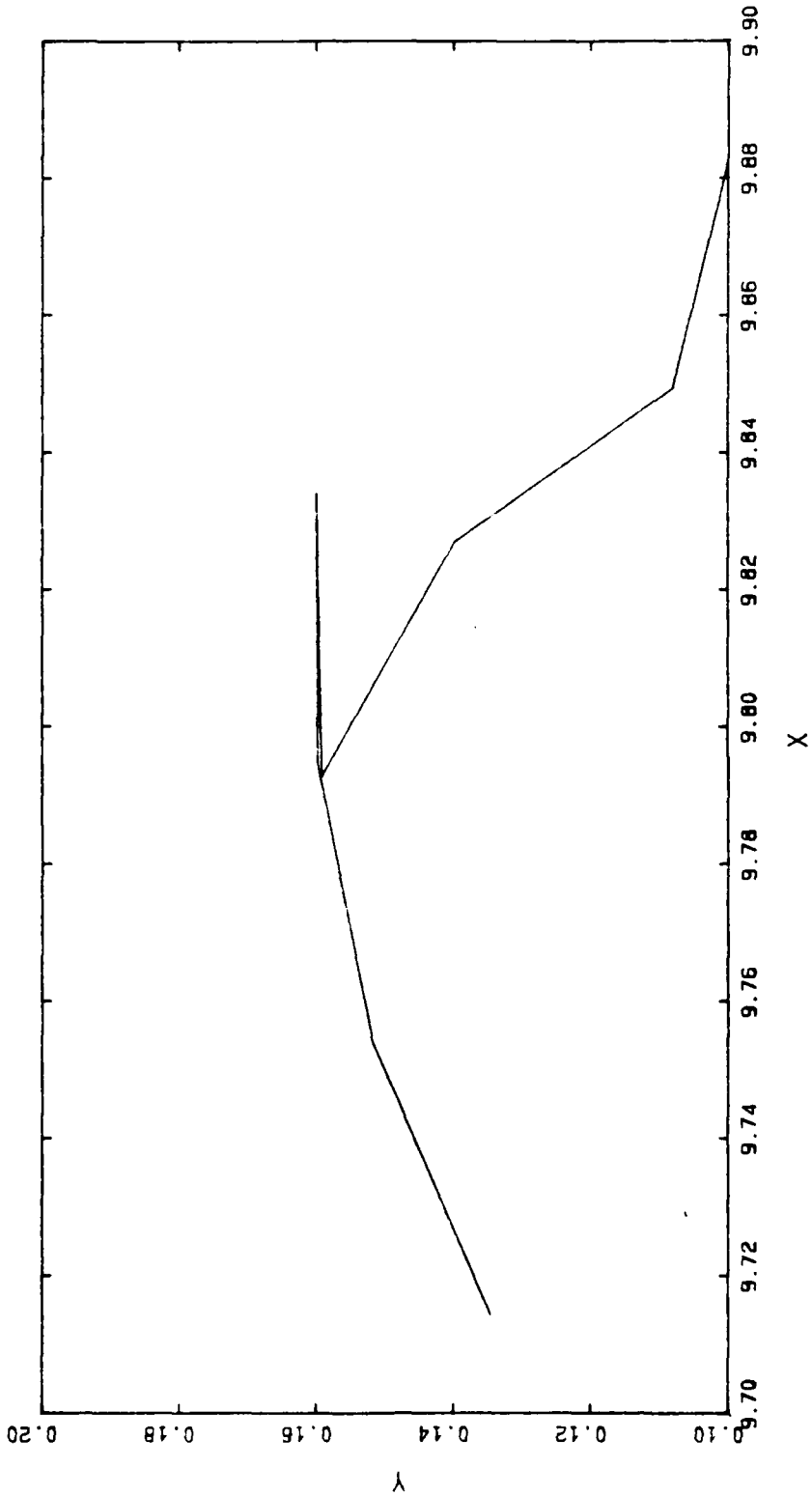

A2 2275 43.2199

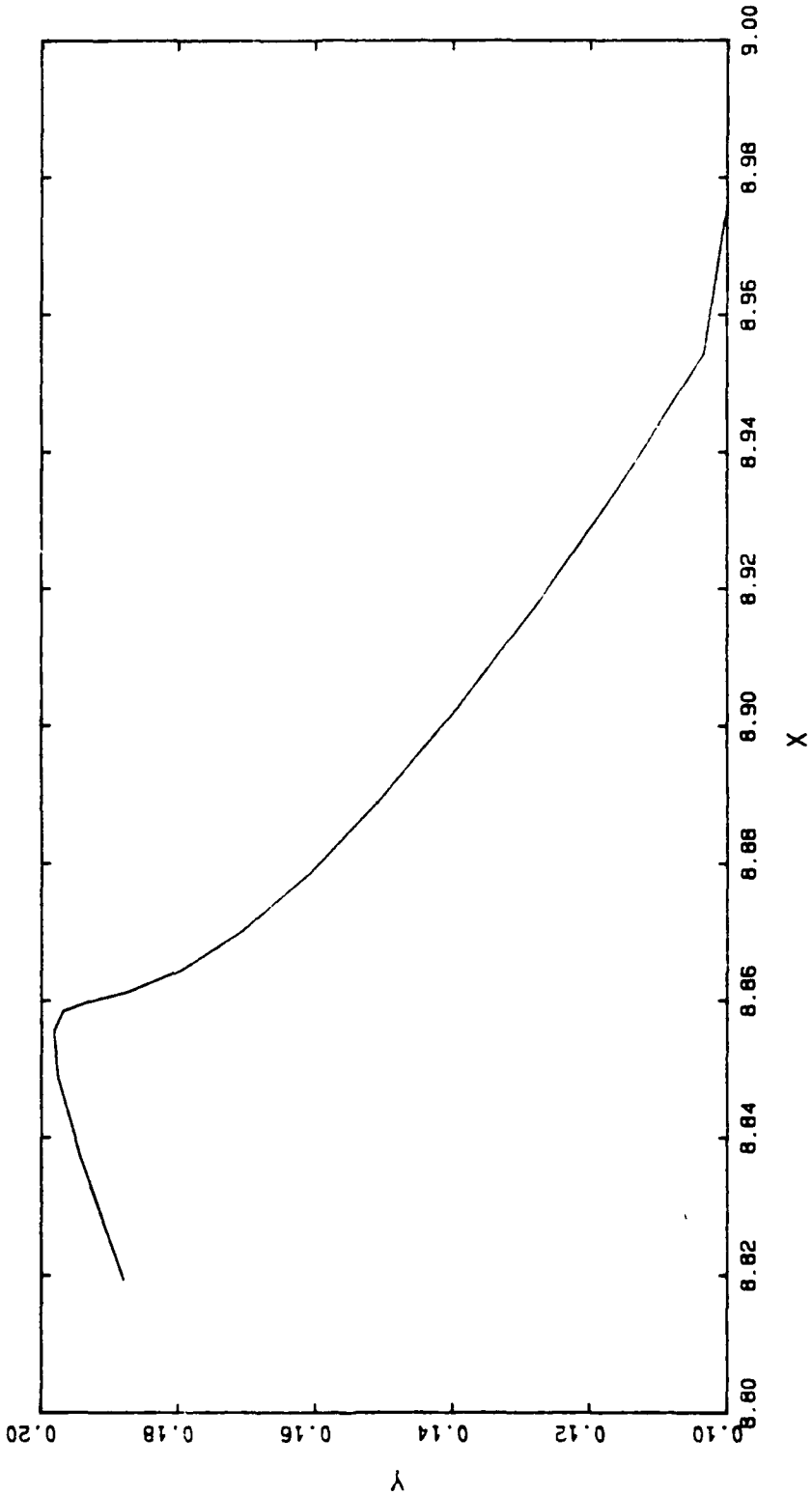

A2 2525 43.3072

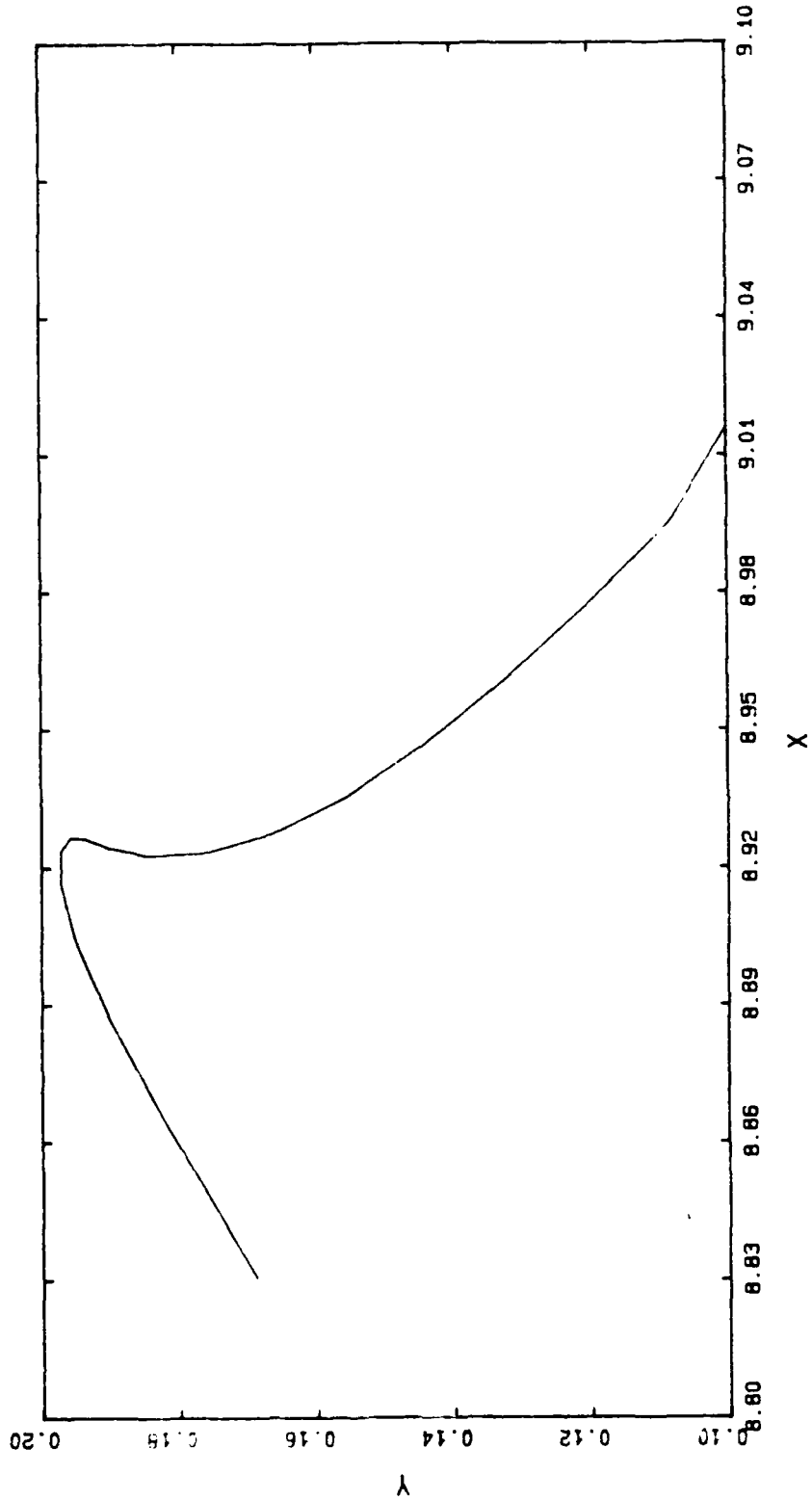

A2 2675 43.3387

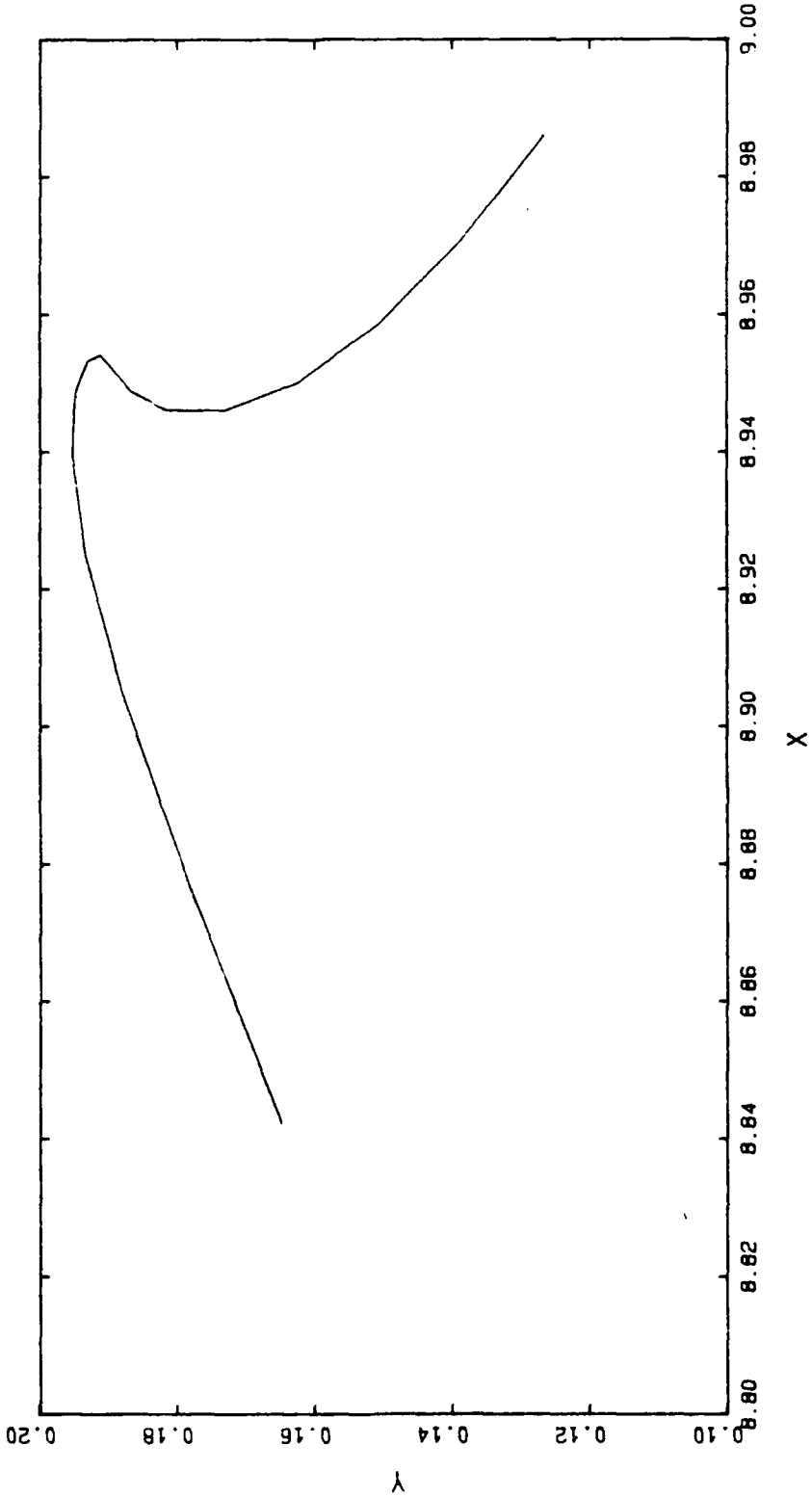

A2 2875 43.3768

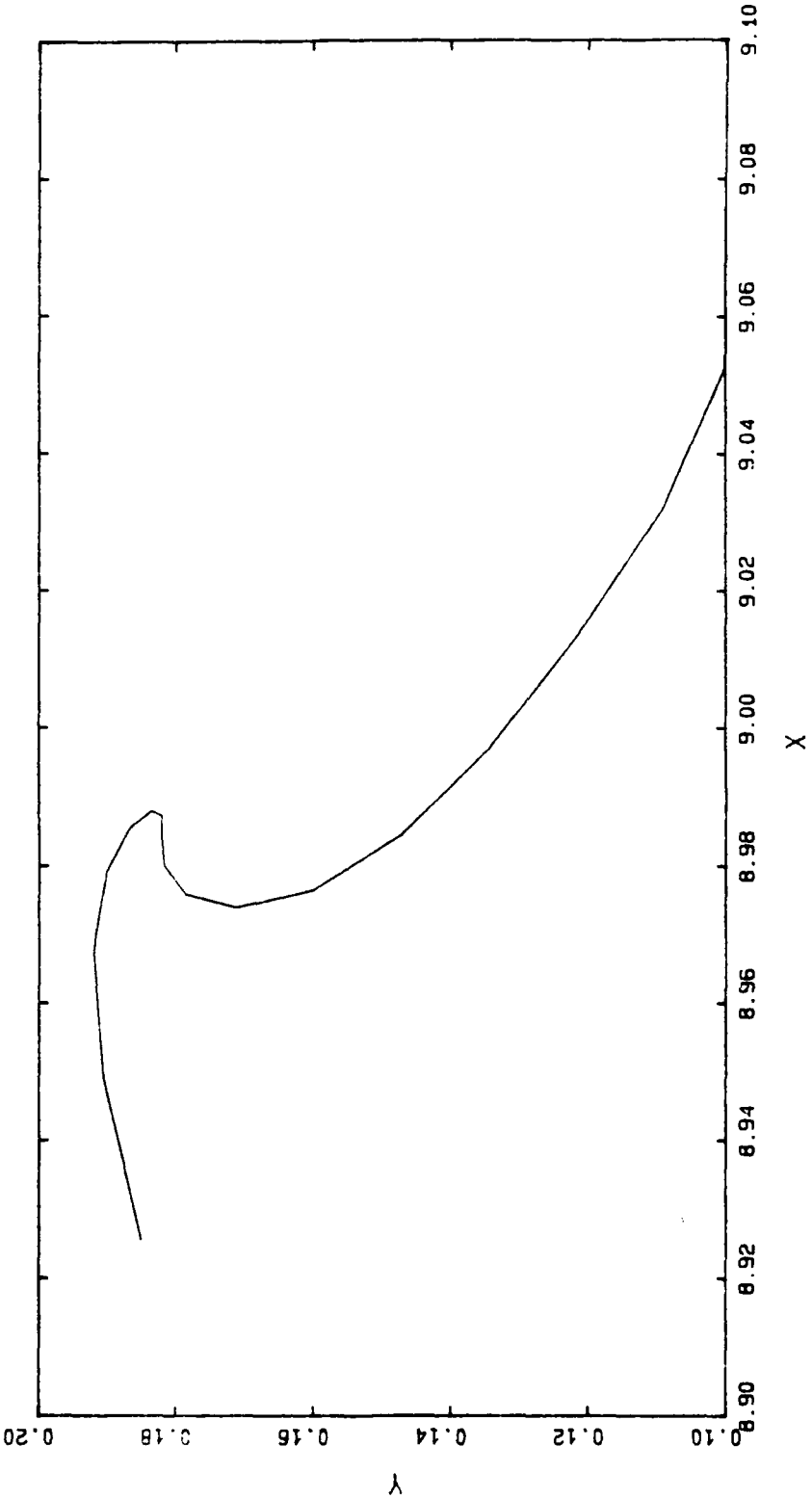

A2 3075 43.4146

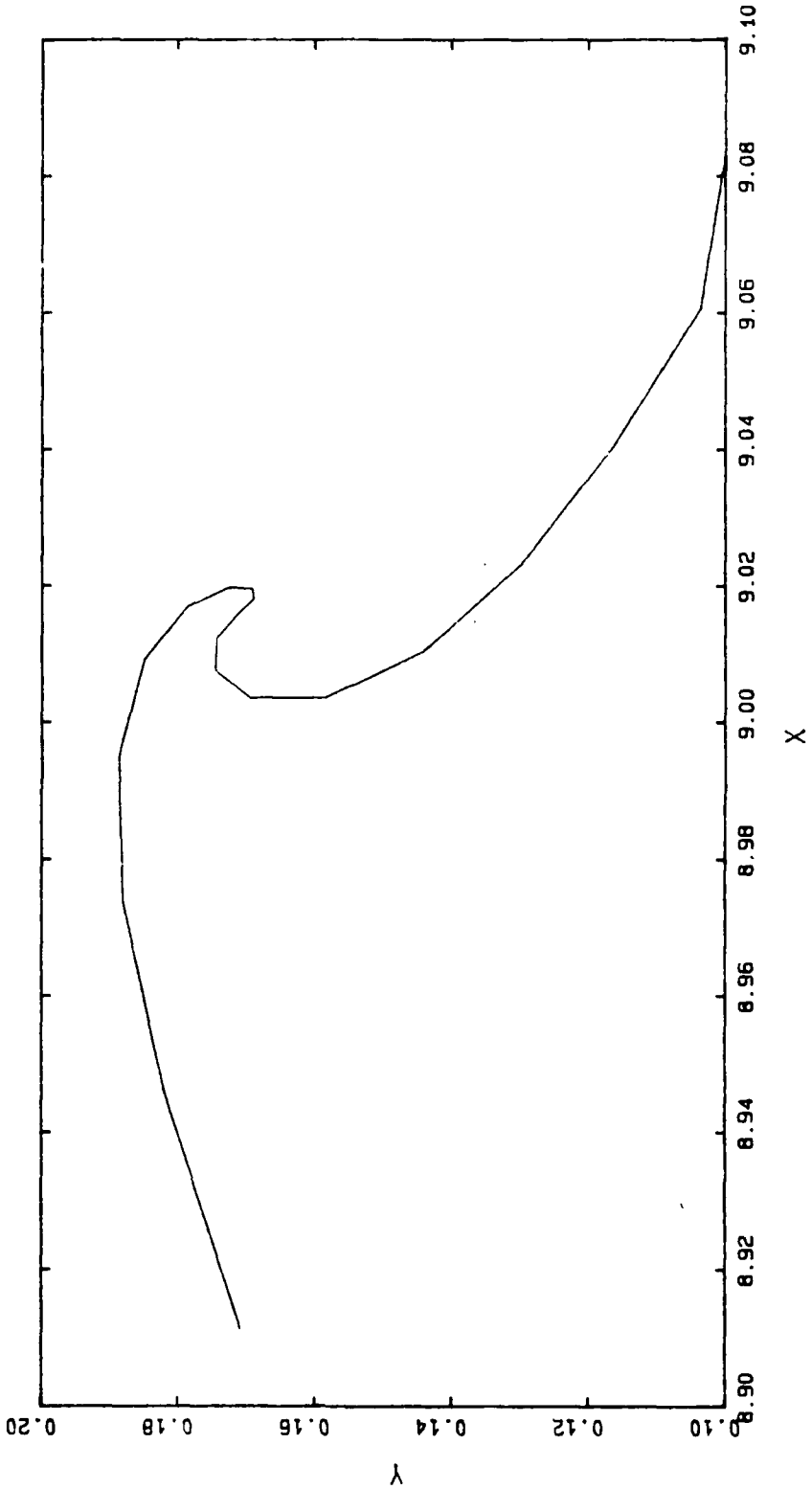

A2 3175 43.4336

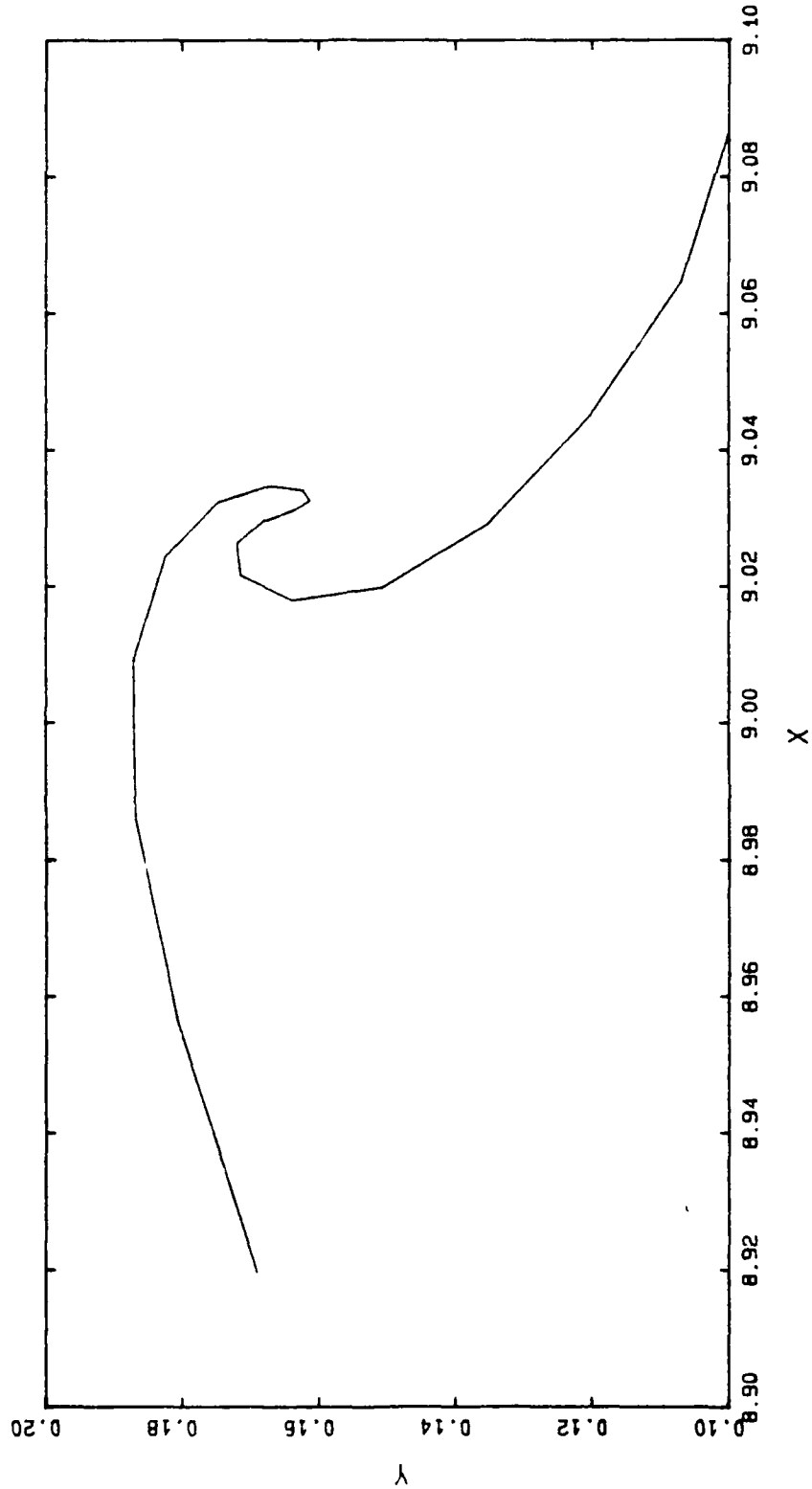

A2 3275 43.4622

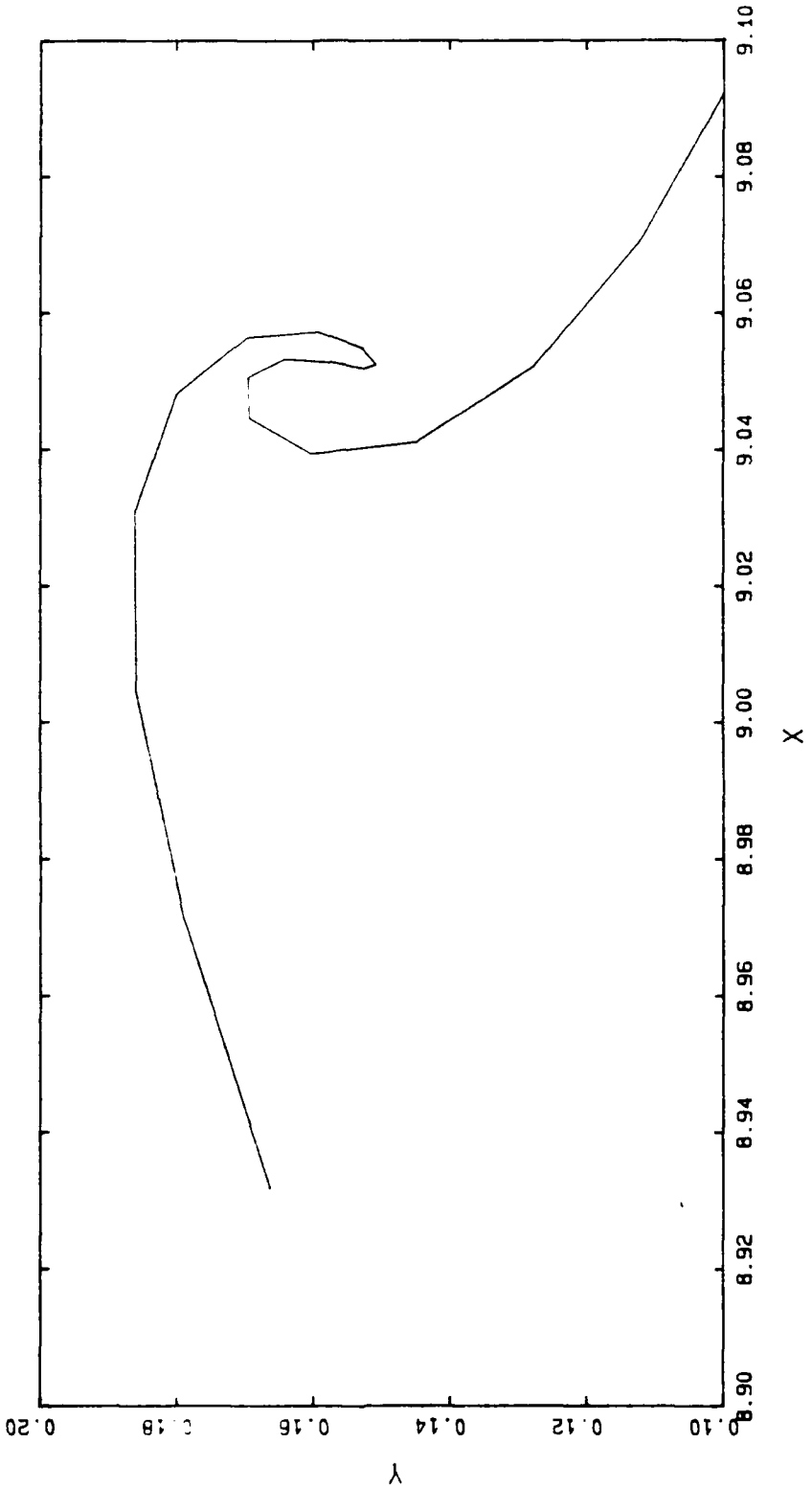

A2 3475 43.5147

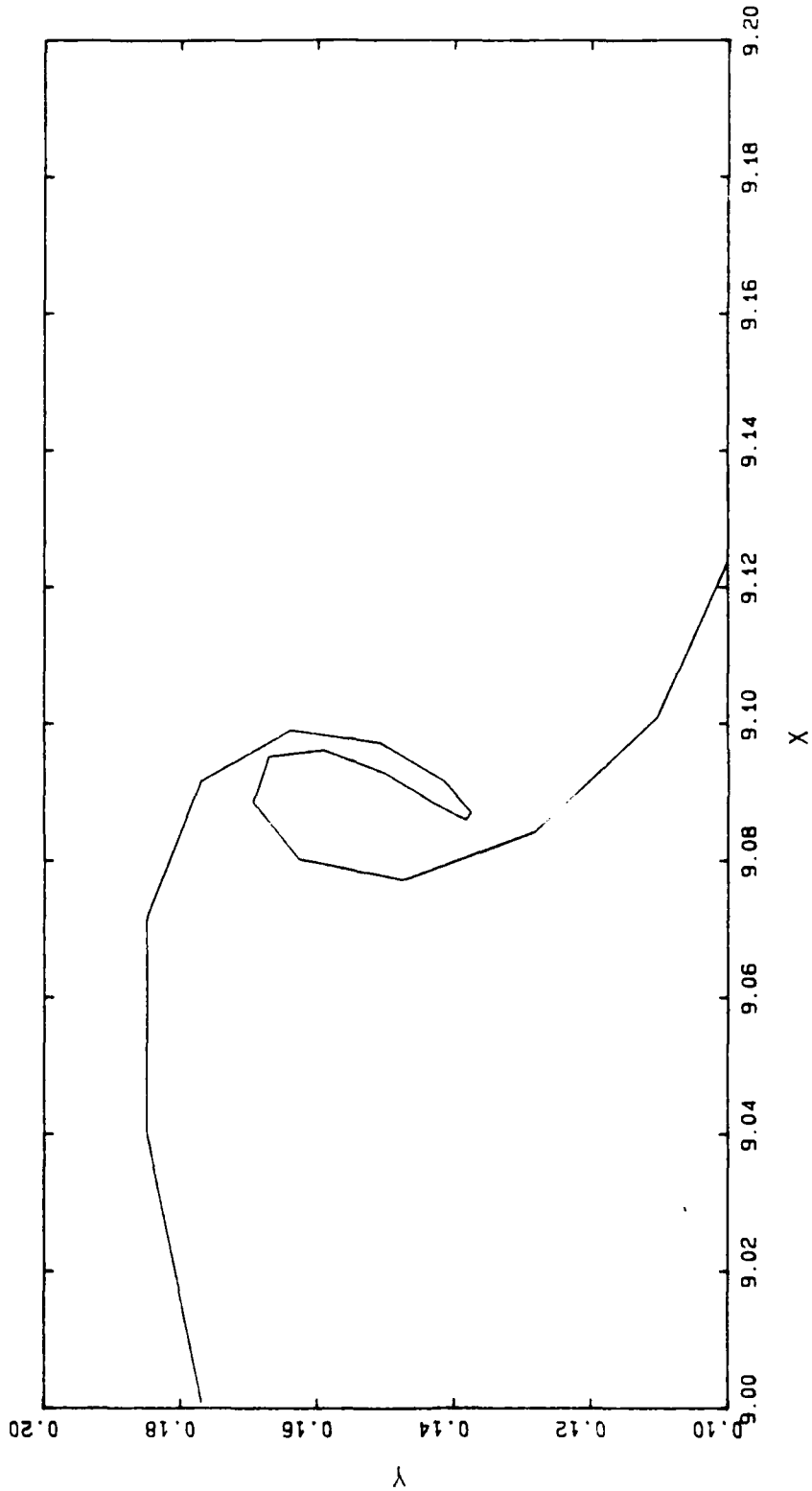

A2 3555 43.5347

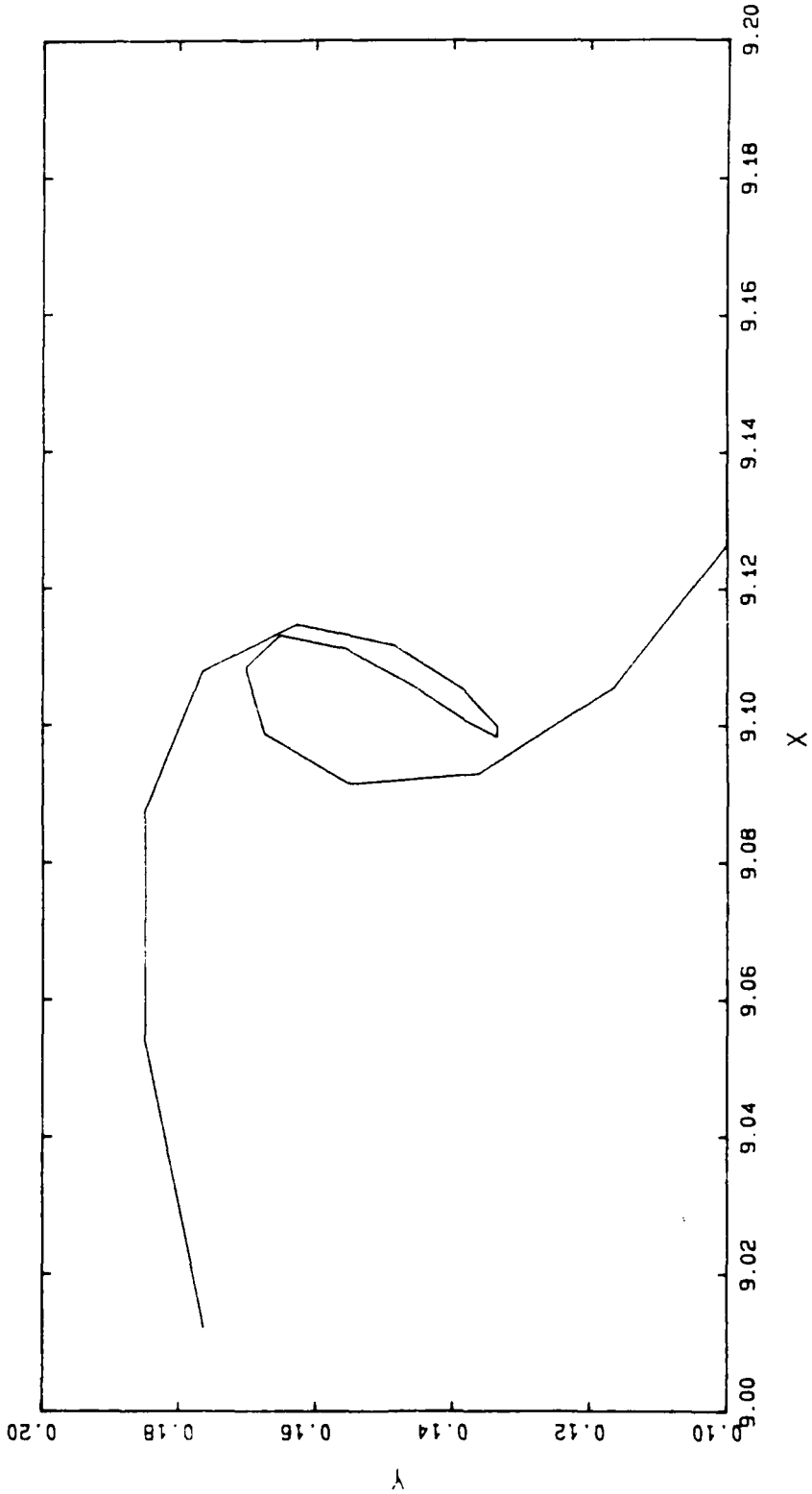

A2 3565 43.5366

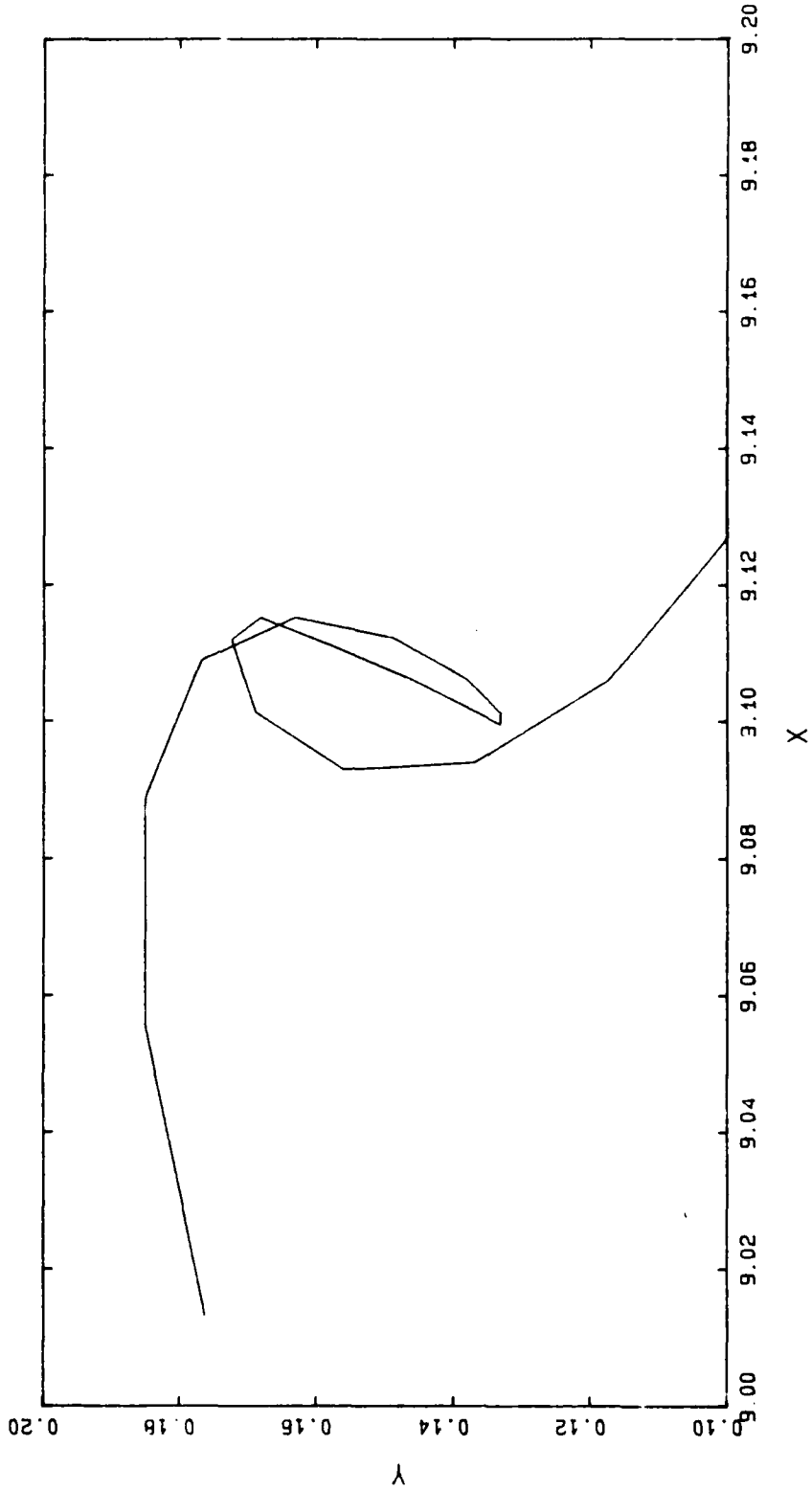

A3 400 19.3077

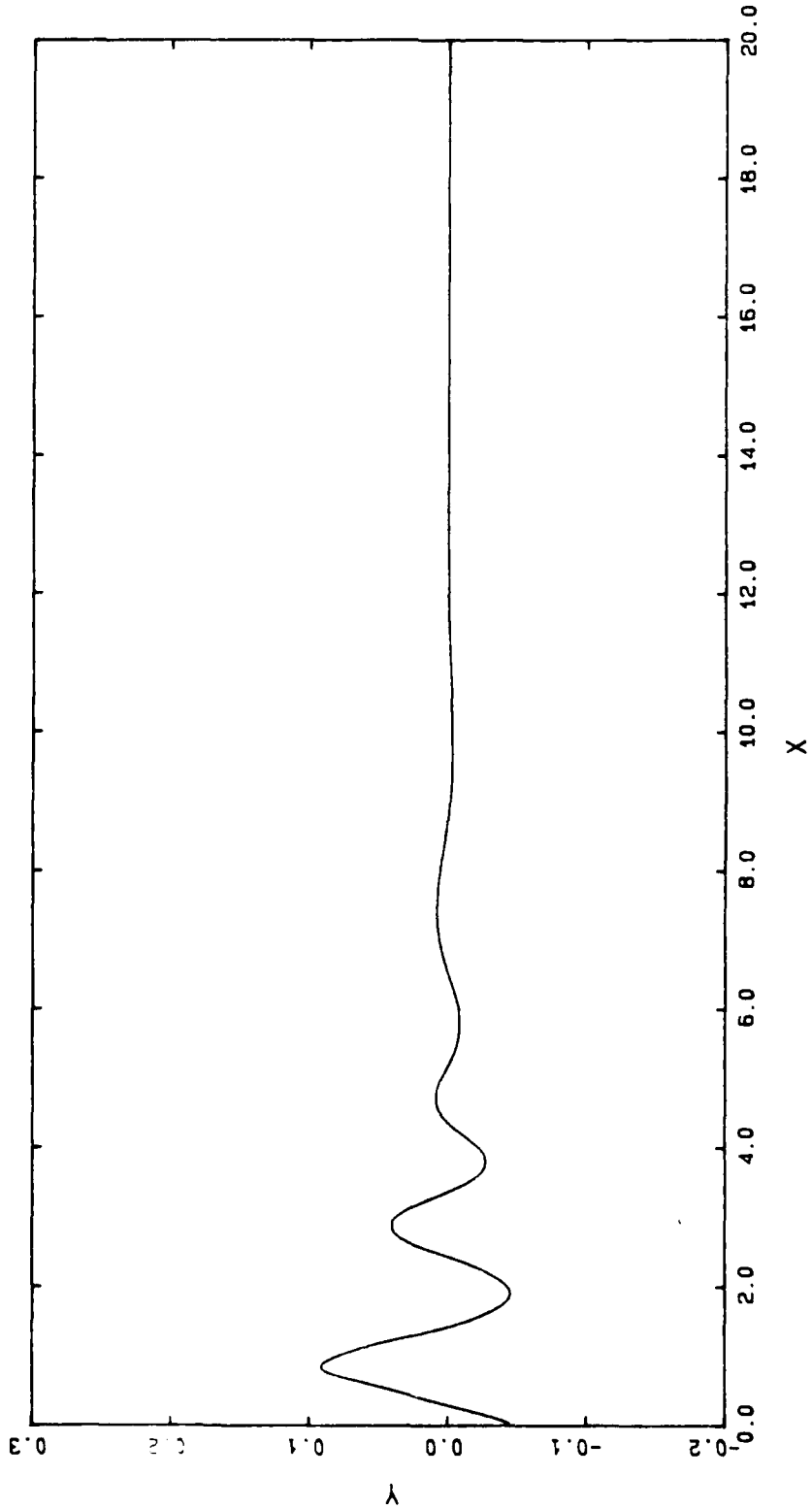

A3 800 27.3905

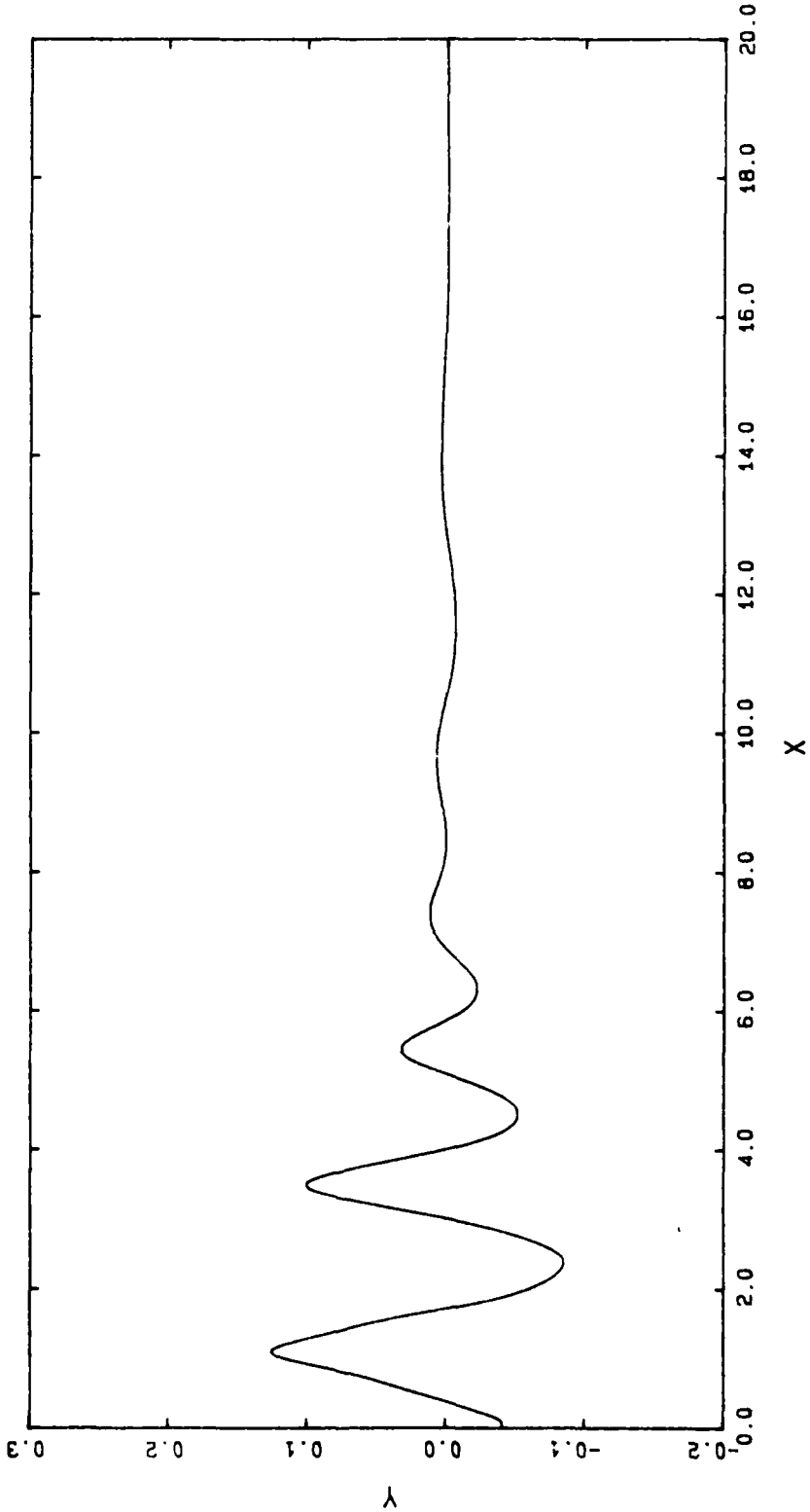

A3 1200 34.3658

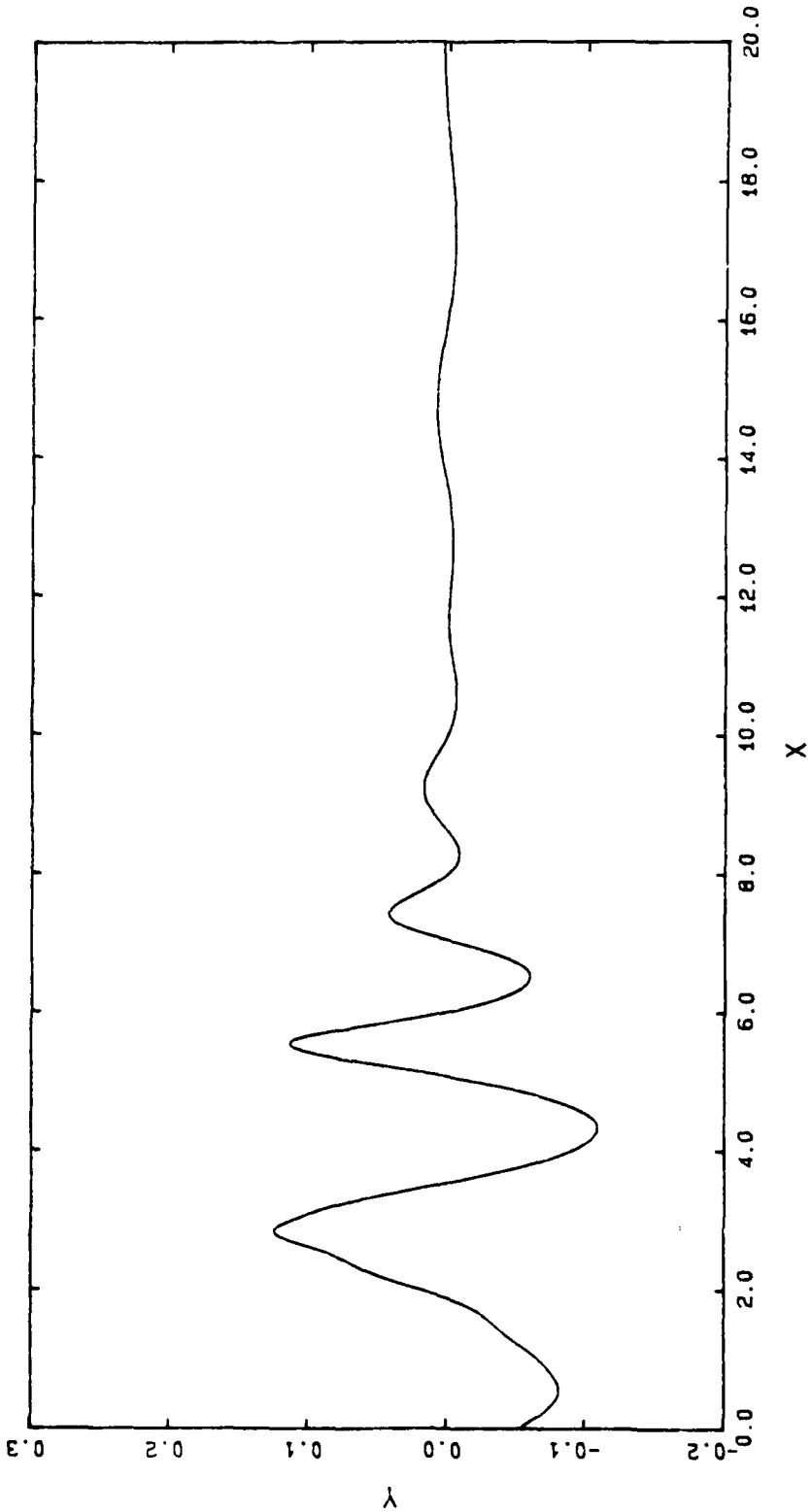

A3 1600 40.3975

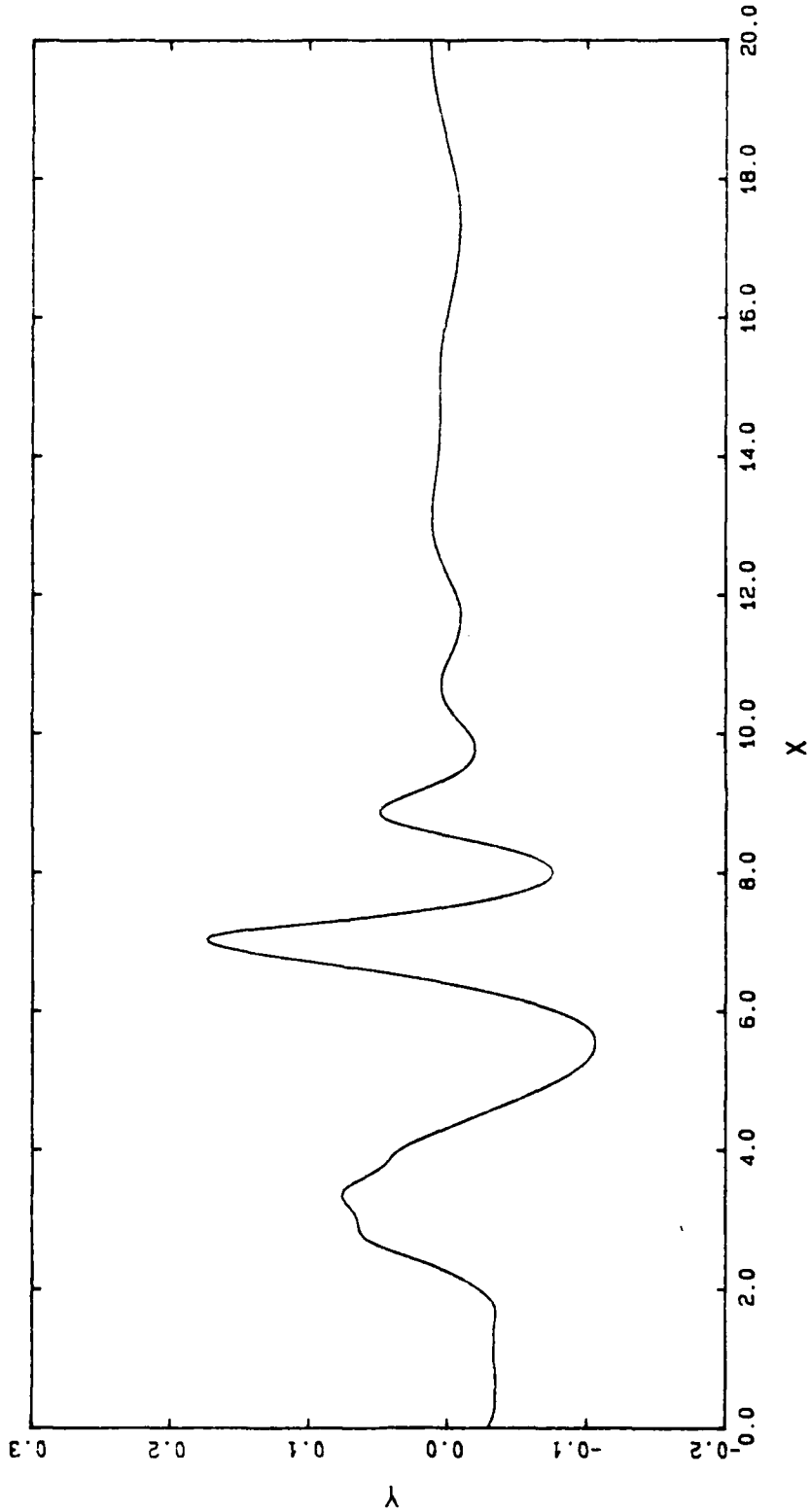

A3 2000 44.3151

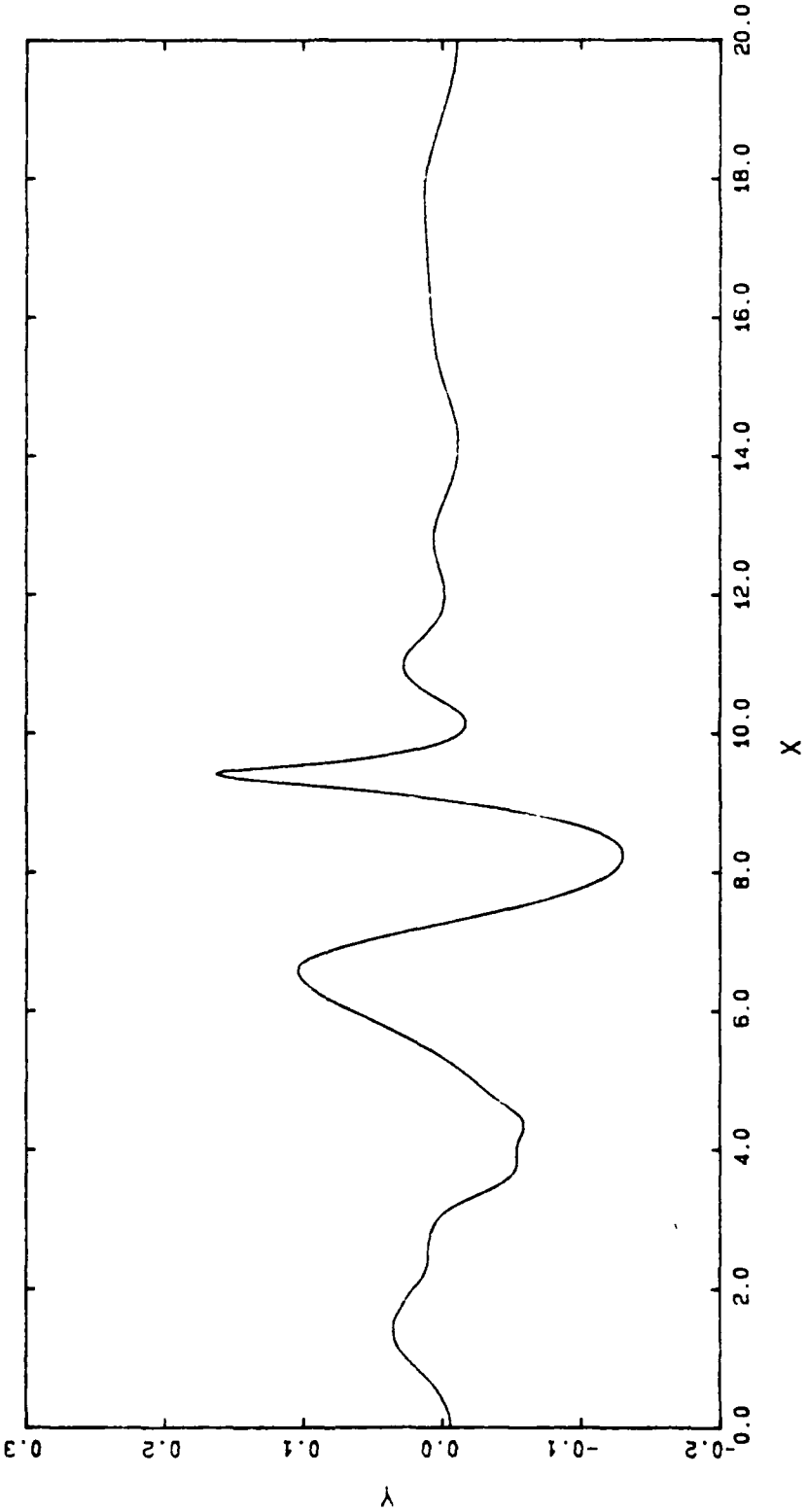

A3 2100 45.3224

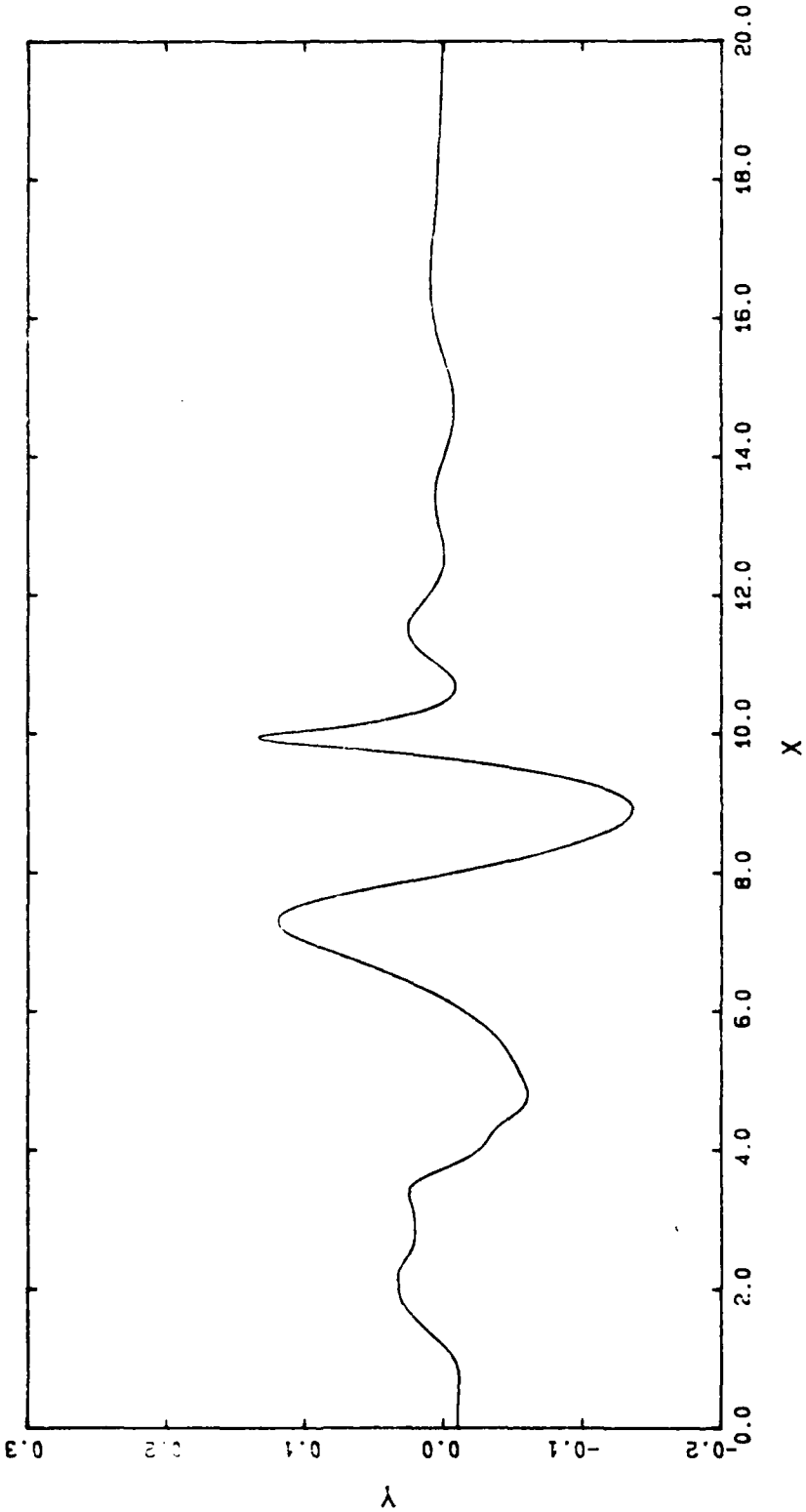

A3 2200 46.6192

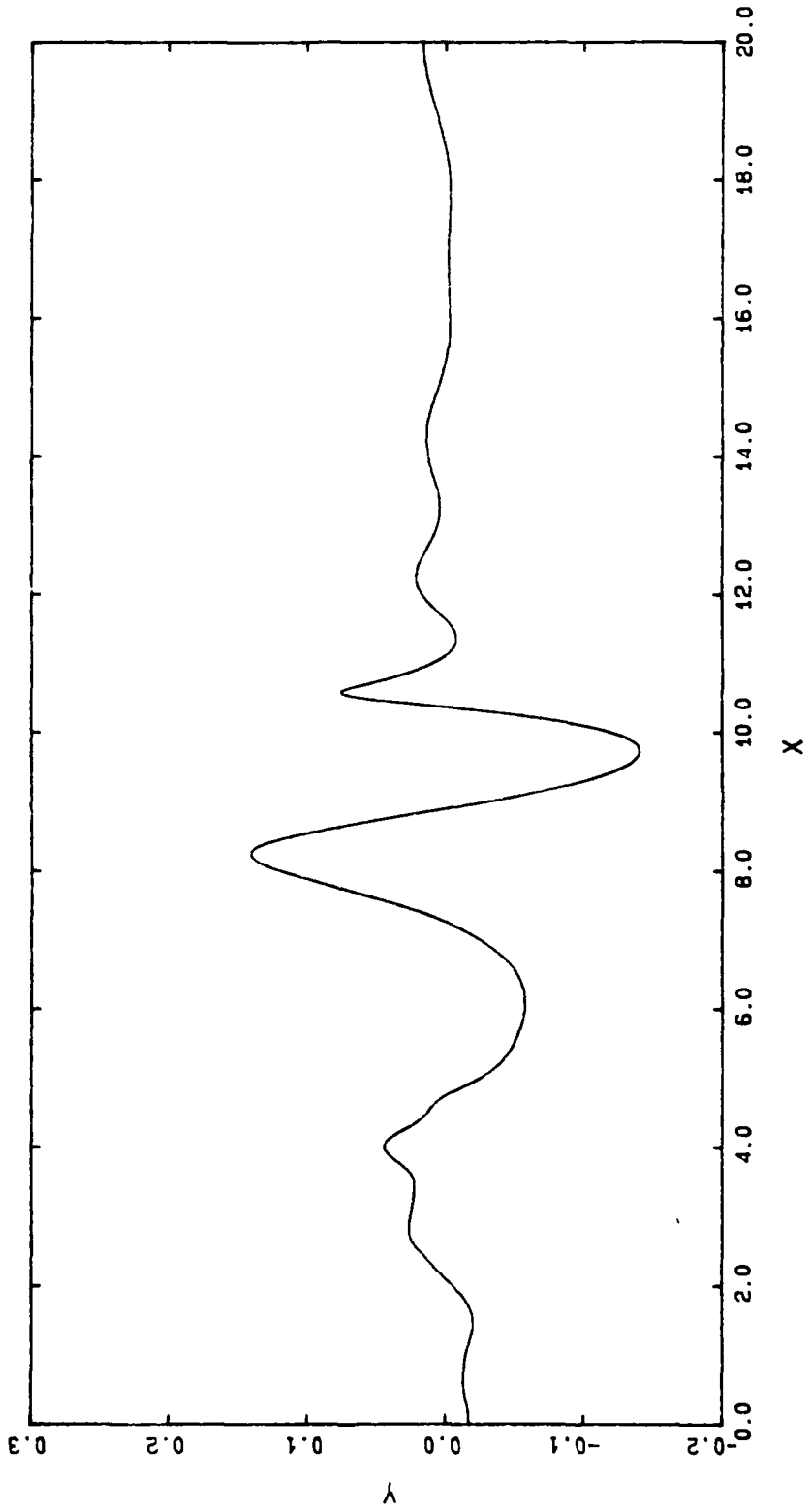

A3 2300 48.2324

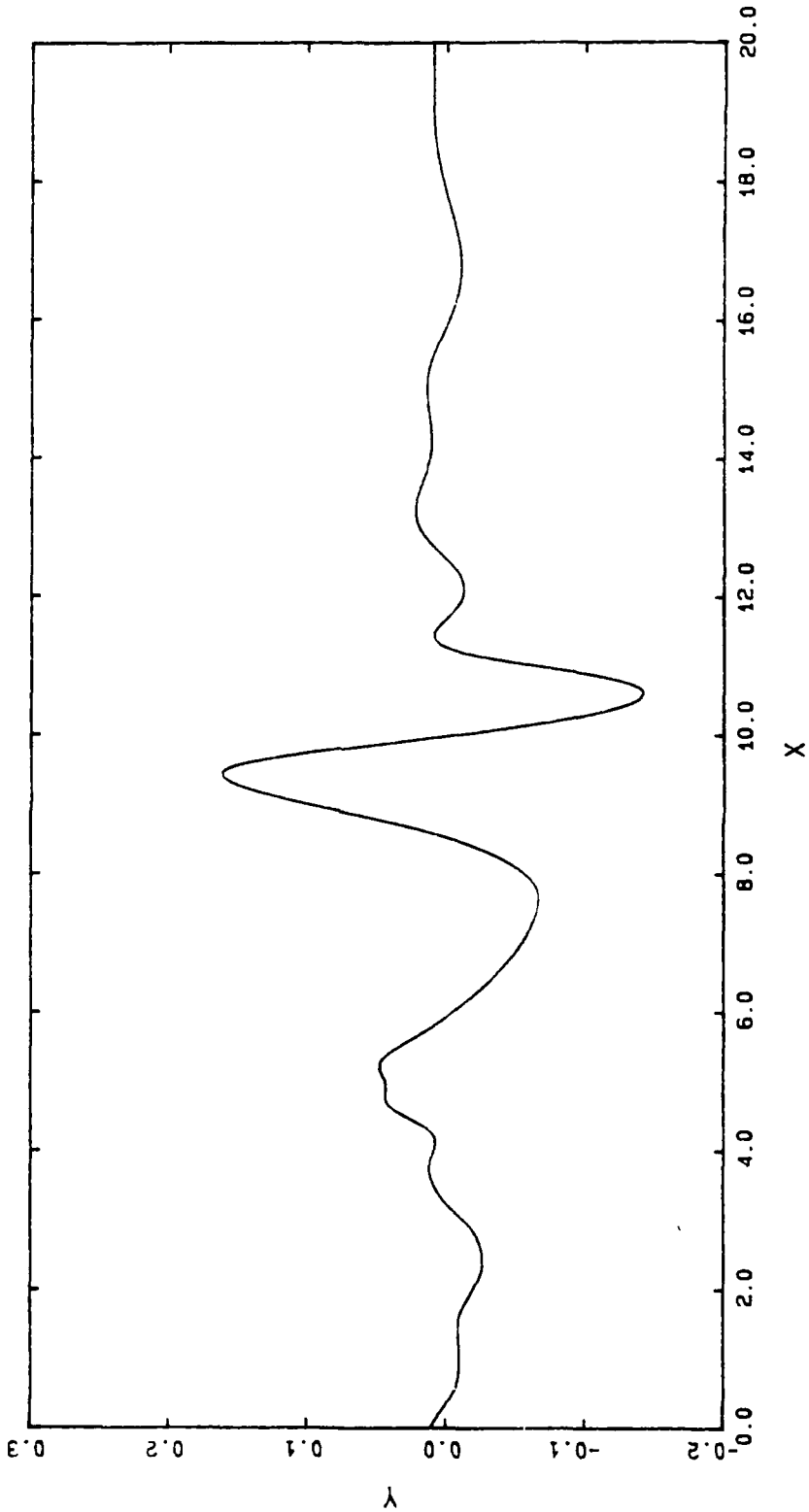

A3 2400 49.4856

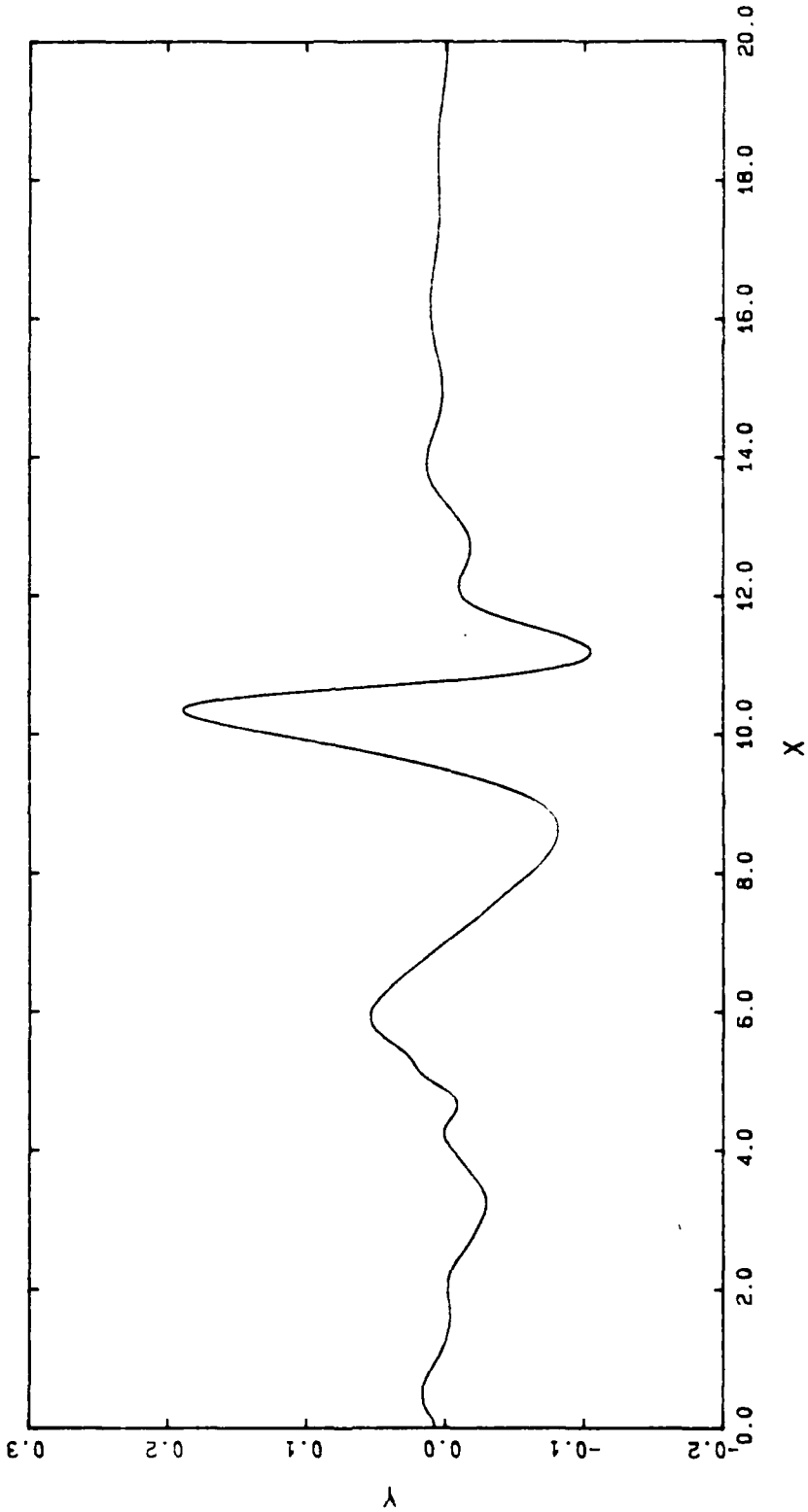

A3 2800 51.8813

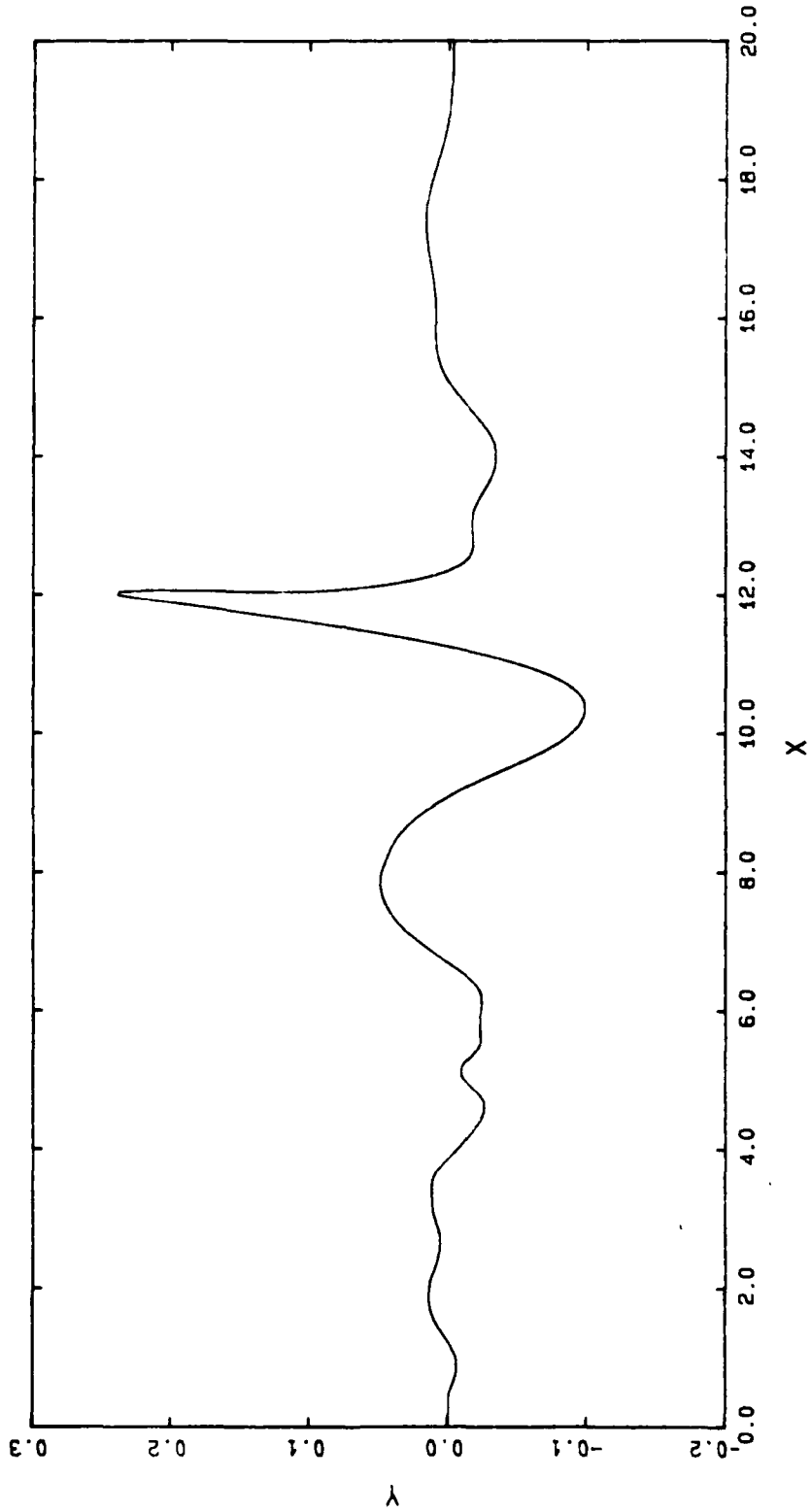

A3 3200 53.7624

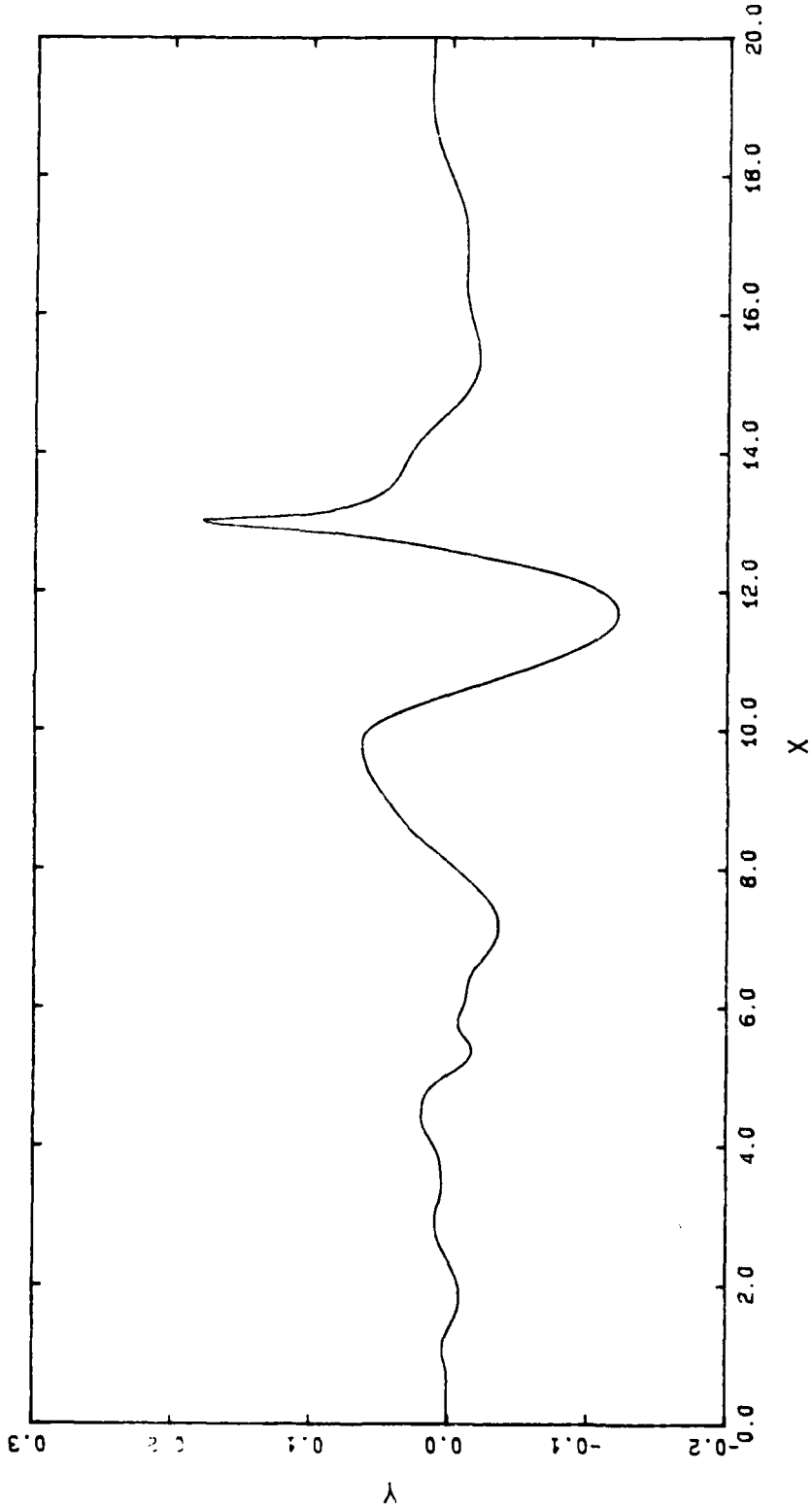

A3A	(1)	3560	51.0968
	(2)	4060	51.3243
	(3)	4260	51.3999
	(4)	4460	51.4743

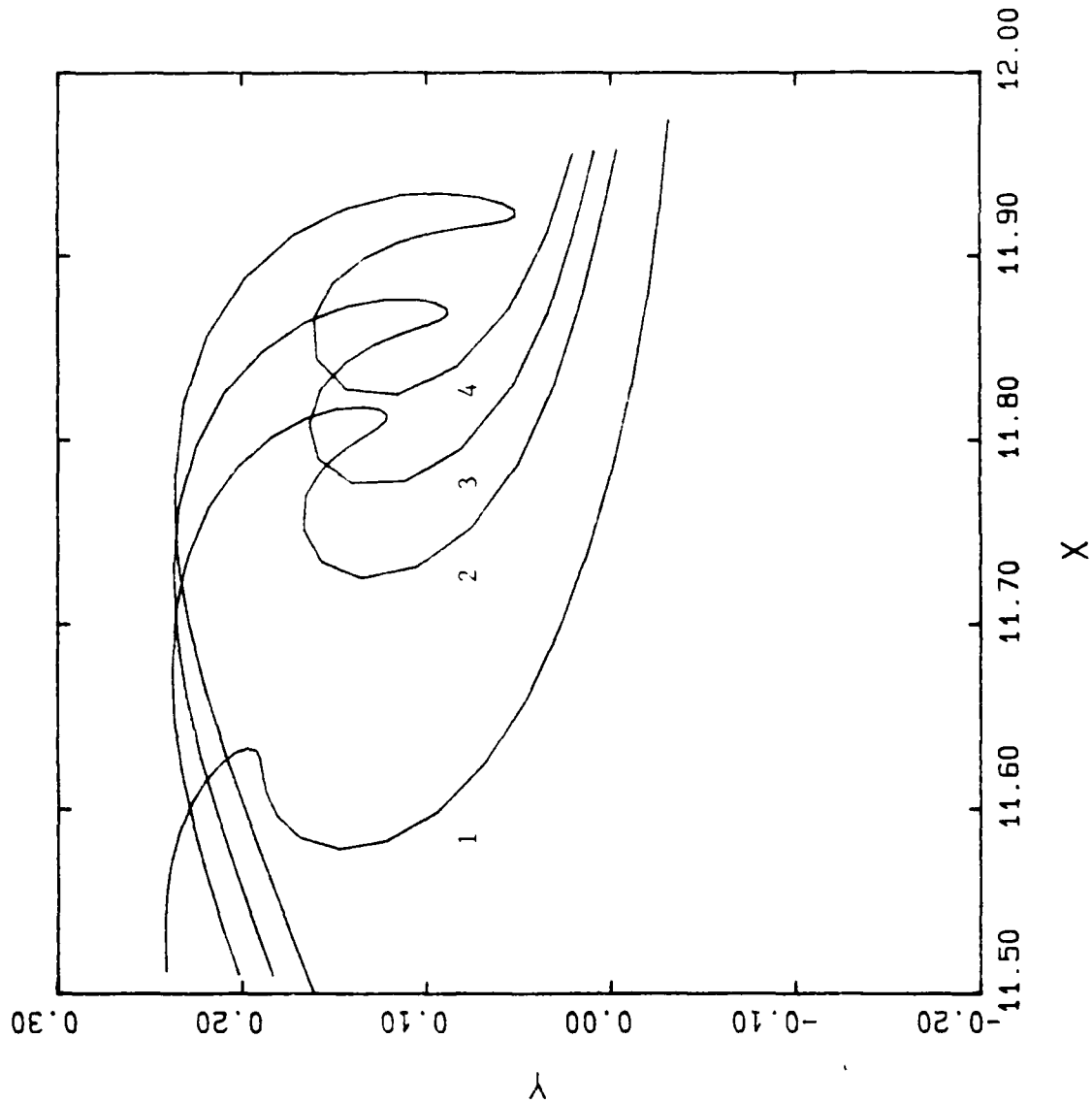

A3B	(1)	3417	50.9411
	(2)	3917	51.1337
	(3)	4117	51.2034
	(4)	4317	51.2797

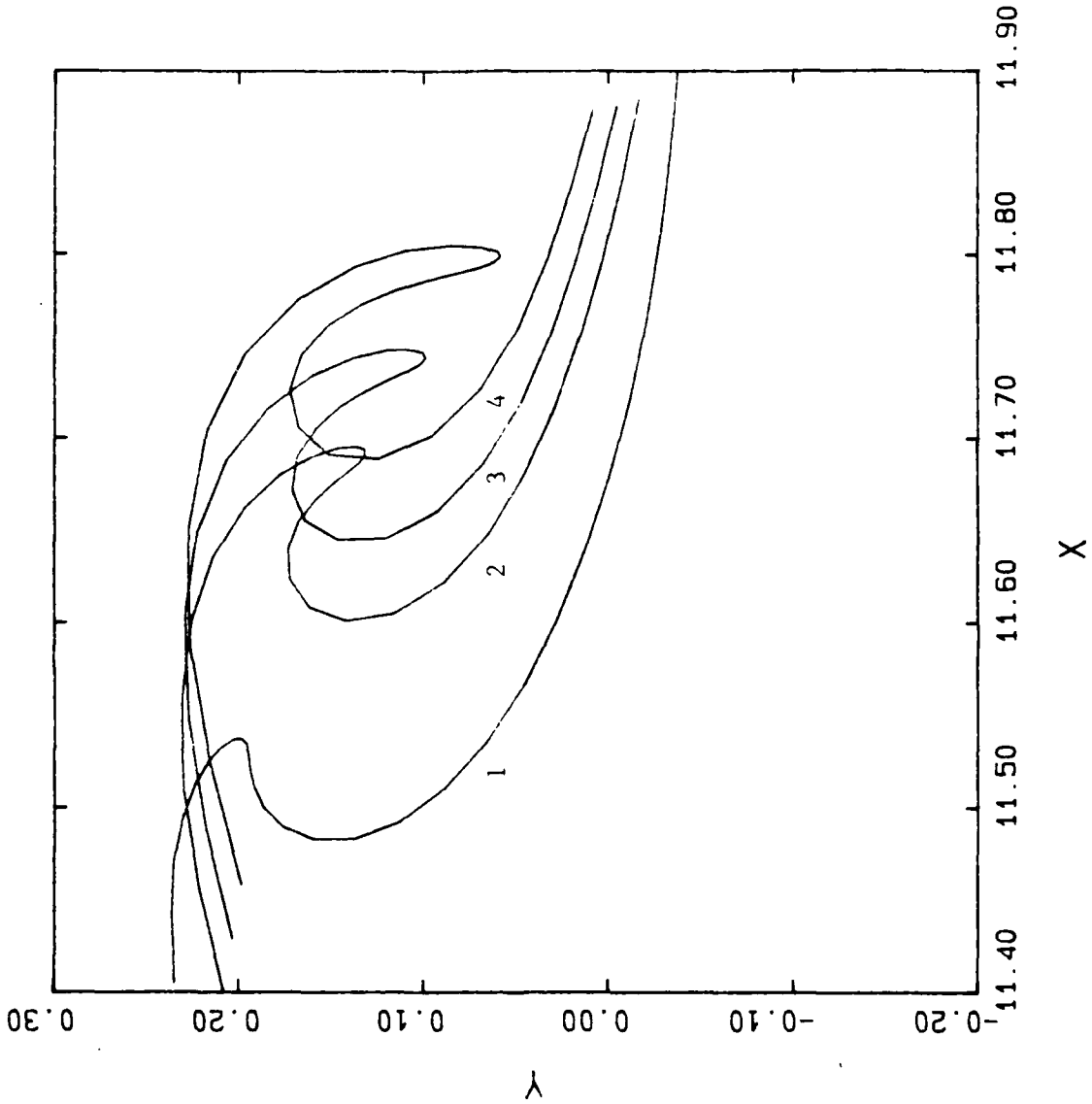

A3C	(1)	3217	50.8396
	(2)	3717	51.0919
	(3)	3917	51.1788
	(4)	4117	51.2639

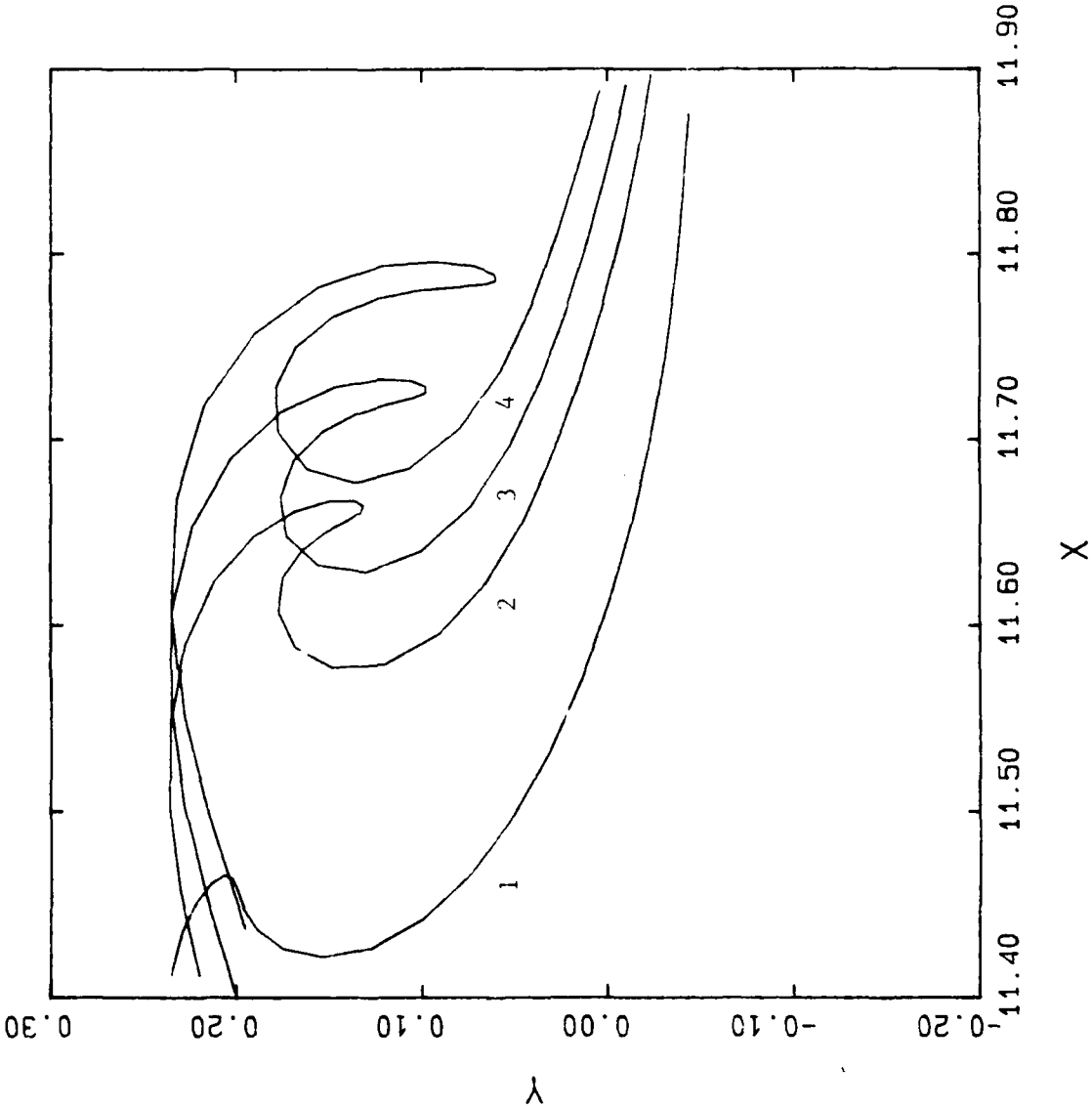

A3D	(1)	3450	50.9077
	(2)	3950	51.0987
	(3)	4150	51.1707
	(4)	4350	51.2399

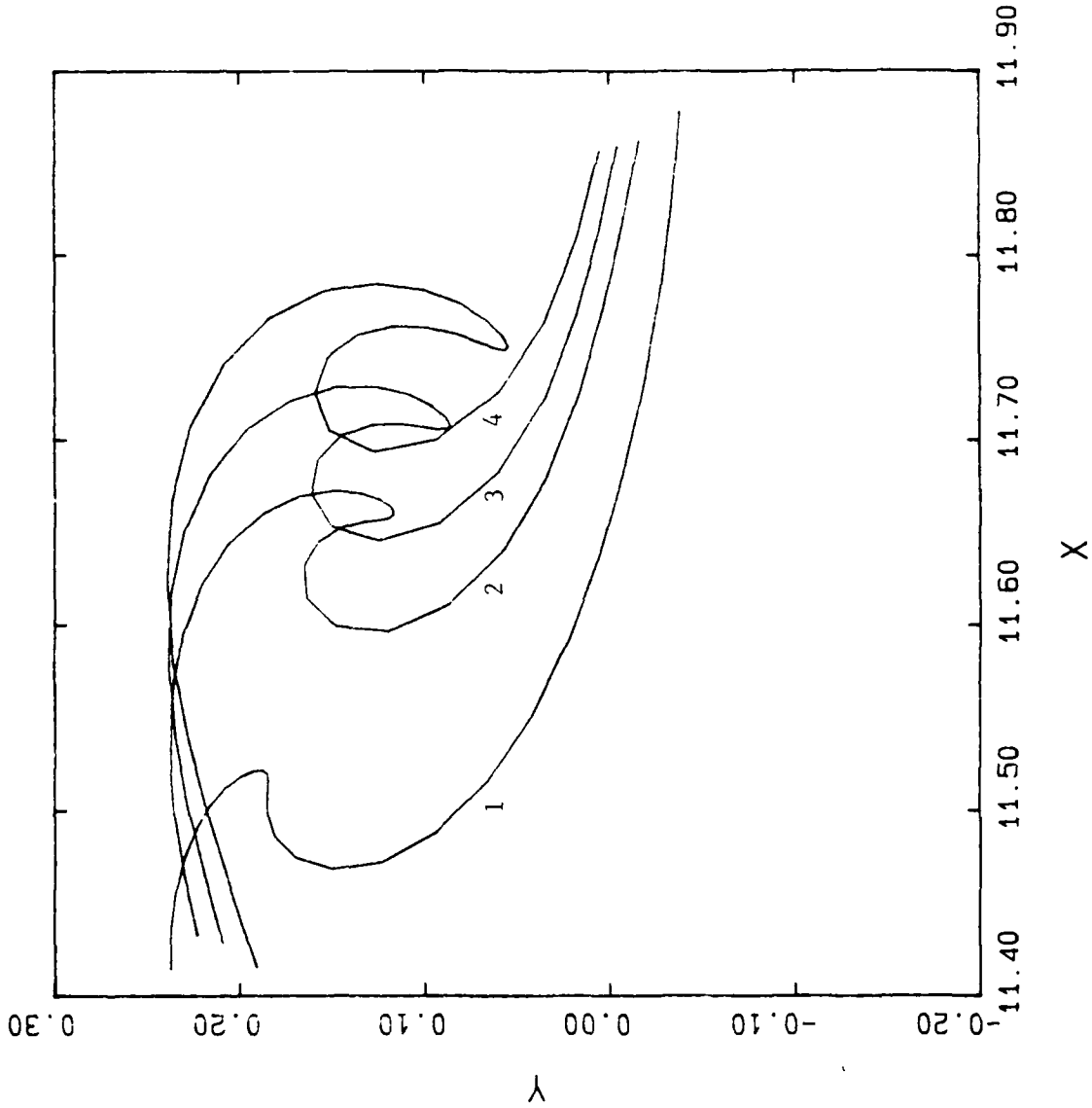

A3E 2645 44.9262

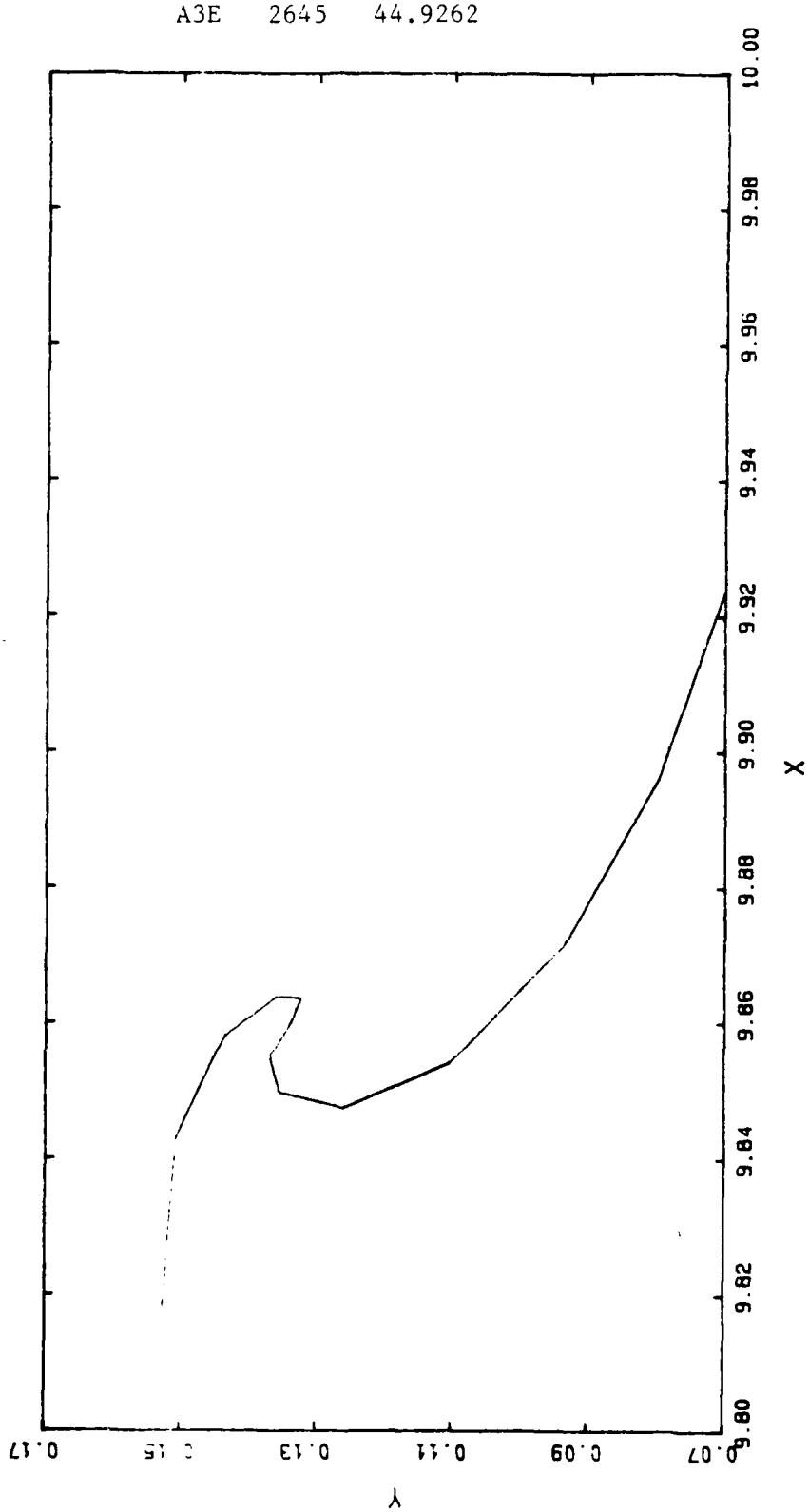

A3E 2695 44.9455

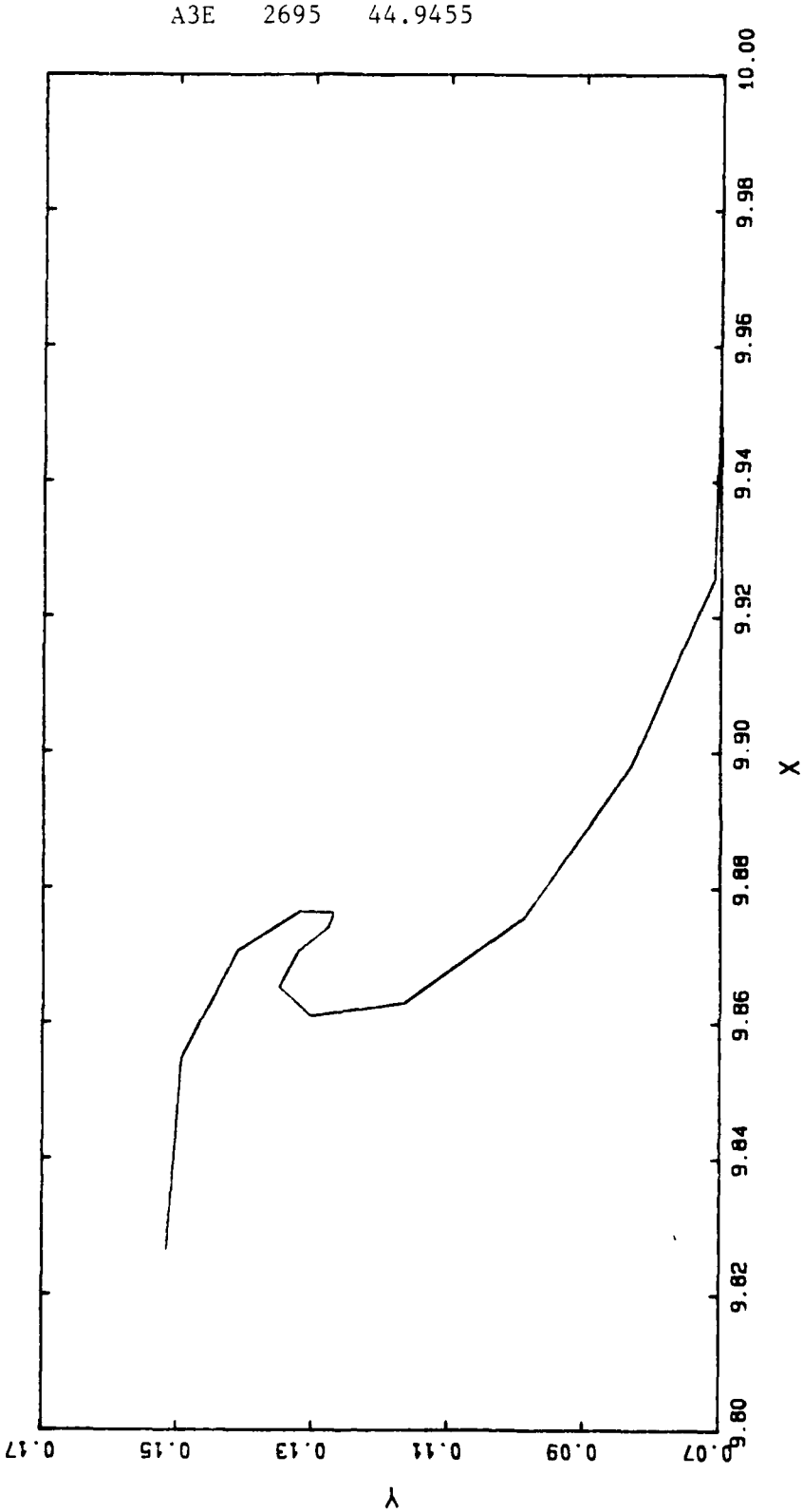

A3E 2745 44.9613

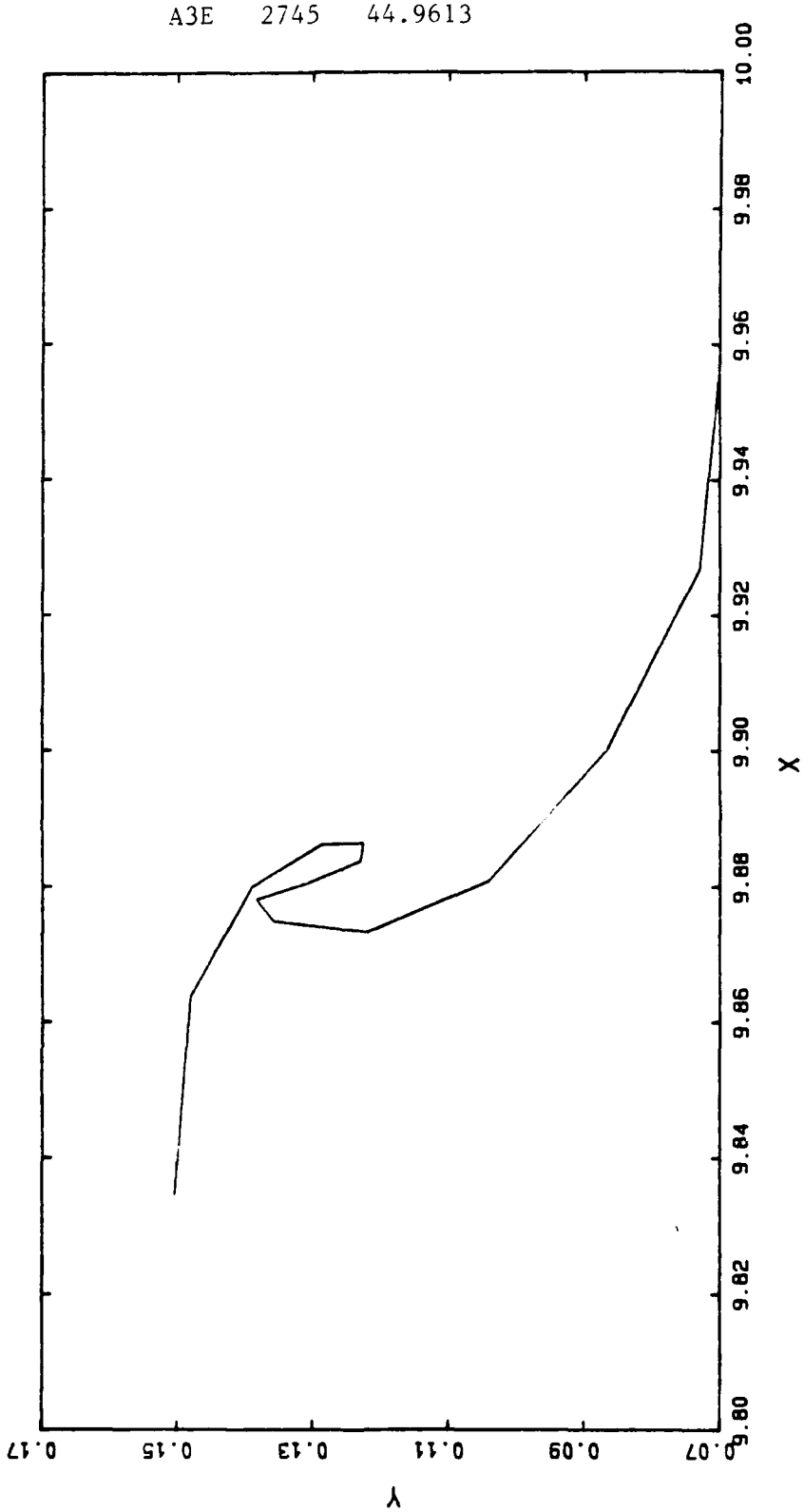

A3F 2665 45.5044

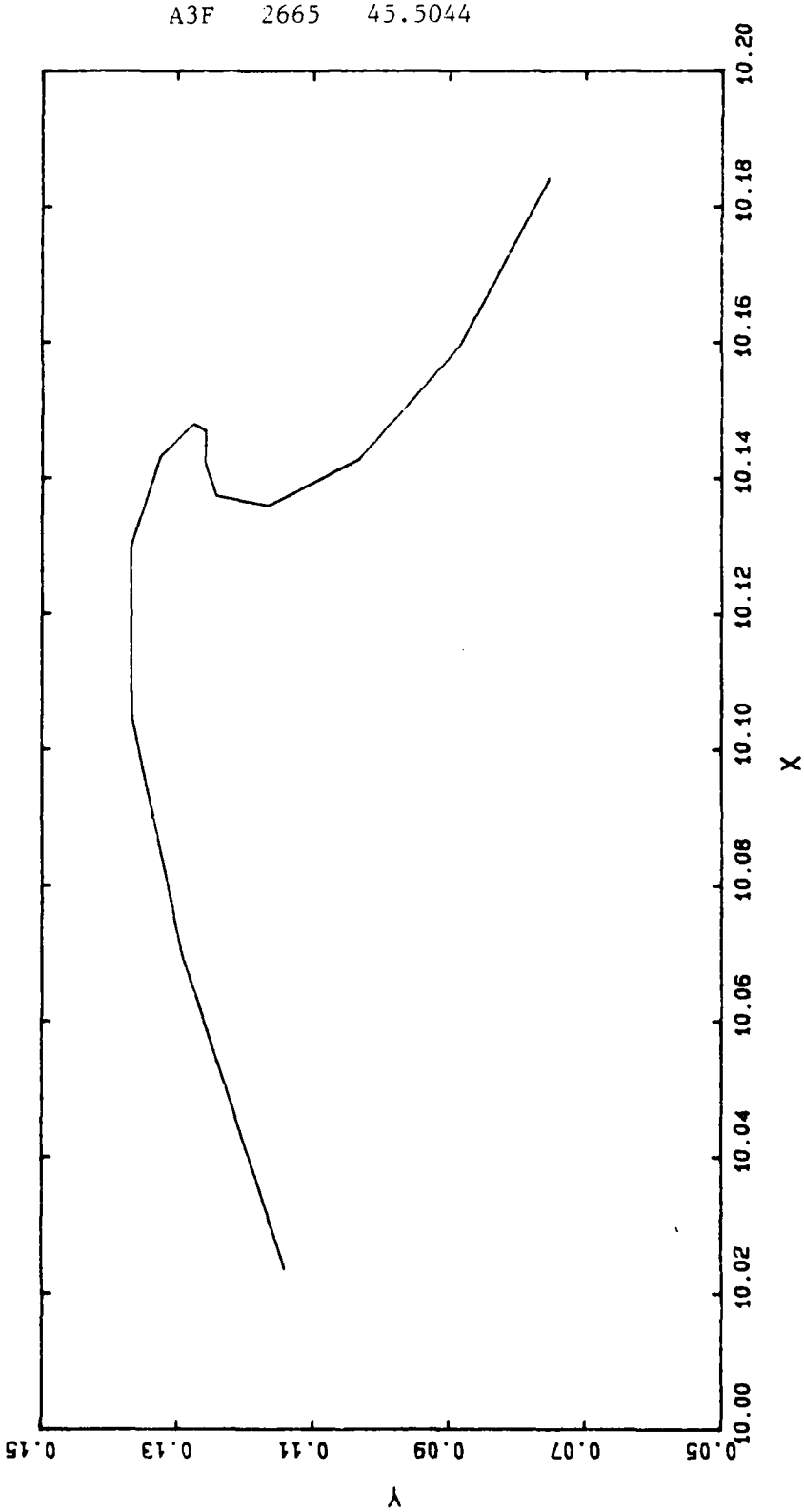

A3F 2715 45.5172

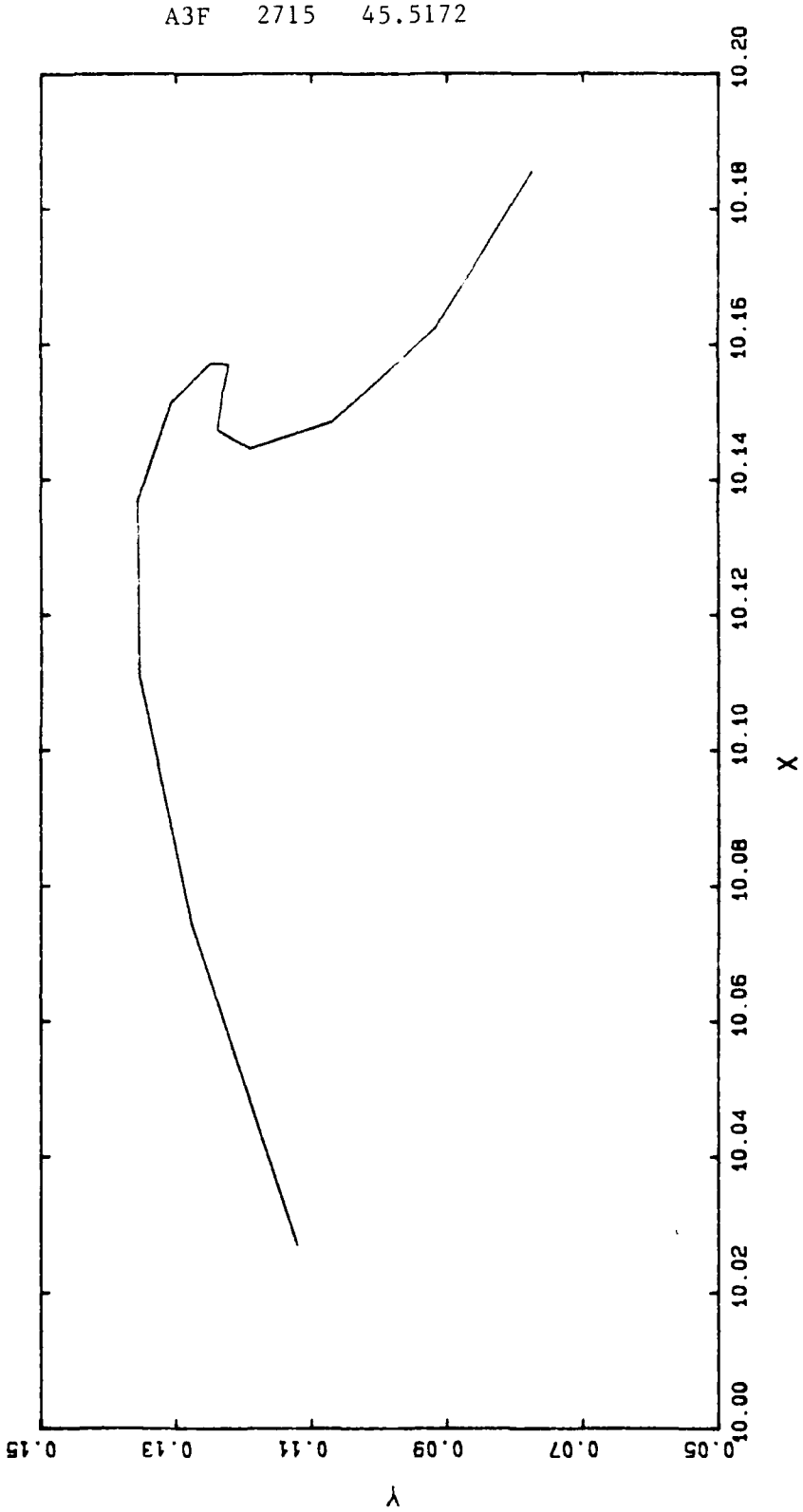

A3F 2745 45.5276

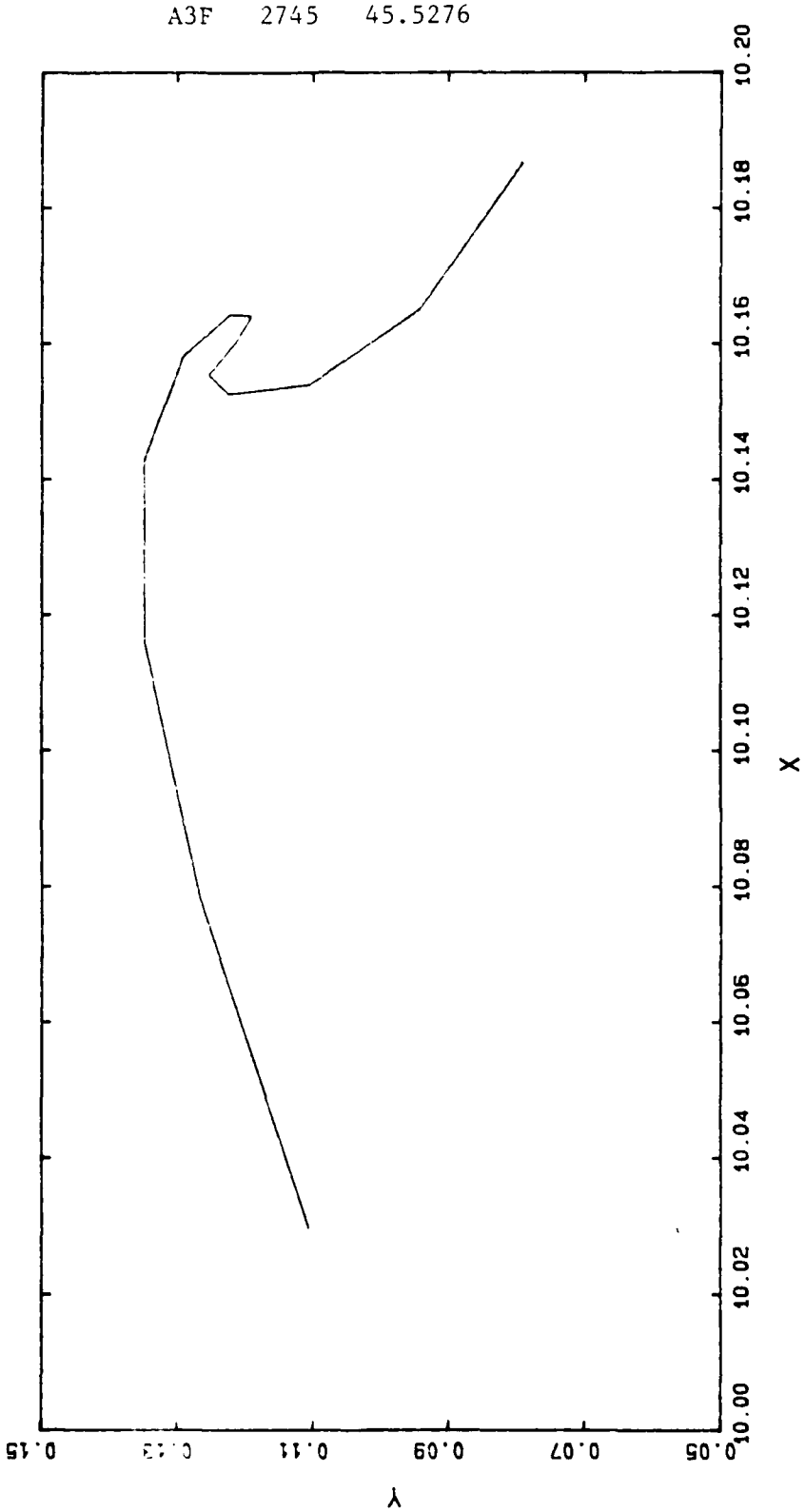

A3F 2755 45.5307

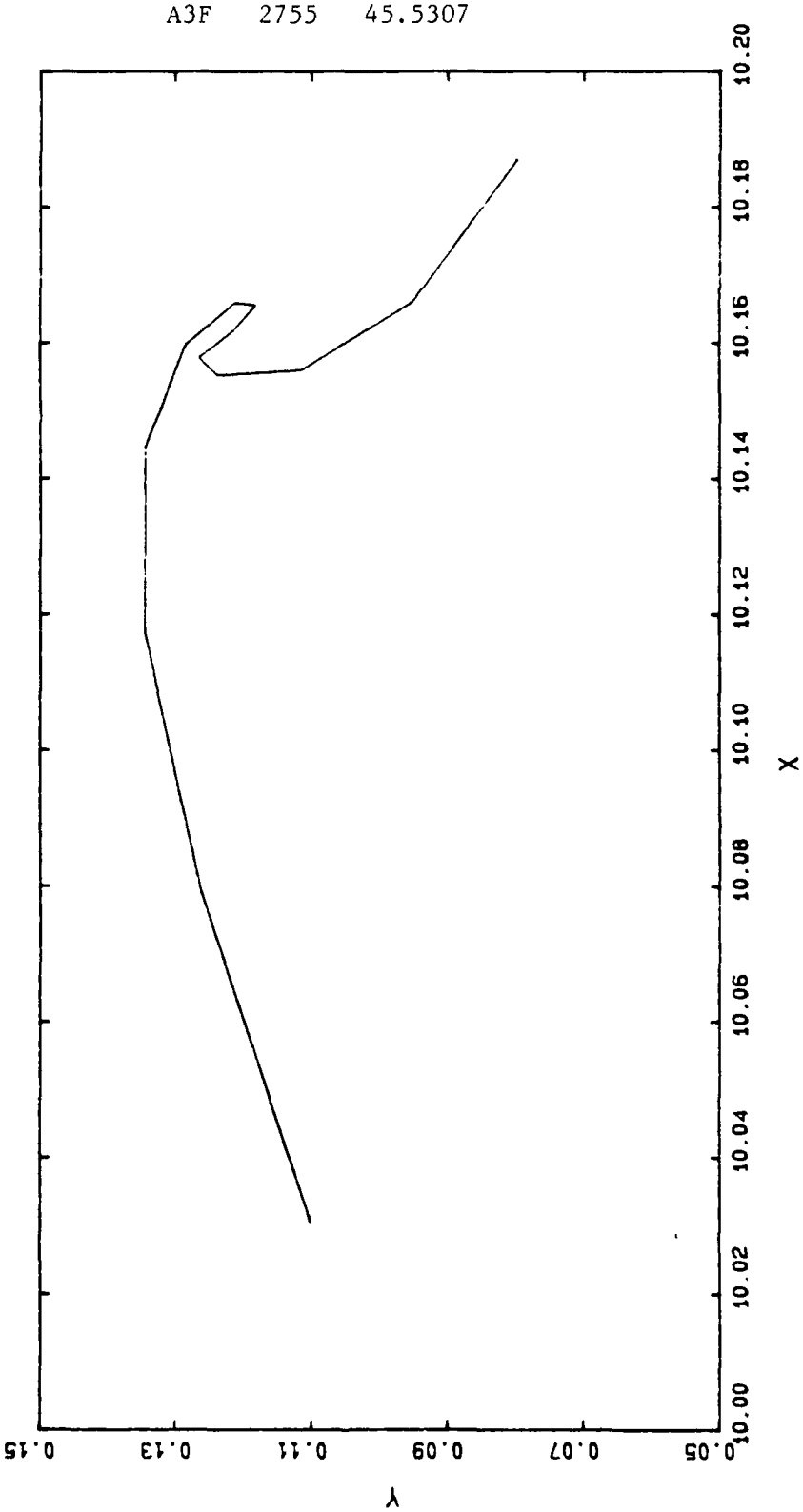

A3F 2765 45.5326

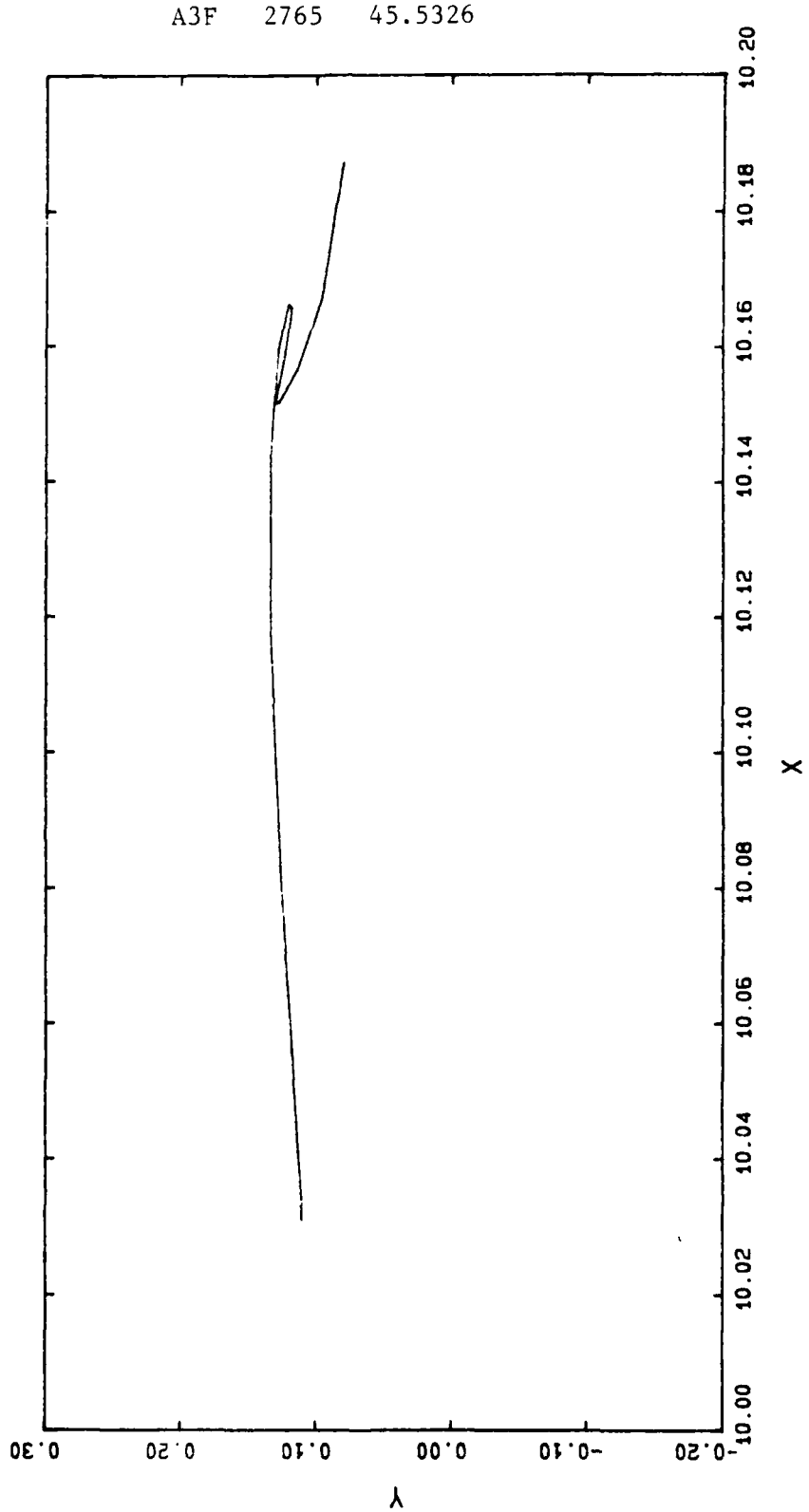

A3G 2836 46.0064

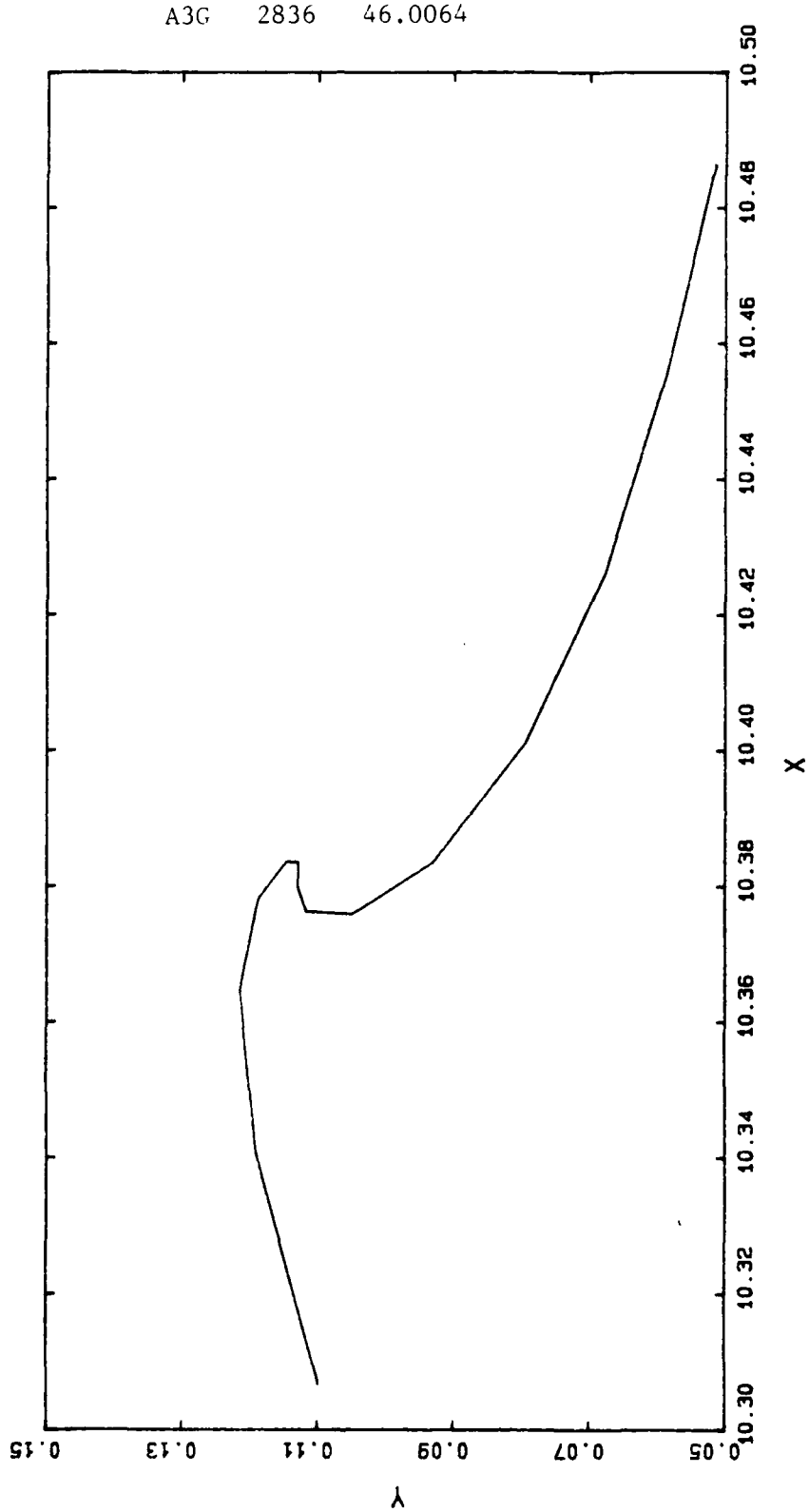

A3G 2886 46.0171

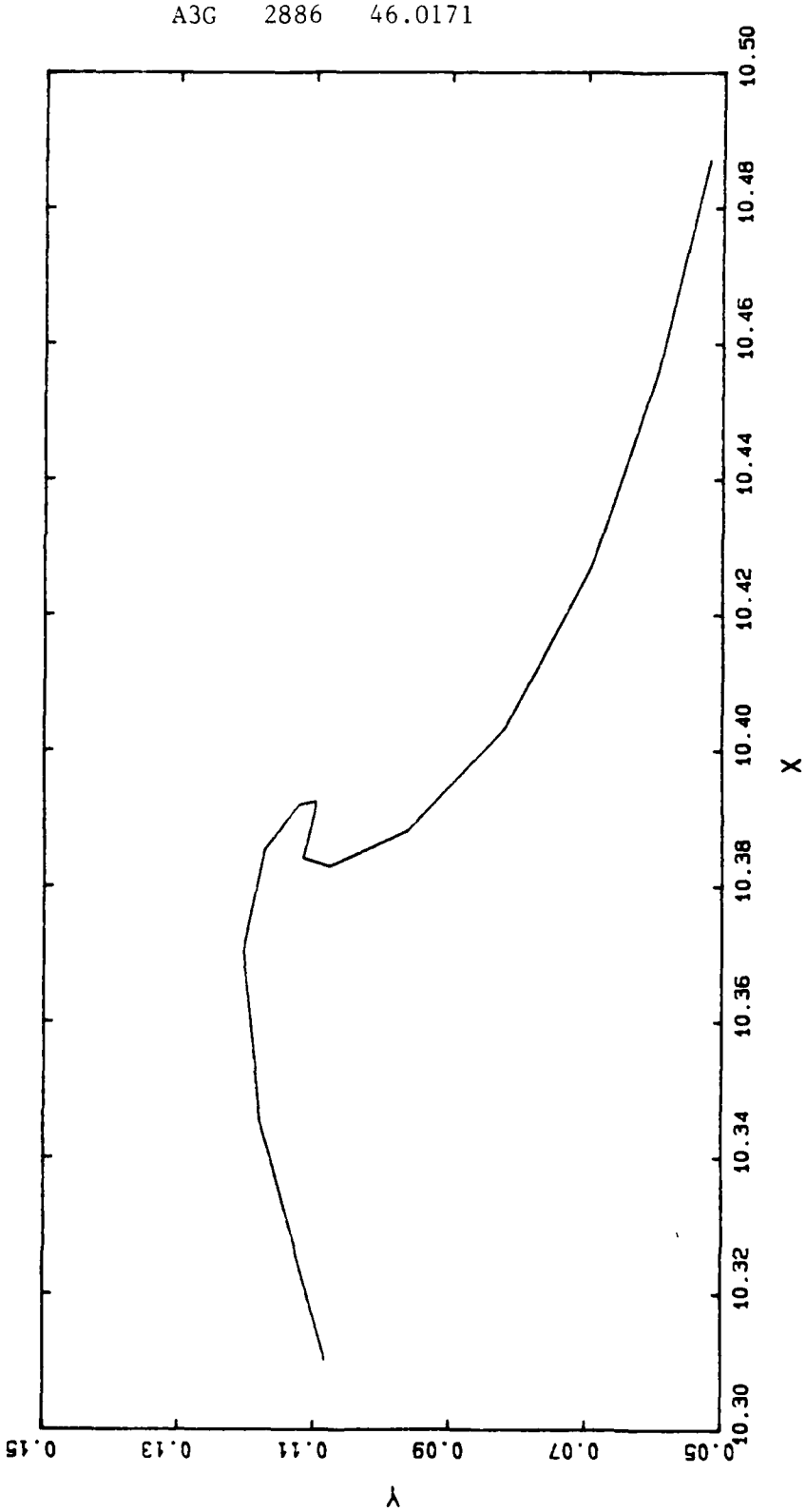

A3G 2906 46.0229

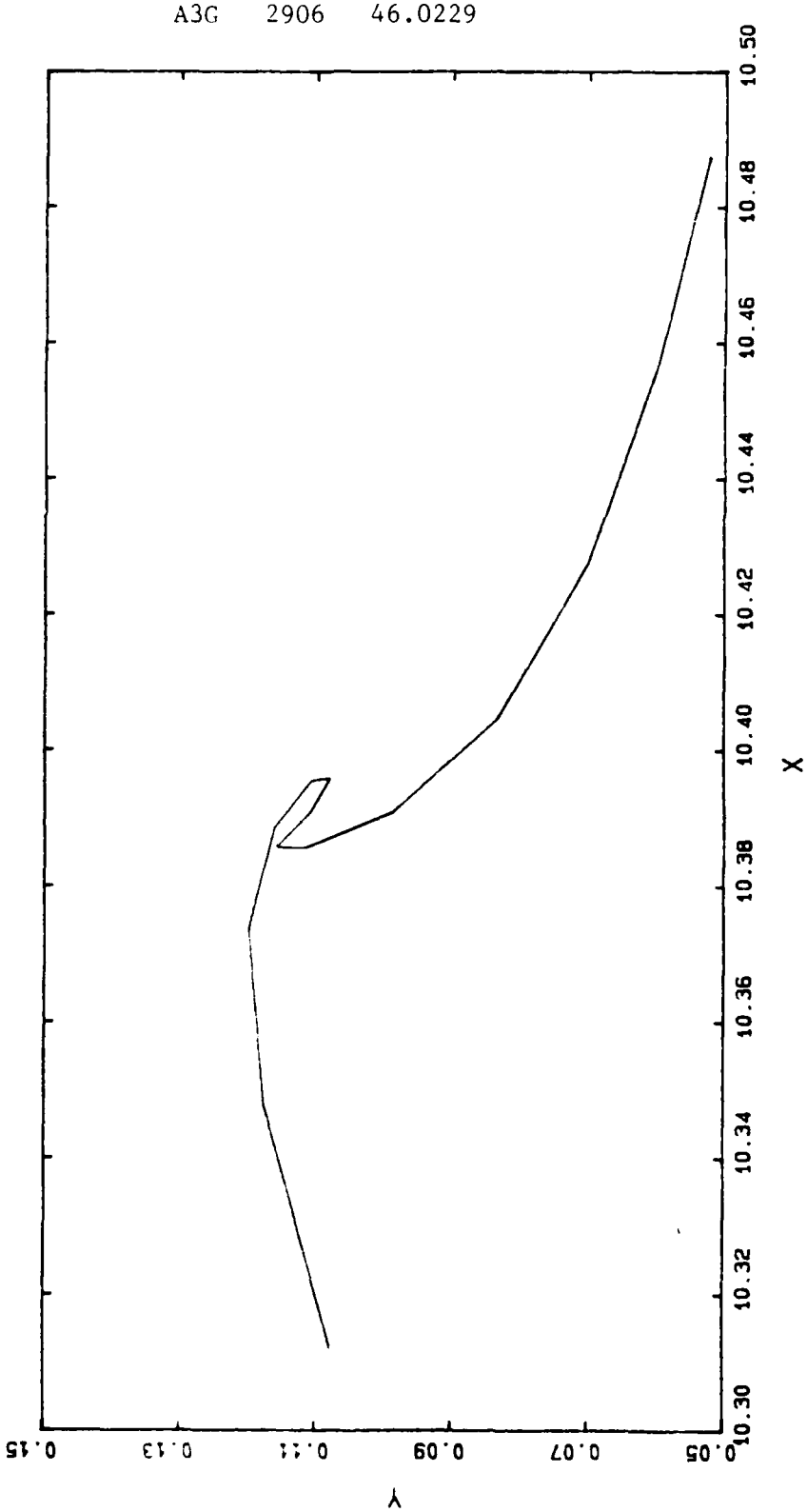

A3G 2916 46.0233

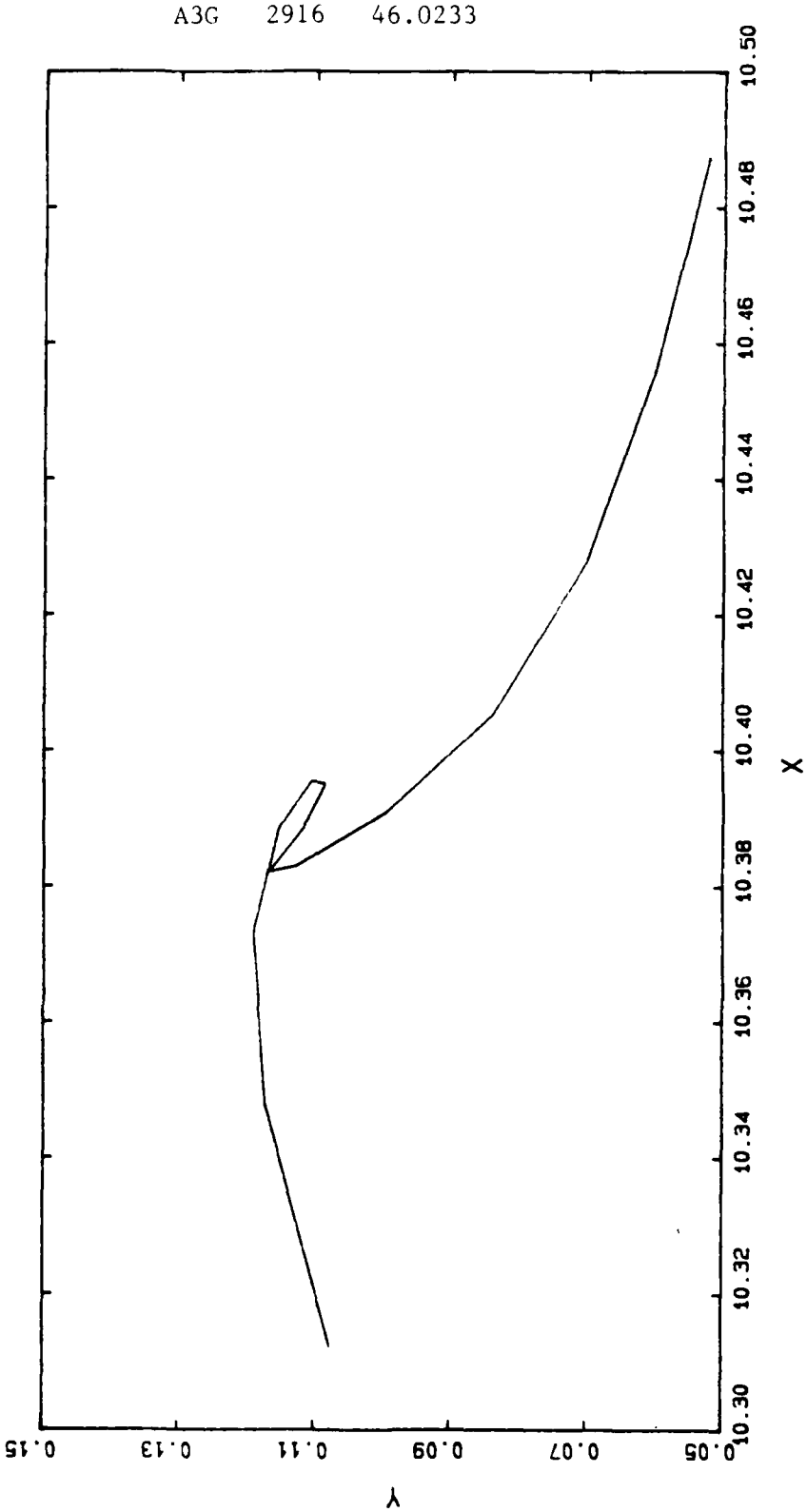

A3G 2936 46.0235

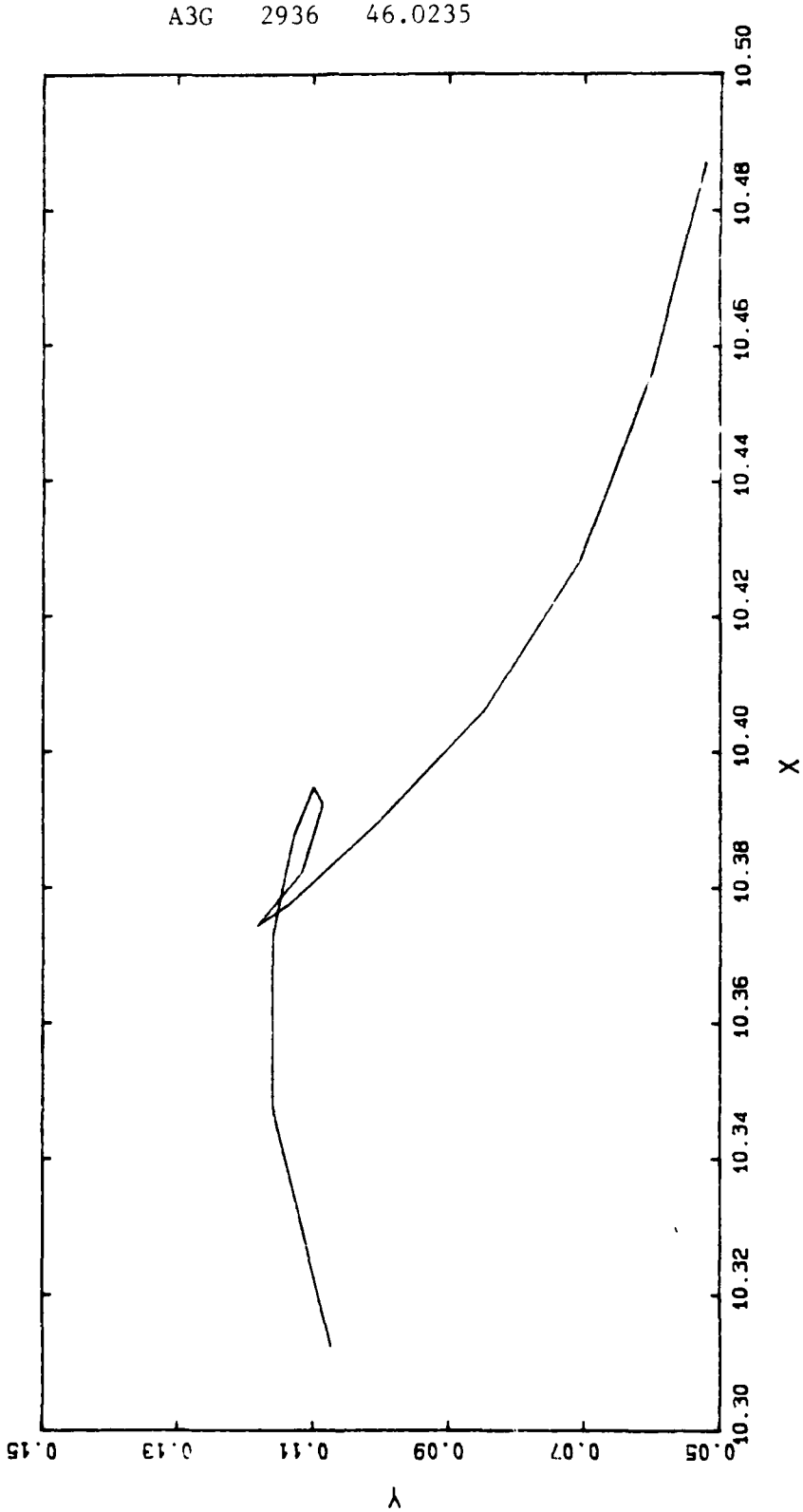

Appendix B

Refer to Chapter 5 for discussion.

B1 2636 47.0380

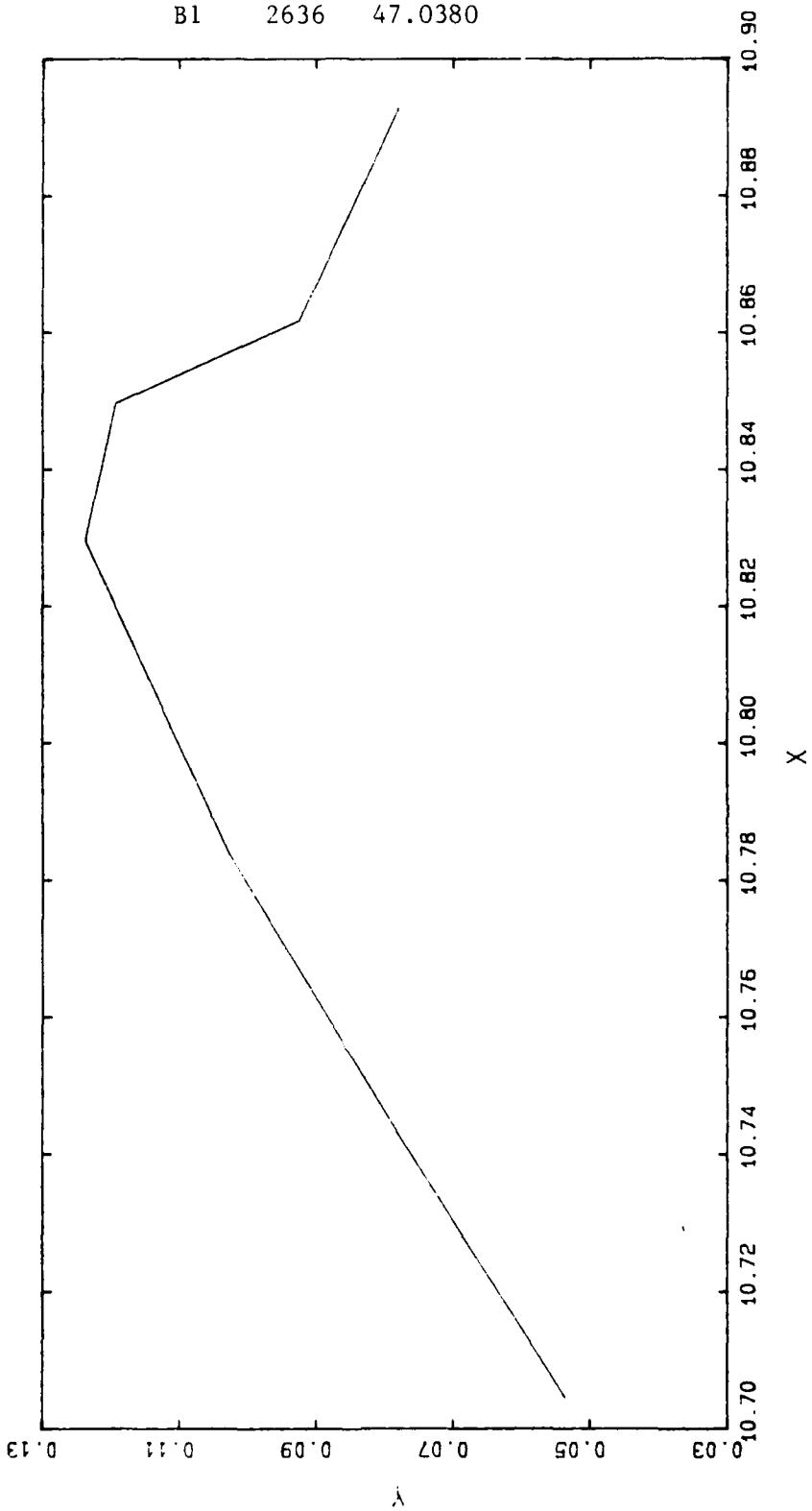

B1 2656 47.2071

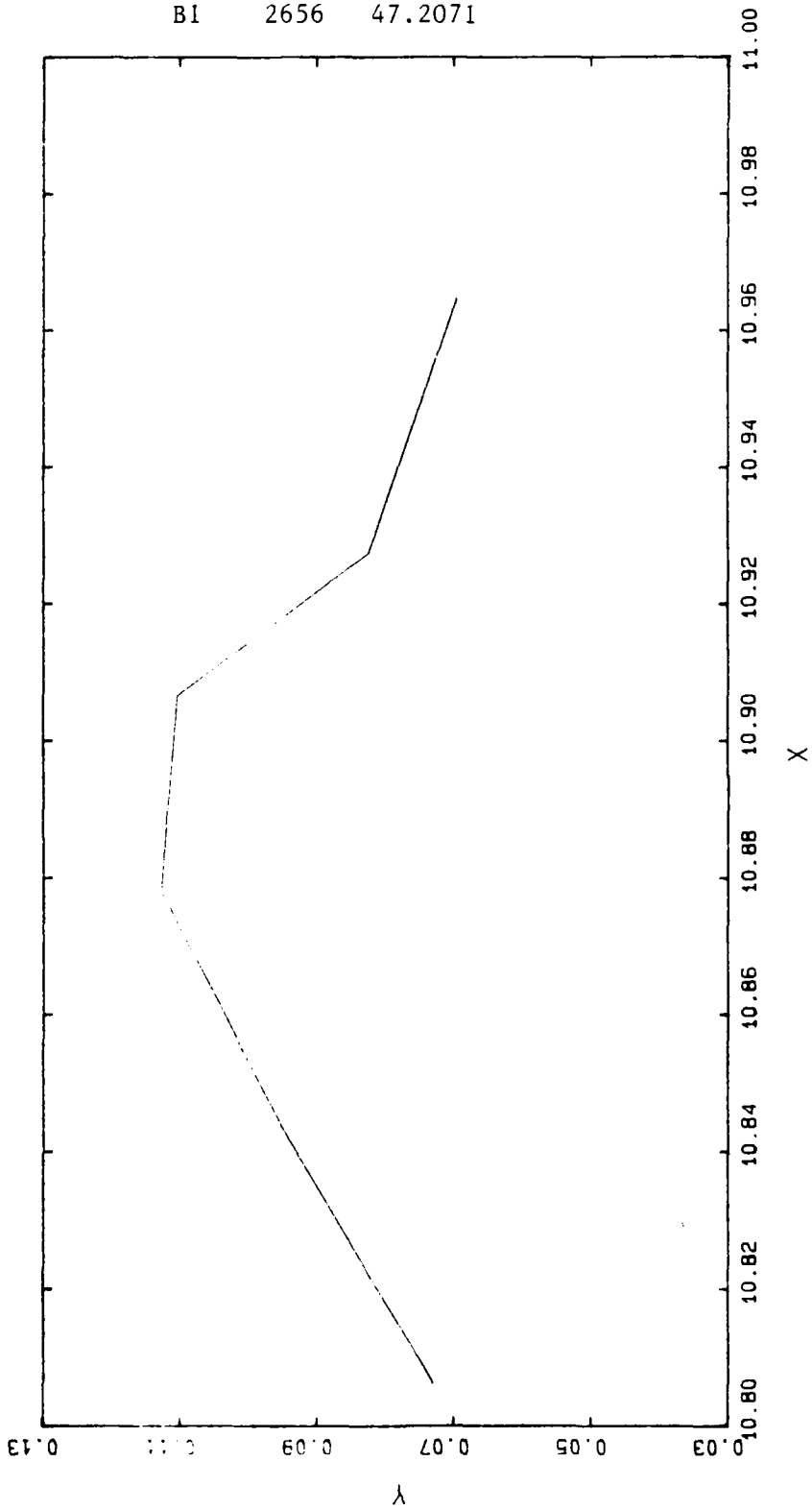

B1 2676 47.3926

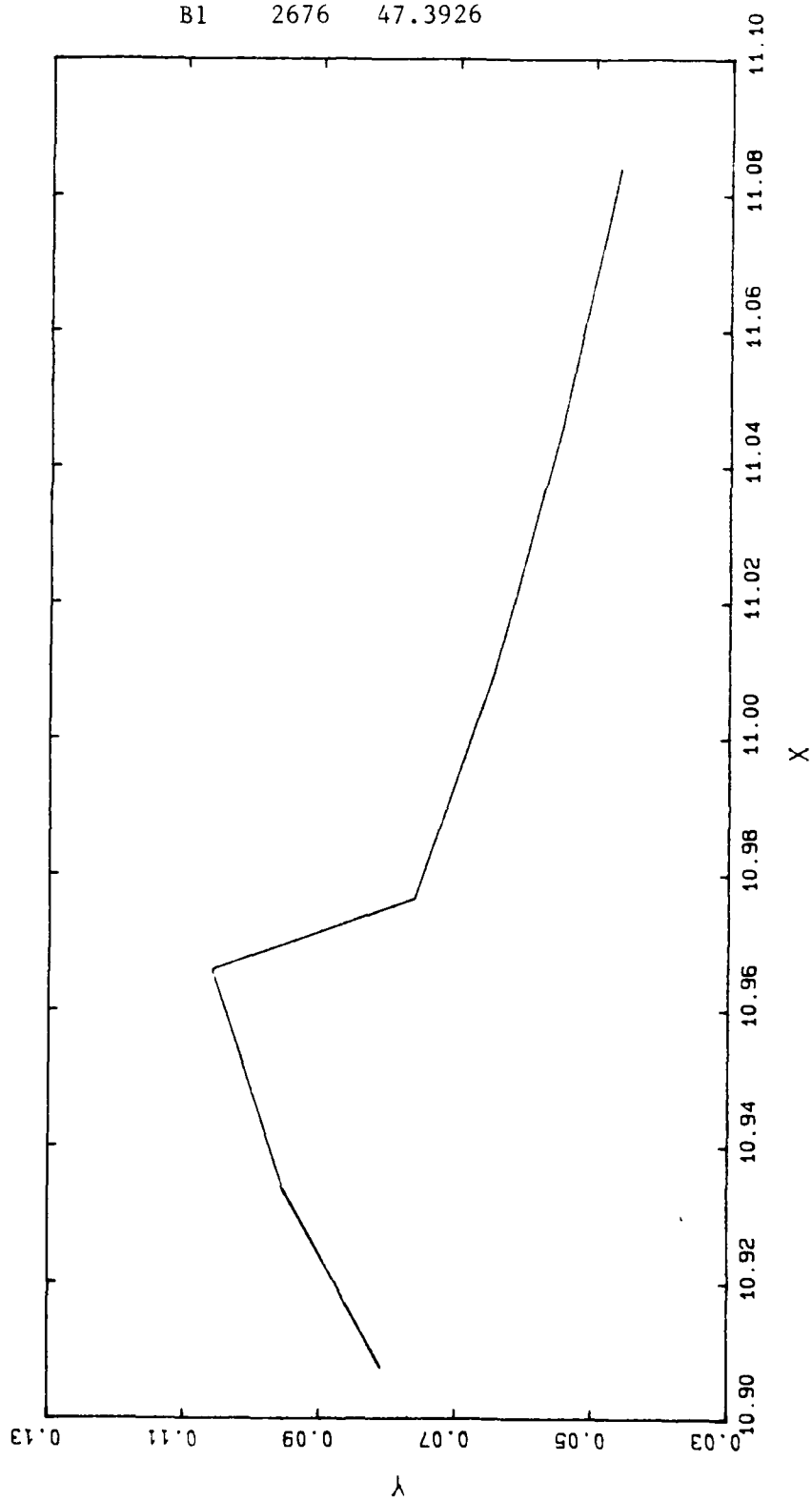

B1 2696 47.5906

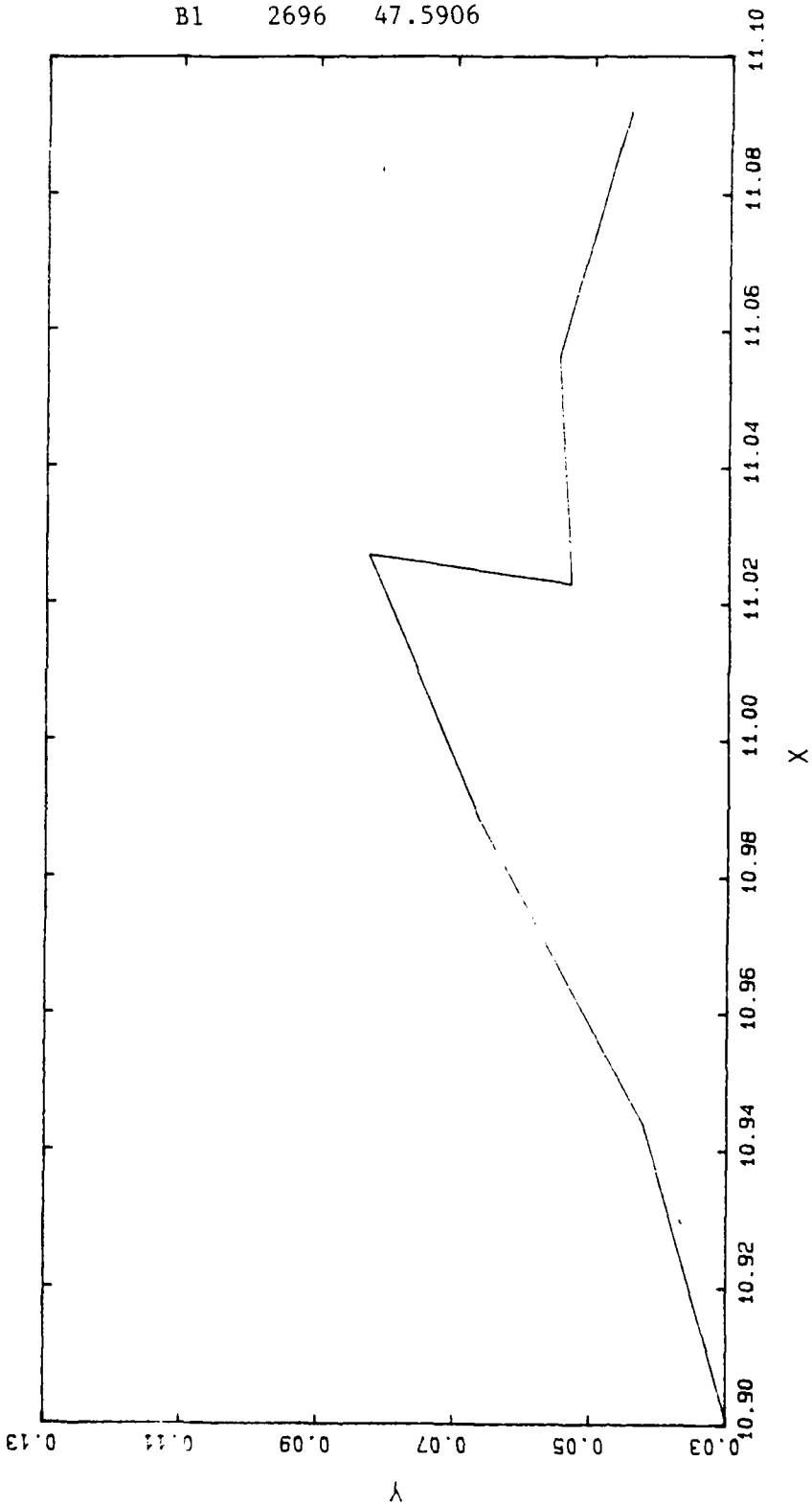

B1 2716 47.6819

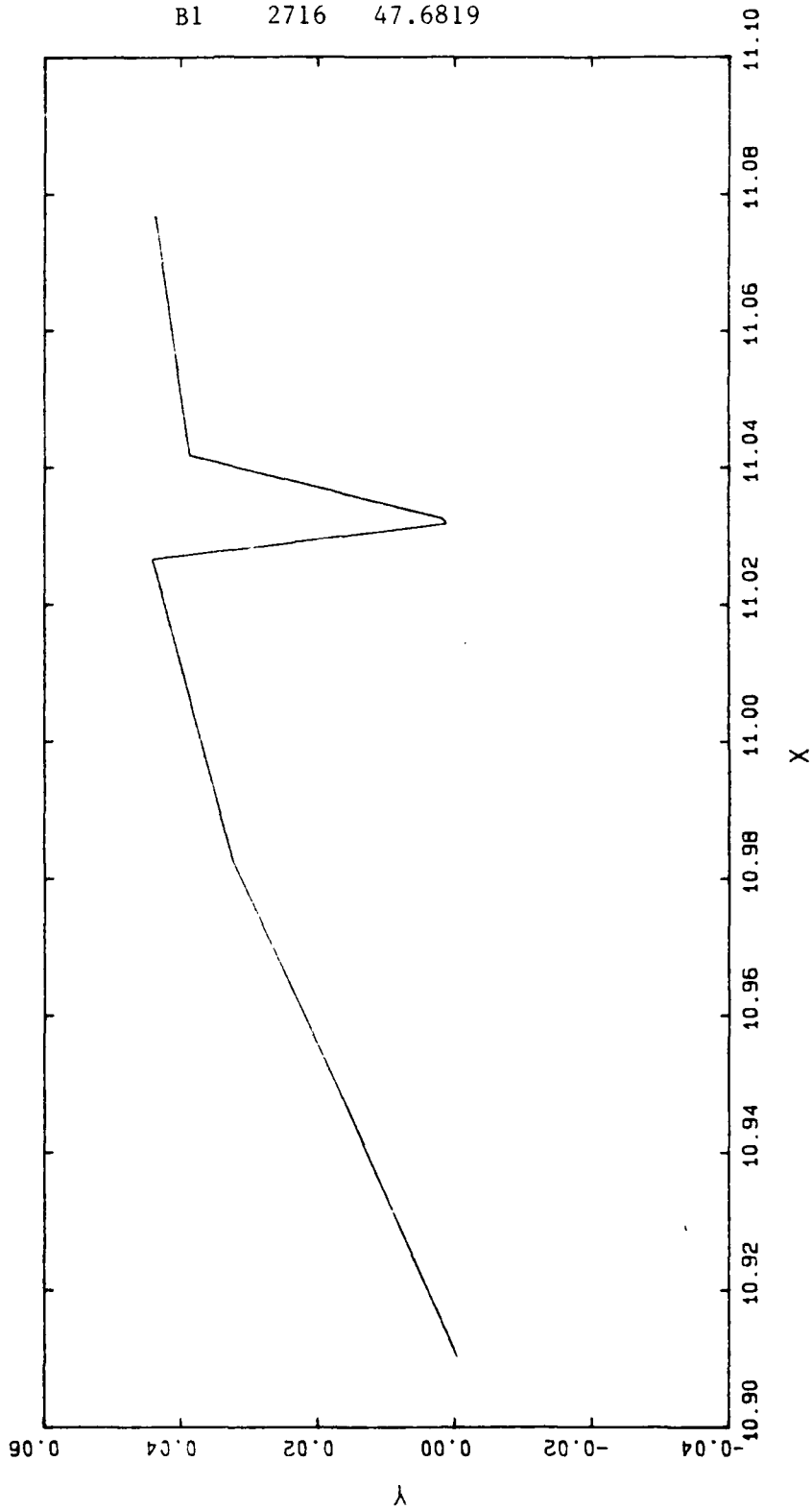

B1 2736 47.6851

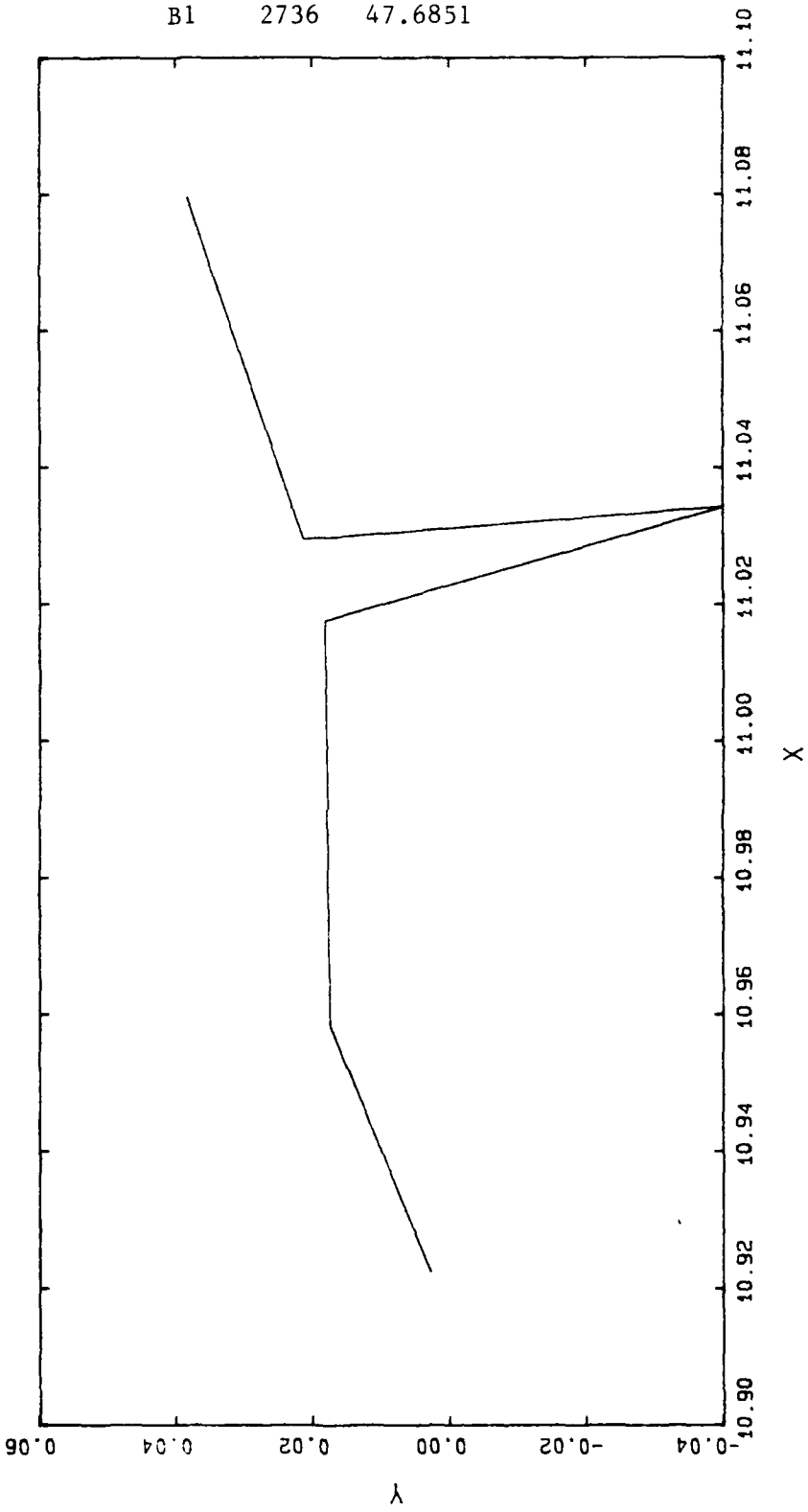

B2 4500 43.7279

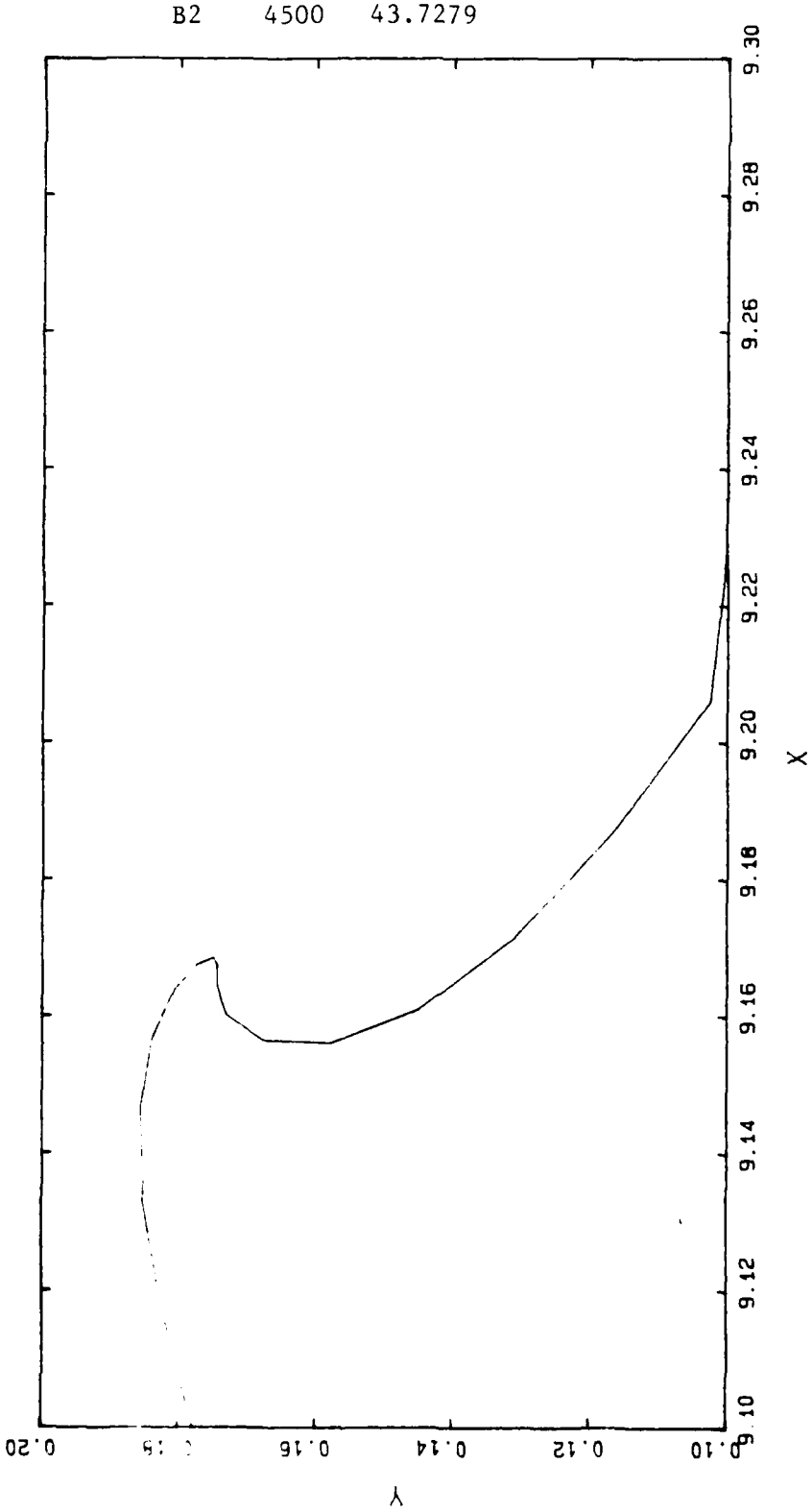

B2 5000 43.8223

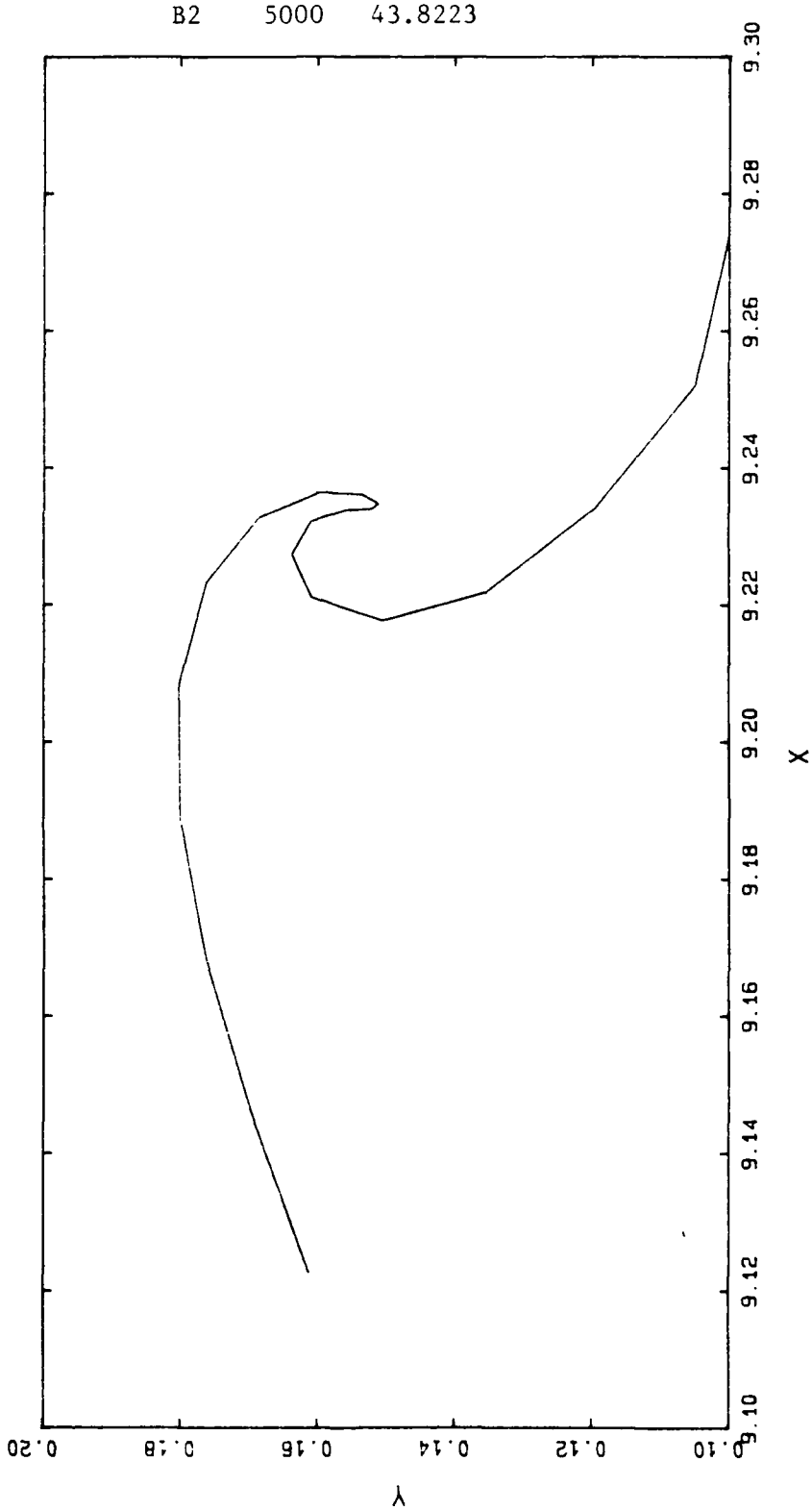

B2 5500 43.9090

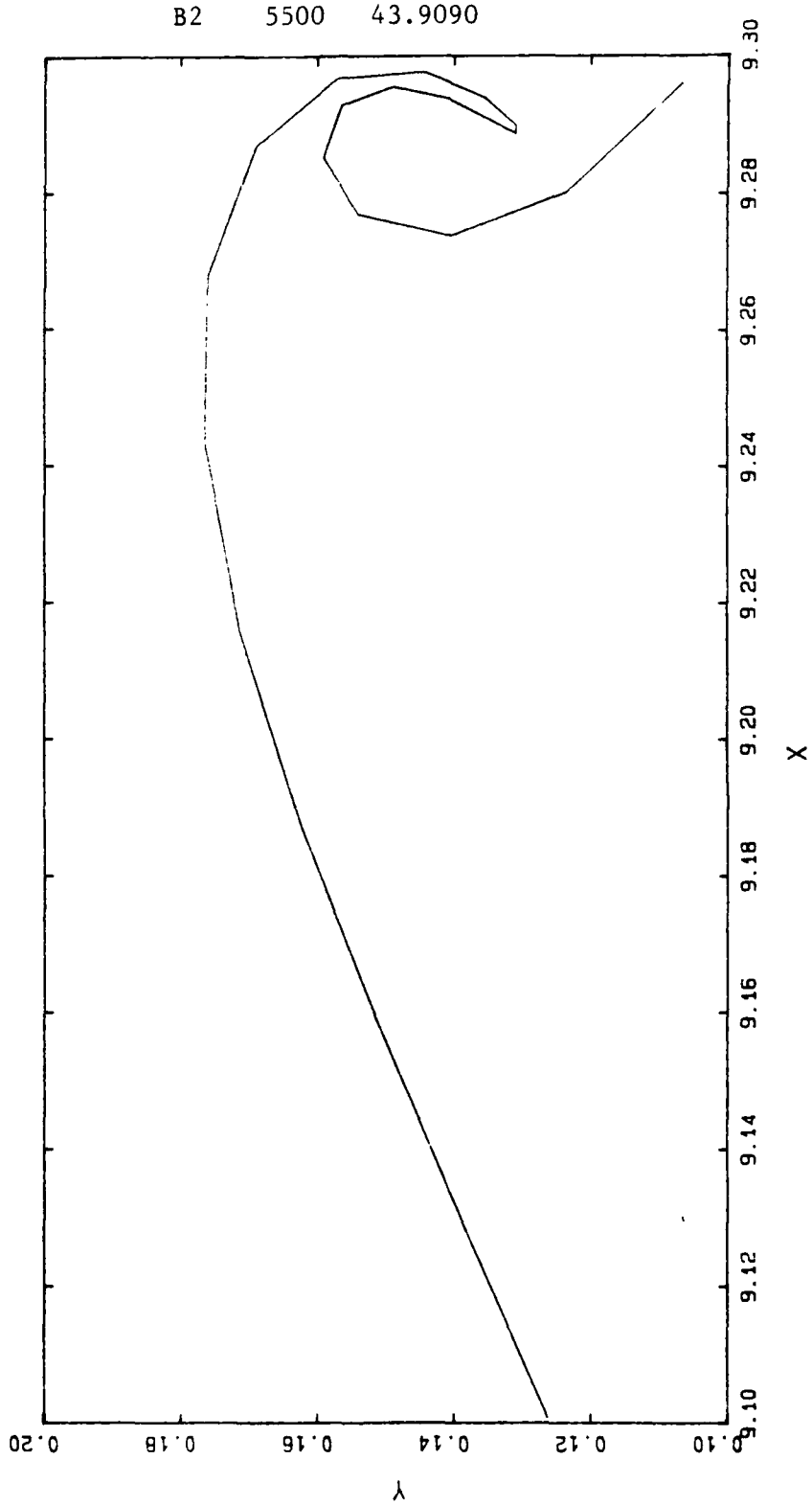

B2 5669 43.9464

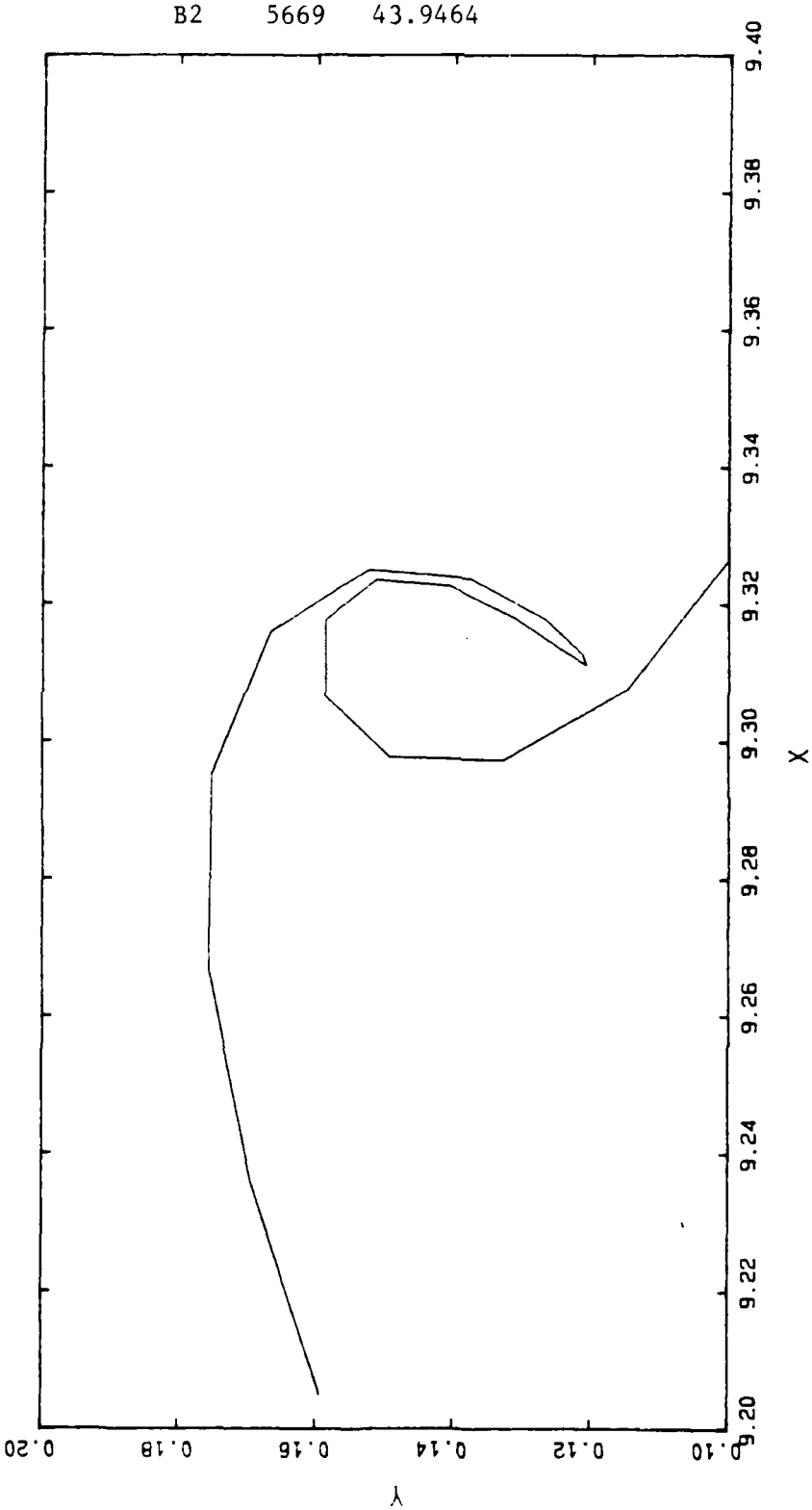

B2 5769 43.9734

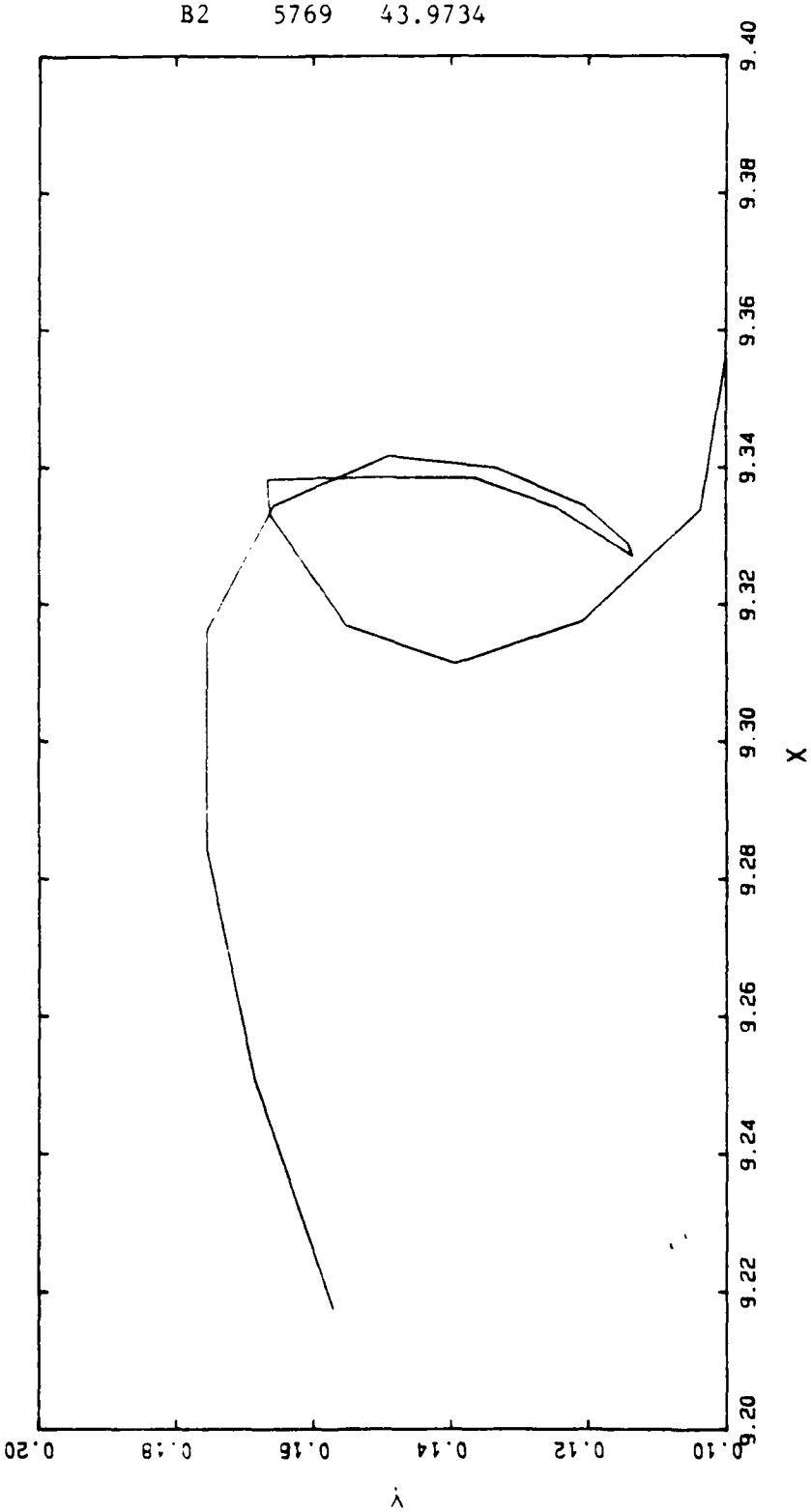

B3 3000 43.2982

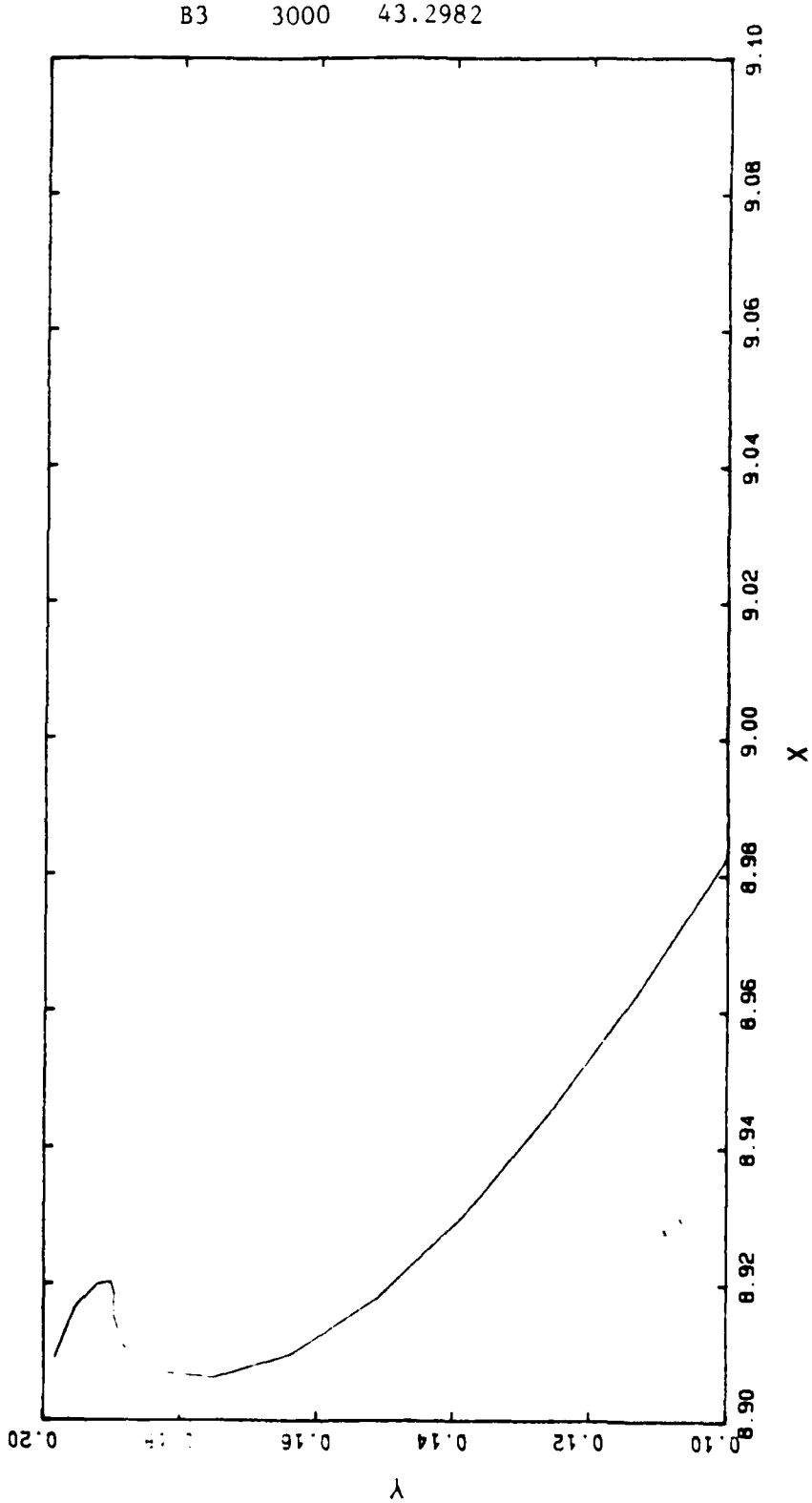

B3 3200 43.3320

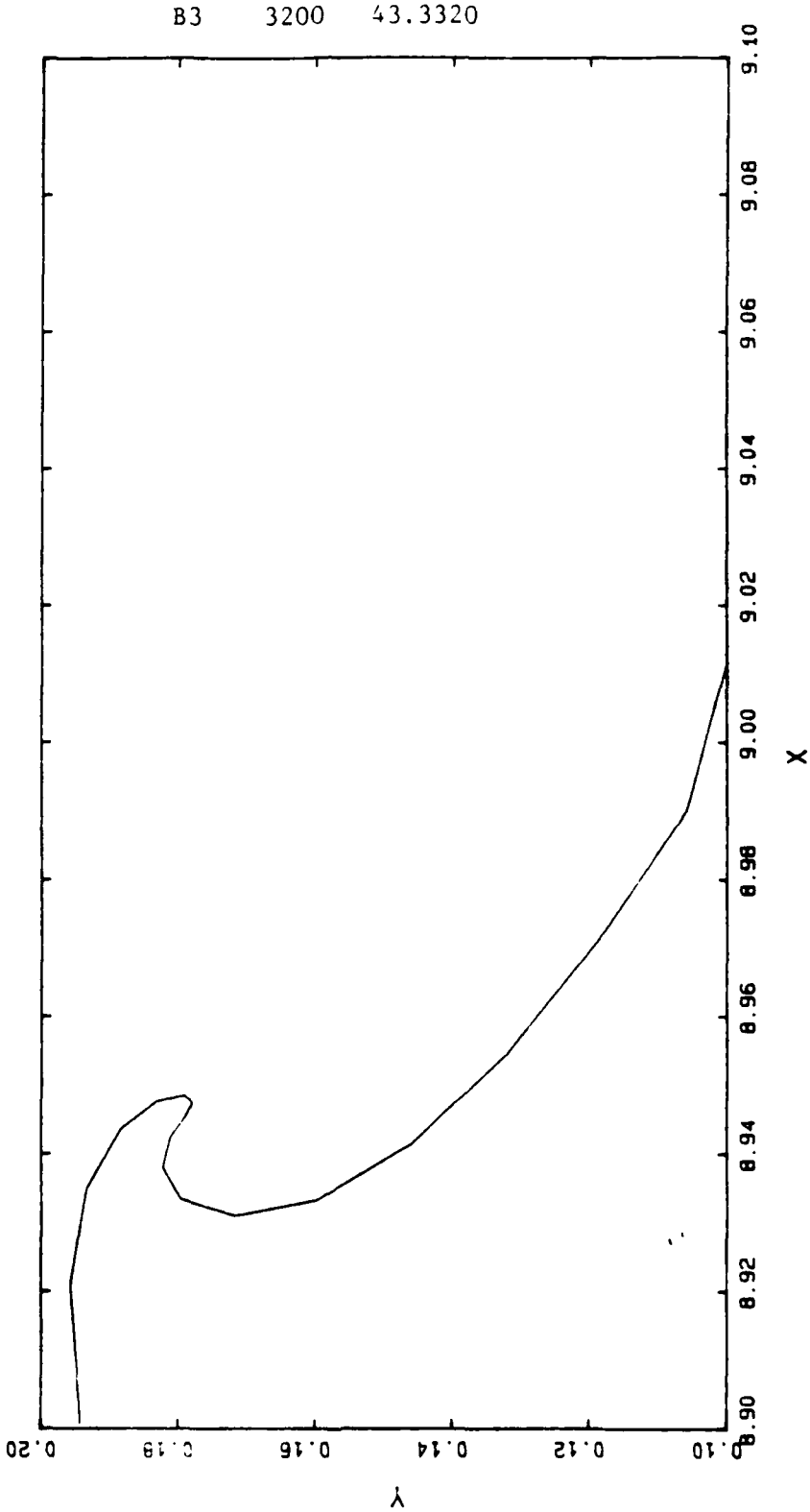

B3 3400 43.3722

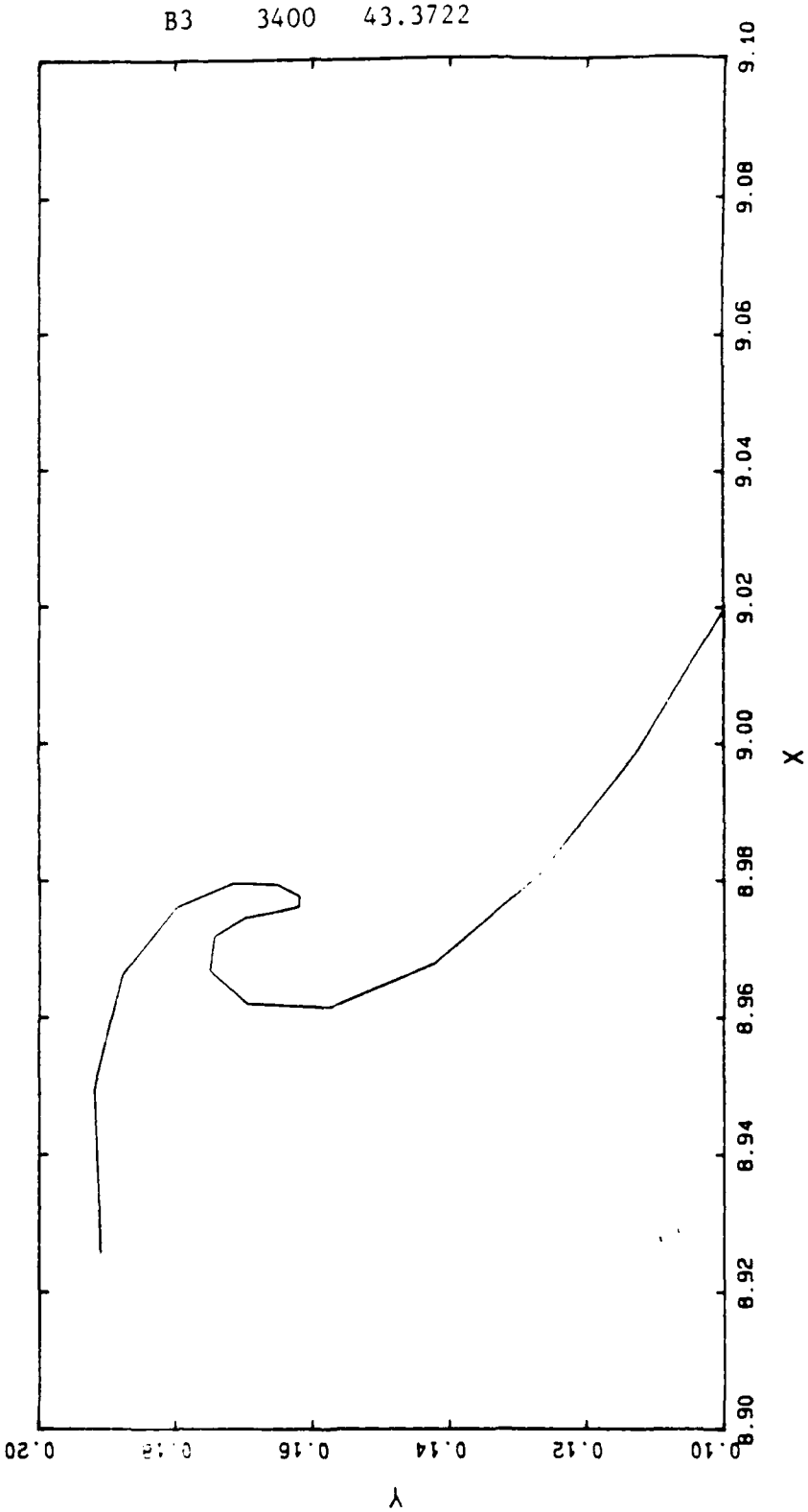

B3 3600 43.4236

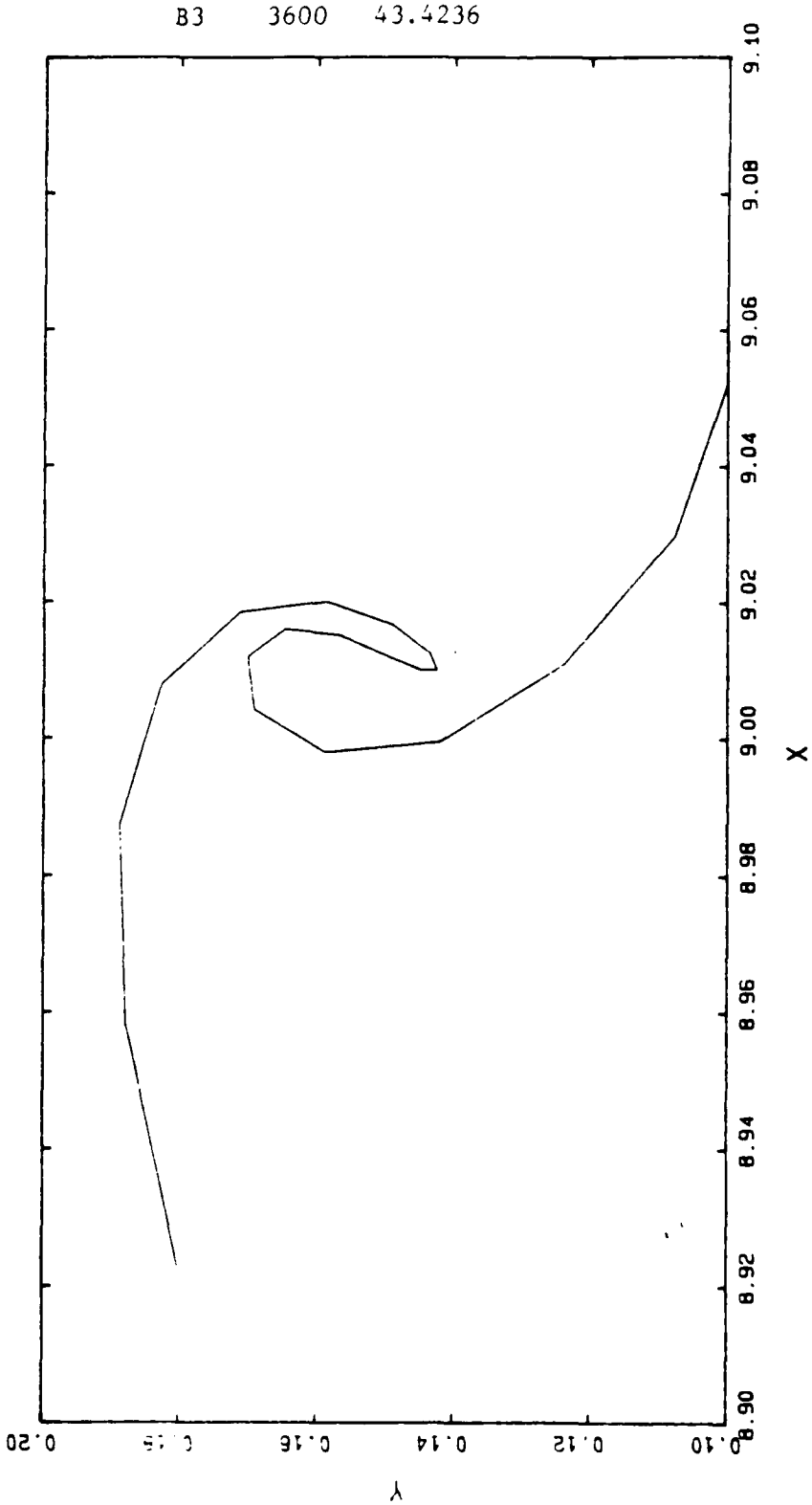

B3 3775 43.4774

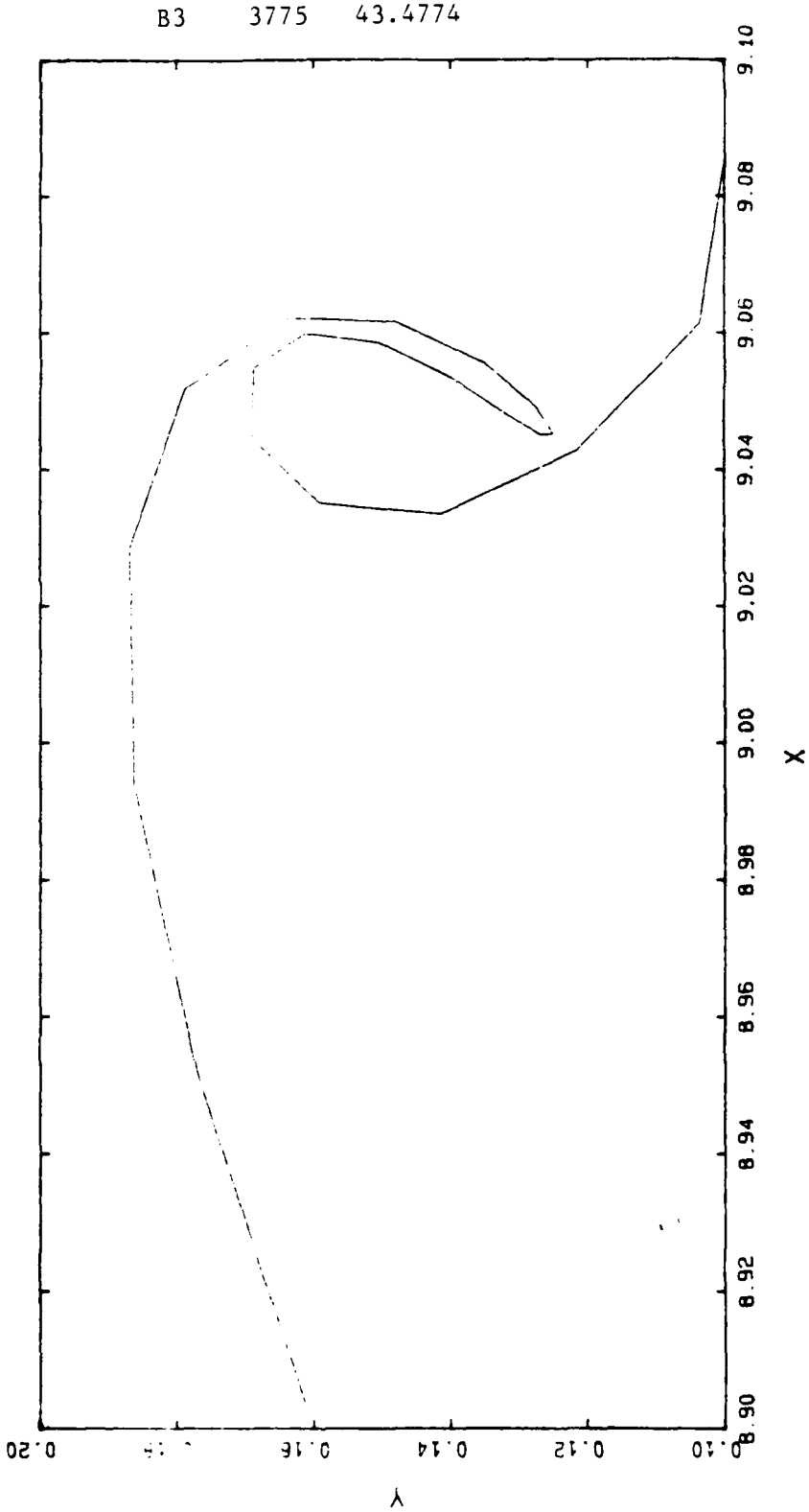

B3 3865 43.5016

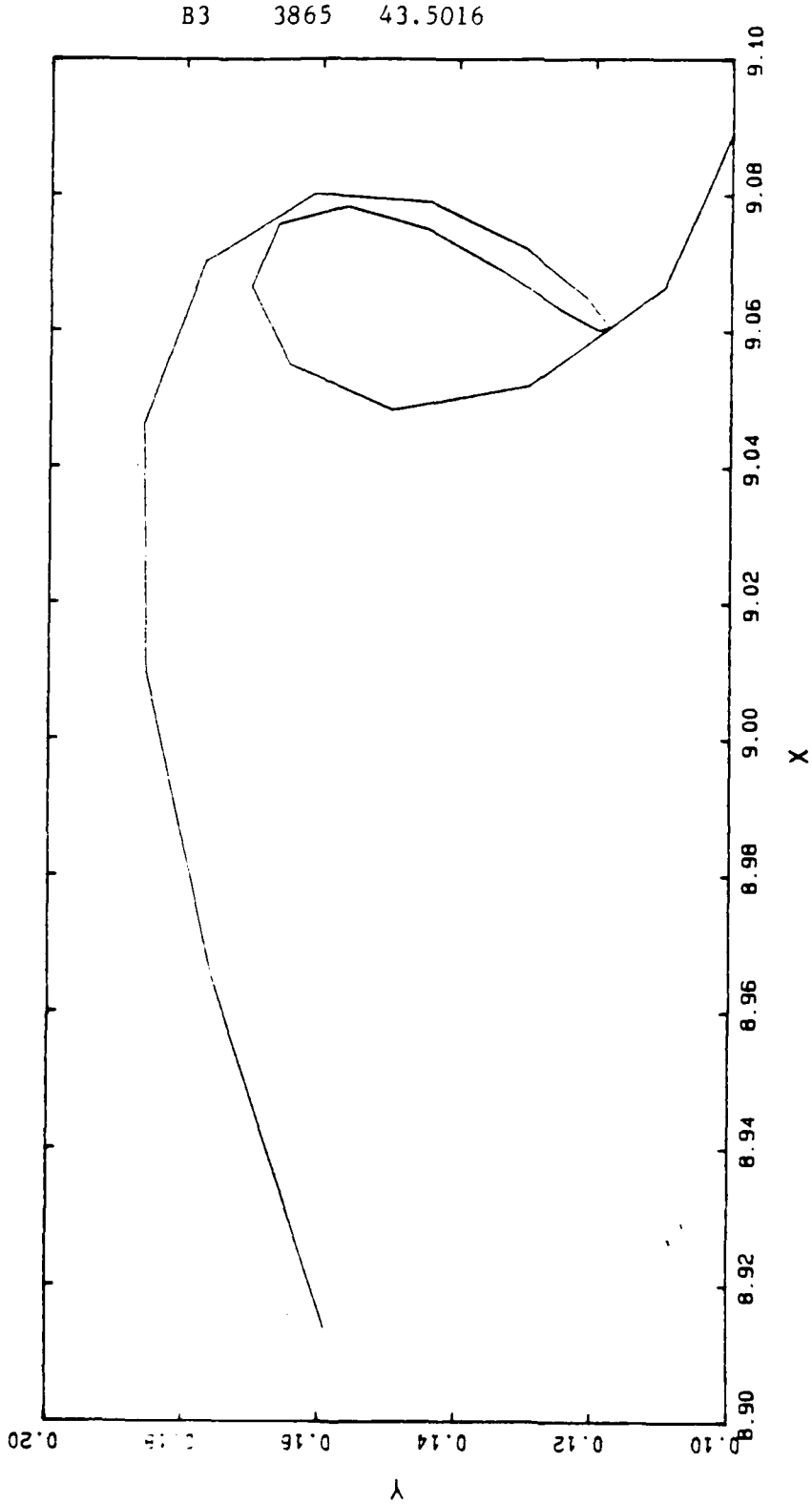

B4 1000 27.0441

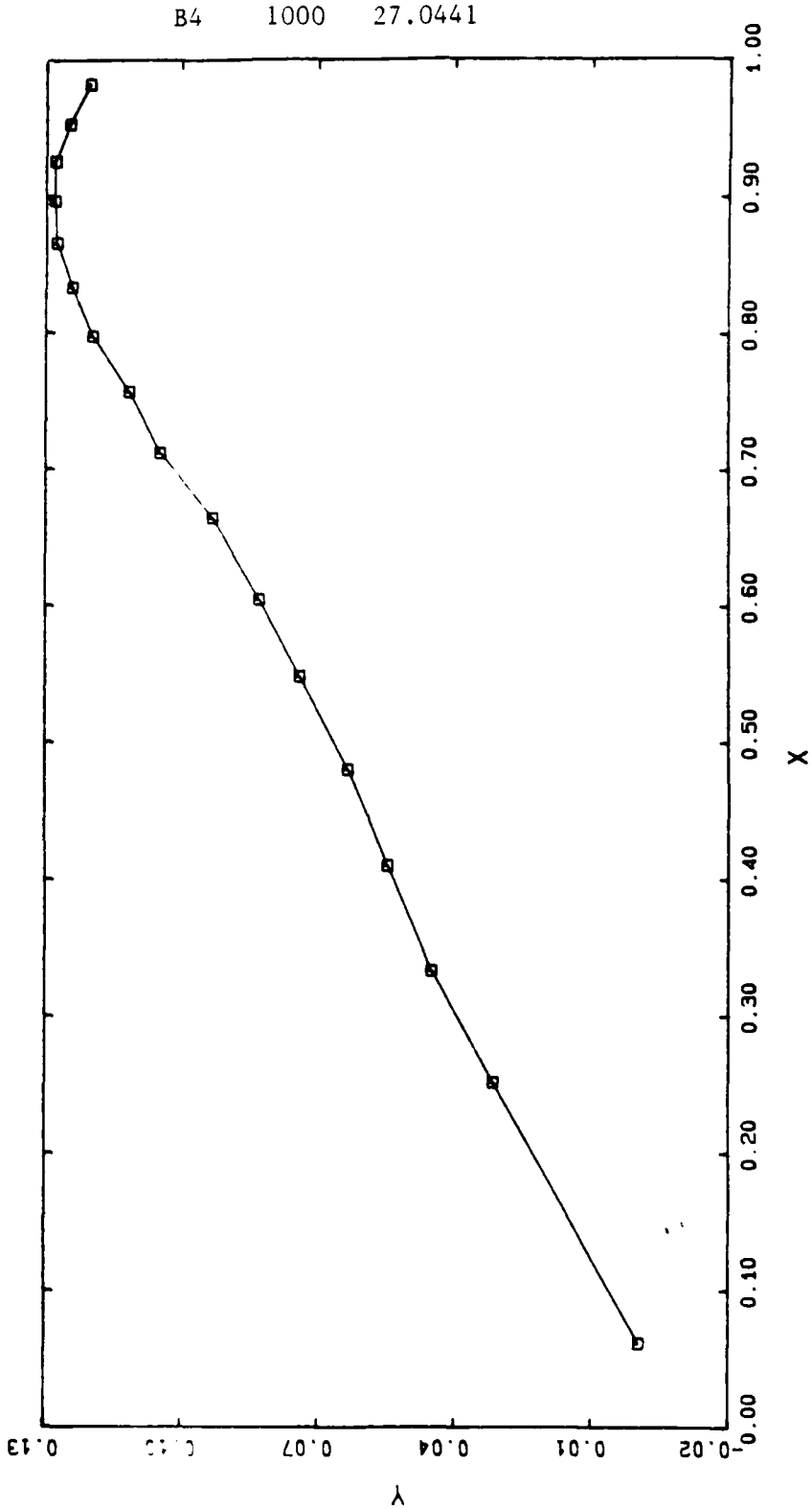

B4 1200 29.1550

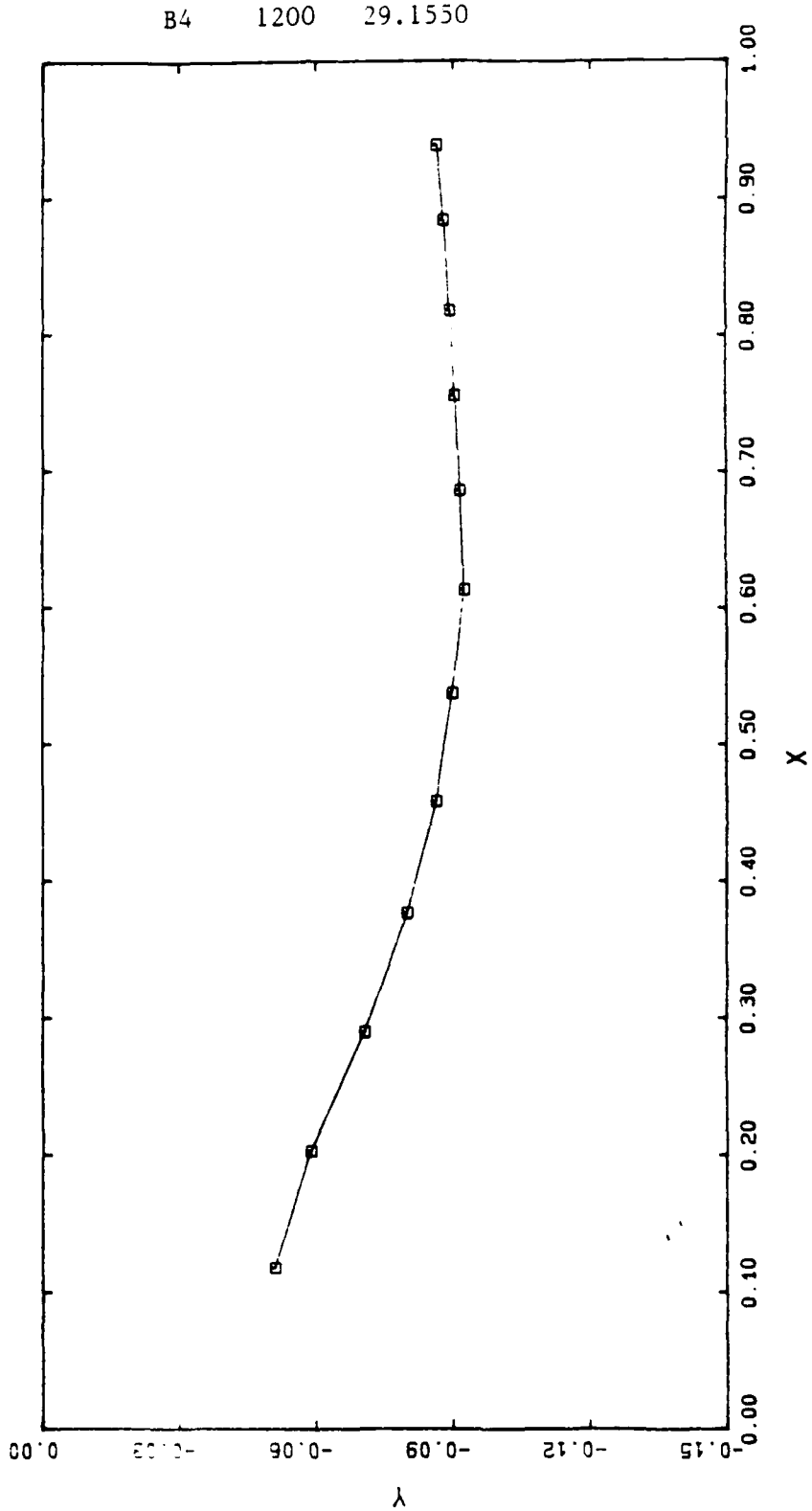

B4 1400 31.0811

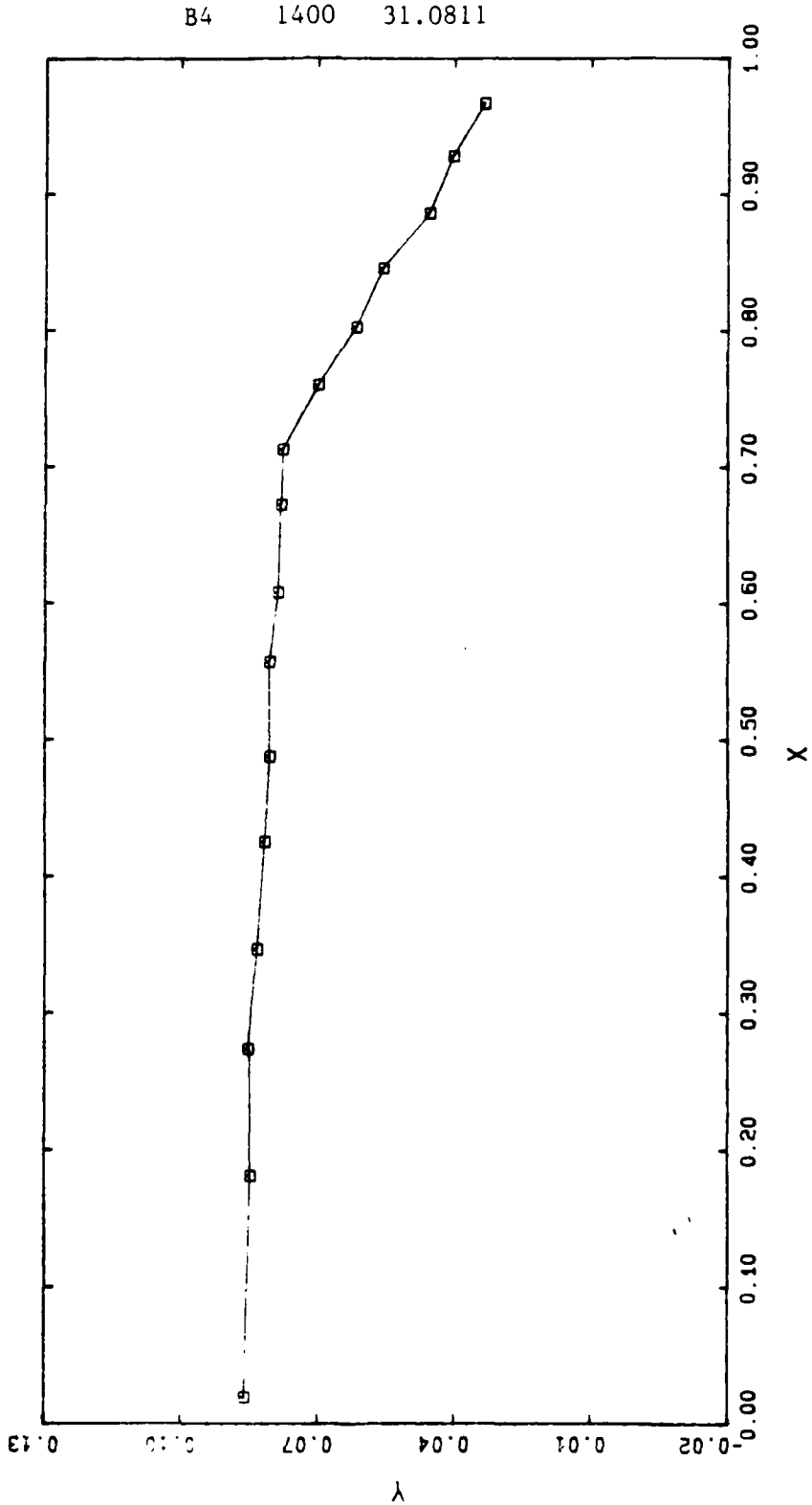

B4 1435 31.4314

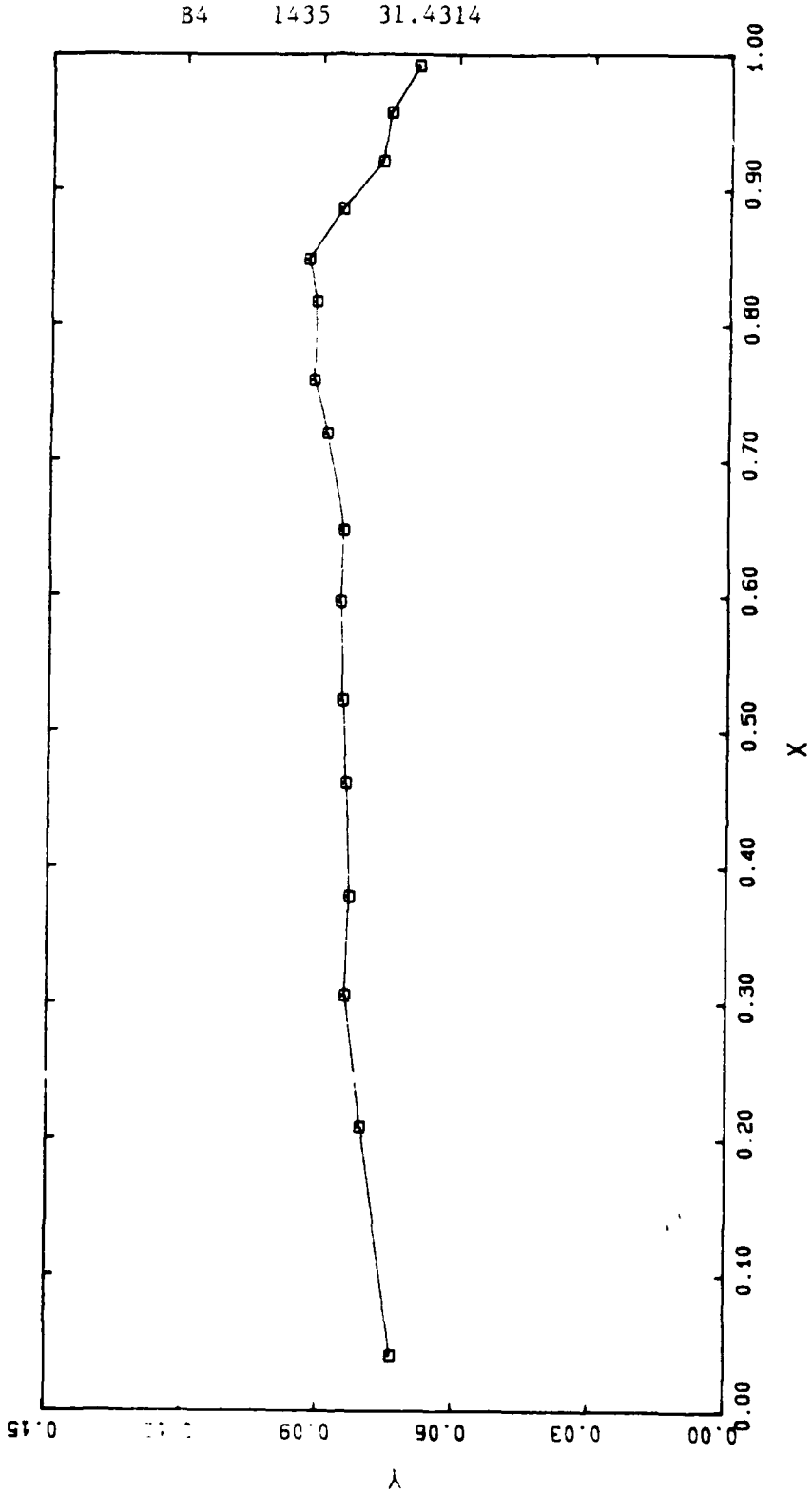

B4 1465 31.7322

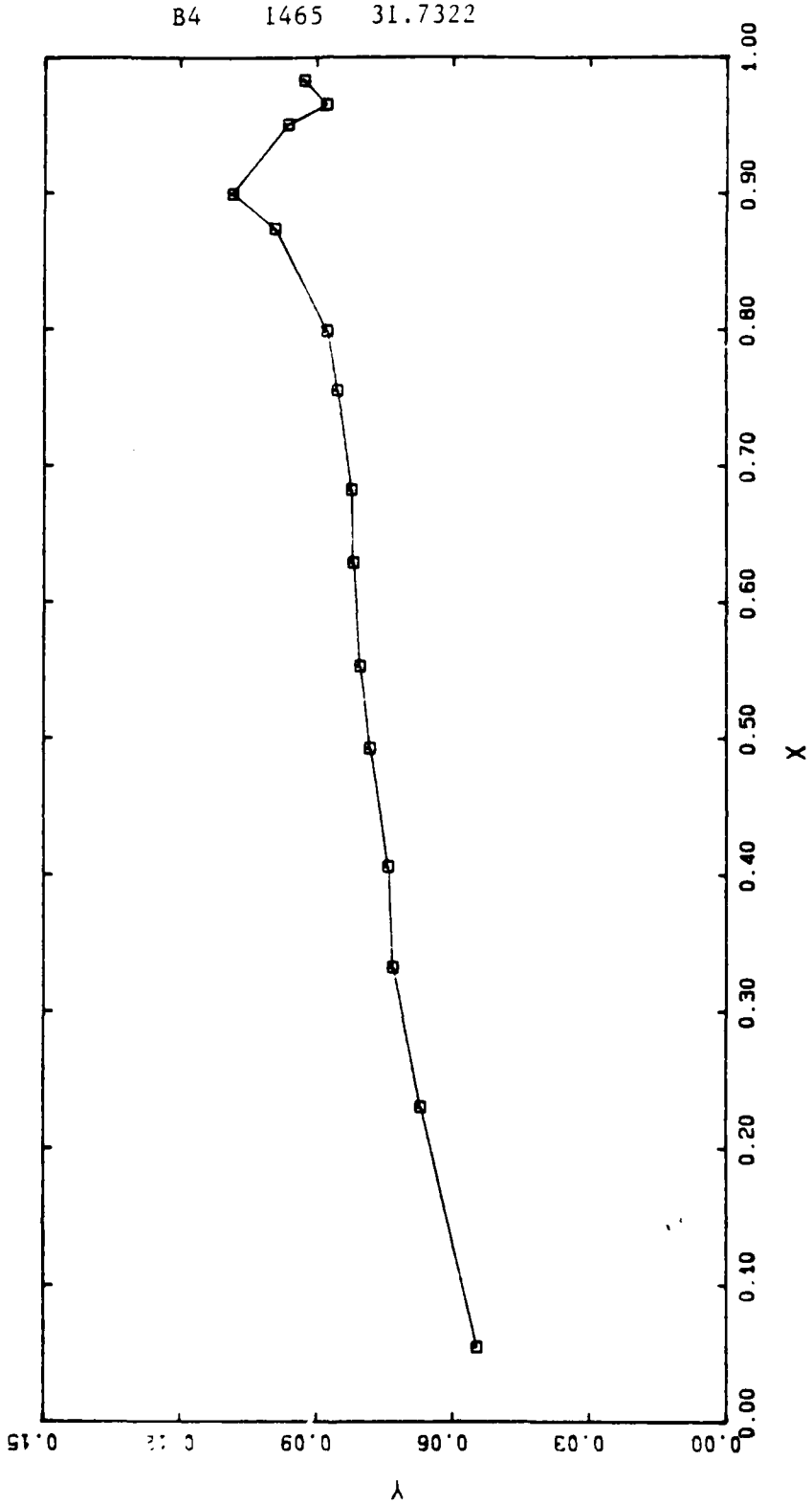

B4 1475 31.7857

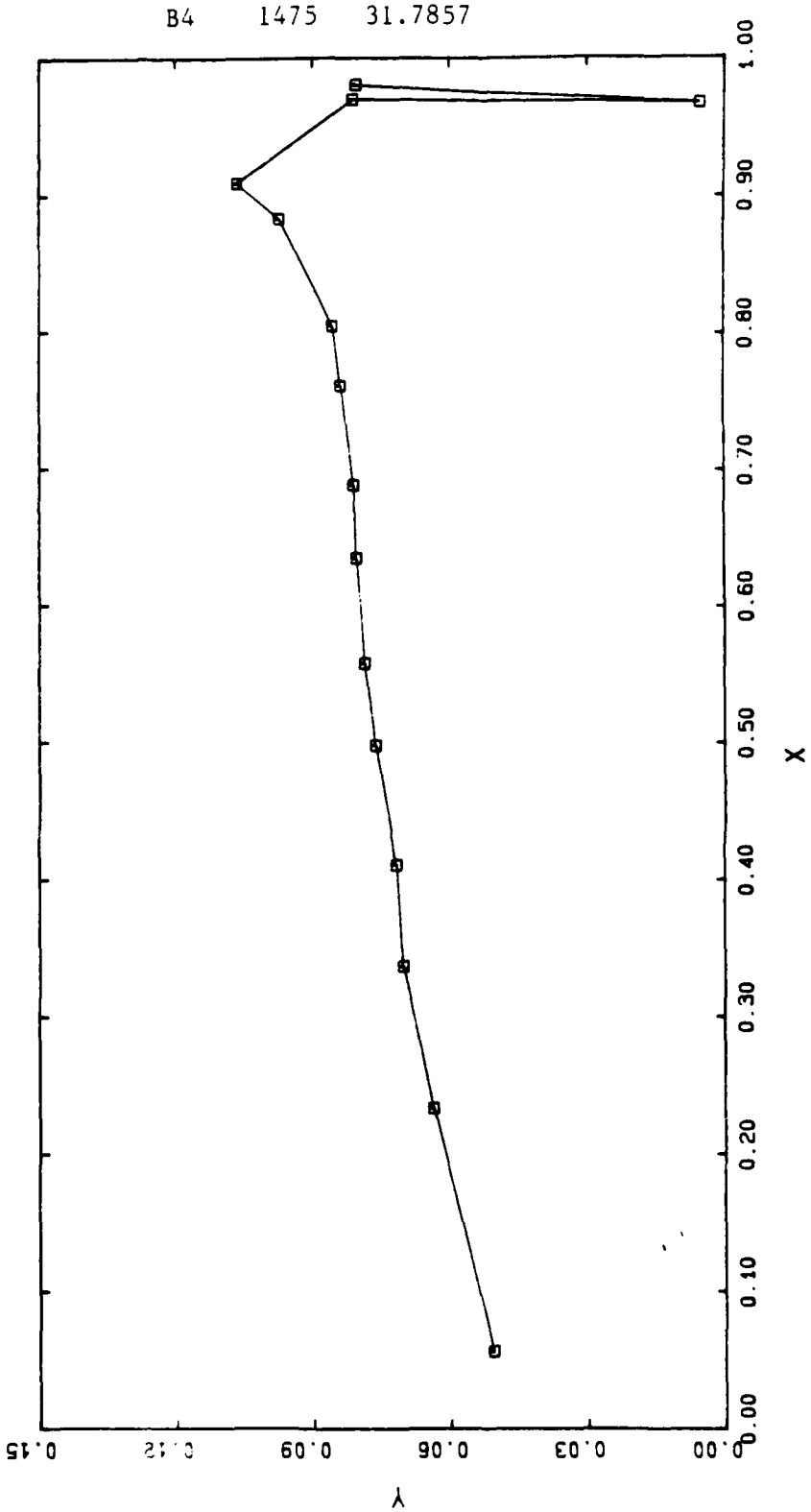

B4 1475 31.7857

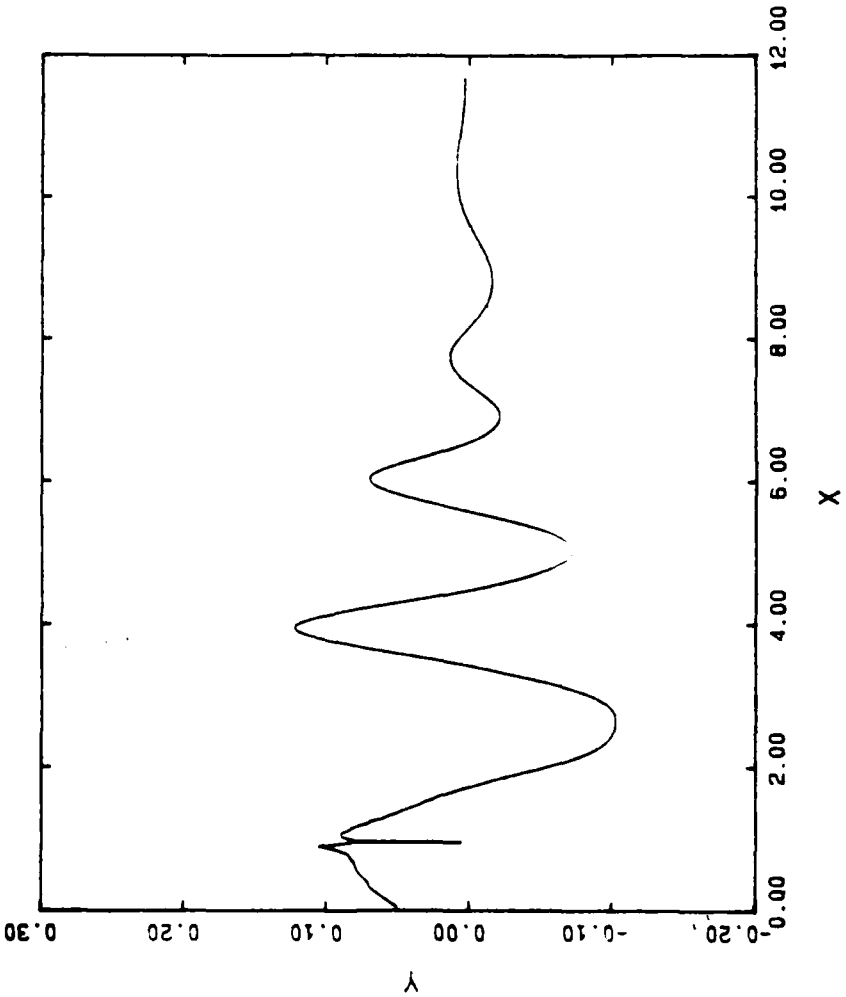

B5 3500 43.7134

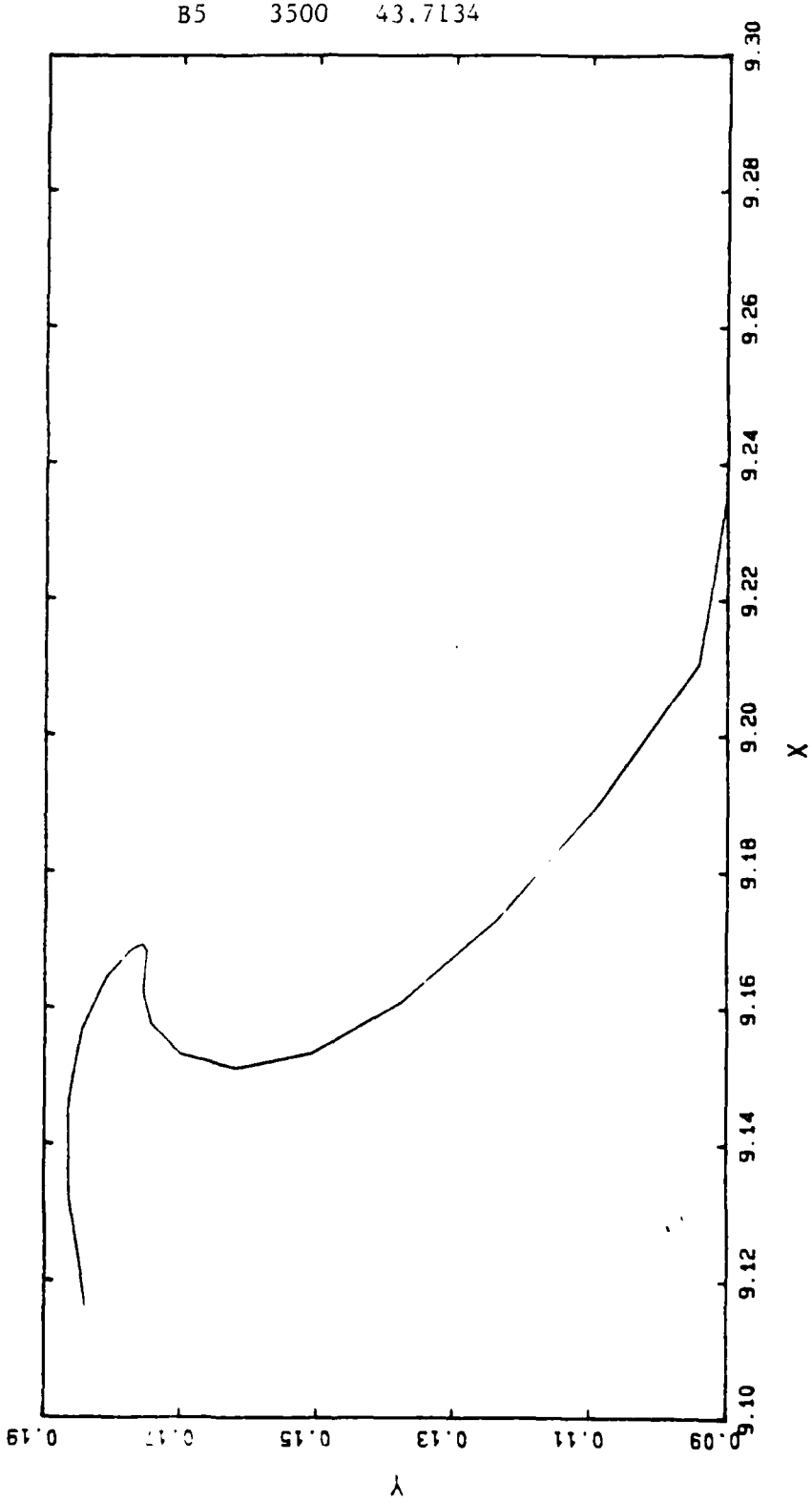

B5 4000 43.7778

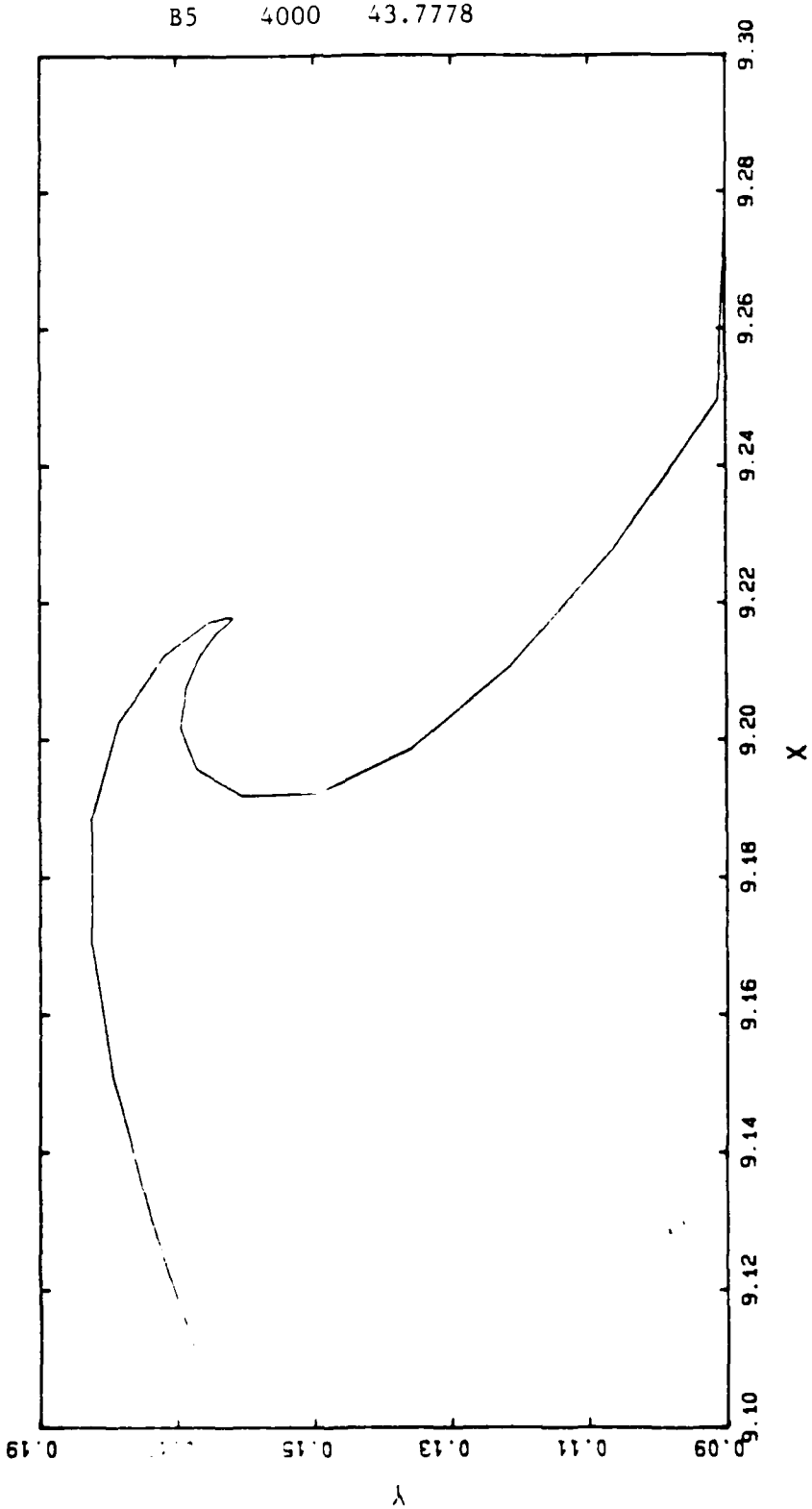

B5 4500 43.8522

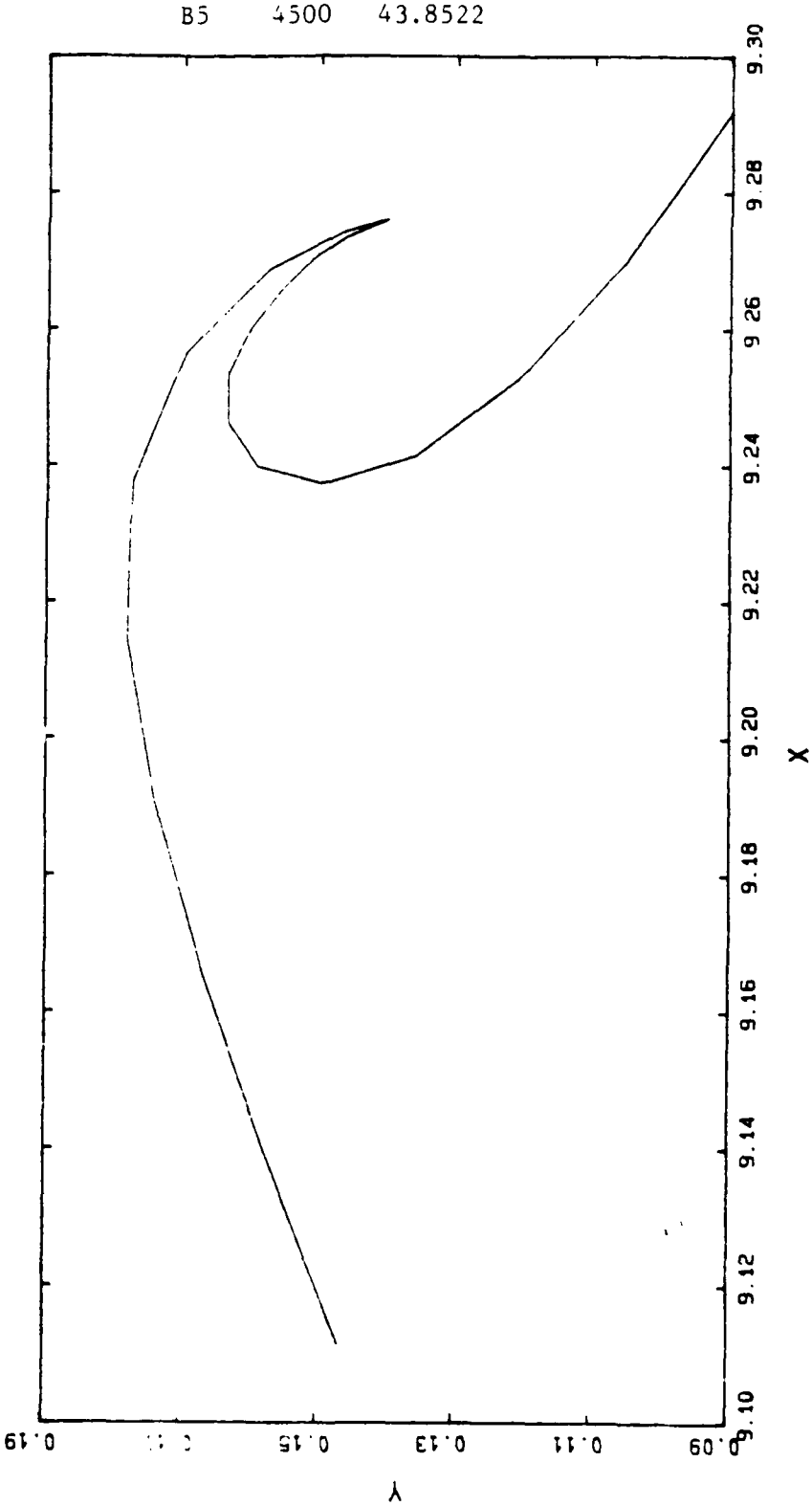

B5 4590 43.8730

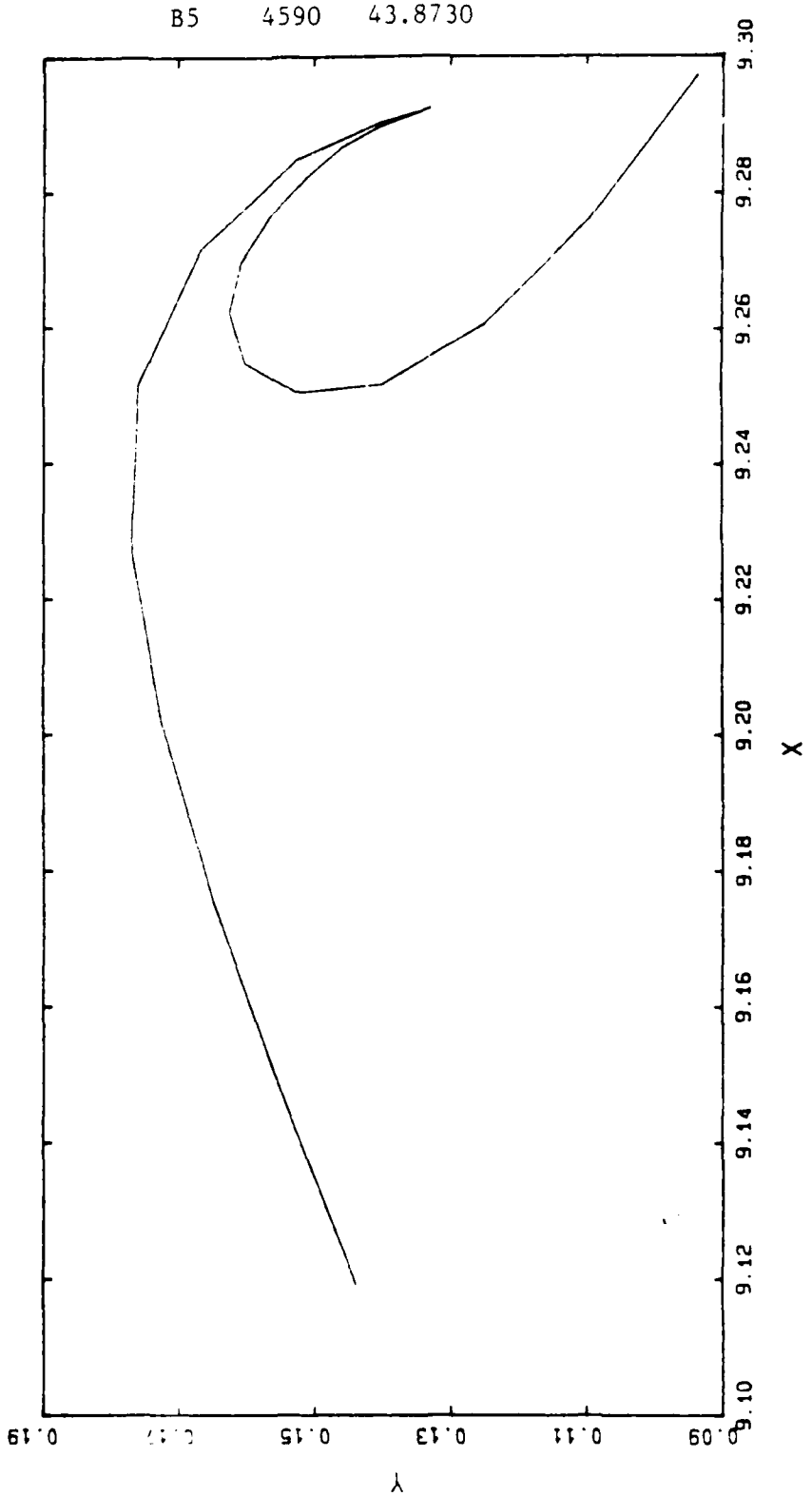

B5 4630 43.8835

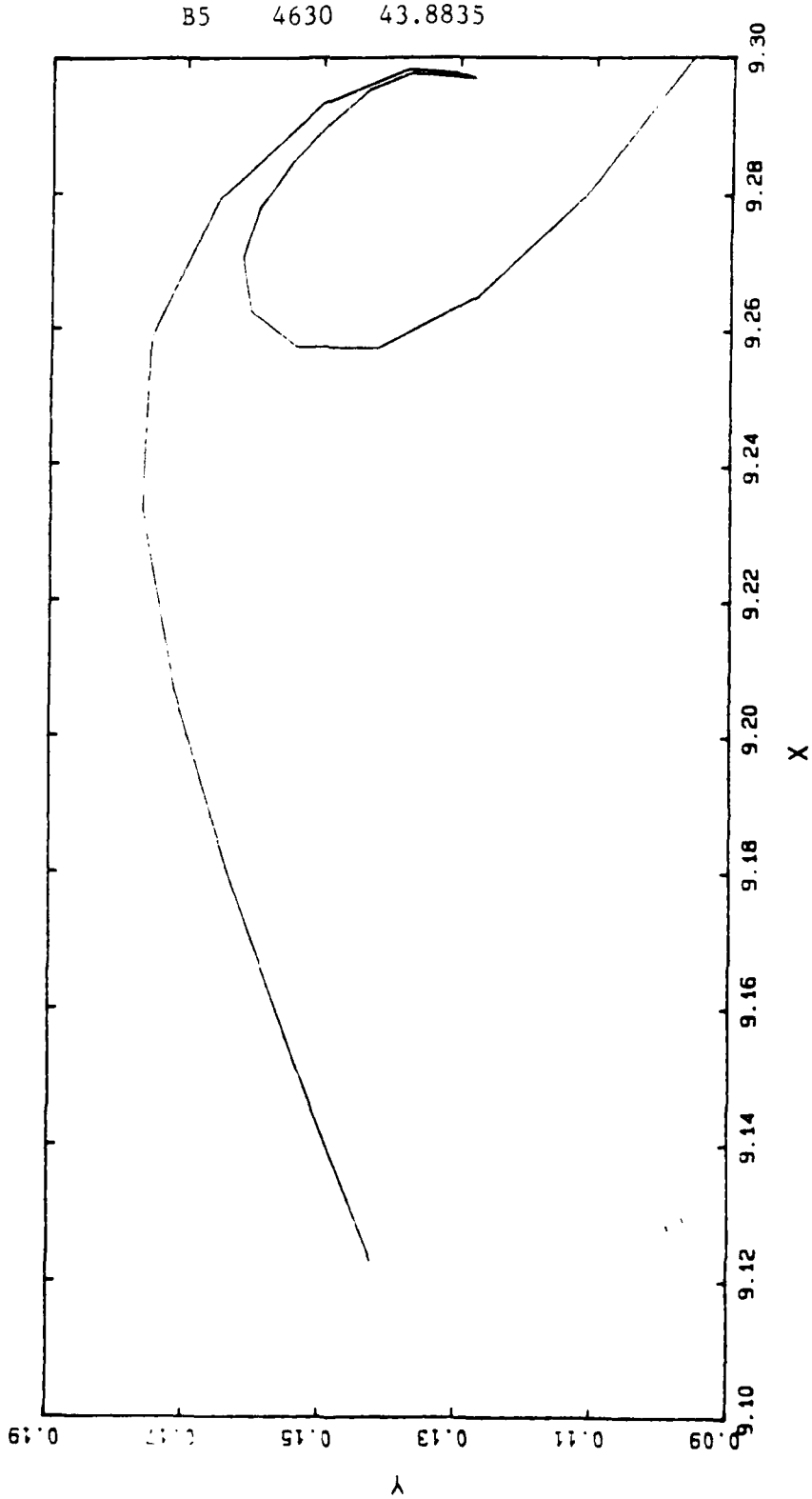

B5 4635 43.8849

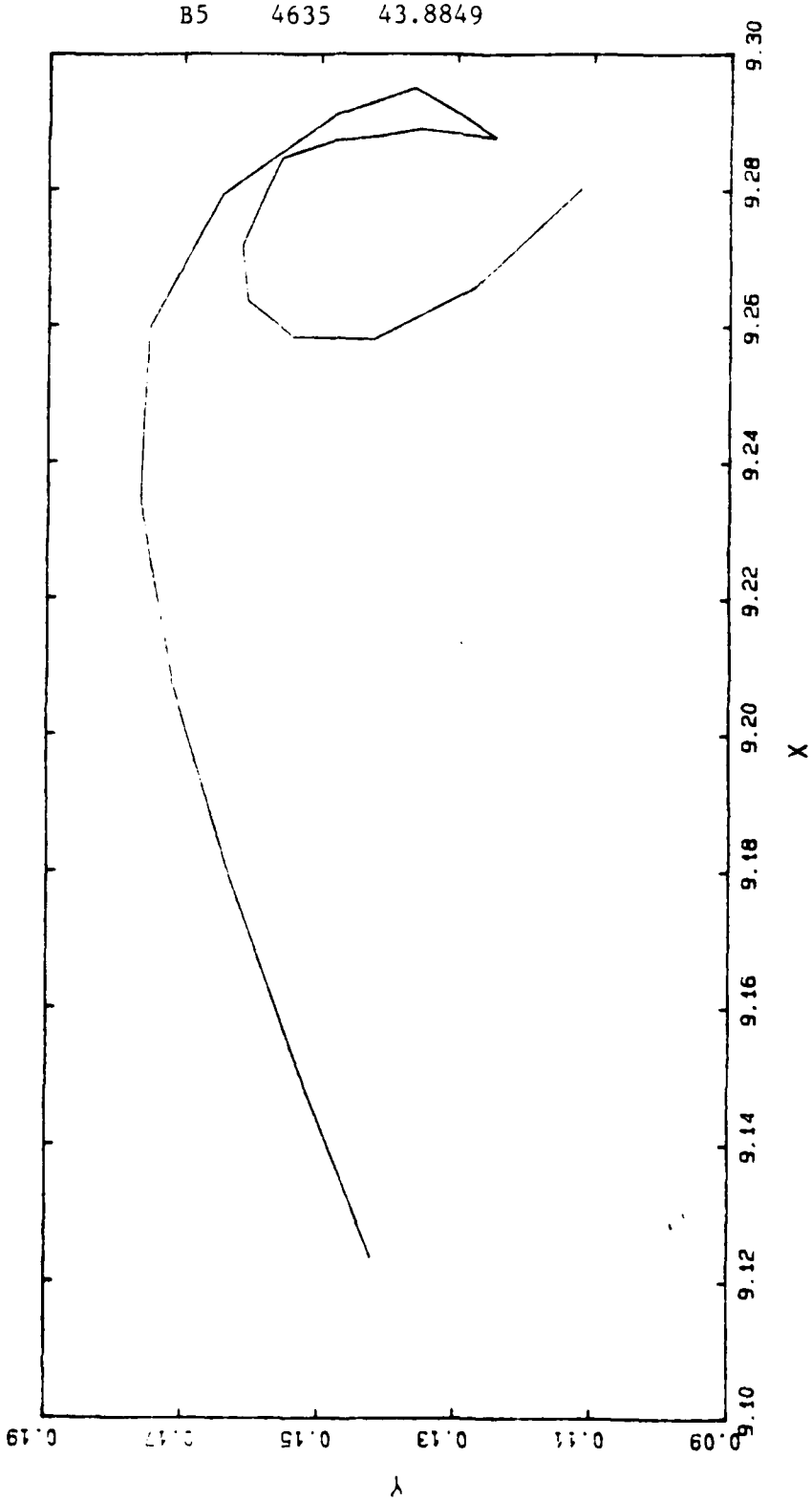

B5 4639 43.8853

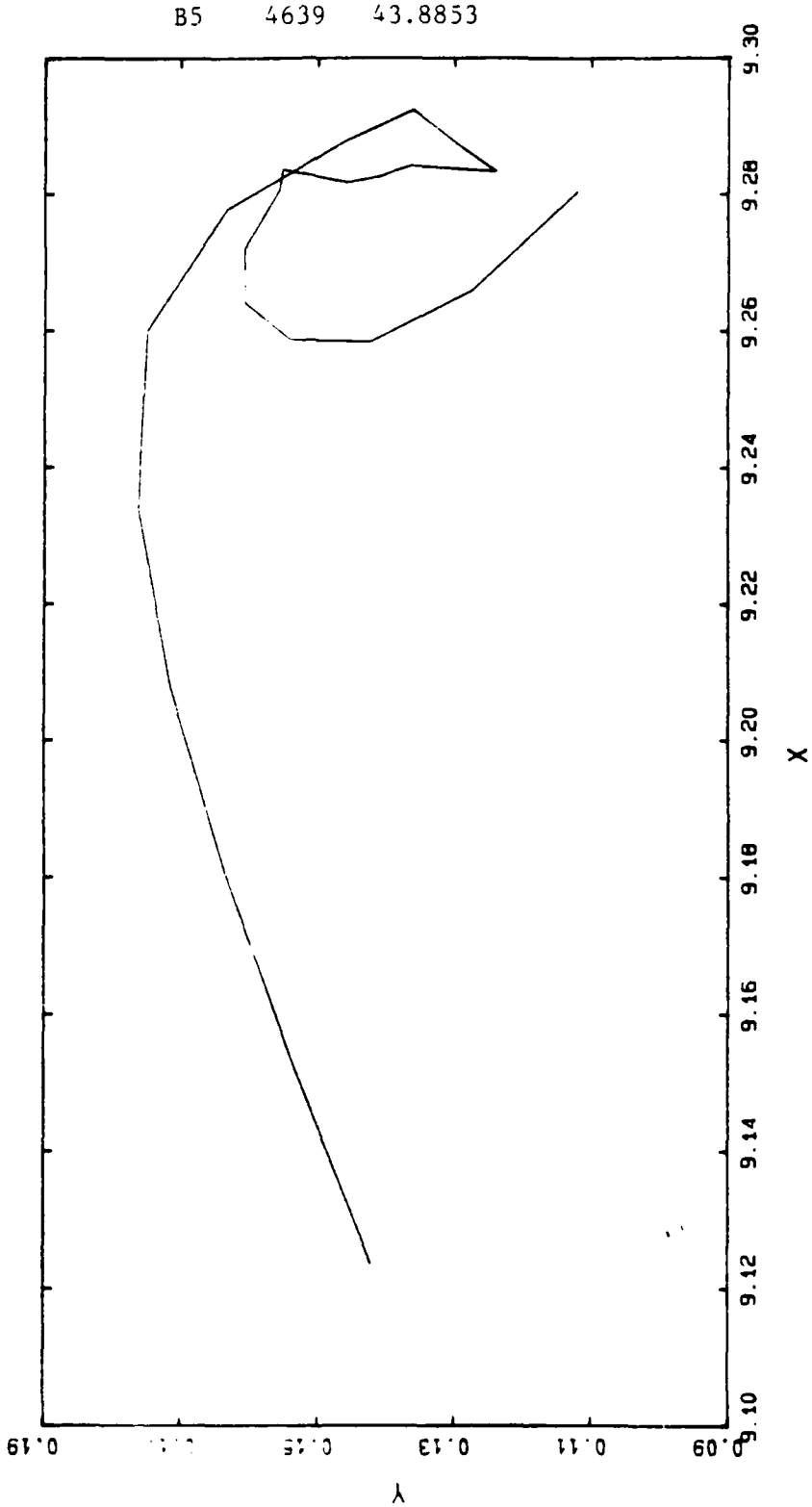

B6 400 19.0570

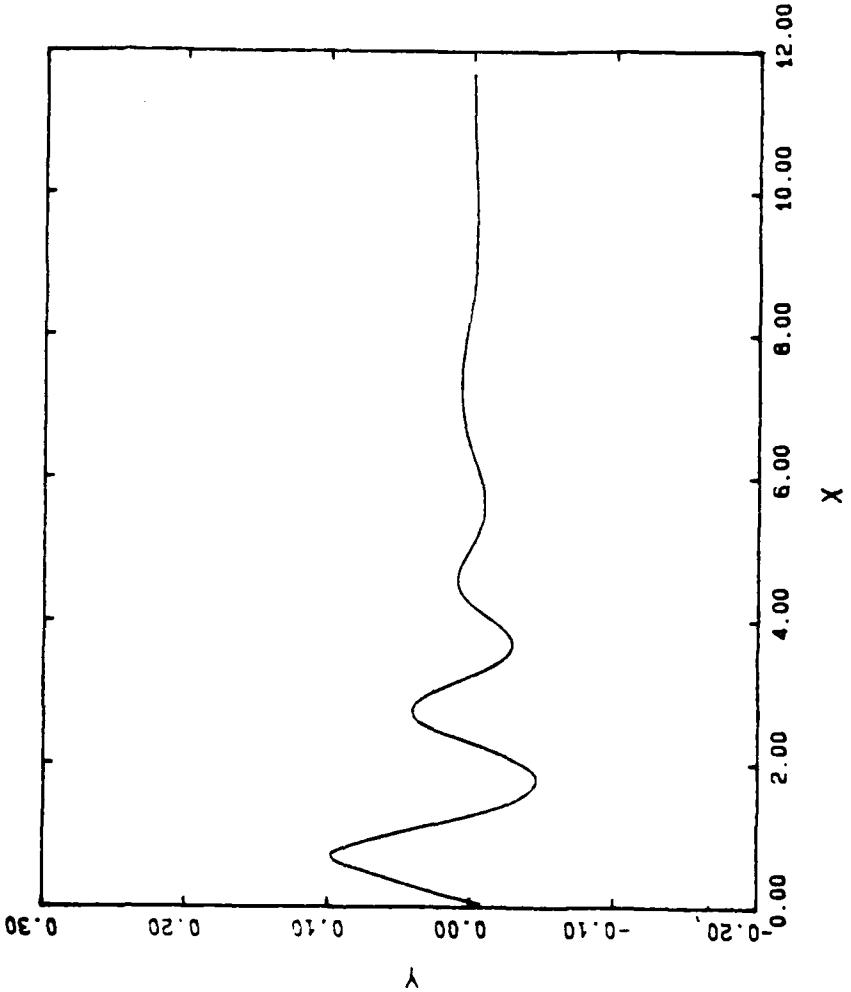

B6 800 27.0111

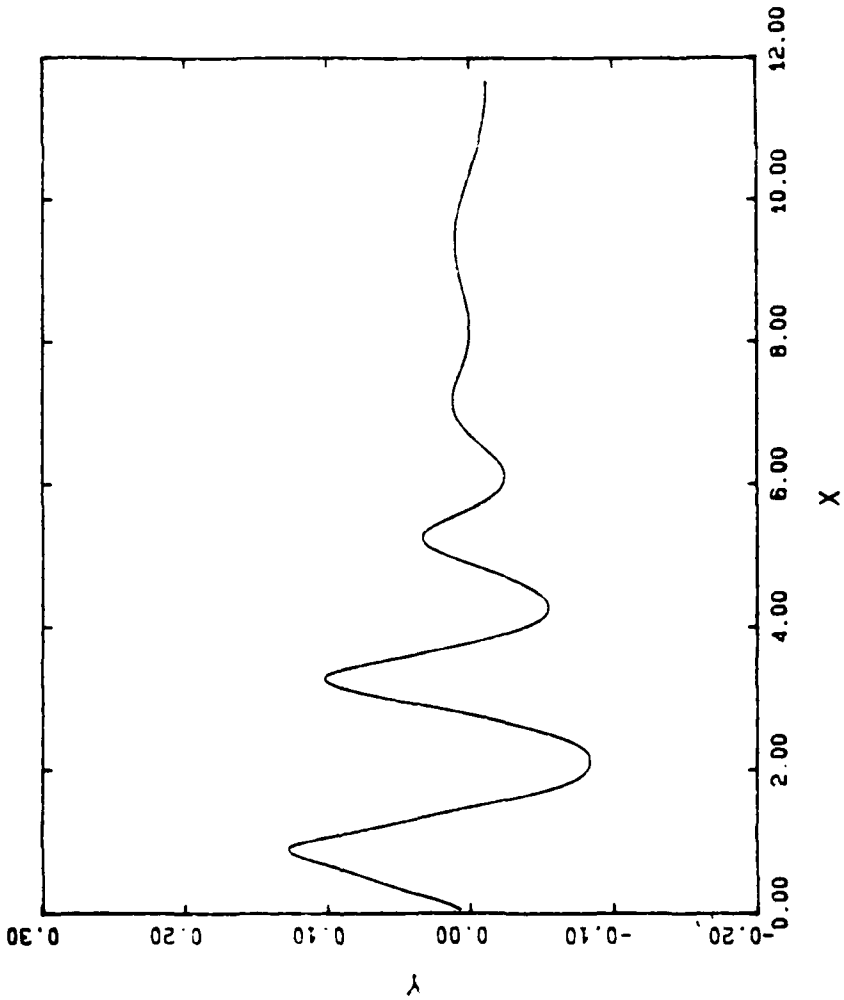

B6 1200 33.8145

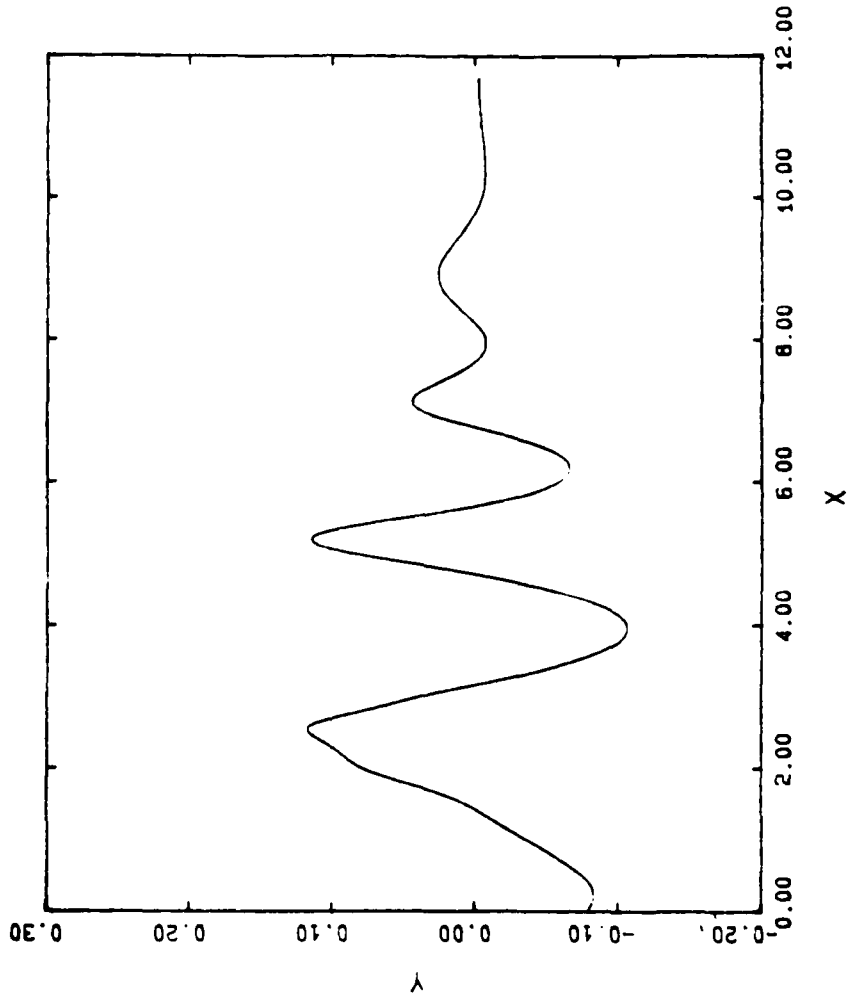

B6 1600 39.8814

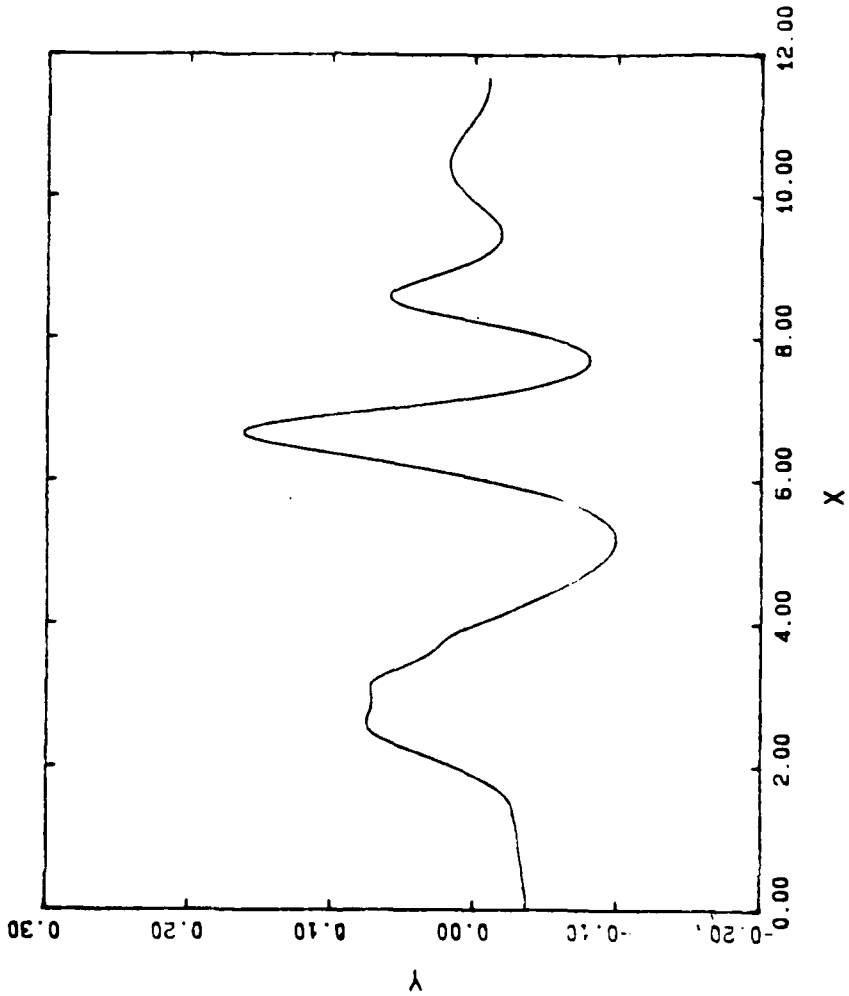

B6 2000 43.8435

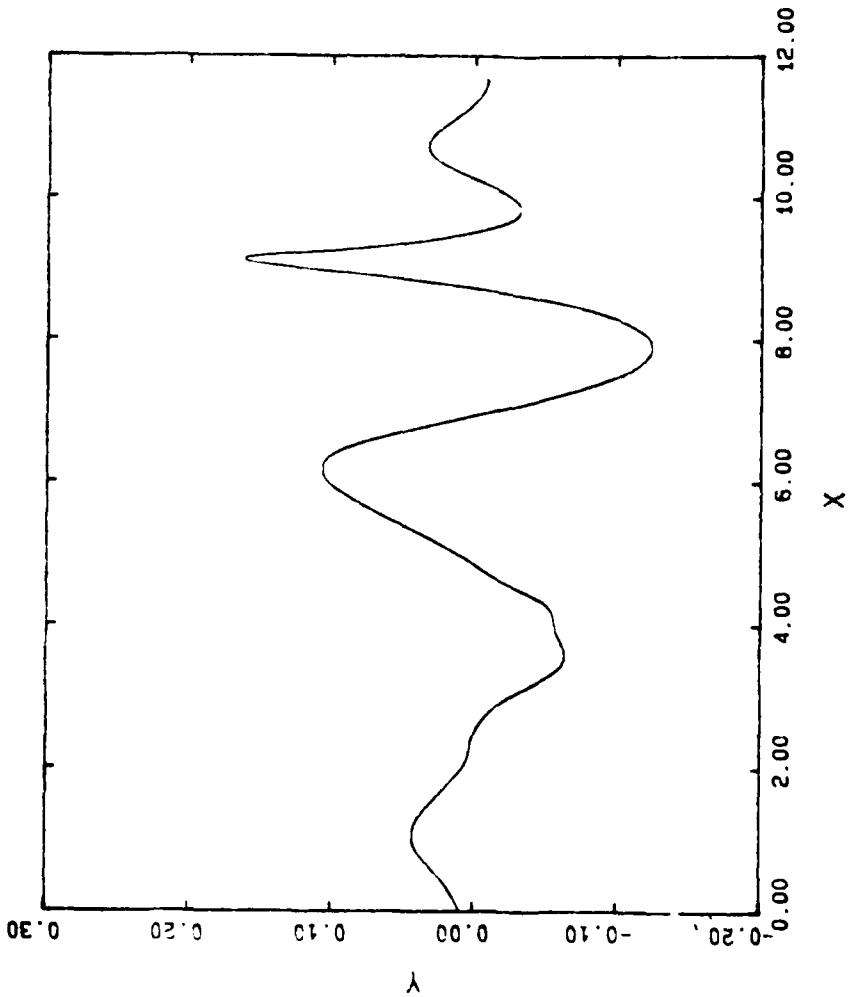

B6 2400 48.7405

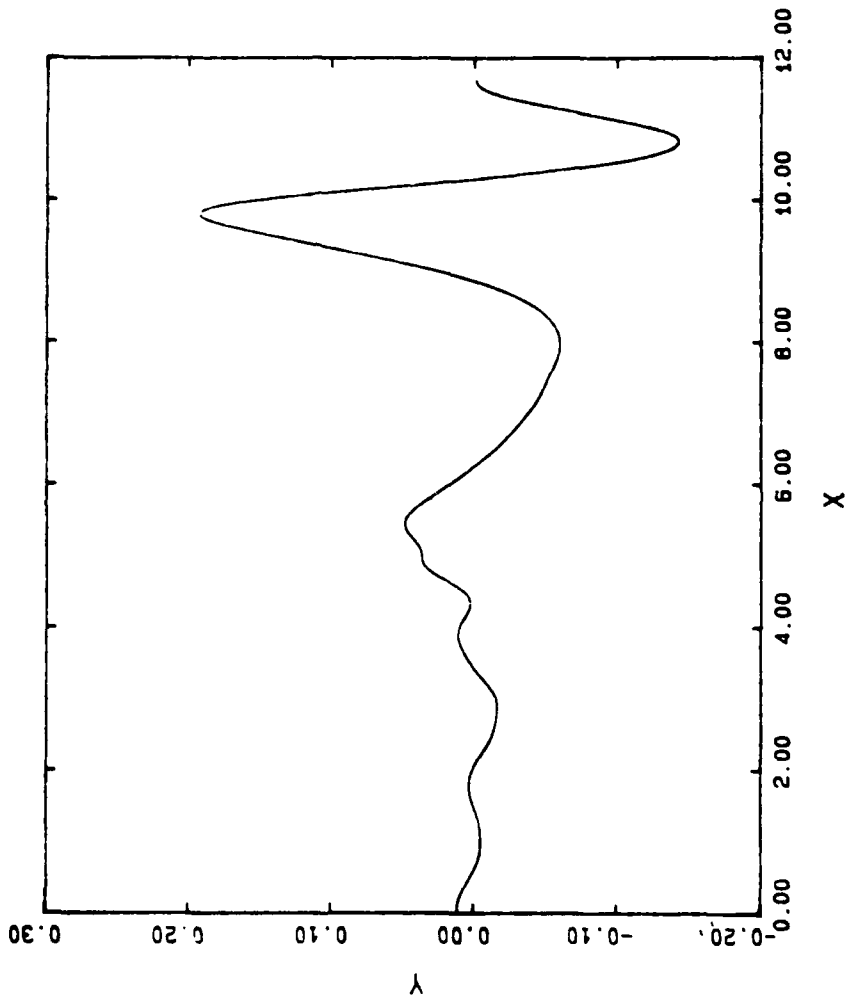

B6 2800 51.2354

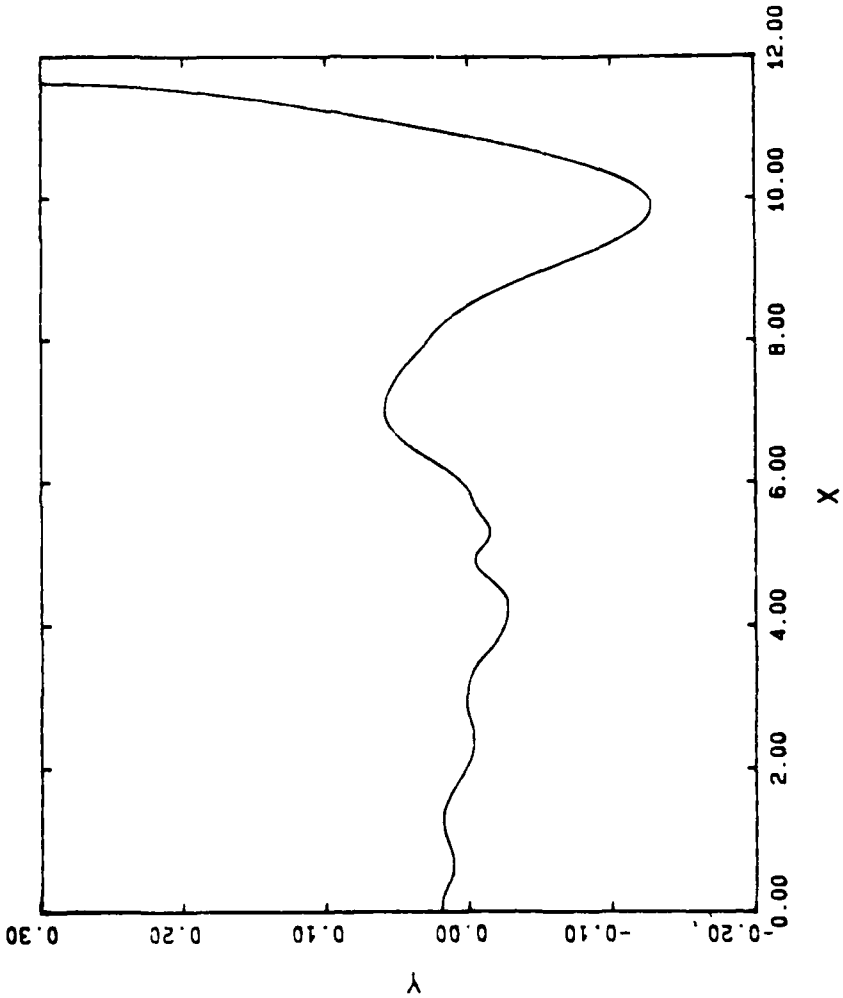

B6A 2740 44.7215

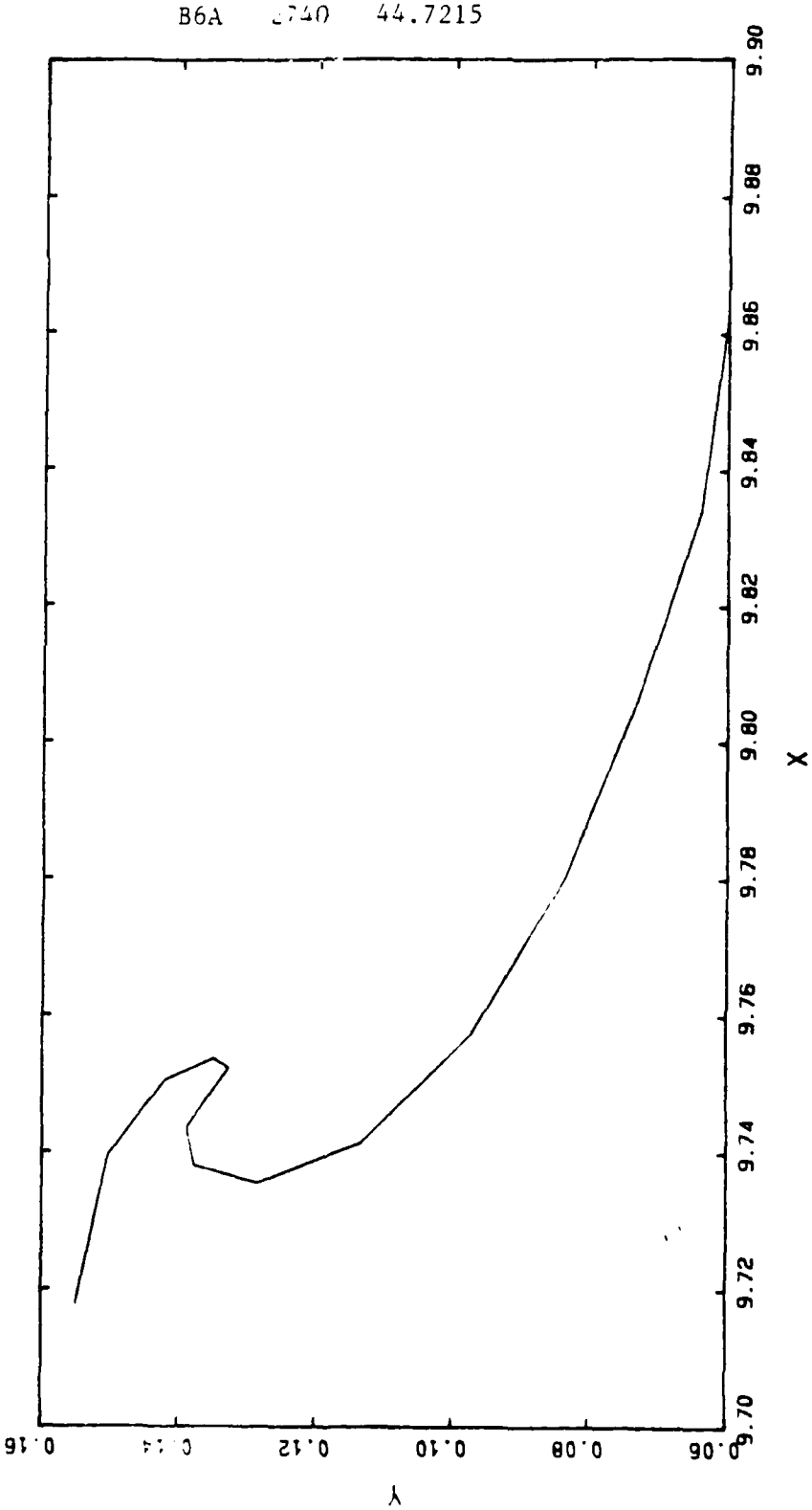

B6A 2790 44.7420

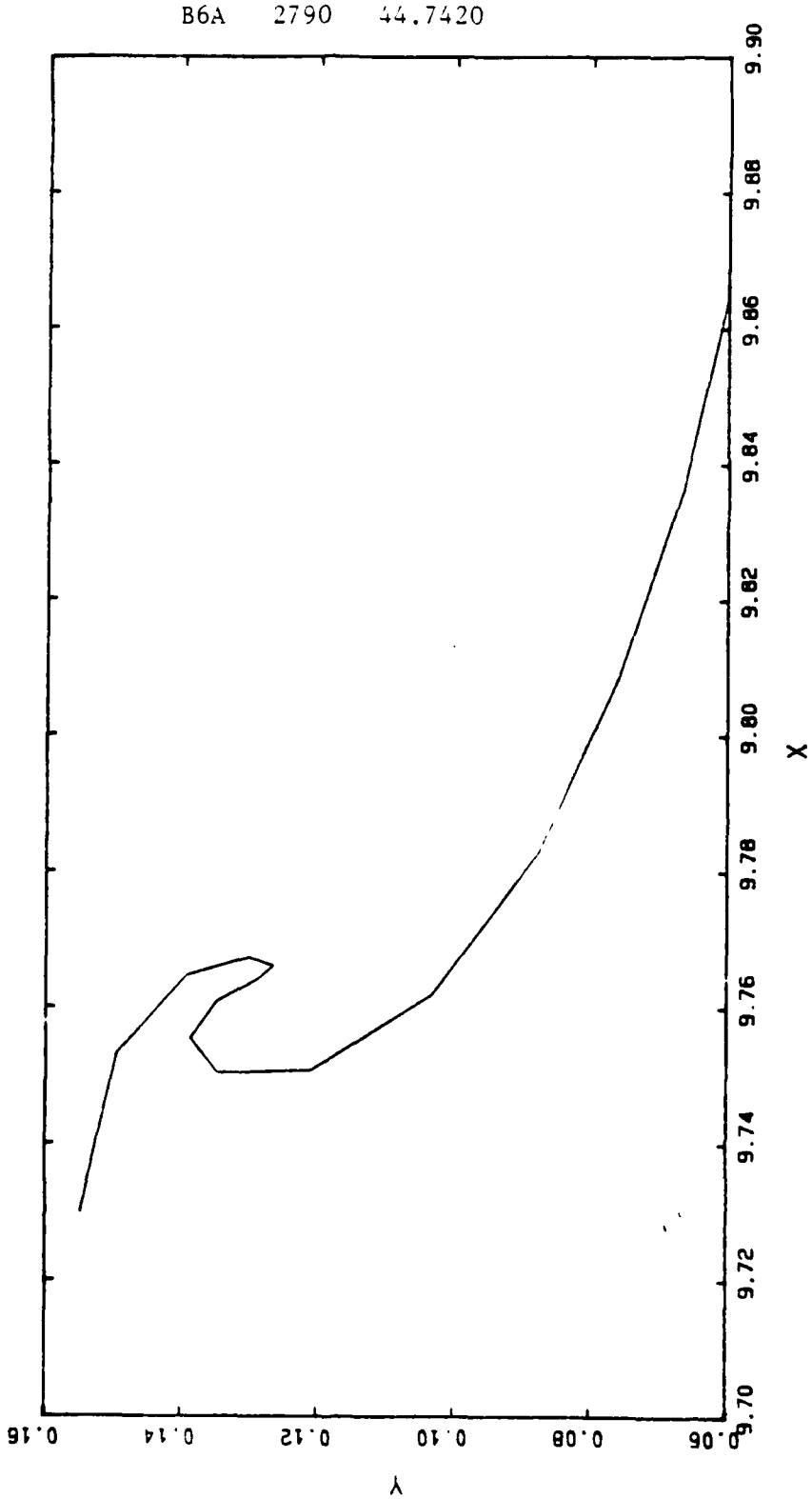

B6A 2830 44.7395

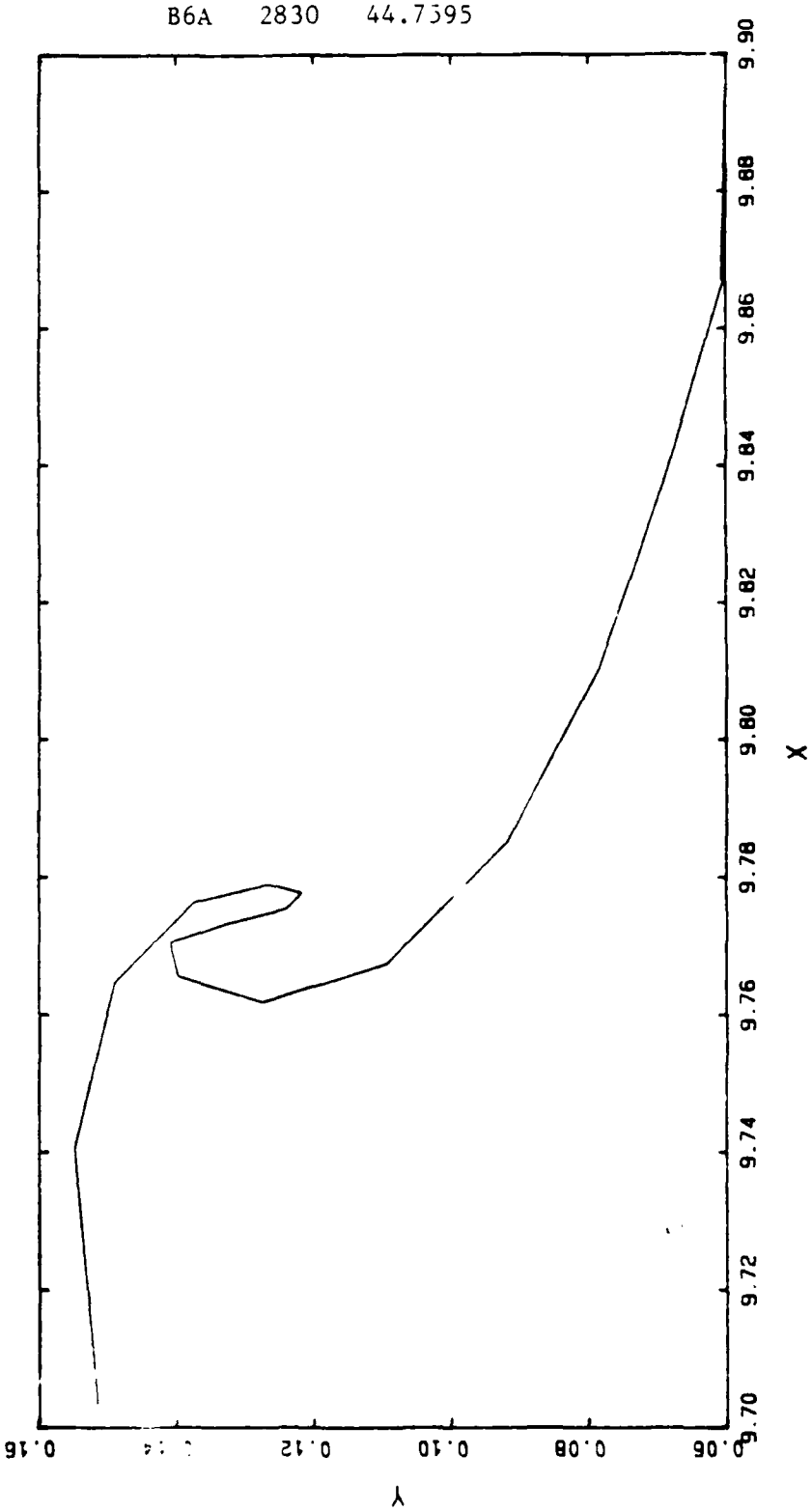

B6A 2840 44.7621

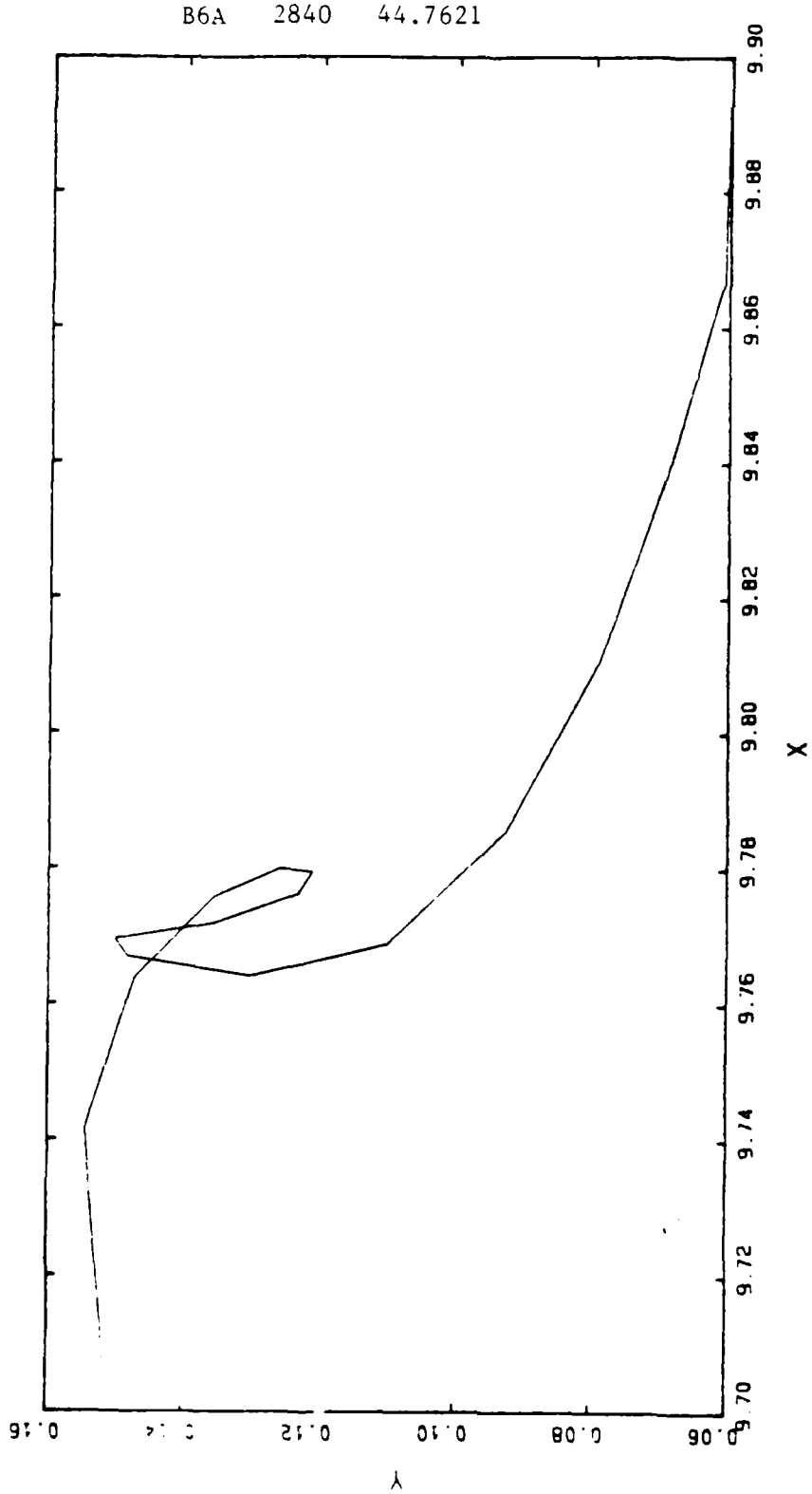

B6B 2822 45.9996

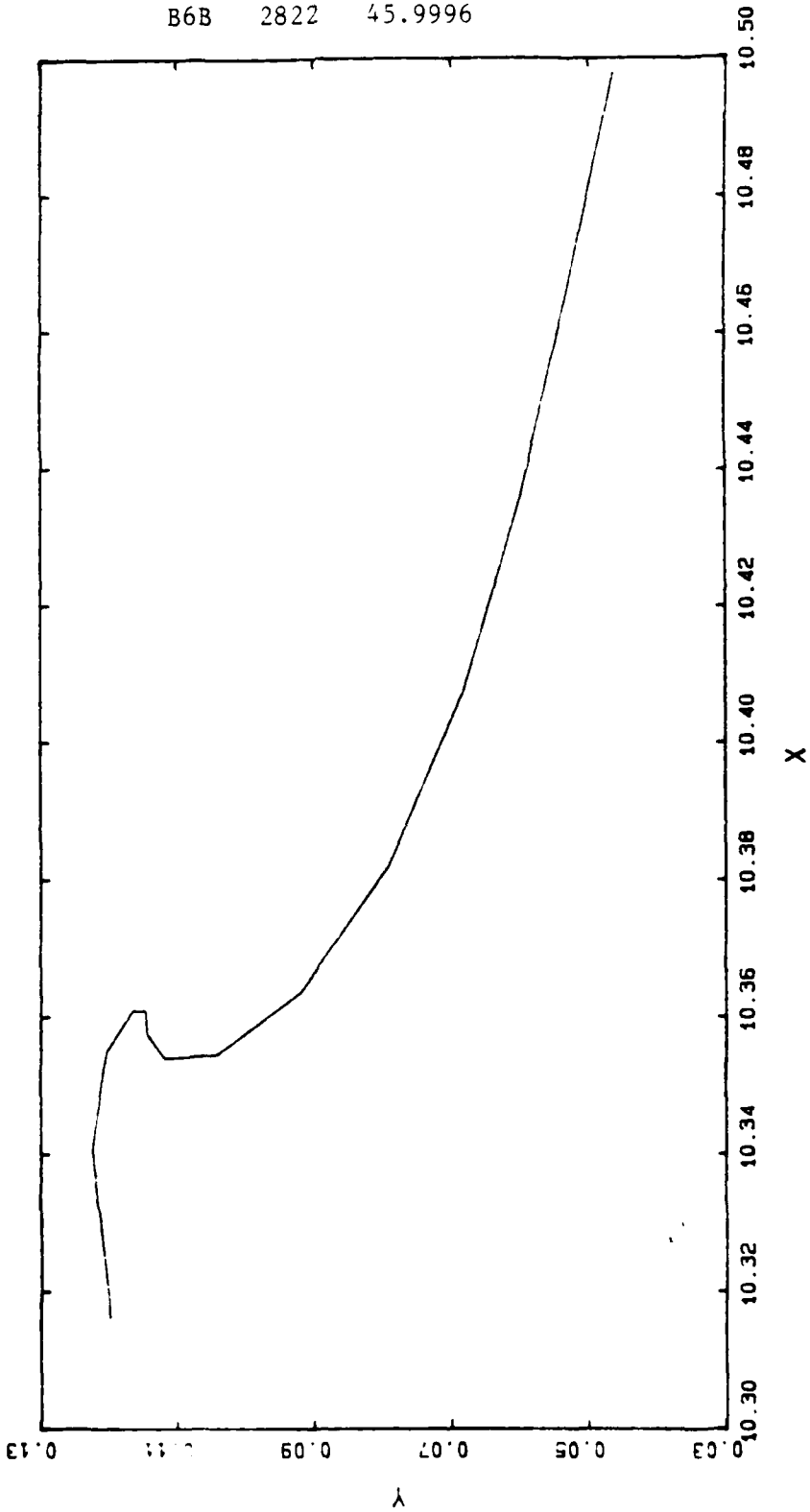

B6B 2872 46.0099

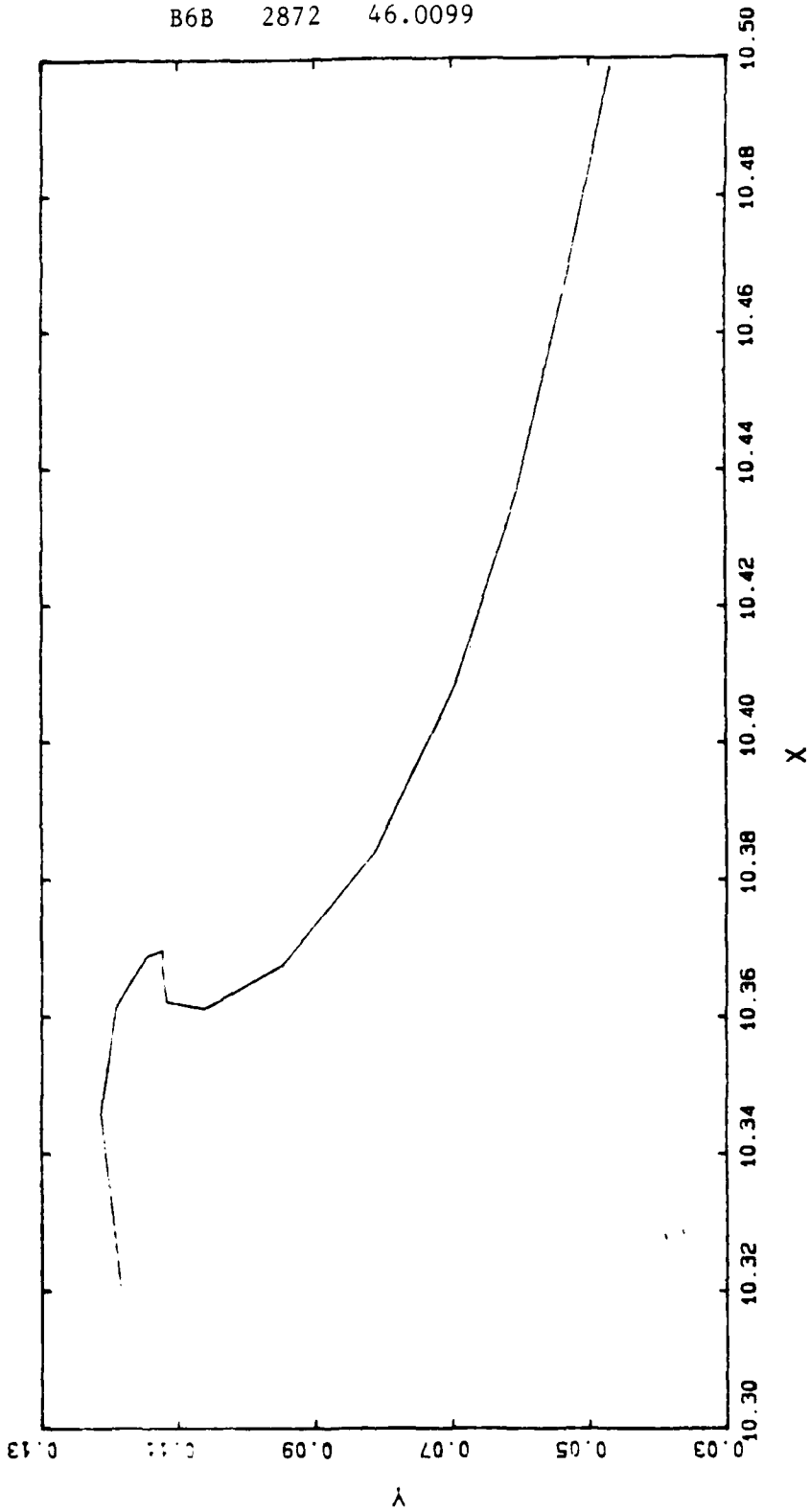

B6B 2902 46.0193

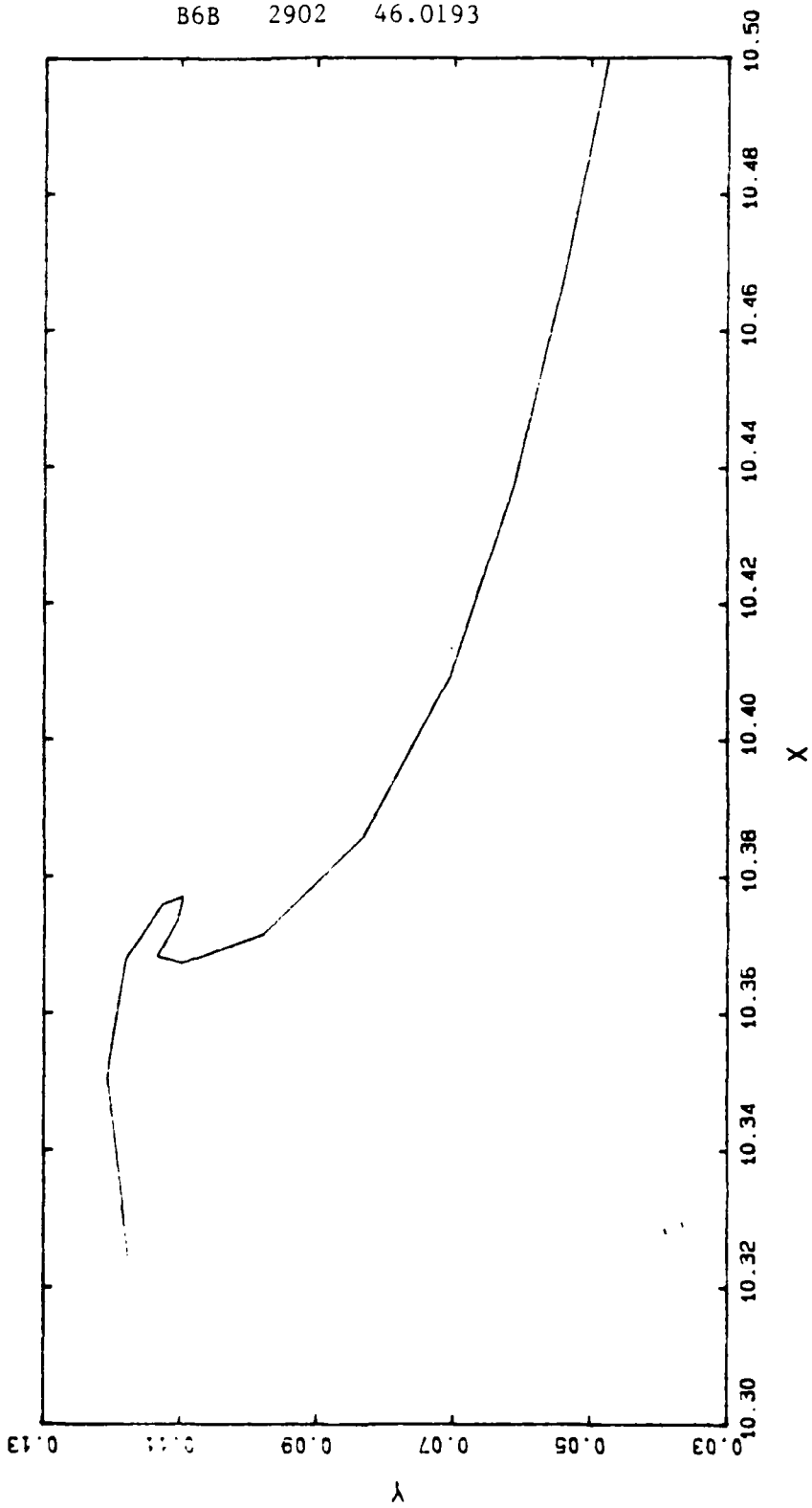

B6B 2912 46.0222

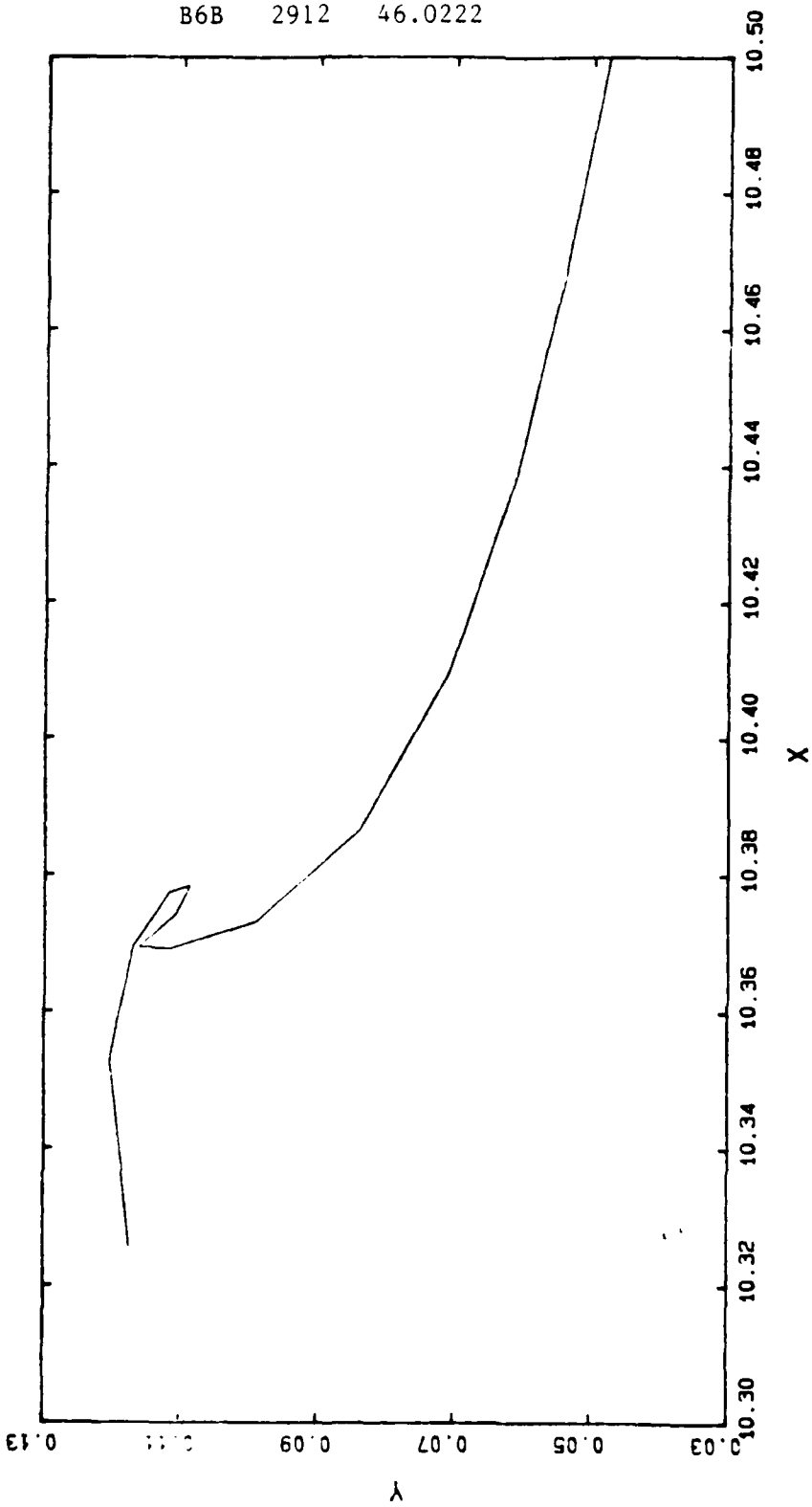

B6C 3640 51.0434

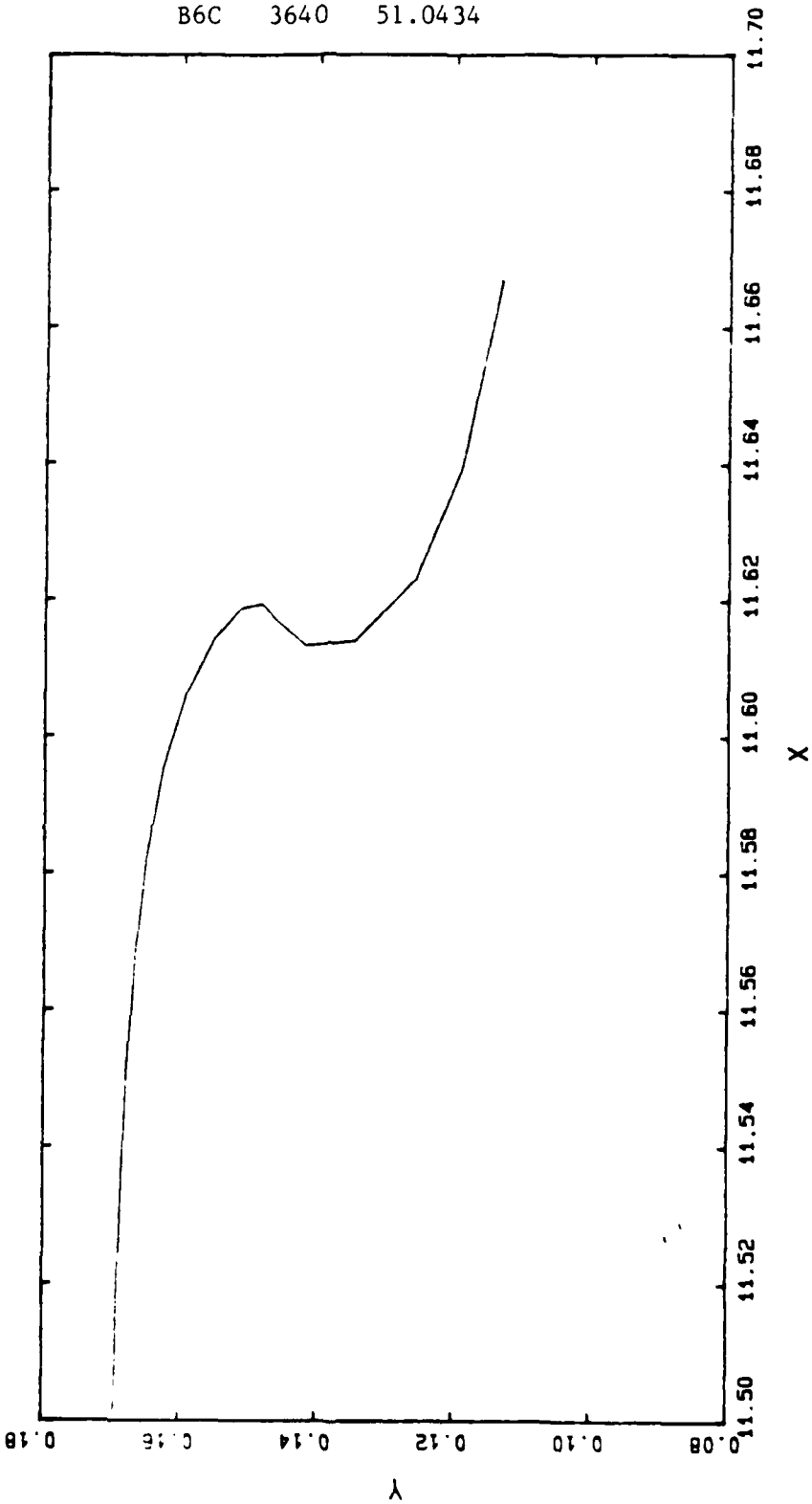

B6C 3690 51.0504

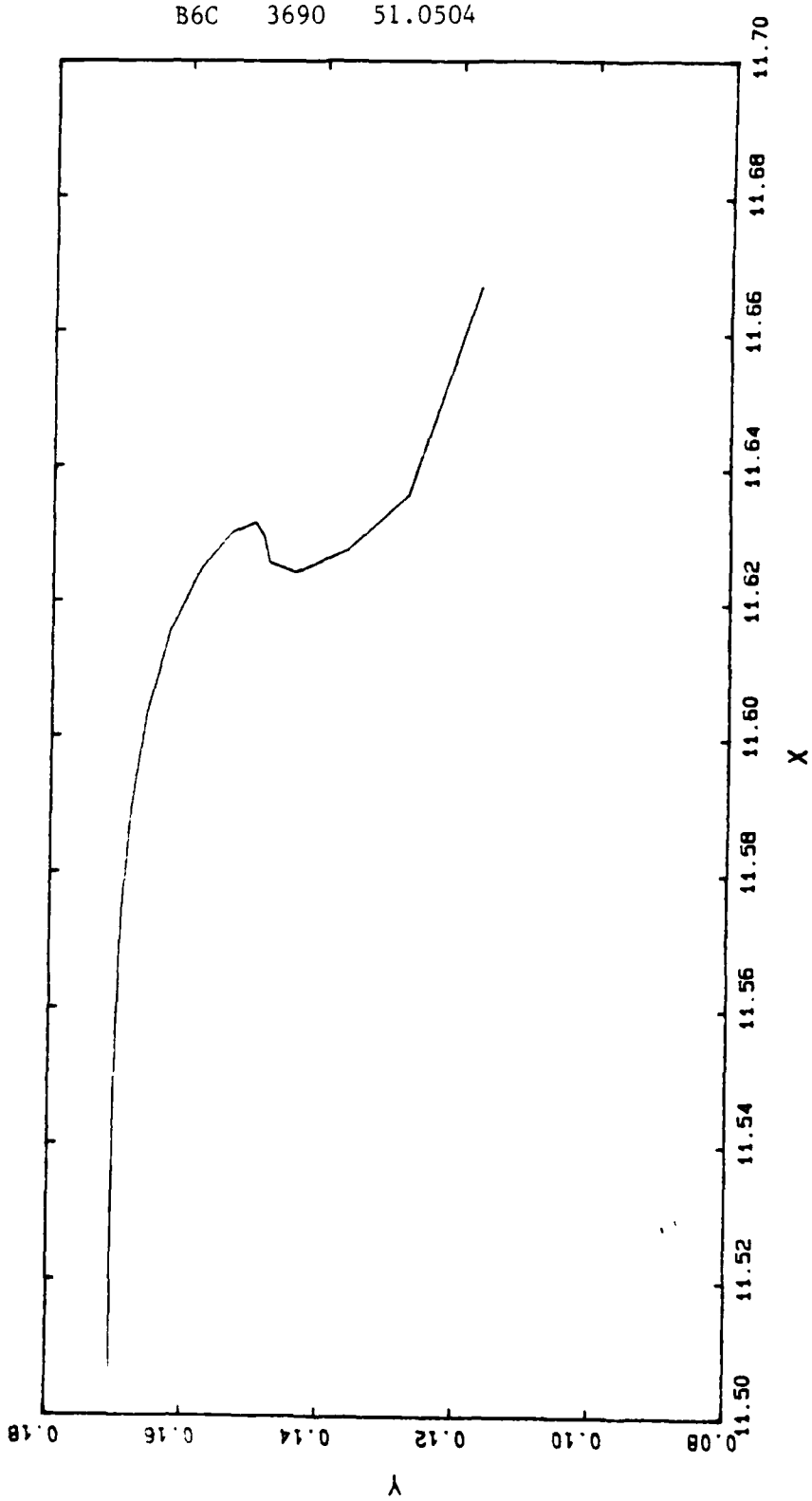

B6C 3730 51.0544

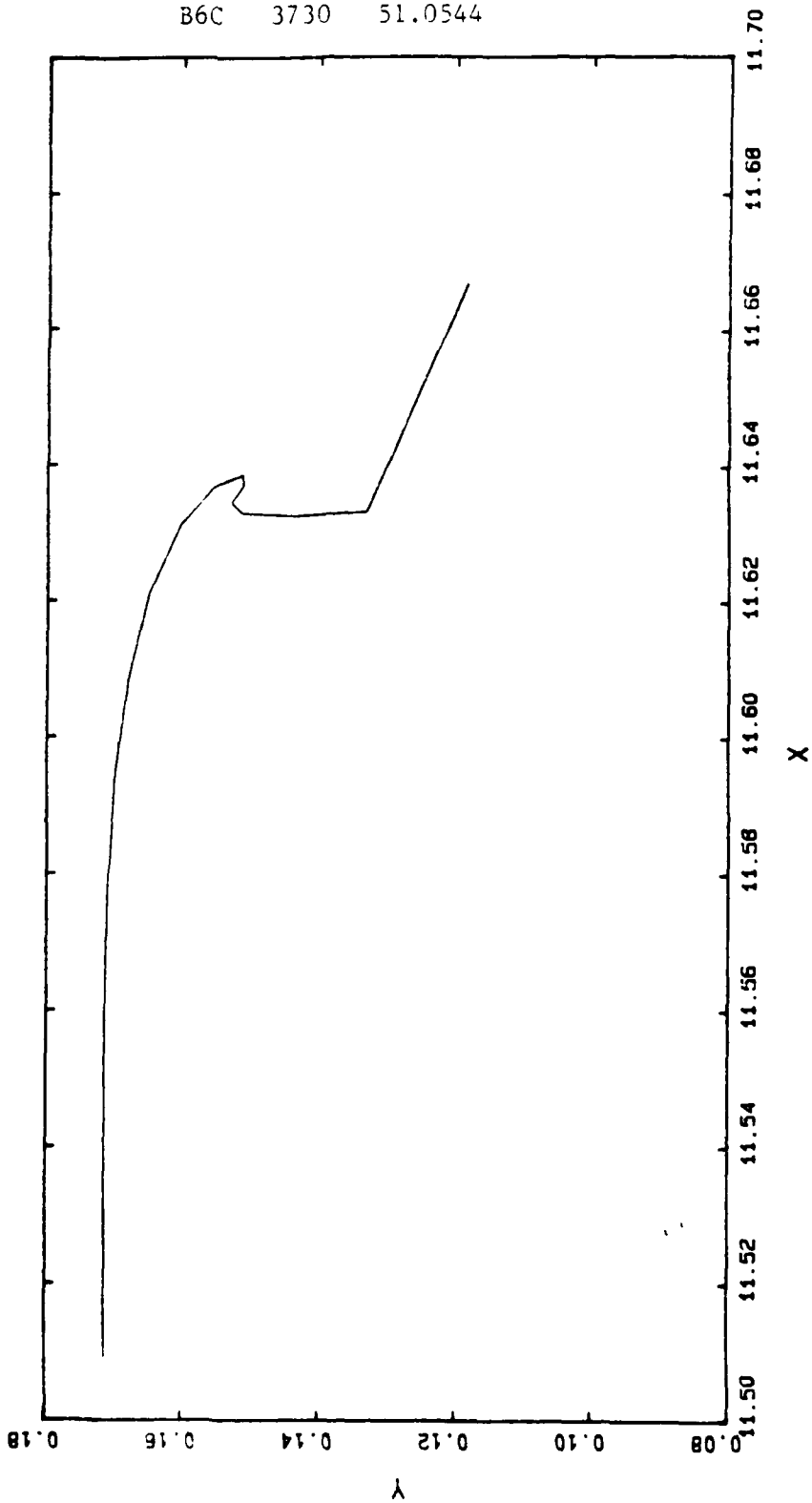

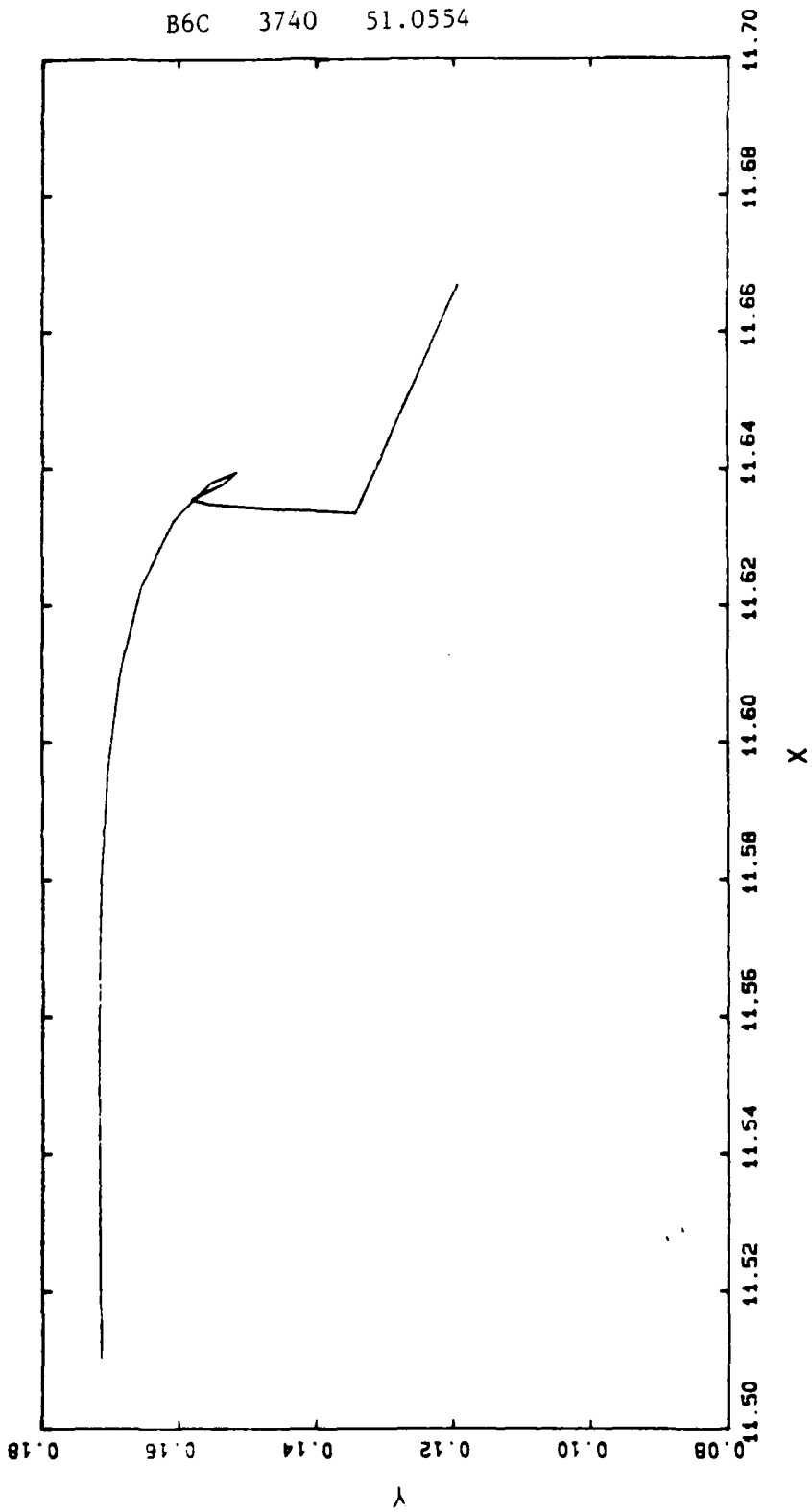
B6C 3740 51.0554
11.50
11.52
11.54
11.56
11.58
11.60
11.62
11.64
11.66
11.68
11.70
X
0.08
0.10
0.12
0.14
0.16
0.18
Y

B6E 3702 51.0215

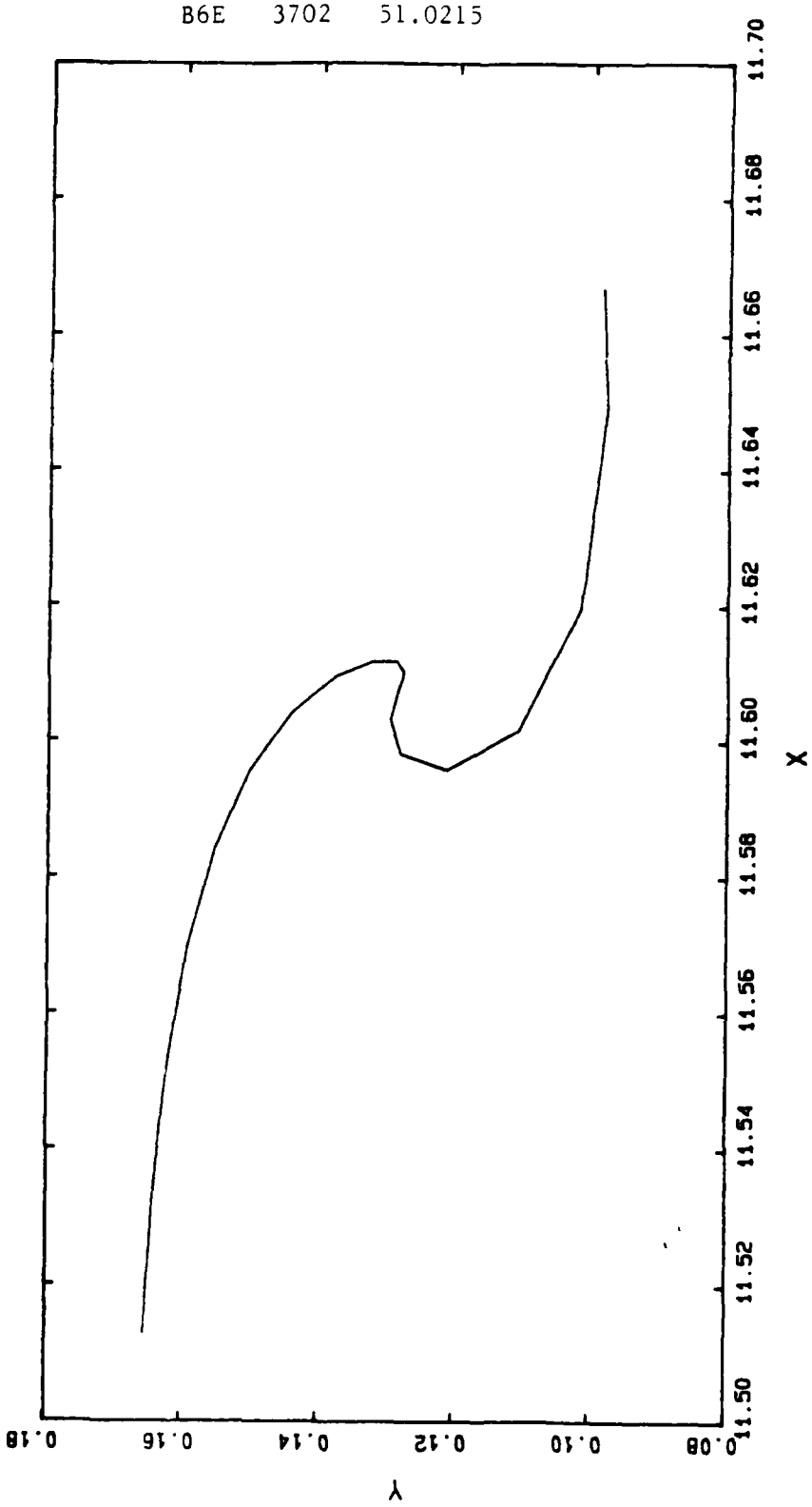

B6E 3752 51.0288

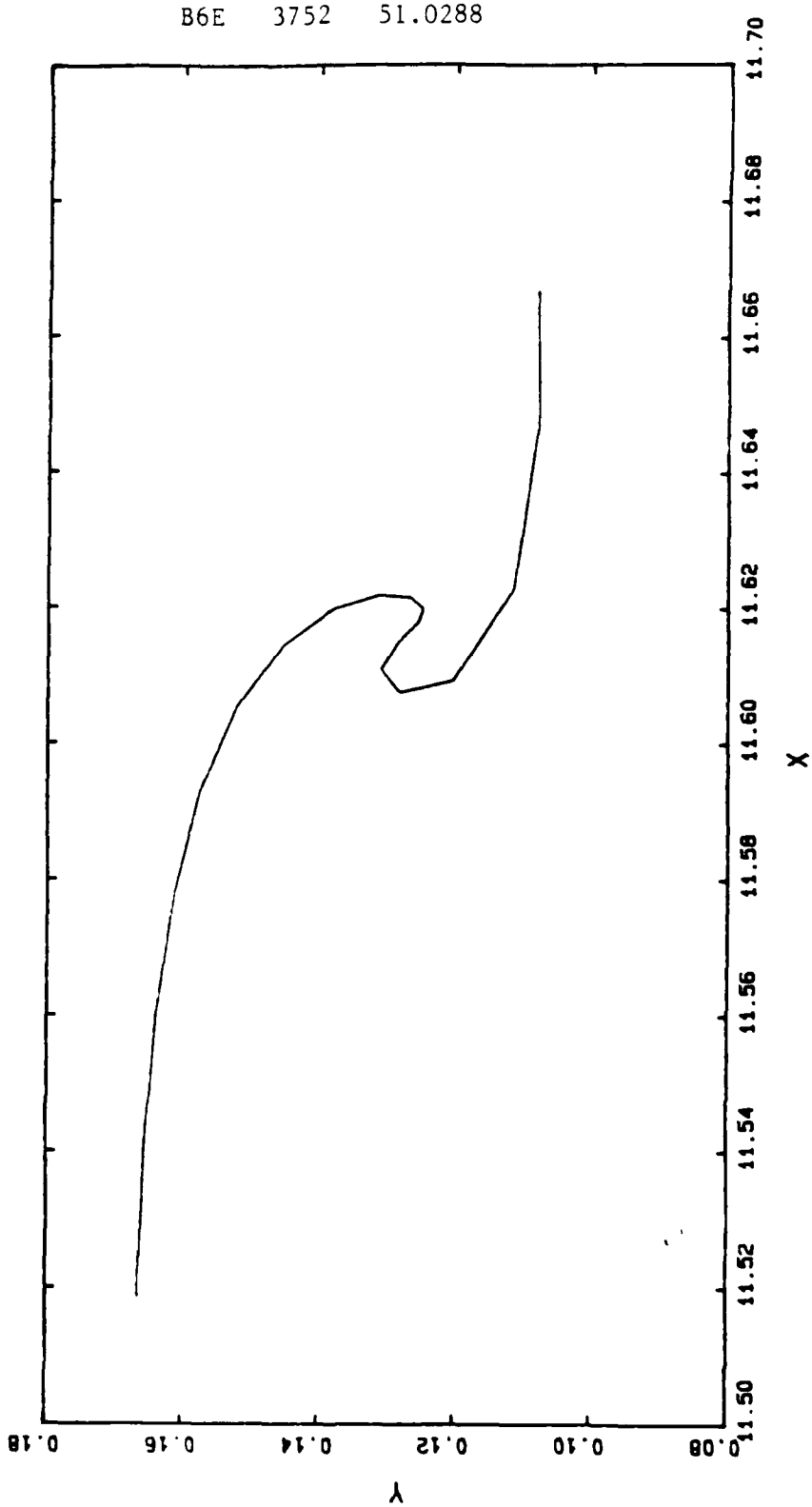

B6E 3772 51.0317

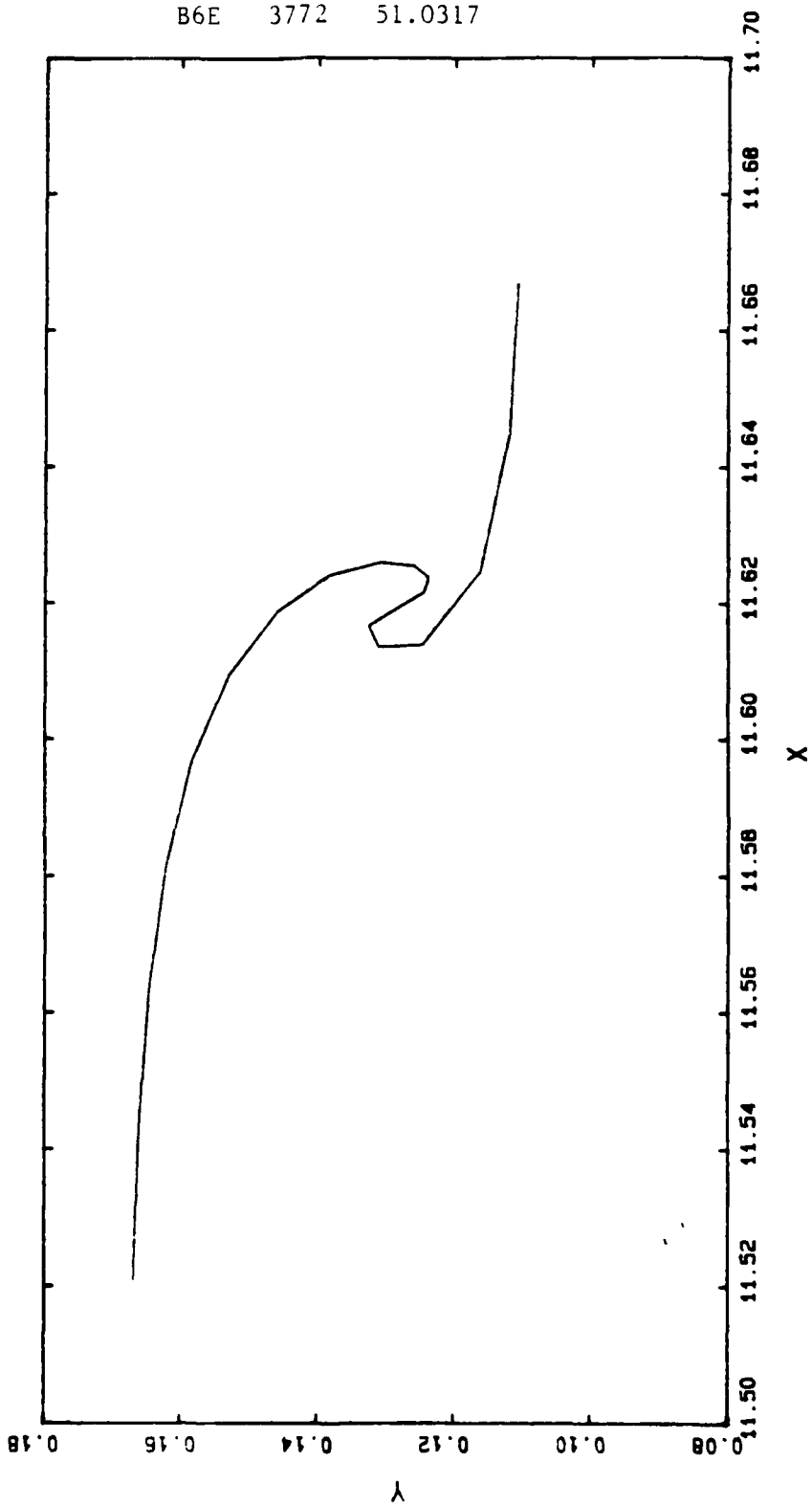

B6E 3792 51.0338

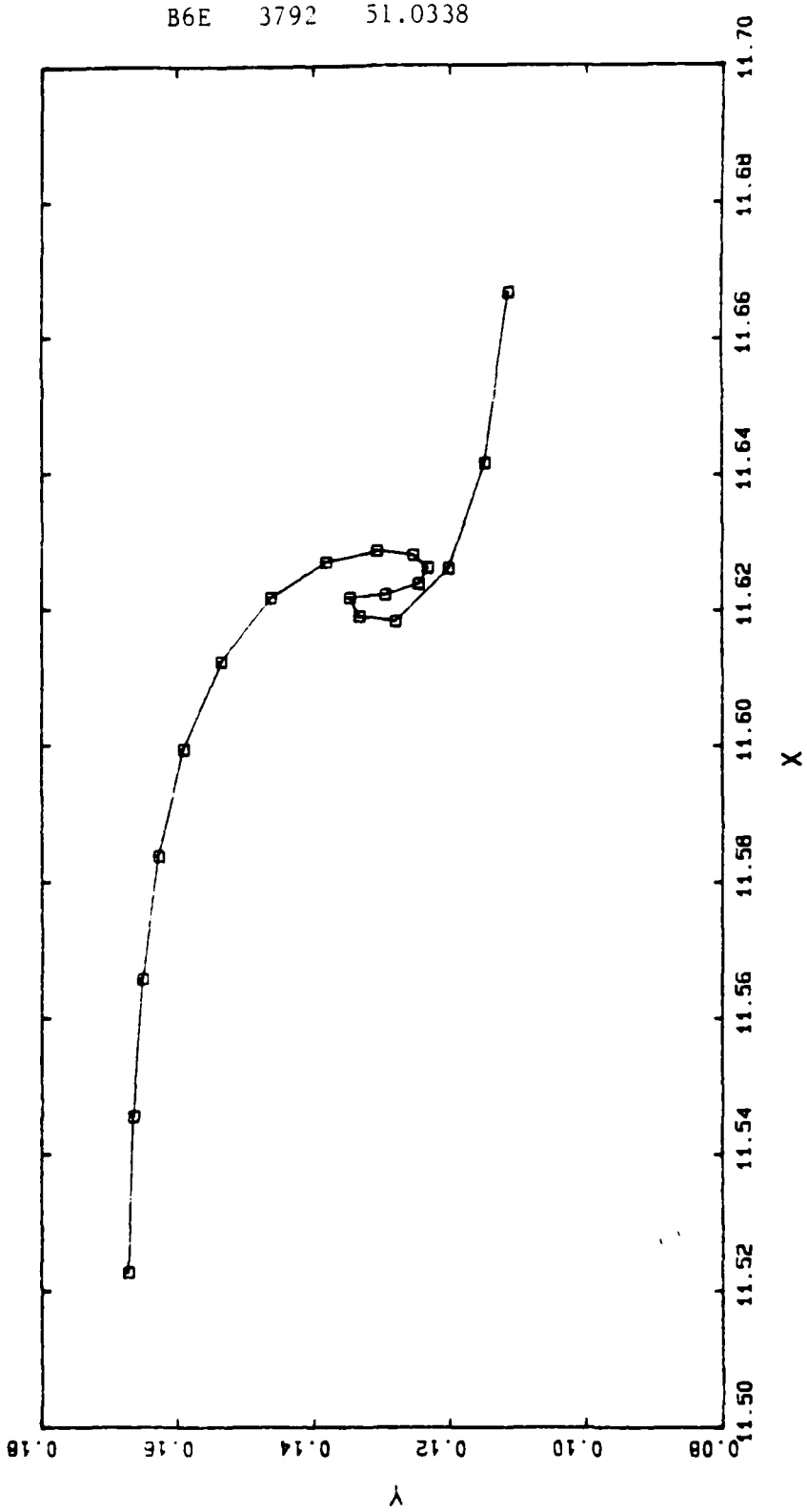

B6E 3792 51.0338

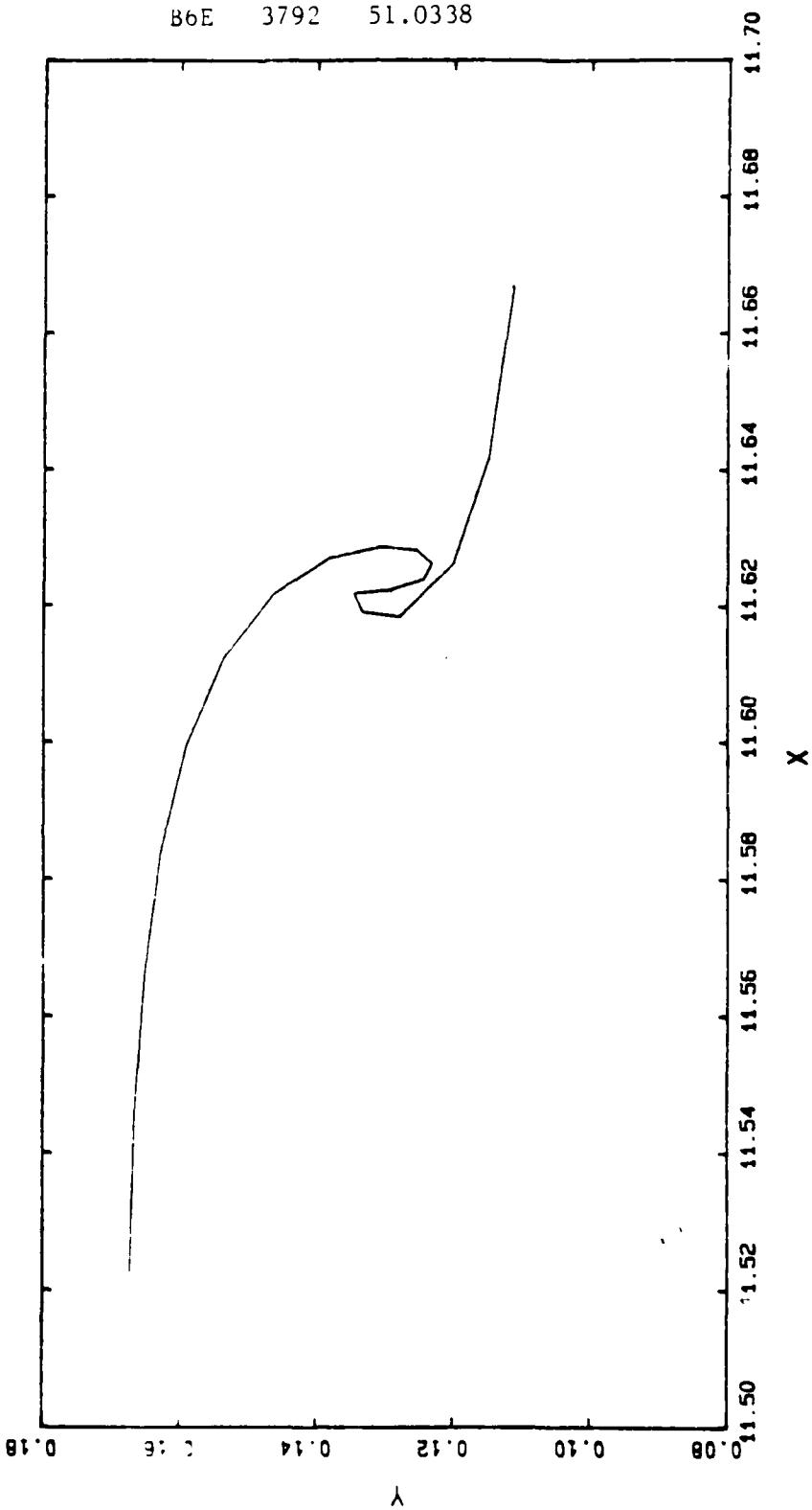

B6E 3802 51.0348

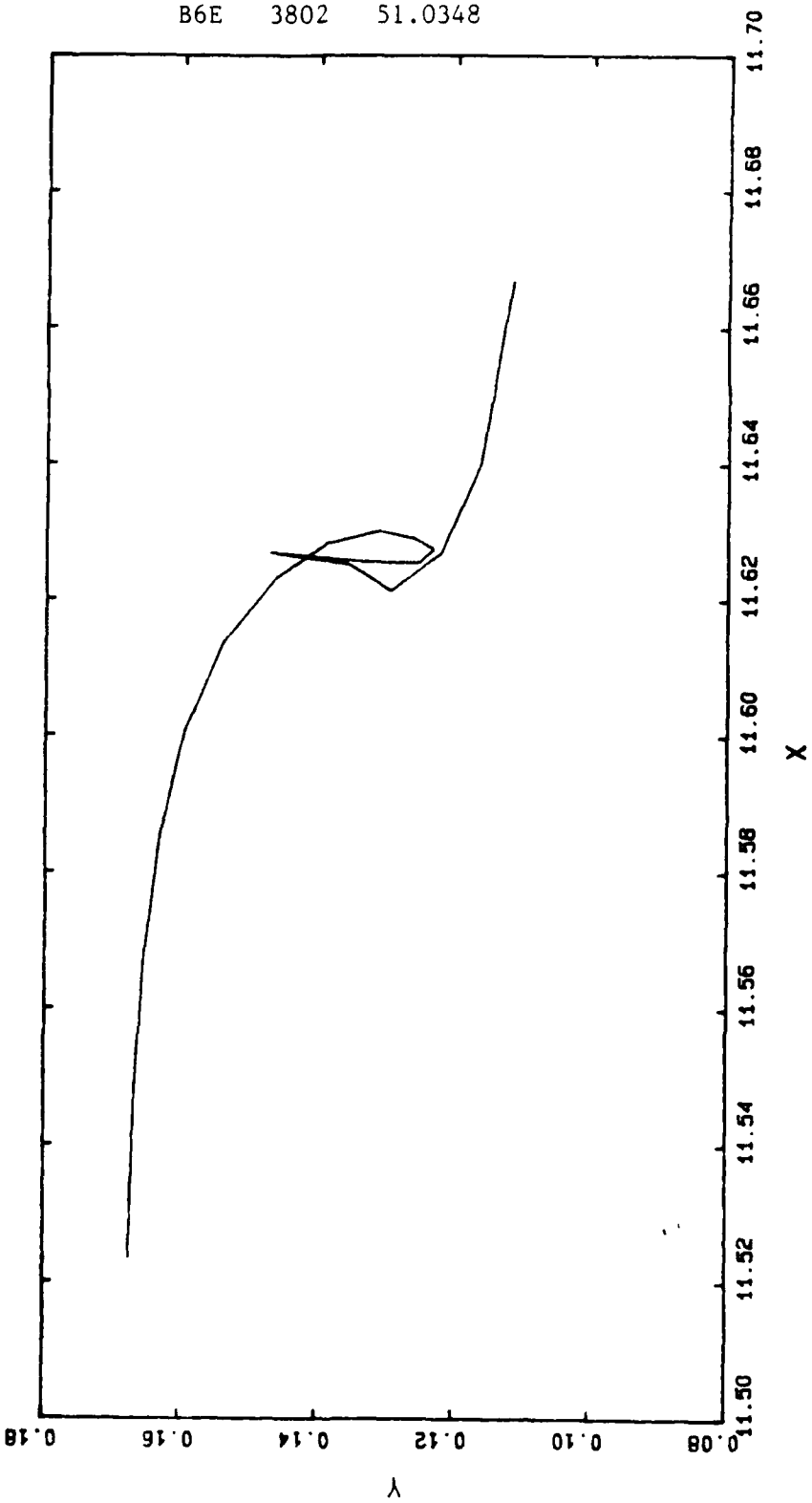

B6F 3562 50.9487

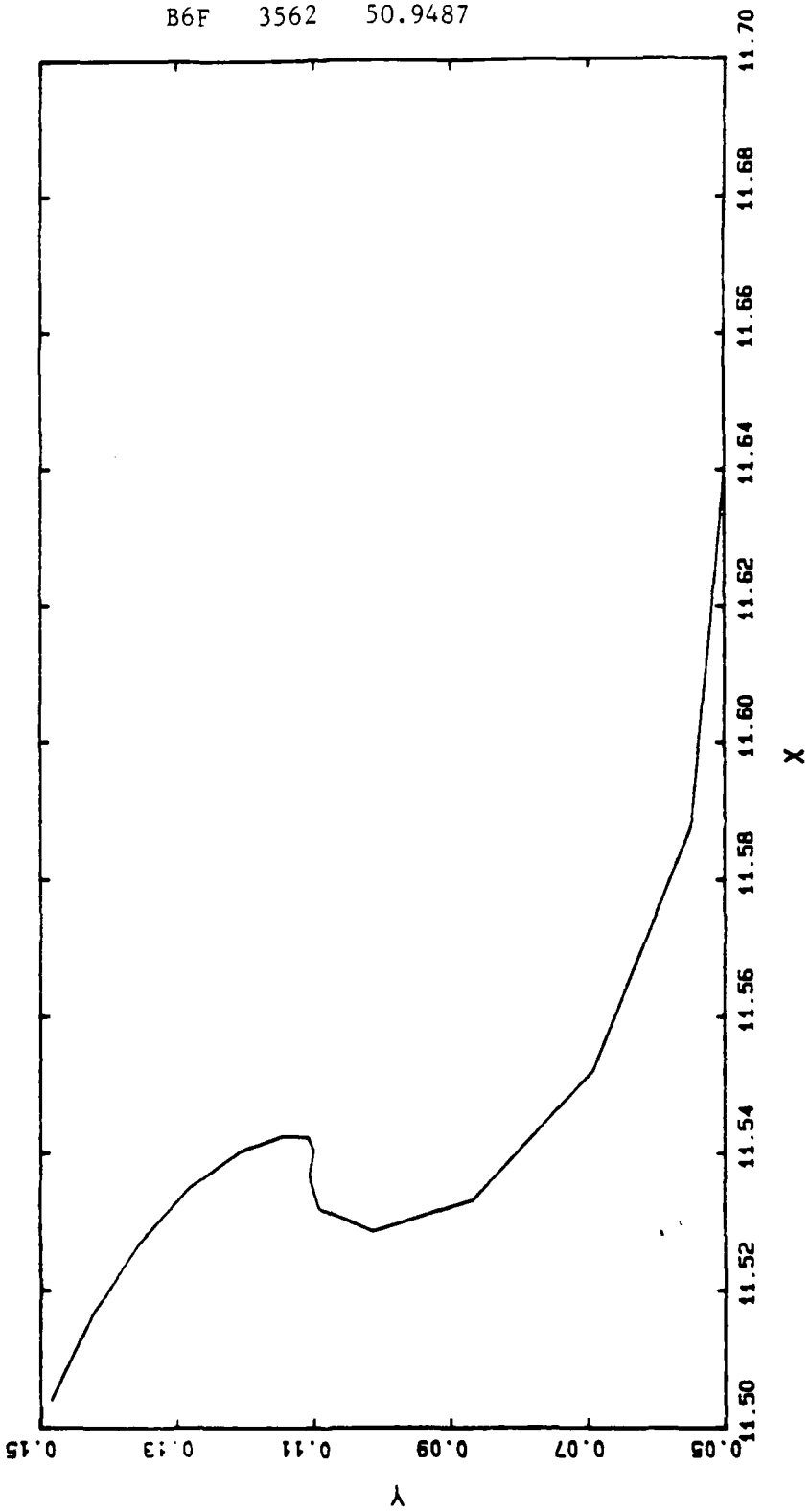

B6F 3612 50.9556

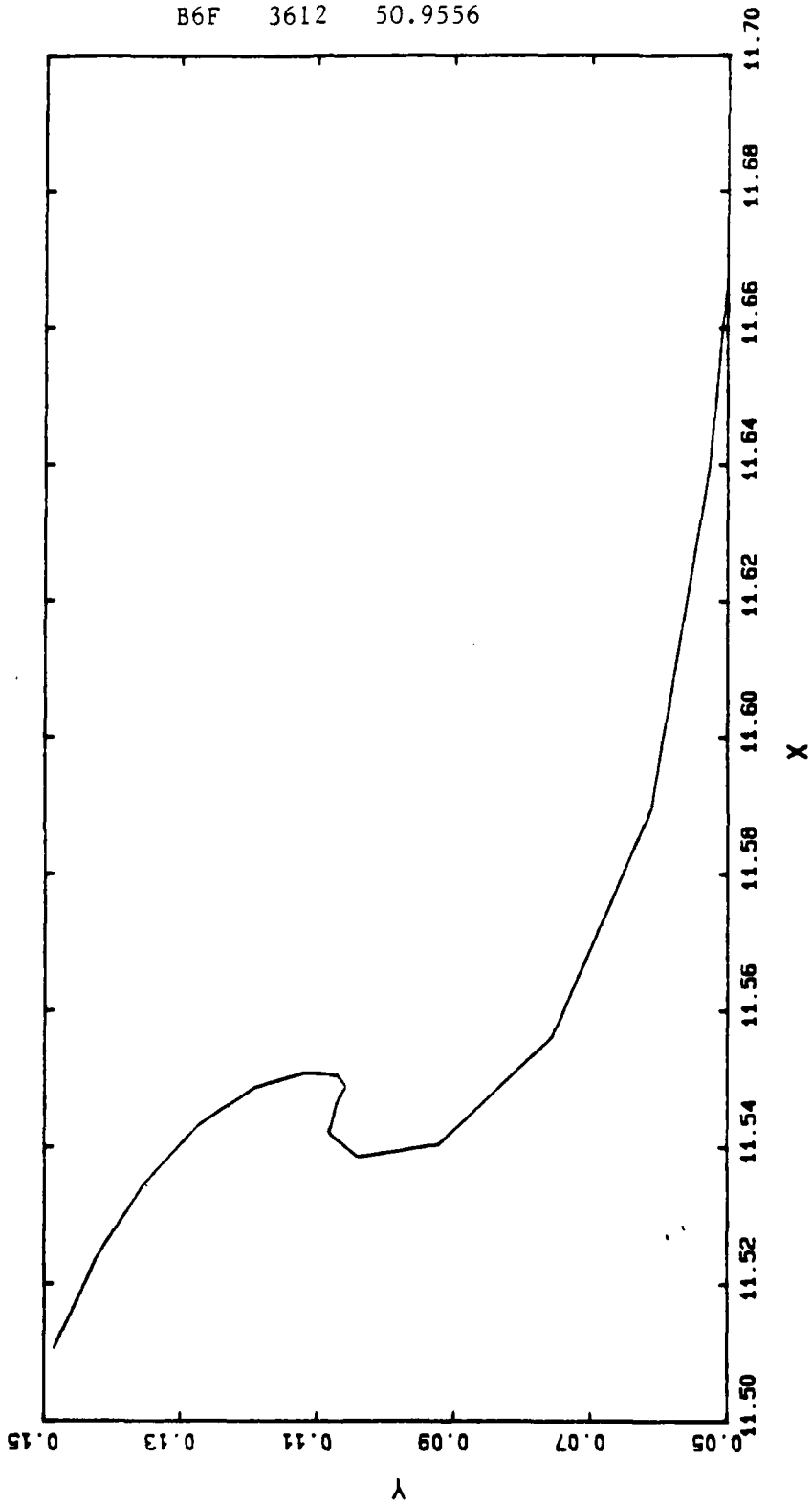

B6F 3632 50.9587

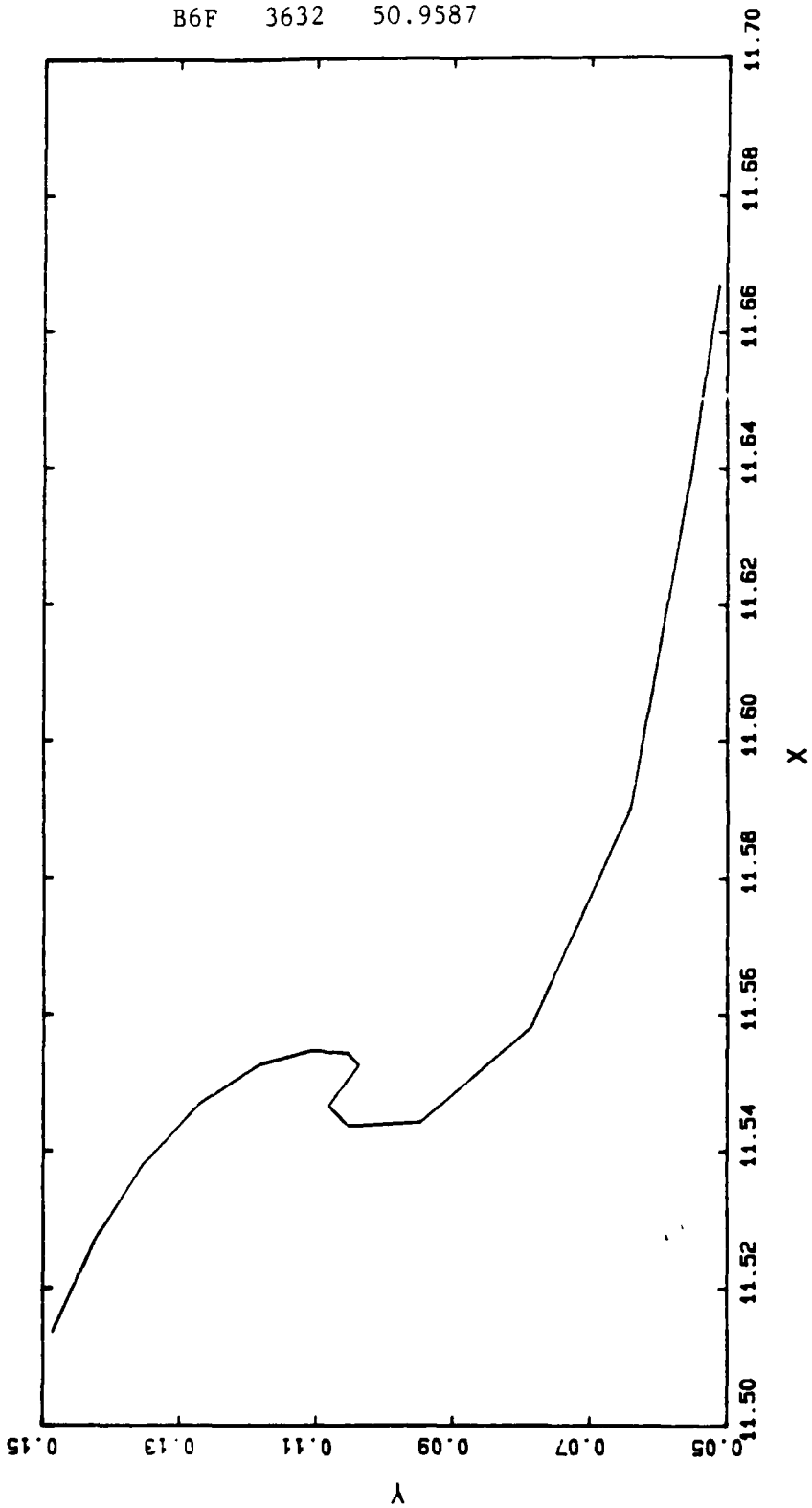

B6F 3632 50.9615

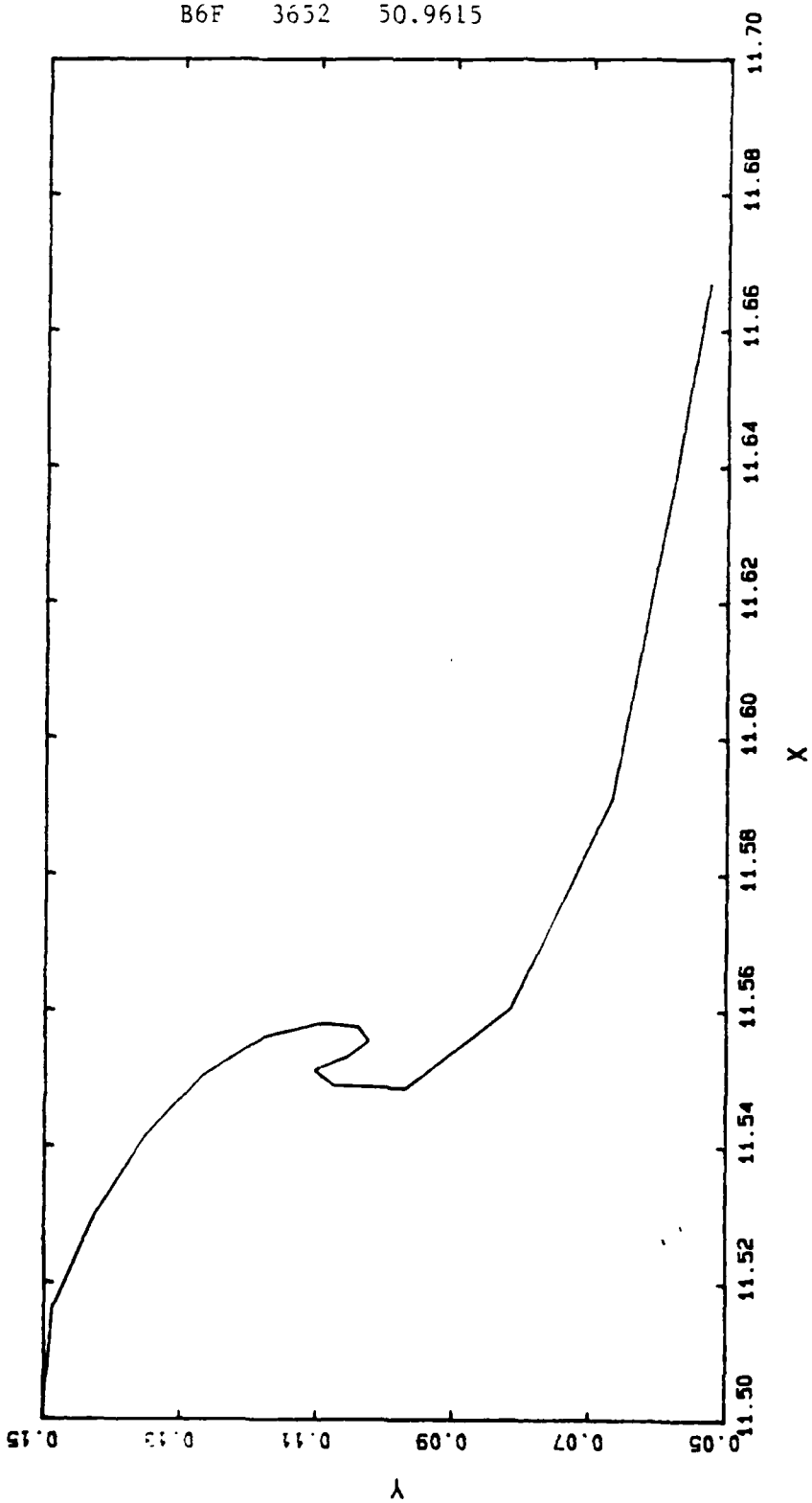

B6F 3662 50.9625

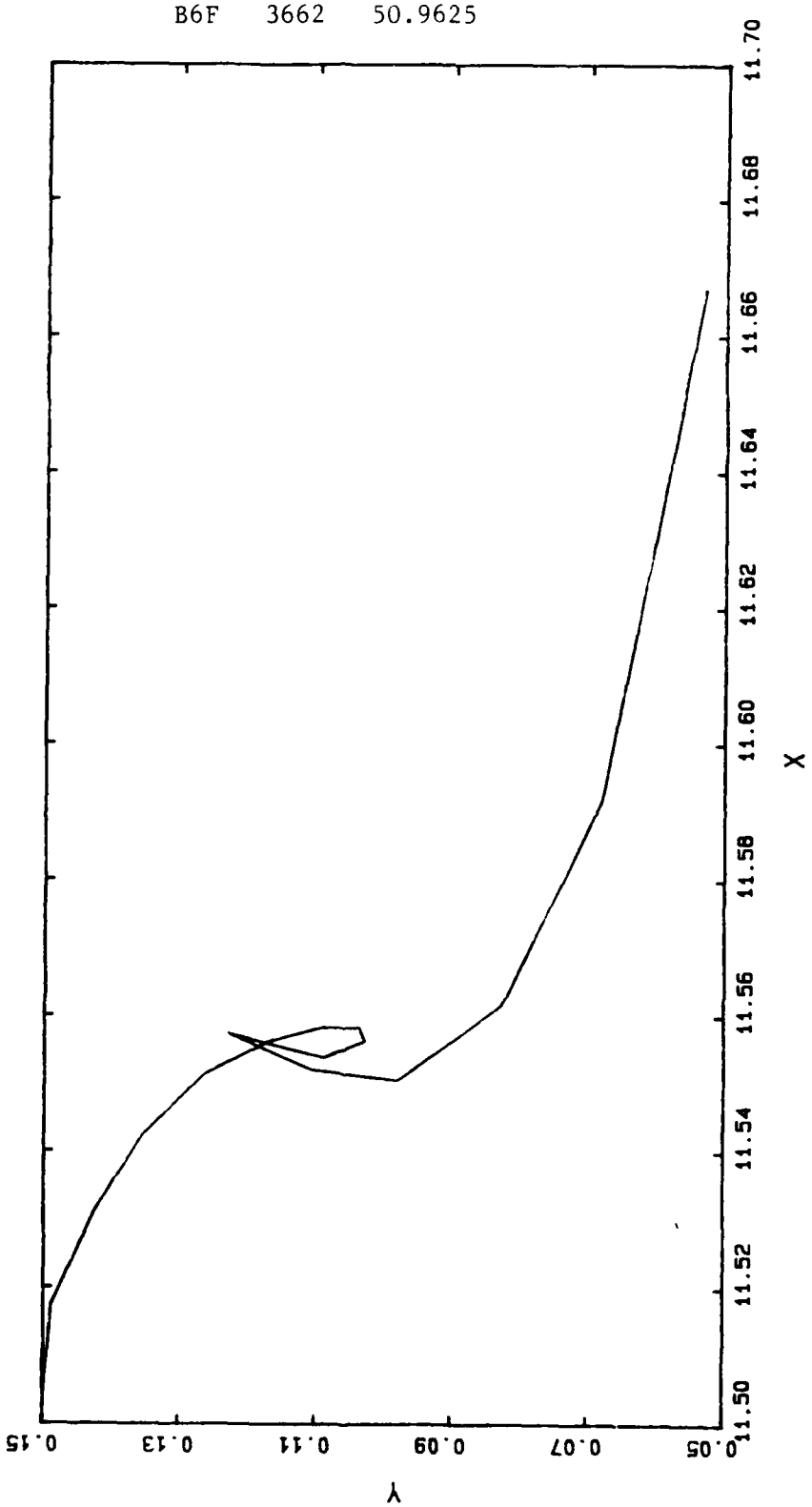

Appendix C

Refer to Chapter 5 for discussion.

C1 3182 50.8486

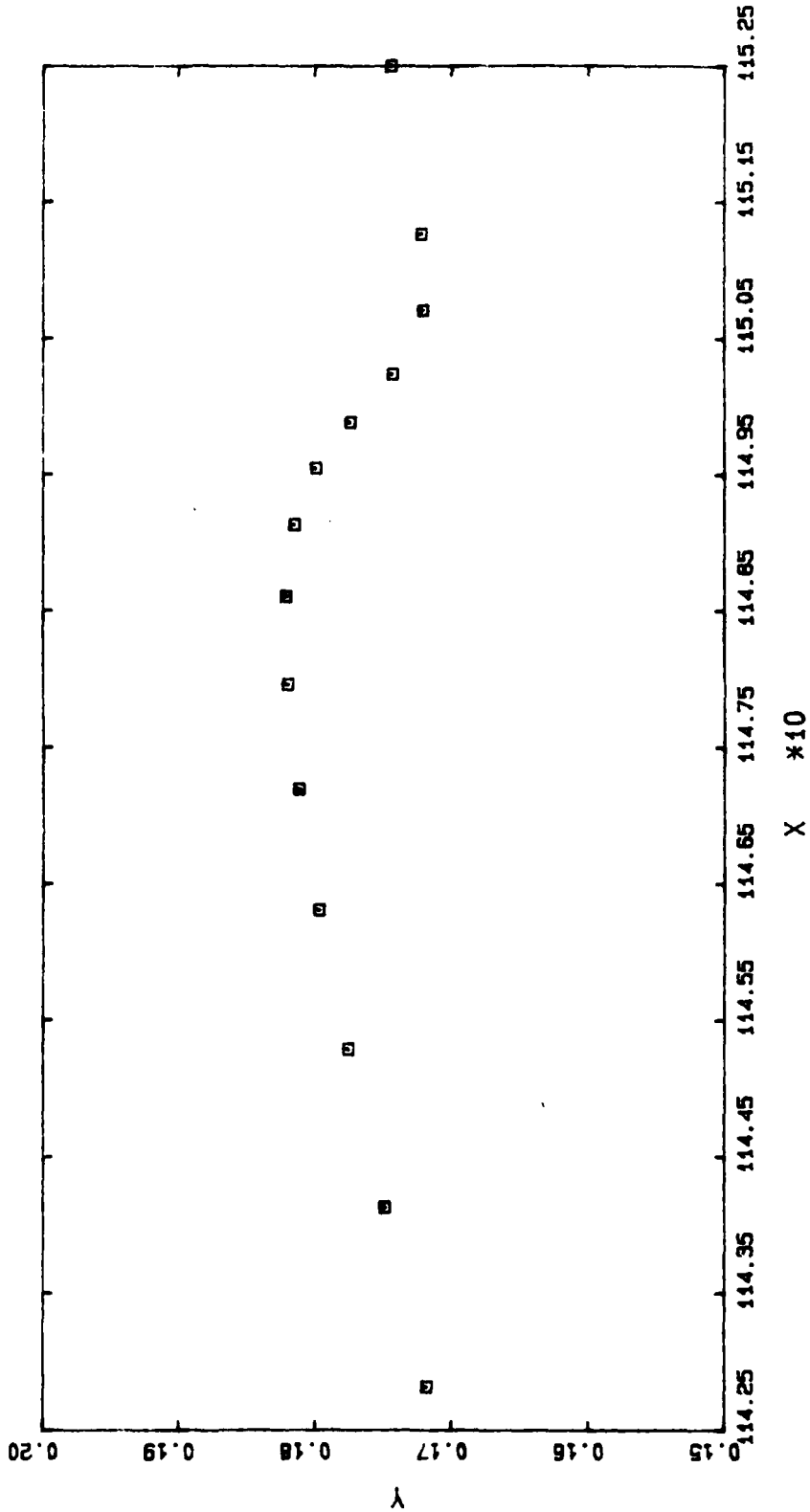

C1 3202 50.8527

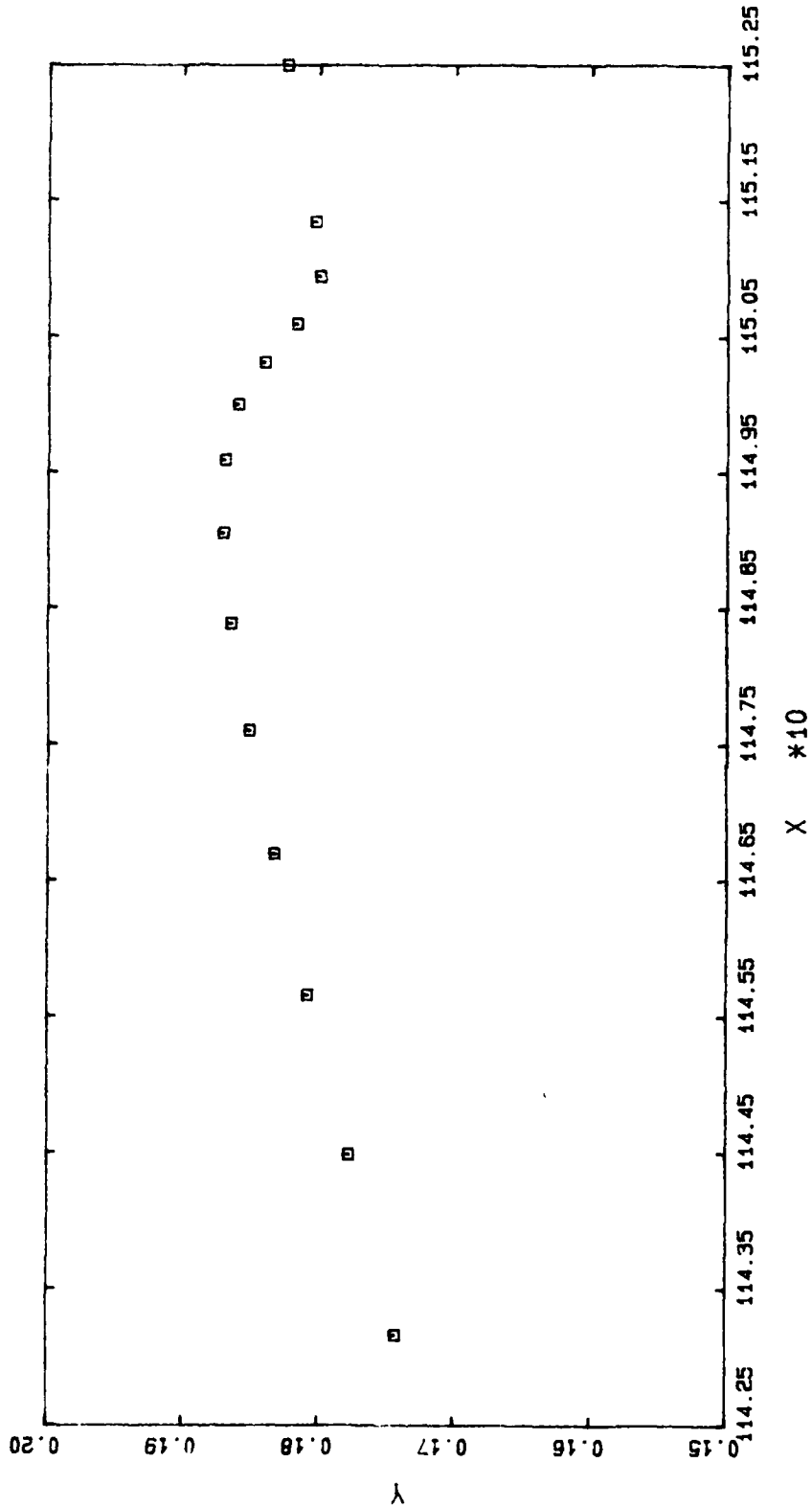

C1 3222 50.8558

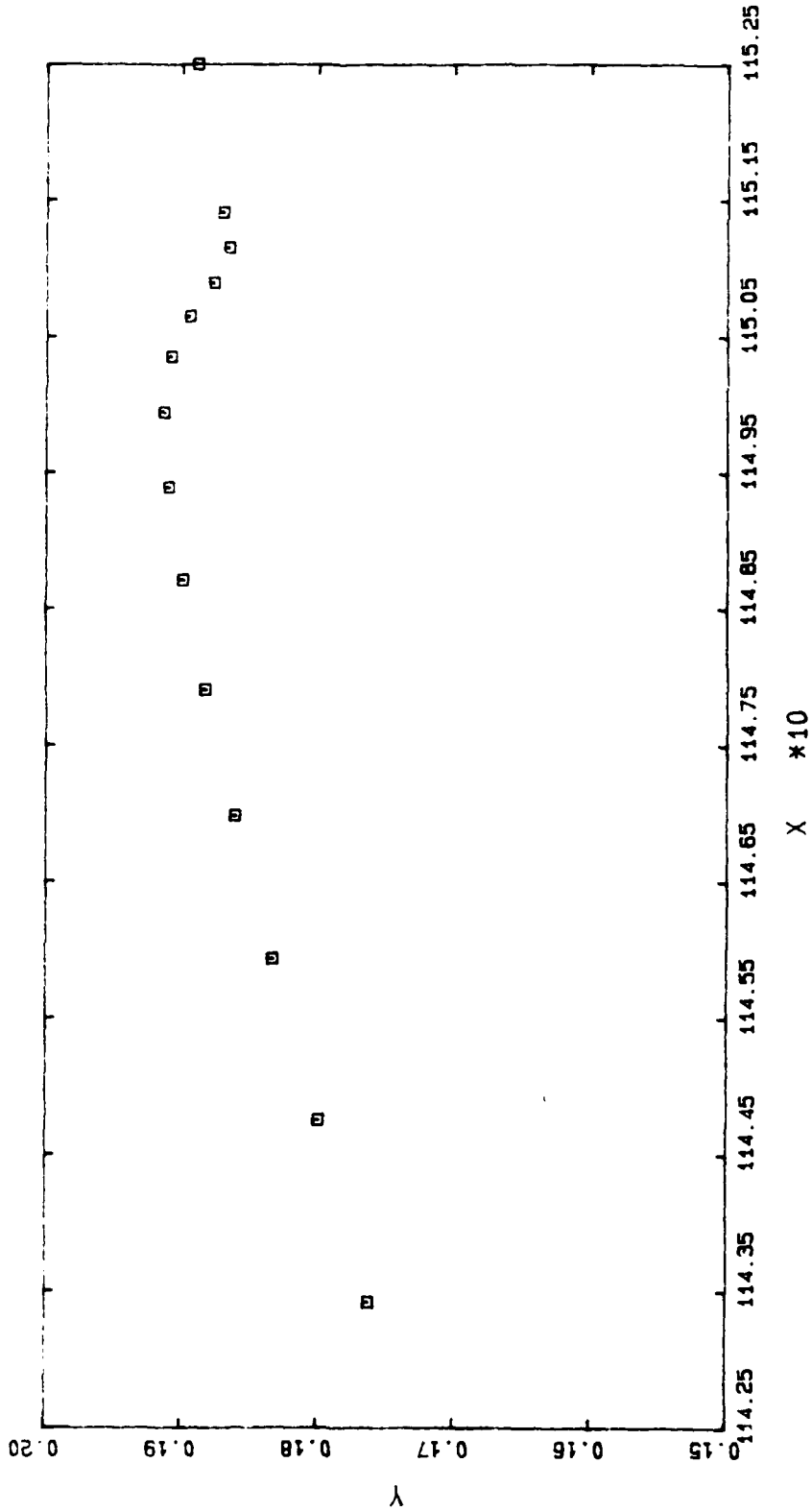

C1 3242 50.8578

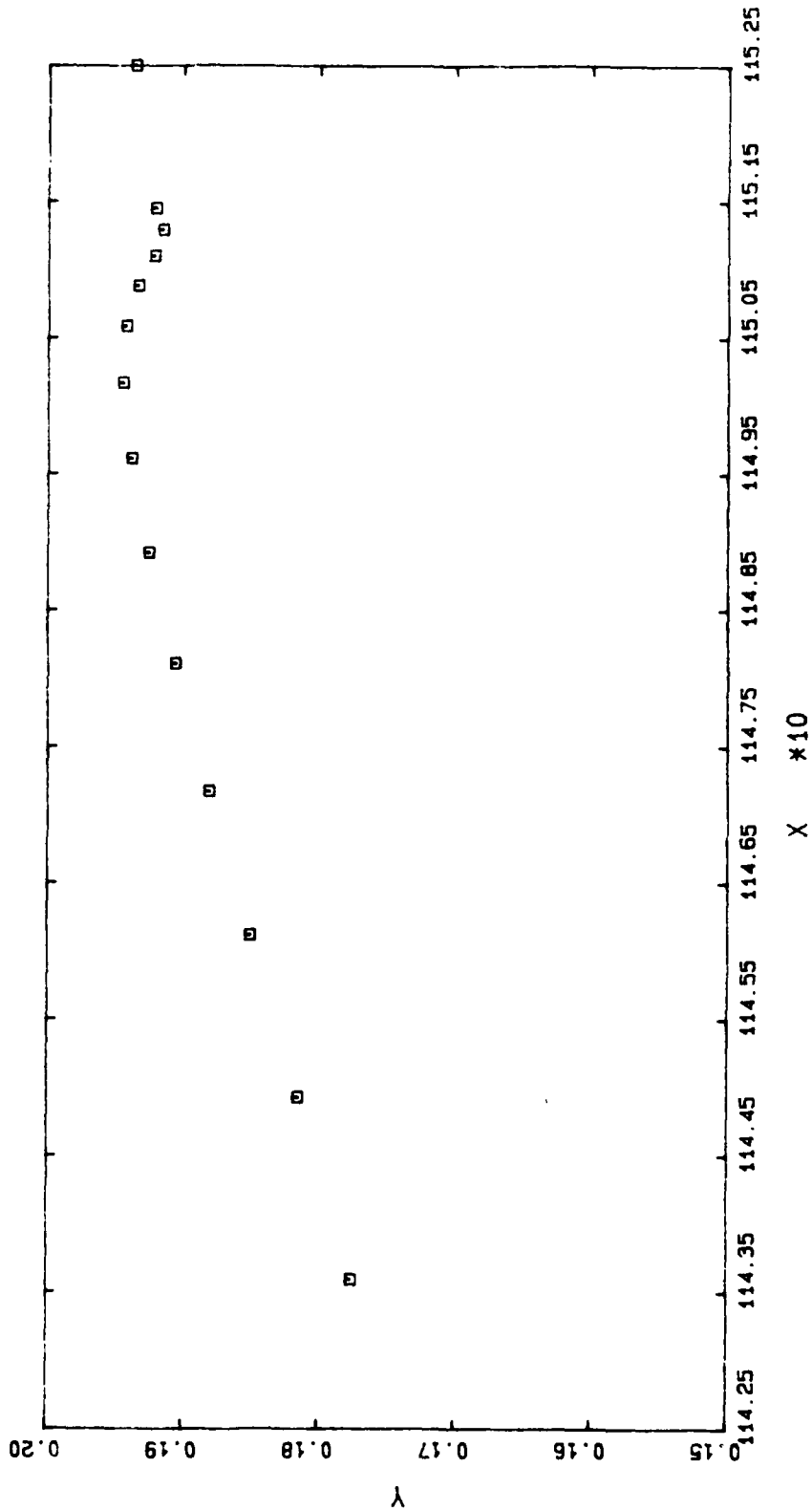

C1 3262 50.8598

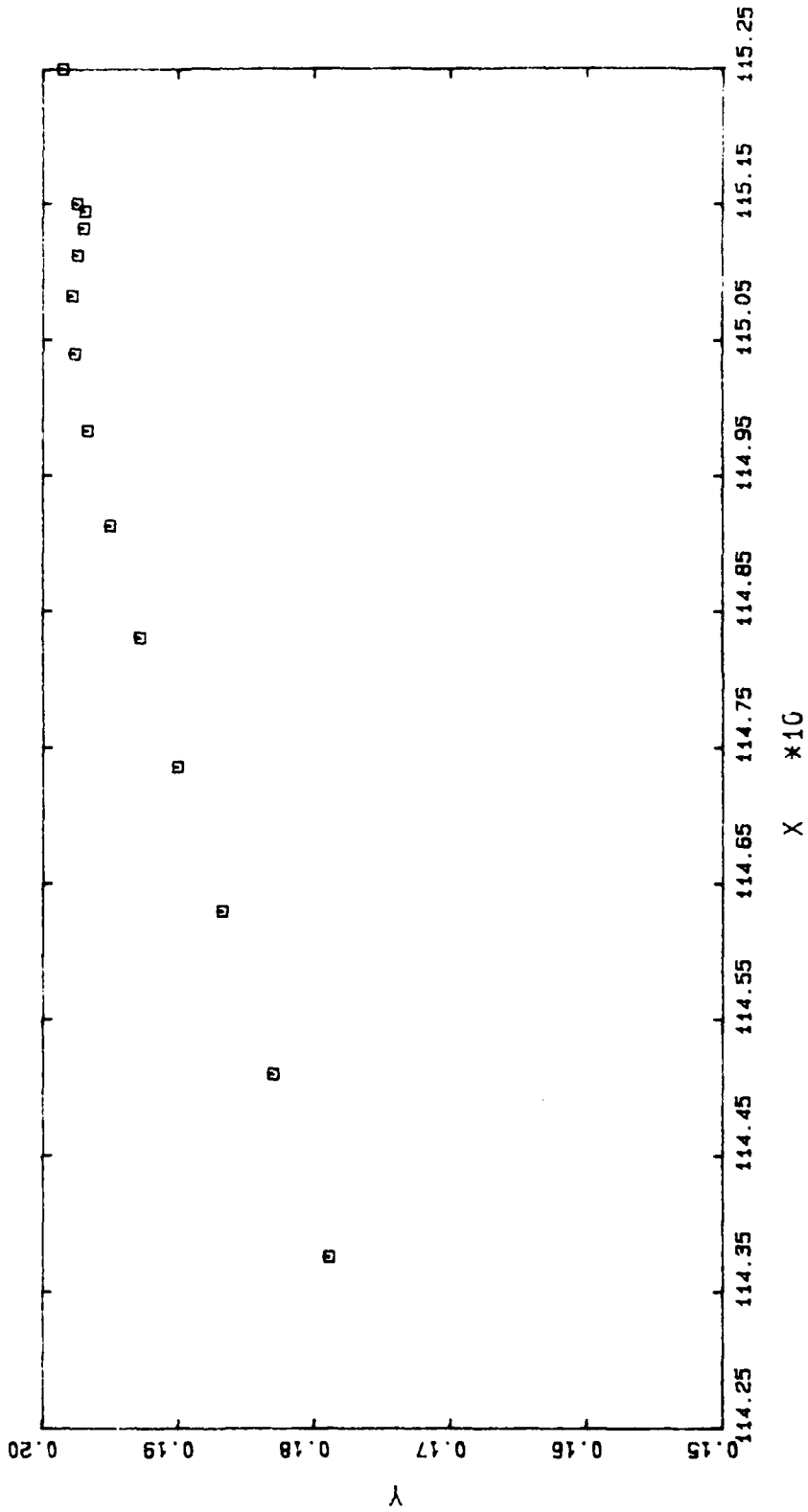

C1 3282 50.8618

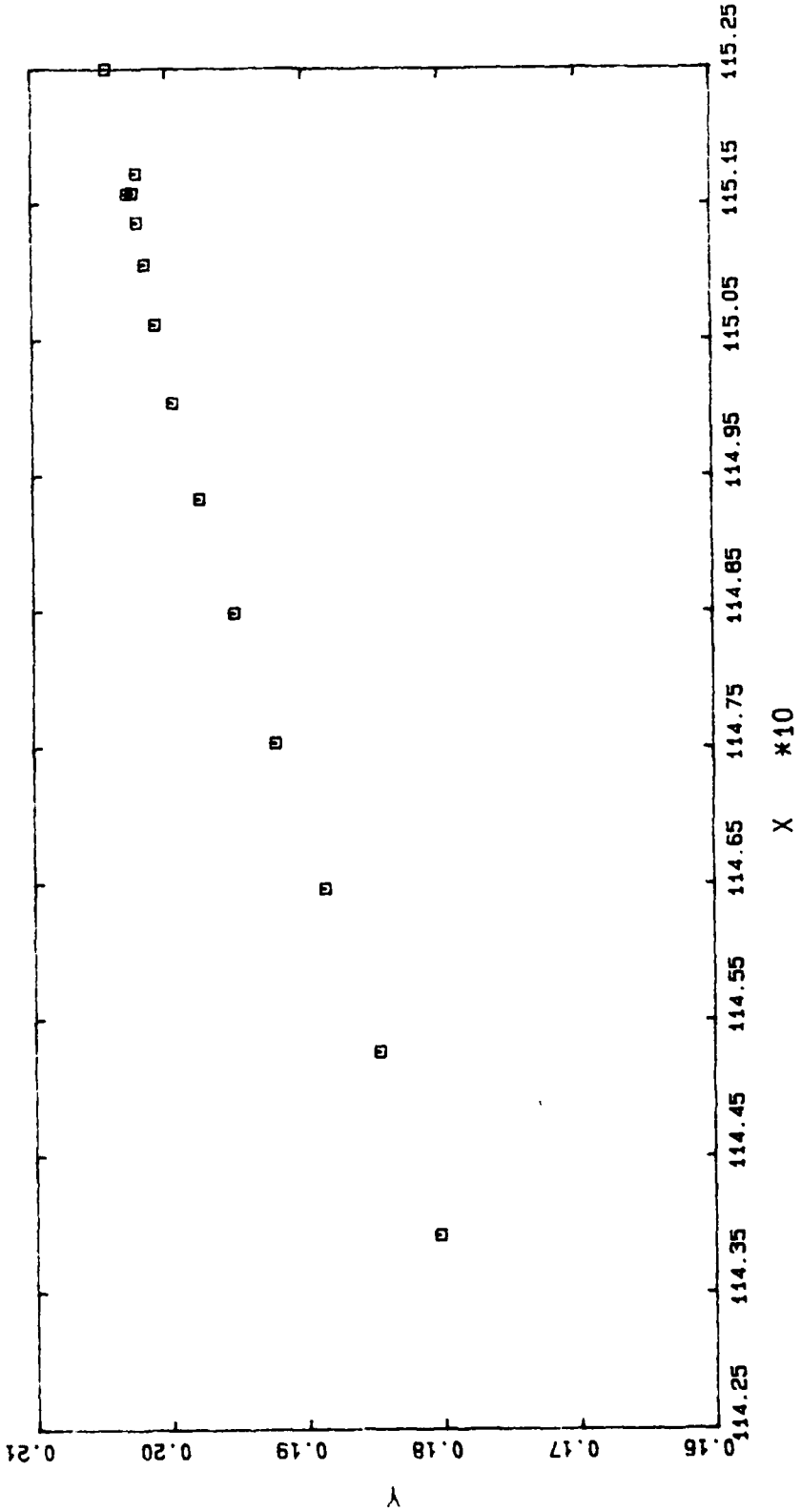

C2 3250 50.8860

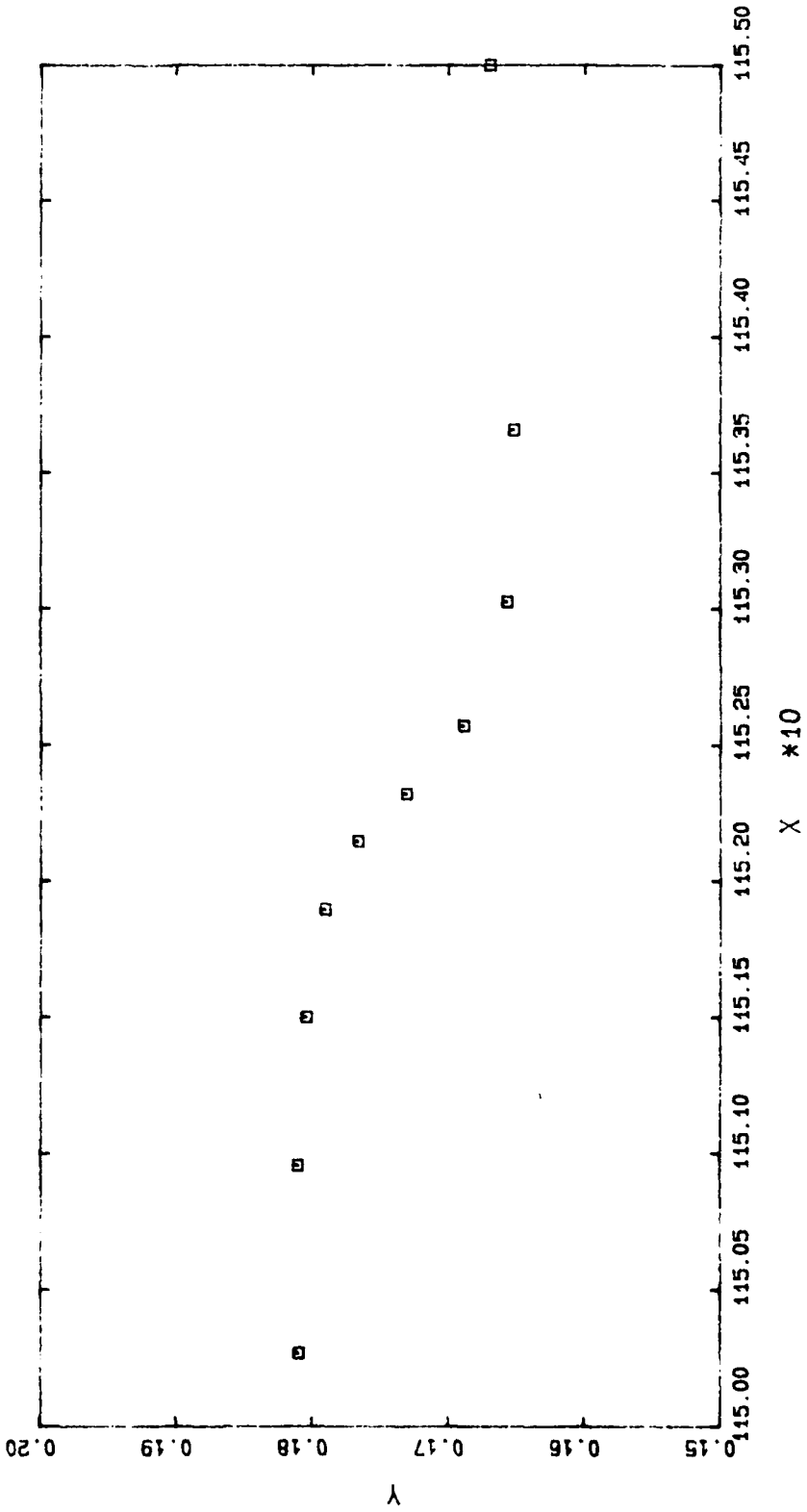

C2 3270 50.8894

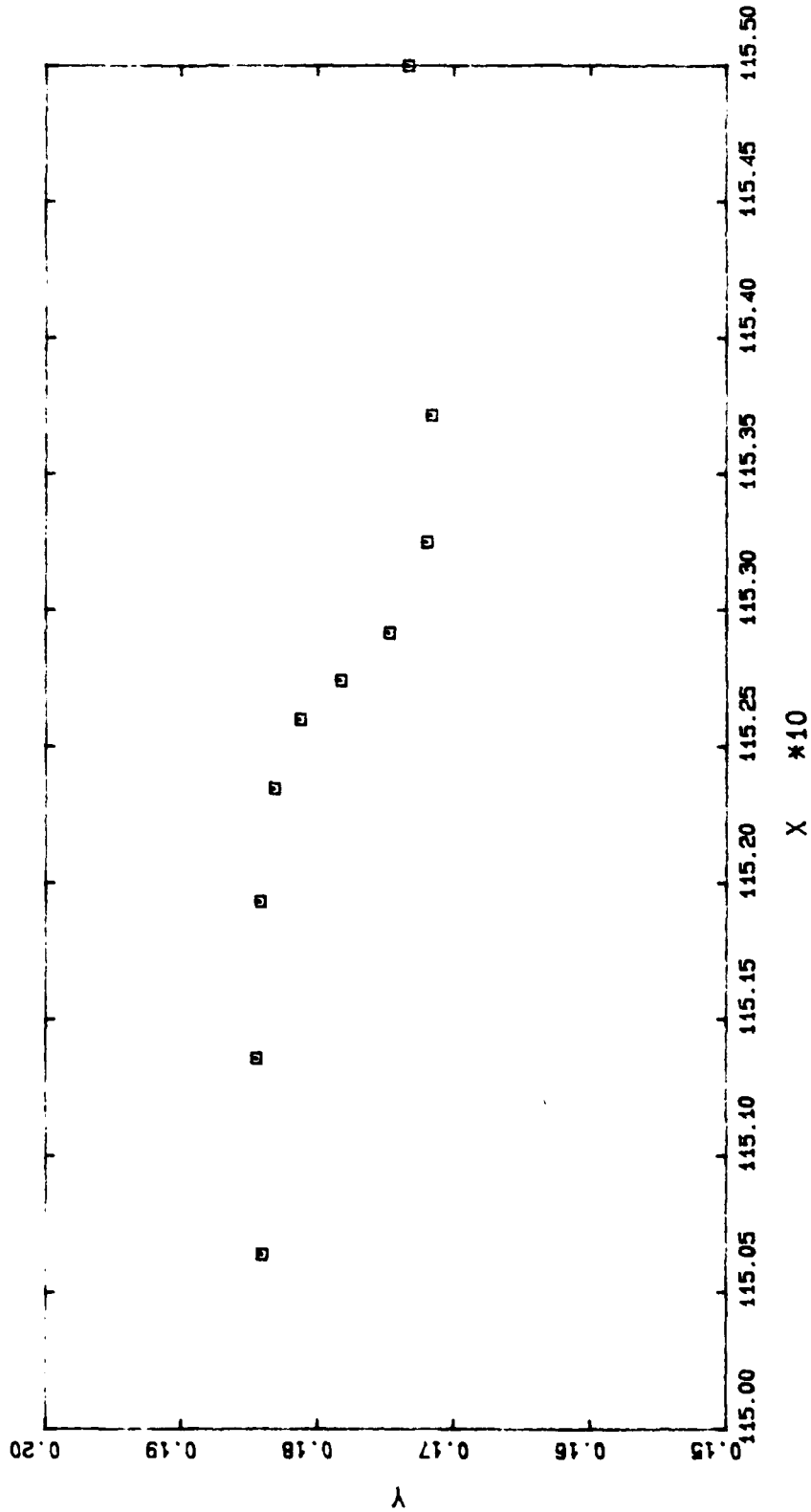

C2 3290 50.8922

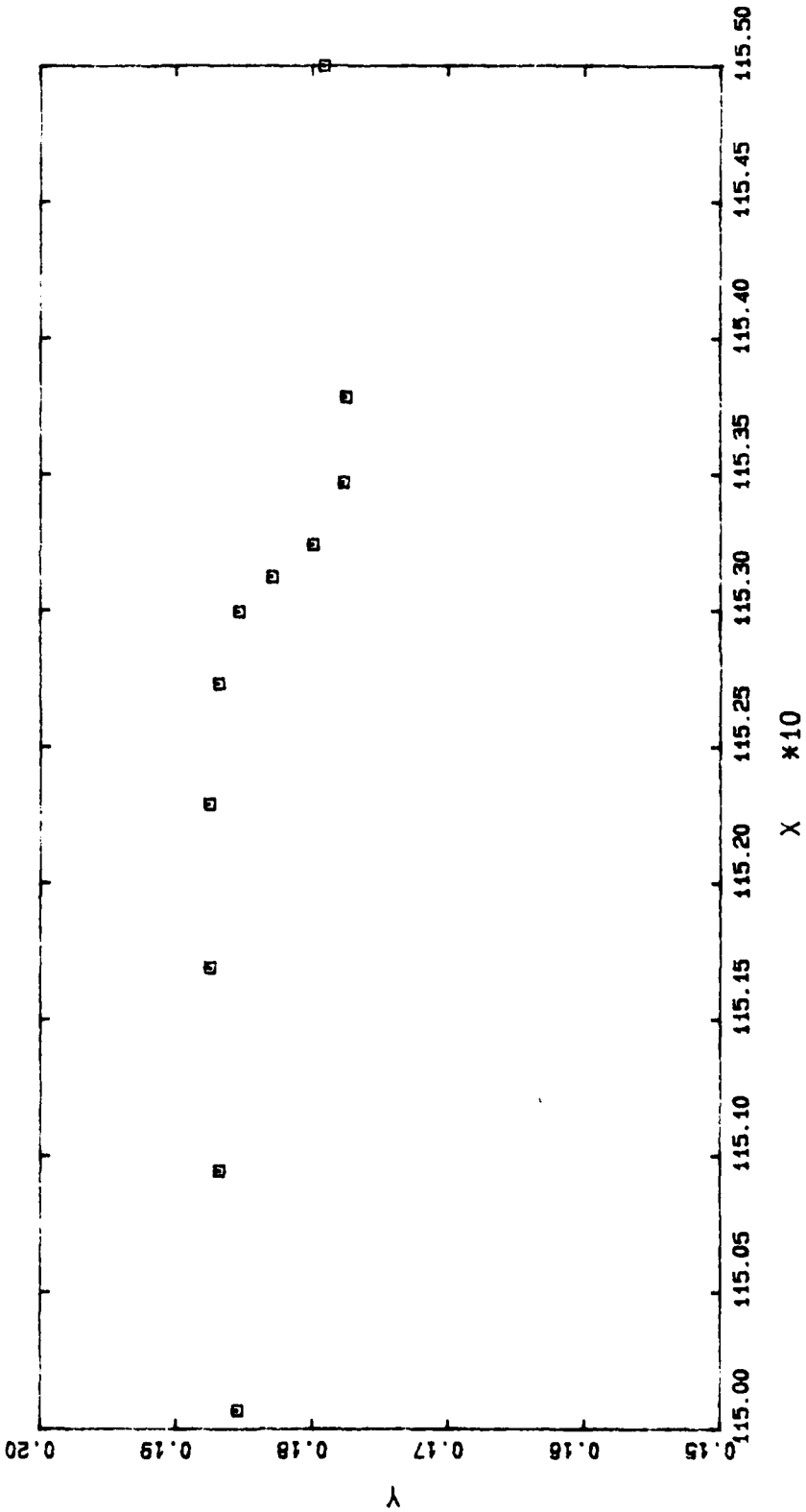

C2 3310 50.8944

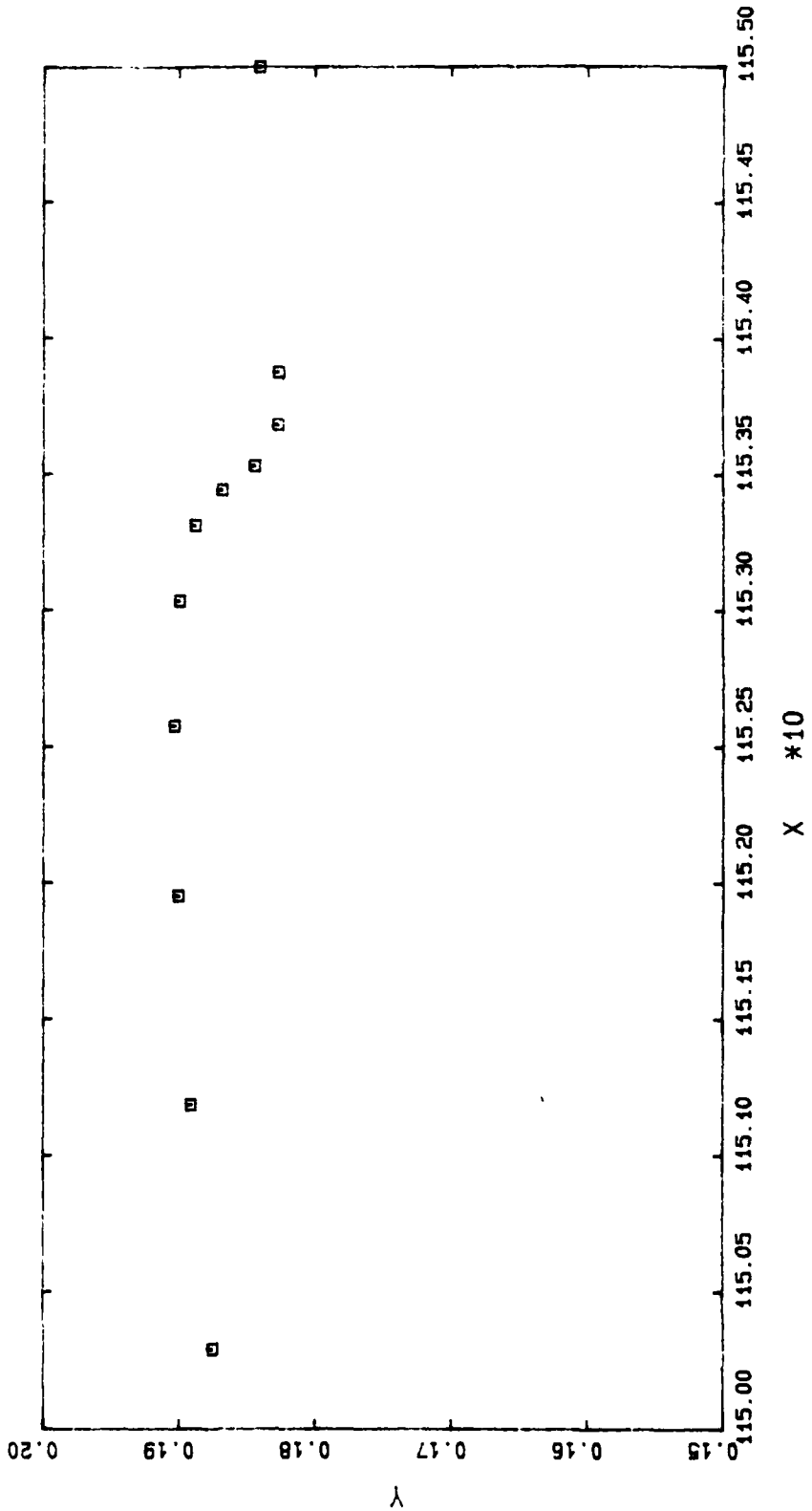

C2 3330 50.8964

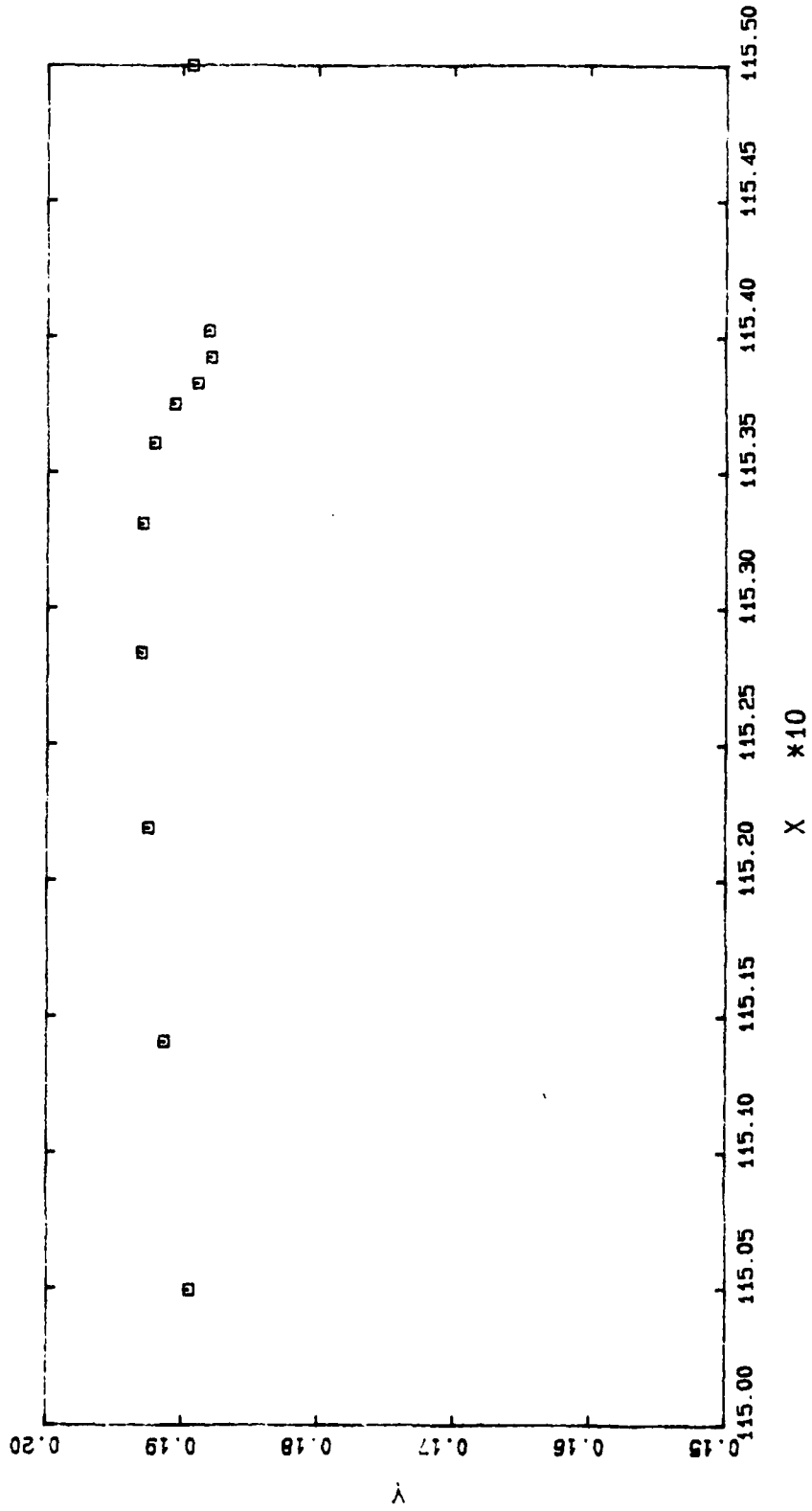

C2 3340 50.8974

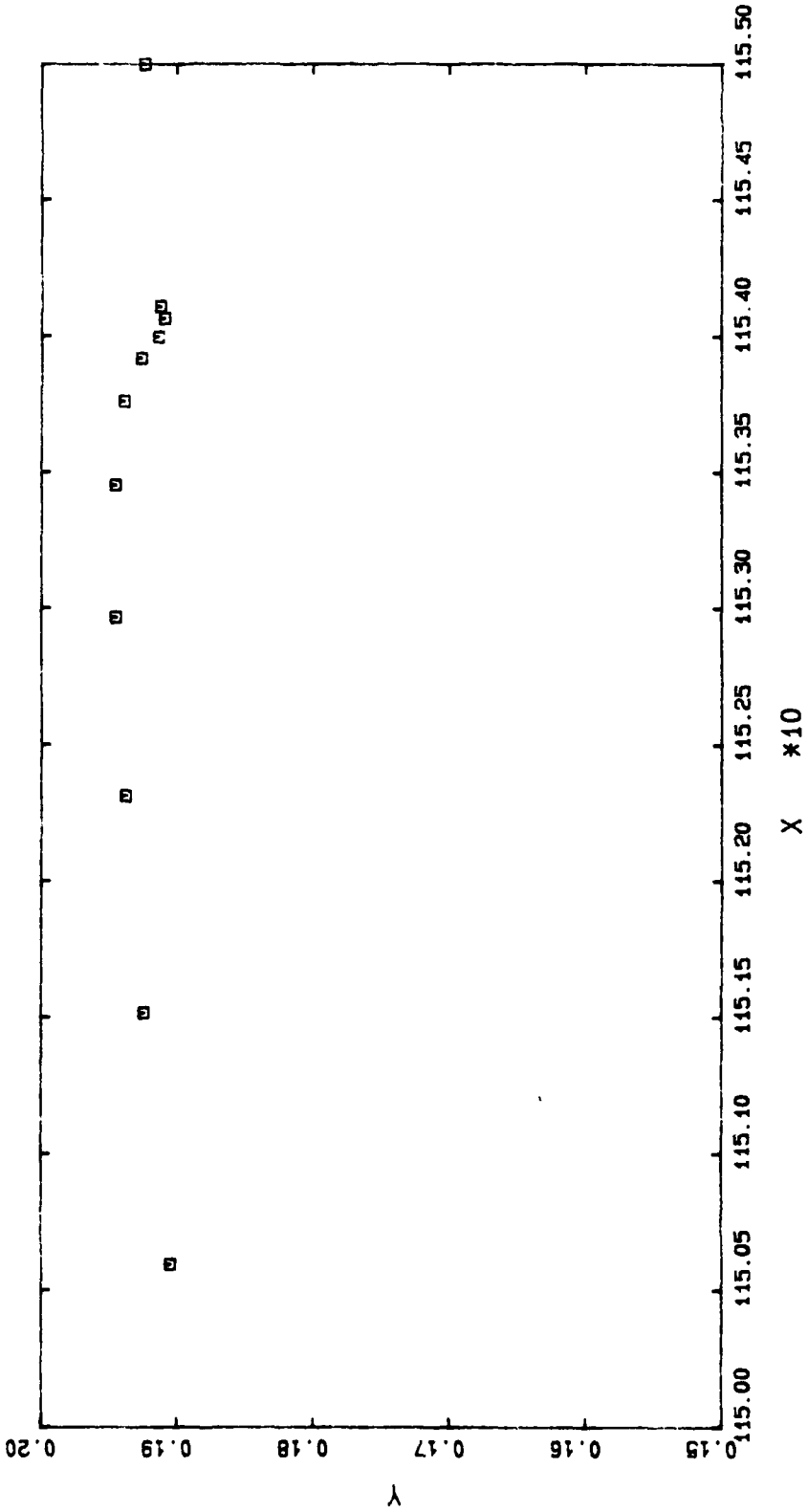

C3 3425 50.9430

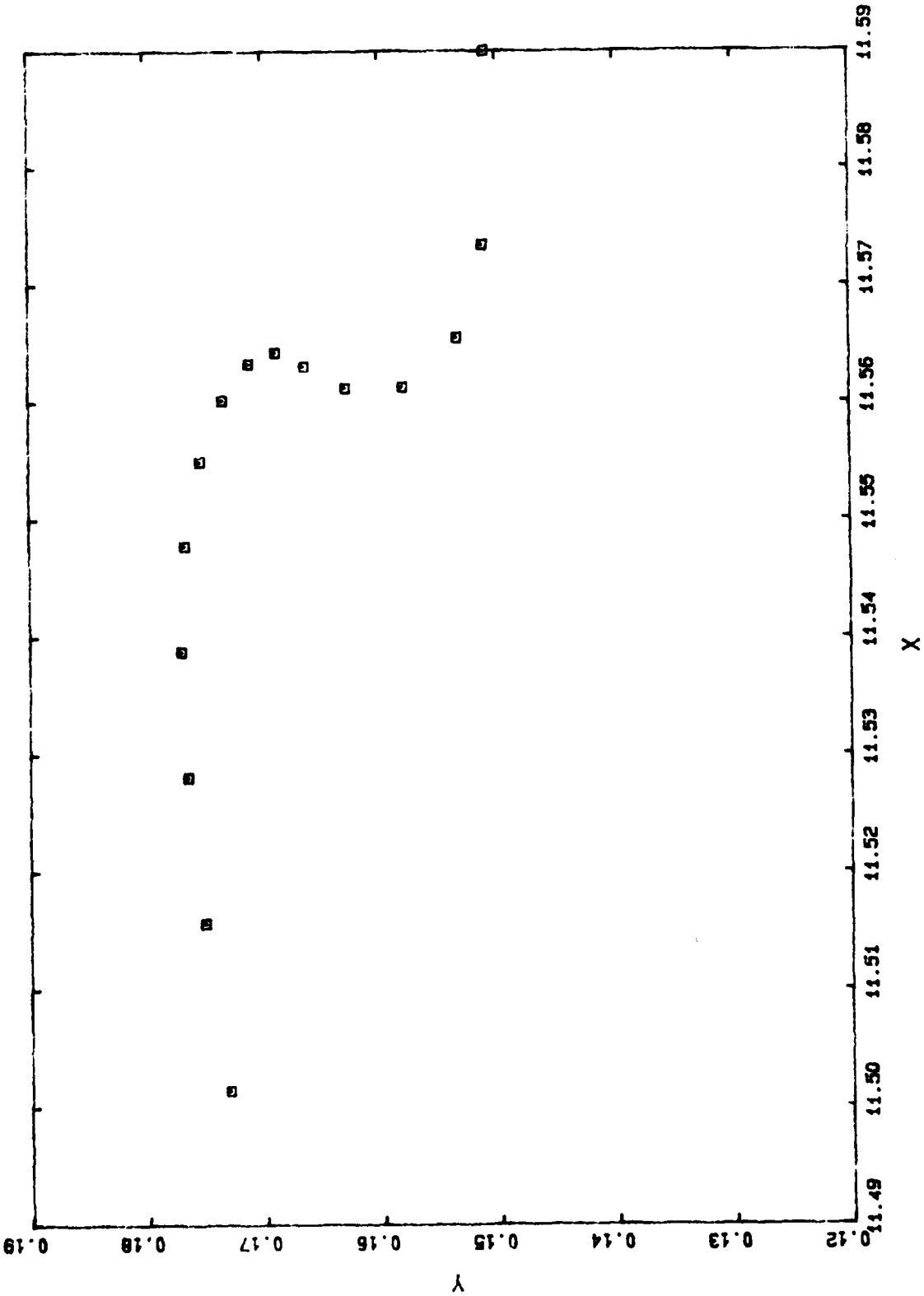

C3 3445 50.9452

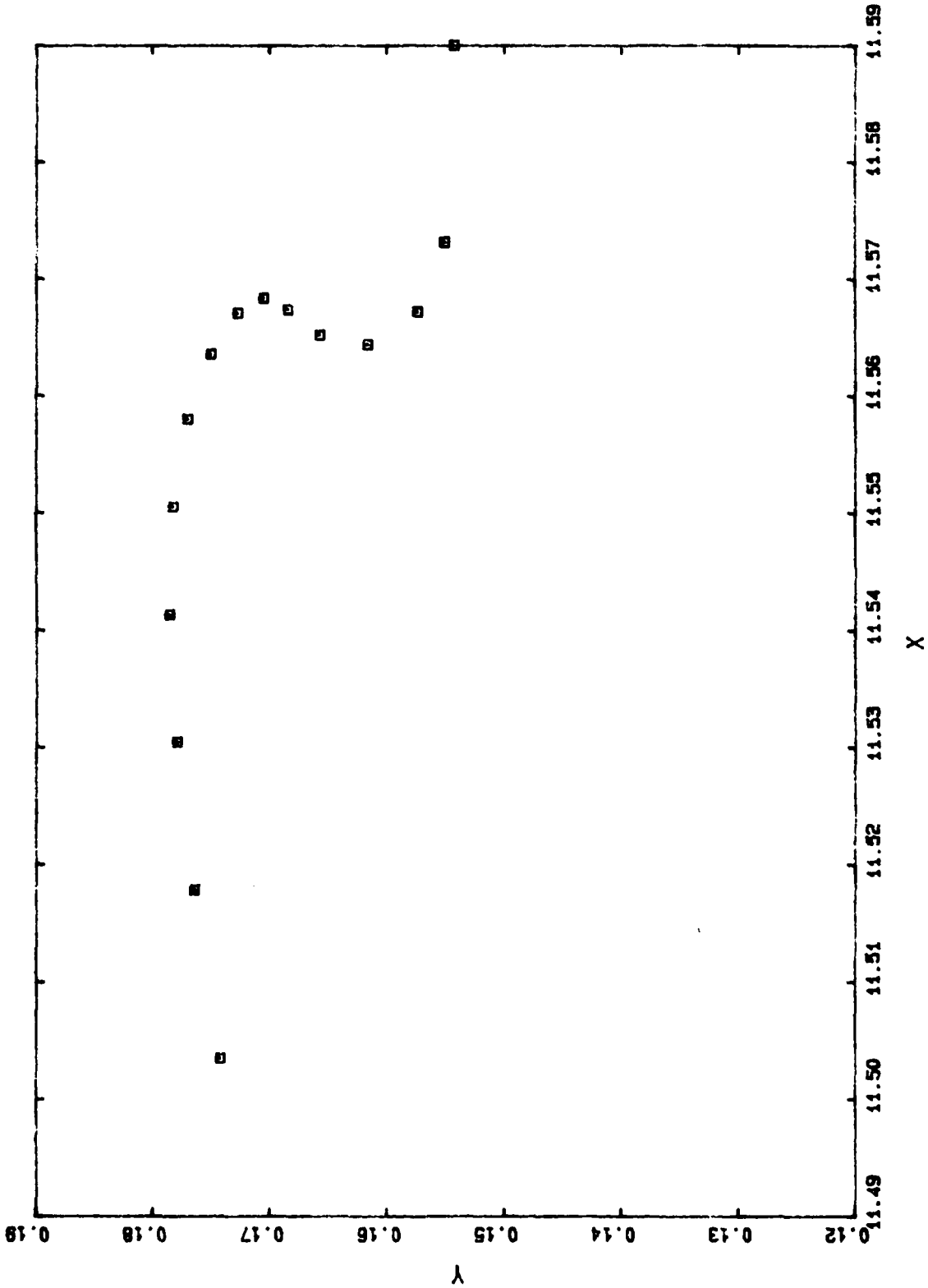

C3 3465 50.9472

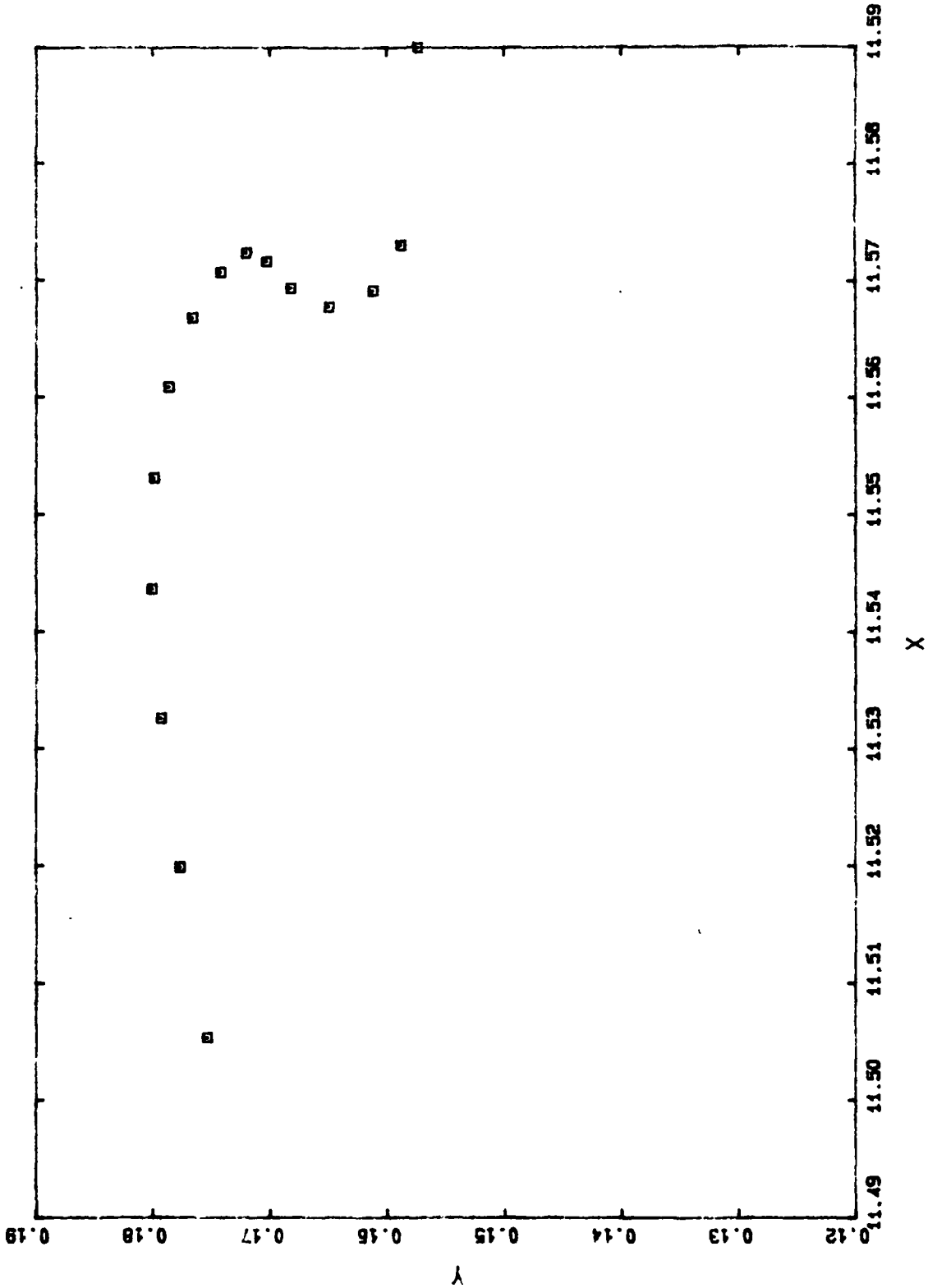

C3 3485 50.9492

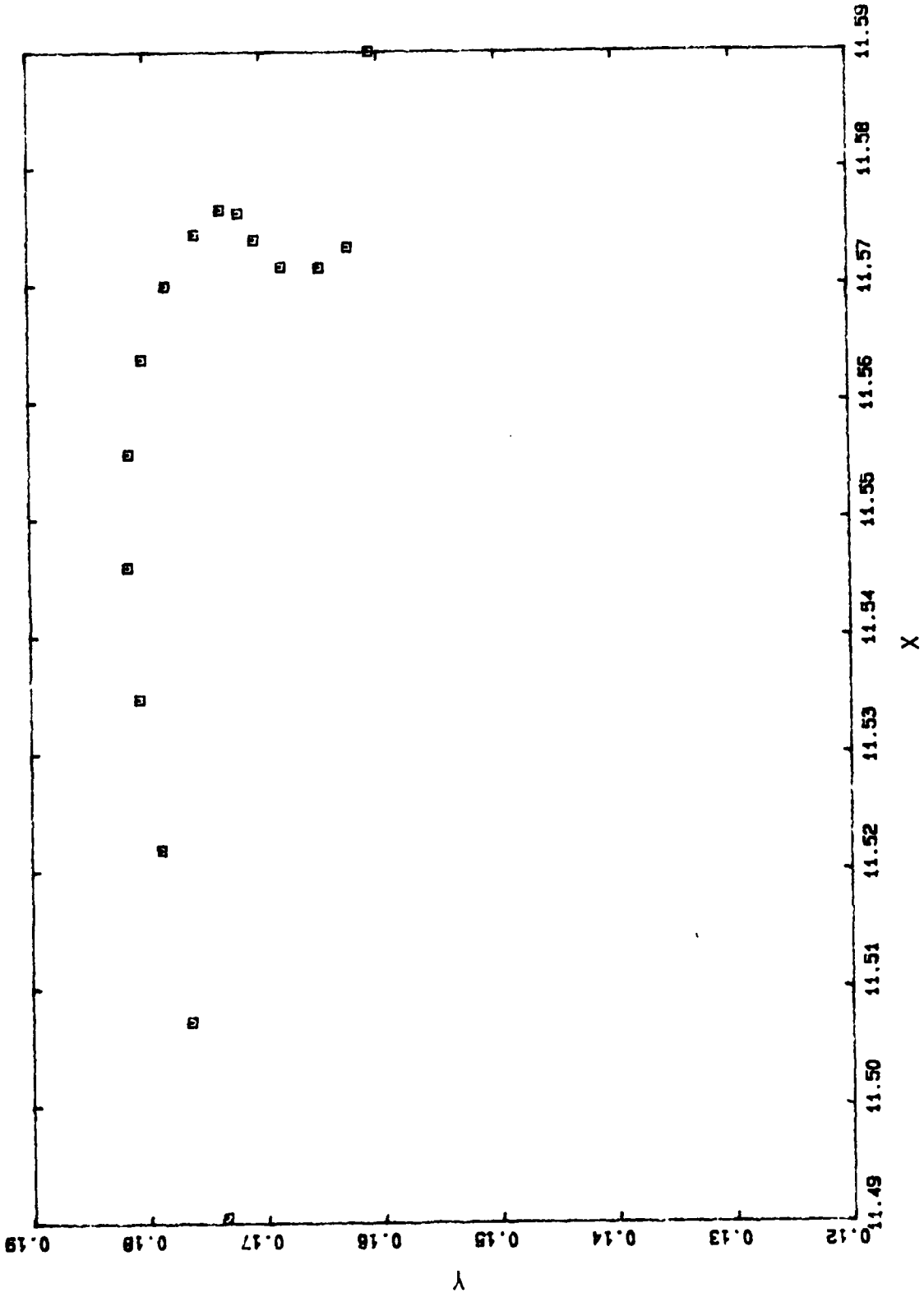

C3 3505 50.9512

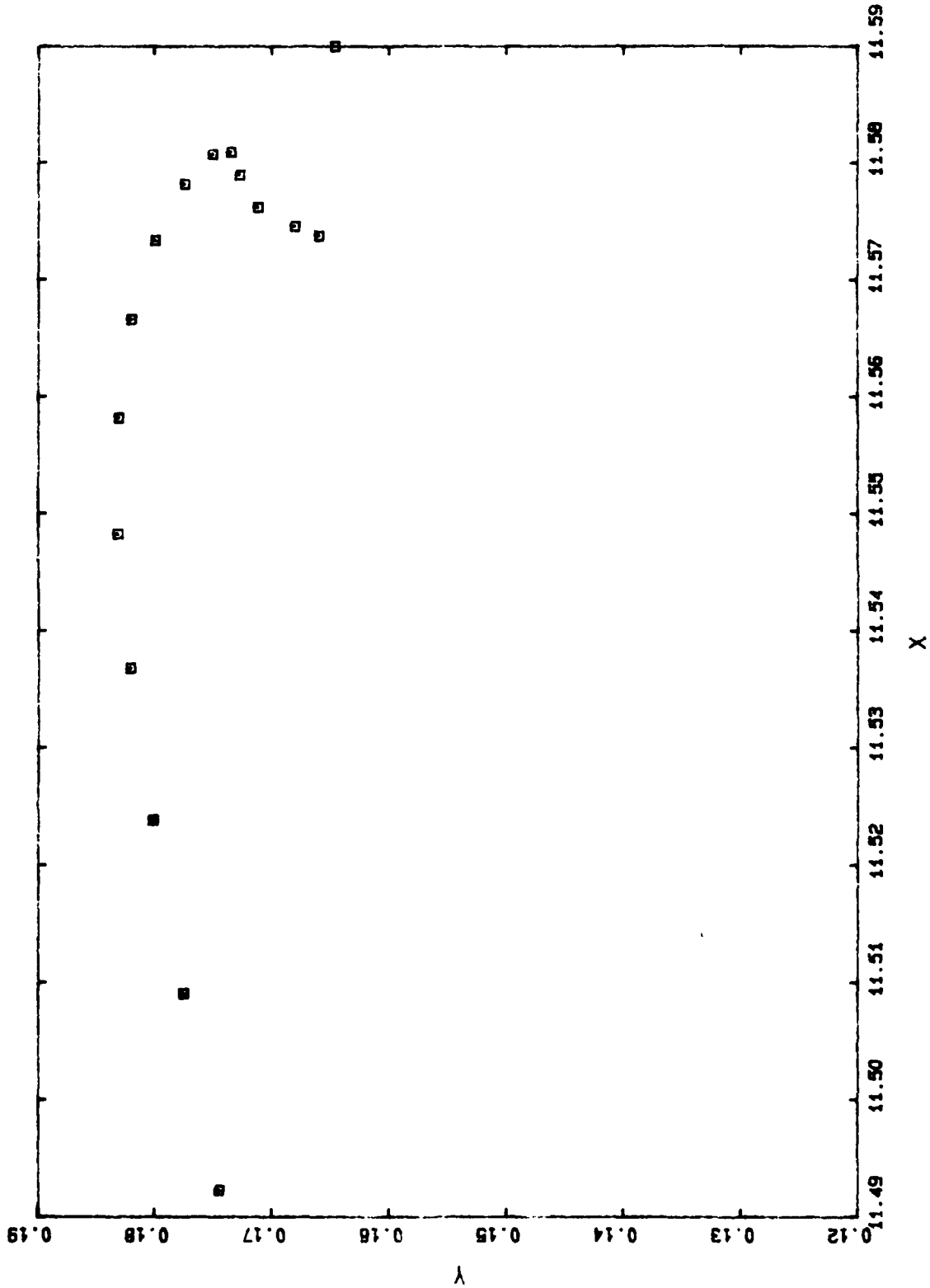

C3 3515 50.9522

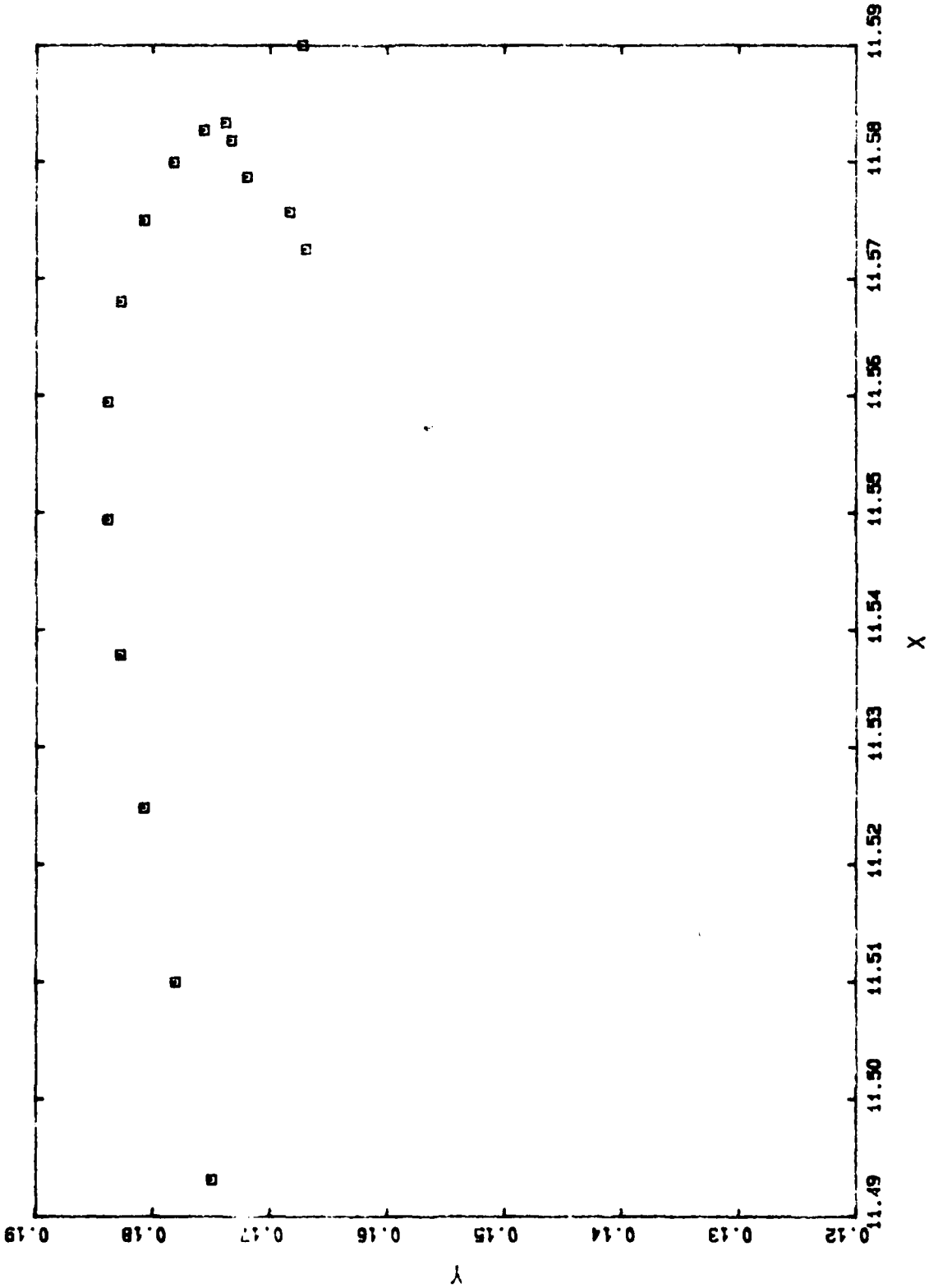

C4 3500 50.9585

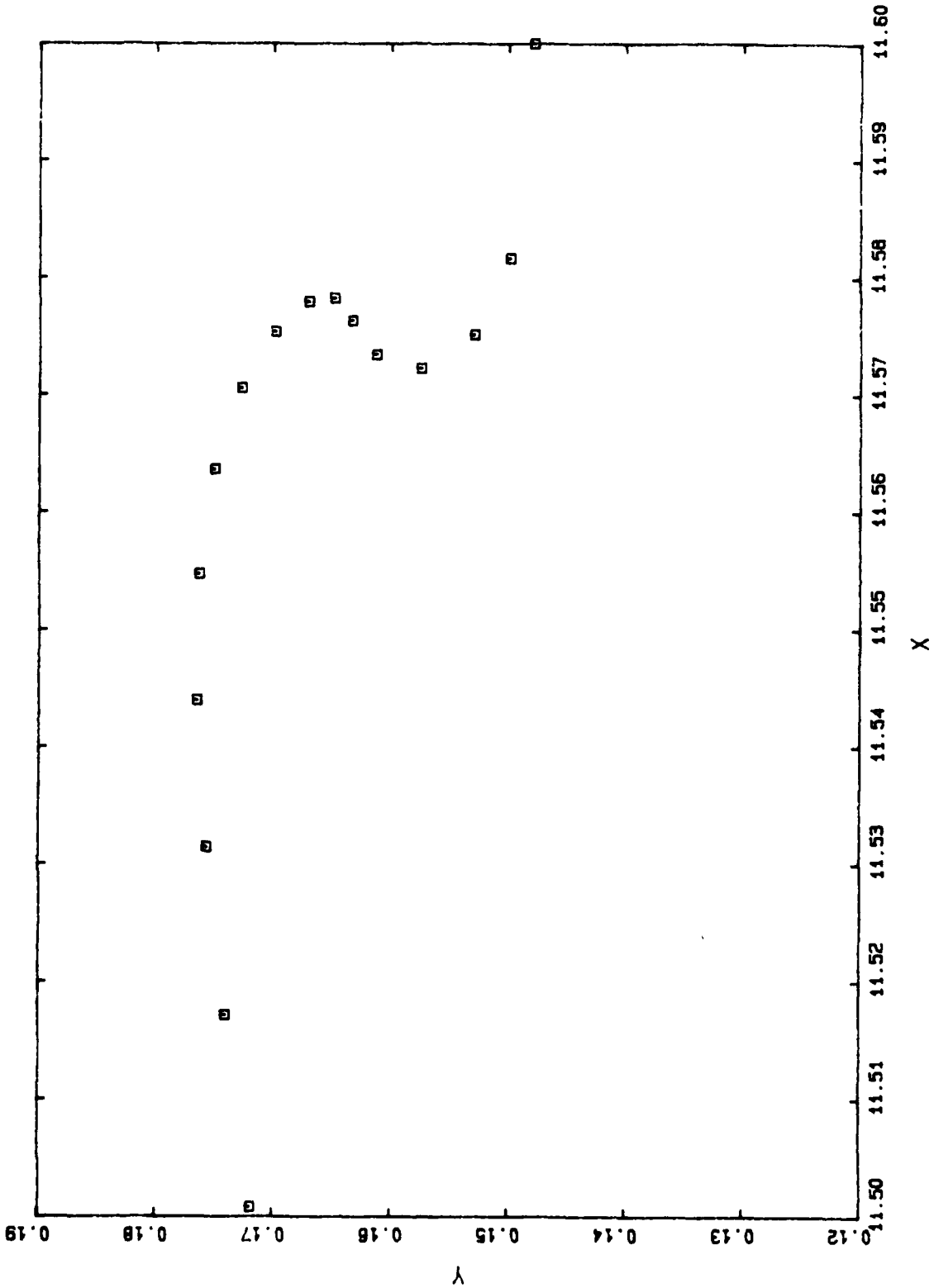

C4 3510 50.9595

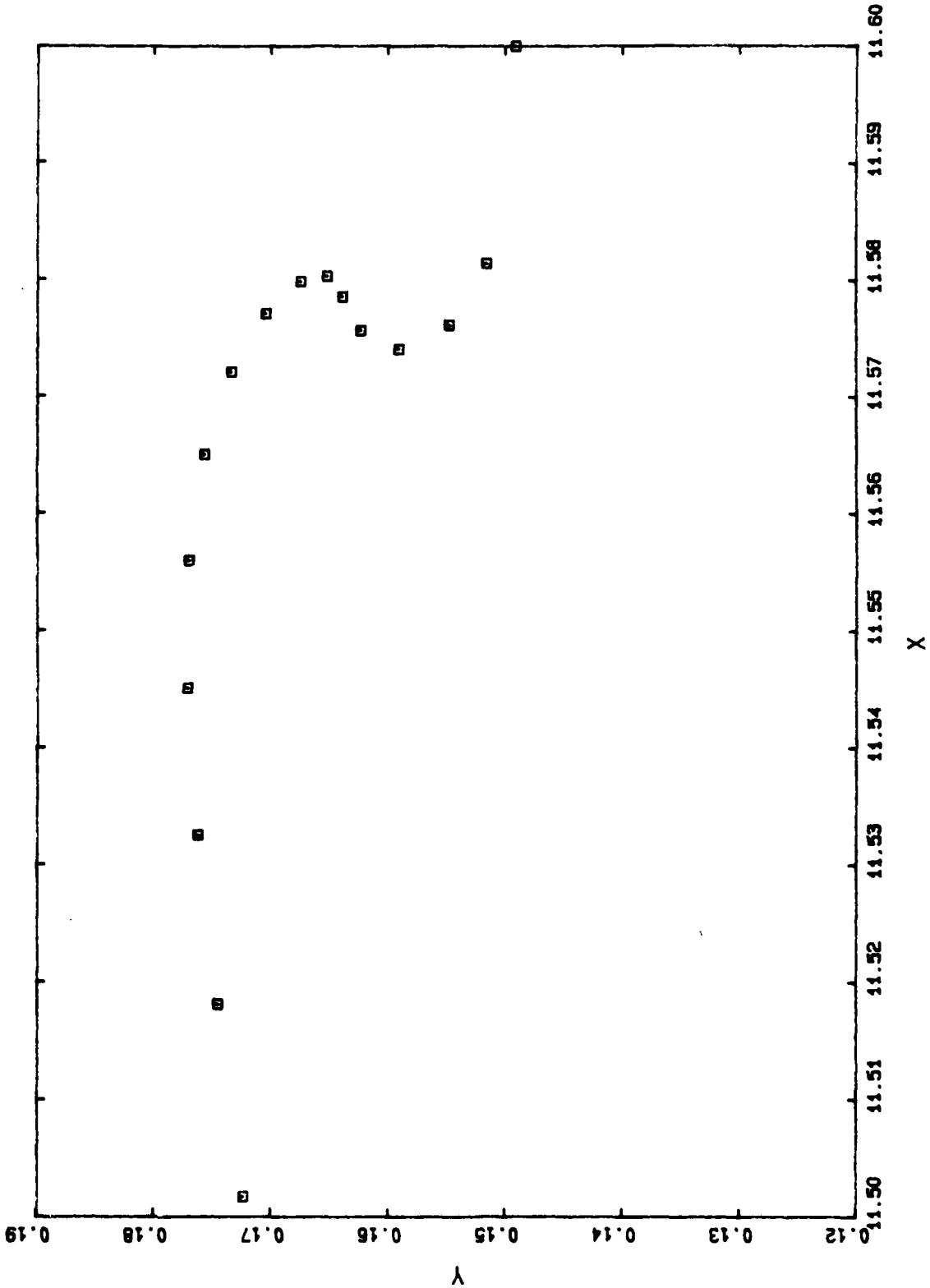

C4 3520 50.9605

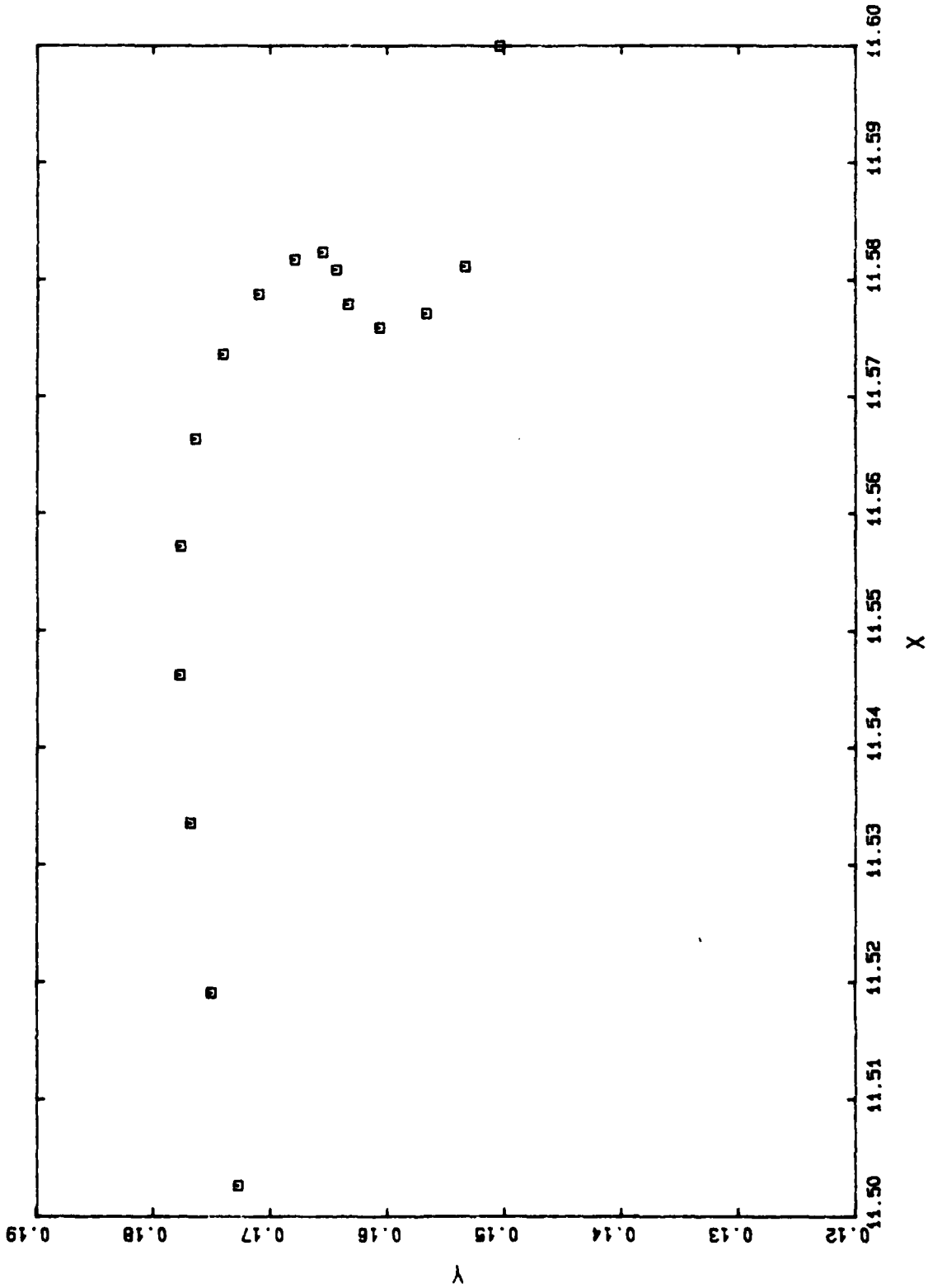

C4 3530 50.9615

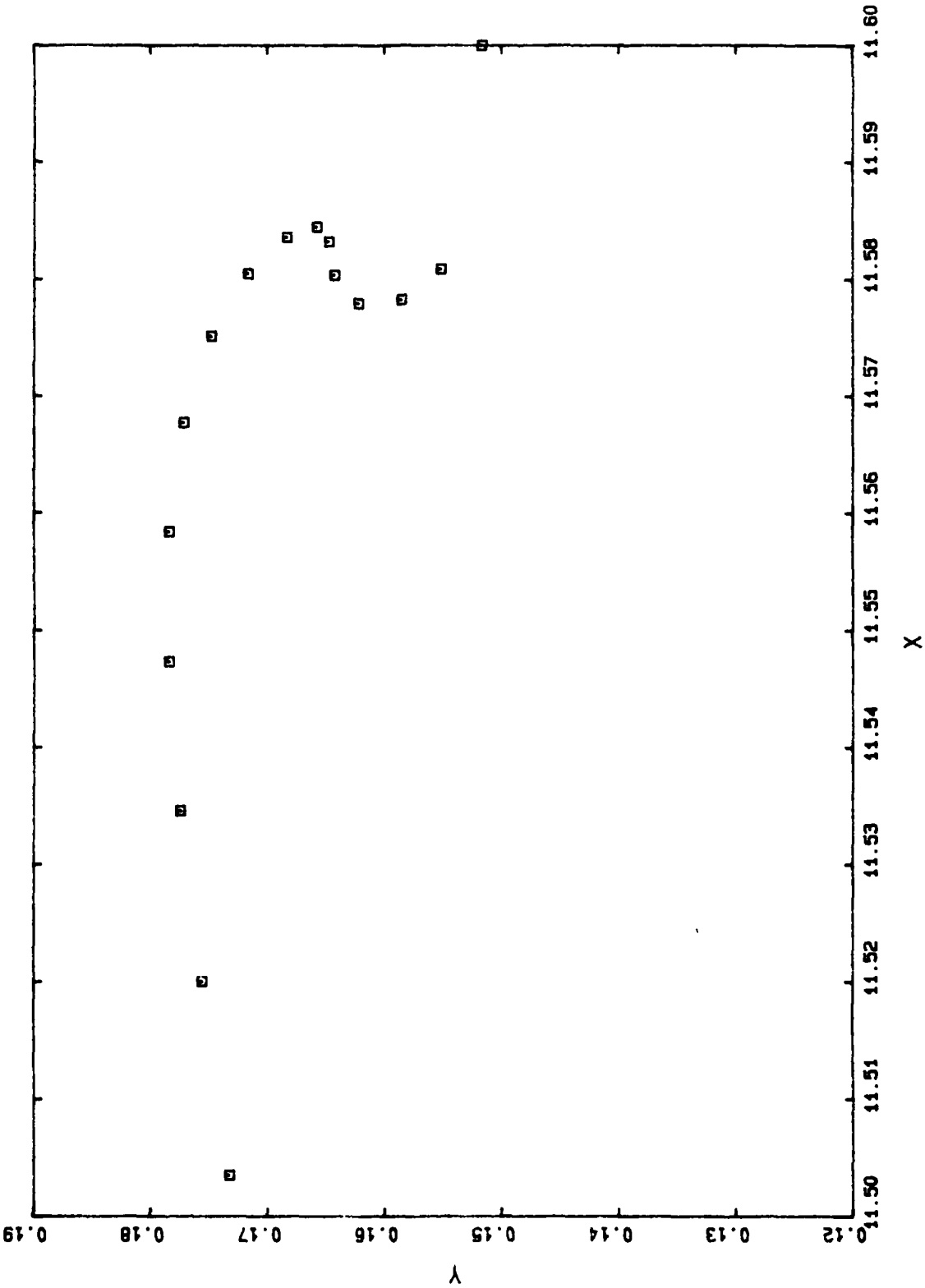

C4 3540 50.9625

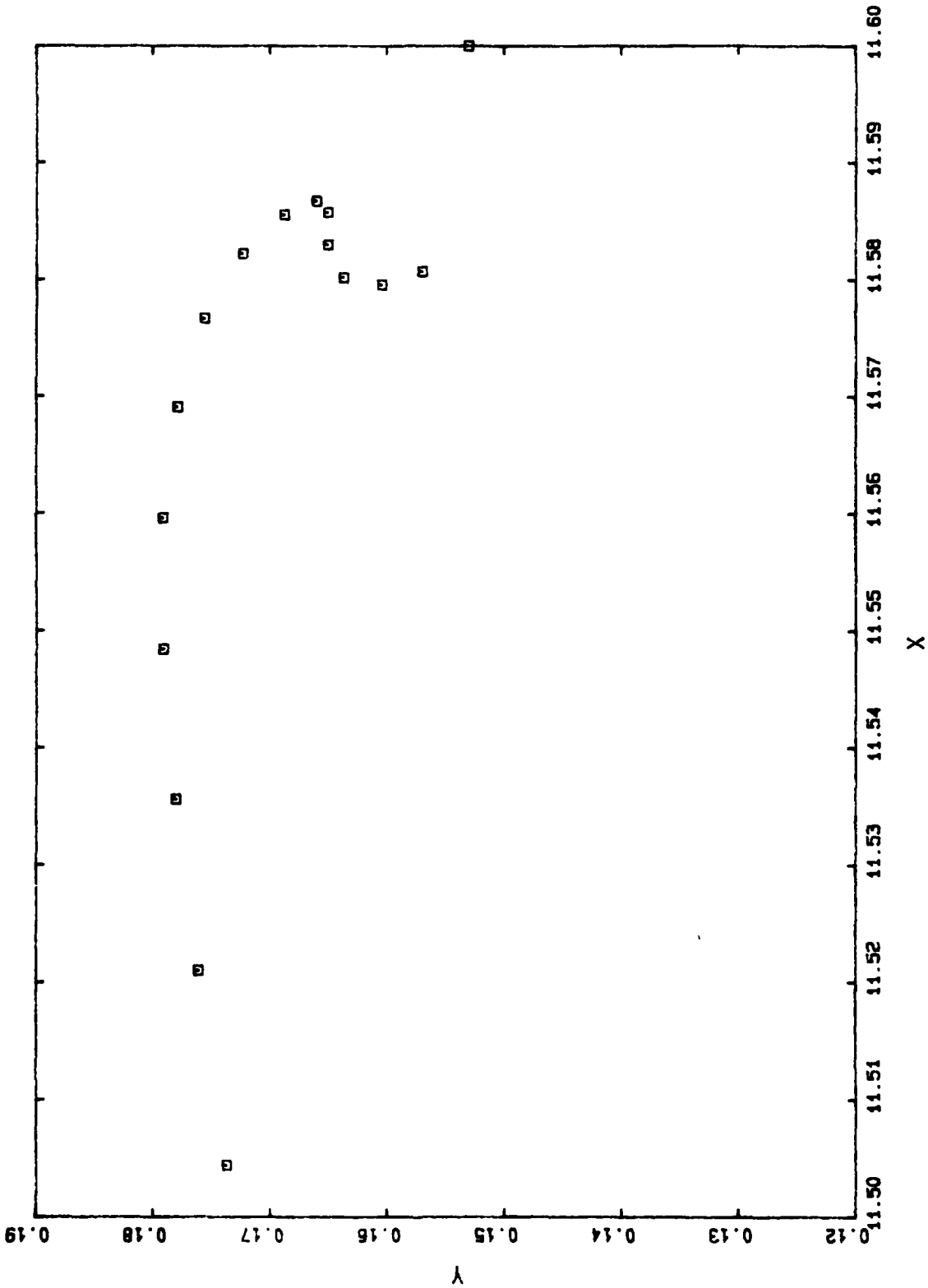

C4 3550 50.9635

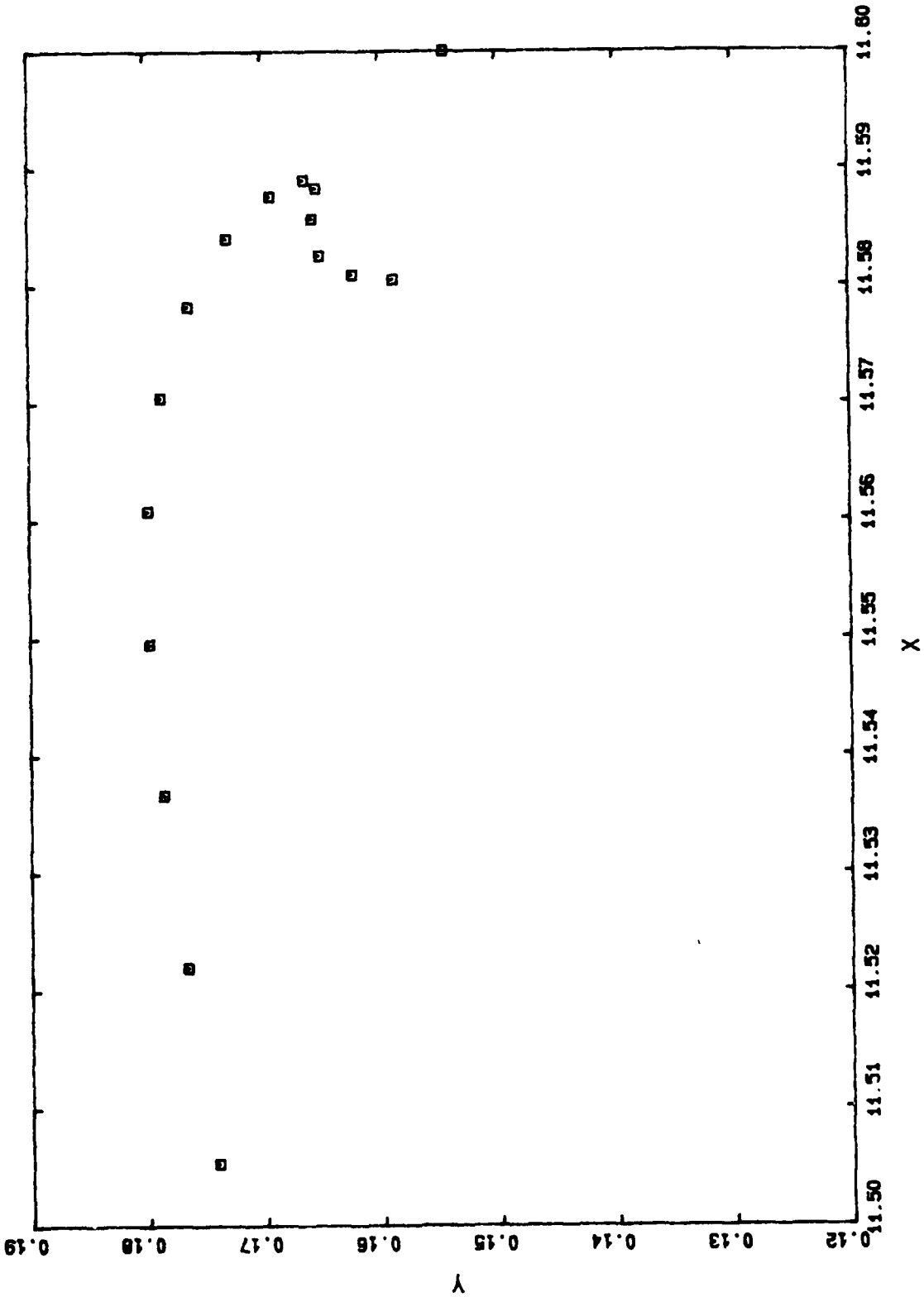

C4 3560 50.9645

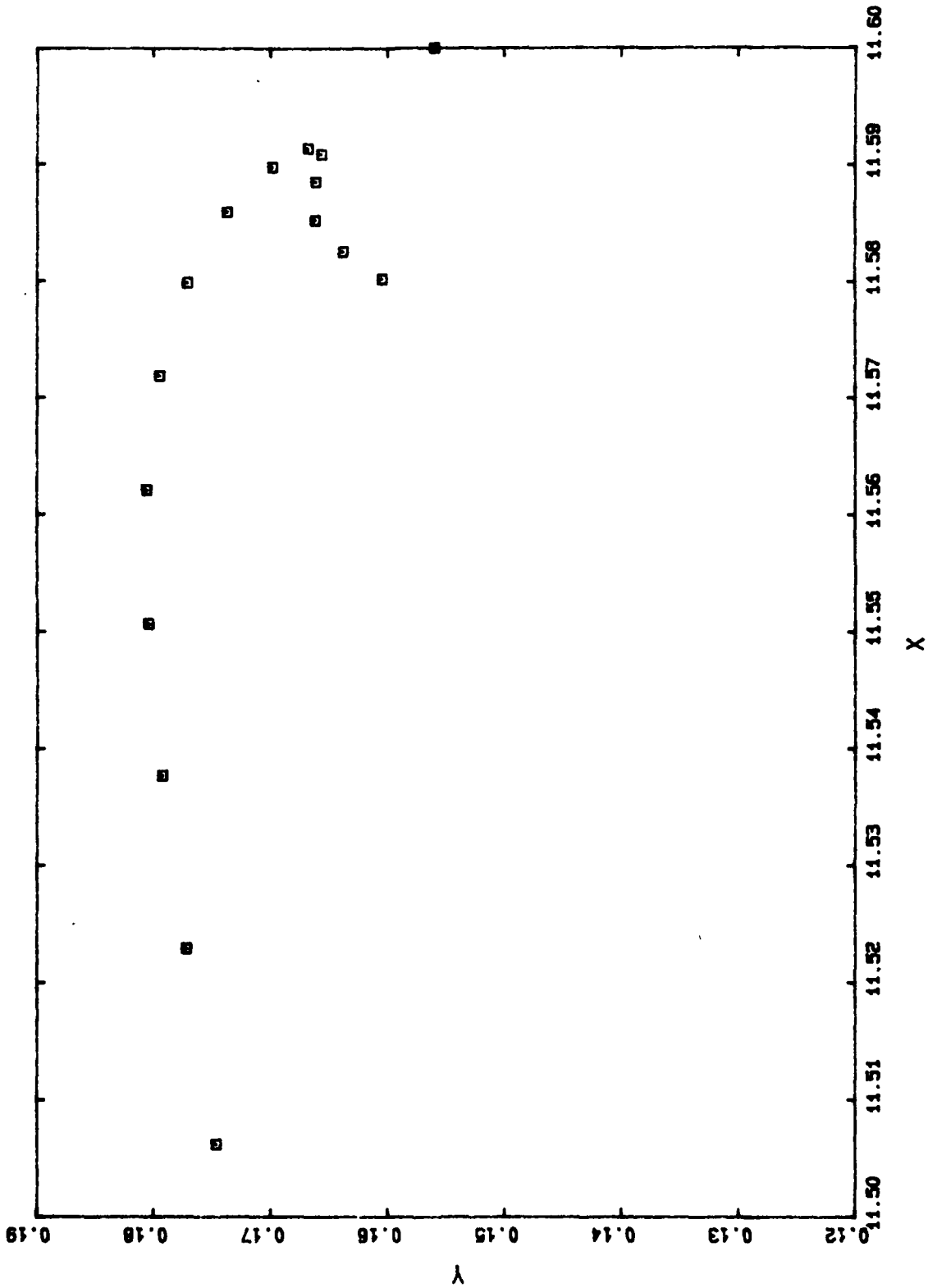

C4 3570 50.9655

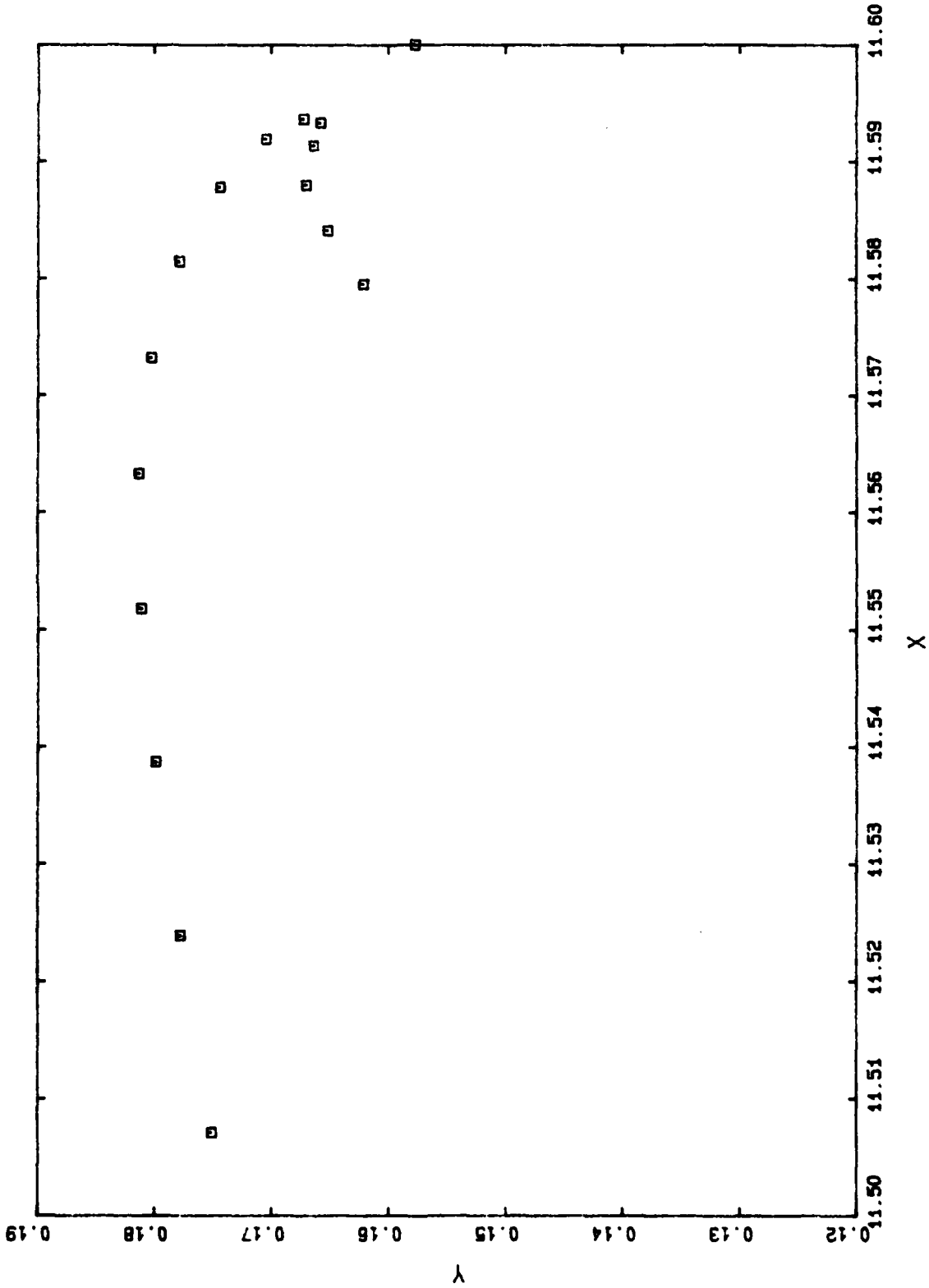

C4 3580 50.9665

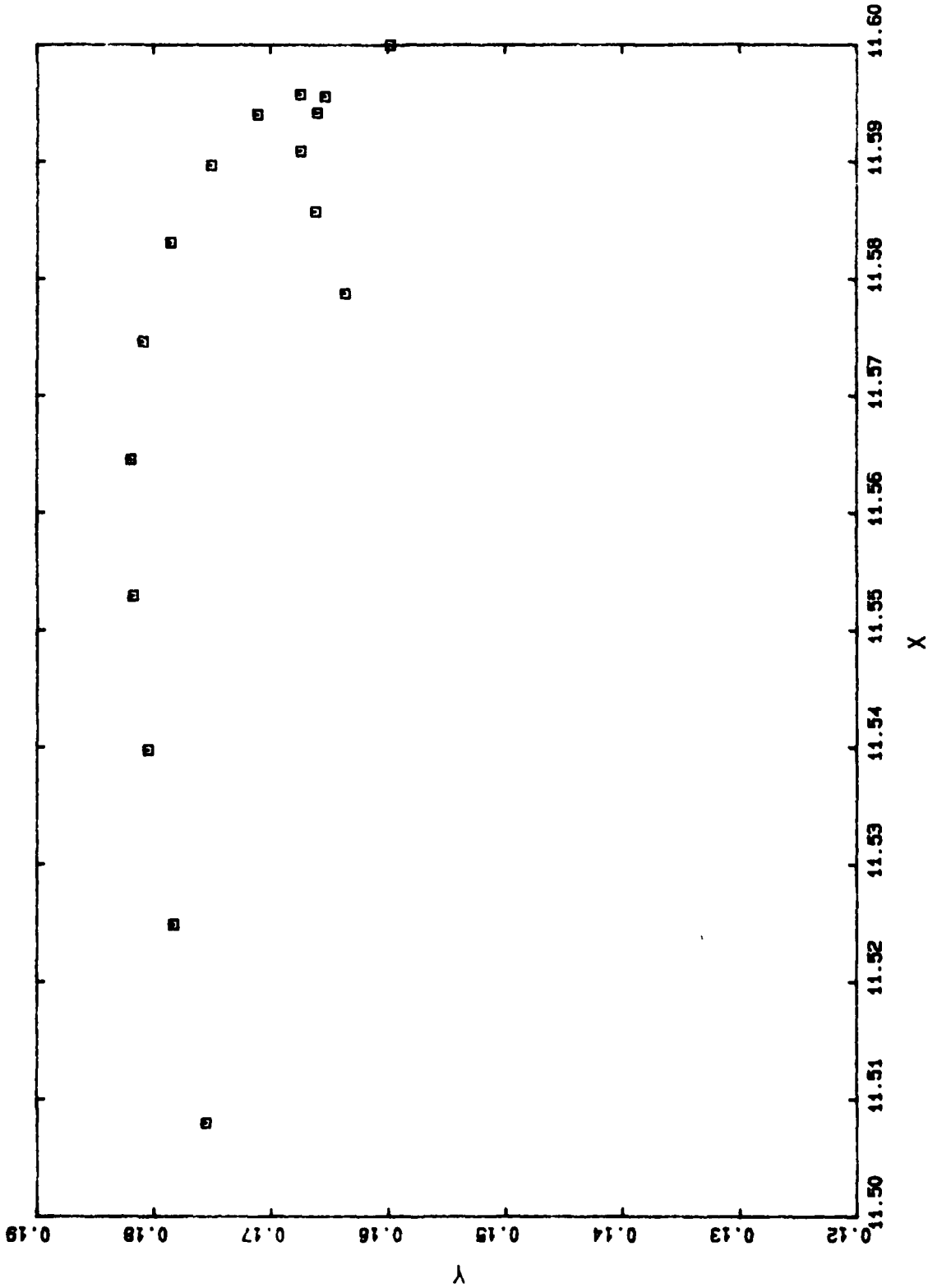

C5 3552 50.9846

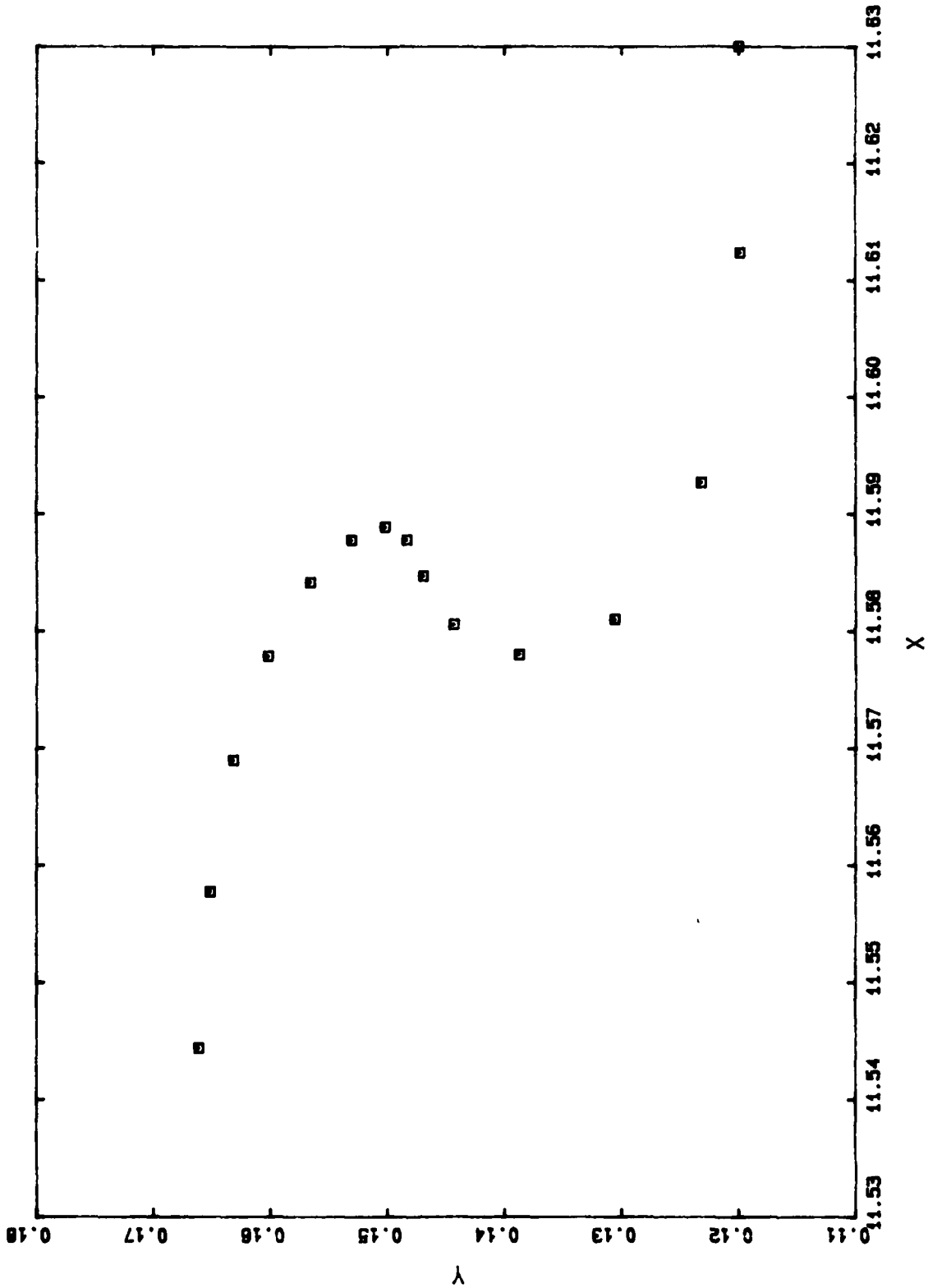

C5 3572 50.9871

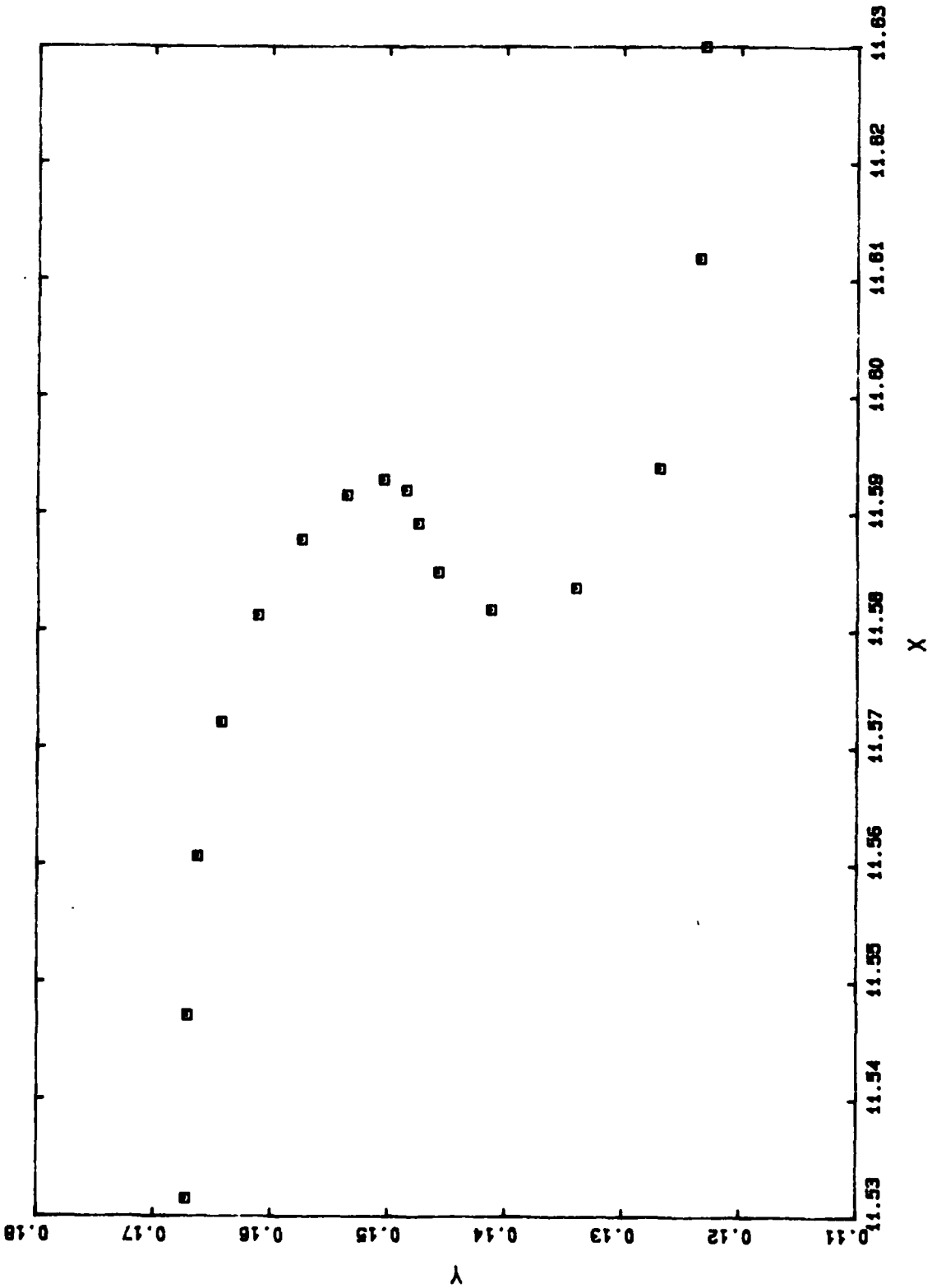

C5 3592 50.9897

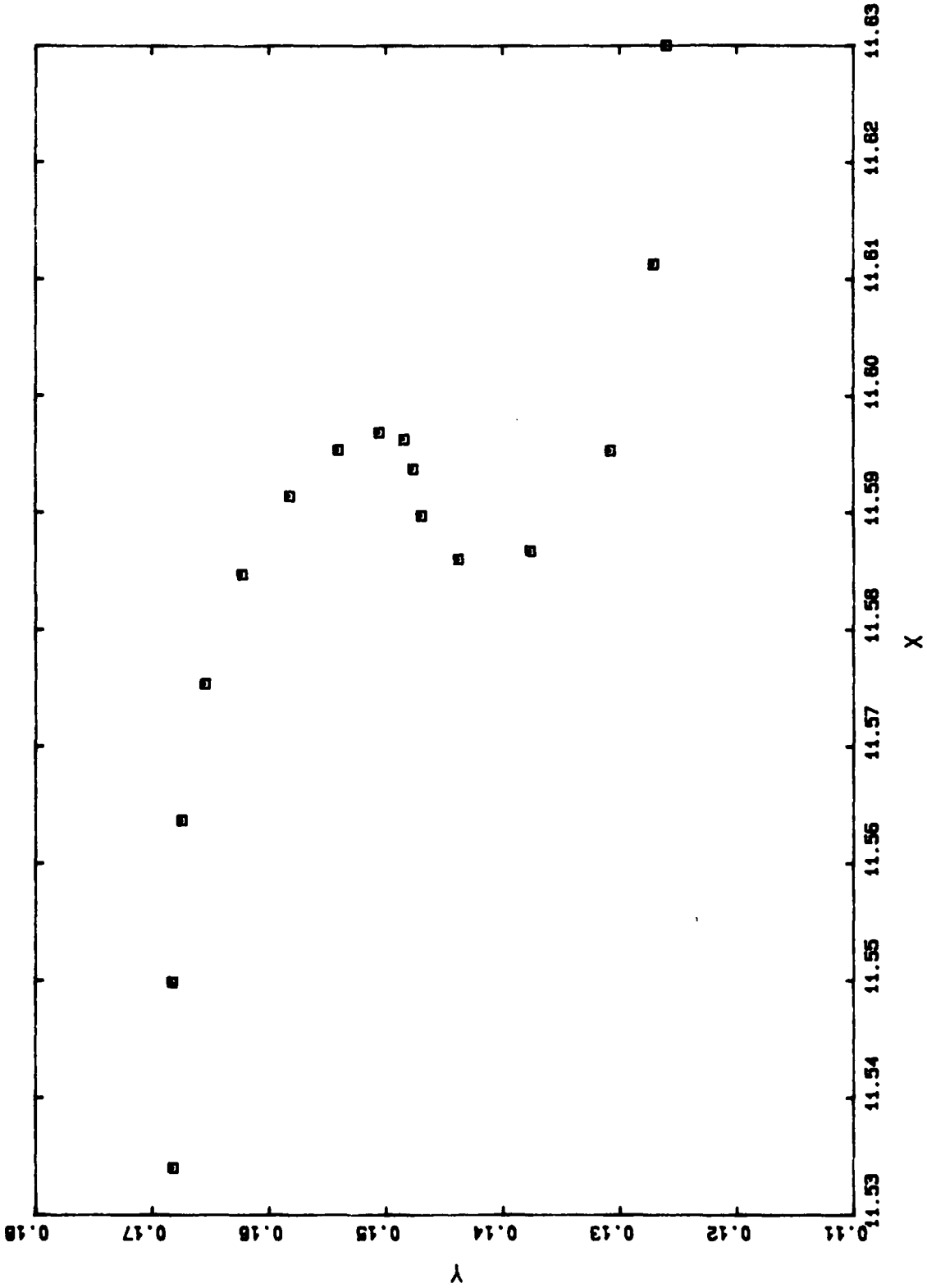

C5 3612 50.9922

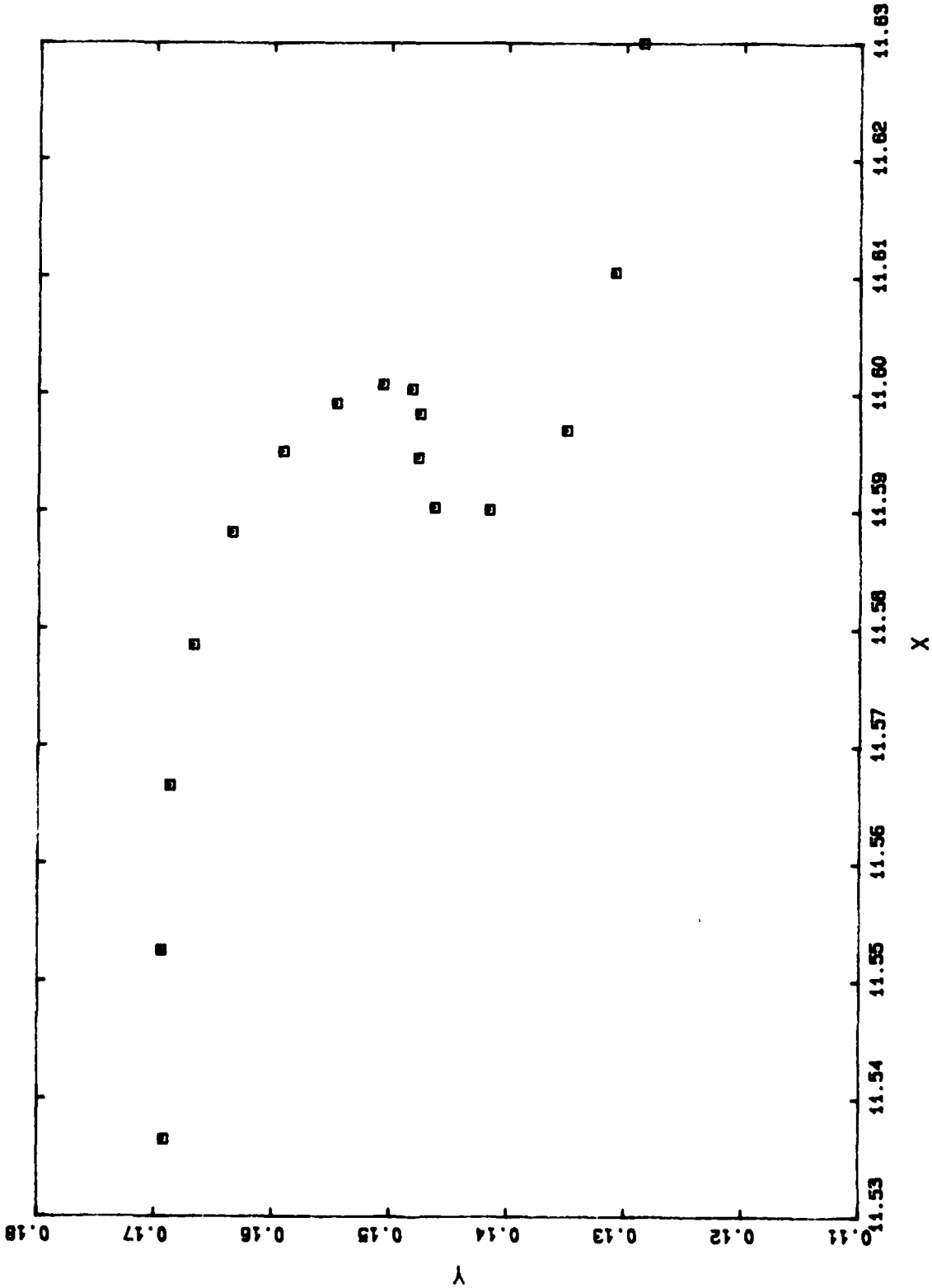

C5 3632 50.9945

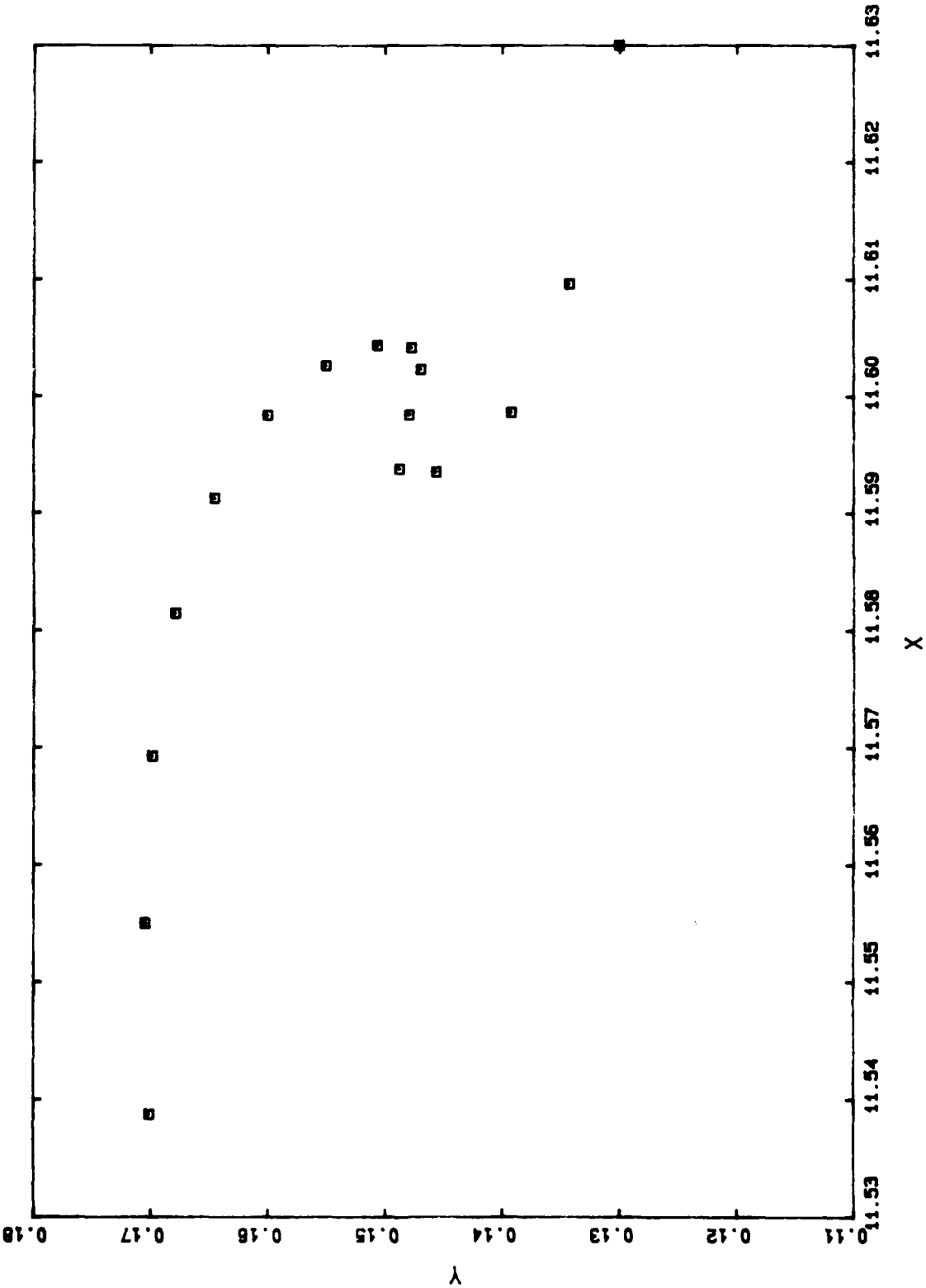

C5 3642 50.9955

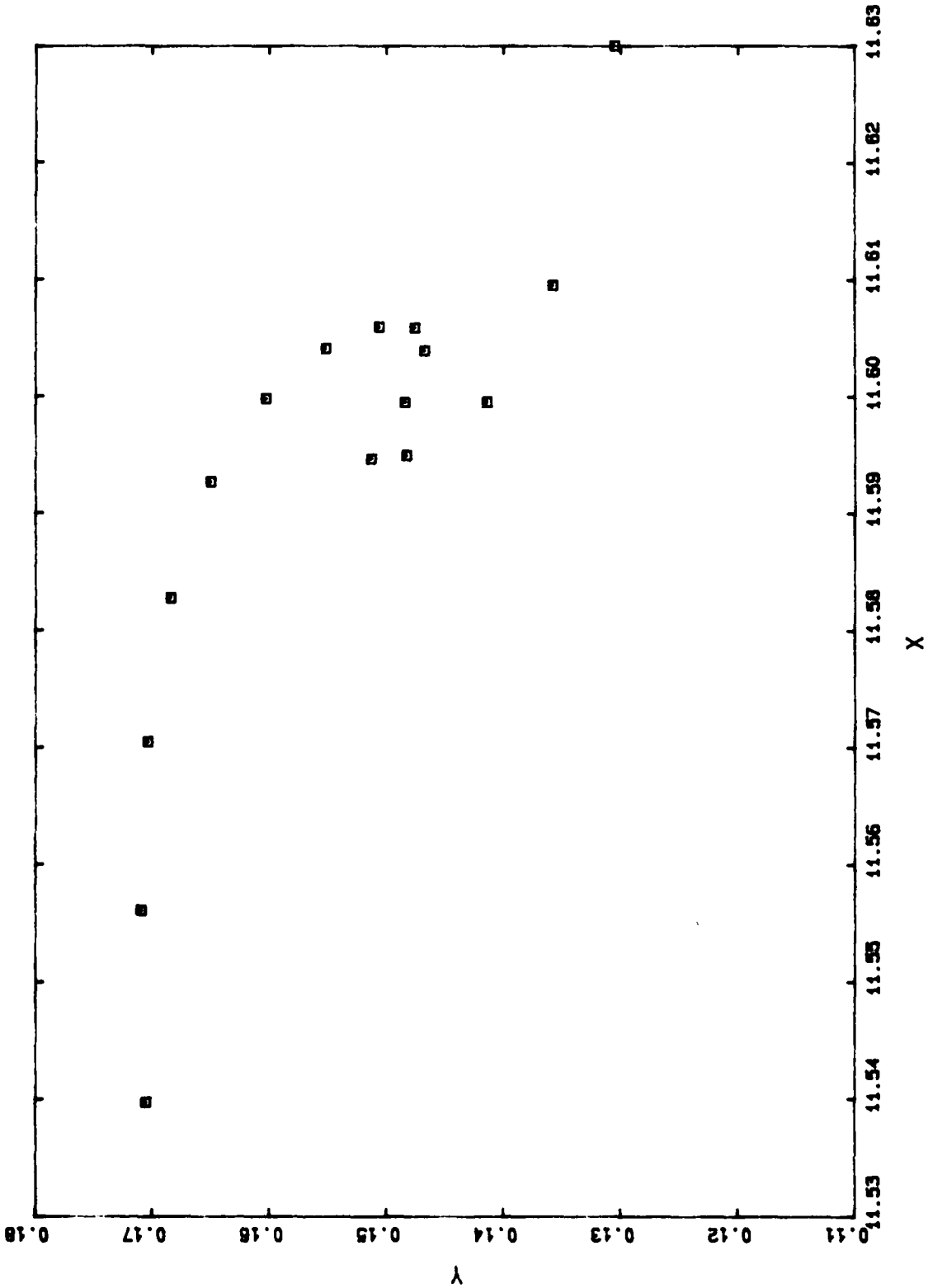

C5 3652 50.9965

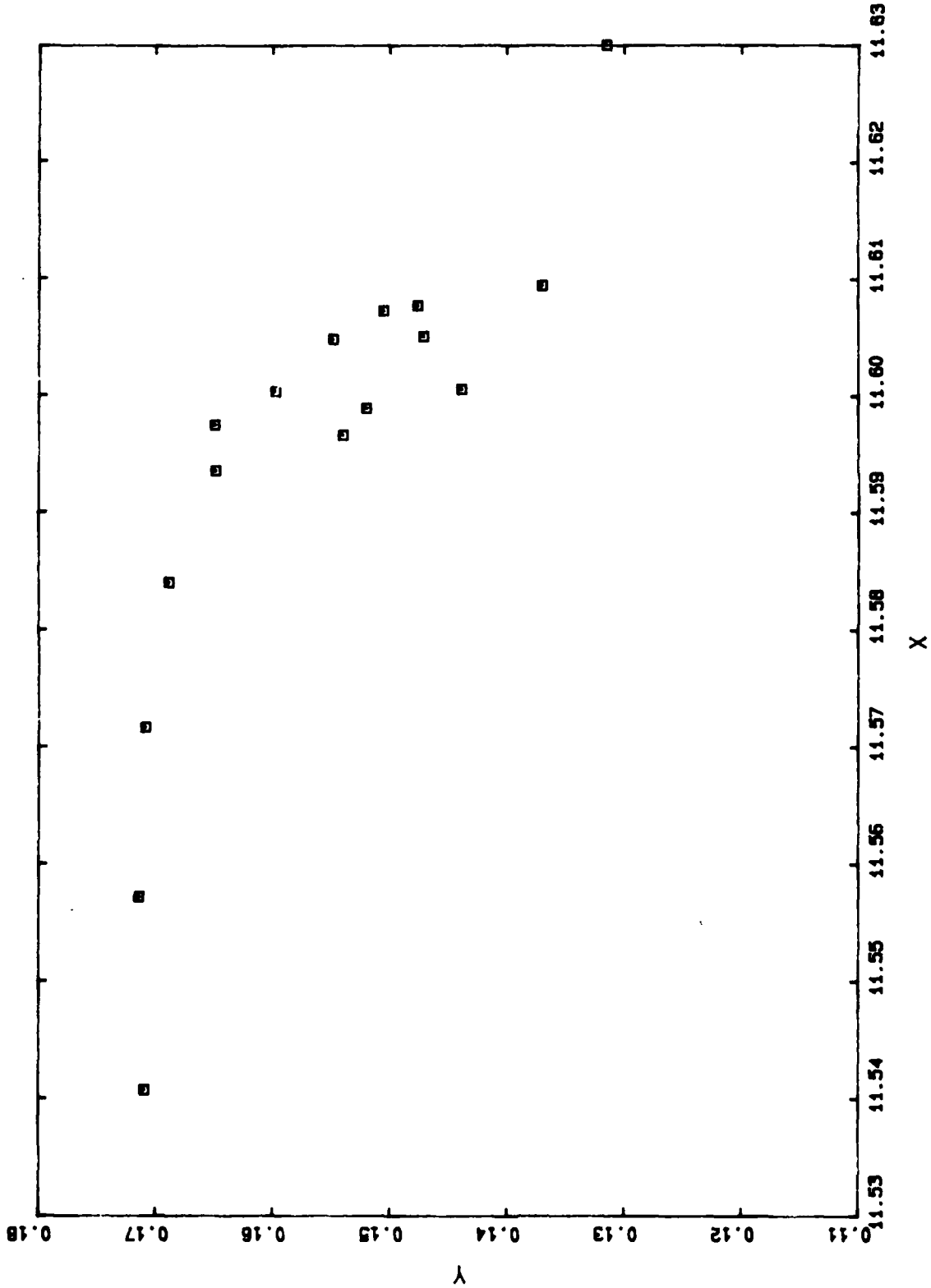

C6 3640 51.0041

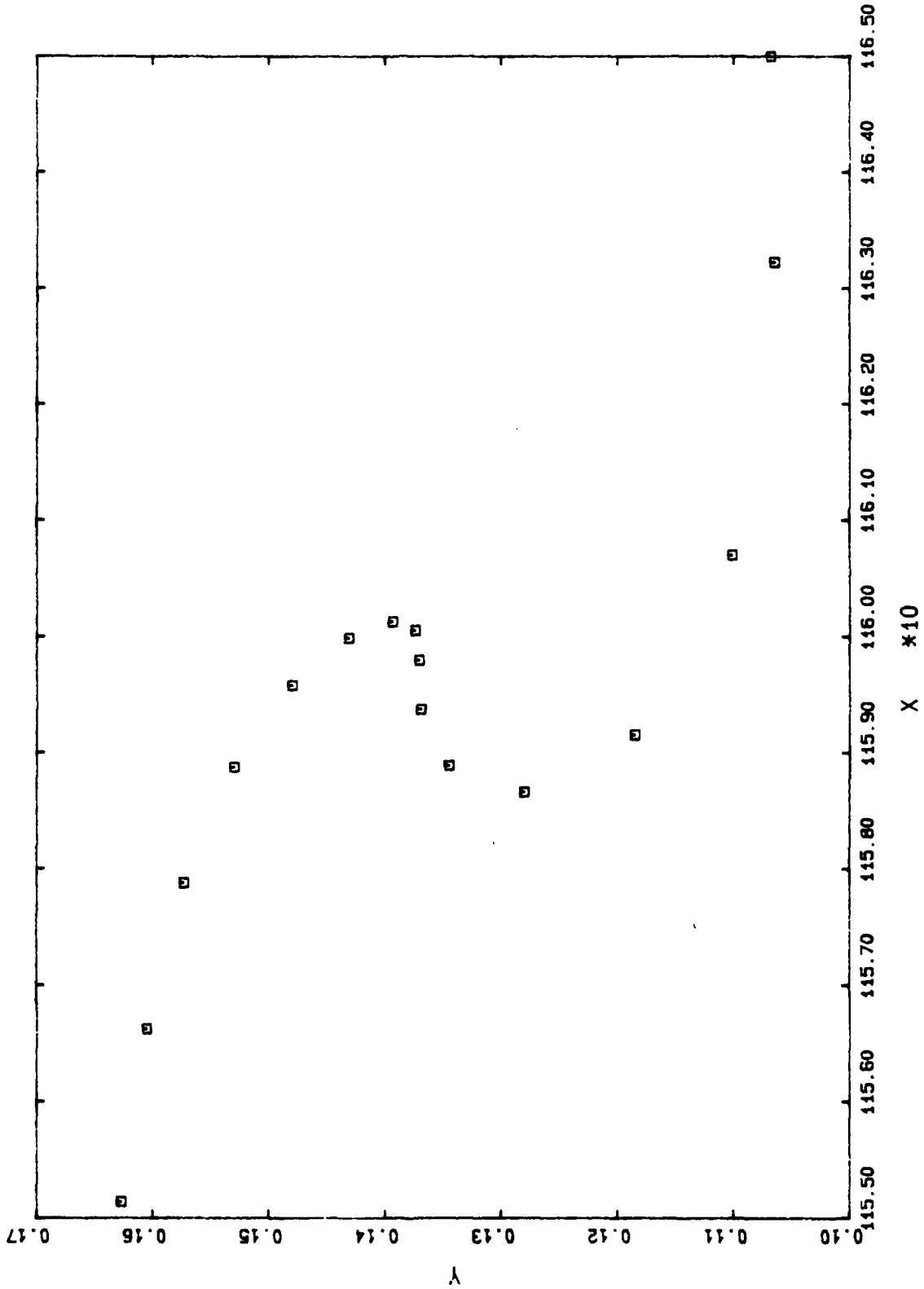

C6 3660 51.0070

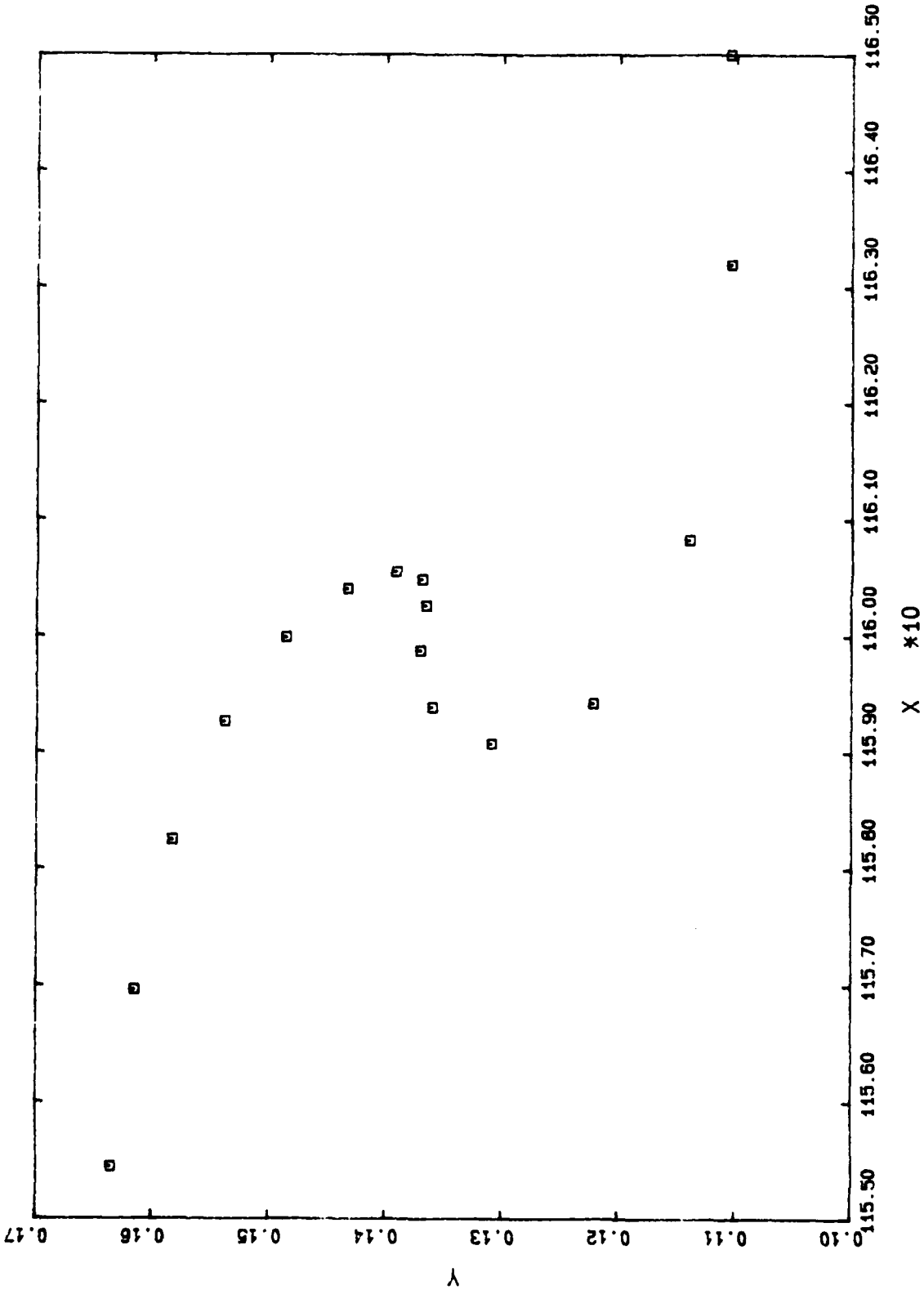

C6 3680 51.0097

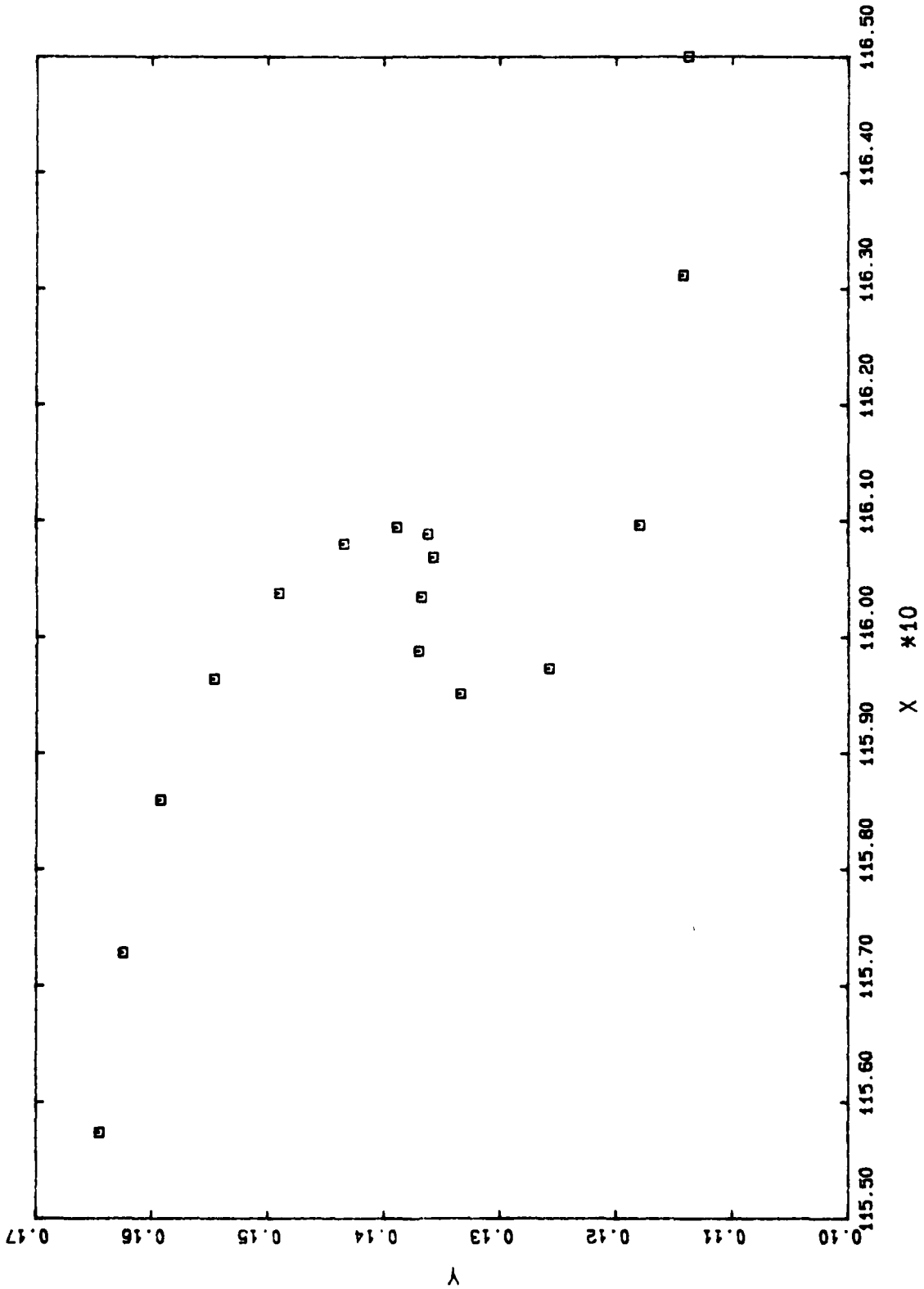

C6 3700 51.0124

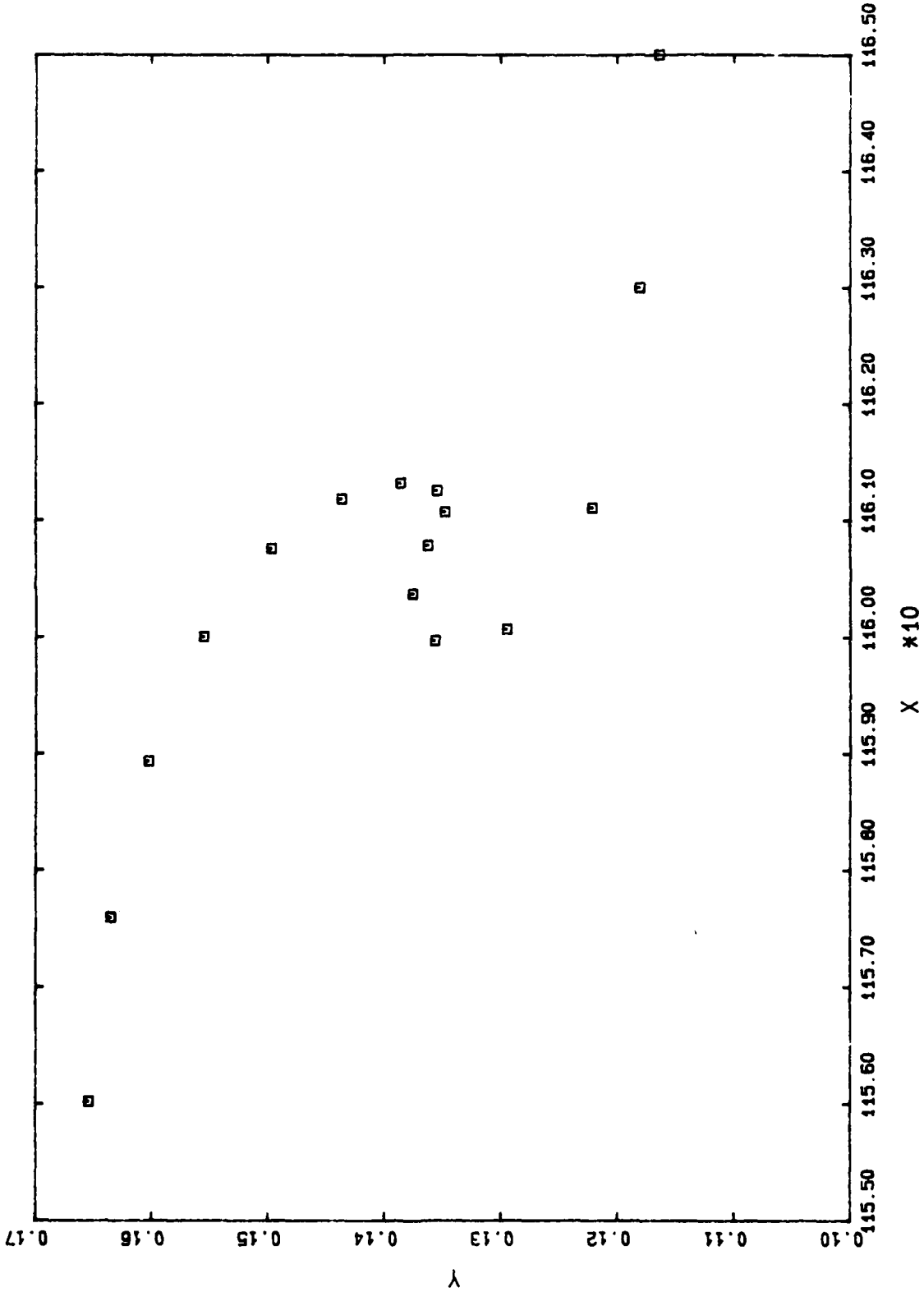

C6 3720 51.0152

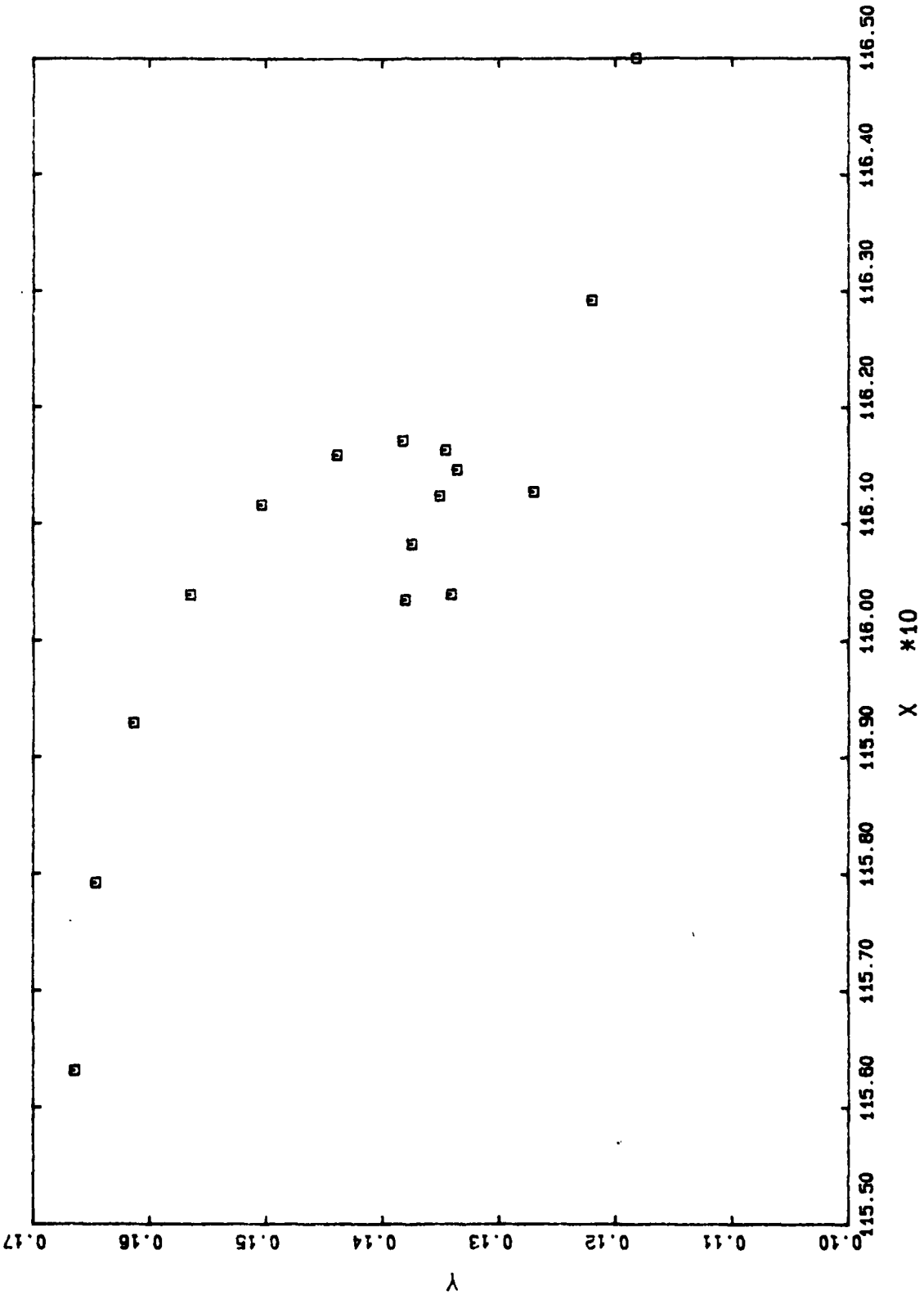

C6 3730 51.0163

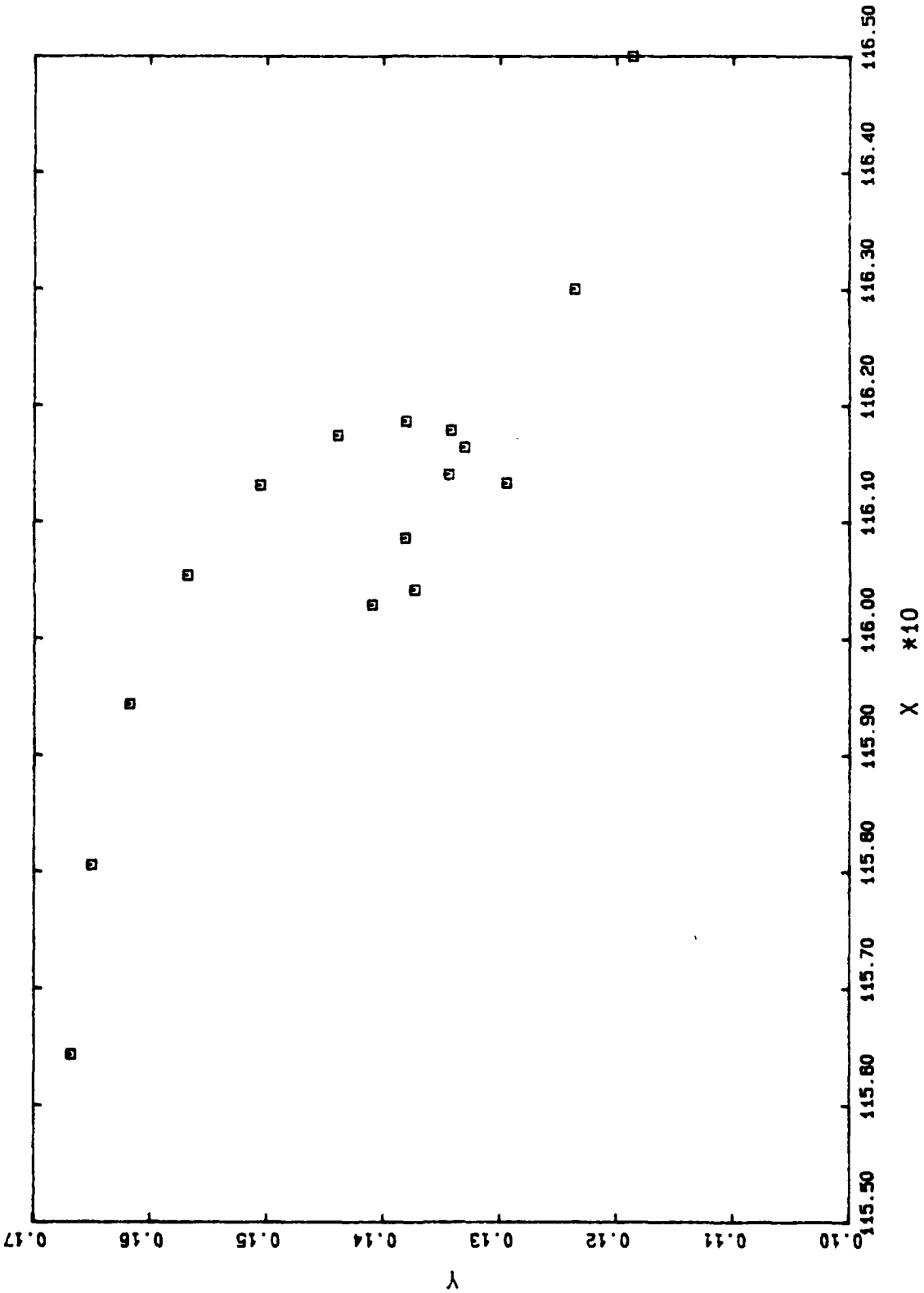

Appendix D

Refer to Chapter 5 for discussion.

D1 3501 50.9586

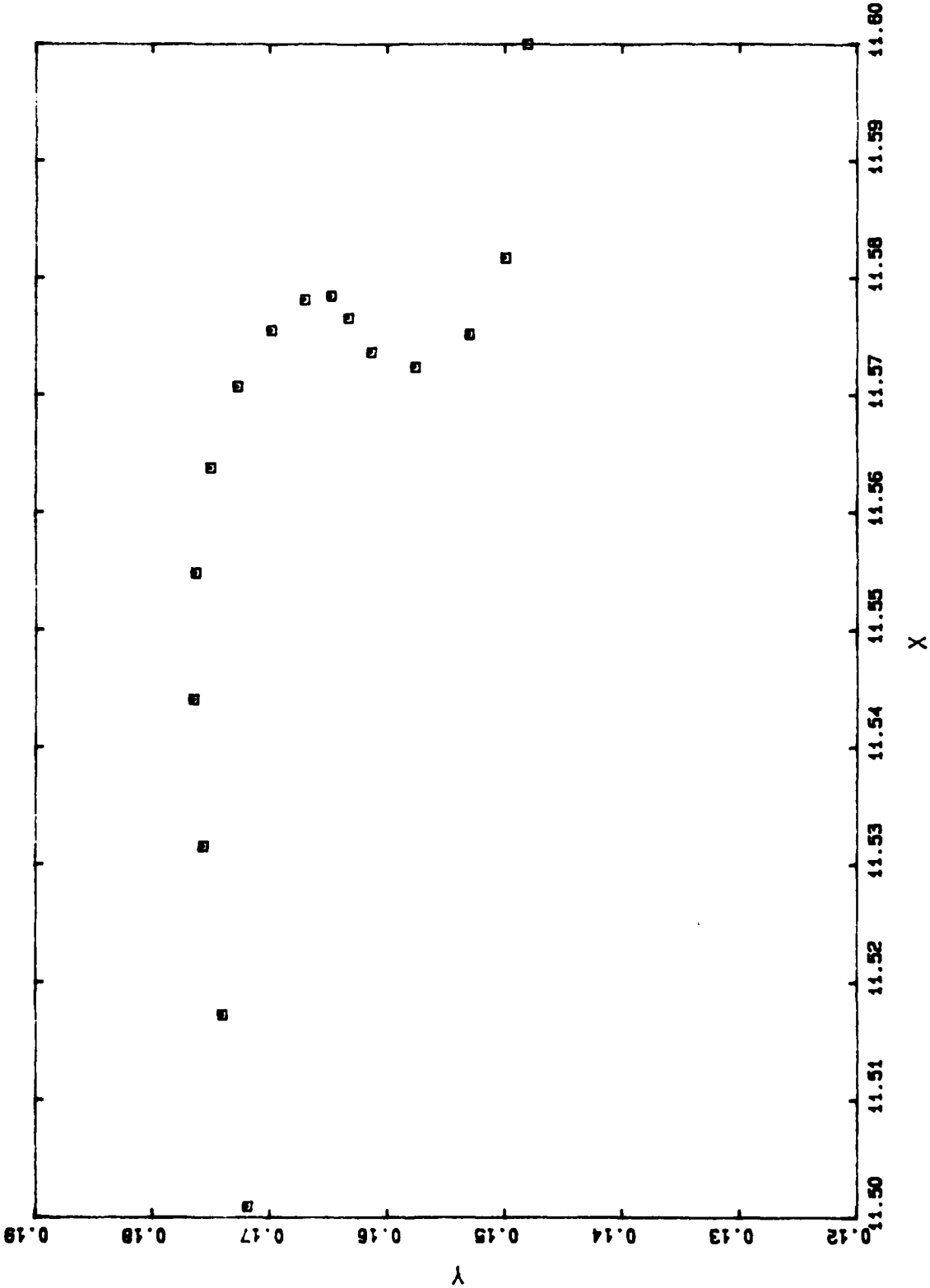

D1 3504 50.9589

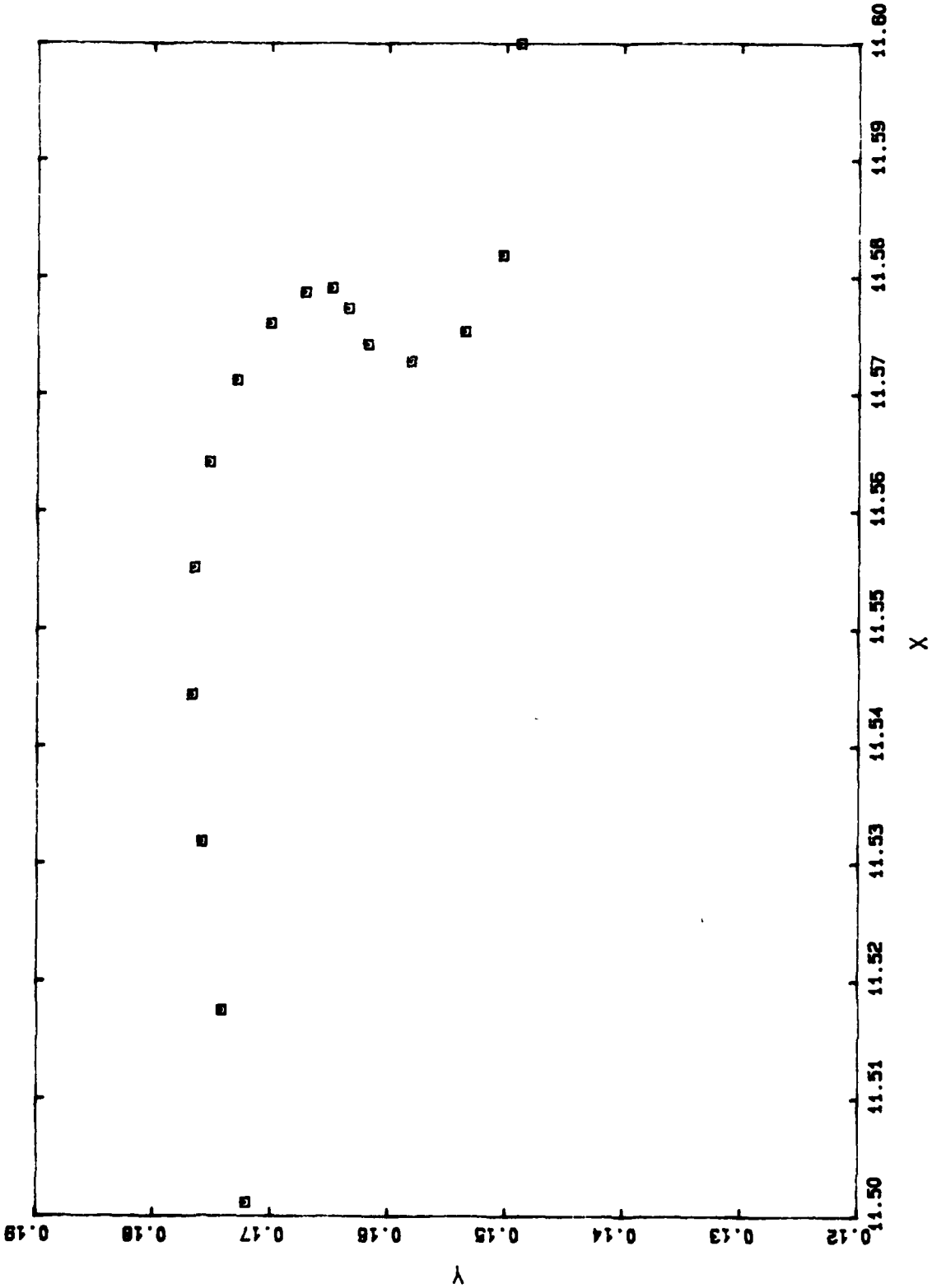

D1 3505 50.9590

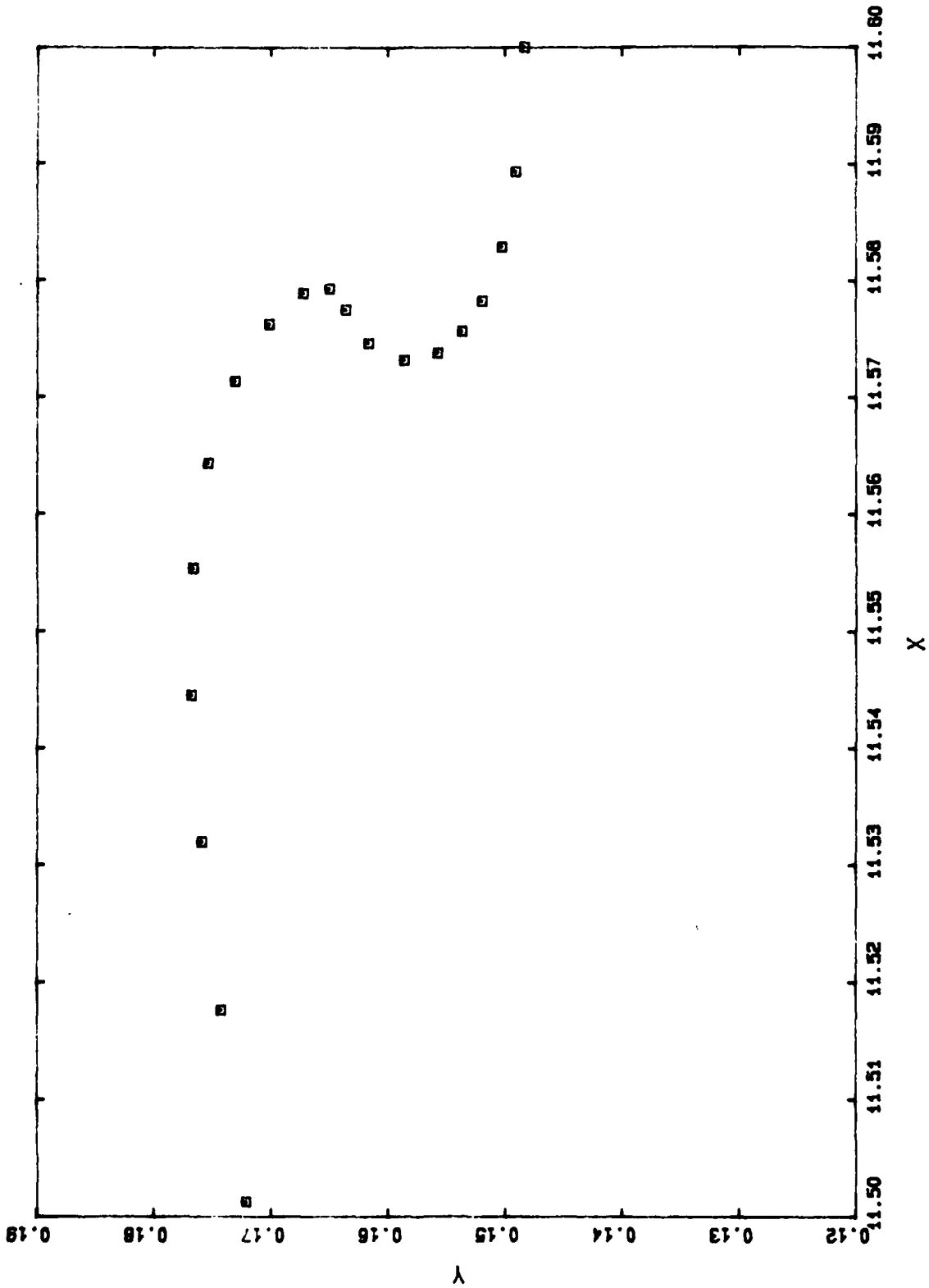

D1 3506 50.9591

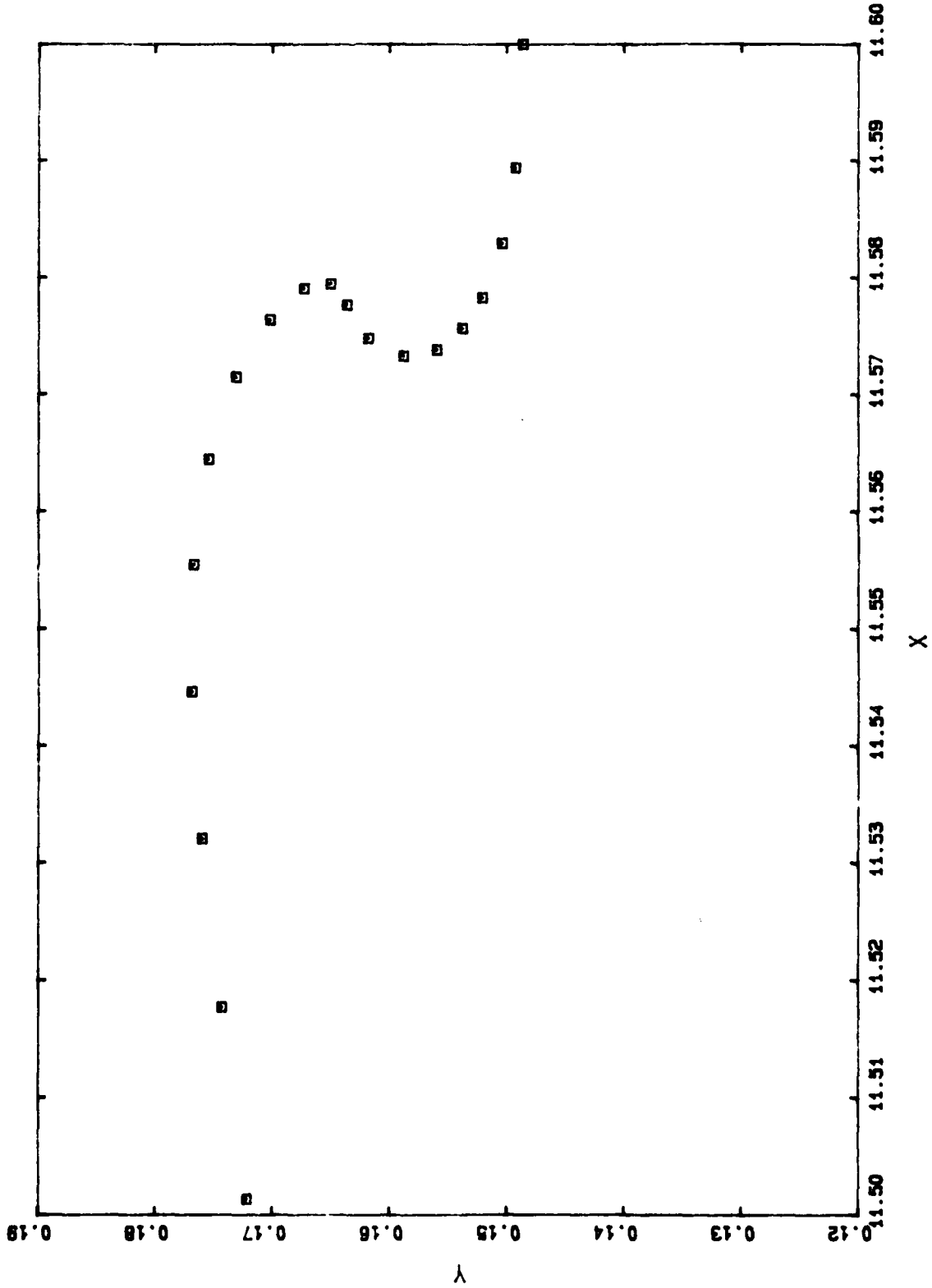

D1 3510 50.9595

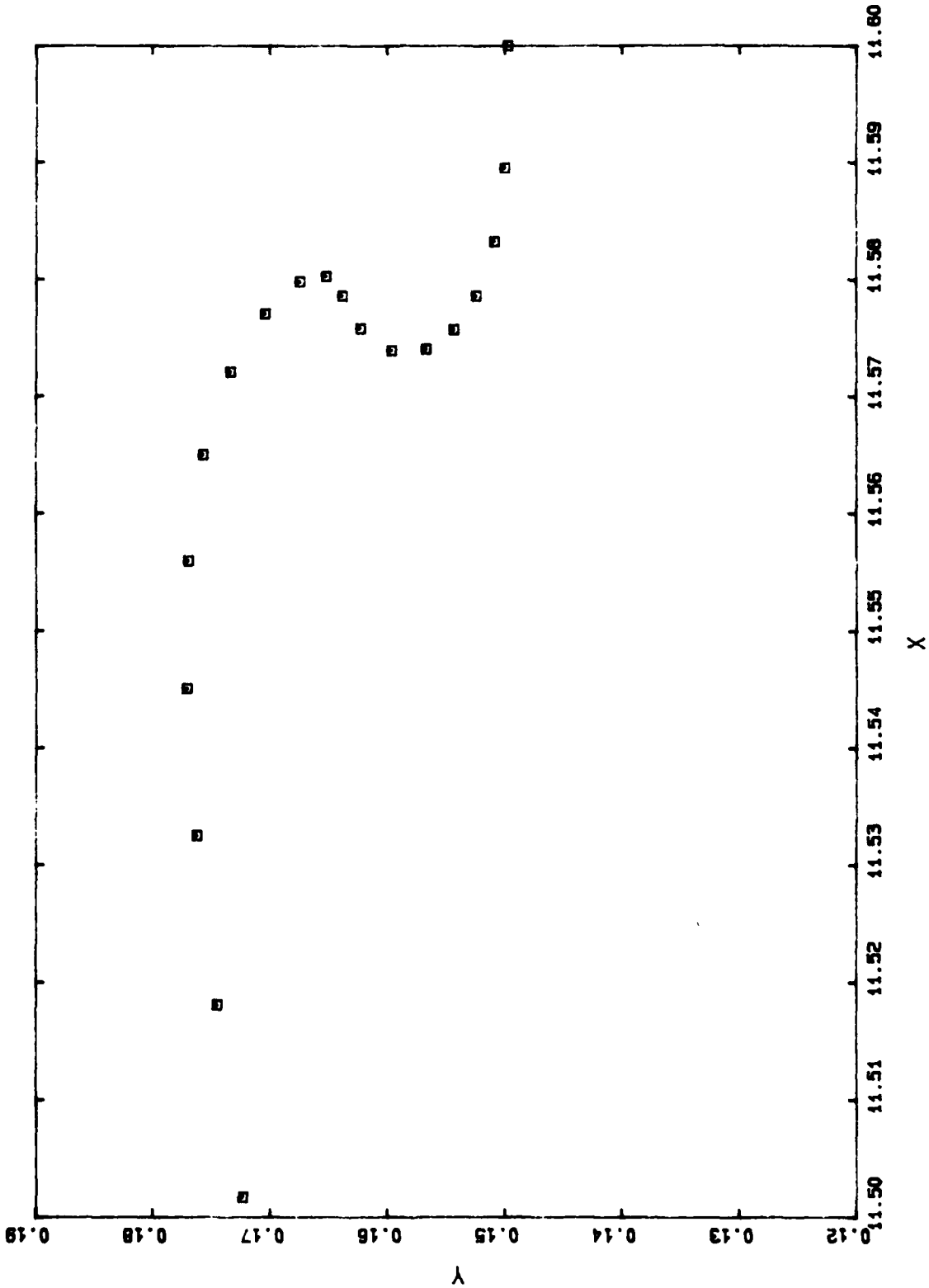

D1 3511 50.9596

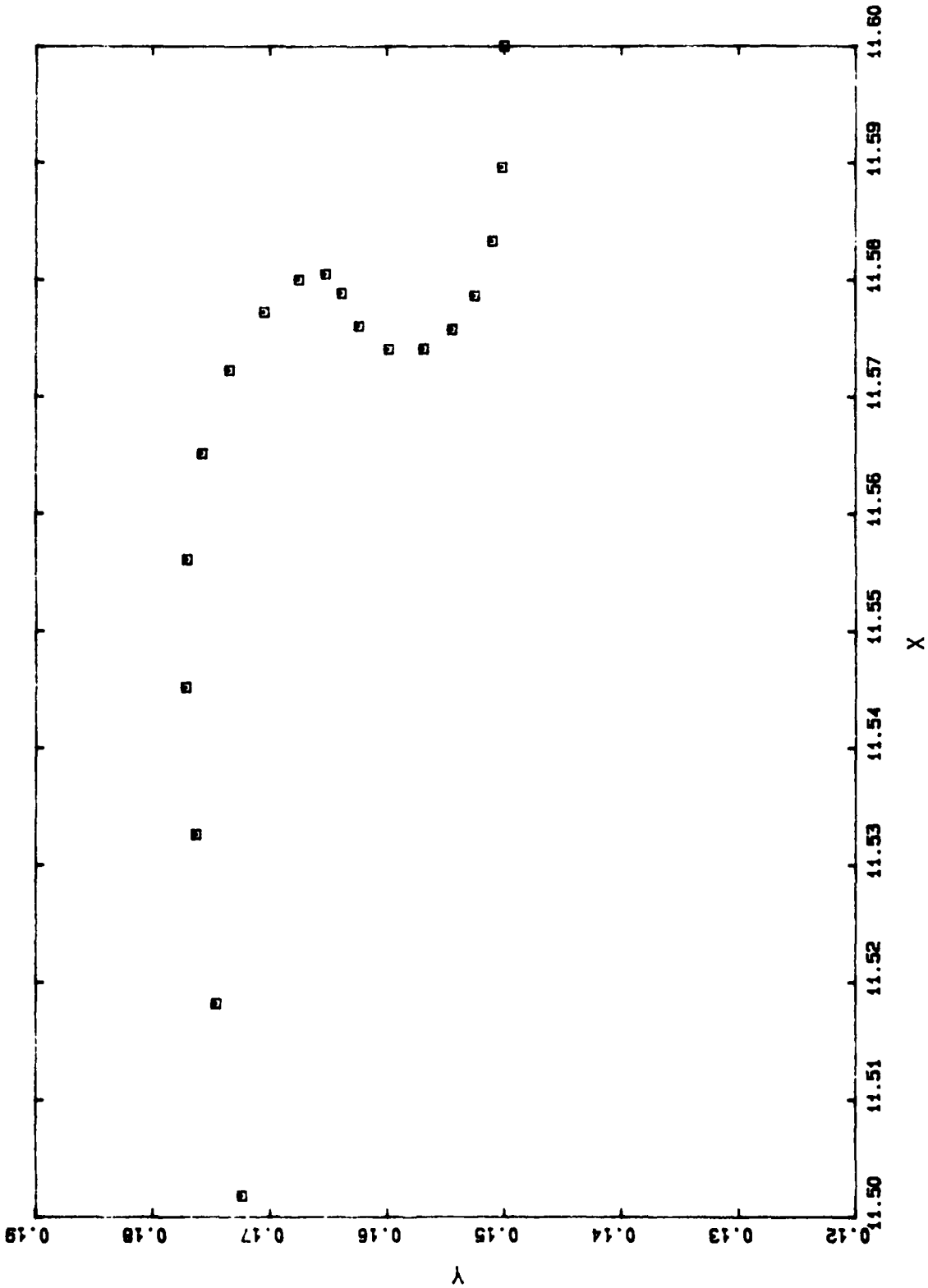

D1 3530 50.9615

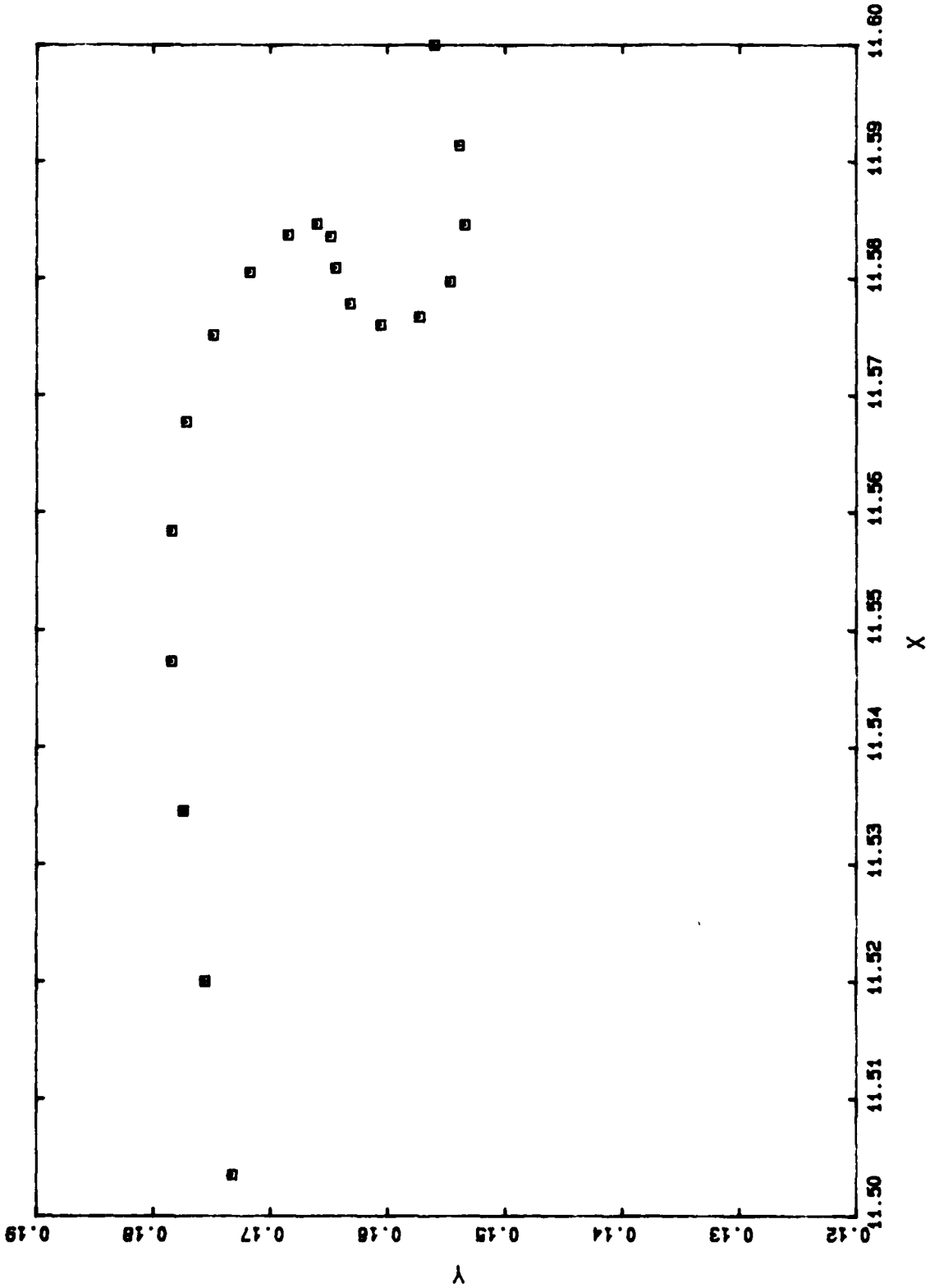

D1 3550 50.9635

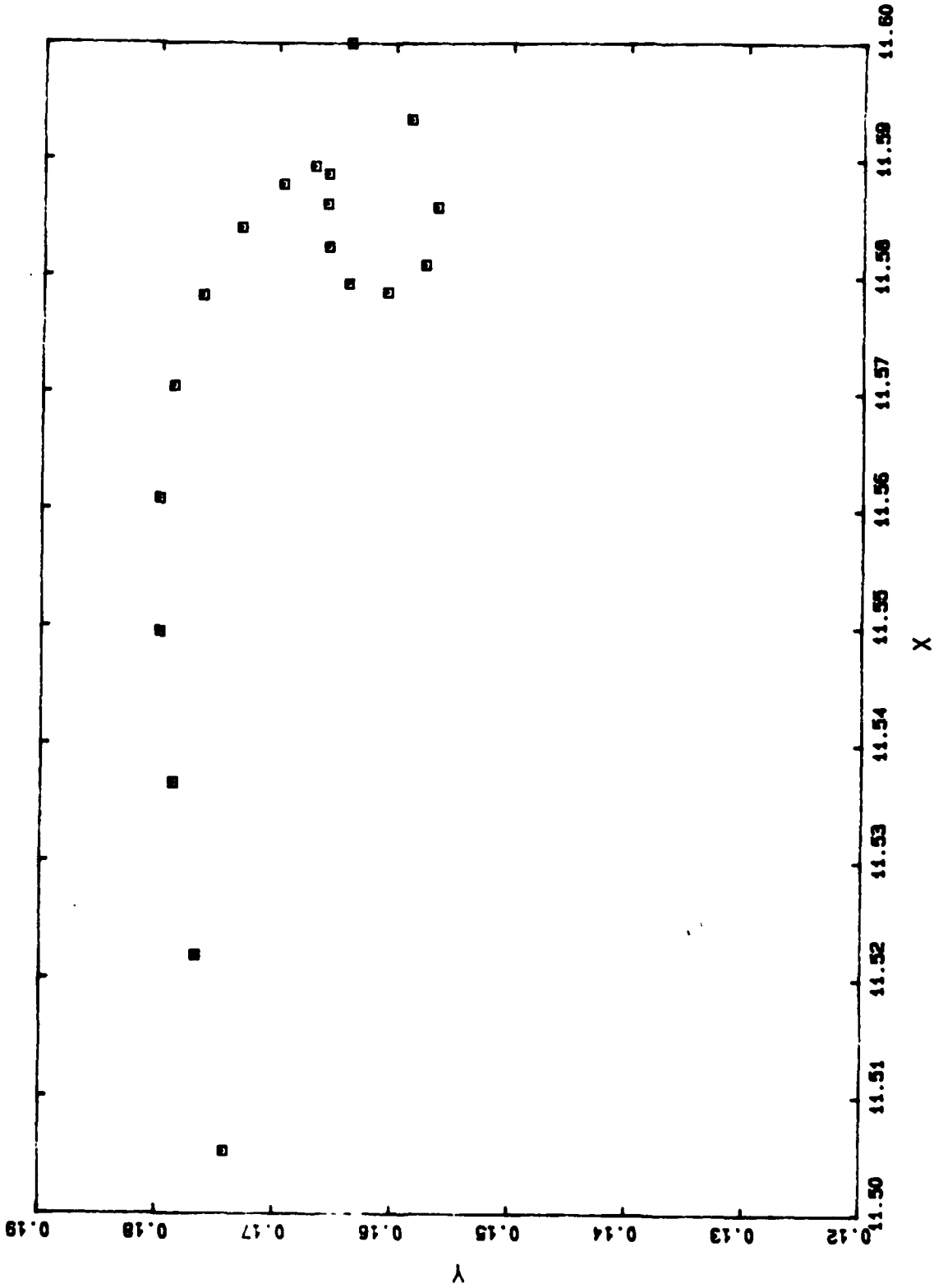

D1 3570 50.9655

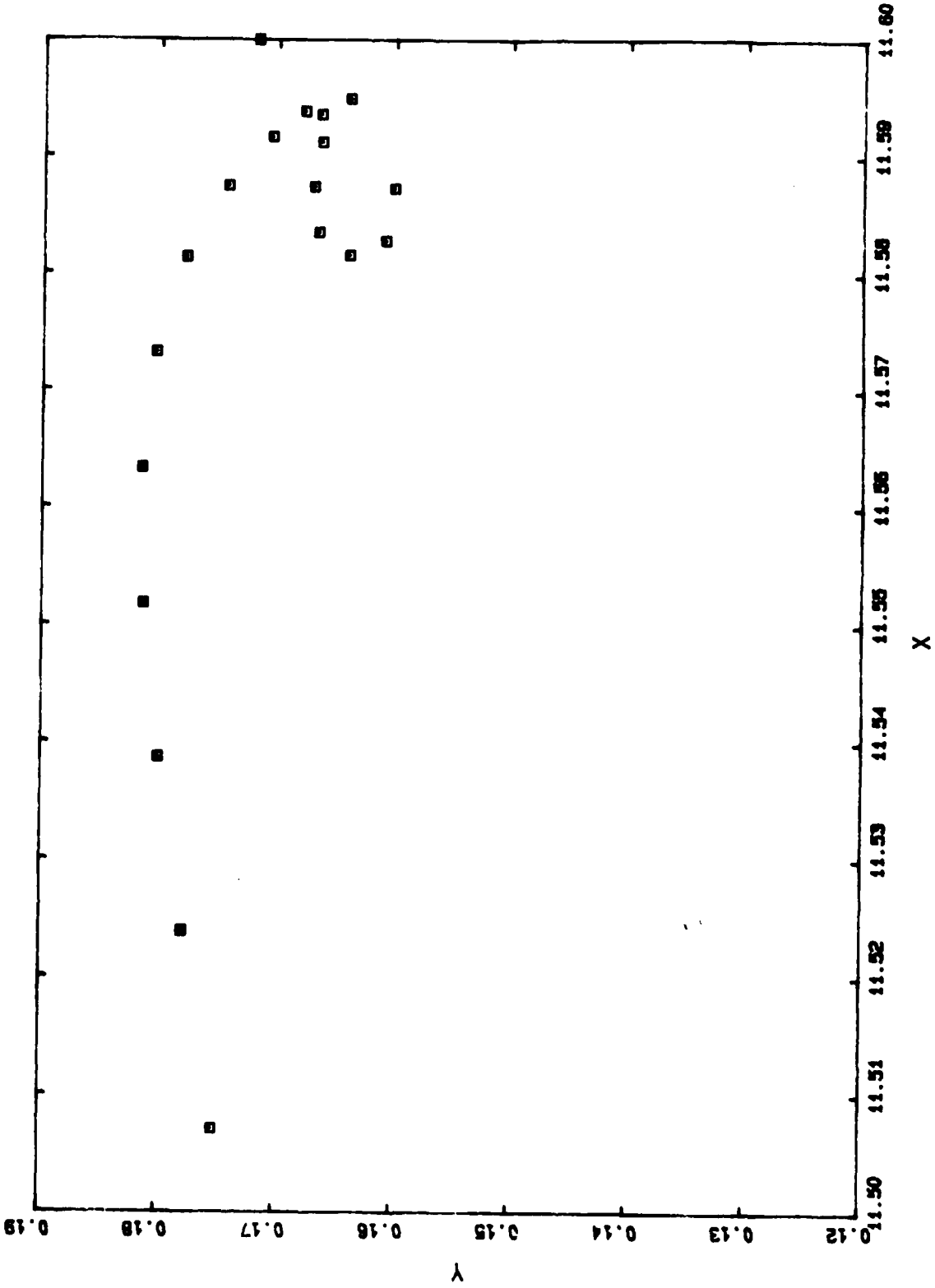

D2 3501 50.9586

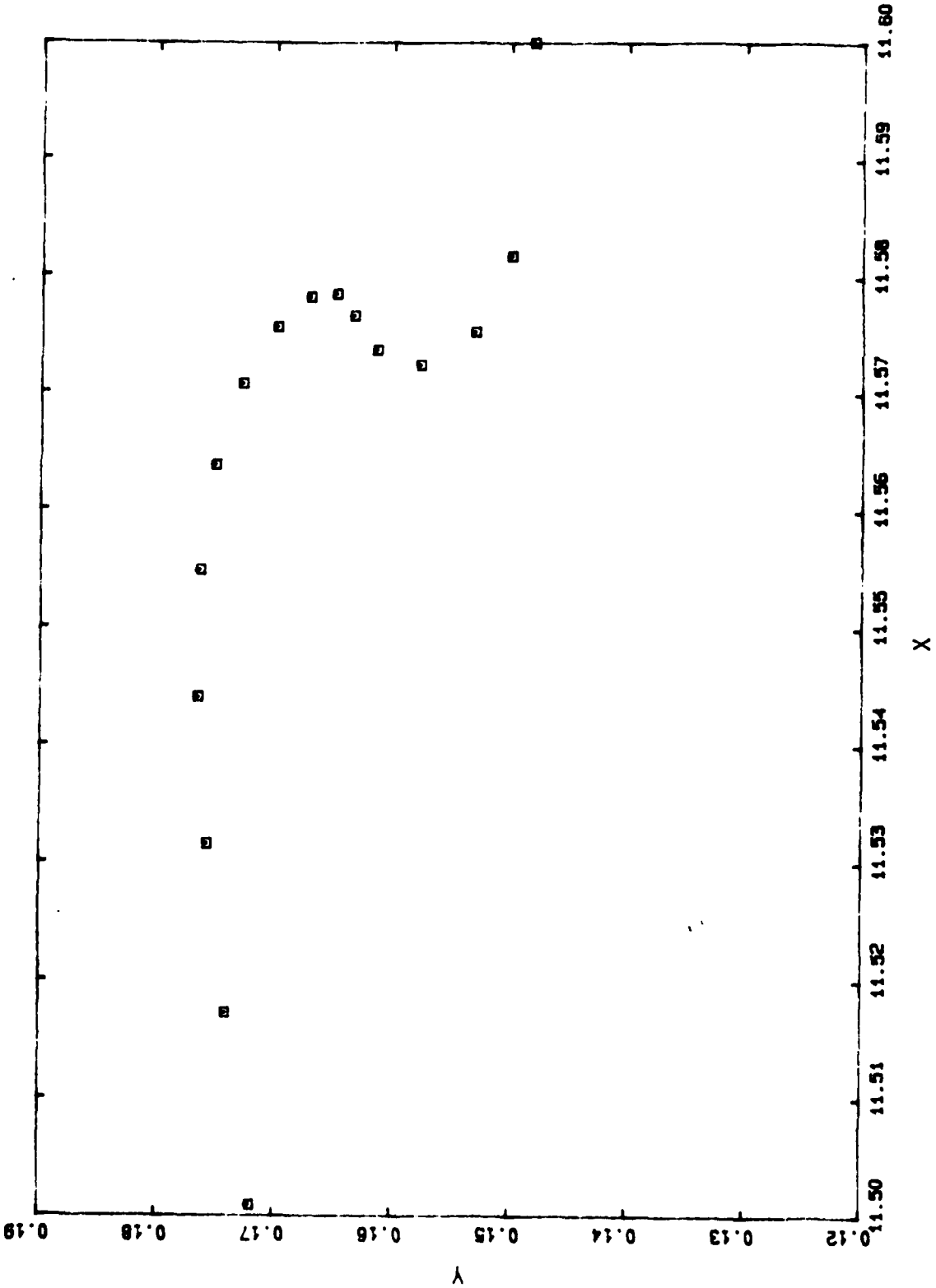

D2 3504 50.9588

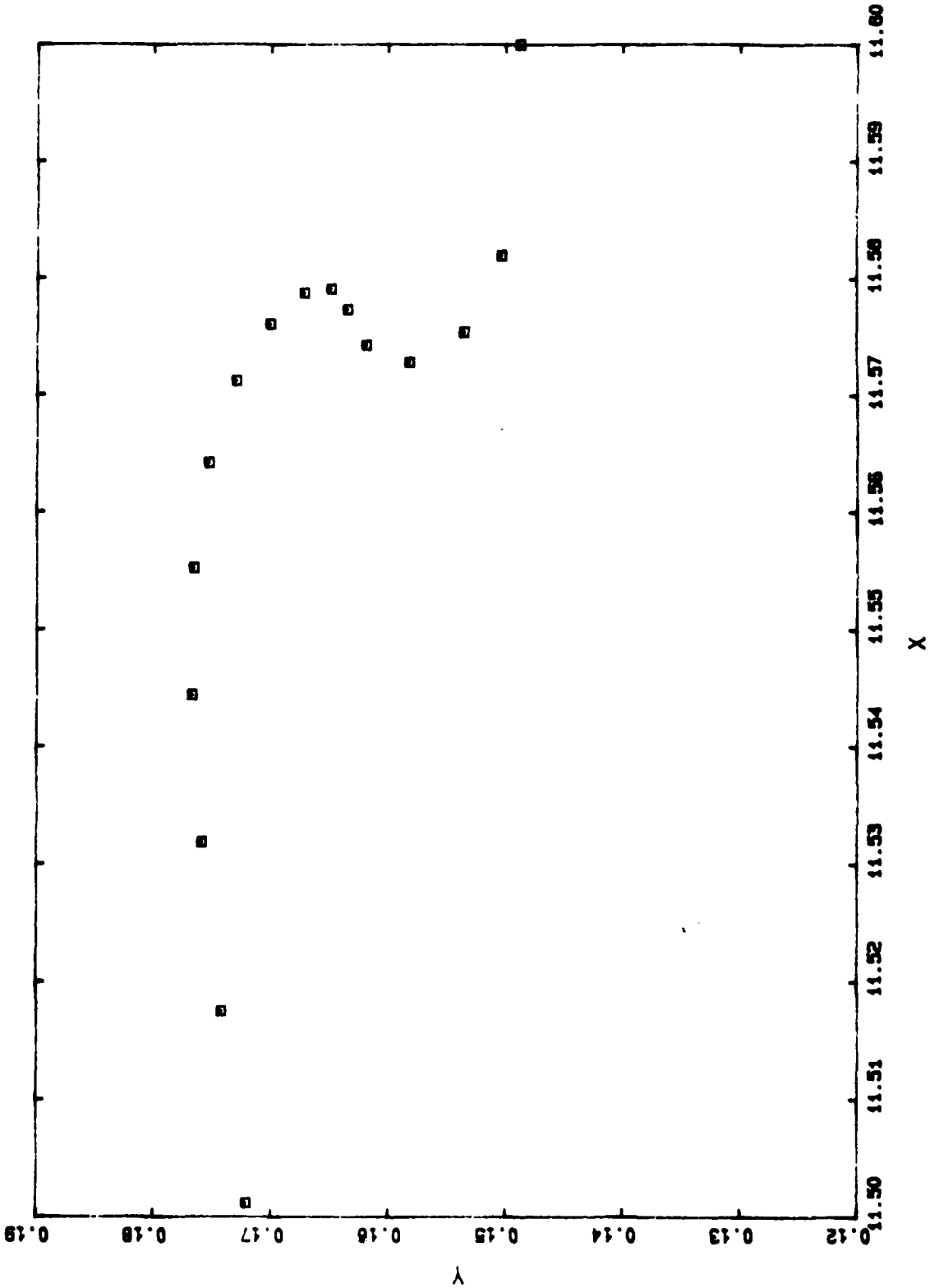

D2 3505 50.9589

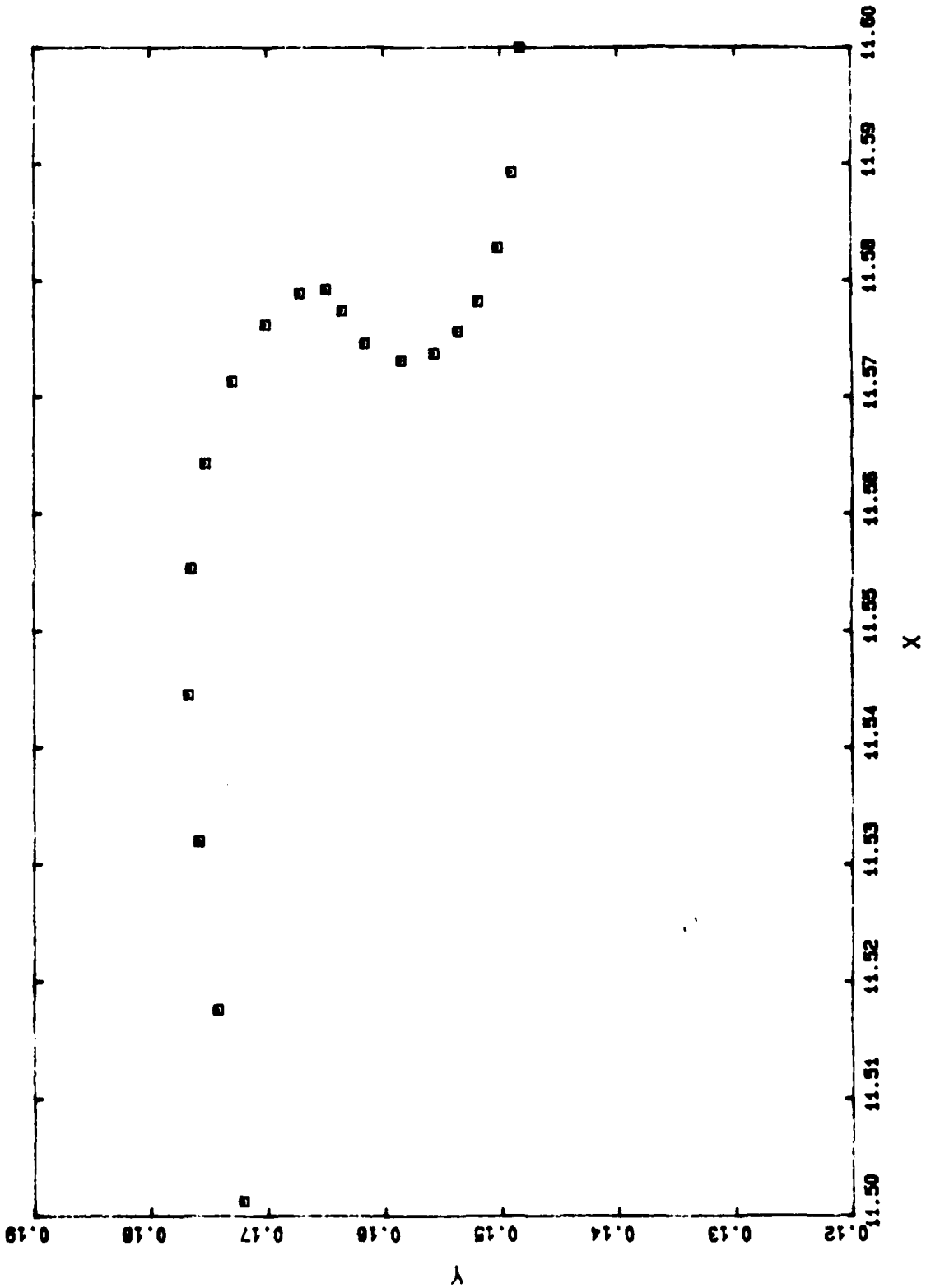

D2 3506 50.9590

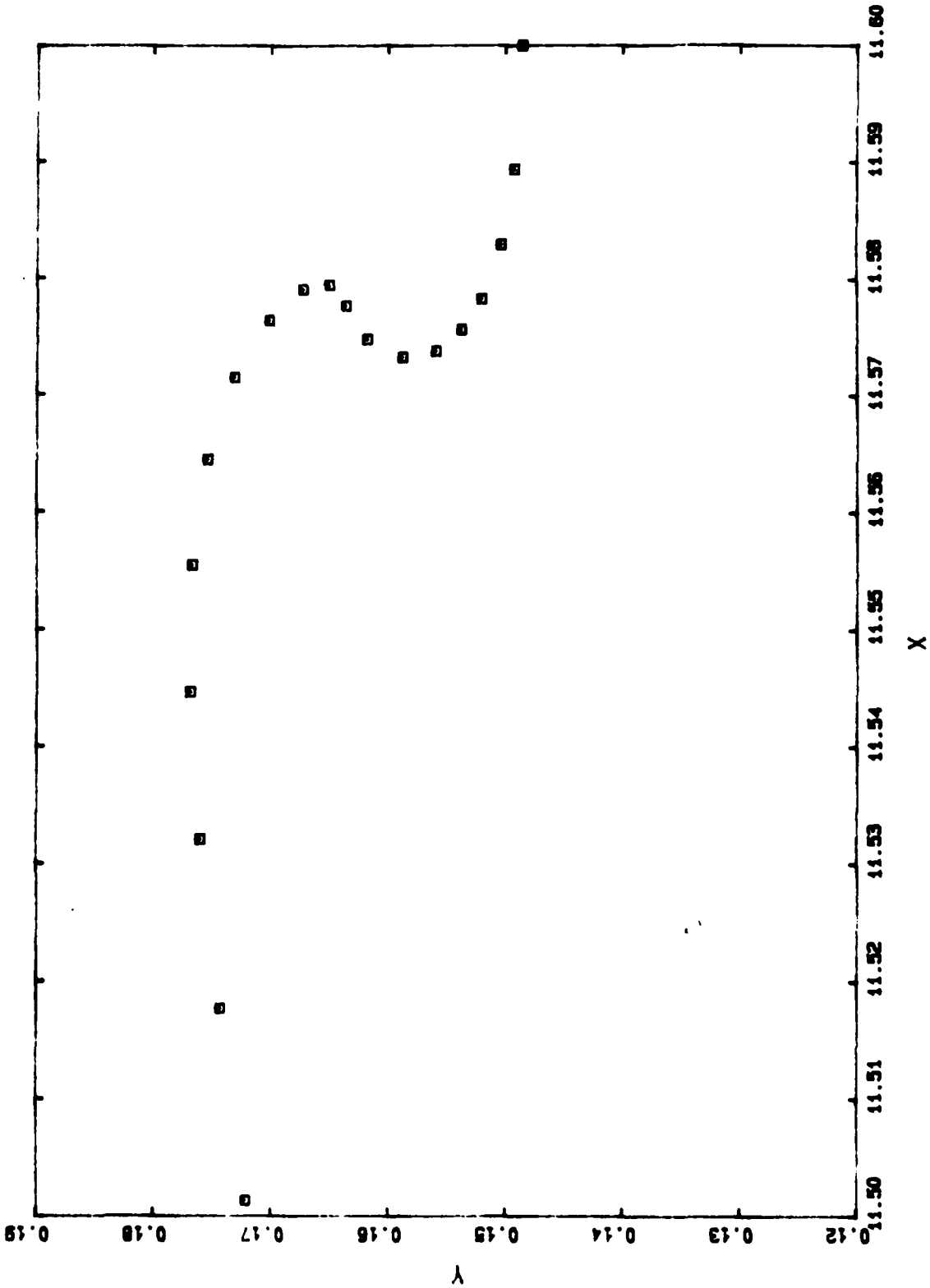

D2 3514 50.9598

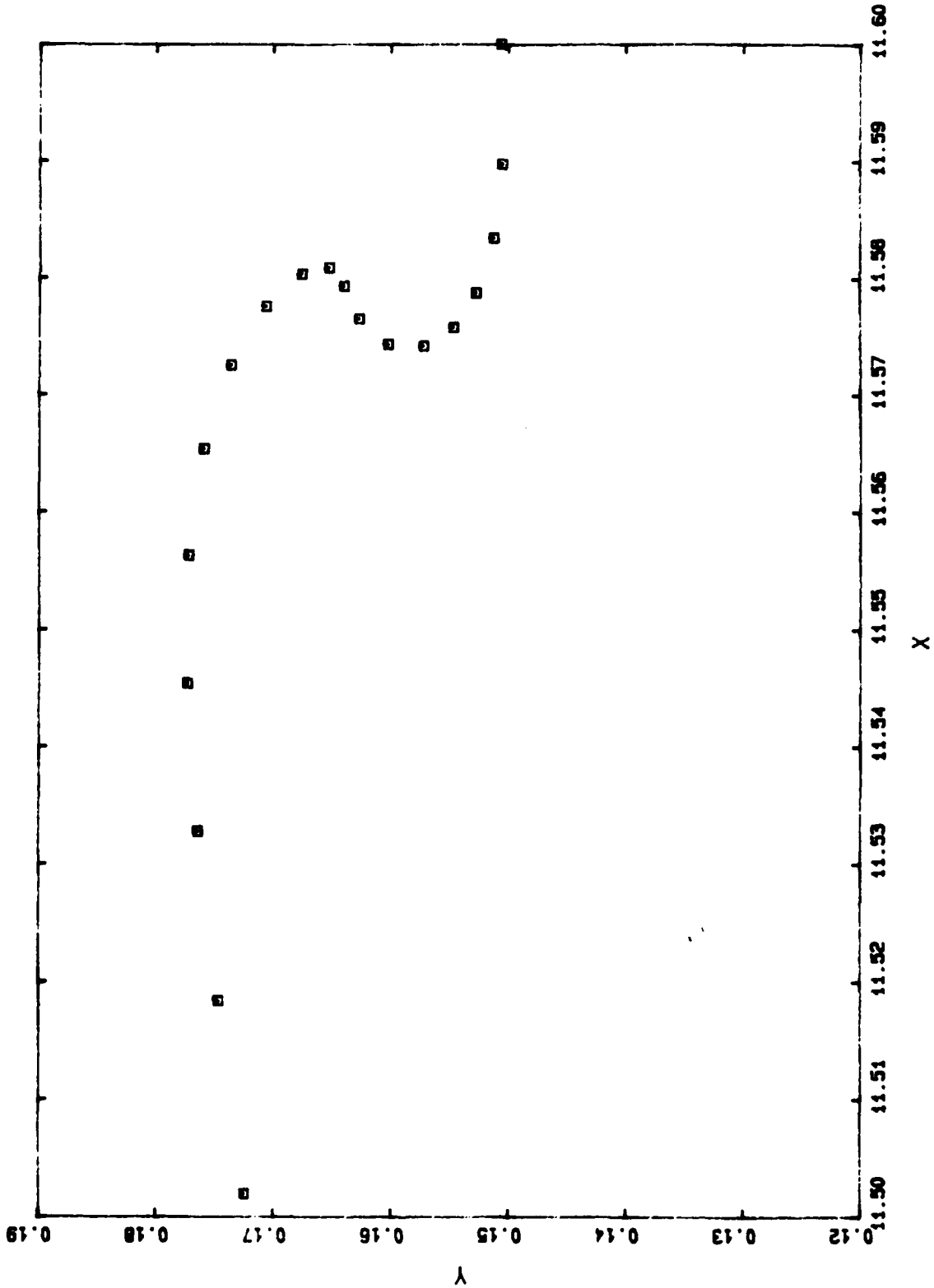

D2 3534 50.9612

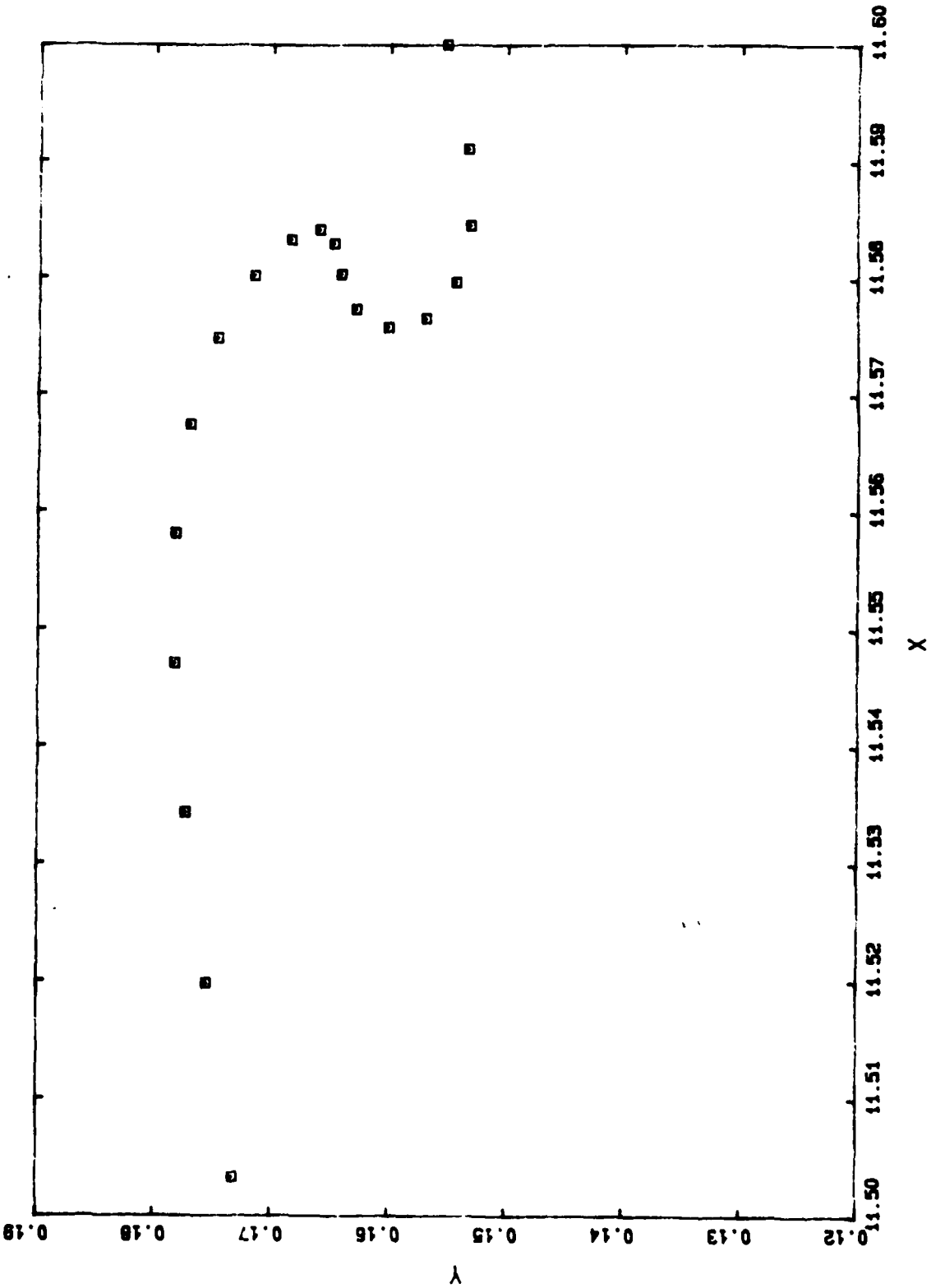

D2 3574 50.9635

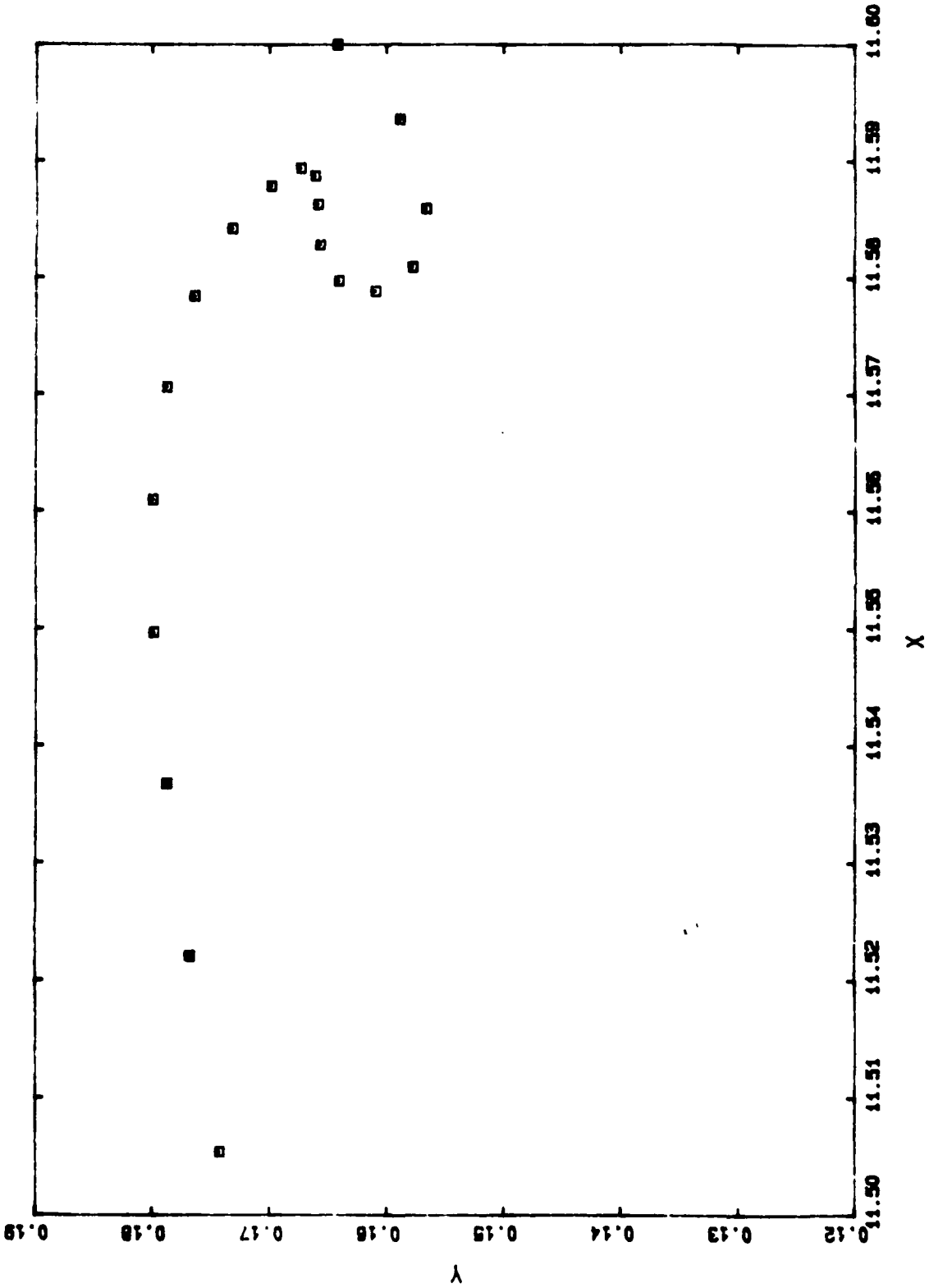

D2 3604 50.9653

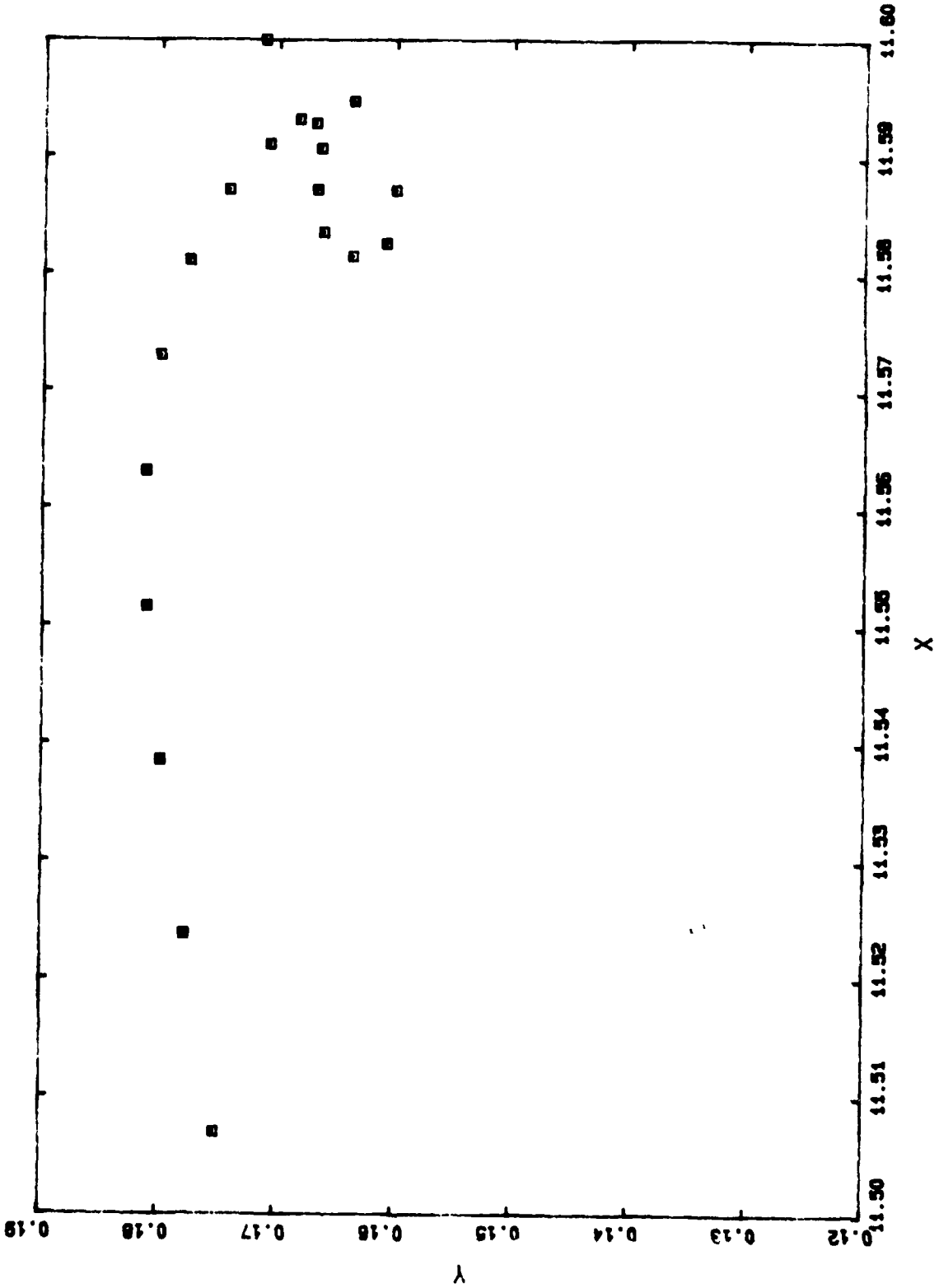

D3 3515 50.9598

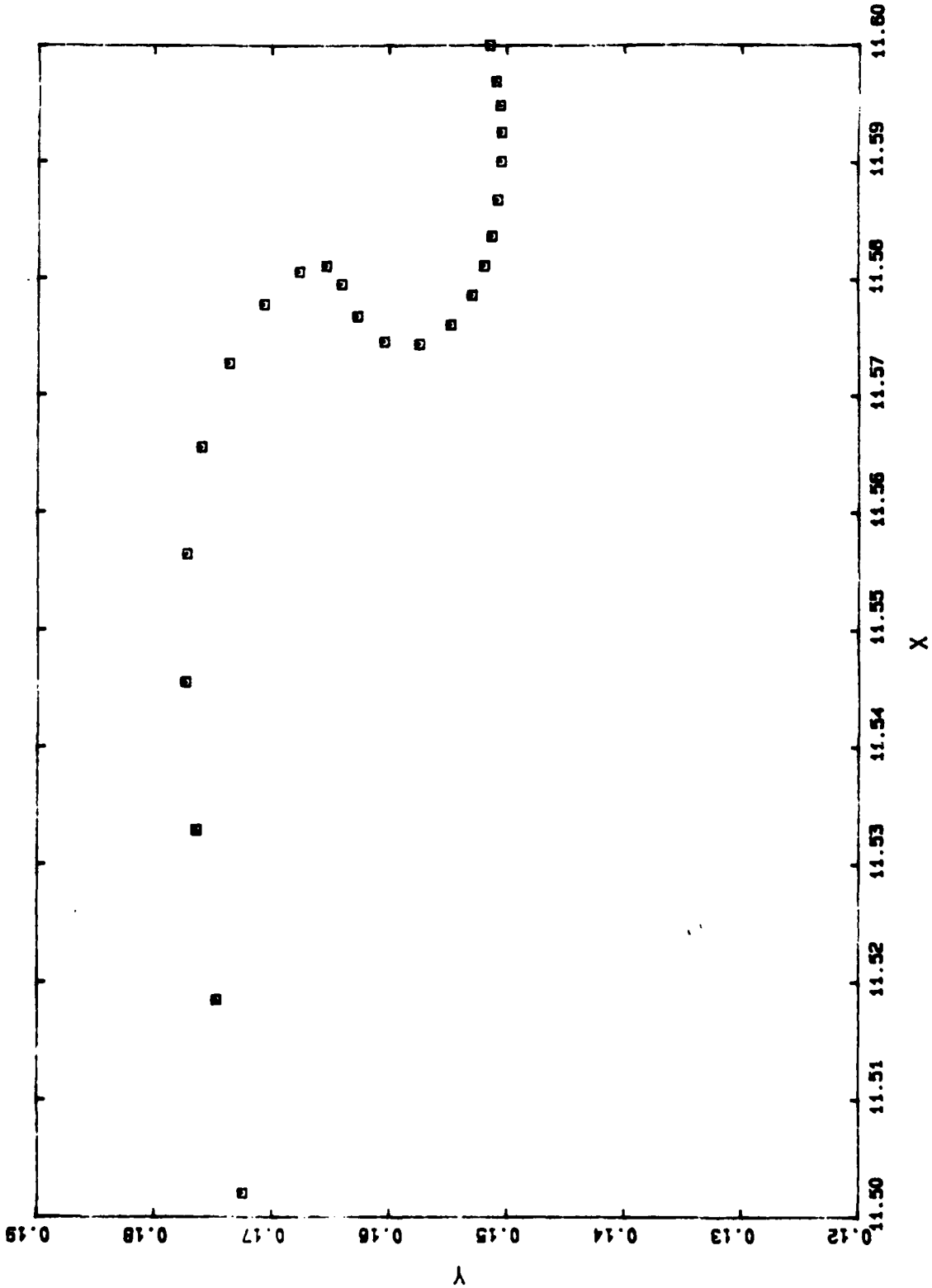

D3 3535 50.9606

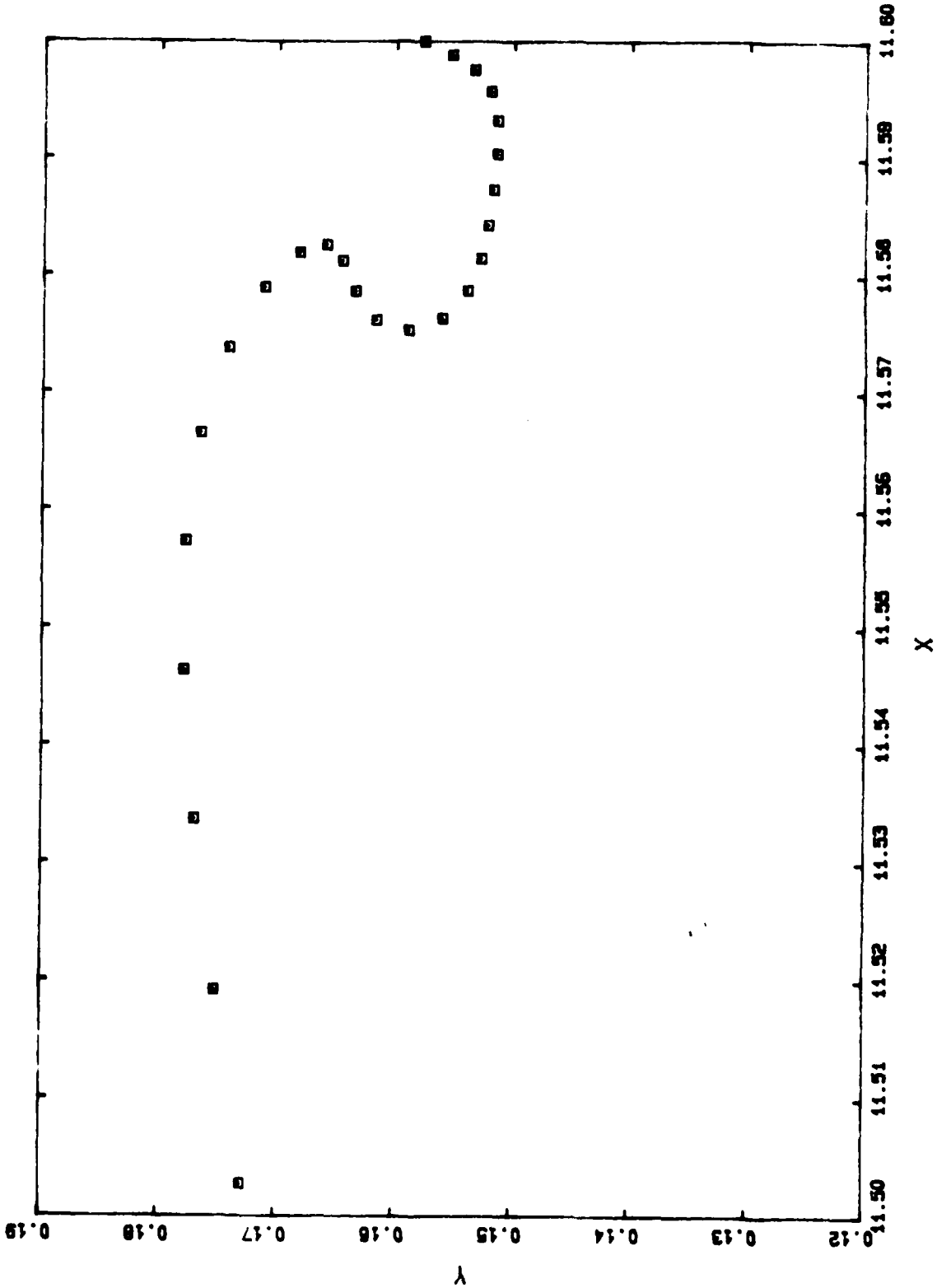

D3 3555 50.9611

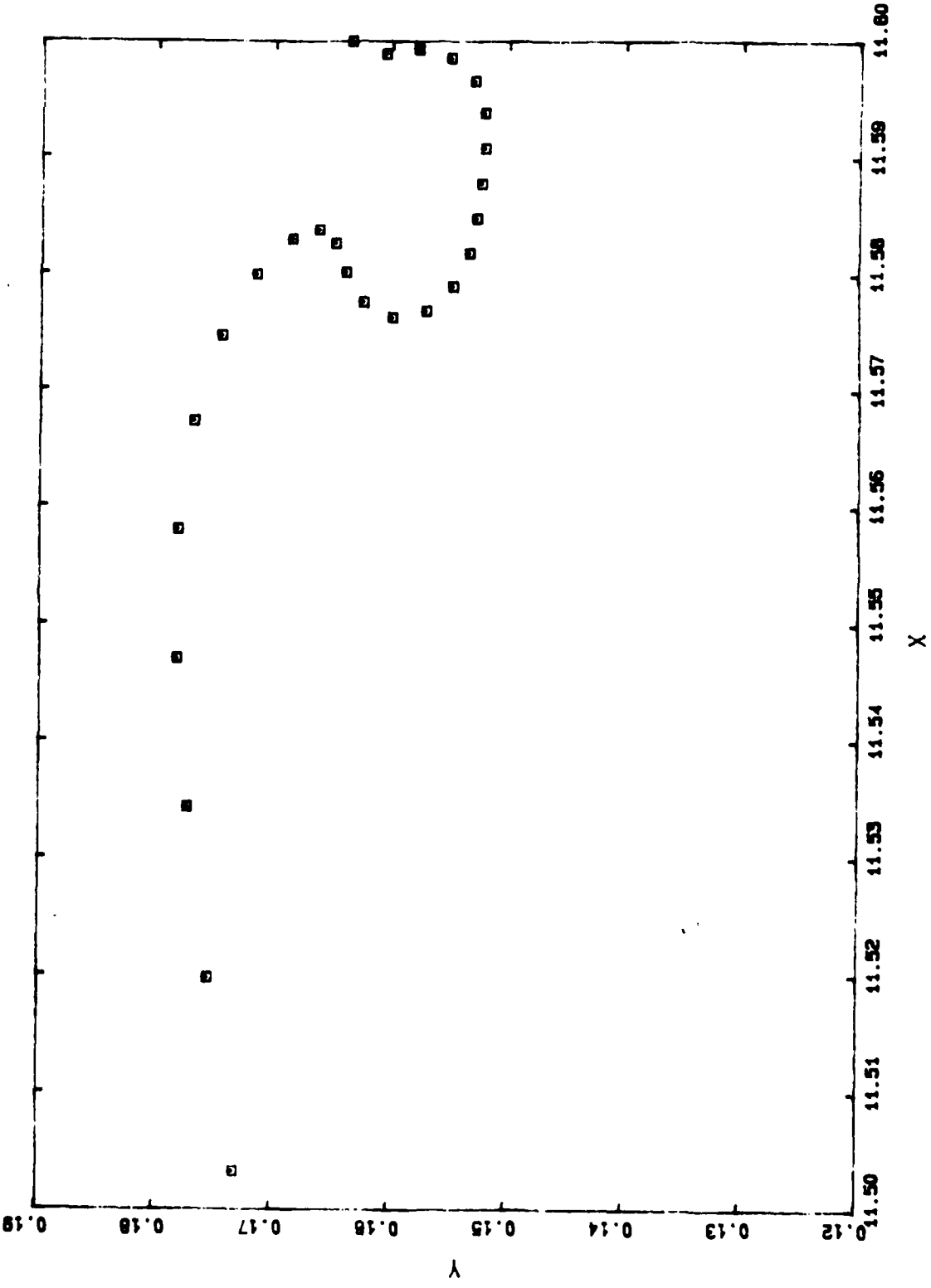

D3 3575 50.9615

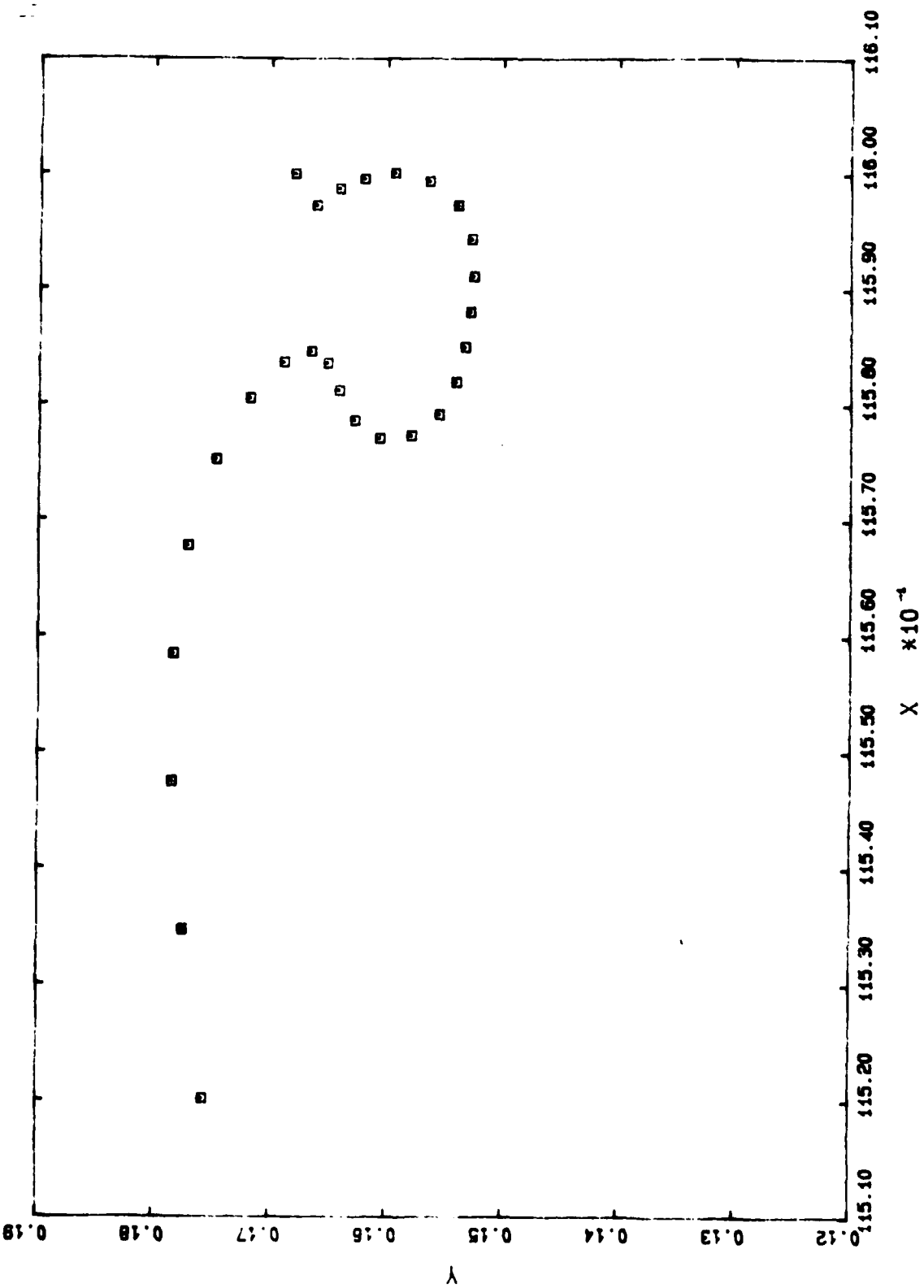

D4 3501 50.9586

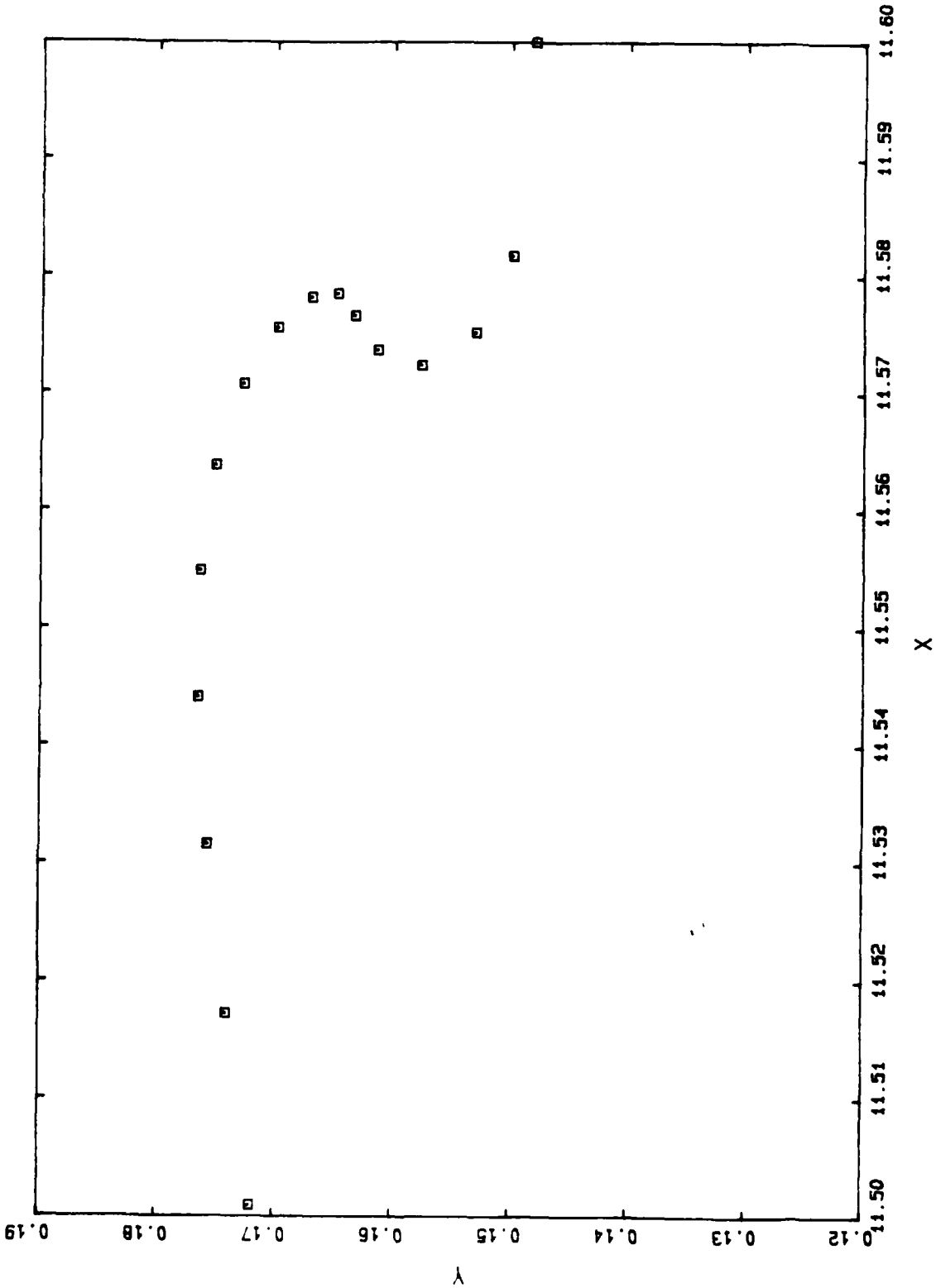

D4 3504 50.9589

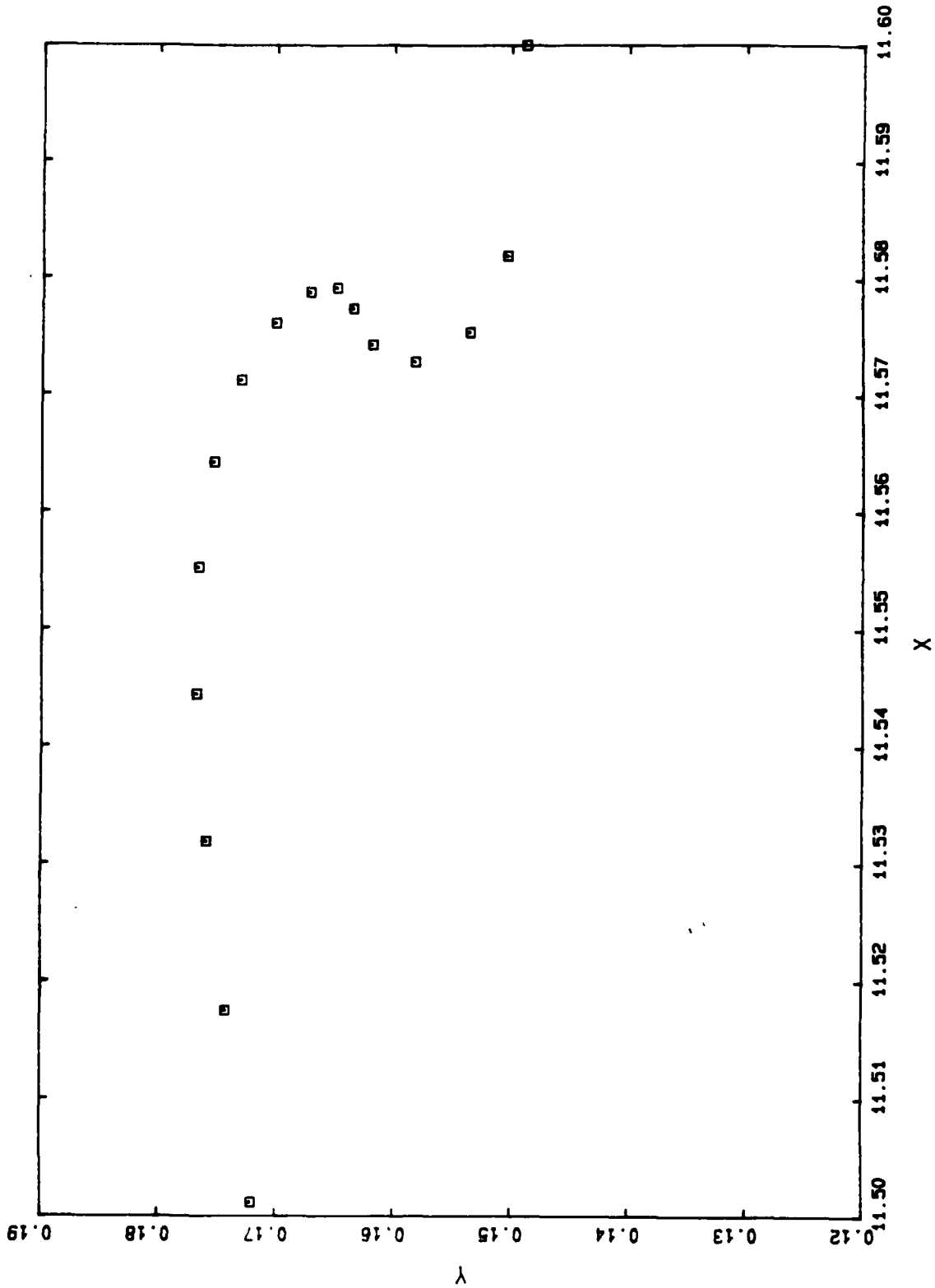

D4 3505 50.9590

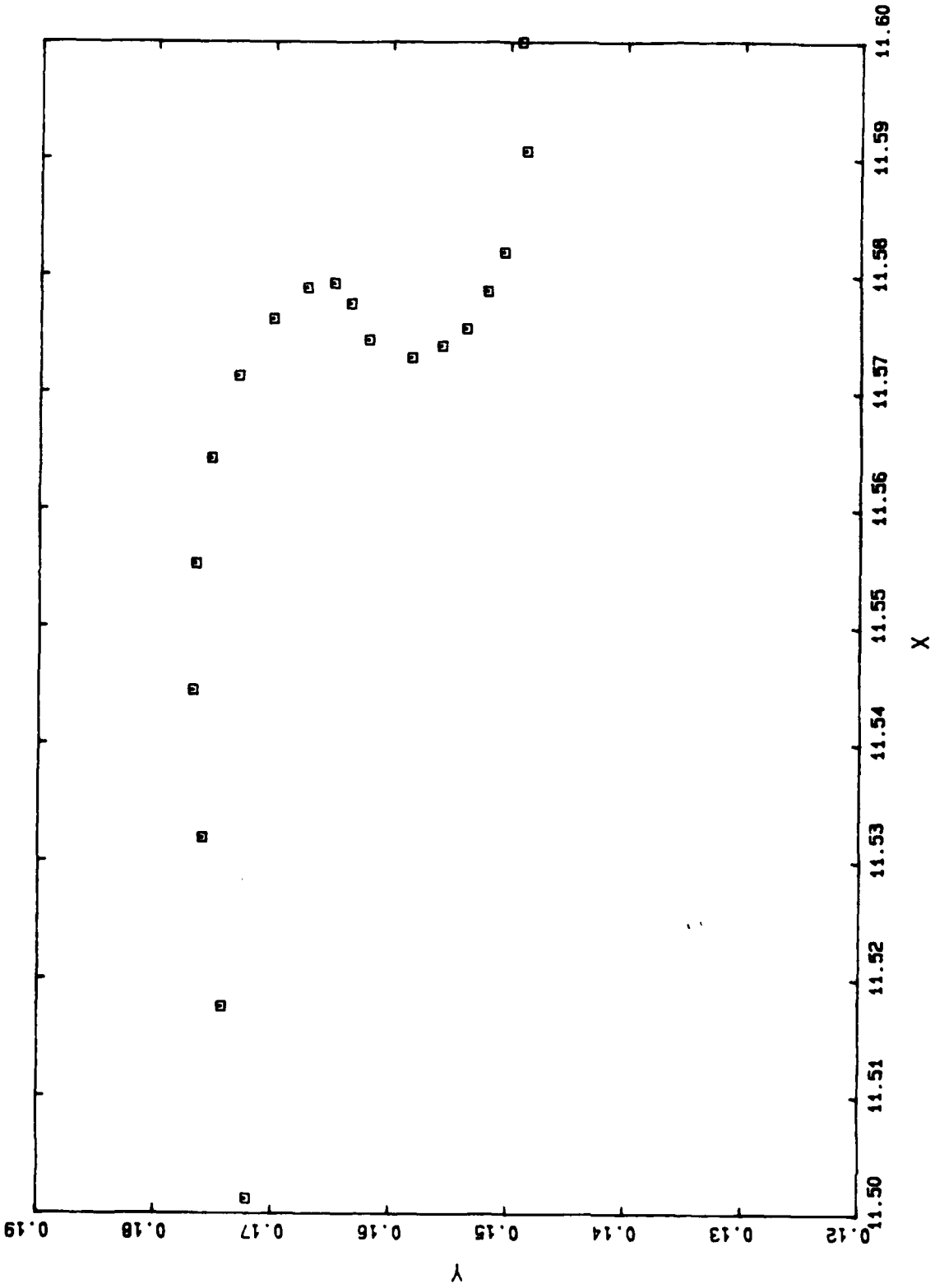

D4 3506 50.9591

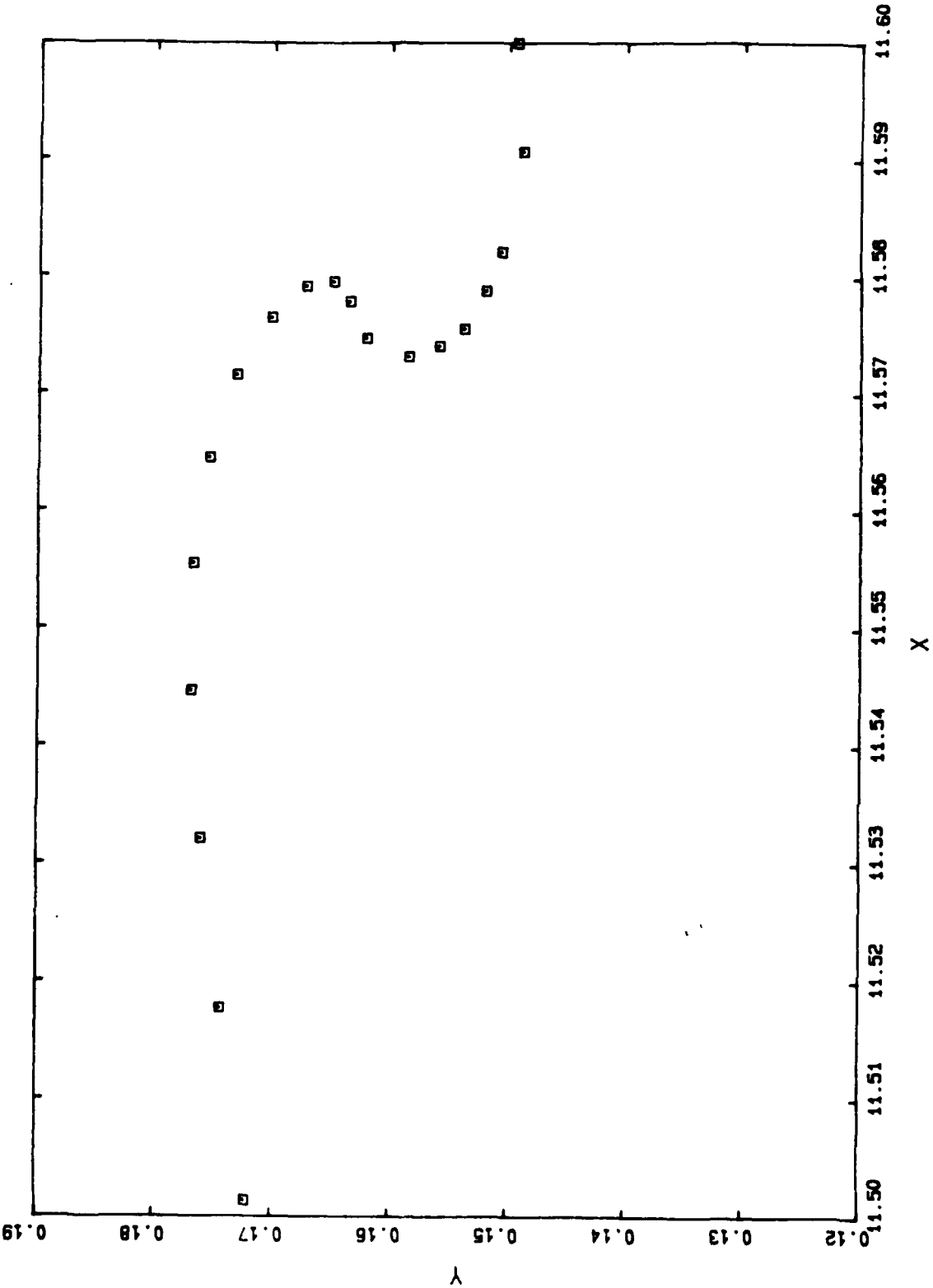

D4 3515 50.9600

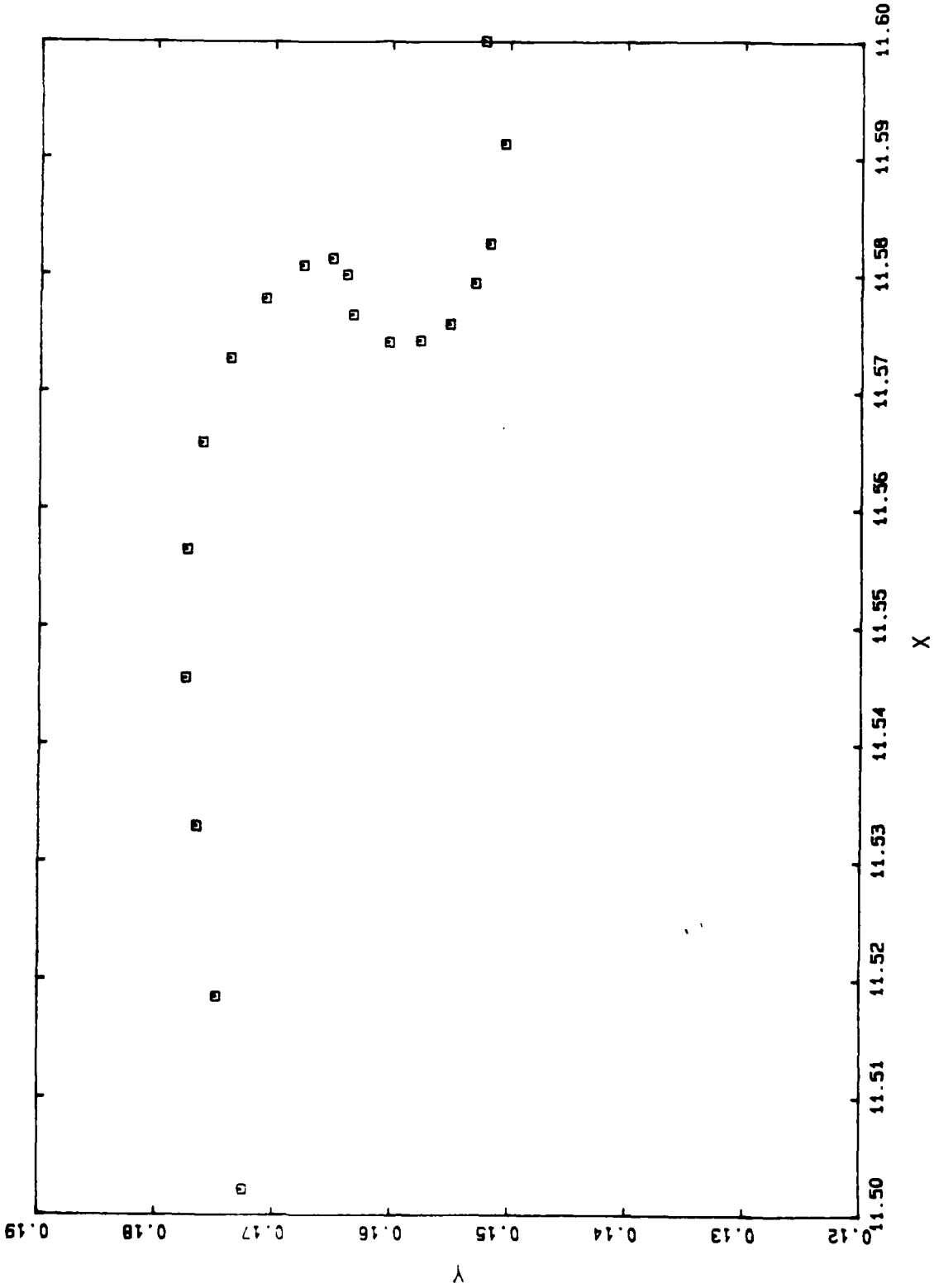

D4 3525 50.9610

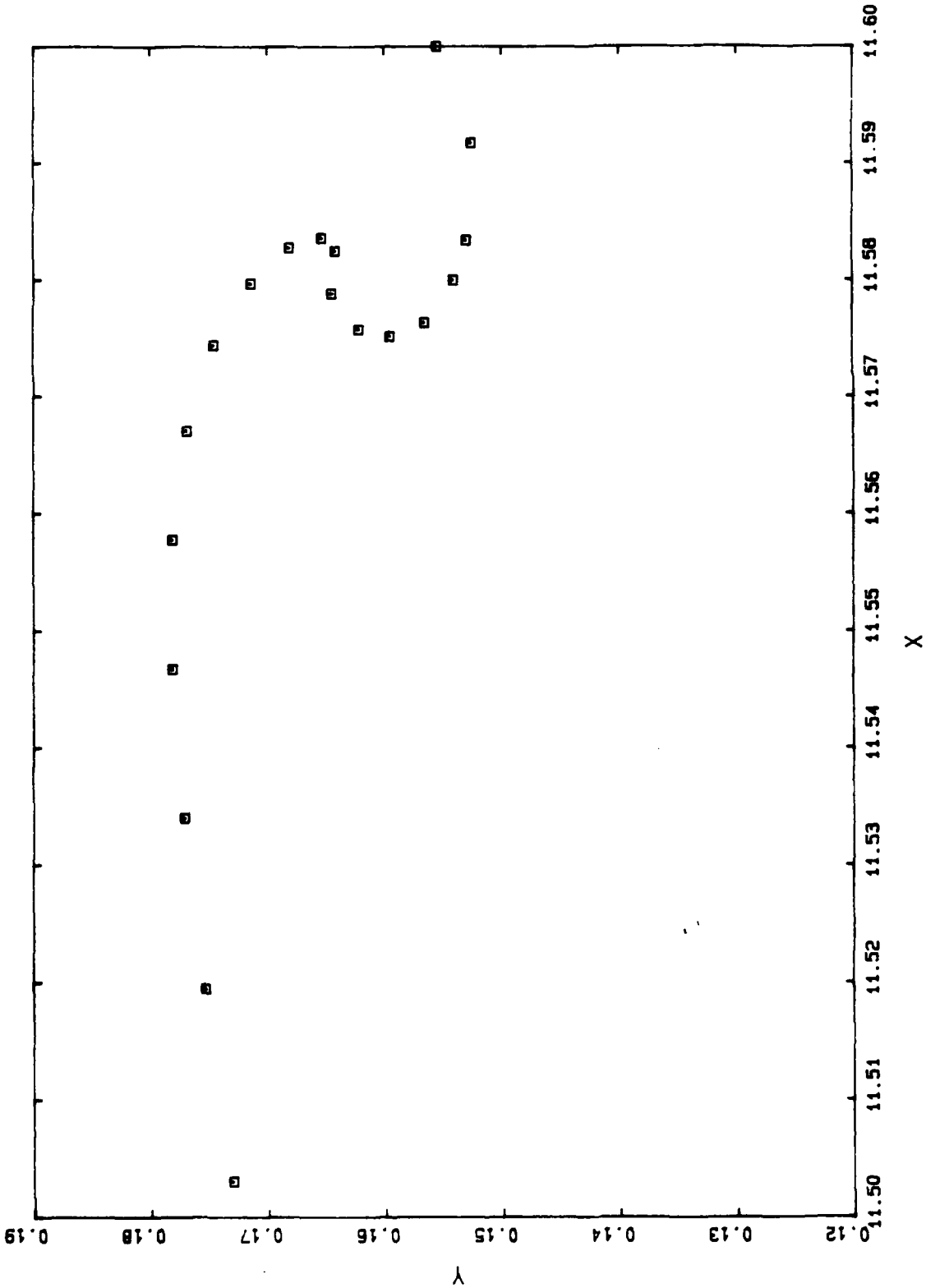

D4 3535 50.9620

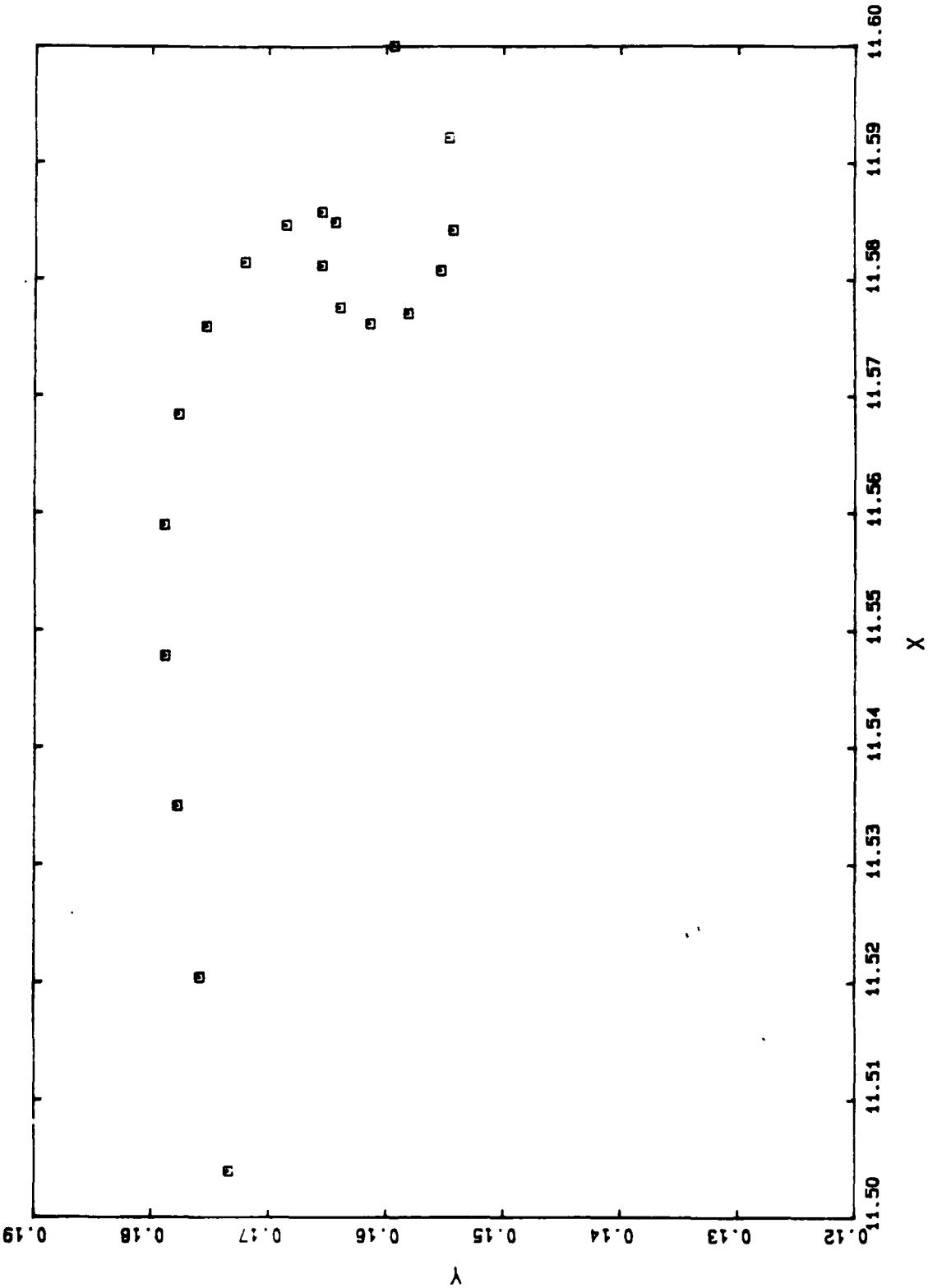

D4 3545 50.9630

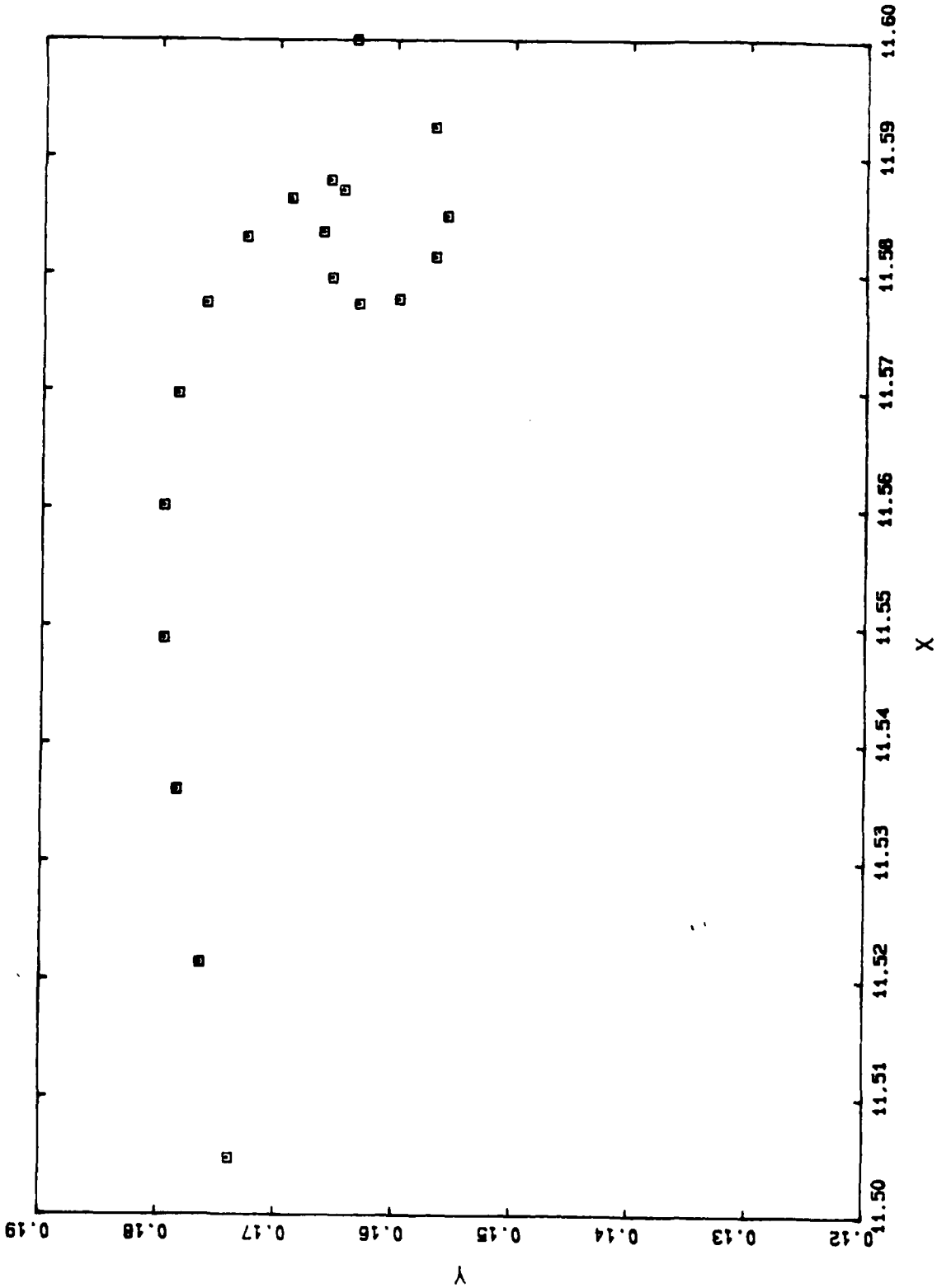

D4 3555 50.9640

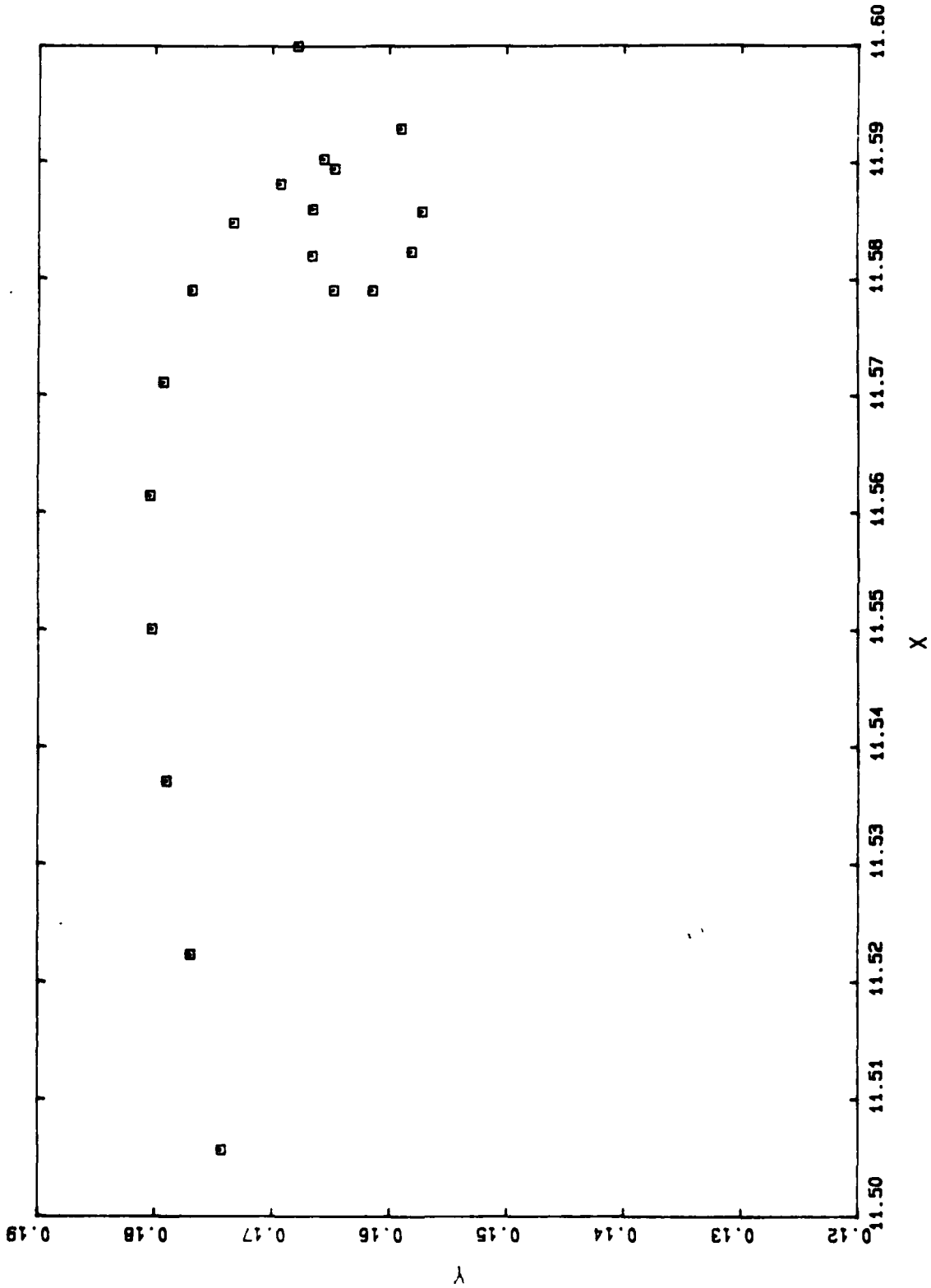

D4 3565 50.9650

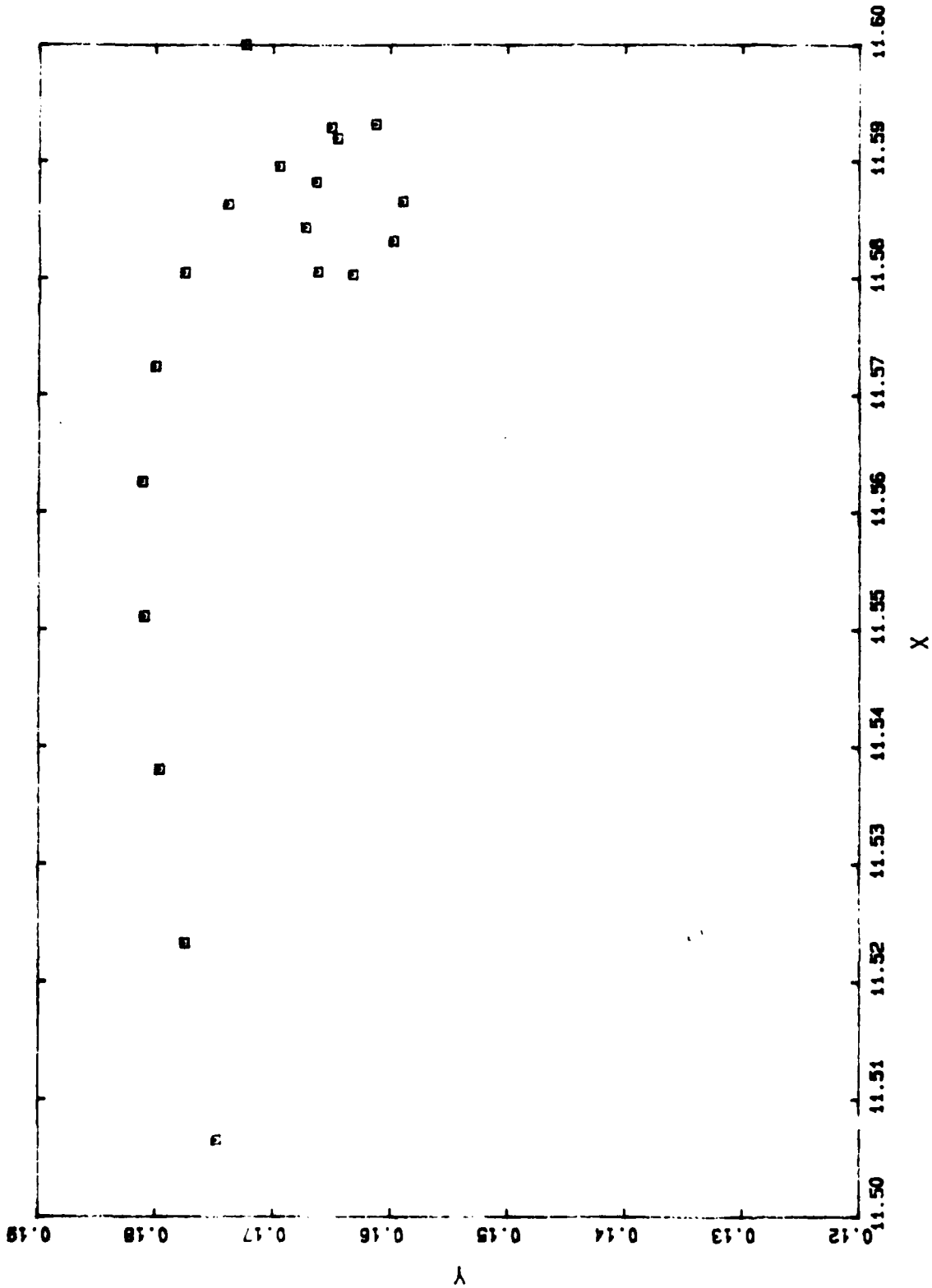

D5 3130 50.8642

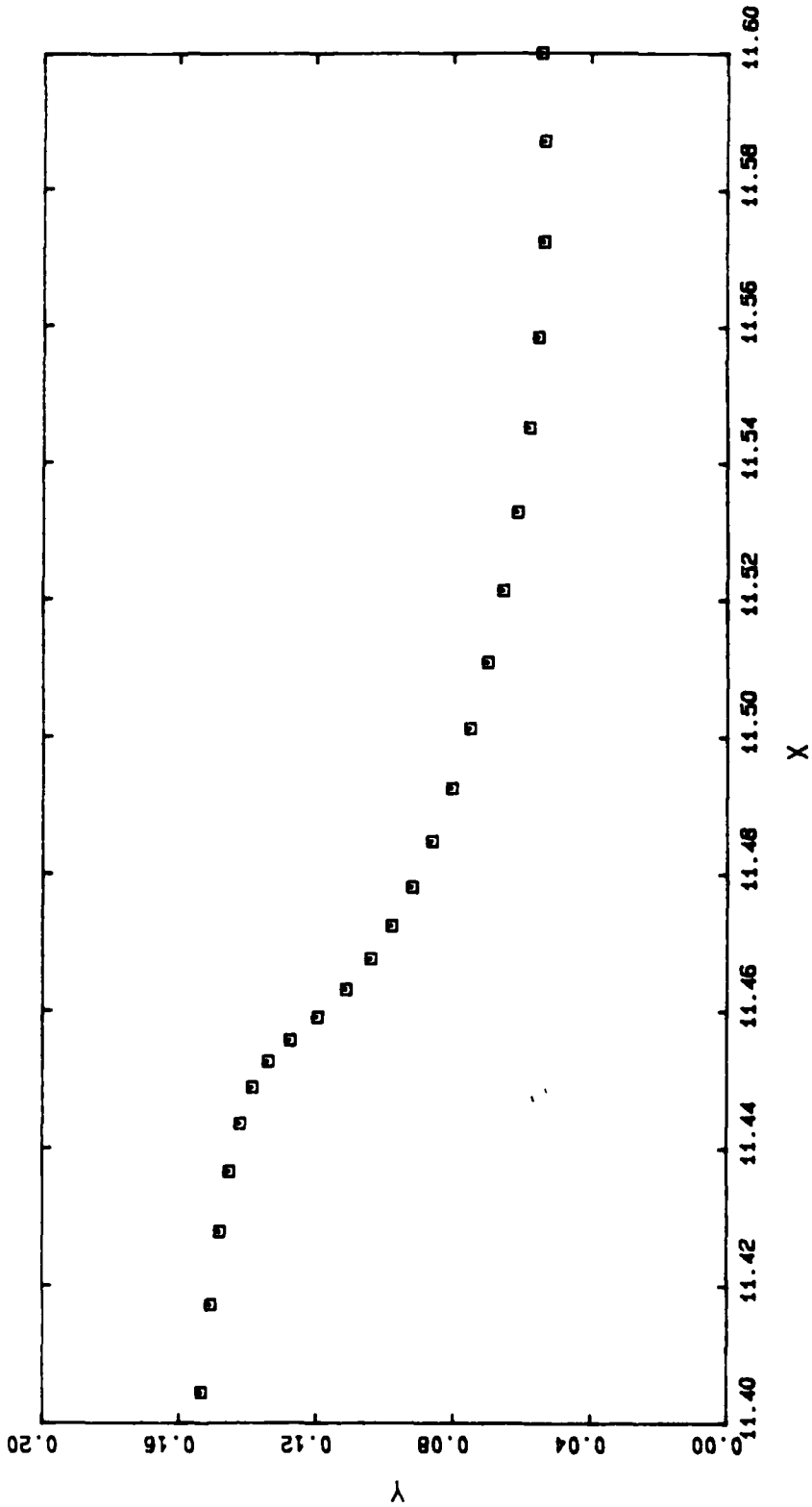

D5 3230 50.9093

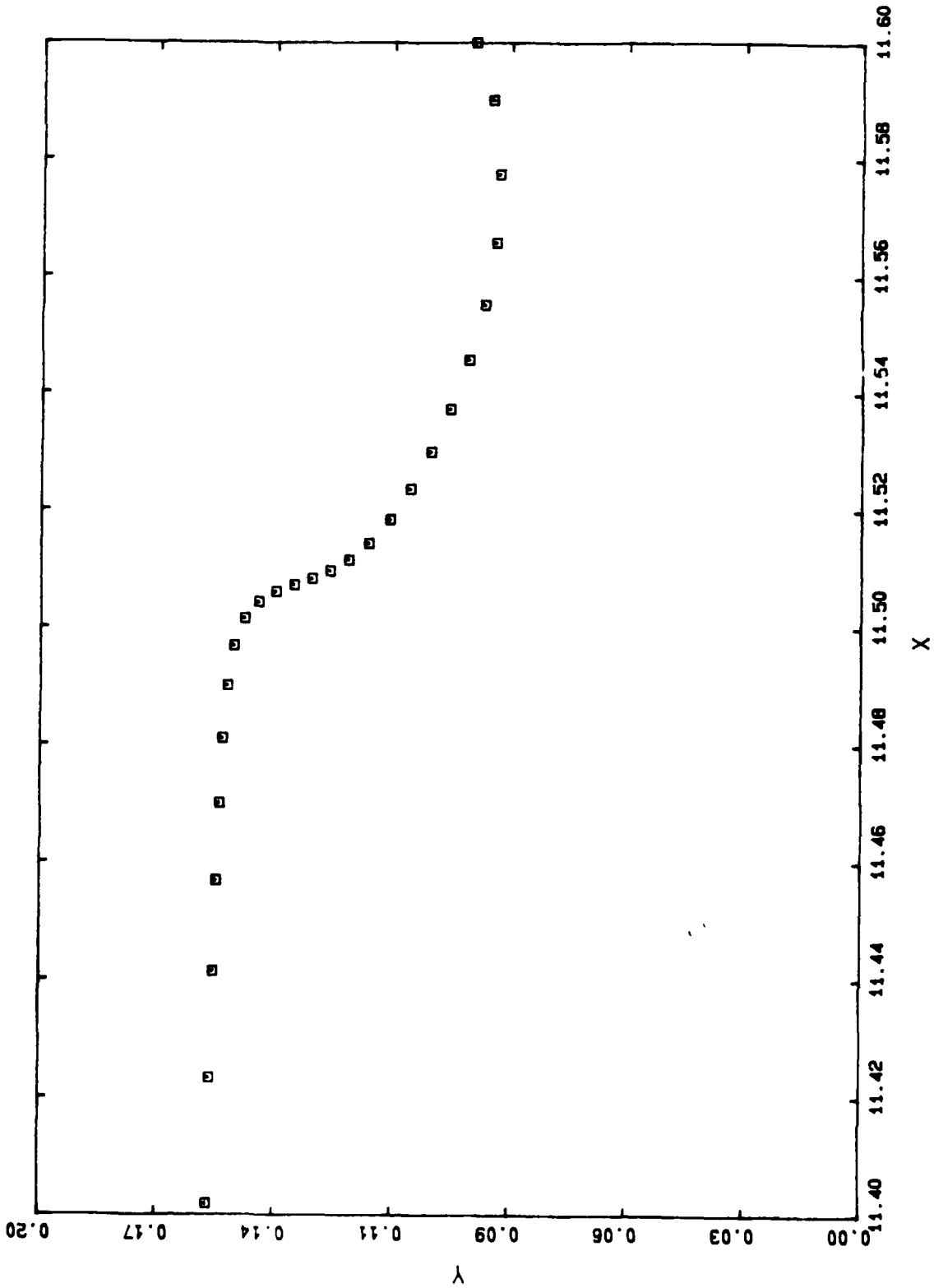

D5 3330 50.9331

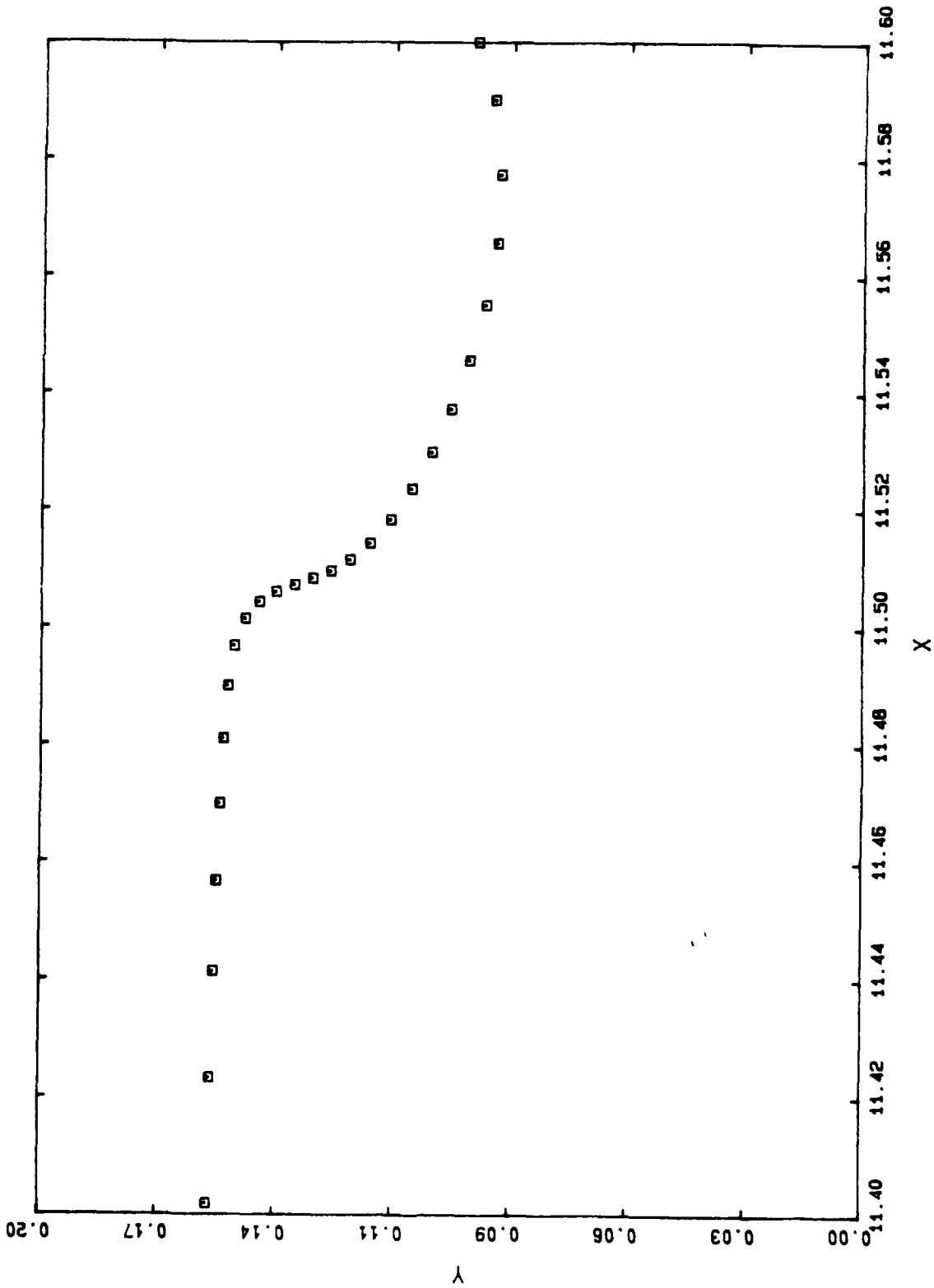

D5 3330 50.9331

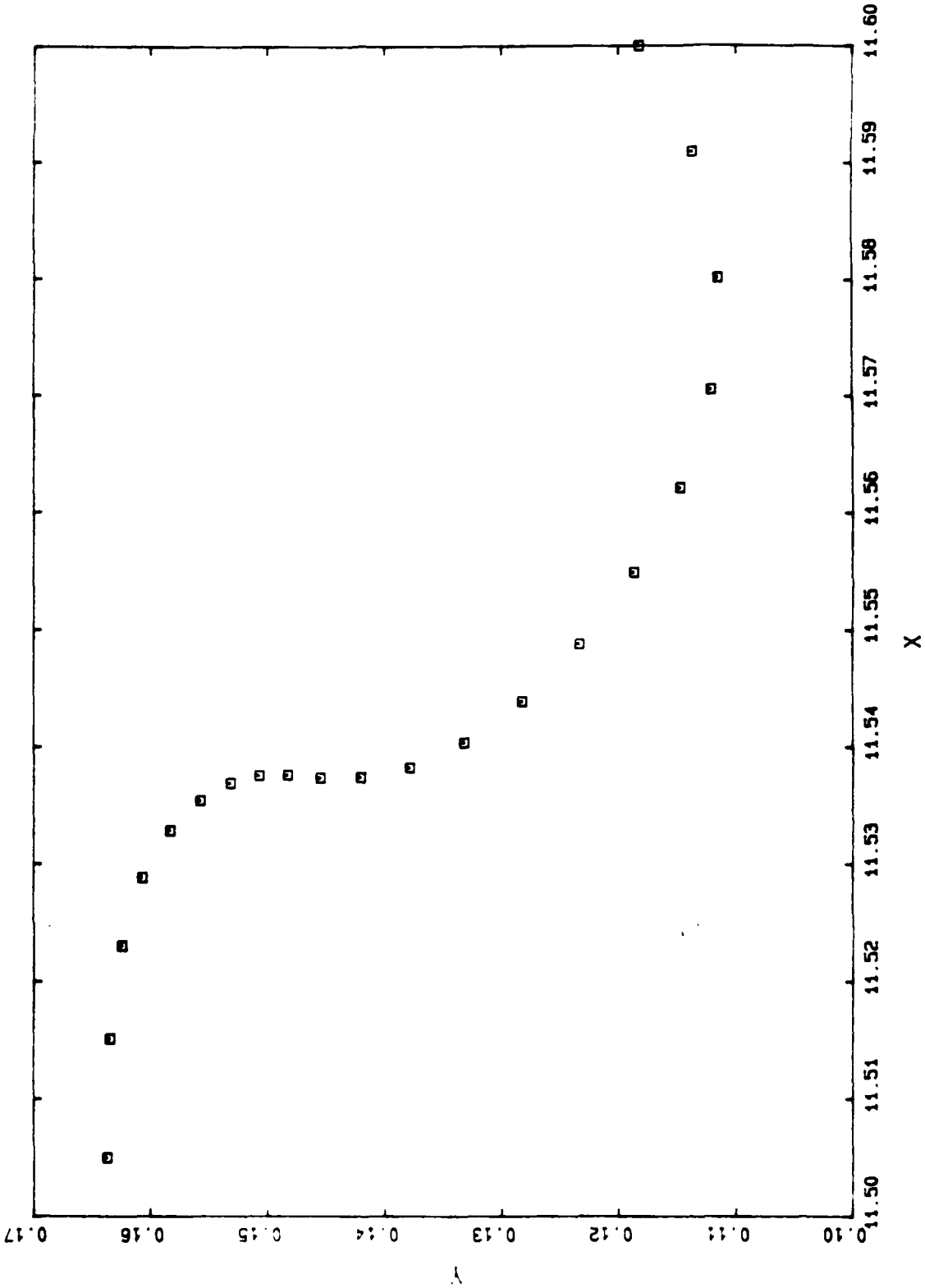

D5 3430 50.9451

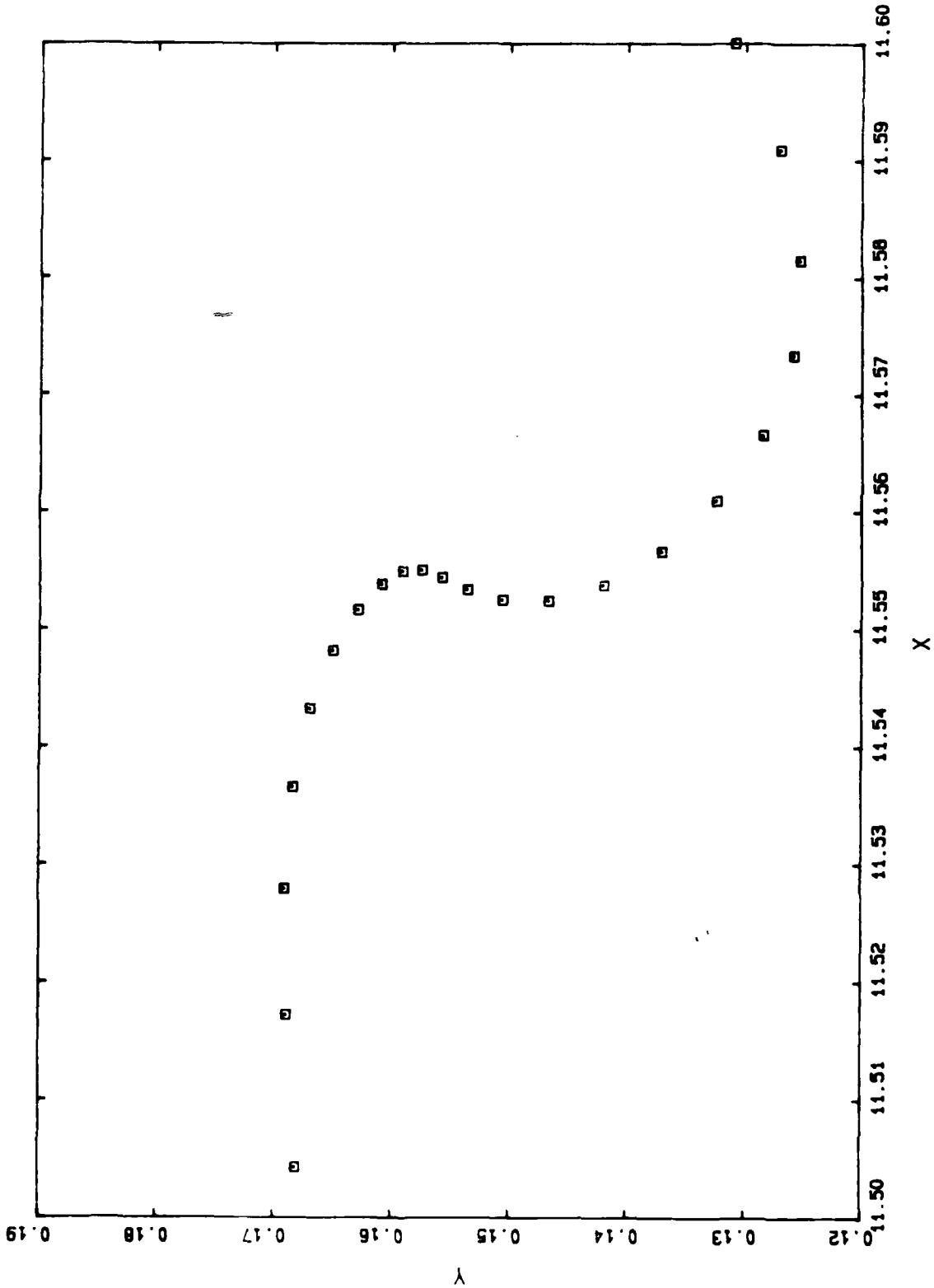

D5 3530 50.9535

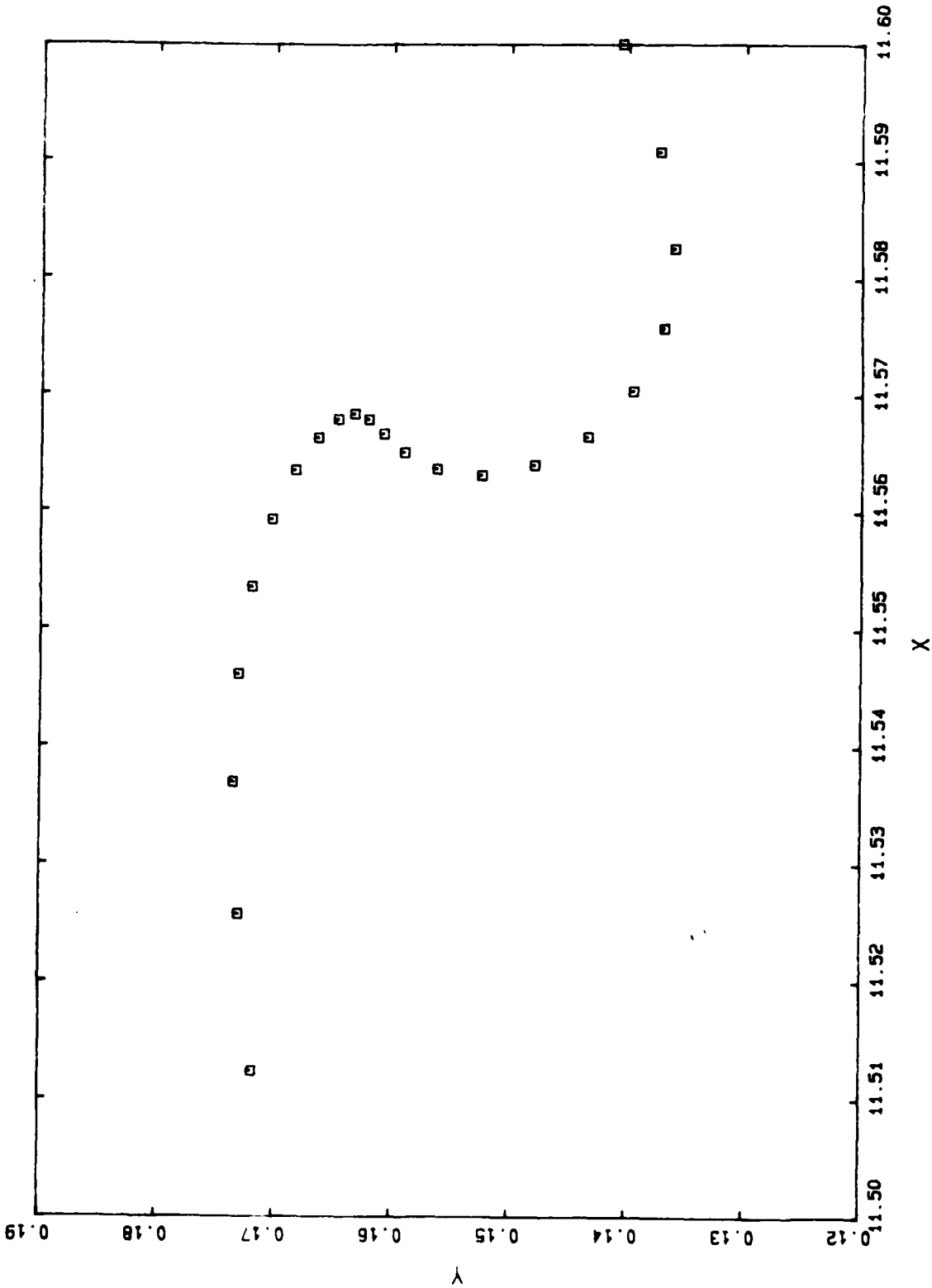

D5 3630 50.9600

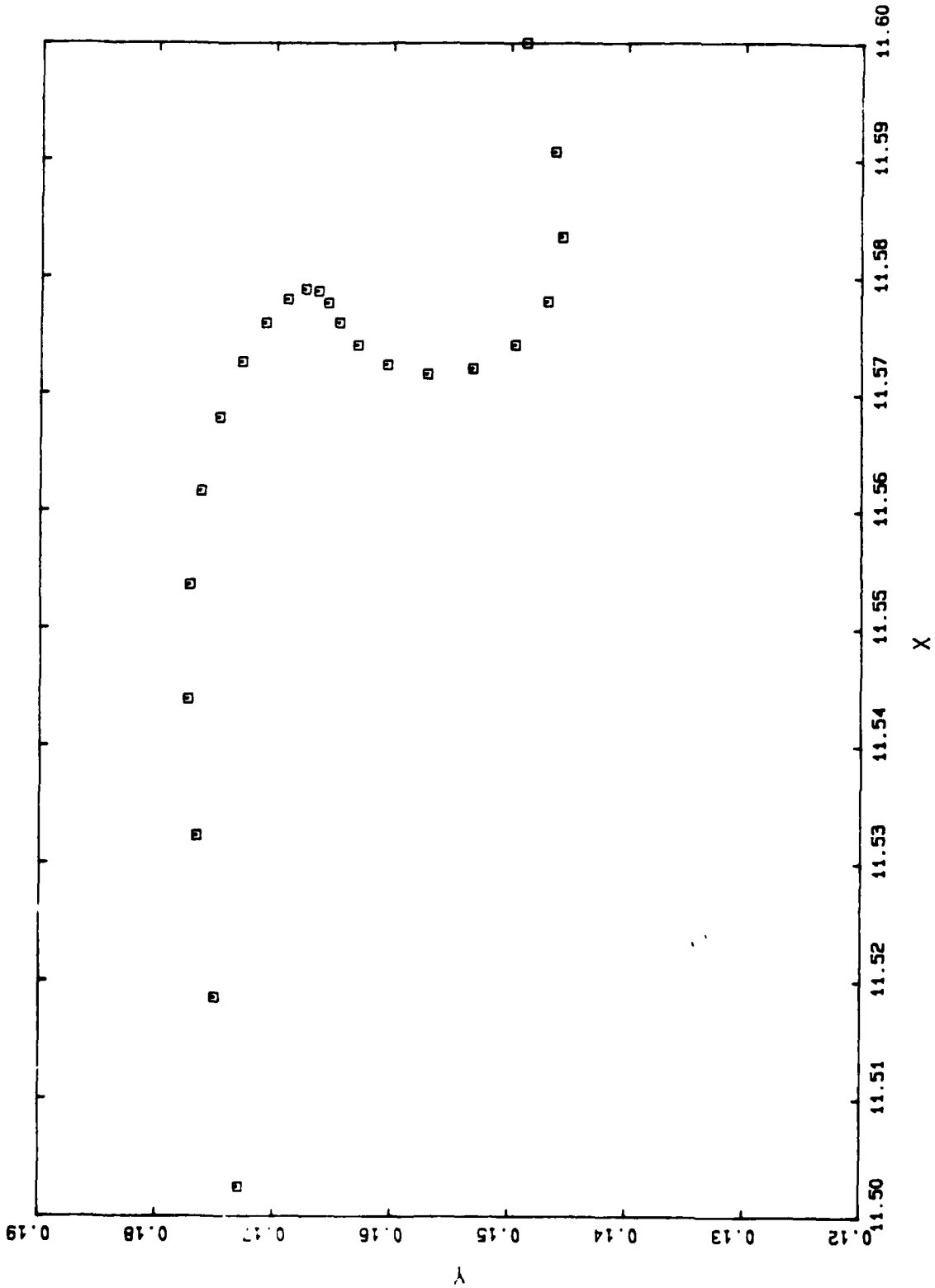

D5 3730 50.9659

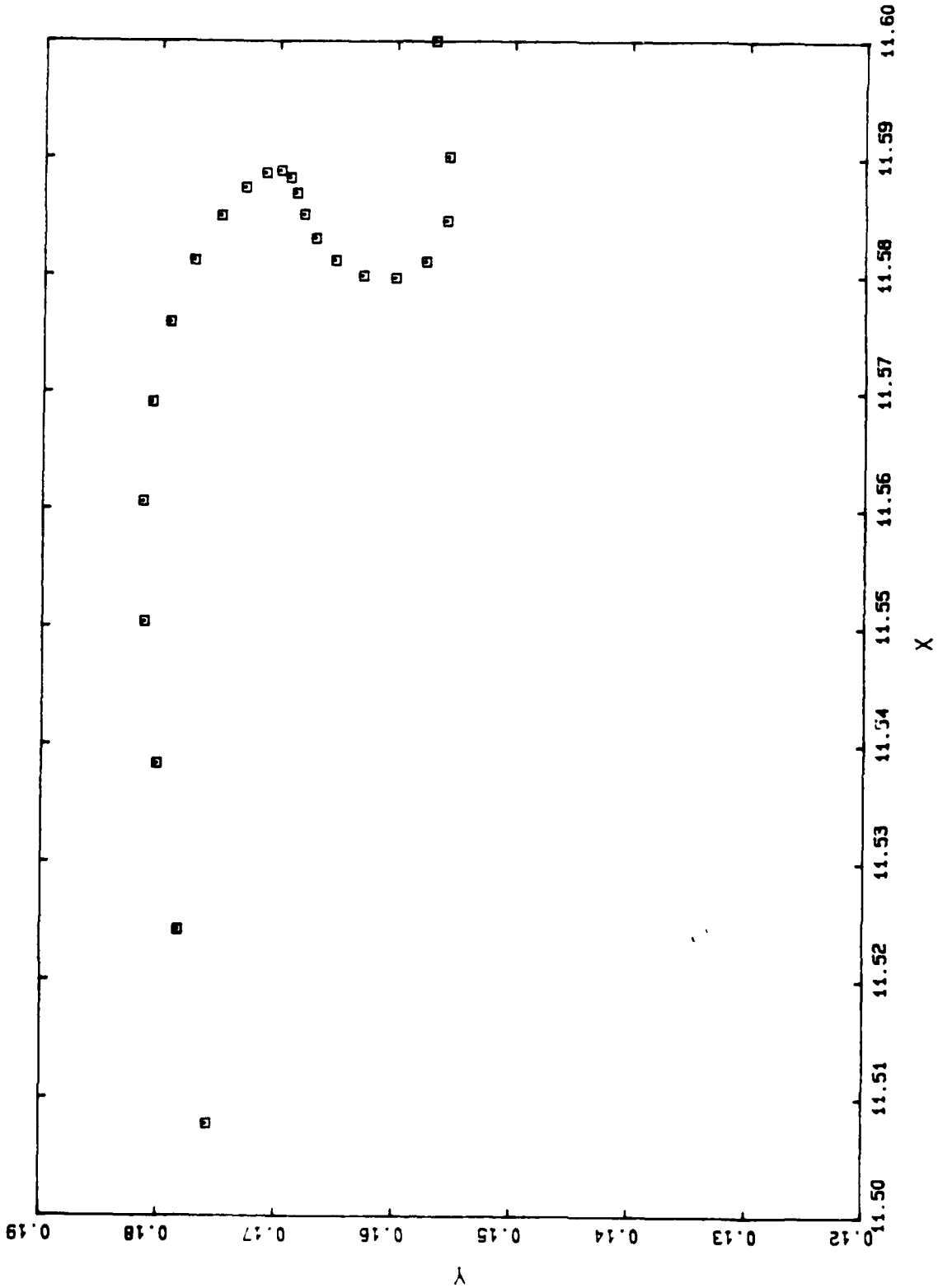

D5 3830 50.9708

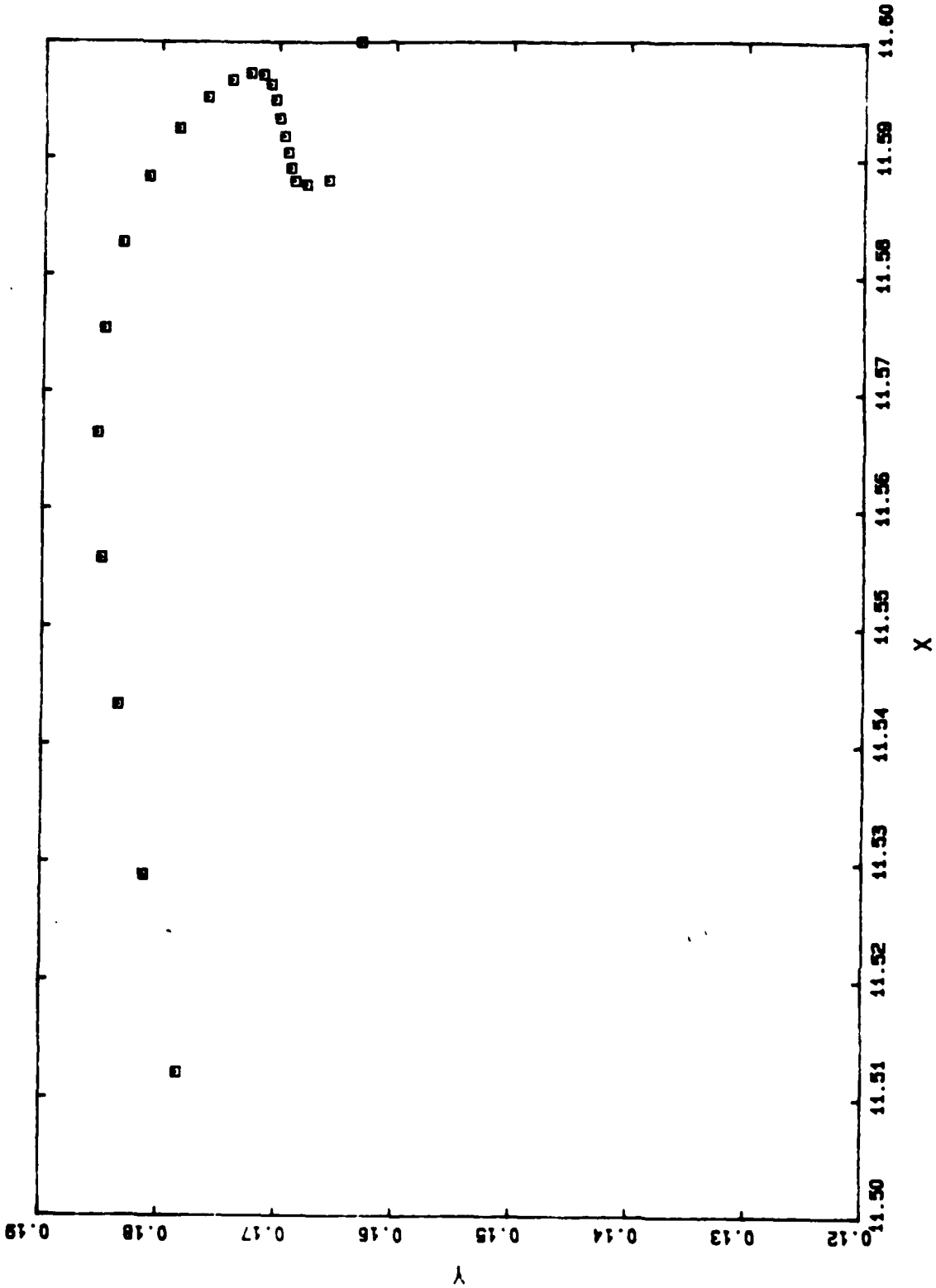

D5 3850 50.9713

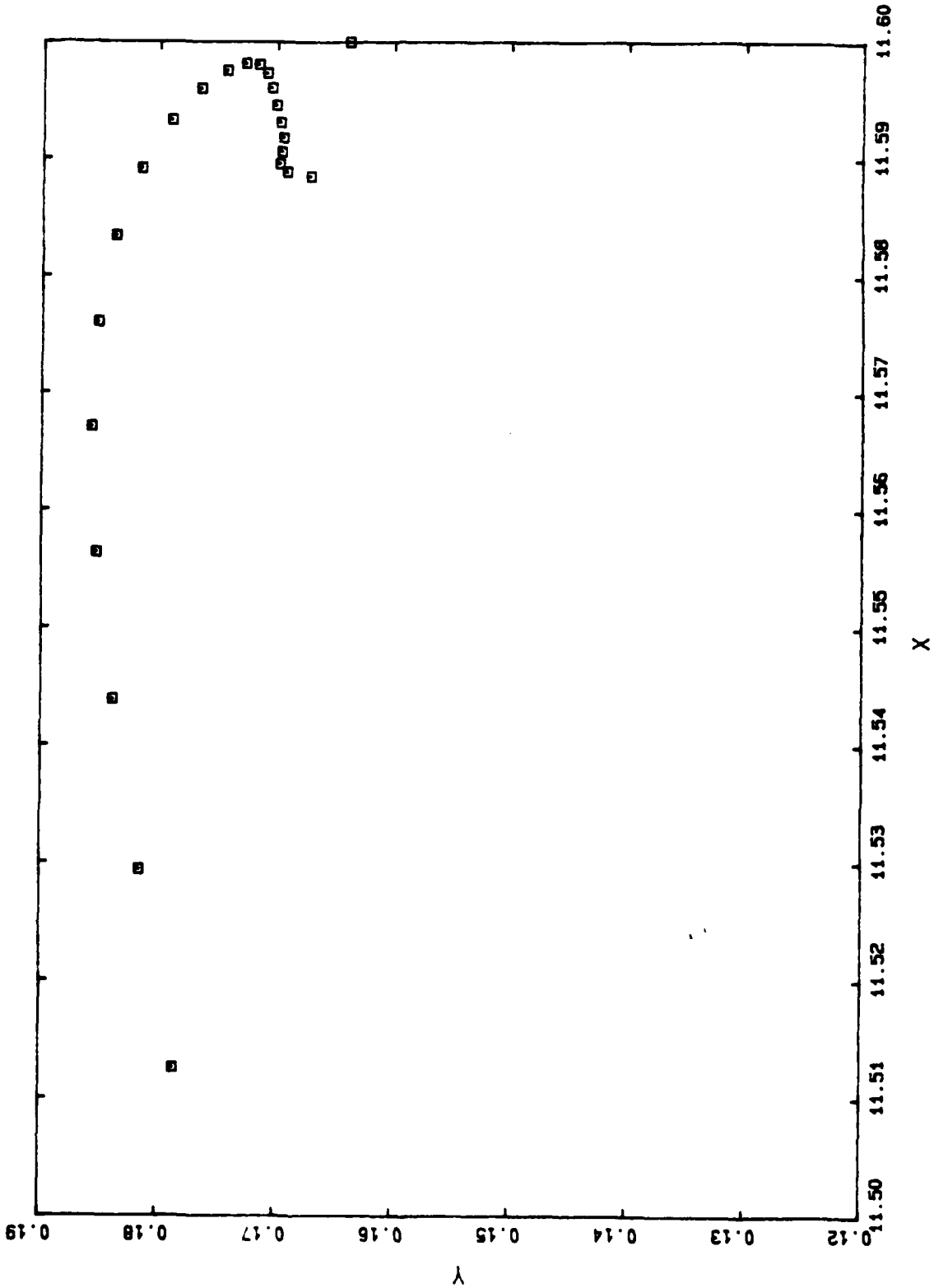

D5 3870 50.9718

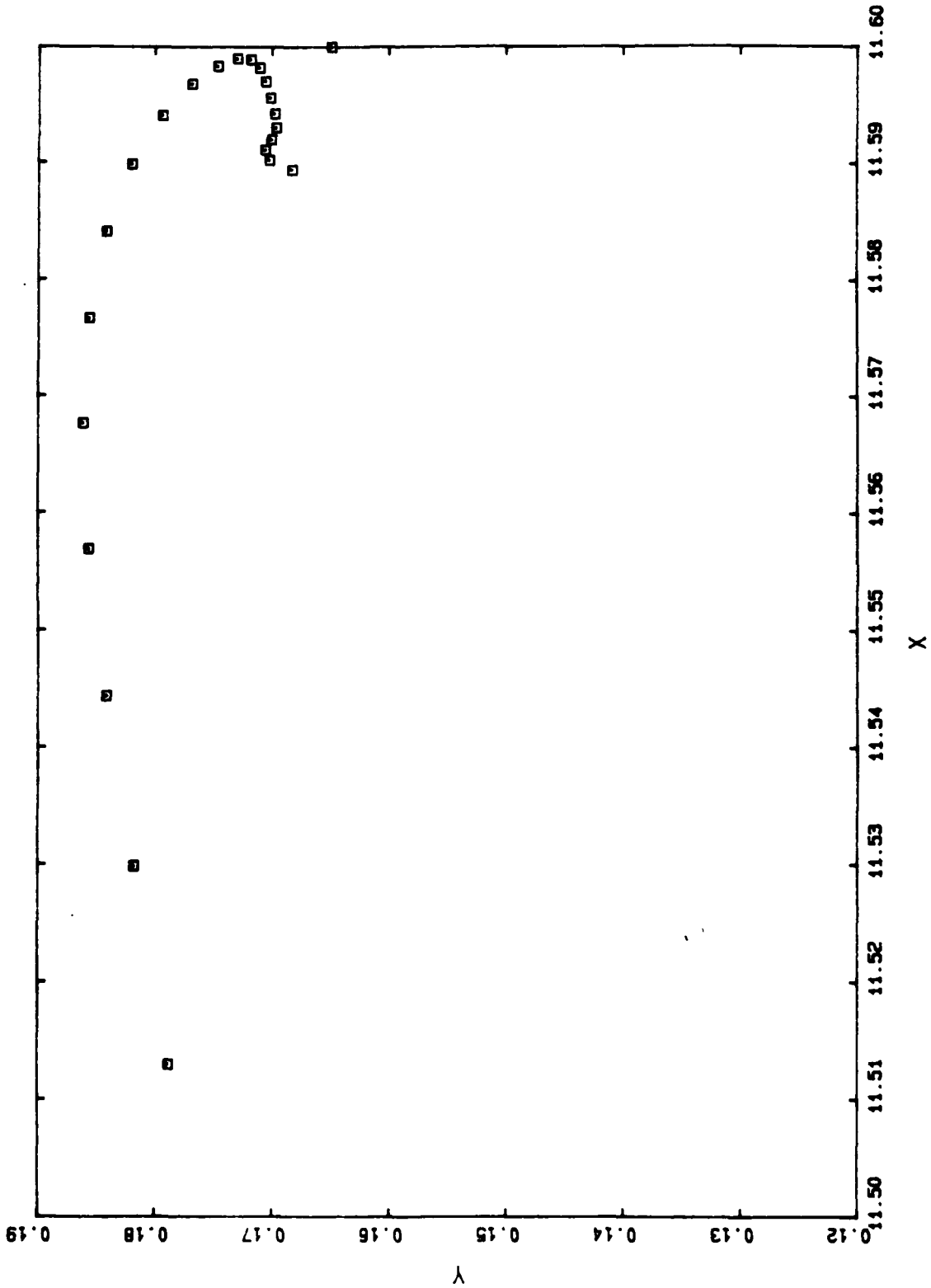

D5 3890 50.9722

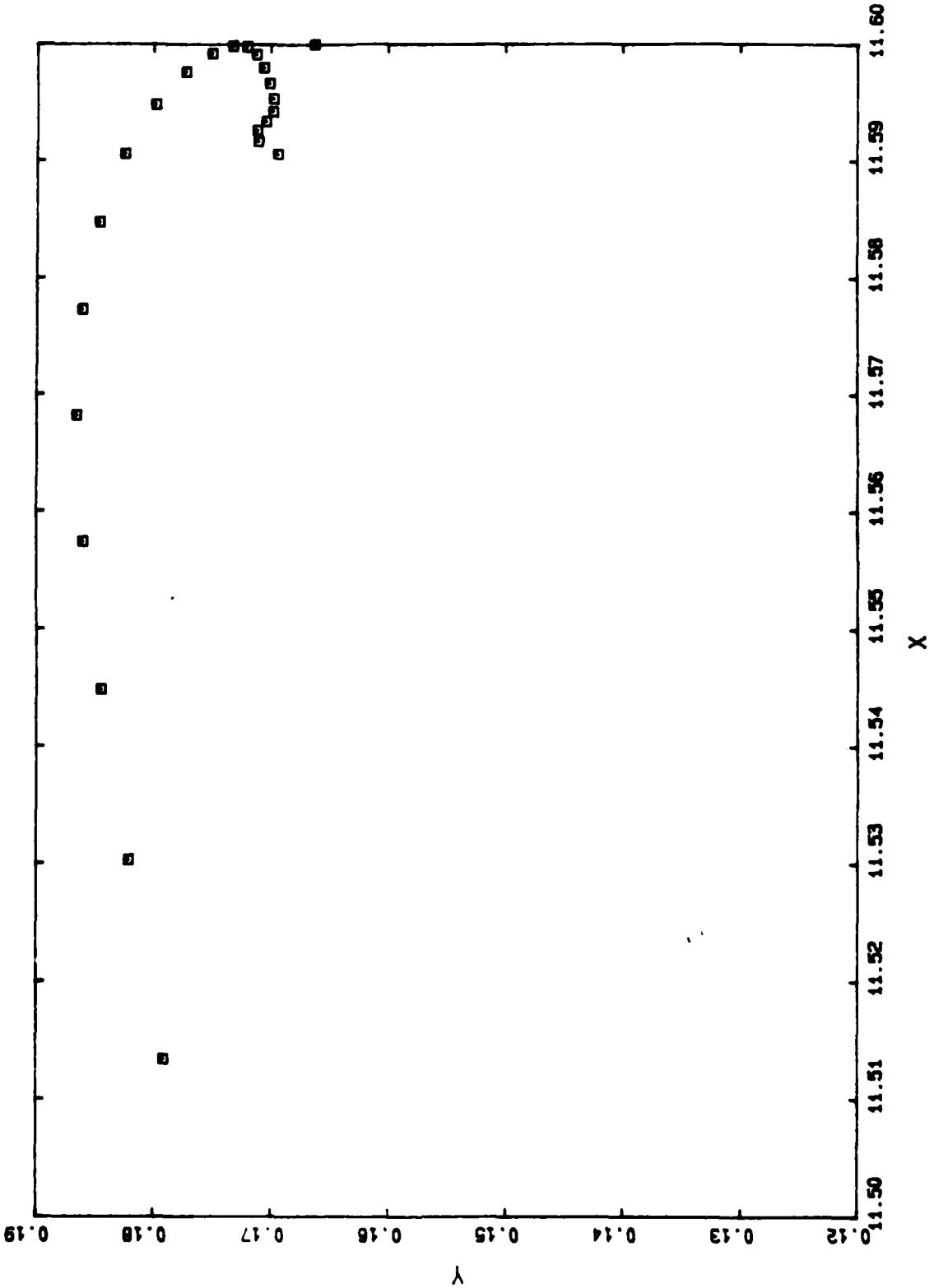

D5 3910 50.9728

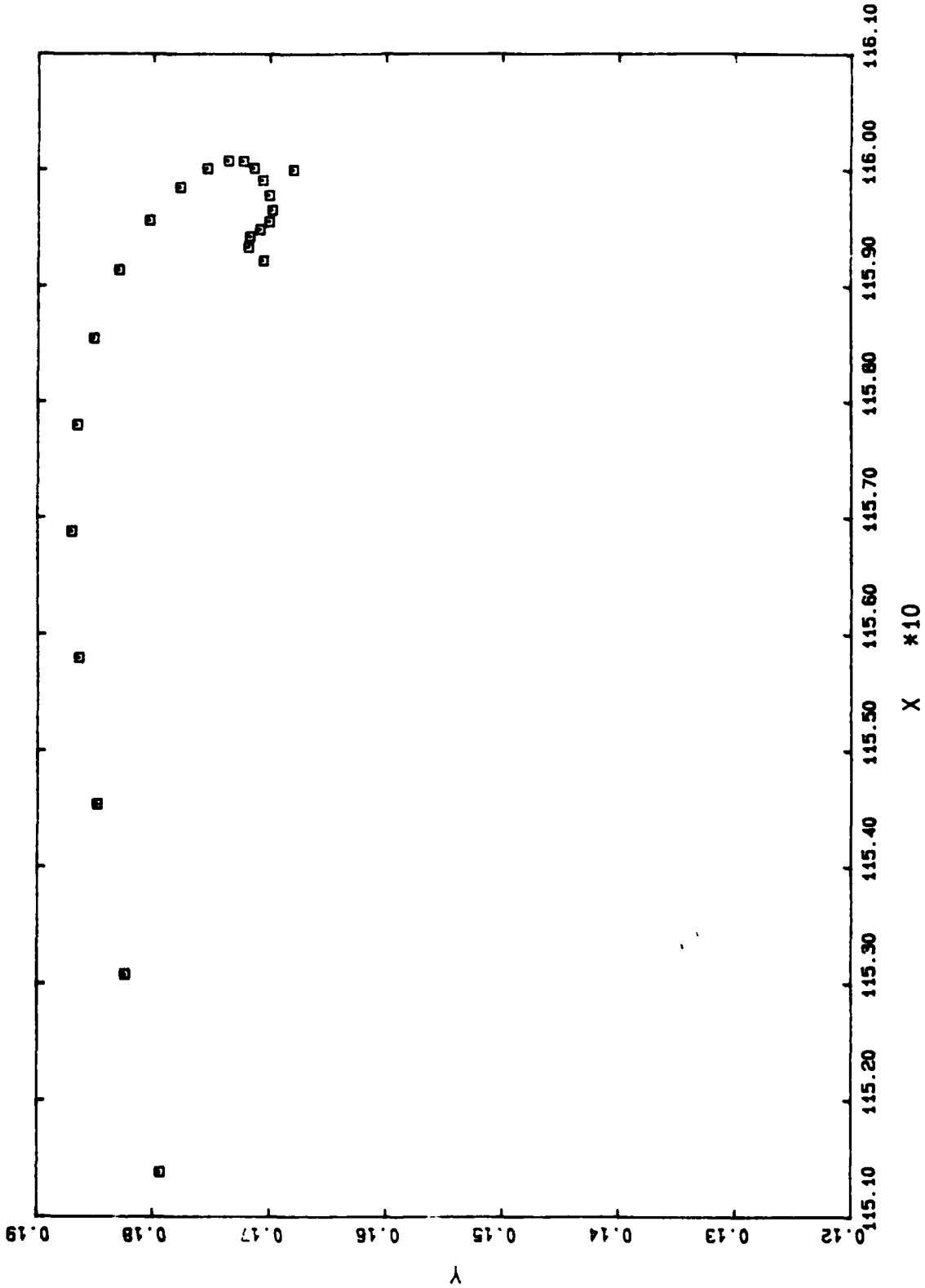

D6 3145 50.8723

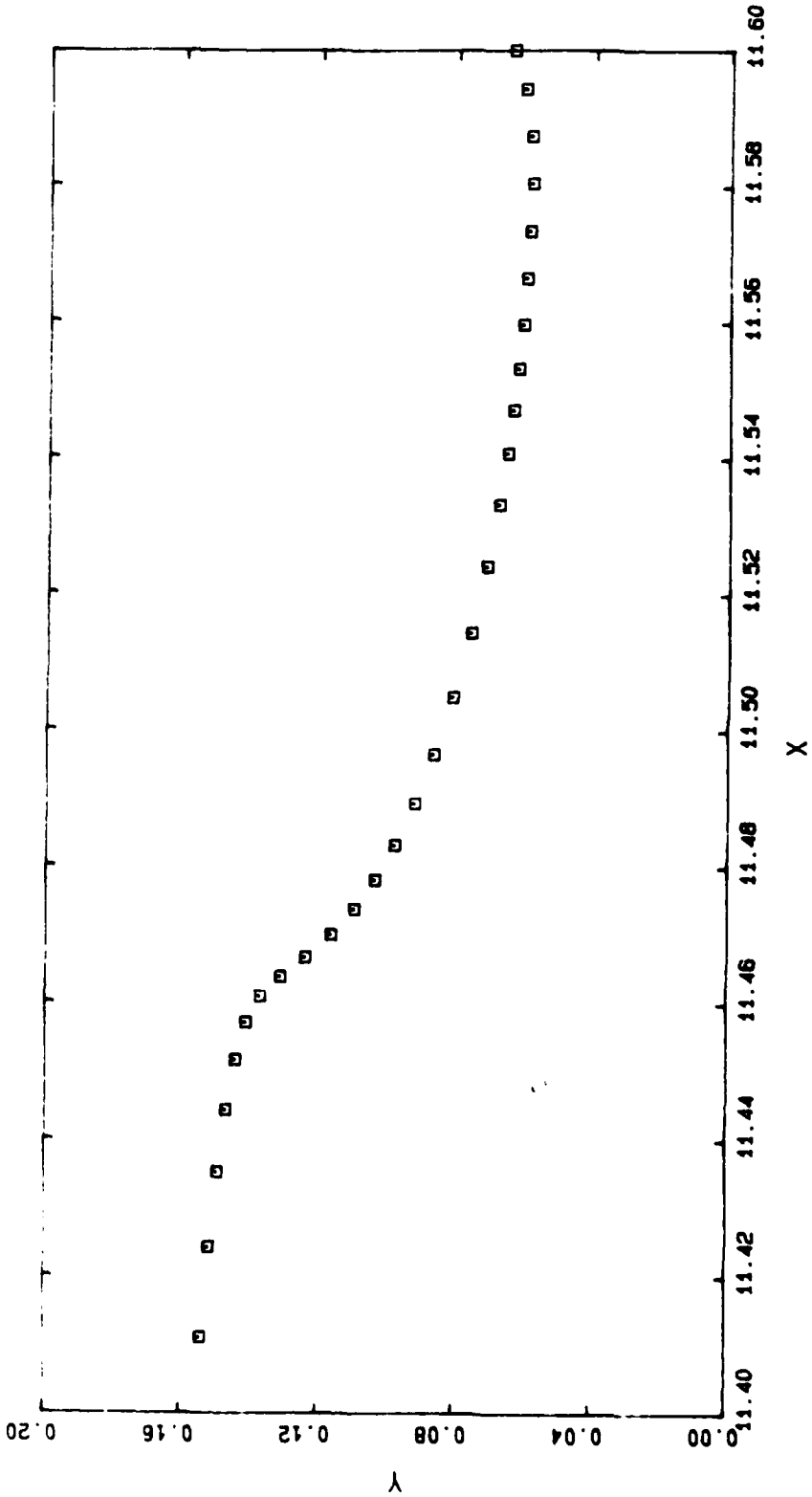

D6 3245 50.9143

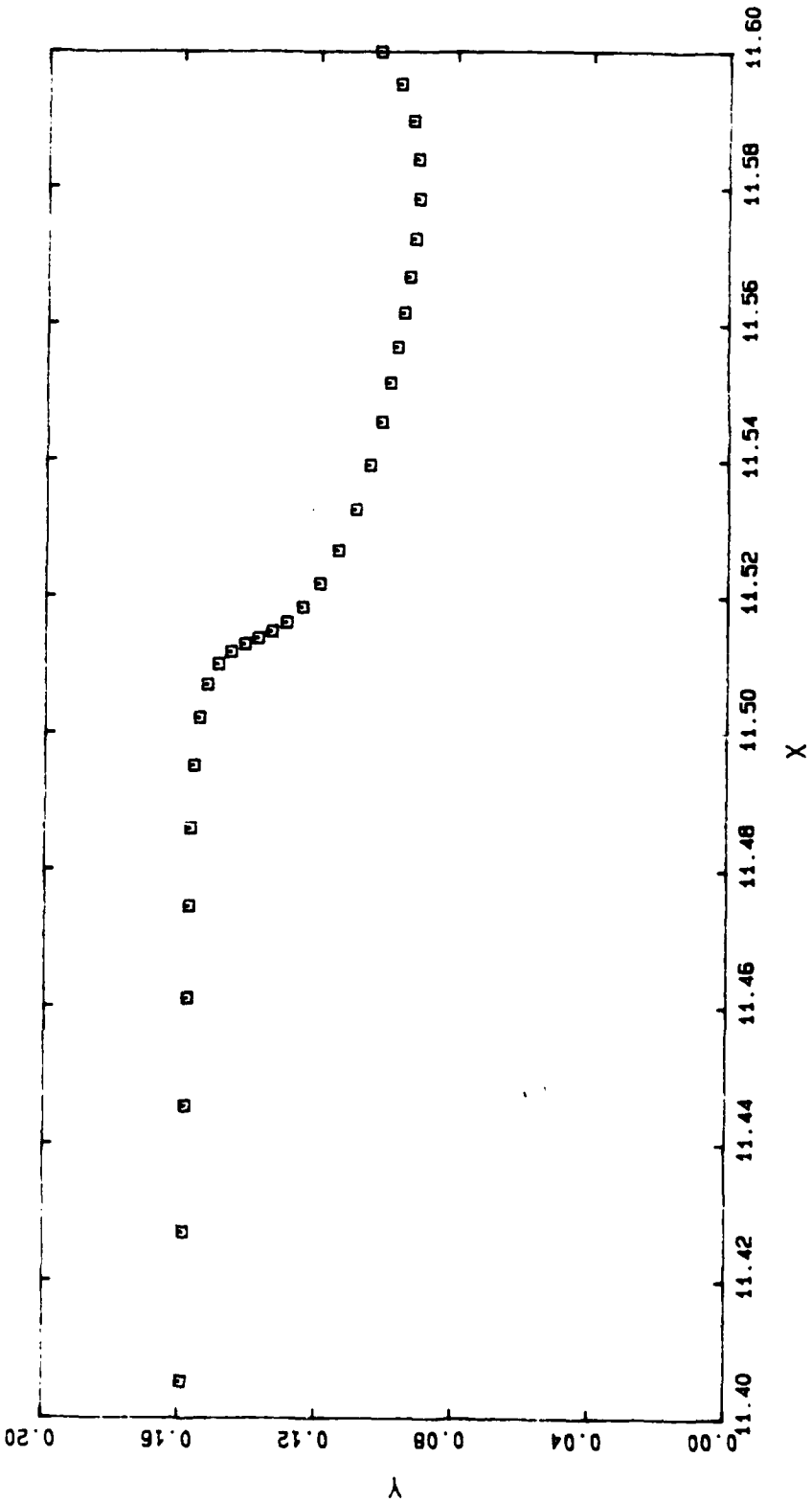

D6 3345 50.9349

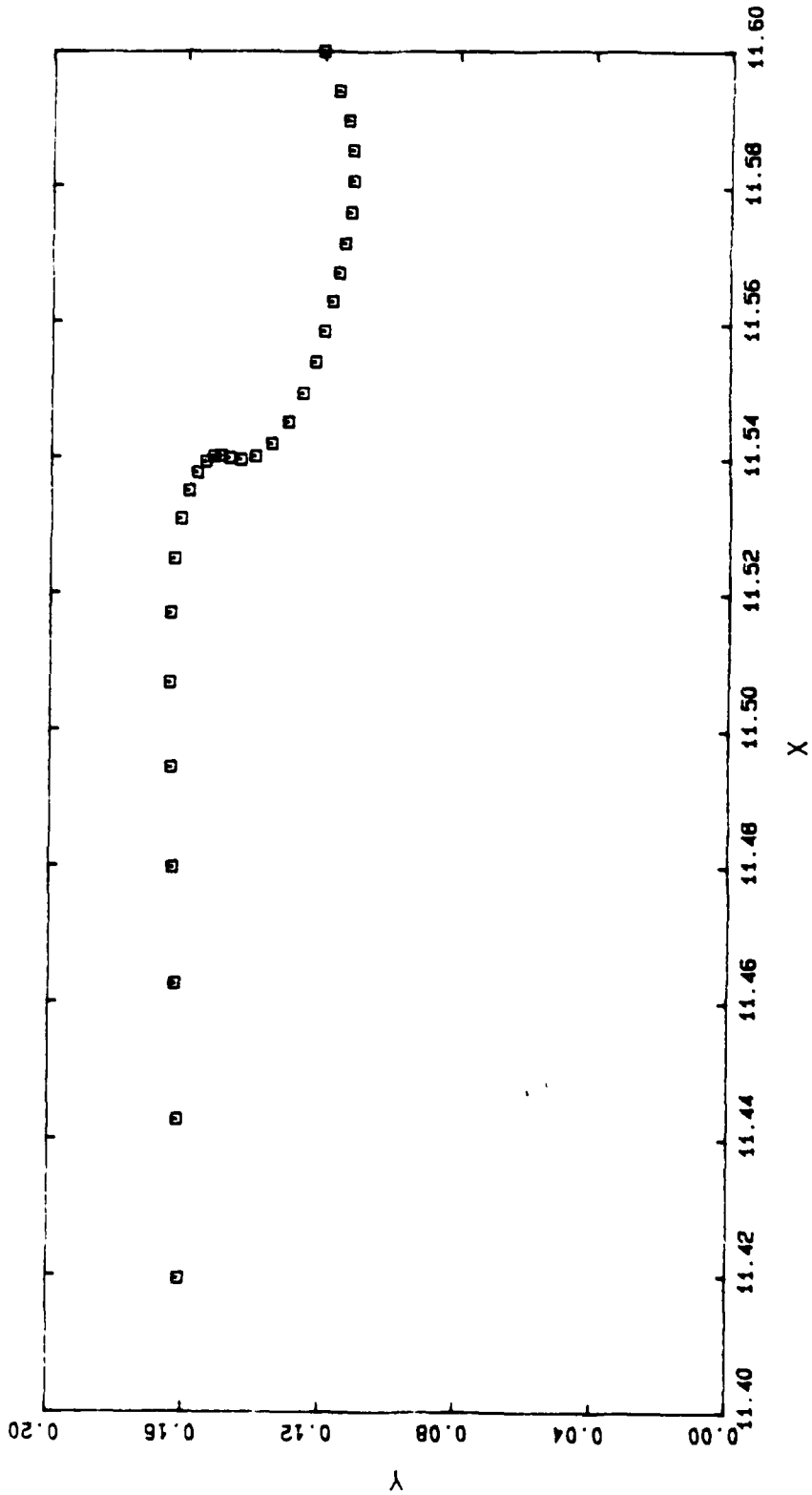

D6 3445 50.9457

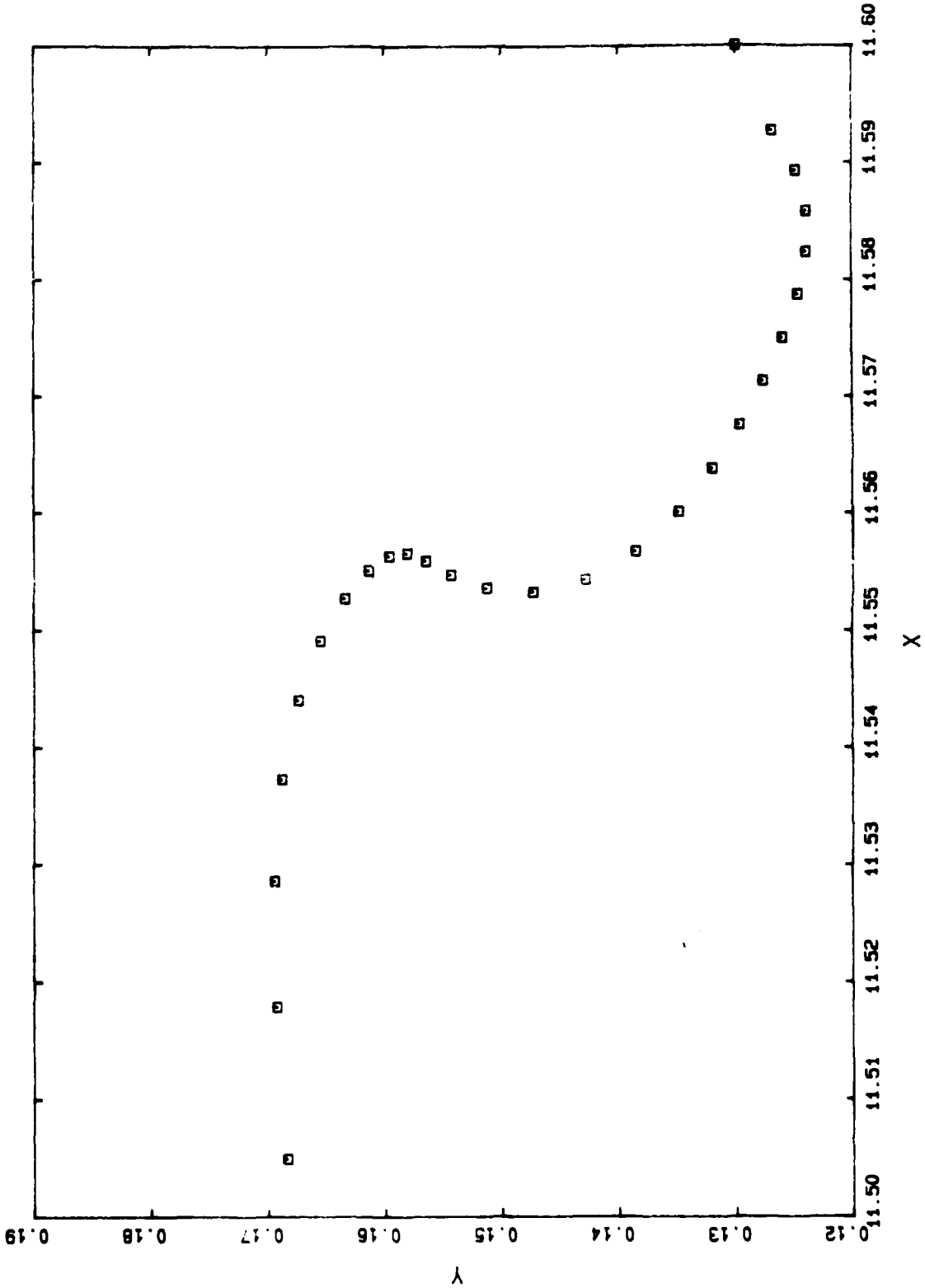

D6 3545 50.9537

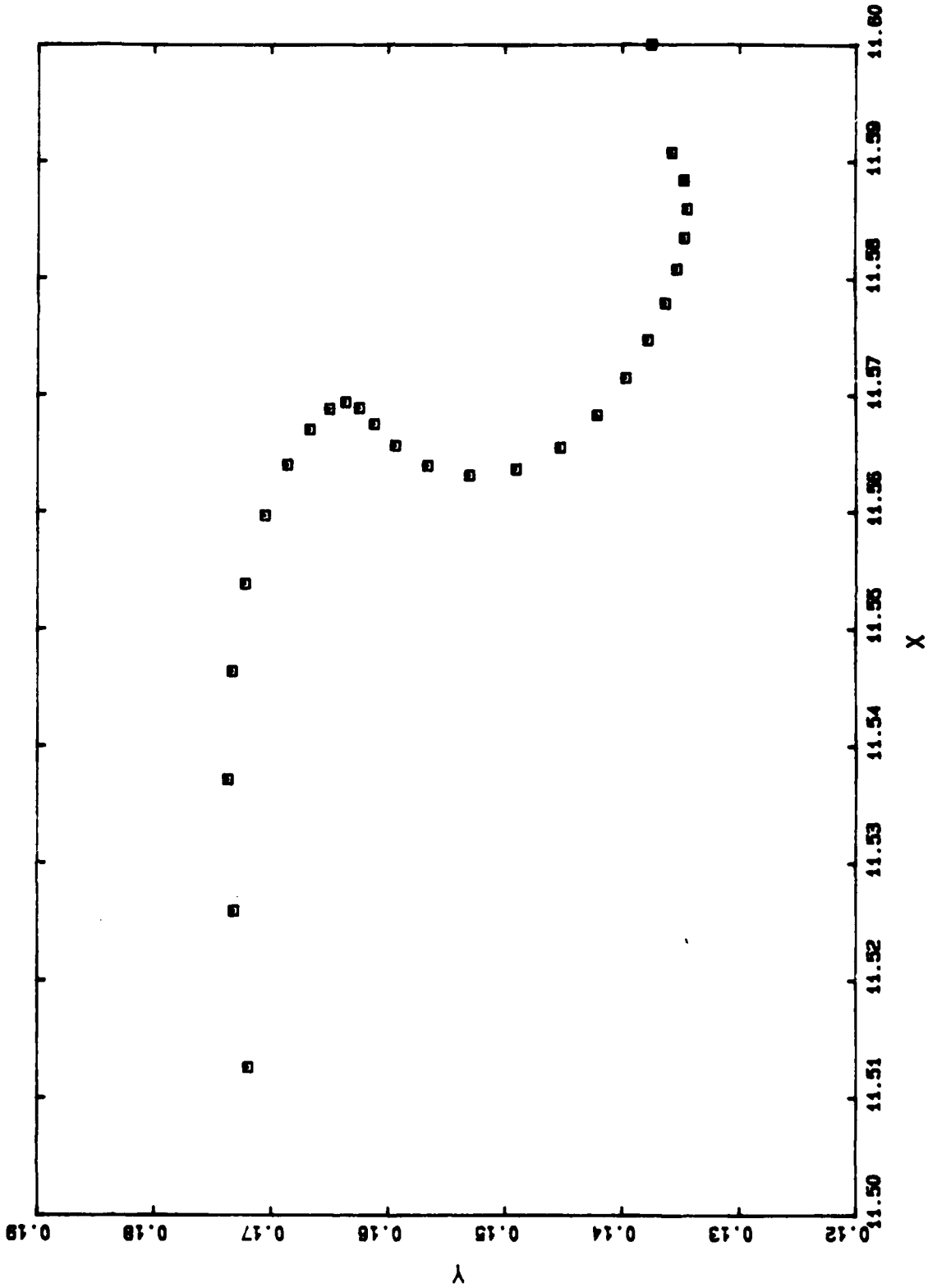

D6 3645 50.9595

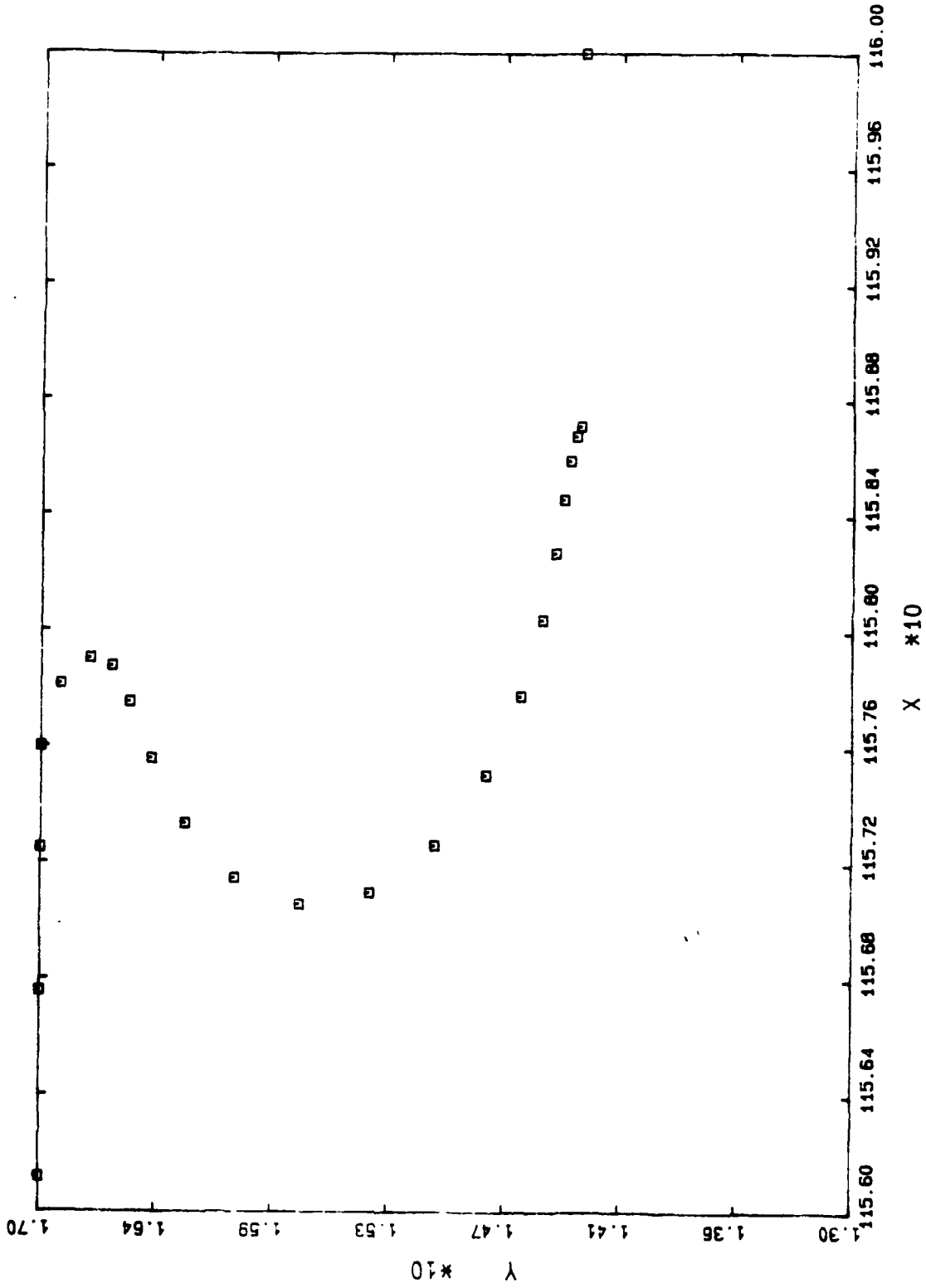

D6 4145 50.9698

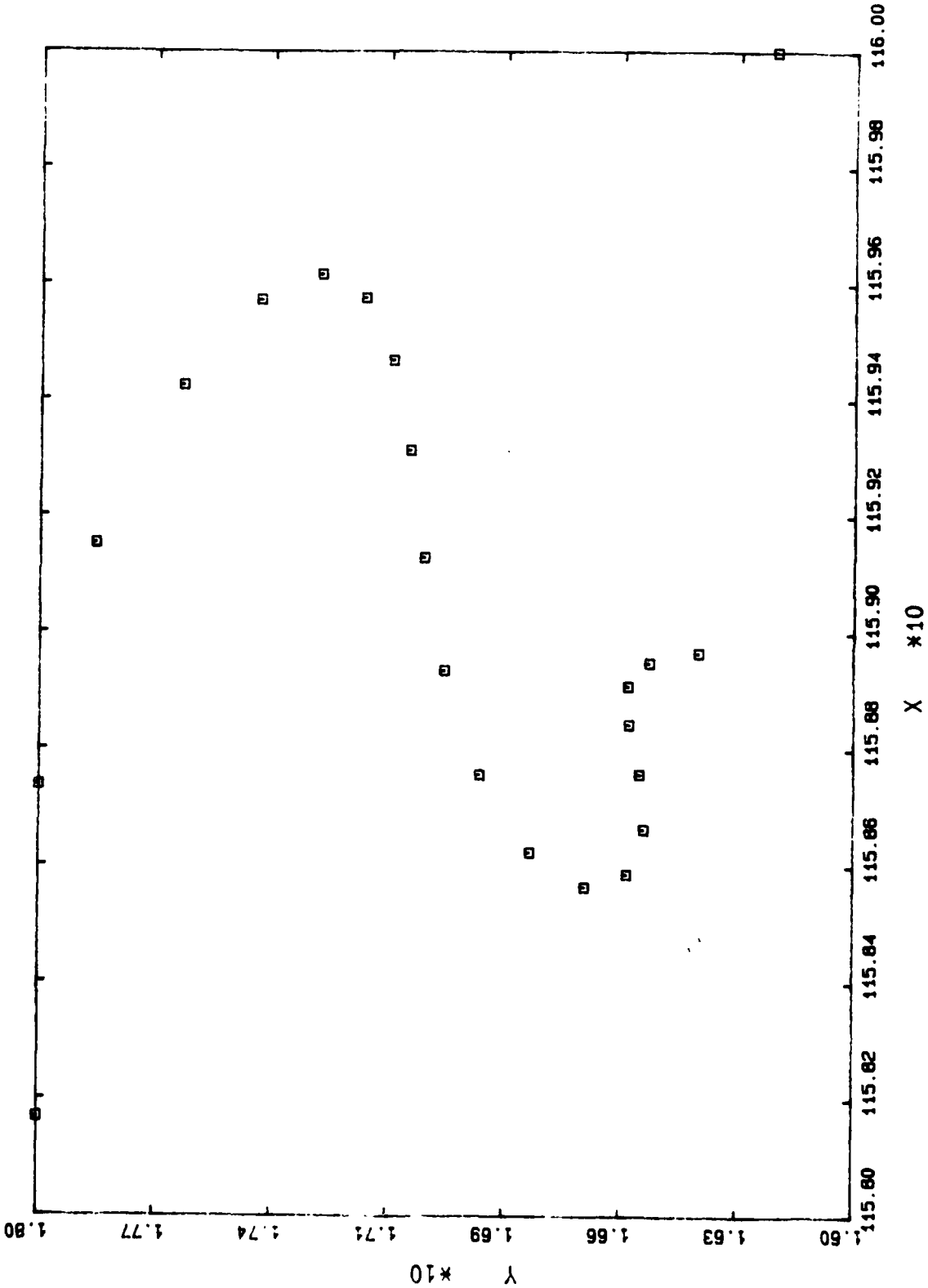

D6 4245 50.9714

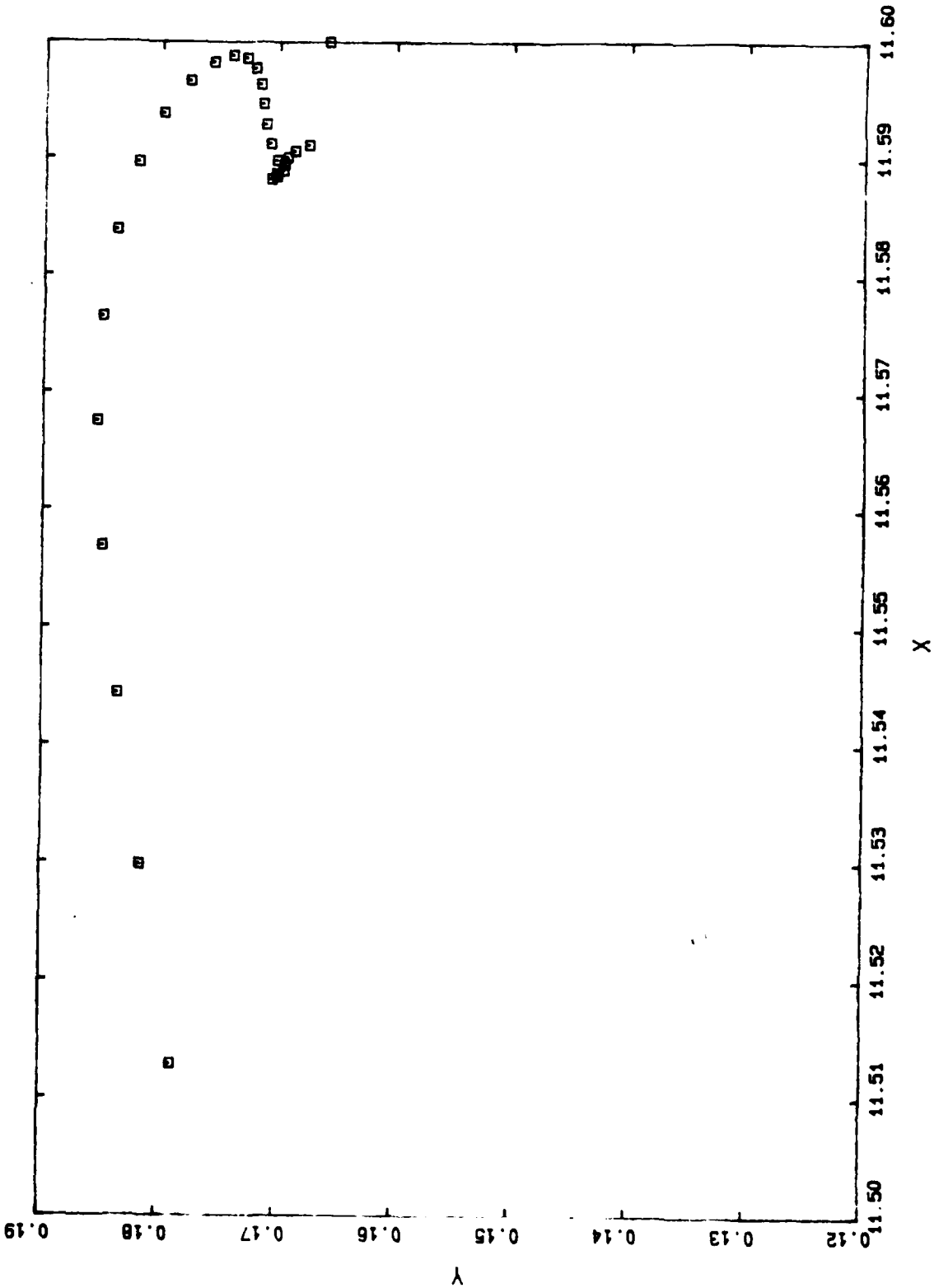

D7 3101 50.8463

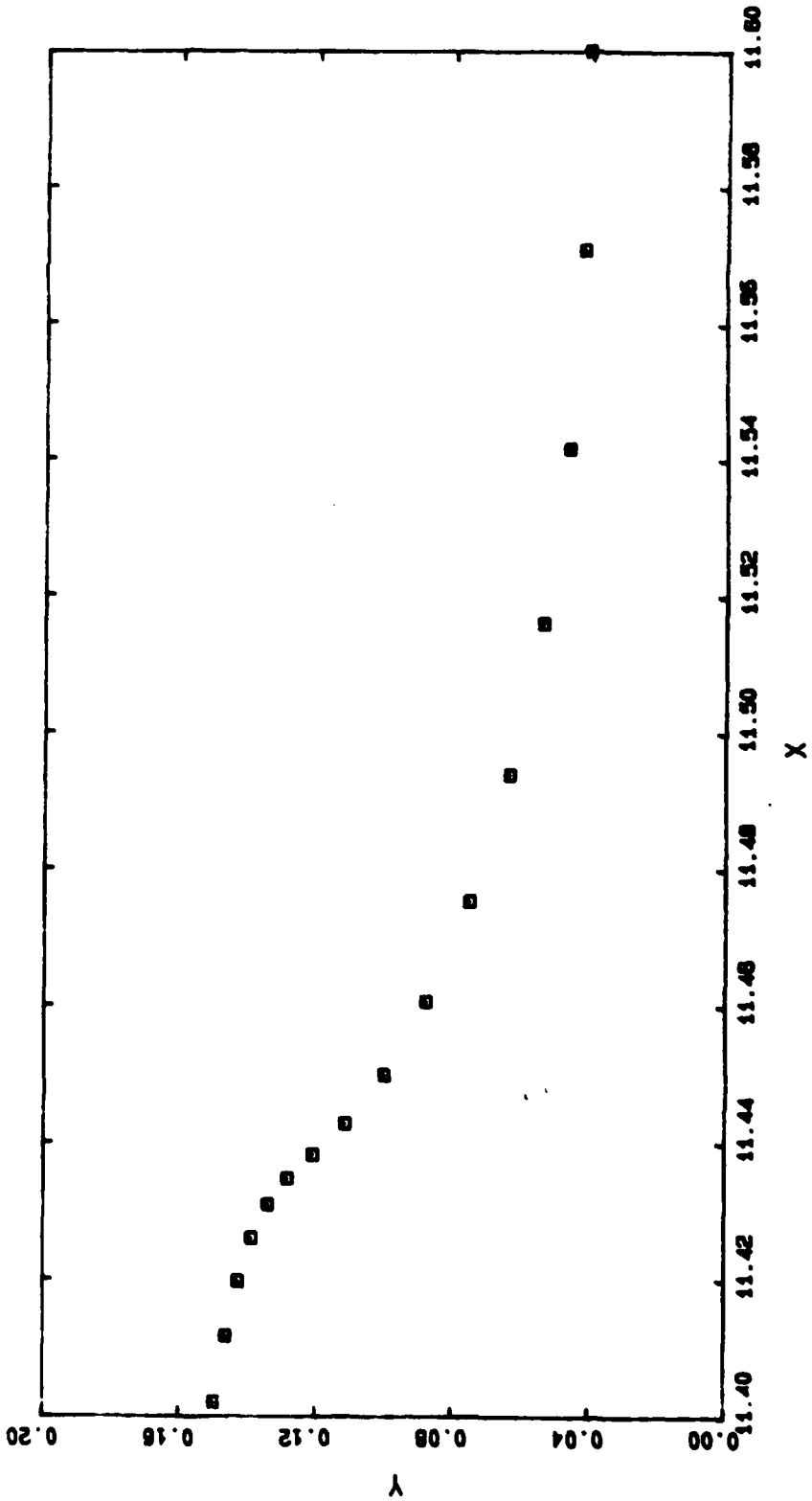

D7 3104 50.8484

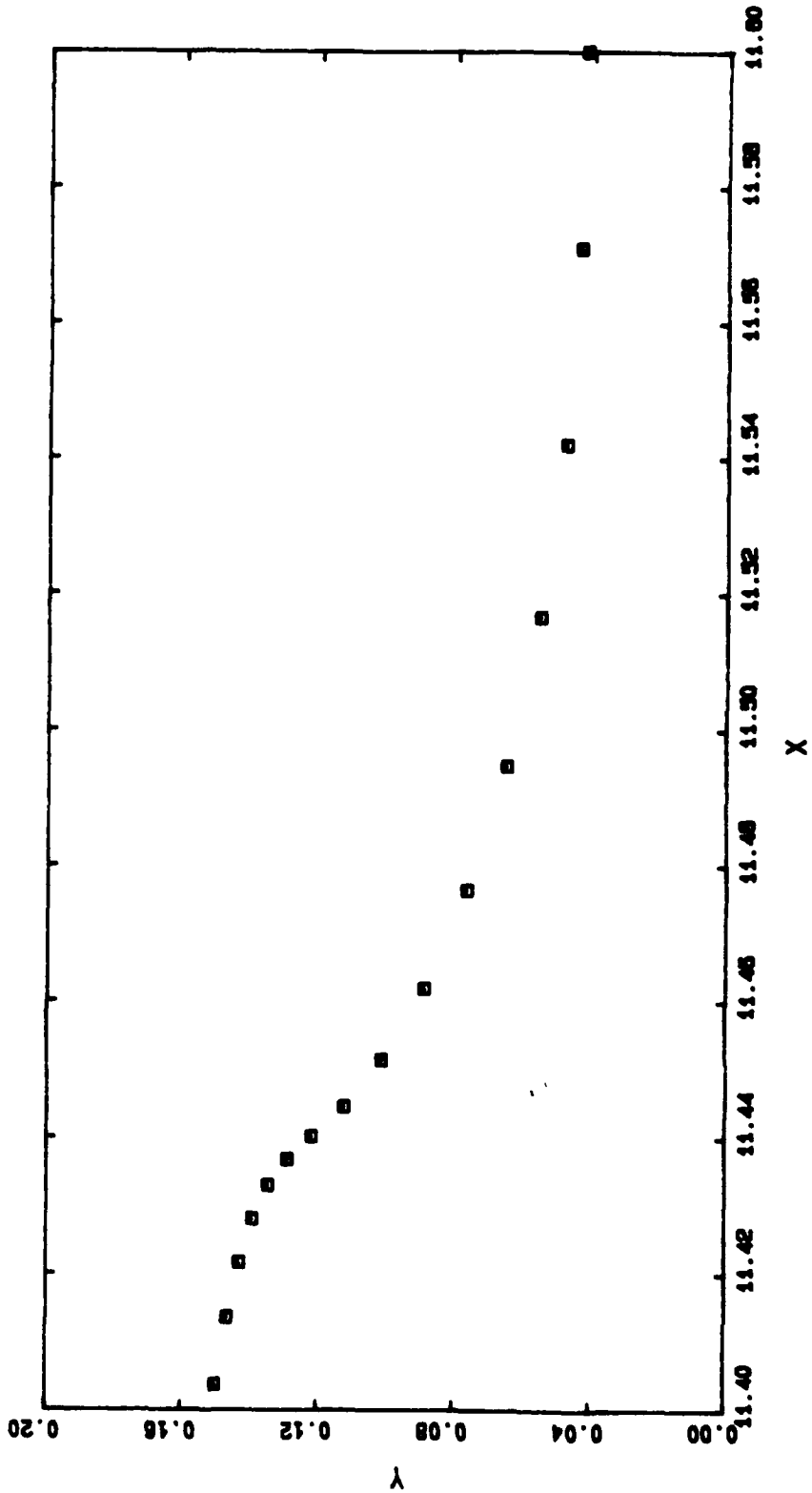

D7 3105 50.8490

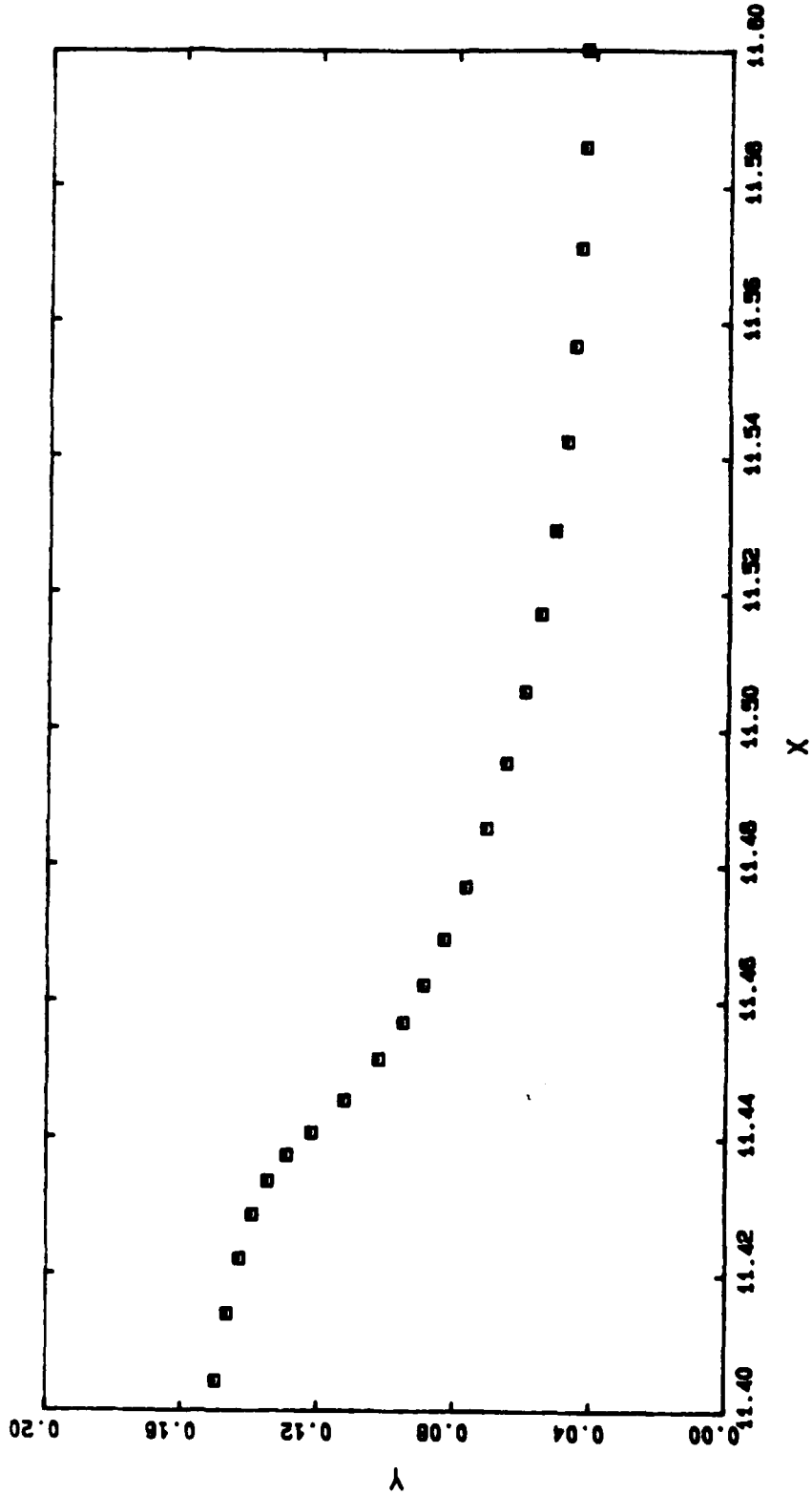

D7 3106 50.8497

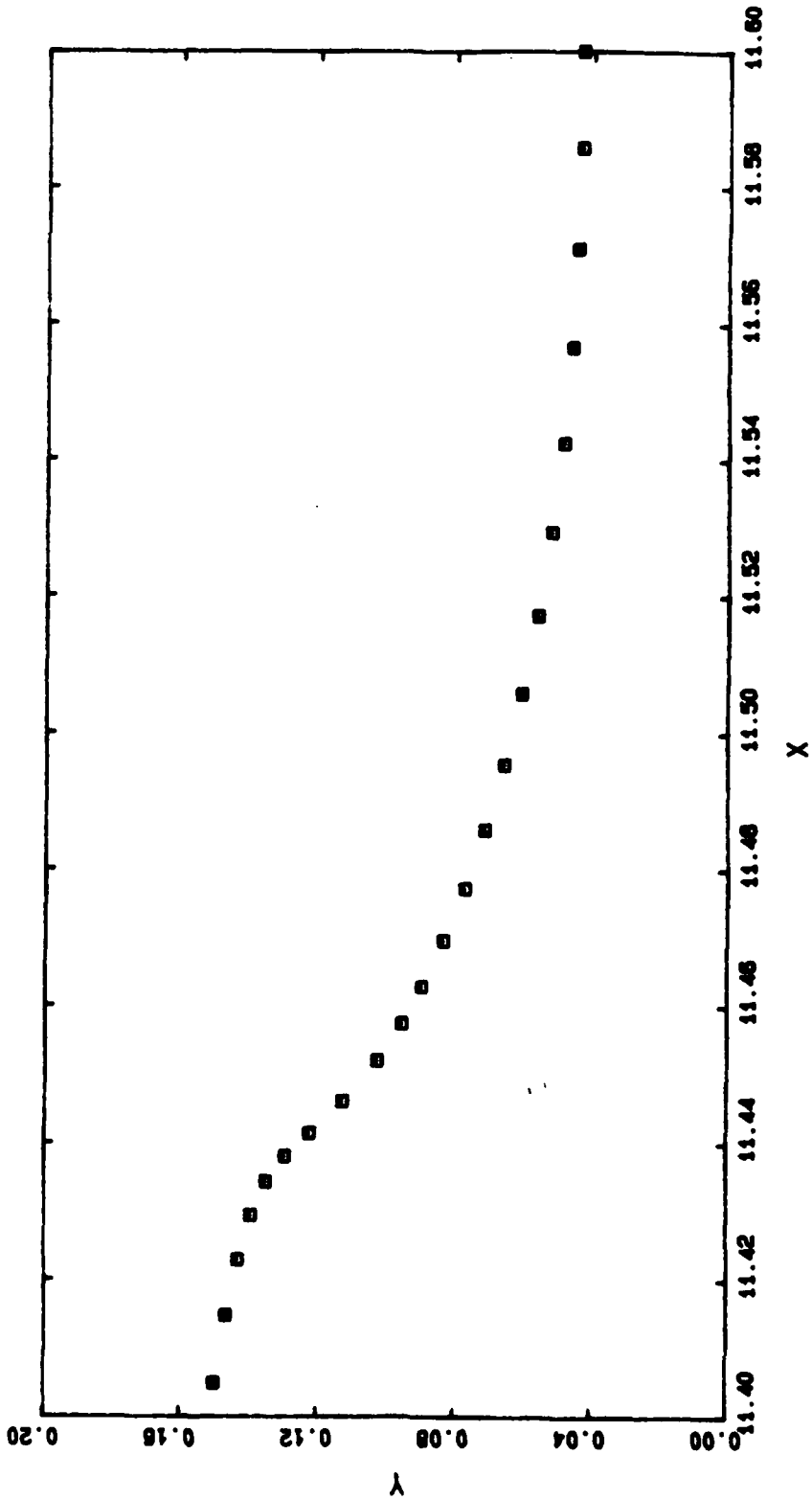

D7 3109 50.8516

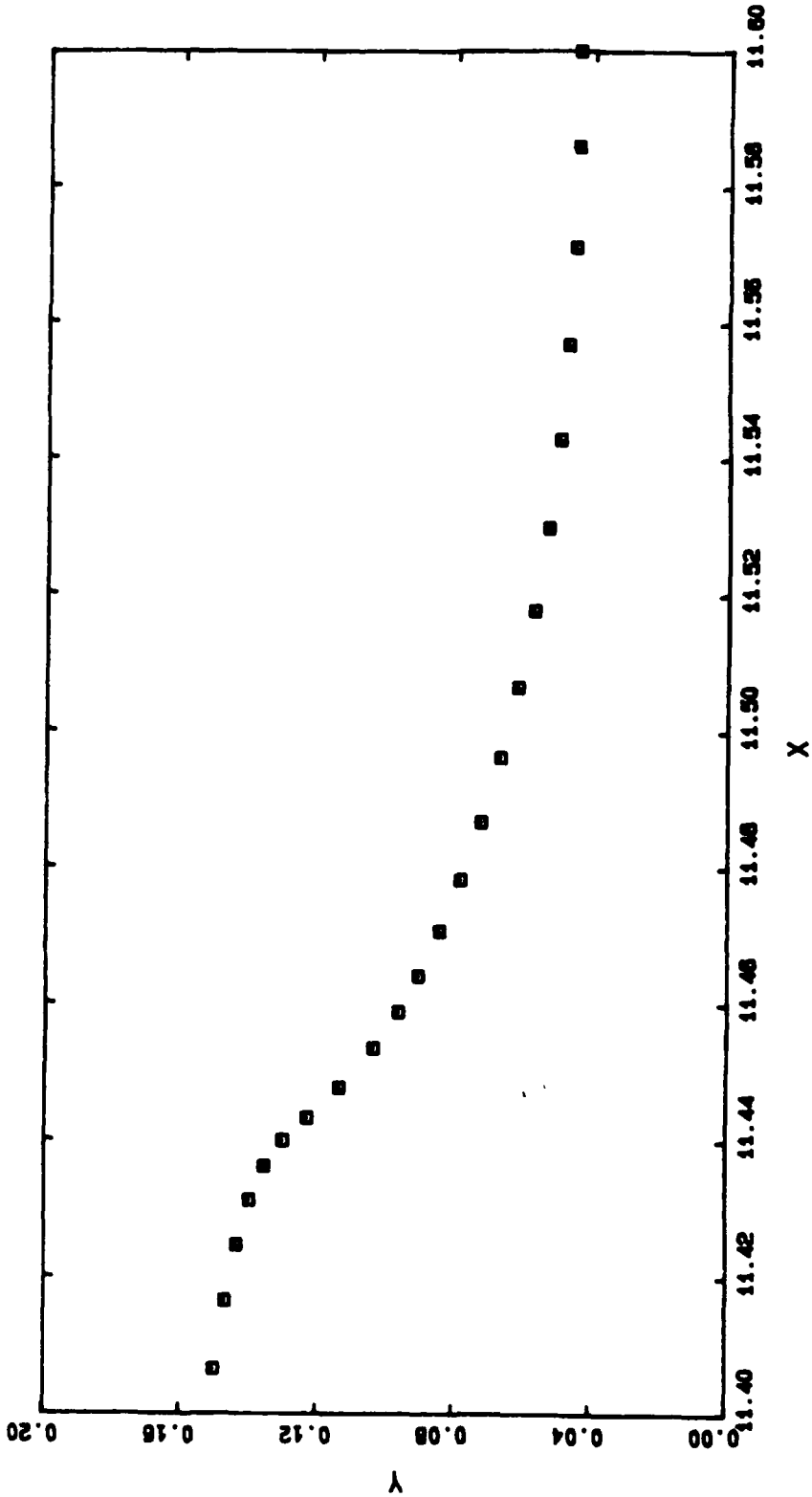

D7 3110 50.8523

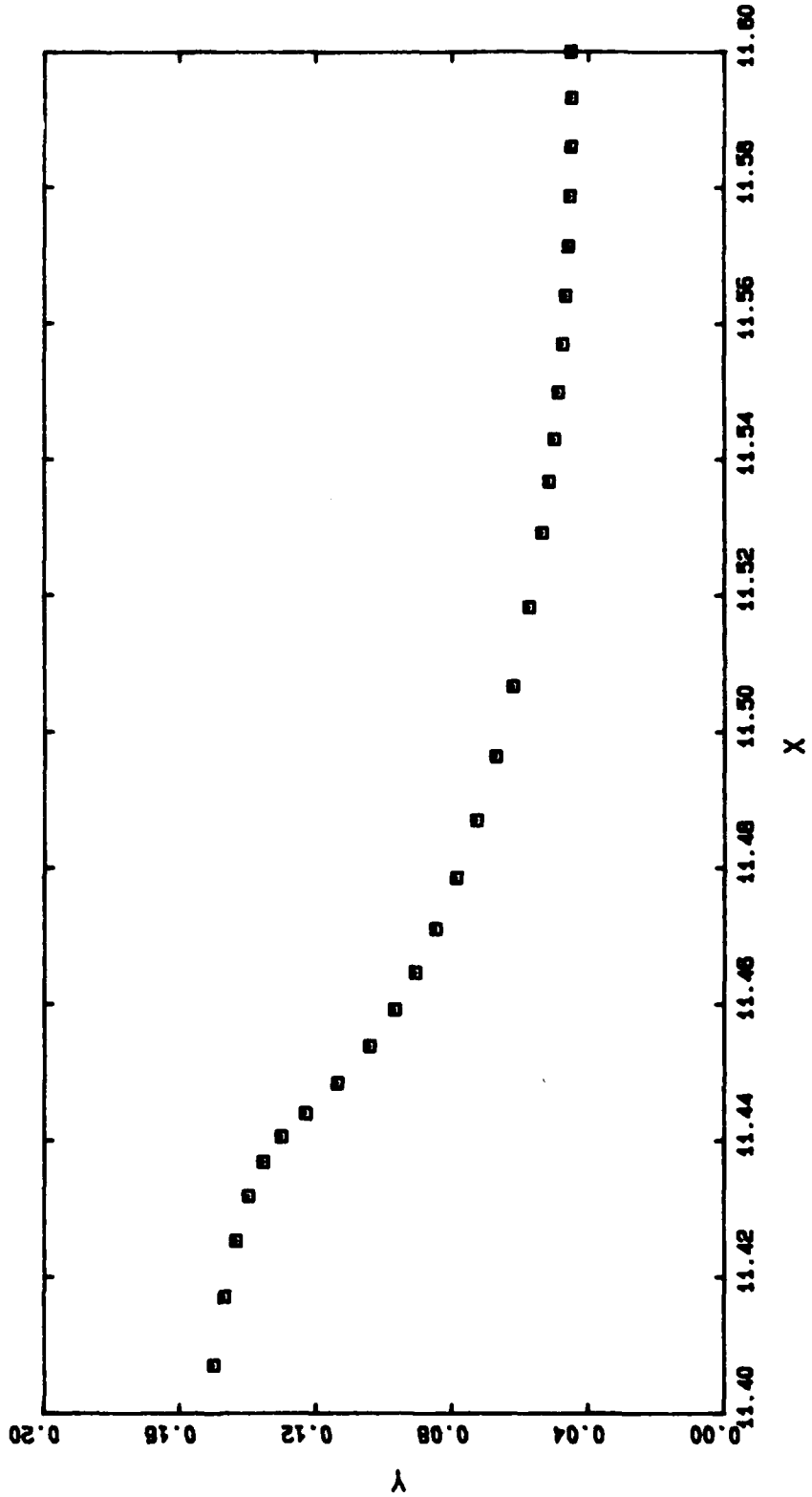

D7 3111 50.8529

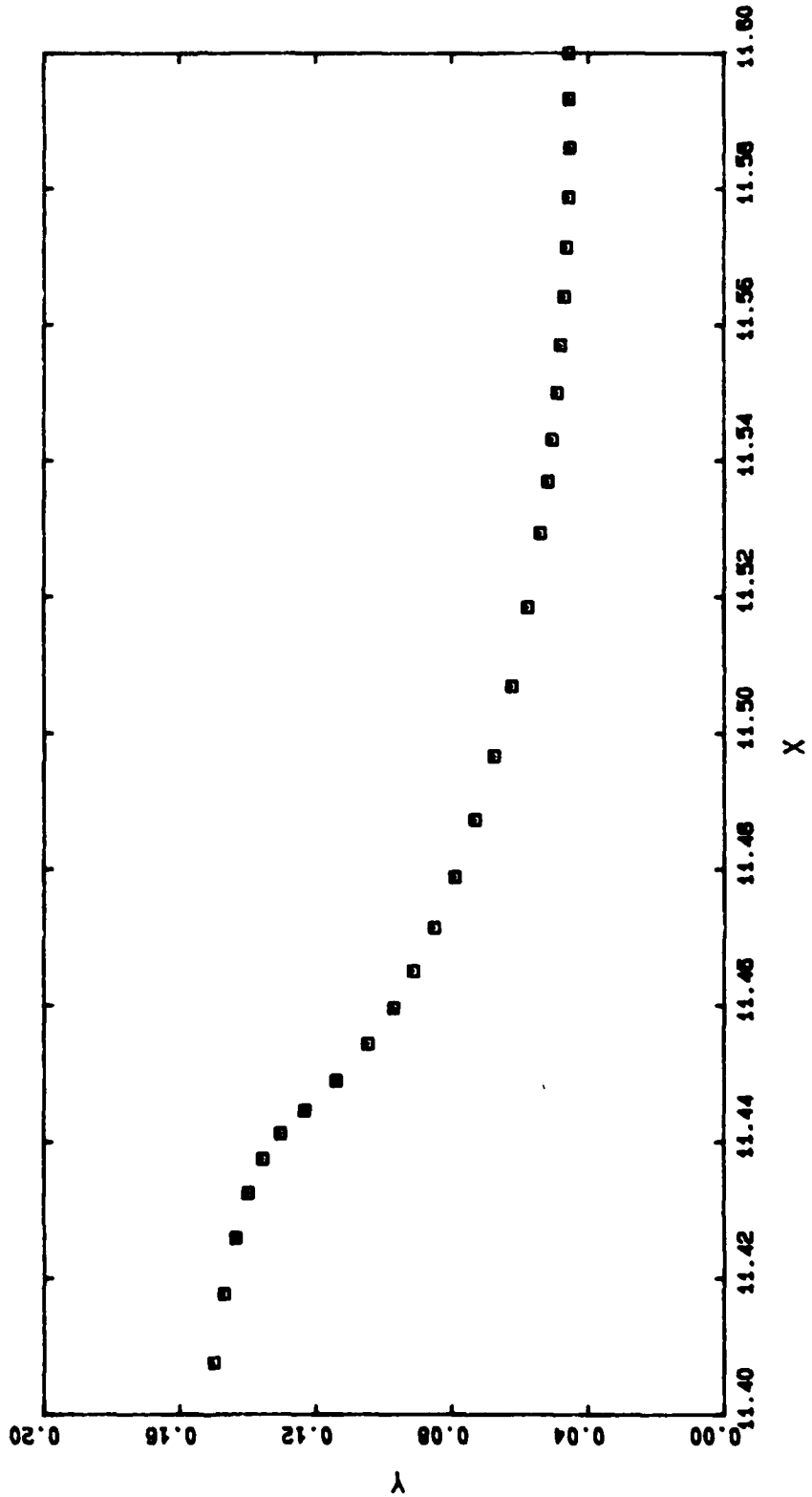

D7 3254 50.9170

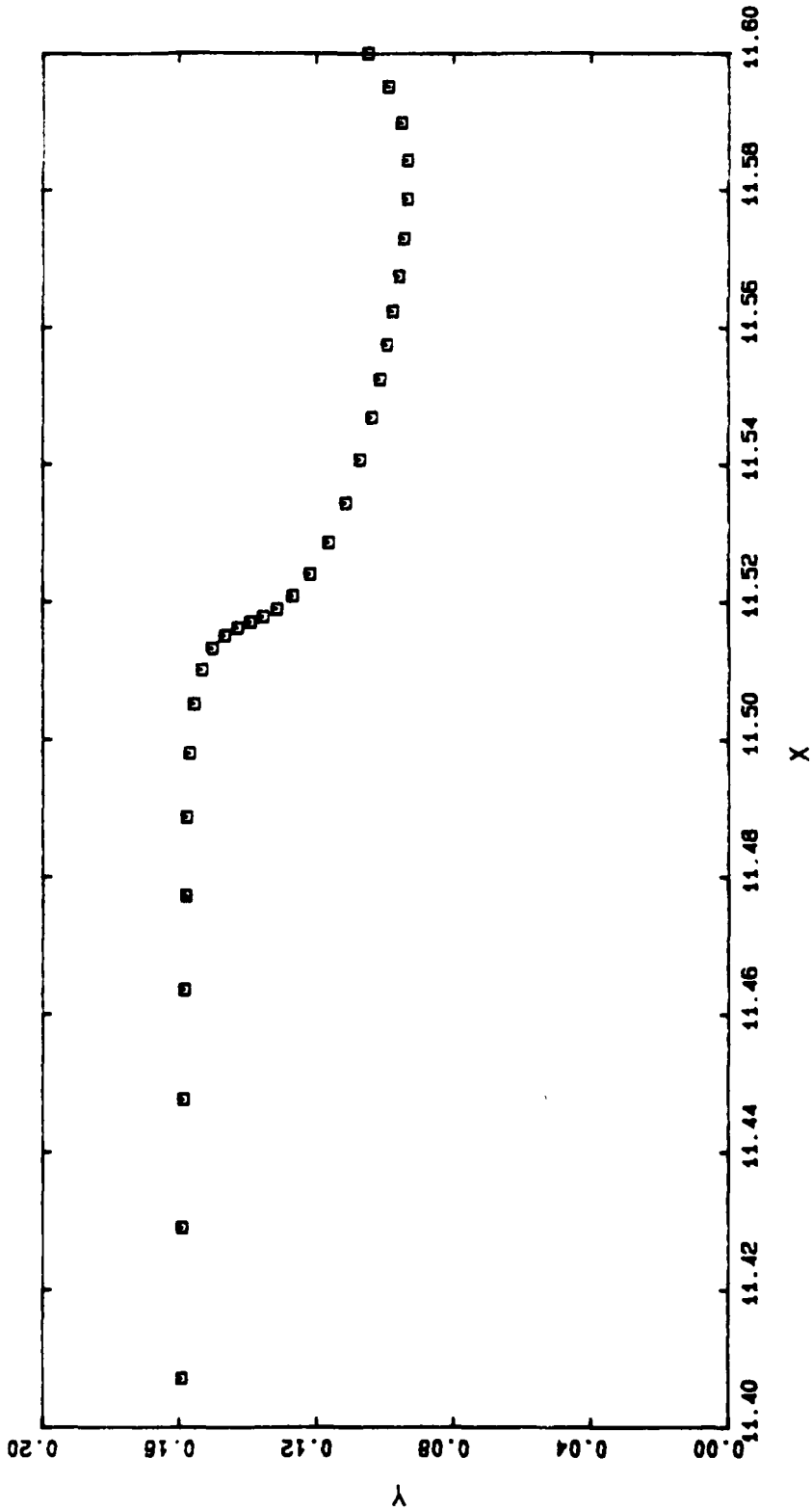

D7 3255 50.9173

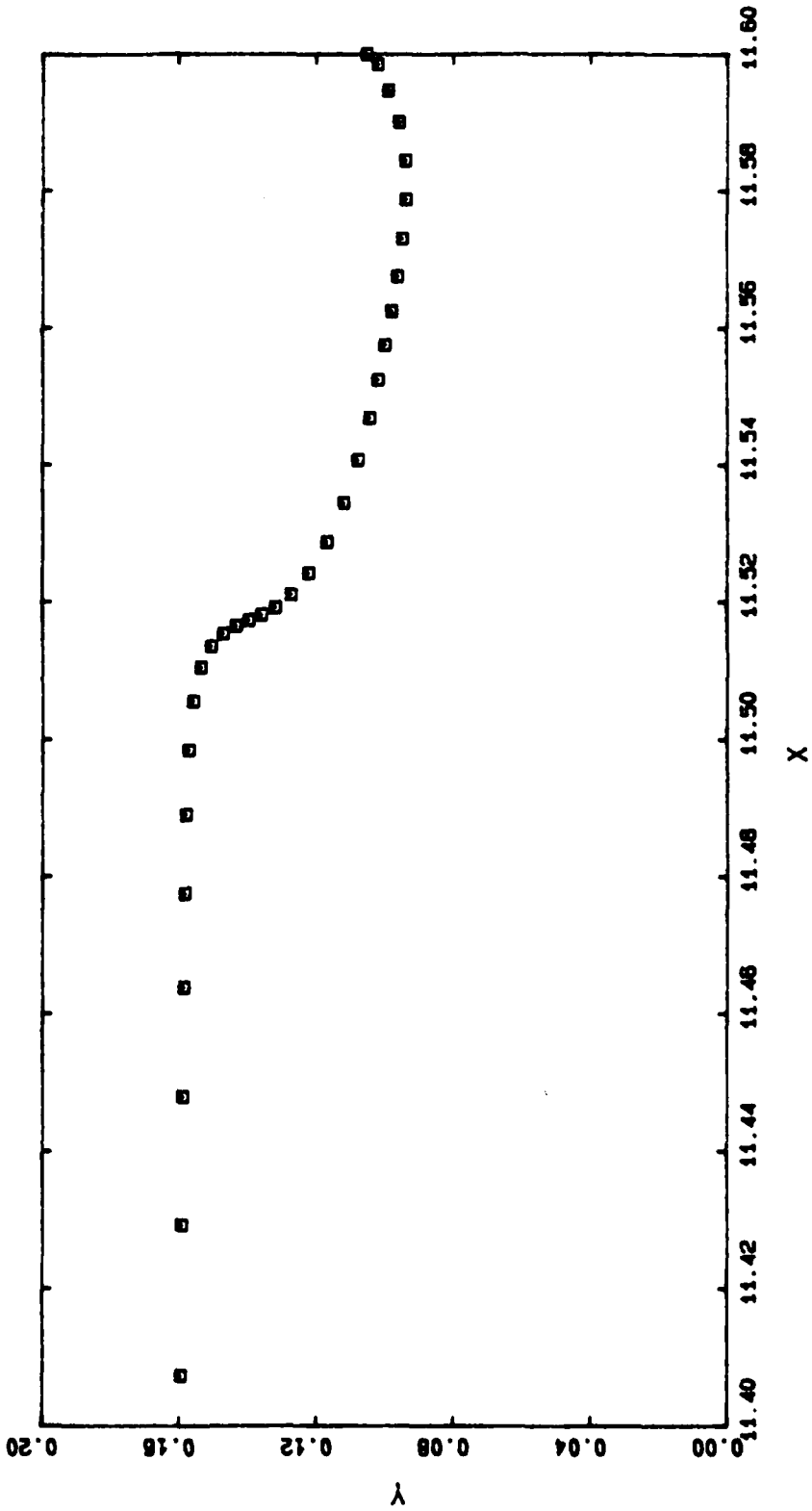

D7 3256 50.9175

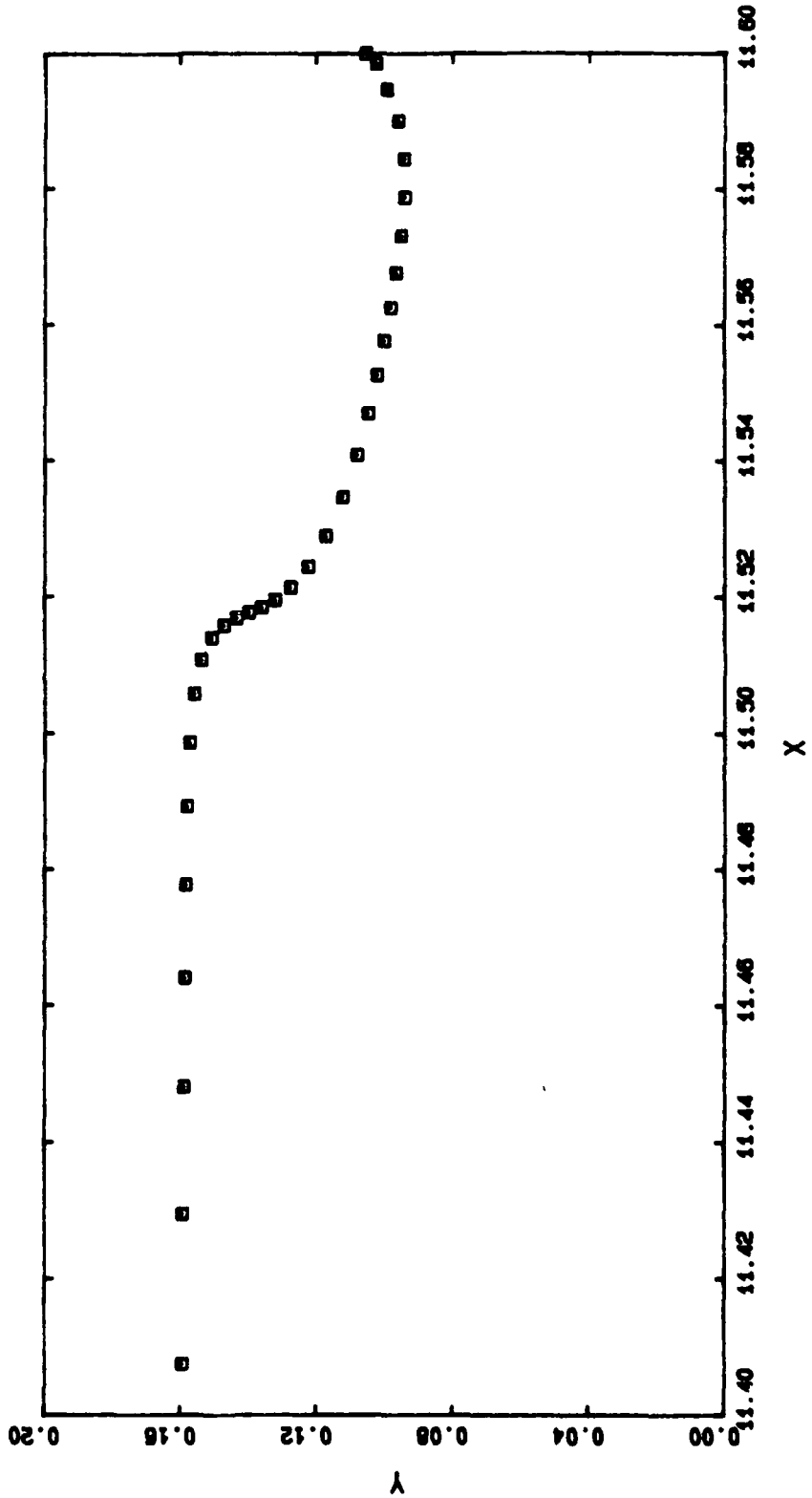

D7 3302 50.9280

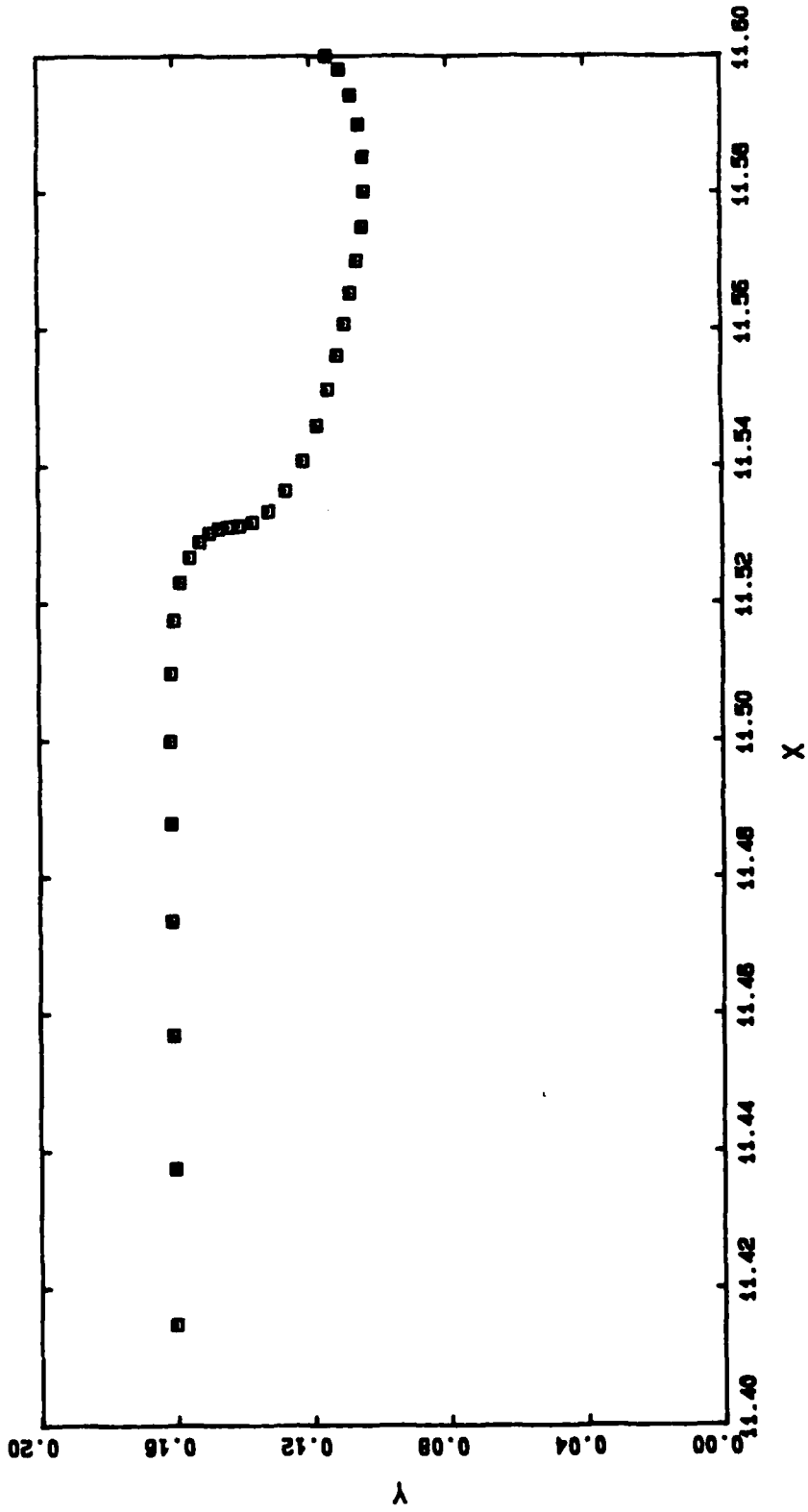

D7 3402 50.9416

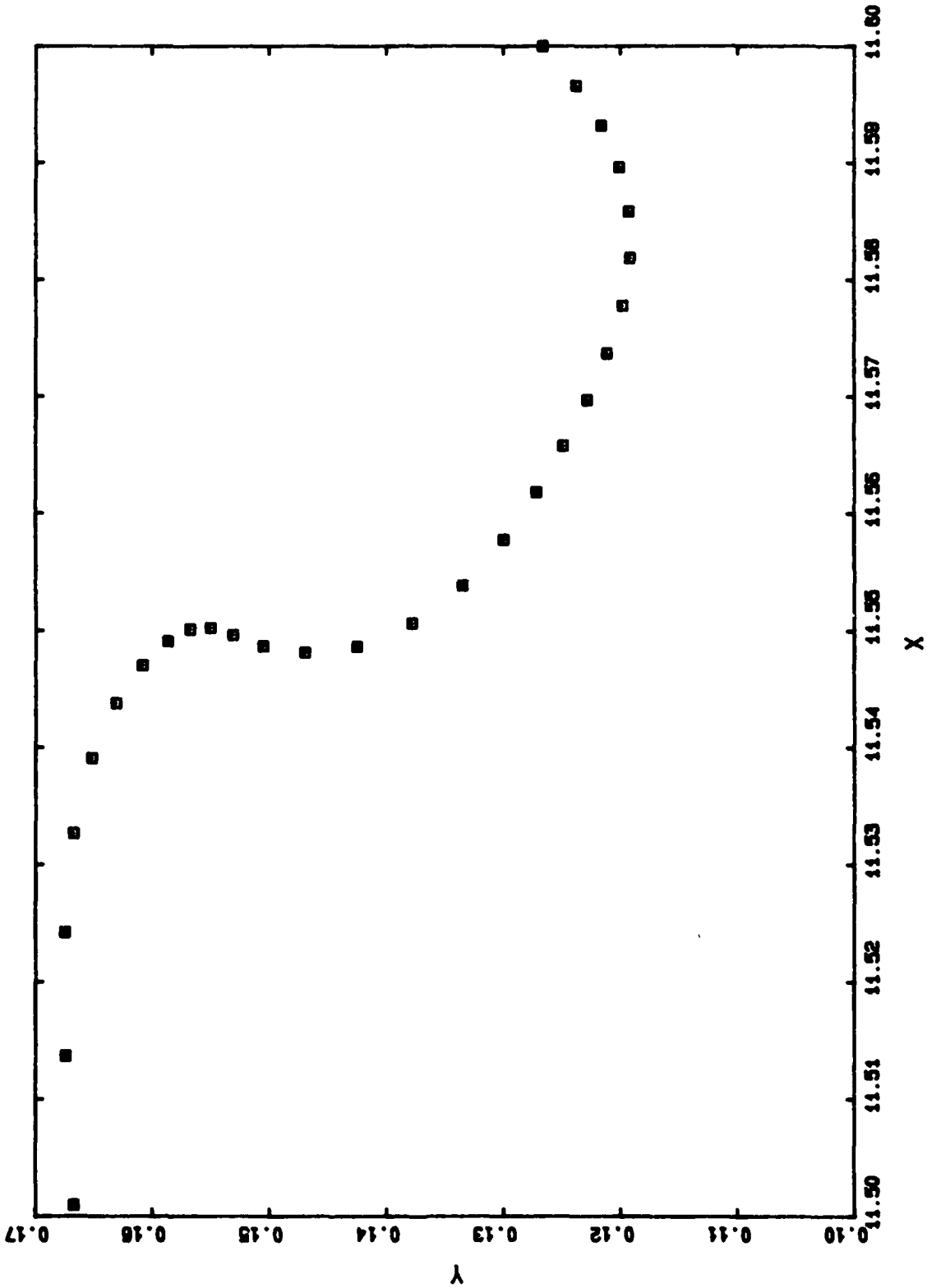

D7 3502 50.9505

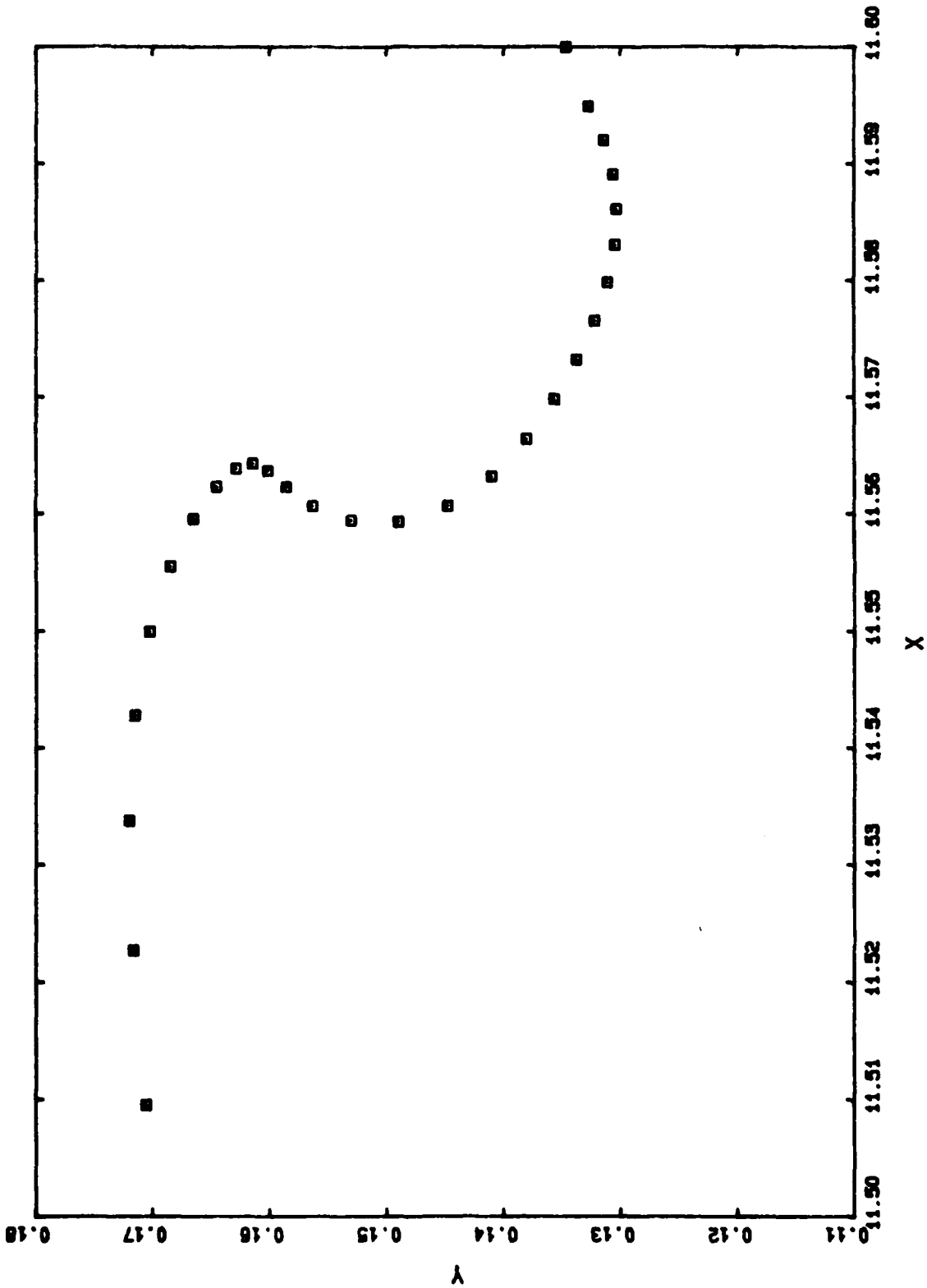

D7 3602 50.9574

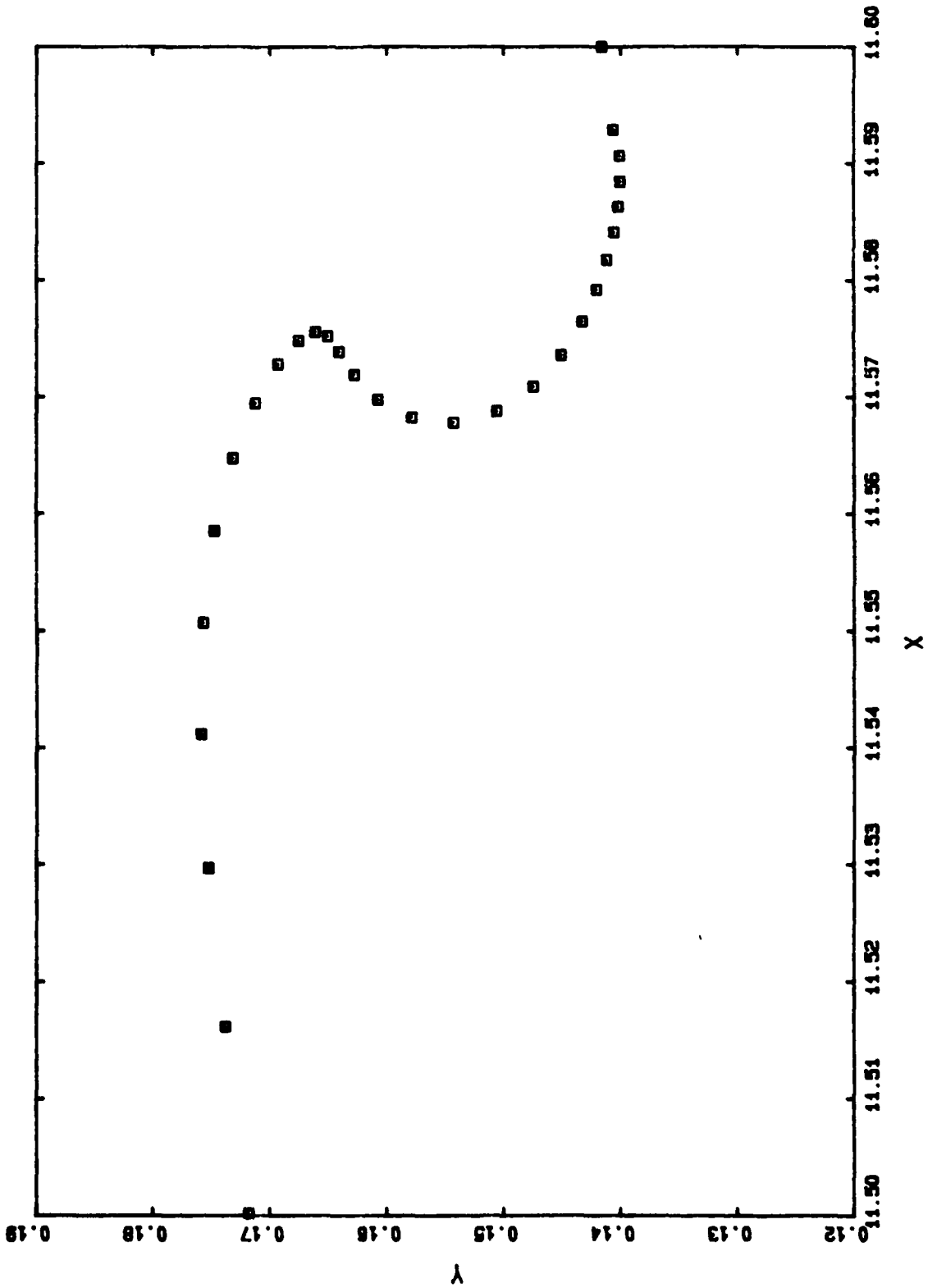

D7 3702 50.9634

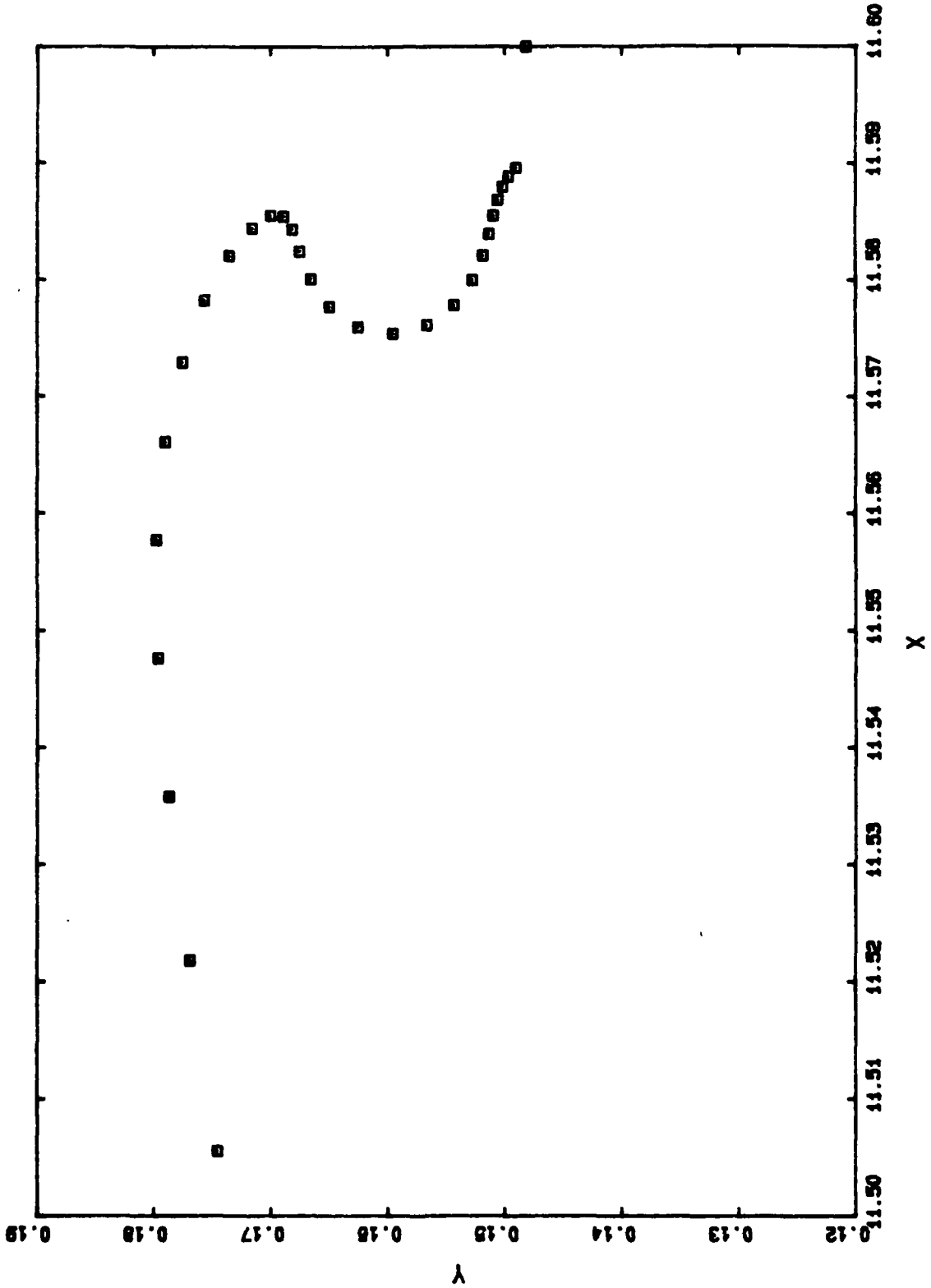

D7 3802 50.9670

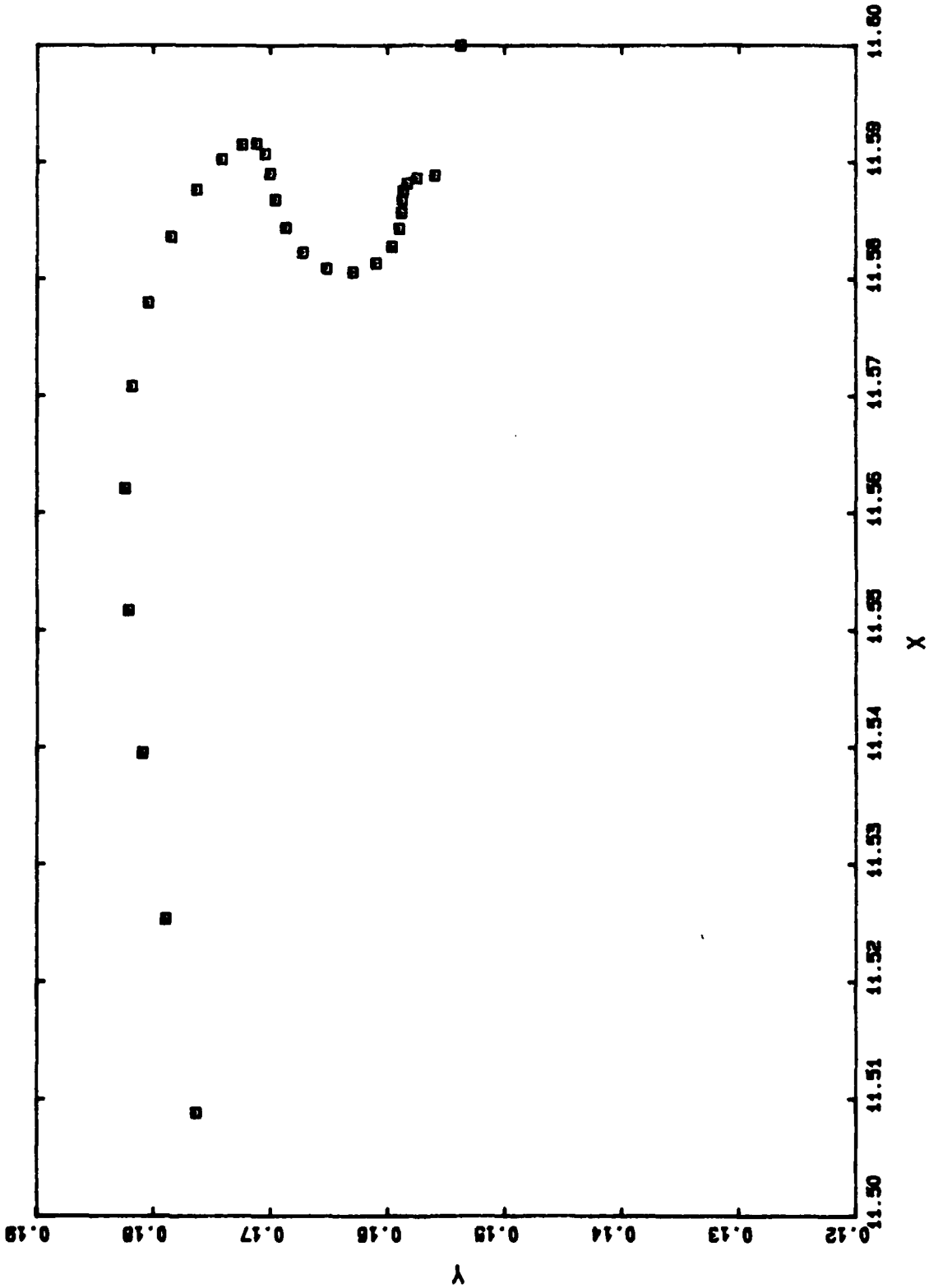

D7 3902 50.9697

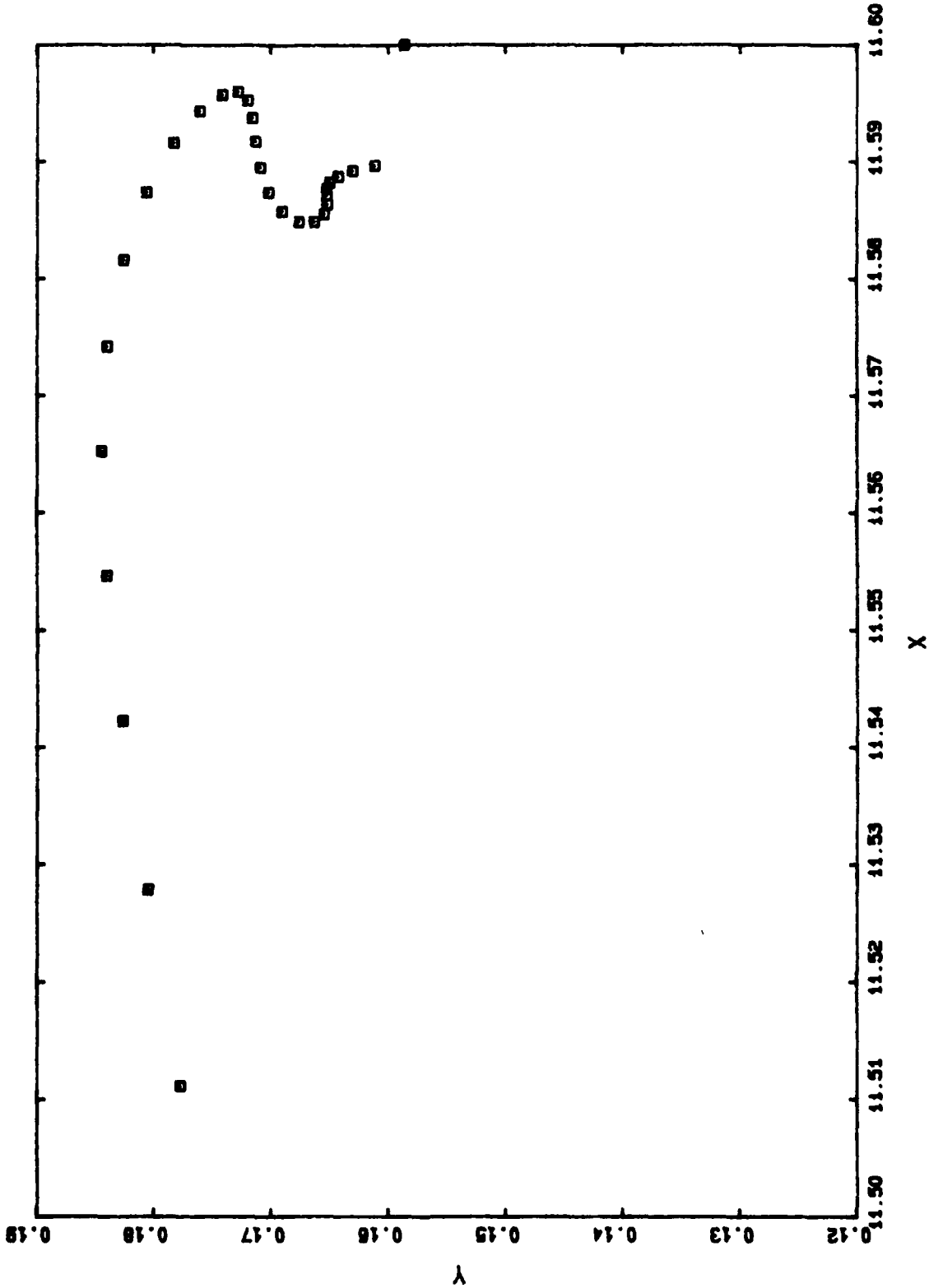

D7 4002 50.9711

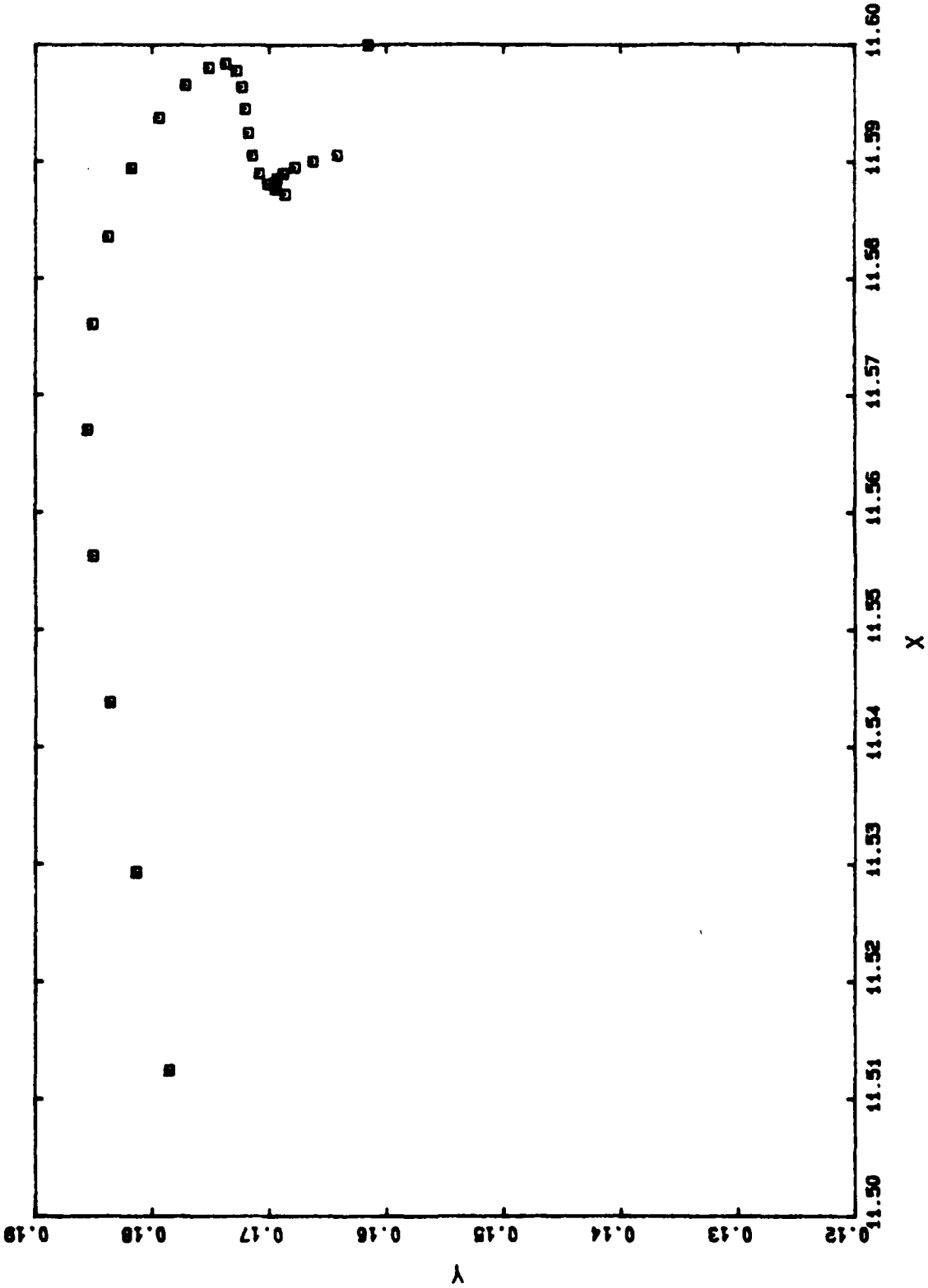

D8 3101 50.8463

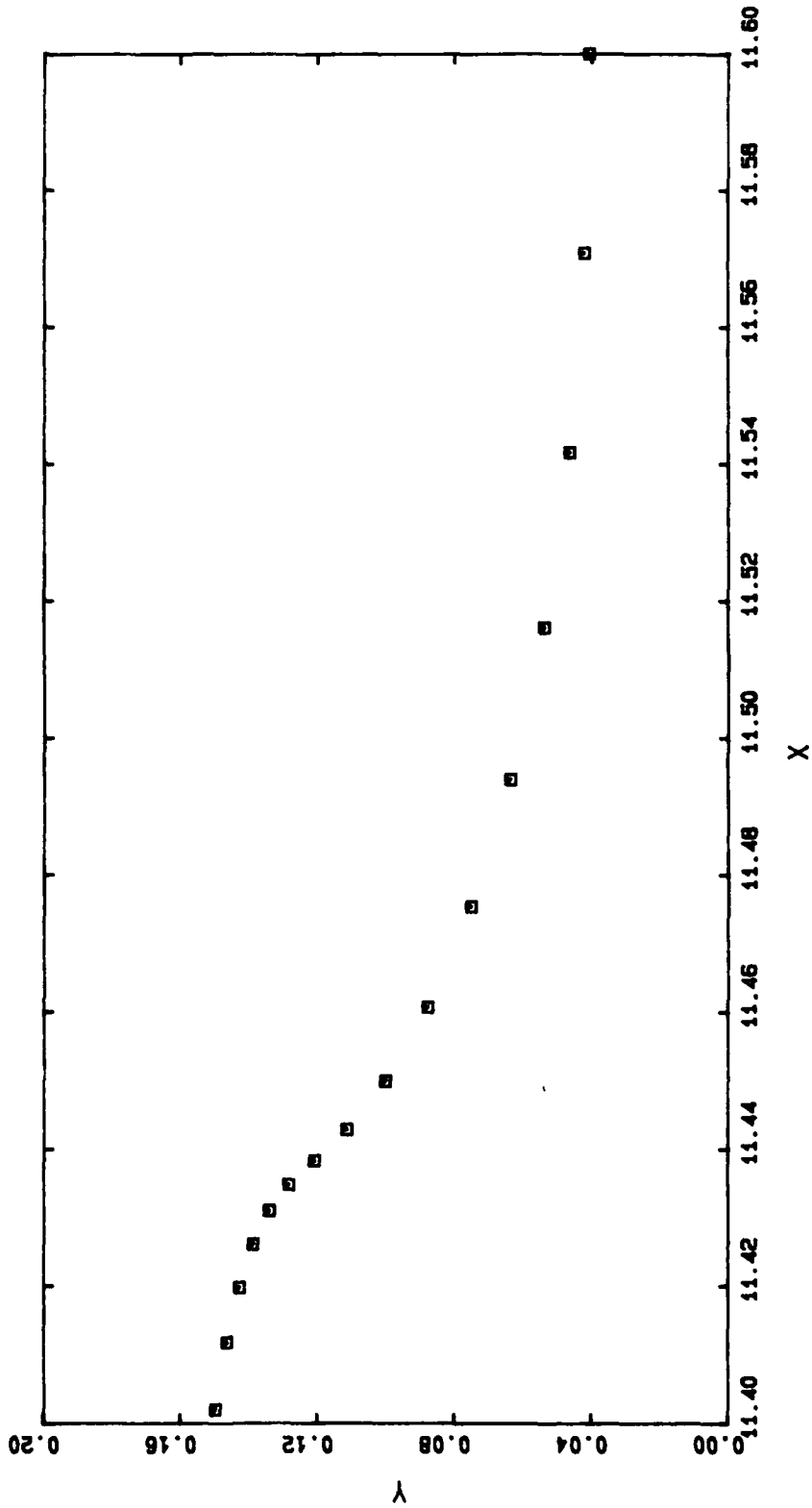

D8 3104 50.8484

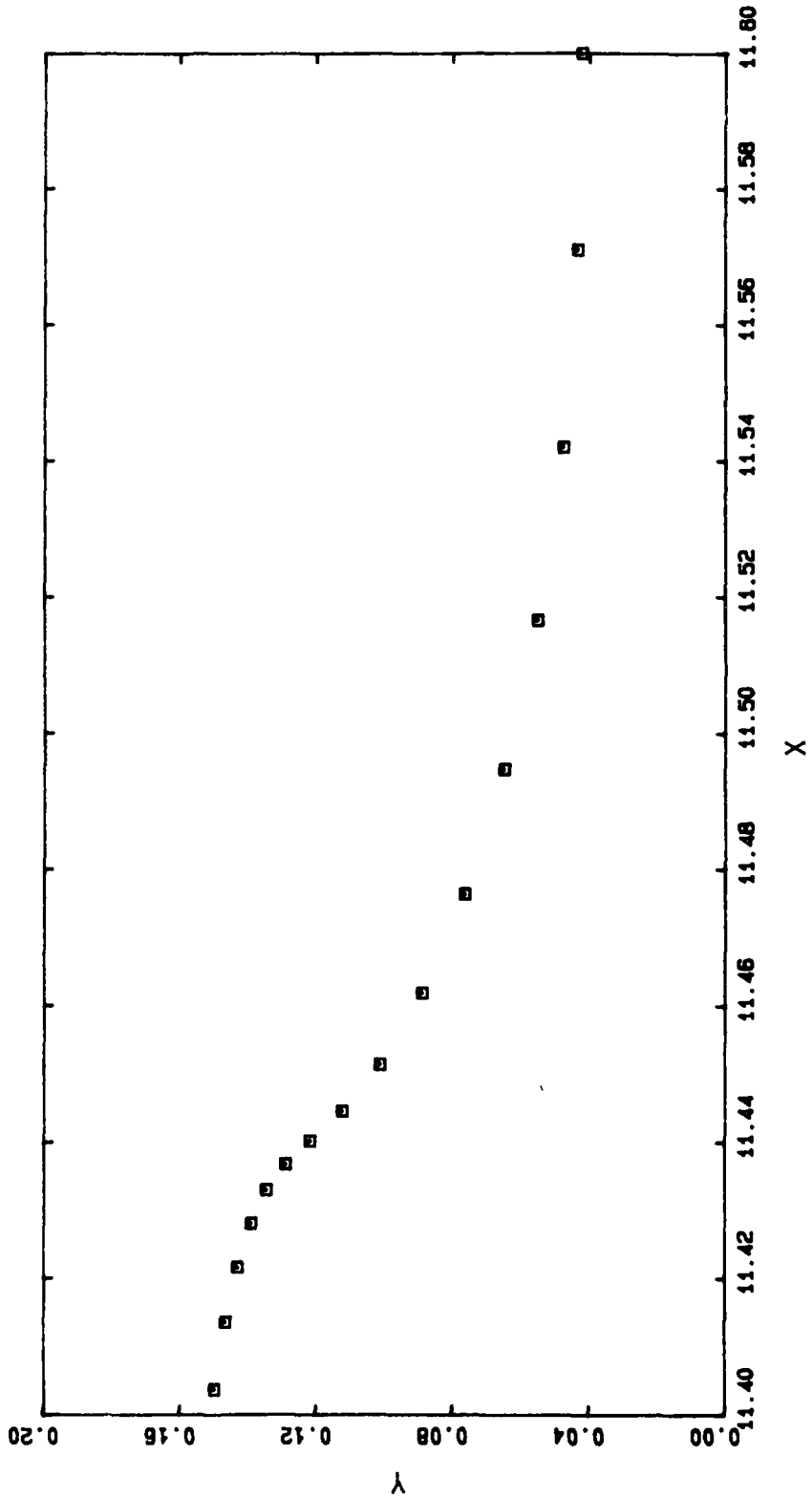

D8 3105 50.8490

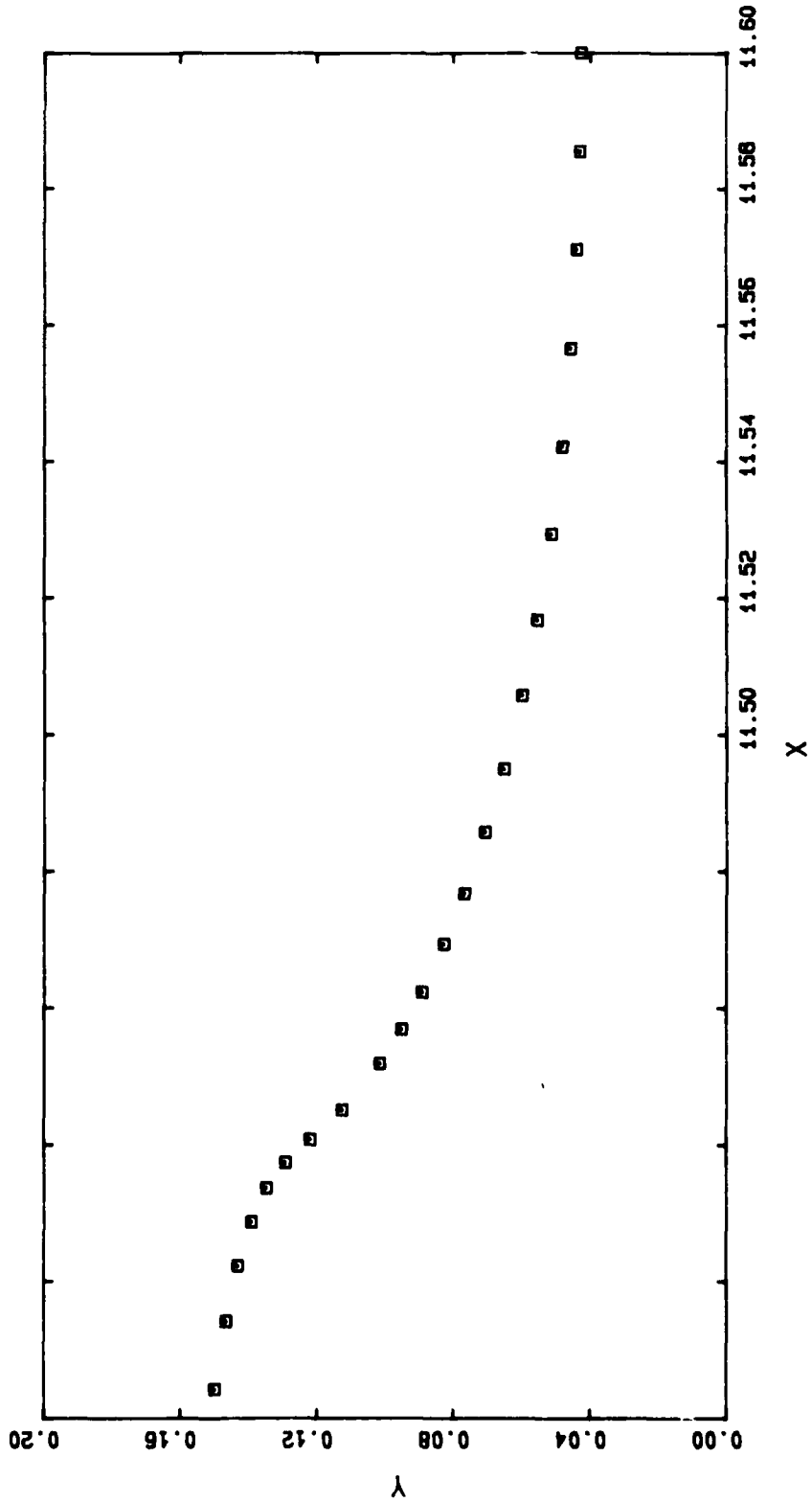

D8 3106 50.8497

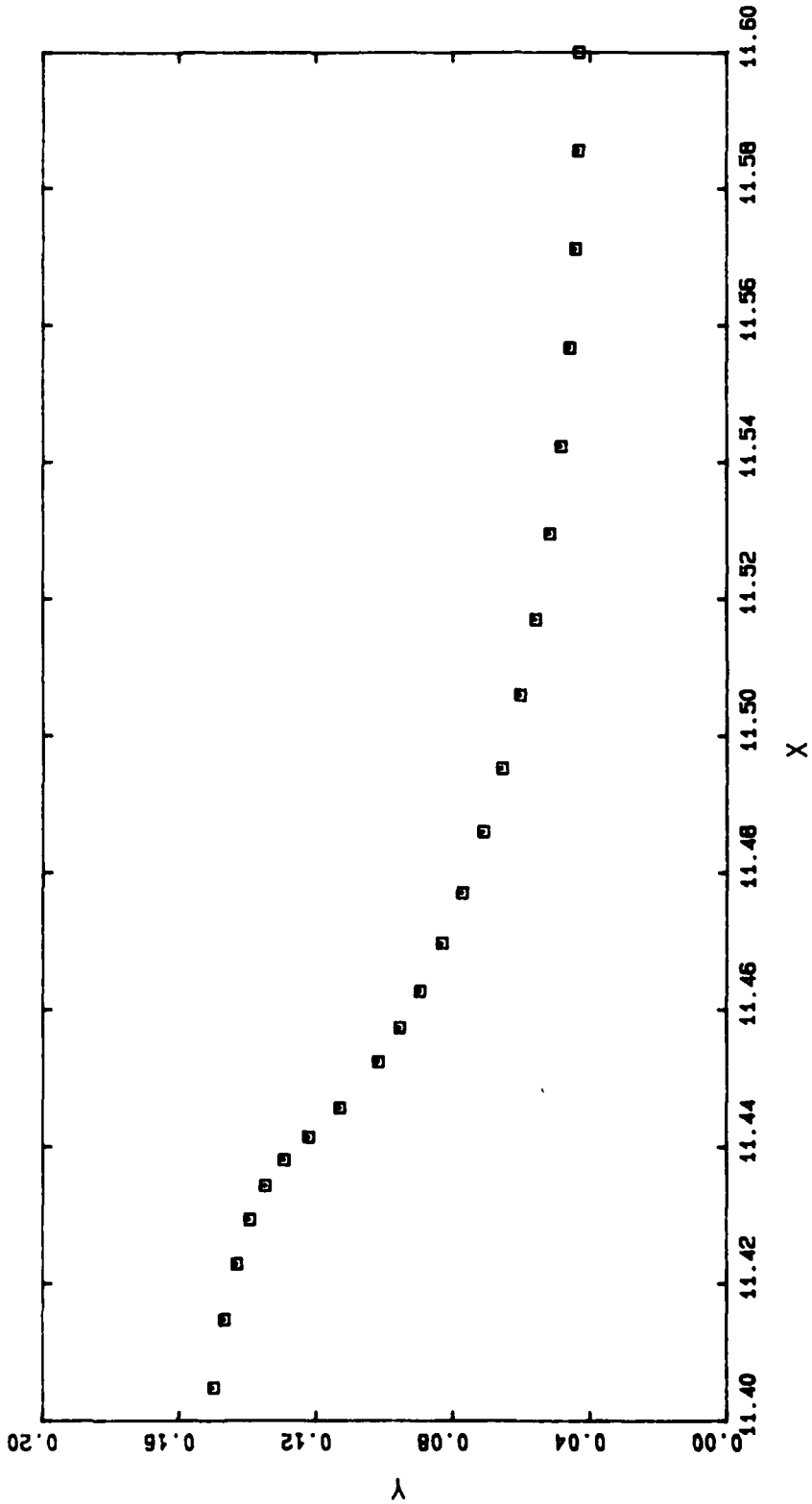

D8 3201 50.8962

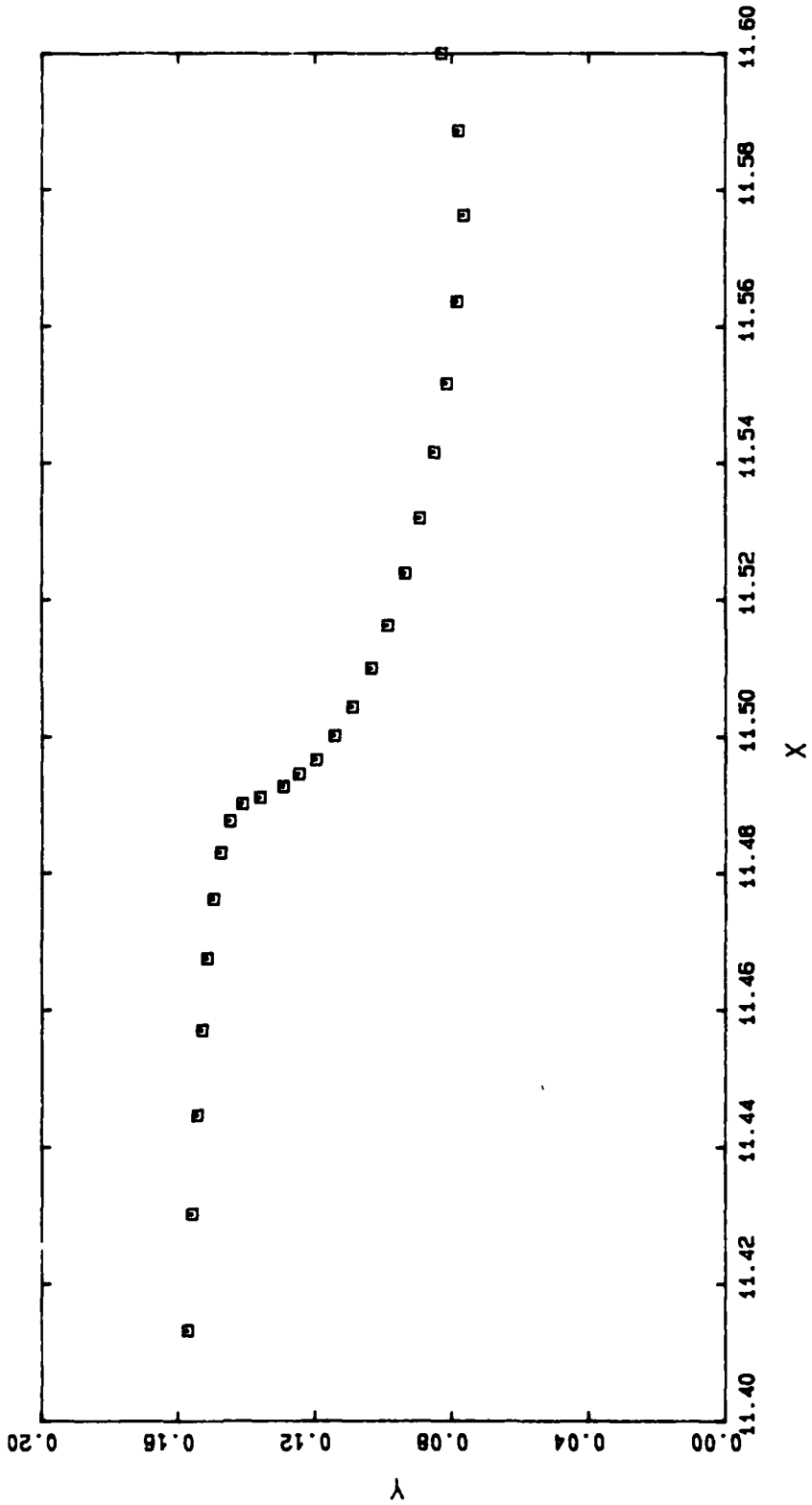

D8 3301 50.9243

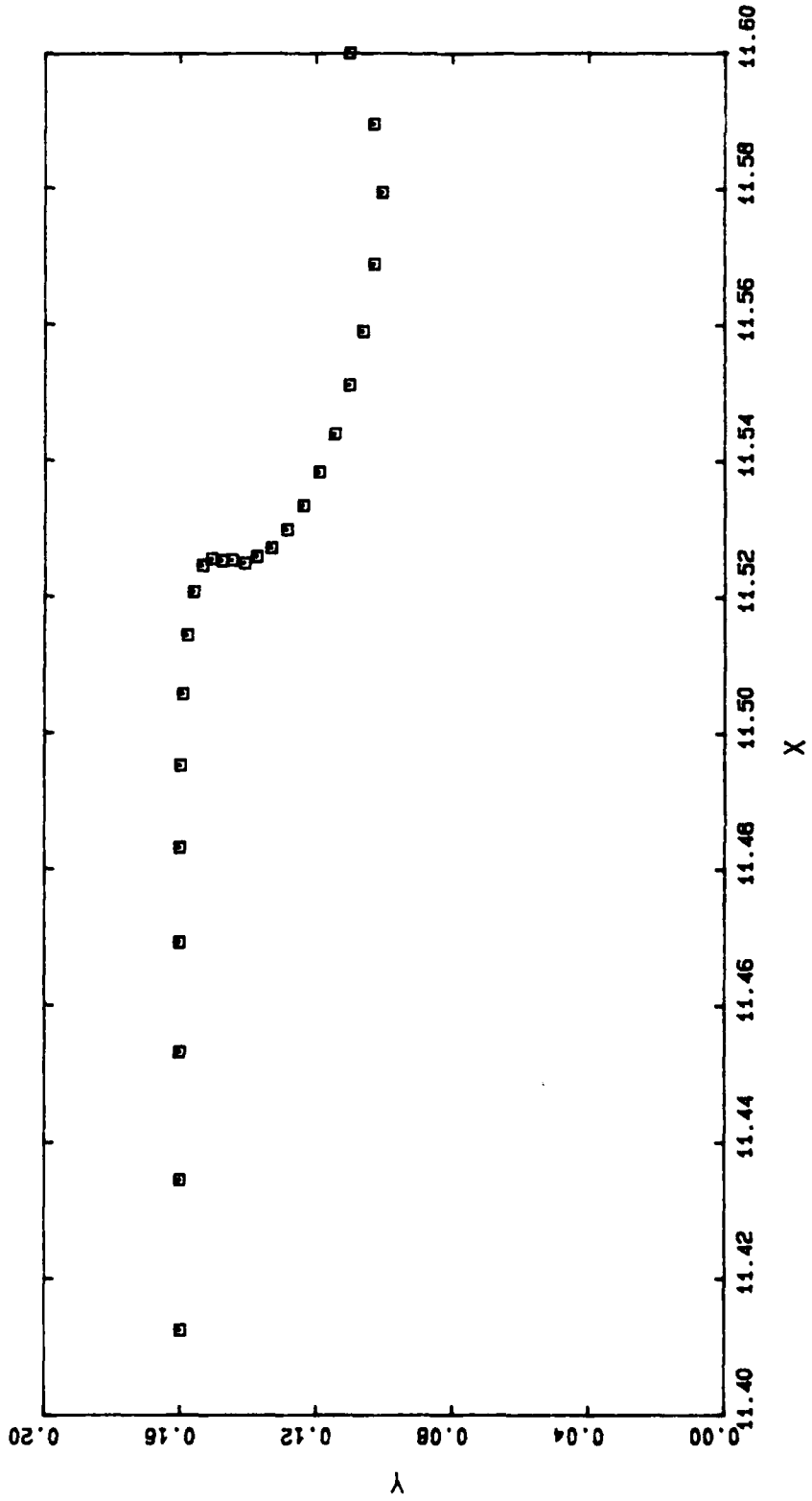

D8 3401 50.9384

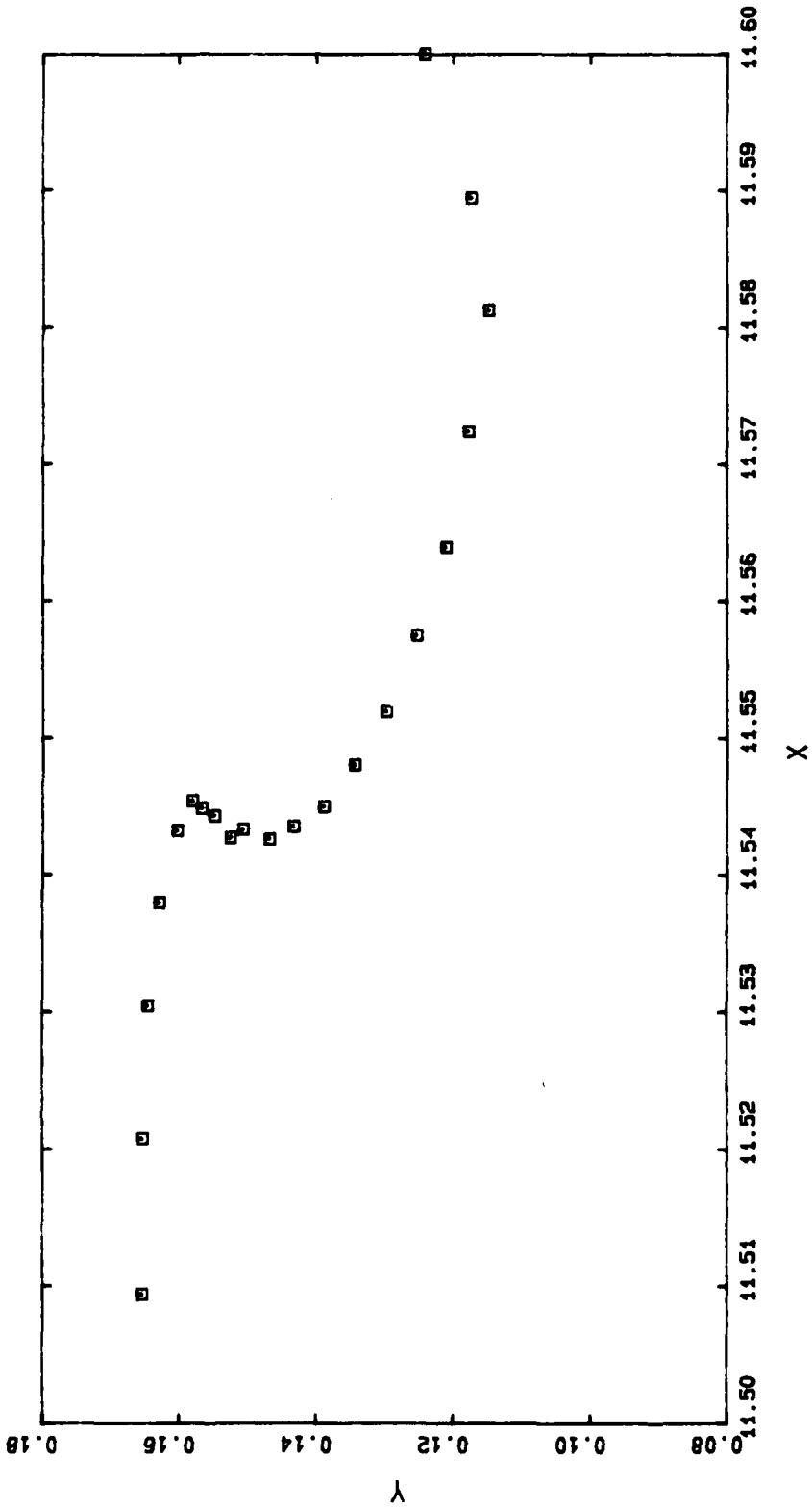

D8 3501 50.9484

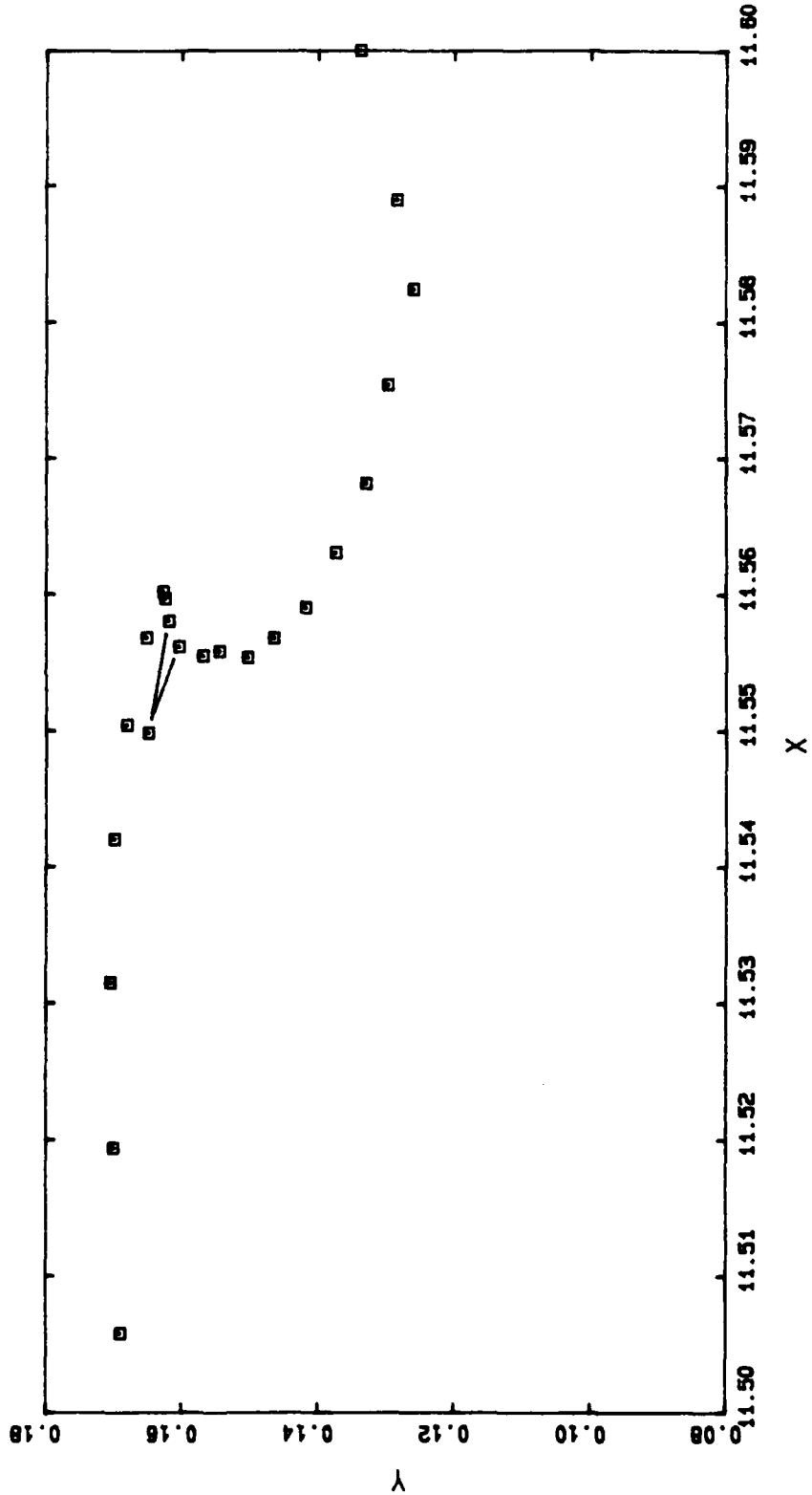

D9 3101 50.8463

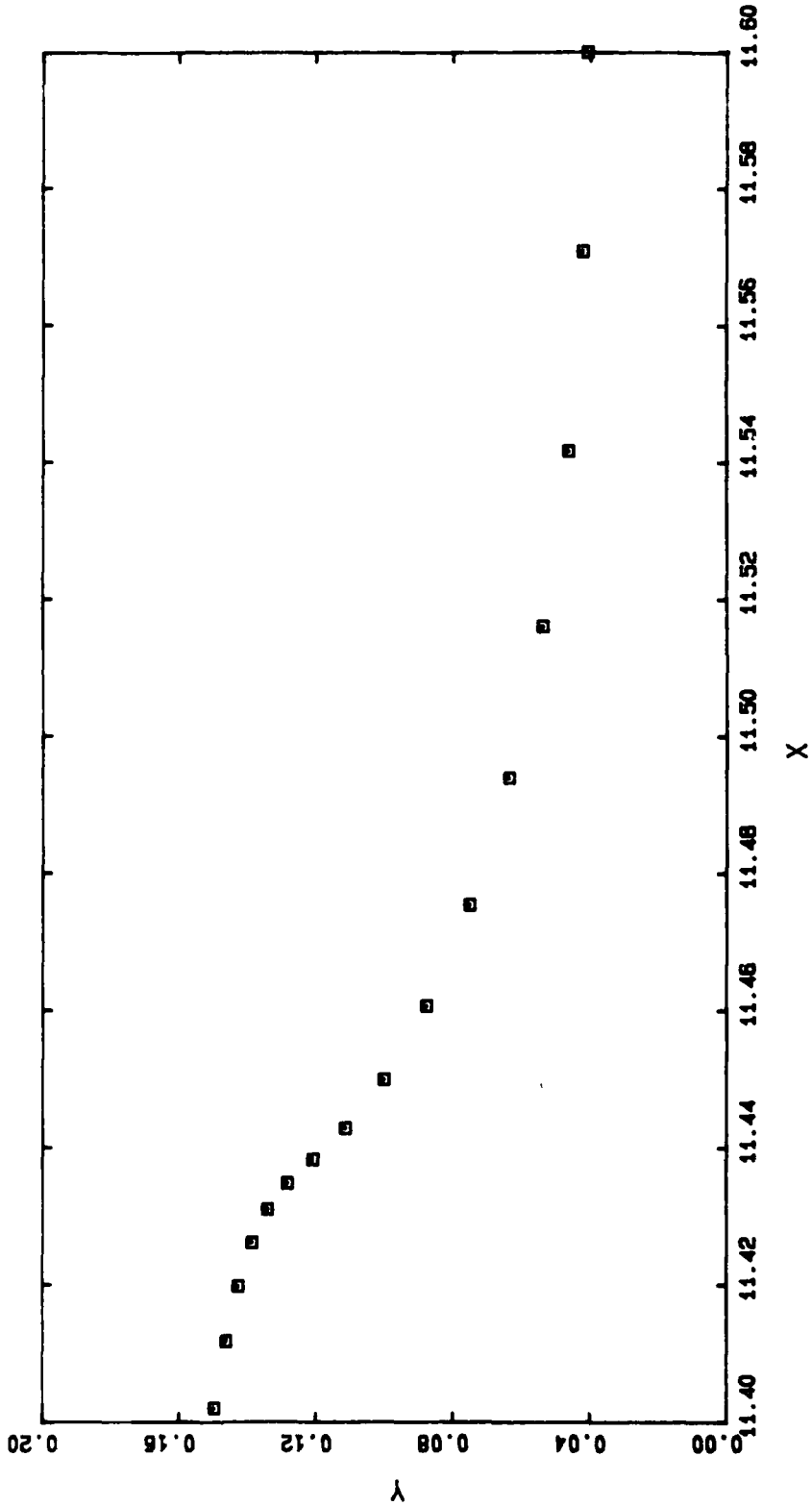

D9 3105 50.8490

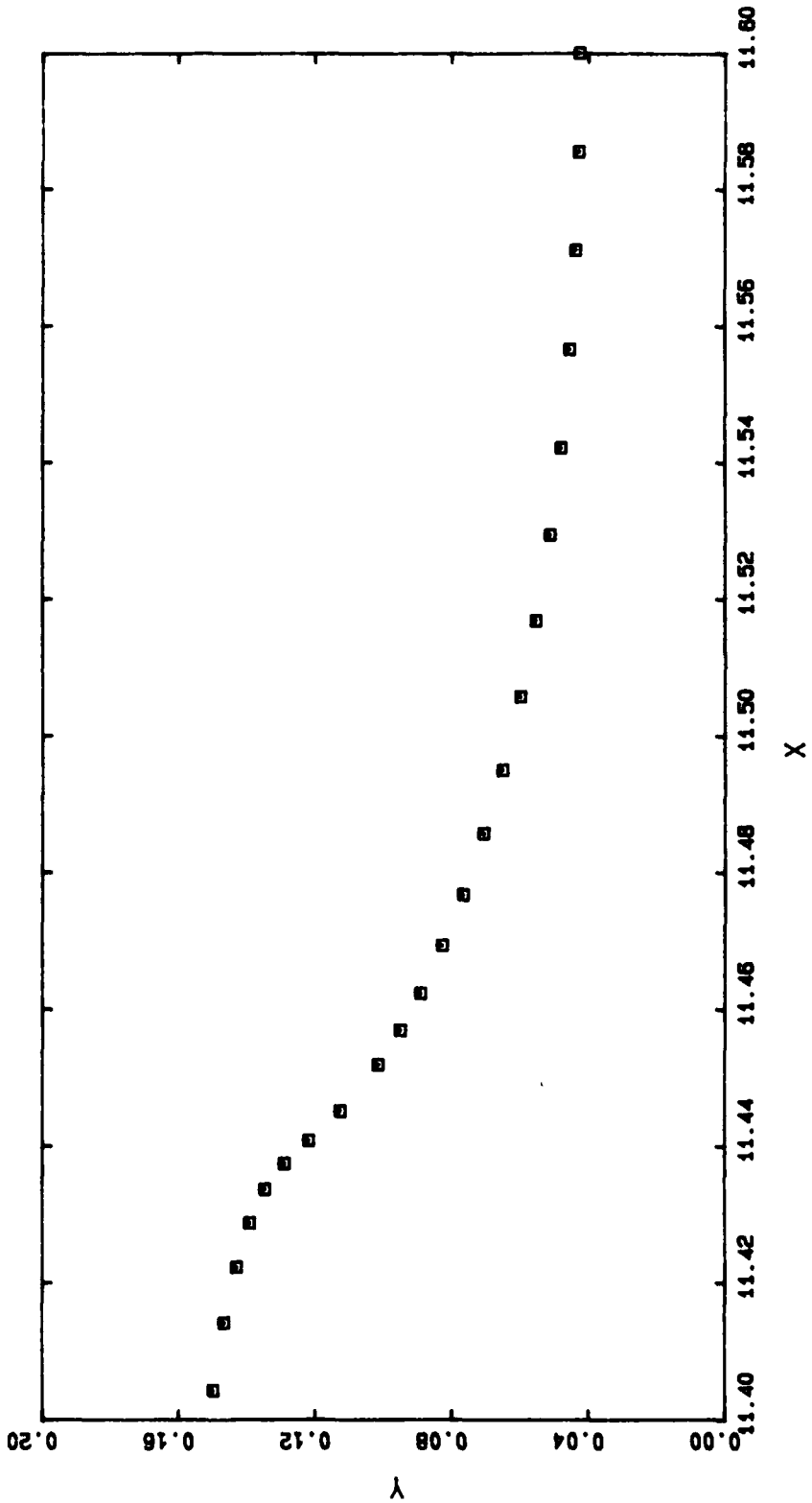

D9 3109 50.8517

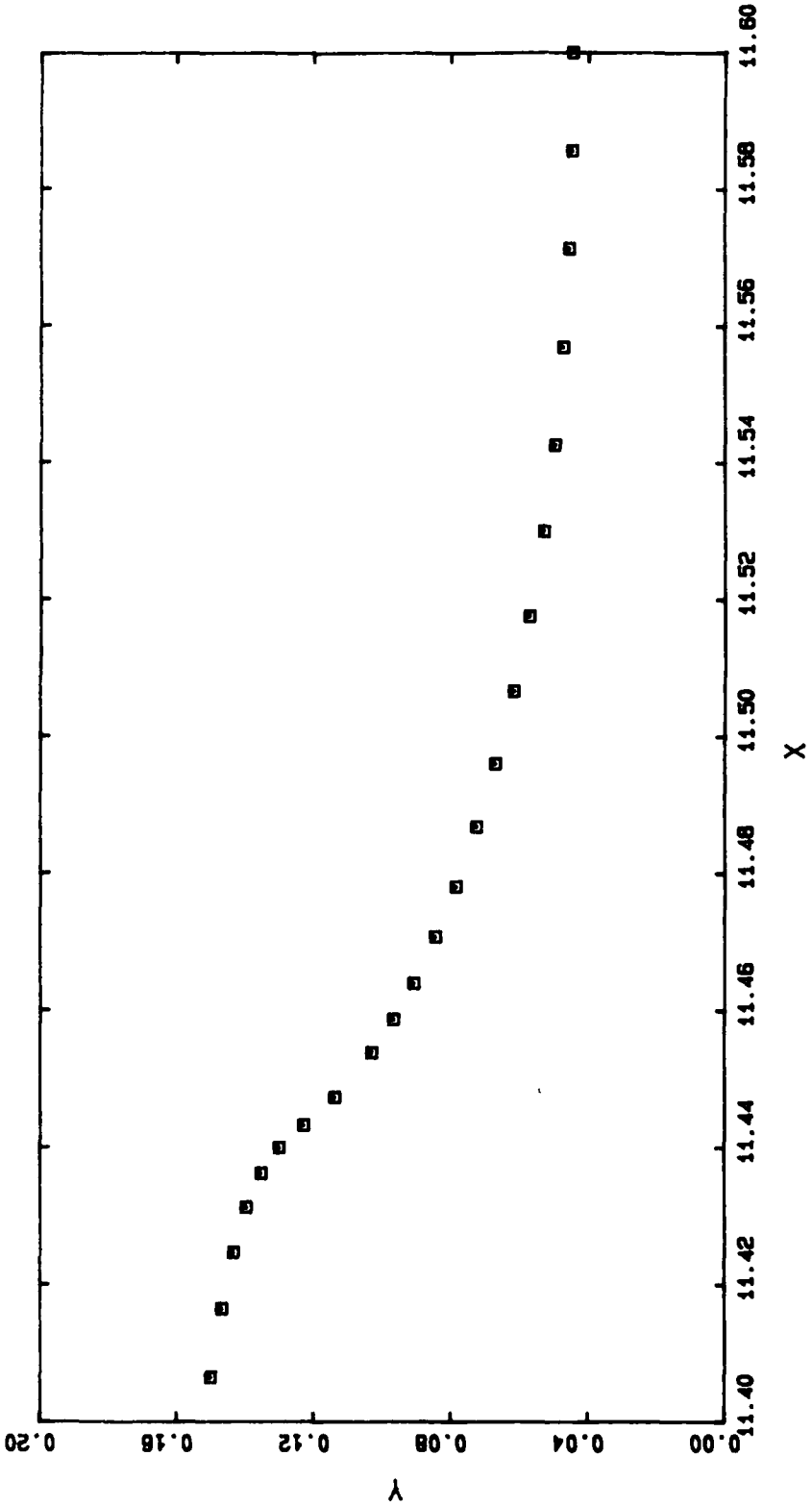

D9 3110 50.8523

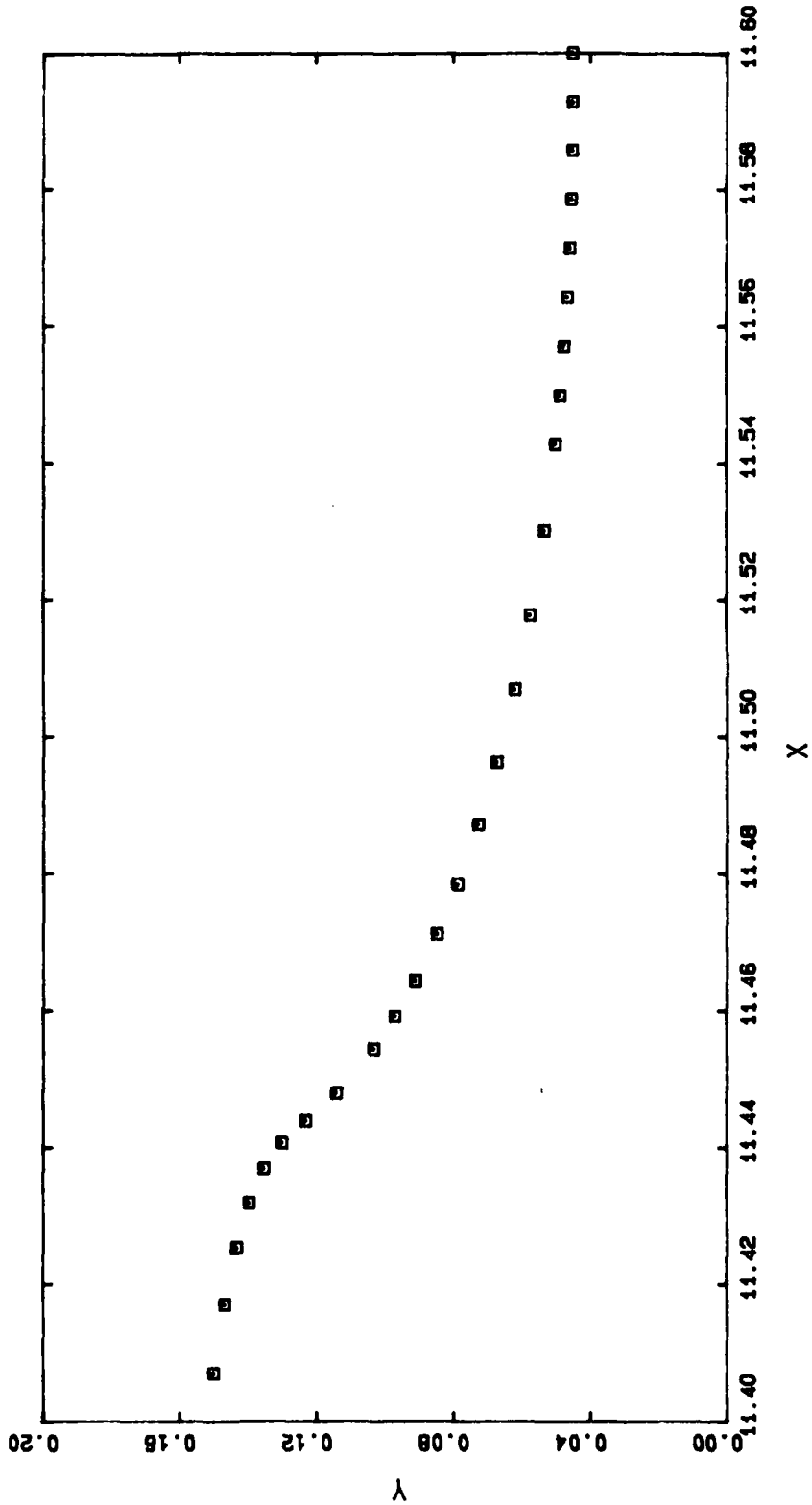

D9 3115 50.8555

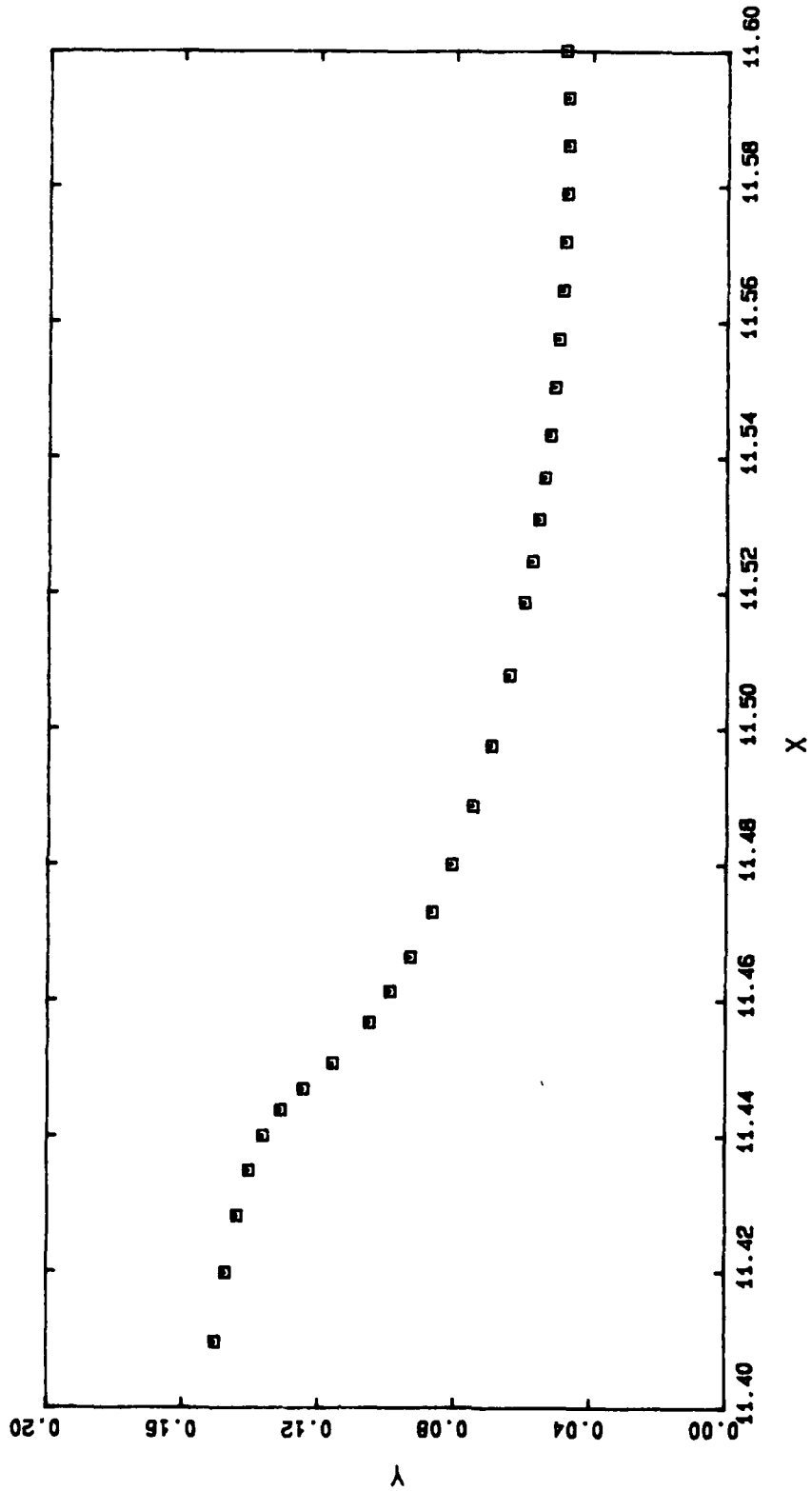

D9 3126 50.8619

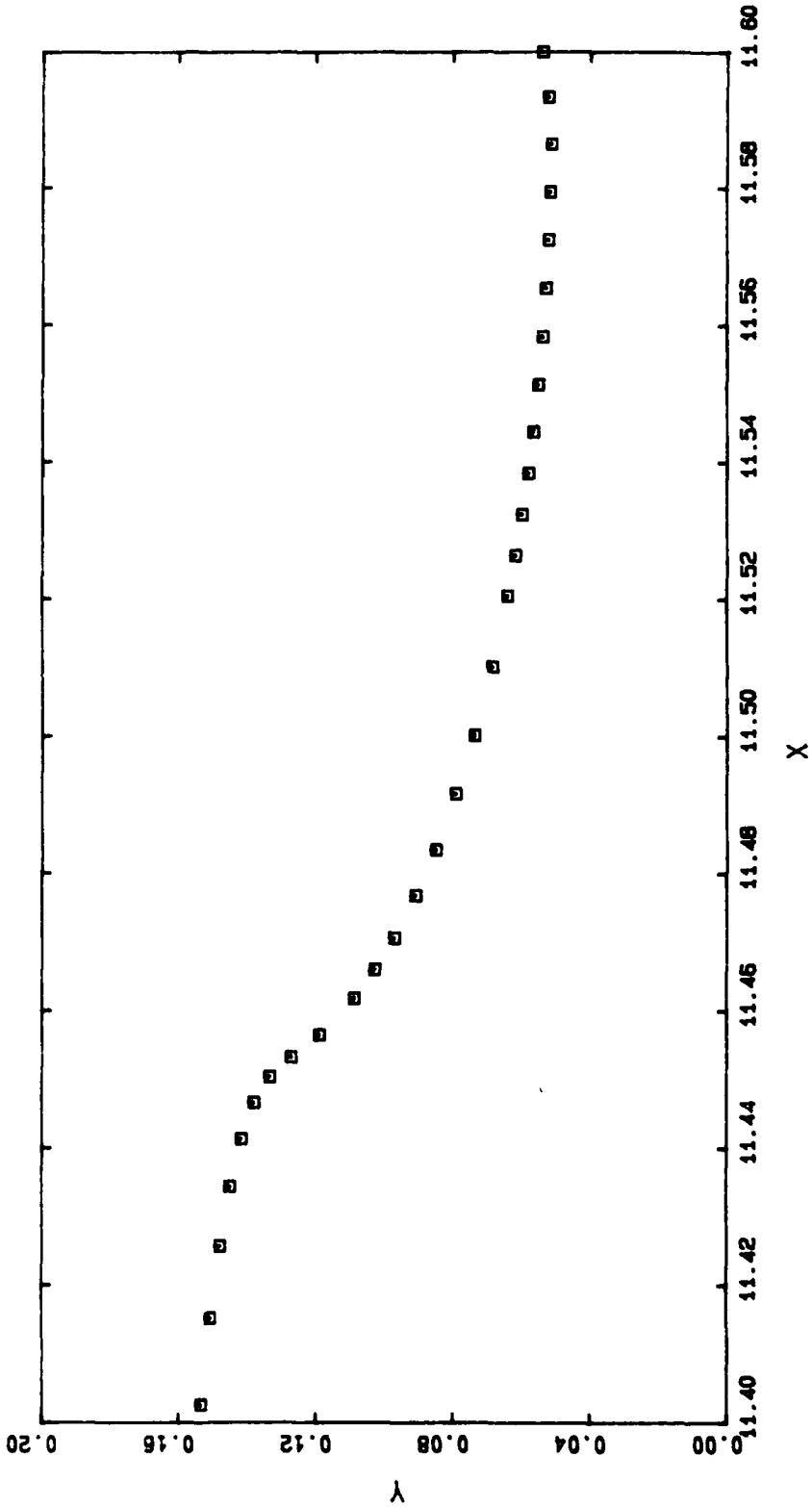

D9 3226 50.9048

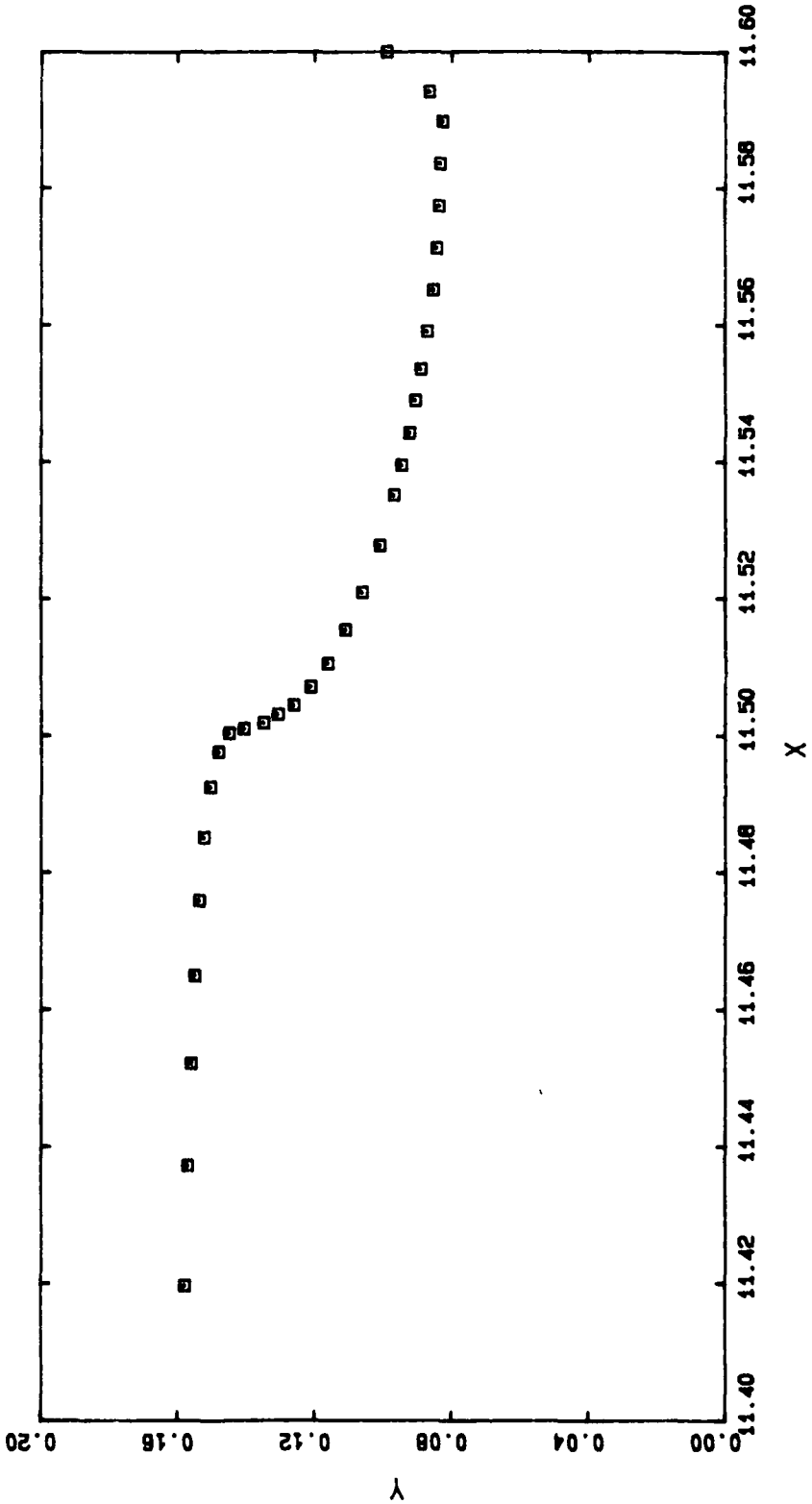

D9 3326 50.9290

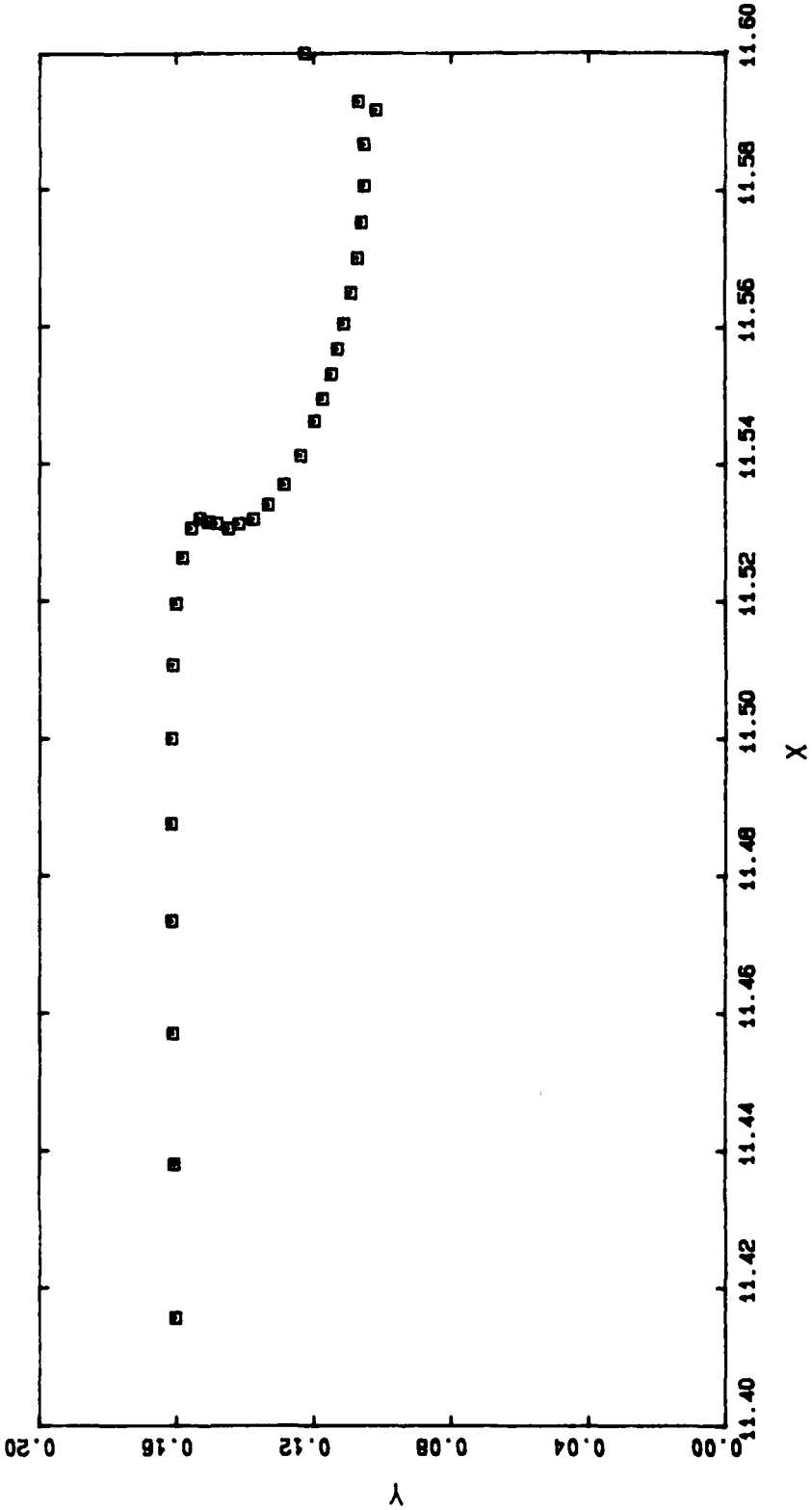

Appendix E

Refer to Chapter 5 for discussion.

E2 3101 50.8463

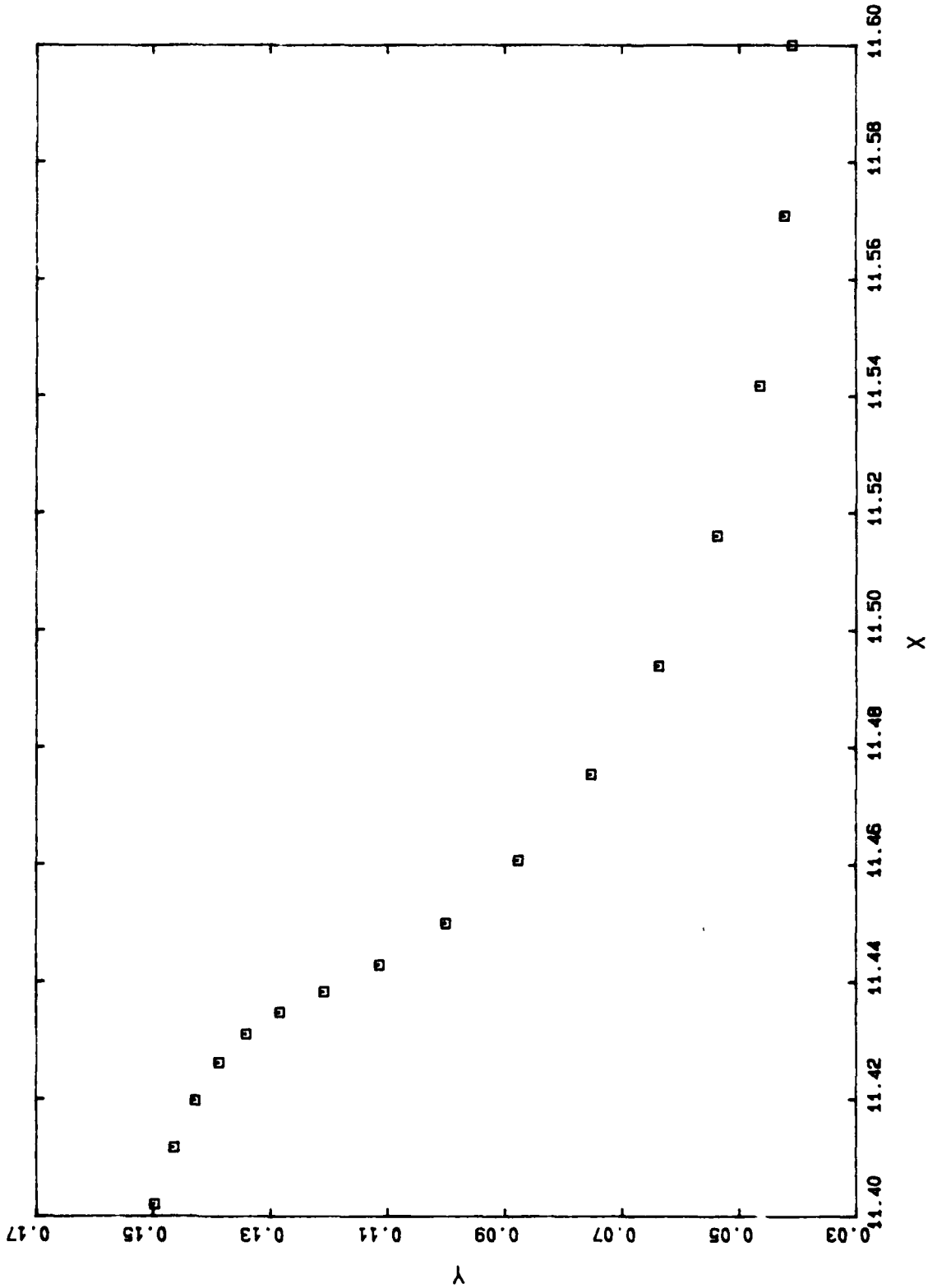

E2 3104 50.8484

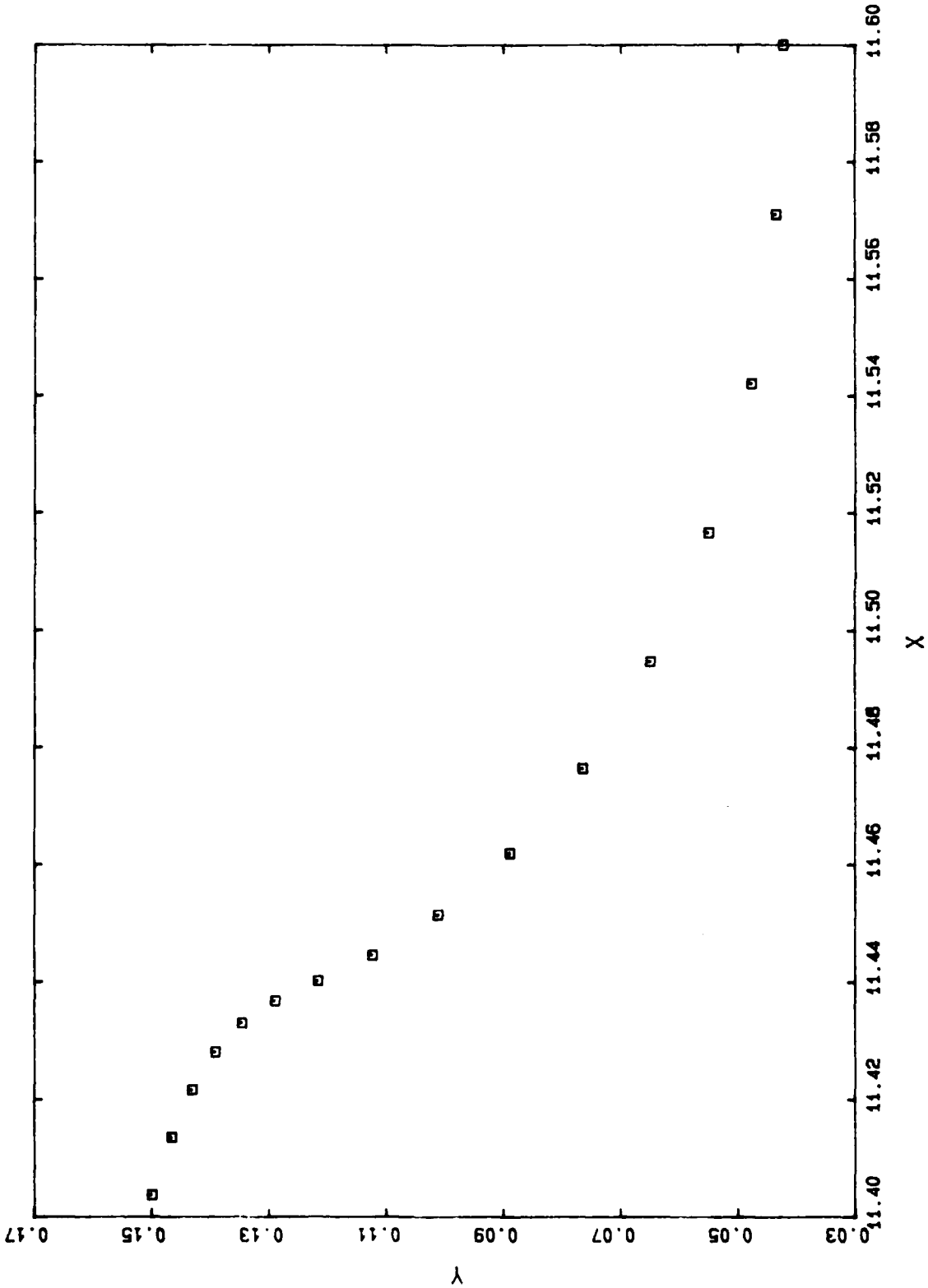

E2 3105 50.8490

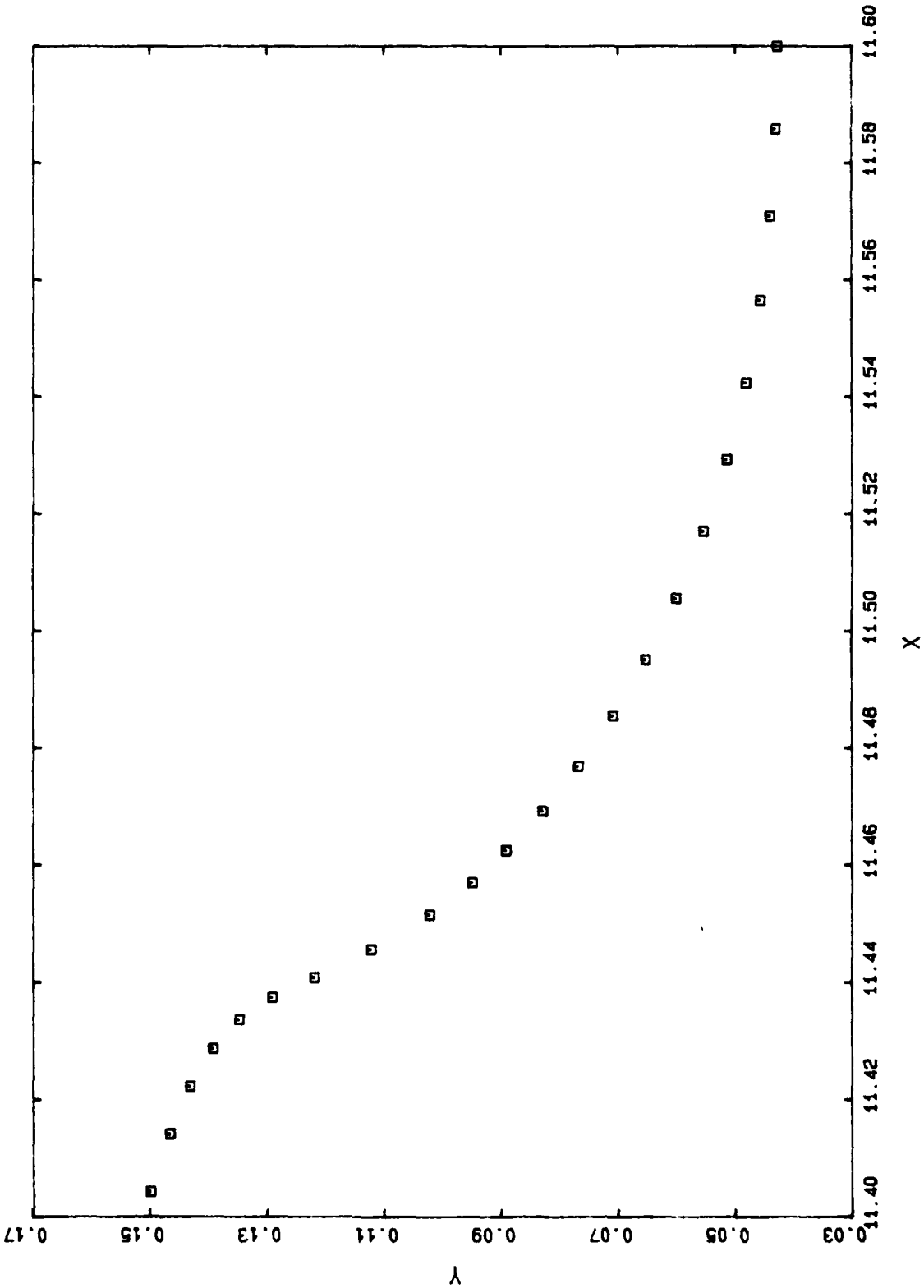

E2 3109 50.8516

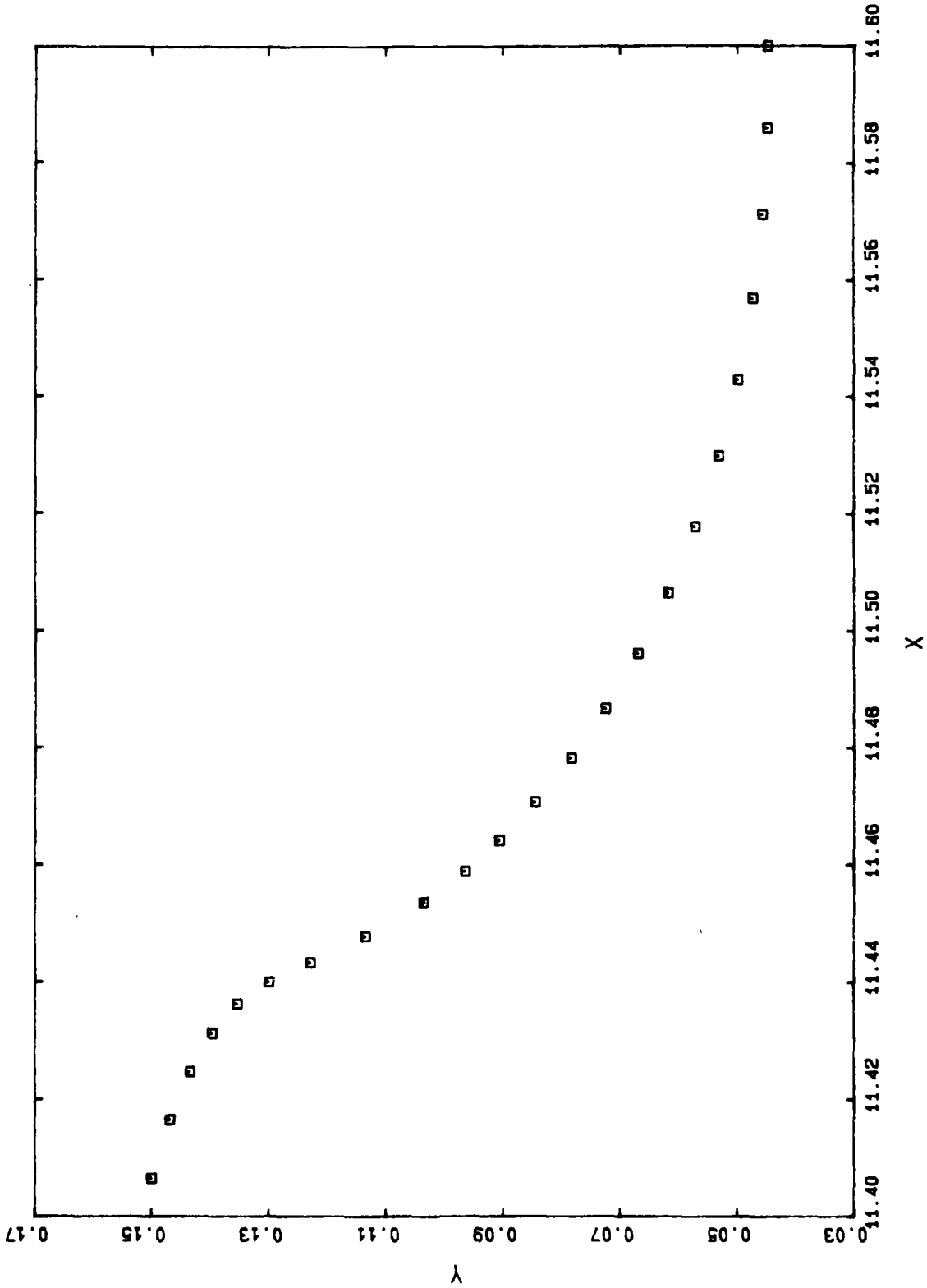

E2 3110 50.8523

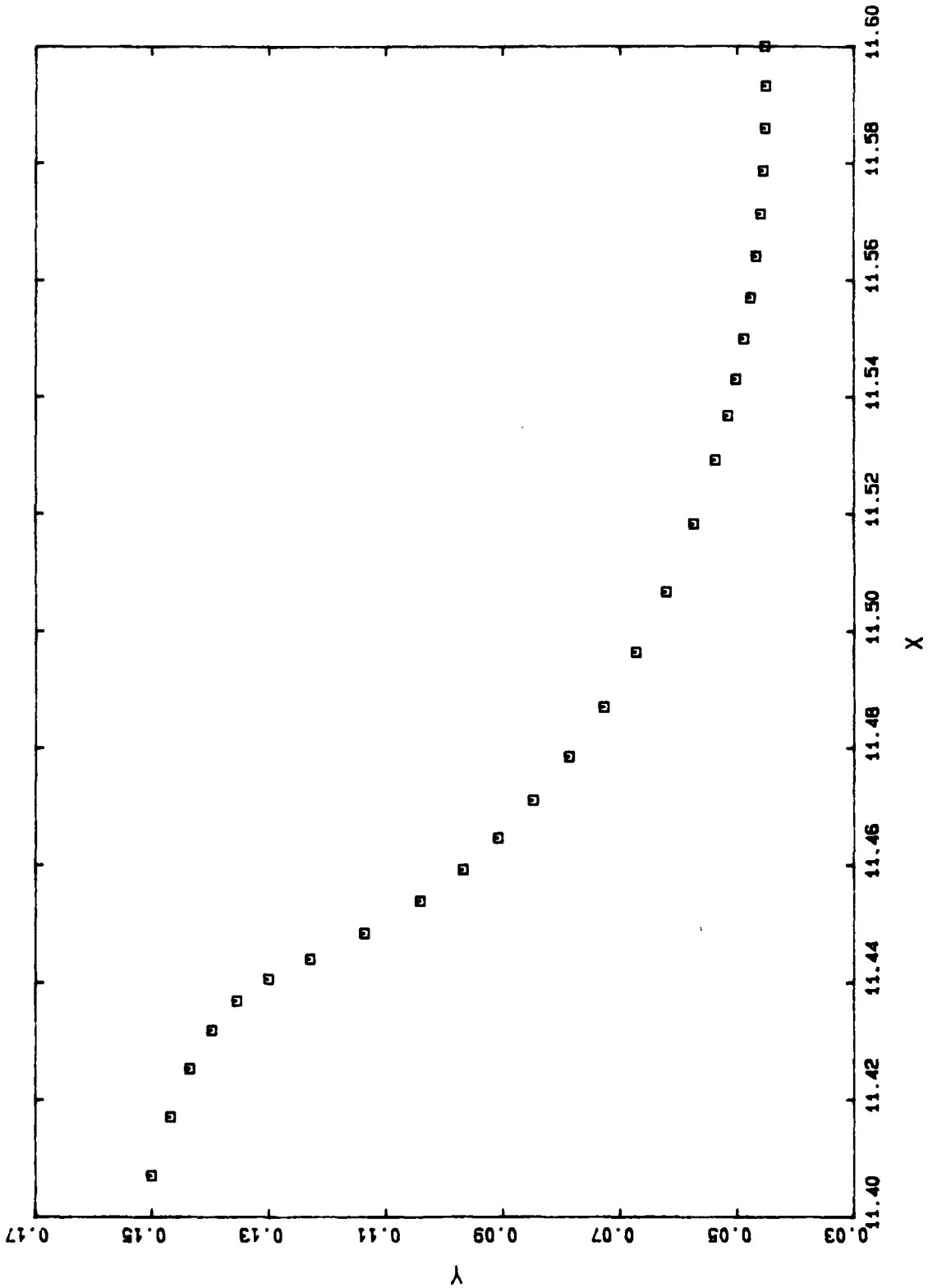

E2 3161 50.8803

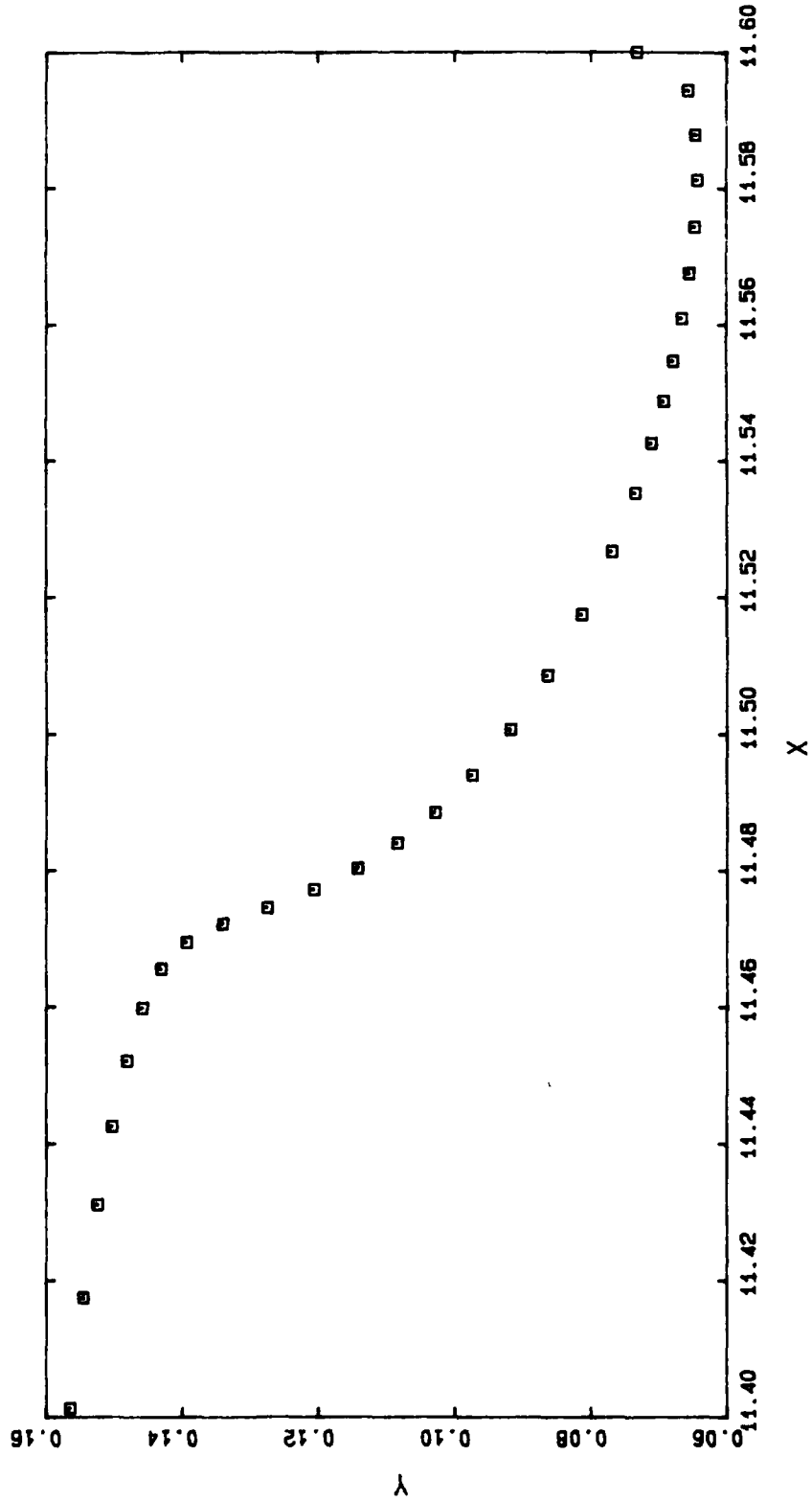

E2 3261 50.9189

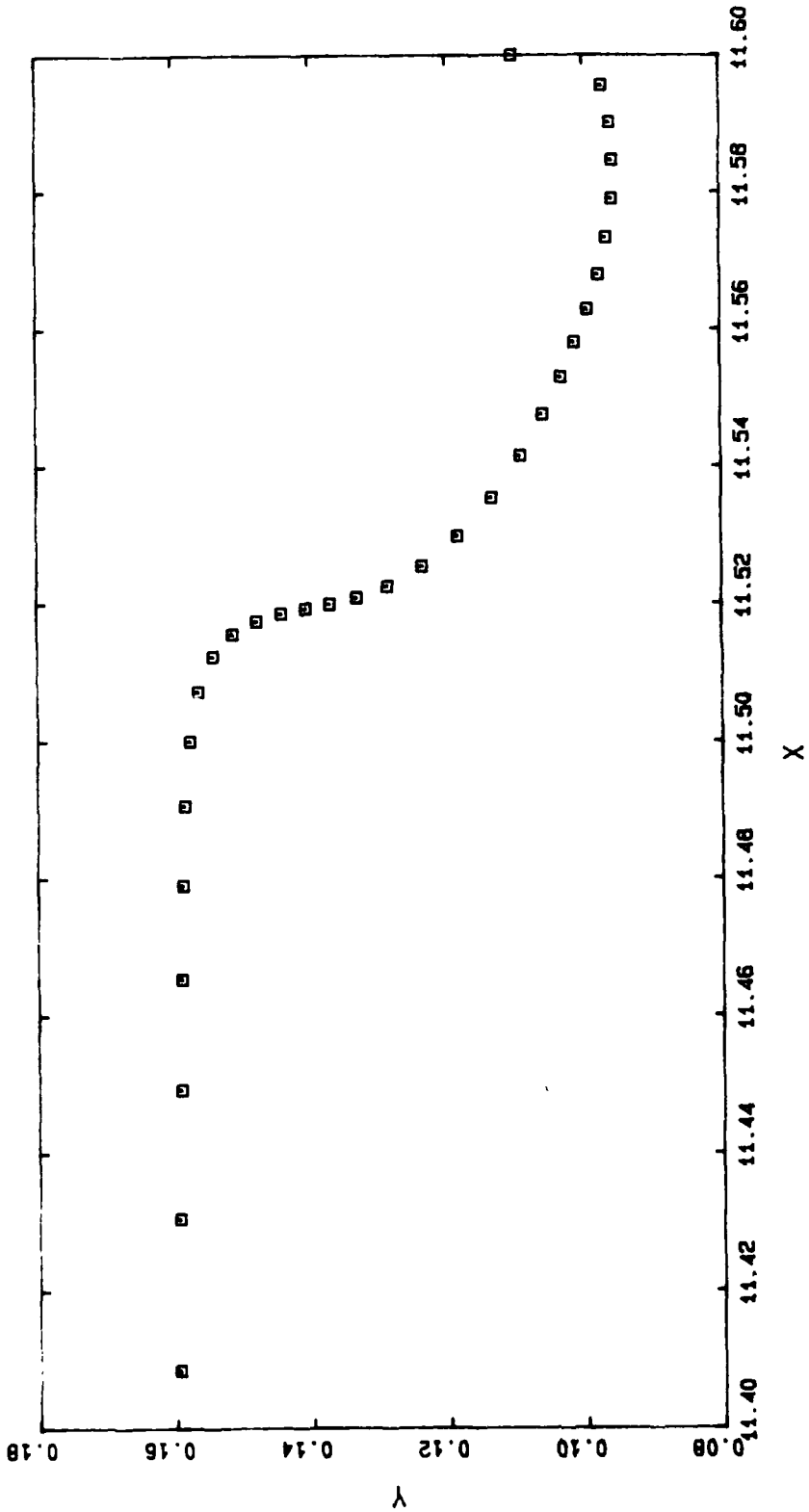

E2 3361 50.9370

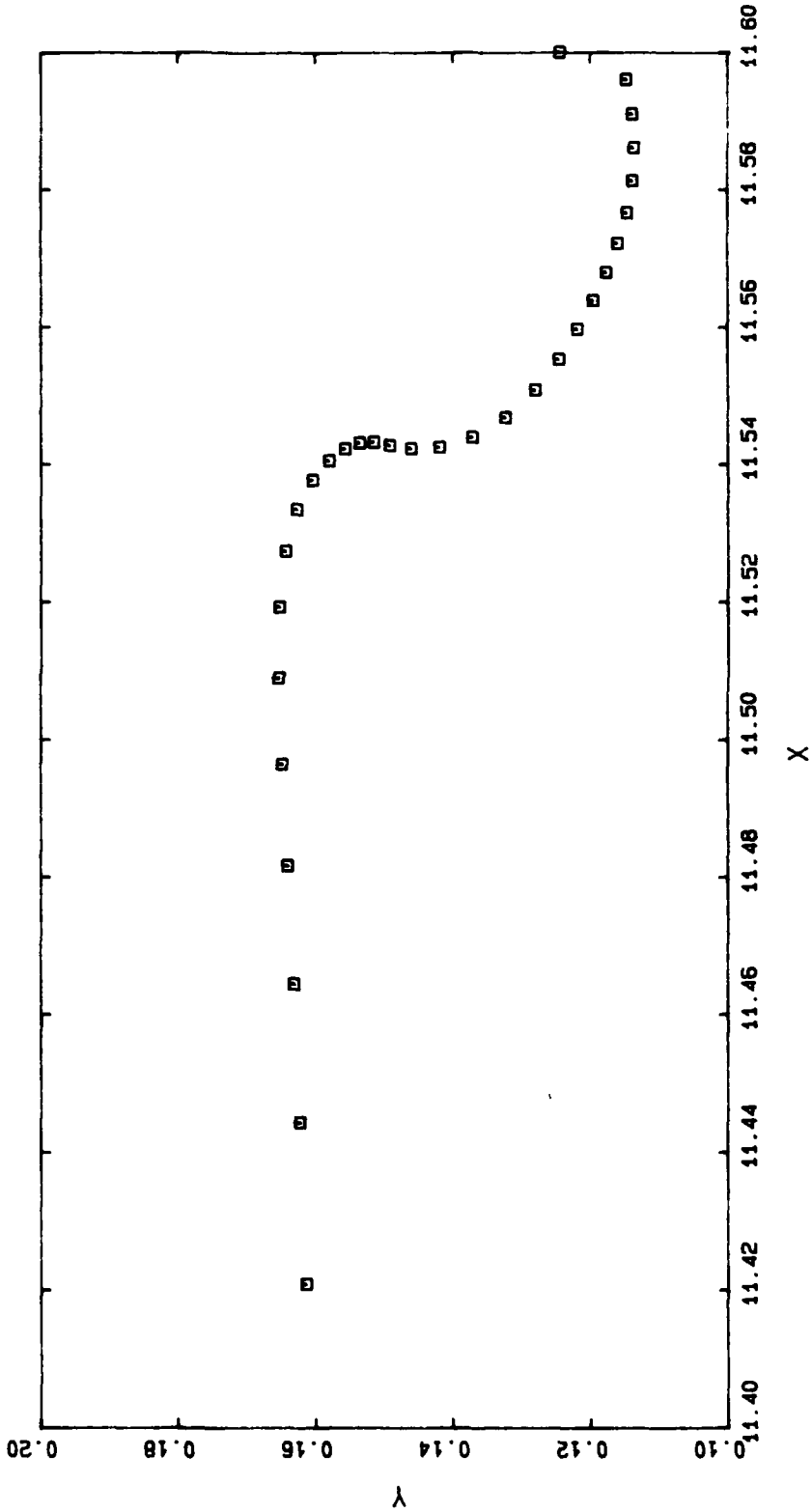

E2 3461 50.9471

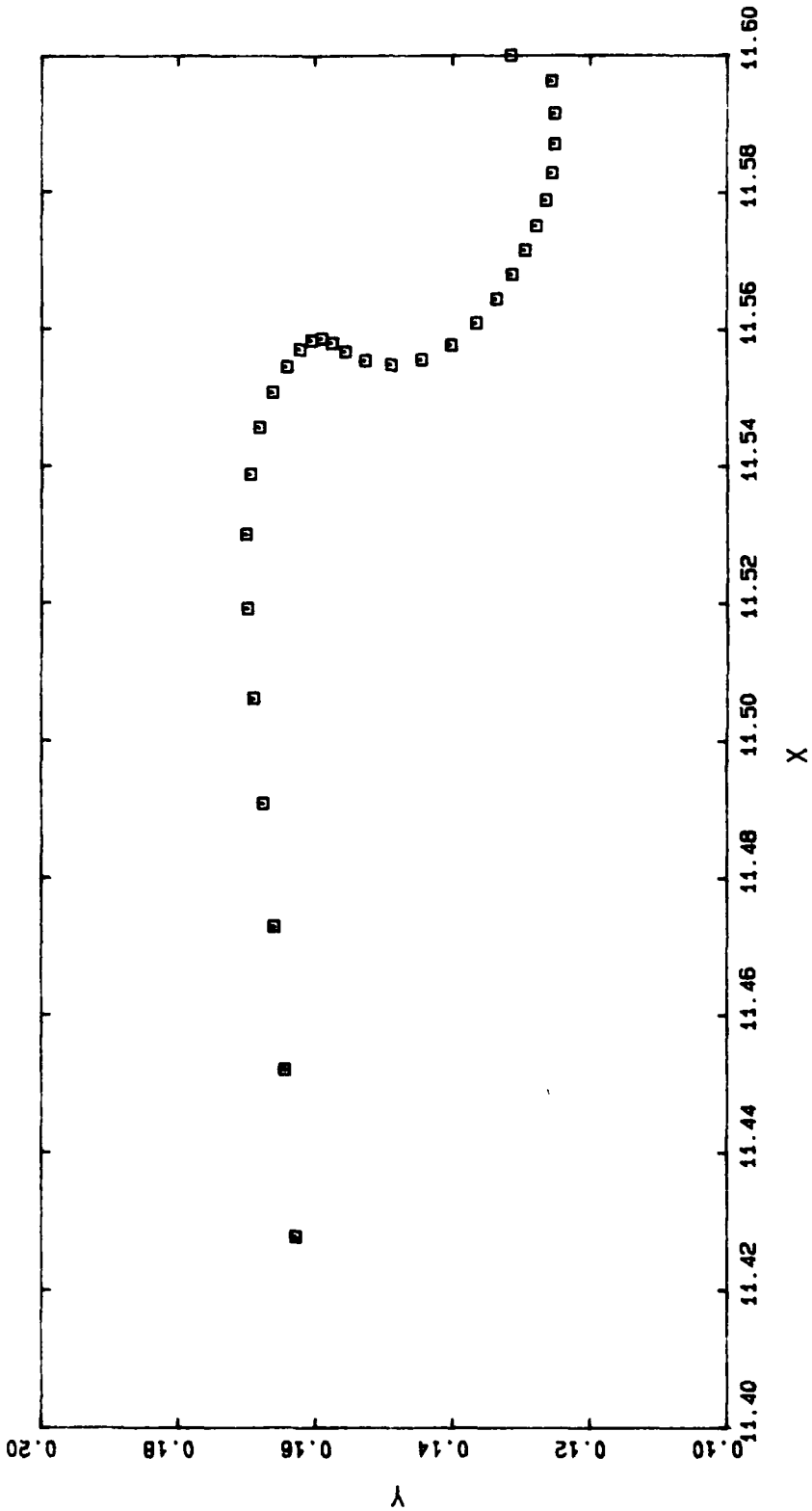

E2 3561 50.9548

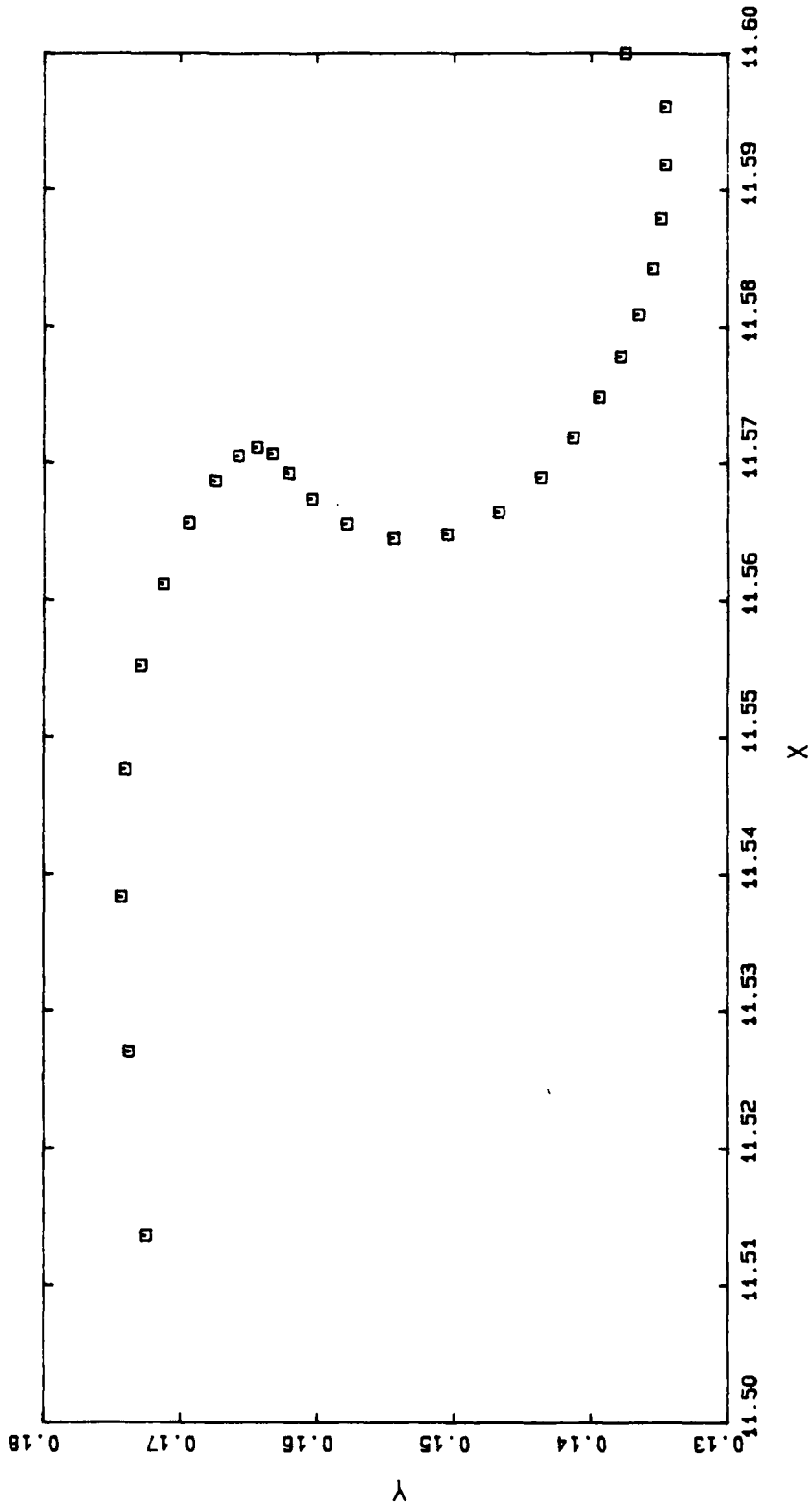

E2 3661 50.9610

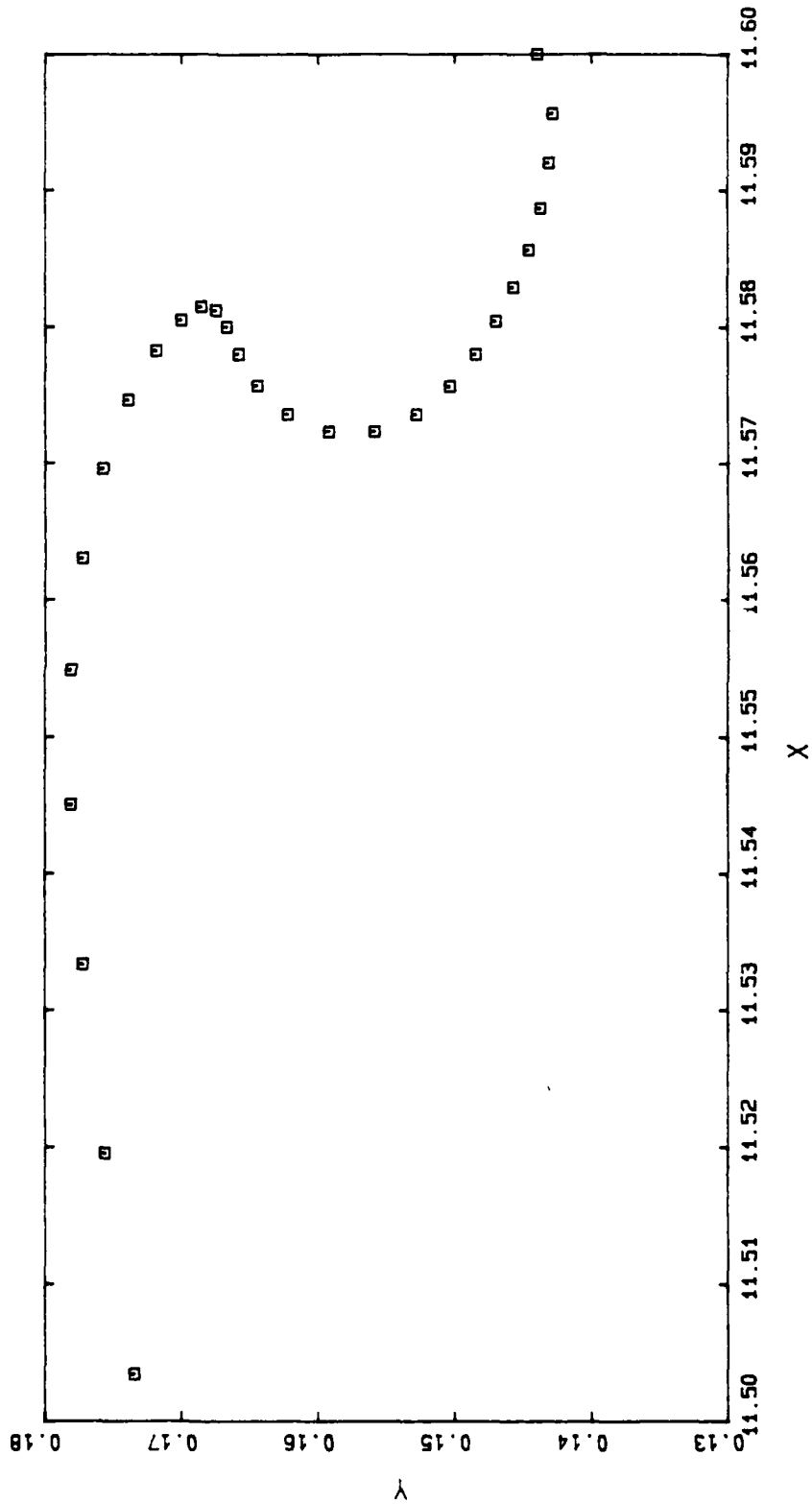

E2 3761 50.9671

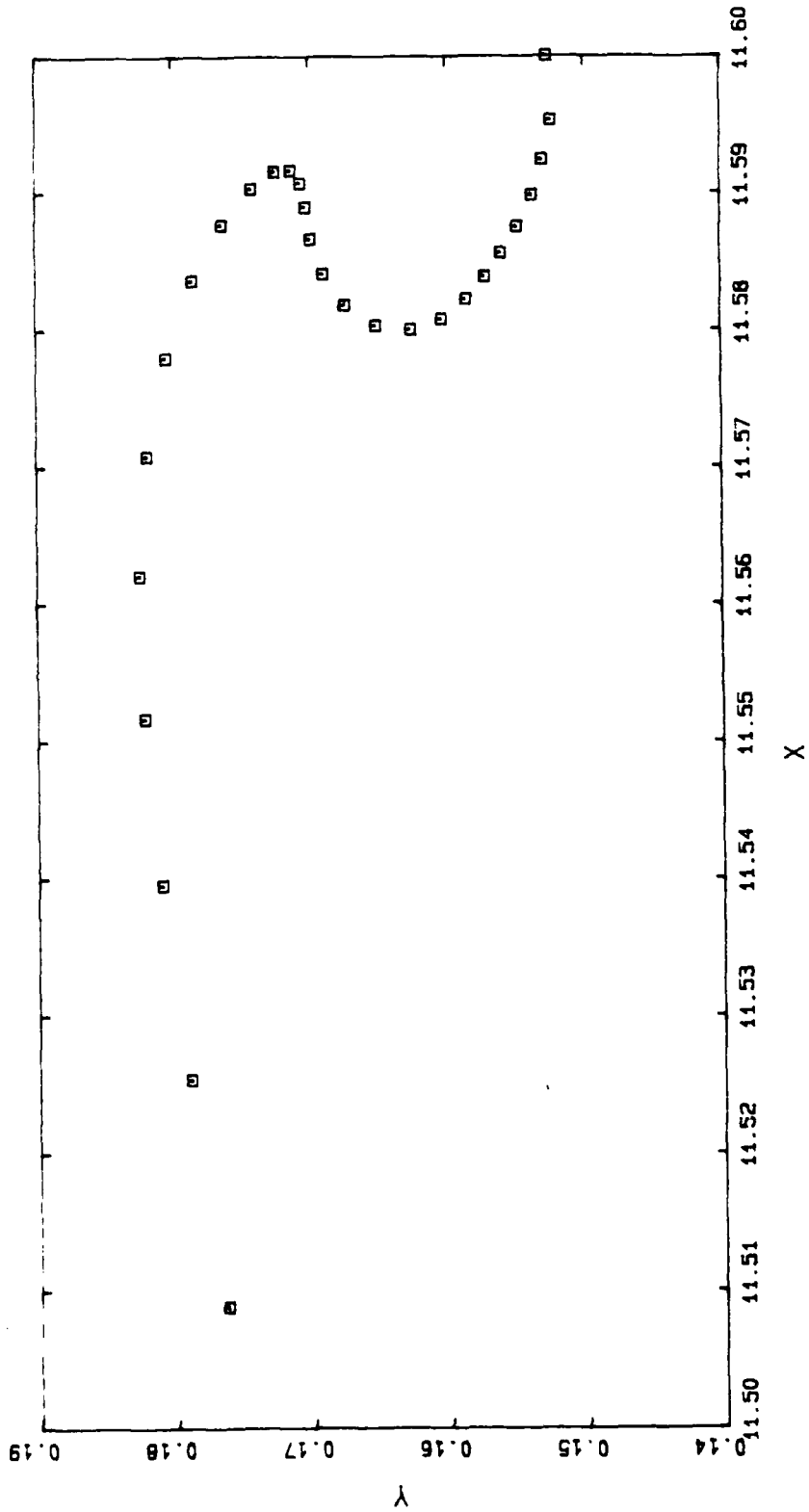

E2 3861 50.9727

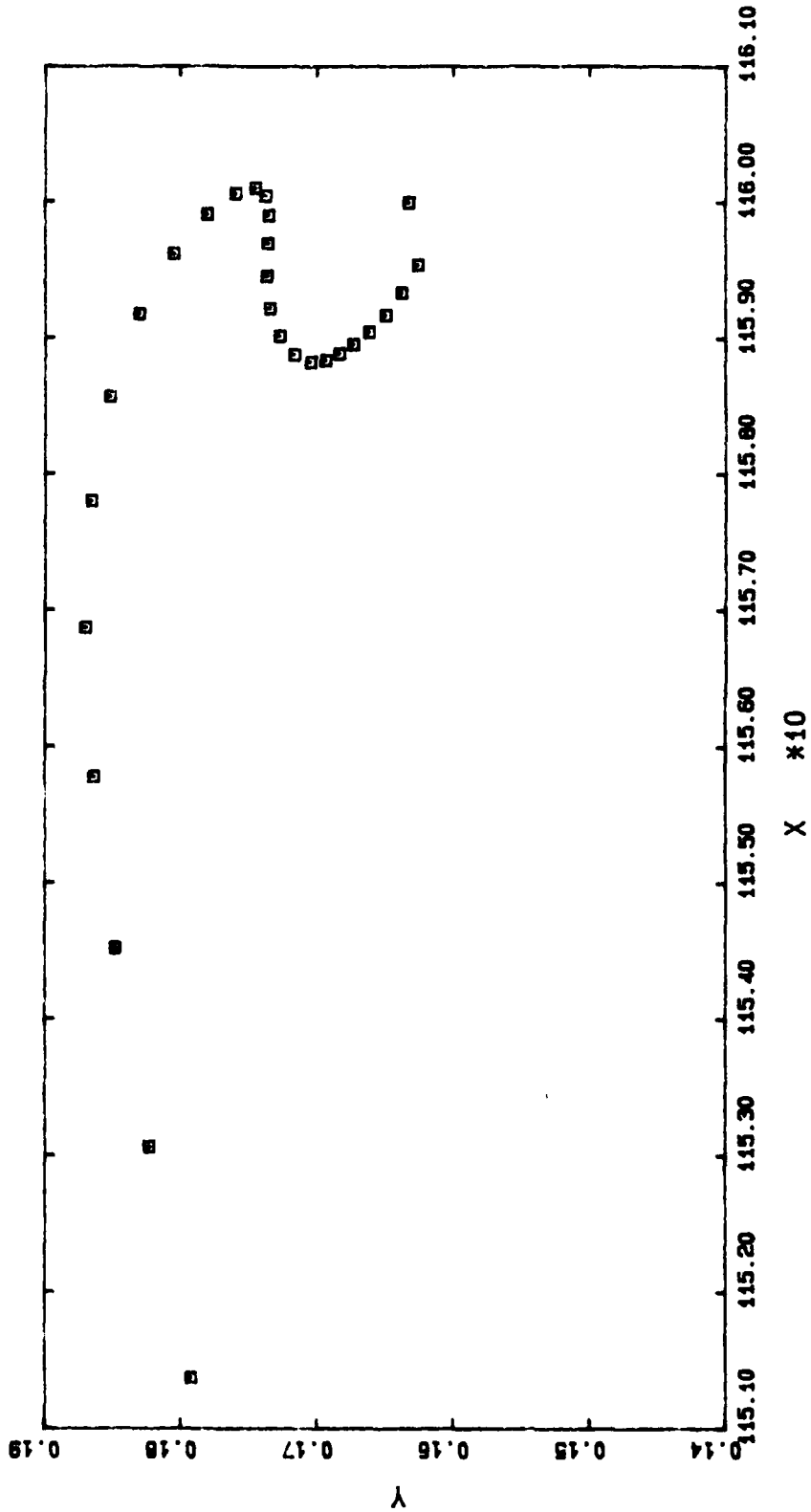

E2 3861 50.9727

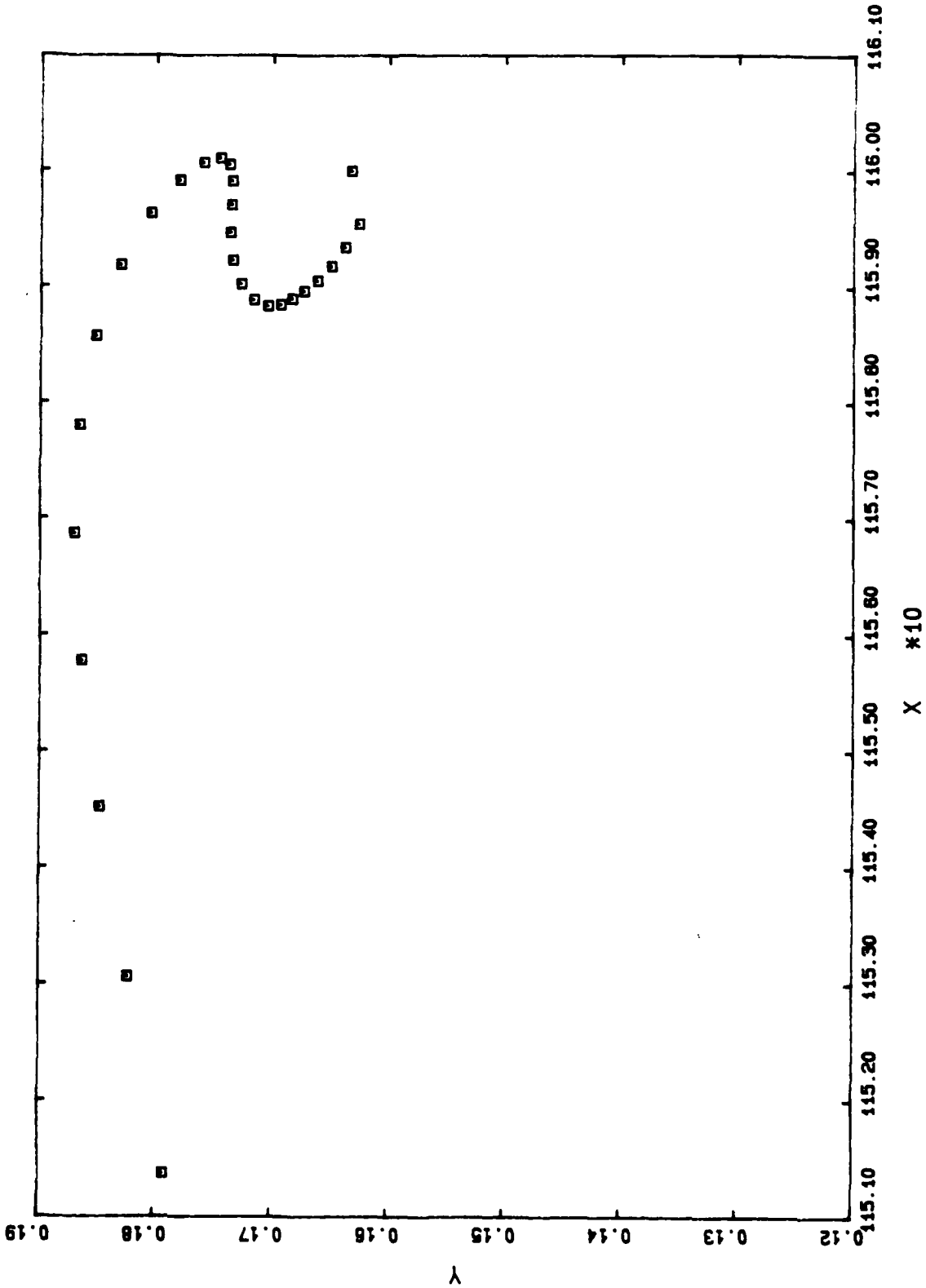

E2 3961 50.9749

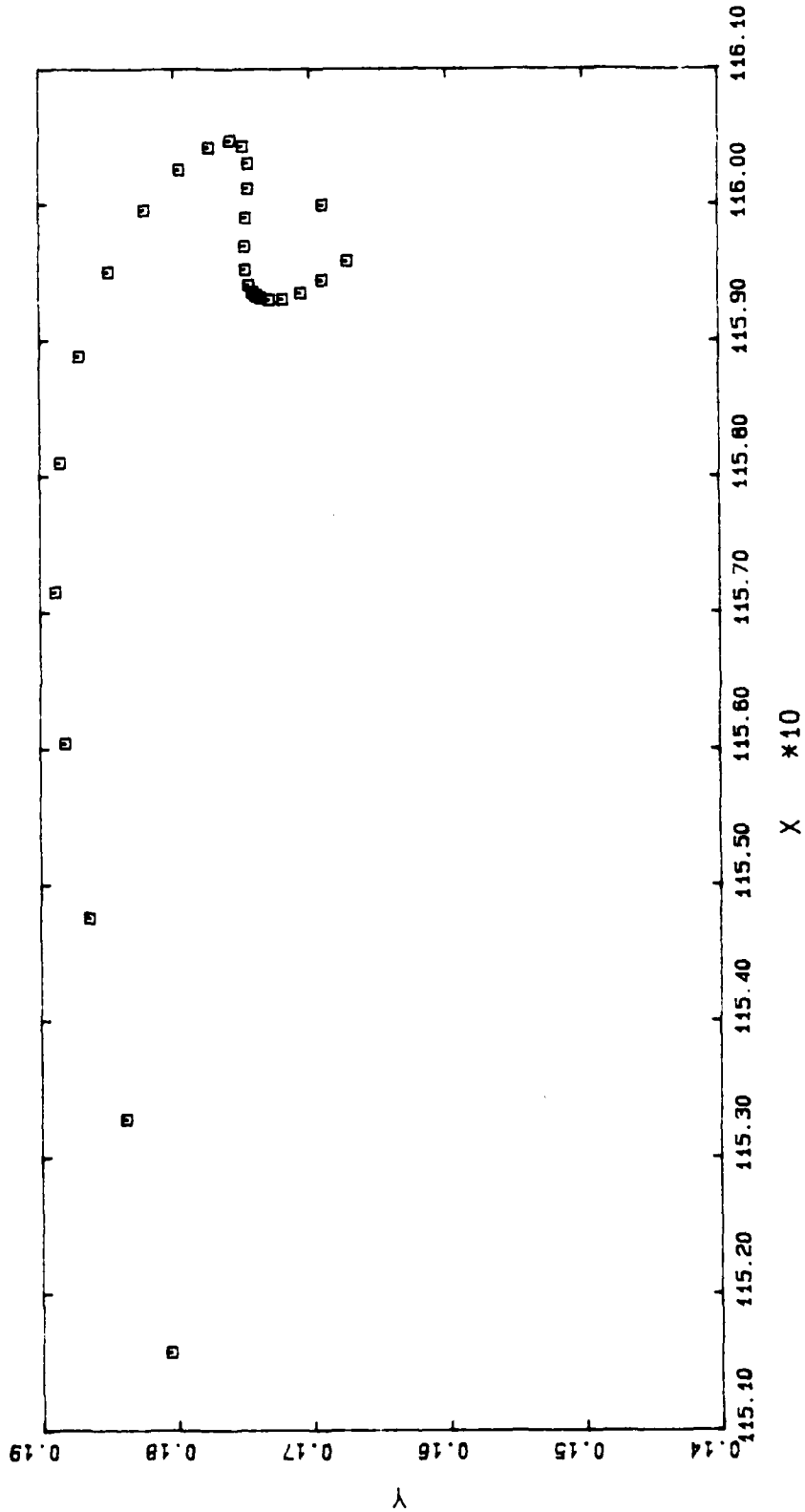

E3 3101 50.8463

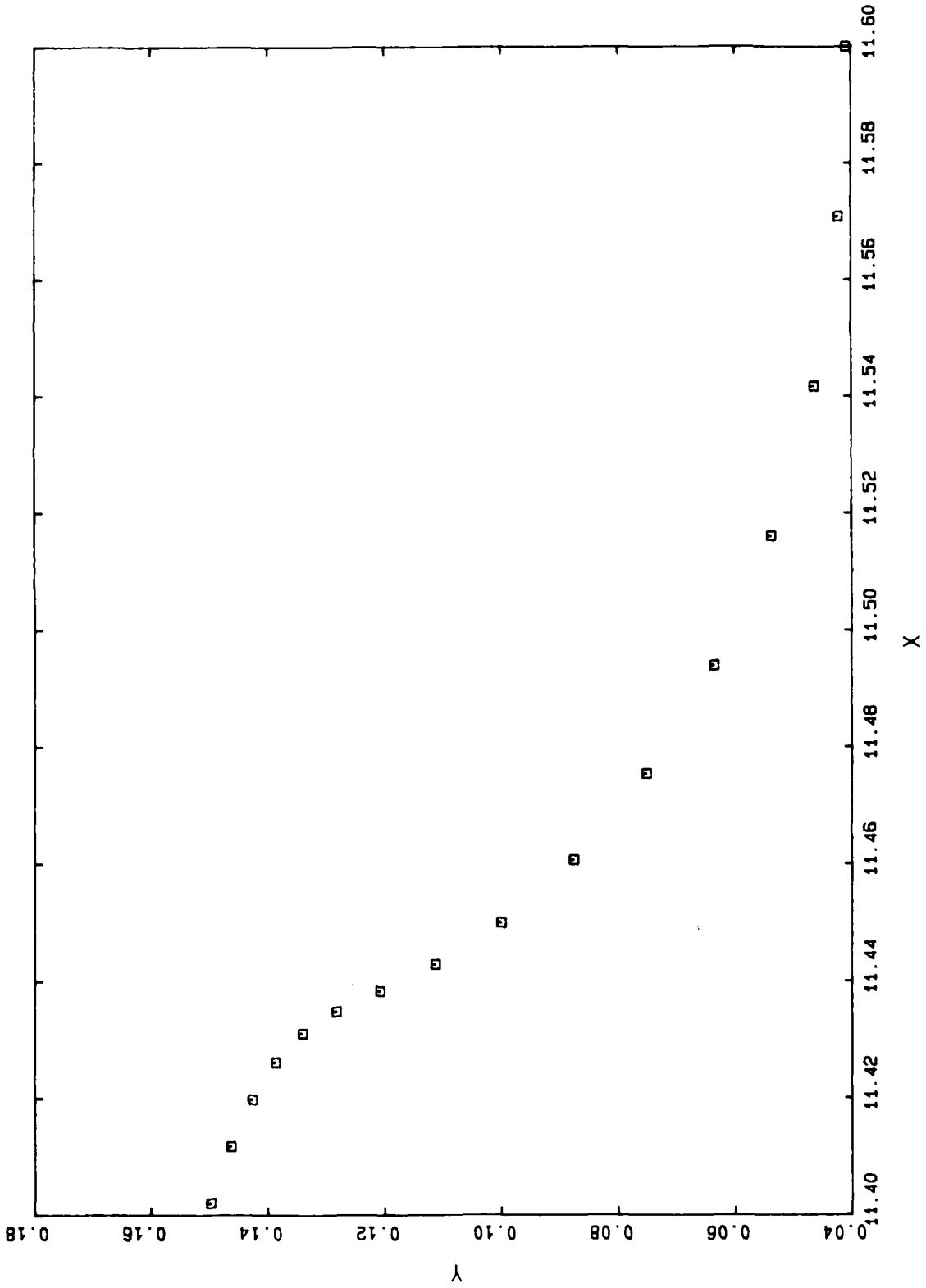

E3 3101 50.8463

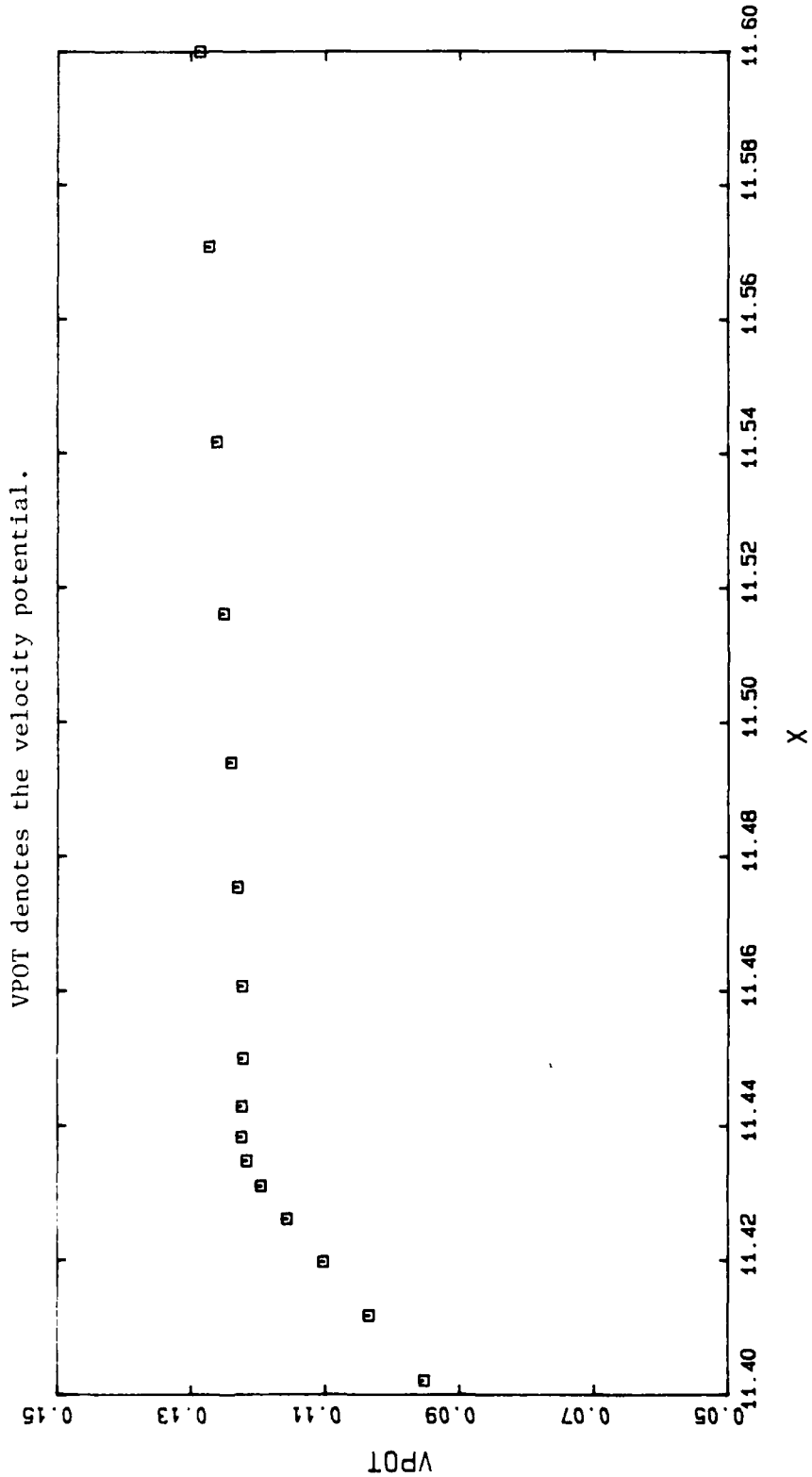

E3 3104 50.8484

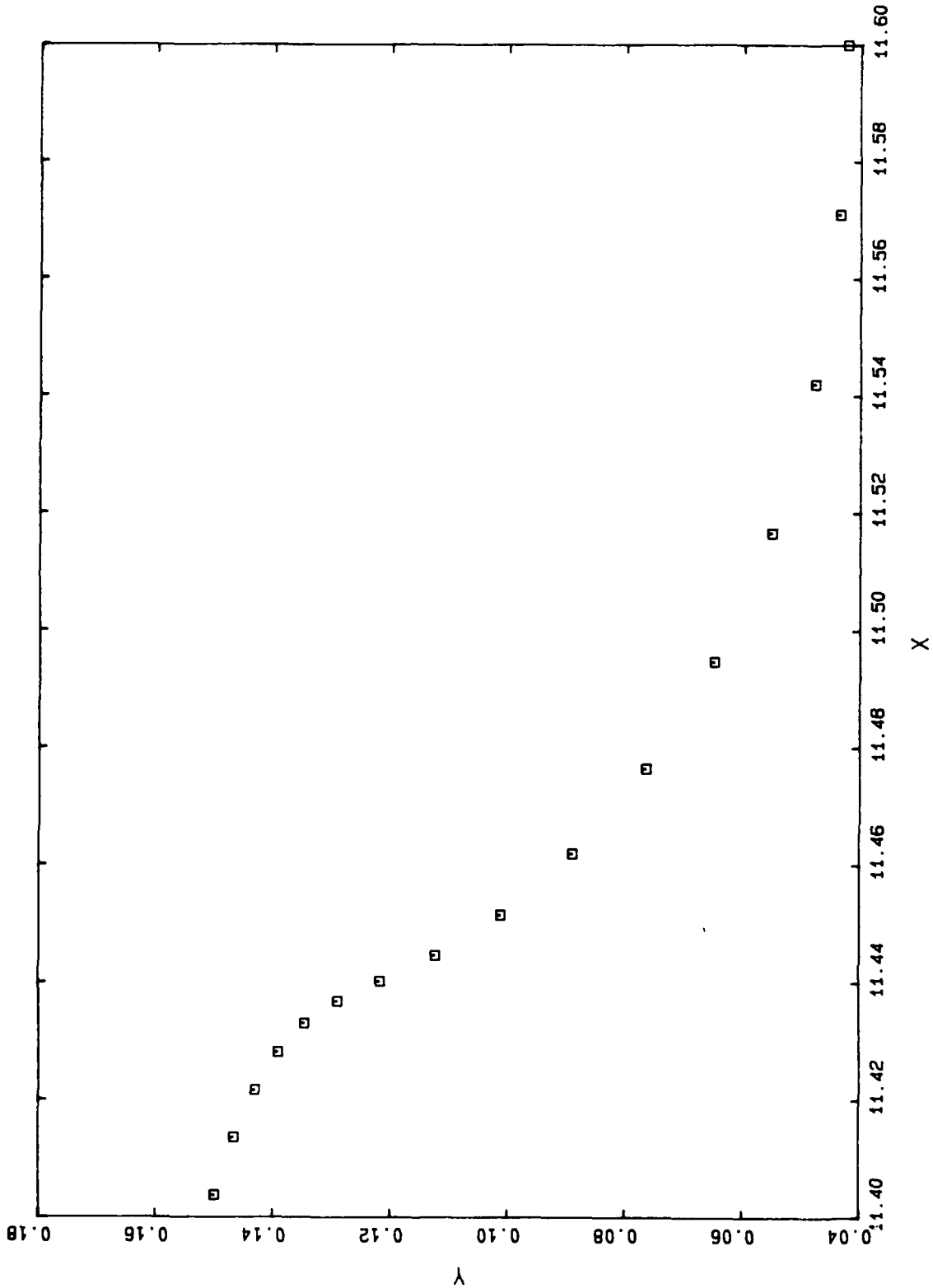

E3 3104 50.8484

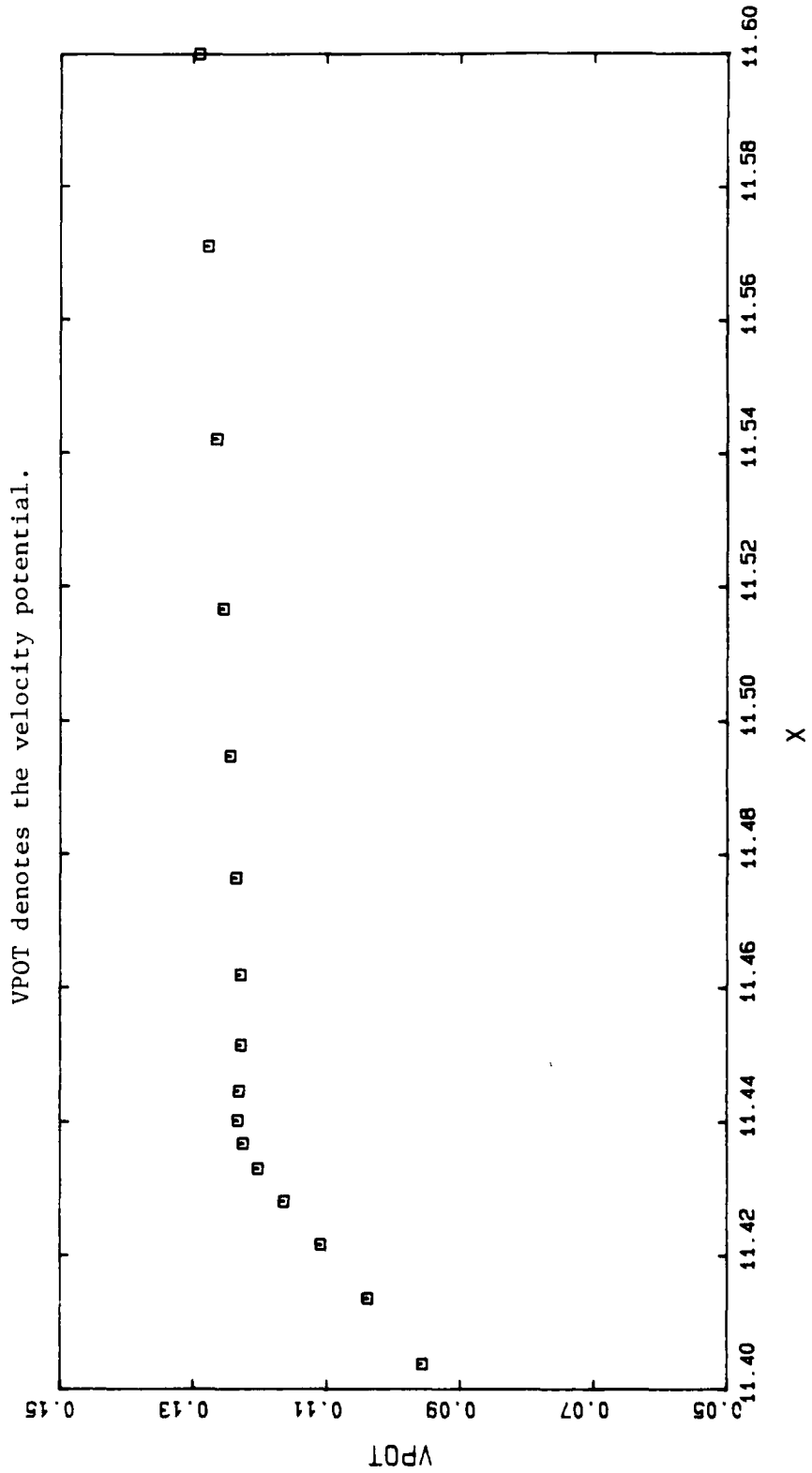

E3 3105 50.8490

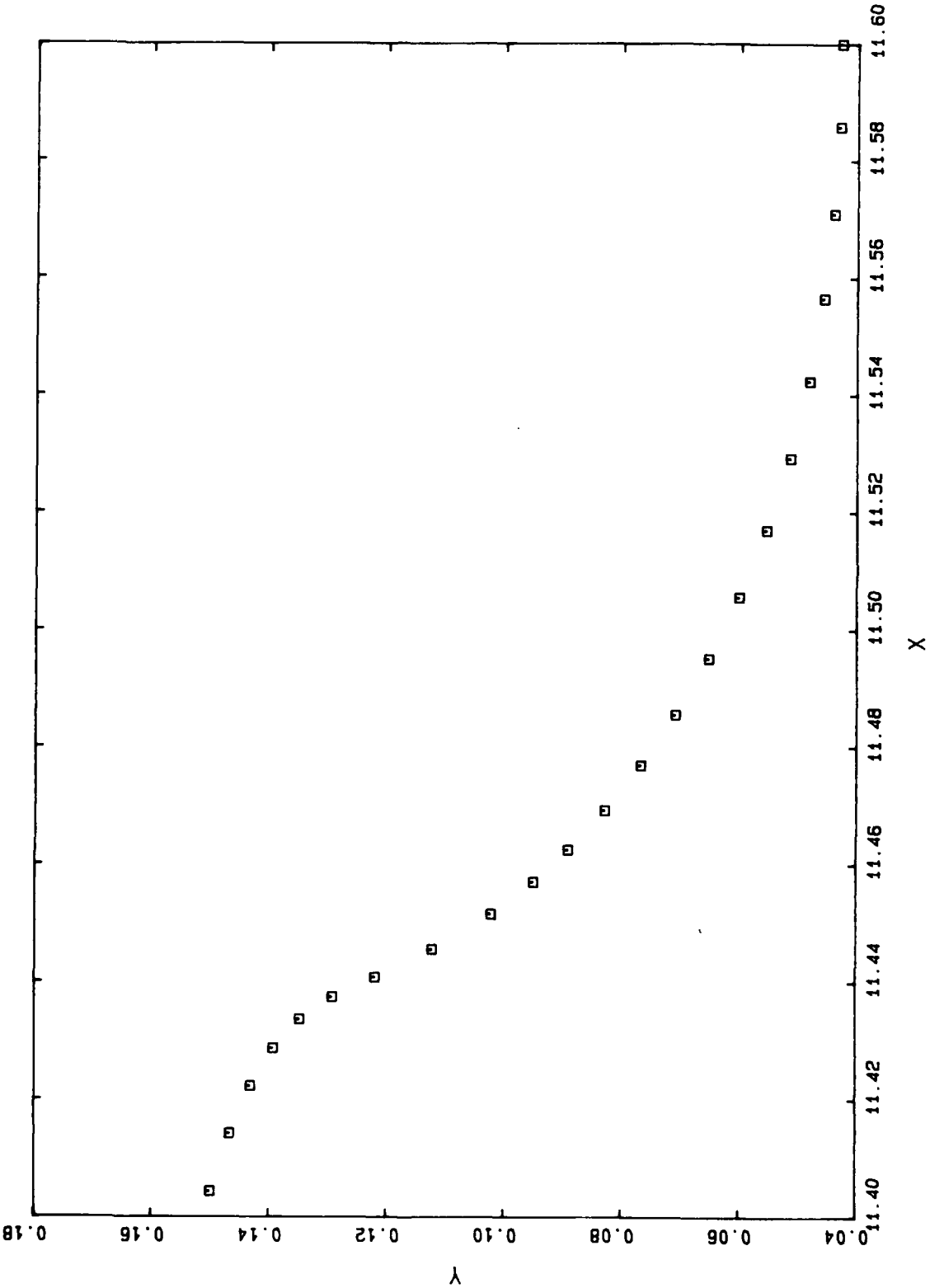

E3 3105 50.8490

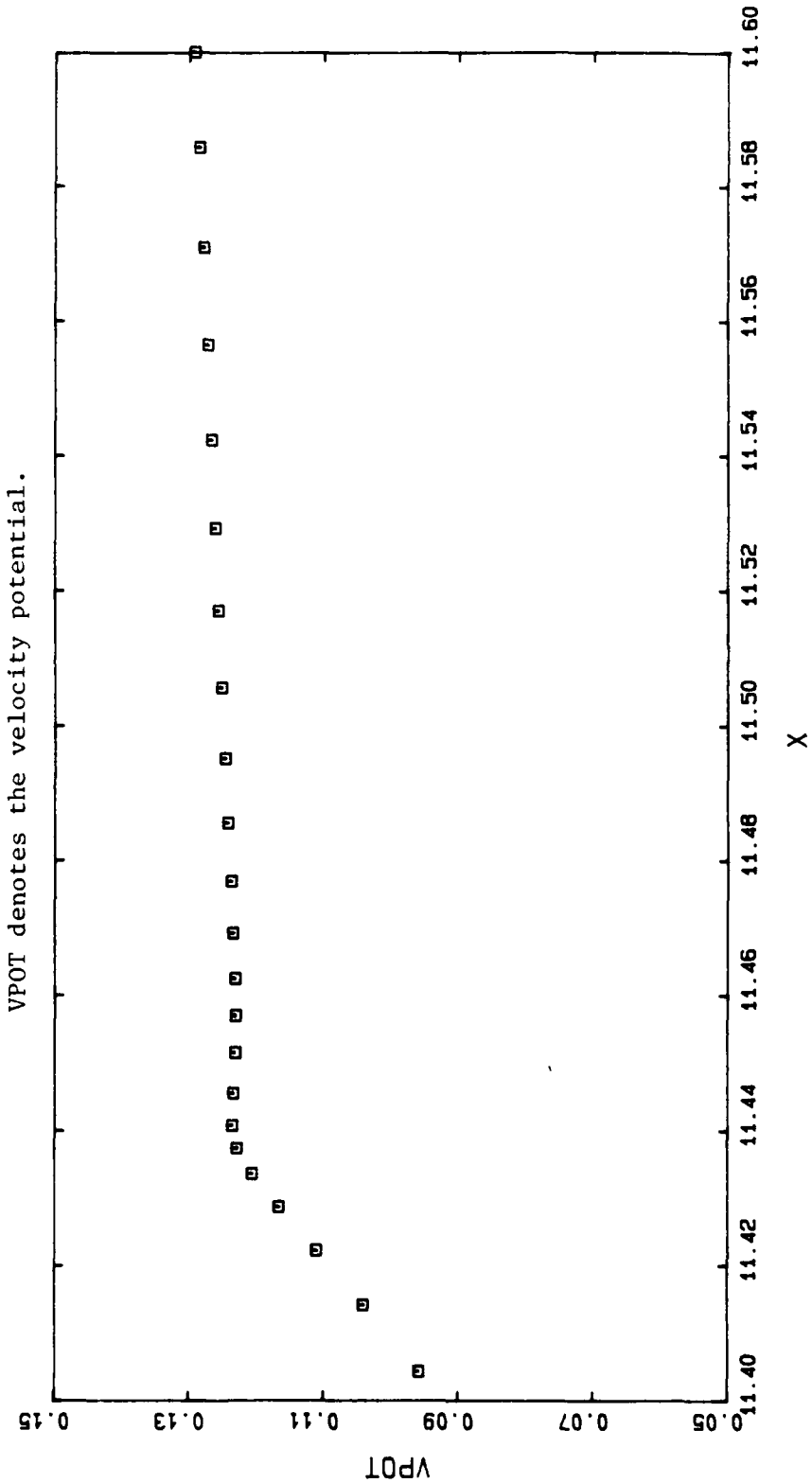

E3 3109 50.8516

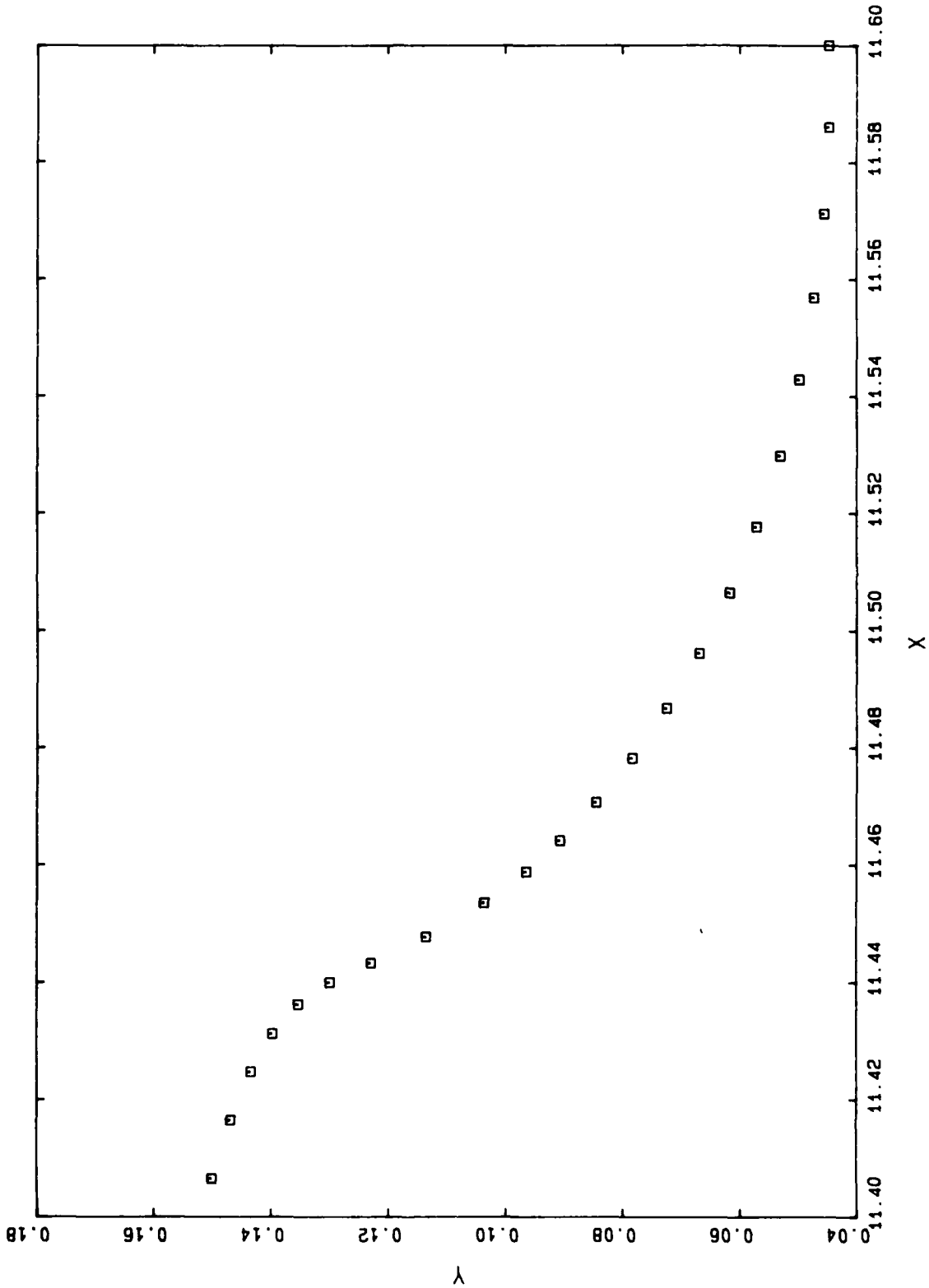

E3 3109 50.8516

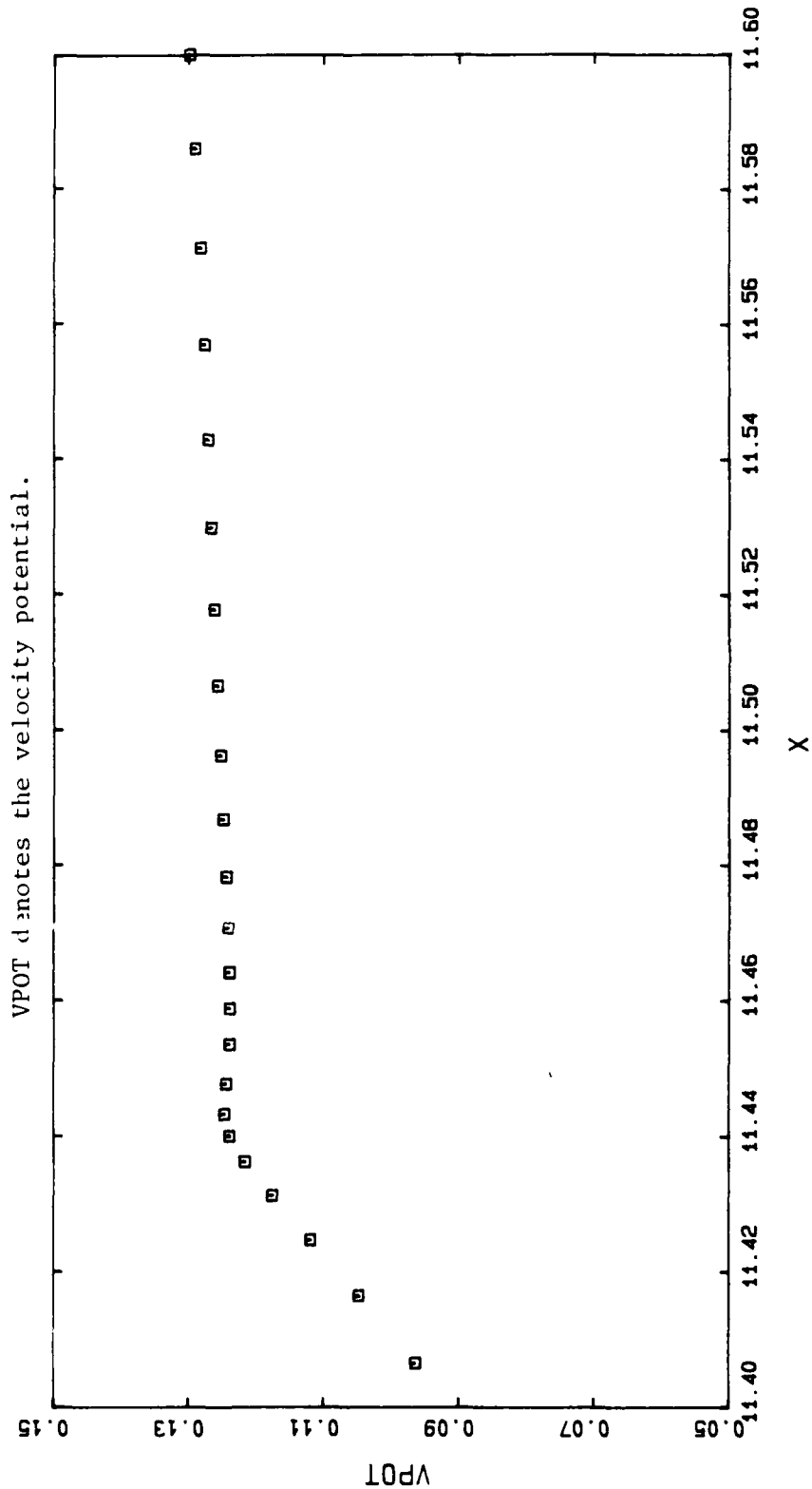

VPOT denotes the velocity potential.

E3 3110 50.8523

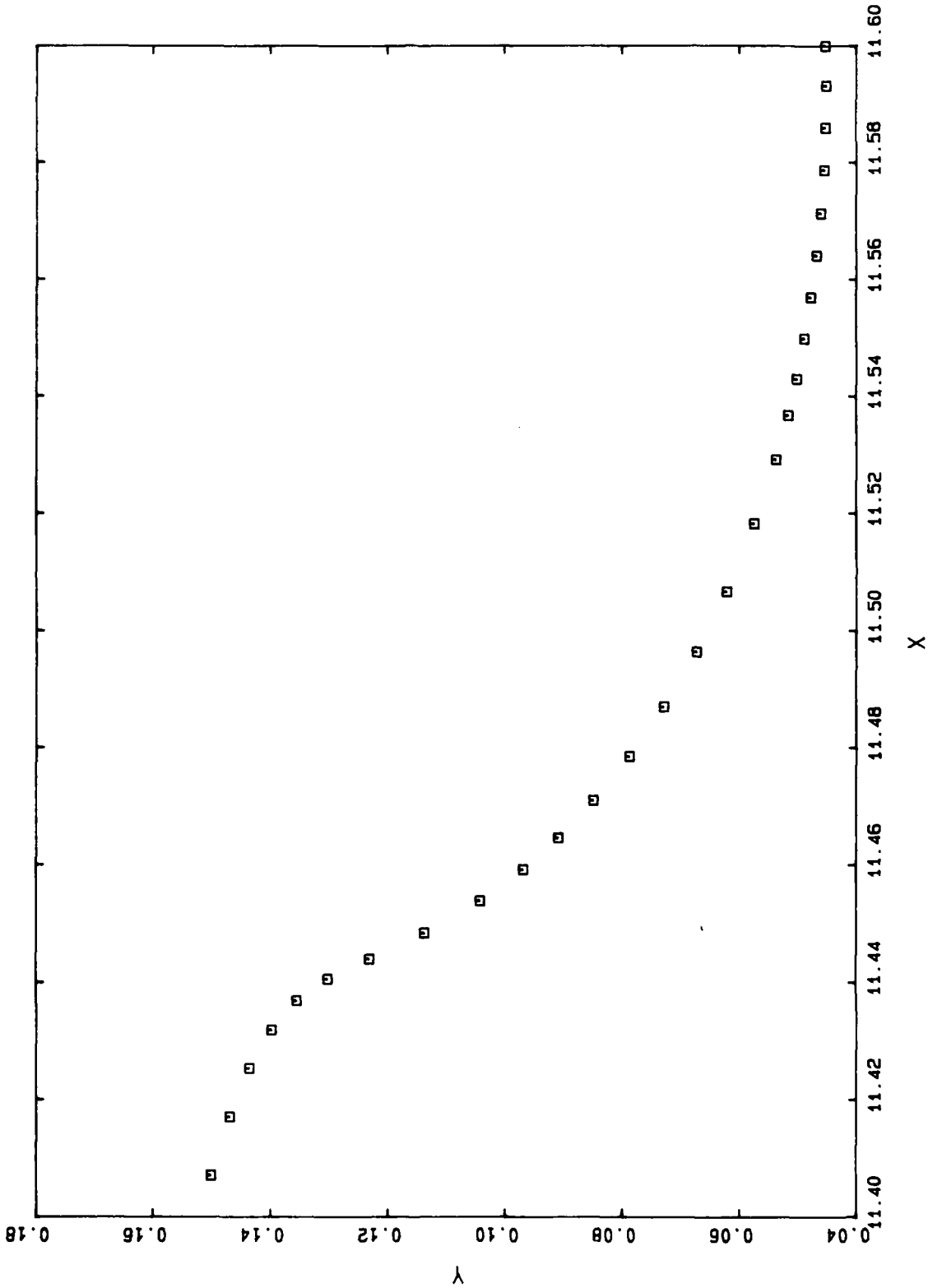

E3 3110 50.8523

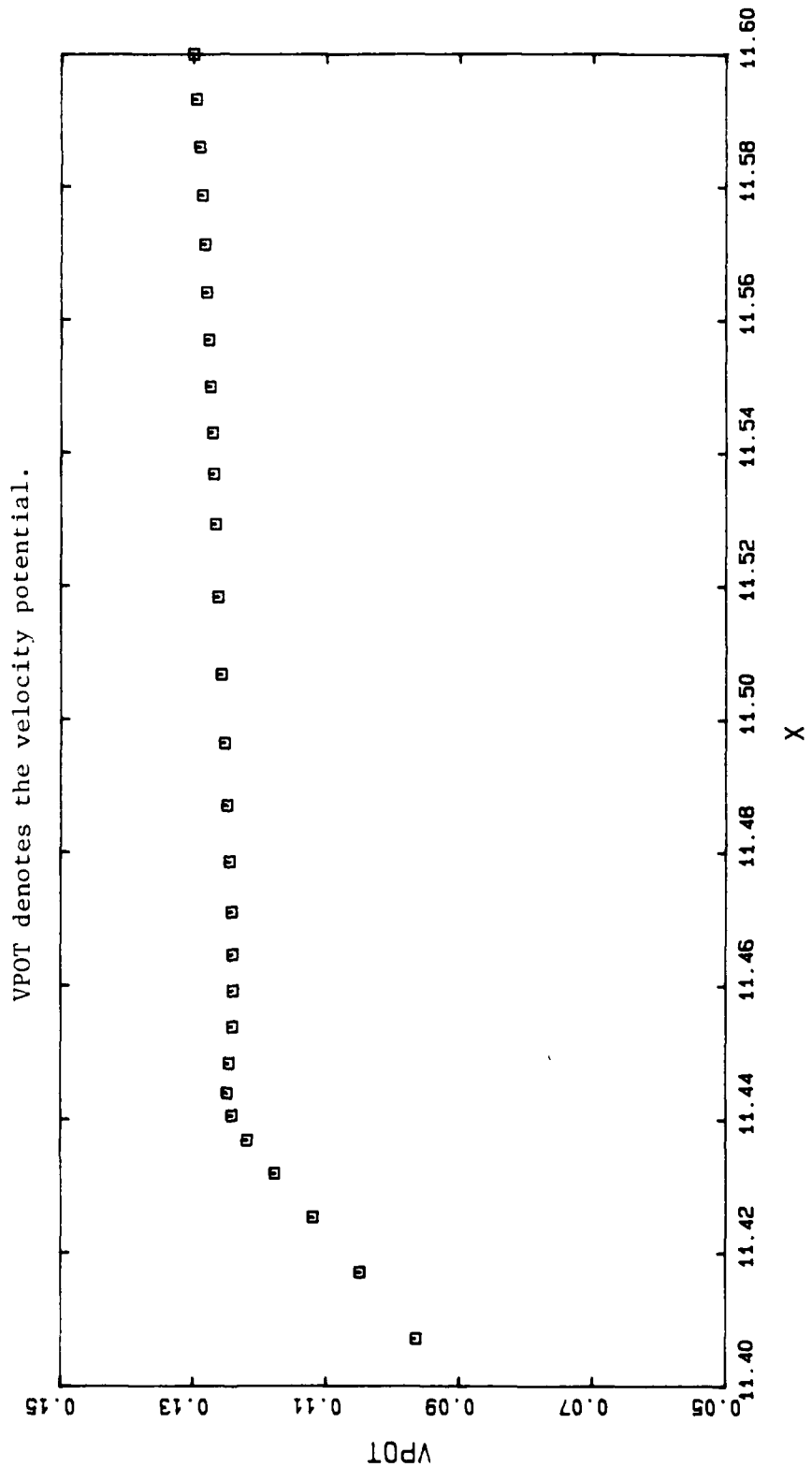

VPOT denotes the velocity potential.

E3 3150 50.8741

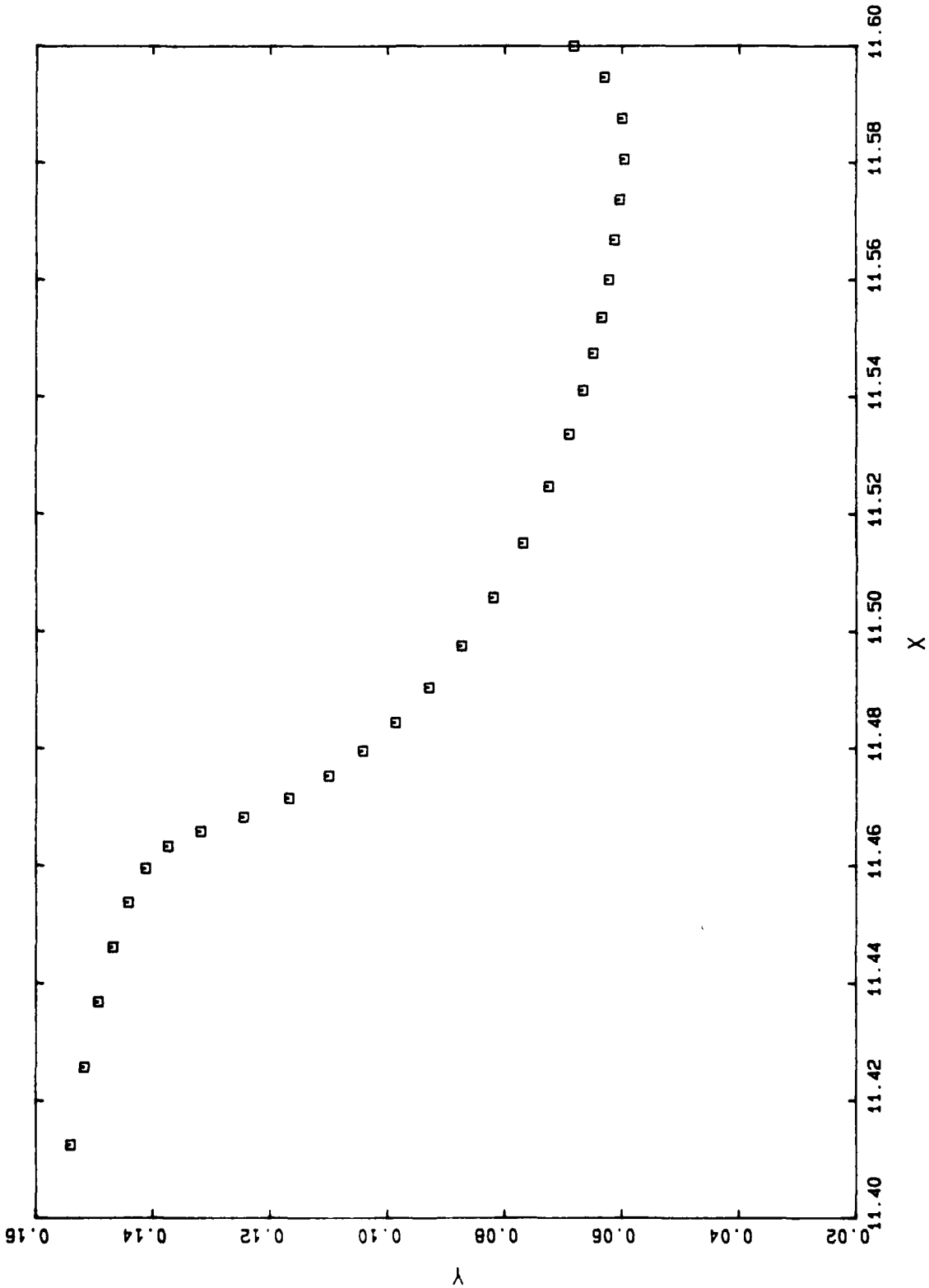

E3 3150 50.8741

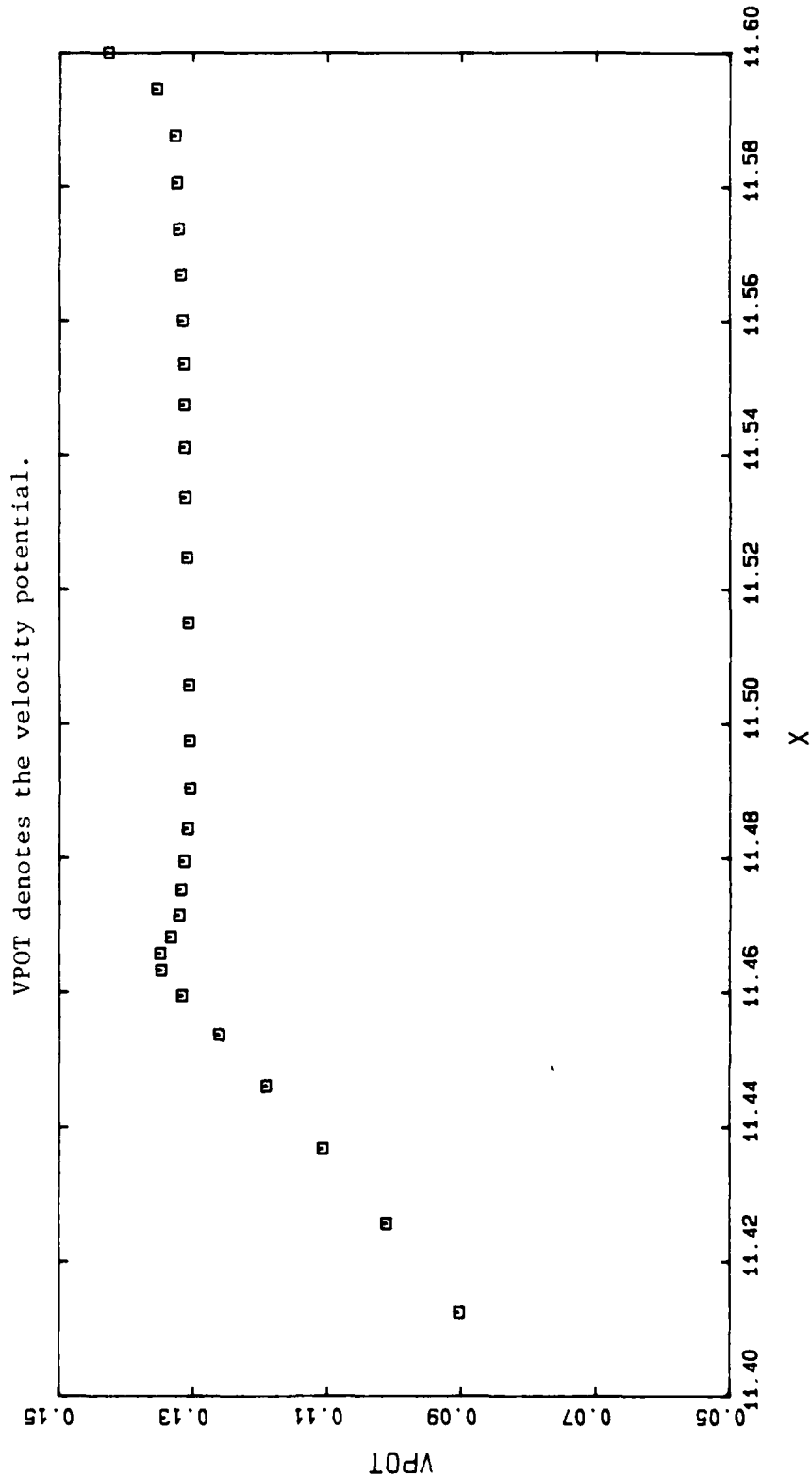

VPOT denotes the velocity potential.

E3 3170 50.8826

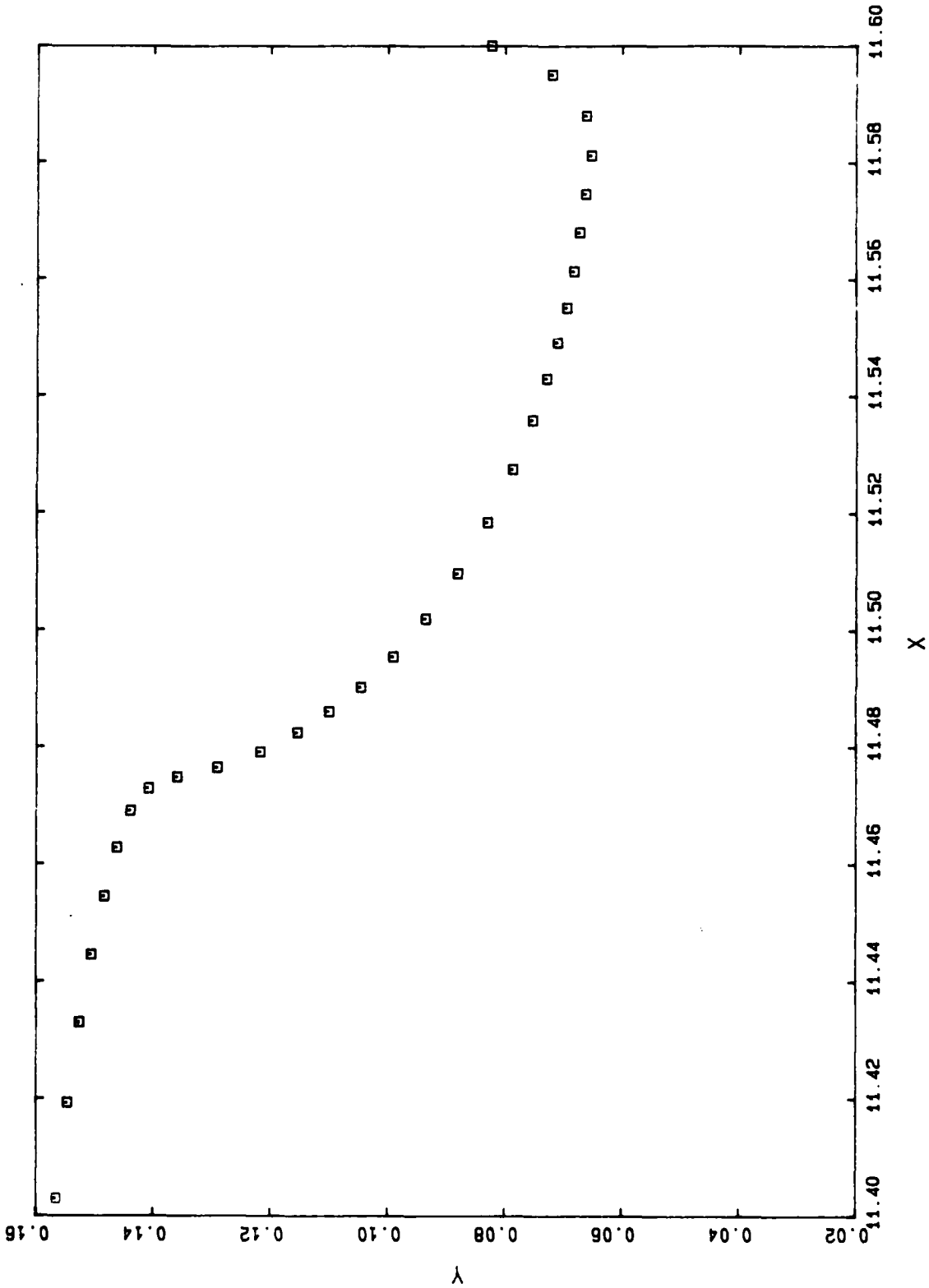

E3 3170 50.8826

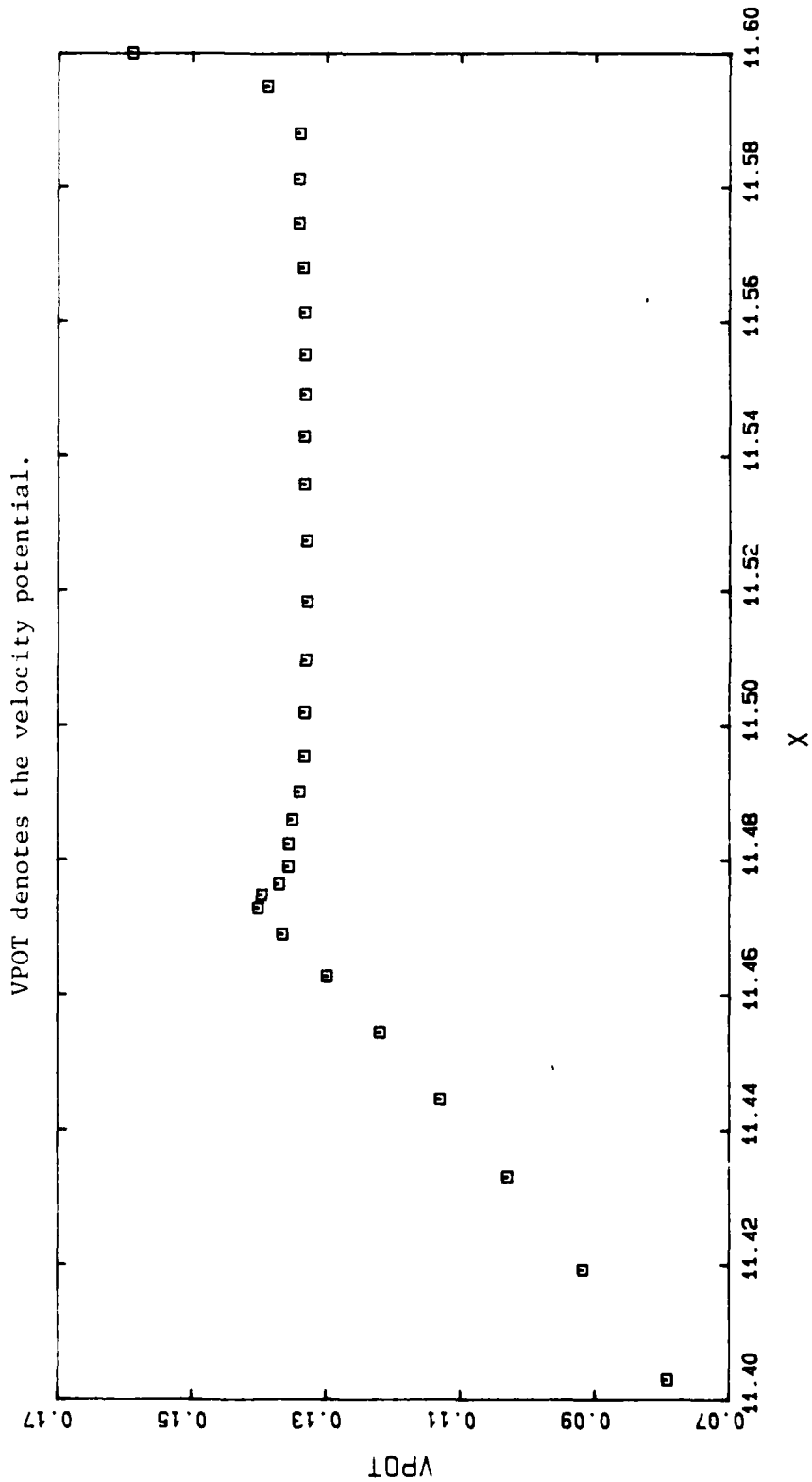

E3 3190 50.8895

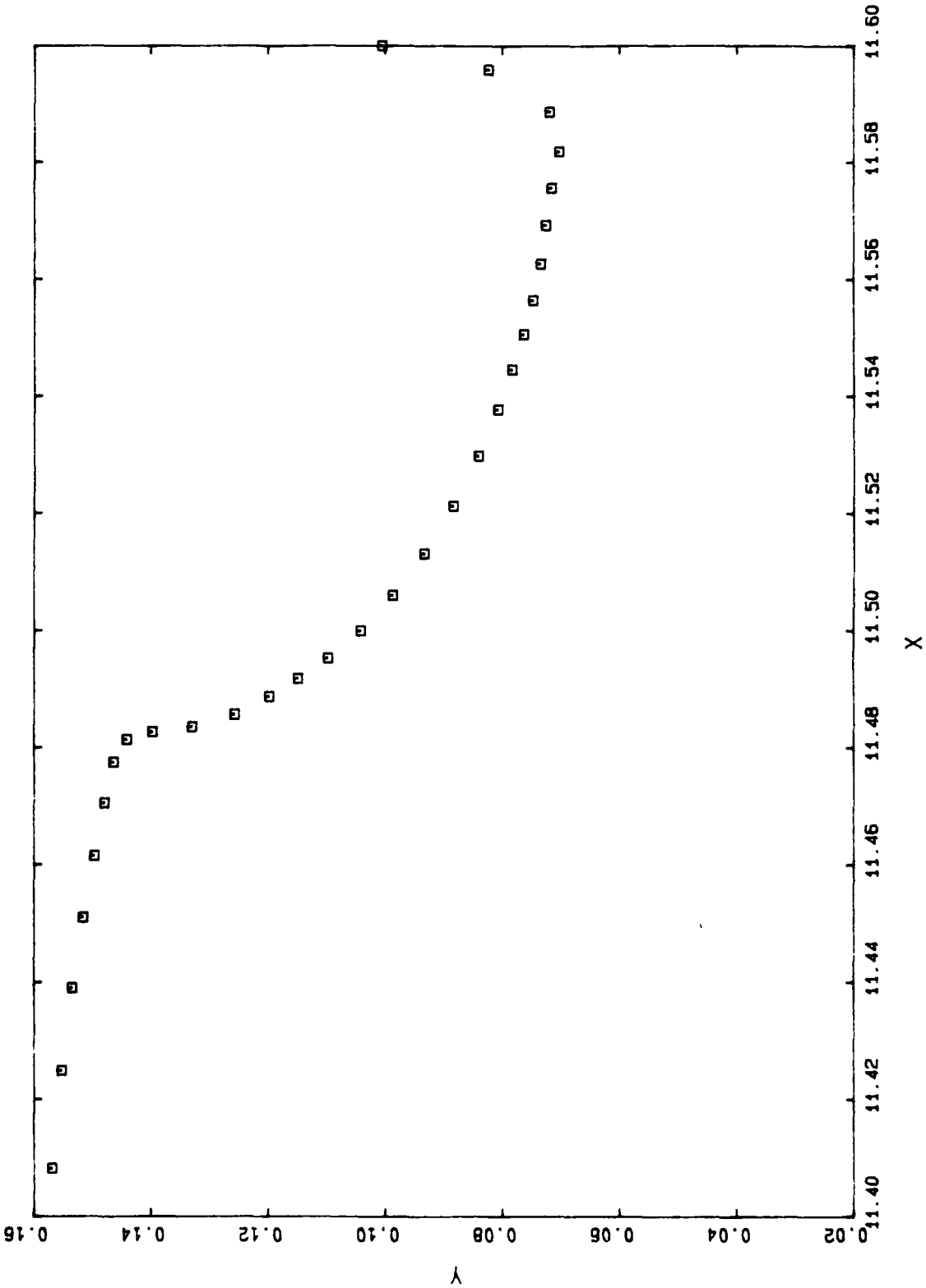

E3 3190 50.8895

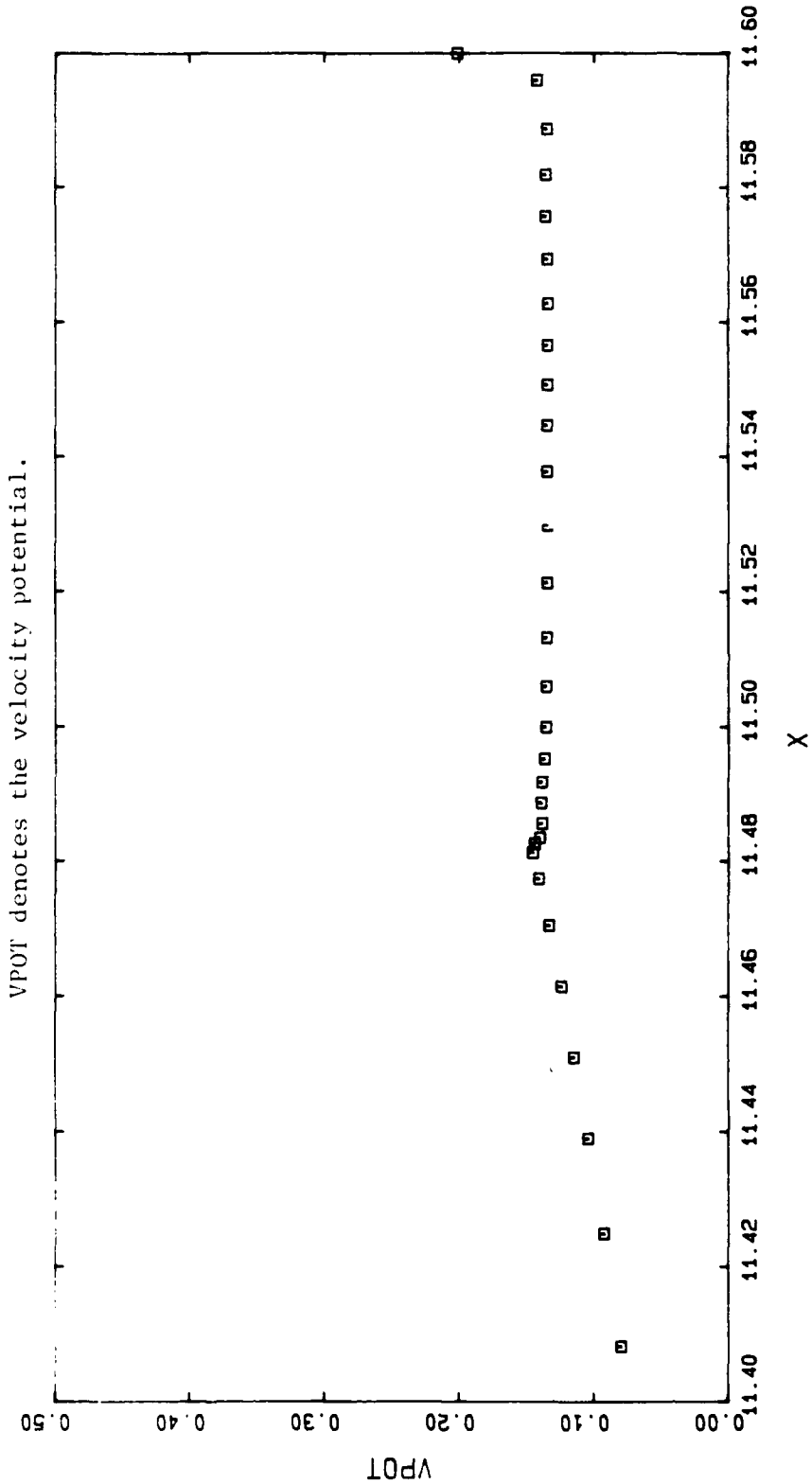

VPOT denotes the velocity potential.

E3 3210 50.8950

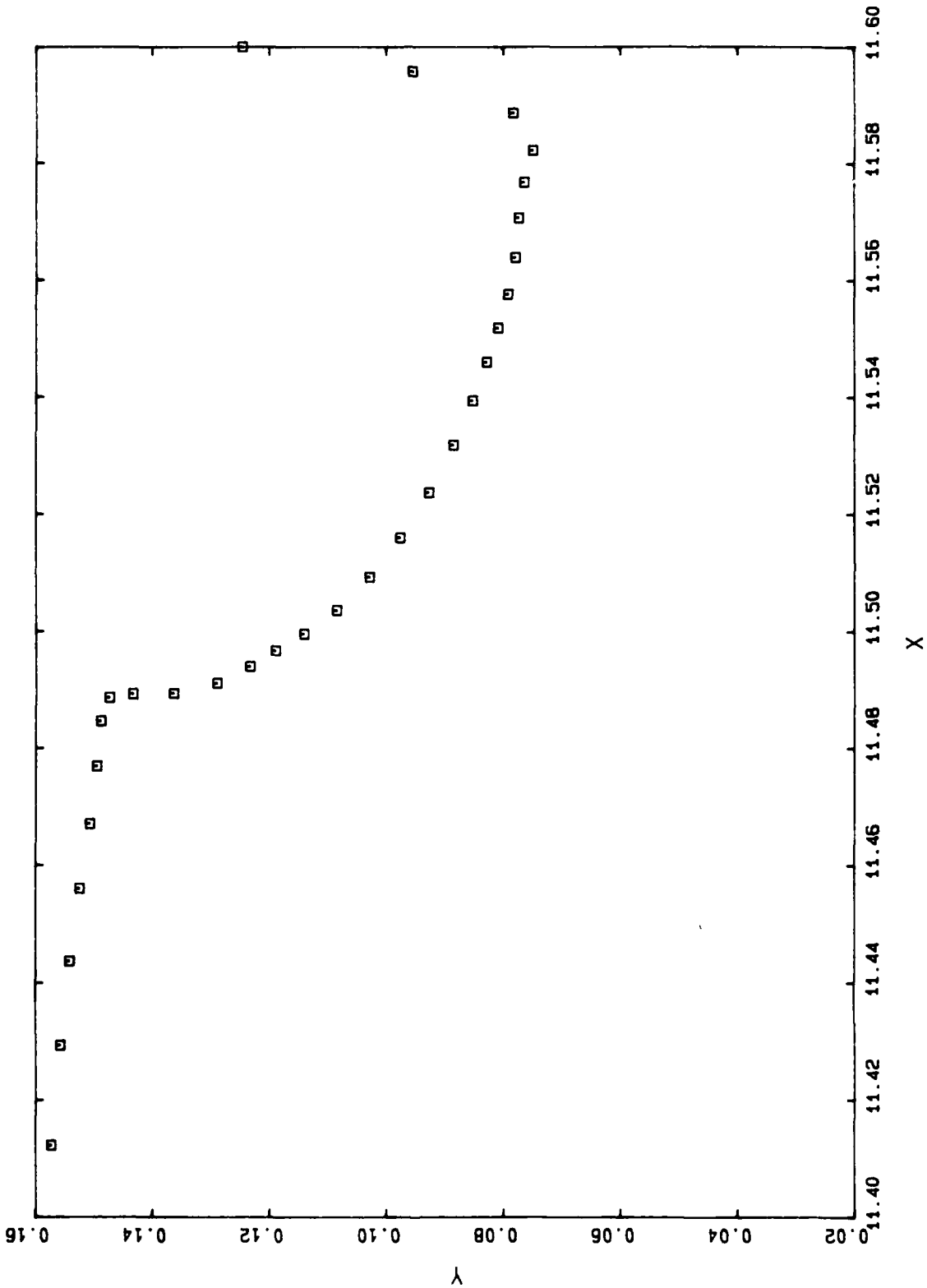

E3 3210 50.8950

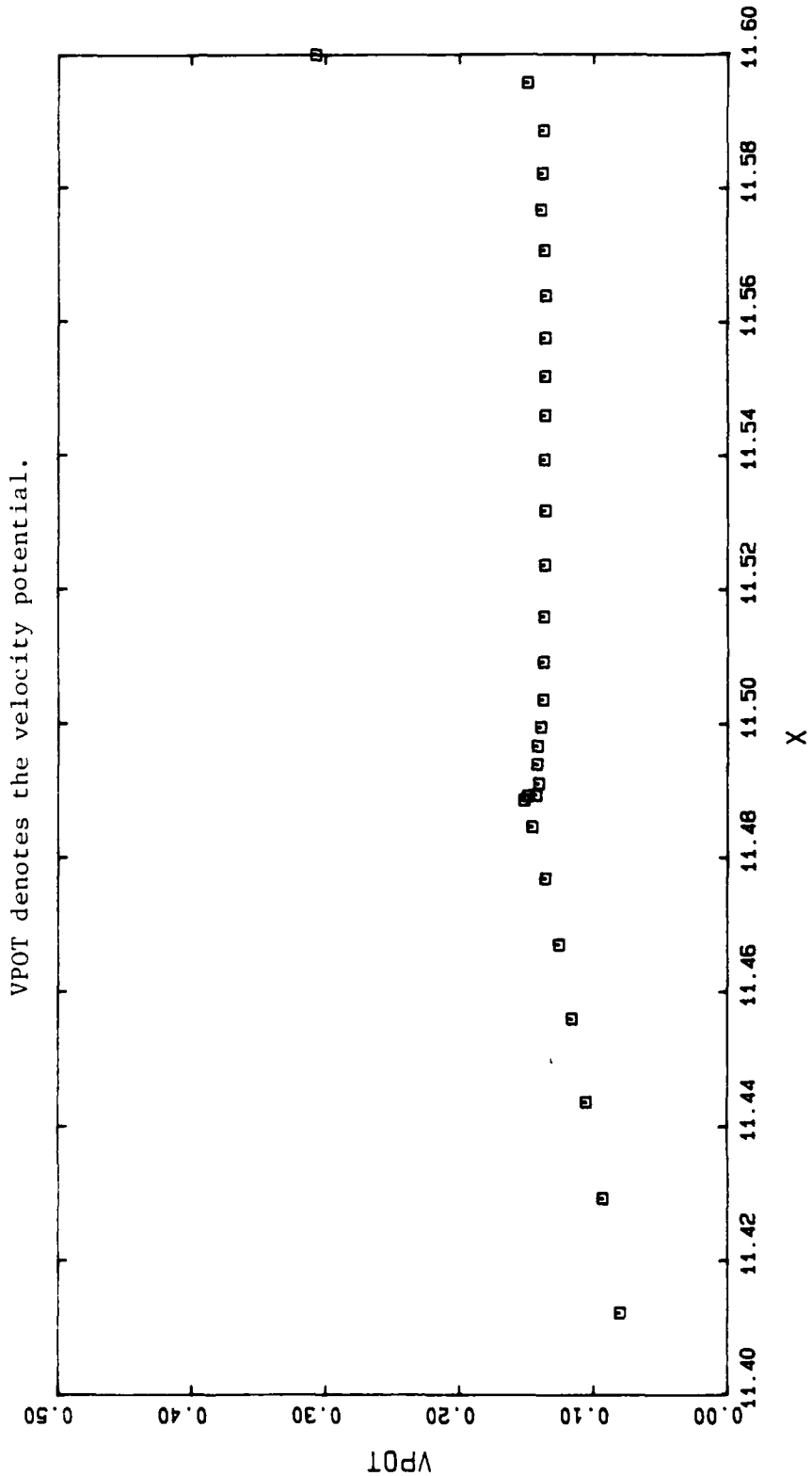

E3 3230 50.8988

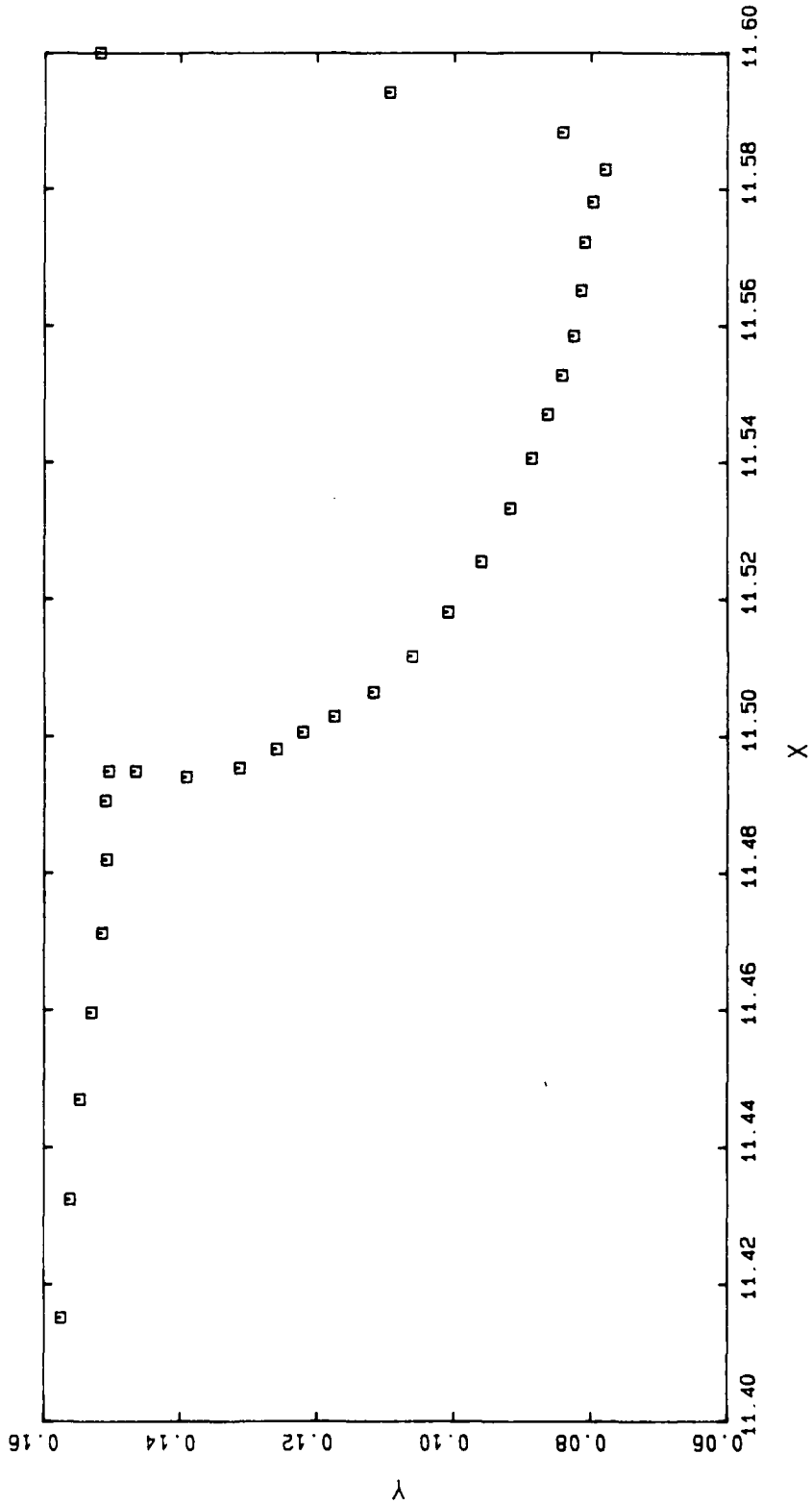

E3 3230 50.8988

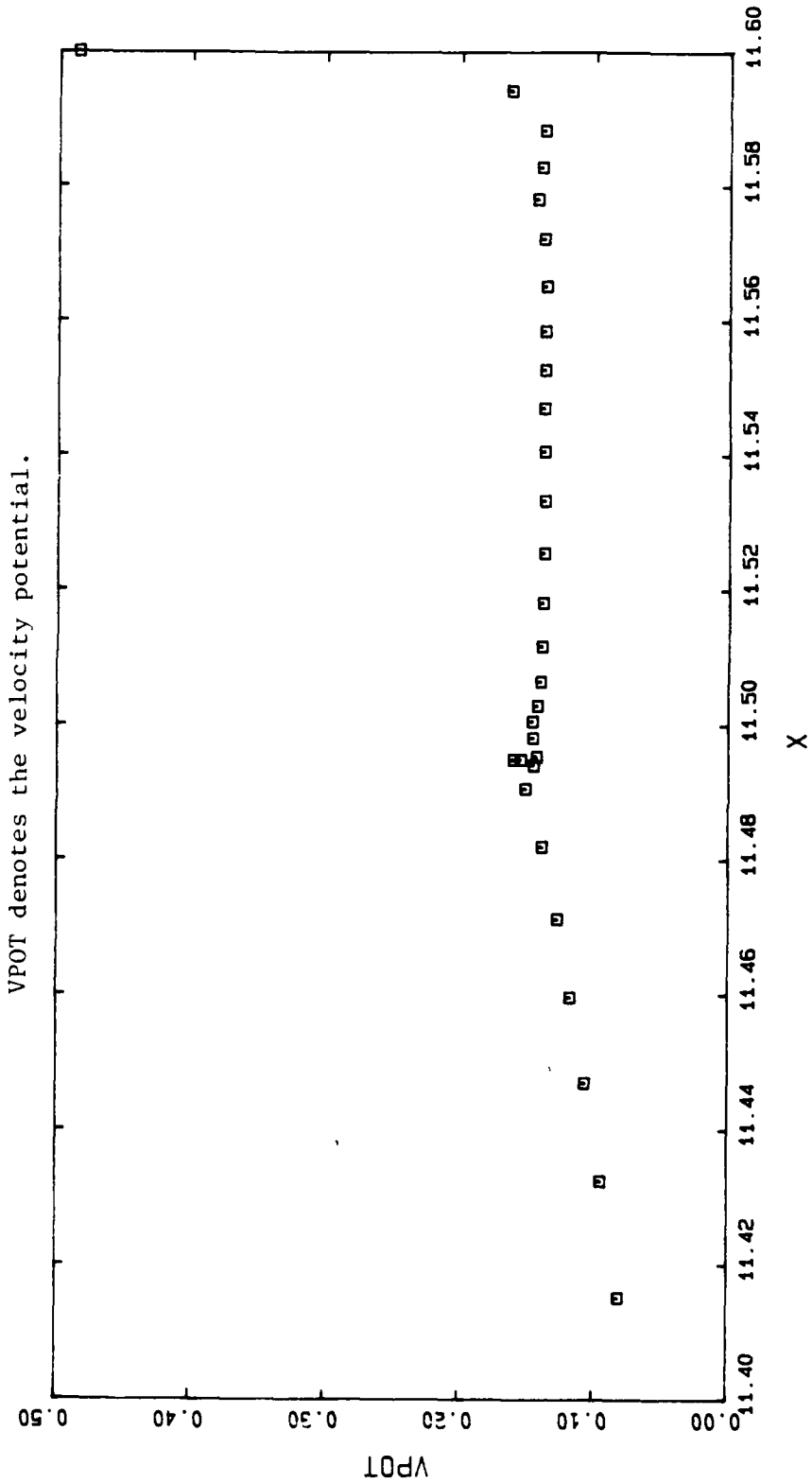

VPOT denotes the velocity potential.

E4 3183 50.8905

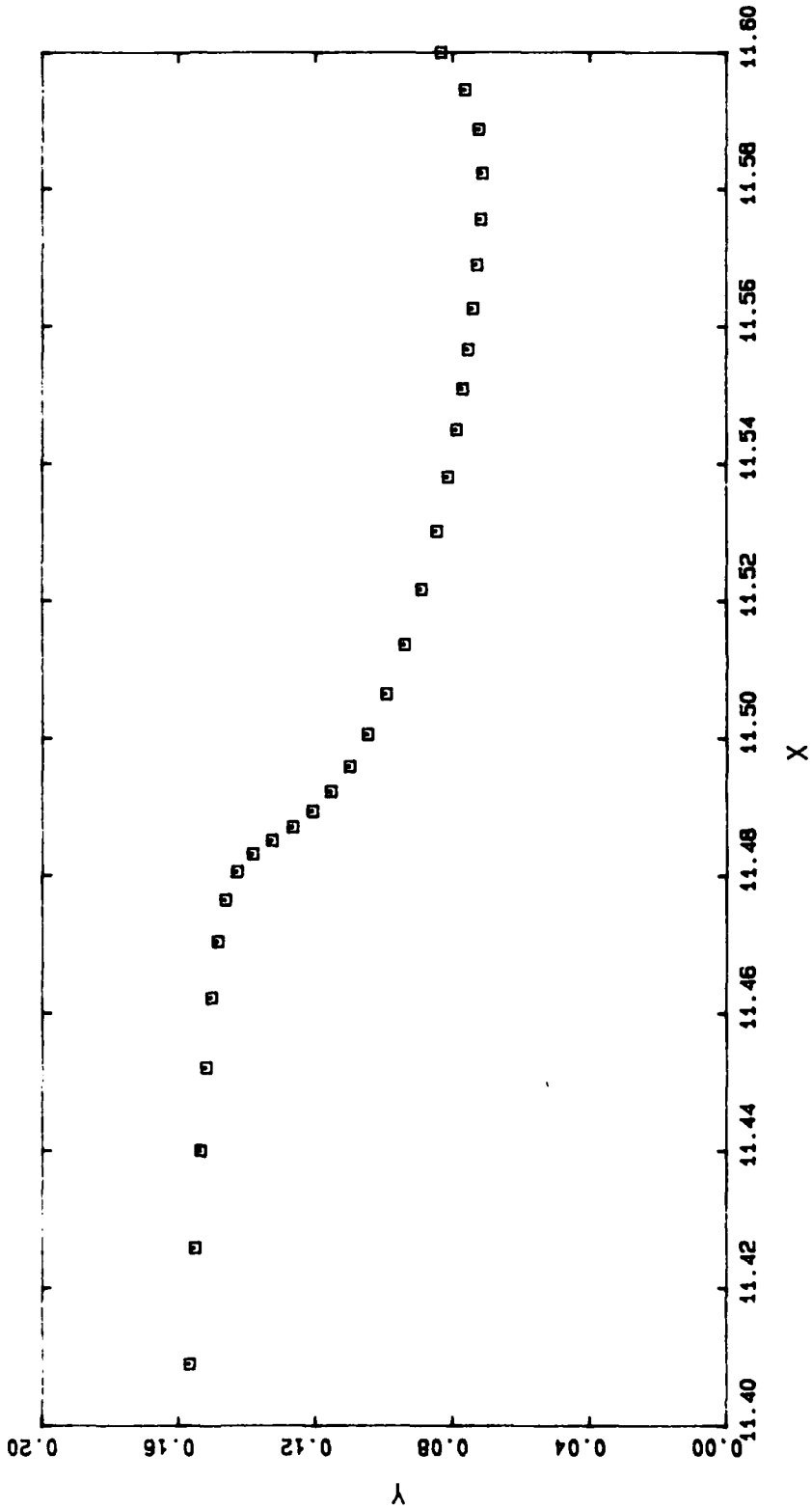

E4 3283 50.9242

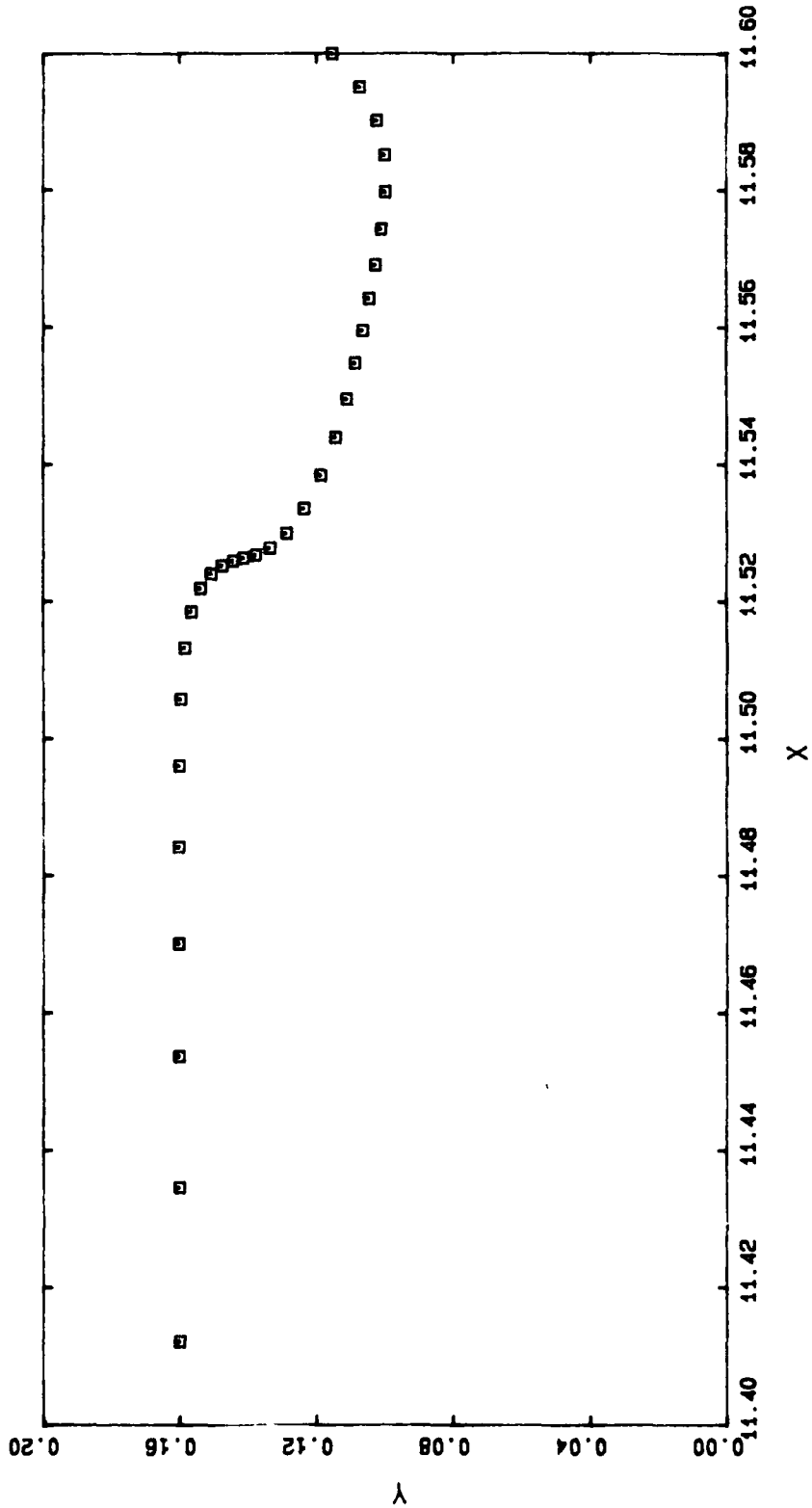

E4 3383 50.9396

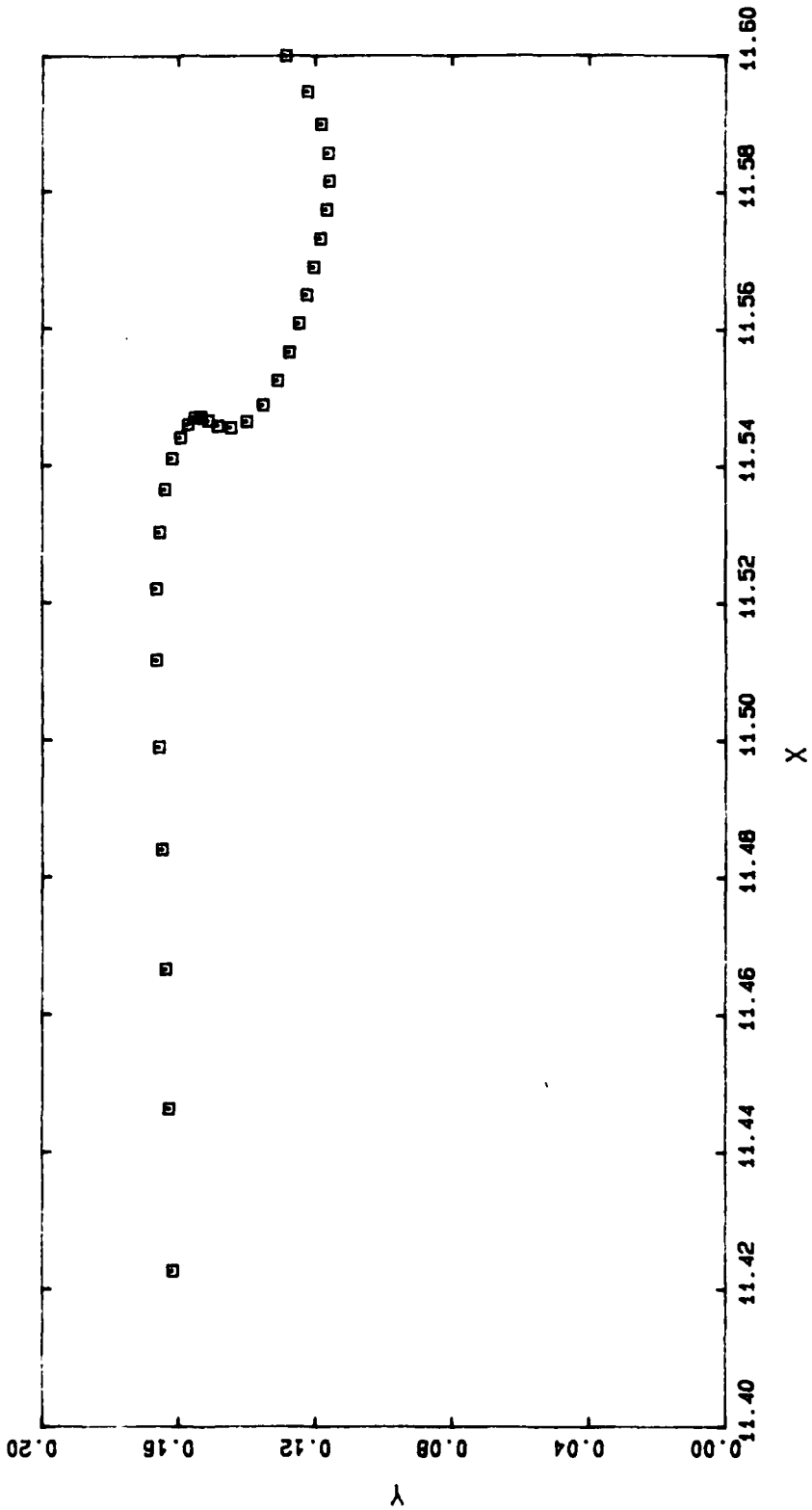

E4 3483 50.9490

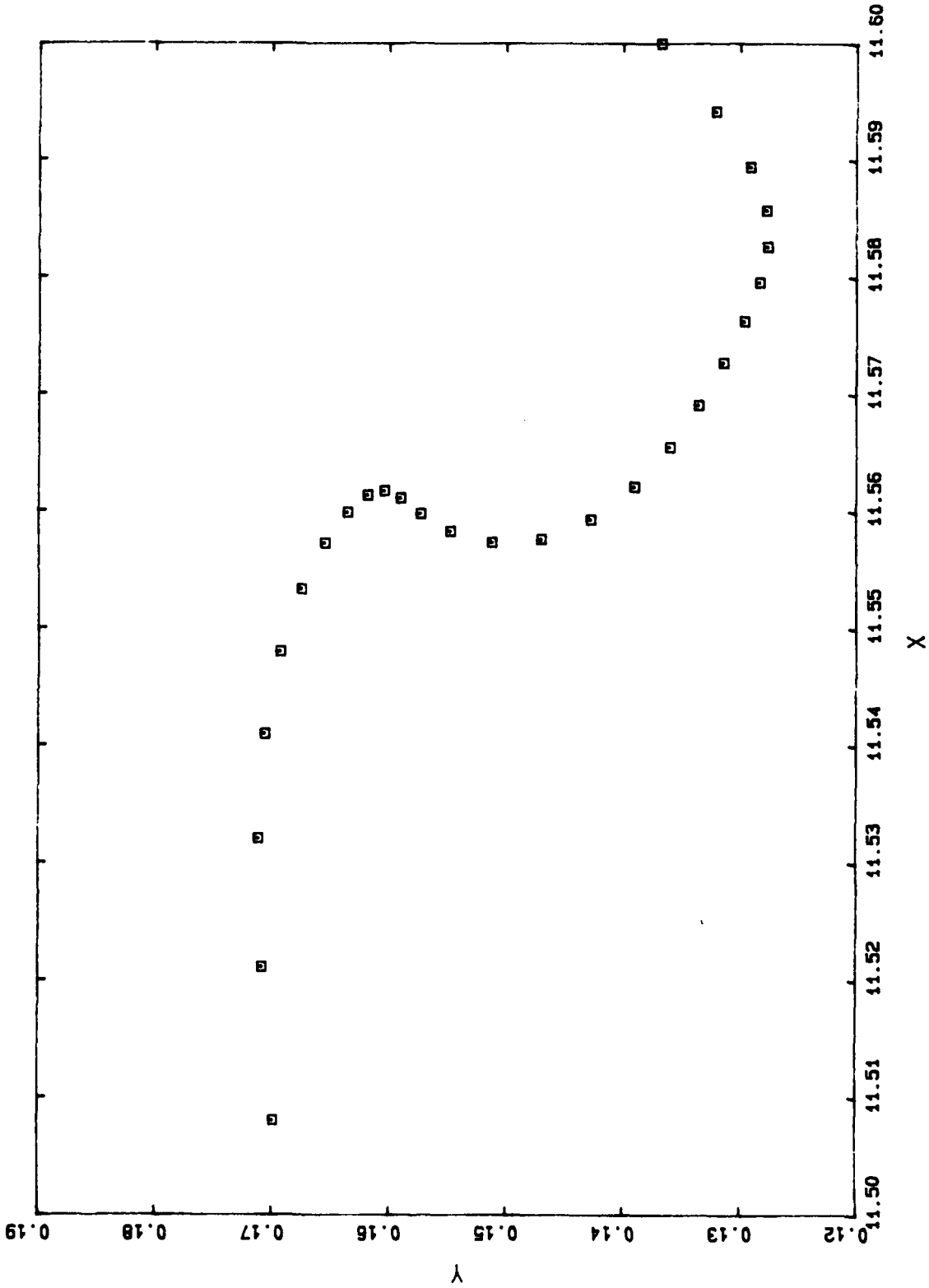

E4 3583 50.9562

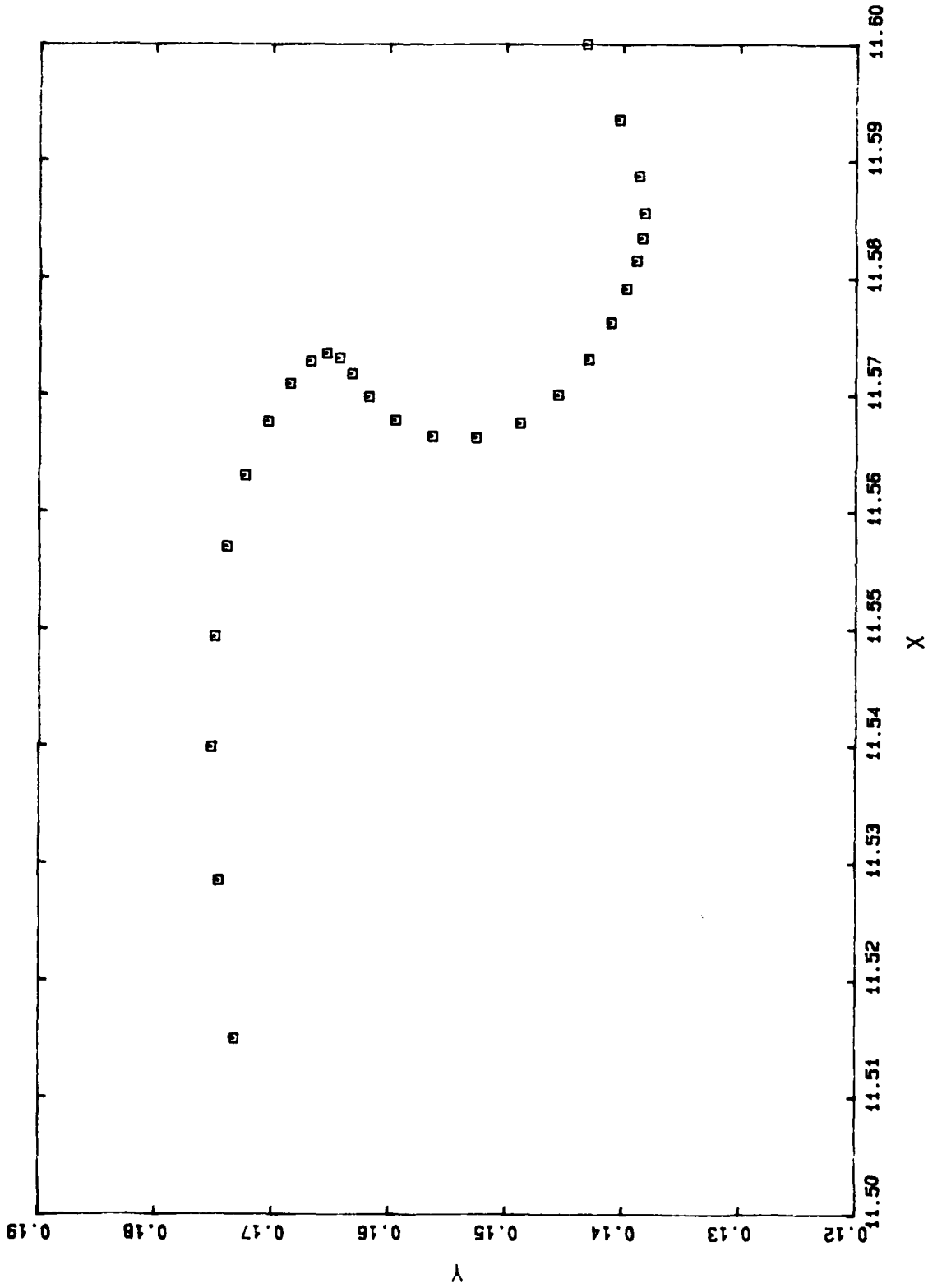

E4 3683 50.9618

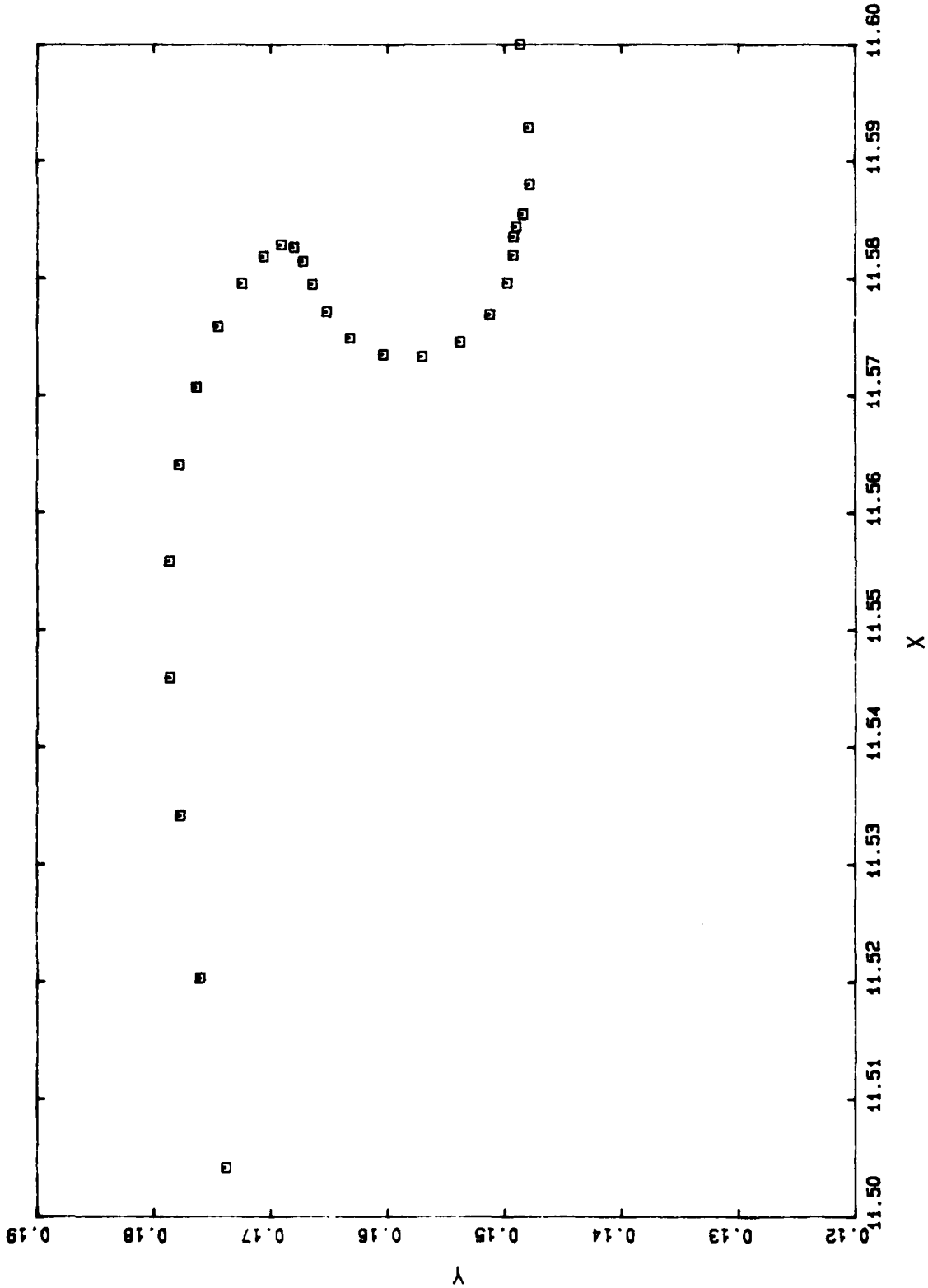

E4 3783 50.9643

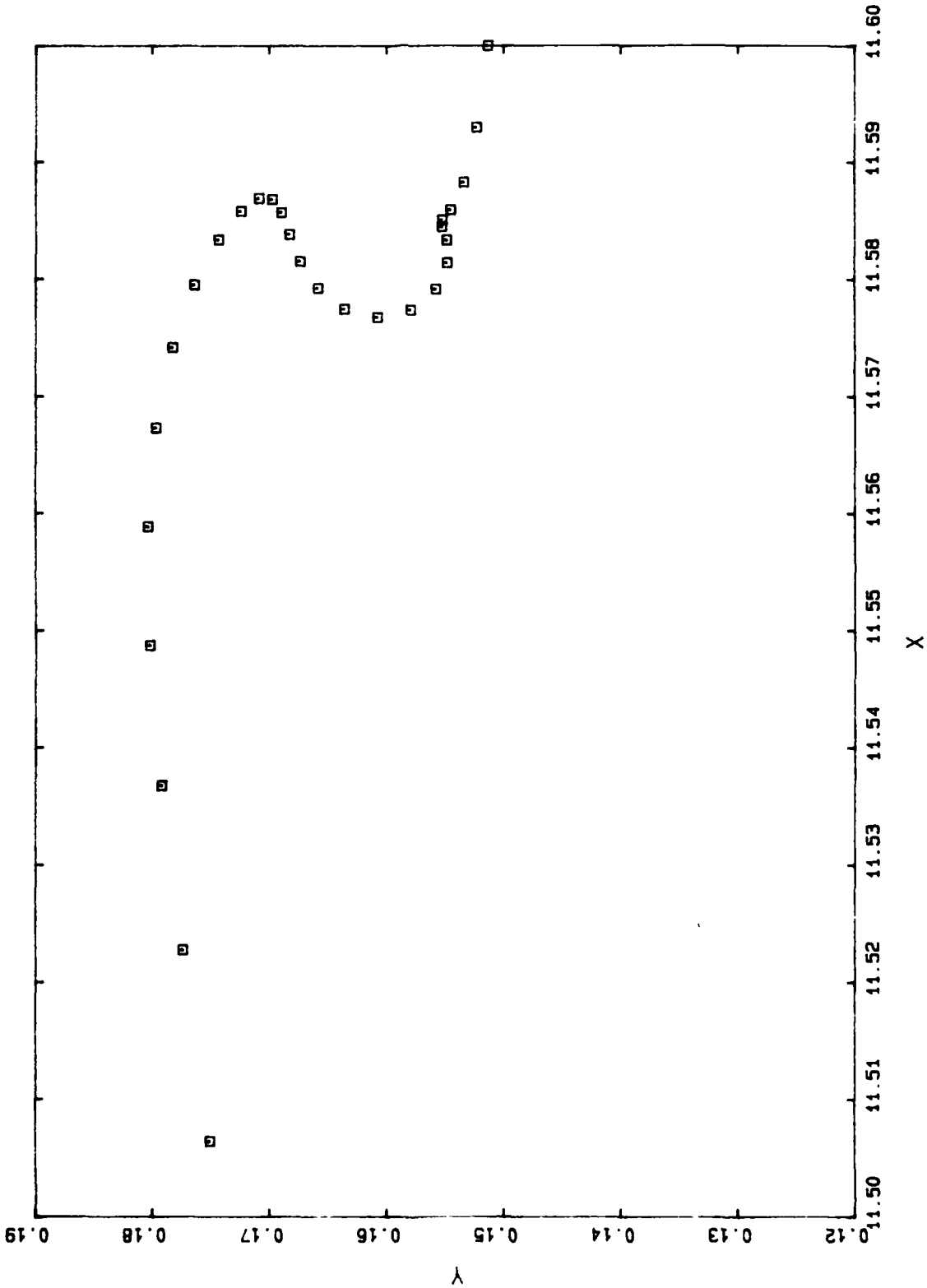

E4 3883 50.9659

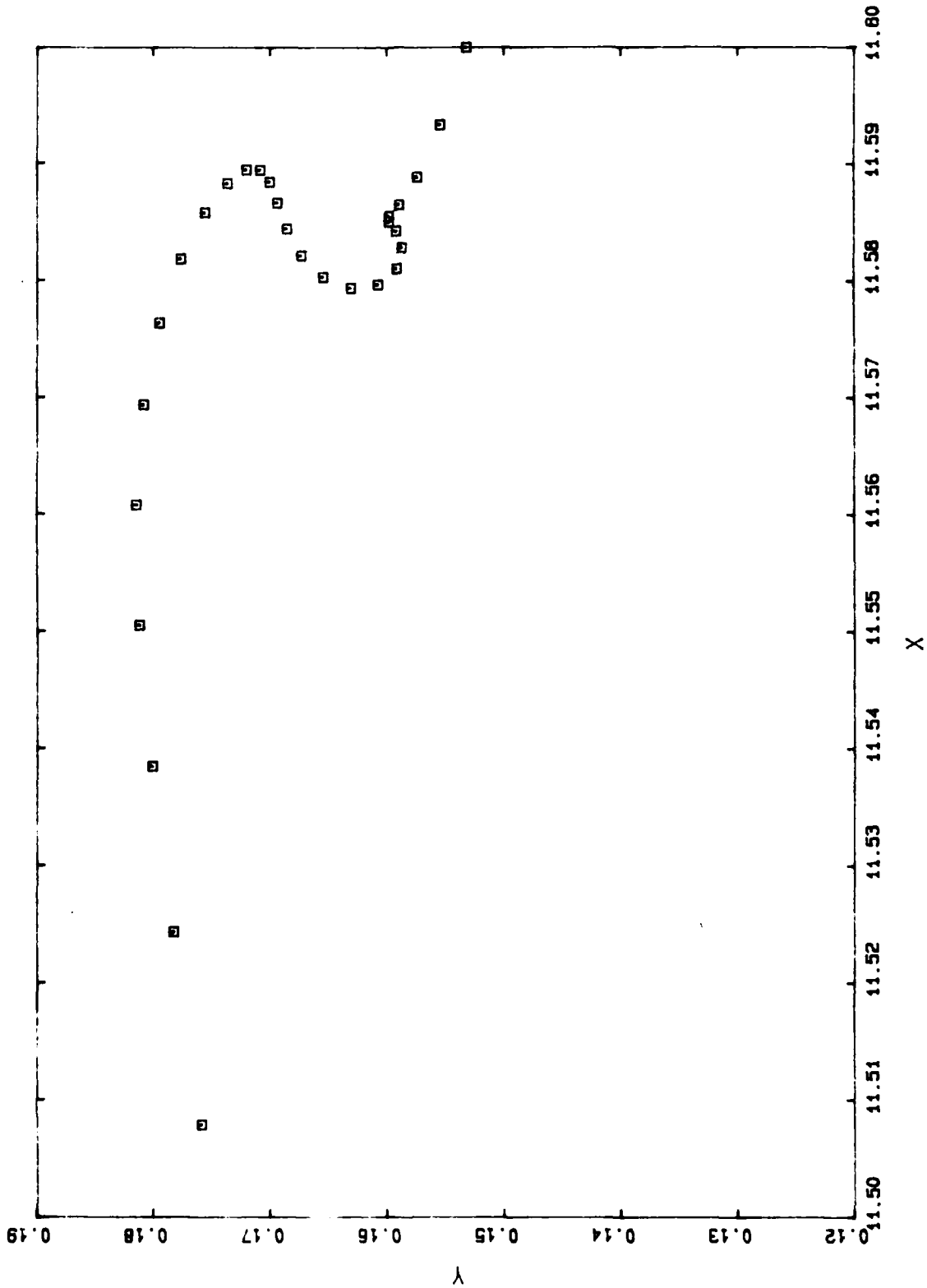

E4 3983 50.9672

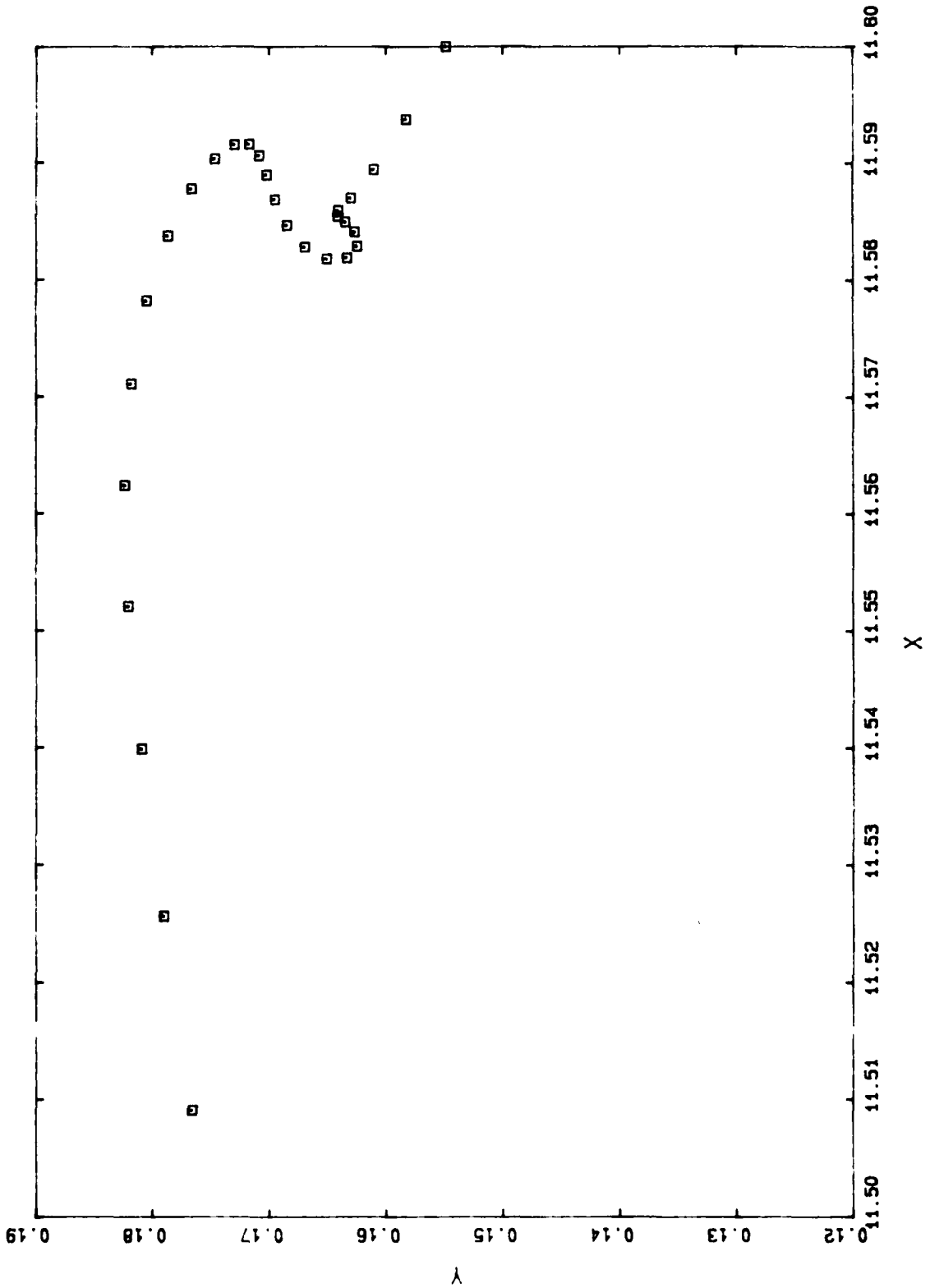

Appendix F

Refer to Chapter 5 for discussion.

F1 3185 50.8914

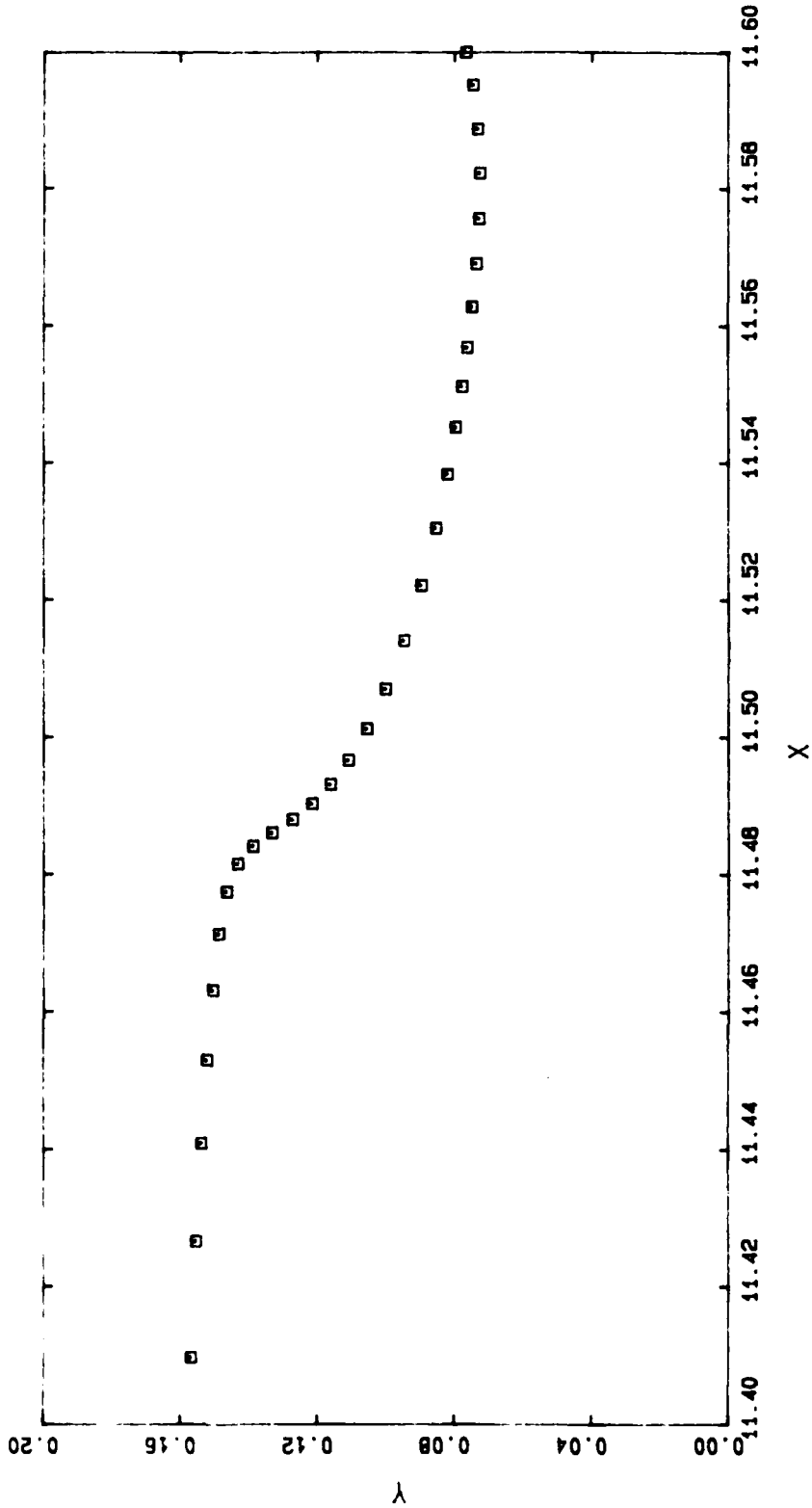

F1 3285 50.9246

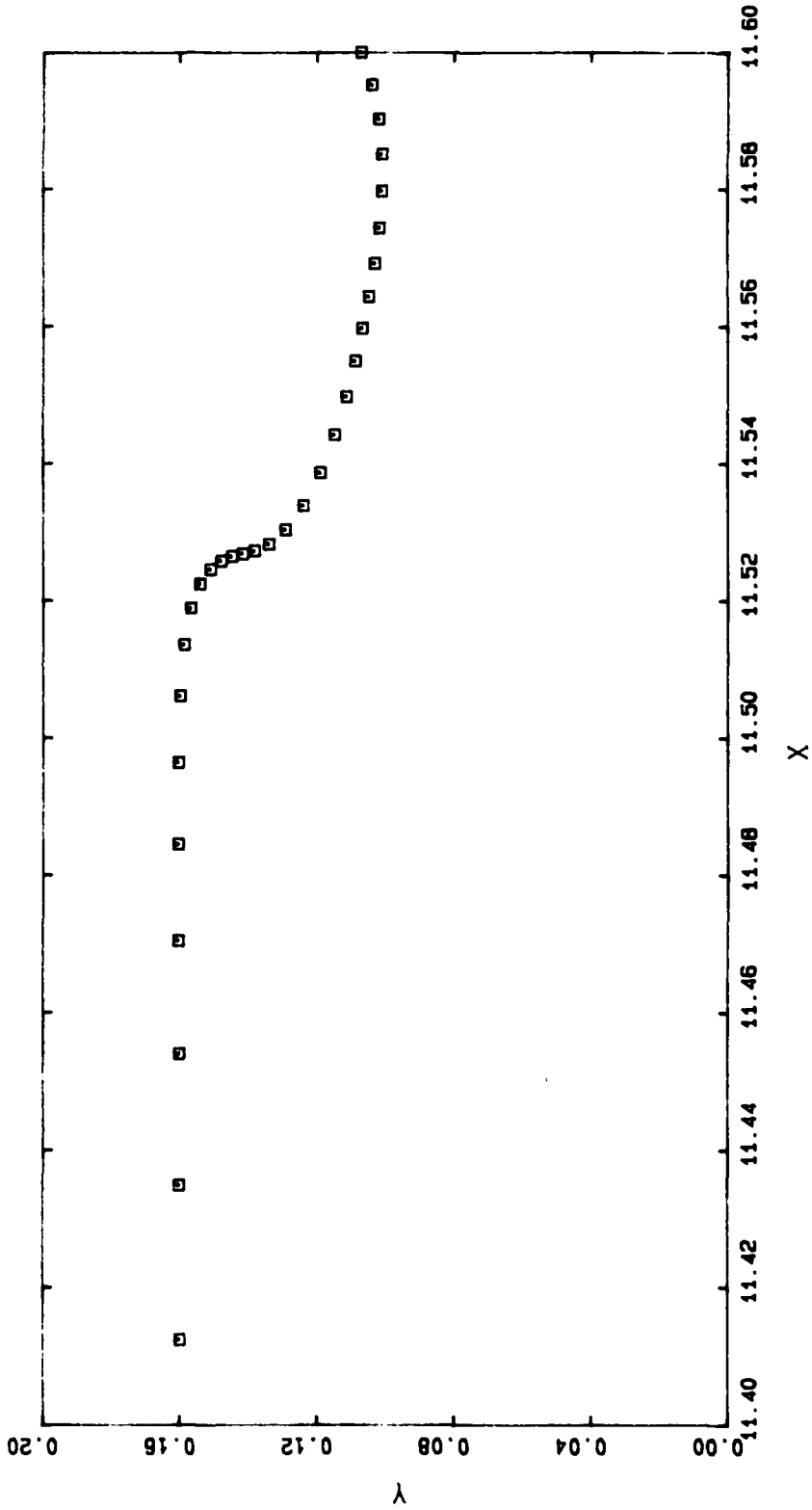

F1 3385 50.9399

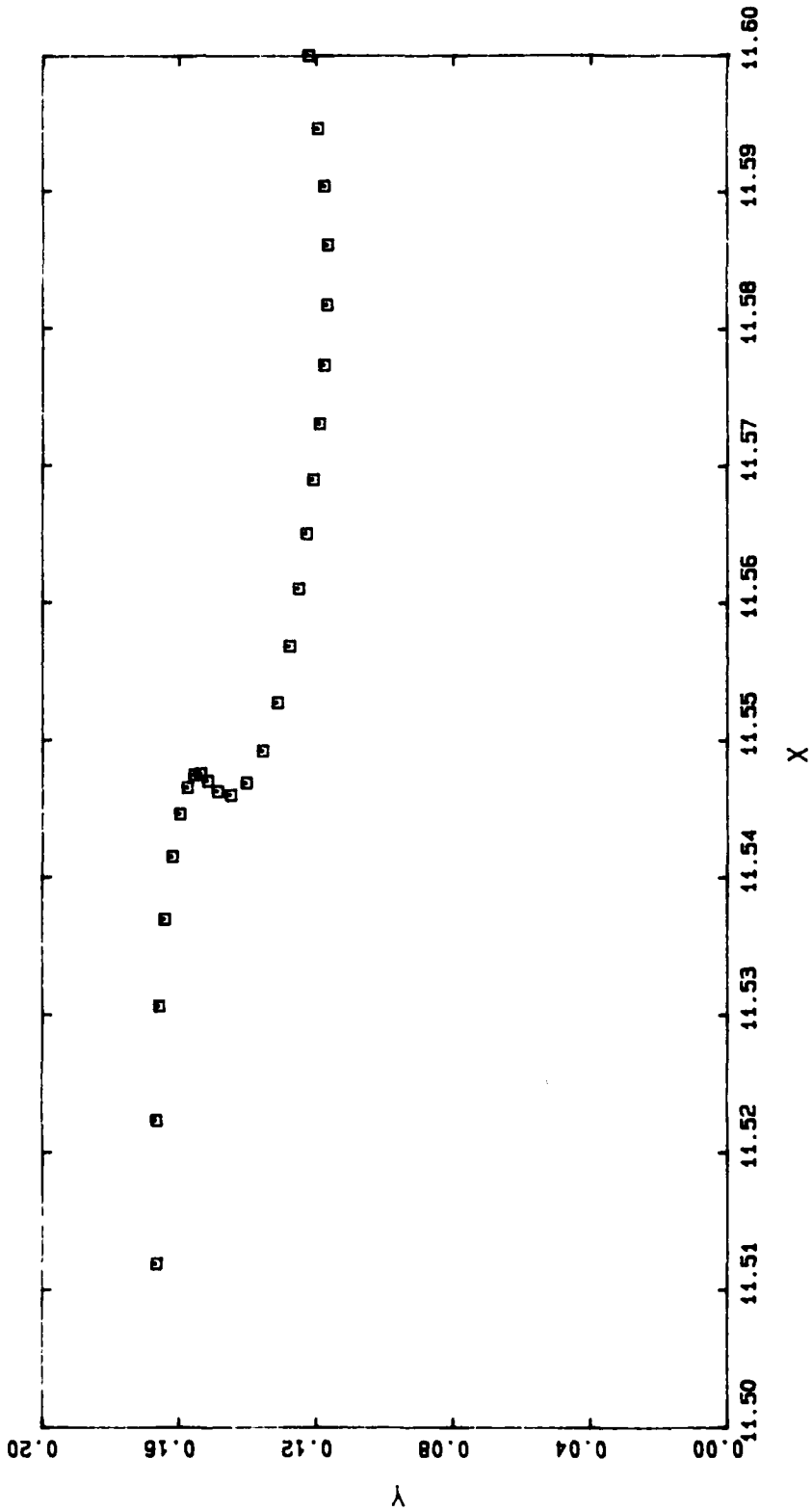

F1 3485 50.9493

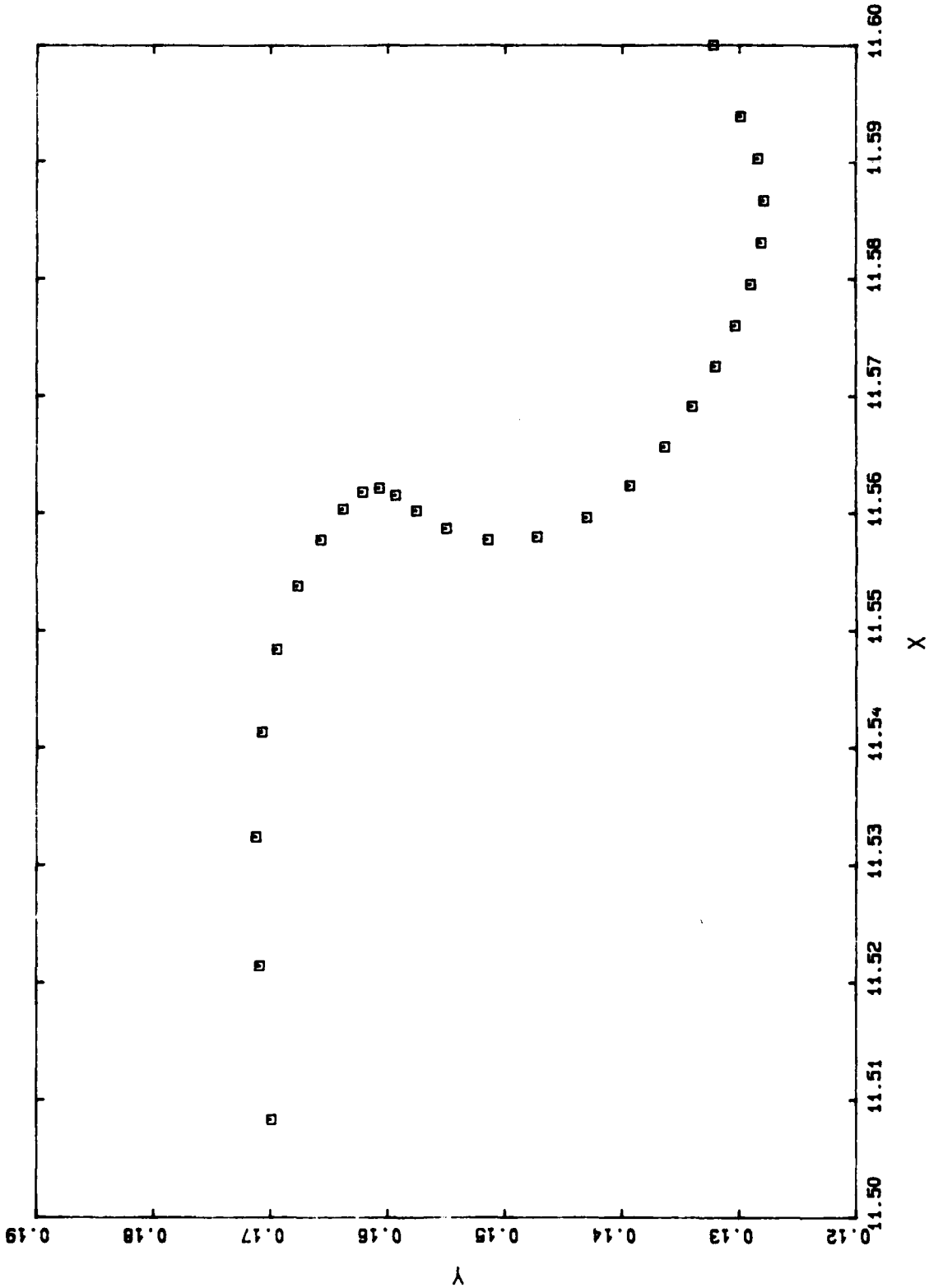

F1 3585 50.9566

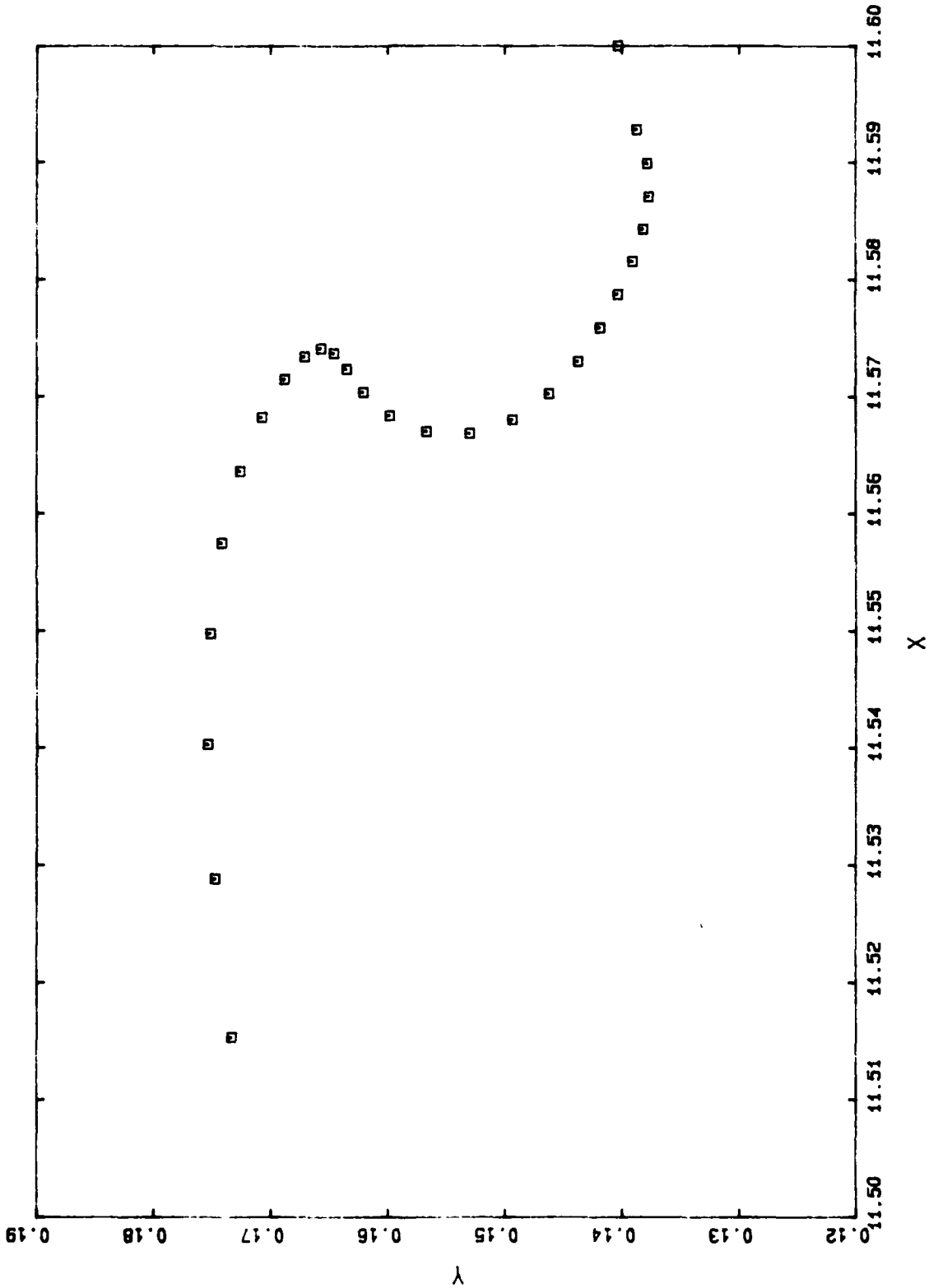

F1 3685 50.9628

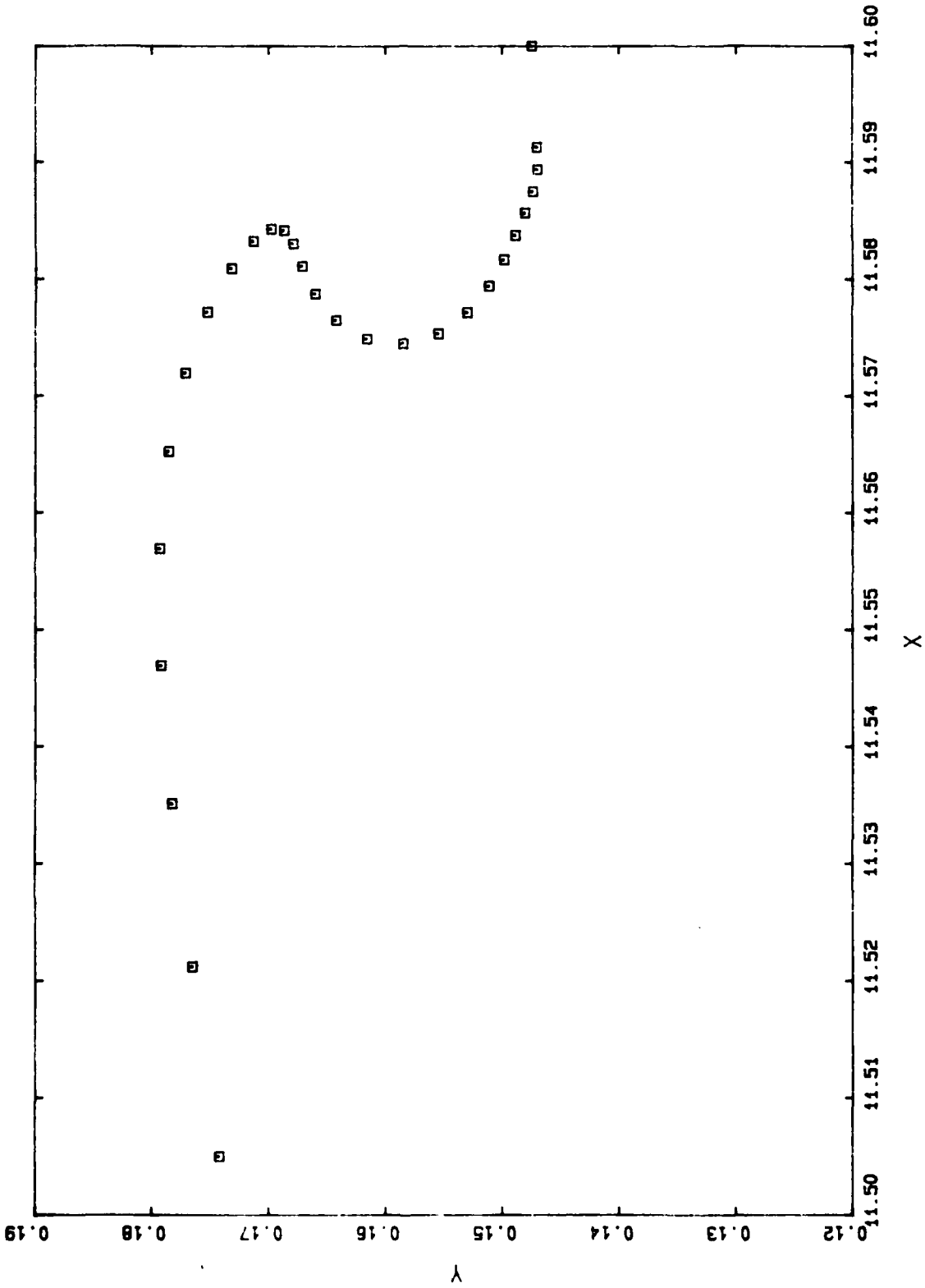

F1 3785 50.9682

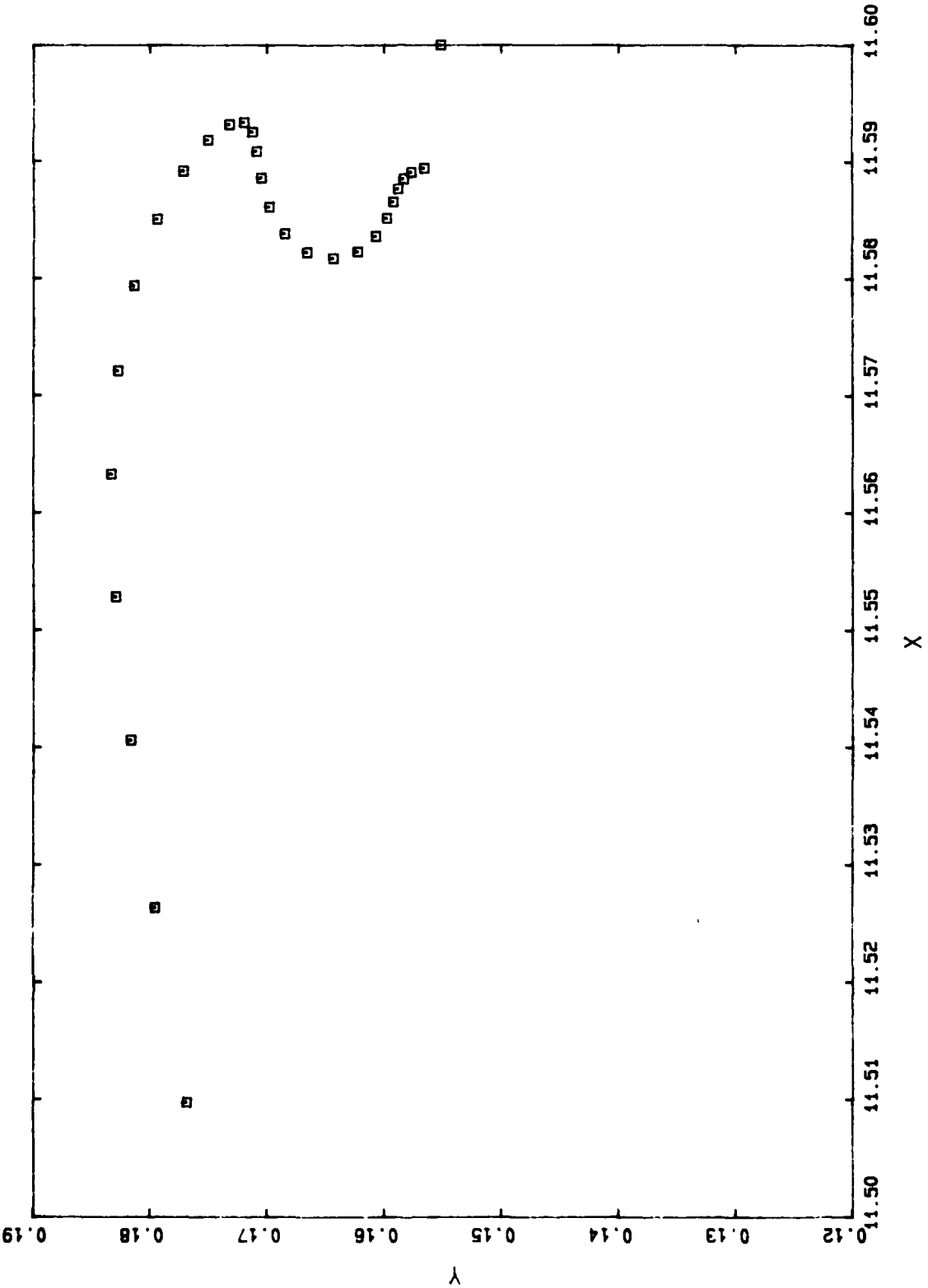

FI 3885 50.9713

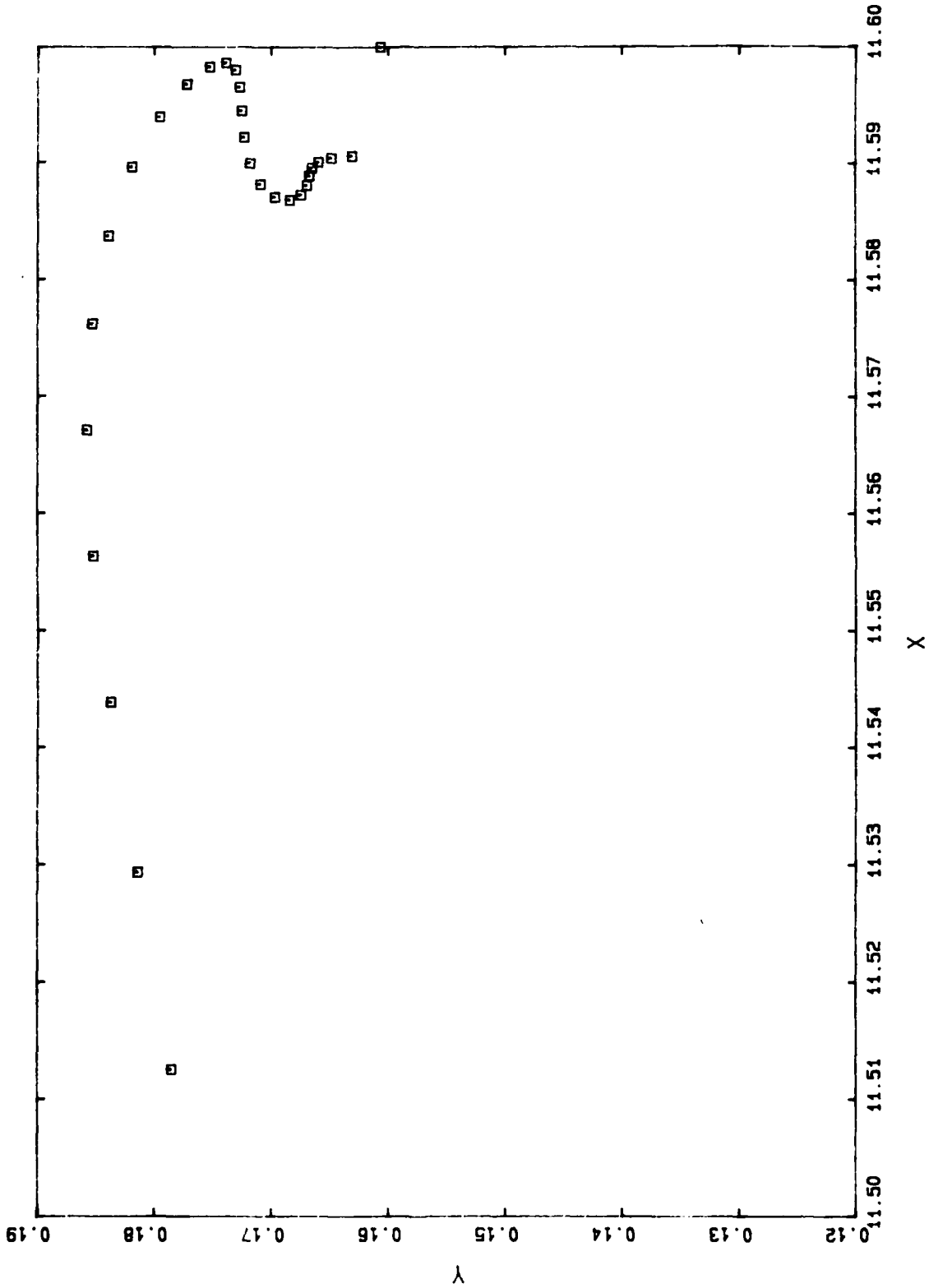

F1 3985 50.9729

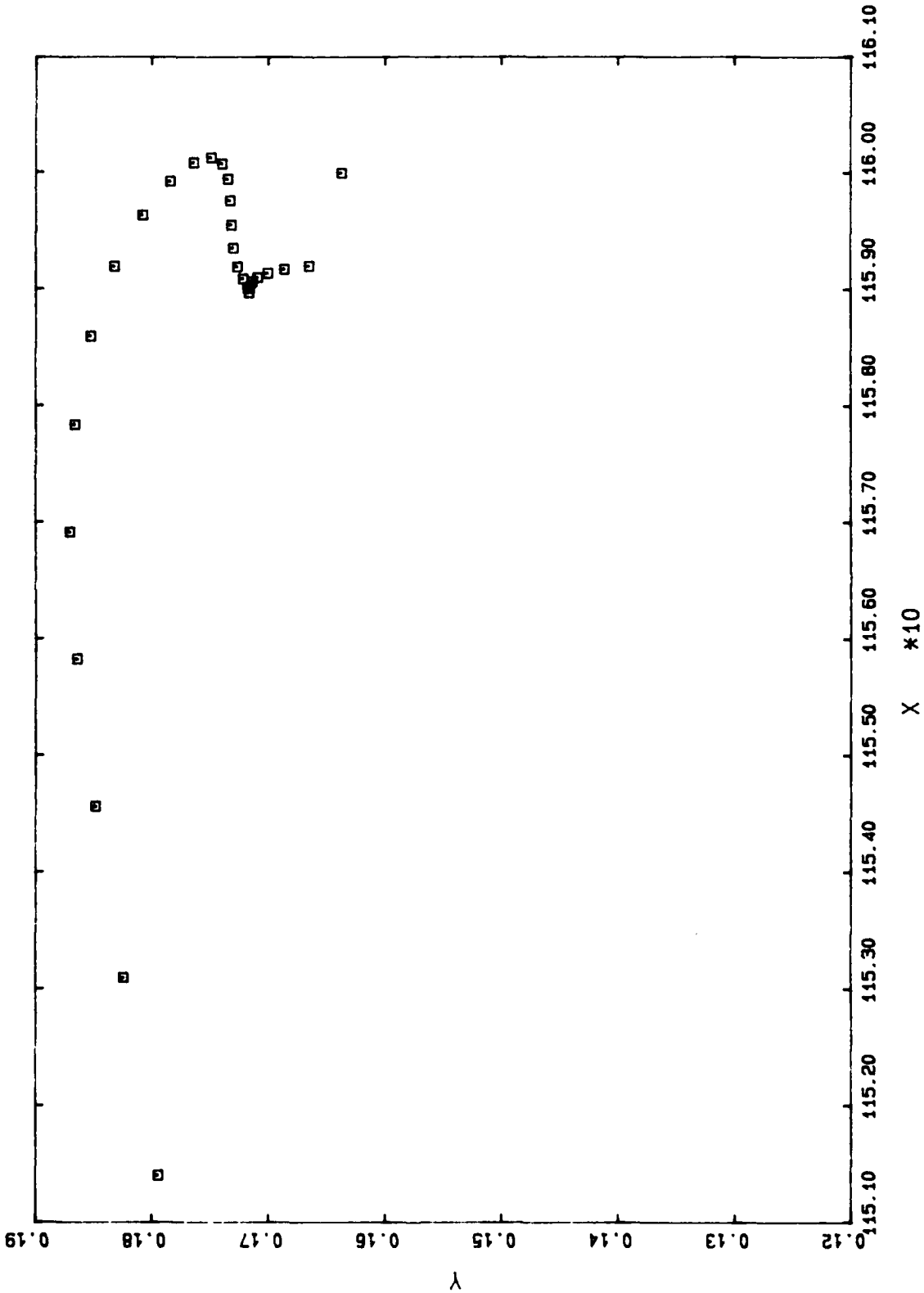

Appendix G

Refer to Chapter 5 for discussion.

G1 3110 50.8523

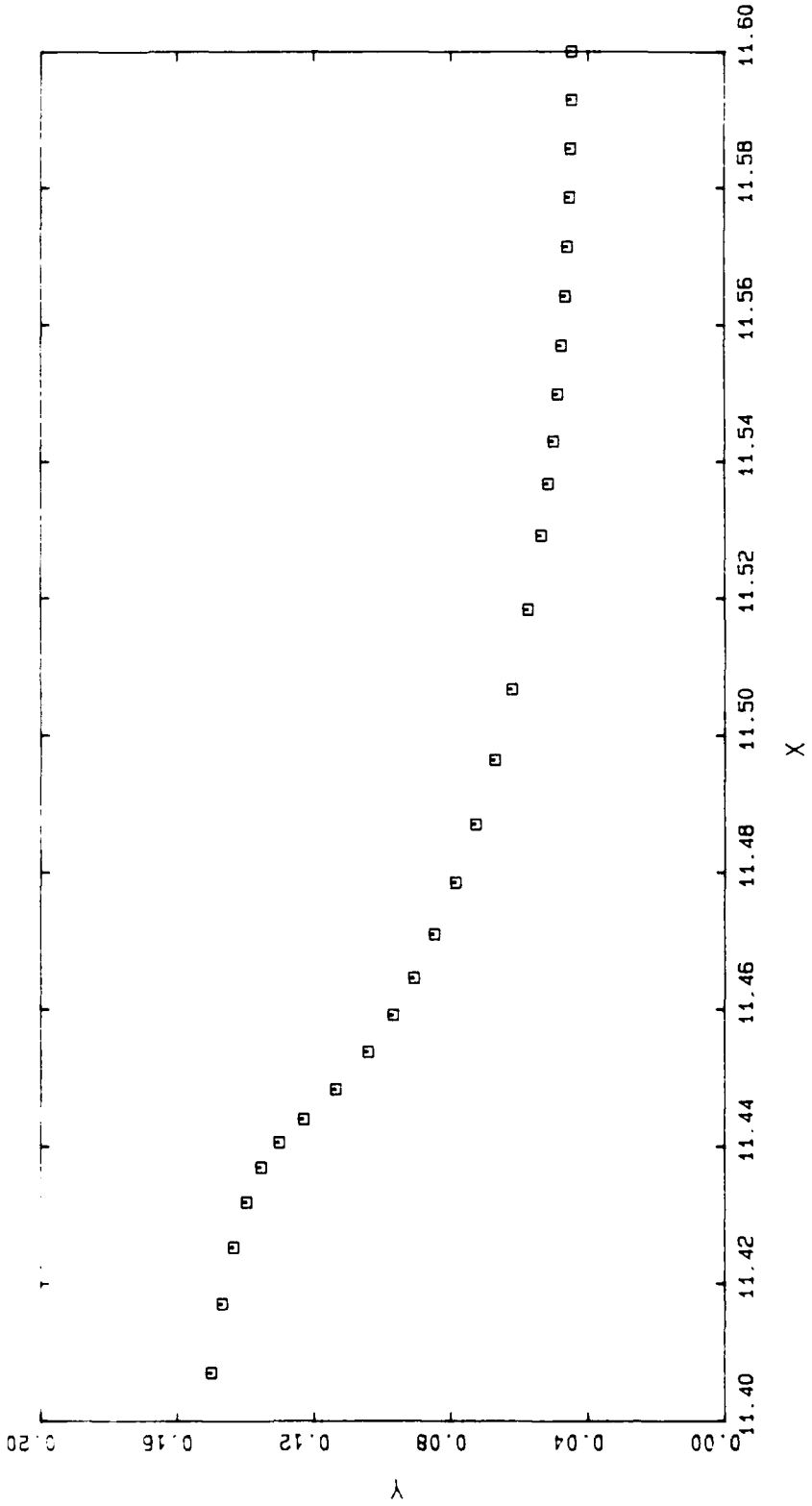

G1 3210 50.9019

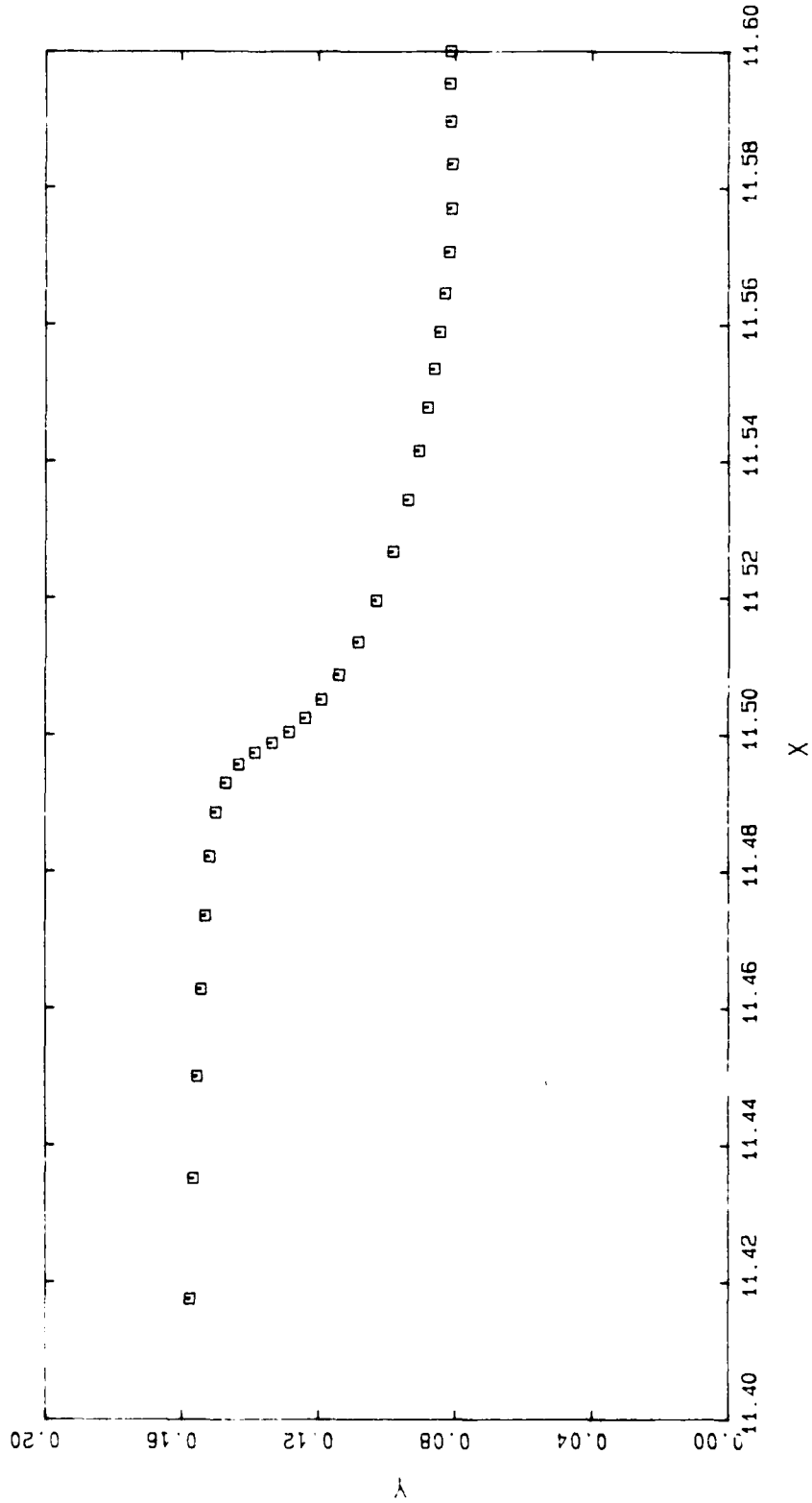

G1 3310 50.9291

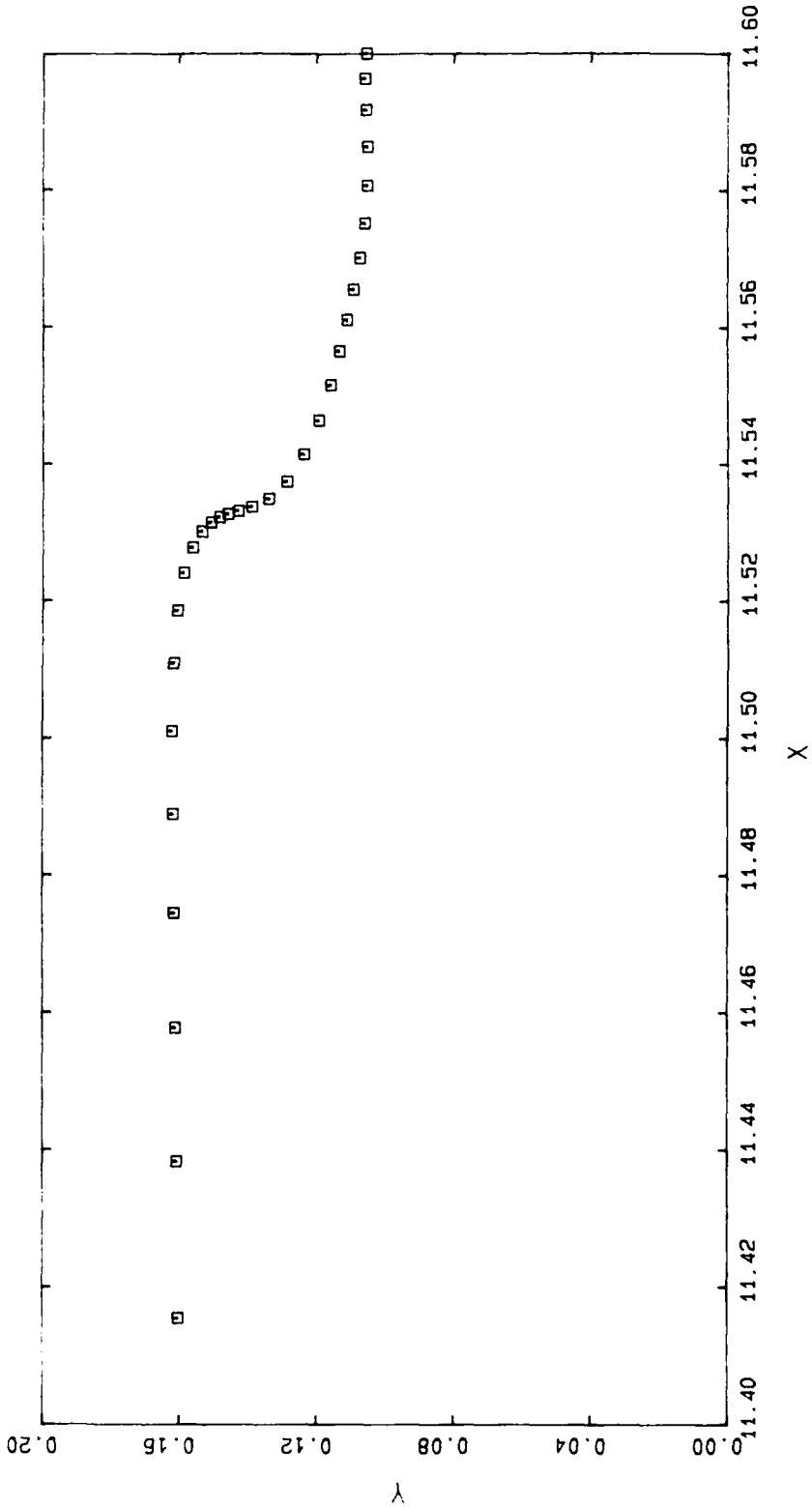

G1 3410 50.9411

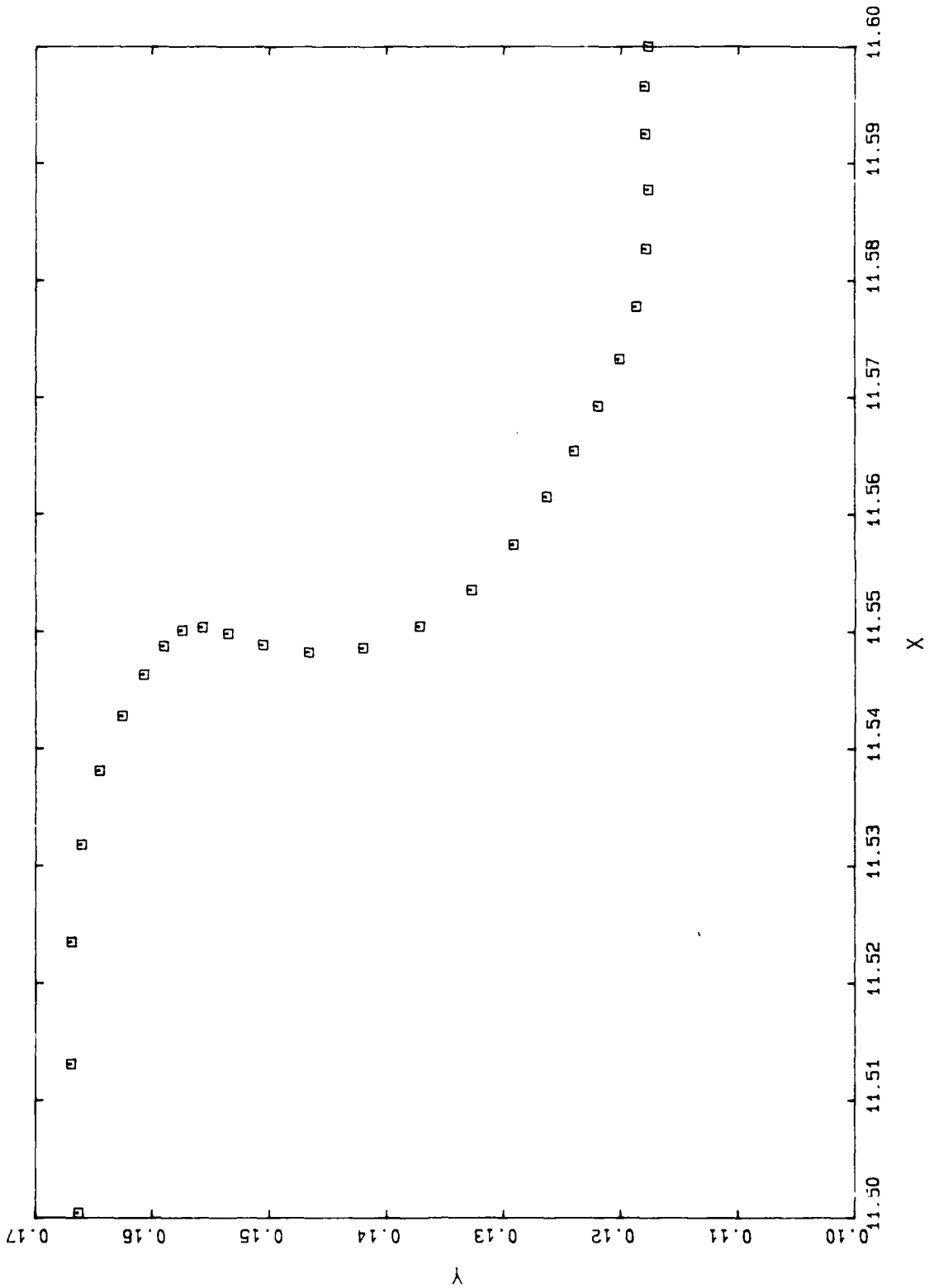

G1 3510 50.9500

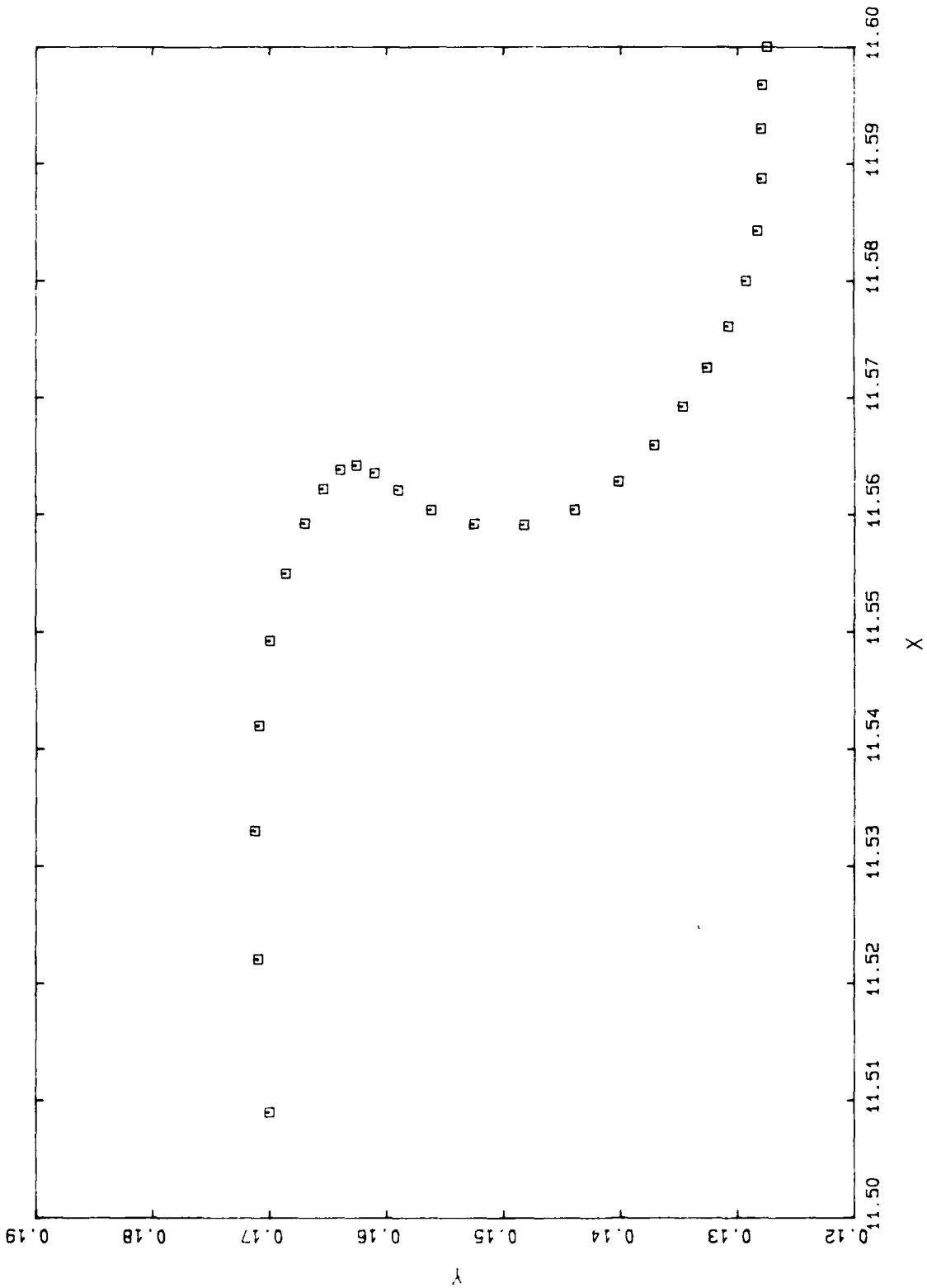

G1 3610 50.9579

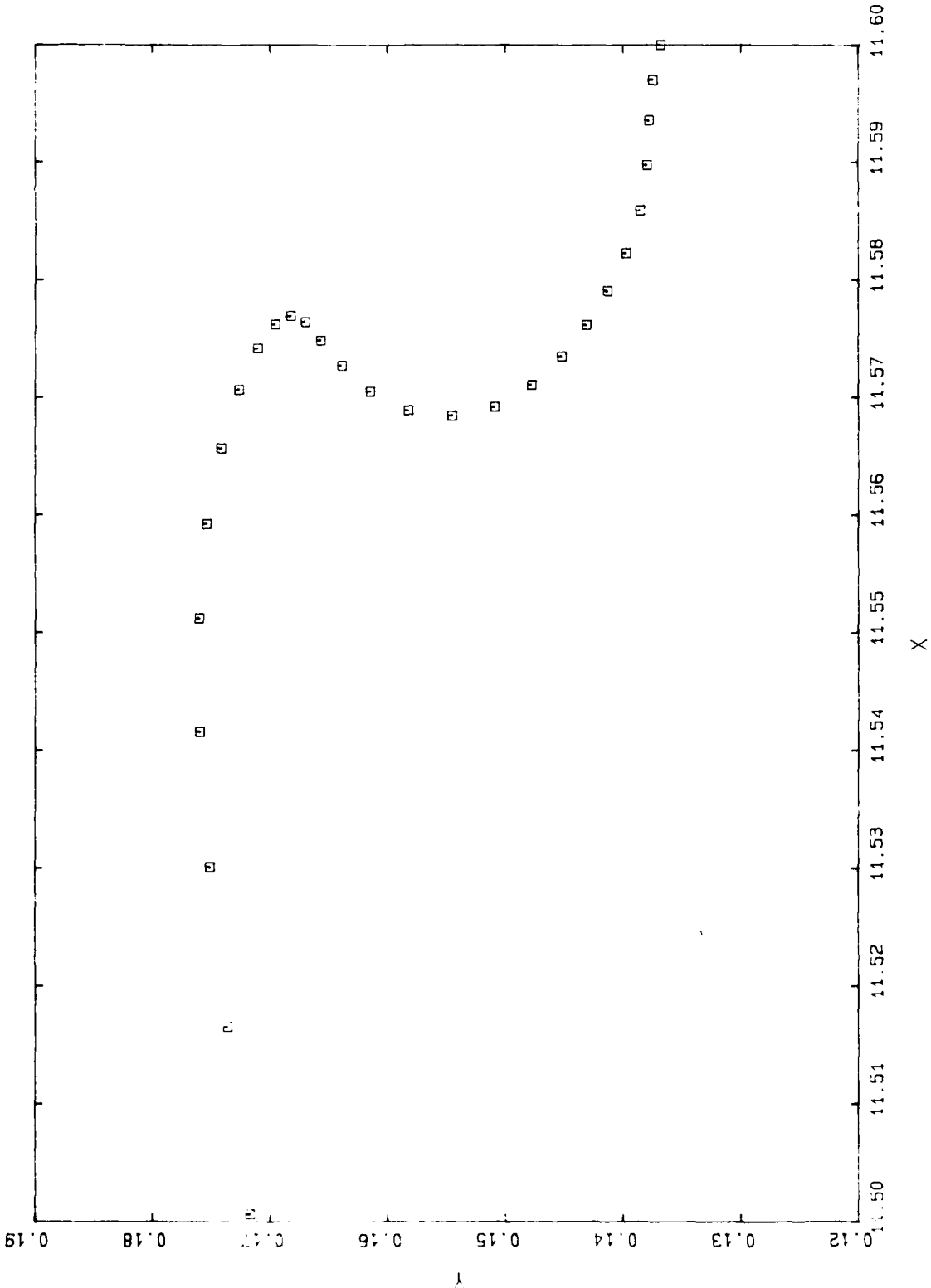

G1 3710 50.9647

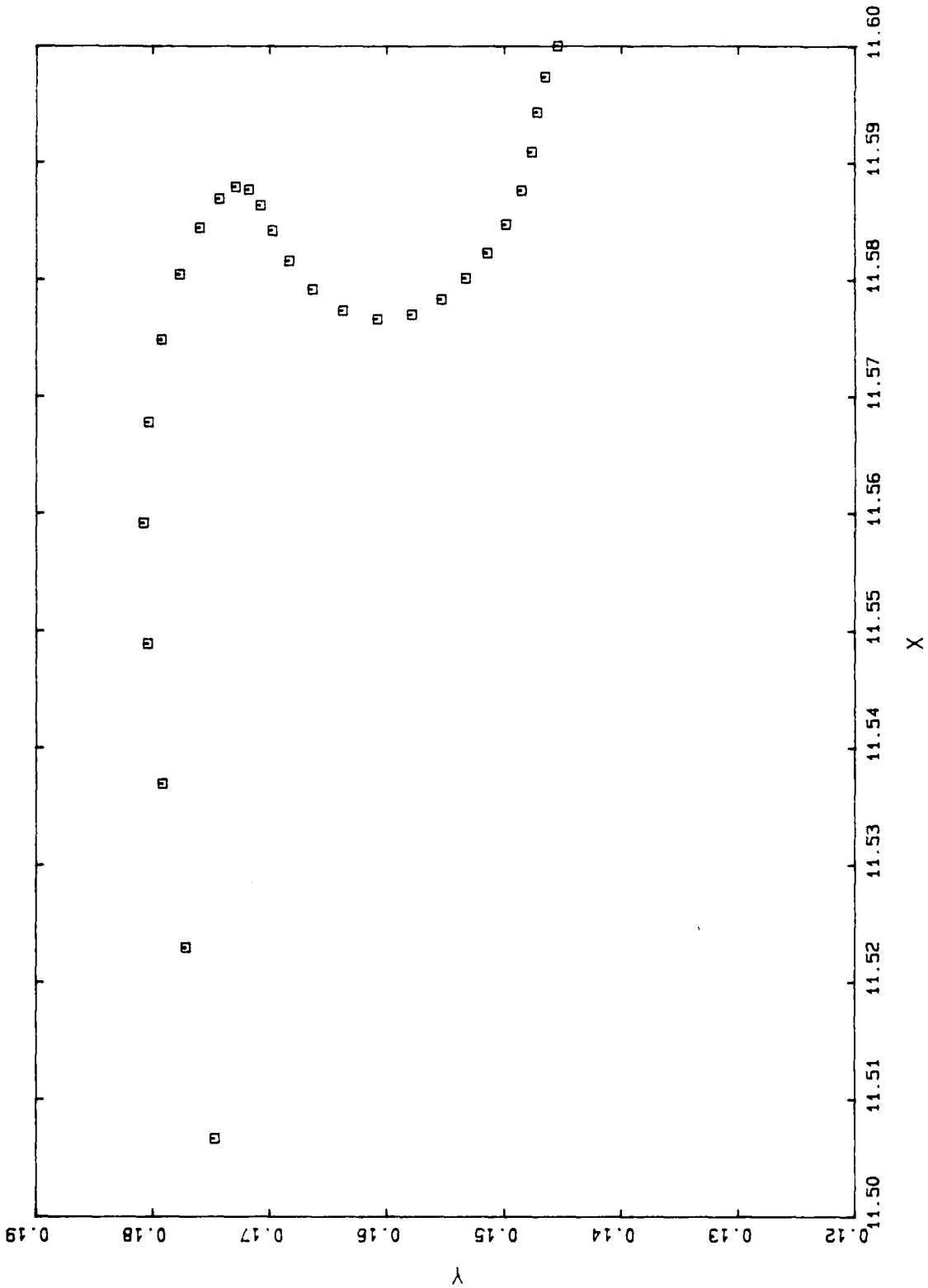

G1 3810 50.9712

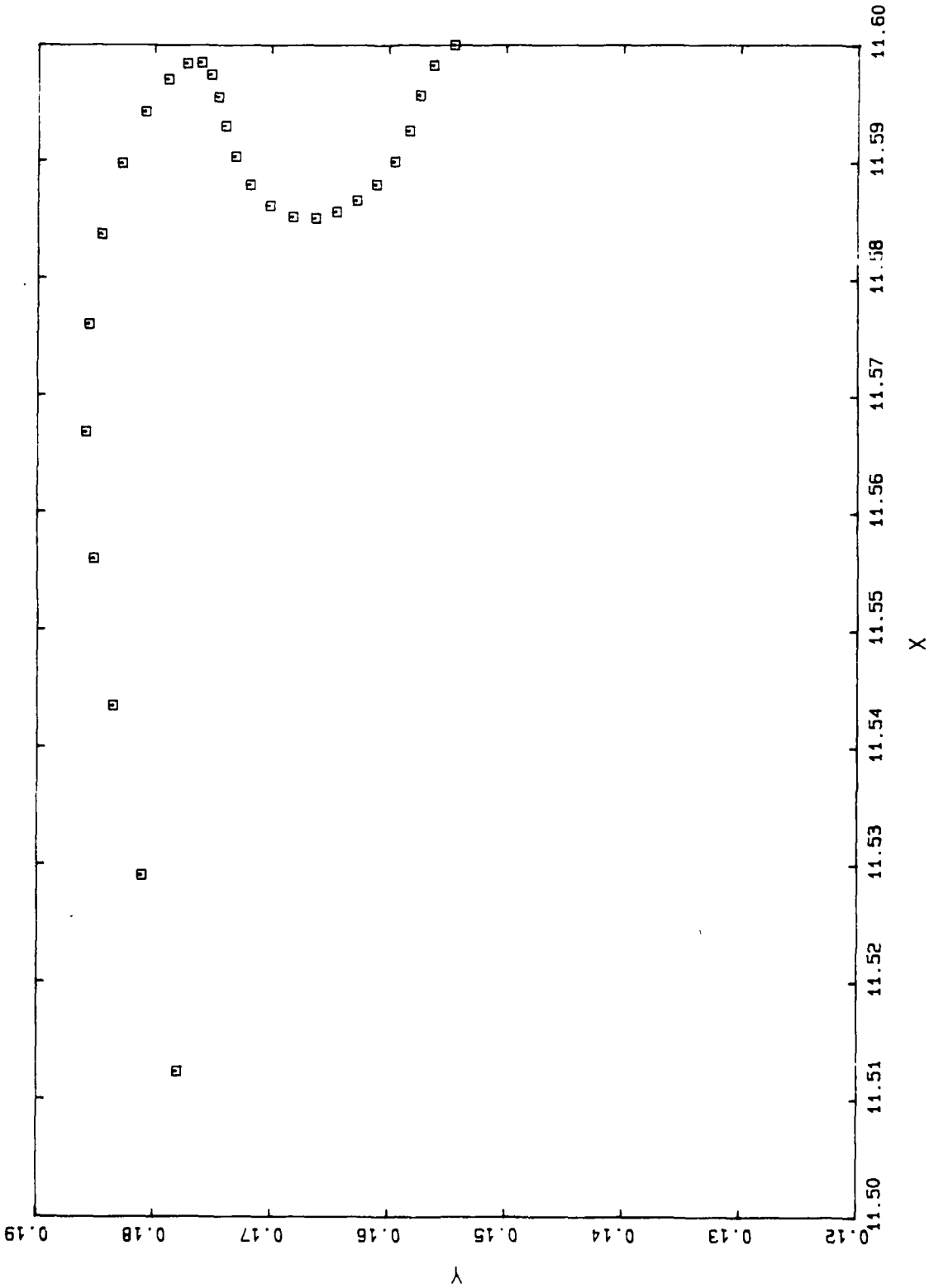

G1 3910 50.9761

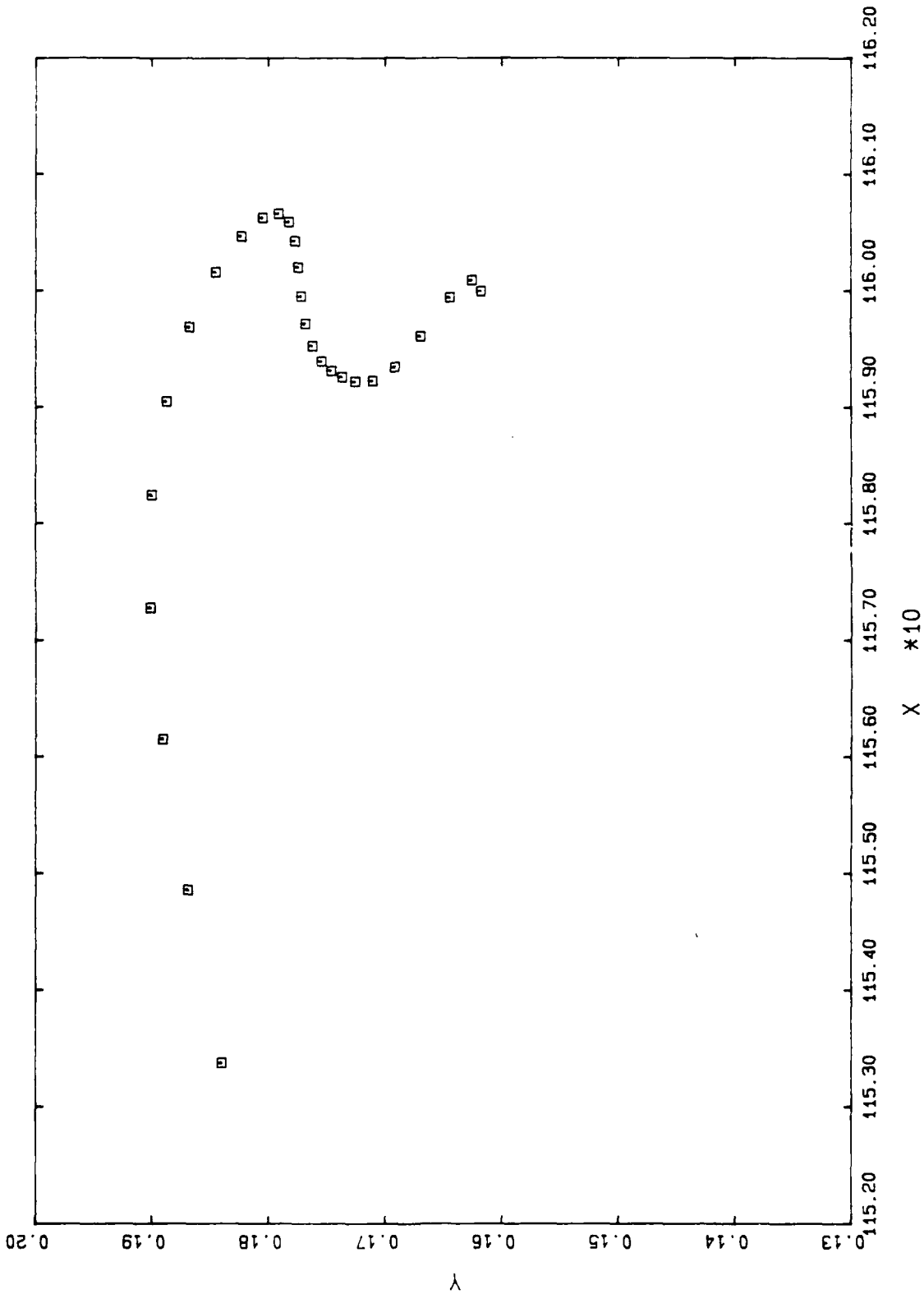

G1 4010 50.9781

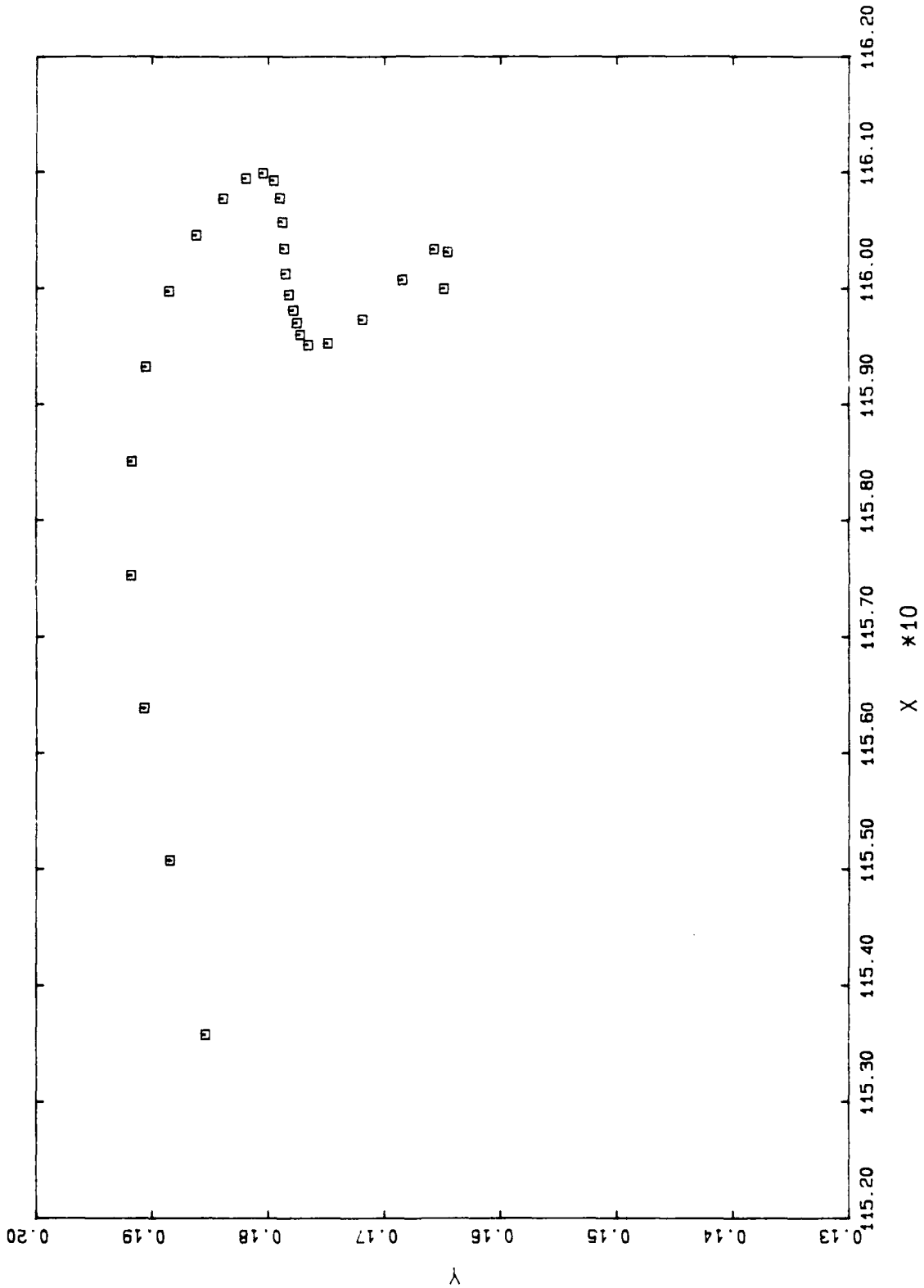

G1 4110 50.9813

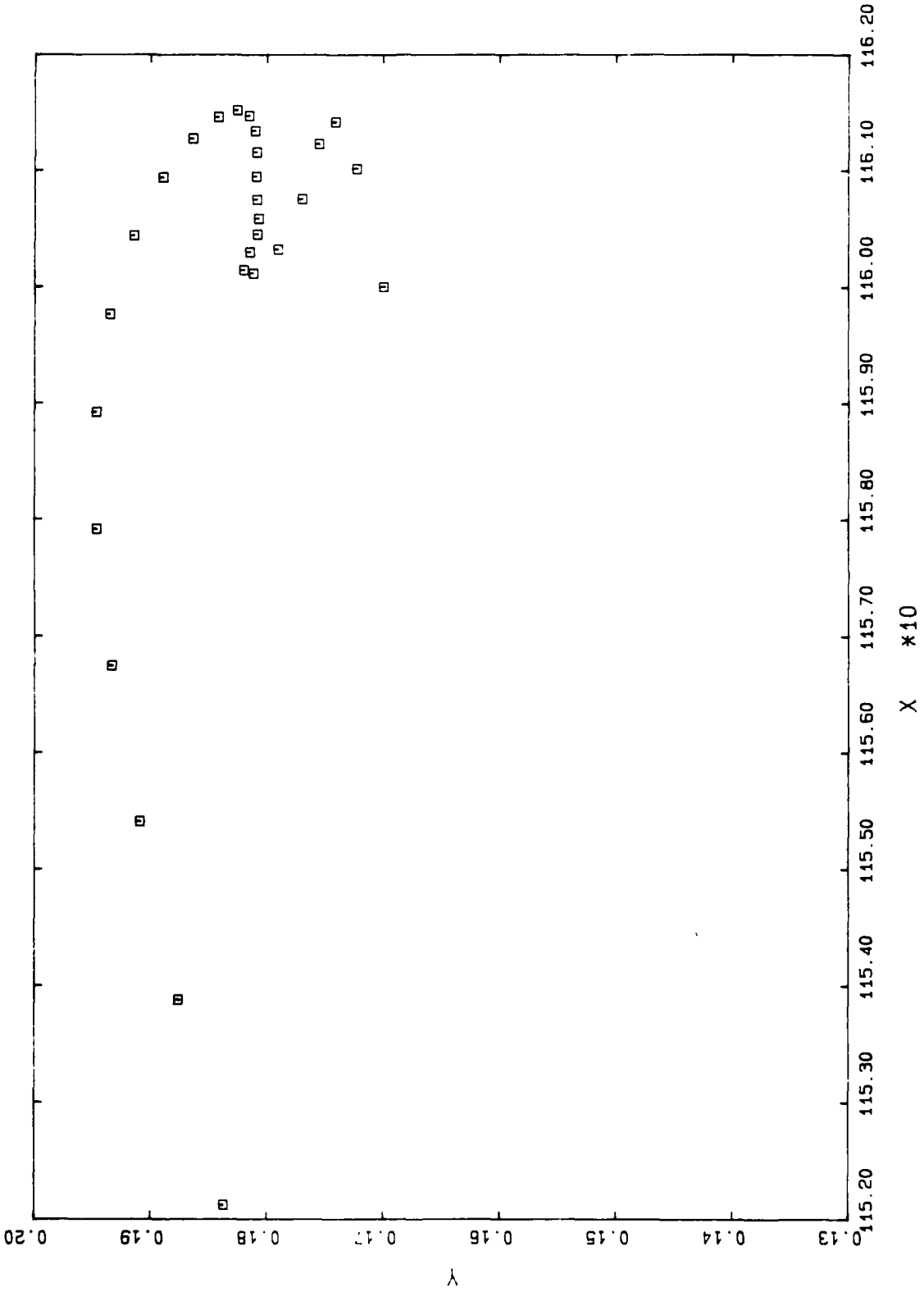

G1 4210 50.9855

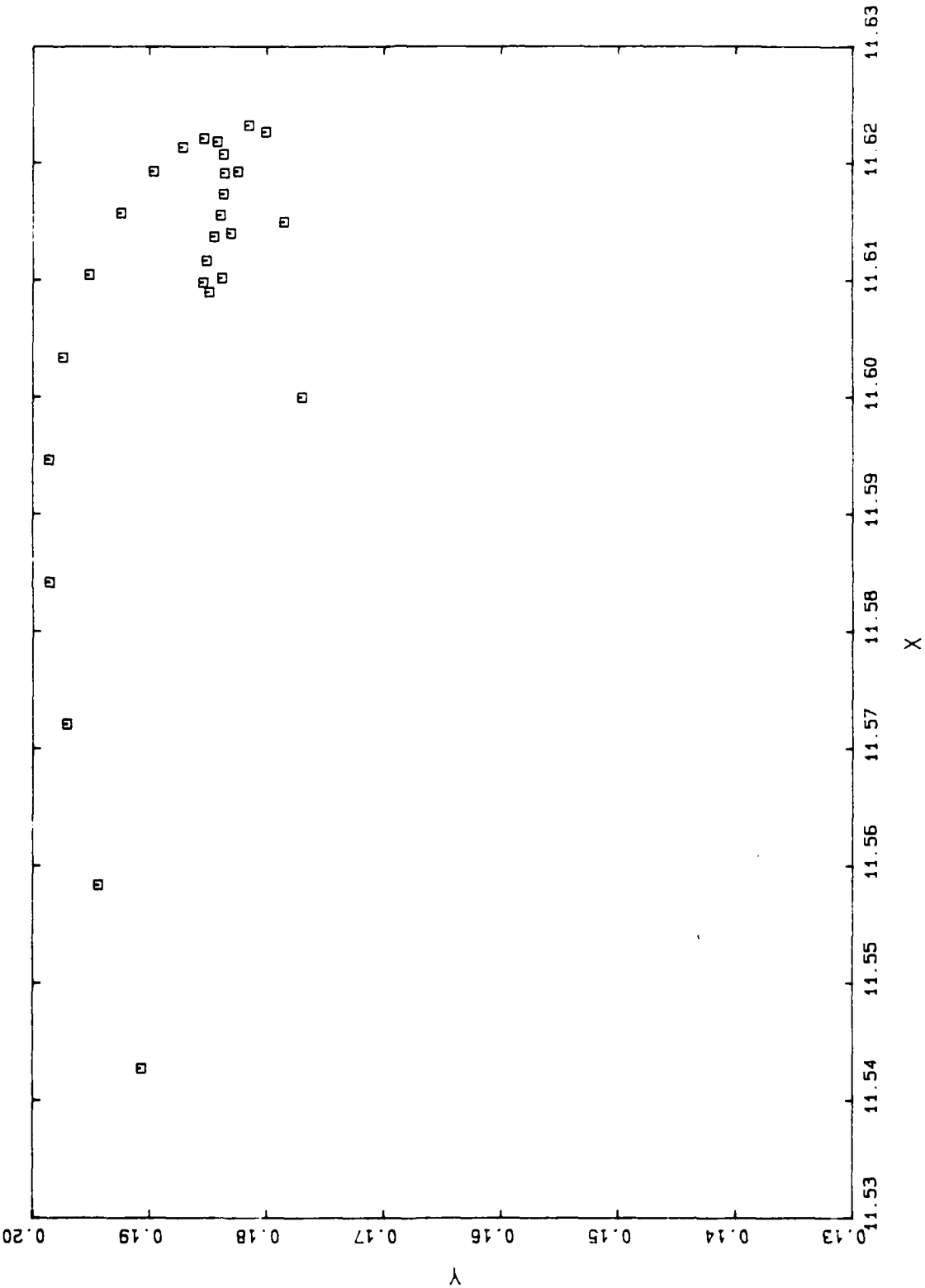

G2 3152 50.8758

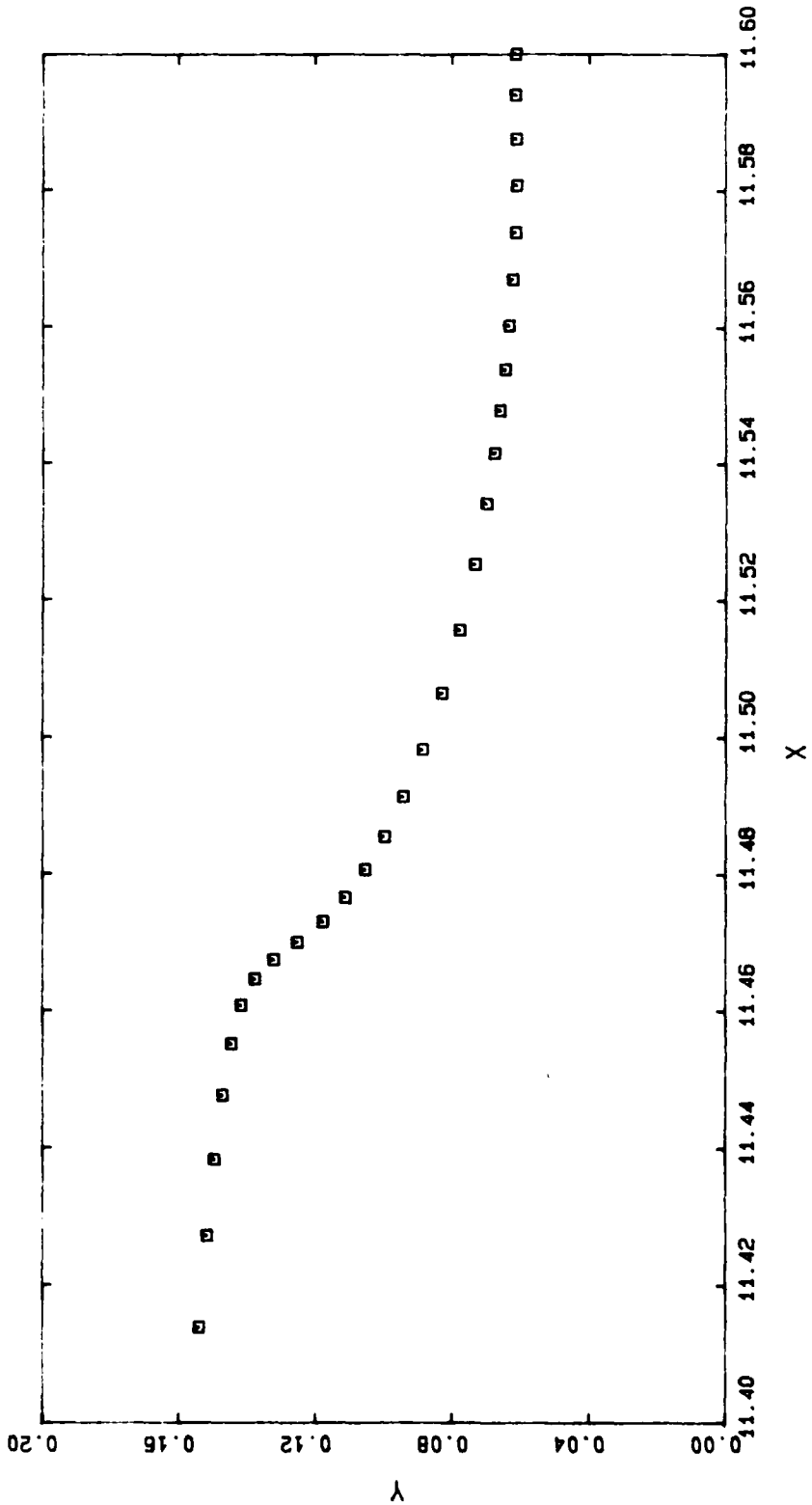

G2 3252 50.9163

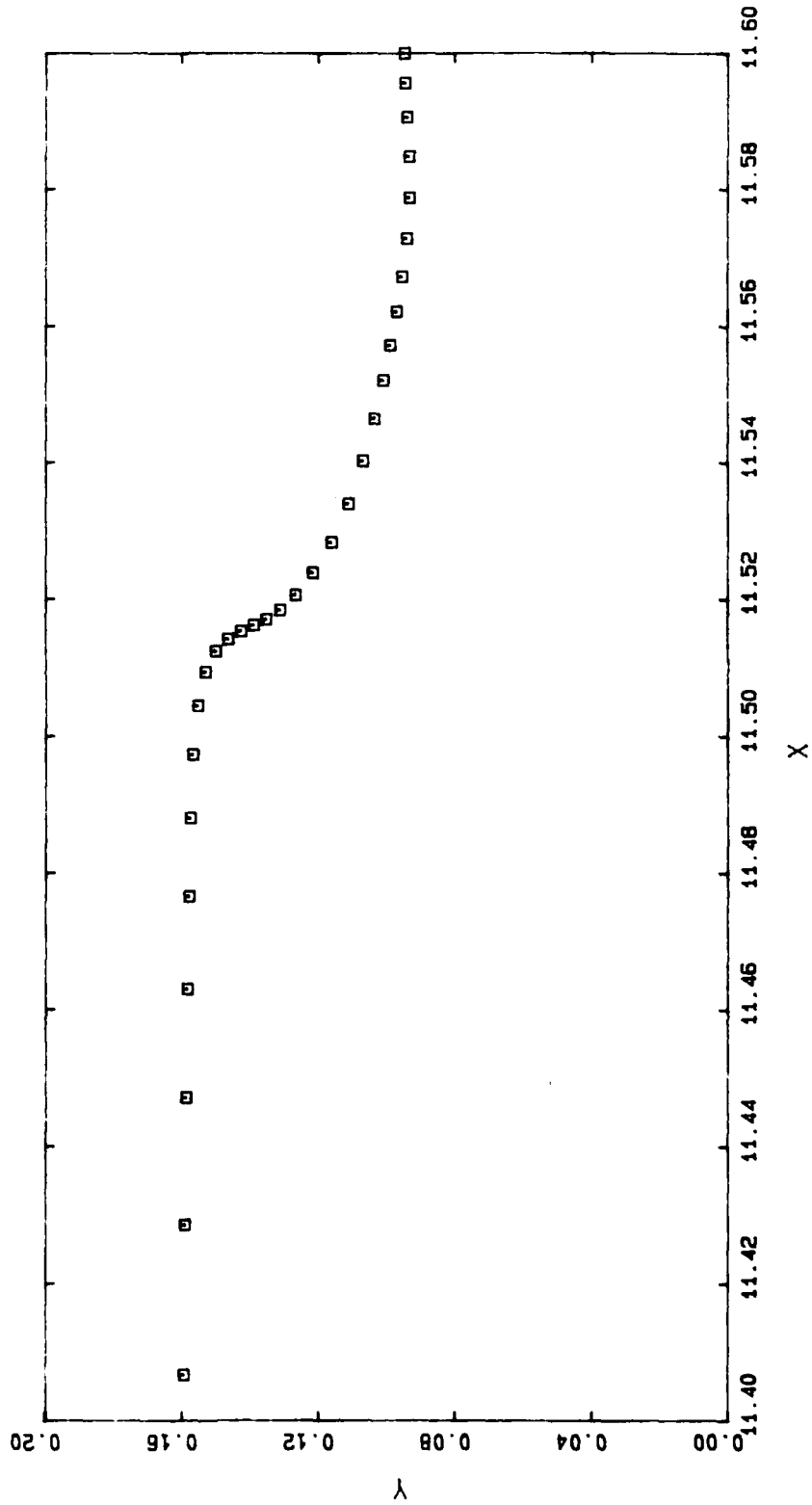

G2 3352 50.9348

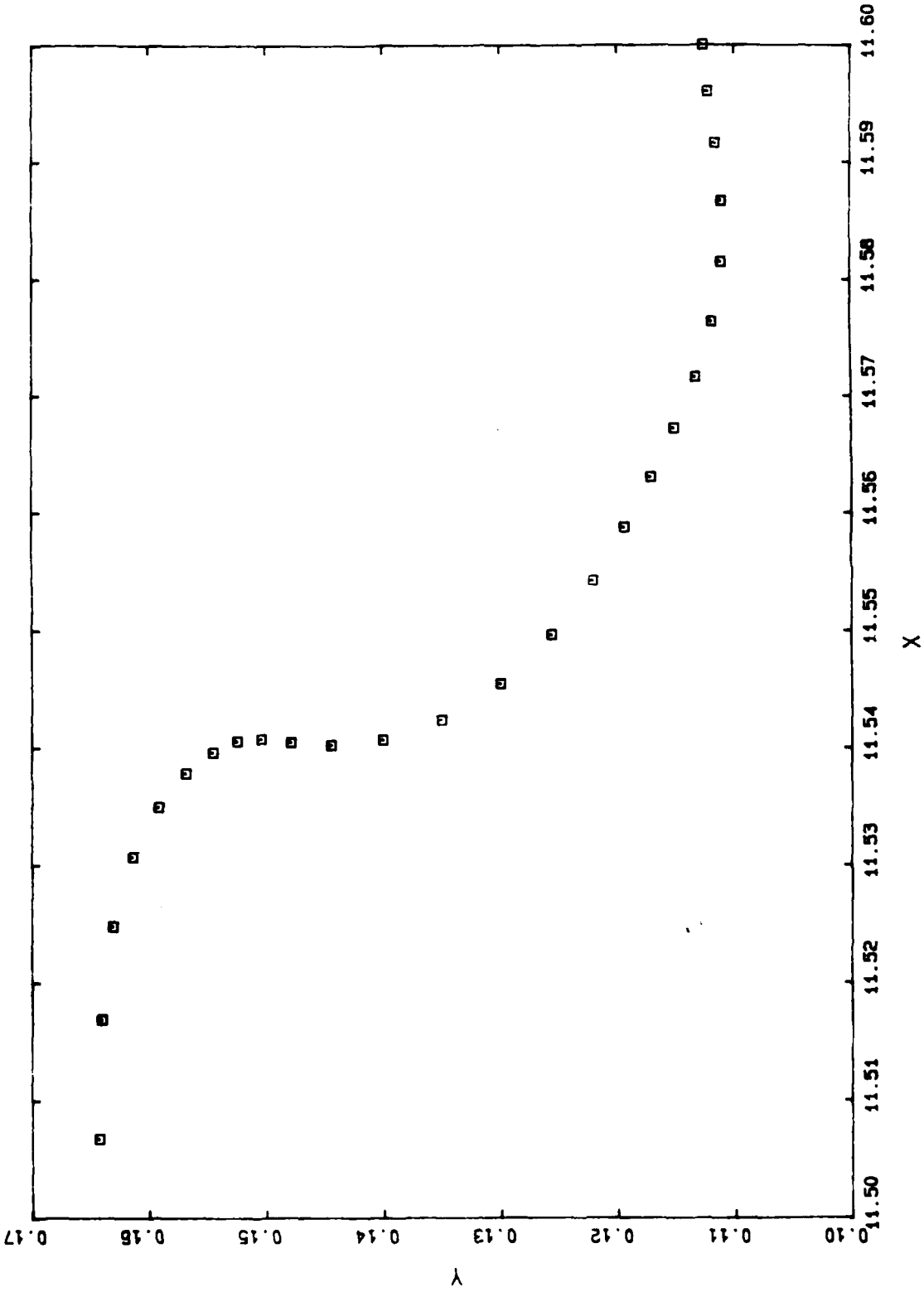

G2 3452 50.9450

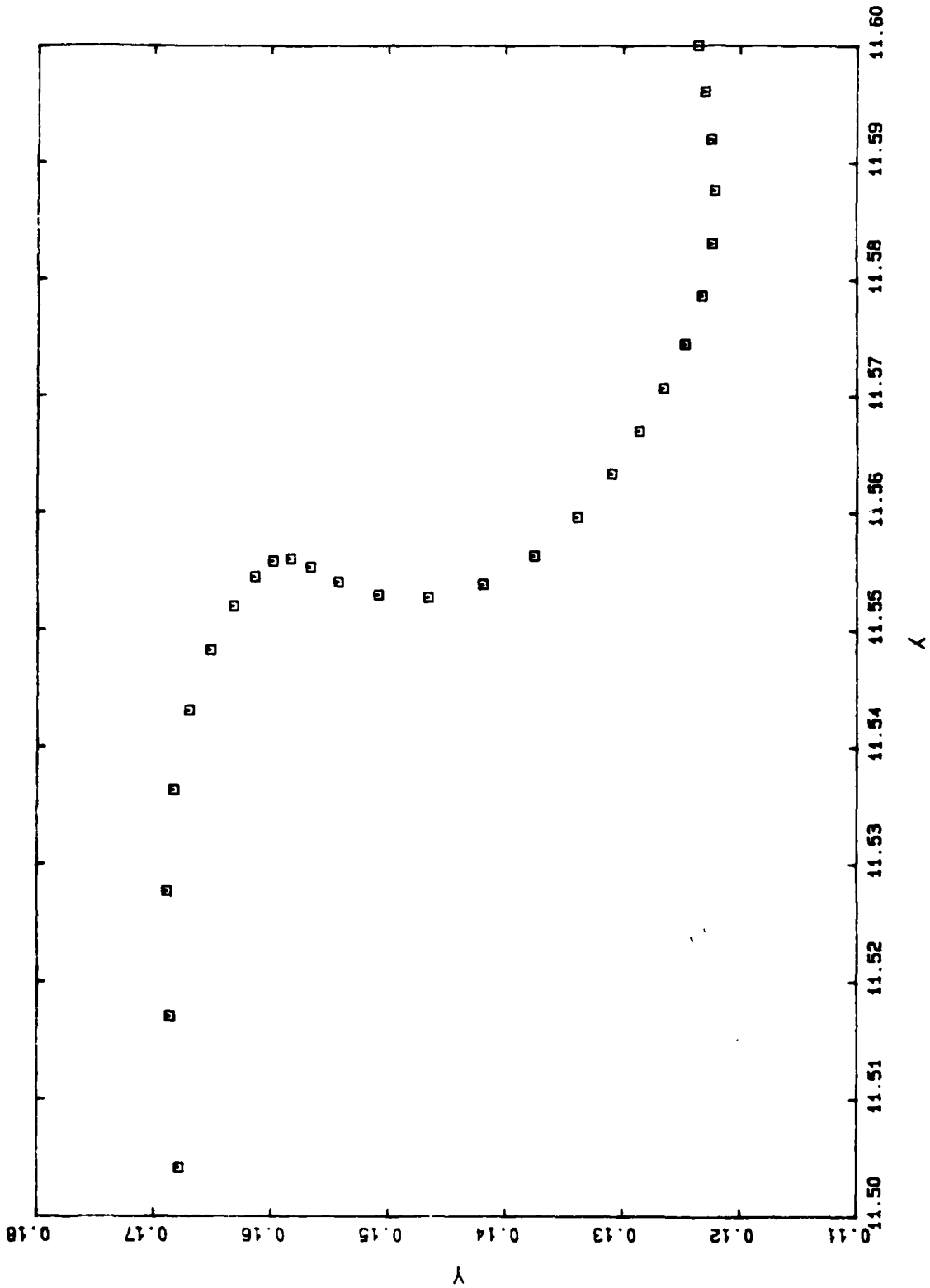

G2 3552 50.9529

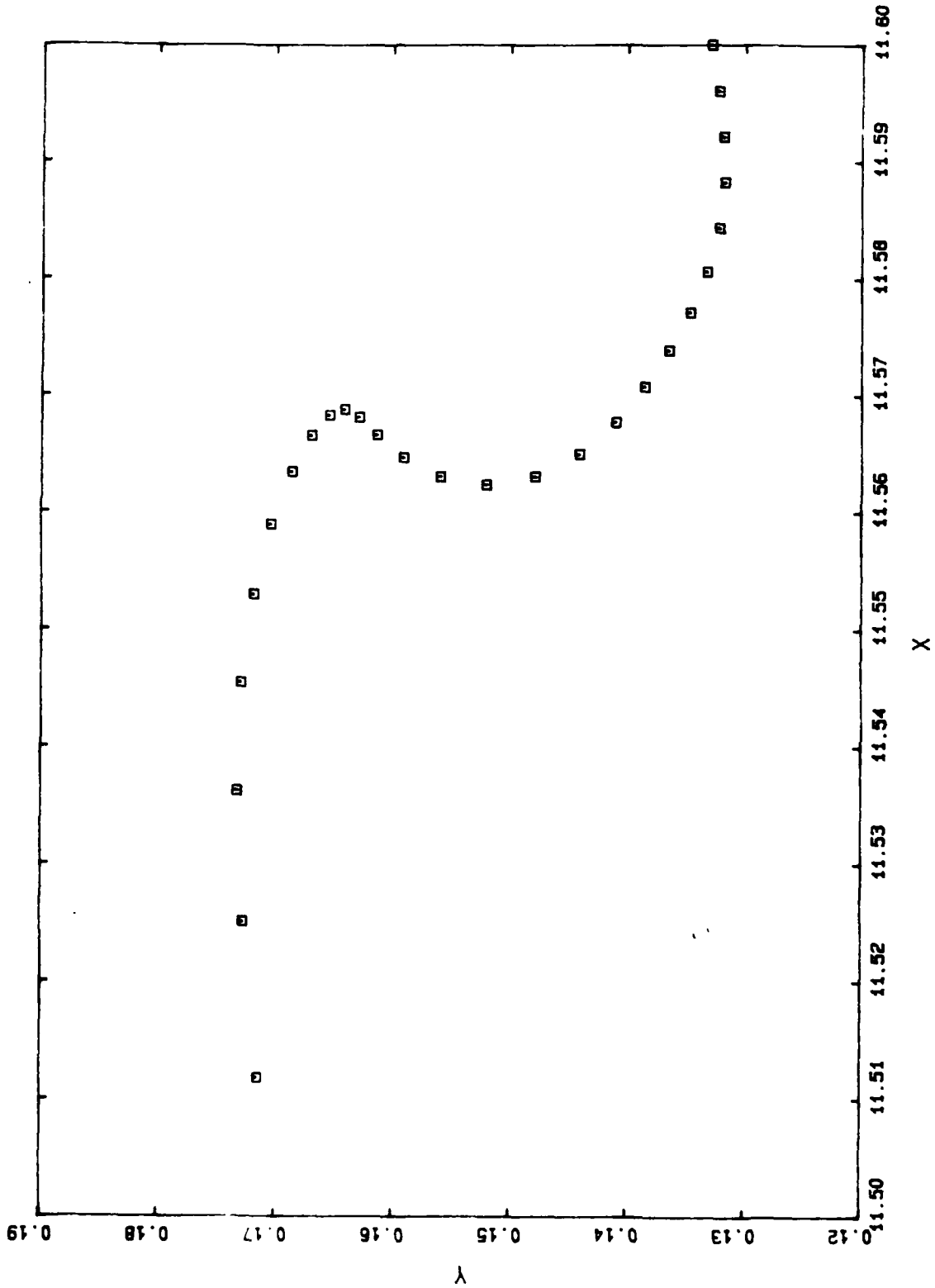

G2 3652 50.9599

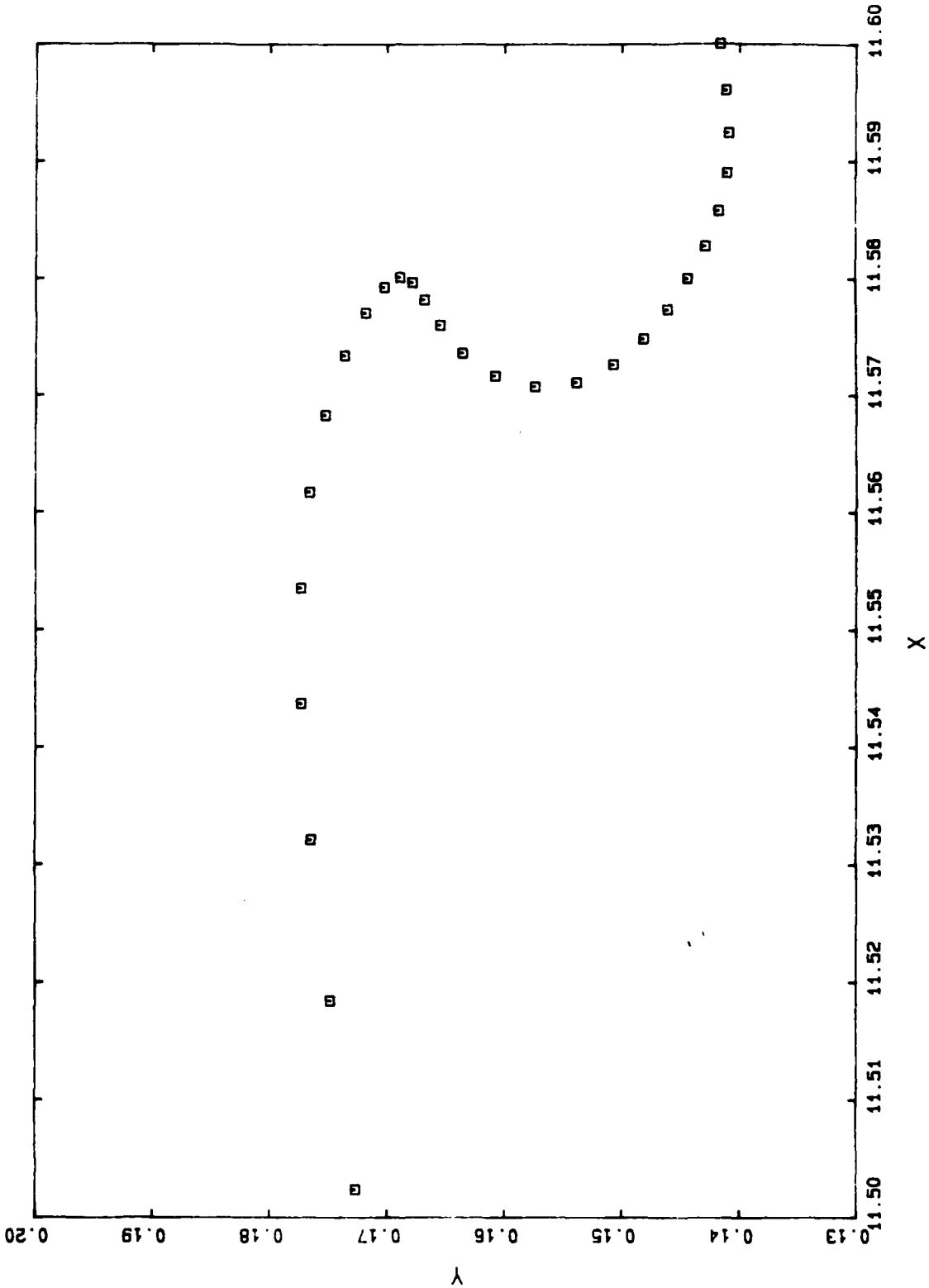

G2 3752 50.9660

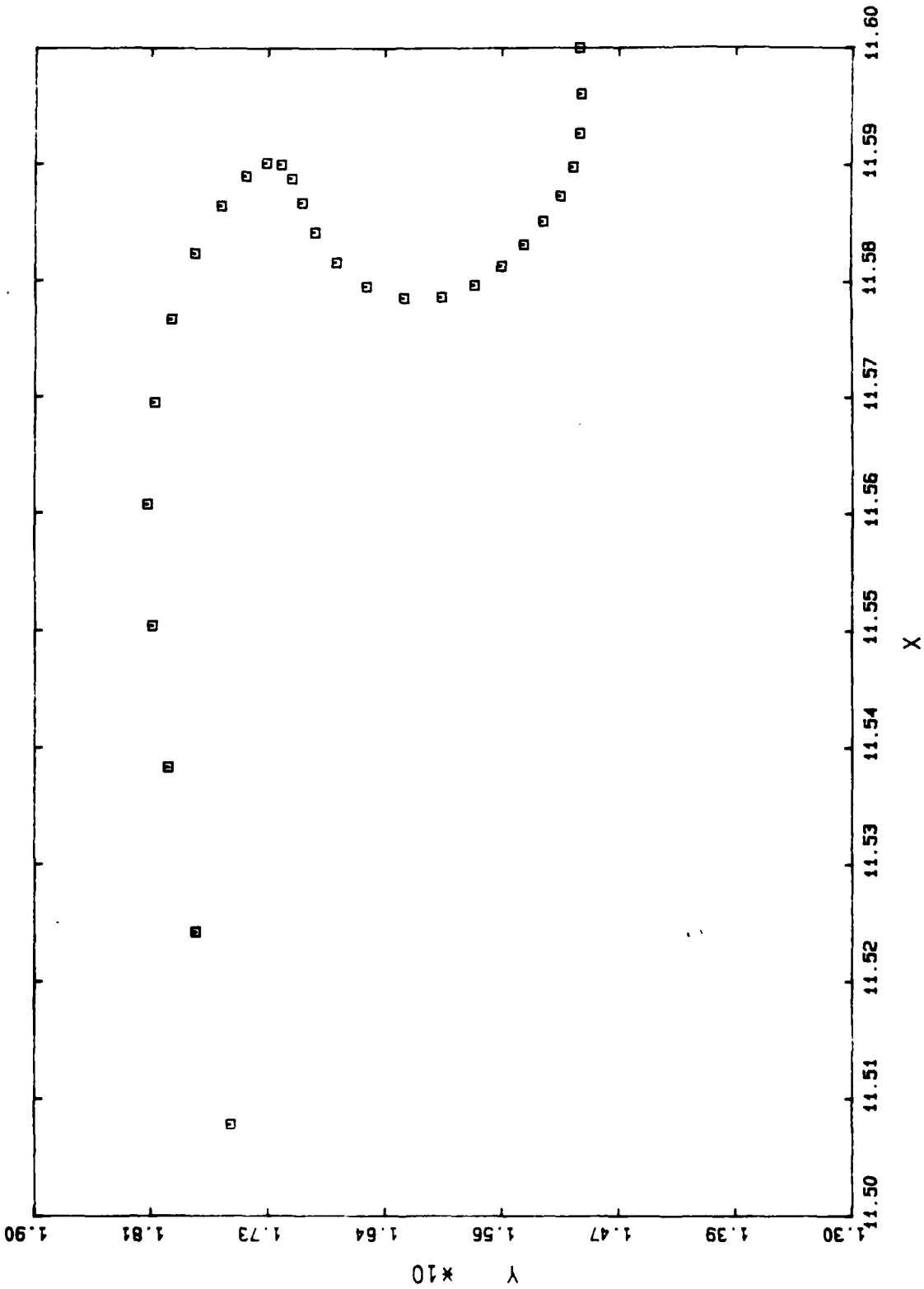

G2 3852 50.9723

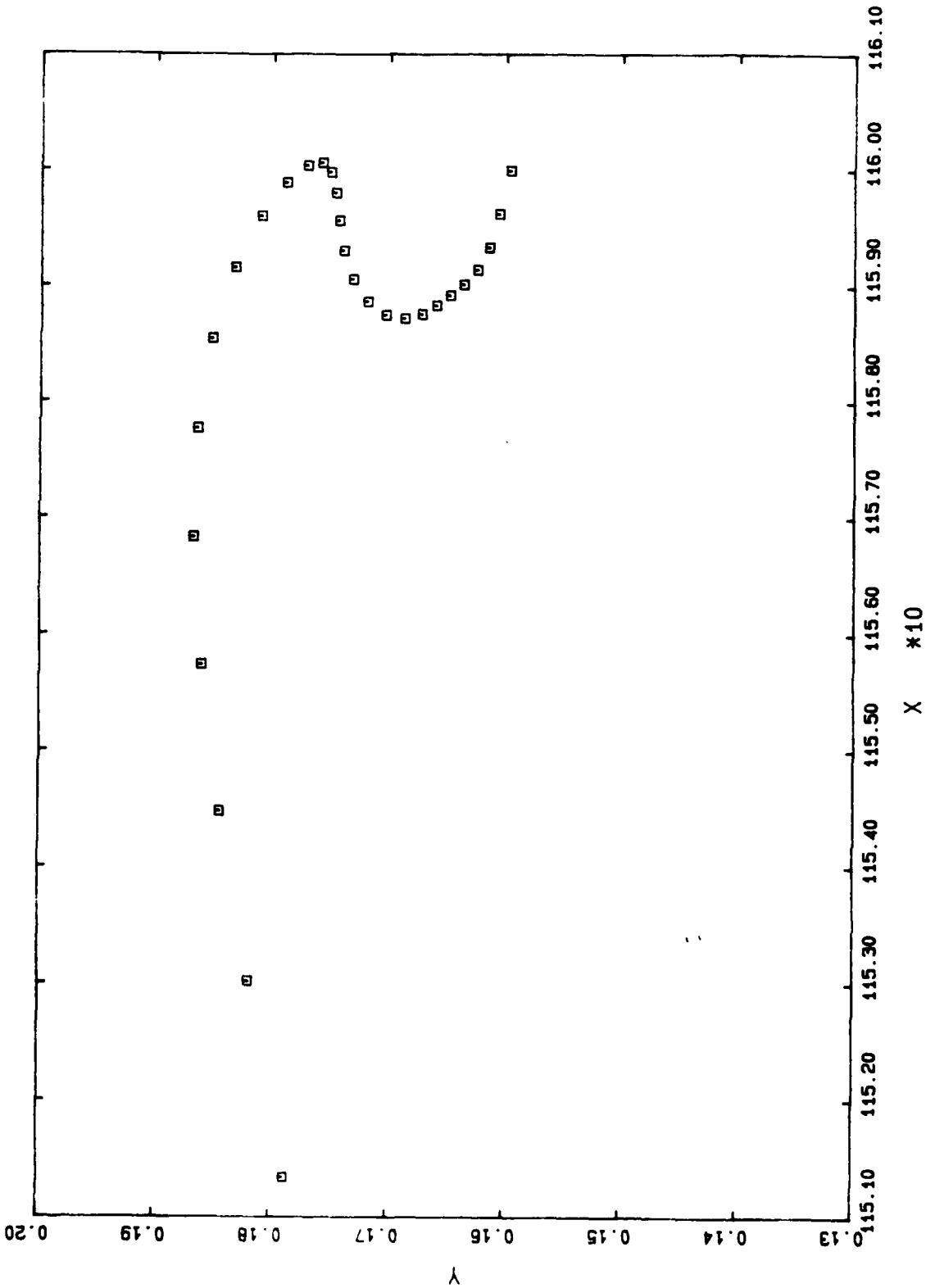

G2 3952 50.9759

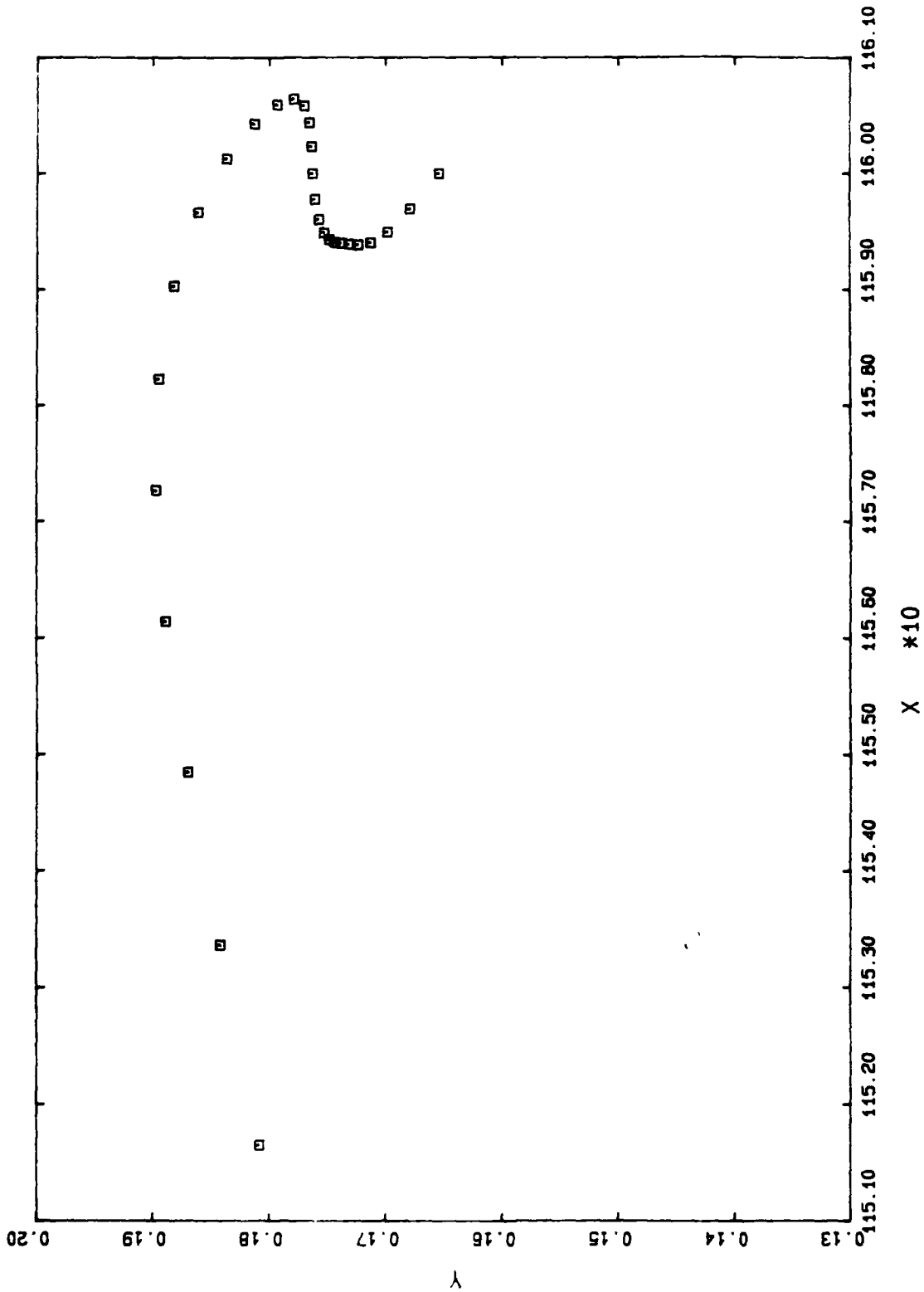

G2 4052 50.9770

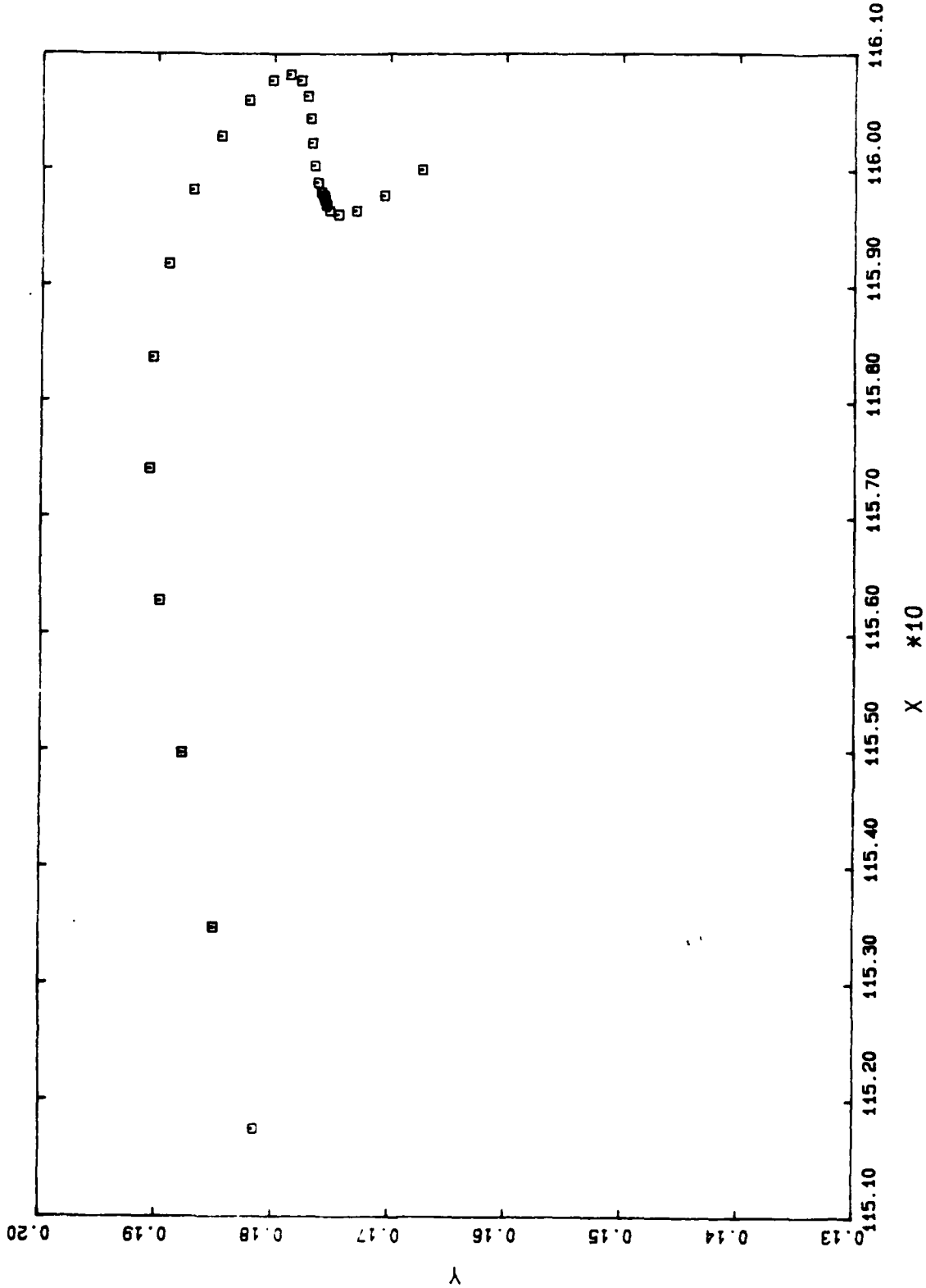

G3 3293 50.9256

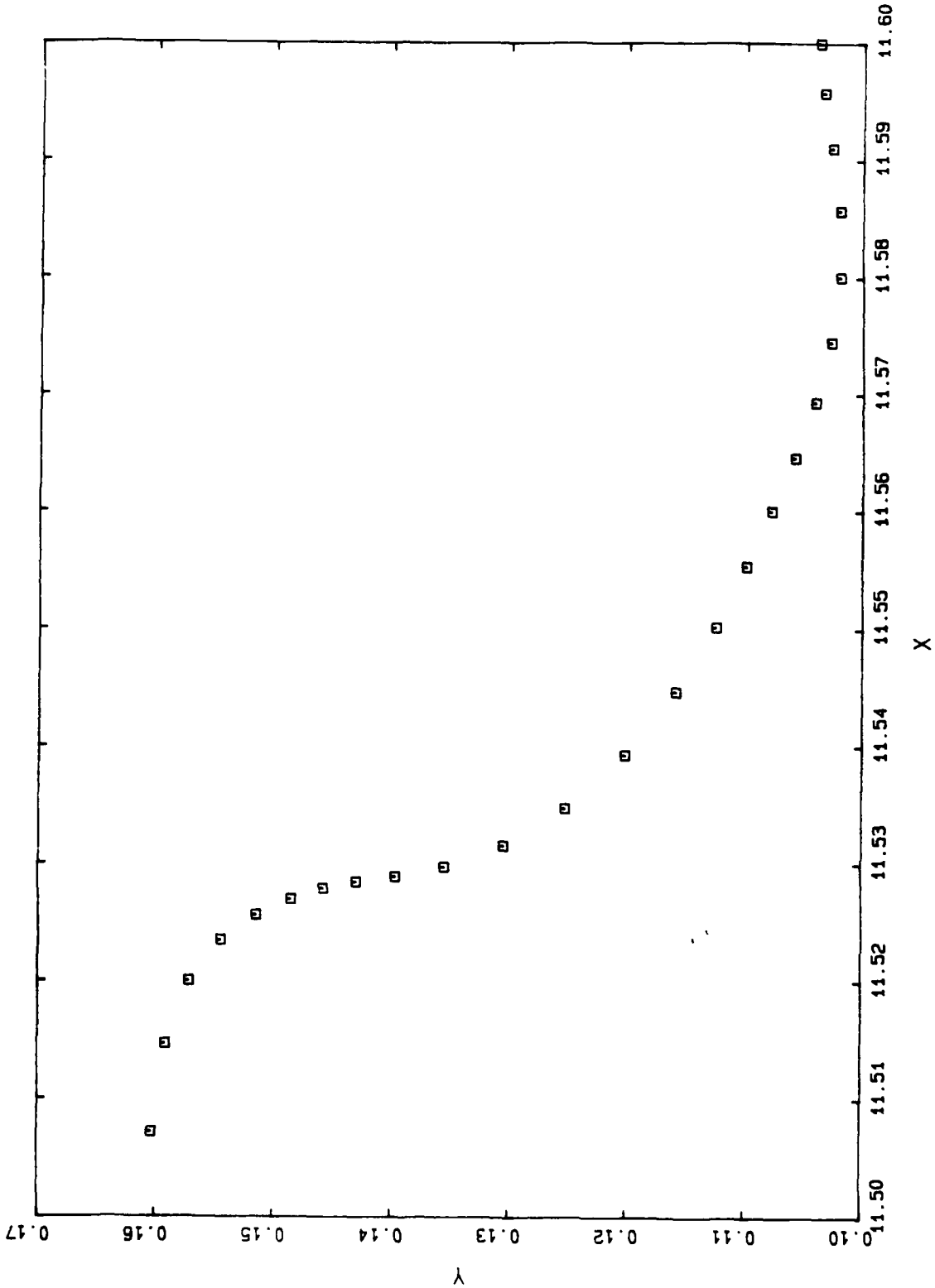

G3 3393 50.9397

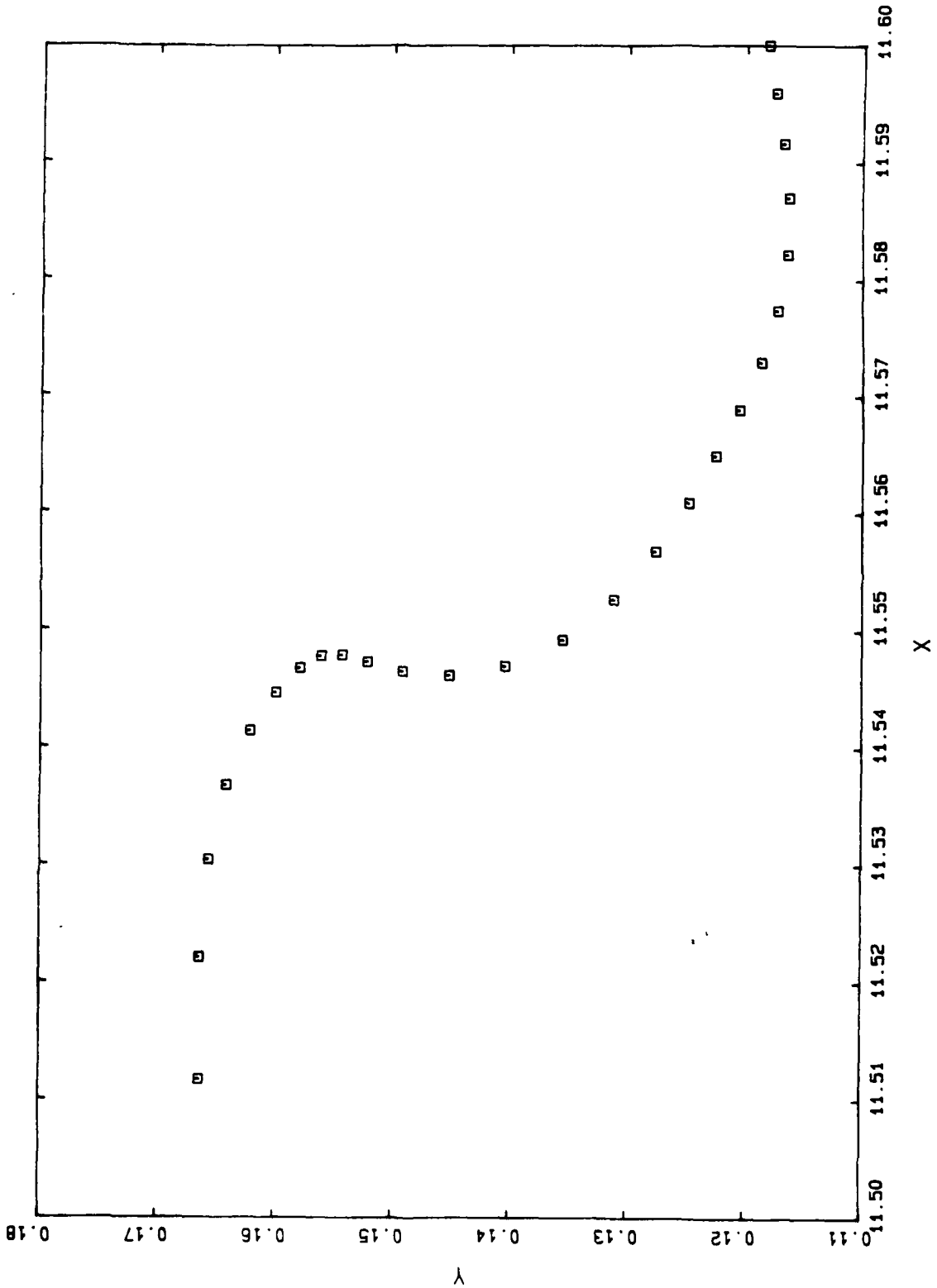

G3 3493 50.9488

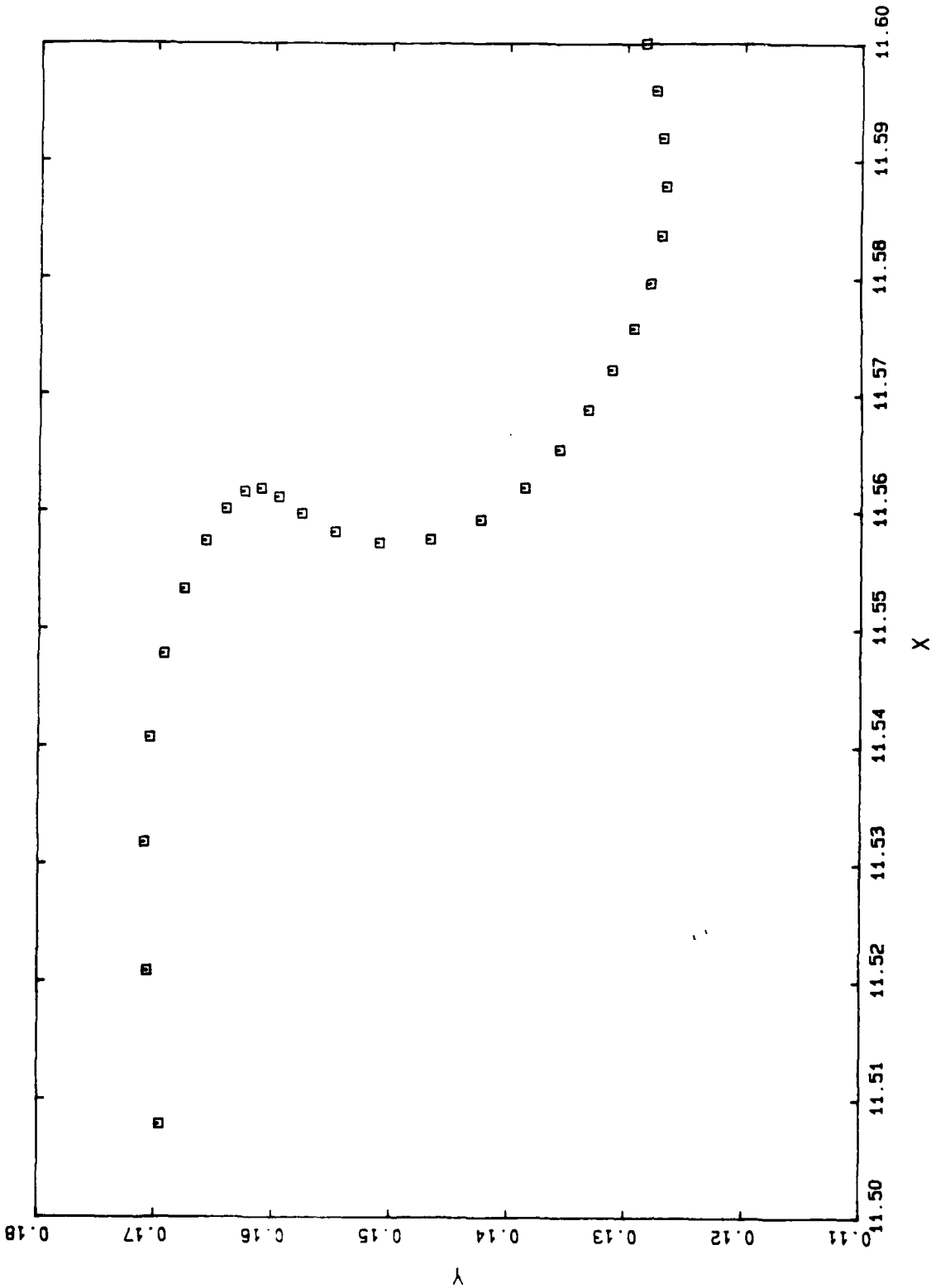

G3 3593 50.9566

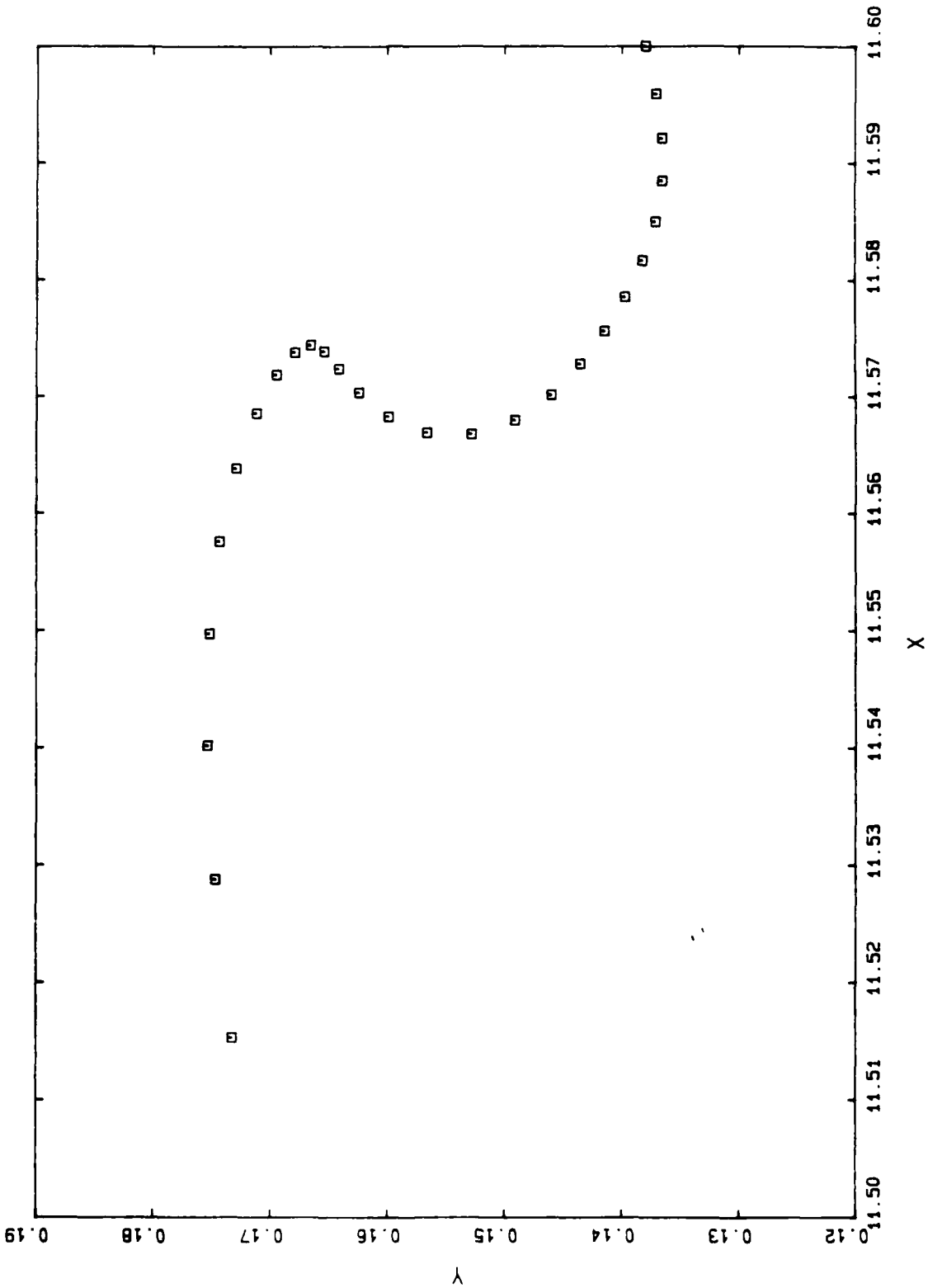

G3 3693 50.9631

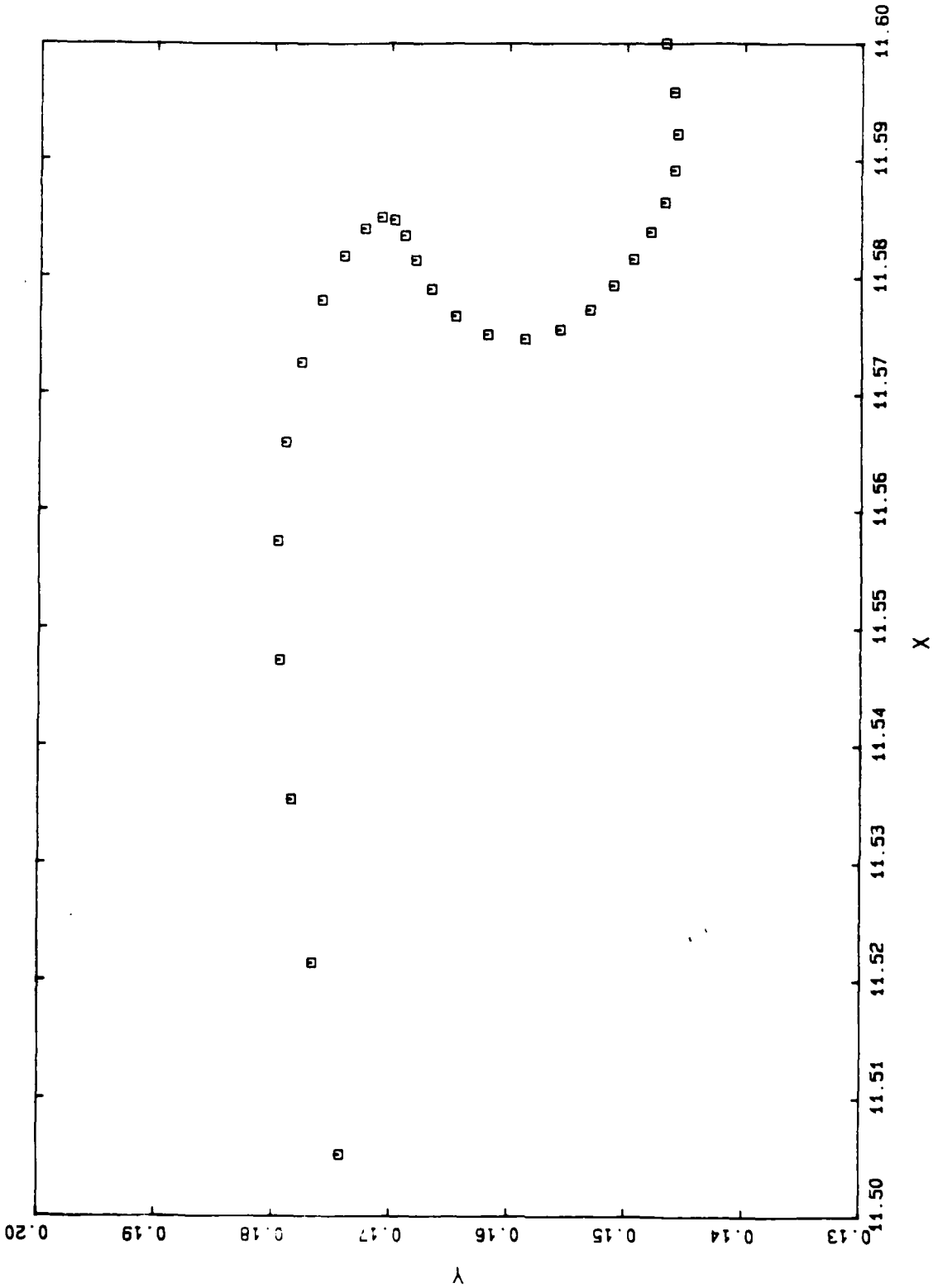

G3 3793 50.9694

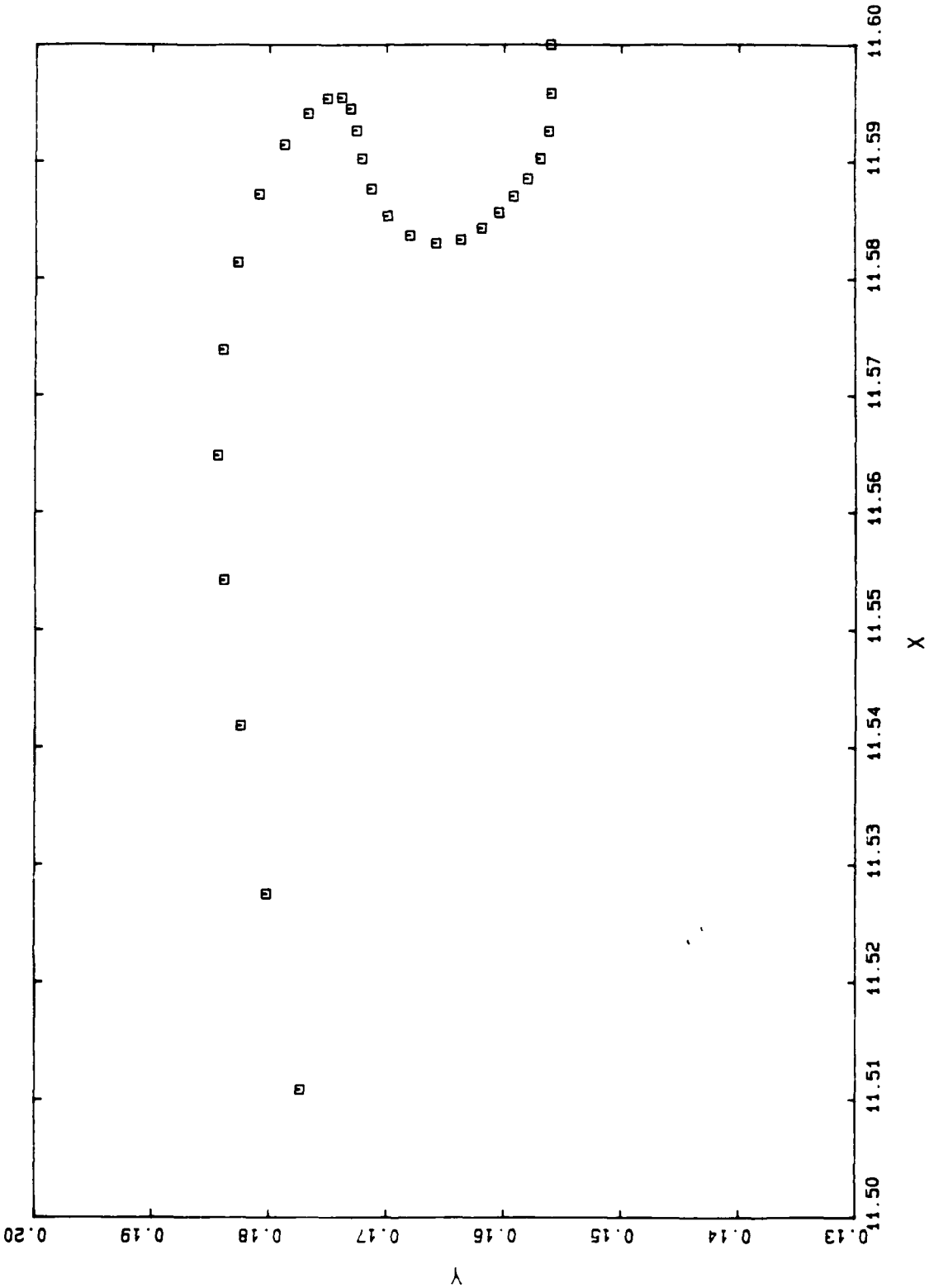

G3 3893 50.9746

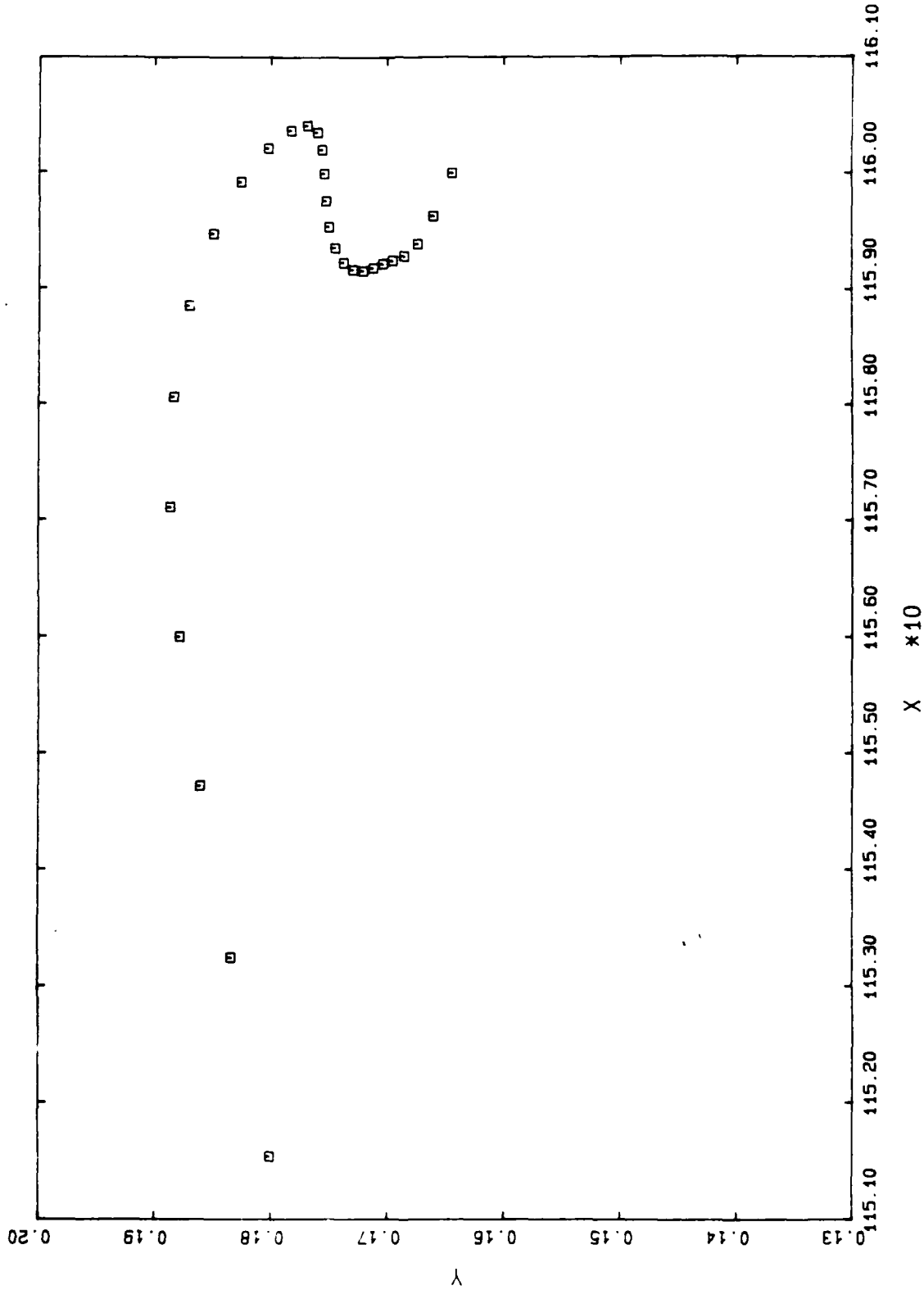

G3 3993 50.9763

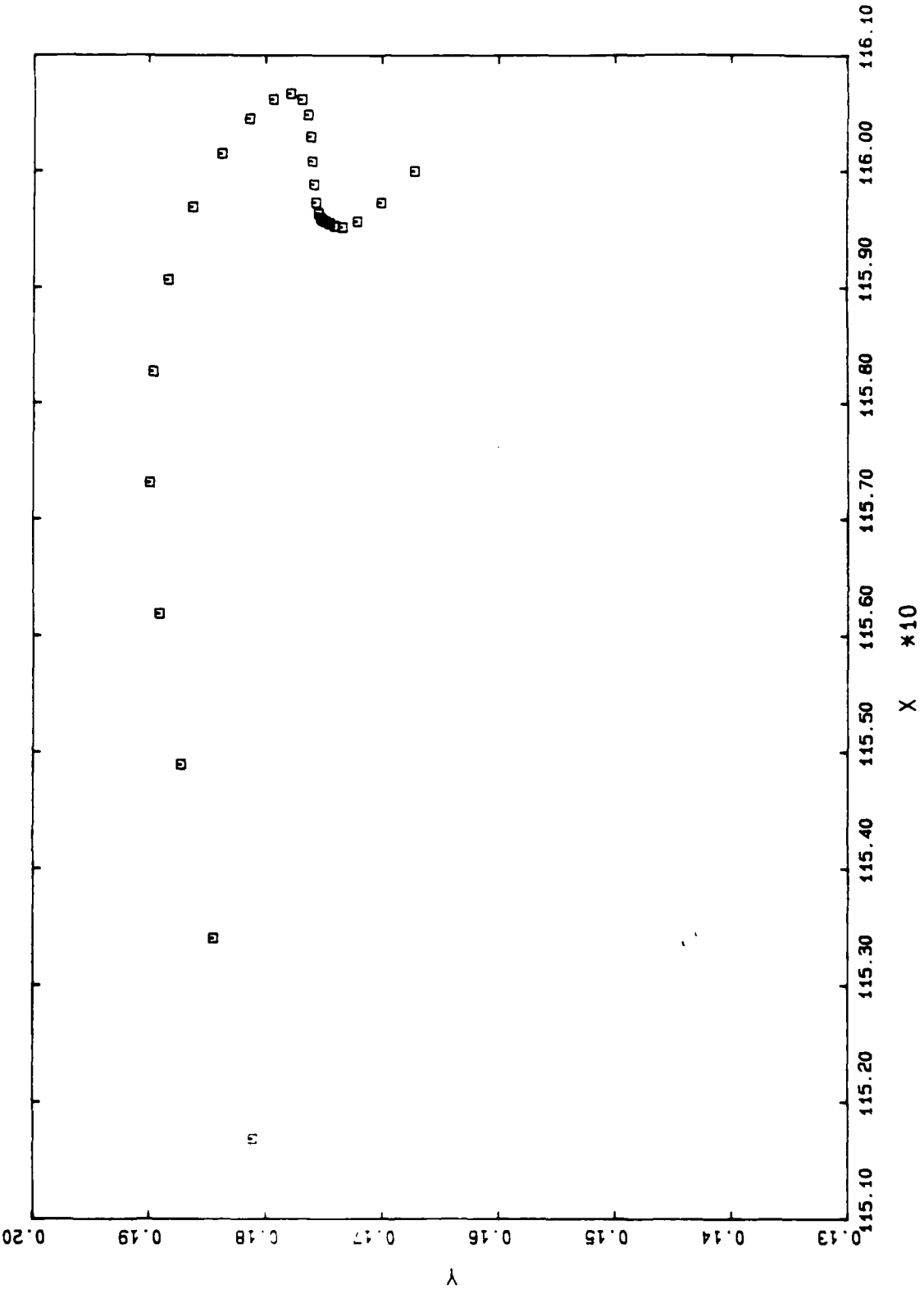

G3 4093 50.9773

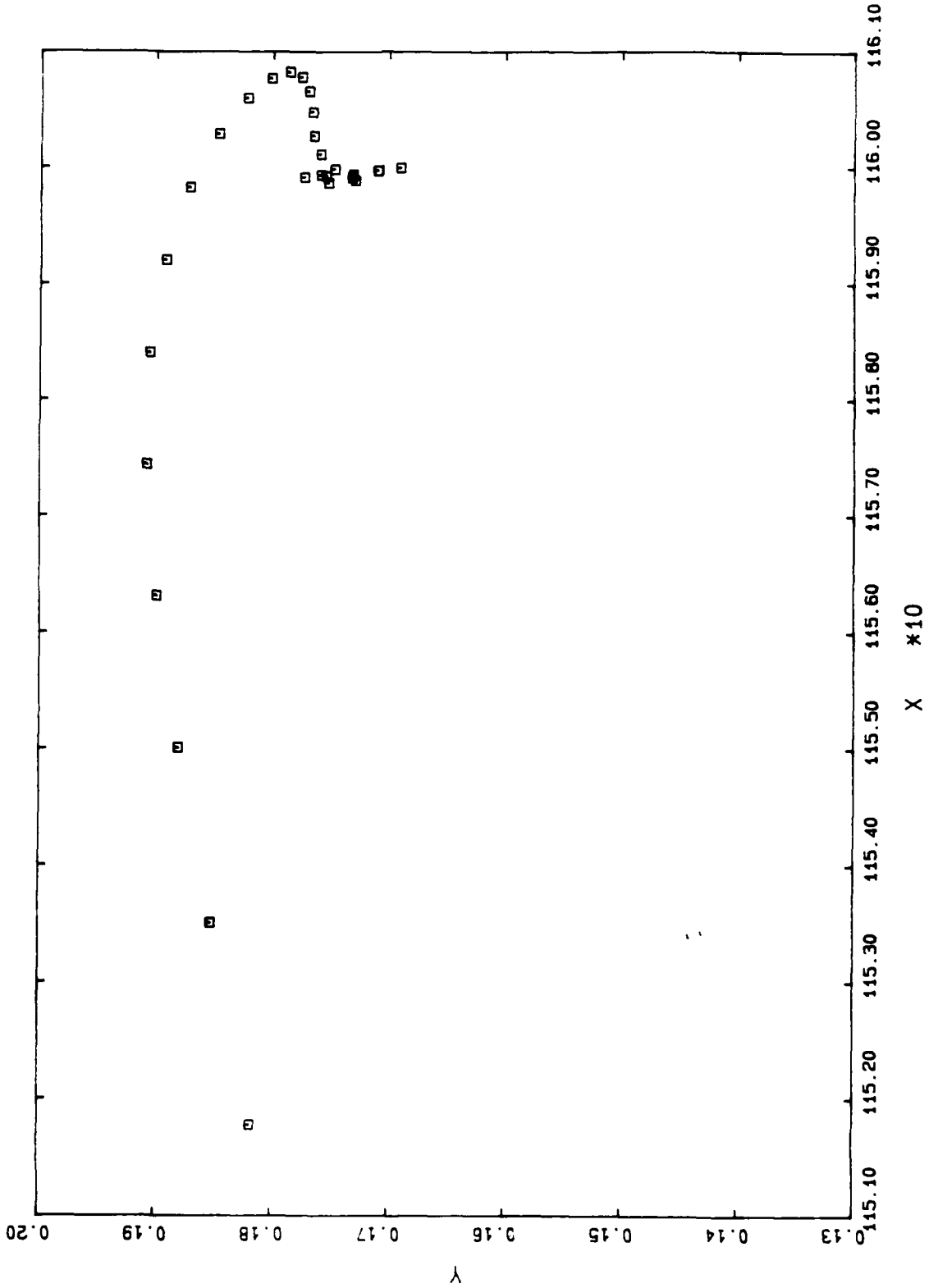

G4 3139 50.8691

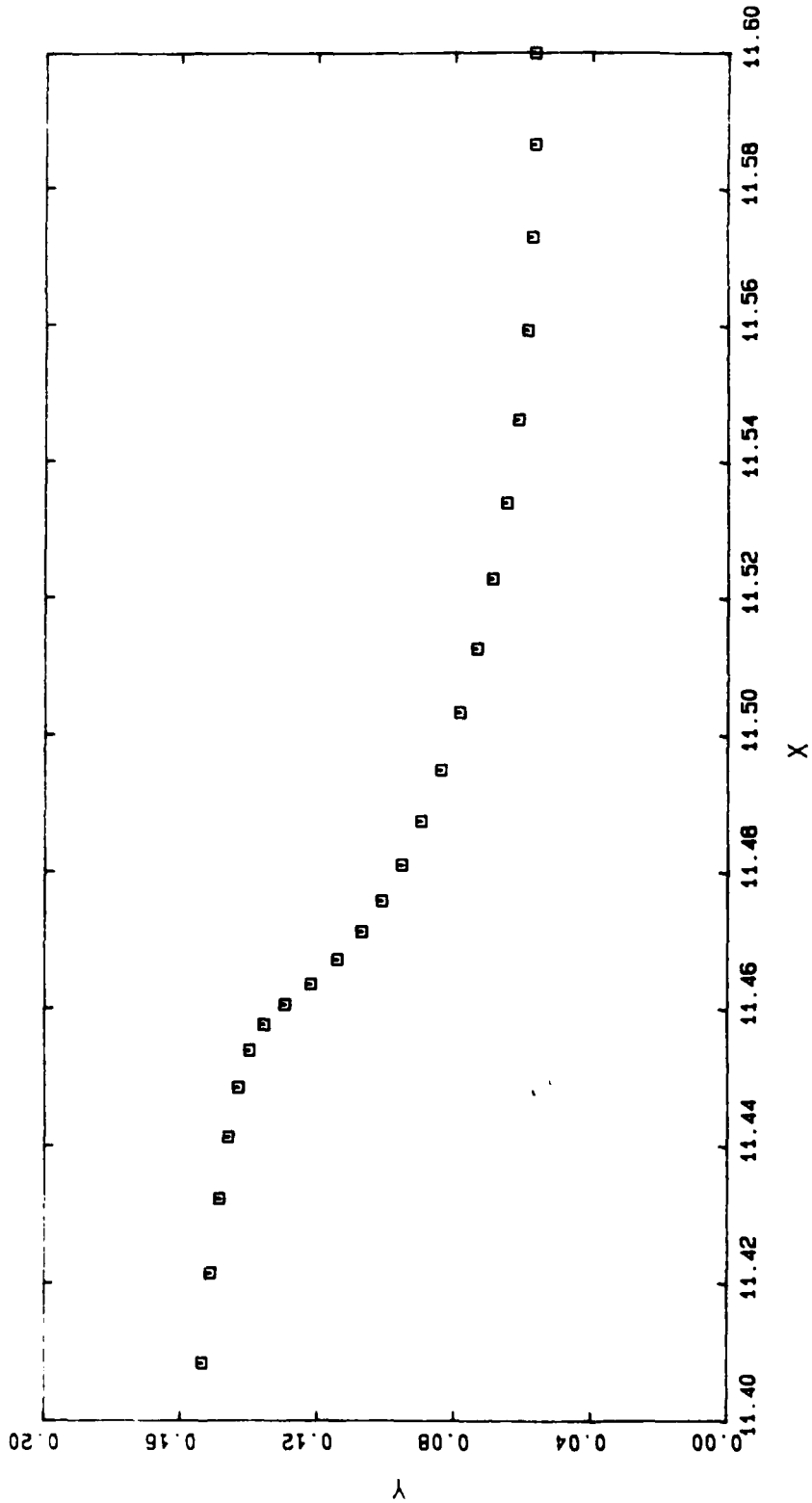

G4 3239 50.9124

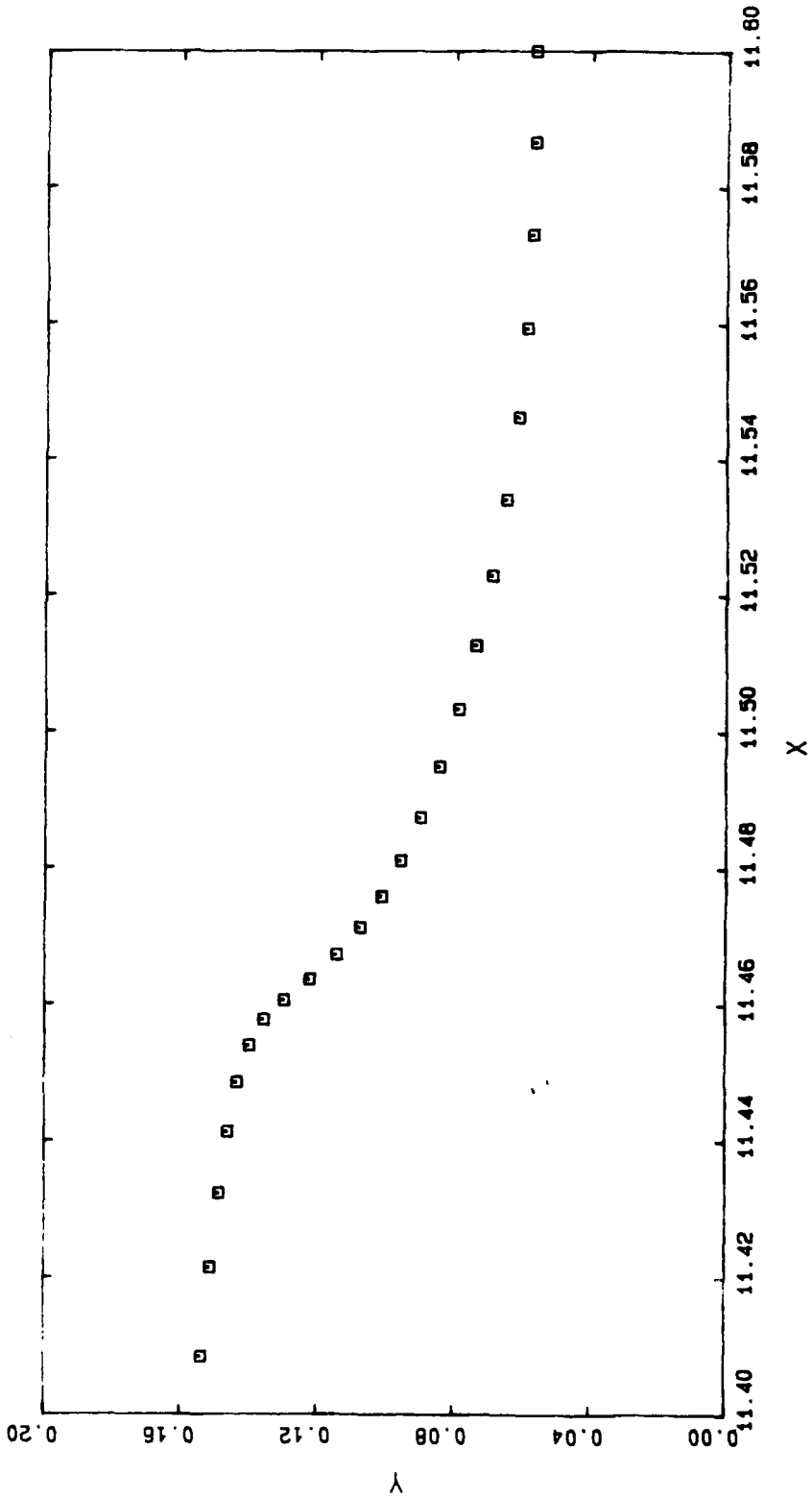

G4 3339 50.9344

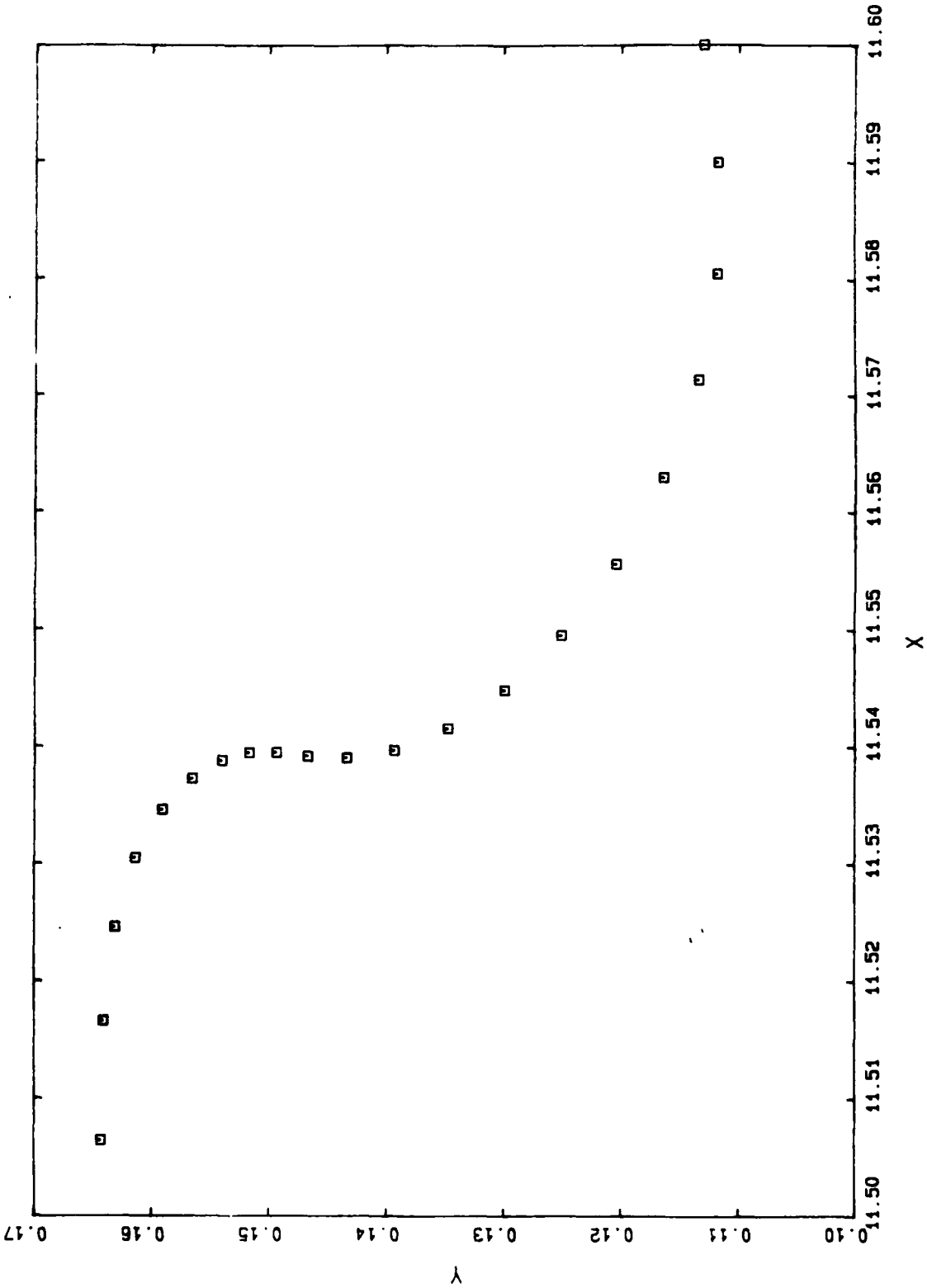

G4 3439 50.9460

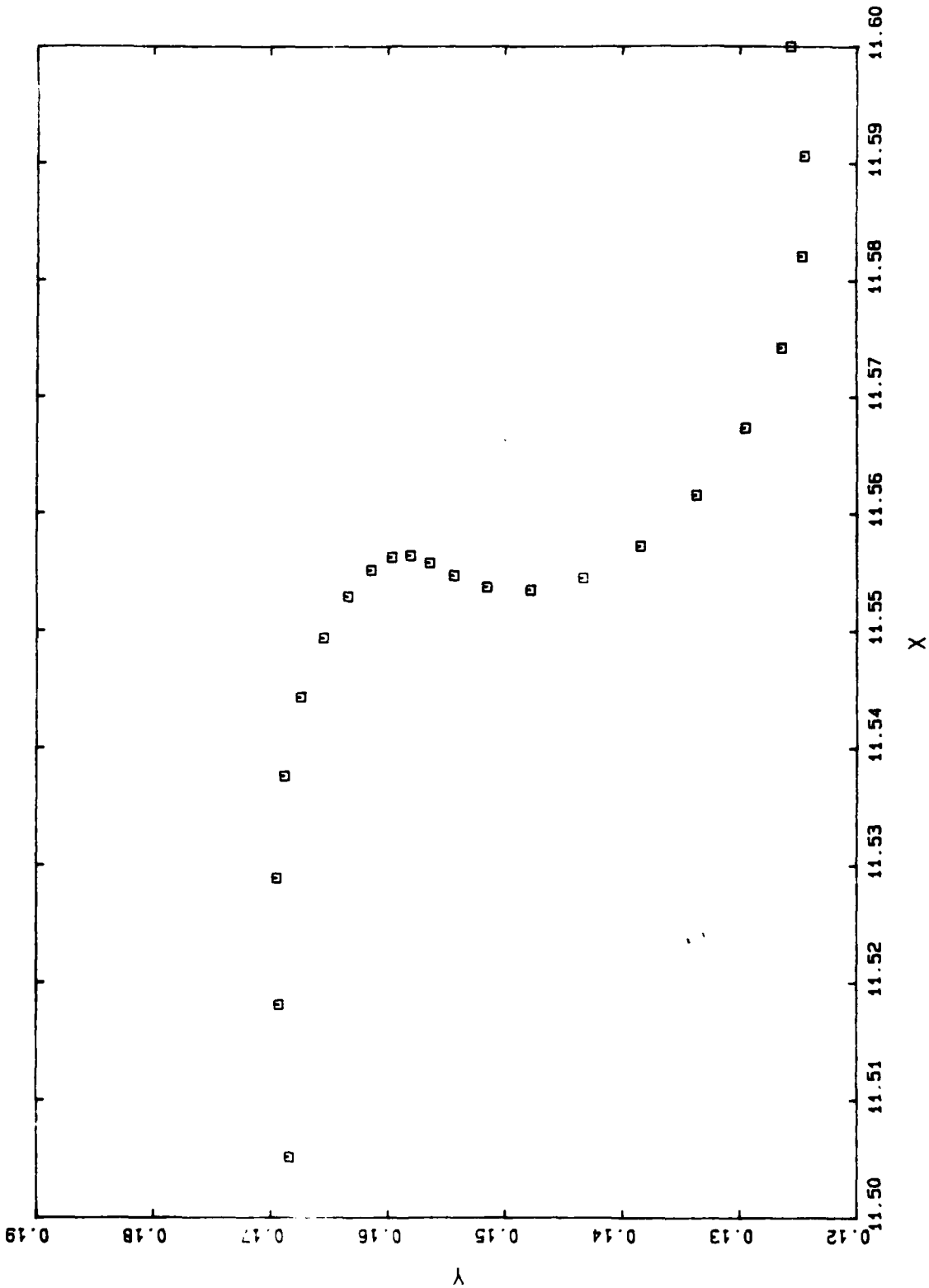

G4 3539 50.9543

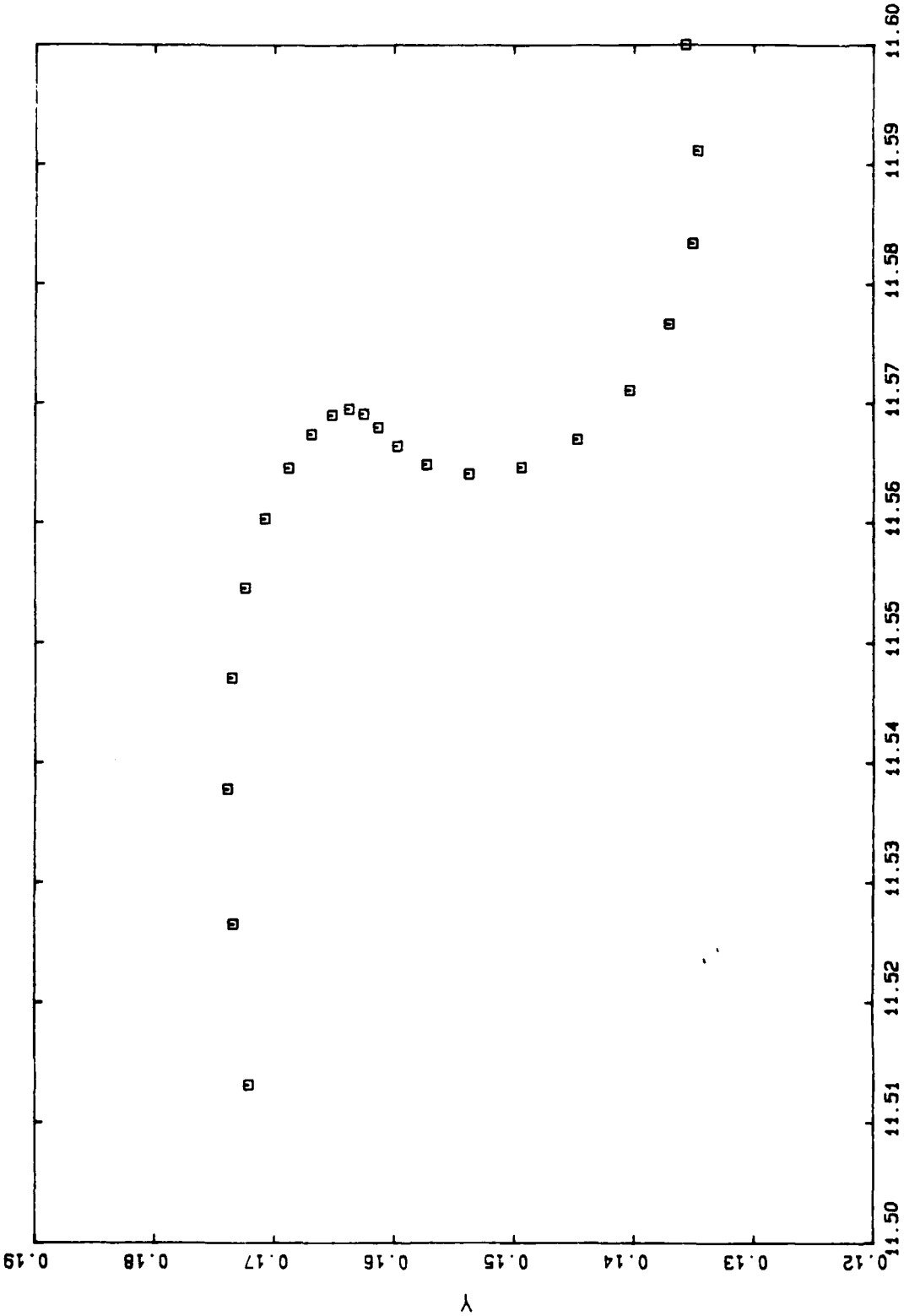

G4 3639 50.9609

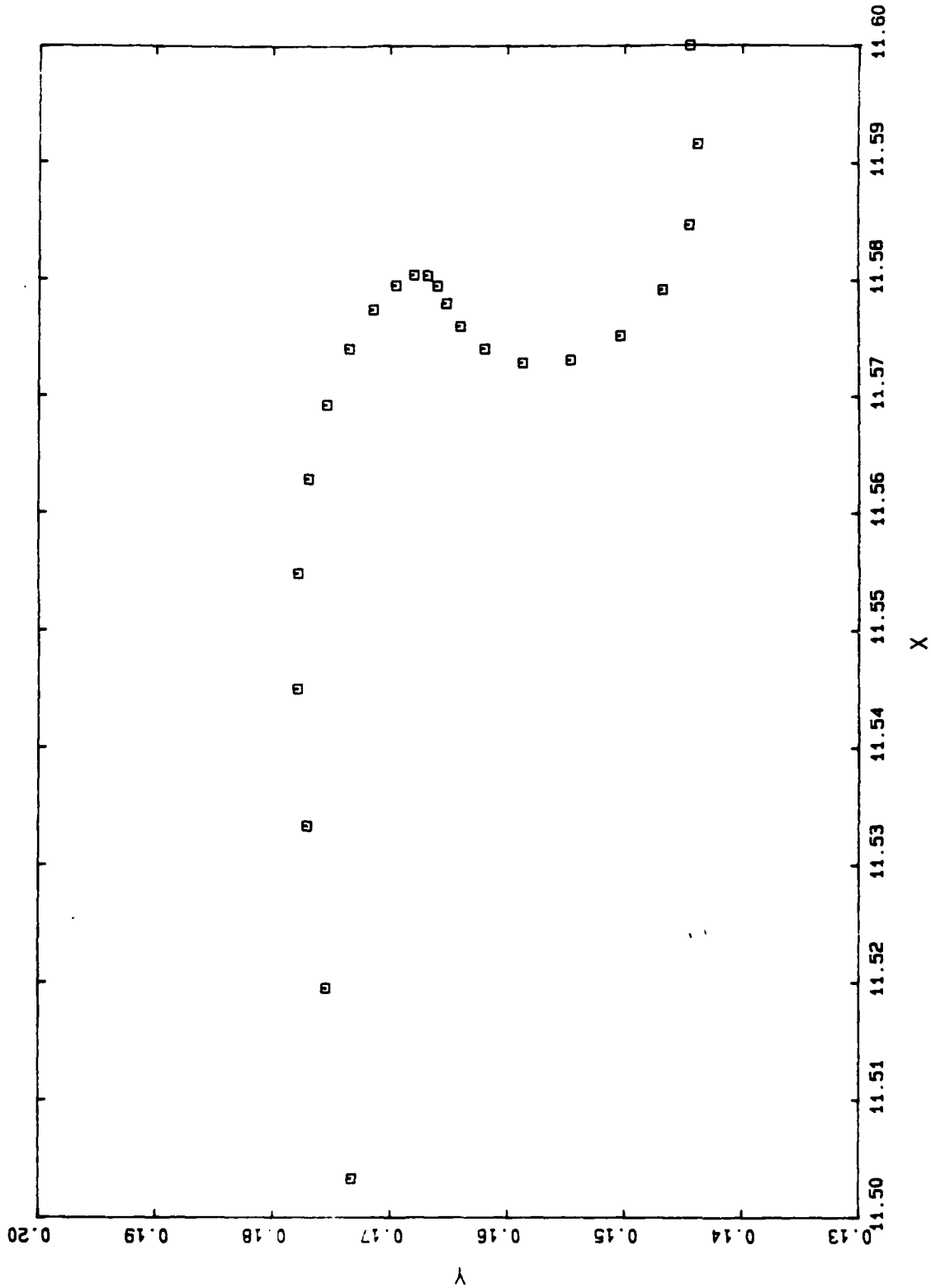

G4 3739 50.9667

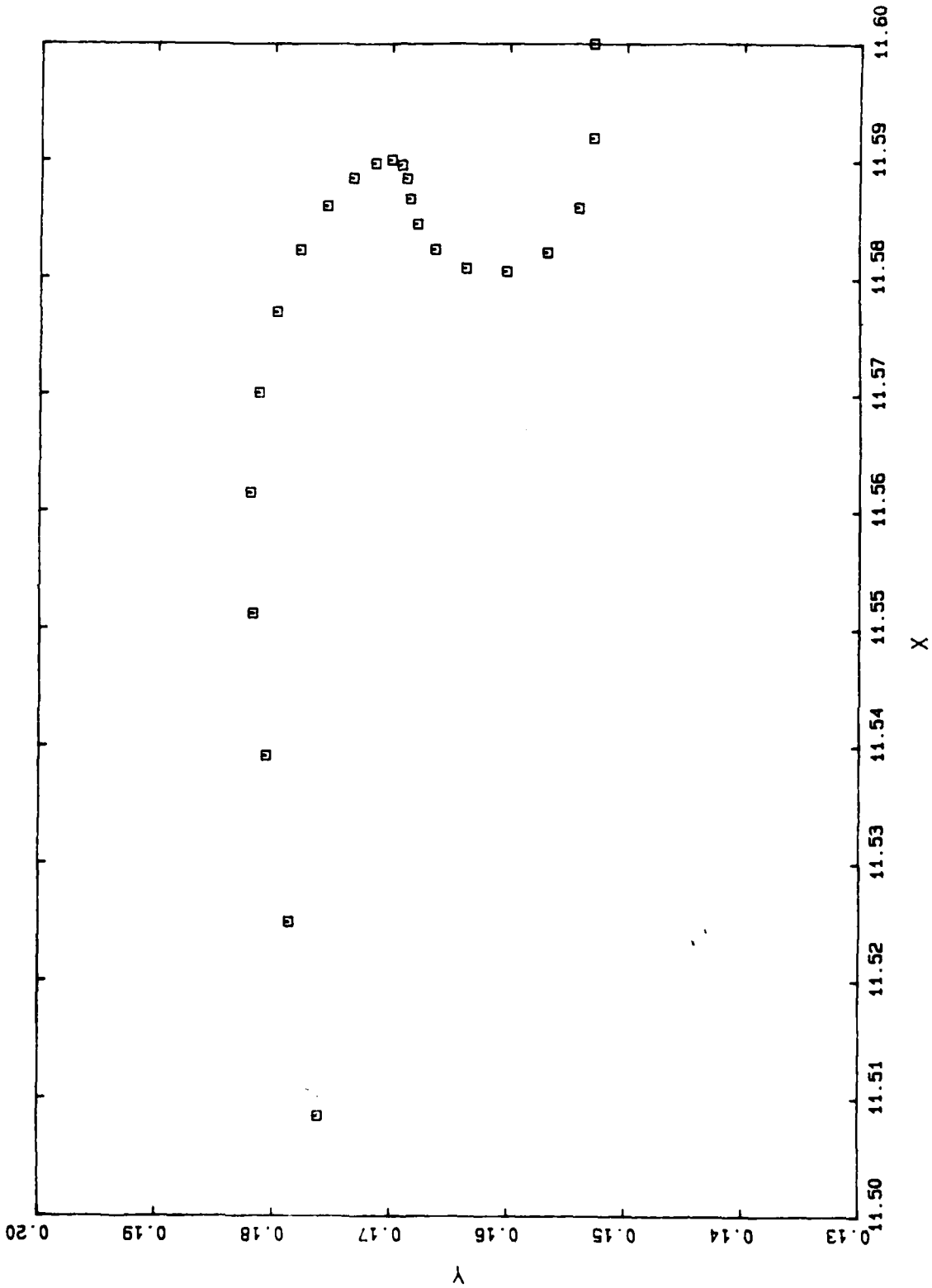

G4 3839 50.9720

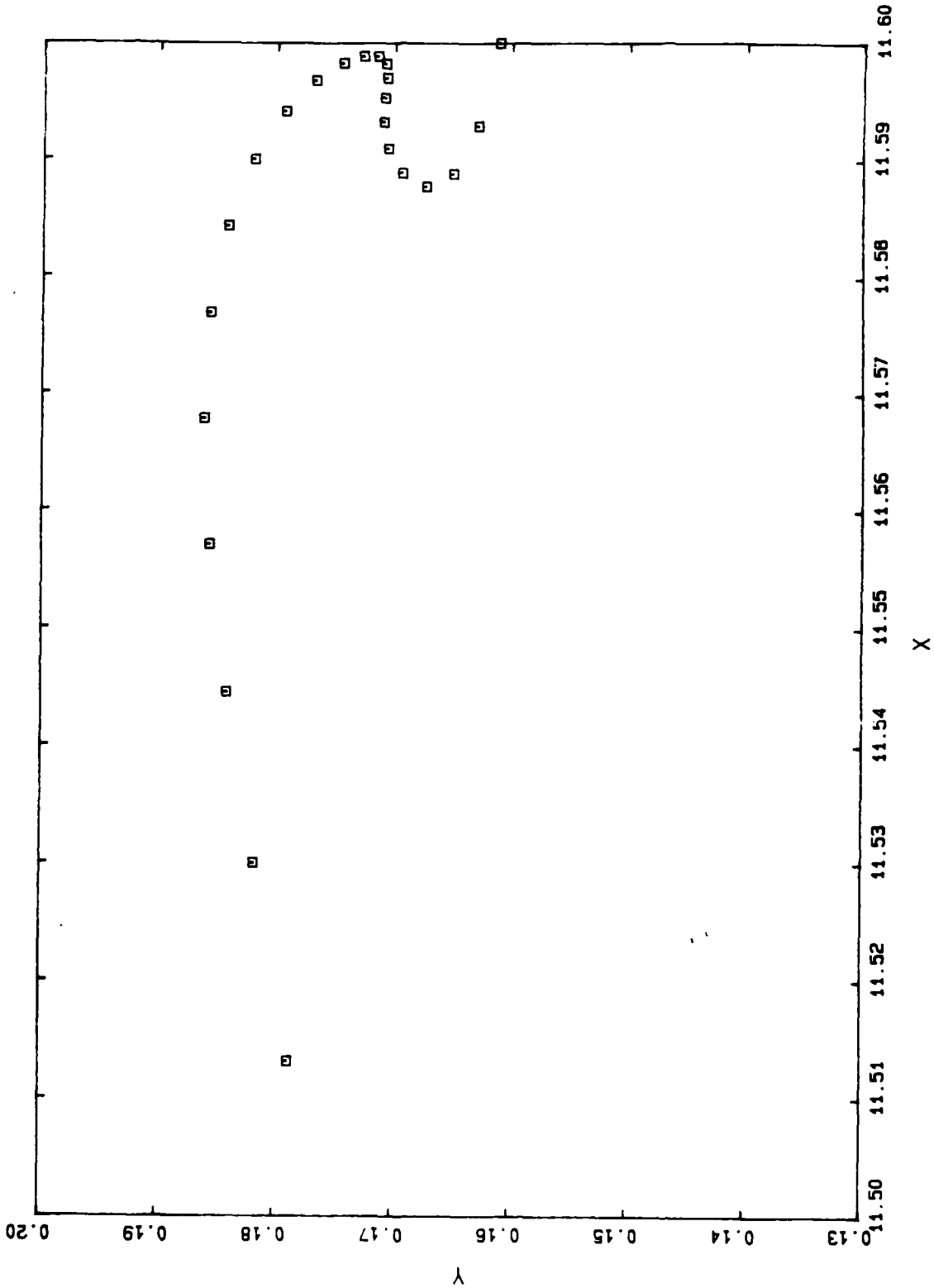

G4 3849 50.9724

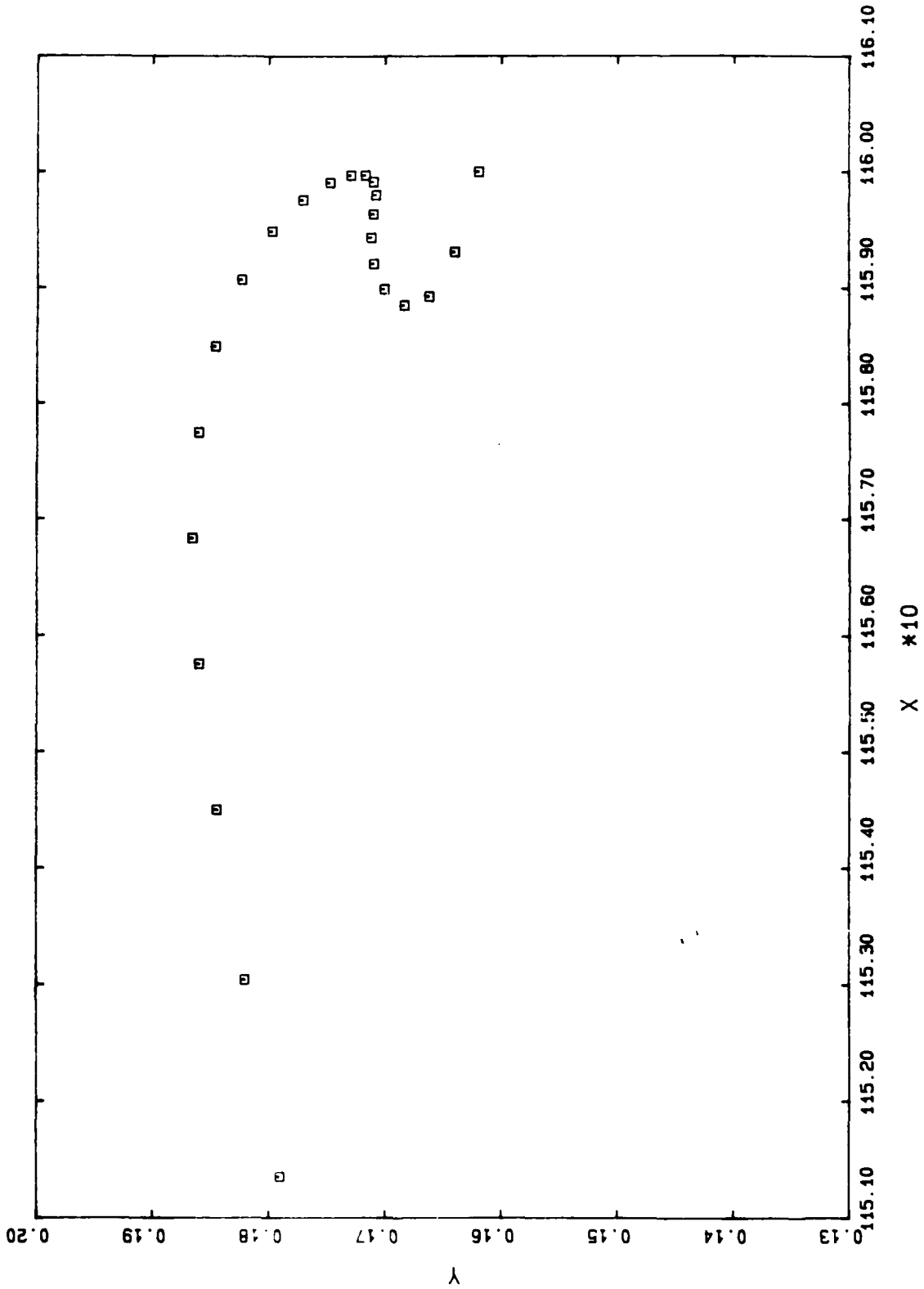

G4 3859 50.9729

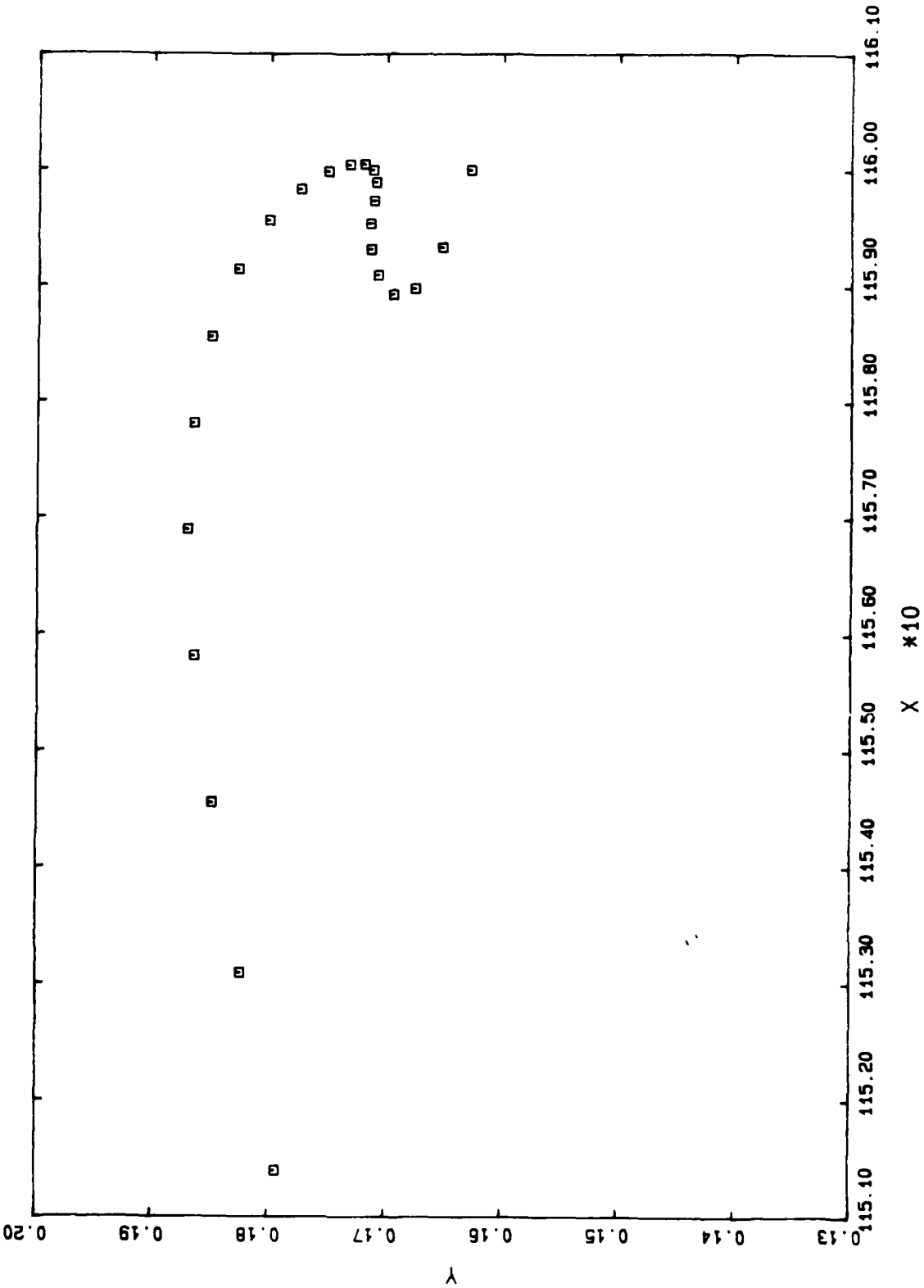

G4 3869 50.9734

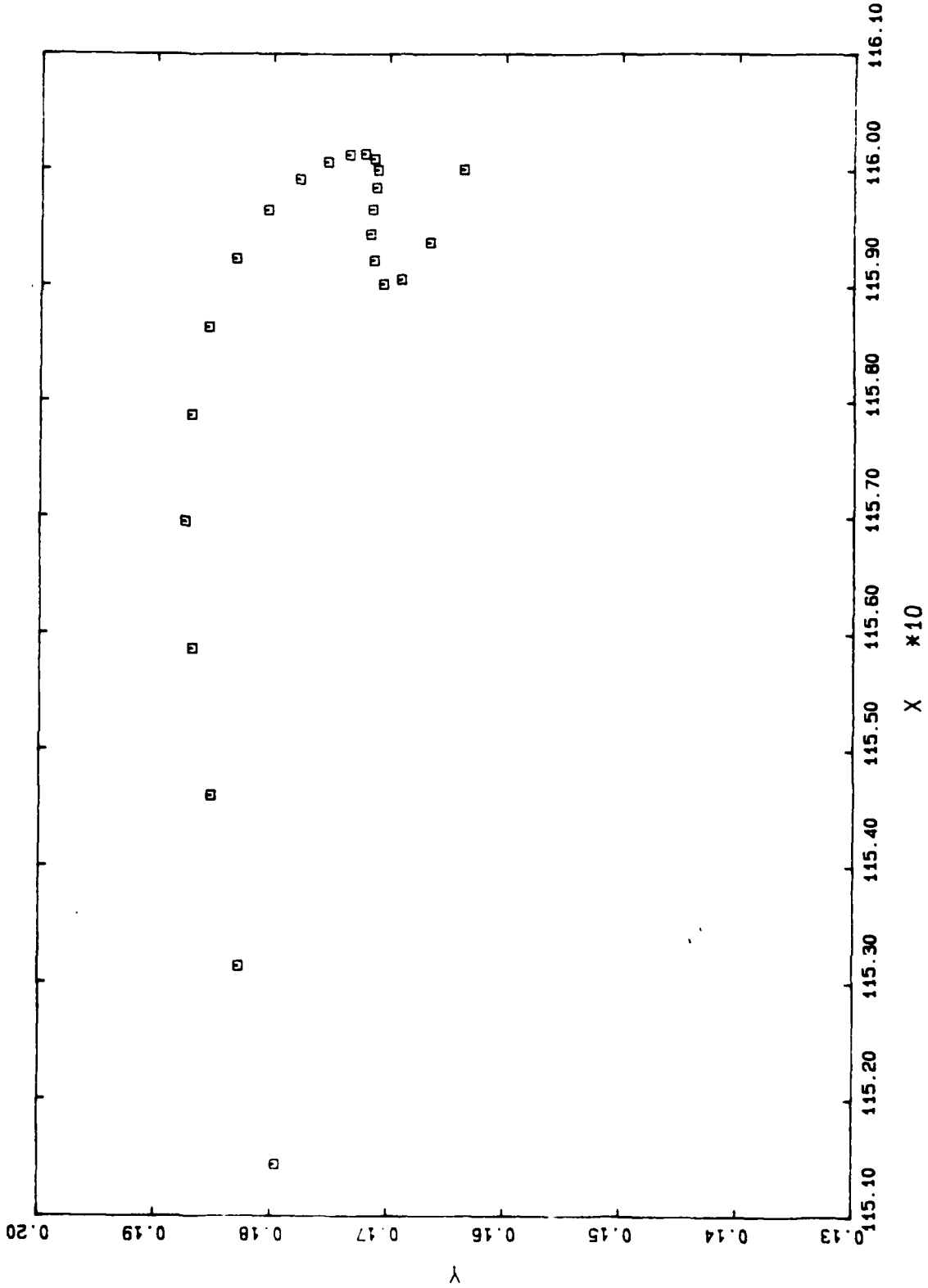

G4 3879 50.9738

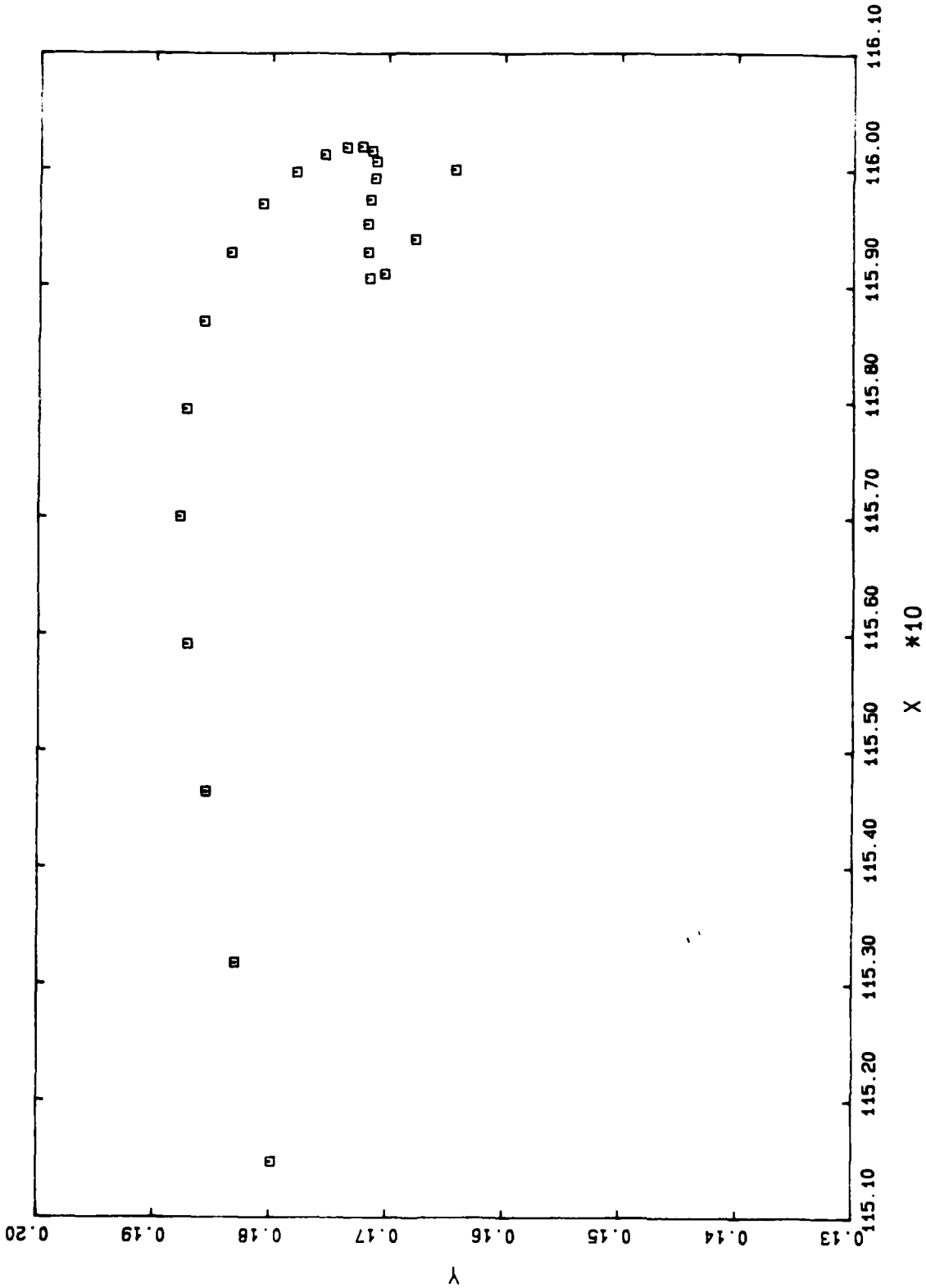

G4 3889 50.9741

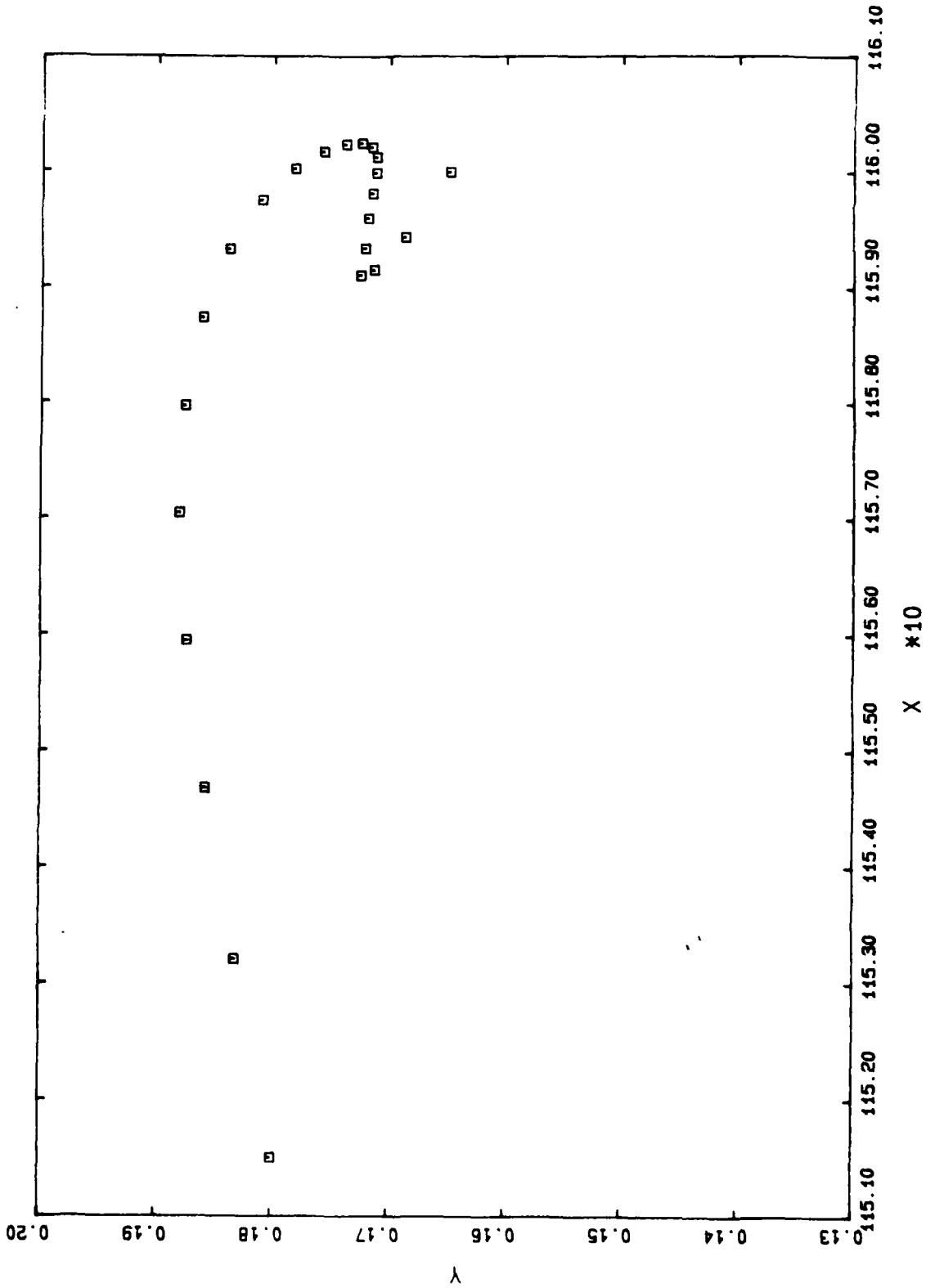

G4 3909 50.9745

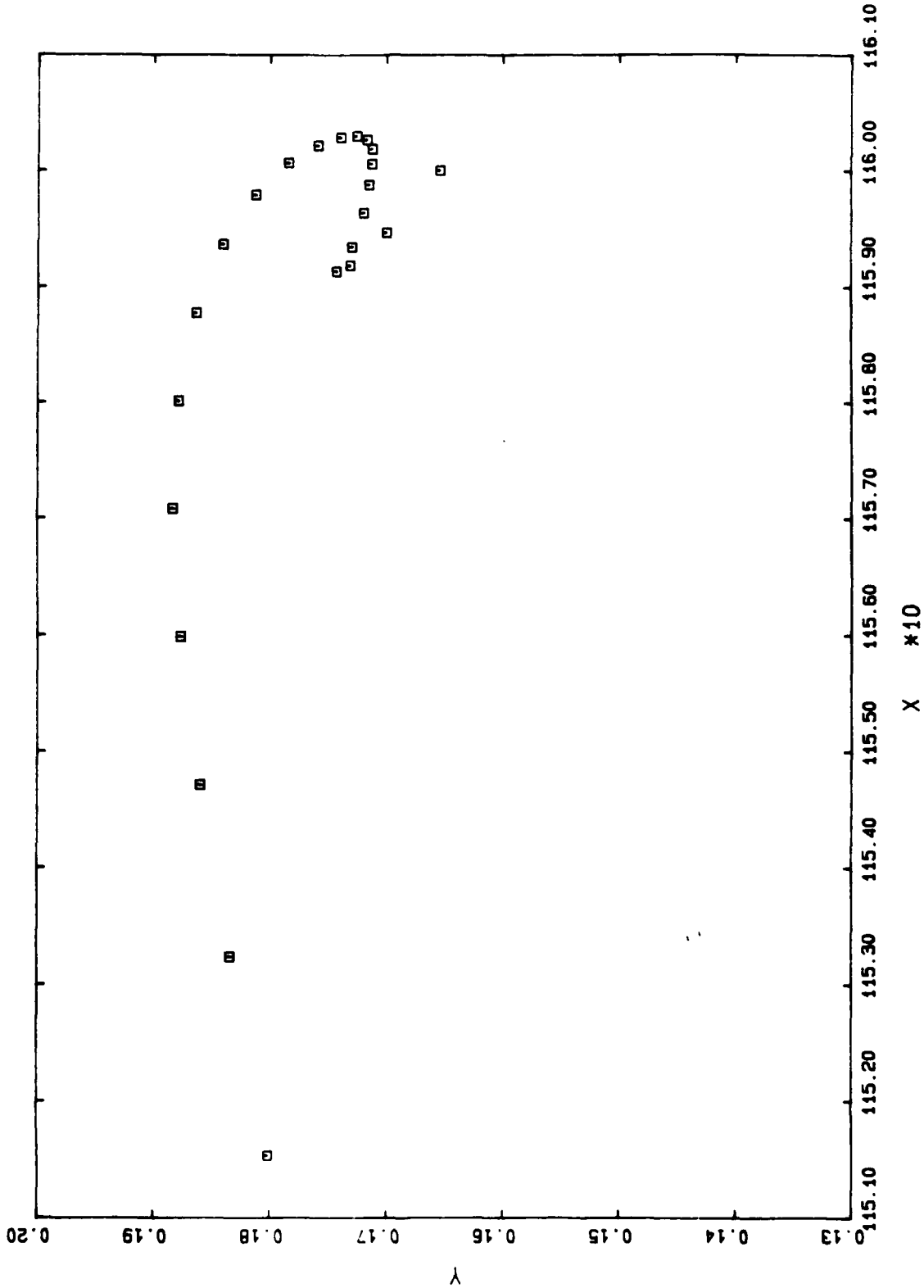

G5 3150 50.8748

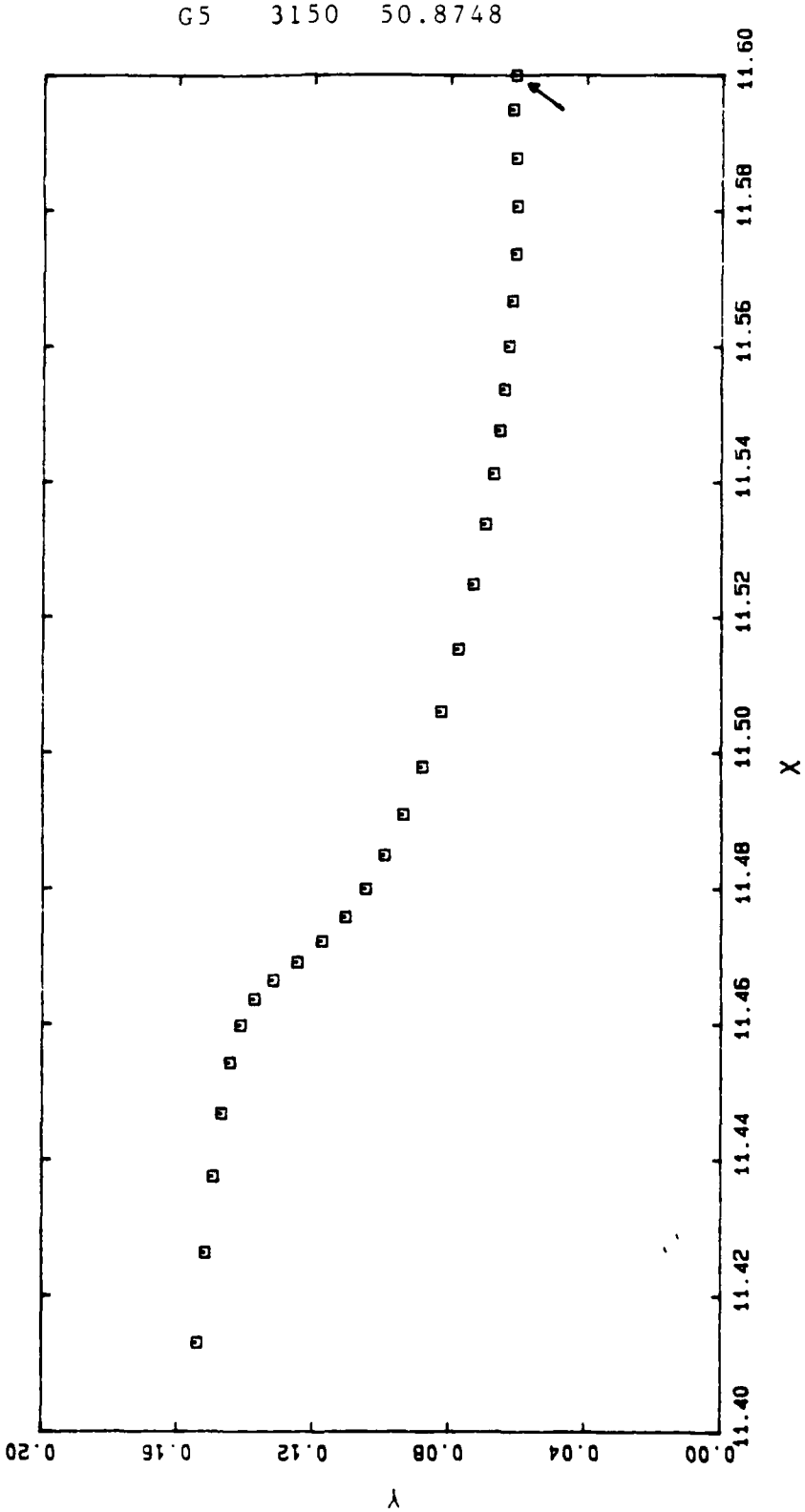

The arrow marks the wall intersection point.

G5 3200 50.8955

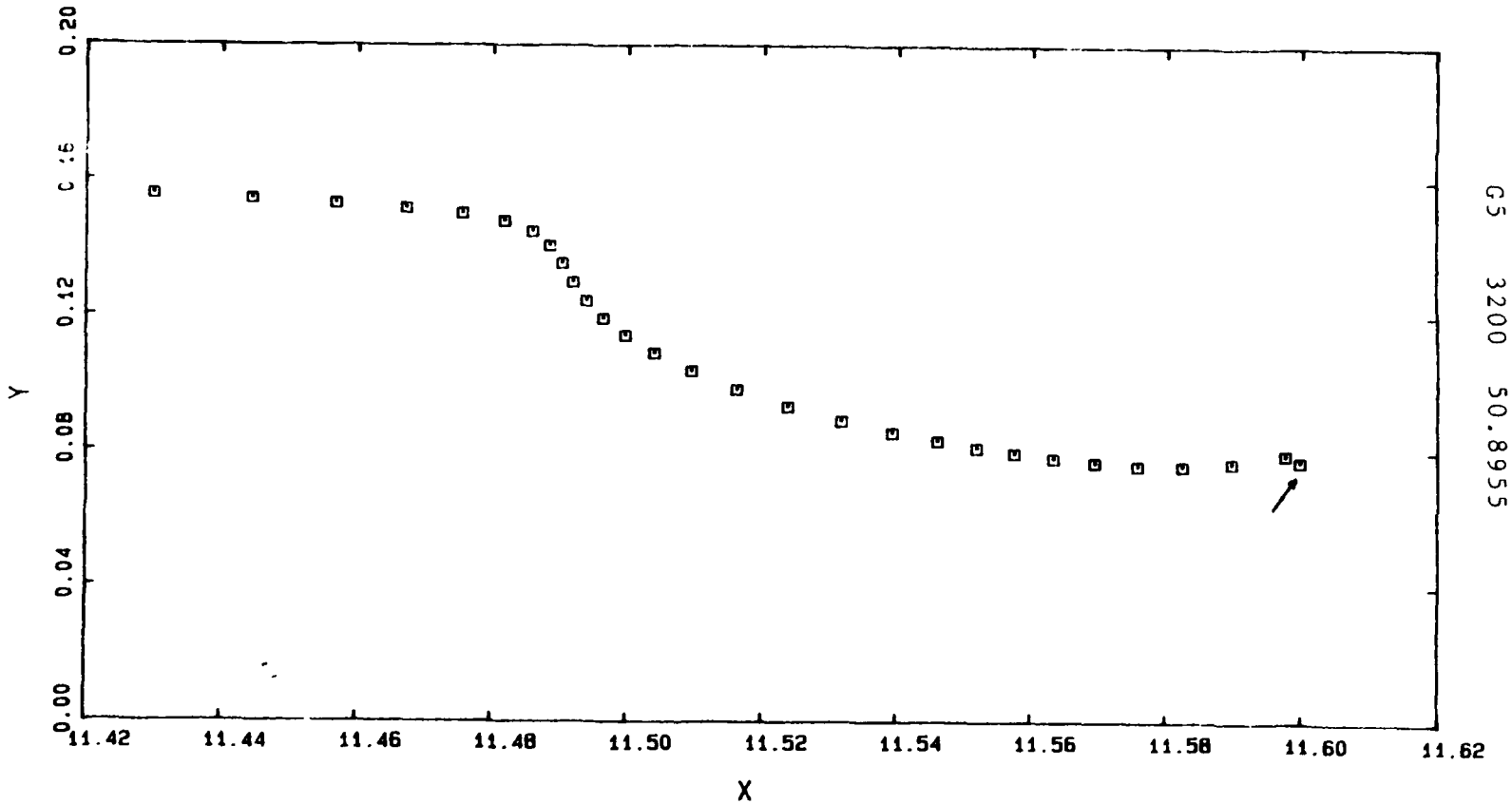

The arrow marks the wall intersection point.

G5 3250 50.9070

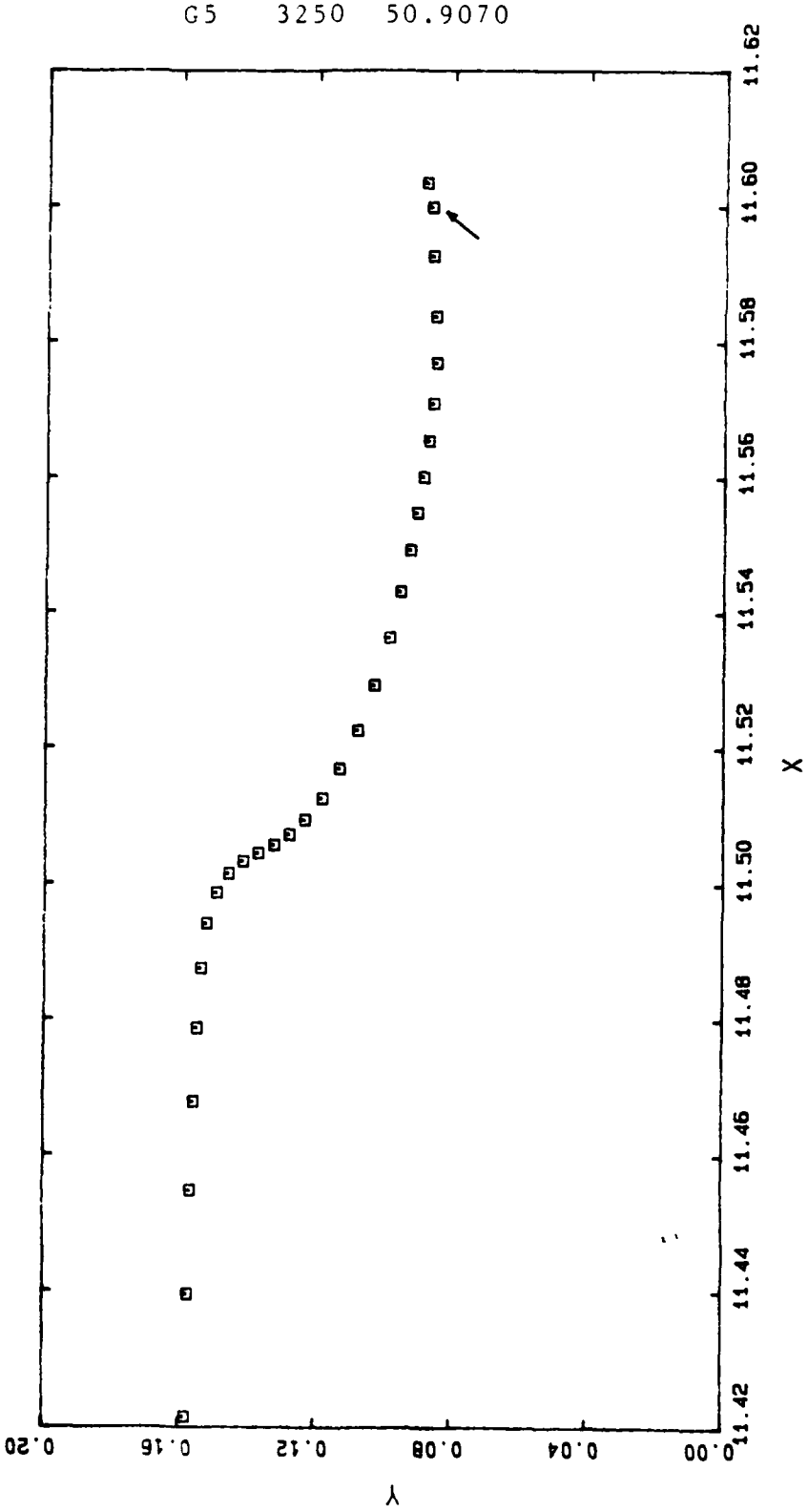

The arrow marks the wall intersection point.

G5 3650 50.9587

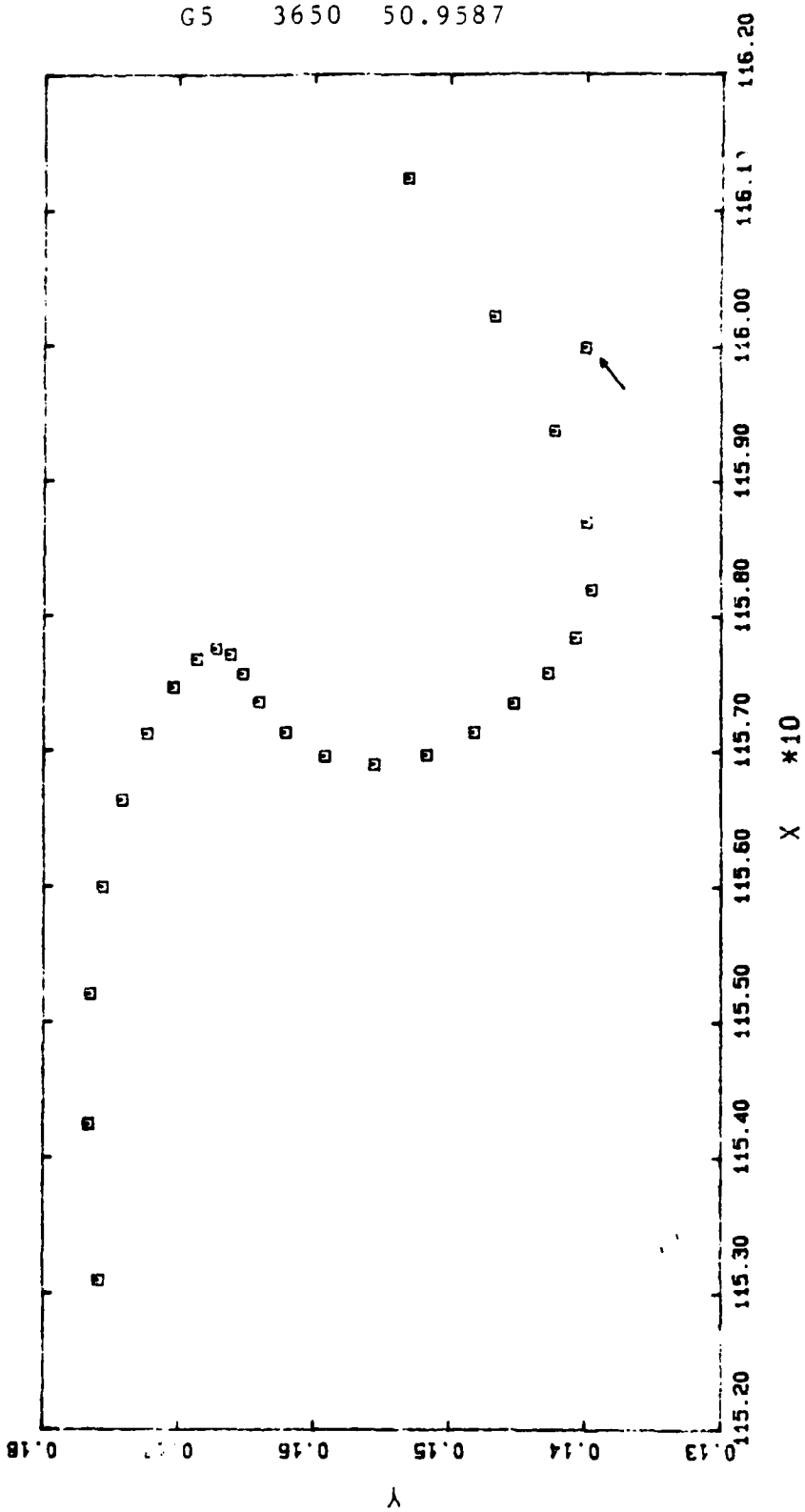

The arrow marks the wall intersection point.

G6 3603 50.9573

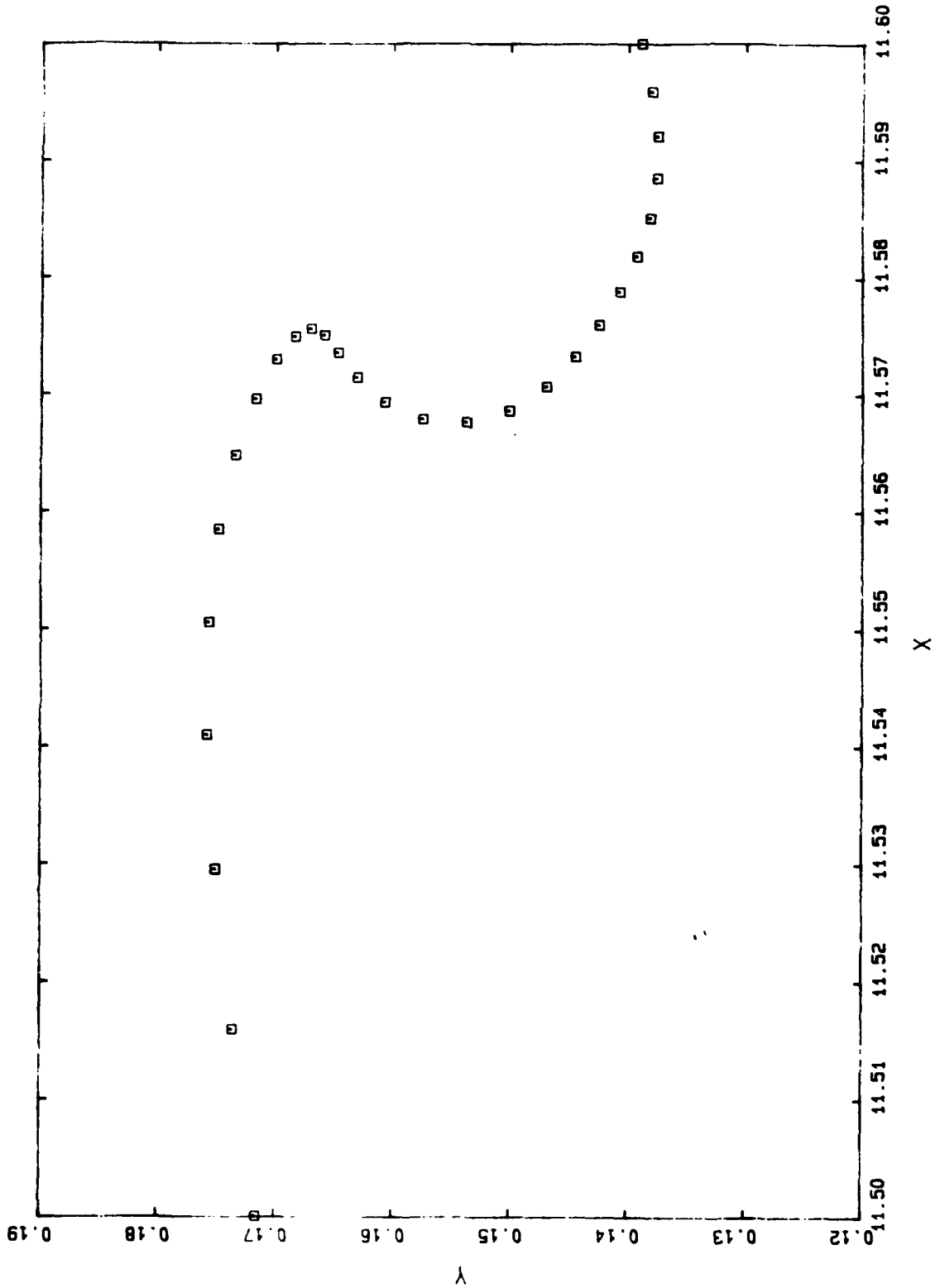

G6 3703 50.9637

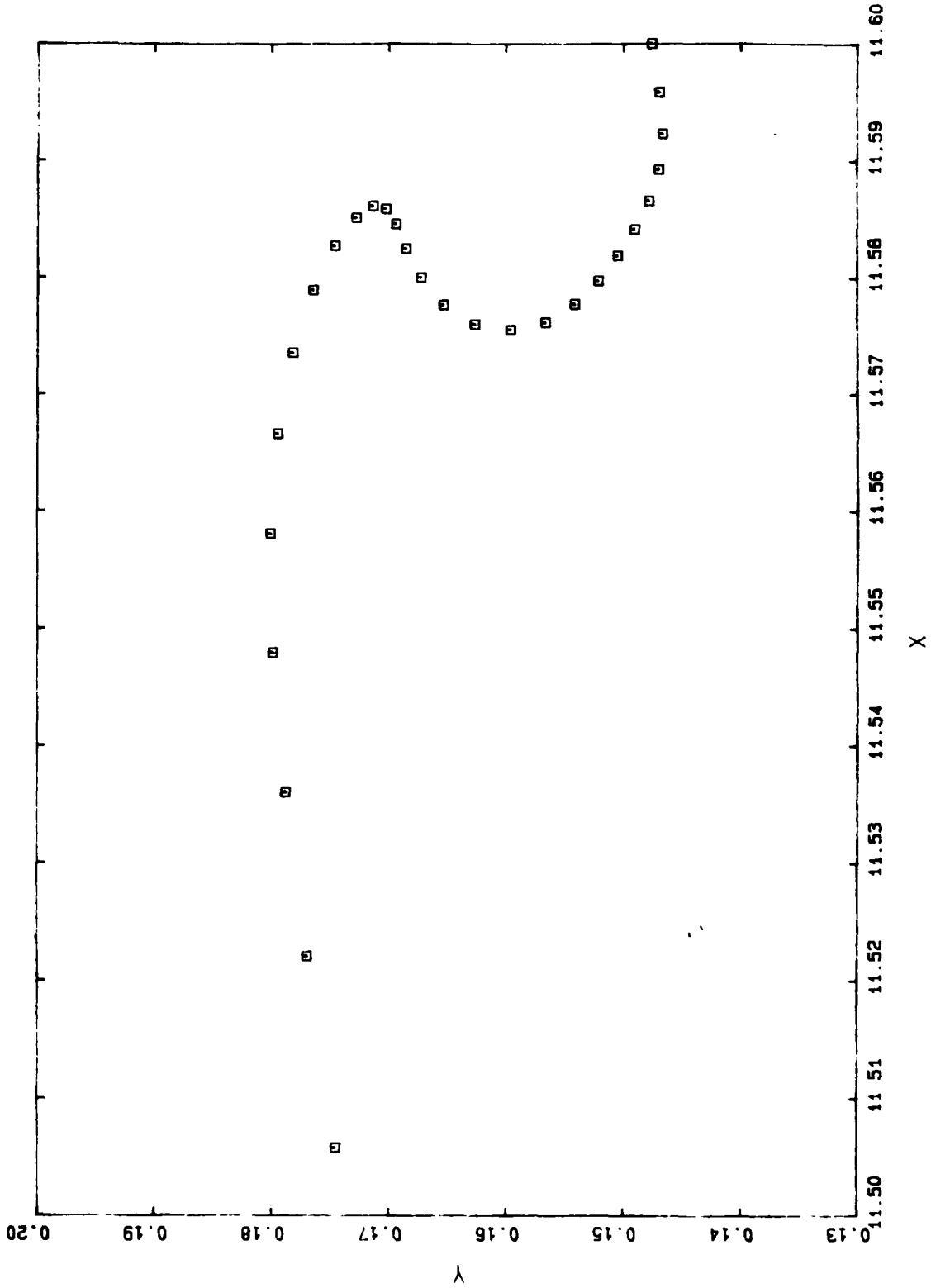

G6 3803 50.9701

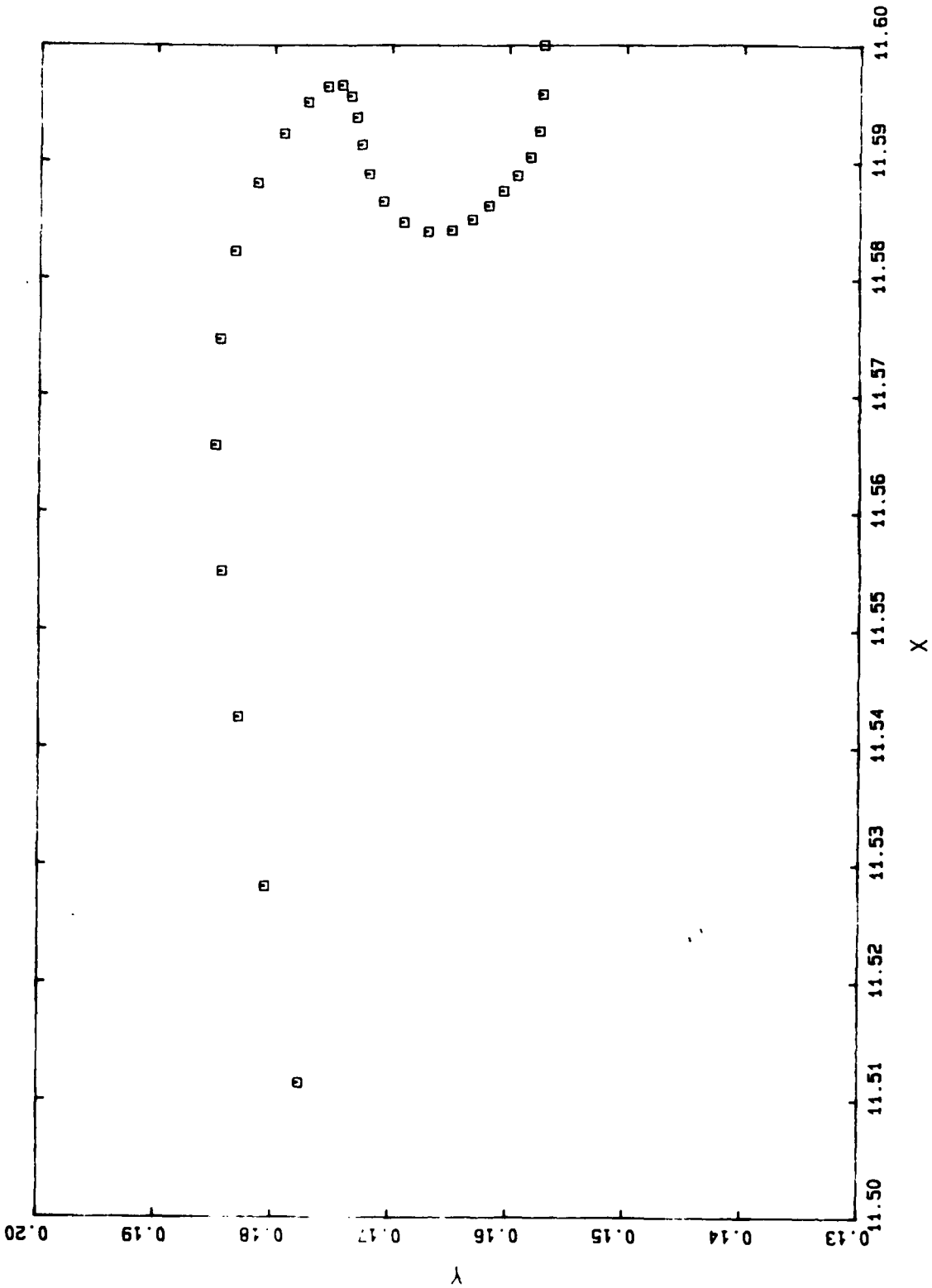

G6 3869 50.9738

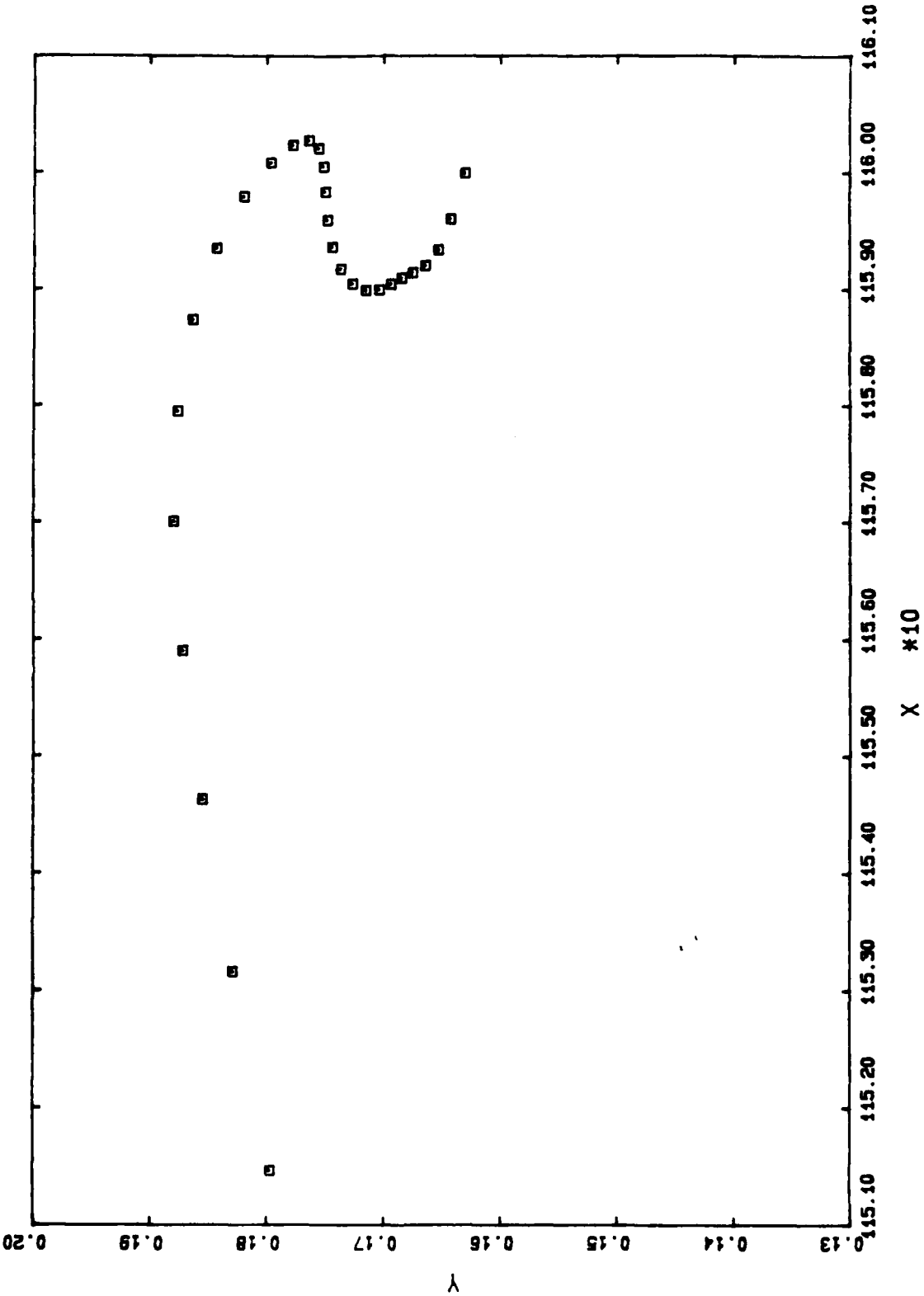

G6 3870 50.9738

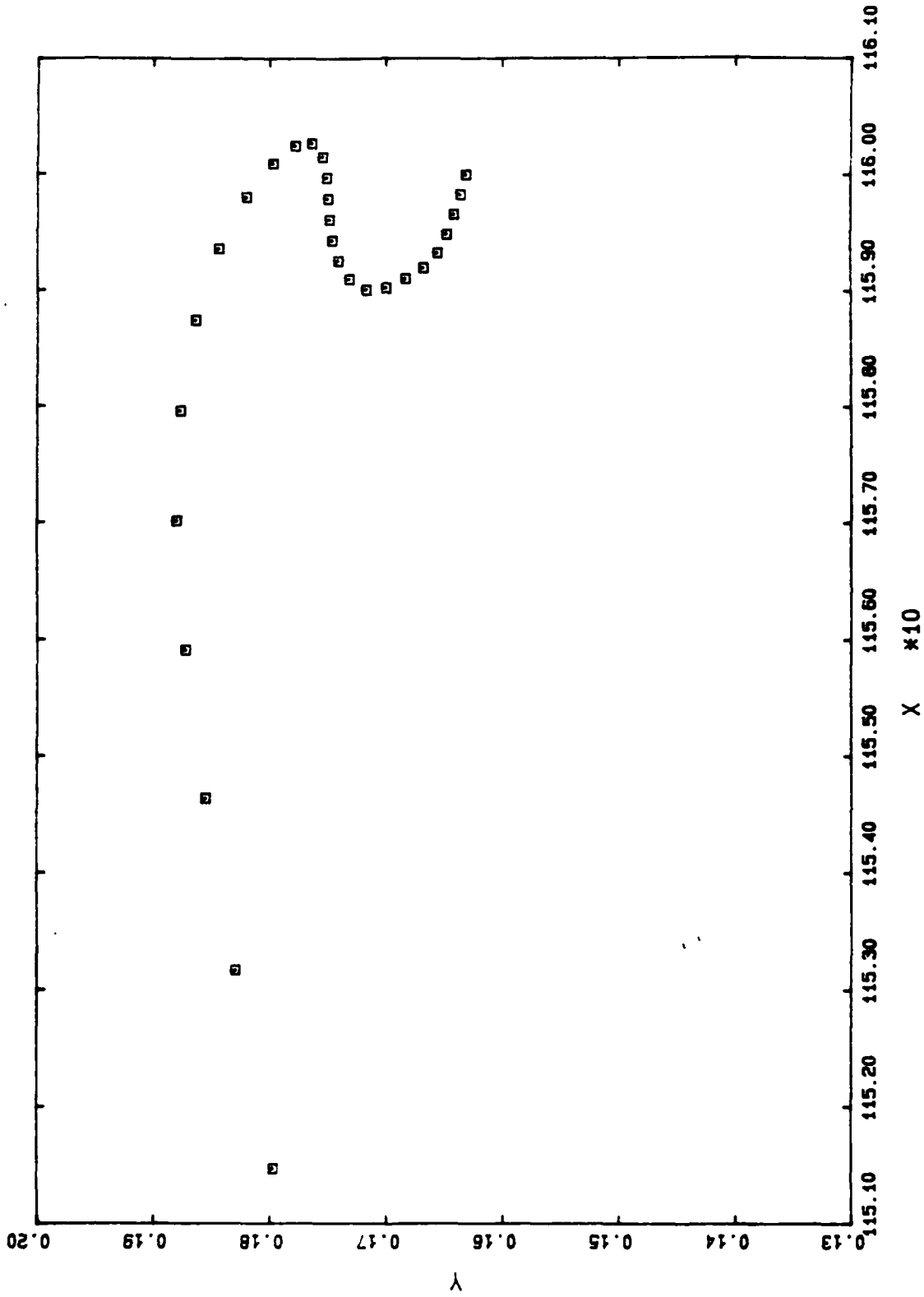

G6 3920 50.9760

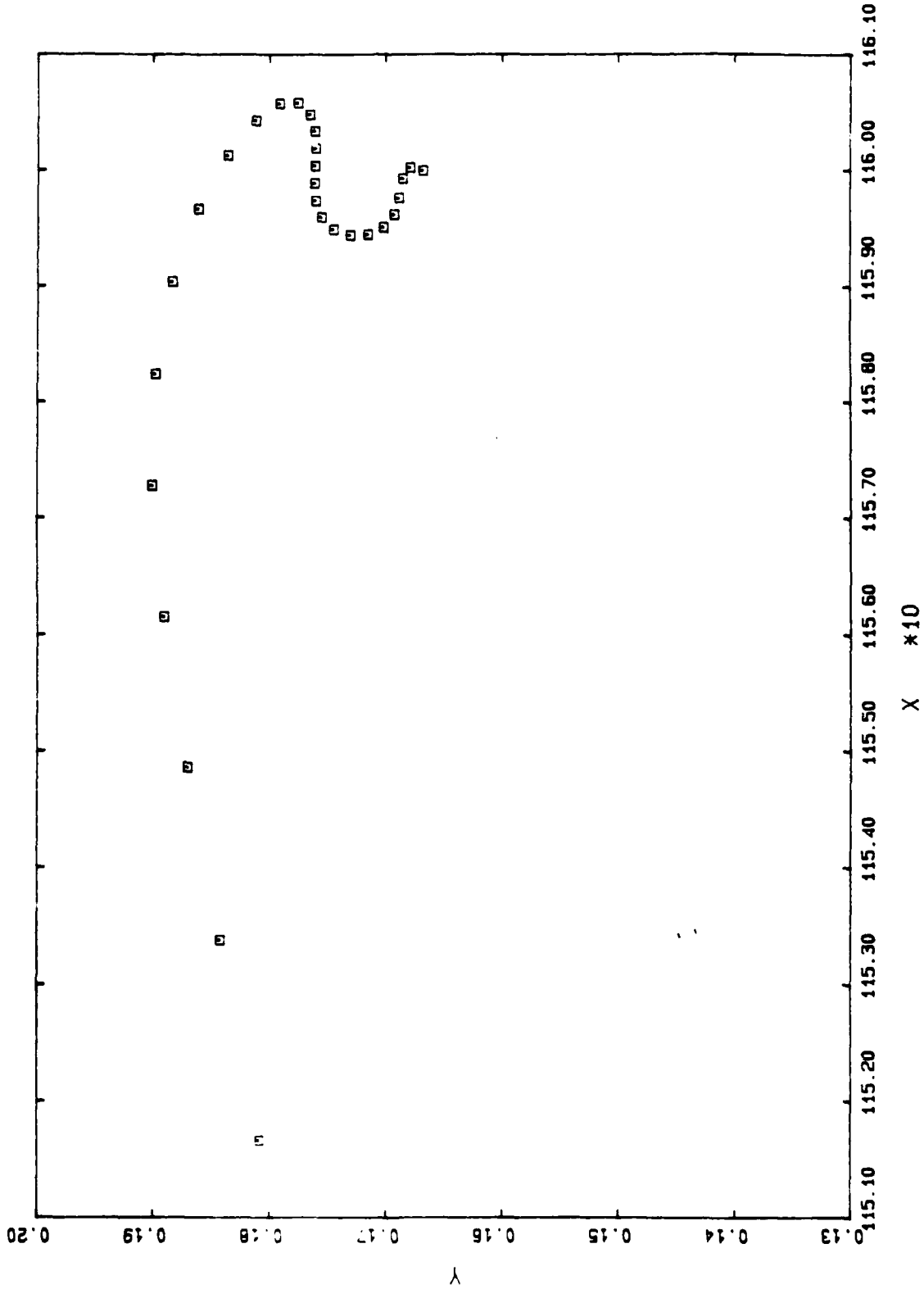

G6 3960 50.9766

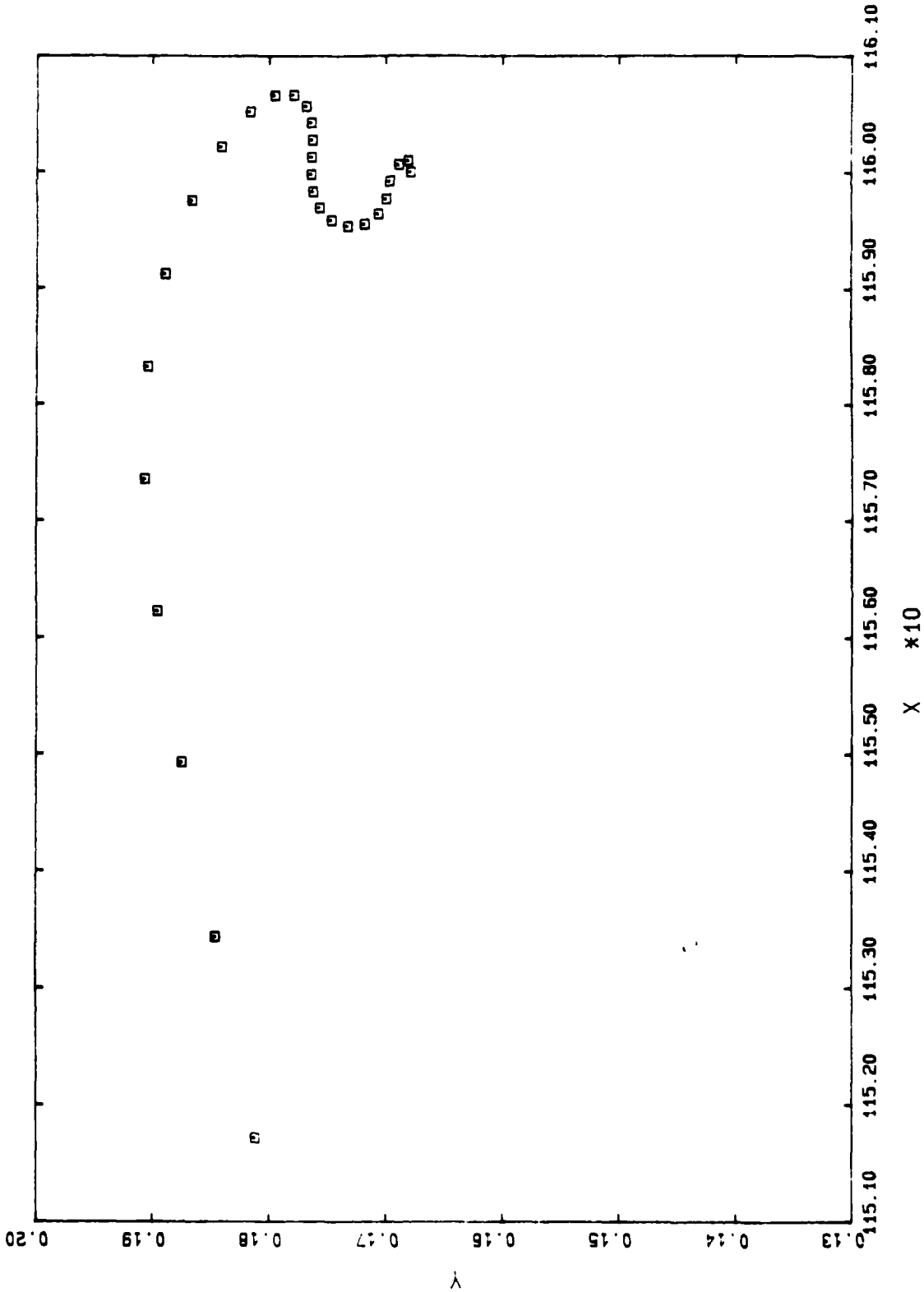

Appendix H

Refer to Chapter 6 for discussion.

H1.1 3851 50.9730

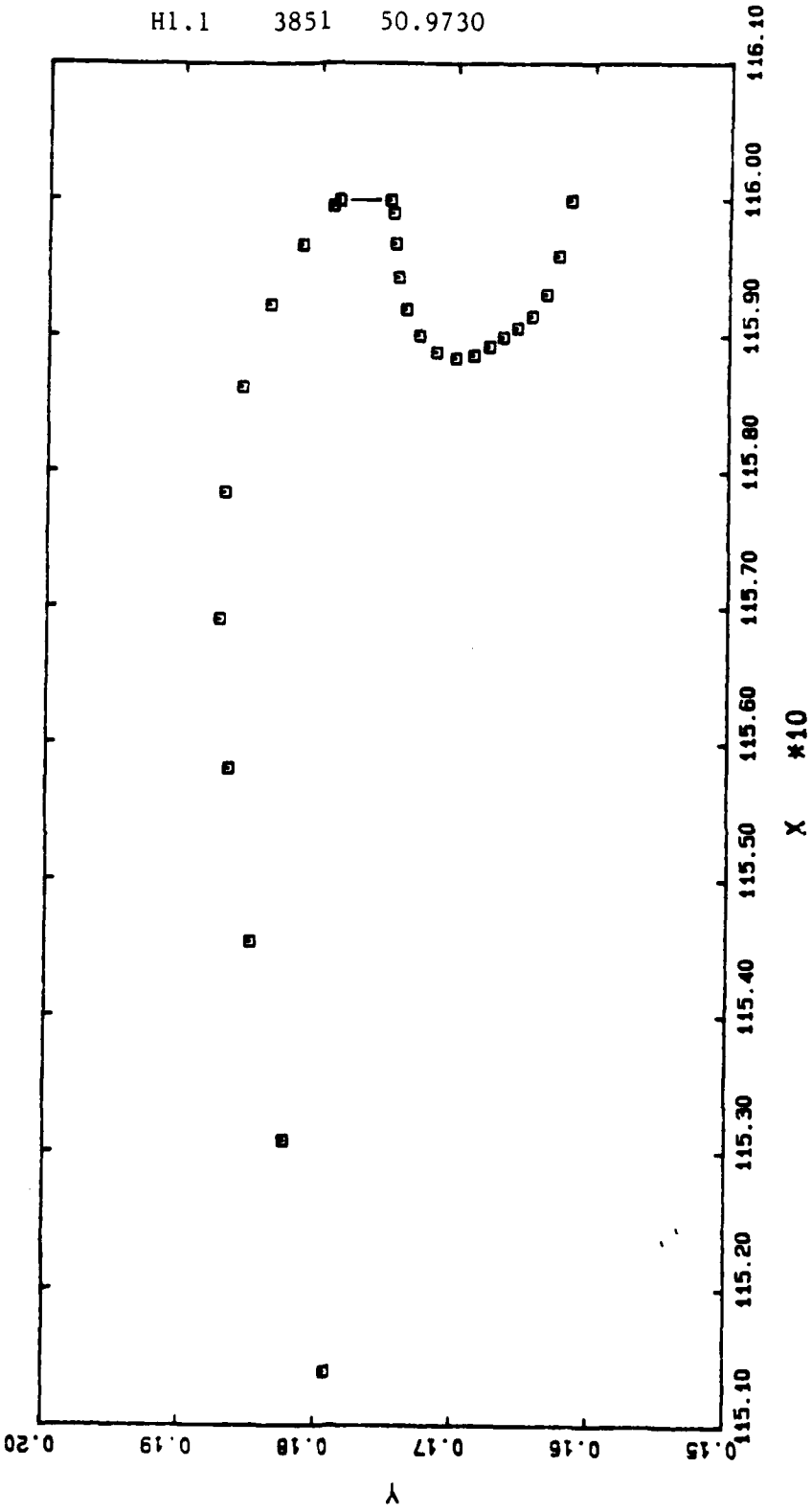

H1.1 3852 50.9730

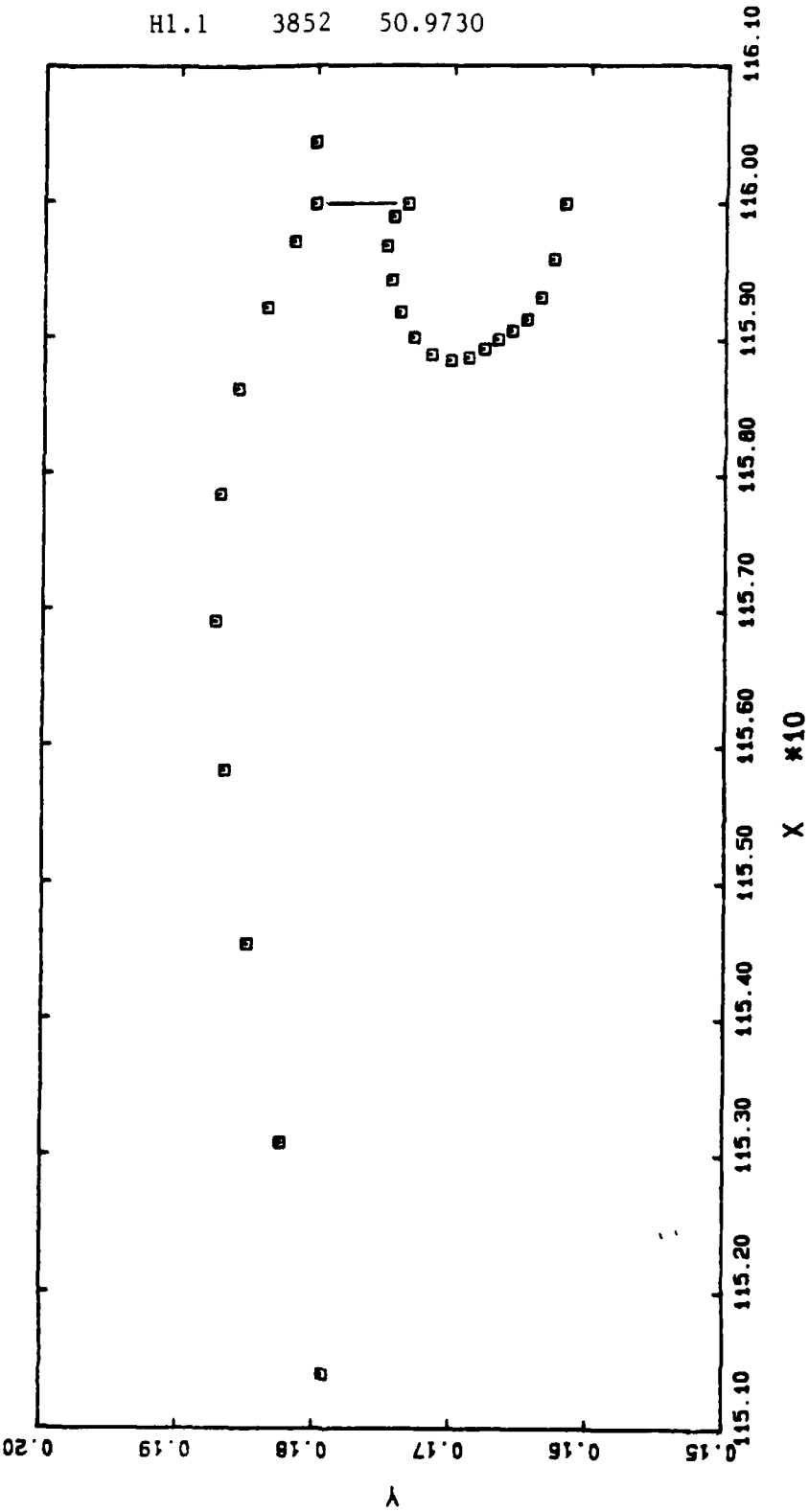

H2.1 3851 50.9730

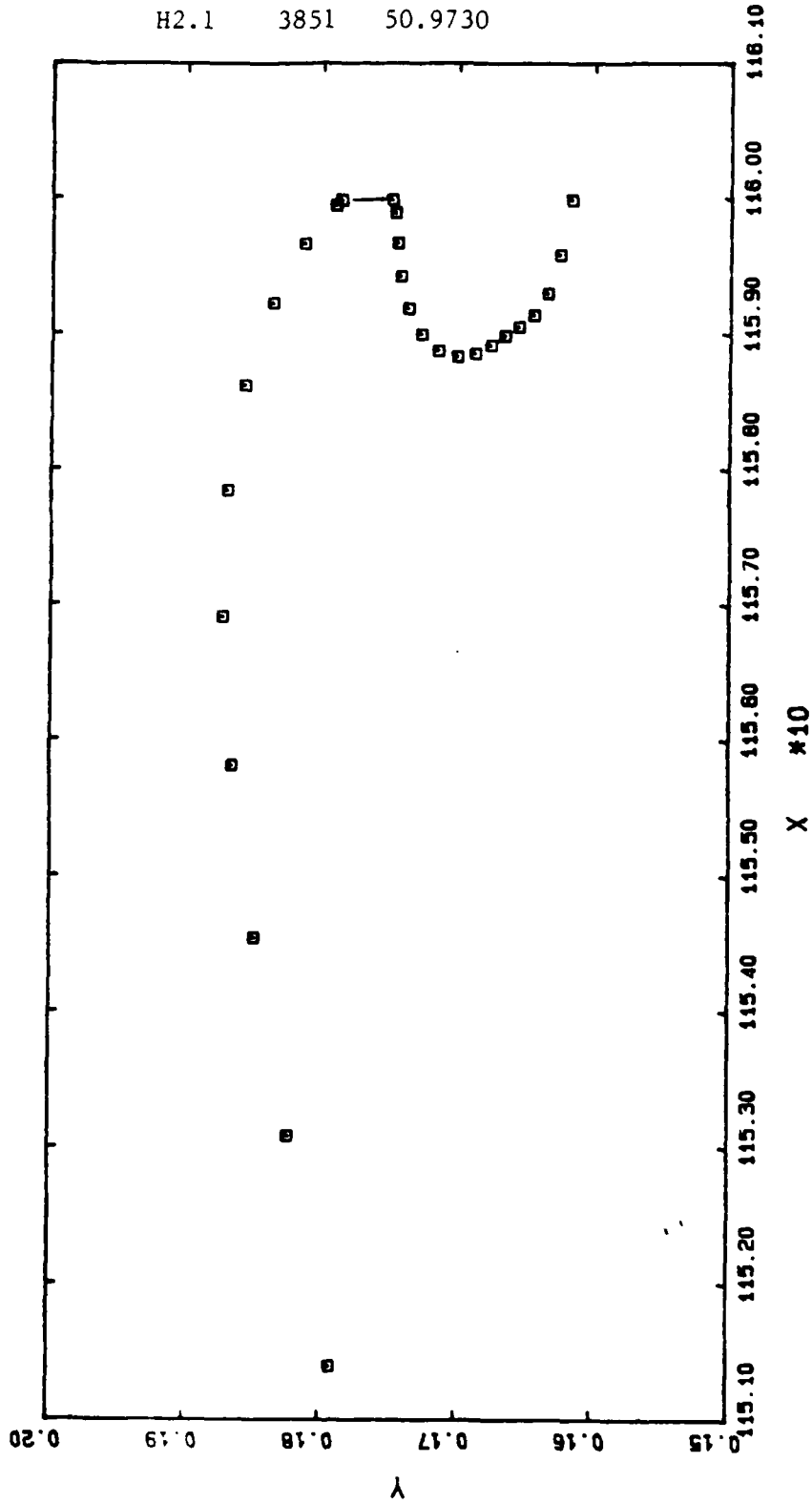

H2.1 3852 50.9730

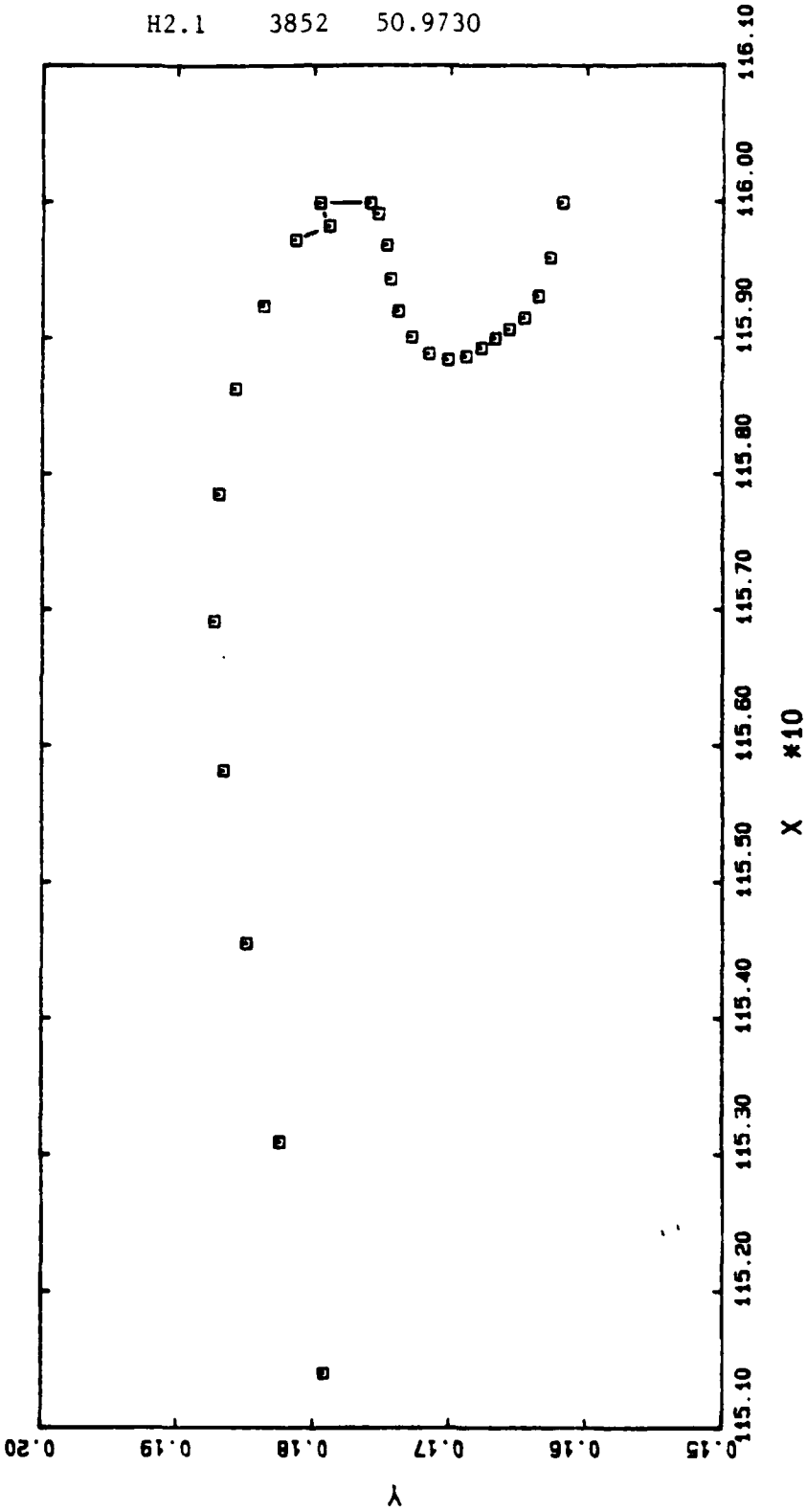

H2.1 3853 50.9731

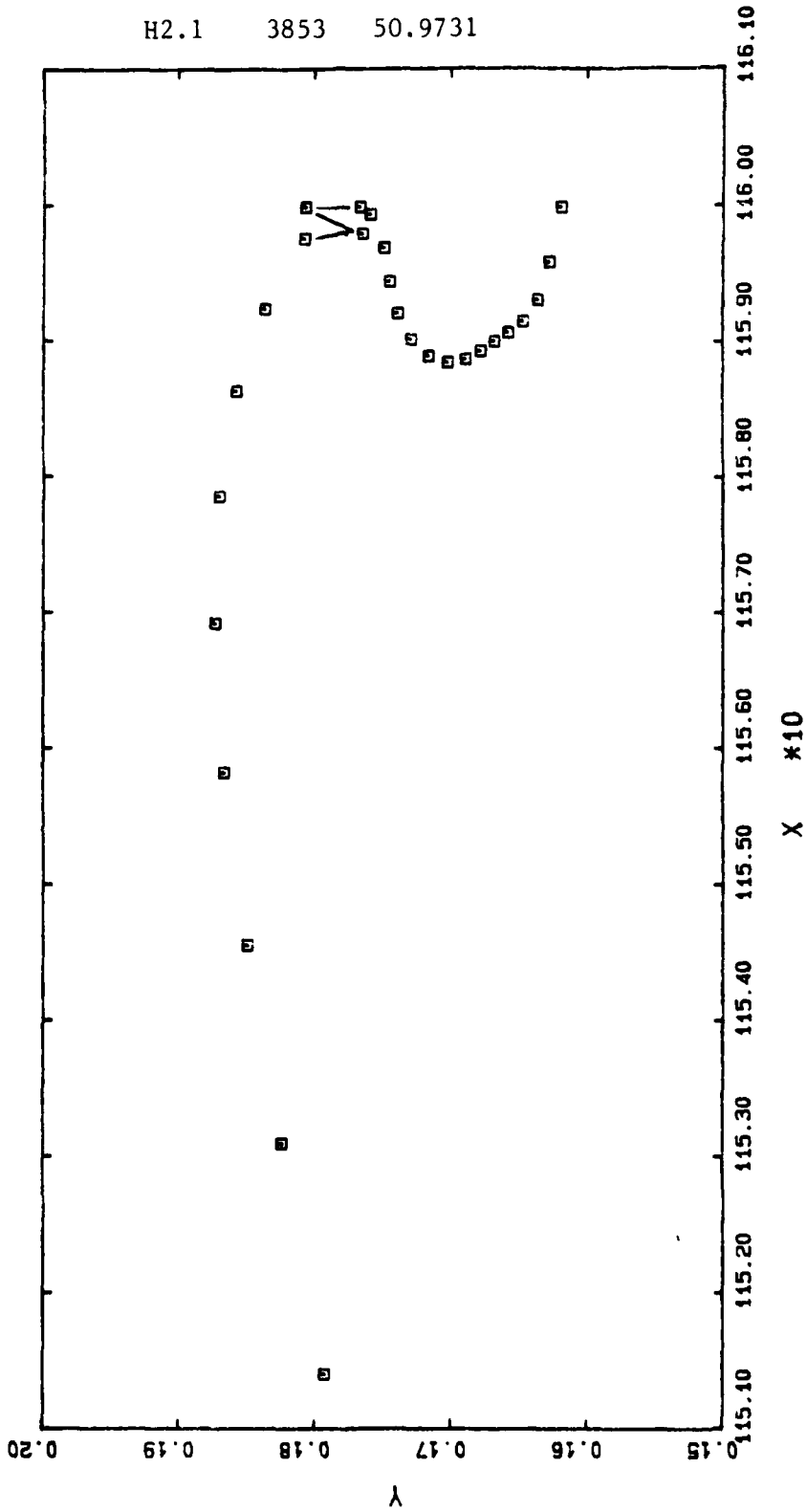

H3.1 3851 50.9730

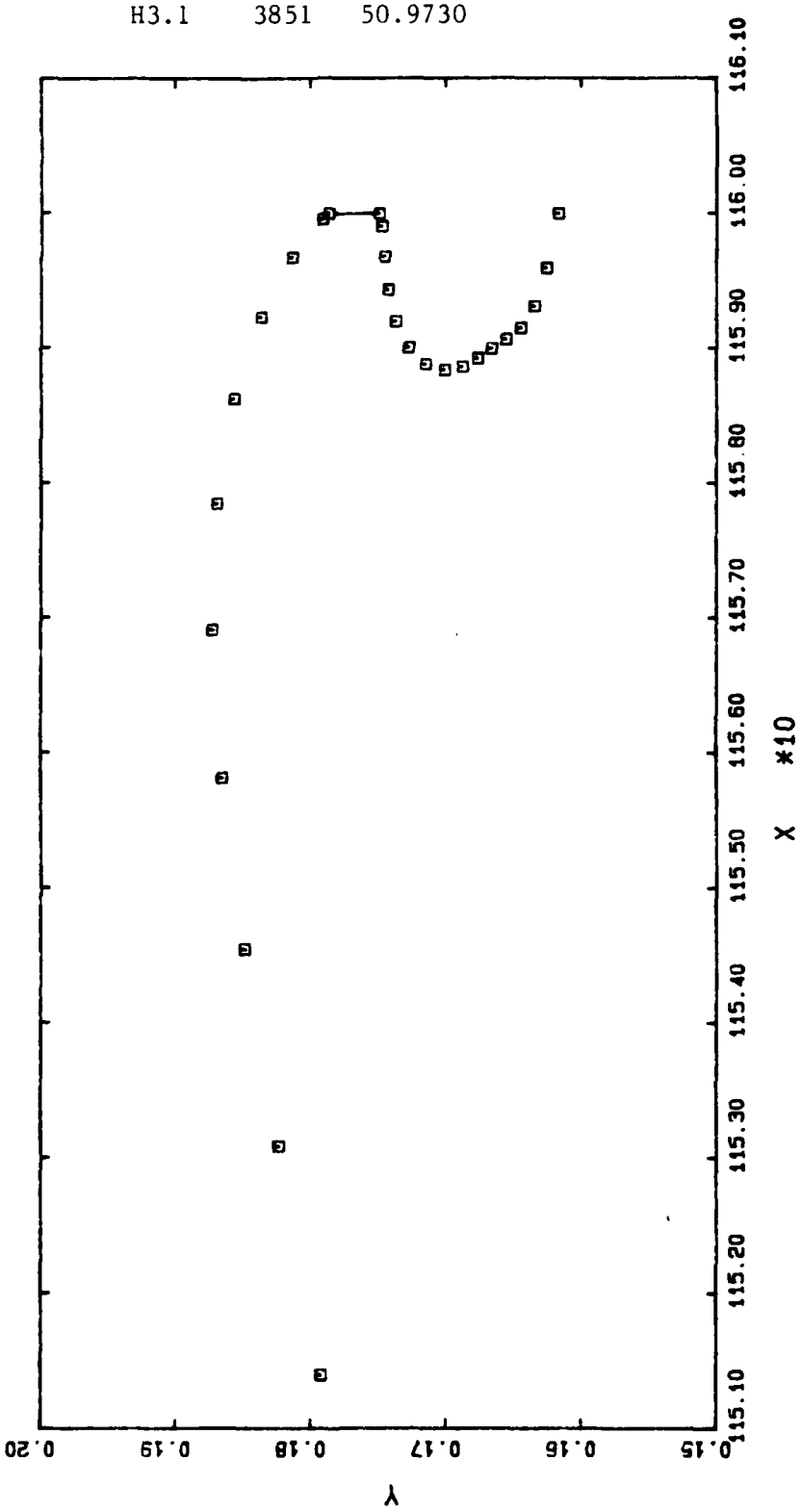

H3.1 3852 50.9730

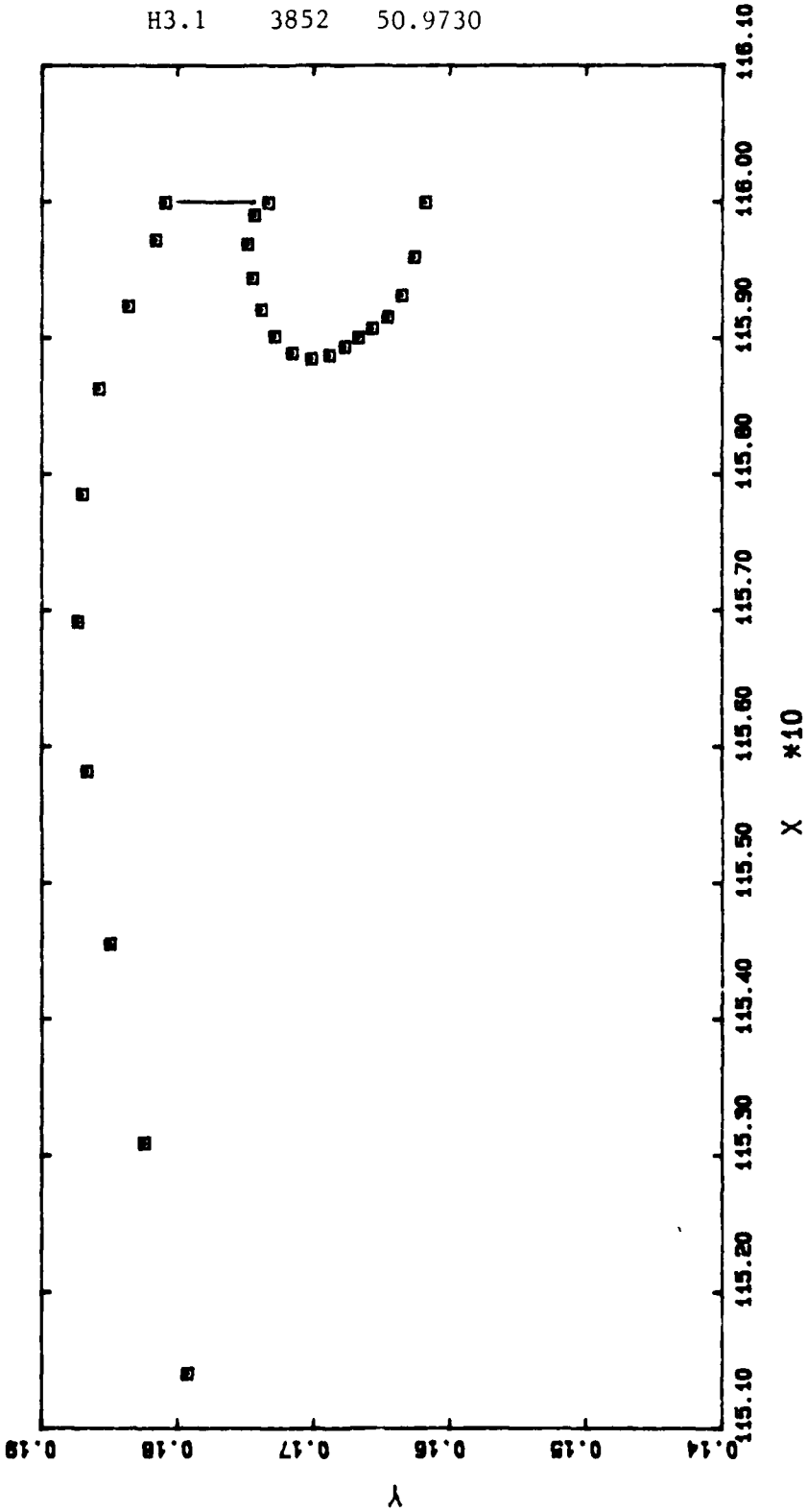

H3.1 3853 50.9731

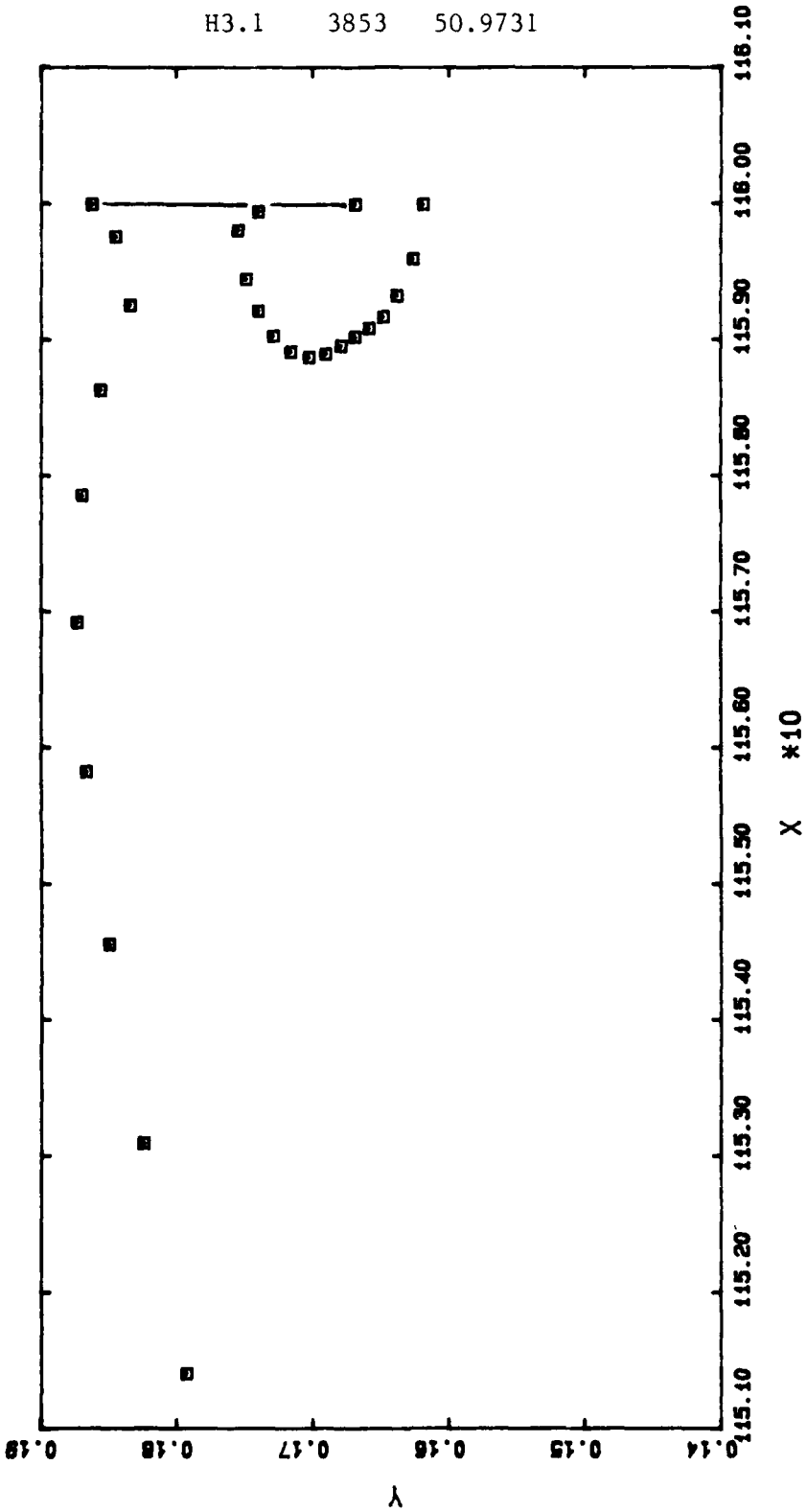

H3.1 3854 50.9731

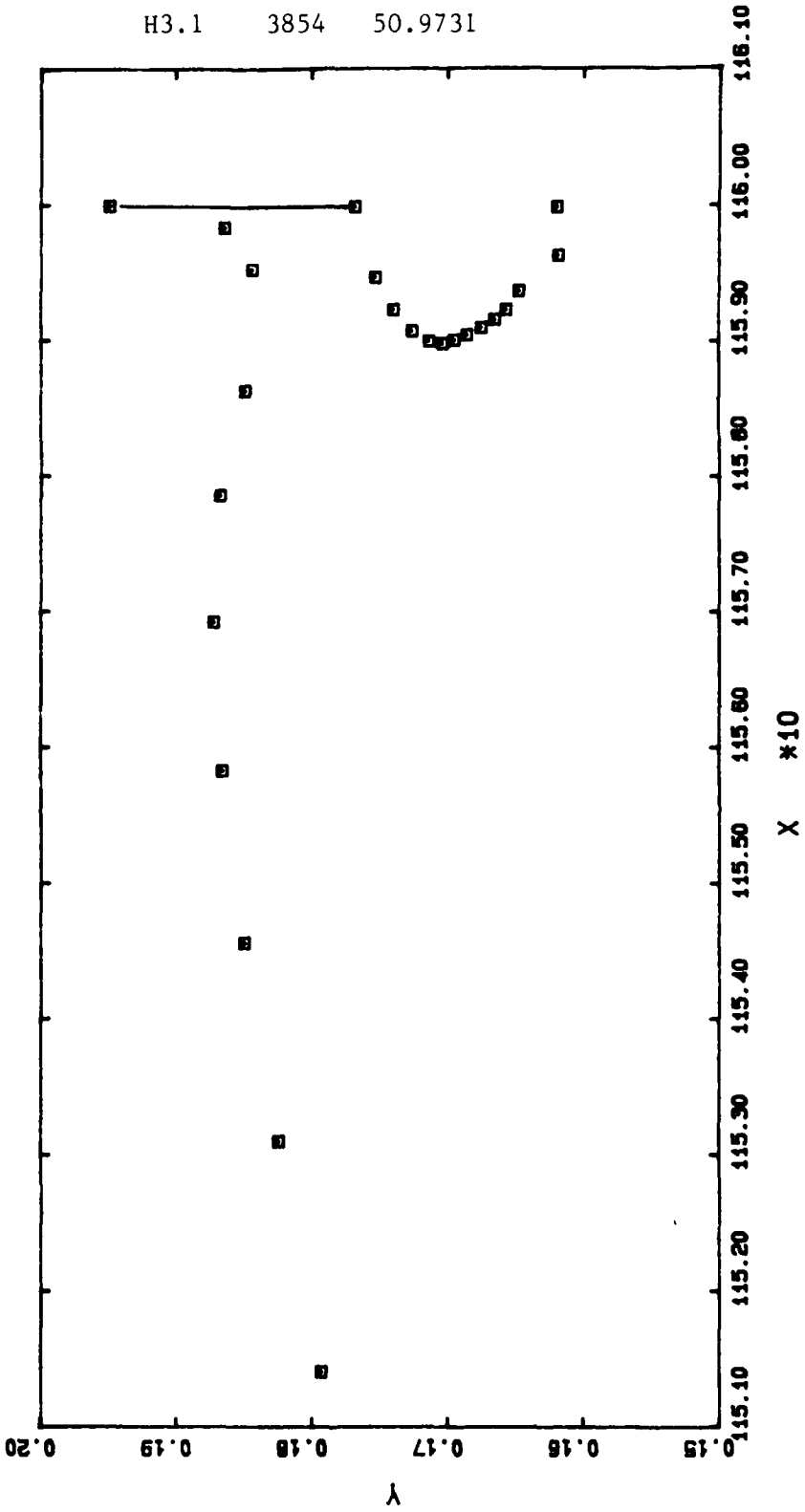

H3.1 3855 50.9732

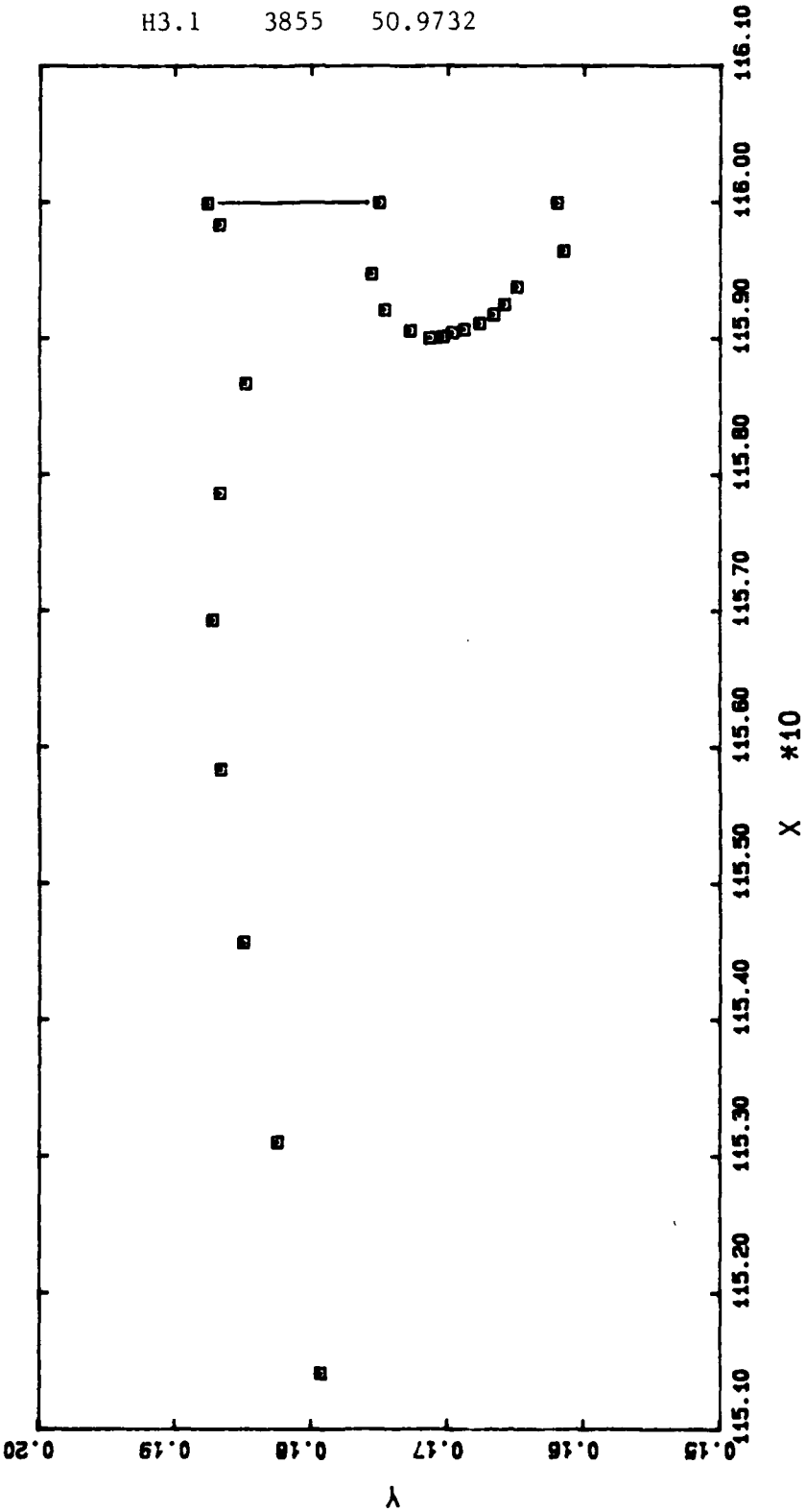

H3.1 3856 50.9732

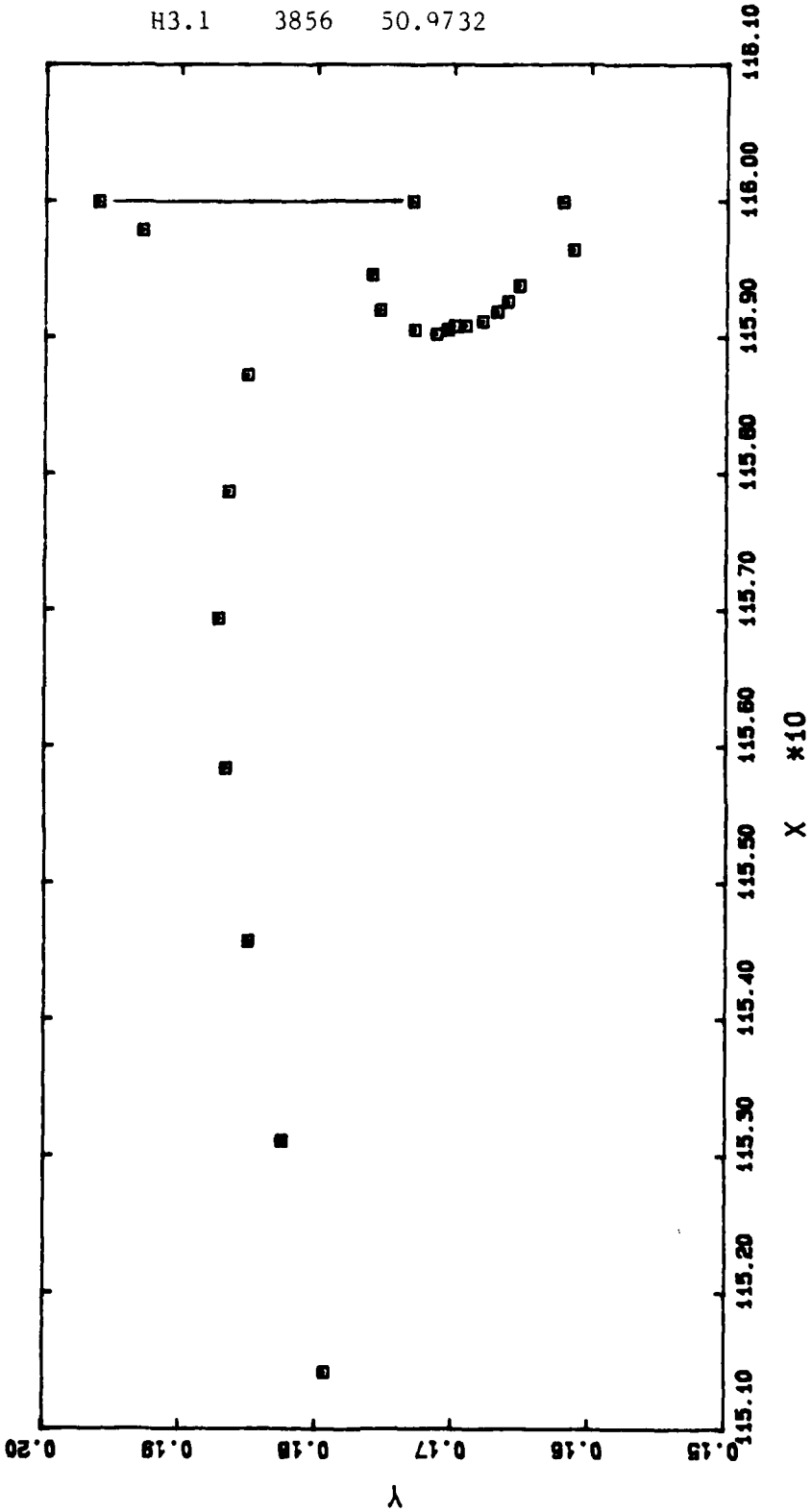

H4.1 3851 50.9730

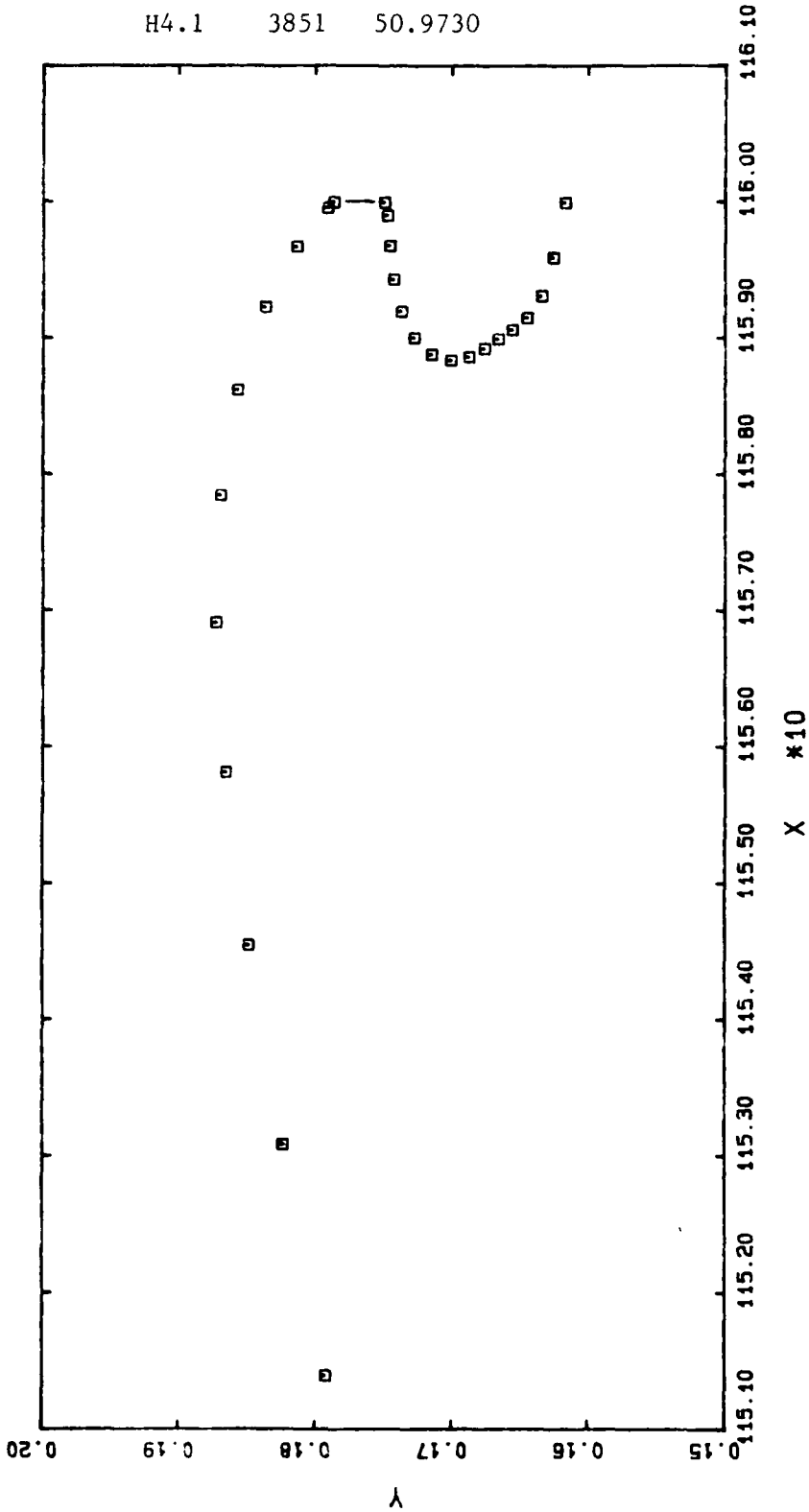

H4.1 3852 50.9730

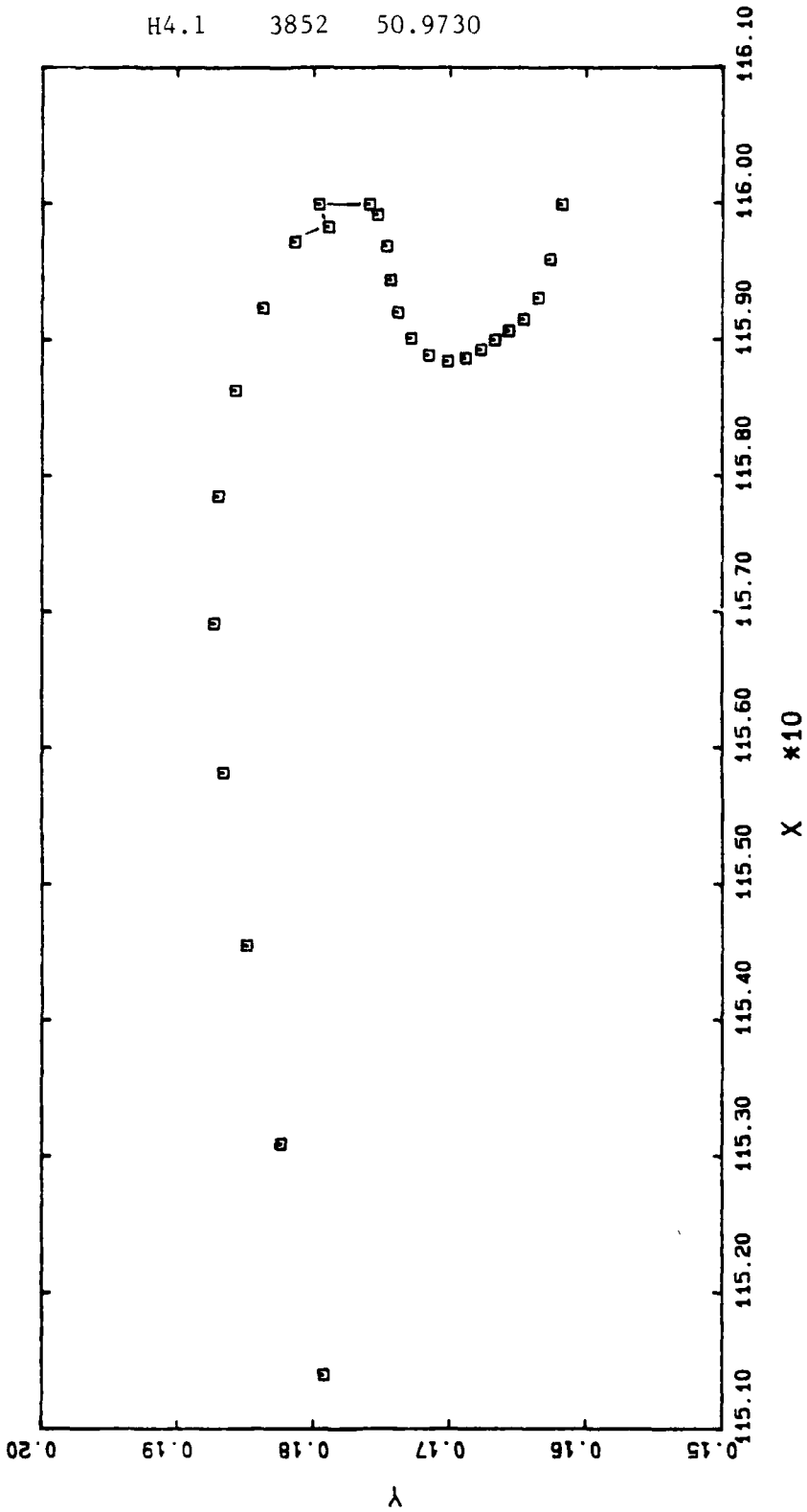

H4.1 3853 50.9731

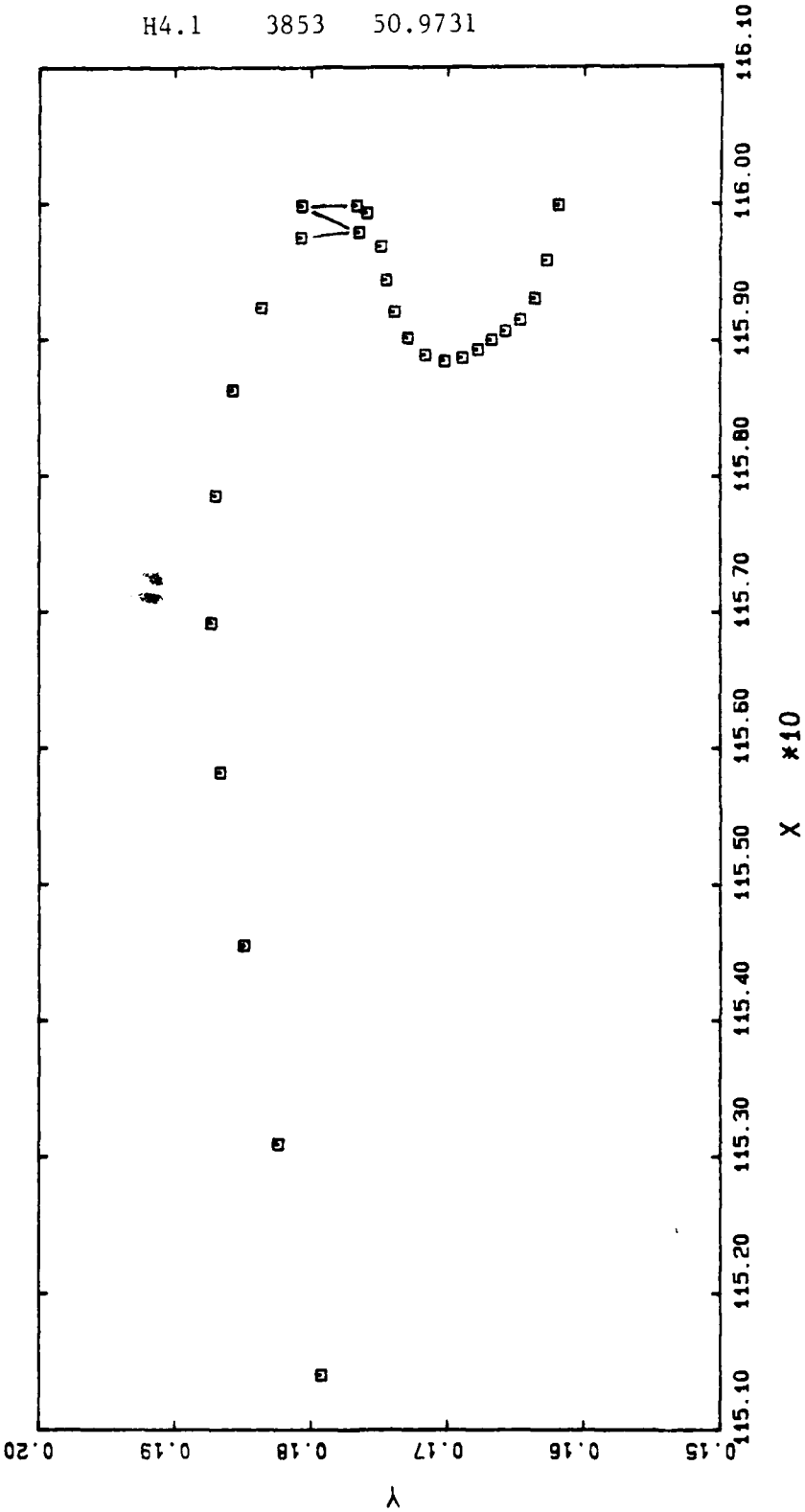

H5.1 3851 50.9730

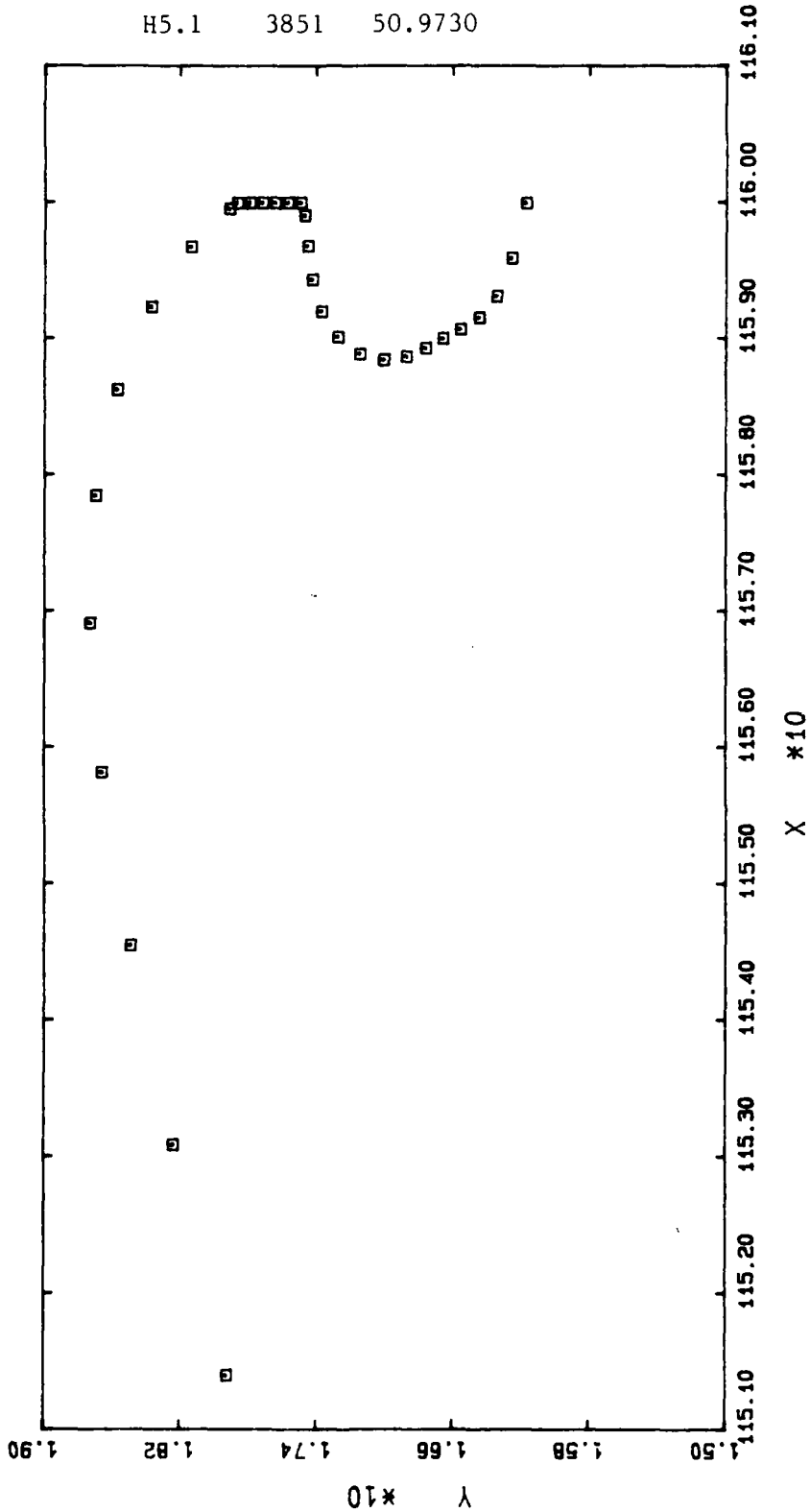

H5.1 3852 50.9730

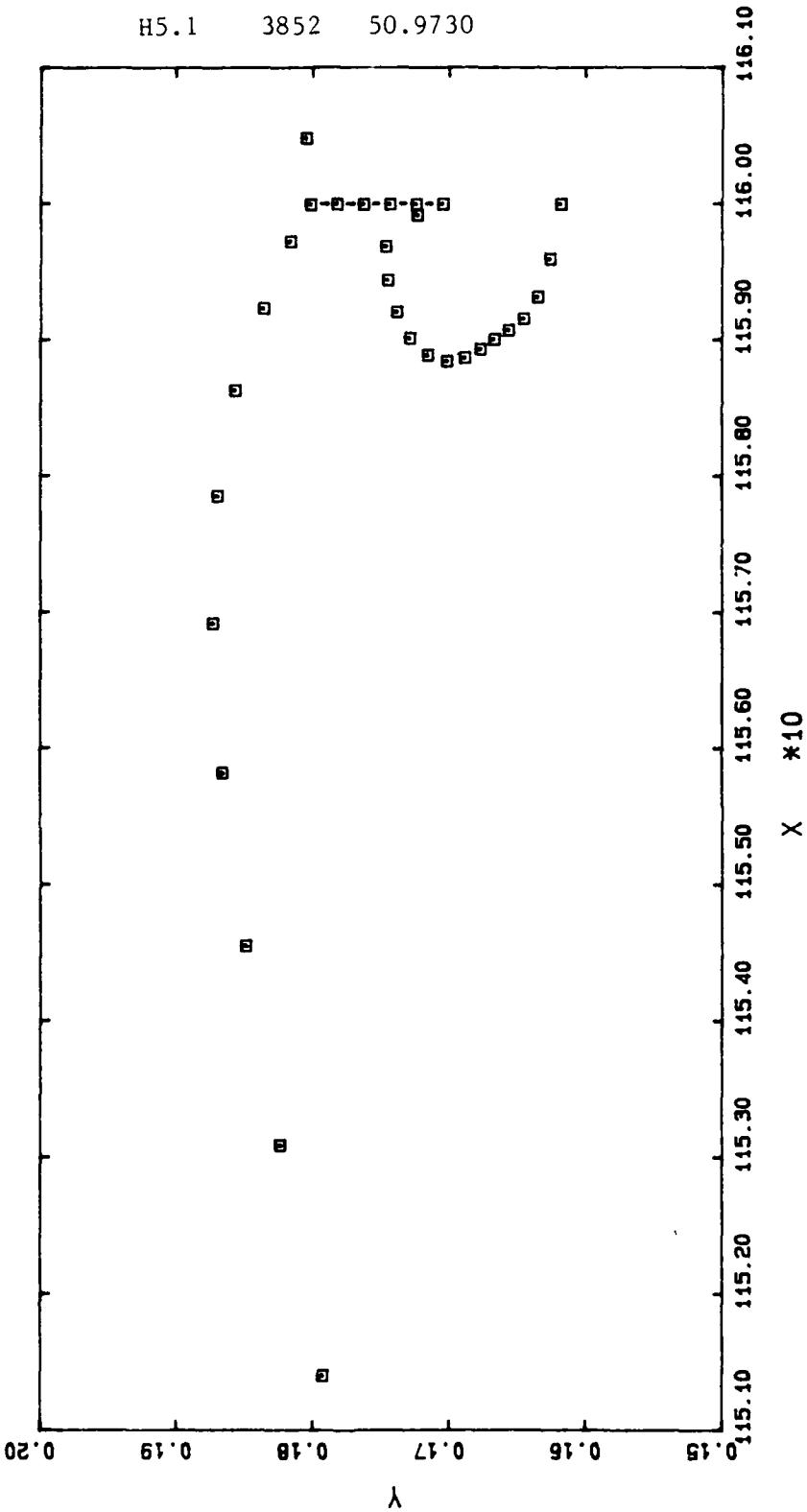

H5.1 3853 50.9731

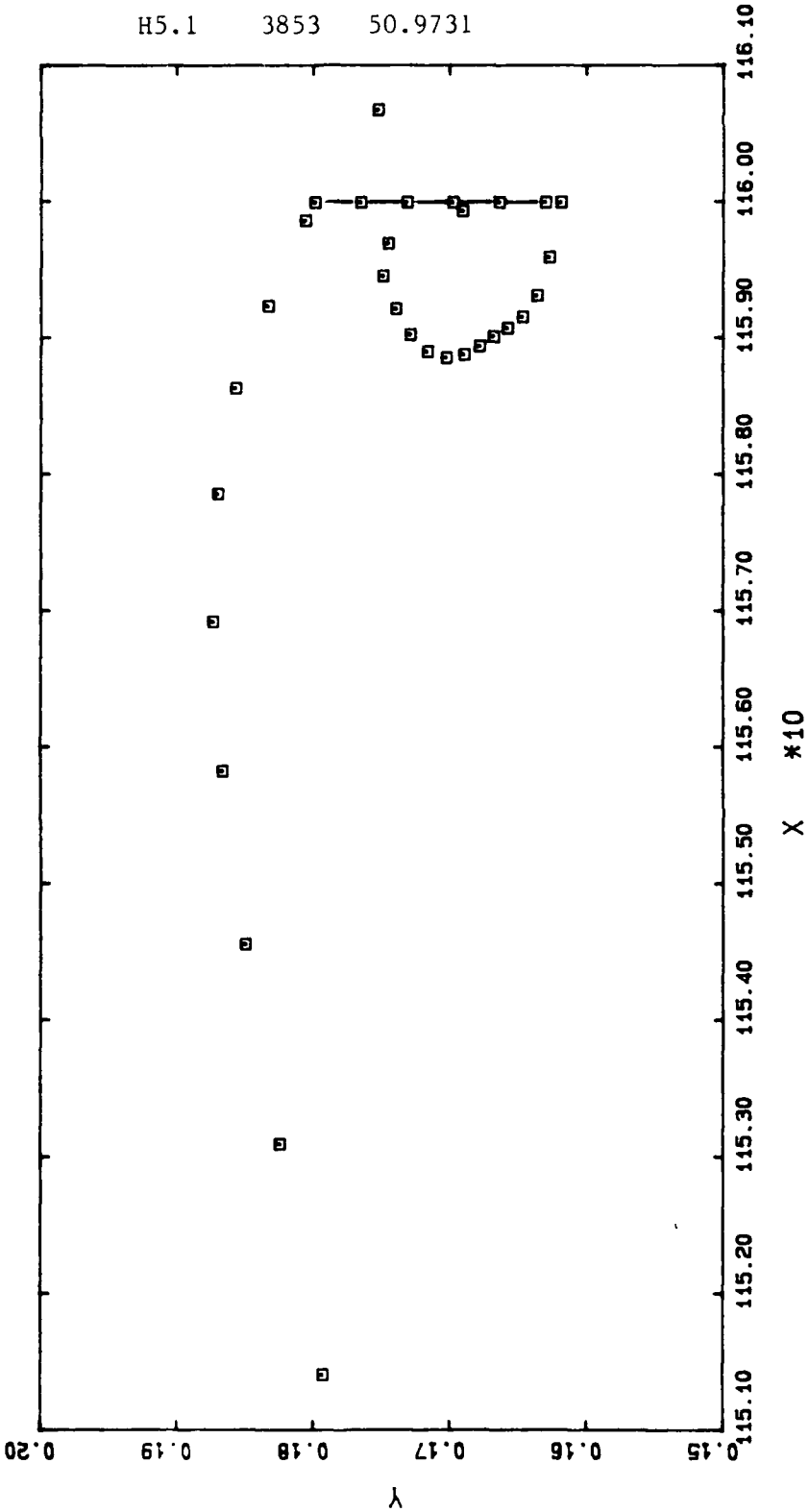

H6.1 3851 50.9730

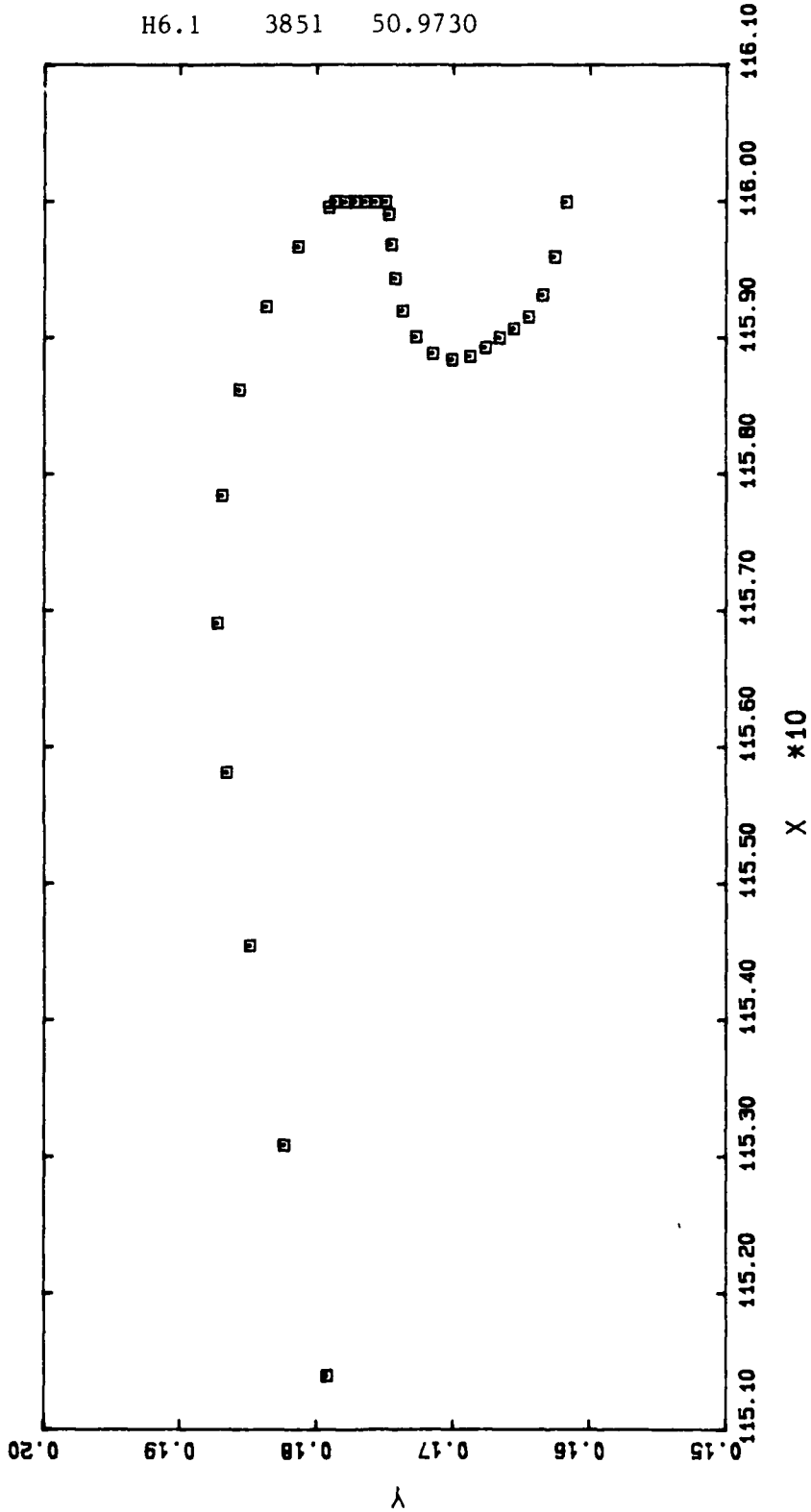

H6.1 3852 50.9730

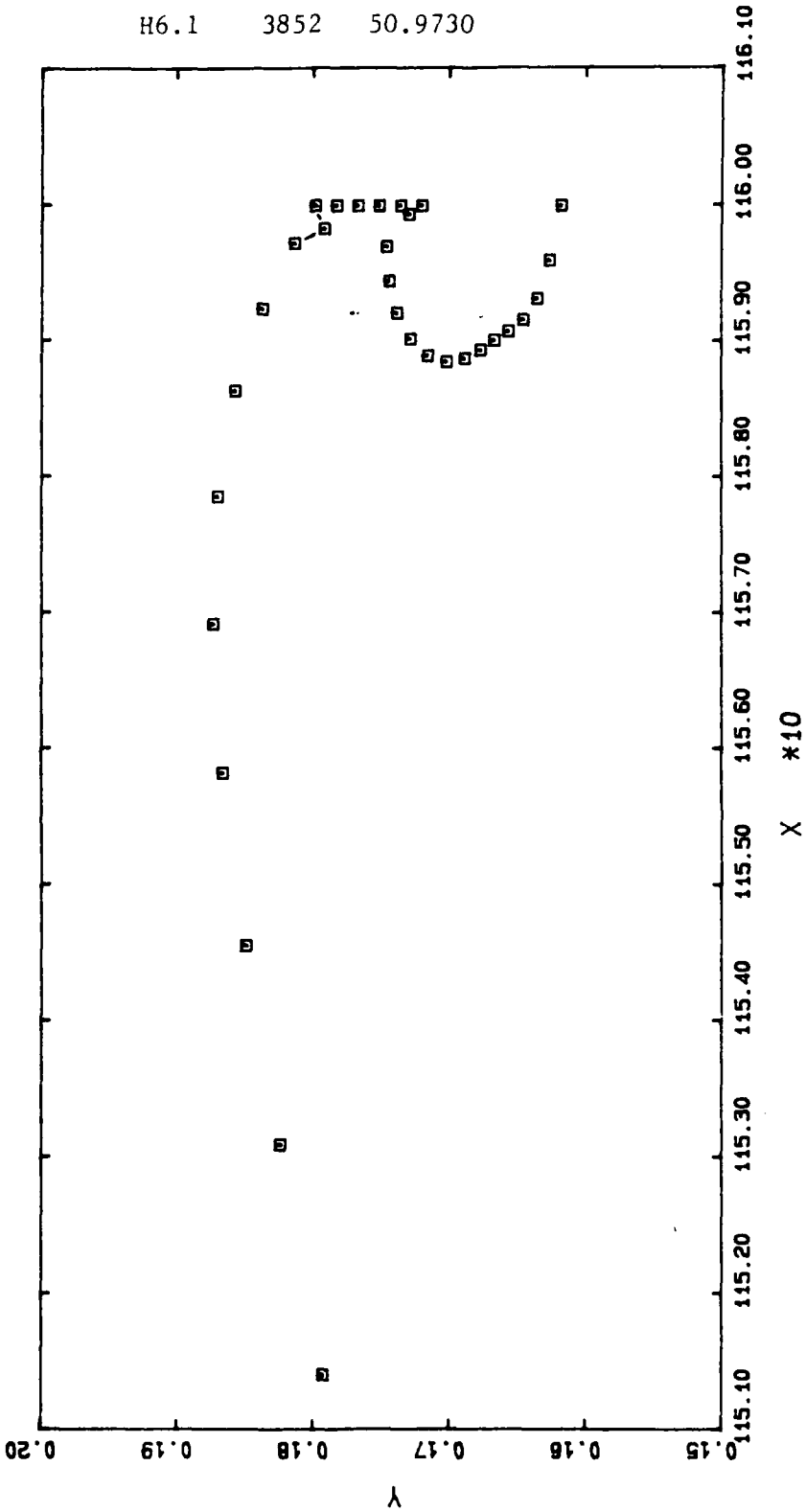

H6.1 3853 50.9731

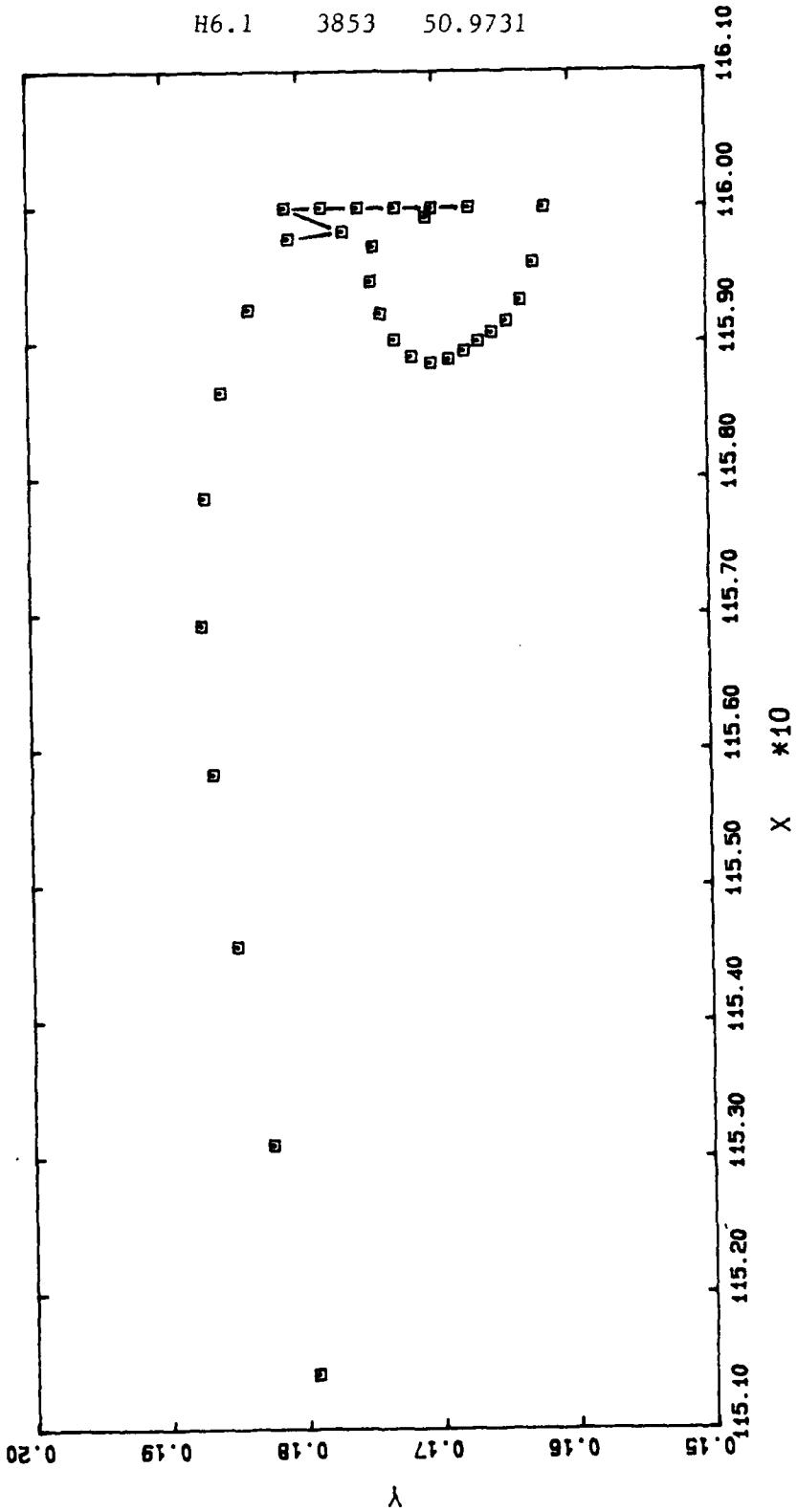

Appendix I

Refer to Chapter 6 for discussion.

I1.1 3871 50.9739

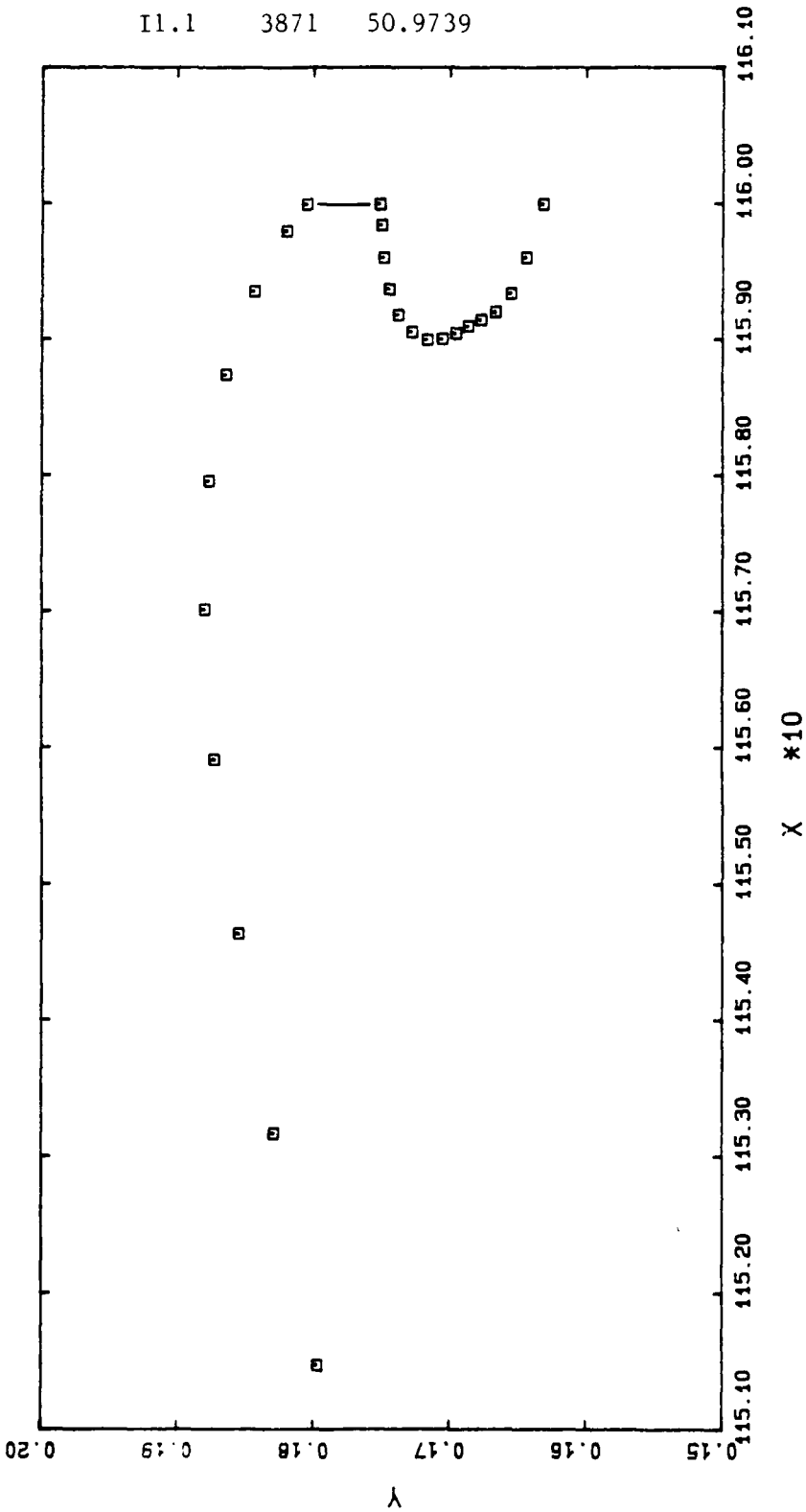

I1.1 3872 50.9739

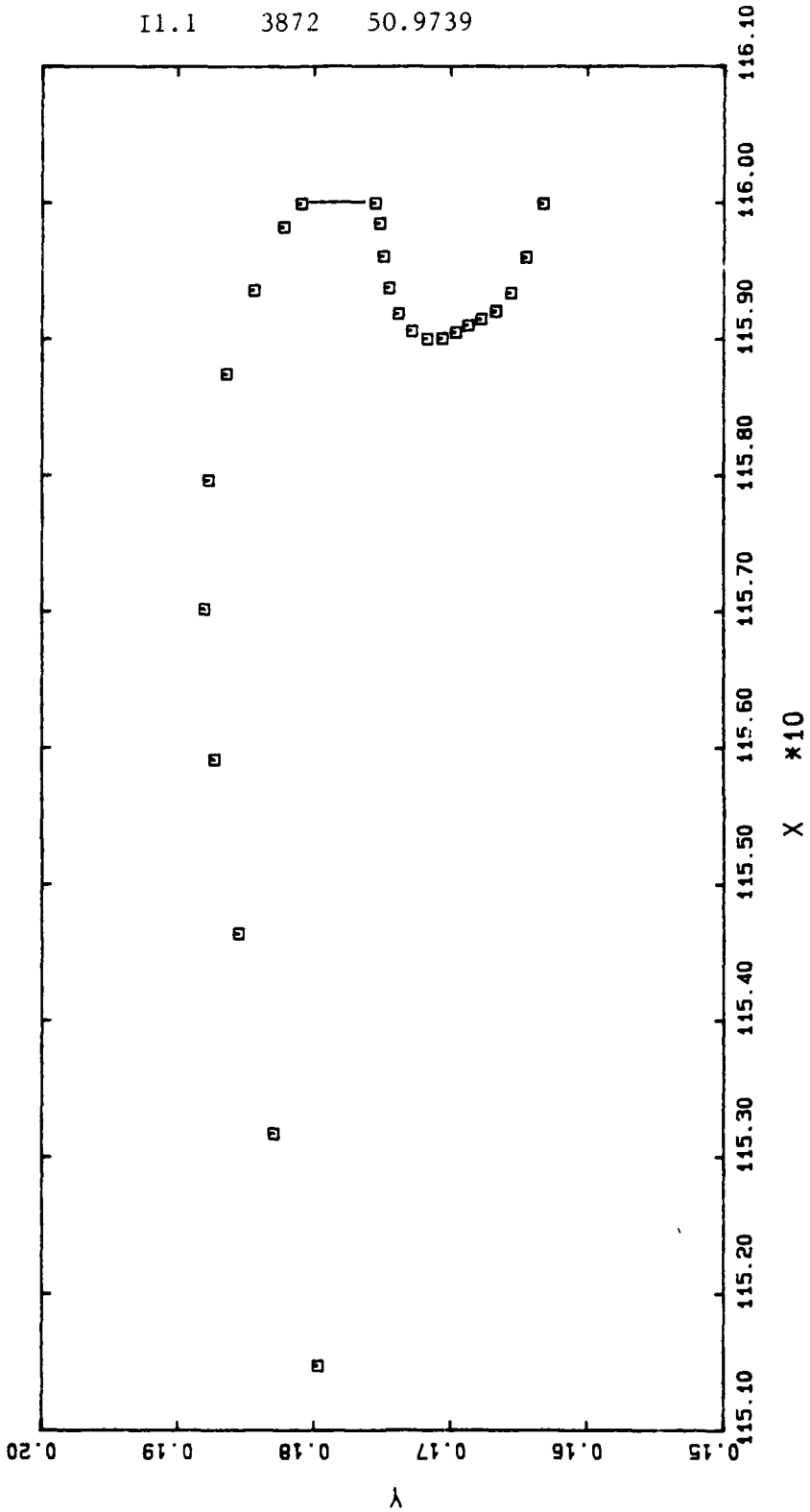

I1.1 3873 50.9739

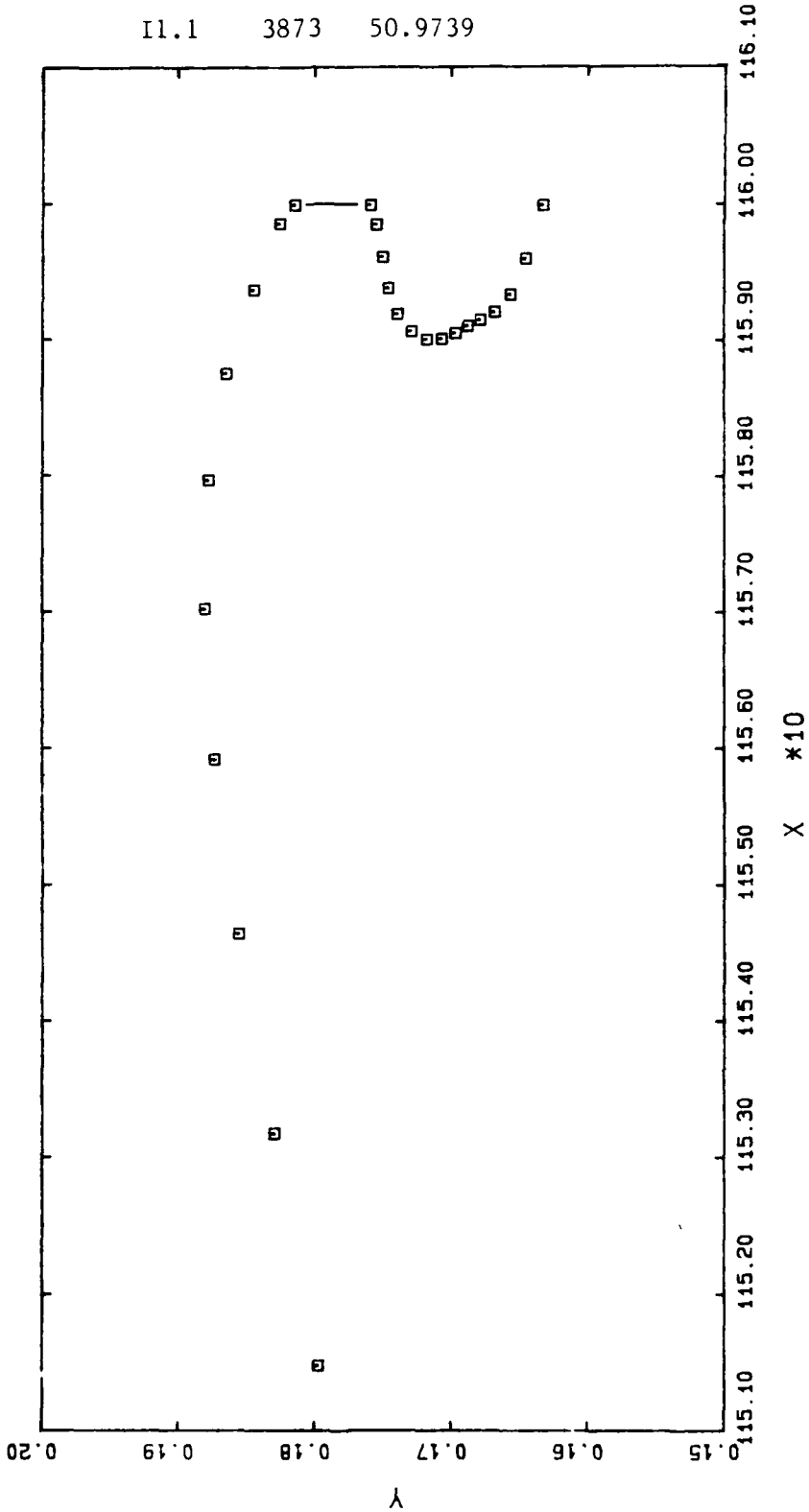

I1.1 3874 50.9740

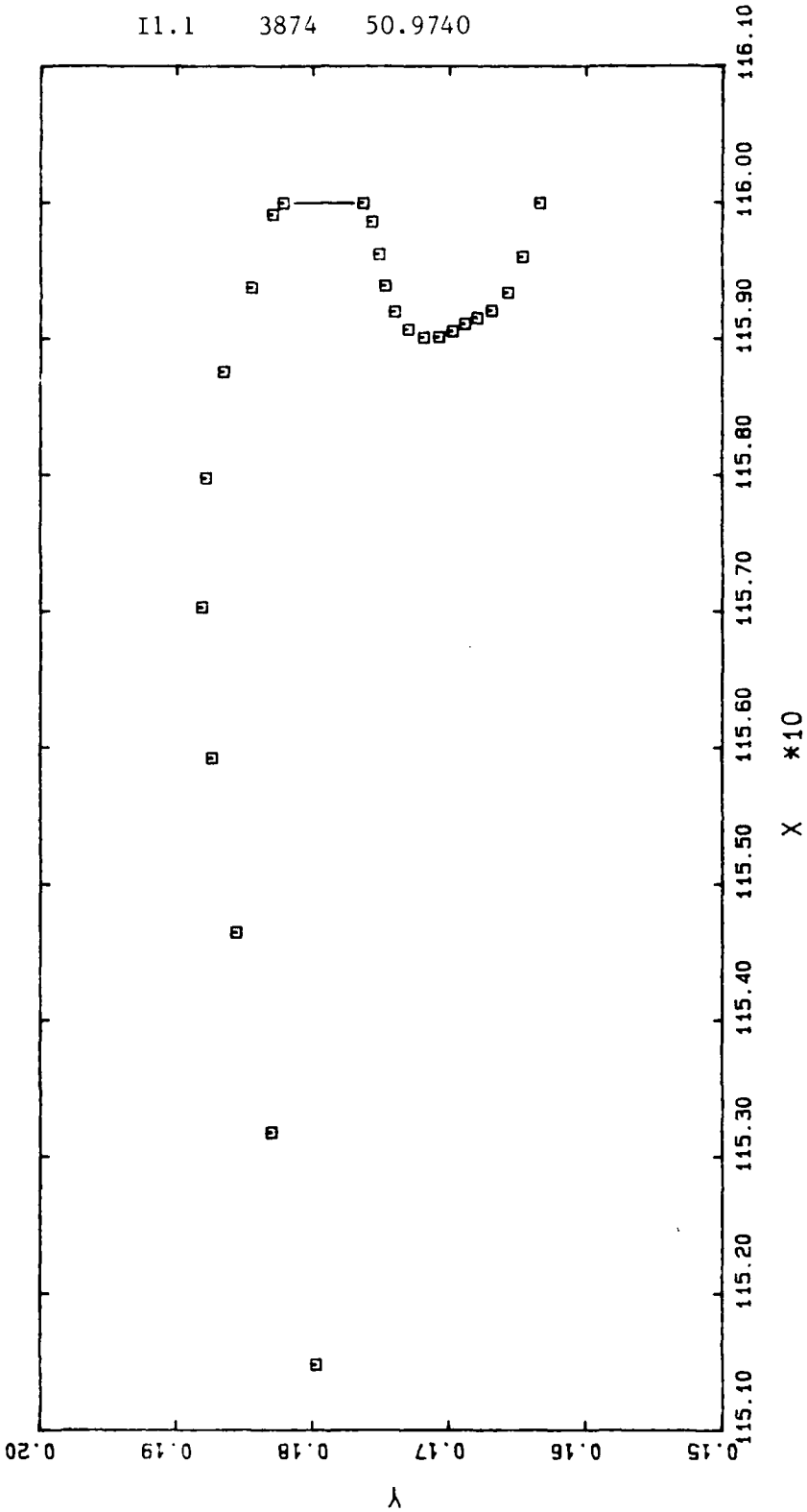

I1.1 3875 50.9740

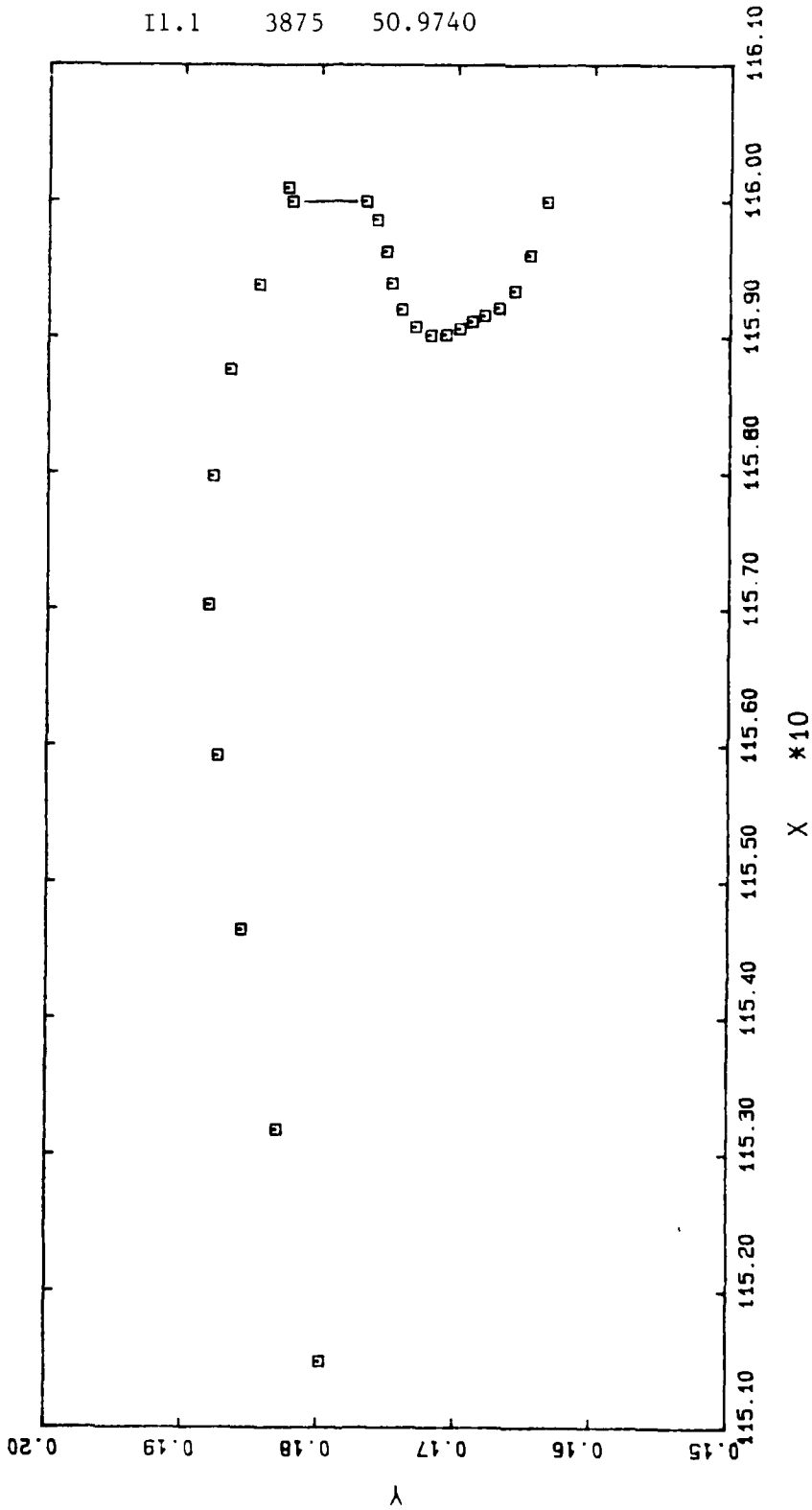

I2.1 3871 50.9739

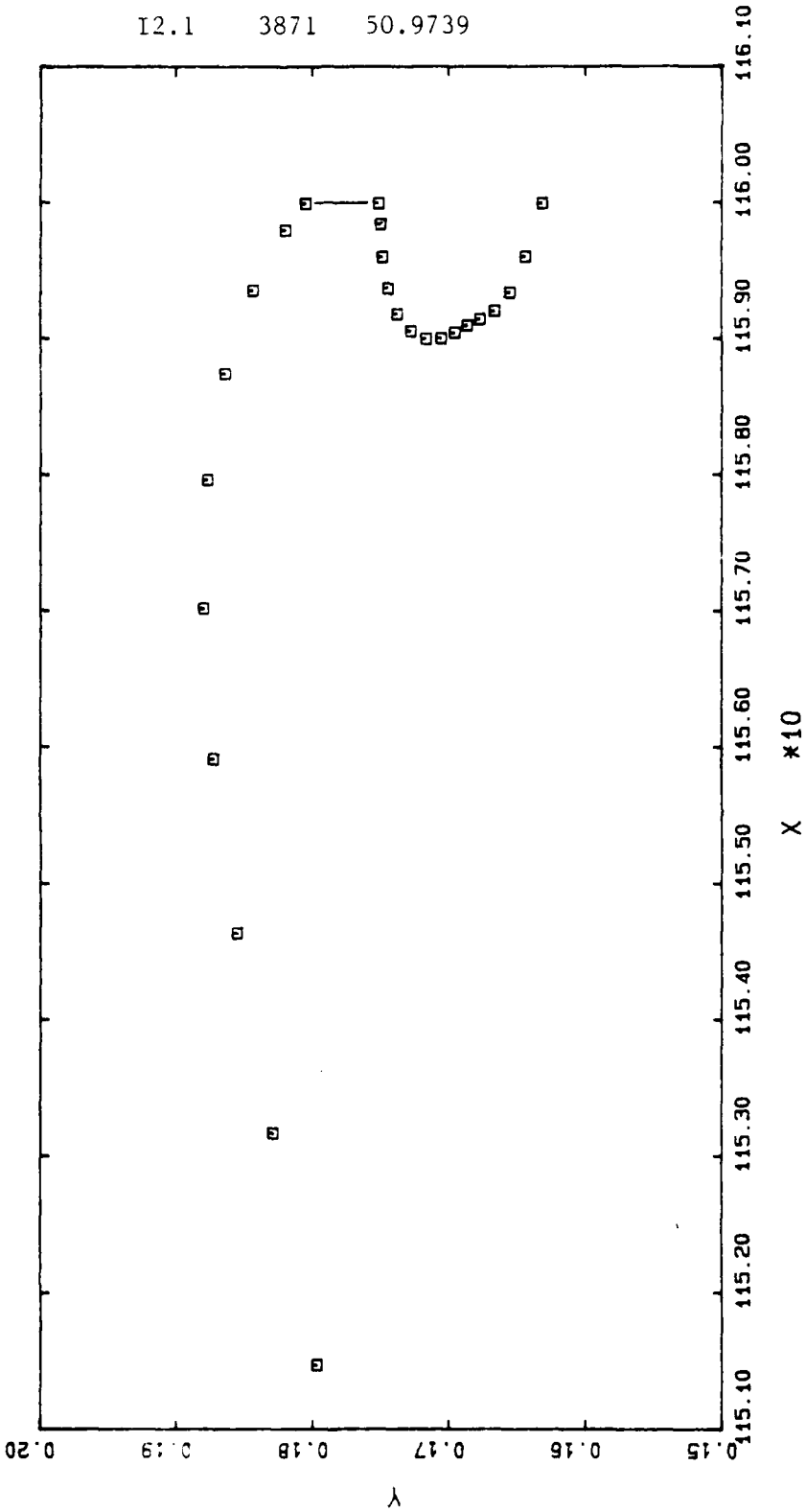

I2.1 3881 50.9742

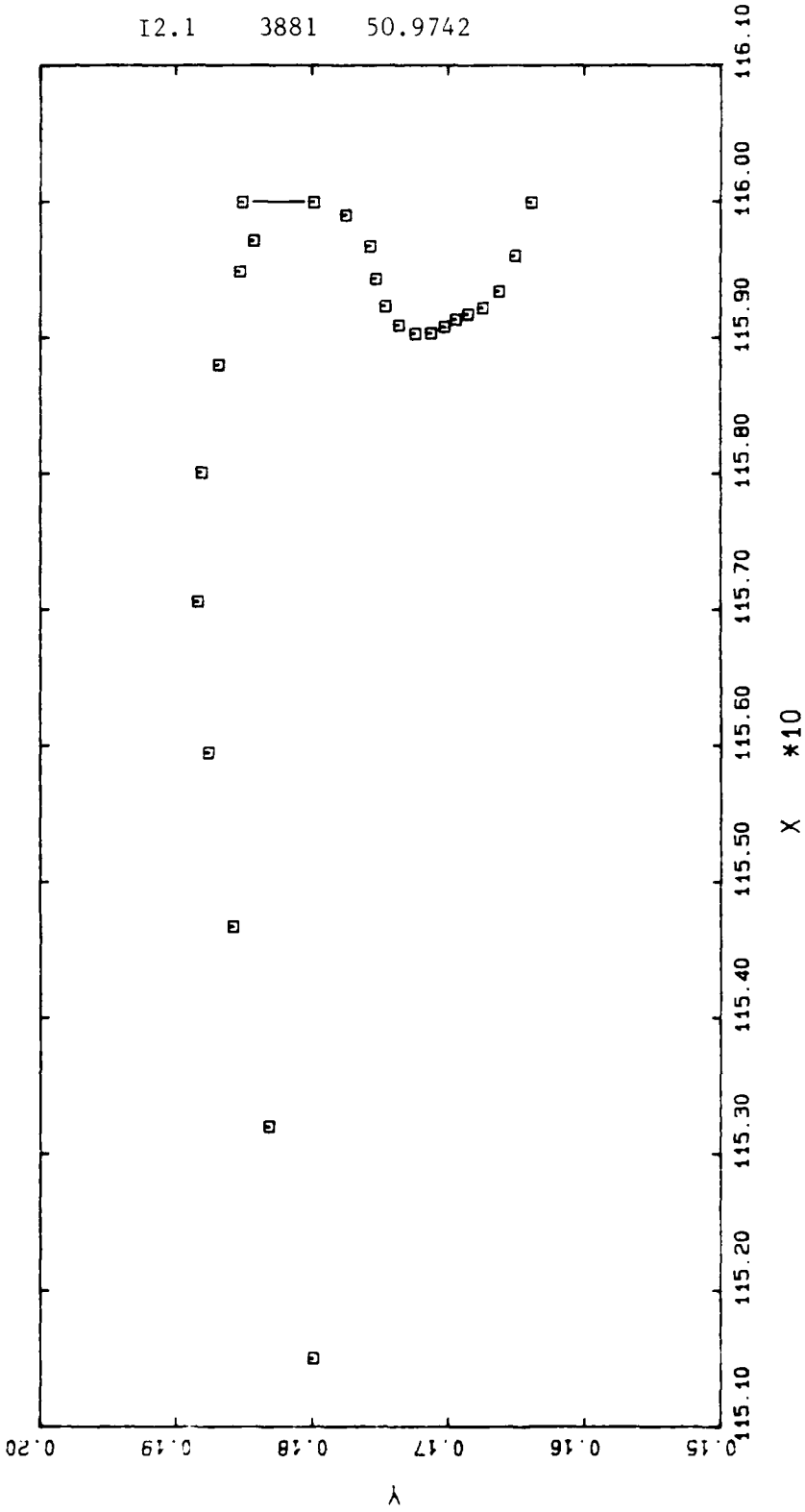

I2.1 3891 50.9746

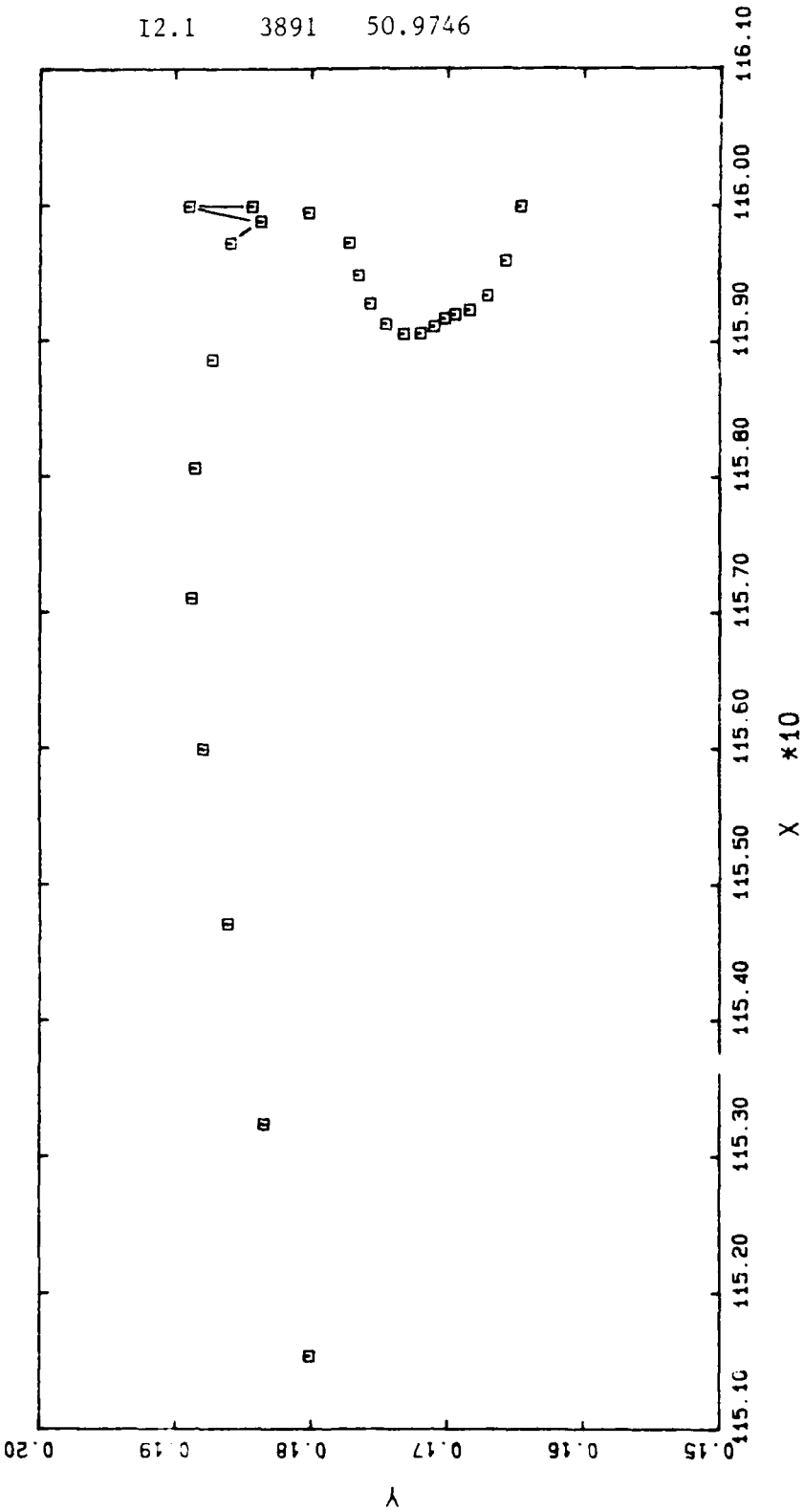

I2.2 3871 50.9739

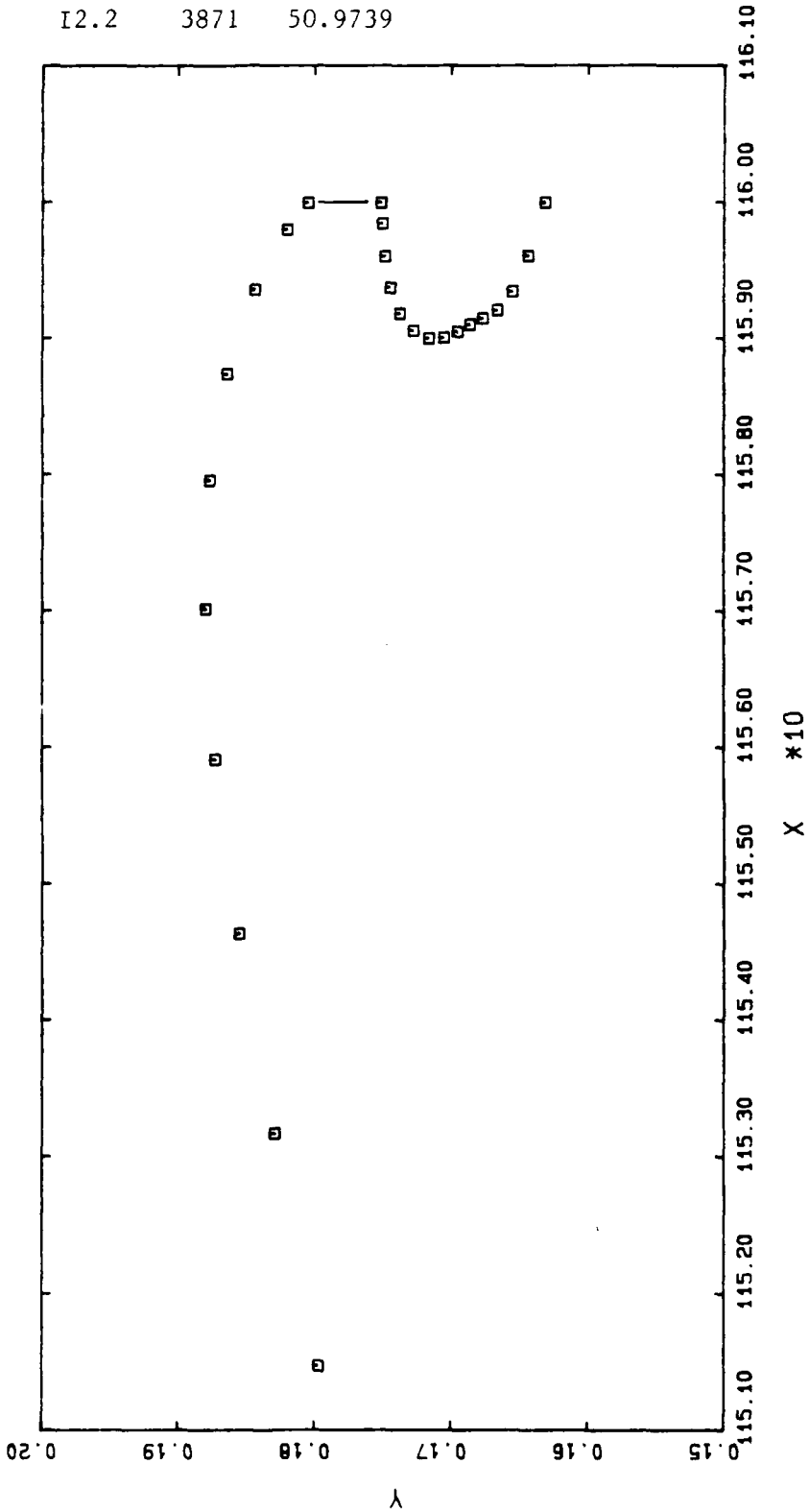

I2.2 3881 50.9742

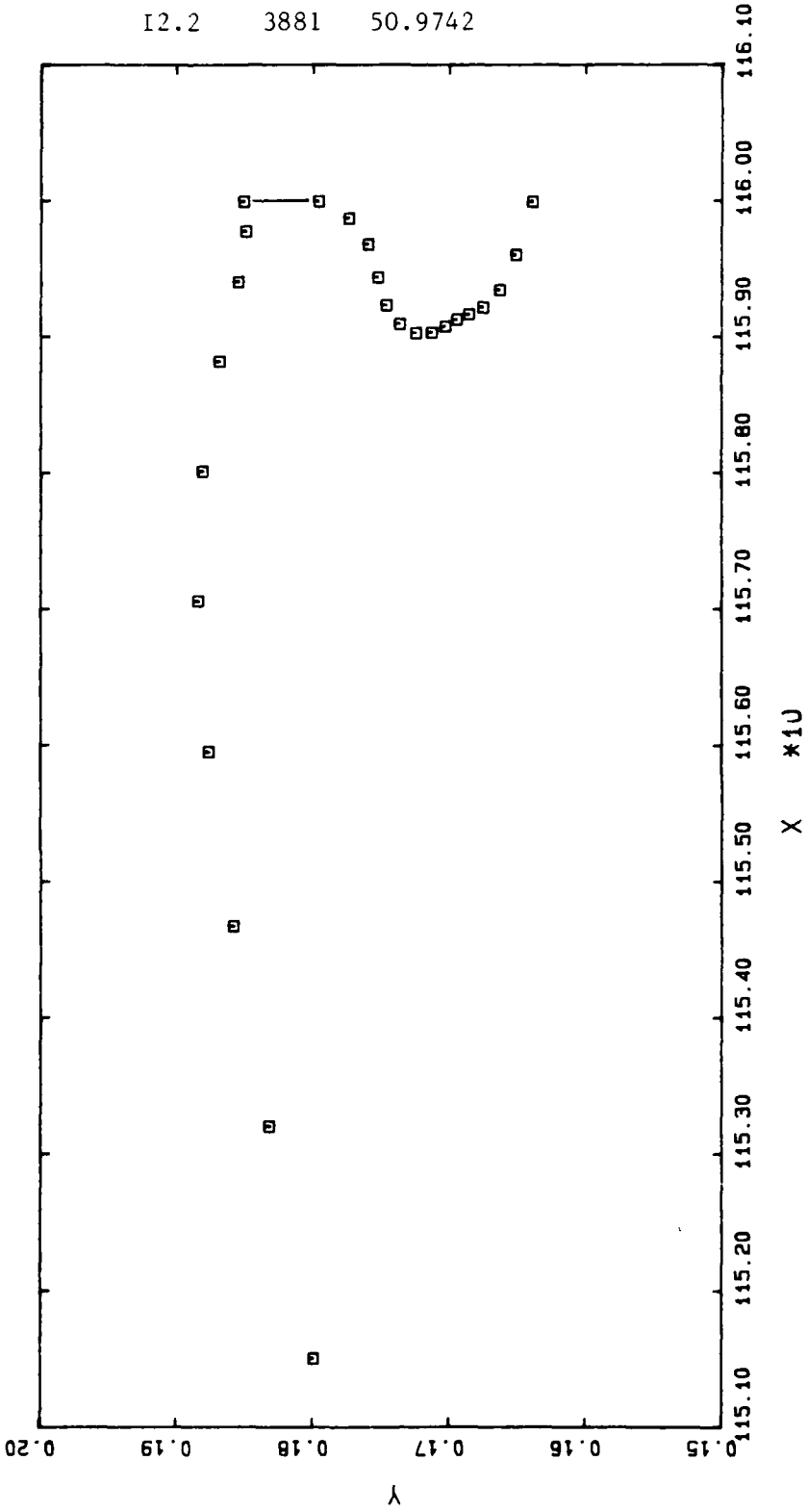

I2.2 3891 50.9746

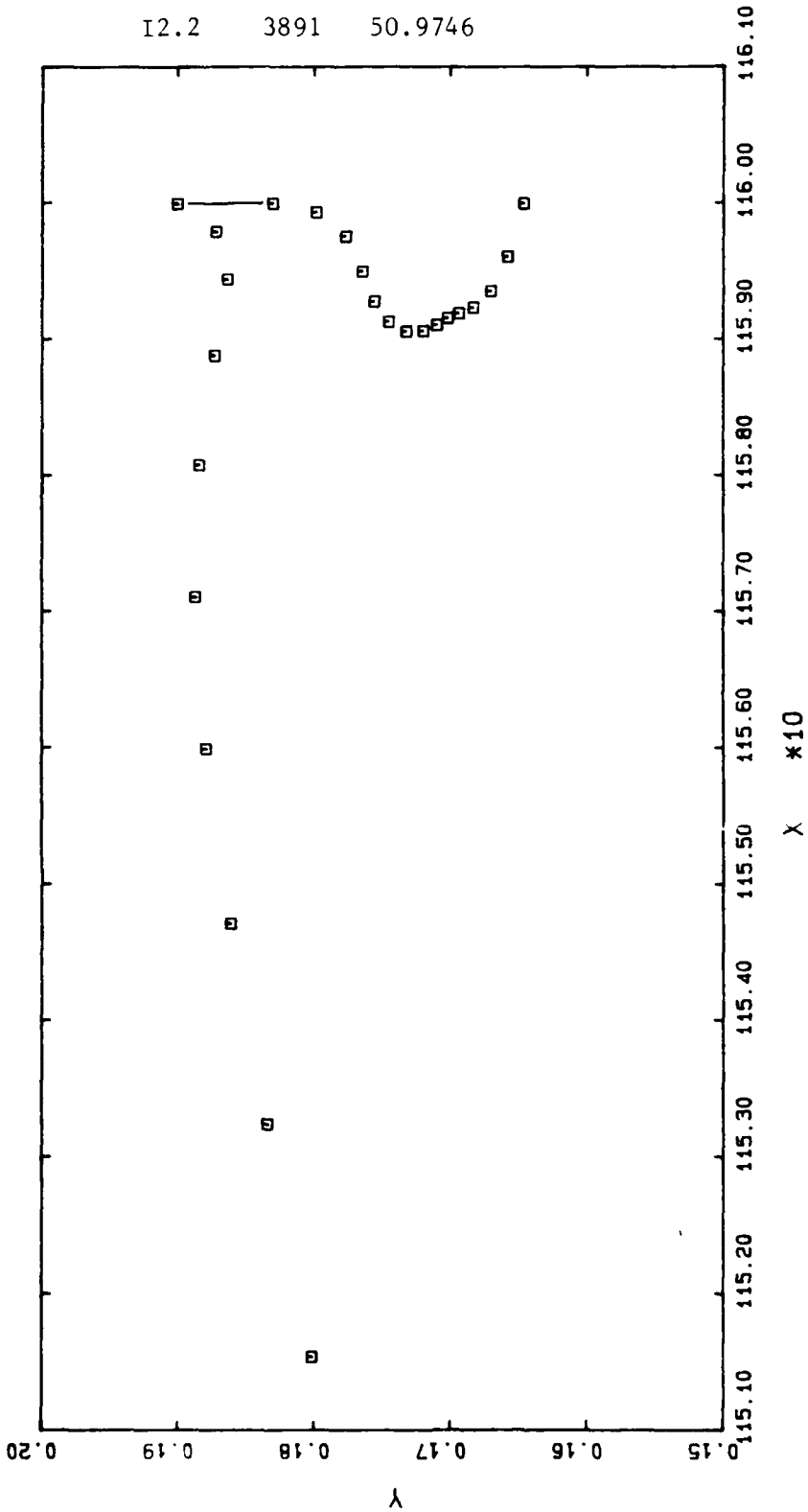

I2.2 3901 50.9750

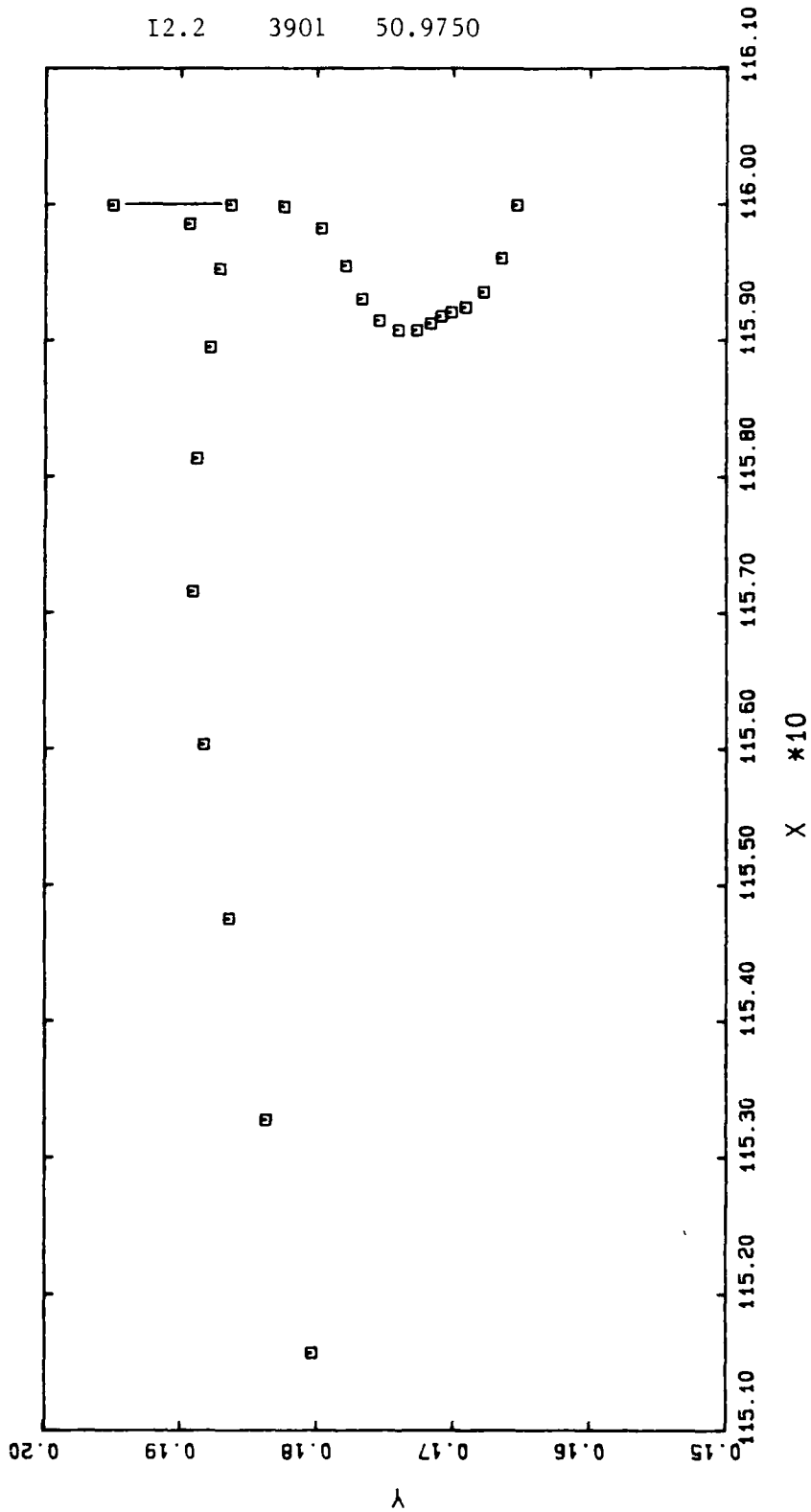

I2.2 3911 50.9754

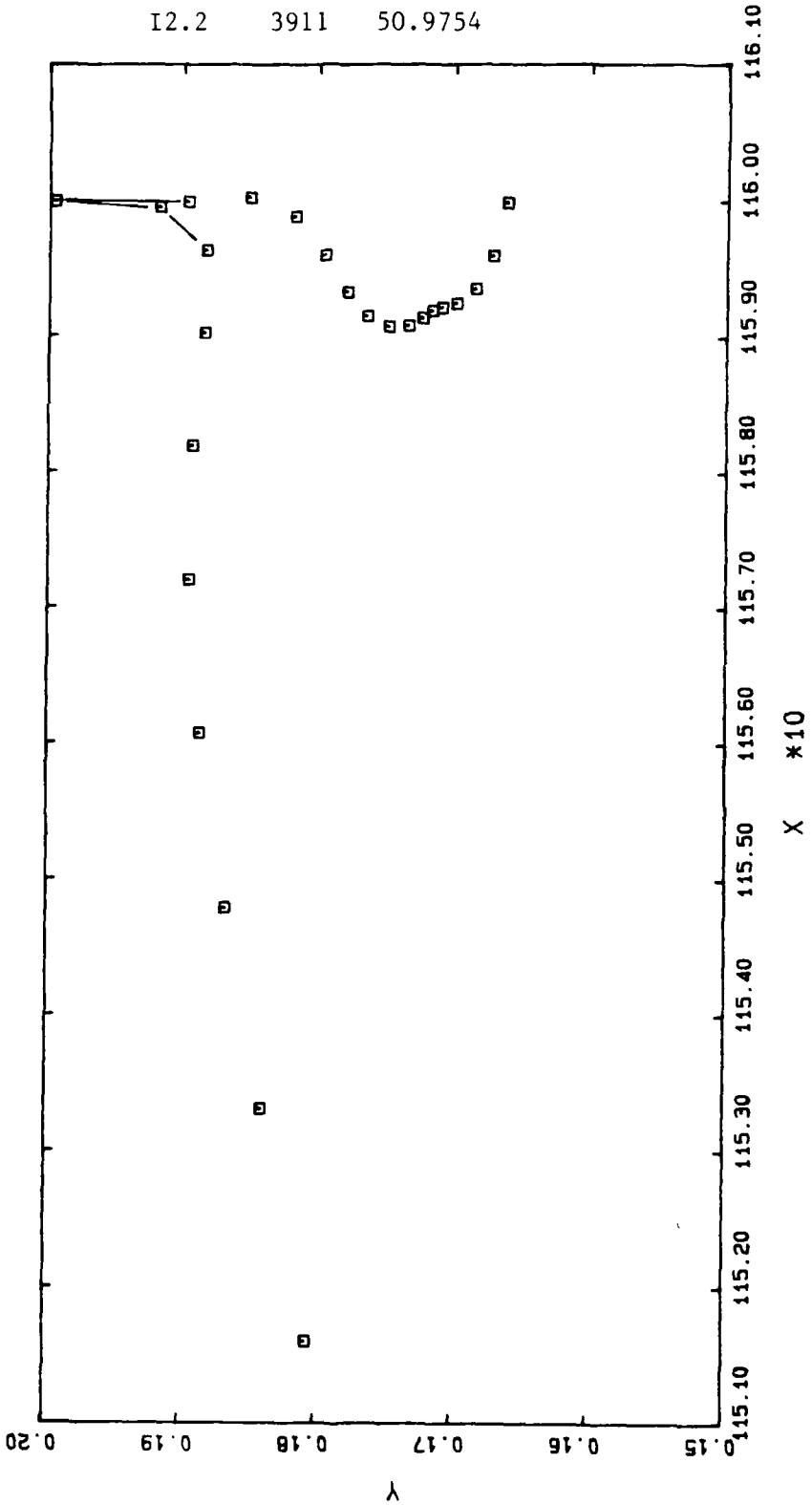

I3.1 3871 50.9739

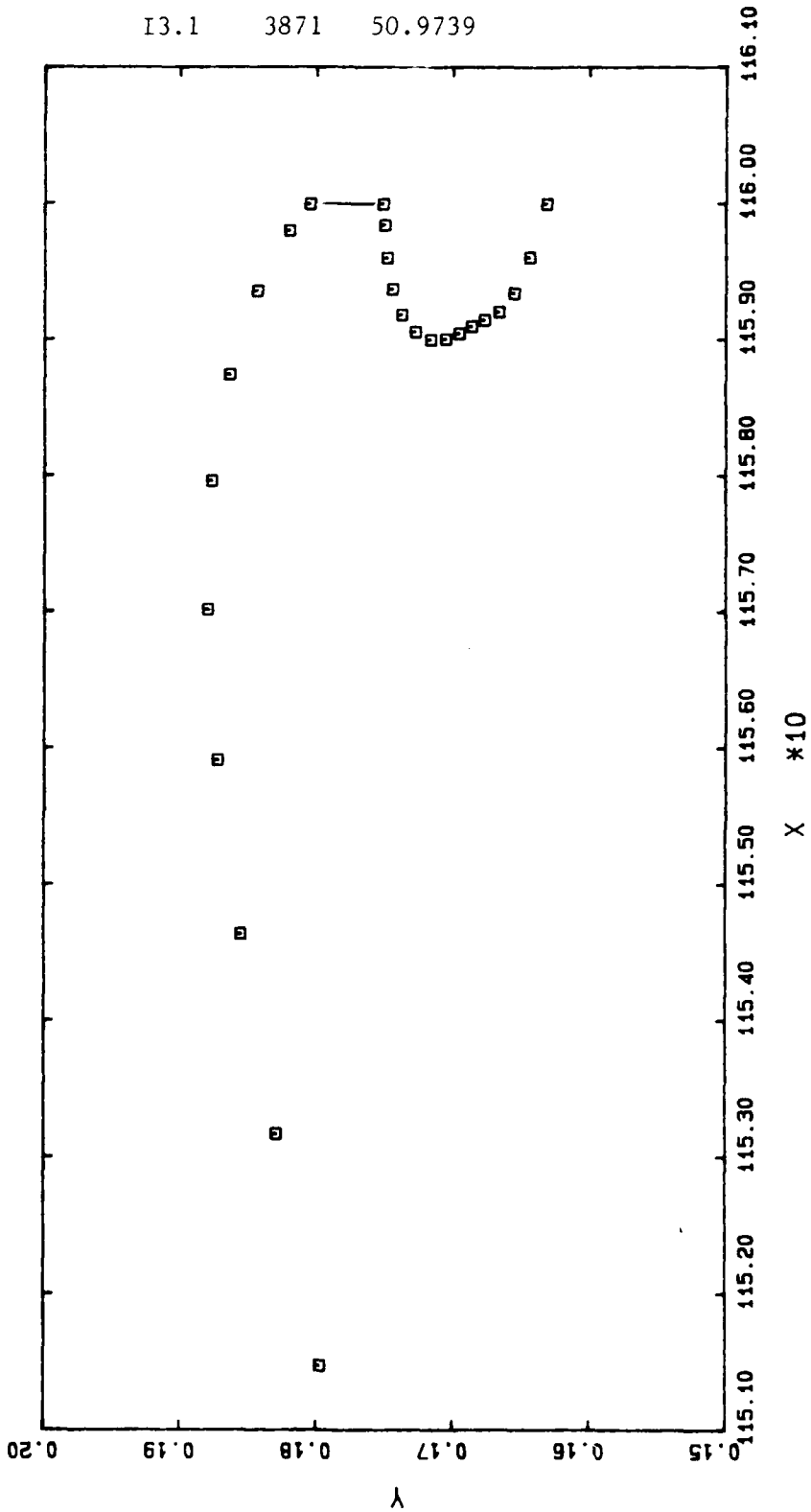

I3.1 3872 50.9739

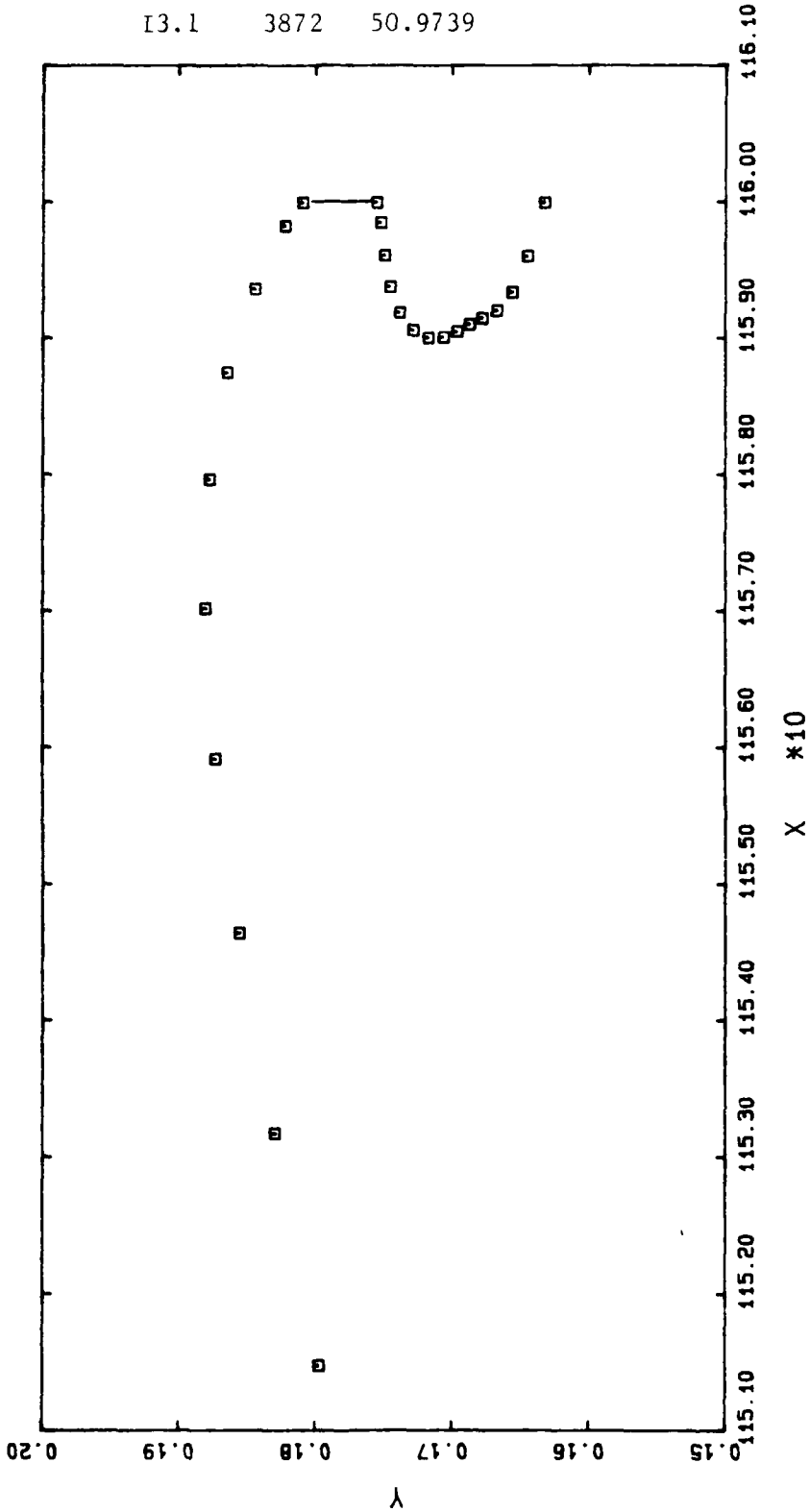

I3.1 3873 50.9739

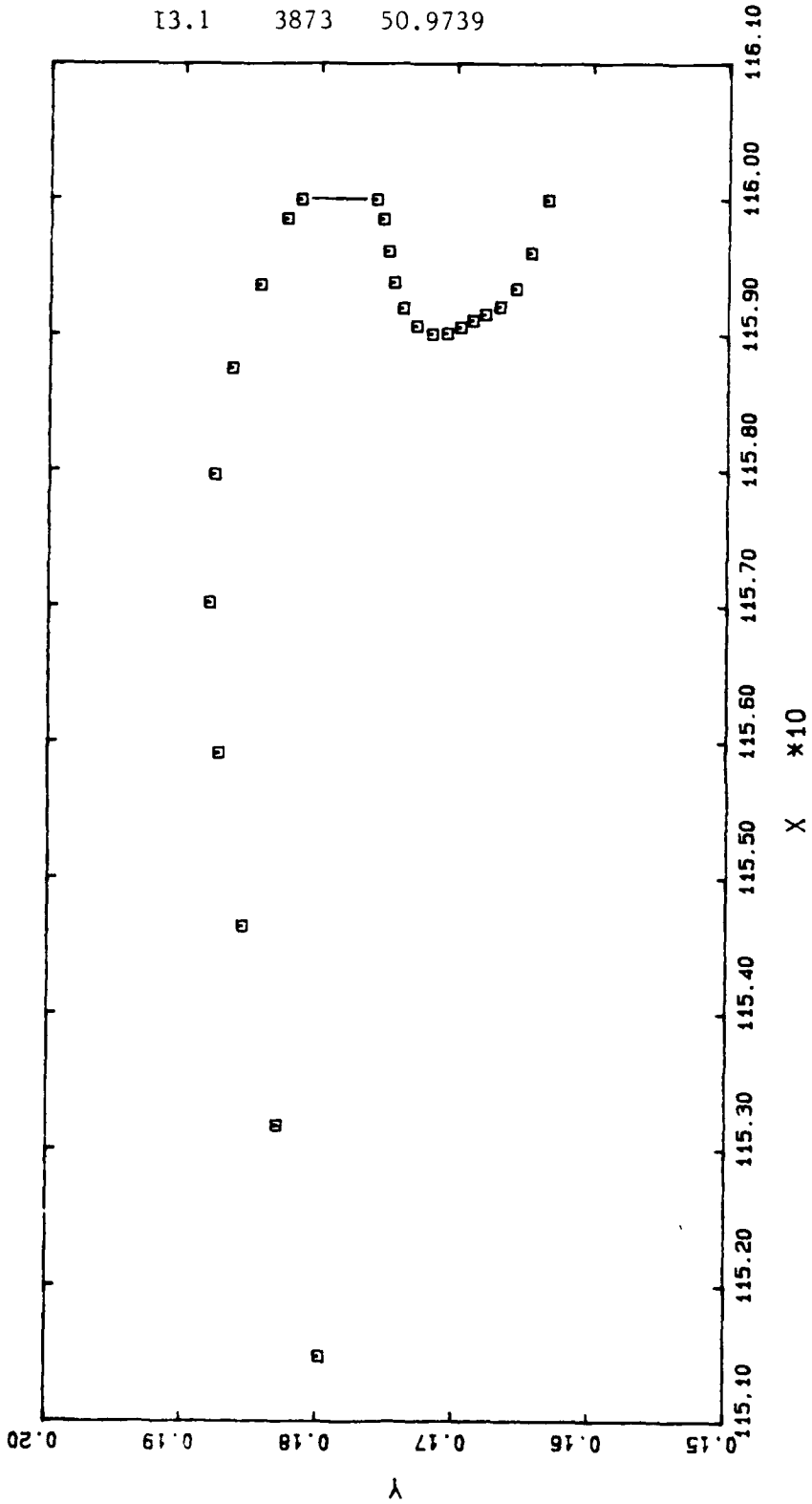

I3.1 3874 50.9740

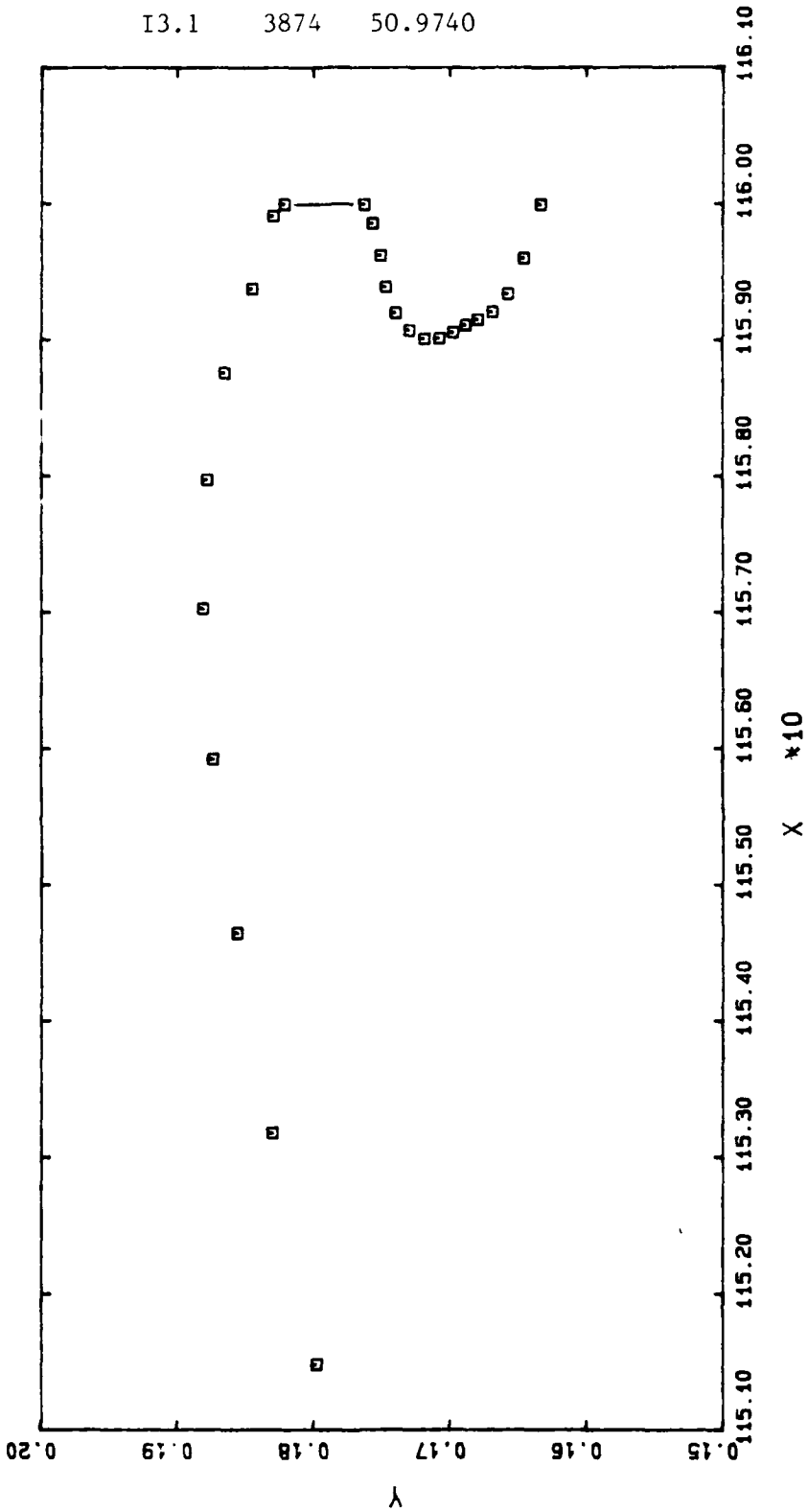

I3.1 3875 50.9740

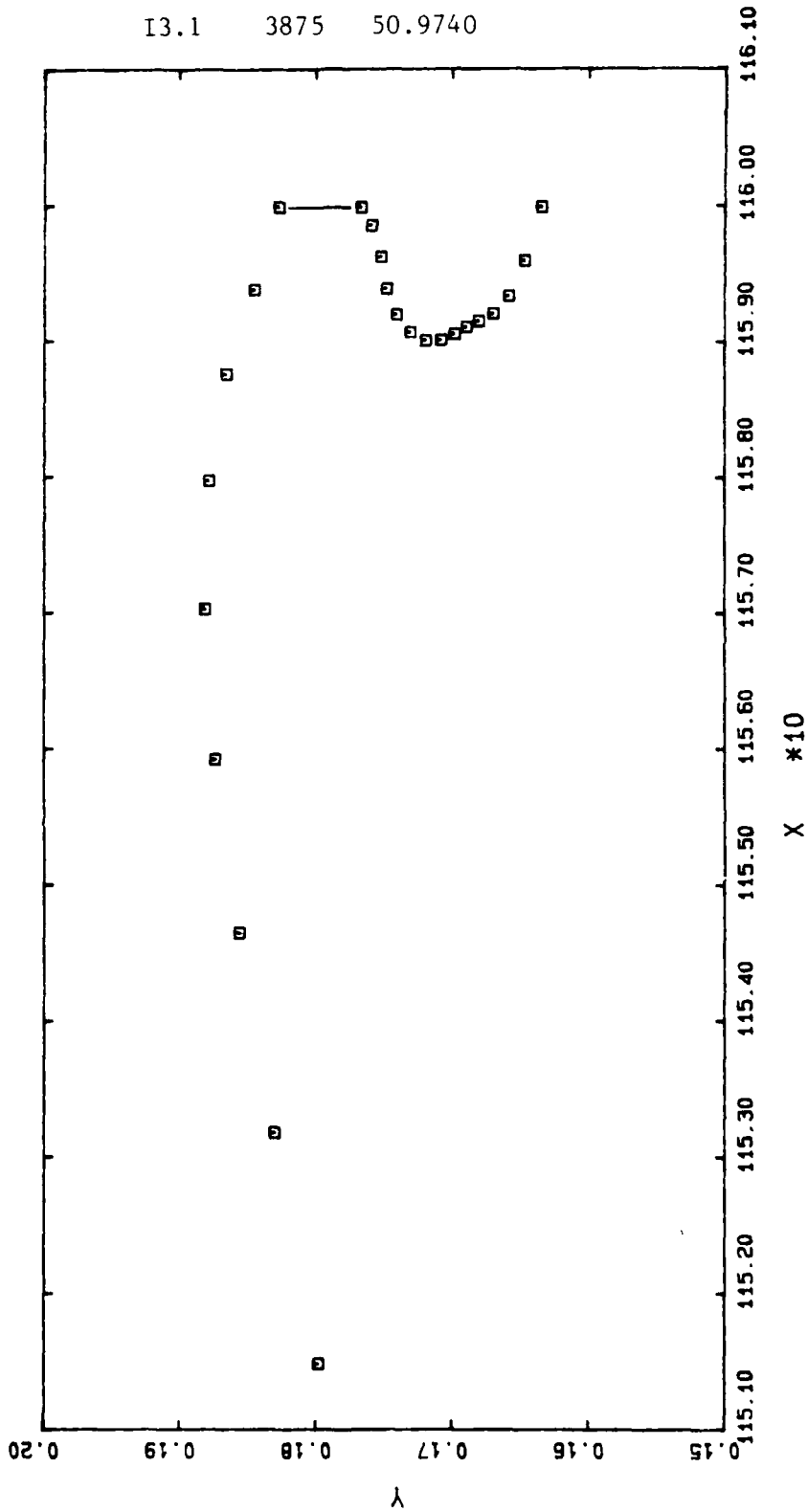

I3.1 3876 50.9741

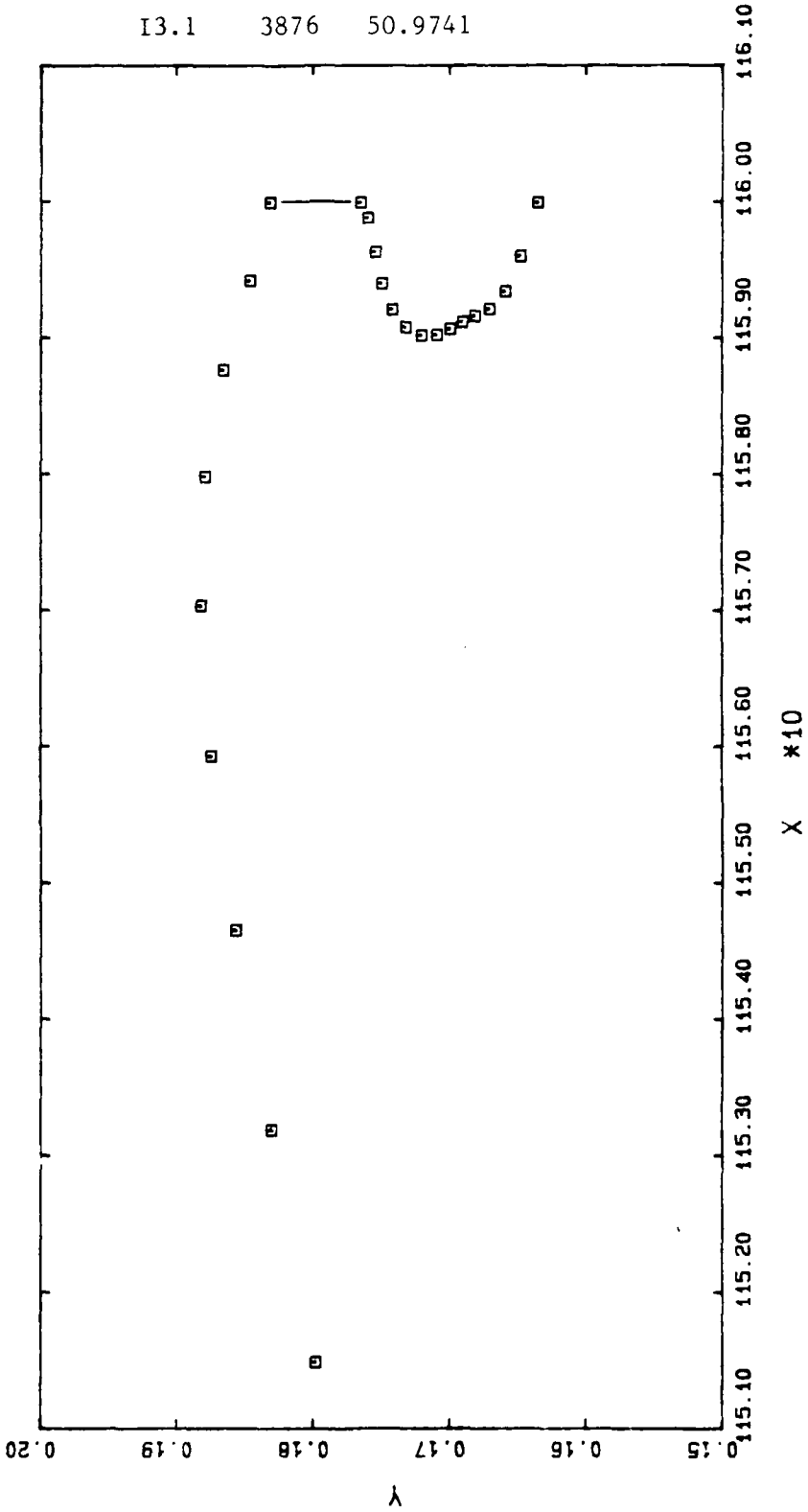

I3.1 3877 50.9741

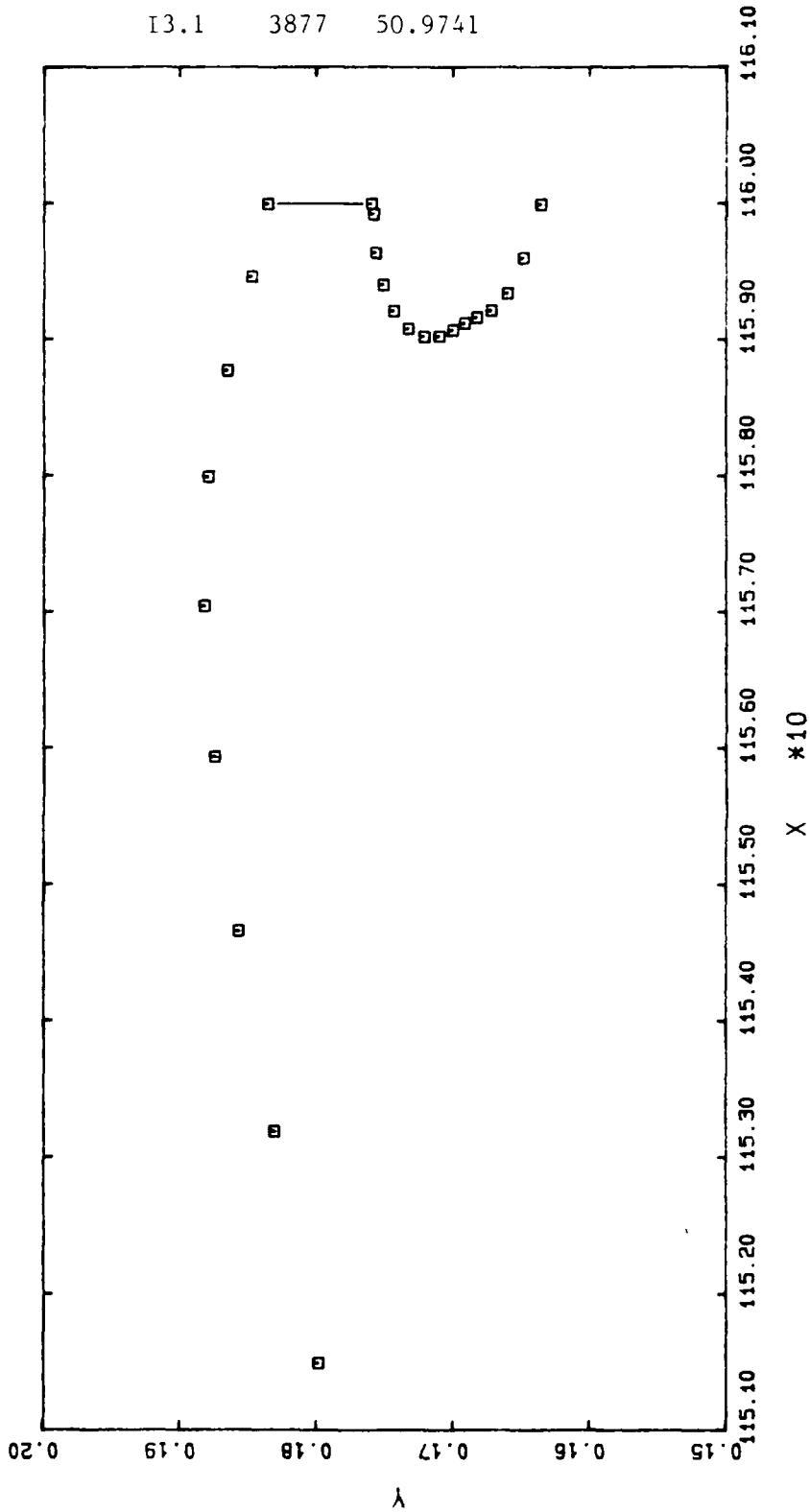

I3.1 3878 50.9741

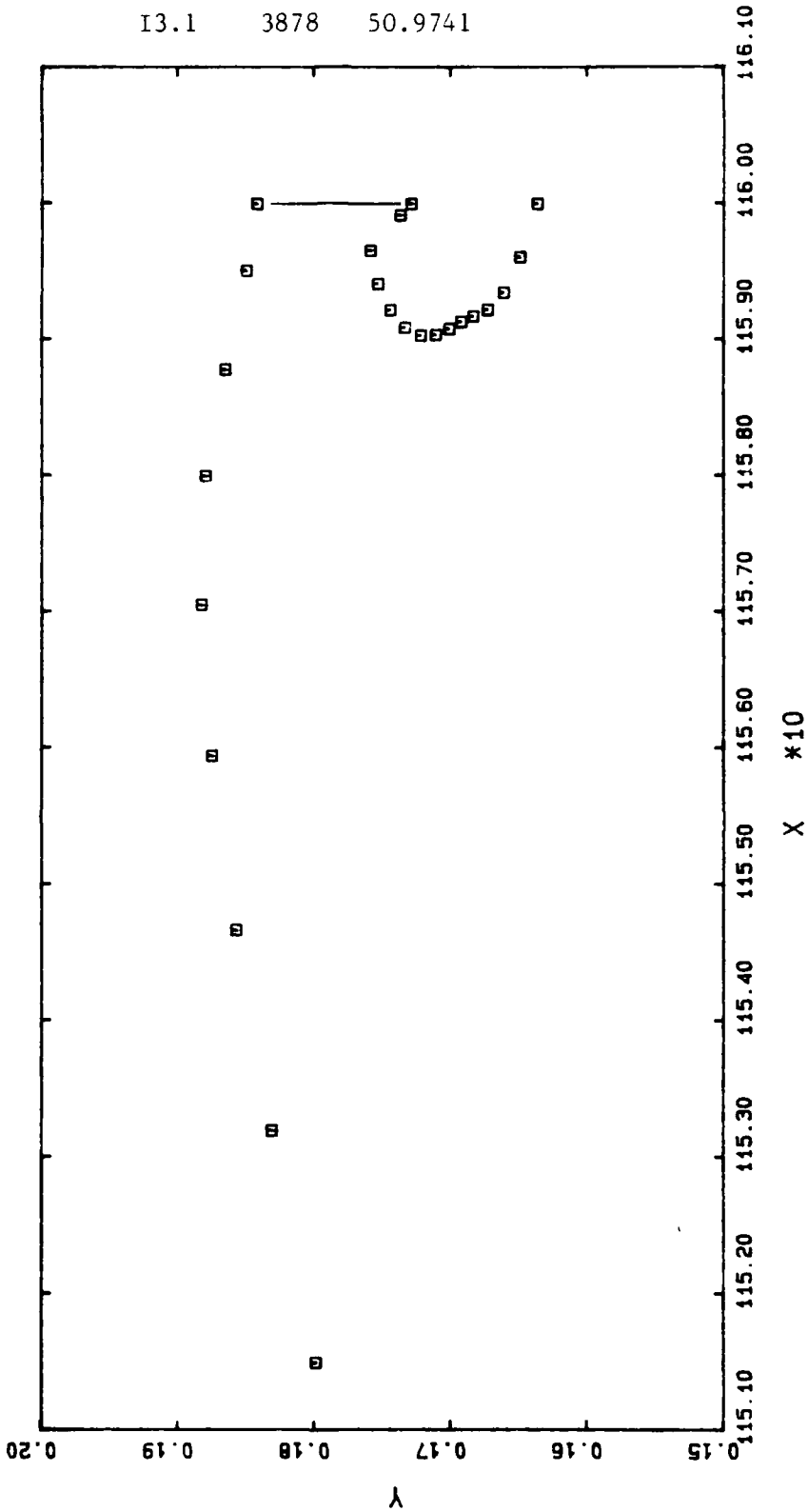

I3.1 3879 50.9742

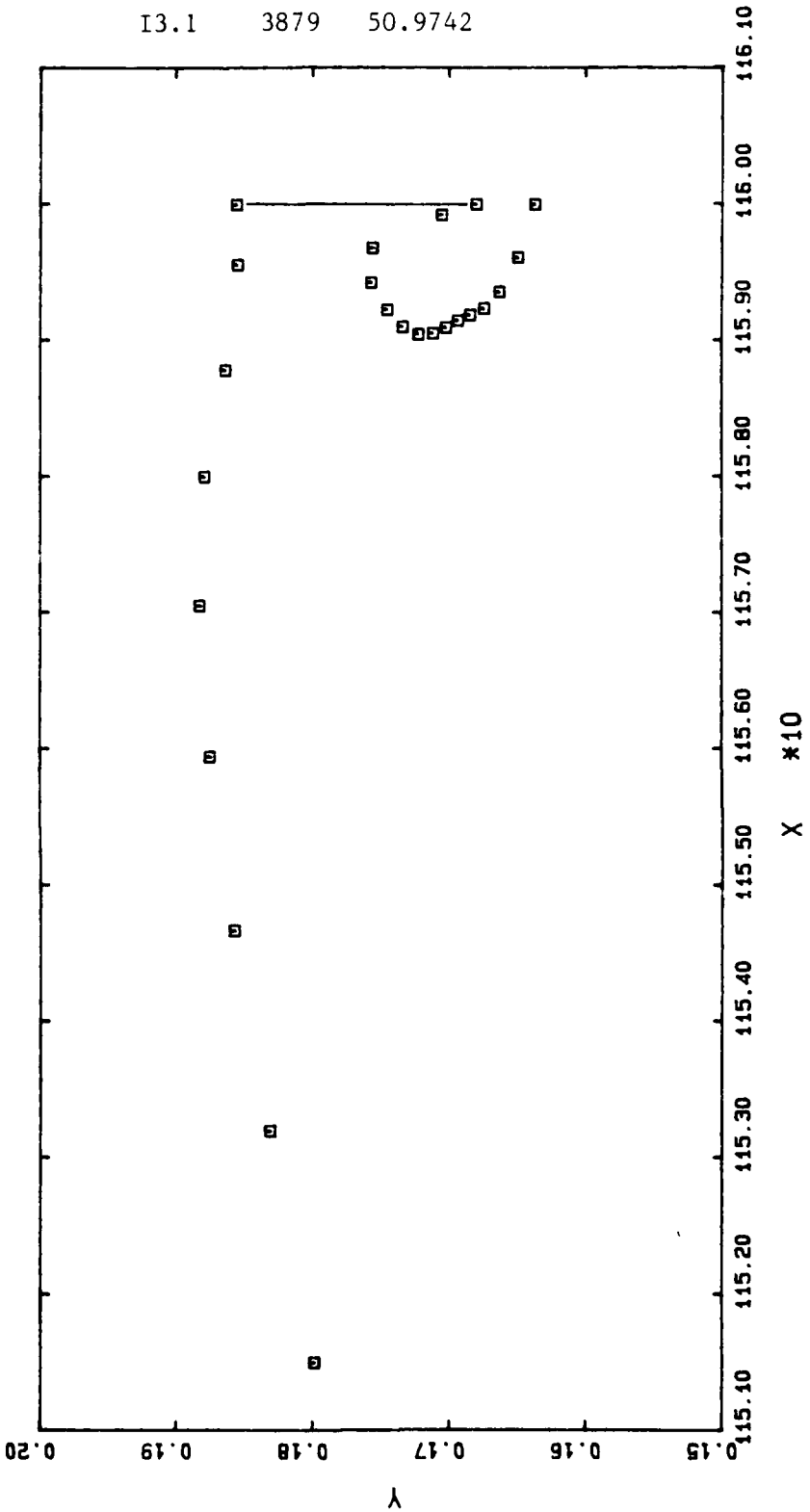

I3.1 3880 50.9742

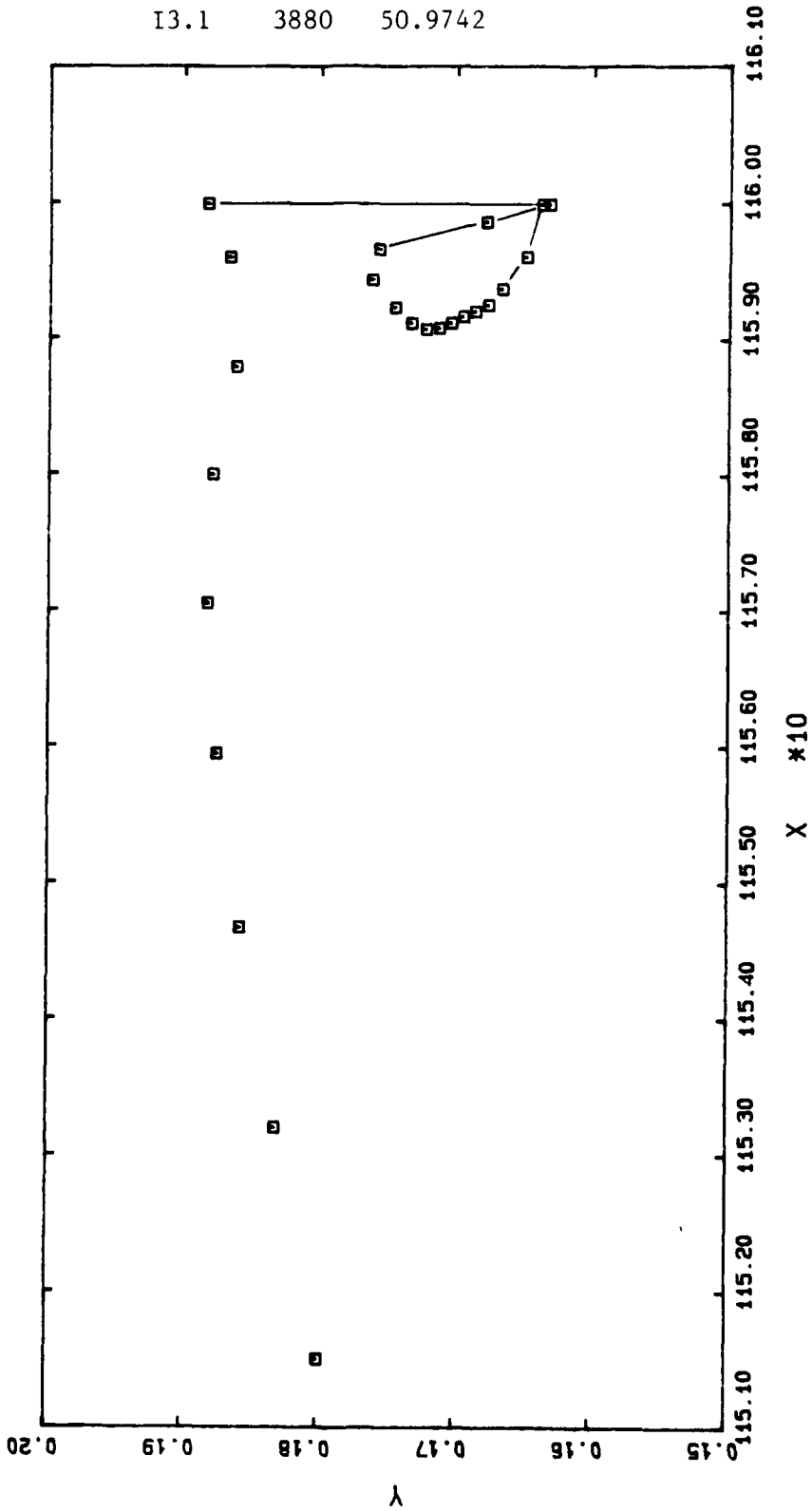

I3.2 3871 50.9739

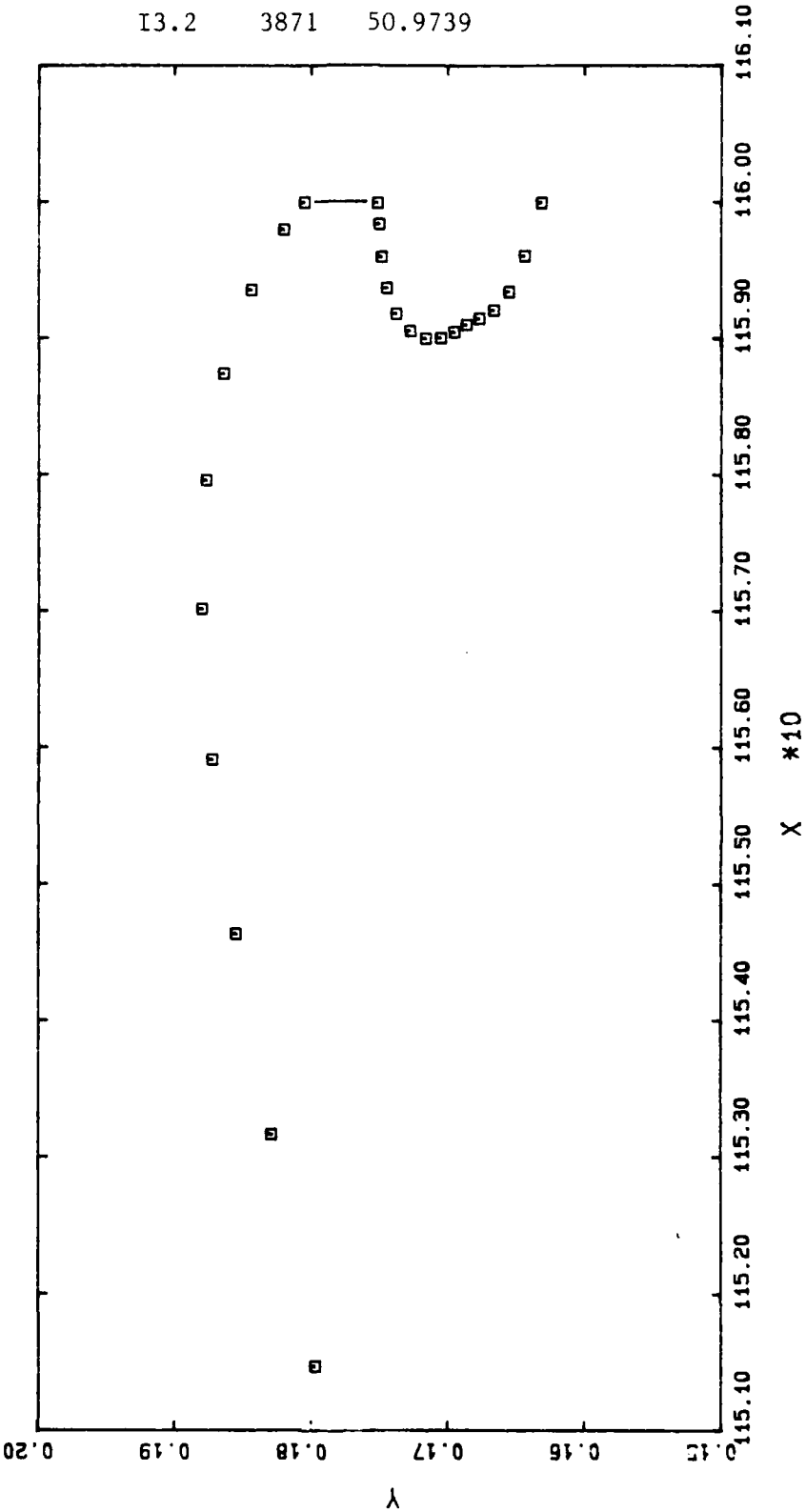

I3.2 3872 50.9739

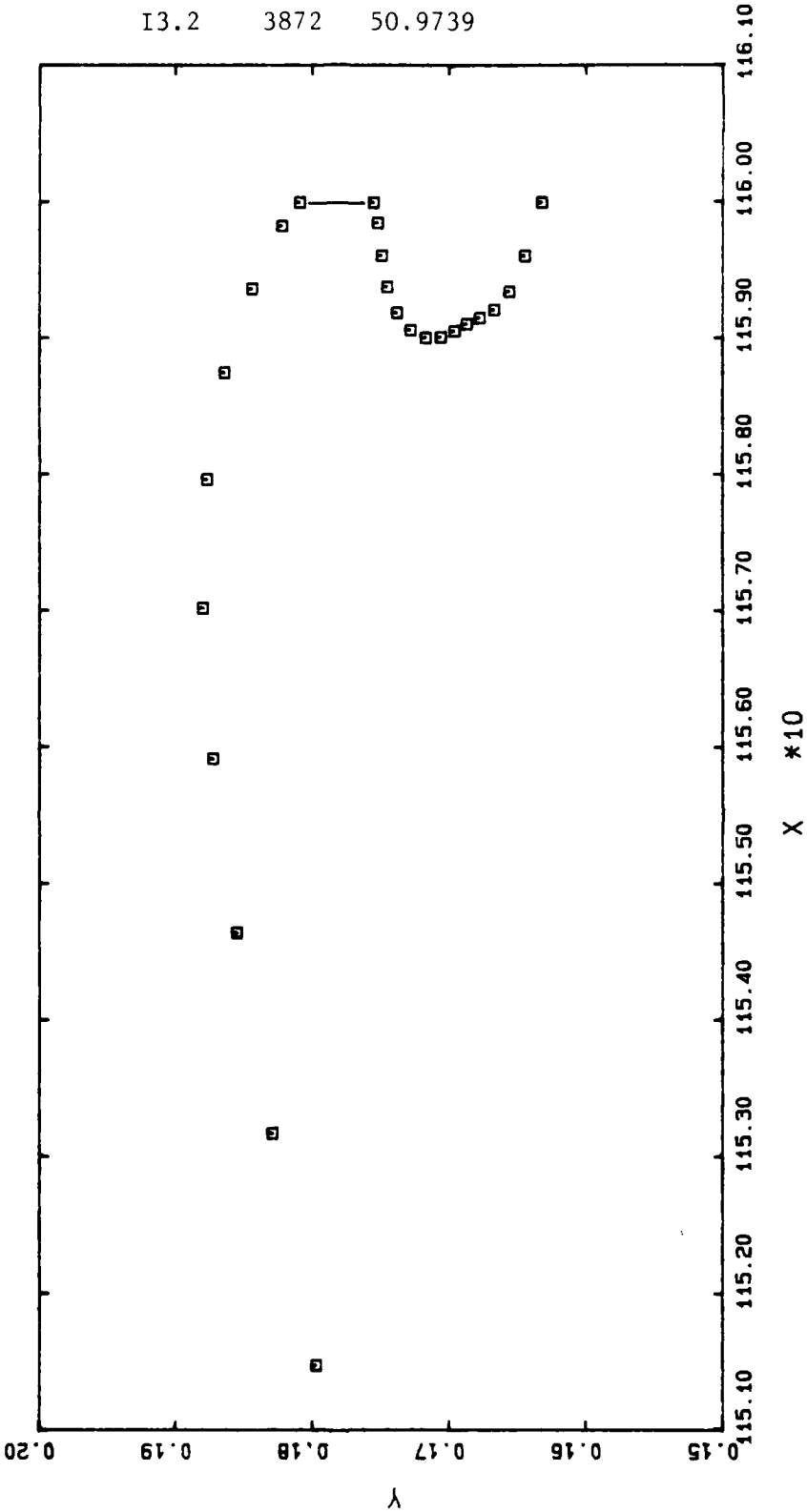

I3.2 3873 50.9739

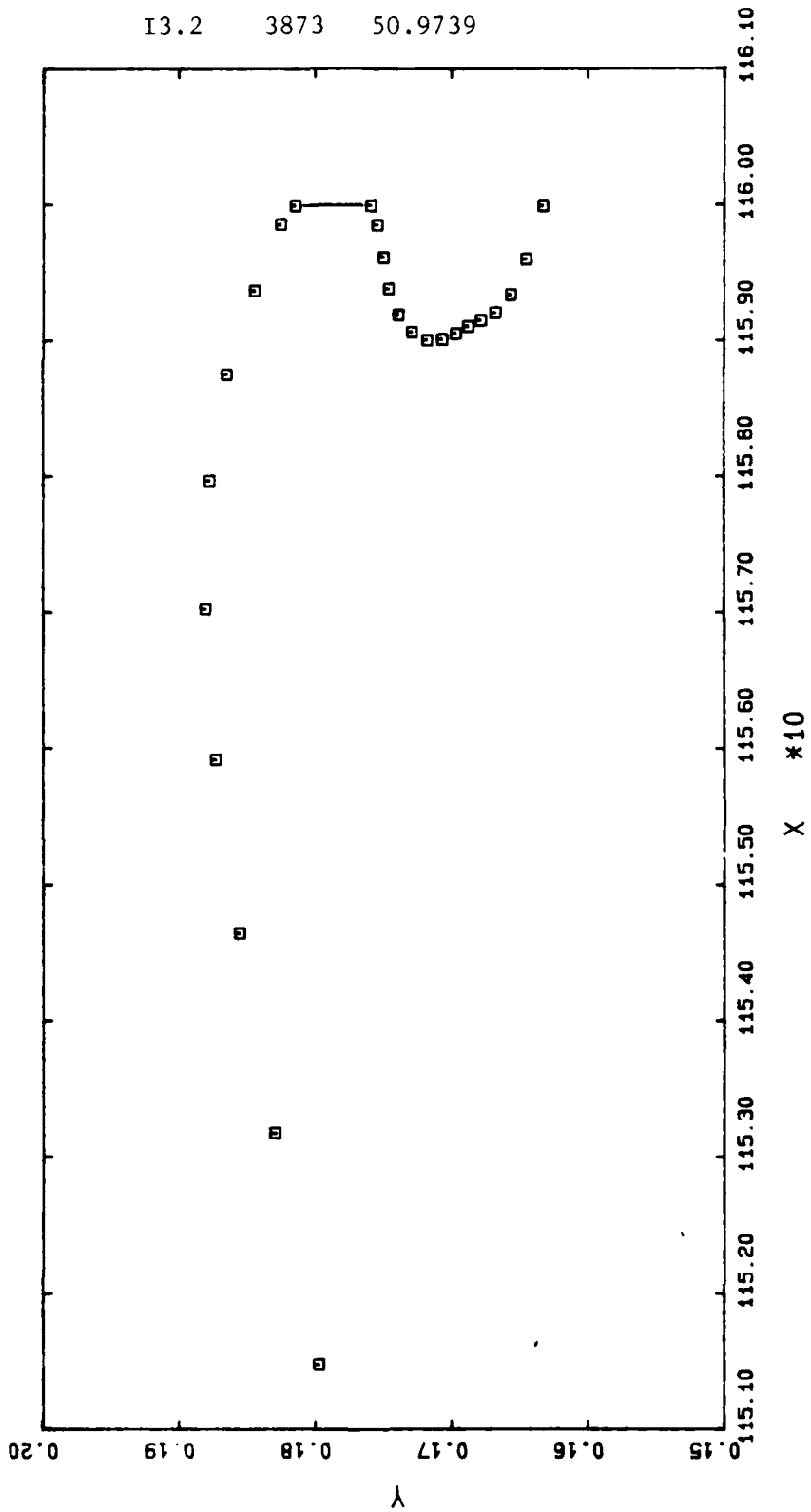

I3.2 3874 50.9740

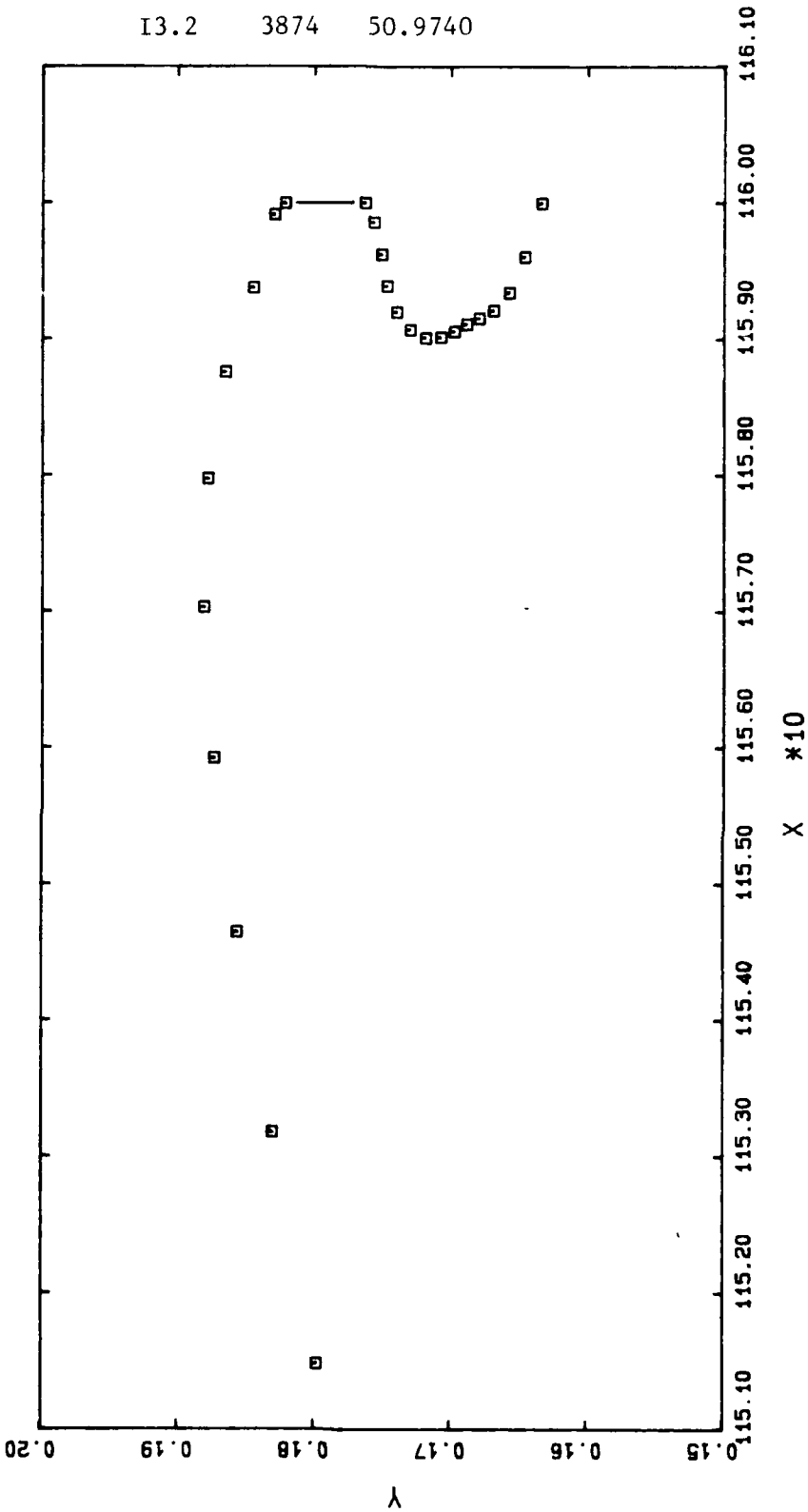

I3.2 3875 50.9740

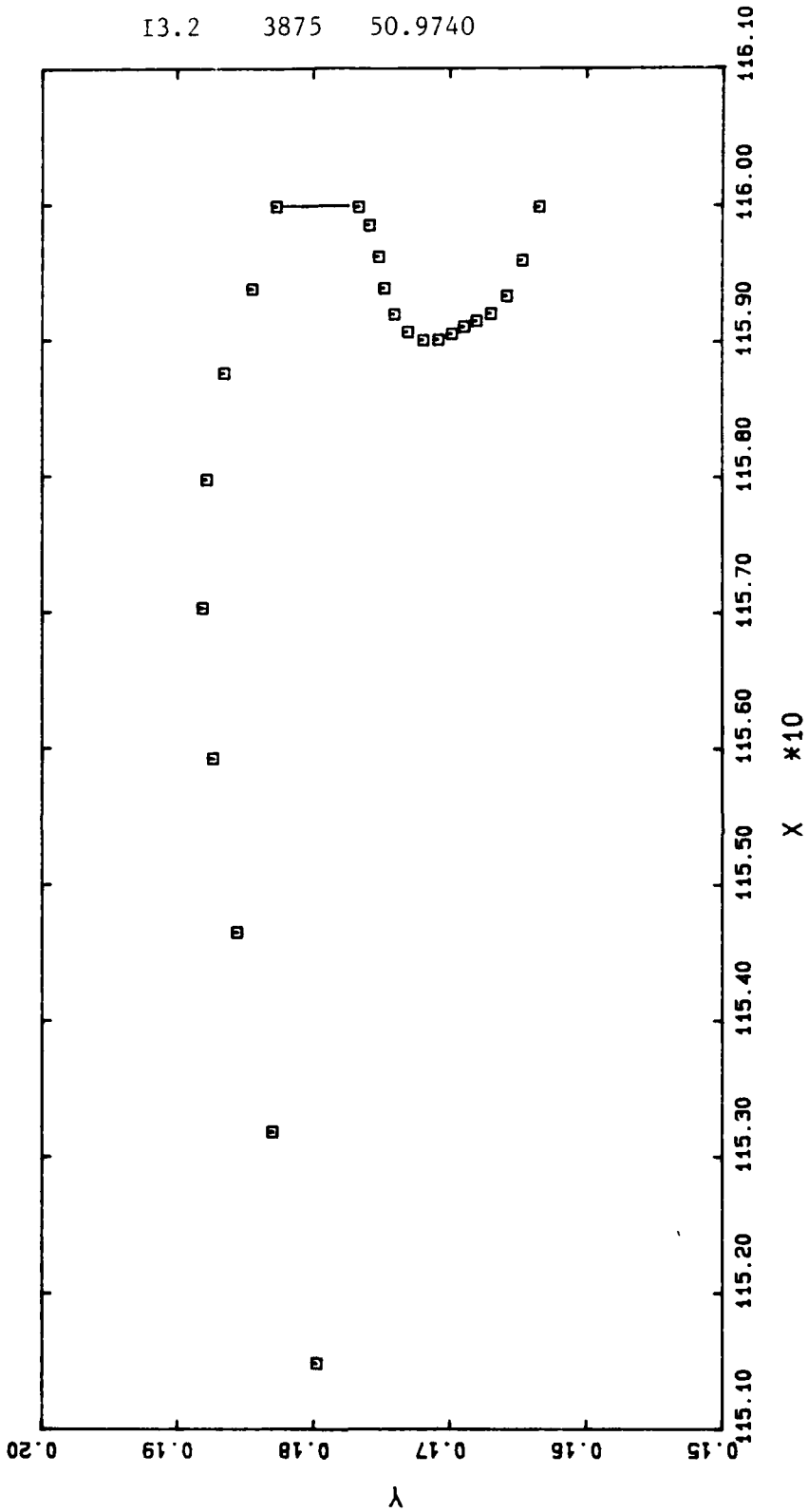

I3.2 3876 50.9741

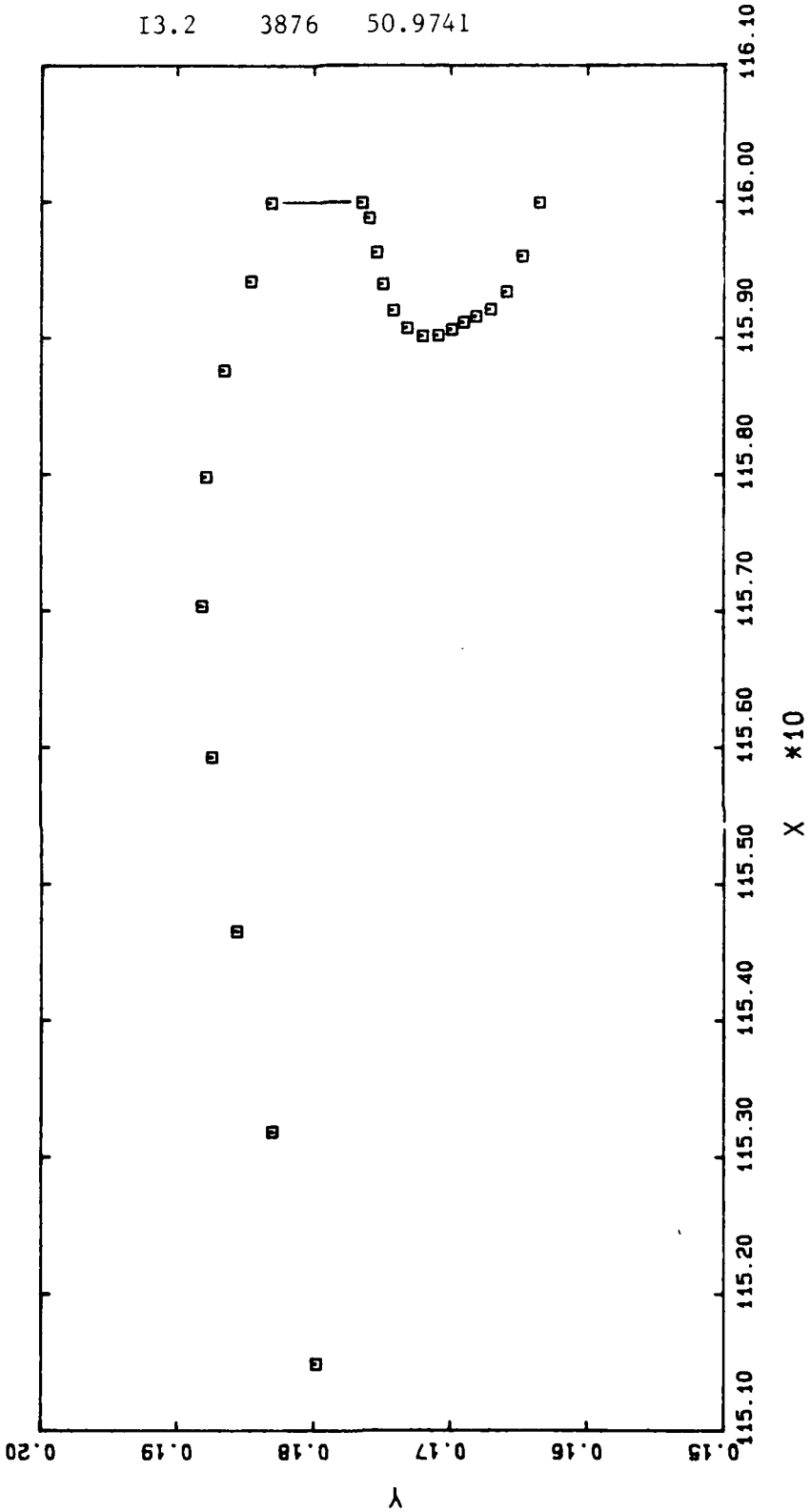

I3.2 3877 50.9741

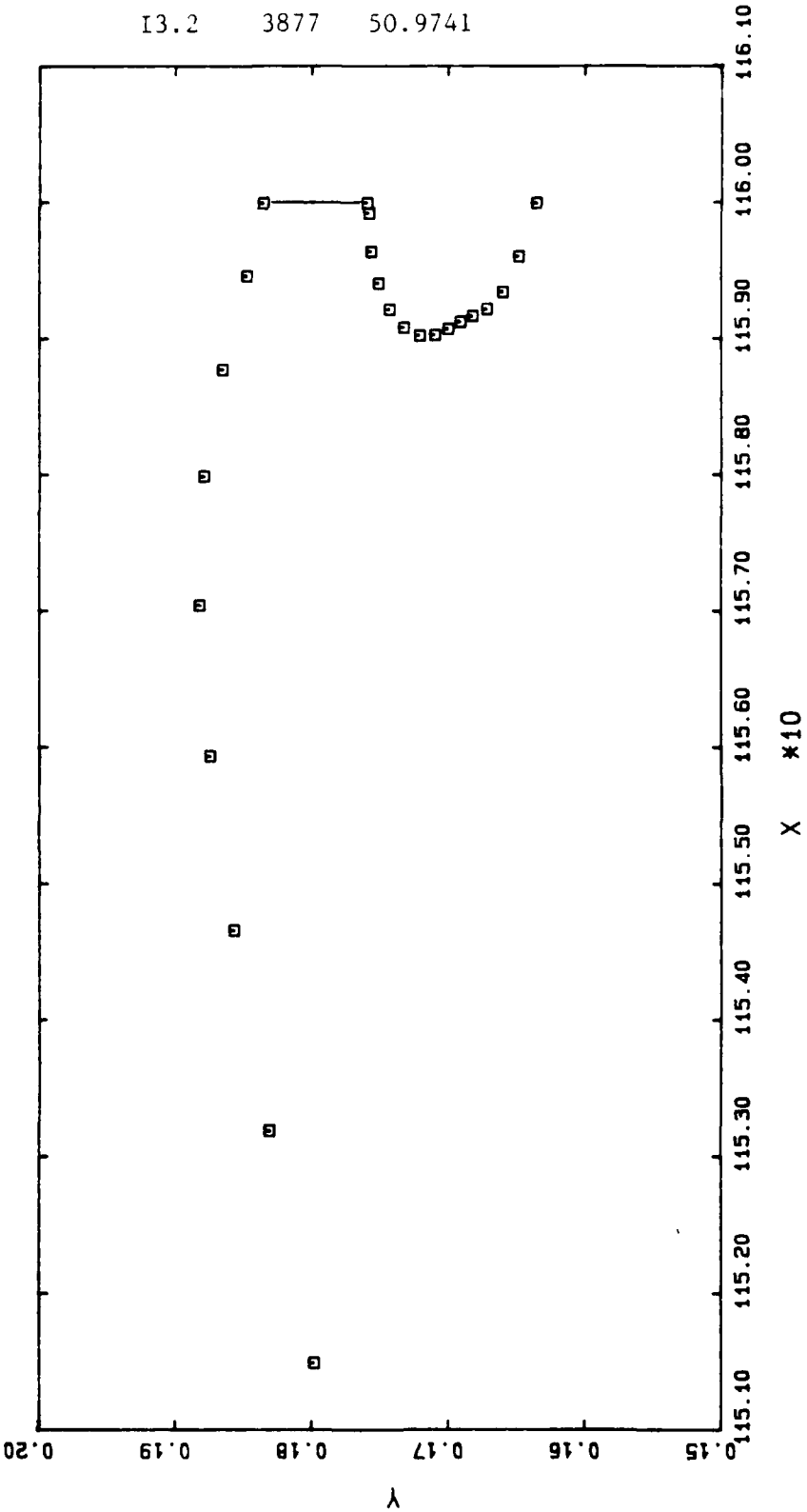

I3.2 3878 50.9741

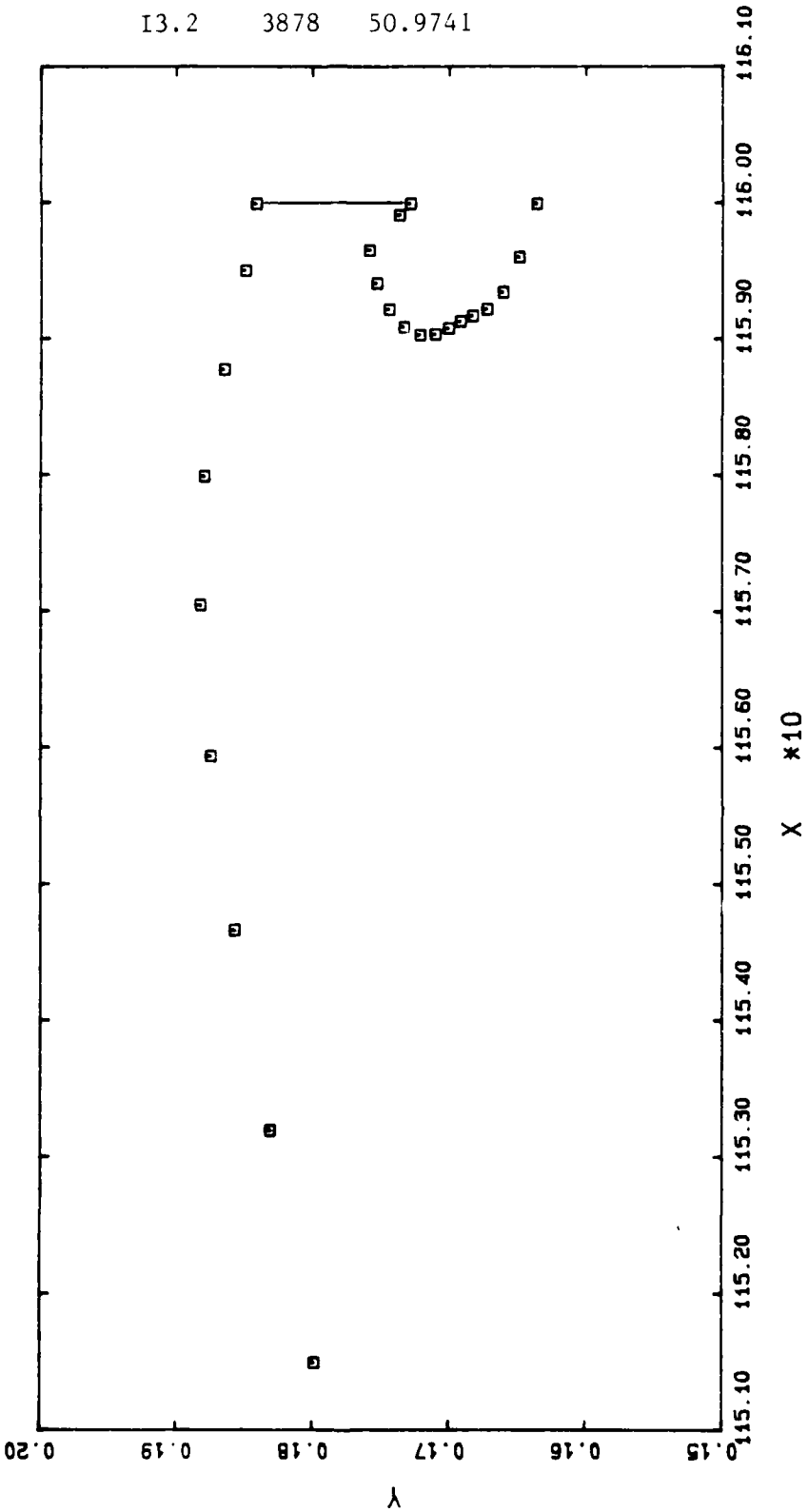

I3.2 3879 50.9742

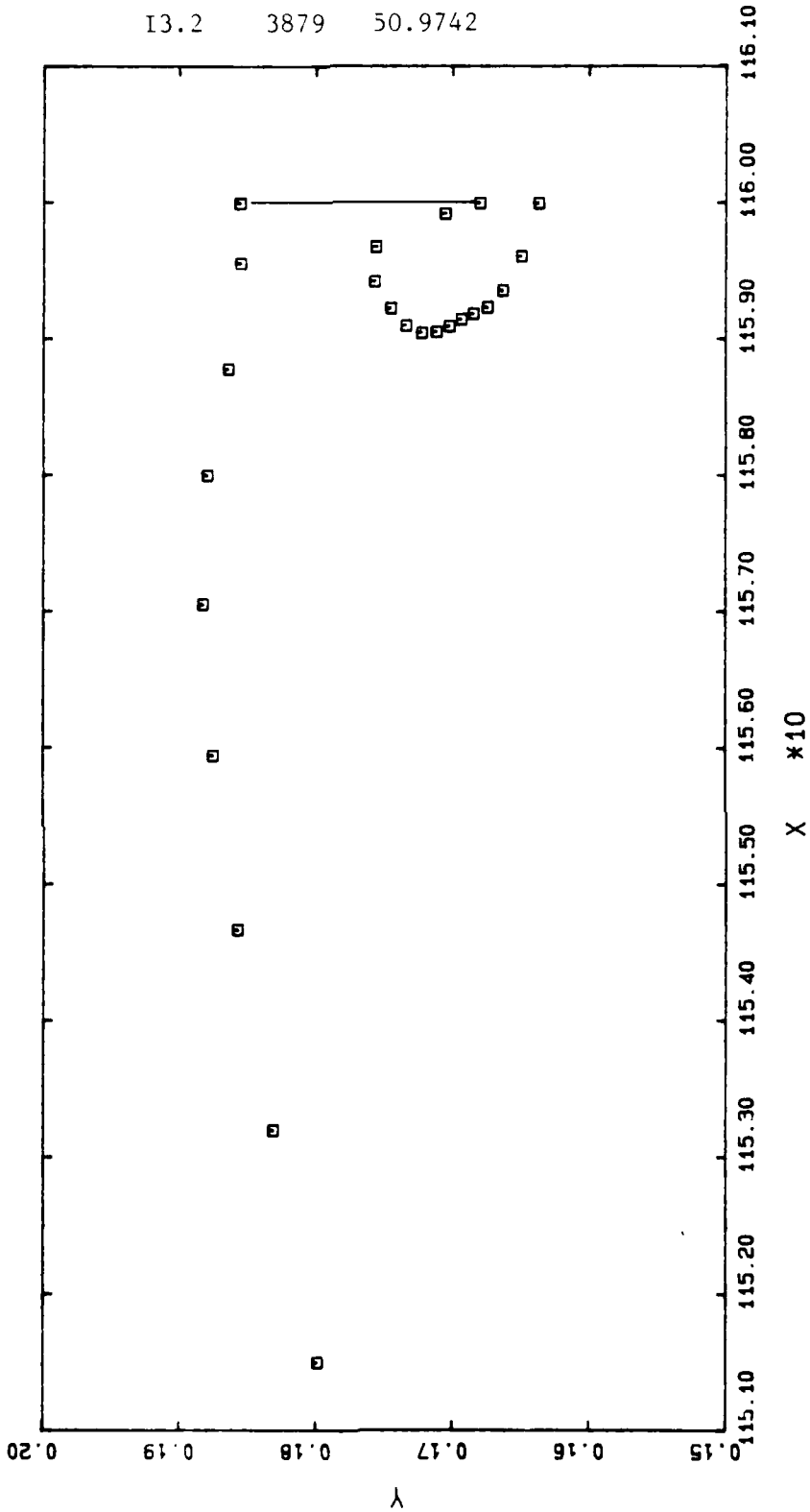

I3.2 3880 50.9742

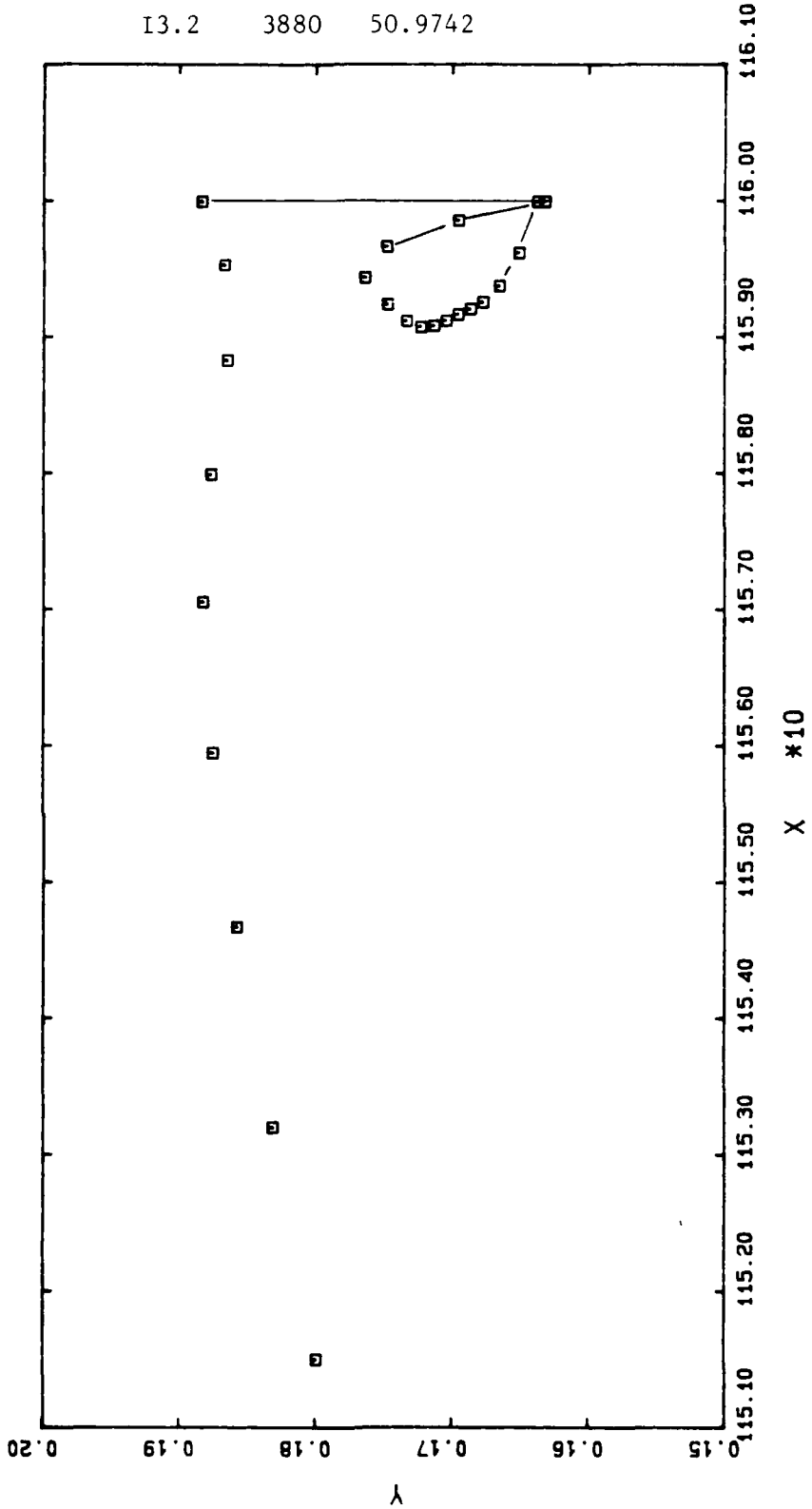

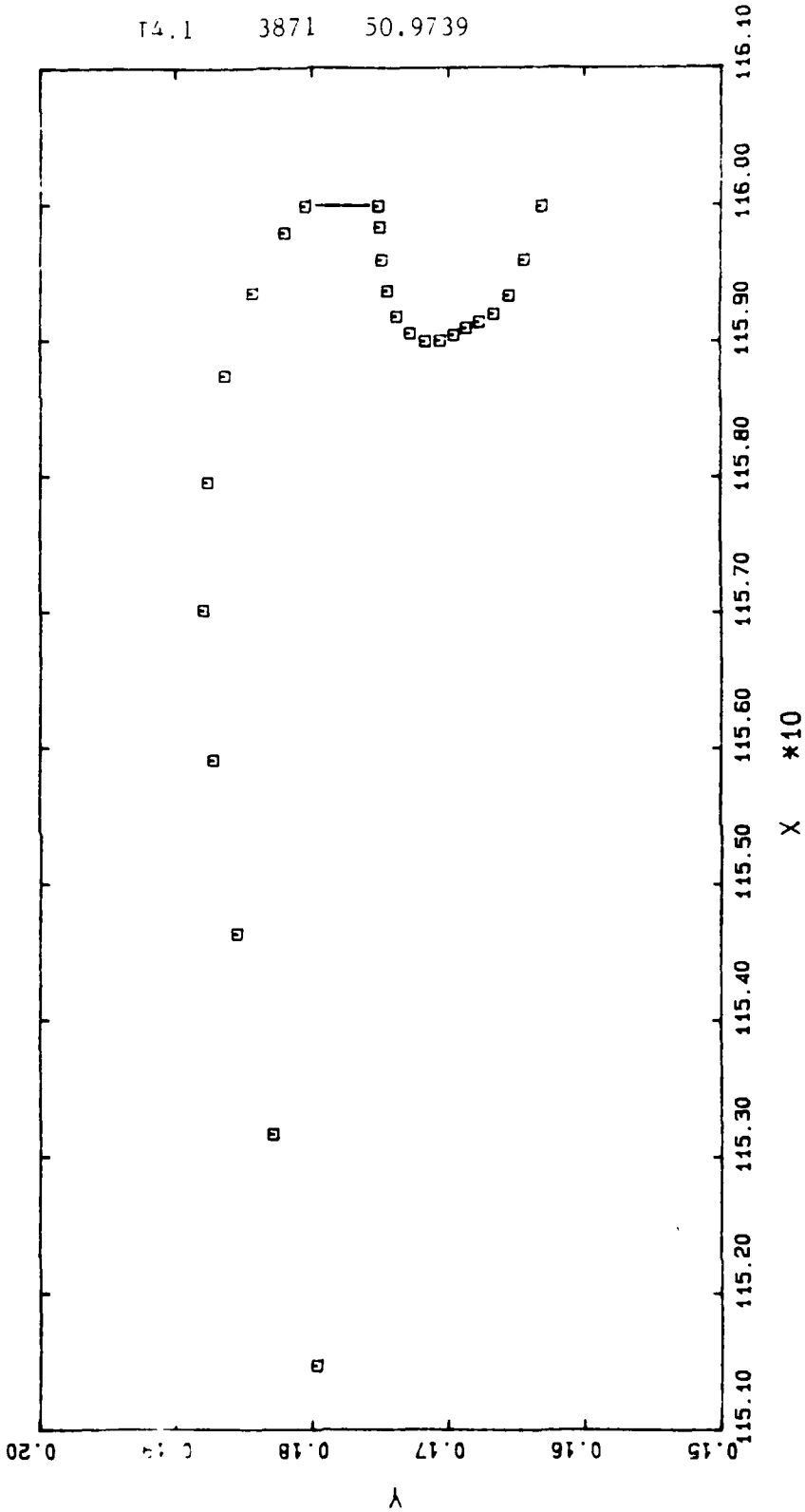
T4.1 3871 50.9739
115.10
115.20
115.30
115.40
115.50
115.60
115.70
115.80
115.90
116.00
116.10
X *10
0.15
0.16
0.17
0.18
0.20
Y

I4.1 3881 50.9742

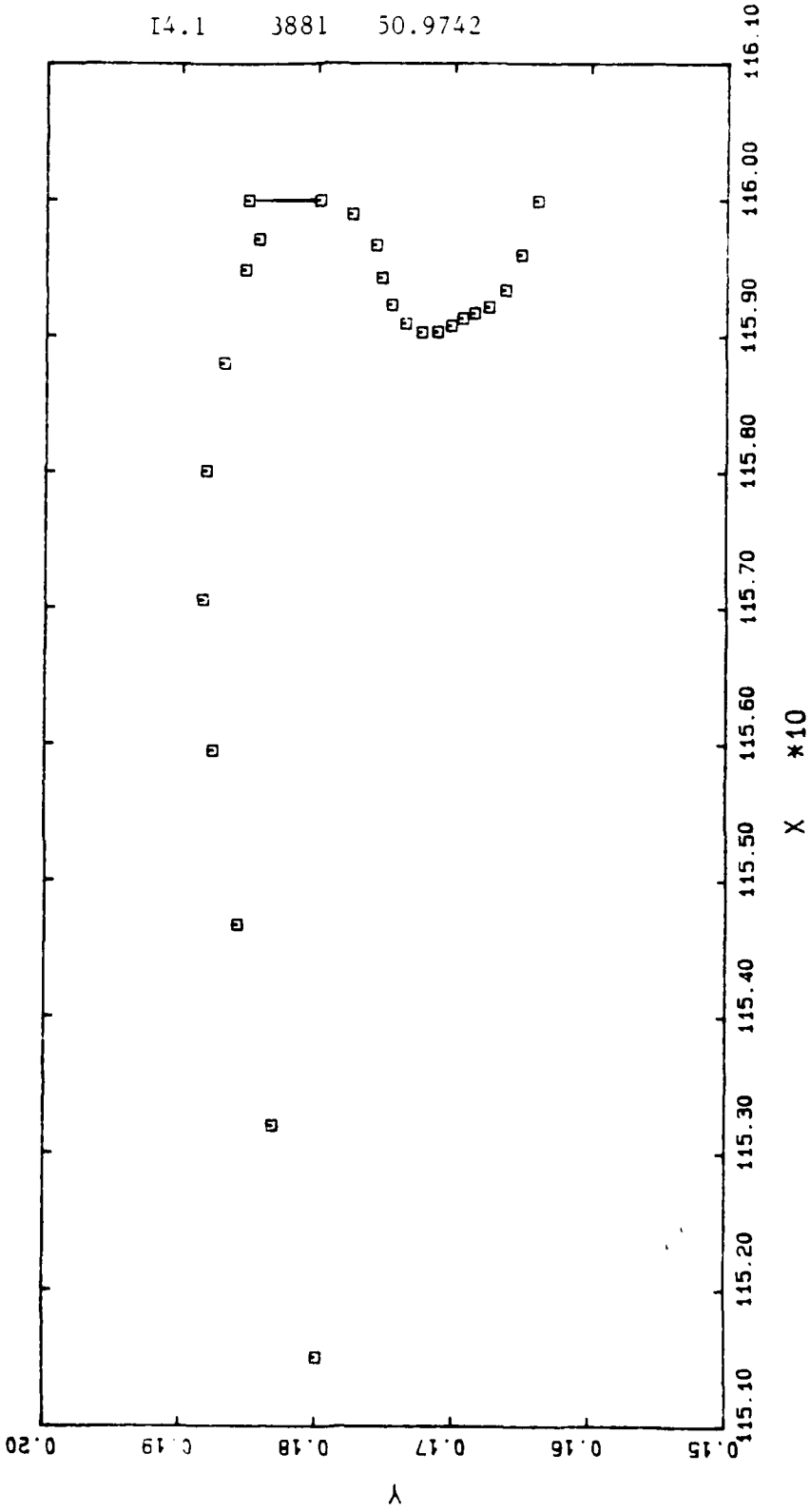

I4.1 3891 50.9746

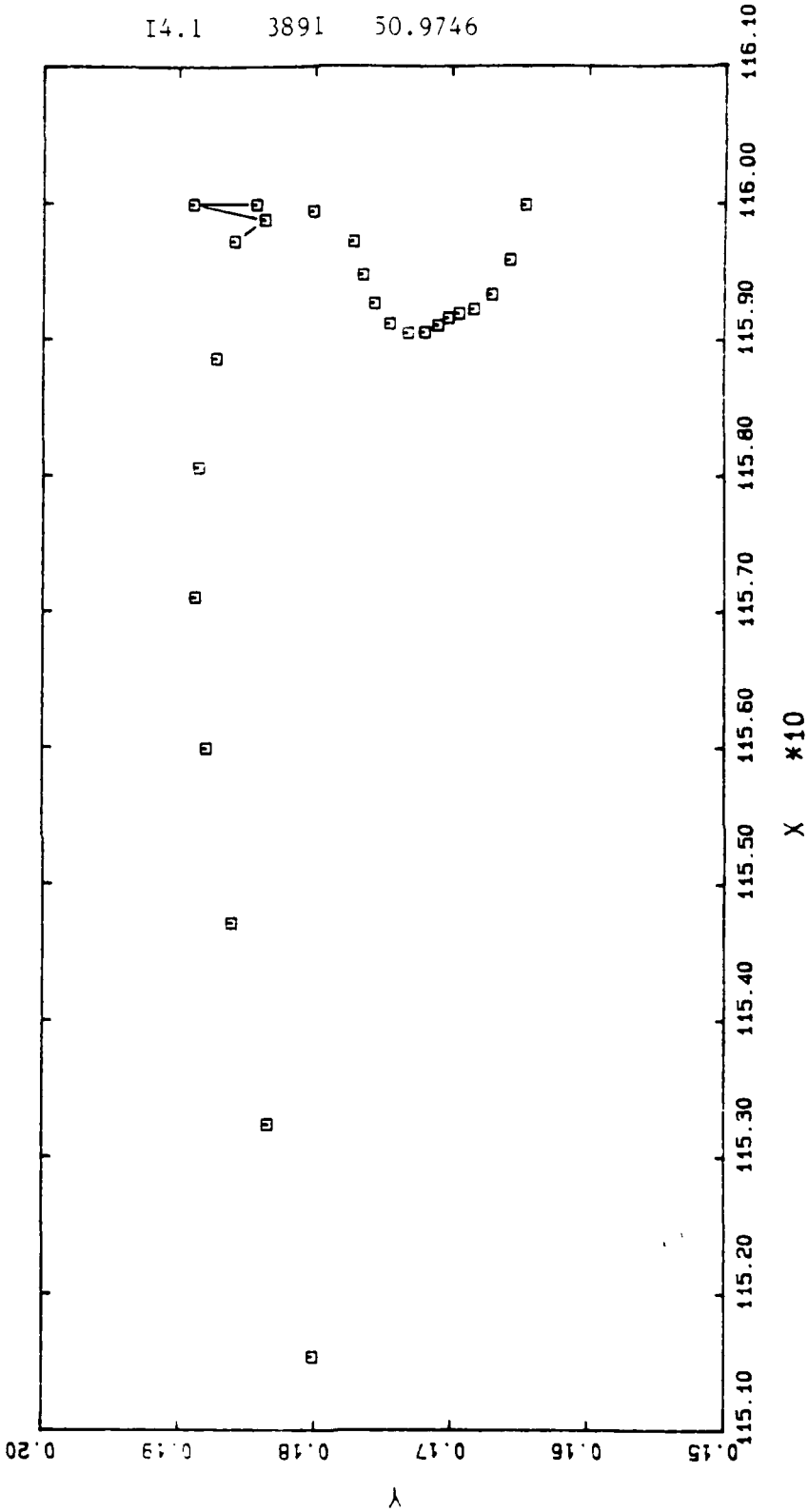

I4.2 3871 50.9739

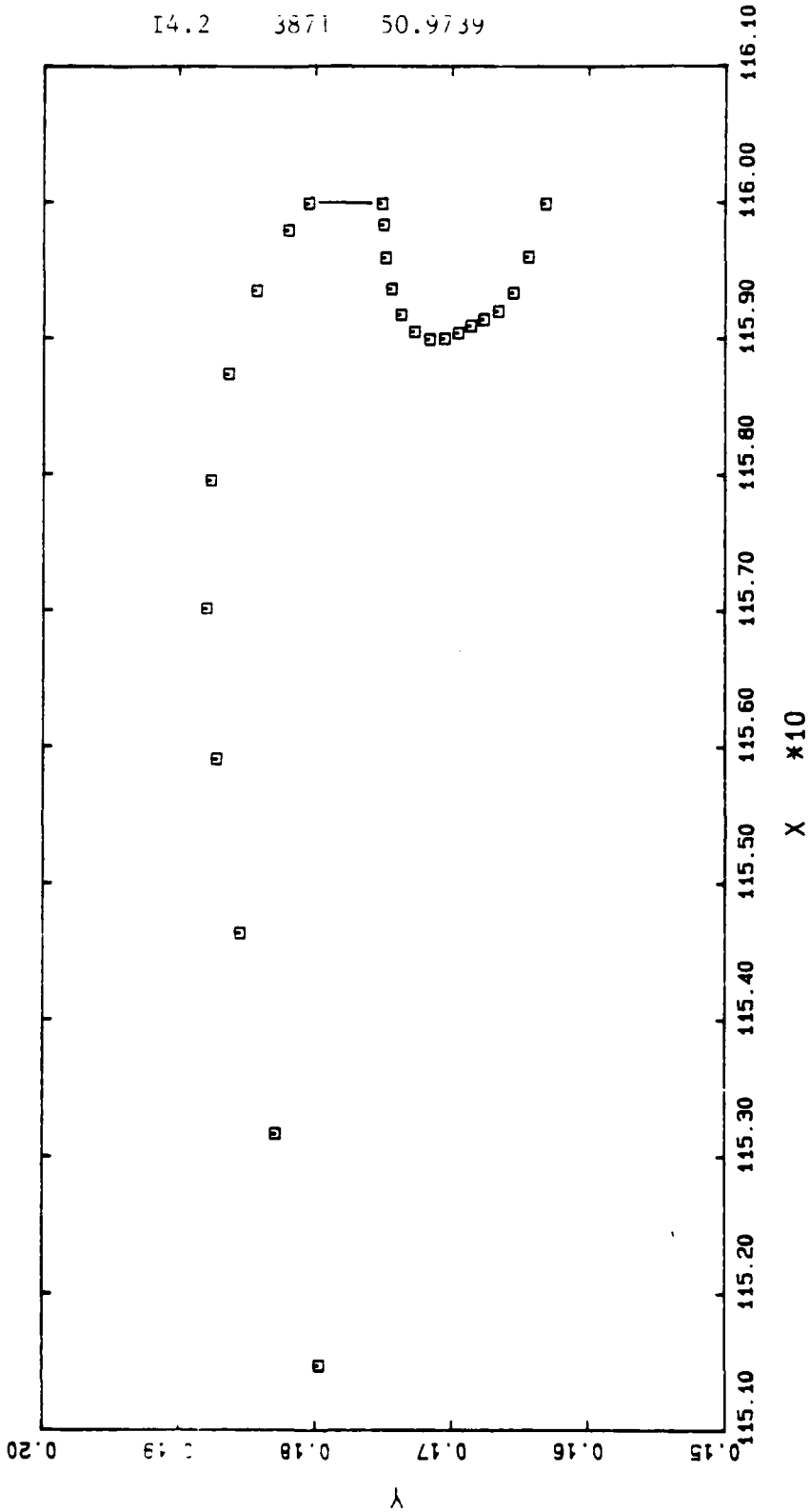

I4.2 3881 50.9742

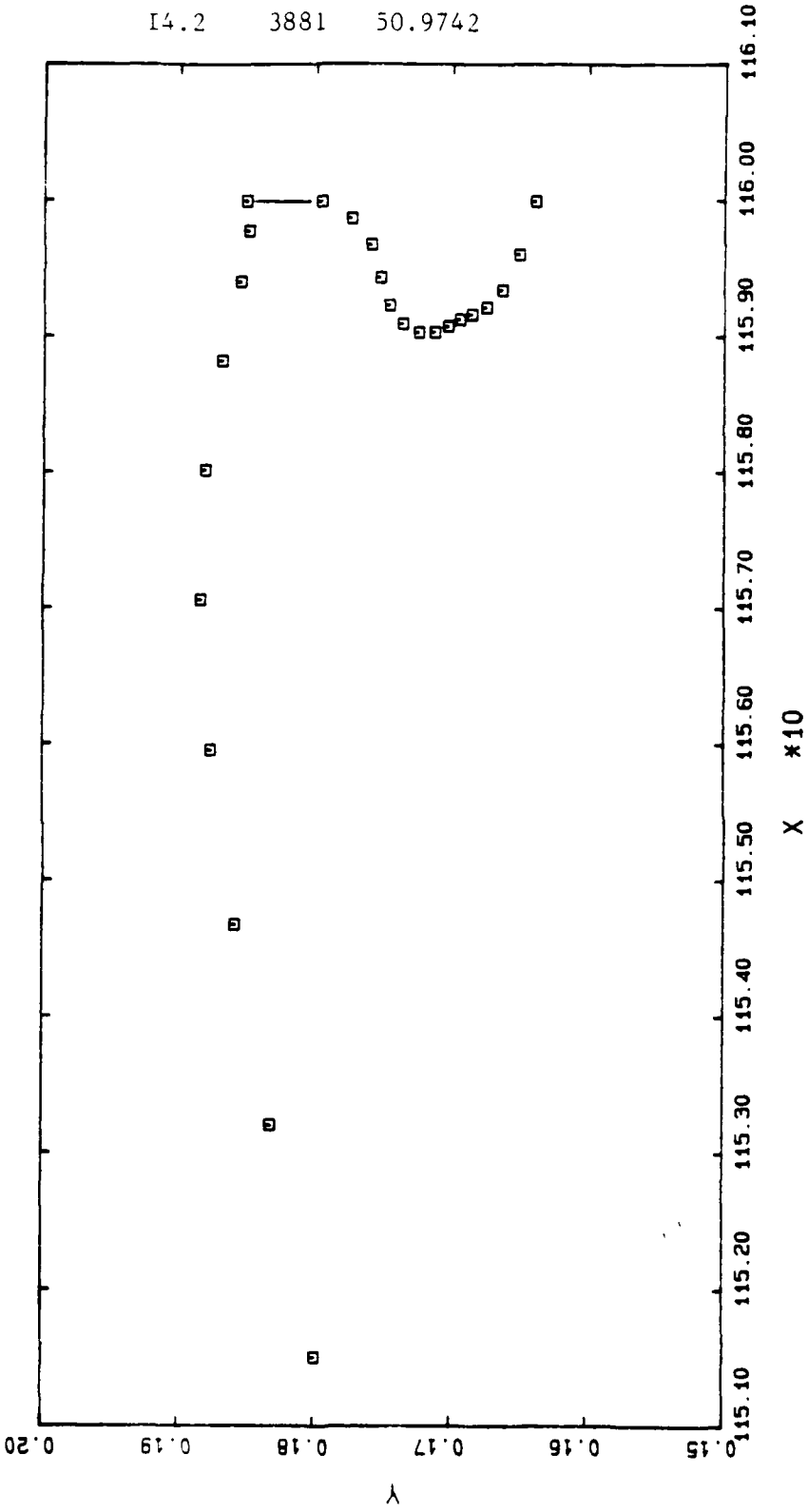

I4.2 3891 50.9746

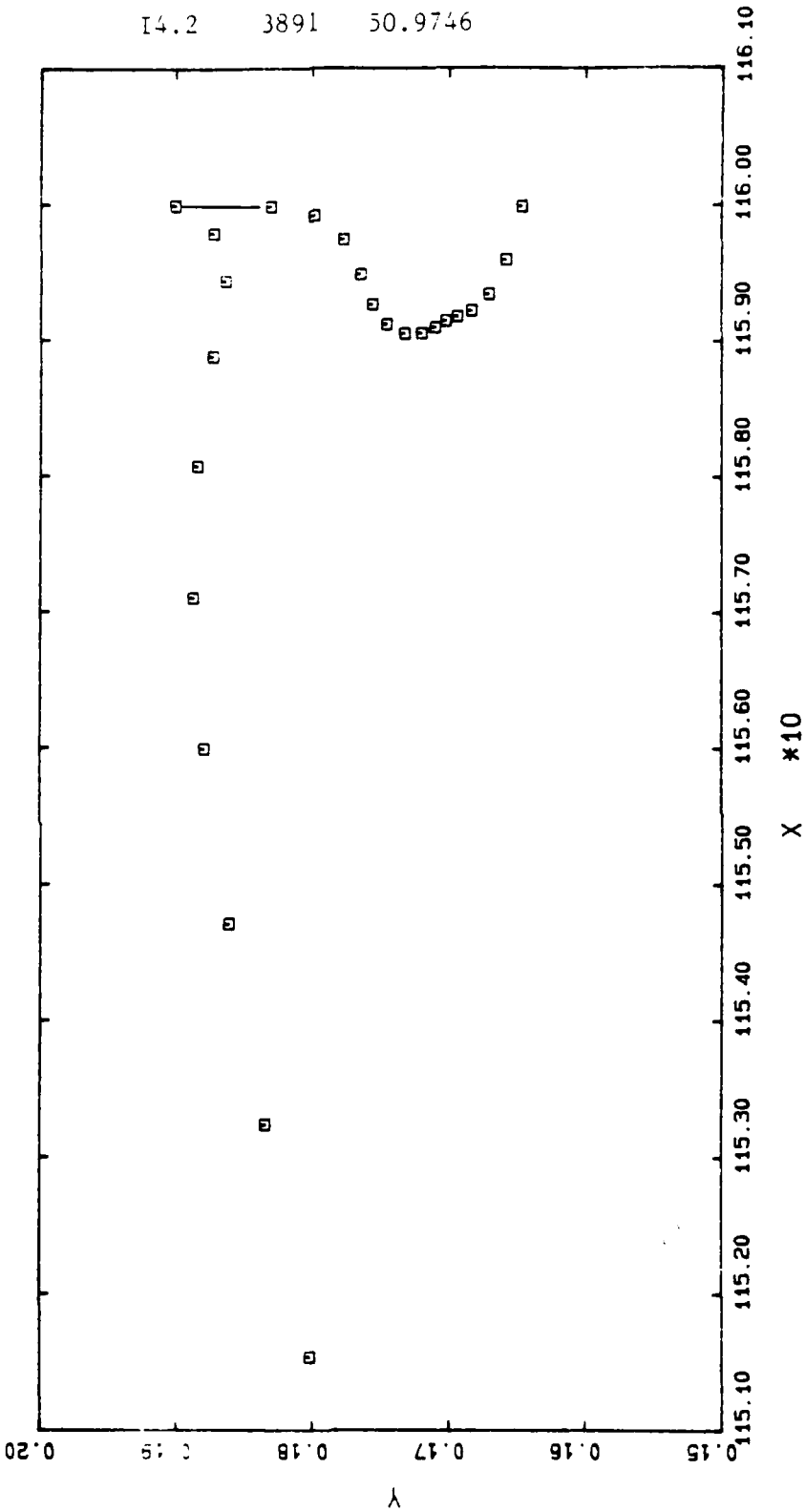

I4.2 3901 50.9750

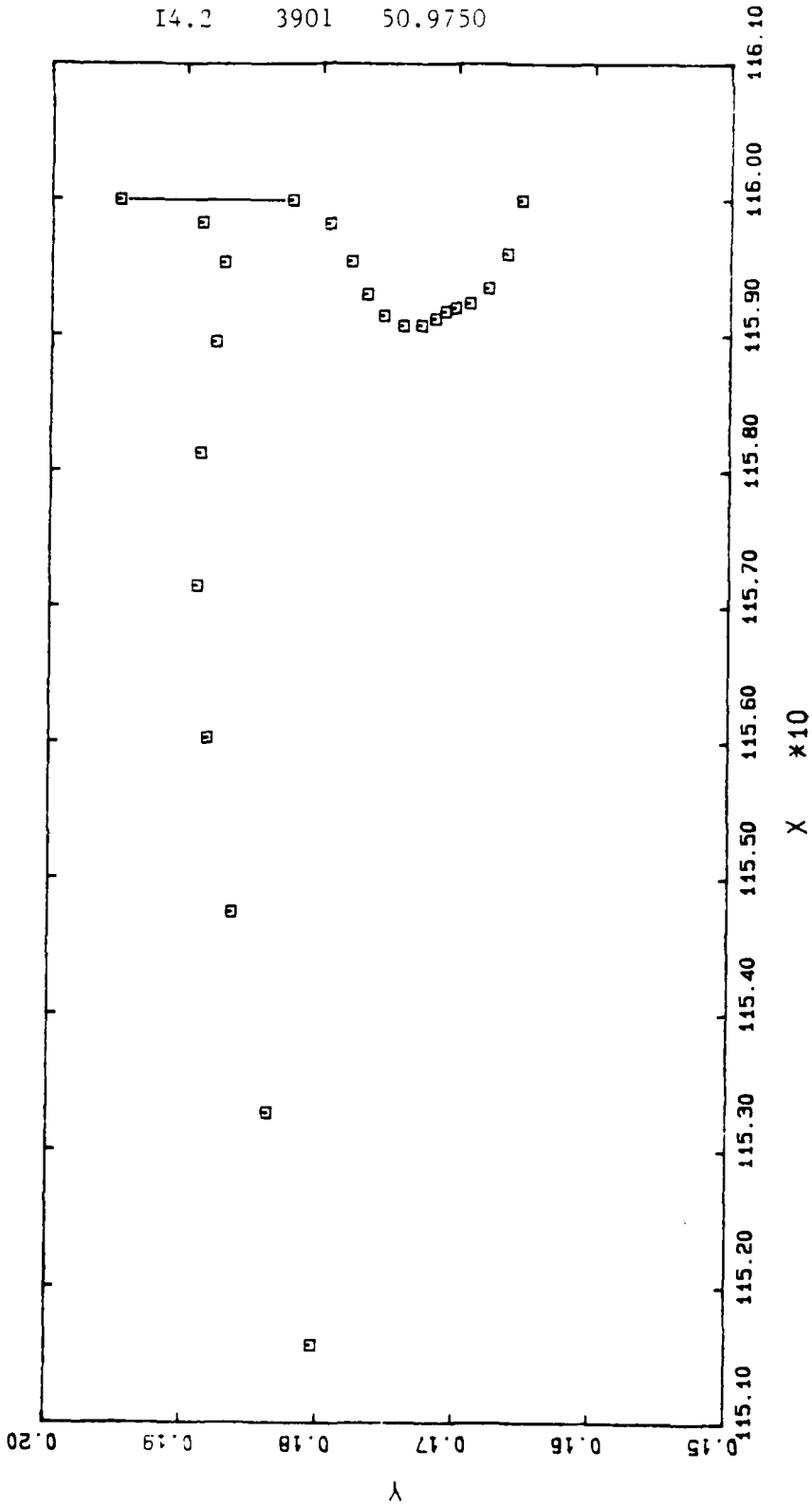

I4.2 3911 50.9754

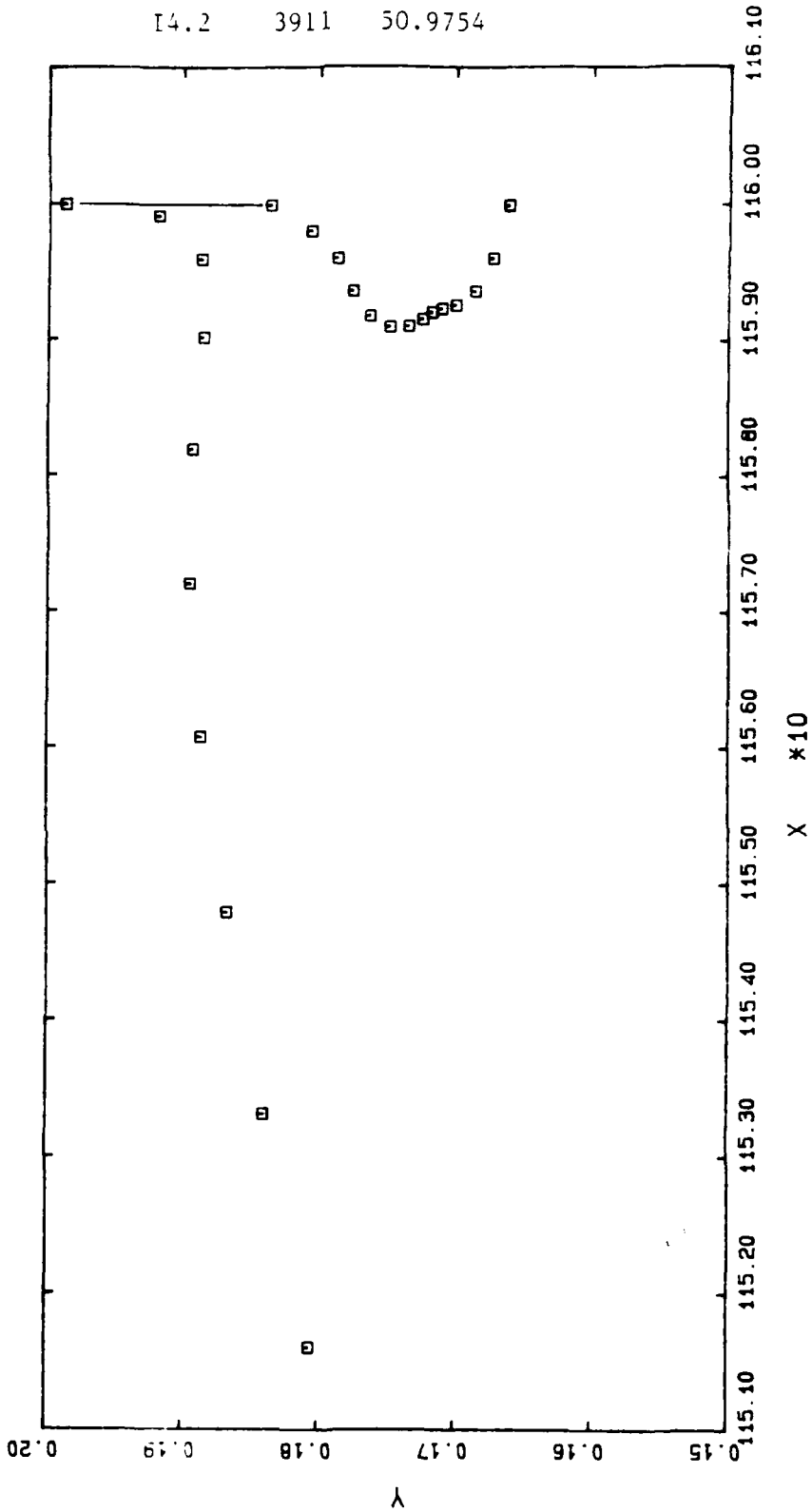

I5.1 3871 50.9739

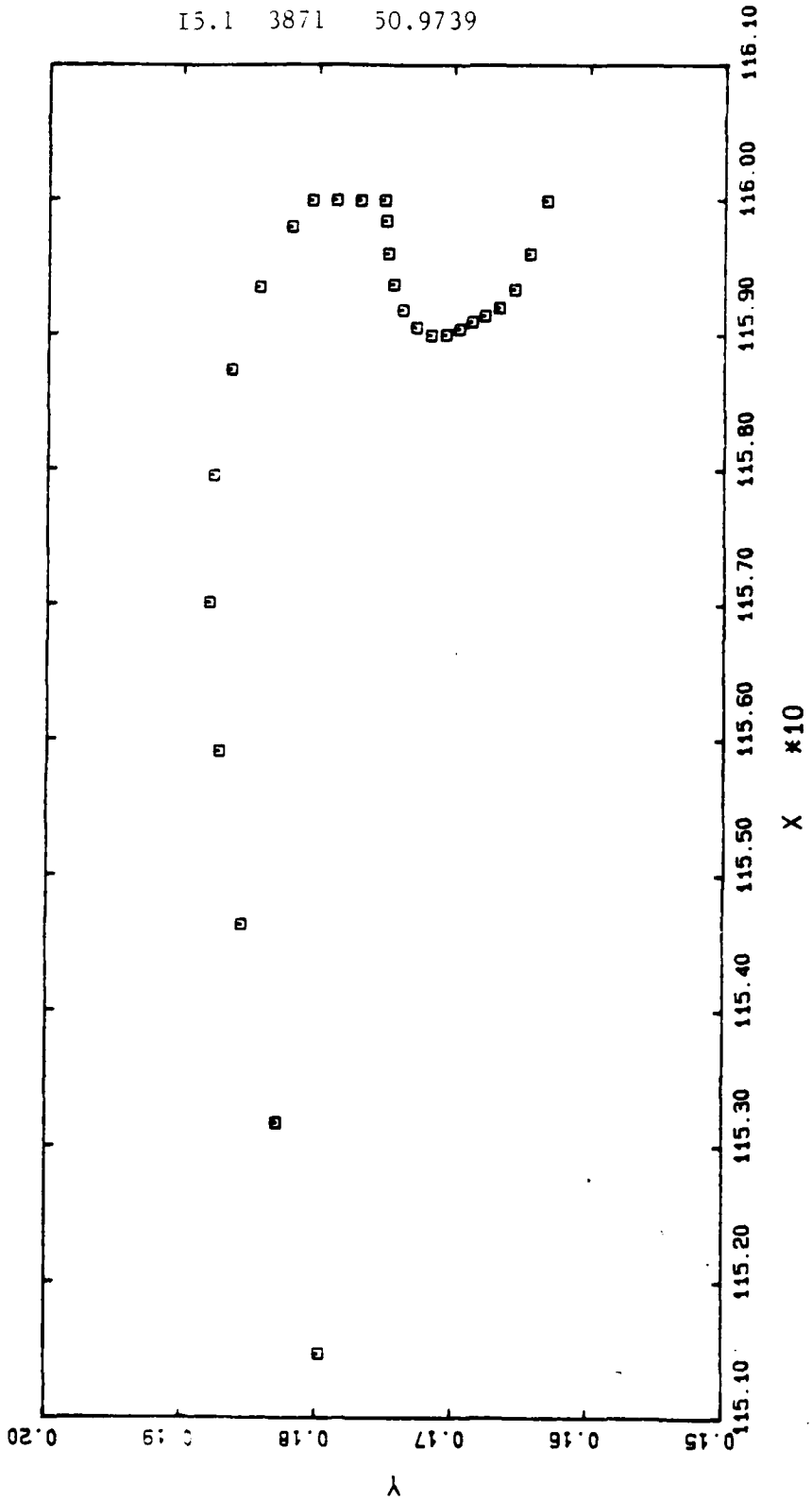

I5.1 3872 50.9739

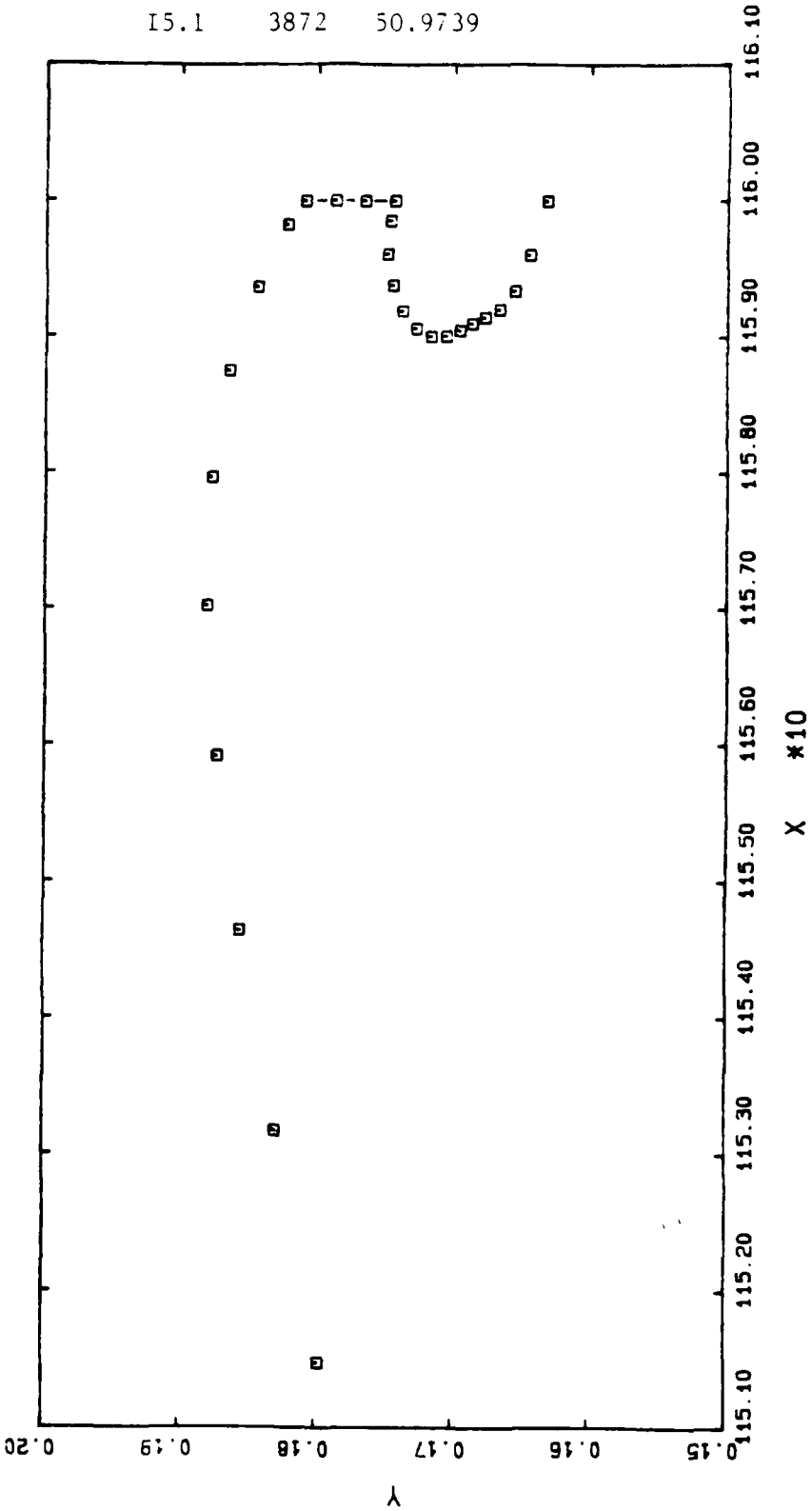

I5.1 3873 50.9739

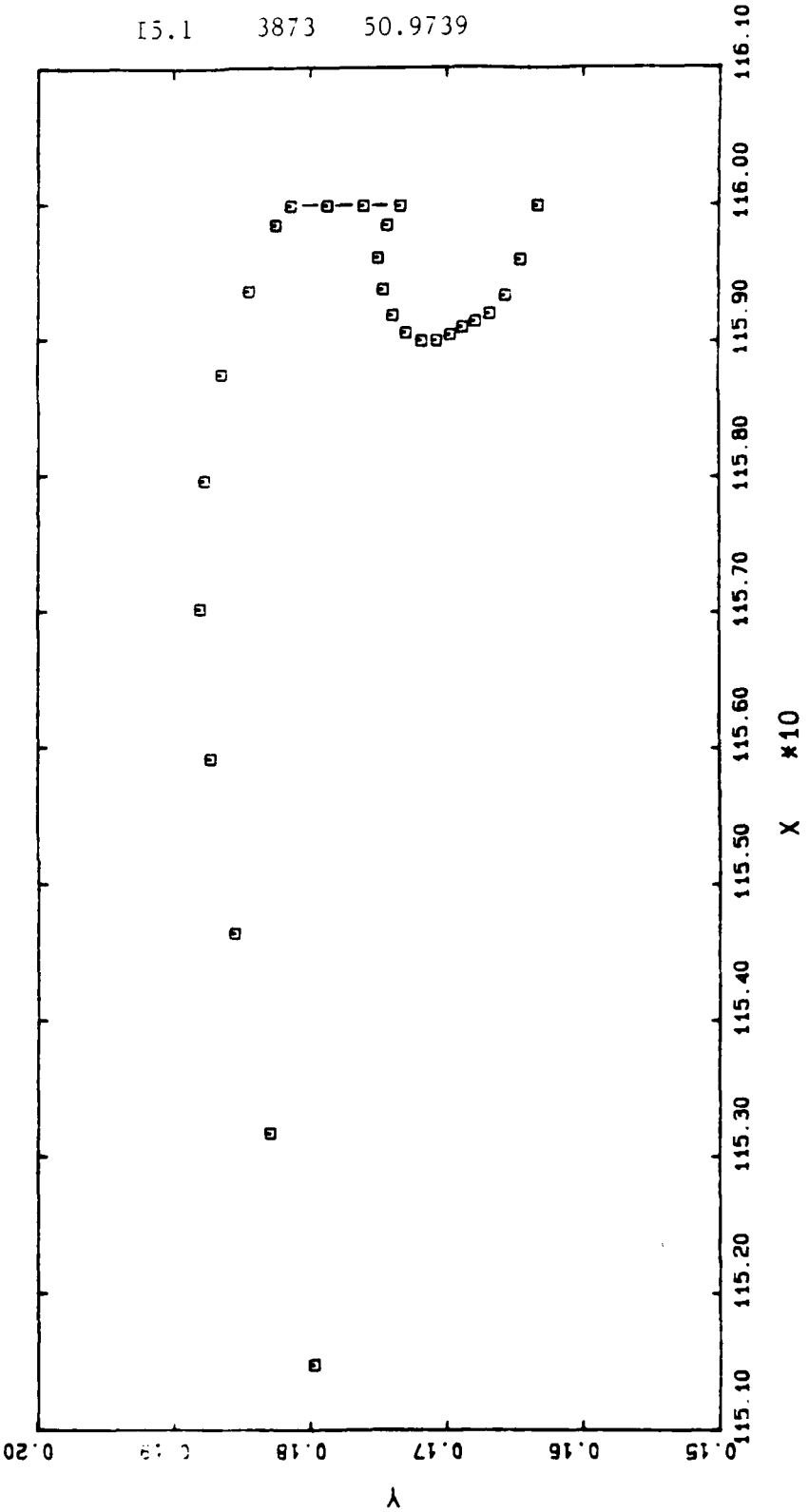

I5.1 3874 50.9740

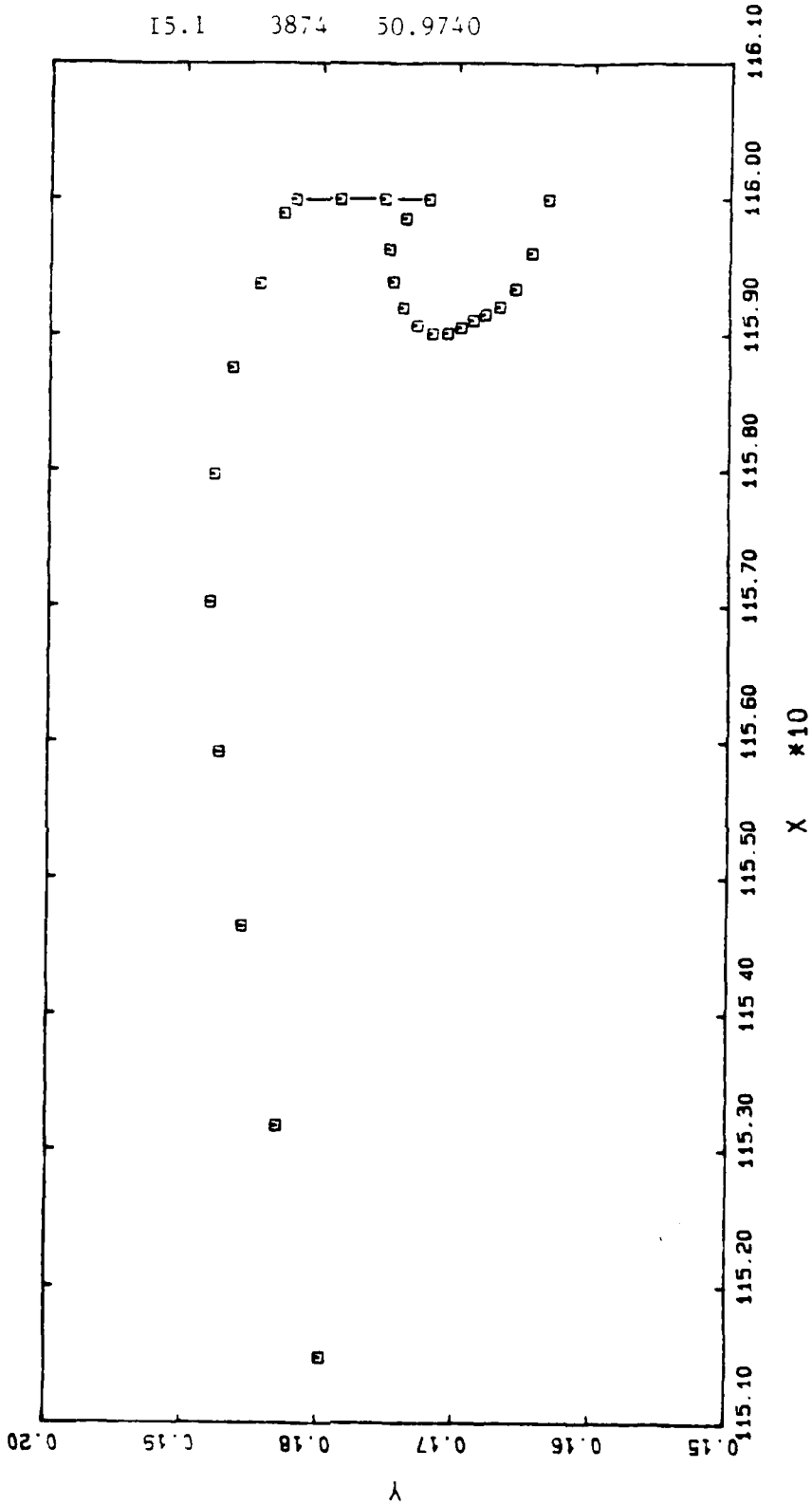

I5.1 3875 50.9740

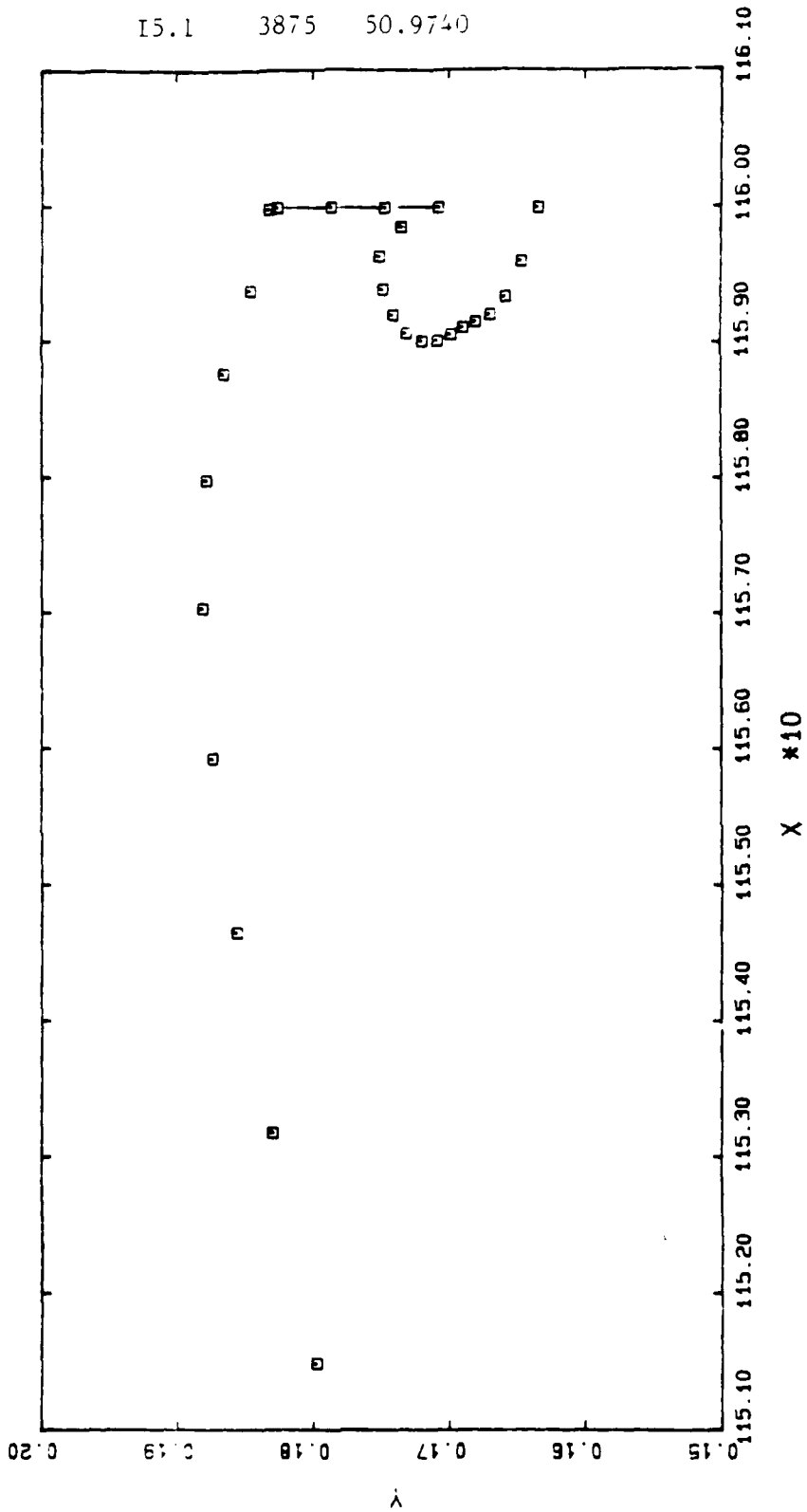

15.1 3876 50.9741

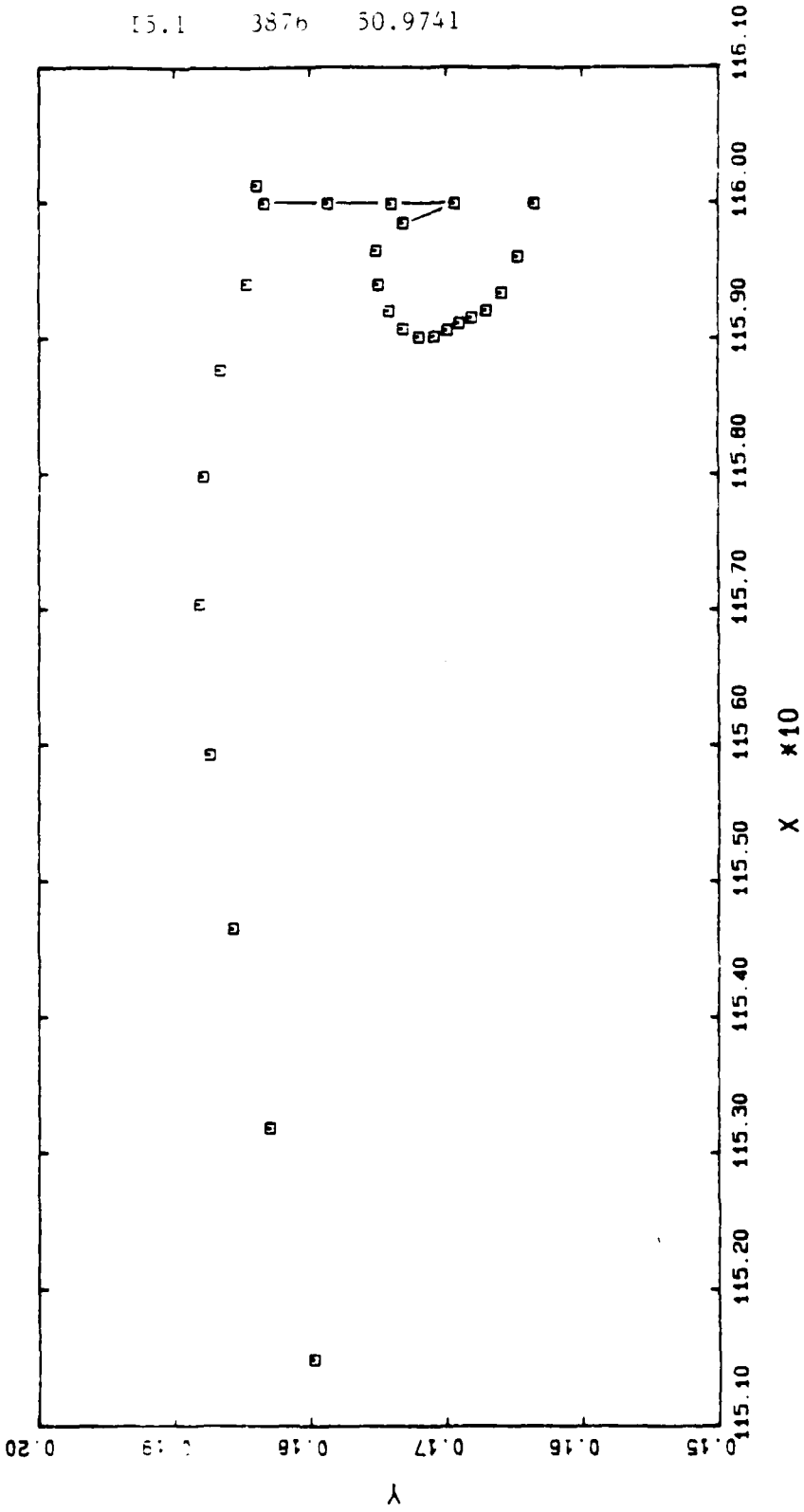

I5.1 3877 50.9741

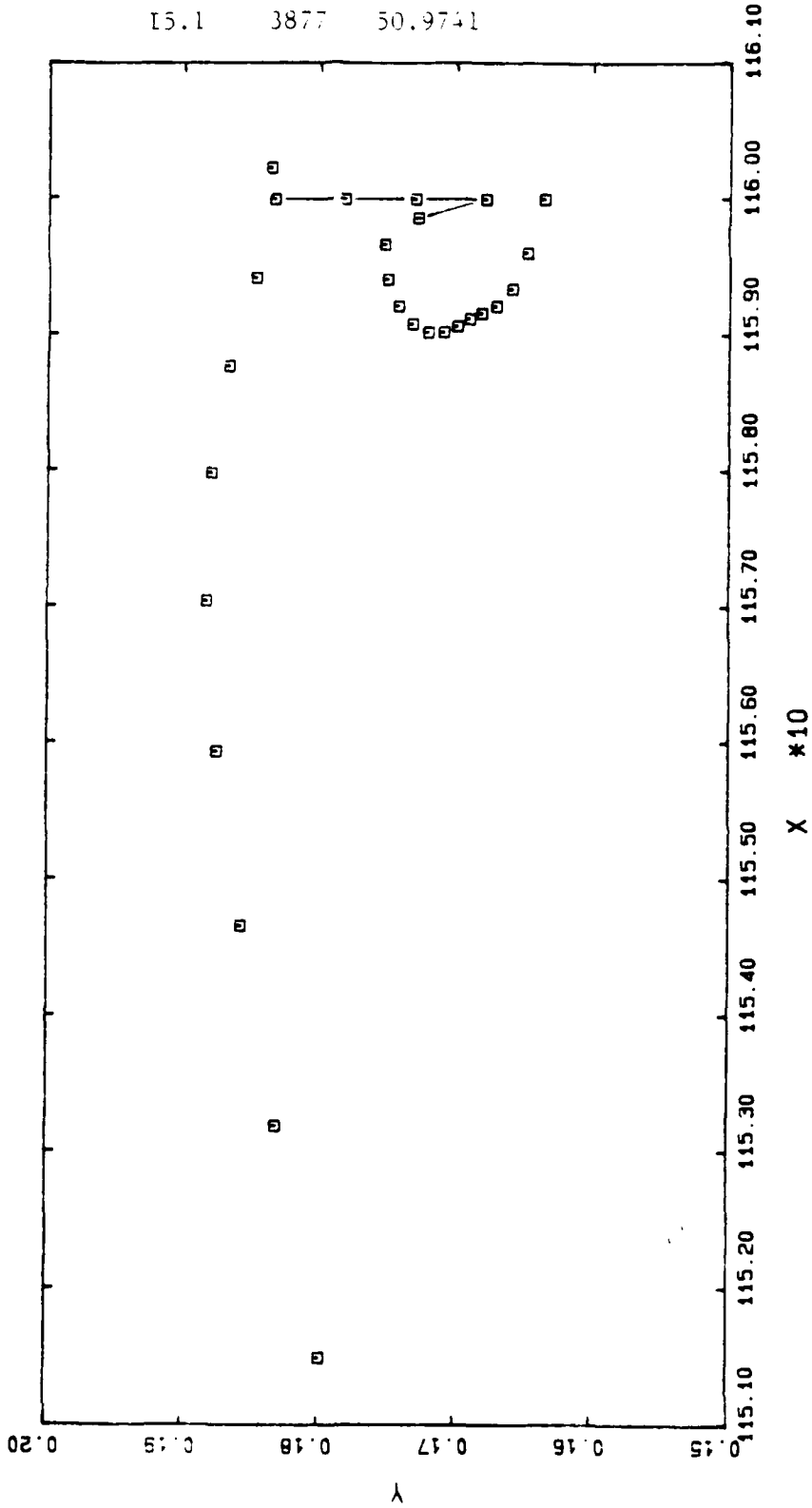

I5.2 3871 50.9739

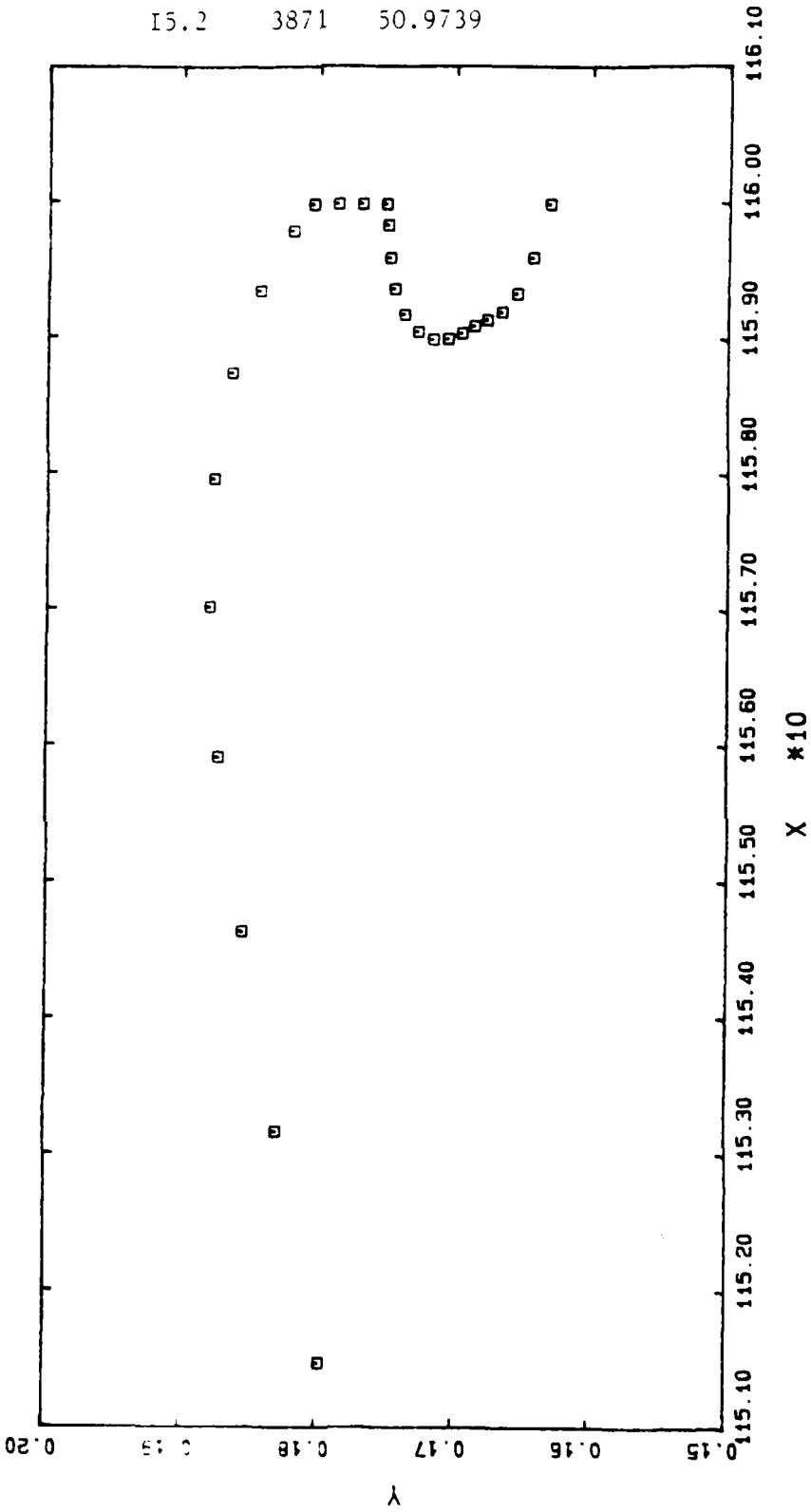

I5.2 3872 50.9739

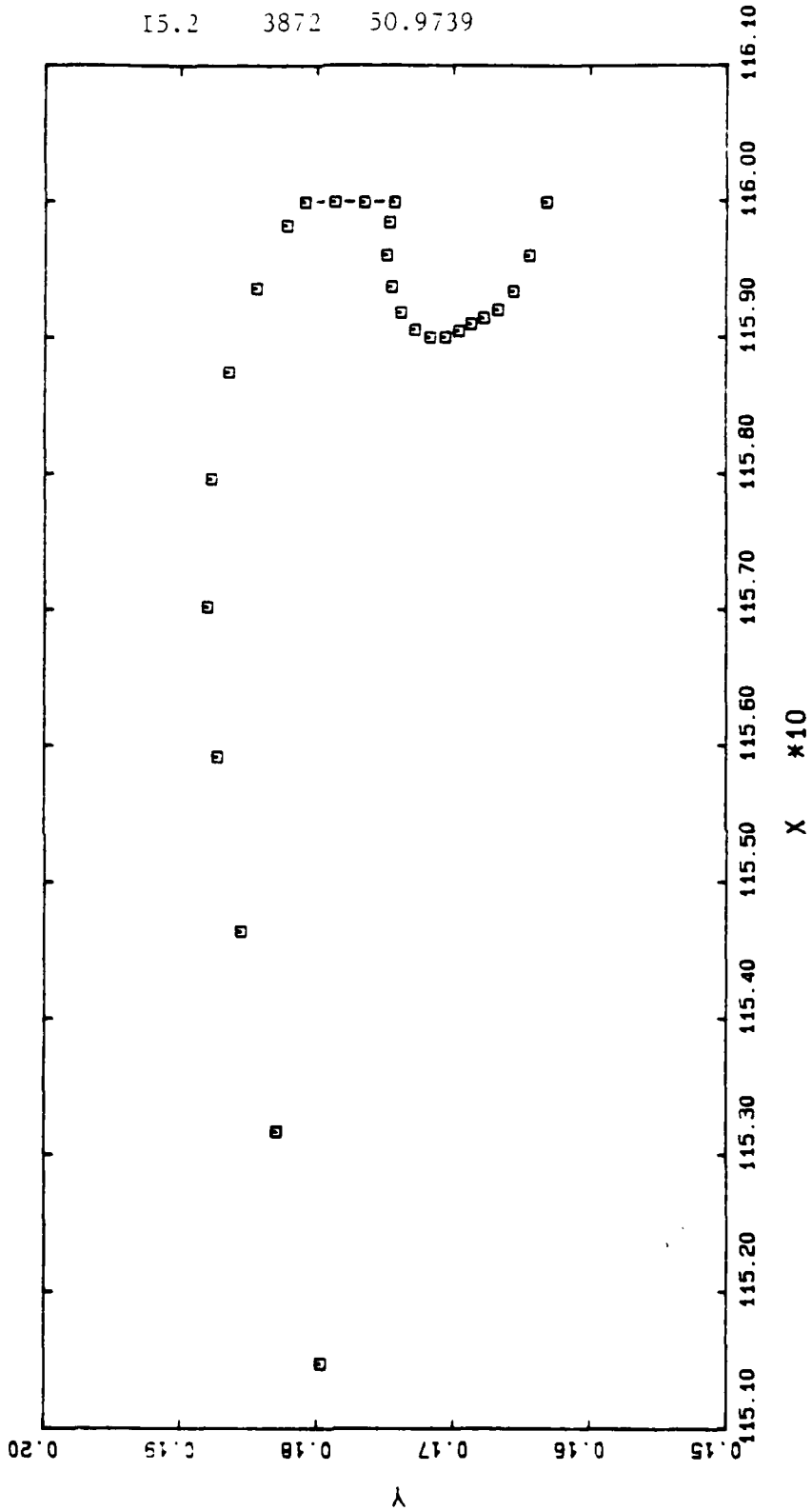

I5.2 3873 50.9739

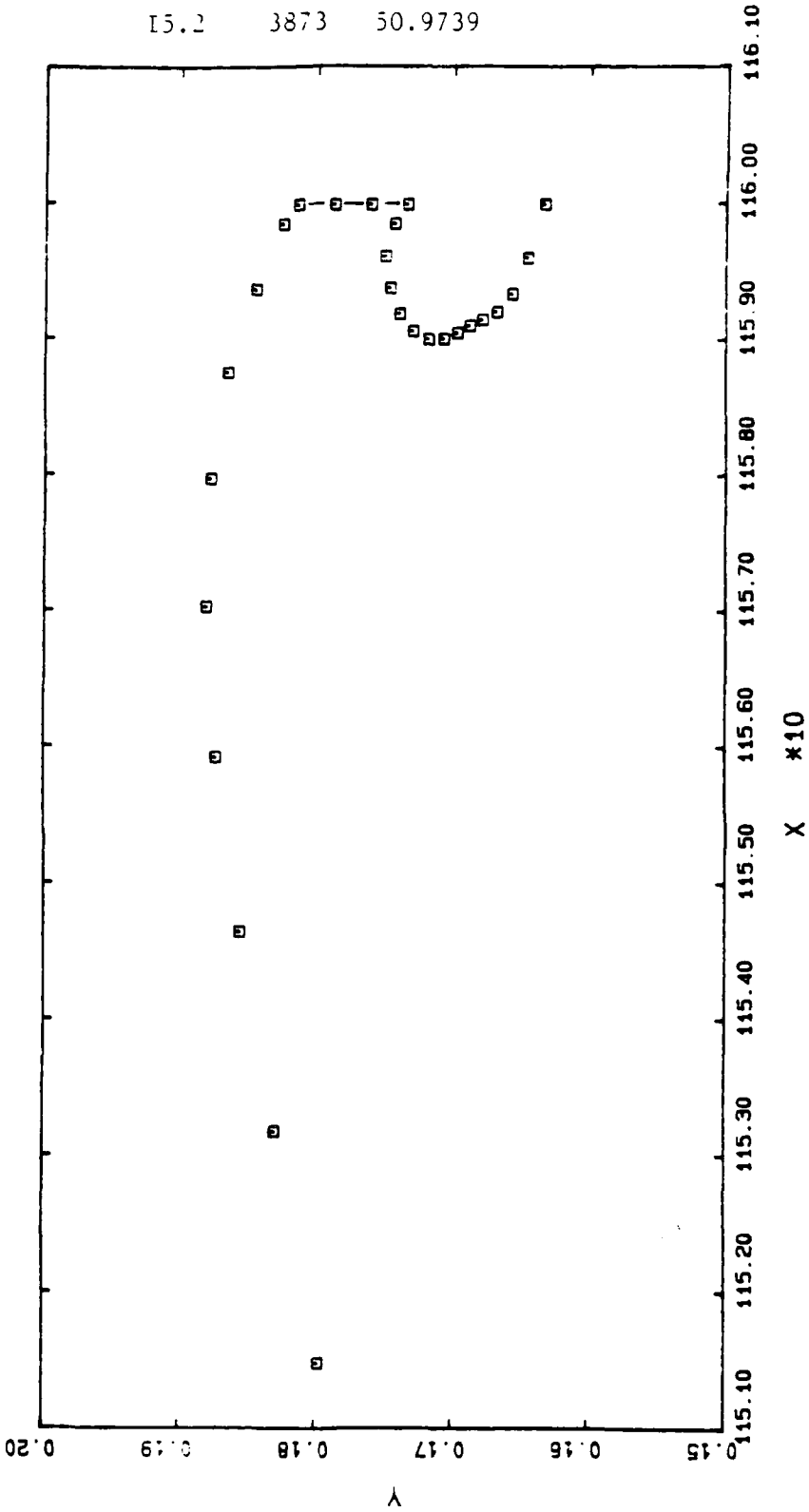

I5.2 3874 50.9740

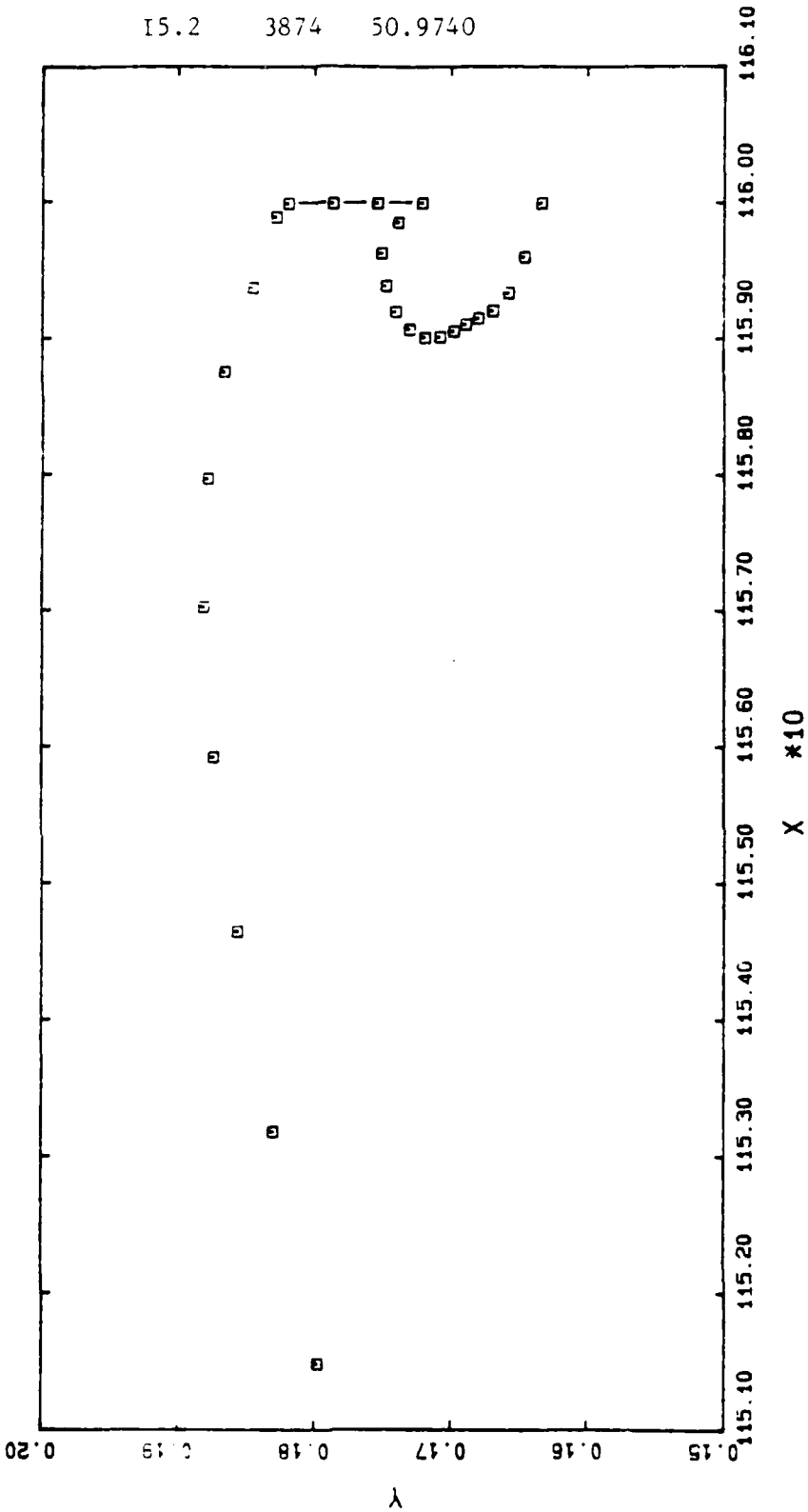

I5.2 3875 50.9740

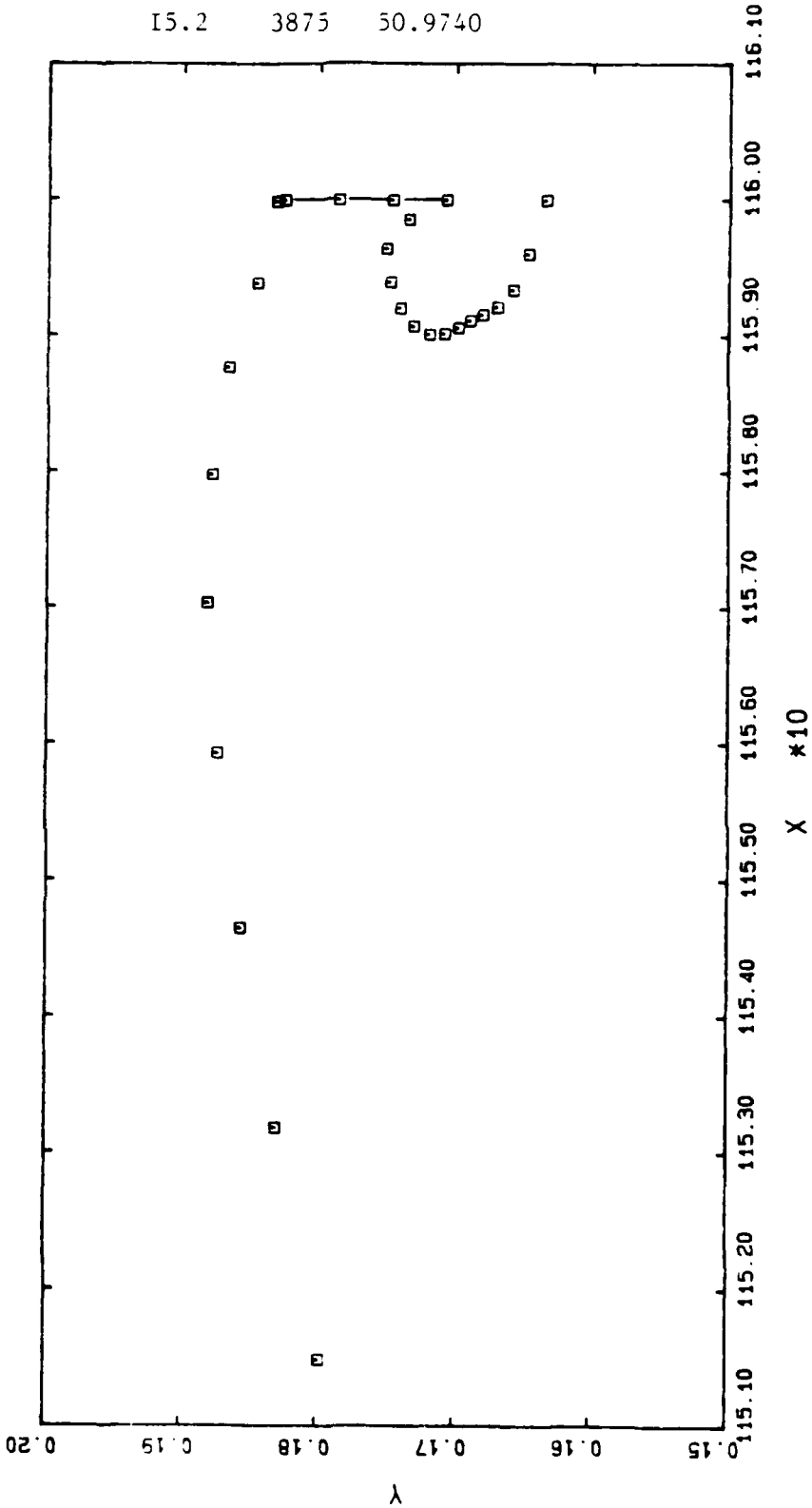

I5.2 3876 50.9741

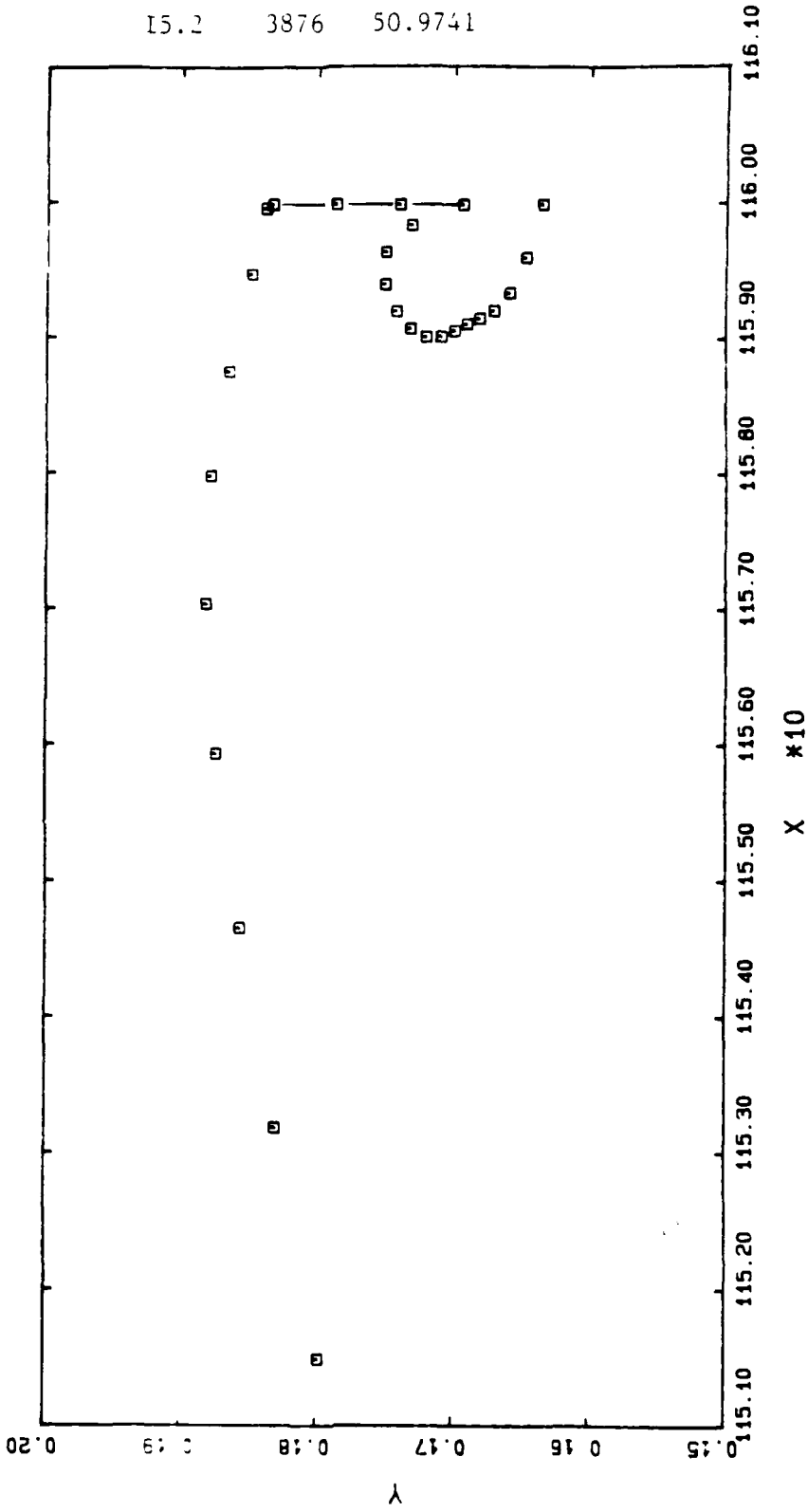

I5.2 3877 50.9741

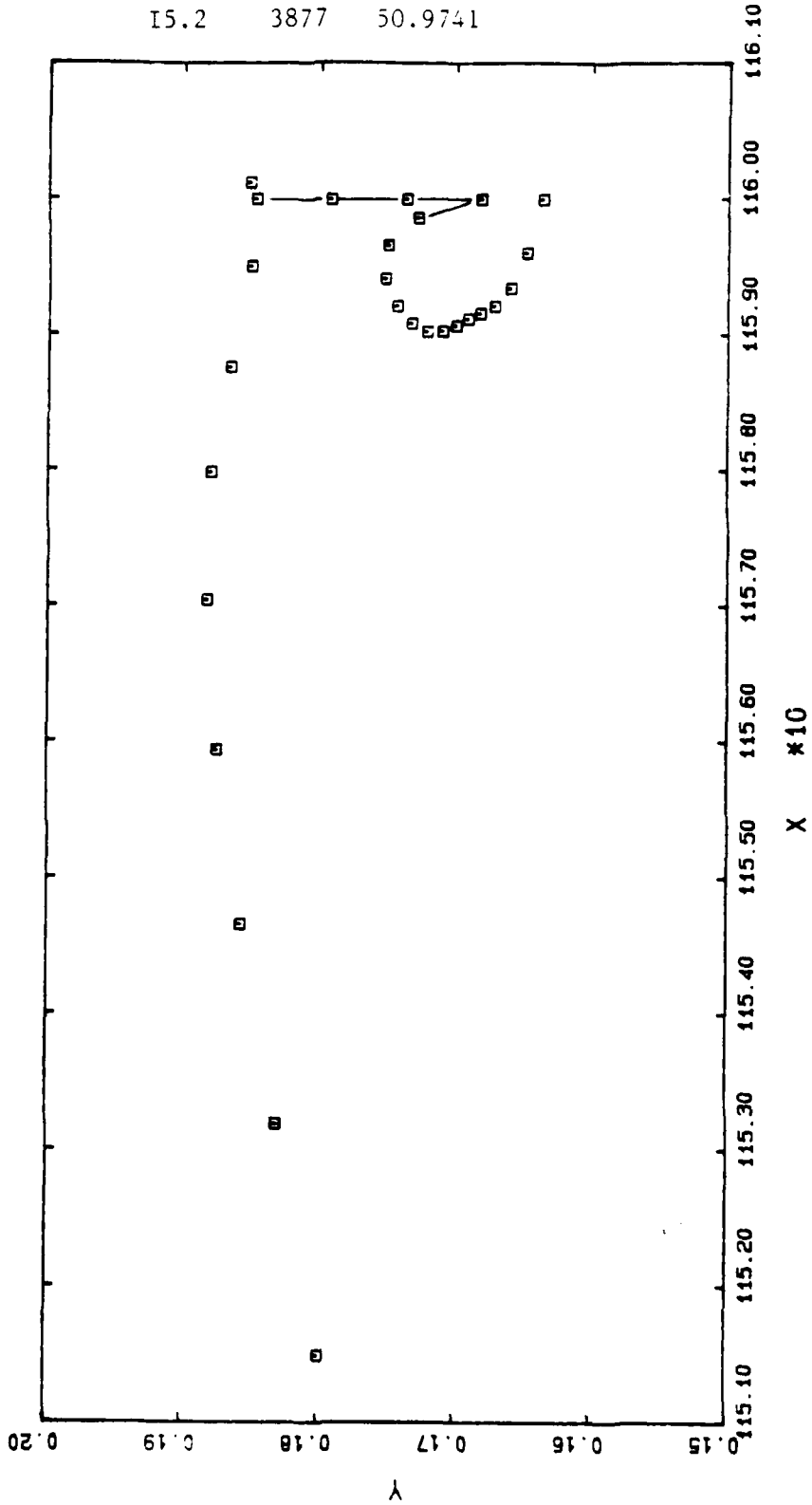

I6.1 3871 50.9739

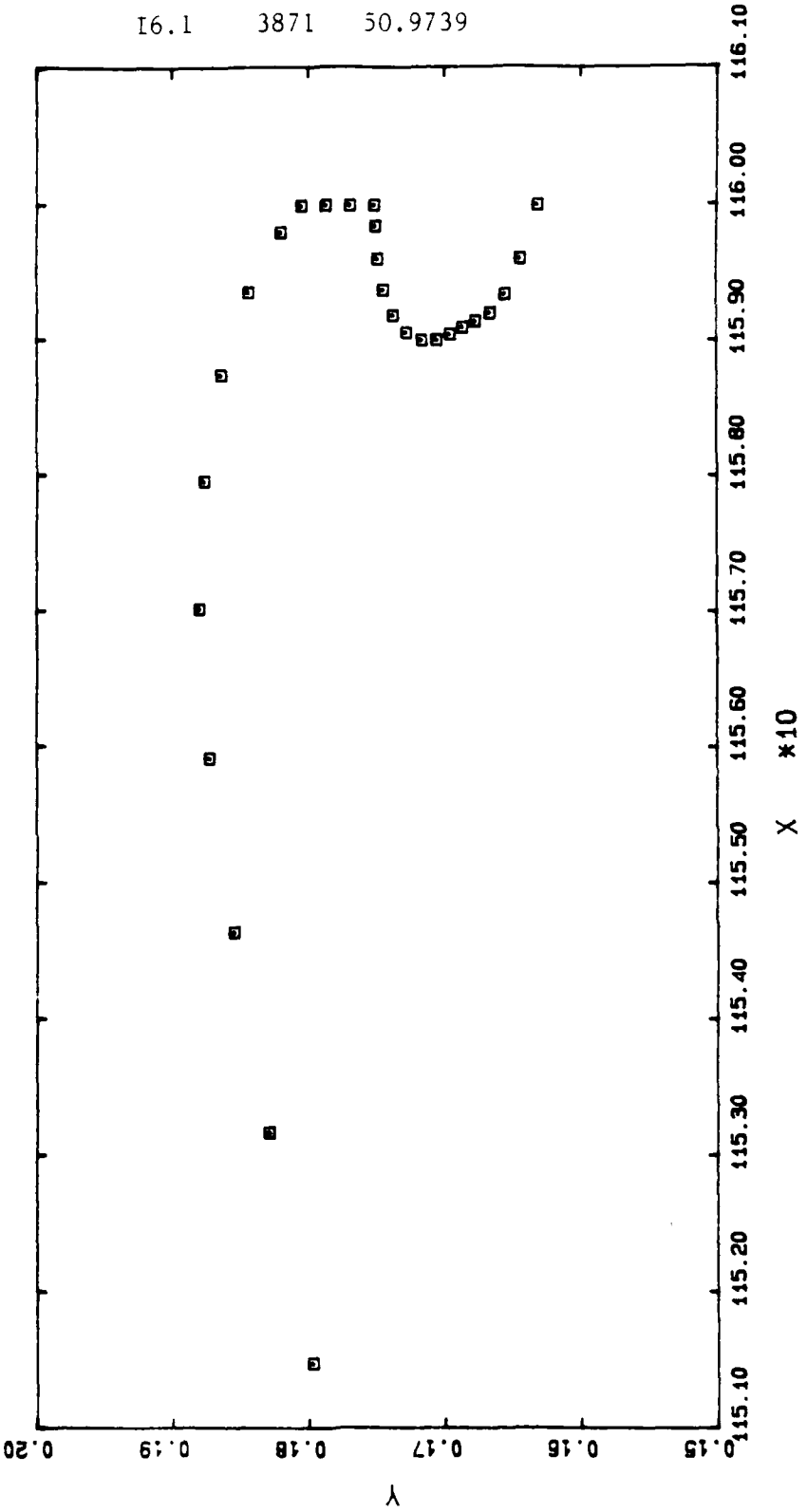

I6.1 3872 50.9739

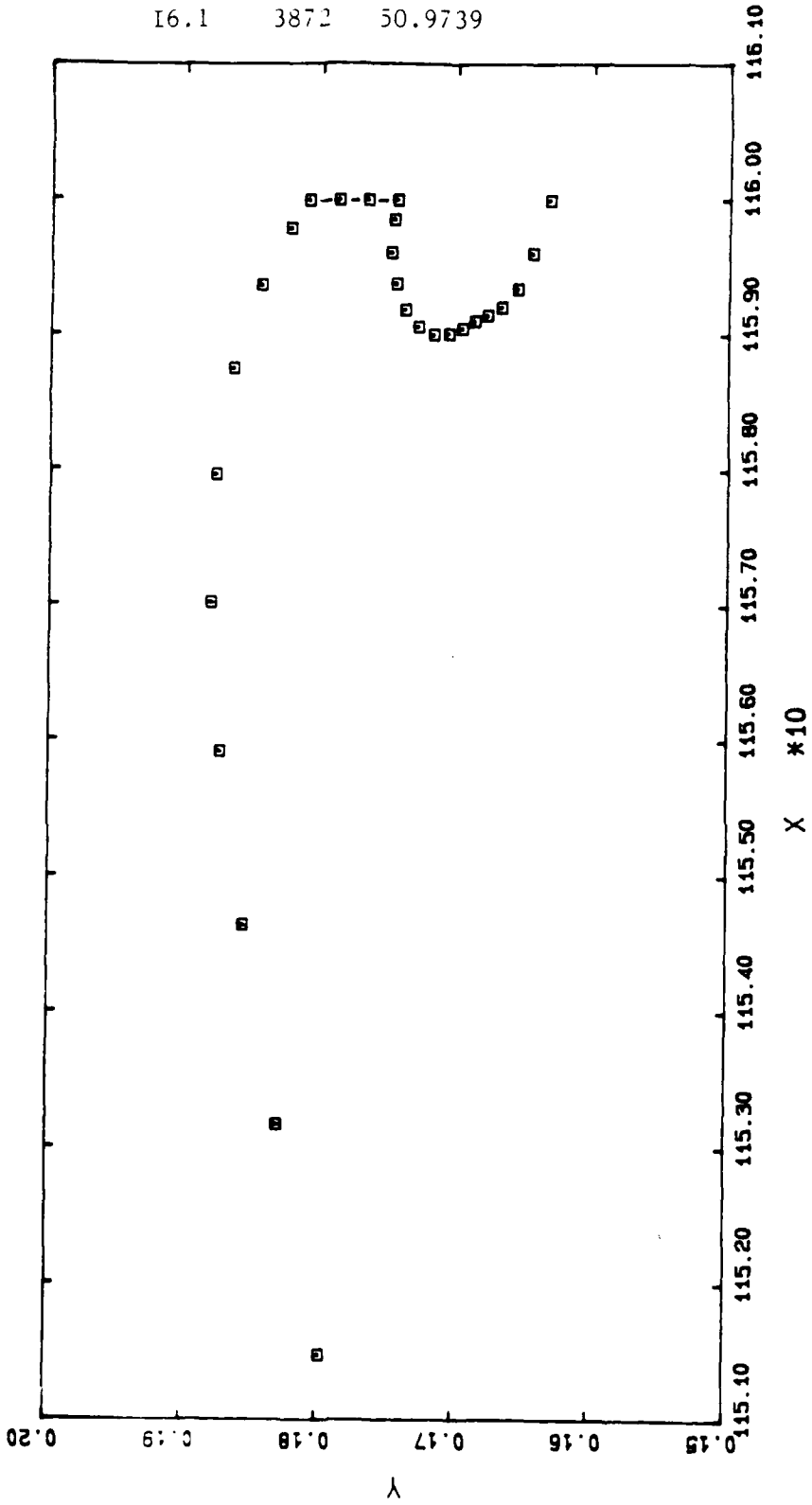

I6.1 3873 50.9739

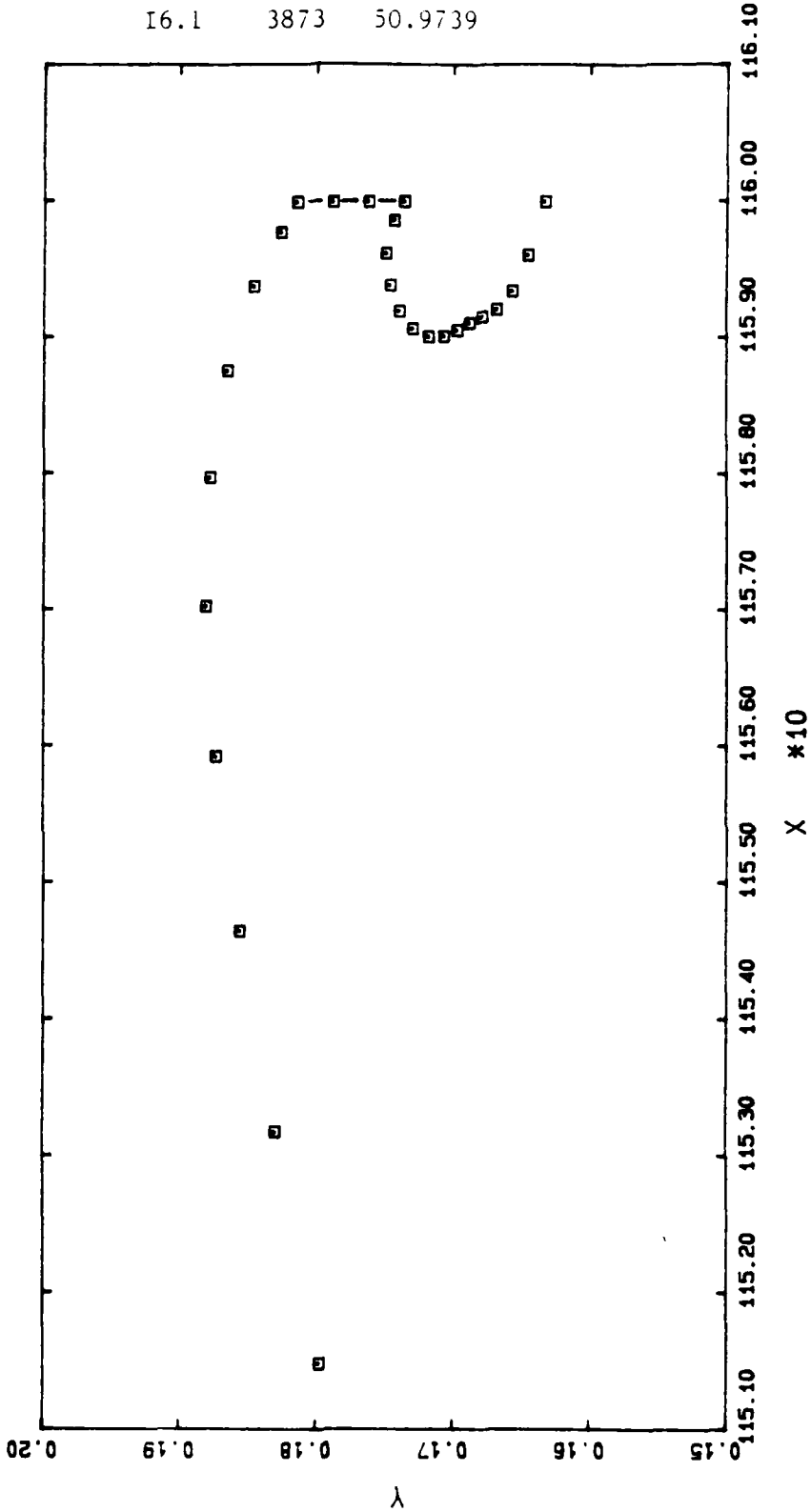

I6.1 3874 50.9740

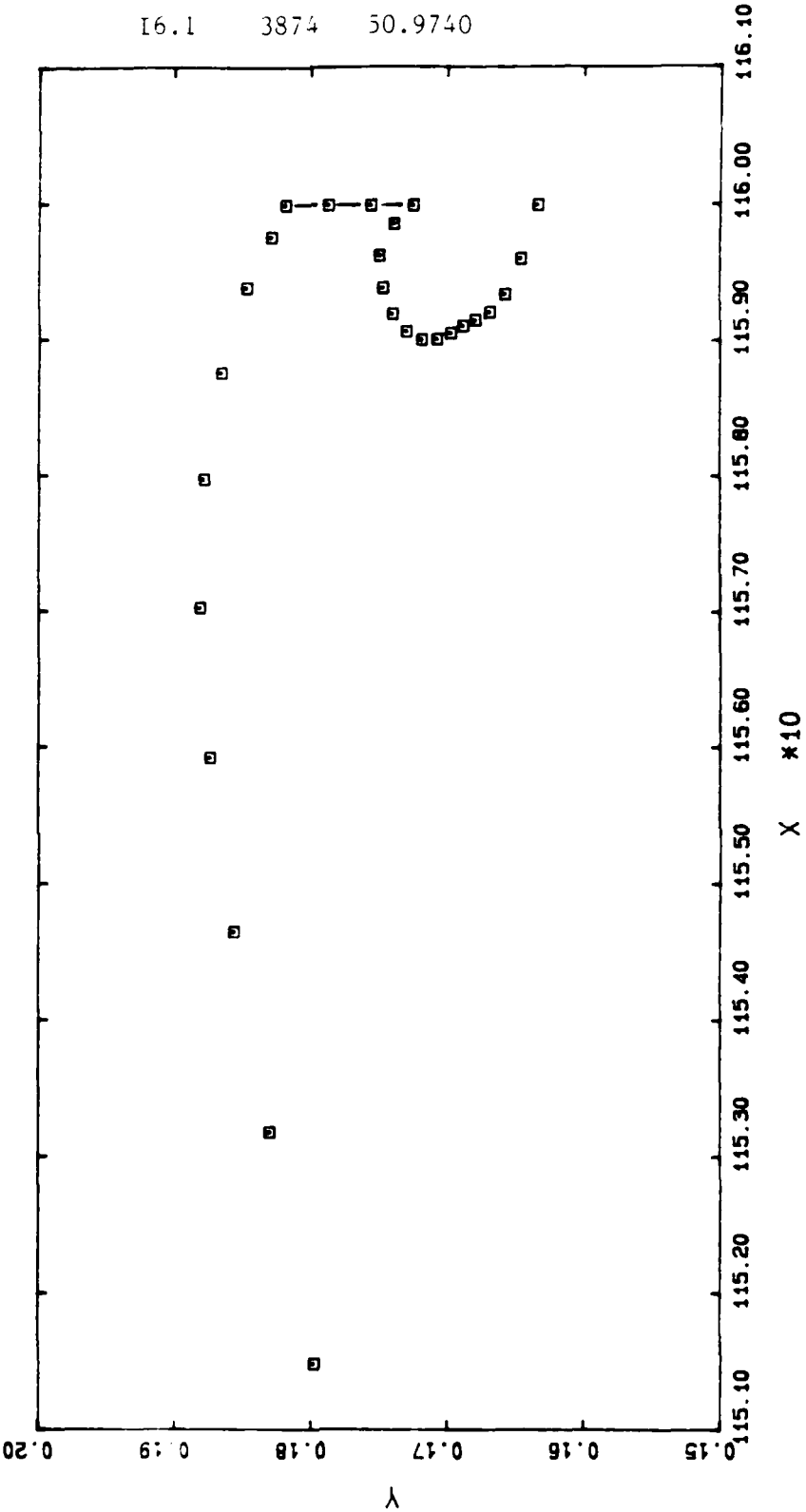

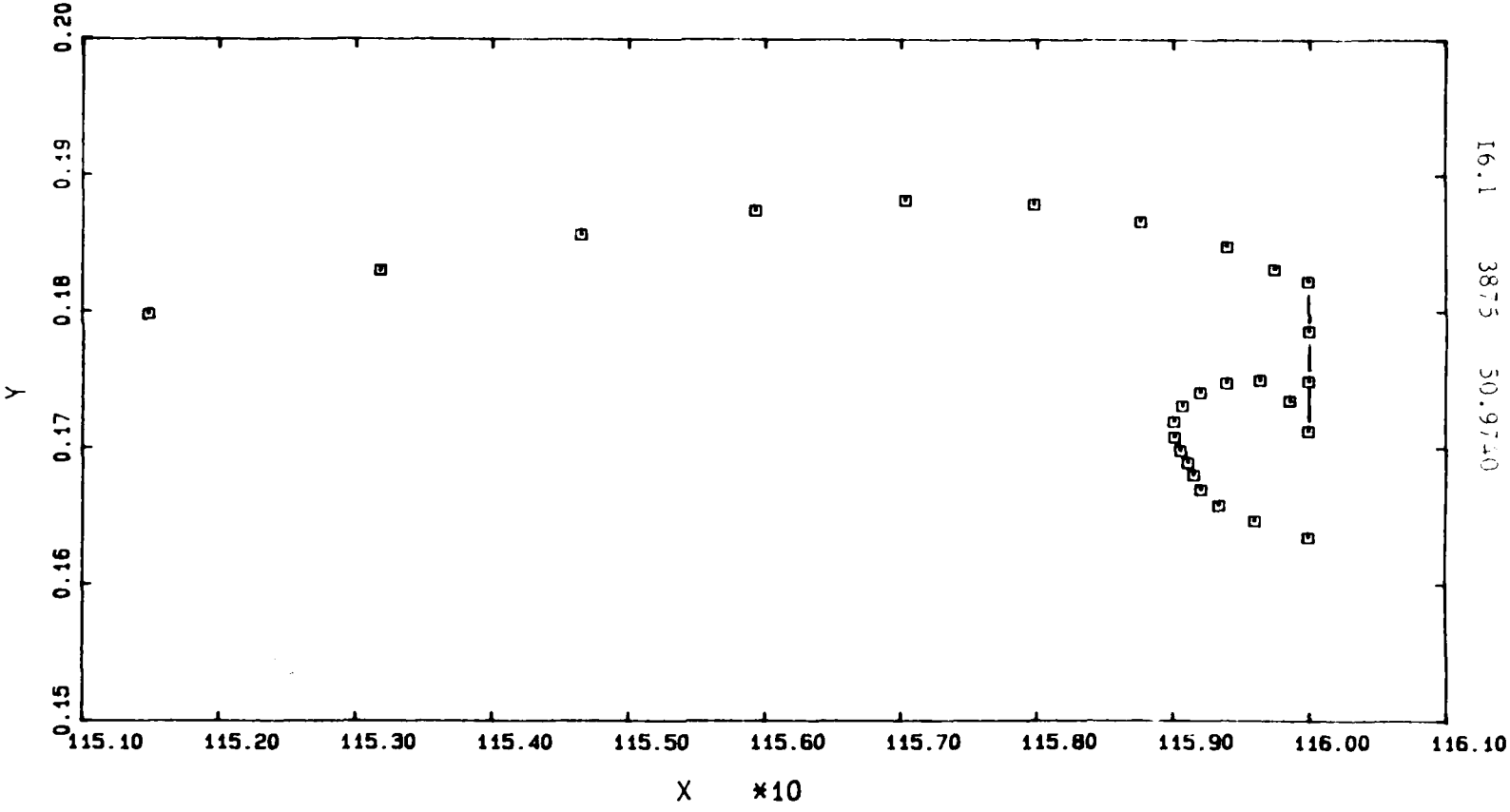

16.1 3875 50.9740

I6.1 3876 50.9741

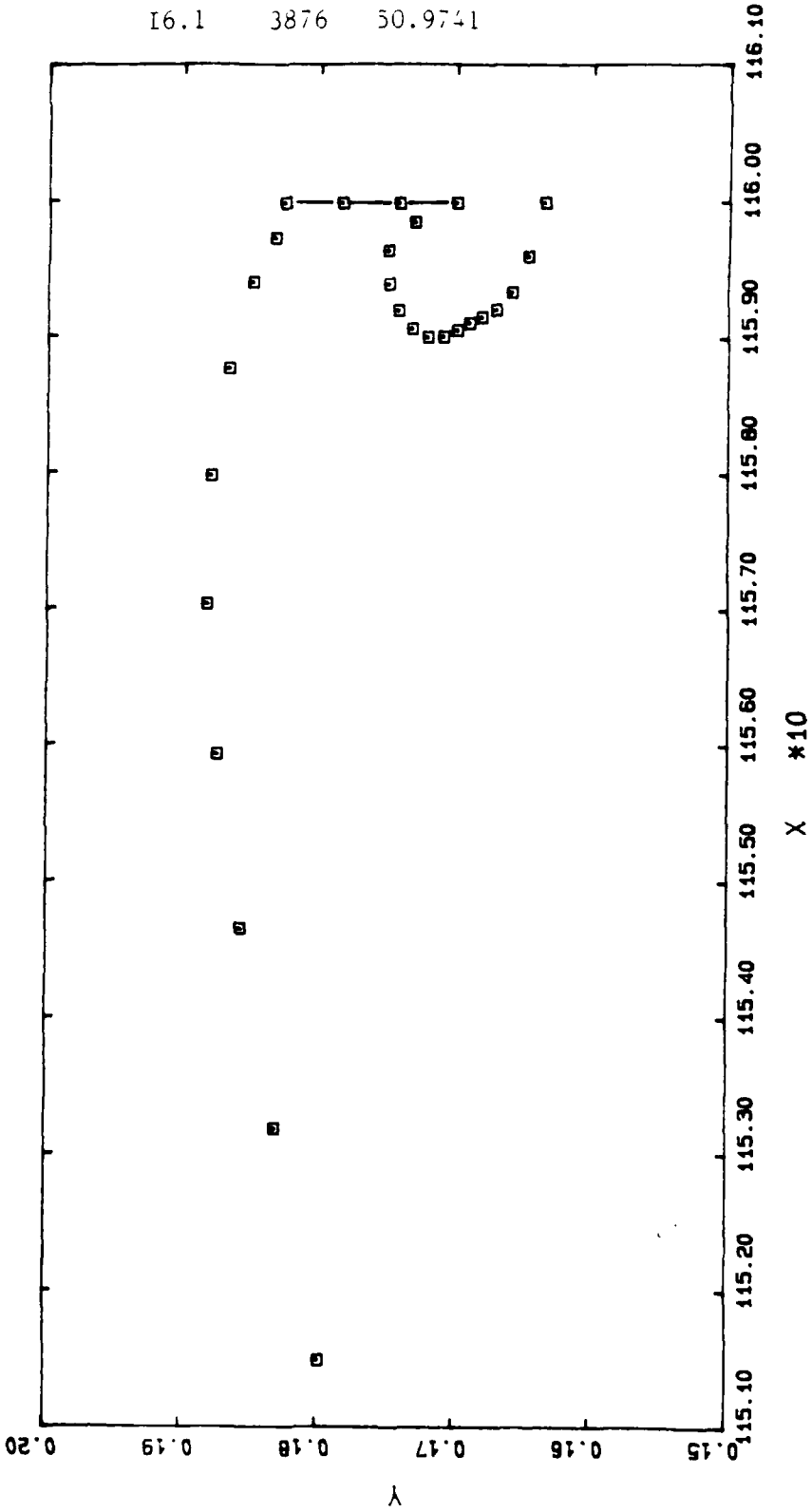

I6.1 3877 50.9741

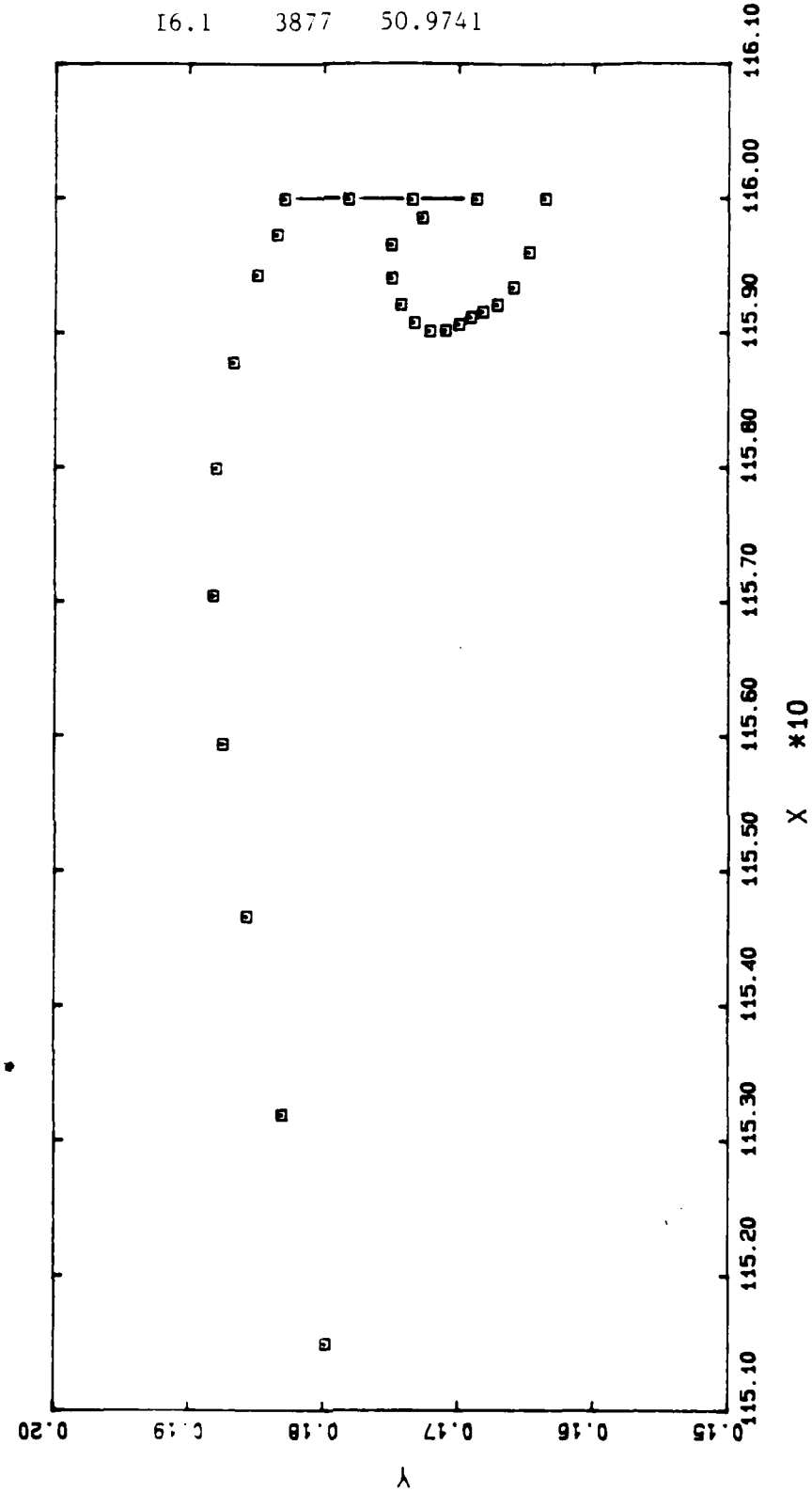

I6.1 3878 50.9741

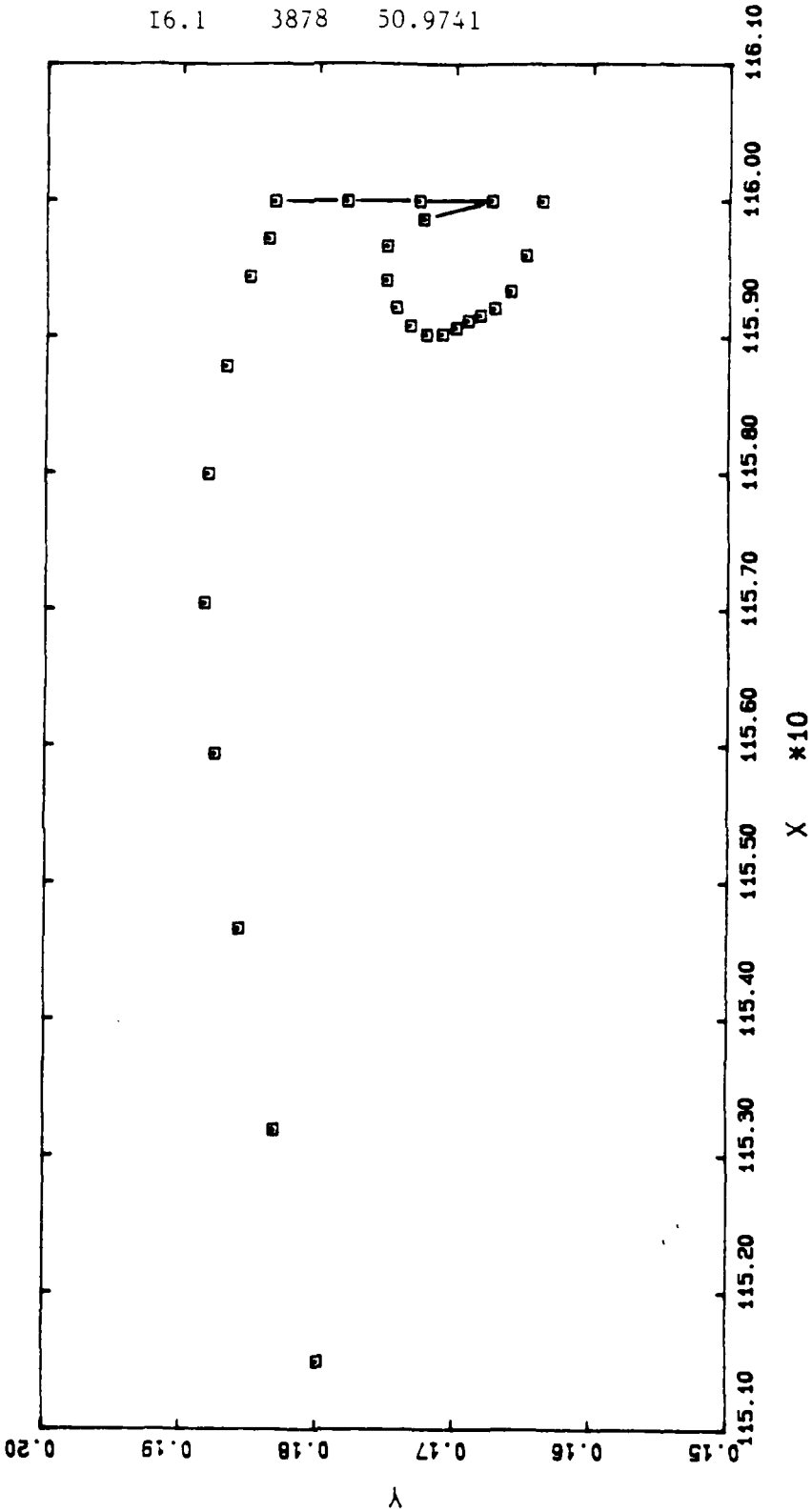

I6.1 3879 50.9742

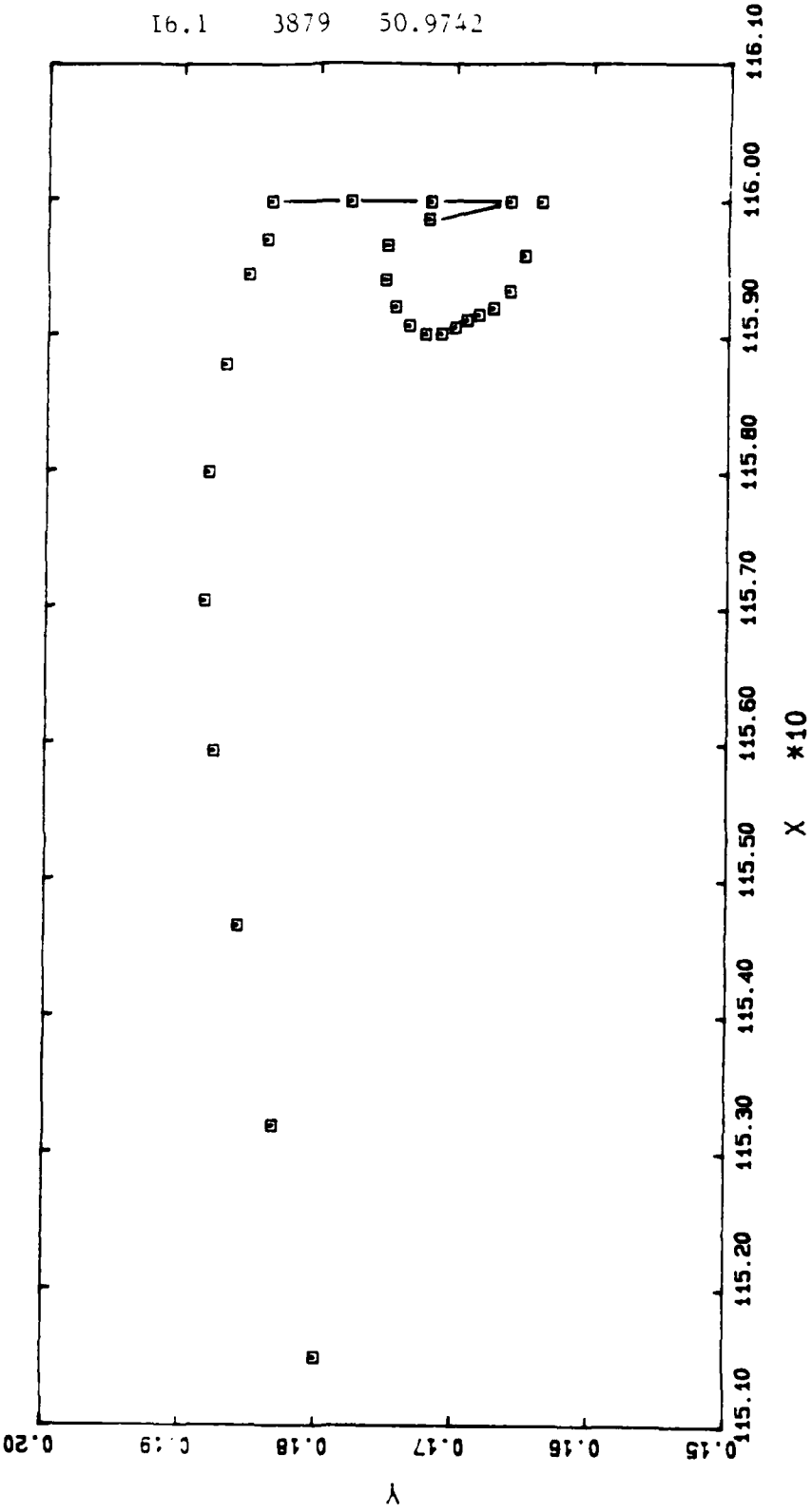

I6.1 3880 50.9742

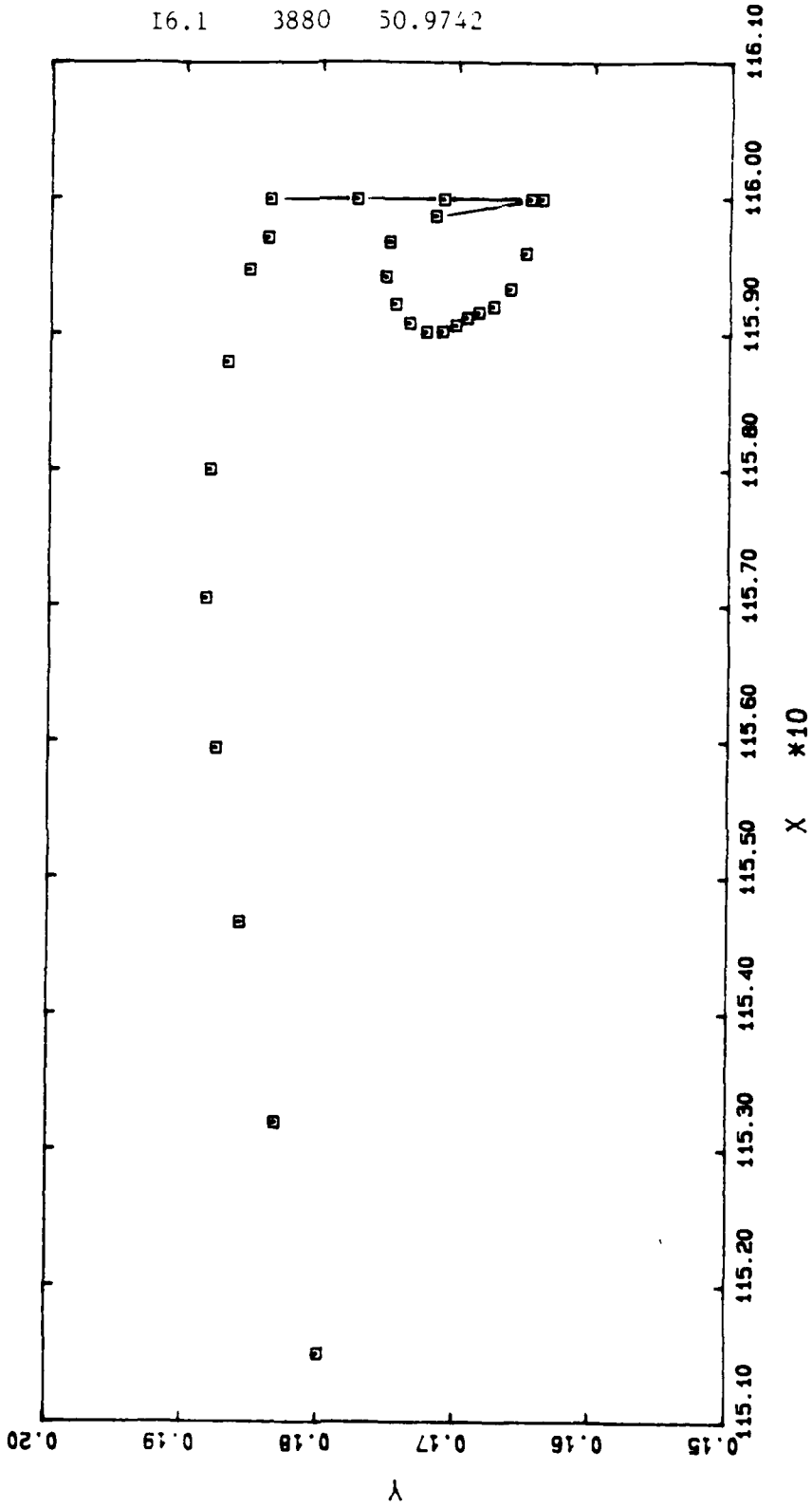

I6.2 3871 50.9739

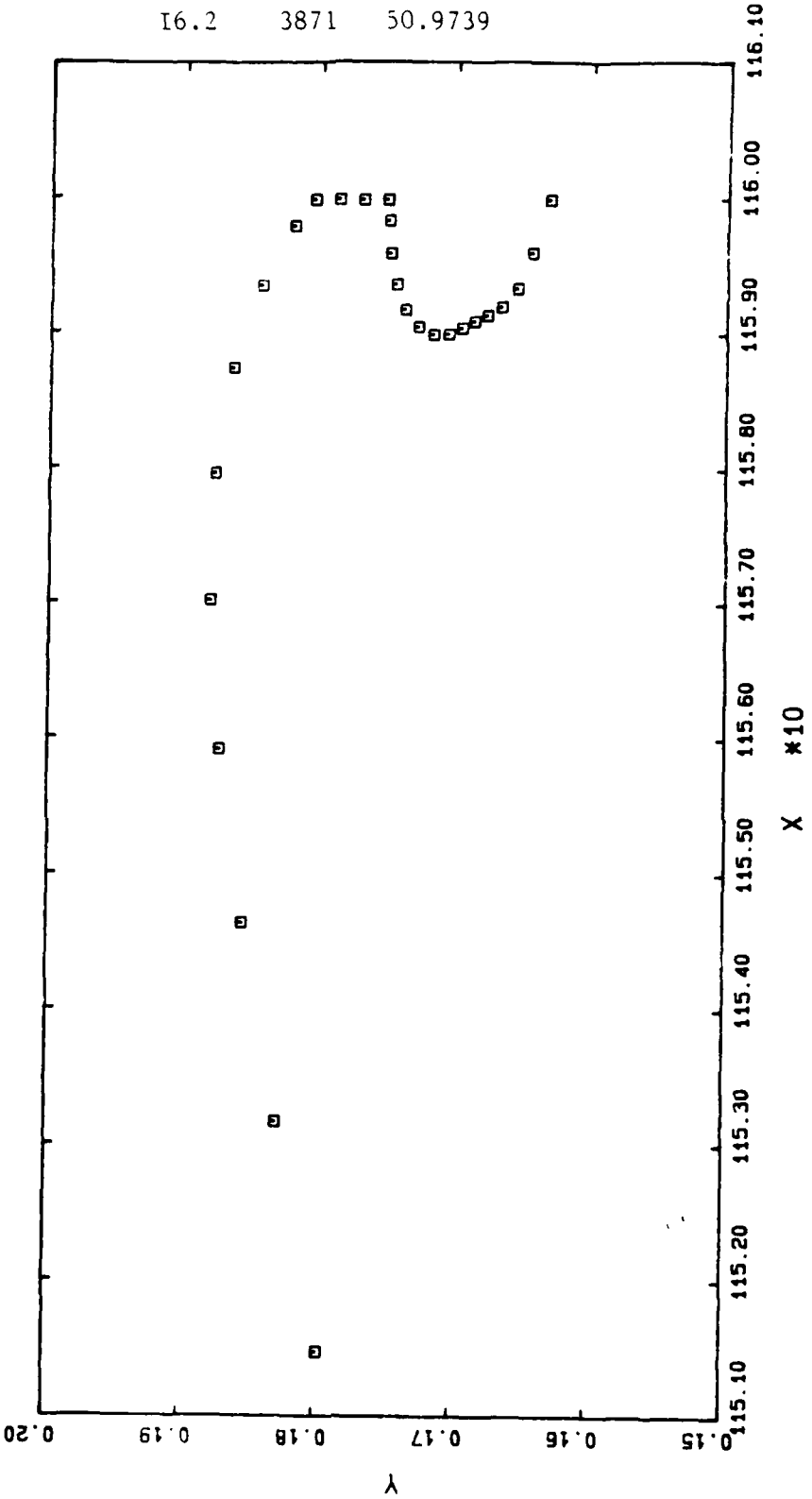

I6.2 3872 50.9739

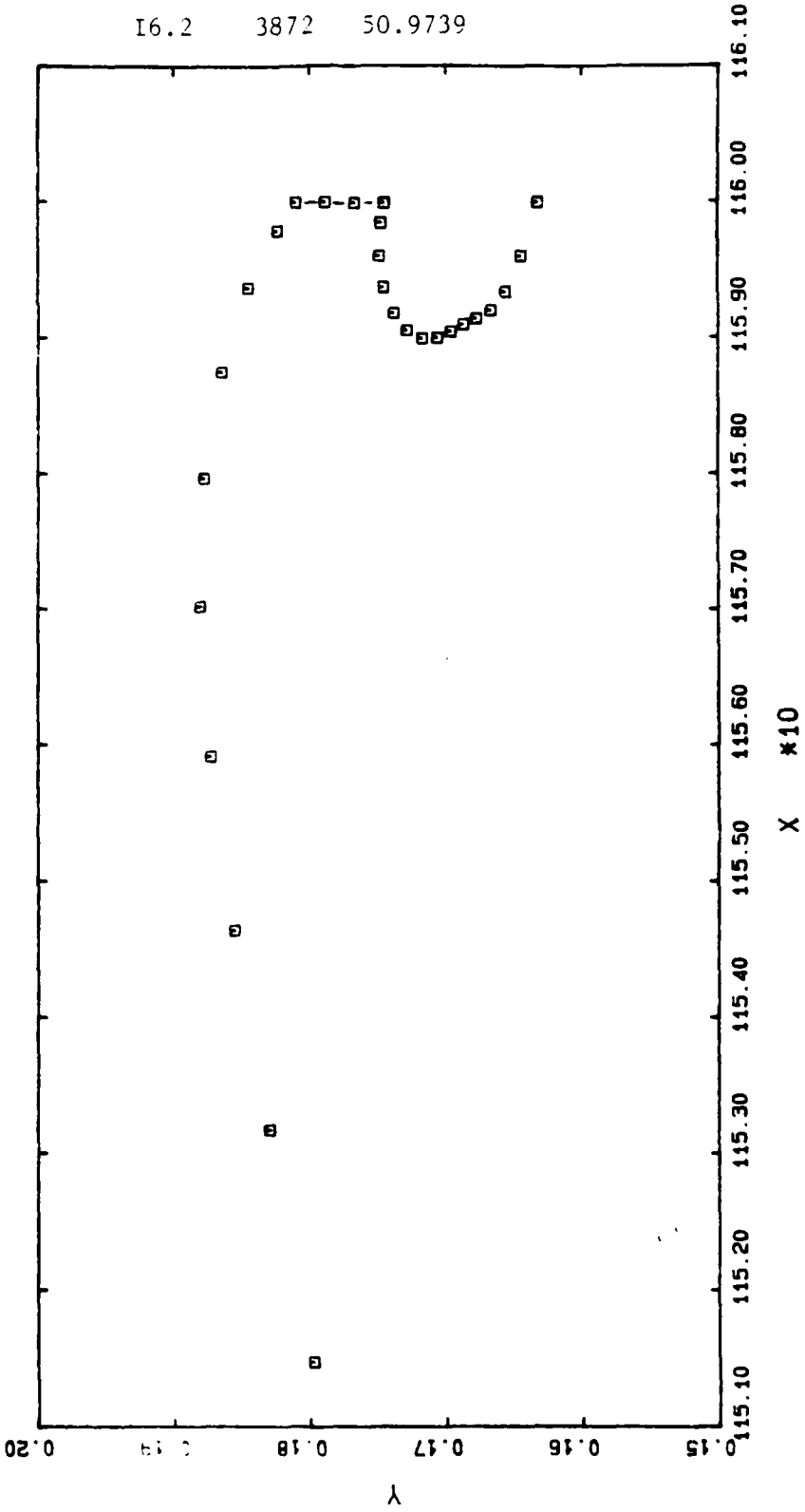

I6.2 3873 50.9739

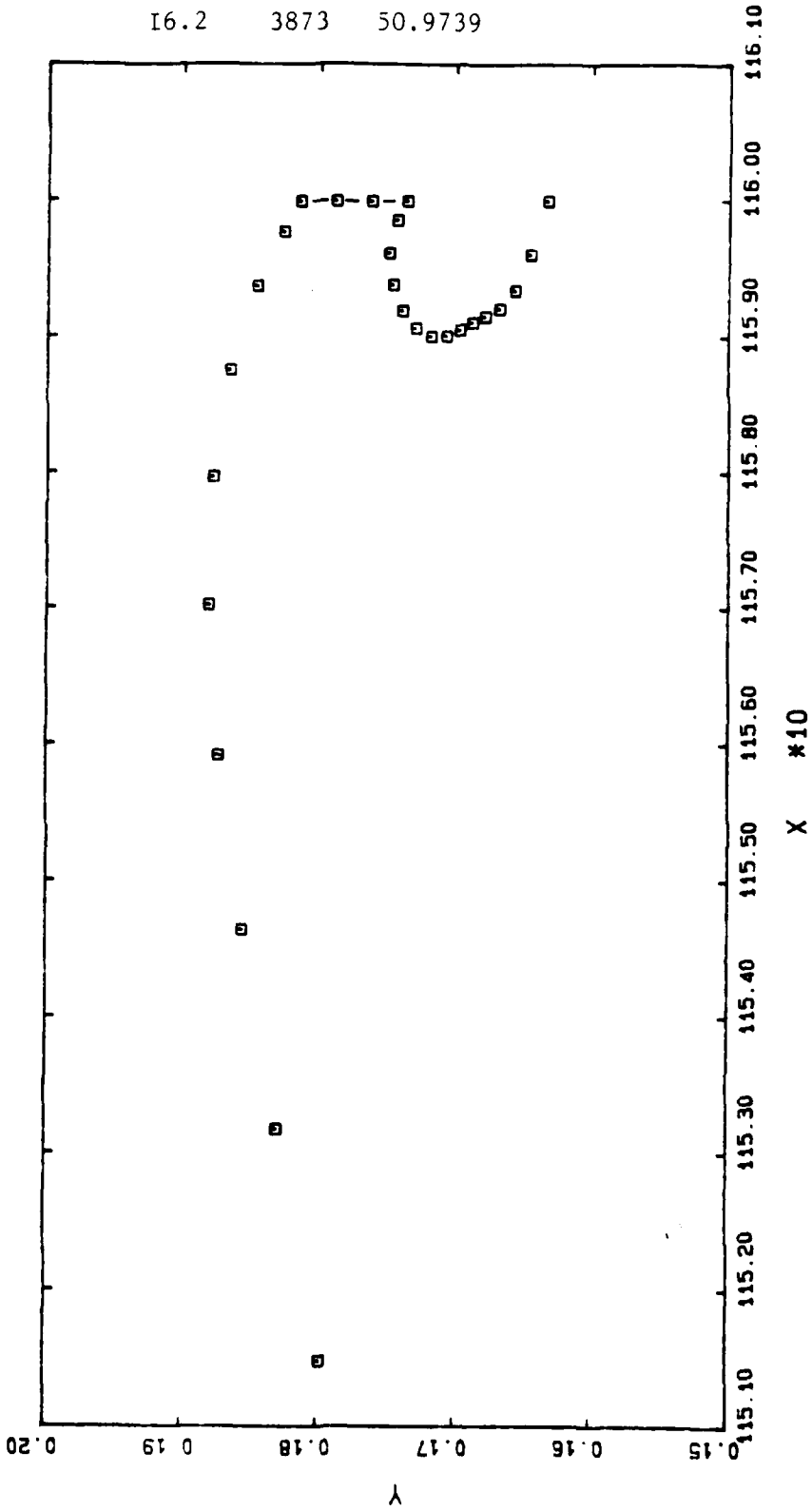

I6.2 3874 50.9740

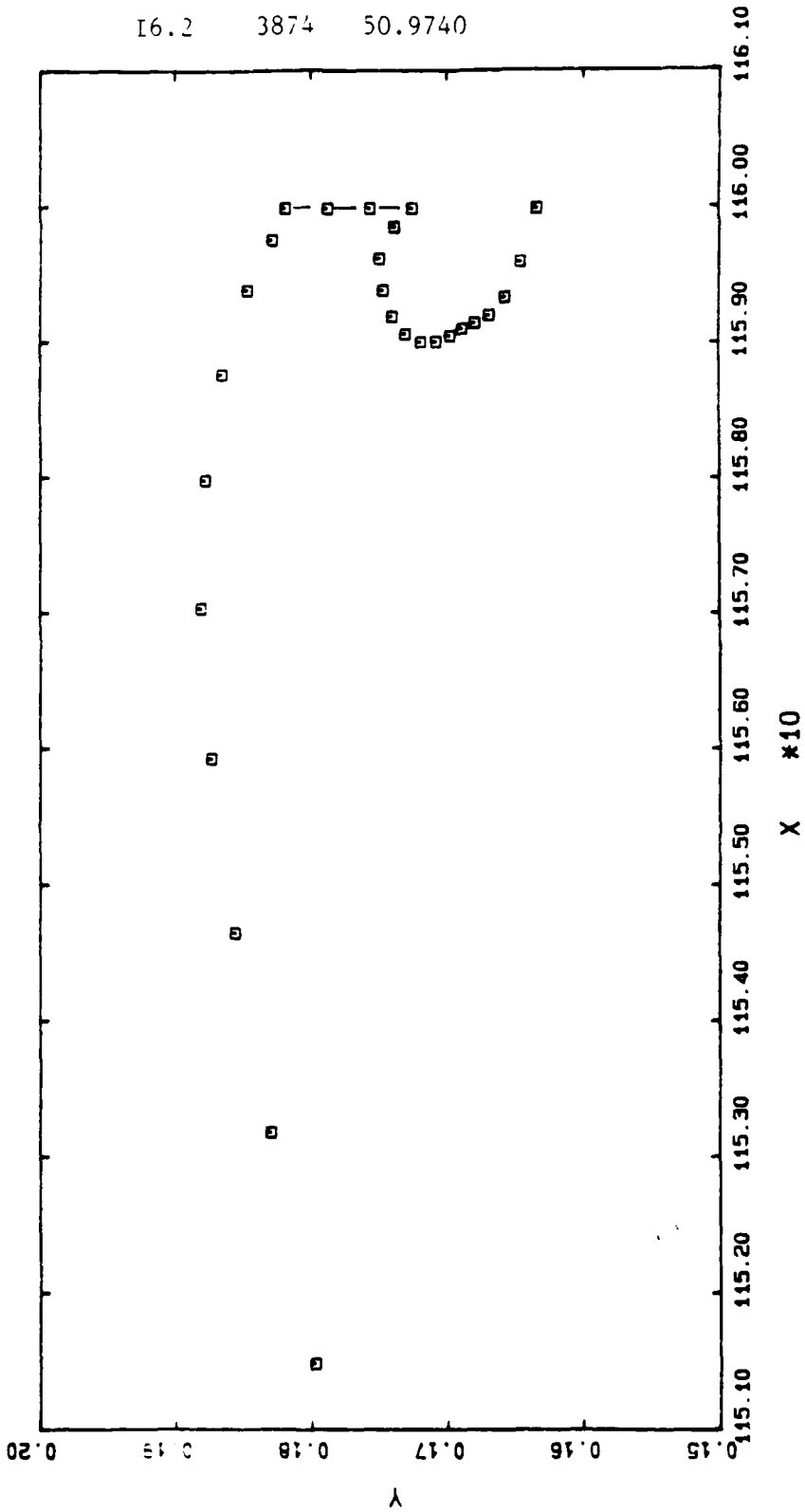

I6.2 3875 50.9740

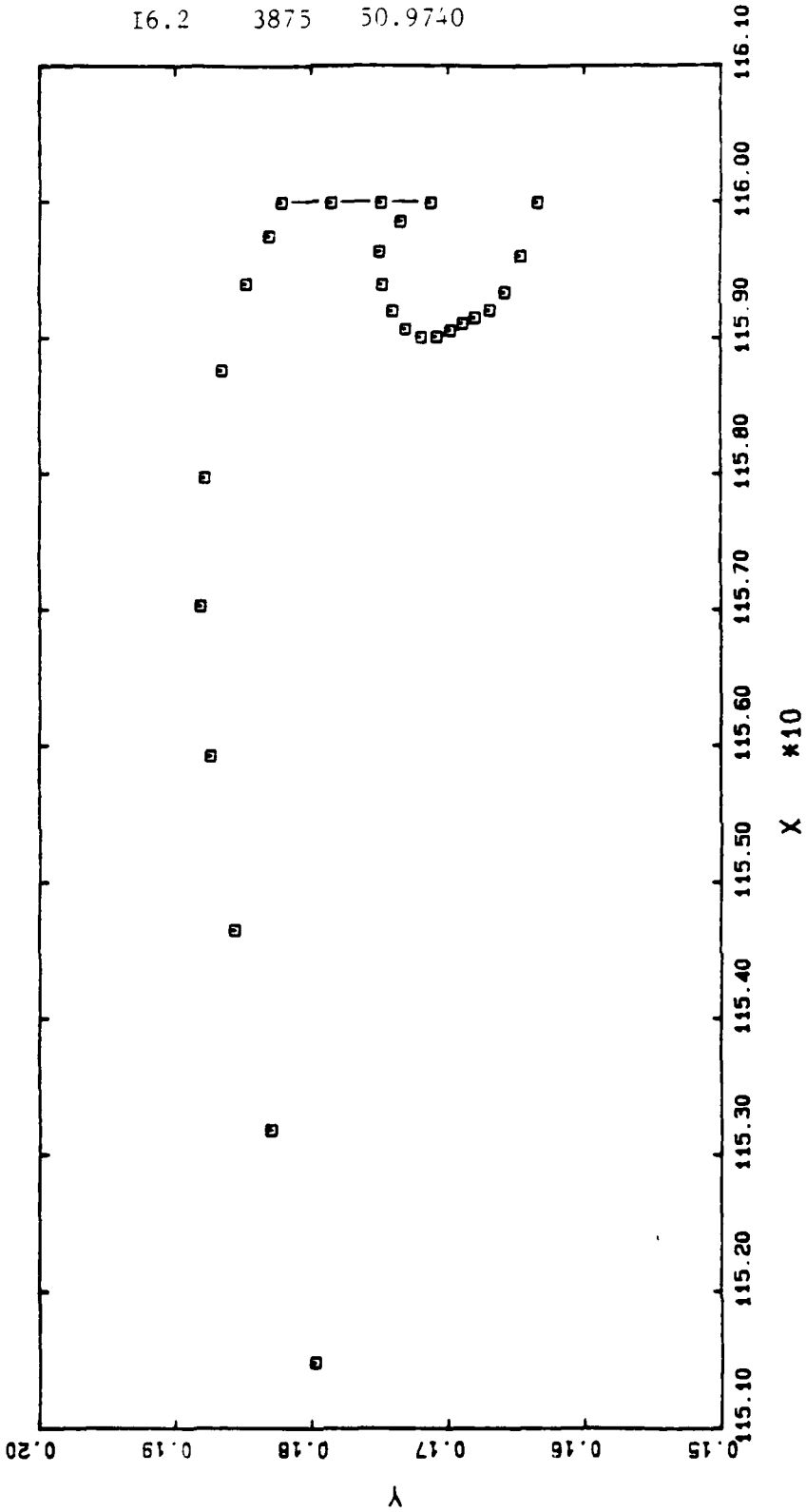

I6.2 3876 50.9741

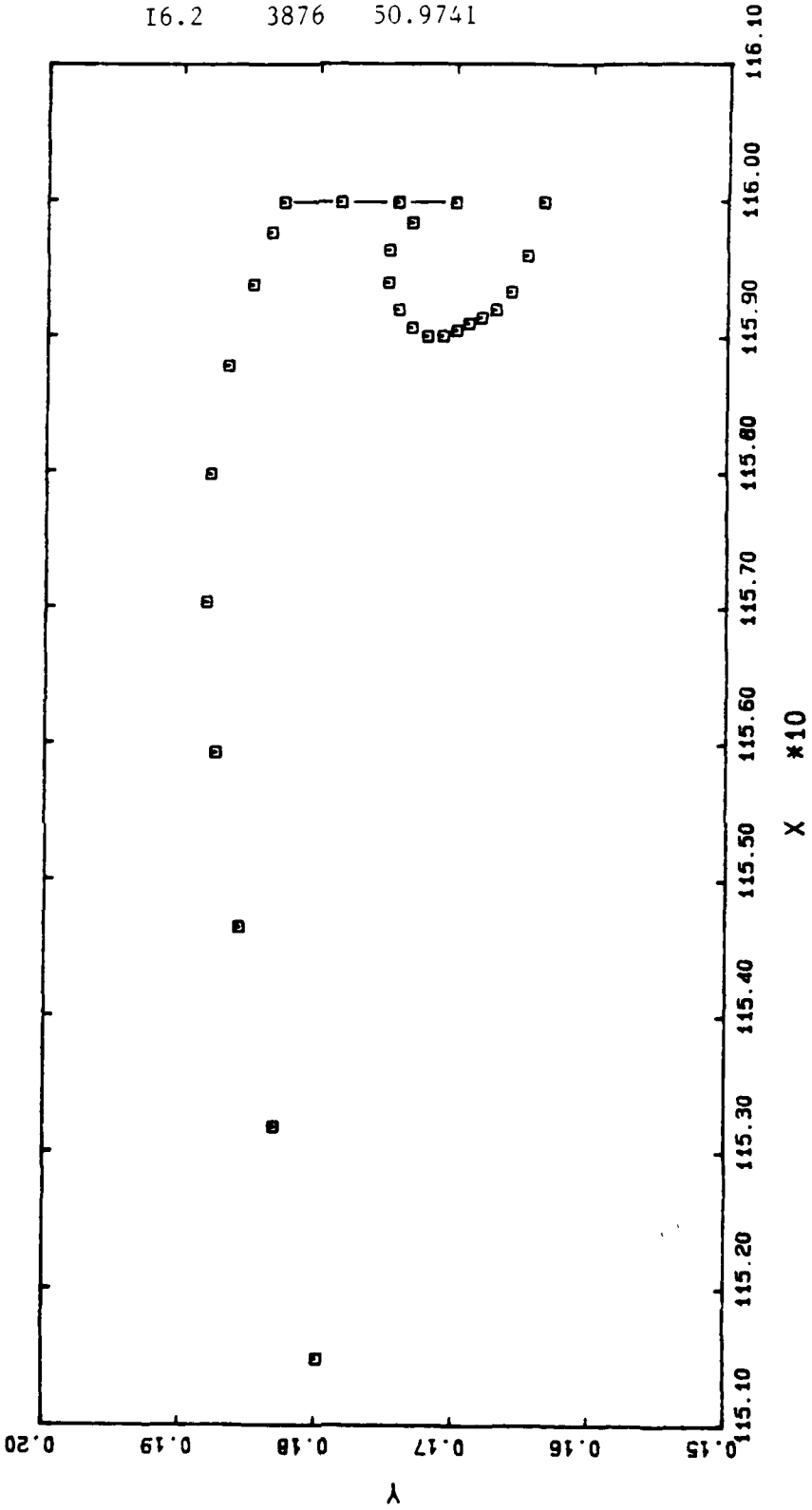

I6.2 3877 50.9741

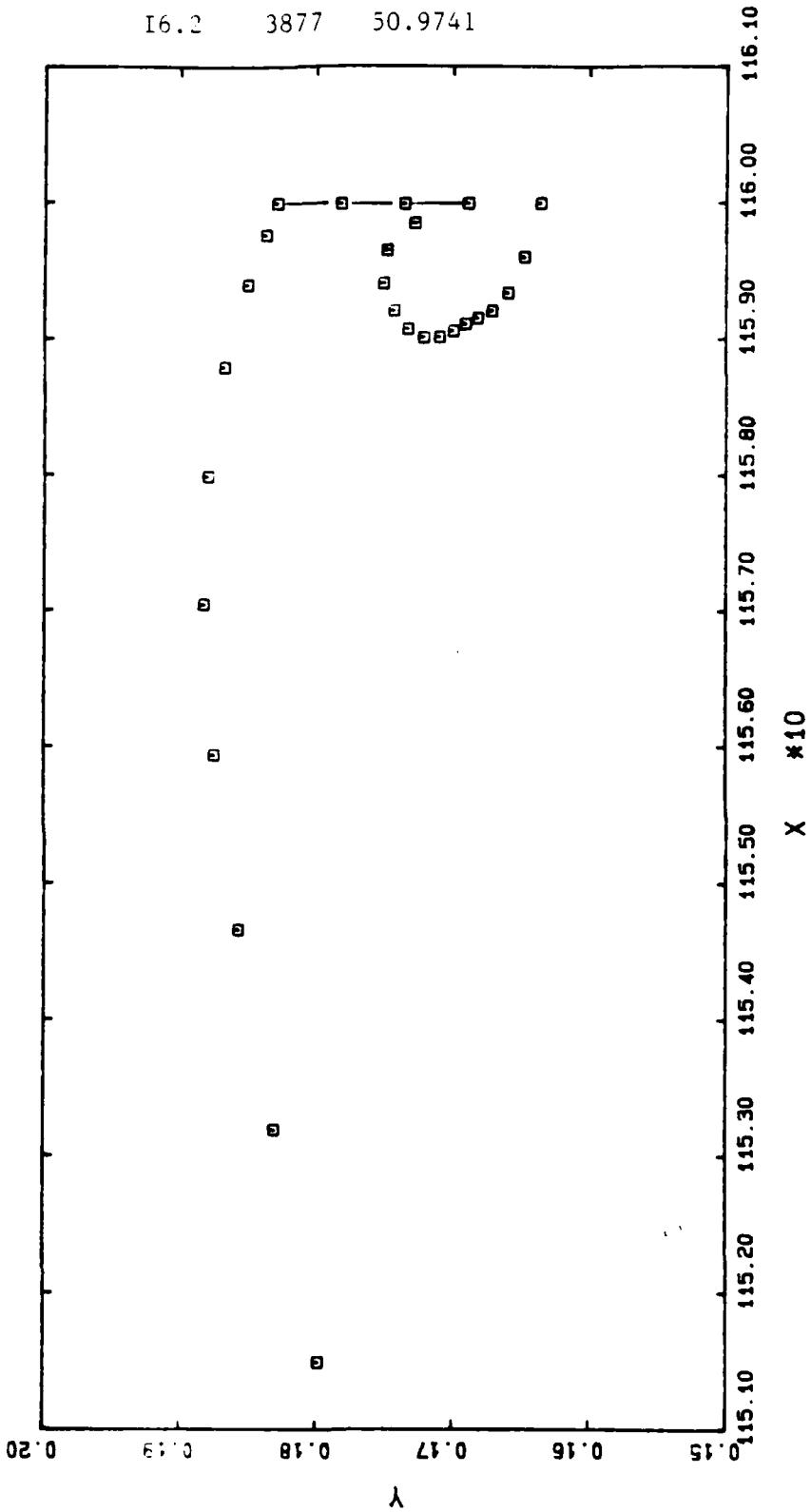

I6.2 3878 50.9741

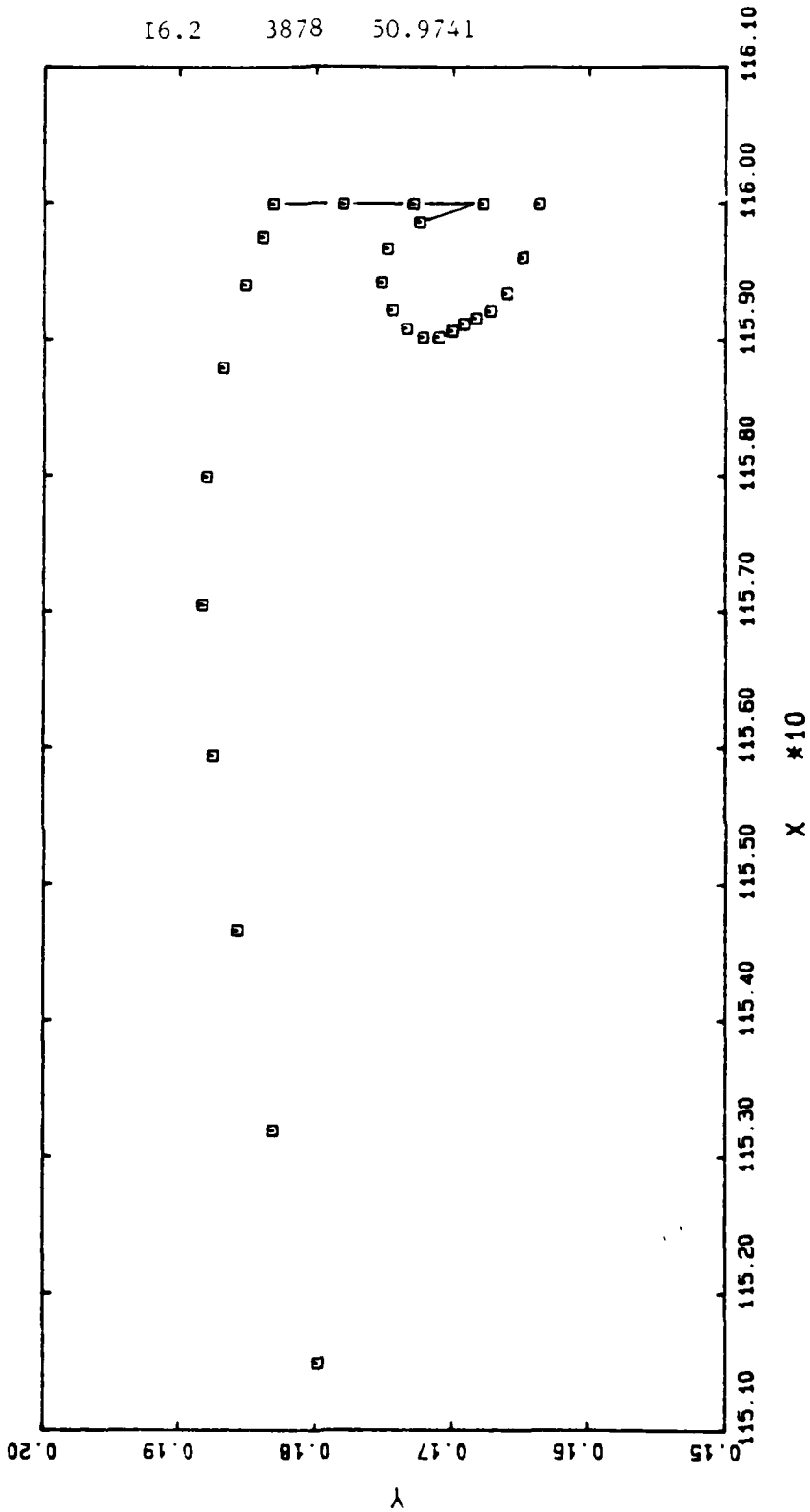

I6.2 3879 50.9742

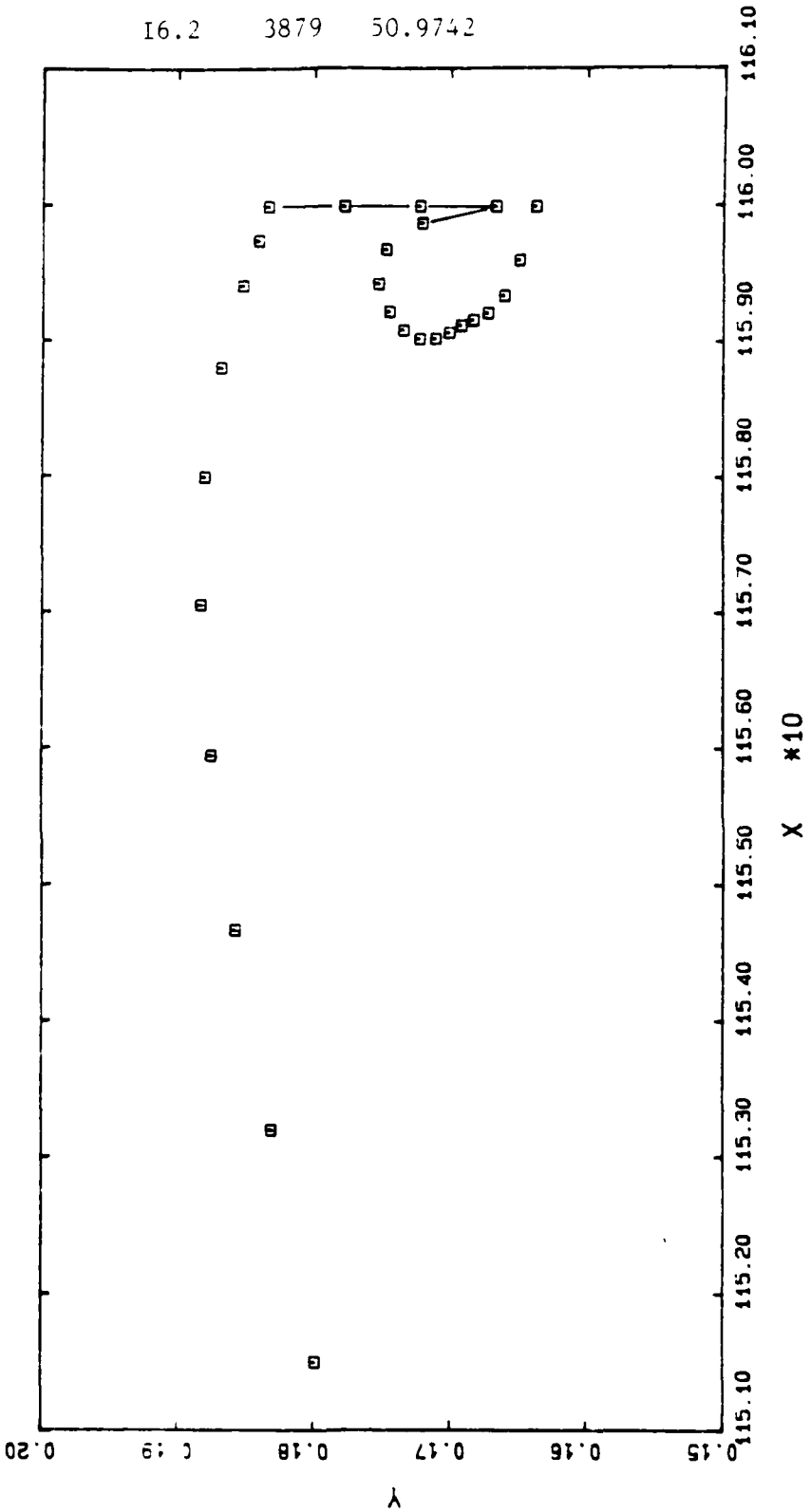

I6.2 3880 50.9742

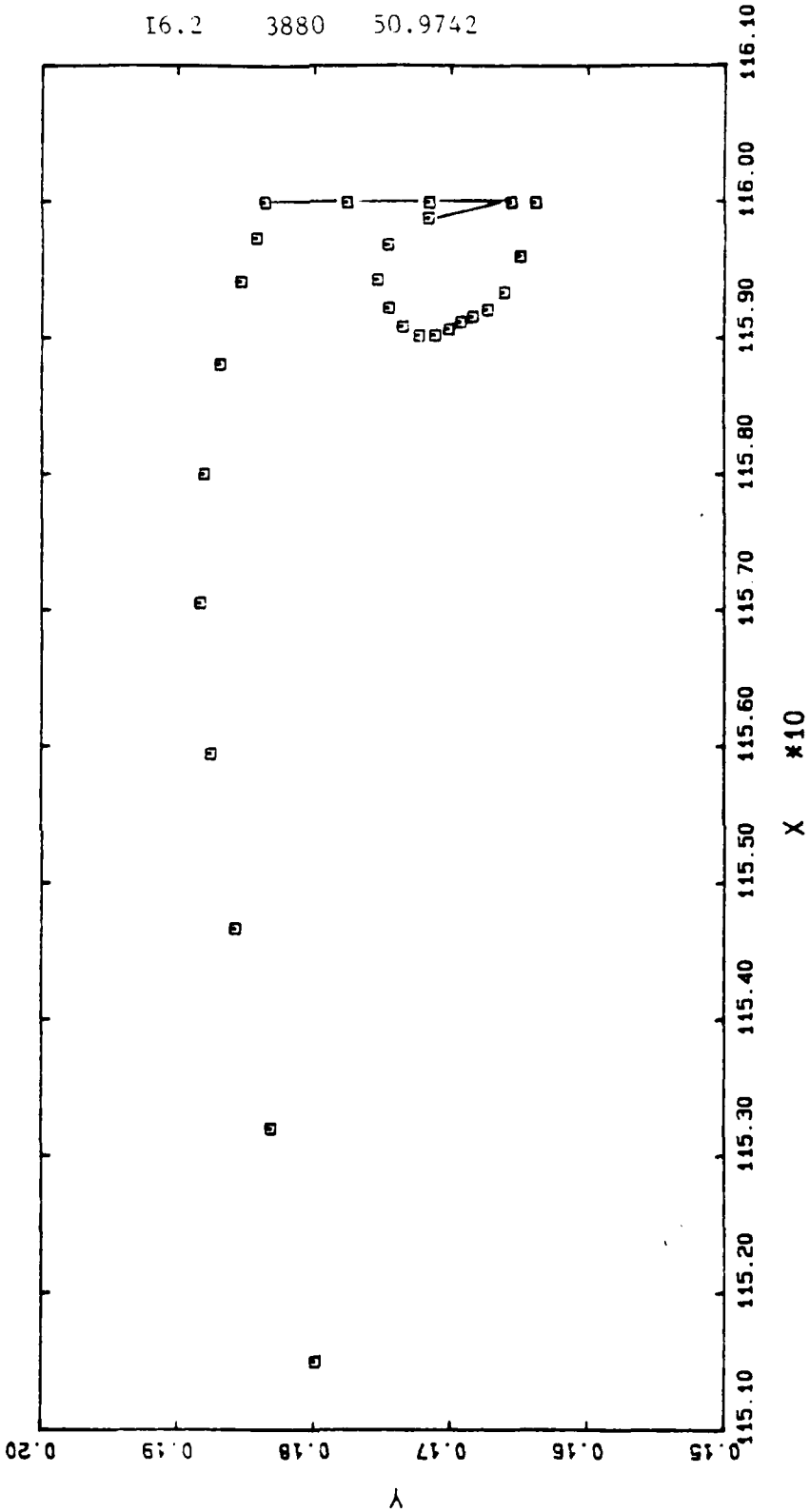

Appendix J

Refer to Chapter 6 for discussion.

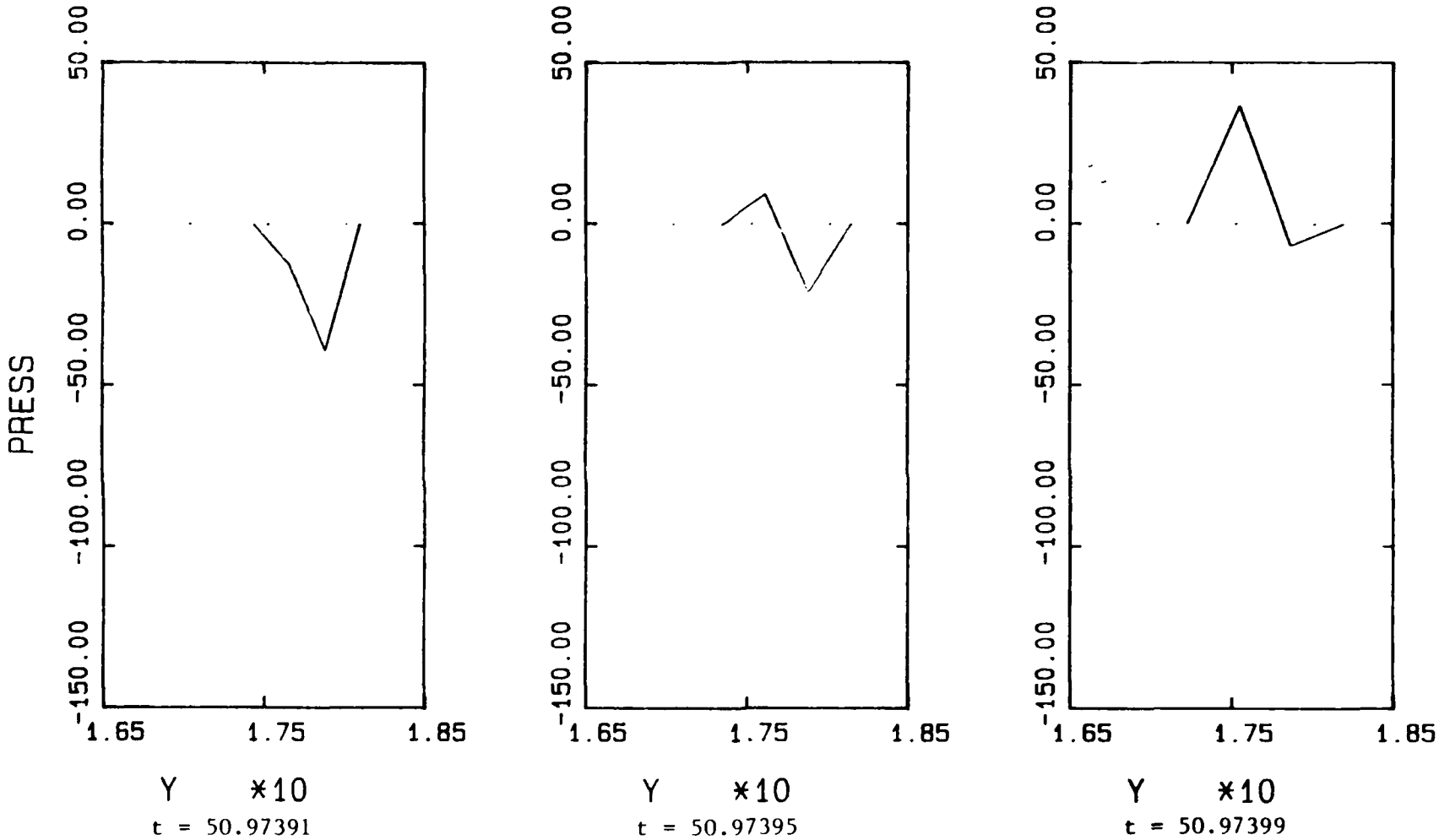

Time history of impact pressure; time step size = 0.00001, no. of points = 4.

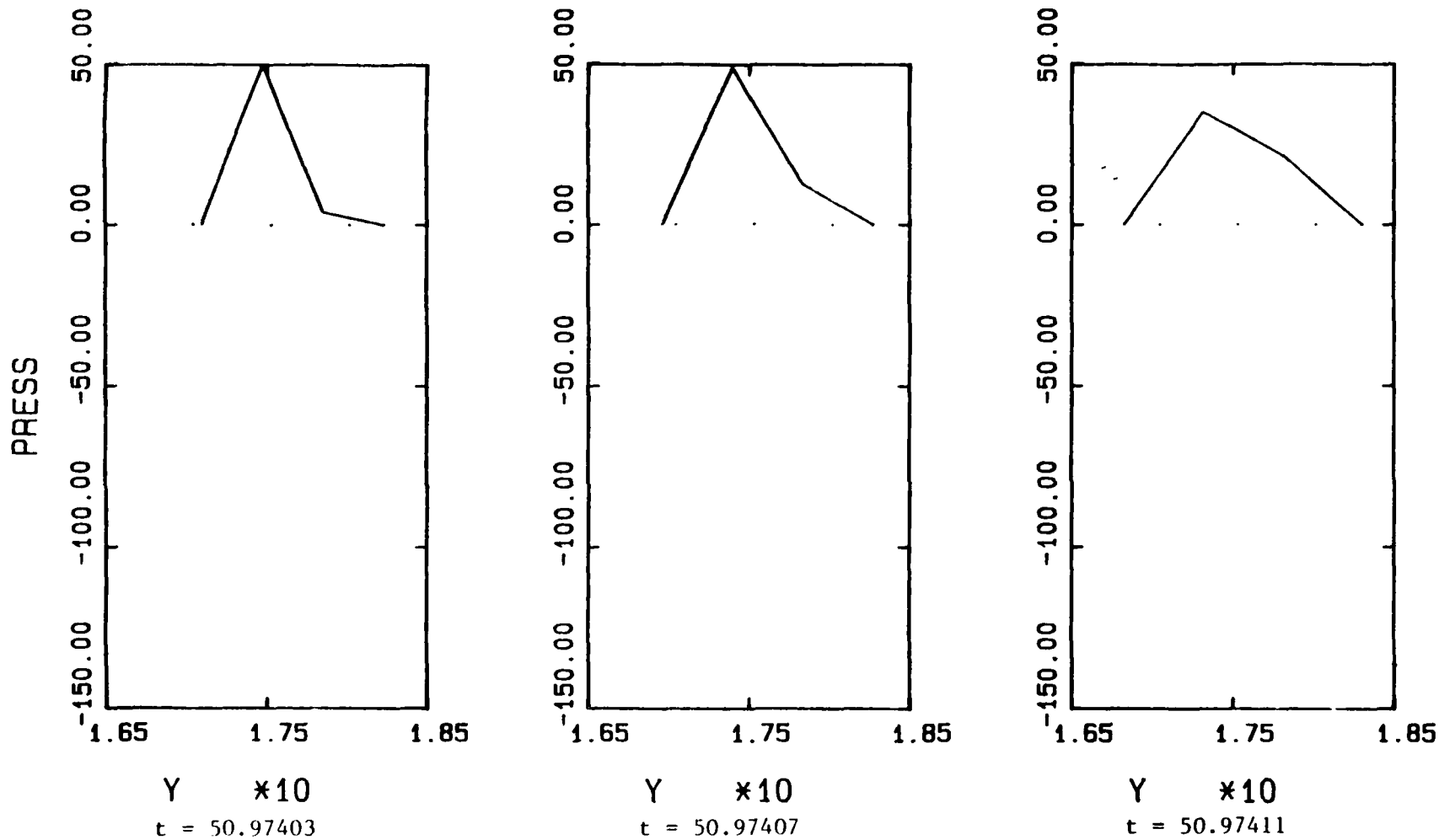

Time history of impact pressure; time step size = 0.00001, no. of points = 4.

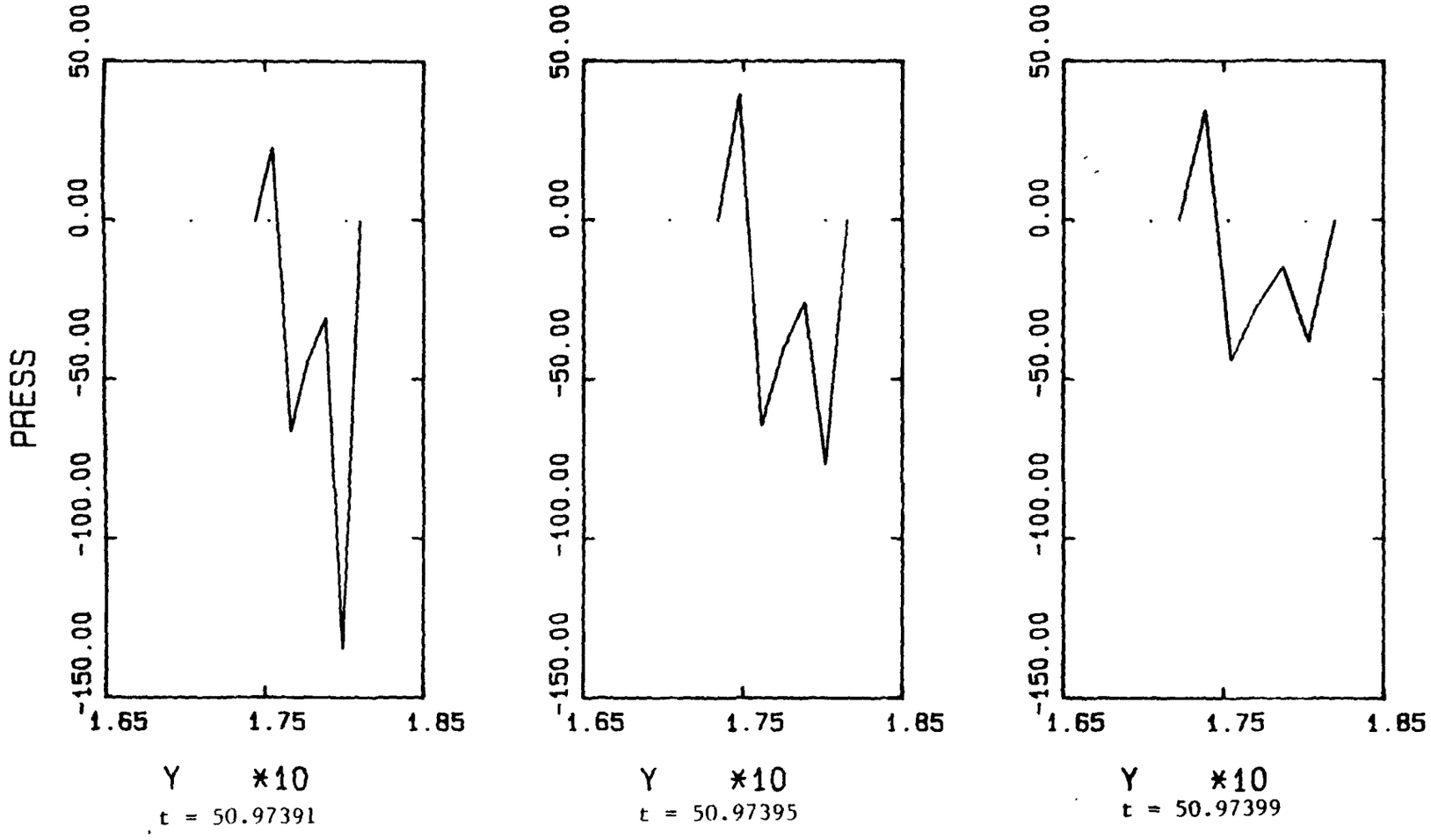

Time history of impact pressure; time step size = 0.00001, no. of points = 7.

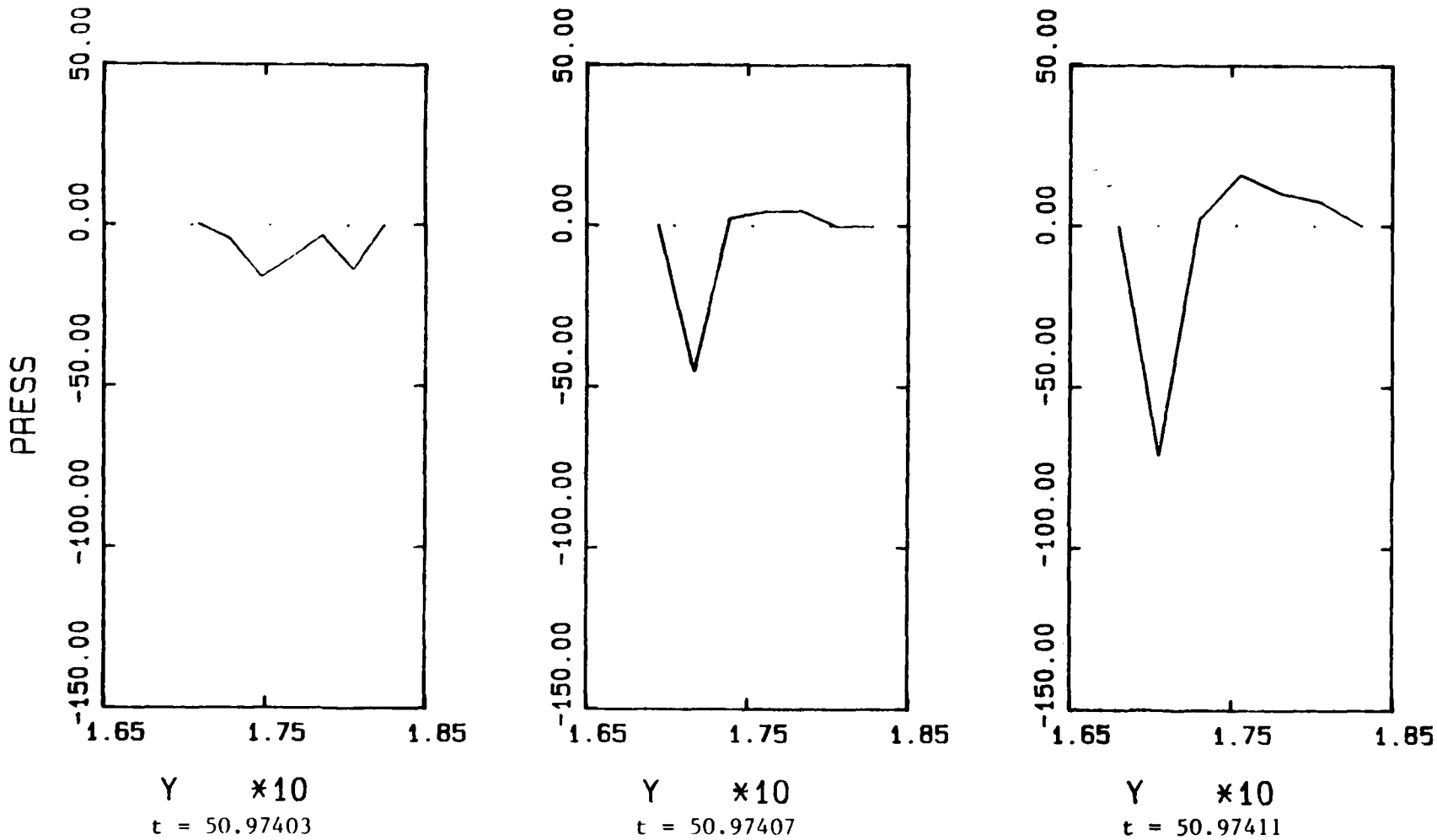

Time history of impact pressure; time step size = 0.00001, no. of points = 7.

References

[1] Chan, E. S.
Deep water breaking wave forces on structures.
PhD thesis, Massacusetts Insitute of Technology, 1985.

[2] Chan, E. S. and Melville, W. K.
Deep-water plunging wave pressures on a vertical plane wall.
Proc. R. Soc. Lond. A. 417:95-131, 1988.

[3] Dommermuth, D. G., Yue, D. K. P., Lin, W. M., Rapp, R. J.,Chan, E. S., and Melville, W. K.
Deep-water plunging breakers: a comparison between potentialtheory and experiments.
J. Fluid Mech. 189:423-442, 1988.

[4] Fink, P. T. and Soh, W. K.
Calculation of vortex sheets in unsteady flow and applications in ship hydrodynamics.
In R. D. Cooper and S. W. Doroff (editor), *Proc. 10th Symp. on Naval Hydro., Cambridge, MA*, pages 463-491. Washington: Government Printing Office, 1974.

[5] Lin, W. M.
Nonlinear motion of the free surface near a moving body.
PhD thesis, Massacusetts Insitute of Technology, 1984.

[6] Lin, W. M., Newman, J. N. and Yue, D. K. P.
Nonlinear forced motions of floating bodies.
In *Proc. 15th Symp. on Naval Hydro., Hamburg*, pages 33-49. Washington: National Academy Press, 1984.

[7] Longuet-Higgins, M. S. and Cokelet, E. D.
The deformation of steep surface waves on water. I. A numerical method of computation.
Proc. R. Soc. Lond. A. 350:1-26, 1976.

[8] Oguz, H. N. and Prosperetti, A.
Surface-tension effects in the contact of liquid surfaces.
J. Fluid Mech. 203:149-171, 1989.

[9] Vinje, T. and Brevig, P.
Nonlinear ship motions.
In *Proc. 3rd Intl Conf. Num. Ship Hydro., Paris*, pages 257-268. Bassin d'Essais des Carenes, France, 1981.